FAST-zero' 15

3rd *International Symposium on*
Future Active Safety Technology
Toward zero traffic accidents

3rd International Symposium on
Future Active Safety Technology
Toward zero traffic accidents

FAST-zero'15

September 9-11, 2015 Gothenburg, Sweden

Proceedings

Editors:

J. Fredriksson
B. Kulcsar
J. Sjöberg

SAFER
VEHICLE AND TRAFFIC SAFETY CENTRE AT CHALMERS

CHALMERS
UNIVERSITY OF TECHNOLOGY

FVEA
SWEDISH VEHICULAR ENGINEERING ASSOCIATION
SVERIGES FORDONSTEKNISKA FÖRENING

IEEE
Advancing Technology for Humanity

ITSS
IEEE INTELLIGENT TRANSPORTATION SYSTEMS SOCIETY

IFAC
INTERNATIONAL FEDERATION OF AUTOMATIC CONTROL

SAE INTERNATIONAL

FISITA

City of Gothenburg

Dear Colleagues,

On behalf of the organizing committee, it is our pleasure to welcome you to Gothenburg, Sweden and the third FAST-zero symposium.

We are happy to have been trusted with the responsibility to organize FAST-zero'15, first time outside Japan, after the two successful events FAST-zero'11 in Tokyo, and FAST-zero'13 in Nagoya. The symposium takes place at Chalmers Conference Centre at Campus Johanneberg, where a major part of the Swedish academic research on traffic safety is carried out. The symposium is co-organized by Chalmers and SAFER - Vehicle and Traffic Safety Centre at Chalmers, which is a competence centre including 34 partners from the academy, society and industry. From this joint competence platform the symposium has been organized in close collaboration with partners in Japan guaranteeing a continuation of the traditions from the earlier symposia.

The quality of the symposium builds on important contributions from many people. To all symposium participants who have submitted technical papers, keynote speakers, International Scientific Committee, and the Organizing Committee - you have done a great job. We want to highlight the invaluable work by the Japanese team and particularly mention Pongsathorn Raksincharoensak and Yasutoshi Horii who have been the bridge between the organizers in Sweden and in Japan.

We hope you will enjoy the symposium!

General Chairs

Jonas Sjöberg, Professor,   Dr. Anna Nilsson-Ehle,
Department of Signals and Systems   Director of SAFER
Chalmers

CHALMERS

SAFER
VEHICLE AND TRAFFIC SAFETY CENTRE AT CHALMERS

Welcome message from International Scientific Committee Chair

Innovation in the field of active safety is the key driving force towards the ultimate goal of realizing zero traffic-accidents. On behalf of the members of international scientific committee of FAST-zero'15, I am very pleased to welcome you to the 3rd symposium in Gothenburg, Sweden and thank you for your great contribution to the symposium. Following the tradition of FAST-zero symposia born in Japan, we organize technical sessions together with excellent keynote lectures by internationally renowned researchers, in order to bring together researchers and engineers to present the current state-of-the art and progress in research and development of active safety technologies.

In this symposium, 96 papers are accepted as technical papers in the technical sessions.   I would like to thank all members of ISC committee who spend their precious time to review and select high-quality papers for the symposium as well as best paper awards. I would like to express my sincere thanks to Cristina Olaverri-Monreal (Austrian Institute of Technology), Benedikt Schonlau (IAV), Andreas Lie (Swedish Transport Administration) and Erik Coelingh (Volvo Cars) as renowned keynote speakers. Especially, besides regular contributions, I would like to thank Cristina Olaverri-Monreal, Keisuke Suzuki, Motoki Shino and Roman Henze for their great cooperation in organizing the invited sessions on special interest topics. For overall arrangement, I would like to thank Balázs Adam Kulcsár and Jonas Fredriksson for the session program arrangement, and Tomas Mckelvey for the symposium award selection process support. Finally, I would like to thank Björn Peters (VTI) for his effort in the technical visit organization.

Without your contributions and active participation, FAST-zero symposium philosophy would not be possible to realize. During the event, I wish that all of you learn a lot of new findings, have fruitful discussions and also build up networks of active safety researchers. Finally, I wish you a pleasant journey and interesting days during FAST-zero'15 symposium in Gothenburg.

Pongsathorn Raksincharoensak,
FAST-zero'15 International Program Committee Chair

Report from Scientific Program Committee

In 2015, the Symposium on Future Active Safety Technology Towards zero traffic accidents has been taken place in Gothenburg, Sweden, triggering lot of research attention from both academia and industry.

The Symposium program is a good synergy of diversified traffic safety topics. Plenary sessions construct the backbone of the technical program, including selected topics on automated driving and human behavior. These two main trends can be observed in the topic selection of the accepted papers. Moreover, novel ideas have been communicated on crash and naturalistic data analysis, active and passive vehicular safety systems, simulator based studies, just to name a few of them. Four invited sessions have been organized, out of which one was on industrial track.

107 presentations can be found in the conference program (number of papers are a bit less due to the fact that industrial submission does not require papers), from 15 countries all around the World. Full Symposium papers have been accepted on the basis of reviewed extended abstracts by using the regular paper format of International Federation of Automatic Control (IFAC). Reviewing extended abstracts gave us the possibility to mobilize the traffic safety research community in order to ensure the quality standards of the Symposium. From paper submission till proceeding creation, an electronic database (www.easychair.org) has been used facilitating the review and program edition process a lot.

Outstanding papers have been nominated to best paper award. Finally, the high level technical program was accompanied by exciting social and technical visits.

We hope that this community will have many more occasion to meet in order to exchange scientific information, to build network, and to contribute to our joint vision: zero-traffic accident.

Balazs Kulcsar, Pongsathorn Raksincharoensak, Chiyomi Miyajima & Jonas Fredriksson
FAST-zero'15 Program Co-Chair

Organizers

FAST-zero'15 is organized by SAFER Vehicle and Traffic Safety Centre and Chalmers University of Technology, in co-operation with Swedish Vehicular Engineering Association.

Co-sponsors

Gold sponsor

IAV automotive engineering is the gold sponsor of the symposium. www.iav.de

Silver sponsor

Iron sponsors

Exhibitors

BECOME AN IFAC AFFILIATE!

If you are interested in Control Engineering you should become an

IFAC AFFILIATE

This gives you the following benefits

- **Free subscription to the IFAC Newsletter**
  - This bimonthly Newsletter contains information about IFAC's technical activities and forthcoming IFAC events all over the world.

- **Automatic inclusion of your name in our mailing lists for forthcoming events in your areas of interest**
  - IFAC organizes about 40 technical meetings all over the world each year

- **Subscription to the IFAC Journals and IFAC Affiliated Journals at a reduced Affiliate rate**
  - Subscription forms can be obtained by marking the appropriate box on the on-line Affiliate Registration Form, or by writing to the IFAC Secretariat directly.

- **Contribution and participation in IFAC's technical work**
  - IFAC at present has more than 40 technical bodies covering all aspects of Automatic Control Engineering

How to join?

Make an on-line registration directly from the IFAC website:

www.ifac-control.org

www.ifac-control.org/about/ifac-affiliate-registration

Organizing Committee FASTzero'15

General Chairs

Jonas Sjöberg
Professor, Research group leader,
Mechatronics, Signals and Systems,
Chalmers University of Technology,
Sweden

Anna Nilsson-Ehle
Director, SAFER,
Sweden.

Program Chair

Balázs Adam Kulcsár
Assistant Professor, Signals and Systems,
Chalmers University of Technology,
Sweden

Program Co-Chairs

Pongsathorn Raksincharoensak
Associate professor, Tokyo University of
Agriculture and Technology, Japan

Chiyomi Miyajima
Assistant Professor, Nagoya
University, Japan

Jonas Fredriksson
Associate Professor, Chalmers University
of Technology, Sweden

Awards Chairs

Pongsathorn Raksincharoensak
Associate professor, Tokyo University of
Agriculture and Technology, Japan

Tomas McKelvey
Professor, Vice Head of Department, Signals
and Systems, Chalmers University of
Technology, Sweden

Finance Chair, main administrator

Lisa Knutsson
Communications Manager, SAFER,
Sweden

Special Session Chairs

Tomas McKelvey
Professor, Vice Head of Department, Signals and Systems, Chalmers University of Technology, Sweden

Motoki Shino
Associate Professor, Department of Human and Engineered Environmental Studies, University of Tokyo, Japan

Keisuke Suzuki
Professor, Kagawa University, Japan

Local Arrangement Chairs

Lars Hammarstrand
Technology Doctor, Signals and Systems, Chalmers University of Technology, Sweden

Lars-Gustaf Hauptmann
Chair, Swedish Vehicular Engineering Association (SVEA), Sweden

Exhibition and Sponsor Chairs

Erik Ström
Professor, Chalmers University of Technology, Sweden

Yasutoshi Horii
Senior Manager, DENSO SALES SWEDEN, Sweden

Yoshiki Miichi
Project Manager, Product Planning Div., Toyota Motor Corporation, Japan

Technical Visit Chair

Björn Peters
Research leader, VTI, Sweden

Program Committee

Motoyuki Akamatsu	National Institute of Advanced Industrial Science and Technology (AIST), Japan
Mattias Althof	Technical University Munich, Germany
Konstantinos Ampountolas	University of Glasgow, GB
Andras Balint	Chalmers University of Technology, Sweden
Christian Berger	Gothenburg University, Sweden
Alberto Broggi	Università di Parma, Italy
Stefan Byttner	Halmstad University, Sweden
Oliver Carsten	University of Leeds, GB
Erik Coelingh	Volvo Car Corporation, Sweden
Bart De Schutter	Delft Institute of Technology, The Netherlands
Shunichi Doi	Kagawa University, Japan
Cristofer Englund	Viktoria Institute, Sweden
Jonas Fredriksson	Chalmers University of Technology, Sweden
Yoshimi Furukawa	Japan
H. Clay Gabler	Virginia Tech - Wake Forest University, USA
Luiz Goes	ITA, Brasil
François Goulette	MINES ParisTech, France
Jack Haddad	Technion, Israel
Lars Hammarstrand	Chalmers University of Technology, Sweden
John H.L. Hansen	University of Texas at Dallas (UTD), USA
Roman Henze	TU Braunschweig, Germany
Yasutoshi Horii	DENSO Europe, Sweden
Giovanni Indiveri	University of Salento, Italy
Makoto Itoh	University of Tsukuba, Japan
Peter Kronberg	Volvo AB, Sweden
Ferit Kucukay	TU Braunschweig, Germany
Balazs Kulcsar	Chalmers University of Technology, Sweden
Jean-Philippe Lauffenburger	Université de Haute Alsace, France
Tomas McKelvey	Chalmers University of Technology, Sweden
Yoshiki Miichi	Toyota Motor Corporation, Japan
Chiyomi Miyajima	Nagoya University, Japan
Reza Moheimani	University of Newcastle, Australia
Jonas Mårtensson	KTH, Sweden
Lena Mårtensson	KTH, Sweden
Masao Nagai	Japan Automobile Research Institute, Japan
Henk Nijmeijer	TU Eindhoven, The Netherlands
Cristina Olaverri	AIT Austrian Institute of Technology GmbH, Austria
Björn Peters	VTI, Sweden
Pongsathorn Raksincharoensak	Tokyo University of Agriculture and Technology, Japan
Erik Rosén	Autoliv, Sweden
Sergio Savaresi	Politecnico di Milano, Italy
Selpi	Chalmers University of Technology, Sweden
Rini Sherony	Toyota, USA
Motoki Shino	The University of Tokyo, Japan
Steven Shladover	University of California PATH Program, USA
Jonas Sjöberg	Chalmers University of Technology, Sweden
Miguel Ángel Sotelo	University of Alcalá
Johan Stahre	Chalmers University of Technology, Sweden
Christoph Stiller	Karlsruher Institut für Technologie (KIT), Germany
Erik Ström	Chalmers University of Technology, Sweden
Keisuke Suzuki	Kagawa University, Japan
Hadj Hamma Tadjine	IAV, Germany
Kazuya Takeda	Nagoya University, Japan
Ljubo Vlacic	Griffith University, Australia
Takahiro Wada	Ritsumeikan University, Japan
Hidehisa Yoshida	National Defense Academy (NDA), Japan

Keynote speakers

Dr. **Cristina Olaverri Monreal**, AIT Austrian Institute of Technology GmbH Innovation Systems Department Business Unit Technology Experience, Austria

Title: Road Users and Human Machine Interaction

Wednesday, September 9, 08:50, Room: Runan

Dr. **Cristina Olaverri Monreal** received the Ph.D. degree and M.Sc. degree in computer science, computational linguistics and phonetics in cooperation with BMW, from the Ludwig-Maximilians University in Munich, Germany, in 2002 and 2006, respectively. Currently, she is a senior scientist and research group lead with the Austrian Institute of Technology, where her focus is on innovative forms of mobile and ubiquitous interaction, and advanced approaches to human mobility also focusing on a vehicular context. Her experience in the areas of Human Factors and Human-Machine Interaction provides the foundation to minimize the barrier between users and technical systems focusing on the perception of the environment in complex, dynamic scenarios that are critical to decision-making processes. Her research interests lie in multi-functional systems for in-vehicle information and entertainment; overall efficiency of user and system utilization; driver behavior; simulation tools and research concerning Intelligent Transportation Systems (ITS). Dr. Olaverri has been engaged for several years as a member of technical committees, a referee for international conferences on ITS and a (co)-organizer of scientific events. She is the chair of the IEEE ITS Society's Technical Activities Committee on Human Factors in Intelligent Transportation Systems and member of the IEEE ITS Society's Technical Activities Committee on Artificial Transportation Systems and Simulation. She is also the program co-chair for the International IEEE Conference on Intelligent Transportation Systems (ITSC15) and the general chair and (co-)organizer of the Human Factors in Intelligent Vehicles Workshop (HFIV'12, HFIV'13, HFIV'14, HFIV'15) within the IEEE IV'12, IV'13, IV'14 and IV'15. Additionally, she is the general chair and (co-)organizer of the special session on Intelligent Cooperative Driving, and Autonomous Connected Vehicles (ICD & ACV 2014, ICD & ACV 2015), within the International Conference on Collaboration Technologies and Systems (CTS). Currently, Dr. Olaverri is Member of the Board of Governors (BoG) of the IEEE Intelligent Transportation Systems Society (ITSS) (Jan 1, 2015 to Dec 31, 2017), associate editor of the IEEE Transactions on Intelligent Transportation Systems and editor of the ITS Research Lab Spot Light column in the IEEE ITS Magazine. 2013-2014 she was guest editor of the special issue on "Human Factors in Intelligent Vehicles" (HFIV) of IEEE Transactions on Intelligent Transportations Systems (IEEE T-ITS).

Dipl.-Ing. **Benedikt Schonlau**, Head of Department Active Safety & Lighting Functions, IAV GmbH, Germany

Title: Highly automated driving: Whom can you trust?

Thursday, September 10, 08:30, Room: Runan

Benedikt Schonlau finished his degree in Mechatronics in 2005 at the Ostwestfalen-Lippe University of Applied Sciences (Germany). Starting in the field of function development for Driver Assistance and Active Safety he has been working for IAV in Chemnitz for over 10 years now. Between 2007 and 2011 Mr. Schonlau worked as project manager on the topic PreCrash. Since 2012 he is Head of Department Active Safety and Lighting Functions. In this role he is responsible for the worldwide establishment of IAV competencies in this field. He has a track record of fundamental research on these topics which is documented by numerous publications by IEEE, VDI and SAE. He is a member in Car2Car communication consortium as well as in ITS Niedersachsen.

Professor **Anders Lie**, PhD, Swedish Transport Administration, Sweden

Title: Road traffic safety, automated cars and infrastructure – potentials and possibilities

Friday, September 11, 08:30, Room: Runan

Anders Lie, Ph.D. in the field of medicine, is specialist in traffic safety working for the Swedish Transport Administration. He has held his position there since 1995. Anders Lie has been an active partner in the development of the Vision Zero. He has furthermore set-up in depth studies of all fatal crashes in Sweden starting from 1997. From the start he has been representing Sweden as a board member in the Euro NCAP crash test co-operation. Anders Lie has further been active in the development of a Management System Standard for Traffic Safety (ISO 39000).

Anders Lie has written over 50 scientific papers within the field of vehicle safety and is active in many international co-operations. His research is focused on evaluation of new vehicle safety technologies and Vision Zero. The research is also looking at how the introduction of new safety technologies can be followed and integrated in modern management systems such as ISO 39001. In September 2014 Anders Lie was appointed as adjunct professor at Chalmers University of Technology.

Dr. **Erik Coelingh**, Volvo Cars, Sweden

Title: Drive Me – Self-driving cars for sustainable mobility

Friday, September 11, 15:10, Room: Runan

Erik Coelingh, Ph.D. is Senior Technical Leader for Safety and Driver Support Technologies with the Volvo Car Corporation and Adjunct Professor at Chalmers University of Technology in Gothenburg Sweden. He received the M.Sc. and Ph.D. degrees in electrical engineering from the University of Twente, Enschede, The Netherlands, in 1995 and 2000, respectively.

After his studies he joined Volvo Car Corporation and worked in several projects on vehicle control and active safety. He was responsible for the first application of collision mitigation by braking on the Volvo S80 in 2006 and led the advanced engineering activities for Pedestrian Detection with Full Auto Brake which was launched in 2010. Currently he is responsible for Volvo's technical strategy for safety and driver support technologies and works actively on research and development of various collision avoidance and automated driving features, such as e.g. the Drive Me project.

Copyright Agreement

Program at a glance

Tuesday, September 8, 2015

18:30-20:00
Welcome Reception & Registration
Location: Dicksonska Palatset, Parkgatan 2, Gothenburg

Wednesday, September 9, 2015

08:00
Registration & Coffee

08:30-08:50
Opening ceremony
Room: Runan

08:50-09:35
Keynote 1: Road Users and Human Machine Interaction
Dr. Cristina Olaverri Monreal, AIT Austrian Institute of Technology GmbH, Innovation Systems Department Business Unit Technology Experience, Austria
Room: Runan

09:35-10:00 Coffee & Green Tea Break

Room: Palmstedtsalen	*Room: Scaniasalen*	*Room: Runan*
10:00-11:40 Automated driving - safety and reliability I	10:00-11:40 Pedestrian safety	10:00-11:40 Traffic systems
11:40-12:40 Lunch Break		
12:40-14:45 Safety analysis	12:40-14:45 Automated driving - driver behaviour	12:40-14:45 Safety oriented driver modelling and analysis
14:45-15:10 Coffee & Green Tea Break		
15:10-16:55 Driver analysis	15:10-16:55 Driver analysis and support systems	15:10-16:55 Risk assessment
16:55-21:00 Technical Demos at AstaZero *(Pre-registration mandatory)*		

Thursday, September 10, 2015

08:00
Coffee & Green Tea

08:30-09:15

Keynote 2: Highly automated driving: Whom can you trust?

Dipl.-Ing. Benedikt Schonlau, Head of Department Active Safety & Lighting Functions, IAV GmbH , Germany

Room: Runan

09:15-09:40 Coffee & Green Tea Break

Room: Palmstedtsalen	*Room: Scaniasalen*	*Room: Runan*
09:40-11:45 Detection, sensing and localization	09:40-11:45 Safety on crossing	09:40-11:45 Automated driving

11:45-13:00 Lunch Break

Room: Palmstedtsalen	*Room: Scaniasalen*	*Room: Runan*	12:45-15:15 Technical Visit at Lindholmen (Group 1) *Pre-registration mandatory*
13:00-14:40 Estimation techniques for active and passive safety	13:00-14:40 Automated driving - vehicle platoons	13:00-14:40 Autonomous driving and crash analysis	

14:40-15:20 Coffee & Green Tea Break			14:45-17:15 Technical Visit at Lindholmen (Group 2) *Pre-registration mandatory*
Room: Palmstedtsalen	*Room: Scaniasalen*	*Room: Runan*	
15:20-17:00 Traffic safety	15:20-17:00 Driving dynamics	15:20-17:00 Crash and naturalistic data	

18:30-23:00

Banquet dinner

Location: Universeum, Södra Vägen 50, Gothenburg

Friday, September 11, 2015

08:00
Coffee & Green Tea

08:30-09:15

Keynote 3: Road traffic safety, automated cars and infrastructure – potentials and possibilities
Prof. Anders Lie, Swedish Transport Administration, Sweden.

Room: Runan

09:15-09:40 Coffee & Green Tea Break

Room: Palmstedtsalen	*Room: Scaniasalen*	*Room: Runan*
09:40-11:20 Analysis and Modeling for Driver Performance I	09:40-11:20 Safety and driver assistant systems	09:40-11:20 Vehicle Automation and Connected Safety

11:20-12:40 Lunch Break

12:40-14:45 Analysis and Modeling for Driver Performance II	12:40-14:45 Safety system evaluation	12:40-14:45 Safe driving and simulators

14:45-15:10 Coffee & Green Tea Break

15:10-15:55

Keynote 4: Drive Me – Self-driving cars for sustainable mobility

Dr. Erik Coelingh, Volvo Cars, Sweden

Room: Runan

15:55-16:20

Prize and closing ceremony

Room: Runan

Conference Program

Asymmetric Collision Risk Spacing Policy for Longitudinal Control of Autonomous Driving Vehicle

S. Tak*, H. Yeo. **, †

**Department of Civil and Environmental Engineering, Korea Advanced Institute of Science and Technology, Daejeon, Korea,
(e-mail: taksehyun@kaist.ac.kr)*

***Department of Civil and Environmental Engineering, Korea Advanced Institute of Science and Technology, Daejeon, Korea,
(e-mail: hwasoo@kaist.ac.kr)*

Abstract: Spacing policy for autonomous vehicles is one of the important issues because it is highly related to the safety on the roads, efficiency of vehicles, and user satisfaction of autonomous vehicles. Many researchers have developed several spacing policies for autonomous vehicle control. Most of the spacing policies are mainly focused on the control scheme such as string stability and safety. So, the issues related to user satisfaction and possible effect of autonomous vehicles on manual vehicles are less considered especially in the mixed traffic situation of autonomous and manual vehicles. In this study, we propose an Asymmetric Collision Risk(ACR)-based spacing policy based on the analysis on collision risk and driving behavior. The proposed spacing policy is compared with other spacing policies by simulating with trajectories of human drivers. Based on the simulation results, the performance of each spacing policy is compared in terms of vehicle operation, CO_2 emission and safety. The results show that ACR spacing policy has similar pattern with the human driver with smoother trajectory and less acceleration/deceleration actions. In terms of road efficiency and environment, the proposed ACR spacing policy shows the second best performance next to Safety Spacing policy. However, in terms of safety in mixed situation of manual and autonomous vehicles, ACR spacing policy is superior to other spacing policies with zero occurrence of critical event. By considering overall performance, the proposed ACR spacing policy is expected to generally show good performance in the mixed traffic situation of manual and autonomous vehicles.

Keywords: Adaptive Cruise Control, Spacing Policy, Longitudinal Control

1. INTRODUCTION

Intelligent Transportation System (ITS) is designed not only to improve the safety and efficiency of road, but also to provide convenient services to drivers. In an effort to meet these purposes, various technologies are proposed such as collision warning system, accident detection system, and adaptive cruise control system. These systems can effectively improve the safety and efficiency on the road, however, in recent years, the decreasing rate of accident occurrences and the improvement of efficiency are almost standstill. An innovative system is needed in order to further improve the people's safety in vehicle operations.

Among various technologies, autonomous vehicle, which autonomously controls longitudinal and later movements with information from installed sensors and communication, is one of promising technology to further improve the safety. Autonomous vehicle is initially designed to improve the driving comfort and convenience by relieving driver from vehicle manoeuvrings. Due to the smaller reaction time and smaller time gaps between two consecutive vehicles than human driver, the autonomous vehicle can also further improve the safety and efficiency of vehicles.

The performance of an autonomous vehicle is highly related to the spacing policy (or range policy) of the autonomous vehicle. The spacing policy refers to the desired state that ACC system attempts to maintain from the preceding vehicle, and vehicle performances such as vehicle safety, traffic flow stability, and user acceptance are greatly related to the spacing policy of autonomous vehicle. To enhance the various aspects of autonomous vehicle, various types of spacing policy such as Constant Spacing Policy (CSH), Constant Time Headway spacing policy (CTH), Safety Spacing policy (SS), Human Driving Behavior-based spacing policy (HDB), and Variable Spacing policy (VS) are proposed. Constant Spacing Headway (CSH) was suggested by Shladover to improve the road capacity especially for the platoon driving (Shladover 1991). CSH can significantly increase the road capacity with tight following distances. However, for high string stability, it requires very accurate information on leader vehicles with very short time interval and it is not feasible in the mixed traffic situation of autonomous vehicle and manual vehicle.

Constant Time Headway policy (CTH) is the most common spacing policy, which is applied to longitudinal control of vehicle by automakers and researchers (Wang & Rajamani 2004; Swaroop & Rajagopal 2001). Unlike the CSH, the information used in CTH can be easily obtained. In CTH, the

desired spacing of the subject vehicle is proportional to the velocity. Due to the easy implementation of the spacing policy, much works have been done in the study of longitudinal vehicle control with CTH spacing policy (Nouveliere & Mammar 2003; Nouveliere 2007). However, CTH spacing policy is not appropriate for used in high density traffic situation and traffic flow stability cannot be ensured by using the simple application of standard CTH spacing policy.

To make an appropriate spacing policy in high density traffic situation and improve the safety aspect of the longitudinal vehicle control, Safety Spacing (SS) policy was proposed (Zhao & Kamel 2010). SS policy mimics the human driving behavior especially focusing on the safety. In the SS policy, the desired spacing of the subject vehicle is determined by the speed and vehicle's braking distance. SS policy can render the vehicle safe no matter how severe the deceleration of vehicle is, by keeping a safe spacing according to vehicle state (velocity and spacing) and maximum braking performance. Furthermore, SS policy can provide more stable traffic flow and improved traffic capacity compared to CTH spacing policy. However, the study on SS policy is based on the extreme sample scenario, so the possible various traffic situations are not considered. The applicability in mixed traffic situation is not guaranteed.

To improve the traffic flow and stability constraints, Human Driving Behavior (HDB) spacing policy is proposed based on an averaged human range policy (Zhou & Peng 2005). The HDB spacing policy is the form of a quadratic curve, which is obtained from the observed data of human driving behavior. The HDB spacing policy can render the critical density higher than human driver and render the maximum sensitivity to external stimuli lower than human driver. However, this study is compared to the Gipps' car following model, so it is limited to show the practical effects of HDB spacing policy on traffic flow and string stability. It is also limited to show the human driving behavior in various traffic situations, because HDB spacing policy is based on the averaged driver behavior.

To overcome the limitation of CTH and improve the traffic flow and road capacity, Variable Spacing (VS) policy is proposed (Wang & Rajamani 2004). The VS policy is simulated in various traffic situations such as sudden brakes of preceding vehicle, a slower moving preceding vehicle, and a lane changing vehicle. The VS spacing policy shows improved safety, string stability, and road capacity compared to CTH spacing policy. However, VS spacing policy is still tested in virtual trajectories of preceding vehicles, so the effect of VS spacing policy in the mixed traffic situation of autonomous vehicle and manual vehicle is not clearly proved.

In previous studies, spacing policy and the associated control law can be evaluated from the point of view of string stability, traffic flow stability, and traffic flow capacity (Santhanakrishnan & Rajamani 2003). Most studies are based on virtual trajectories of preceding vehicles and rarely consider possible situations in the mixed traffic situation of autonomous vehicle and manual vehicle. In terms of being applied in mixed traffic situation, the existing studies on spacing policy have some limitations. First, the effect of mechanical movement of vehicle, which shows different movement to a manually driven vehicle, on safety of following human driver is not considered. The autonomous vehicle is always along with the surrounding manual vehicles especially when the market penetration rate is low. In this context, mechanical movement of autonomous vehicle can render the following human driver unsafe because human driver drives a vehicle based on the assumption that the trajectory of preceding vehicle is similar to the human behavior especially when the market penetration rate of autonomous vehicle is low. Therefore, the possible effect of autonomous vehicles on the road to the safety of following human drivers must be evaluated. Second, the microscopic driving behavior in the previous spacing policy studies is rarely considered. The autonomous vehicle is designed to replace the role of human driver. Similar movement of autonomous vehicle with that of human driver is required to improve the user acceptability. However, the existing spacing policy is rarely based on the more detailed, microscopic driving behavior of human driver and only few studies are based on the averaged driving behavior. Third, other important issues such as CO_2 emission are not considered.

To enhance the limitation of current studies, a new spacing policy, which shows the similar vehicle movement to the human driving, is proposed. This new spacing policy is based on the relationship between human driving behavior and estimated collision risk. The new spacing policy is evaluated and compared to other spacing policy in terms of similarity to human driver, road efficiency, CO2 emission, and possible effect on safety of following human driver. For the comparison analysis, each spacing policy is simulated with the human trajectory data to be simulated in a mixed environment of autonomous vehicle and manual vehicle.

2. NEW SPACING POLICY

2.1 Collision Risk and Driving Behavior

To be acceptable to human drivers, the movements of autonomous vehicles must be similar to the driving behavior of manual vehicles. Among various psychological factors, collision risk of driver is highly related to the celebration behaviour of driver in the previous studies (Wåhlberg 2006a; Wåhlberg 2007; Wåhlberg 2006b; Tak et al. 2015). Based on this knowledge, we analyze the microscopic driving behavior and identify the relationship between the estimated collision risk and driving action.

The relationship between the estimated collision risk and driving action is analyzed in both speed-spacing plane and relative speed-spacing plane to show different aspects of driving behavior. The collision risk in car-following situation is estimated by the Deceleration-based surrogate safety measure (DSSM), which shows the balanced estimated performance in various traffic situation such as acceleration phase and deceleration phase (Tak et al. 2015). DSSM is based on the minimum stopping distance constraint to prevent collision and is mathematically expressed as:

$$
\begin{aligned}
K &= [x_n(t) - x_{n-1}(t) + s_{n-1}] + [2 \cdot v_n(t) + a_n(t) \cdot \tau] \cdot \frac{\tau}{2} \\
&\quad - \left[v_{n-1}(t)/2 + \frac{(a_{n-1}(t) + b_{max,n-1})}{4} \cdot \frac{(a_{n-1}(t) - b_{max,n-1})}{L_{n-1}} \right] \\
&\quad \cdot \frac{(a_{n-1}(t) - b_{max,n-1})}{L_{n-1}} \\
&\quad + \left[v_n(t)/2 + a_n(t) \cdot \tau + \frac{(a_n(t) + b_{max,n})}{4} \cdot \frac{(a_n(t) - b_{max,n})}{L_n} \right] \\
&\quad \cdot \frac{(a_n(t) - b_{max,n})}{L_n}
\end{aligned} \tag{1}
$$

$$
b_n(t) = b_{max,n-1}(t) \cdot \frac{[v_n(t) + a_n(t) \cdot \tau]^2}{[2 \cdot K \cdot b_{max,n-1}(t) + v_{n-1}(t)^2]} \tag{2}
$$

$$
DSSM_{Sub,n}(t) = \frac{b_n(t)}{b_{max.n}} \tag{3}
$$

where $a_n(t)$ is the acceleration rate of following vehicle at time t, $a_{n-1}(t)$ is the acceleration rate of leader vehicle at time t, $b_{max.n-1}$ is the maximum braking rate of leader vehicle, which represents the vehicle's mechanical deceleration performance, $b_n(t)$ is the needed deceleration rate of following vehicle to avoid the accident at time t, $b_{max.n}$ is the maximum braking rate of following vehicle, $v_{n-1}(t)$ is the speed of leader vehicle at time t, $v_n(t)$ is the speed of following vehicle at time t, L_{n-1} is the maximum variation of acceleration of leader vehicle, L_n is the maximum variation of acceleration of following vehicle, $v_n(t+\tau)$ is the expected speed of following vehicle after τ, $x_{n-1}(t)$ is the location of leader vehicle at time t, $x_n(t)$ is the location of following vehicle at time t, τ is the perception reaction time, and s_{n-1} is the length of leader vehicle.

Fig. 1 shows the relationship between estimated collision risk and driving action in a speed-spacing plane. This plot shows how driver adjusts the speed of subject vehicle in response to collision risk based on the concept of asymmetric driving behavior (Yeo et al. 2008; Yeo & Skabardonis 2011; Yeo 2008). The black dotted circles and black solid circles in Fig. 1 are the cases that the driver start the acceleration or deceleration action to adjust collision risk. In the areas near the black dotted circles, which are occurred during the deceleration process, the high collision risks are occurred right before the state of subject vehicle reaches to the deceleration action point line. The collision risks are sharply decreased after the driver starts deceleration action. In the areas near the black solid circles, which are occurred during the acceleration process, the high collision risks are occurred right before the state of subject vehicle reaches A-curve, which is boundary curve from acceleration side. The collision risks are decreased after the state of subject vehicle is reached to the A-curve as the subject vehicle maintains a constant speed. The collision risks are gradually reduced until the state of subject vehicle reaches to the acceleration action point line.

Fig. 2 shows the relationship between estimated collision risk and driving action in a relative speed-spacing plane. This plot shows how a driver differently reacts to collision risk when the relative speed is increasing and decreasing based on the concept of 'action point model' (Brackstone & McDonald 1999; Delorme & Song 2001). The collision risk significantly changed before and after the action points, which are marked with black dotted circles. After the action points, which are

occurred when the preceding vehicle is slower than subject vehicle, the estimated collision risk is sharply decreased. After the action points, which are occurred when the preceding vehicle is faster than subject vehicle, the estimated collision risk of DSSM shows the increasing trend and high collision risk is also observed.
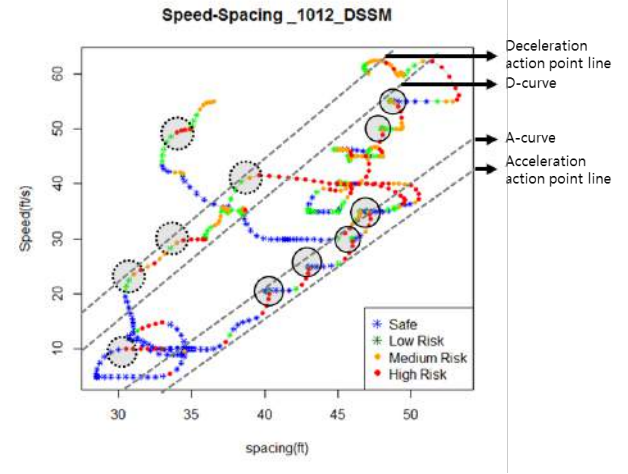
Fig. 1. The relationship between estimated collision risk (DSSM) and driving action (acceleration and deceleration) in a speed-spacing plane (example case).
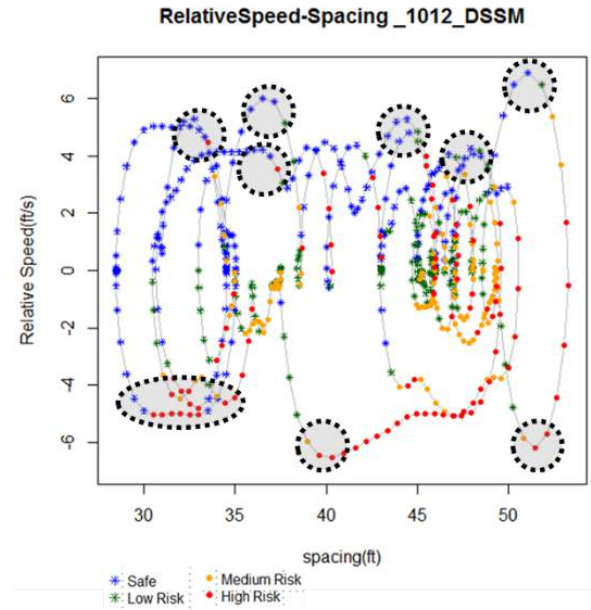
Fig. 2. The relationship between estimated collision risk (DSSM) and driving action (acceleration and deceleration) in a relative speed-spacing plane (example case).

This relationship between collision risk and acceleration and deceleration behavior is also observed in the DSSM (collision risk)-time plane. Fig. 3 shows the changes in DSSM in the car following situation. Blue dots represent the acceleration actions and red dots represent the deceleration actions. The gray line is the trend of DSSM. In Fig. 3, the collision risk and acceleration and deceleration action show the similar pattern with Fig. 1 and the different patterns in acceleration process

and deceleration process are more clearly observed. During the acceleration process, the driver gradually increases the speed based on the continuous interaction to collision risk, which represents external stimuli. In the acceleration process, initially the driver increases the speed until the collision risk is somewhat increased and maintain the constant speed. After the collision risk is reduced due to the constant speed, the driver increases the speed again and the collision risk is also increased. The amount of acceleration is generally same or larger than the amount of previous acceleration. The peak value of DSSM is also increased compared to the peak value of DSSM during the previous acceleration. The acceleration behavior and the trends of acceleration and collision risk are observed in most acceleration processes.

(a) DSSM collision risk _ example 1
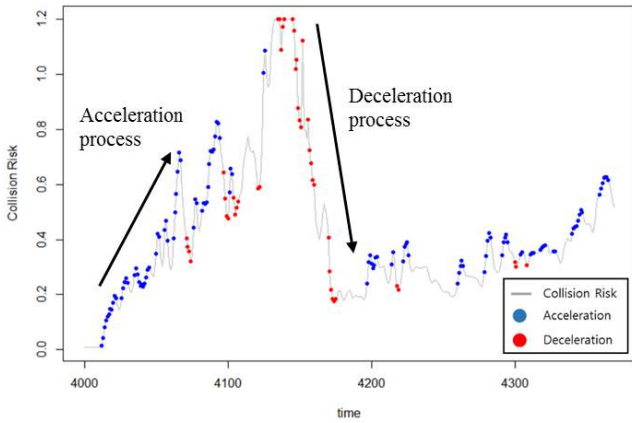
(b) DSSM collision risk _ example 2
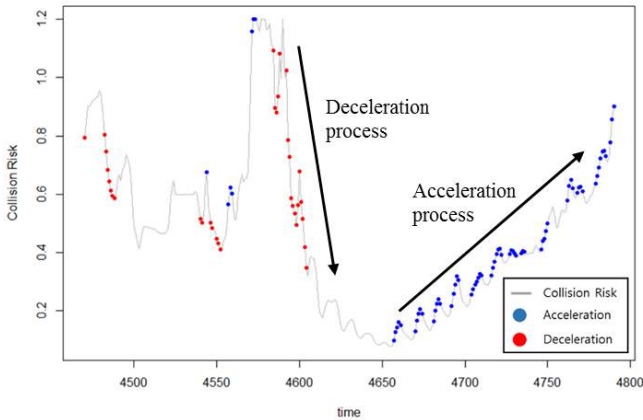
Fig. 3. The relationship between DSSM (collision risk) and driving behaviour in collision risk-time plane

2.2 Collision Risk-based Spacing Policy

In the analysis of relationship between the collision risk and driving behavior, the results show that the driver adjusts acceleration and deceleration based on the estimated collision risk of subject vehicle in the car-following situation. When the collision risk is high, the driver decelerates to reduce the collision risk to certain level. In contrast, when the collision

risk is low, the driver accelerates until the collision risk reach certain level. Based on these driving behaviors, we propose the Asymmetric Collision Risk(ACR) spacing policy as follows:

$$
\begin{aligned}
&a_{des,n}(t)\\
&= \begin{cases}
a_{max}(t) \cdot \dfrac{(TH_{acc} - DSSM_{Sub,n}(t))}{Std_{up}}, & DSSM_{Sub,n}(t) < TH_{ac}\\
0, & TH_{dec} \leq DSSM_{Sub,n}(t) \leq TH_{acc}\\
-b_{max.n} \cdot \dfrac{(TH_{dec} - DSSM_{Sub,n}(t))}{1.2 - TH_{dec}}, & DSSM_{Sub,n}(t) > TH_{de}
\end{cases}
\end{aligned} \quad (4)
$$

The value for making decision on acceleration and deceleration actions is determined based on the calculated DSSM value ($DSSM_{Sub,n}(t)$). The longitudinal control algorithm consists of three parts. (1) The subject vehicle increases the speed proportionally to the difference between TH_{acc} and calculated DSSM. TH_{acc} is the reference point for determining the acceleration action and 0.7 is used for that value in this study. The frequent acceleration action is prevented and the intensity of acceleration rate is increased by decreasing the TH_{acc}. (2) The subject vehicle maintains the current speed when the calculated $DSSM_{Sub,n}(t)$ is between TH_{acc} and TH_{dec}. (3) The subject vehicle reduces the speed proportionally to the difference between TH_{dec} and calculated $DSSM_{Sub,n}(t)$. TH_{dec} is the reference point for determining the deceleration action and 0.85 is used for that value in this study. By changing the TH_{dec} value, the degree of risk taking is determined. For example, the driver who wants to reduce the collision risk can decrease the TH_{dec}. On the other hand, the driver who does not wants frequent braking can increase the TH_{dec} up to 1.0. TH_{acc} and TH_{dec} can be adjusted depending on the user preferences and system objectives

3. CASE STUDY

In order to evaluate the performance of each spacing policy, this study uses the Next Generation Simulation (NGSIM) trajectory data collected from a highway site called I-80 in California, US (Anon 2006). The NGSIM data have been used for validation and calibration of microscopic traffic models by many researchers (Thiemann et al. 2008; Lu & Skabardonis 2007). Especially, the NGSIM data can well represent both uncongested and congested traffic flow conditions. So, it is useful for studying the effect of newly proposed algorithm in the various traffic situations.

To simulate the spacing policy in various traffic situations, we extract the car–following cases, which do not have any disturbances such as cut-in vehicle, lane changing, and accidents. In this context, we extract the total 926 car-following cases from the NGSIM trajectories and classify the car-following cases based on the maximum speed, minimum speed, average speed, and standard deviation of speed by using the k-mean clustering method. Fig. 4 shows the clustering results of car-following cases. The car-following cases are clustered into 4 clusters: high average speed with medium standard deviation cases (1), low standard deviation of speed cases (2), high standard deviation of speed cases (3), and low average speed with medium standard deviation cases (4). Each cluster represents different car-following cases. High average

speed with medium standard deviation cases (1) represent the car-following cases in high speed with moderate shockwave. Low standard deviation of speed cases (2) represent the car-following cases in high speed without shockwave. High standard deviation of speed cases (3) represent the car-following cases with severe shockwave. Low average speed with medium standard deviation cases (4) represent the car-following cases in low speed with moderate shockwave.
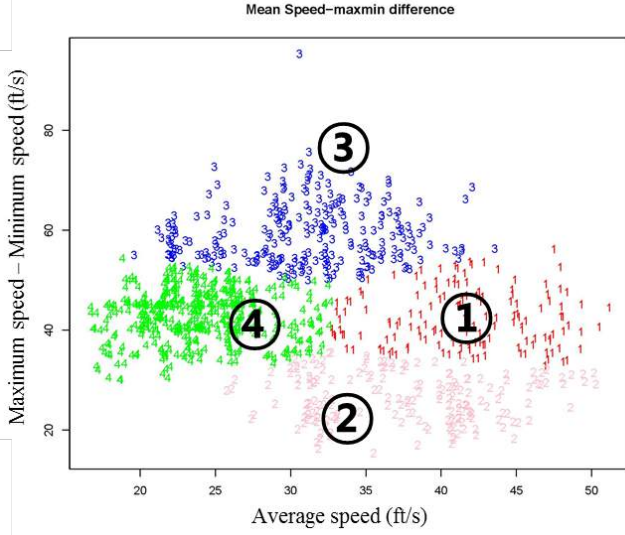
Fig. 4. Clustering result

4. COMPARISON ANALYSIS

The performance of the proposed ACR spacing policy is compared with those of other spacing policies, such as Constant Time Headway policy (CTH), Safety Spacing policy (SS), Human Driving Behavior spacing policy (HDB), and Variable Spacing policy (VS), based on the microscopic trajectory data. The details on each spacing policy is in Table 1.

The performance of each spacing policy is evaluated in terms of similarity to human driver, road efficiency, CO_2 emission, and possible effect on safety of following human driver. The vehicle operation characteristics are analyzed based on the average speed, standard deviation of speed, acceleration amount, and deceleration amount. Based on this analysis, the possible effects of various spacing policies on the road performance are evaluated and the similarity between human driver and autonomous vehicle is also evaluated. The CO_2 emission is estimated by VT-Micro model to evaluate the effect of autonomous vehicle on the environment (El-Shawarby et al. 2005). The effect on safety is evaluated based on the frequency of the critical event, which indirectly represents the dangerous situation. The critical event such as severe deceleration renders the human following driver dangerous, and it is highly related to the accidents caused by following vehicle. In this section, severe deceleration, which is common critical event, is used to measure the safety and -13ft/s² is used as the threshold value for critical situation.

Table 1. Spacing policies for comparison analysis

CTH	$a_{des,n}(t) = -1/h \cdot (v_n(t) - v_{n-1}(t) + \lambda \cdot \delta_i)$ $\delta_i = x_{n-1} - x_n + h \cdot v_n(t) + L,$
SS	$a_{des,n}(t) = -(\lambda \cdot \delta_i + x_{n-1} - x_n)/(t - \frac{\gamma}{b_{max,n}} \cdot v_n(t))$
HDB	$R_n(t) = A + T \cdot v_n(t) + G \cdot v_n(t)^2$ $a_{des,n}(t) = \left(1 - \tau \cdot \frac{T_v}{T_a}\right) \cdot a_n(t-1) + \frac{\tau}{T_a} \cdot \dot{R}_n(t) + \frac{\tau \cdot \lambda}{T_a} \cdot \epsilon_n(t)$
VS	$S(v_n(t))(t) = \frac{1}{\rho_m(1 - v_n(t)/v_f)}$ $a_{des,n}(t) = -\rho_m(v_f - v_n(t))(1 - \frac{v_n(t)}{v_f})(\dot{\epsilon}_n + \lambda \delta_n)$

where, $v_n(t)$ is the speed of subject vehicle, $v_{n-1}(t)$ is the speed of preceding vehicle, λ is a control gain, x_{n-1} is the location of subject vehicle, x_n is the location of preceding vehicle, h is the time headway, L is a constant that includes the vehicle length (sn-1) of leader vehicle, L is a constant distance that includes the vehicle length, k ia a time delay of the longitudinal control system, γ is a safety coefficient, d_n is a subject vehicle's braking distance, $b_{max,n}$ is the maximum braking performance of the subject vehicle, R is the desired spacing, A is the clearance at standstill, T and G are the coefficients, τ is the time constant, T_a is a control gain, $a_n(t-1)$ is the acceleration at time t, q is the convergence rate of the sliding surface, $S(v_n(t))(t)$ is the desired distance at time t, ρ_m is a density parameter, v_f is a speed parameter.

5. COMPARISON RESULTS

Fig. 5-11 show the simulation results of five spacing policies in various traffic conditions. The performance of five spacing policies are compared to human driver to show the effect of the autonomous vehicle and similarity between the movement of autonomous vehicle and the movement of manual vehicle. Fig. 5 shows the average spacing of autonomous and manual vehicle in four different traffic situations. The proposed ACR spacing polity show the most similar average spacing to the human driver in all traffic situations. SS, HDB, and VS show the smaller average spacing compared to human driver and CTH shows much large average spacing than human driver. Among five spacing policies, HDB uses the road with shortest spacing. The manual and autonomous vehicle shows the different spacing depending on the traffic situations.

Except for CTH spacing policy, human driver and autonomous vehicle show the longest average spacing in the high average speed with medium standard deviation case because the human driver and autonomous vehicle shows the increasing trend of spacing as the speed of vehicle increases. However, CTH spacing policy shows the highest average spacing in the high standard deviation of speed case. CTH spacing policy is mainly designed to be used in the free flow traffic state or in the situation when the speed of subject vehicle is similar to that of preceding vehicle. In the low standard deviation of speed case and high speed with low standard deviation case, the

situation where the speed difference between preceding and subject vehicle is large is occurred less frequently than other two traffic situations, so the average spacing is relatively small. However, in the high standard deviation of speed case and low average speed with medium standard deviation case, the situation where the speed difference between preceding and subject vehicle is large is frequently occurred especially after the vehicle meets the shockwave. In this situation, the vehicle with CTH spacing policy does not follows the preceding vehicle with close spacing and it is the reason why CTH spacing policy shows the large average spacing when the standard deviation of speed is high.
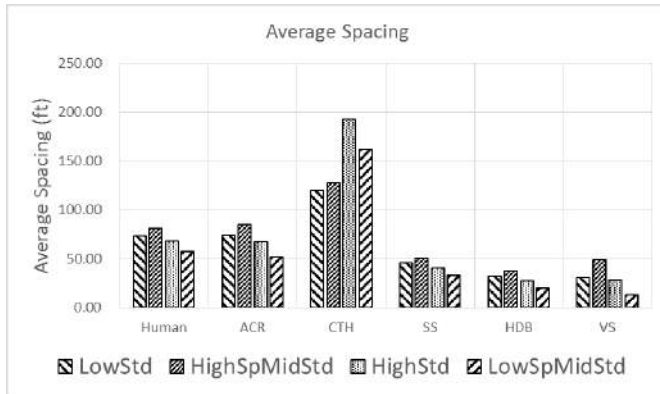
Fig. 5. Comparison of average spacing (ft)
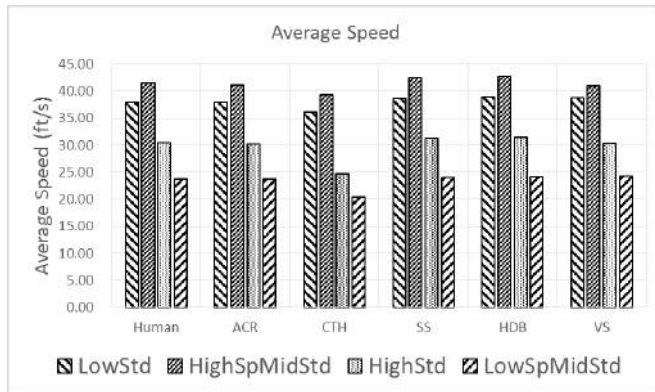
Fig. 6. Comparison of average speed (ft/s)
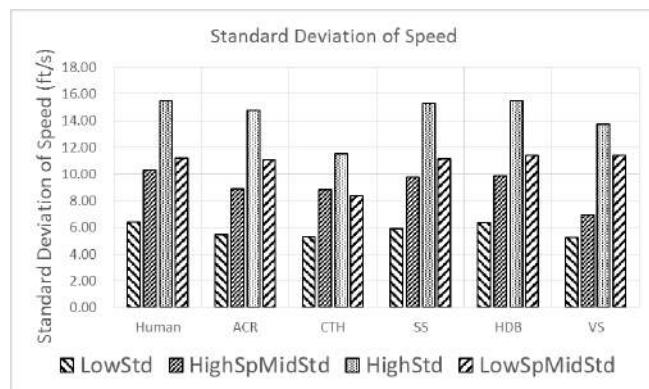
Fig. 7. Comparison of standard deviation of speed (ft/s)

Fig. 6 and Fig. 7 show the average speed and standard deviation of speed in four different traffic situations. Unlike the results on average spacing analysis, human driver and five spacing polies generally show the similar trends and values in all traffic situations except for CTH spacing policy. In detail, the ACR spacing policy is slightly more similar to human driver in terms of average speed with low standard deviation. With this result, the ACR spacing policy is expected that it shows more smoothed trajectory with similar speed to human driver. The CTH spacing policy show the lowest standard deviation of speed in all traffic situations and the magnitude of reduction is large in the high standard deviation of speed case. This result indirectly shows that CTH spacing policy can render the large fluctuation trajectory smooth and this effect leads to the elimination of possible negative influence caused by the shockwave. However, this positive effect of CTH spacing policy is due to the loss of spacing and it is directly related to the loss of road capacity.

The capacity of the road is highly related to the average spacing and average speed of vehicle. With a same preceding vehicle, a spacing policy, which shows both low average spacing and high average speed, has a huge possibility to improve the road capacity when apply to the autonomous vehicle. In this perspective, SS and HDB spacing policy can increase the road capacity with low average spacing.
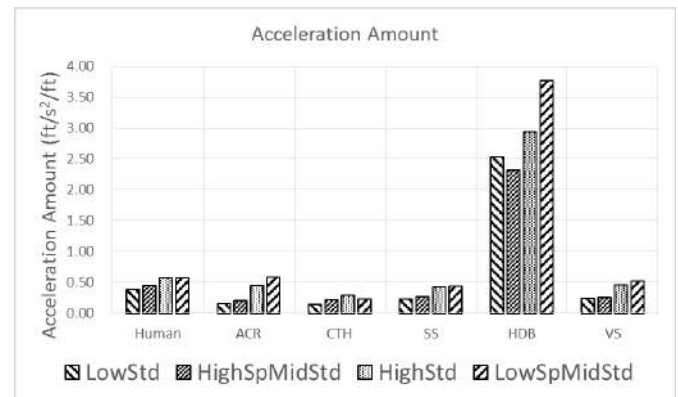
Fig. 8. Comparison of total acceleration (ft/s^2)
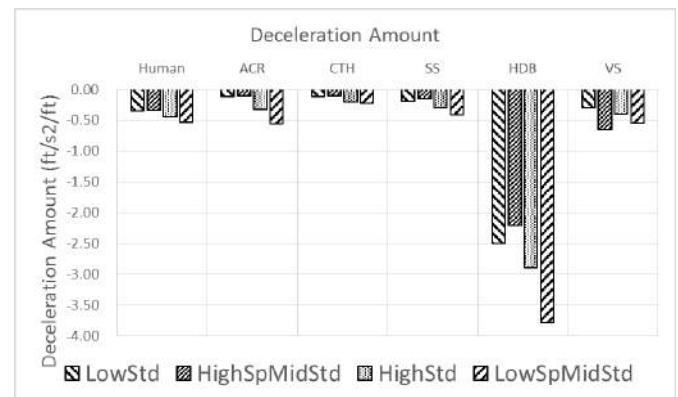
Fig. 9. Comparison of total deceleration (ft/s^2)

Fig. 8 and Fig. 9 show the total acceleration and deceleration amount during the car-following in different traffic situations. This analysis indirectly shows the fuel consumption of vehicle and indirectly shows the feelings on movement of autonomous vehicle because not only the frequent acceleration and

deceleration actions but also frequent changes in acceleration and deceleration behavior render the human in the vehicle distressing. Except HDB spacing policy, human driver and other spacing policy show the similar acceleration and deceleration amount during the whole car-following situation in the all traffic situations with same trend. Both acceleration and deceleration amount are increased as the standard deviation of speed increases, so the high standard deviation of speed case and the low average speed with medium standard deviation case show higher absolute values than other traffic states. These trend is caused by the negative influence of shockwave, which produces and propagates the stop-and-go traffic, in the high standard deviation of speed case and the low average speed with medium standard deviation case.

The proposed ACR shows smaller absolute amount of acceleration and deceleration compared to human driver especially in high average speed with medium standard deviation case and low standard deviation of speed case. By considering the result in average spacing and average speed, the proposed ACR shows the similar trajectory to the human driver with less acceleration and deceleration actions. The HDB shows the worst performance in the acceleration and deceleration analysis. In the HDB spacing policy, more acceleration up to 16 times and more deceleration up to 22 times are occurred compared to proposed ACR. The HDB spacing policy is not feasible in the perspective of acceleration and deceleration actions.

Fig. 10 shows the comparison of CO_2 emission of manual and autonomous vehicles in the different traffic situation. In the CO_2 emission, all spacing policies shows the similar pattern according to the traffic situations. Highest CO_2 emission observed in the low speed with medium standard deviation case and second highest CO_2 emission is observed in high standard deviation case.

Comparing the CO_2 emission of human driver, ACR, CTH, and SS spacing policies generally reduce the CO_2 emission in all cases. In the high speed of low standard deviation case, the reduction rate of CO_2 emission is up to 4% in ACR spacing policy and CTH spacing policy, 2% in SS spacing policy. In the high standard deviation case and low standard deviation case, the reduction rates of CO_2 emission are 3% in ACR spacing policy, 4% in CTH spacing policy, and 2% SS spacing policy. However, the CO_2 emission of HDB and VS spacing policy is much larger than that of human driver with larger fluctuation according to the traffic situations. Especially, HDB spacing policy more emits CO_2 than human driver. In the perspective of CO_2 emission, the ACR and CTH spacing policies shows the better performance than other spacing policies with small changes in CO_2 emission according to the to traffic situations.

Fig. 11 shows the average frequency of critical event caused by the autonomous vehicles. The critical event is highly related to the collision risk of both the subject vehicle and following vehicle and this renders the following vehicle significantly dangerous especially when the following vehicle is driven by human. In this section, the critical event is defined by the sever deceleration below -13ft/s². As shown in Fig. 11, the ACR and CTH spacing policies rarely generate the critical event and

especially, in the ACR spacing policy, there are no critical event. In the mixed traffic situation of manual and autonomous vehicle, the proposed ACR spacing policy may be most safe among five spacing policies. Other spacing policies such as SS, HDB, and VS spacing policy generate many critical event. Among these spacing policies, the frequency of critical event is extremely high in HDB spacing policy and this is related to the frequent acceleration and deceleration action of HDB spacing policy. The important findings of this analysis is that the frequency of the critical events of SS, HDB, and VS spacing policies is increased as the standard deviation of speed is increases.
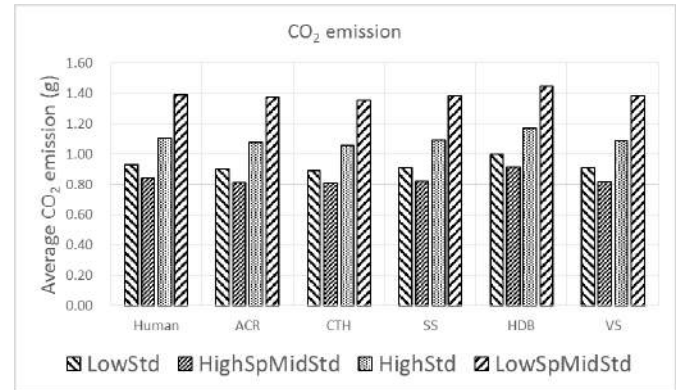
Fig. 10. Comparison of average CO2 emission (g)
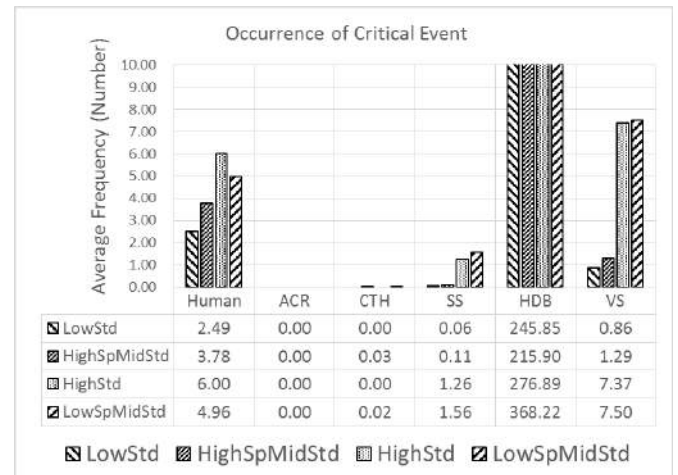
Fig. 11. Comparison of Average frequency of critical event

6. CONCLUSION

In this paper, we propose an Asymmetric Collision Risk (ACR) spacing policy based on the analysis of relationship between collision risk and driving behaviors such as acceleration and deceleration actions. The performance of the proposed ACR spacing policy is compared to that of other spacing policies and human driver based on the simulation with human leader vehicle. The results show that ACR spacing policy shows the similar pattern to the human driver with smoother trajectory and less acceleration/deceleration actions.

In terms of positive impacts on road efficiency and environment, overall, SS spacing policy shows the better performance than other spacing policies. Due to the relatively lager average spacing of ACR spacing policy, the proposed

ACR spacing policy shows the second best performance next to the SS spacing policy. However, in terms of safety for mixed situation of manual and autonomous vehicles, ACR spacing policy is superior to other spacing policies with zero occurrence of critical event. Proceeding from what has been said above, ACR spacing policy is expected to generally show the good performance in the mixed traffic situation of manual and autonomous vehicles.

7. ACKNOWLEDGEMENTS

8. REFERENCES

Anon, 2006. NGSIM - Next Generation Simulation. Available at: http://ngsim-community.org/.

Brackstone, M. & McDonald, M., 1999. Car-following: a historical review. Transportation Research Part F: Traffic Psychology and Behaviour, 2(4), pp.181–196. Available at: http://www.sciencedirect.com/science/article/pii/S13698 4780000005X [Accessed July 21, 2014].

Delorme, D. & Song, B., 2001. Human driver model for SmartAHS. California Partners for Advanced Transit and Highways (PATH). Available at: http://escholarship.org/uc/item/8qn889mt.pdf [Accessed March 19, 2015].

El-Shawarby, I., Ahn, K. & Rakha, H., 2005. Comparative field evaluation of vehicle cruise speed and acceleration level impacts on hot stabilized emissions. Transportation Research Part D: Transport and Environment, 10(1), pp.13–30.

Lu, X. & Skabardonis, A., 2007. Freeway traffic shockwave analysis: Exploring NGSIM trajectory data. Transportation Research Board 86th Annual Meeting, No. 07-301.

Nouveliere, L., 2007. Experimental vehicle longitudinal control using a second order sliding mode technique. Control Engineering Practice. Available at: http://www.sciencedirect.com/science/article/pii/S09670 66106002255 [Accessed March 15, 2015].

Nouveliere, L. & Mammar, S., 2003. Experimental vehicle longitudinal control using second order sliding modes. In IEEE, ed. American Control Conference, 2003. Proceedings of the 2003. IEEE. Available at: http://ieeexplore.ieee.org/xpls/abs_all.jsp?arnumber=124 2466 [Accessed March 15, 2015].

Santhanakrishnan, K. & Rajamani, R., 2003. On spacing policies for highway vehicle automation. Intelligent Transportation Systems, IEEE Transactions on, 4(4), pp.198–204.

Shladover, S., 1991. Longitudinal control of automotive vehicles in close-formation platoons. Journal of dynamic systems, measurement, and control, 113(2), pp.231–241.

Available at: http://dynamicsystems.asmedigitalcollection.asme.org/ar ticle.aspx?articleid=1405551 [Accessed March 15, 2015].

Swaroop, D. & Rajagopal, K.R., 2001. A review of constant time headway policy for automatic vehicle following. In IEEE, ed. Intelligent Transportation Systems, 2001. Proceedings. 2001 IEEE. IEEE, pp. 65–69.

Tak, S., Kim, S. & Yeo, H., 2015. Development of a Deceleration-Based Surrogate Safety Measure for Rear-End Collision Risk. IEEE Transactions on Intelligent Transportation Systems, In press.

Thiemann, C., Treiber, M. & Kesting, A., 2008. Estimating acceleration and lane-changing dynamics from next generation simulation trajectory data. Transportation Research Record: Journal of the Transportation Research Board, 2088(1), pp.90–101.

Wåhlberg, A. af, 2007. Aggregation of driver celeration behavior data: Effects on stability and accident prediction. Safety science. Available at: http://www.sciencedirect.com/science/article/pii/S09257 53506001007 [Accessed June 6, 2013].

Wåhlberg, A. af, 2006a. Driver celeration behavior and the prediction of traffic accidents. International Journal of Occupational Safety and …. Available at: http://www.ciop.pl/18288 [Accessed June 6, 2013].

Wåhlberg, A. af, 2006b. Speed choice versus celeration behavior as traffic accident predictor. Journal of safety research. Available at: http://www.sciencedirect.com/science/article/pii/S00224 37506000041 [Accessed June 6, 2013].

Wang, J. & Rajamani, R., 2004. The impact of adaptive cruise control systems on highway safety and traffic flow. Proceedings of the Institution of Mechanical Engineers, Part D: Journal of Automobile Engineering, 218(2), pp.111–130.

Yeo, H., 2008. Asymmetric microscopic driving behavior theory, University of California, Berkeley: ProQuest.

Yeo, H. & Skabardonis, A., 2011. Microscopic fundamental relationships between vehicle speed and spacing in view of asymmetric traffic theory. In Intelligent Transportation Systems (ITSC), 2011 14th International IEEE Conference on. IEEE.

Yeo, H., Skabardonis, A. & Halkias, J., 2008. Oversaturated freeway flow algorithm for use in next generation simulation. Transportation Research Record: Journal of the Transportation Research Board, 2088(1), pp.68–79. Available at: http://trb.metapress.com/index/0kpu7835q85730qm.pdf [Accessed March 27, 2015].

Zhao, J. & Kamel, A. El, 2010. Coordinated throttle and brake fuzzy controller design for vehicle following. Intelligent Transportation Systems (ITSC), 2010 13th International IEEE Conference on. IEEE. Available at: http://ieeexplore.ieee.org/xpls/abs_all.jsp?arnumber=562 5158 [Accessed March 15, 2015].

Zhou, J. & Peng, H., 2005. Range policy of adaptive cruise control vehicles for improved flow stability and string stability. Intelligent Transportation Systems, IEEE Transactions on, 6(2), pp.229–237.

Traffic safety at intersections: a priority based approach for cooperative collision avoidance

Gabriel R. Campos[1,2], **Paolo Falcone**[2], **Jonas Sjöberg**[2]

[1] *DEIB, Politecnico di Milano, Italy*
Email: `gabriel.rodriguesdecampos@polimi.it`
[2]*Department of Signals and Systems,*
Chalmers University of Technology, Sweden.
Email: `paolo.falcone,jonas.sjoberg@chalmers.se`

Abstract: In this paper, we consider the coordination problem of multiple autonomous vehicles at traffic intersections. In particular, we exploit a cooperative, sequential conflict resolution approach based on a pre-defined decision order. Using an optimal control formulation, we show how coordination can be ensured by solving two local problems where collision avoidance is enforced as time-dependent state constraints. We will analyse the feasibility of a given sequence with respect to different decision criteria and present simulation results supporting our results.

Keywords: Safety systems, Conflict resolution, Cooperative control, Autonomous driving

1. INTRODUCTION

The development of new Intelligent Transportation Systems (ITS) has enabled safer, smarter, and greener transport systems [Behere et al. (2013)]. Recent research has been focusing, among others, in prevention and mitigation of accidents, reduction of greenhouse gas emissions and efficiency in terms of energy and infrastructure utilization. Such efforts are fuelled by alarming statistics on road accident fatalities and the rapidly growing number of vehicles on the road. According to the World Health Organization, 1.24 million people died in traffic accidents during 2013 and as many as 50 million people suffered non fatal injuries, and this number can increase up to 1.9 million by 2020 if no action is taken [World Health Organisation (2013)]. Even if fatalities and injuries numbers render safety more compelling than efficiency, the effects of inefficient road transportation (e.g., traffic congestions, pollutants, greenhouse gasses and fuel consumption) on the environment, health and finance are also significant. For instance, road transportation is currently responsible for 16.5 percent of the anthropogenic greenhouse gas emissions [International Energy Association (2013)], and congestion locks down most major cities during rush hours. According to estimates by the U.S. Treasury, 7 billion liters of gas is wasted through congestion in the U.S. alone, which together with wasted time and productivity incurs a cost of over 100 billion dollars annually [U.S. Department of Treasury (2012)].

A particular interesting problem, both from a safety and efficiency point of view, is collision avoidance at traffic

intersections [Hafner et al. (2013); Doerzaph et al. (2008); Alexander et al. (2011)]. In Europe, intersections-related accidents are responsible for 21% of traffic related deaths and 43% of the non-fatal injuries [Simon et al. (2009)]. Similar numbers have been reported from the U.S. [National Traffic Highway Safety Association (2010)]. Due to the high risk of accidents, these traffic scenarios are among the most regulated ones, with vehicles guided simultaneously by traffic lights, signs, road-markings and right-of-way rules. As a consequence, they often form bottlenecks in the traffic system and even when not causing congestion, existing coordination rules are inherently inefficient, enforcing unnecessary decelerations and stops and thereby wasting both fuel and time.

Cooperative ITS have the potential to improve traffic flow and safety near intersections, without relying on inefficient traffic lights or error-prone human control. Instead, vehicles equipped with communication devices, have to coordinate and agree on how to cross the intersection without collisions. Informally, the *coordination problem* amounts to deciding the control functions for the individual vehicles that allow them to safely reach their destination. It consequently entails avoiding both collisions and traffic deadlocks, and doing so in a manner compatible with the physical capabilities and constraints of the vehicles. Note that the coordination problem has, in general, infinitely many solutions corresponding to different control functions and different crossing orders, i.e., temporal orders under which the vehicles occupies the critical regions. In today's traffic system, the strategy resulting from the interplay between human drivers, signal infrastructure and traffic rules gives *one* of the many solutions. However, as noted in the introduction, this particular strategy suffers from inefficient performance, and can, due to the presence of human drivers, unintentionally lead to constraint violations (collisions). Given a performance metric, we can also

set an *optimal coordination problem*, where the best of all feasible solutions to the coordination problem is sought.

Cooperative conflict resolution problems for autonomous vehicles at road intersections is a subject that has attracted a lot of research efforts recently. For instance, several works focused on the coordination problem based on the multi-agent systems paradigm and a rule-based approach [Dresner and Stone (2004, 2005, 2008); Kowshik et al. (2011)]. Other works, instead, used Model Predictive Control (MPC) coordination strategies [Kim and Kumar (2014); Hult et al. (2015); Campos et al. (2013, 2014)]. For instance, [Hult et al. (2015)] exploits the structure of the centralized, finite time optimal control problem, in order to propose an approximate solution, while [Campos et al. (2013)] considered a fully decentralized solution to the intersection conflict resolution problem, based on sub-optimal decision-making heuristics, using the concept of *decision sequence*. This results were later extended in [Campos et al. (2014)], where authors proposed a low complexity receding horizon control framework. It is worth mentioning that collision avoidance has also been approached from an active safety point of view, where the driver is overridden in case safety is compromised. Among others, [Hafner et al. (2011, 2013)] exploited hybrid systems theory and [Ahn et al. (2014); Bruni et al. (2013); Colombo and Del Vecchio (2015); Colombo and Del Vecchio (2012)] a scheduling-based approach, where the equivalence between the verification problem and the feasibility of a scheduling problem is presented.

In this paper, we consider a fully decentralized solution to the intersection conflict resolution problem, suitable for fully autonomous vehicles (contrary to [Hafner et al. (2011, 2013)], which focus on intervention). We abstract from the (many) implementation issues and focus on the fundamental aspects of the underlying decision making problems. Our solution relies on a cooperatively pre-determined decision order (enabling sequential decision making)for the computation of optimal collision-free trajectories (contrary to [Colombo and Del Vecchio (2012)], which focuses on feasible crossings sequences and not optimality). This work complements our previous results [Campos et al. (2013, 2014)], by considering general decision orders and providing a comparison in terms of feasibility for different decision criteria.

The rest of this paper is organized as follows. Section 2 presents the problem formulation while Section 3 addresses the centralized control formulation. In Section 4, a sequential and decentralized approach is presented, where formal feasibility conditions are derived for a given decision order. Finally, Section 5 presents some simulations results supporting the theoretical contributions of this paper and Section 6 some final conclusions.

2. SYSTEM DESCRIPTION

Consider $N > 1$ autonomous vehicles/agents approaching a traffic intersection as shown in Figure 1. For each agent i, we assume that:

- a path is given and is known;
- the assigned path is perfectly followed;
- the acceleration along the path can be varied;
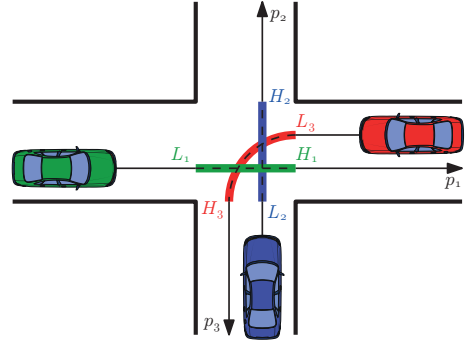
Fig. 1. Illustration of the considered scenario. Several autonomous vehicles approach an intersection defined by a range of positions over pre-defined paths. Vehicles are supposed to approach the intersection with a desired speed, where the variable of control is the longitudinal acceleration.

- all vehicles have synchronized clocks and are located before the intersection at the initial time instant.

Let $x_i = [p_i \ v_i]^T \in X_i = P_i \times V_i$ denote the state of each vehicle $i \in \mathcal{N} = \{1, \ldots, N\}$, where $p_i \in P_i$, $v_i \in V_i$ and P_i and V_i represent the sets of all admissible (scalar) longitudinal positions and velocities along the path, respectively. Each agent is modeled as a discrete time double integrator

$$x_i(t+1) = A \ x_i(t) + B \ u_i(t), \qquad (1)$$

where $A = [1 \ 1; 0 \ 1]$ and $B = [0 \ 1]^T$. Furthermore, we assume that a full measurement of the state $x_i(t)$ is available at all times. Throughout the rest of the article, t is considered to be the current time such that $(\cdot)(t+k)$ denotes the predicted value of variable $(\cdot)$ at time $t+k$, computed at time t.

As a part of the assigned driving task, each agent i has a given reference (i.e., desired) velocity denoted by $v_{di} \in V_i$. Furthermore, let $x = [x_i^T, \ldots, x_N^T]^T, y = [y_i^T, \ldots, y_N^T]^T, u = [u_i^T, \ldots, u_N^T]^T, v_d = [v_{di}, \ldots, v_{dN}]^T$ denote the state, the input, the output, and the desired velocity vector, respectively, for the entire system composed of N vehicles. The following constraints are also taken into account:

(1) **Actuator limitations**

To ensure that the control input u_i (longitudinal acceleration) is within the admissible actuator range, each vehicle is assumed to be subject to:

$$u_i^{\min} \ \leq \ u_i(t) \ \leq \ u_i^{\max}, \qquad \forall t \ \geq 0, \qquad (2)$$

which yields $U_i = \{ u_i | \ u_i \in [u_i^{\min}, u_i^{\max}] \}$.

(2) **State constraints**

Vehicles' velocities are constrained such that

$$0 < \ v_i^{\min} \ \leq \ v_i(t) \ \leq v_i^{\max}, \qquad \forall t \ \geq 0, \qquad (3)$$

which yields $V_i = \{ v_i | \ v_i \in [v_i^{\min}, v_i^{\max}] \}$.

(3) **Safety constraints**

The proposed collision avoidance solution relies on the design local controllers preventing a given vehicle of accessing the intersection if it is already occupied by any other vehicle. We introduce the following definitions.

Definition 1. (**Critical set**). For each agent $i \in \mathcal{N}$, let Cr_i denote the *critical set*, i.e., the set of all positions along the path where a collision is possible and defined as

$$\mathrm{Cr}_i \triangleq \{ x_i \in X_i | \ p_i \in [L_i, H_i] \}, \tag{4}$$

where $L_i < H_i$ are bounds on the position along the path of vehicle i defining the intersection. Note that these parameters are dependent on the geometry of the workspace and are time-invariant.

Definition 2. (**Occupancy interval**). For each agent $i \in \mathcal{N}$, the *occupancy interval* of the intersection for a given predicted control sequence can be expressed as

$$\Gamma_{i,t} \left(x_i(t), u_i(t), u_i(t+1), \ldots \right) = \{k | \ x_i(k) \in \mathrm{Cr}_i\}, \tag{5}$$

where $x_i(t + 1)$ is given by (1) and $\{u_i(t), u_i(t + 1), \ldots\}$ denotes a control sequence. In order to simplify the notation, we will consider throughout the rest of the paper $\Gamma_{i,t}$ as the shorthand form of $\Gamma_{i,t} \left(x_i(t), u_i(t), u_i(t+1), \ldots \right)$.

From Def. 2 the following collision avoidance constraint follows

$$\Gamma_{i,t} \cap \Gamma_{j,t} = \emptyset, \forall \ i, j \in \mathcal{N}, j \neq i. \tag{6}$$

For the sake of clarity, if at time t the condition $p_i(t) < L_i$ holds, we will state that agent i is "before" the critical set, while if $p_i(t) > H_i$ holds we will say that the agent is "after" the critical set. Finally, we introduce the polytopes Ω_i and Υ_i as the set of states corresponding to the vehicle being before and after the intersection, respectively, and are defined as

$$\Omega_i = \{x_i | \ v_i^{\min} \leq v_i \leq v_i^{\max}, \ 0 \leq p_i \leq L_i\},$$

and $\Upsilon_i = X / \{\mathrm{Cr}_i \cup \Omega_i\}$, see Figure 3.

3. CENTRALIZED PROBLEM FORMULATION

Consider the following global cost function

$$J_{\mathrm{centr},t} = \sum_{k=0}^{\infty} \|v(t+k) - v_d\|_Q^2 + \|u(t+k)\|_R^2, \tag{7}$$

where, $R \succ 0$ and $Q \succeq 0$ are block diagonal weighting matrices of appropriate dimensions penalizing the control signal and the deviation of the agent's speed from the desired value, respectively. The formal centralized problem for traffic coordination at traffic intersections is given by

$$\min_{[u(t),u(t+1),\ldots]} J_{\mathrm{centr},t} \tag{8}$$

$$\text{subject to: } (1), (2) \text{ and } (3), \ \forall \ i \in \mathcal{N}$$

$$(6), \ \forall \ i, j \in \mathcal{N}, j \neq i.$$

The solutions to (8) consists of the best possible strategies with respect to (7), given the geometry of the coordination scenario, the initial state configuration and the limitations
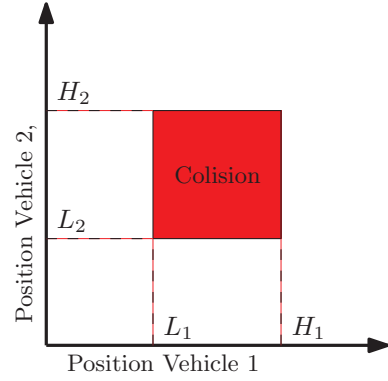
Fig. 2. Schematic illustration of a two vehicle collision accordingly to Definition 1 and (6). The red area contains the infeasible (forbidden) state space combinations and corresponds to collisions between vehicles 1 and 2.

and capabilities of each vehicle. However, the structure of (8) raises serious computational complexity issues related to the prediction horizon length and the number of involved vehicles. Indeed, even a formulation of (8) over a finite time horizon W, yet large, might be computationally prohibitive. In order to tackle this issue, we propose in the sequel a low complexity decentralized solution based on a pre-defined decision order.

4. DECENTRALIZED PROBLEM FORMULATION

Due to the collision avoidance constraints (6), problem (8) is computationally prohibitive and non-convex, see Figure (2). However, a low complexity approximate solution of problem (8), based on the sequential solution of $2N - 1$ convex problems, can be formulated by assuming the existence of a decision order [Campos et al. (2013, 2014)]. In the context of this article, a decision order defines the sequence in which the different agents will solve their local optimization problems. The following definition is introduced.

Definition 3. (**Decision order**). Let $\mathcal{N} = \{1, \ldots, N\}$ be the set of vehicles and $\mathcal{O}$ a permutation of $\mathcal{N}$ defined according to a given criterium θ_i. Then $\mathcal{O}$ is considered to be the *decision order*, where $(\mathcal{O})_m$ denotes the m-th element in the order. Furthermore, $\mathcal{O}$ can be partitioned, with respect to each vehicle $i = (\mathcal{O})_m$, into $\mathcal{O}_i^b$ and $\mathcal{O}_i^a$: the first set contains the indices of all agents $j \neq i$ appearing before i in the decision order, while the second includes the indices of the vehicles appearing after agent i.

Considering a decision order, a sequential approach is proposed here. It is assumed that the first agent on the decision order will progress according to a local unconstrained optimization problem, which will broadcast the expected occupancy interval of the intersection. This will then be used by the remain vehicles on the decision order to enforce collision avoidance in their respective local optimization problems (problems (14) and (15) presented later in this paper).

4.1 Priority ordering

The main idea behind the proposed decentralized approach relies on a pre-defined decision order establishing in which sequence agents will solve their local optimization problems. How to define a meaningful decision order, however, is still an open problem. Here, we consider commonly used heuristics for priority assignment. We will also propose a novel criteria able to incorporate the individual degree of freedom of each vehicle.

(1) **First In First out (FIFO):** FIFO algorithms are methods for organizing and manipulating a queue of operations, widely spread in different technical fields. They can also be applied to intersection crossing where the vehicle arriving first to the intersection, or "head" of the queue, is processed first. In the context of this paper, vehicles getting to the intersection earlier will then gain priority in the decision sequence $\mathcal{O}$.

(2) **Distance to intersection:** Another intuitive, commonly used decision criteria is based on the distance between each vehicle and the collision point. In the context of this paper, such algorithm has the advantage of handling eminent collisions first, while keeping far-way agents at the end of queue. Nevertheless, such approach is incapable of incorporating the effective control freedom of each vehicle.

(3) **Time to react:** The concept behind this approach relies on the set of state configurations that will lead to an unavoidable collision. For example, it is possible that an agent, once it detects a possible collision with another agent, is unable to control its future trajectory in such a way that it can influence the time instants at which it will occupy the intersection. Based on such an argument, we are interested in determining if it exists a trajectory leading a vehicle to the critical set in a finite number of steps, under any feasible control input [Campos et al. (2013)]. The following definition, taken from [Borrelli et al. (2014)], will be used in the sequel to define the degree of freedom of each vehicle.

Definition 4. (**One-step robust controllable set**). Consider a system given by

$$x(t+1) = f(x(t), w(t)),$$

where $x(t) \in X, w(t) \in W,$ and $t \geq 0$. We denote the one-step controllable set to the set $\mathcal{T}$ as

$$\mathrm{Pre}(\mathcal{T}, \mathcal{W}) \triangleq \{x \in X \ : \ f(x, u) \in \mathcal{T}, \forall w \in \mathcal{W}\}.$$

In a intersection scenario, it is clear that the individual degree of freedom of a vehicle is defined by its range of feasible control inputs. Exploiting the notion of one-step robust controllable set, we introduce here the concept of *attraction set* denoted by $\mathcal{A}_i, \forall i \in N$. Using reachability analysis tools, the set $\mathcal{A}_i$ is defined as:

$$\mathcal{A}_i(\mathbf{Cr_i}) = Pre(\mathbf{Cr_i}, U_i) \qquad (9)$$
$$= \{x_i(t) \ \in X_i : x_i(t+1) \in \mathbf{Cr_i}, \forall \ u_i \in U_i\}.$$

In other words, the set $\mathcal{A}_i$ includes all possible state configurations that will lead the agent, unavoidably, to its *critical set* $\mathbf{Cr_i}$ in one step. The reader can refer to [Borrelli et al. (2014)] for further details on
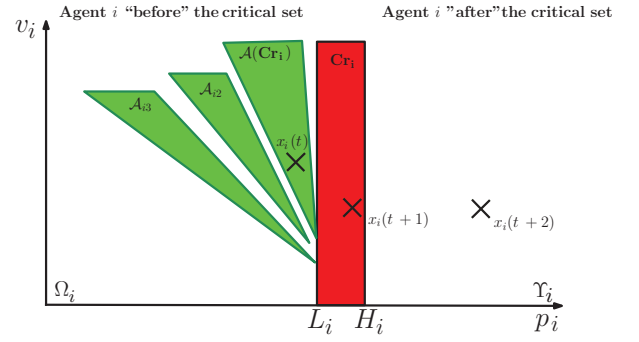
Fig. 3. Illustration of the attraction sets $\mathcal{A}_i^z$ and the critical set $\mathbf{Cr_i}$.

reachability/controllability analysis. In a general way, define now:

$$\mathcal{A}_i(\mathcal{T}) = Pre(\mathcal{T}, U_i)$$
$$= \{x_i(t) \ \in X_i : x_i(t+1) \in \mathcal{T}, \forall \ u_i \in U_i\}.$$

where $\mathcal{T}$ is usually referred to as the target set. Denote $\mathcal{A}_{i1} = \mathcal{A}_i(\mathbf{Cr_i})$. By performing backward sequential calculations, it is possible to compute the super-set $\mathcal{A}_i^z$ including all the *attraction sets* that will drive vehicle i to $\mathbf{Cr_i}$ in at most z steps such that:

$$\mathcal{A}_i^z = [\mathcal{A}_{i1}, \mathcal{A}_{i2}, \cdots, \mathcal{A}_{iz}], \qquad (10)$$

where $\mathcal{A}_{in} = \mathcal{A}_i(\ \mathcal{A}_{i(n-1)})$. Note that the scalar z is not a chosen parameter but it rather depends on the structure of the problem. In other words, z is the largest scalar before the backward reachability calculations result in an empty set. For the sake of clearness, an illustrative schema is presented in Figure 3.

It follows from (4) and (10) that both $\mathbf{Cr_i}$ and $\mathcal{A}_i^z$ are time invariant, therefore offering precious information regarding the individual degree of freedom of each agent. We therefore propose to use such concepts to establish cooperation among agents. In order to introduce some logical fairness in the protocol and to compensate the natural drawbacks of a sequential decision procedure, in consider int this work a *control priority* defined in a proportionally inverse way with respect to the values of the "Time to react", defined as follows:

Definition 5. (**Time to react** Δ_i^{TR}). Consider the state $x_i(t)$ at the current time instant t. The time interval until the vehicle reaches any set n of $\mathcal{A}_i^z$ (if vehicle keeps its desired profile) is considered to be the **time to react** Δ_i^{TR}. By definition, it follows that the agent's will enter, unavoidably, into $\mathbf{Cr_i}$ in $\Delta_i^{TR} + n$ steps, $n \in \{1, \ldots, z\}$.

In other words, priority will be given to the agent lying closer to its attraction set, *i.e.*, the agent with the lowest Δ_i^{TR} value, then to the agent with the second smallest Δ_i^{TR} and so on. Such policy is motivated by the claim that the agent with the lower Δ_i^{TR} has, among all vehicles, the lowest individual degree of freedom.

4.2 Formulation of two convex optimization problems

Consider that the intersection is already occupied by an agent j during some time interval $\Gamma_{j,t}$. Thus, only two options are therefore valid for any other agent: (i) crossing the intersection before; (ii) crossing the intersection after. Extending this line of thought, a decentralized scheme can be set up where each agent in the decision order restricts its choices to pass the intersection before or after *all* the preceding vehicles in the decision order. Note that this approach is no longer optimal, since not all crossing orders are explored [1]. Note that the computational complexity of the proposed algorithm is linear with the vehicles number N, relying on the sequential computation of $2N - 1$ quadratic programming problems. For the general case of N vehicles (with $N!$ potential crossing orders), the proposed approach reduces the number of possible crossing orders to $2^{(N-1)}$ and considers only one of them.

Keeping the same performance metrics as in (7), the local objective associate to each agent $i \in \mathcal{N}$ is given by

$$J_{i,t}^d = \sum_{k=0}^{W} \|v_i(t+k) - v_{di}\|_{Q_i}^2 + \|u_i(t+k)\|_{R_i}^2, \quad (11)$$

where W is a very large prediction horizon and $R_i \succ 0$ and $Q_i \succeq 0$ are weighting matrices of appropriate dimensions. We can informally define the following two problems:

- **Problem A (Informal Statement):** Find the optimal control policy such that agent i enters the intersection only after *all* preceding agent(s) $j \in \mathcal{O}_i^b$ have exited.

- **Problem B (Informal Statement):** Find the optimal control policy such that agent i exits the intersection before *any* preceding agent(s) $j \in \mathcal{O}_i^b$ enters.

For agent i, let $\Psi_{i,t} = \bigcup_{j \in \mathcal{O}_i^b} \Gamma_{j,t}$ be the union of the occupancy intervals of all preceding vehicles in $\mathcal{O}$. Collision avoidance is then ensured if

(1) For Problem A, the earliest entry time for agent i is given by

$$t_{i,t}^a = \max_{m \in \Psi_{i,t}} \{m\} + \delta_i^a. \quad (12)$$

(2) For Problem B, the latest exit time for agent i is given by

$$t_{i,t}^b = \min_{m \in \Psi_{i,t}} \{m\} - \delta_i^b. \quad (13)$$

Here δ_i^b, $\delta_i^a \in \mathbb{Z}_+$ are safety time gaps between two occupancy intervals. We are now ready to formulate Problems A and B as two convex optimization problems where collision avoidance is enforced by state constraints. Thus, we have

Problem A:

$$\min_{[u_i(t),u_i(t+1),\dots]} \quad J_{i,t}^d \quad (14)$$
$$\text{subject to:} \quad (1), (2) \text{ and } (3),$$
$$p_i(t_{i,t}^a) \in \Omega_i.$$

Problem B:

$$\min_{[u_i(t),u_i(t+1),\dots]} \quad J_{i,t}^d \quad (15)$$
$$\text{subject to:} \quad (1), (2) \text{ and } (3),$$
$$p_i(t_{i,t}^b) \in \Upsilon_i.$$

Assuming that both Problem A and B have a solution, each vehicle will then choose the solution associated with the lowest $J_{i,t}^d$.

4.3 Feasibility analysis

From problems (14) and (15), one can easily conclude that the proposed conflict resolution algorithm relies on two optimization problems over two different horizons: one guaranteeing that a vehicle i can reach Υ_i in $(t_{i,t}^b - t)$ steps (i.e., accelerating and crossing first); the other ensuring that the agent can remain within Ω_i in $(t_{i,t}^a - t)$ steps (i.e., slow down and take the last position). The following definition is taken from [Borrelli et al. (2014)] and is used in the sequel to derive feasibility conditions of a given decision order.

Definition 6. (One-step and R-step controllable sets). Consider a system subject to external inputs given by

$$x(t+1) = f(x(t), u(t)),$$

where $x(t) \in X, u(t) \in U,$ and $t \geq 0$. We denote the one-step controllable set to the set $\mathcal{T}$ as

$$\mathrm{Pre}(\mathcal{T}) \triangleq \{x \in X \ : \exists u \in U \text{ s.t. } f(x,u) \in \mathcal{T}\}.$$

Furthermore, the R-step controllable set $\mathrm{K}^R(\mathcal{T})$ to the set $\mathcal{T}$ is defined recursively as

$$\mathrm{K}^m(\mathcal{T}) \triangleq \mathrm{Pre}(\mathrm{K}^{m-1}(\mathcal{T})) \cap X, \quad \mathrm{K}^0(\mathcal{T}) = \mathcal{T},$$

where $m \in \{1, \dots, R\}$.

For a given decision order, the following conditions hold [Campos et al. (2014)].

Proposition 1. (Local feasibility). Let the state of an agent $i \in \mathcal{N}$, driven by dynamics (1), be $x_i(t) \in X_i$ at time t. Given a decision sequence $\mathcal{O}$, agent i has a feasible solution if and only if **at least one** of the following conditions is satisfied

$$x_i(t) \in \mathrm{K}_i^{(t_{i,t}^a - t)}(\Omega_i), \quad (16a)$$

$$x_i(t) \in \mathrm{K}_i^{(t_{i,t}^b - t)}(\Upsilon_i), \quad (16b)$$

It follows from Def. 6 that if condition (16a) is satisfied, then $\exists u_i \in U_i$ such that vehicle i can remain within Ω_i in $(t_{i,t}^a - t)$ steps. On the other hand, if condition (16b) is satisfied, then there exists a feasible control input that can drive the system to the target set Υ_i in $(t_{i,t}^b - t)$ steps. Thus, if one of these is satisfied, there exists at least one feasible control sequence satisfying the safety constraints.

Proposition 2. (Global feasibility). Consider a set of N systems driven by dynamics (1) such that $x(t) \in X$. At time t, a decision order $\mathcal{O}$ is feasible if and only if Proposition 1 is satisfied for each element in $\mathcal{O}$, except the first one.

Proposition 1 and Proposition 2 present local and global feasibility conditions for a given decision order $\mathcal{O}$, respectively. More precisely, they allow us to verify feasibility

---

[1] As an example, take the three vehicle case, with a decision sequence $\mathcal{O} = \{1, 2, 3\}$. Considering the proposed algorithm, only four possible crossing orders $\{1,2,3\}$, $\{3,1,2\}$, $\{2,1,3\}$ and $\{3,2,1\}$ are considered, whereas sequences $\{1,3,2\}$ and $\{2,3,1\}$ are discarded.

of an order by performing set-membership tests according to Proposition 1 and 2. From an implementation point of view, this can help to reduce the computational load considering that the derivation of the backward reachable sets can be locally pre-computed.

Remark 1. Note that the concept of *decision sequence* has been extended in [Campos et al. (2014)] to a receding horizon control (RHC) framework. For any given decision sequence, it was shown that highly complex coordination scenarios can be simplified into simple and scalable RHC problems. More precisely, the local problems are divided into a finite-time optimal control problem, where collision avoidance is enforced as terminal constraints, and an infinite horizon control problem that is solved offline.

5. SIMULATION RESULTS AND DISCUSSION

Consider a system of three vehicles ($N = 3$) as represented in Figure 1. Here, the safety parameter δ has been chosen as $\delta = [\ \delta^b \ \ \delta^a \ ]^T = [1 \ 1]^T$ and $L_i = 100$ and $H_i = 130$, $\forall i \in \mathcal{N}$. Furthermore, vehicles are heterogeneous with respect to the control constraints such that $U_i \neq U_j$, $\forall i, j \in \mathcal{N}$. For each agent, the initial state is given by $x_i(0) = [p_i(0) \ v_{di}]^T$ such that $x_1(0) = [7 \ 8.2]^T, x_2(0) = [4 \ 5.95]^T, x_3(0) = [70 \ 3.3]^T$. This yields $\Gamma_{1,t} = \{10 - 15\}, \Gamma_{2,t} = \{17 - 21\}$ and $\Gamma_{3,t} = \{10 - 18\}$. If no collision avoidance procedures are implemented, i.e., if all agents respect their pre-defined trajectory, then a collision can occur from $t = 10$ until $t = 21$.

In the sequel, we will discuss the advantages of the proposed sequential approach. As previously mentioned, there are several heuristics that can be used to define a decision order, as considered in the context of this paper. However, not all criteria θ_i offer the same performance and feasibility properties. In this work we are interested in the local and global feasibility of the decision order accordingly to Propositions 1 and 2. Note that the order $\mathcal{O}$ is assumed to be defined from the lowest to the highest value of $\theta_i, \forall i \in N$. Our goal is to show the advantages, in terms of feasibility, of a decision order based on time to react of the different vehicles, as proposed in this work. For comparison purposes, we consider other common decision criteria θ_i based on: (i) First In First Out (FIFO) protocols; (ii) distance to intersection.

For the different criteria, the resulting orders and feasibility arguments are presented in Table 1. Recall the intuition behind the concepts "time to react" and the attraction sets. Able to incorporate the individual degree of freedom of each vehicle, we claim here that such an approach leads to a deeper and comprehensive understanding of the current traffic situation, allowing therefore the derivation, from a fairness and feasibility point of view, of better priority relations/orders. The analysis of Table 1 supports our claims in terms of feasibility. Indeed, if a decision order is based on the "time to react", this leads to a feasible solution allowing agents to cross safely the intersection. On the other hand, however, the remaining criteria do not guarantee global feasibility, since both problems (14) and (15) are unfeasible for vehicle 1. This is shown in Figure 4, where the results of set-membership conditions

(a)

(b)
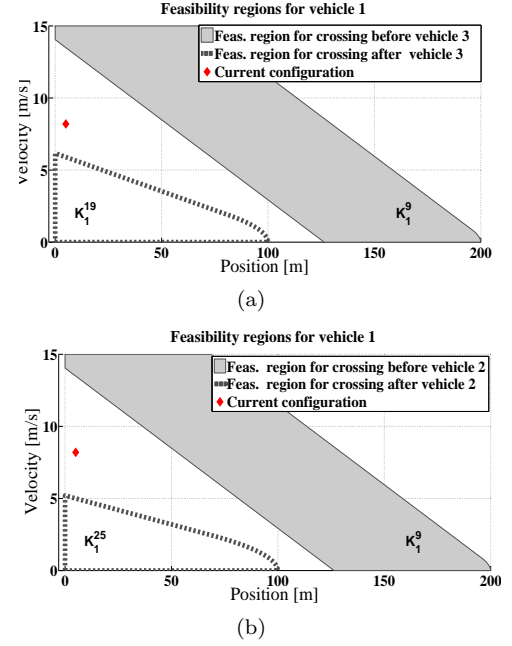
Fig. 4. Feasibility regions for vehicle 1: (a) for an order $\mathcal{O} = \{3, 1, 2\}$ defined with respect to a FIFO algorithm; (b) for an order $\mathcal{O} = \{3, 2, 1\}$ defined with respect to approaching speed $\|p_i(0) - L_i\|$. In both figures, the current state (red dot) does not belong to any of the presented sets, therefore compromising the global feasibility of the corresponding order.
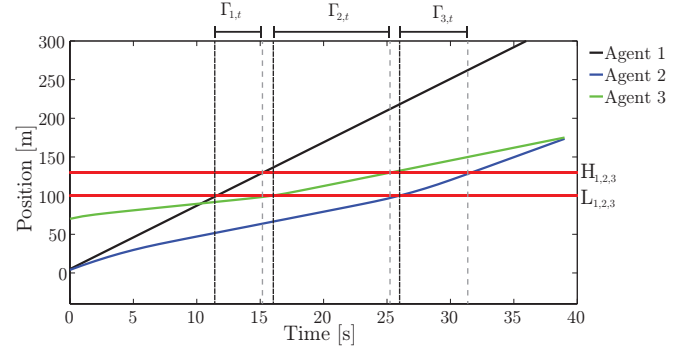
Fig. 5. Evolution of the agents' trajectories according to proposed sequential algorithm. The intersection is represented by the horizontal red lines and the black and grey dashed lines represent the entrance and exit time instants, respectively.

(accordingly to Proposition 1 and 2) are presented. In both figures one can see that the current configuration of vehicle 1 does not belong to any of the sets (derived using reachability theory). Accordingly to these results, vehicle 1 is: **(i)** unable to cross before vehicle 3 (in Fig. 4(a) and (b), $x(t) \notin K_1^9$); **(ii)** unable to cross after vehicle 3 (in Fig. 4(a), $x(t) \notin K_1^{19}$); **(iii)** unable to cross the intersection after vehicle 3 and 2 (in Fig. 4(b), $x(t) \notin K_1^{25}$).

Finally, Figure 5 presents the trajectories of the different vehicles according to the proposed control protocol for a decision order $\mathcal{O} = \{1, 3, 2\}$. Here, the critical set Cr_i is represented by the horizontal red lines and the black and grey dashed lines represent the entrance and exit times,

θ_i	"time to react"	$\|p_i(t) - L_i\|$	FIFO
Order $\mathcal{O}$	$\{1, 3, 2\}$	$\{3, 2, 1\}$	$\{3, 1, 2\}$
Feasibility	Feasible	Unfeasible	Unfeasible

Table 1. Decision orders $\mathcal{O}$ and feasibility conclusions with respect to different θ_i.

defining $\Gamma_{i,t}, \forall i \in \mathcal{N}$. One can observe that a collision is avoided, since the different $\Gamma_{i,t}$ never intersect. We recall that in the proposed approach time-dependent state constraints are enforcing collision avoidance conditions, see (14) and (15). According to the proposed algorithm, agent 1 (with highest priority) keeps its desired trajectory, crossing the intersection during $12 < t < 15$. Based on this information, agent 3 solves problems (14) and (15), choosing the best local solution. The same procedure is later performed by agent 2.

6. CONCLUSIONS

In this paper, we presented a cooperative conflict resolution approach for traffic intersections, based on a sequential approach. The proposed solution offers several advantages such as low complexity and scalability. In fact, its per agent complexity with respect to the number of agents remains constant since collision avoidance is enforced through local state constraints at given time steps. Furthermore, due to its low computational requirements, the proposed structure can also be cast into a RCH framework. Finally, this novel control formulation has also the merit of allowing the derivation of (easily verifiable) feasibility conditions for a given sequence. Throughout simulation results, we showed that a decision order based on the time to react, as proposed in this paper, guarantees global feasibility of the order whenever other decision criteria do not. To complement these results, future research should focus on the optimality analysis and experimental implementation of such approaches.

REFERENCES

Ahn, H., Colombo, A., and Del Vecchio, D. (2014). Supervisory control for intersection collision avoidance in the presence of uncontrolled vehicles. In *American Control Conference*, 867–873.

Alexander, P., Haley, D., and Grant, A. (2011). Cooperative intelligent transport systems: 5.9-ghz field trials. *Proc. IEEE*, 99, 1213–1235.

Behere, S., Törngren, M., and Chen, D.J. (2013). A reference architecture for cooperative driving. *Journal of Systems Architecture*, 59(10, Part C), 1095 – 1112.

Borrelli, F., Bemporad, A., and Morari, M. (2014). Predictive control for linear and hybrid systems. In preparation.

Bruni, L., Colombo, A., and Del Vecchio, D. (2013). Robust multi-agent collision avoidance through scheduling. In *Decision and Control (CDC), 2013 IEEE 52nd Annual Conference on*, 3944–3950.

Campos, G.R., Falcone, P., and Sjöberg, J. (2013). Autonomous cooperative driving: a velocity-based negotiation approach for intersection crossing. In *IEEE Conference on Intel. Transportation Systems*.

Campos, G.R., Falcone, P., Wymeersch, H., Hult, R., and Sjöberg, J. (2014). A receding horizon control strategy for cooperative conflict resolution at traffic intersections. In *IEEE Conference on Decision and Control*.

Colombo, A. and Del Vecchio, D. (2015). Least restrictive supervisors for intersection collision avoidance: A scheduling approach. *IEEE Transactions on Automatic Control*.

Colombo, A. and Del Vecchio, D. (2012). Efficient algorithms for collision avoidance at intersections. In *ACM Conference on Hybrid Systems: Computation and Control*.

Doerzaph, Z.R., Neale, V.L., Bowman, J.R., Viita, D.C., and Maile, M. (2008). Cooperative intersection collision avoidance system limited to stop sign and traffic signal violations (CICAS-V) Subtask 3.2 interim report: Naturalistic infrastructure based driving data collection and intersection collision avoidance algorithm development. Technical report, National Highway Traffic Safety Administration.

Dresner, K. and Stone, P. (2004). Multiagent traffic management: a reservation-based intersection control mechanism. In *Autonomous Agents and Multiagent Systems, 2004. AAMAS 2004. Proceedings of the Third International Joint Conference on*, 530–537.

Dresner, K. and Stone, P. (2005). Multiagent traffic management: An improved intersection control mechanism. In *Proceedings of the fourth international joint conference on Autonomous agents and multiagent systems*, 471–477. ACM.

Dresner, K.M. and Stone, P. (2008). A multiagent approach to autonomous intersection management. *J. Artif. Intell. Res.(JAIR)*, 31(1), 591–656.

Hafner, M., Cunningham, D., Caminiti, L., and Del Vecchio, D. (2013). Cooperative collision avoidance at intersections: Algorithms and experiments. *Trans. Intel. Transportation Systems*, 14(3), 1162–1175.

Hafner, M.R., Cunningham, D., Caminiti, L., and Del Vecchio, D. (2011). Automated vehicle-to-vehicle collision avoidance at intersections. In *ITS World Congress*.

Hult, R., Campos, G.R., Falcone, P., and Wymeersch, H. (2015). An approximate solution to the optimal coordination problem for autonomous vehicles at intersections. In *American Control Conference*.

International Energy Association (2013). CO_2 Emissions from fuel combustion.

Kim, K.D. and Kumar, P. (2014). An mpc-based approach to provable system-wide safety and liveness of autonomous ground traffic. *IEEE Transactions on Automatic Control*, 59(12), 3341–3356. doi: 10.1109/TAC.2014.2351911.

Kowshik, H., Caveney, D., and Kumar, P. (2011). Provable systemwide safety in intelligent intersections. *Trans. on Vehicular Technology*, 60(3), 804–818.

National Traffic Highway Safety Association (2010). Crash Factors in Intersection-Related Crashes: An On-Scene Perspective.

Simon, M., Hermitte, T., and Page, Y. (2009). Intersection road accident causation: A European view. *21st International Technical Conference on the Enhanced Safety of Vehicles*, 1–10.

U.S. Department of Treasury (2012). A new economic analysis of infrastructure investment.

World Health Organisation (2013). Global Status Report on Road Safety.

Distance Constraint Model for Automated Lane Change to Merge or Exit

Quoc Huy Do*, Hossein Tehrani**, Masumi Egawa**, Kenji Muto**, Keisuke Yoneda*, Seiichi Mita*

**Research Center for Smart Vehicles of Toyota Technological Institute, 2-12 Hisakata. Nagoya, 468-8511, JAPAN
(Tel: +81-52-802-1822; e-mail: { huydq,yoneda,smita }@ toyota-ti.ac.jp)
** Corporate R&D Div.3, DENSO CORPORATION, 1-1, Showa-cho, Kariya-shi, Aichi-ken, 448-8661, JAPAN
(Tel: +81-566-25-57558; e-mail: {hossein_tehrani, masumi_egawa, kenji_Muto}@ denso.co.jp).*

Abstract: Lane change is a complicated maneuver and that causes many severe highway accidents. Automatic lane change has great potentials to reduce the number of accidents. Previous researches mostly tried to find an optimal trajectory that can be applied for simple lane change. They do not consider time/distance constraints for doing the lane change during the merging/exiting. Through analysis of human driver lane change data, we propose a multi segments behavior and motion model to mimic the human driver operation. We developed a simulation platform in PreScan and evaluated the proposed automatic lane change model for challenging scenario in the merging/exiting.

Keywords: Automated Guided Vehicle, Autonomous Control, Driver Models

1. INTRODUCTION

Statistical data of highway traffic accidents shows the human error is a major reason for about 90% of accidents (Volvo 2013). Lane change manoeuvre is a cause for many severe highway accidents due to wrong estimation of surrounding environment or wrong manoeuvre. Currently, ADAS or automated driving proved their great potentials to reduce the impact of human errors through providing warning, semi or fully automated solutions. Previous researches in fully automated driving systems designed for lane change or overtake manoeuvres, can be divided into rule-based (Fletcher, et al., 2009), or utility-based (Dolan & Litkouhi, 2010), approaches. The lane changing trajectory is generated according to the vehicle states, surrounding vehicles and road information, and then the control laws are designed to use on-board sensors to track the generated trajectory.

In (Kasper , et al., 2014), authors introduce an object-oriented Bayesian network approach for traffic scene modelling for lane change manoeuvres detection. Bayesian network was also used by Schubert et al (2010) for lane change situation assessment and decision making. Other related researches focus on manoeuvre prediction. In (Friedman et al., 2009) authors trained Bayesian belief networks for the prediction of lane changes. A dynamic Bayesian network is also used by Gindele et al. (2012) for behaviour and trajectory prediction. The fuzzy logic was used by Naranjo et al (2008) for solving the modelling lane change decision making problems. They use fuzzy controllers that mimic human behaviour and reactions during overtaking manoeuvres. Simon and Markus (2013) applied an online Partially Observable Markov Decision Process to solve the decision making for lane change. Brechtel et al (2011) apply probabilistic MDP-Behavior planning for cars. Ardelt et al (2012) presented a probabilistic approach to build a lane change framework for automated vehicle. In (Jula et al.,

2000) presented the collision avoidance by analyzing the kinematic of the vehicle then calculated the minimum safety space requirement for doing the lane change. However, they provided a more general framework rather than focusing on lane change decision situations in particular.

Most of discussed researches try to predict the behaviour of surrounding vehicle or are based on the kinematic functions and try to find an optimal trajectory for lane-changing (Ziegler et al., 2014). They ignore the host vehicle lane change behaviour model for complicated scenarios or in the presence of time/distance constraint for merging/exiting of the highway. To exactly understand the human lane change model, we have conducted lane change experiments at Japan highway. The results of the human lane change motion analysis already published by the authors (Tehrani et al., 2014). Through analysis of human lane change data including neighbour vehicles and motion/behaviour data, we realized that the human model is not a single stage. In this paper, we propose a multi segments behaviour and motion model to mimic the human driver lane change operation. At "behaviour segment", the host vehicle tries to adjust the longitudinal distance, position or relative velocity to make or find suitable free space in front and the destination lane. At "motion segment", the host vehicle starts lateral motion and enters into the destination lane. The proposed method is able to solve and generate solution a for complicated lane change scenario.

The structure of this paper is as follows; Section 2.1 explains our automatic vehicle's lane change flowchart. Section 2.2 introduces our scenario modelling approach. The behaviour decision and velocity planning are presented in section 2.3 and 2.4. The lane change motion planning is described in section 2.5. Section 3 presents our simulation for merging in and exiting situation. Finally, the conclusion is given in section 4.

2. LANE CHANGE MODEL

Through experiments, we learned that the human driver model is not just the turning of steering wheel and it starts at seconds before the steering. As shown in Fig. 1 (a), turning the steering wheel starts at time 7.6 thought the human driver has already started to decelerate and reduce the vehicle speed from 19.5 m/s to 16.7 m/s. We see the driver has to decelerate to keep safe space from the front vehicle (black vehicle) and wait to let the blue vehicle to pass it. In this paper, we propose a two-segment behavior/motion lane change model as shown in Fig. 1 (b). In segment 1, the driver adjusts the longitudinal speed and makes safe space based on the positions and relative velocities of surrounding vehicles. The driver behavior in segment 1 is highly dependent on the number of surrounding vehicles, distances and their relative velocities. There are other important parameters such as road curvature, visibility condition or behavior of the surrounding vehicles. We also found that time/distance constraint is also a critical factor to select the suitable behavior at segment 1. It occurs when we try to merge into highway traffic or exit from
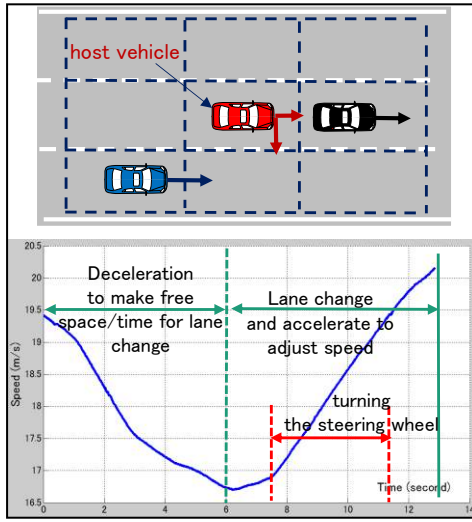
(a) Human lane change data.
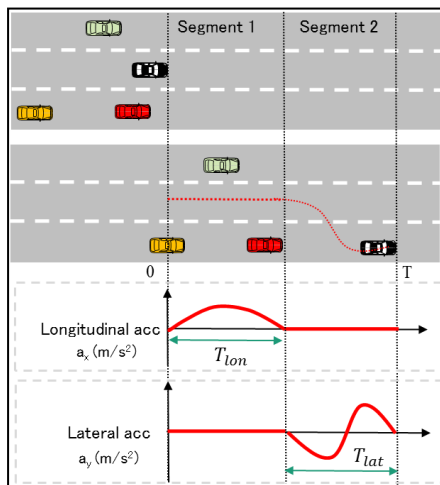
(b) Two segments model.

Fig. 1. Two segments lane change model.

the highway. By analyzing different cases of human lane change data, we extracted the following behaviors for the segment 1.
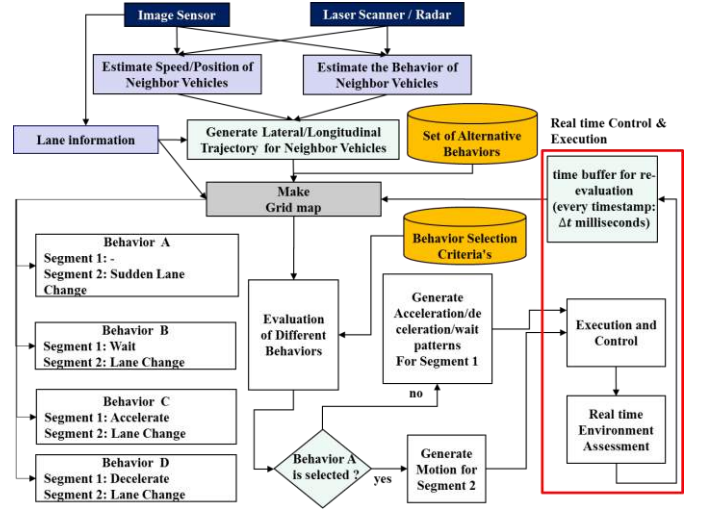
Fig. 2 Automatic lane change flowchart.

$$B = \{do\ lane\ change(LC), wait, accelerate, decelerate, evasive\} \quad (1)$$

Although, it is difficult to develop a general behavior model but we can propose a standard model that guarantee the safety and smoothness of the lane change operation. For example, if there is enough space at the destination lane, we can turn the steering wheel and *do the lane change (LC)*. If the relative speed of the approaching vehicles in the destination lane is relatively high, we may prefer to wait until find enough free space. In this case, we may even do *deceleration* to reduce the time or traveled distance. The deceleration behavior may be useful in the case of time/distance constraint when we have to change the lane to exit from the highway. In the other case, when the relative speed of the neighbor vehicles in the destination lane is relatively low, we may *accelerate* to pass the neighbor vehicles for doing the lane change. If we have a sudden change in the behavior of the surrounding vehicles during the lane change (sudden acceleration, deceleration or lane change), we may need *evasive* maneuver to avoid accident. In the other hand, the road curvature and speed limits and kinematic constraints of the vehicles such as maximum speed or acceleration have also impact on the driver behavior.

2.1 Lane Change Flowchart

Automatic lane change is integration of sensing/perception, planning (behavior & motion) and control. The behavior/motion flowchart for doing the lane change is shown in Fig. 2. It starts with estimation of motion parameters/ position of neighbor vehicles to estimate their trajectories. Based on the driving lane information and the behavior/motion parameters of the neighbor vehicles, we are able to estimate a trajectory for a certain period [0~T]. By using the trajectory data points $(t, x(t), y(t))$, we estimate the occupancy grid map of current and future state of the surrounding environment. In the following, we briefly explain the main components of the lane change flowchart.

2.2 Situation Modelling

We model the current lane change situation into a state occupancy grid as in the Fig. 3. This state grid is attached to the vehicle position.

$$d_{ego} = \beta . length_{host}$$
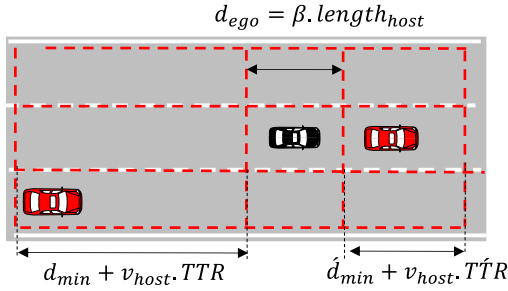
Fig. 3. Environment grid modelling.

The grid cell's width and orientation are equal to the lane width. The middle cell length d_{ego} is equal to the ego vehicle length plus a safety distance at the front and back size. The gird's front cell size is calculated based on the current velocity and time to react.

$$d_{safe} = d_{min} + v_{host} * TTR \qquad (2)$$

where d_{min} is a human defined minimum safety distance; v_{host} is the current ego vehicle's velocity, and TTR is time to react in case of some emergency situation happening (e.g. the car in the front suddenly stops). The space needed is depent on the ego vehicle's speed and the surrounding vehicle's speed. A longer distance is needed when the vehicle is travelling at high speed. The scenario around the ego vehicle can now be modelled into a grid of 8 states and labelled/numbered as in Fig.4. Each cell in the grid has one state of either "empty" or "occupied".

Occupied
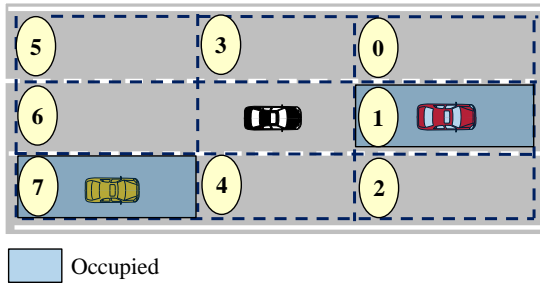
Fig. 4. Observation grid state.

If cell (1) is "empty" then it means there is no obstacle inside the space that's required in front of ego vehicle. Similar meaning is applied for other cells. That means if cell (0),(1),(3), and (5) are "empty", the ego vehicle has sufficient space to perform the left side lane change. Besides, if the entire surrounding vehicles travel with a relatively equal speed then it is also possible to change to right side lane. Similarly, when the vehicle is travelling at the right-most lane, corresponding right side cells are set to be occupied.

By discretization the surrounding environment to a nine-cell grid, we are able to present different states to do the lane change. We have eight surrounding cells in the occupancy grid that can be free (cell value = 0) or occupied (cell value = 1) then we have totally 2^8 =256 states. Since the vehicle only perform either the left side or right side lane changing

maneuverer, we can temporarily ignore the other side's cell so that the number of state can be reduced to $2^5 = 32$ states.

For merge-in maneuver from a side road to main lane, according to traffic rules, a direct cut-in is considered dangerous or unsafe maneuver and Figure 5.a) illustrates a proper merge in maneuver. We apply the grid state model from the entrance of the ramp road. Figure 5.b) illustrates an exiting from main line situation, the vehicle needs to change own lane to the exit lane before it passes the lane end.
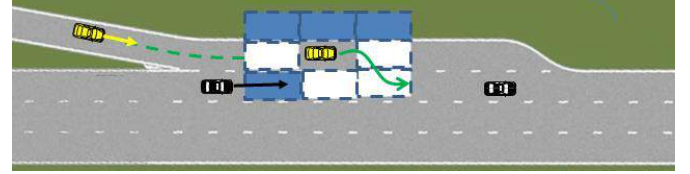
a) Proper merge in maneuver.
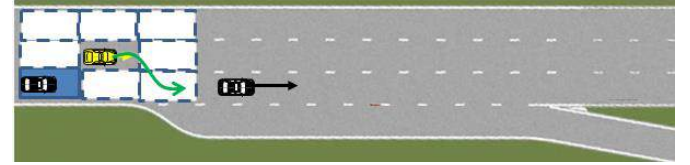
b)Lane change for exitting from main line traffic.
Fig. 5. Merge in and exit lane.

2.3 Behaviour Generation

For every state, we consider different alternative behaviors as shown in Fig. 6. For the occupancy grid state in Fig. 6, different following behaviors are available to do the lane change;

● **Case A:** The host vehicle just waits until the right lane
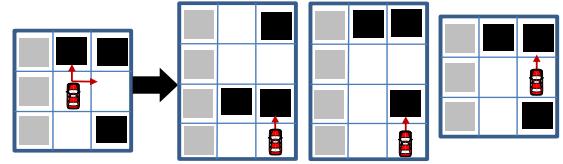
Case : A   Case : B   Case : C

Fig. 6. Different available behavior and motion for lane change.

approaching vehicles passes it and the right lane becomes free to do right lane change.

● **Case B:** In this case, the host vehicle decelerates and enters to the right lane. It is preferable behavior when we have to do the lane change at limited time/distance (for example exit point in the highway).

● **Case C:** In this case, the host vehicle does the lane change as there is enough space and the relative velocities of the vehicle in the right lane is not high.

To have exact understanding of different behaviors, we categorized 32 (2^5) occupancy gird states (left or right lane change) to the following main four categories. We limit the behavior alternatives based on the categories to reduce the calculation time. Different categories for occupancy grid states are shown in Fig. 7, and we explain the characteristics of each categories and available alternative behaviors for each state. The categories and alternative behaviors are

defined based on our experiments from analyzing the human driver data for different lane change scenarios.

- **Category A:** We have two alternative behaviors for occupancy grid states. We either wait or do the lane change based on the relative speed and distance to the neighbor vehicles.

(a) Category A

(b) Category B

(c) Category C

(d) Category D

Fig. 7. All 32 states models for right lane change and available alternative behaviours for each of them.

- **Category B:** We have more alternative behaviors for states in this category. We may do the lane change but

sometimes acceleration/deceleration or wait is preferable to do safer/smoother lane change. In the case of time/distance constraint, acceleration/deceleration may necessary to satisfy the lane change limitations.

- **Category C:** It is related to complicated state during lane change. In this category, the right cell of the host vehicle is occupied and suitable behavior should be selected to provide free space at the destination lane. We may accelerate, decelerate or wait for states in this category.

- **Category D:** We have to wait for doing the lane change and any other behavior may cause danger.

For situation that has more than one behavior option, we prefer the waiting and deceleration action since it provides the vehicle more time to perform lane change maneuver. We define an evaluation function which consists of three main parts including safety, smoothness (comfortable) and the operation time (travelled distance) to select the suitable behaviour for each state.

2.4 Velocity Planning (Behaviour Segment)

According to the decided behavior, we calculate the corresponding desired vehicle's velocity profile. The acceleration/deceleration patterns are presented in the form of a function that considers ego vehicle position, velocity and the target leading/behind vehicle.

In Fig 8, we illustrate the vehicle acceleration behavior when a leading vehicle is present in the neighboring lane. In this scenario, our vehicle decides to accelerate and pass the leading vehicle. The acceleration is continued till sufficient safe distance is achieved, before performing the lane change maneuver.
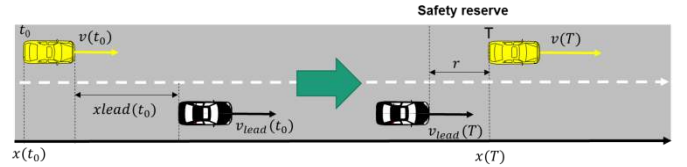
Fig. 8. Vehicle acceleration for passing.

The ego vehicle's acceleration is calculated based on (3):

$$\ddot{x} = 2(x_{lead}(t_0) - x(t_0) + T(v_{lead}(t_0) - v(t_0)) + r)/T^2 \tag{3}$$

where $x(t_0), v(t_0)$ are the vehicle position and velocity at time t_0; $x_{lead}(t_0), v_{lead}(t_0)$ are leading vehicle position and velocity at time t_0; T is the operation time horizon; r is a safety reserving distance and calculated through leading vehicle velocity and time to react TTR

$$r = d_{min} + v_{lead}(T) * TTR \tag{4}$$

Similarly, for other decisions, we can calculate the vehicle desired position and corresponding velocity profile. This velocity profile will be used for trajectory planning.

To generate smooth and comfort acceleration/deceleration motion, we minimize the following cost function;

$$J = \int_0^T (\omega_{dist}[\Delta d(t)]^2 + \omega_{acc}[\ddot{x}(t)]^2)dt \tag{5}$$

This cost function is similar to the method presented in (Geiger et al., 2012) though the operation time T is fixed. In our approach, the operation time T is not fixed to have more degree of freedom for behavior in segment 1. The error in the safety distance ($\Delta d(t)$) is calculated by the following;

$$\Delta d(t) = x_{lead}(t) - r + t * \dot{x}_{lead}(t) - x(t) \quad (6)$$

We use quartic polynomial to generate acceleration/deceleration motion (D. Althoff, et al., 2012).

$$x(t) = b_4 t^4 + b_3 t^3 + b_2 t^2 + b_1 t + b_0 \quad (7)$$

We estimate the coefficients $b_i (i = \overline{0,4})$ by considering vehicle constraints (maximum acceleration/deceleration and speed), desired velocity and operation time. We sample from valid range of operation time T and final velocity $\dot{x}(T)$ to generate alternative longitudinal trajectories while considering the boundary conditions including maximum and minimum acceleration $\ddot{x}_{max}, \ddot{x}_{min}$.

2. 5 Motion Segment

To model a geometric path during a lane change, literature show often approaches using 5th degree polynomials [10, 11]. Polynomial function provides a geometric modelling of the vehicle trajectory that responds to the realistic demands of the maneuver. Quintic polynomials as following, used to generate alternative lateral trajectories

$$y(t) = a_5 t^5 + a_4 t^4 + a_3 t^3 + a_2 t^2 + a_1 t + a_0 \quad (8)$$

The equation coefficients $a_i (i = \overline{0,4})$ are calculated considering dynamic constraints (boundary conditions for lateral acceleration) and values of the position, velocity and acceleration at initial and endpoint. We are able to get the initial velocity and acceleration of vehicle from the CAN and generate alternative lateral trajectories by changing operation time T. We sample T from valid range of operation time and end conditions to generate alternative lateral trajectories c considering the boundary conditions including $\ddot{y}_{max}, \ddot{y}_{min}$ and $\kappa(t) \leq \frac{\ddot{y}_{max}}{\dot{x}(t)^2}$ to avoid slip.

We optimize the lateral motion by minimizing the following cost function that includes lateral jerk, heading error and smoothness as shown in Fig. 9;

$$J = w_{jerk} \int_0^T \dddot{y}^2(t) + w_{heading}[\kappa(T) - \kappa_{road}]^2 + w_{smoothness} \int_0^T \frac{\dot{\kappa}(t)^2}{\sqrt{\dot{x}(t)^2 + \dot{y}(t)^2}} \quad (9)$$
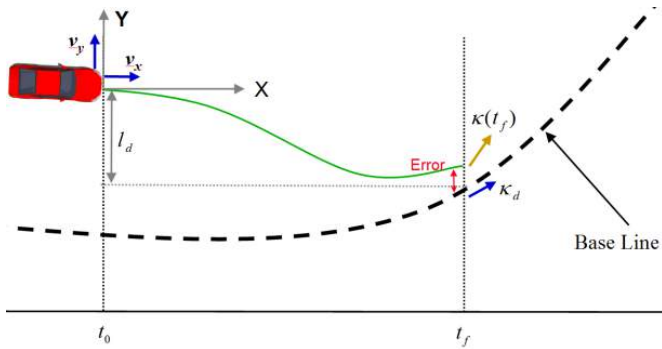
Fig. 9. Lateral trajectory optimization.

3. SIMULATION

To evaluate and test the proposed model, we developed a simulation platform on the PreScan. It includes different modules for sensing, behaviour/motion planning, trajectory estimation of neighbour vehicles and control. Figure 10 shows simulation results for the lane change scenario in the case of distance constraint for exiting the highway (host vehicle is red and it is going to do right lane change to exit the highway). Refer to the Fig. 7, current observation grid status belongs to Category C and the host vehicle can select between *acceleration*, *deceleration* and *wait* behaviour.
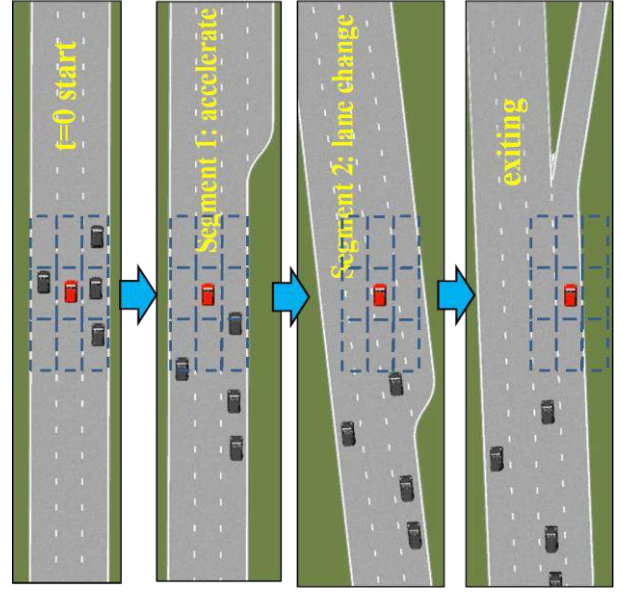
Fig. 10. Lane change simulation for exiting with acceleration behaviour.
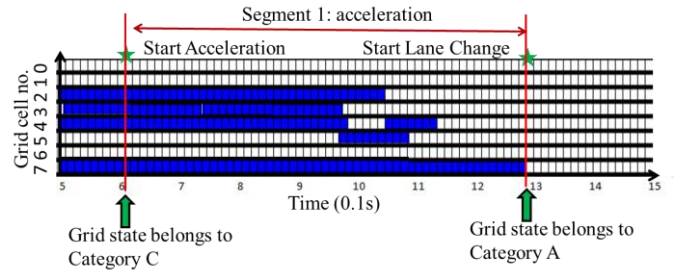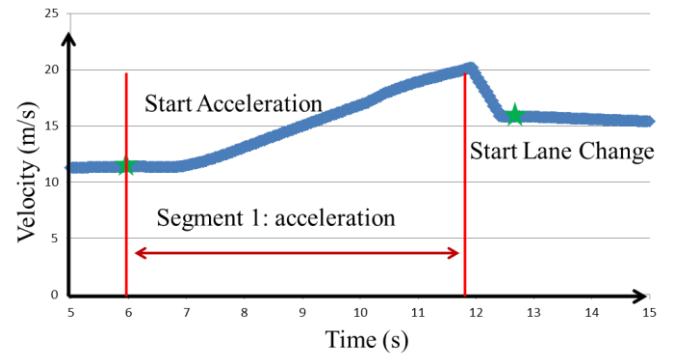
a) Observation grid.

b) Velocity profile.

Fig. 11. Lateral position, velocity profile and observation grid state for acceleration behaviour.

Considering the time constraint for exiting and neighbour`s vehicle speed at the left lane, the *acceleration* or *deceleration* behaviours are preferable to meet the time constraint for doing the lane change. As the left lane neighbour's vehicles speed are lower than the host vehicle`s speed, the *acceleration* behaviour is selected for segment 1 and the velocity profile is generated as shown in Fig. 11(b). By doing acceleration, the host vehicle evaluates the state of the grid and when the state falls into Category A, it starts to do the left lane change. The state of observation gird is shown in Fig. 11 (a) and we are able to select suitable behaviour based on the grid state.
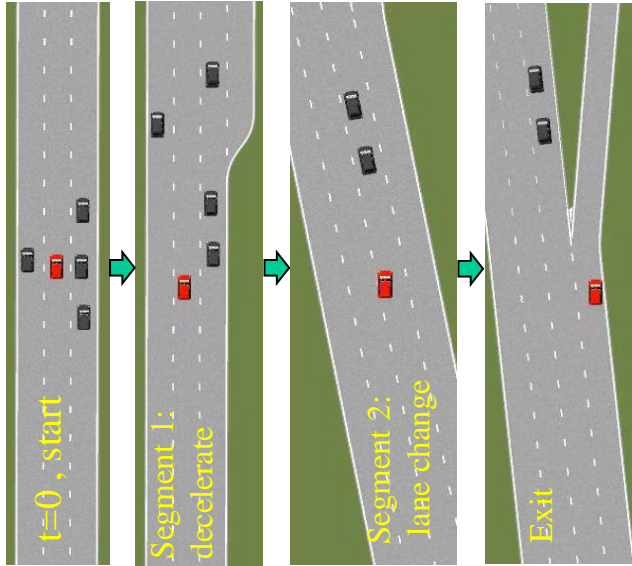
Fig. 12. Lane change simulation for exiting with deceleration behaviour.
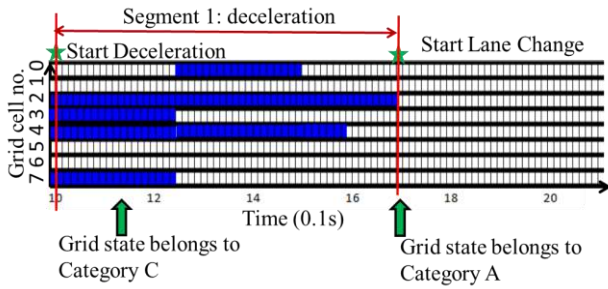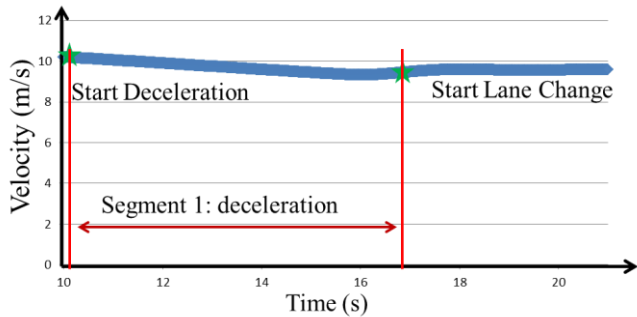
a) Observation grid.

b) Velocity profile.

Fig. 13. Velocity profile and observation grid state for deceleration behaviour.
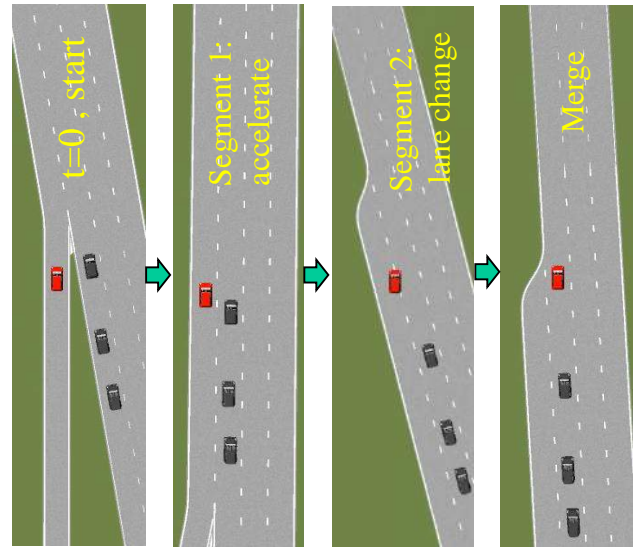
Fig. 14. Lane change simulation for merge in with acceleration behaviour.
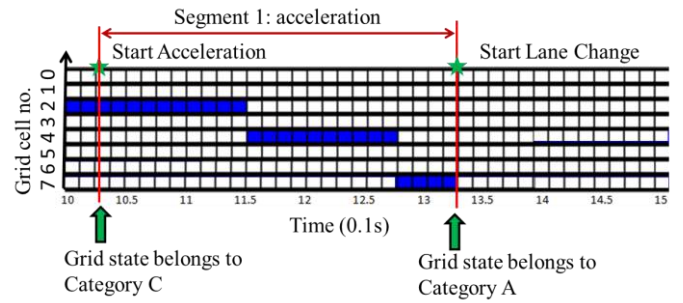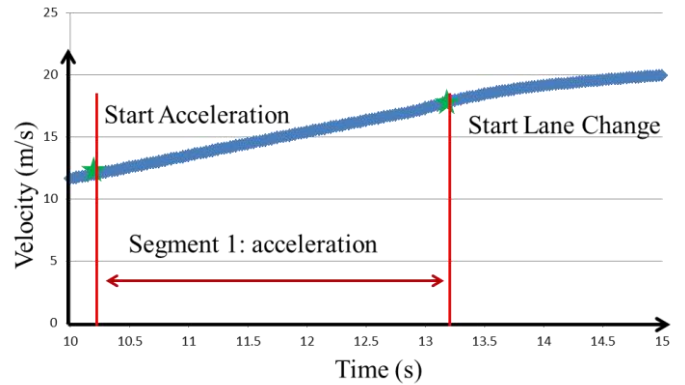
a) Observation grid.

b) Velocity profile.

Fig. 15. Velocity profile and observation grid state for acceleration behaviour.

In these experiments, the host vehicle is travelling at speed of 12 m/s. The exit lane distance is 150m. The grid cell's width is equal to lane's width = 3.5m. The reaction time (TTR) is 1 second. Notice that, in this stage, we do not consider the interaction between drivers. Figure 12 also illustrates a lane change process for exiting, however, this time, the deceleration behaviour was chosen. In this case, left lane neighbour` vehicles speed are higher than the host vehicle's speed and the velocity profile is generated as shown in Fig. 13(a). As shown in Fig. 13 (b) the host vehicle try to change

the state of the grid and when the state falls into Category A, it starts to do the left lane change. Figure 14, 16 show merging simulations to the highway. Same as exiting, the host vehicle selects the suitable behaviour based on in current state of observation gird and do the lane change when the grid state falls into category A. The suitable behaviour from acceleration and deceleration is selected based on the neighbour' vehicles speed and distances. We extracted the relative speed ranges and distances by doing lane change experiments at highway and recording the human behaviour at different scenarios. As shown in Fig.11 when the vehicle applies acceleration behaviour, although it take shorter time to reach suitable lane change state, the vehicle needs to deceleration since it comes close to the exiting-lane's entrance. If the ego vehicle applies deceleration behaviour as shown in Fig. 13, it took longer time to find suitable state for lane change. Similar situation happens for enter-lane cases as in Fig.15 and Fig.17.

4. CONCLUSIONS

In this paper, a behaviour/motion model for automatic lane change at highway has been proposed. The proposed model is mainly inspired by human driver lane change and behaviour data and can handle difficult lane change scenarios. The observation grid state was presented to model the environment/situation. The occupancy grid states are categorized and alternative behaviours are defined for each corresponding category. In the future, we are going to do lane change experiments by human drivers to extract the reference samples and learn the behaviour selection function. Our current behaviour model does not consider the interaction between the vehicles so that in future work, our model will involve it.

REFERENCES

Althoff, D., Buss, M., Lawitzky, A., Werling, M., and Wollherr, D. (2012). On-line Trajectory Generation for Safe and Optimal Vehicle Motion Planning. *AMS 2012*, pp. 99-107.

Ardelt, M., Coester, C. and Kaempchen N. 2012. Highly automated driving on freeways in real traffic using a probabilistic framework. in *IEEE Transactions on Intelligent Transportation Systems*, vol. 13, no. 4, pp. 1576-1585.

Brechtel, S., Gindele, T. and Dillmann, R. (2011). Probabilistic MDP-behavior planning for cars. *14th International IEEE Conference on Intelligent Transportation Systems*, pp.1537-1542.

Dolan, W. and Litkouhi, B. (2010). A prediction- and cost function-based algorithm for robust autonomous freeway driving. *2010 IEEE Intelligent Vehicles Symposium (IV)*, pp. 512–517.

Fletcher, L. et al. (2009). *The DARPA Urban Challenge*, volume 56 of Springer Tracts in Advanced Robotics, pp. 509–548. Springer Berlin Heidelberg.
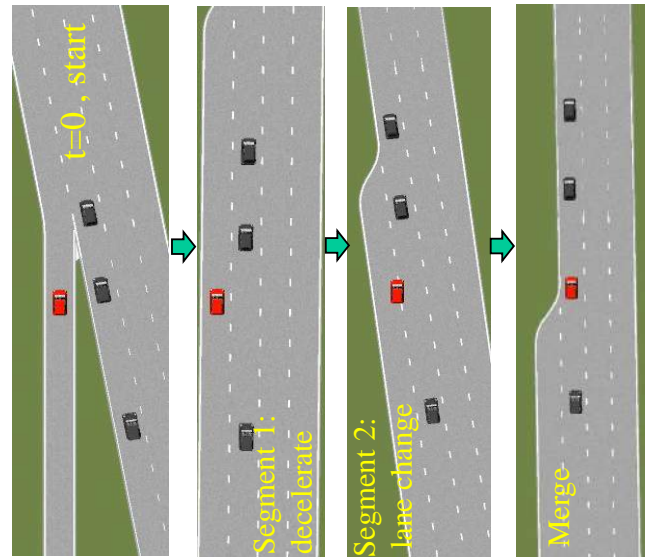
Fig. 16. Lane change simulation for merge in with deceleration behaviour.
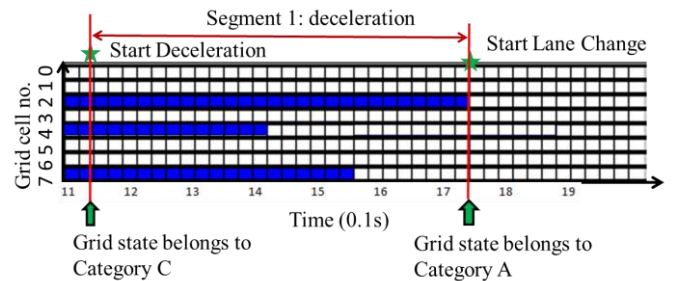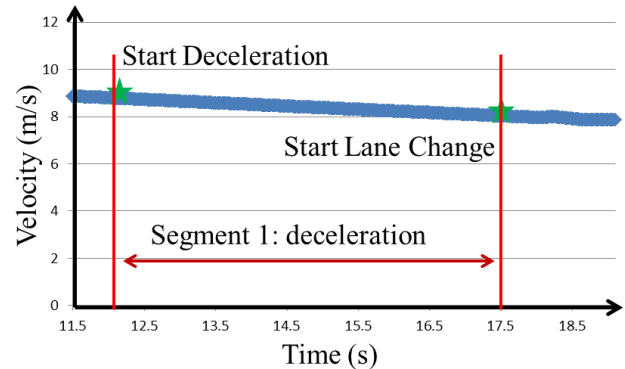
a) Observation grid.

b) Velocity profile.

Fig. 17. Velocity profile and observation grid state for deceleration behaviour.

Geiger, A A., Lauer, M., Moosmann, F., Ranf, B., et al. (2012). Team AnnieWAY's Entry to the 2011 Grand Cooperative Driving Challenge. *IEEE Transactions on Intelligent Transportation Systems*, vol 13, no 3, pp. 1008 – 1017.

Jula, H., Kosmatopoulos, E. and Ioannou, P. 2000. Collision avoidance analysis for lane changing and merging. *IEEE Transactions on Vehicle Technology*, vol. 49, pp.2295 - 2308.

Kasper, D., Weidl, G., Dang T, et al. (2014). Object-Oriented Bayesian Networks for Detection of Lane Change Maneuvers. *Intelligent Transportation Systems Magazine*, Vol. 4, No. 1, pp.19-31.

Naranjo, J. E, Gonzalez, C., Garcia, R. and de Pedro, T. (2008). Lane-Change Fuzzy Control in Autonomous Vehicles for the Overtaking Maneuver. *IEEE Transactions on Intelligent Transportation Systems*, vol. 9, no. 3, pp. 438-450.

Schubert, R., Schulze, K. and Wanielik, G. (2010). Situation Assessment for Automatic Lane-Change Maneuvers. *IEEE Transactions on Intelligent Transportation Systems*, vol. 11, no. 3, pp. 607-616.

Simon, U. and Markus, M. (2013). Probabilistic Online POMDP Decision Making for Lane Changes in Fully Automated Driving. *Proceedings of IEEE Conference on Intelligent Transportation Systems*, pp.2063-2070.

Tehrani, H., Muto, K., Yoneda, K. and Mita, S. (2014). Evaluating human & computer for expressway lane changing. *IEEE Intelligent Vehicles Symposium Proceedings*, pp. 382 – 387.

Volvo Trucks, European Accident Research and Safety Report.[Online]http://www.volvotrucks.com/SiteCollectionDocuments/VTC/Corporate/Values/ART%20Report%202013_150dpi.pdf, 2013.

Ziegler, J., Bender, P., Dang, T. and Stiller, C. (2014). Motion planning for Bertha - a local, continuous method. *Proceedings of Intelligent Vehicles Symposium*, Dearborn, Michigan, USA, pp. 450-457.

Full Spectrum Camera Simulation for Development of Automated Driving Applications

René Molenaar*, Raymond de Vries*, Robin van der Made*.

* TASS International, the Netherlands

Abstract: Cameras are an essential component of many Advanced Driver Assistance Systems (ADAS) such as Lane Departure Warning, Lane Keeping Assistance, Automatic Emergency Braking, Traffic Sign Recognition and Night Vision. With the ongoing evolution of ADAS towards Automated Driving, the amount of cameras within vehicles as well as the performance of these cameras is only expected to grow. Nowadays automotive cameras are typically sensitive beyond the visual range (i.e. into the near infrared range) They may also use up to 20 bits precision for their internal signal. In order to support the development process of ADAS and Automated Driving Systems by means of simulation, it is required to have detailed physically correct simulation models of these automotive cameras. This paper describes the implementation and validation of a new spectral camera sensor model in the ADAS simulation platform PreScan. The traditional RGB-based camera implementation created images limited to the visual spectrum. In contrast, the new PreScan spectral camera sensor model allows for high color depth, broad spectrum and physically correct image generation. The model provides a real-time simulation of light in the 320-1500nm spectral range which traverses through the various media and lenses before the sensor produces the final image signal. Other important features of this new detailed camera model are a depth resolution of 20 bit per waveband as well as an in—creased dynamic range.

Keywords: Autonomous vehicles, sensors, simulation, cameras.

1. INTRODUCTION

With the increasing deployment of ADAS and the ongoing development towards full vehicle automation, efficient ways of validating such systems are becoming a crucial part of the development process. Simulation is emerging as an important addition to "traditional" test-track tests and field trials as it facilitates an early and automated evaluation process of intelligent vehicle systems. Due to the high complexity of traffic scenarios, solely relying on test-track tests and field trials requires a tremendous effort including driving millions of kilometres. Simulation can bring down the number of test kilometers that needs to be covered before a new ADAS system is launched. Moreover, simulation is a good solution for evaluating the performance of a system in complex or improbable traffic situations which are costly or unsafe to recreate in the real world.

During the past few years, the simulation platform PreScan has emerged as the global standard for virtual development and validation of ADAS, automated driving and connected vehicle applications. PreScan was originally developed by the Netherlands Organization for Applied Scientific Research TNO [1], and has recently been transferred to TASS International [2]. PreScan is in use at many automotive OEMs, Tiers as well as at Universities and Research Institutes around the globe. Applying PreScan saves time and money, and it increases the quality of the final systems that are released onto the market [3,4,5]

Fig. 1. The simulation platform PreScan is the global standard for virtual development and validation of ADAS, automated driving and connected vehicle applications.

Simulations of ADAS systems is used by the automotive industry for several purposes. The first application area is to develop and evaluate vehicle control algorithms. Testing the nominal behaviour of control algorithms can be done with "ground-truth sensor models" which deliver the true undisturbed values of the simulated quantities to the control algorithms under test (e.g. the true position and velocity of vehicles, or the true width and curvature of a lane). If needed, stochastic functions can be imposed onto these idealized sensor readings for a "quick and dirty" evaluation of the system's robustness. We then usually speak about "probabilistic sensor models". These probabilistic models are typically created by measuring the output of sensors in the real-world, comparing these measurements with the output of

a ground-truth reference system, and fitting a noise model onto all these measurement data. Such probabilistic sensor models deliver disturbances with the same order of magnitude as the real sensors would have done.

However, the complex physical "cause-consequence relationships" which are the source of the sensor disturbances (such as the influence of guardrail geometry on radar readings or the influence of adverse light conditions on camera images) are definitely not captured within a probabilistic sensor model. Therefore, a more detailed analysis of the relationship between scenario characteristics and system behaviour requires "physics-based sensor models".

Moreover, there is a second up-and-coming application area of ADAS simulation within automotive companies which is virtual development and validation of sensors and sensor algorithms. Such sensor algorithms are for example used for object detection, object classification and sensor data fusion. By definition, this application area requires very detailed physically correct simulation models of both the environment and the sensor itself. In other words, also here "physics-based sensor models" are needed.

This paper discusses the implementation and validation of one of such "physics-based sensor models": a full-spectrum camera sensor model

2. CAMERA SENSOR SIMULATION

2.1 Traditional RGB-based camera simulation models

Most currently available camera simulation models are using RGB camera sensors, mainly because the current displays are RGB-based and targeted for the human perception (i.e. limited to the visual wavelength range in three channels). However, there are many differences between the human eye and a video camera system. Human experiences are not always accurate when it comes to validating a simulated image. For example, the eye has the ability to see light in the most dark circumstances, where it adapts its dynamic range to groups of receptor cells ("pixels"). A standard camera does not have this ability, and will see nothing but low level noise in such scenes. Although camera sensors have limited dynamic range, a simulated scene should provide a full dynamic range. Different sensors or sensor types have different sensitivity for particular wavelengths.

Typical machine vision algorithms use only the intensity of the light. For quality requirements and specific region of interest localization color information might be needed as well. Red channel color information can be used for traffic light, traffic sign or for car rear-light detection. Hence, sensor manufacturers have designed Red/Clear (RCCC) color filter arrays specifically for automotive use [12]. There are other limitations of using RGB-based systems. Consider for example a simulated image inside a real camera for image processing, such as in a Hardware in the Loop (HIL) setup. This is discussed in more detail below.

In short, the need for more accurate physics-based camera sensor modelling arises from the observation that real life sensors become more advanced and integrated, and their intelligent algorithms become more sensitive to smaller variations. The next section describes the requirements of such an accurate physics-based camera sensor model, as an answer to more demanding sensor model requirements automotive companies have.

2.2 Requirements for an accurate physics-based camera sensor model

Fig. 2 provides a systematic overview of the scene content and the camera model. Light starts at the light sources (sky, sun, headlights, etc), travels through media (air, water, fog, etc.), is reflected from complex materials, and travels through media towards the camera. Subsequently, spectral radiance from the scene first enters the lens system. The optics subsystem modulates the scene representation at the camera lens and generates the spectral radiance image (the optical image), on the sensor plane.
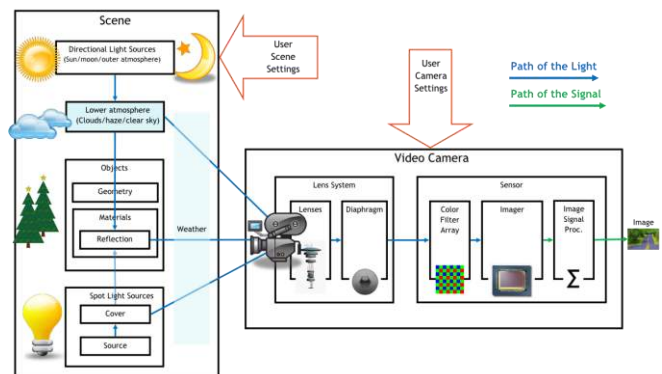
Fig. 2. A systemic view of the spectral scene (left) and the spectral camera sensor (right)

In this subsystem lens effects and artefacts are applied. Colour Filter Arrays allow capturing specific spectra at specific pixels. The shutter determines exposure time. The image sensor consists of a 2D array of pixels, each of which collects an amount of power. These pixels contain photo detectors that convert light into photocurrent. In conventional sensors the photocurrent is integrated during exposure into charge and read out as voltage pixel data. The sensitivity of an image sensor is characterized by its Quantum Efficiency (QE). Noise dependent on temperature, exposure time and other sensor settings impacts the image at this stage. The image processor works on the pixel data and enhance the image by applying a bunch of image processing algorithms, before the ADAS algorithms process the image.

A typical RGB-based camera looks at a three channel (red, green, blue) world with limited precision, matching current image display precisions. To record the amount of light, it uses the perception-based quantity luminance. This is sufficient for the human perception of average scenes in the visual wavelength range. However in low and high lighting conditions, the dynamic range and precision of this approach

is insufficient for current automotive sensor applications. Furthermore, the color filter transmission curves of Color Filter Arrays (CFAs) in general deviate from the tristimulus curves for human perception and different sensors have different sensitivity for particular wavelengths. Such curves, as well as those of lens coatings and light sources (e.g. fluorescent), can be very spiky, which cannot be accurately represented by a three-channel approach. In conclusion, real time performance is required when real cameras are used to process the simulated image.

Finally, the simulated image is required to reproduce the same quality and artifacts present in real images to produce similar results to real images in the ADAS algorithms.

The following list of requirements has been drawn up in order to model an accurate physics-based camera sensor:

• Spectral Based

• High Dynamic Range

• High Colour Depth

• Real time performance

• Physically plausible reflection model

• Reproduce limitations and artefacts of real cameras

Because there is a continuous pressure on the automotive industry to work cost-effectively, automotive camera systems are typically not high-end. This means they will be subject to a number of artefacts which can impact the performance of the ADAS application. For estimating the usability for a certain application, it is crucial to know the parameter ranges, within which the ADAS algorithm performs successfully. These ranges are influenced by artefacts, such as distortions and blur, which influence the color and intensity of the light and subsequently the electrical signals induced in the imager.

2.3. The PreScan spectral camera sensor

The new PreScan spectral camera sensor model that has been developed is a multispectral high dynamic range camera. It meets the demand for a more accurate physically based sensor simulation, and distinguishes itself from a typical camera in two important ways. First, it measures light as a physical quantity at high precision and large range. The radiance is recorded as desired in either W/m2.sr or photons/s.m2.sr. In contrast to graphics-based light models, the light equations of the spectral world obey energy conservation and Helmholtz reciprocity. Second, it measures the detailed spectrum of the light entering the camera. The light spectrum has a variable spectral resolution (number of wavelength bands) and can extend beyond the visual into the near infrared.

The radiance data results of the Spectral Camera should be recorded and communicated to the user. For this the OpenEXR file format has been used. An OpenEXR file contains a complete image (width x height) for each wavelength band. The Spectral Camera can also provide

RGB HDR images for visual inspection. OpenEXR is a high dynamic-range (HDR) image file format developed by Industrial Light & Magic for use in computer imaging applications. OpenEXR's features include a higher dynamic range and color precision than existing 8- and 10-bit image file formats (e.g. 16-bit or 32-bit floating point pixels) [7]. The Image format can also store arbitrary channels, specular, diffuse, alpha, RGB, normals, and various other types of channels in one file. The OpenEXR (.exr) files containing channels for each wavelength band can be imported into Matlab by using a script. This script reads the OpenEXR data and stores it in the Matlab workspace as an array for further processing.

The Image Systems Evaluation Toolbox (ISET) is a software package in MATLAB to simulate different imaging optics, sensor electronics and image processing pipelines. ISET provides clients with the ability to specify explore and optimize the parameters of an image-processing pipeline for different imaging conditions and hardware. The principles of ISET are well described in a research paper [8]. Instead of using the default sensor and optics module in PreScan, the spectral data can be imported into Matlab, and used in ISET to simulate the optics, imager and processing.

Validation tests are developed that validate physical plausibility of the rendering pipeline. For example physical laws such as energy conservation can be checked since all values in the simulation are known. Simple experiments containing a single object and a single light are used for theoretical validation. Reference material like real world measured data or accurate physics based simulation software (e.g. PBRT [9]) can be used to further validate the rendering pipeline. The results of the spectral camera can also be compared to the RGB pipeline to investigate the added value. More validation tests and comparison checks under different conditions are being developed to increase the confidence and applicability of physics based sensors.

Benchmarking experiments are developed to track performance requirements. Elements and aspects of the scene can be benchmarked individually and integration tests are used to measure performance of a complete pipeline in scenarios that well represent common camera-based automotive applications.

3. APPLICATION EXAMPLES OF THE PRESCAN SPECTRAL HDR CAMERA SENSOR MODEL

3.1 Vehicle detection

Vehicle detection is an essential part of environmental awareness. This is a challenging task, because the continuously changing landscape along the road and the various lighting conditions that depend on the time of day and weather are not known in advance. It is achieved by using color, edge and motion information for e.g. template matching and temporal differencing.

More specifically, rear lights are used to detect cars, while their distance is derived from the image based on a flat road

plane assumption [10]. To reduce the search time for rear lights, only the red component of each image frame is analyzed. For cars at less than 10 m distance, a threshold that is very close to the brightest possible value, e.g. 98%, is used, because at such small distances bright rear lights cause "blooming effects" in CCD cameras, especially in poorly lit highway scenes, at night or in tunnels [10]. For proper rear light detection algorithms these properties and artifacts need to be accurately modelled. The presence of the sun in the camera view (e.g. low sun conditions) causes glare, and can severely interfere with proper vehicle detection and recognition. At night time, dusk and dawn, a similar role is played by headlights of approaching vehicles [11].

The sky and the sun are the dominant sources of light in common daytime scenarios. To simulate these scenarios with the spectral HDR camera, the image-based RGB skybox in PreScan's traditional camera model is replaced by a physics-based analytic model of the daytime sky [12]. The sun position and corresponding clear sky, turbidity and ground albedo can be configured by the user. The sky model includes the complete visual spectrum, and is stored in multiple shader language-supported memory structures called cubemaps. It stores for each direction, the complete spectrum and radiance value of the light coming from that direction. For memory efficiency reasons, the sky's cubemap is set to a certain resolution, matching the rather low gradients occurring in the sky. However, the sun disc itself is calculated from a separate analytic model. Moreover, it cannot be stored in the same low resolution cubemap, since we expect a sharp circular disc when looking into the sun. Therefore the sundisc is projected into the sky with a separate texture of much higher resolution.

The results of a spectral camera simulation, with the camera looking into the sun, are shown in Fig 3. The glare artifacts (e.g. solar flares and pixel bleeding) are caused by the optics and the imager, which were simulated accurately with the ISET software, using a relatively long exposure time. The simulation result shows that an overexposed image with solar flares can severely influence vehicle detection on the road.
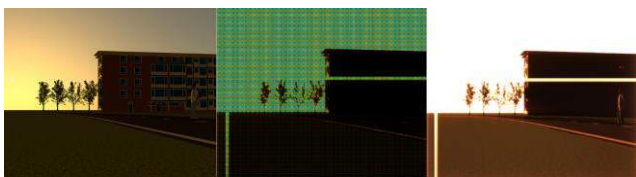
Fig. 3. Post processing a spectral radiance scene (left) from the spectral HDR camera with ISET. Image after applying the Bayer filter (center). Image after demosaicing and processing (right). Please note that the RGB based colors in these printed pictures (left) do not reveal the true wavelengths and radiance values of the images generated by the spectral camera model.

3.2 Pedestrian detection

Compared to vehicle detection, pedestrian detection is even more challenging due to the high variability of their appearance (i.e., different articulated pose, clothes, distance and viewpoint) and the cluttered scenarios usually found in urban environments [13]. It is used in ADAS applications,

such as Collision Warning and Pedestrian Protection Systems. To achieve a robust pedestrian detection, techniques from the domain of computer vision are used. Techniques such as noise filters, thresholding, histogramming, edge detection and pattern detection rely on a realistic input image. Over the years, camera systems have moved from 10 bit to 14 bit and higher for their internal precision of intensity values. They have also exploited the increased spectral response of imager chips in the NIR (Near Infrared) for improved detection capability. This allows them to detect a pedestrian in low lighting and night conditions, at greater distances than before, increasing safety. The perception (RGB) based camera fails to comply to such scenarios. First, it is limited to the visual range of wavelengths (roughly 350nm to 750nm) and uses just three channels (Red, Green and Blue) within that range. Second, the precision of each channel is limited to 8 bit or 256 levels. For a typical outdoor scene the difference between bright and dark areas is many orders of magnitude, for which 256 levels would not suffice.

The spectral HDR camera was designed with different specifications, and can simulate pedestrian detection scenarios adequately. It achieves this by extending the wavelength range to the Near Infrared (up to 1500nm), increasing the precision per channel to 32 bit (21 bit mantissa), and allowing for an arbitrary number of wavelength buckets. See Fig. 4 for a simulation with 20 buckets of 20 nm each. These are technically achieved using advanced shading and texturing techniques, which are configurable through user settings.
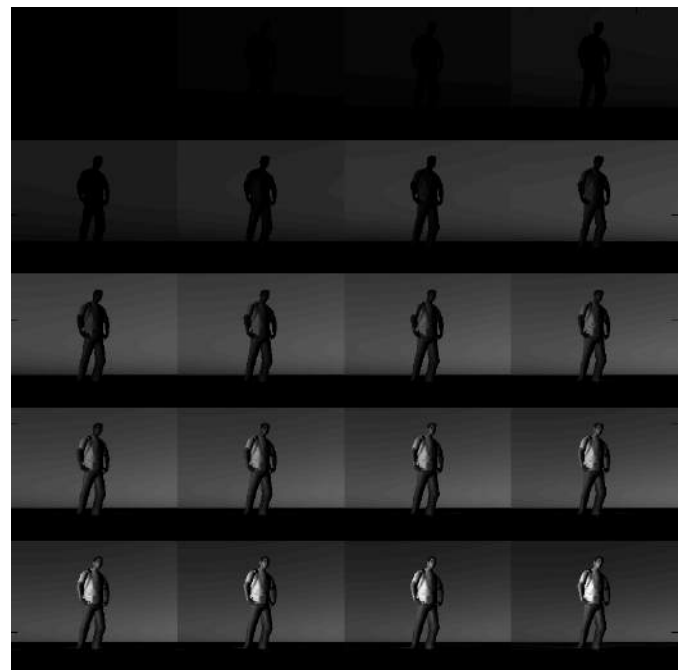
Fig. 4. Simulating a pedestrian in 20 wavelength channels (320-720nm). Please note that the RGB based colors in these printed pictures do not reveal the true wavelengths and radiance values of the images generated by the spectral camera model.

For pedestrian actors, PreScan users can specify variations in clothing materials and variations in skin color in the PreScan Editor. Technically, one can specify the material all the way down to the pixel level, which provides high fidelity input to pedestrian pattern recognition algorithms. This technique not only allows for detailed pedestrian modelling, but is available for all models in PreScan (Fig. 5). Spectral databases can be used to specify the reflectance spectra of the materials and skin. For example, Vrhel et al. [14] provide measurement data of various skin reflectance spectra.
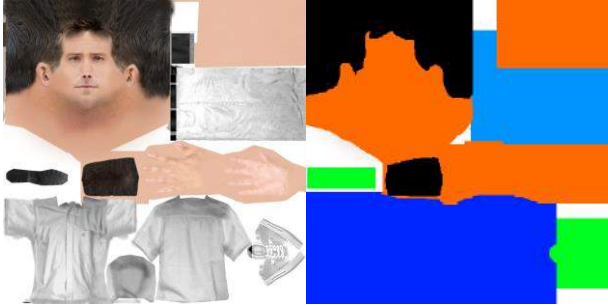
Fig. 5. Pedestrians model regions can be assigned different materials on a per-pixel level, using a color-id texture (right).

3.3 Traffic sign recognition

PreScan supports a wide range of traffic signs in a wide range of categories, like speed limits, warnings, directions, transitions, school area and slope categories. In ADAS application there are two problems: traffic sign detection (TSD) and traffic sign classification (TSC). Some datasets with images of traffic signs are reaching recognition saturation [15] (i.e. most images in the dataset are recognized by the algorithms). In most cases a single frame is used and no temporal information is available. Larger dataset and more variation in weather conditions are needed to further improve the recognition algorithms. Simulation environments are an interesting alternative since traffic sign and weather conditions can be configured. Users can add imperfections to the traffic signs such as dirt, dust or snow. Temporal information is also available. Using the spectral data with specific color filter arrays allows the detection of regions of interest based on red color information in the images. Proper simulation of the optics and sensor are needed to reproduce the artifacts in real images, such as focal problems as described by the Modulation Transfer Function (MTF), motion blurs, or other causes of image quality degradation such as noise.

3.4 Lane marker detection

To test for the robustness of image based lane marker recognition and lane keeping algorithms, configurable wear and tear and fading artefacts to the materials are added to PreScan. Experiments are repeatable with different wear and tear configurations. The materials of the lane lines and asphalt can be configured, e.g. the colours of the lane lines or the asphalt.

Measured spectral reflectance data from various sources can be used in PreScan to define the materials. The USGS Digital Spectral Library is a digital reflectance spectral library that

covers the wavelength range from the ultraviolet to far infrared along with sample documentation [16].
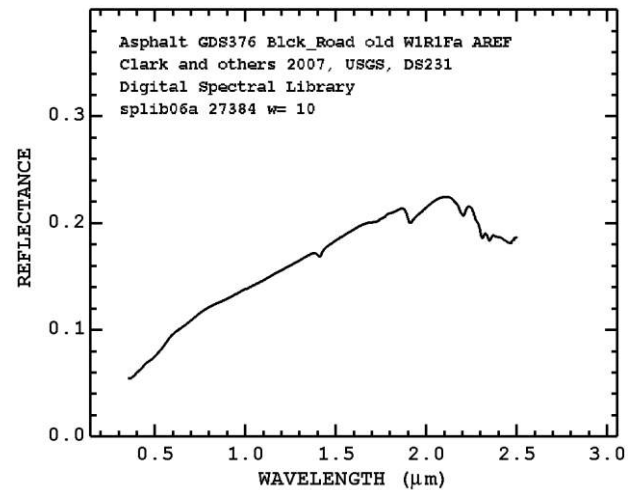
Fig. 6. Sample plot of the reflectance of a weathered asphalt surface taken from the USGS Digital Spectral Library.

The library includes samples of natural and man-made materials (Fig. 6). A subset of common materials prepared for the spectral HDR camera model are included in PreScan. Light arriving at an object's (non-emitting) surface, can be reflected, absorbed and transmitted. For each incoming light direction, the light can be reflected differently in each outgoing direction. The function that maps the fraction of light being reflected for each incoming direction is called the Bidirectional Reflectance Distribution Function (BRDF) [17].

Energy conservation demands that the outgoing energy cannot be larger than the incoming energy. Helmholtz reciprocity states that swapping the incoming and outgoing angles should yield the same value (of the BRDF). Once reflected we look at the part that is reflected in the camera direction. The physical quantity (radiance in Watt/m2.sr or photons/s.m2.sr) that enters the lens system is made available for further processing.

4. IMPLEMENTATION EXAMPLE: HIL SETUP BASED ON INJECTION OF CAMERA IMAGES

PreScan is used in many different ways, both in offline and in online setups. In offline mode, simulated sensor data (e.g. virtual camera images, radar readings, GPS positions) are sent to algorithms which run on a PC (e.g. in Matlab/Simulink or in the ADTF framework). In contrast, when using PreScan in online mode, the virtual sensor data are sent to a real hardware ECU. We are then speaking about "Hardware-in-the-Loop (HIL) simulation". This section gives an example of how the new spectral camera model can be applied in such a HIL simulation setup.

4.1 Projection HIL setup

The PreScan software can be used for HIL applications [18]. HIL setups are typically used to test a control algorithm on the ECU (Electronic Control Unit) which is also going to be applied in the production vehicle. The example given below

describes how PreScan was used as a traditional HIL simulator for testing a Lane Keeping Assistance System (LKAS). Fig.7 shows the set-up in which PreScan generates the images which are projected on a screen in the black box.
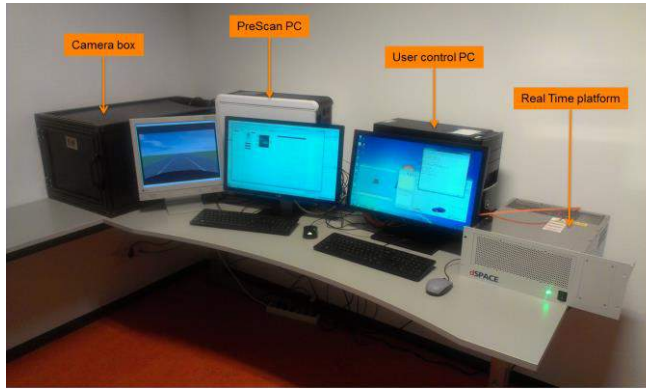
Fig. 7. HIL Set-Up for LKAS System, involving a Real Time (RT) platform for vehicle dynamics simulations, a PreScan PC and a camera projection box.

The camera hardware module with LKAS functionality "looks" at these images and sends out corrective steering wheel adjustments depending on the car's position on the road. Projection occurs in the RGB domain only, since projectors and/or monitors cannot reproduce images in the NIR domain. This is one of the reasons that such a set-up is not suitable for NIR (Near Infra Red). This (RGB-based) type of projection HIL setup is used for functional control algorithm testing but is limited due to the fact that a display is used. The display device often also have limited dynamic range and limited color depth, the computer generated source image follows these limitations in standard graphics pipelines. Higher dynamic range and higher color depth precision allow for less artifacts in image processing algorithms and for example allow better discerning of objects from the background.

4.2 Injection HIL setup

Functionalities that require HDR, infrared and high depth precision cannot be tested in a projection based setup. These limitations can only be removed by using an injection HIL setup and a customized rendering pipeline. The concept of signal projection and injection (Fig. 8) is that projection occurs in front of the sensor head (RF head for radar, lens for camera, etc.) whilst injection occurs somewhere down the processing chain. The simplest type of injection is injection of CAN meta data (object data) where in fact the whole ECU is by-passed. The further upstream, the more difficult it becomes to generate the right type of signal, at the right quality, at the right speed.

When absolute reproducibility is desired one should opt for injection since projection methods are not stable (e.g. lamp output changes over time) or are not properly calibrated. Screen settings determine brightness, colour temperature and contrast ratios of a screen in a projection box like depicted in Fig 7.
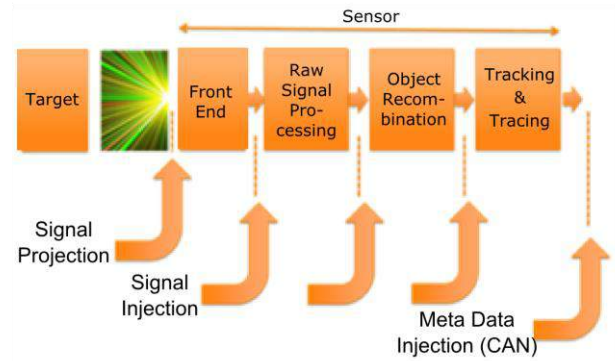
Fig. 8. Projection and Injection at Various System Levels.

Injection is also needed when projection is not possible at all, as mentioned before at high color depths, at high dynamic range and when the detector can sense outside the standard RGB domain (i.e. NIR). Also, injection offers the fastest way possible to inject the images coming from a simulator like PreScan into an ECU under test since there is neither input lag of the displaying device, nor effects caused by the way the frames are built up on the screen. To meet the real time requirements that are imposed by the hardware, the highly parallel structures of hardware accelerated graphics and its programmable graphics pipeline are utilized. Custom shaders that render multiple channels are implemented on the GPU.

Using injection in real hardware and using the corresponding specifications of the optics and sensors in the simulations, OEMs are enabled to evaluate and benchmark different camera systems and different optics and sensor types with different quality and costs in a wide range of simulated conditions.

5. CONCLUSION & OUTLOOK

Current projection-based HIL setups have several limitations that can be resolved by using a spectral based (including NIR), high depth precision and high dynamic range custom graphical pipeline and image injection. Using a new spectral HDR camera model for the PreScan, image based ADAS applications like vehicle, pedestrian, traffic sign and lanemarker recognition can be developed and evaluated for robustness. Moreover, the model makes that different camera systems and different optics and sensor types with different quality and costs can be evaluated and benchmarked.

The spectral radiance data generated by the new spectral HDR camera model can be accurately processed using the default module or external sensor and optics simulation software such as ISET. For an injection HIL setup, this part of the pipeline is implemented on the GPU, allowing direct transfer of the image data and higher frame rates. Other features include enrichment of the scene content, like imperfections to the asphalt and traffic signs, weather effects, support for multiple material models and support for additional measured reflection properties of materials (allowing e.g. retroreflection). Finally, optics and sensor features and artifacts are implemented to accurately follow real world aspects with these systems, like motion blur or depth of field effect.

REFERENCES

[1] Website TNO [Online]. Available: www.tno.nl

[2] Website Prescan [Online]. Available:www.tassinternational.com/prescan

[3] M. Tideman, "Scenario-Based Simulation Environment for Assistance Systems," in *ATZ (Automobiltechnische Zeitschrift)*, vol. 112, No. 2, pp. 32-36, 2010.

[4] M. Tideman and S.J. Janssen, "A Simulation Environment for Developing Intelligent Headlight Systems," in *Proceedings of IEEE IV*, San Diego, USA, 2010.

[5] M. Tideman and M. van Noort. "A Simulation Tool-Suite for Developing Connected Vehicle Systems," in *Proceedings of IEEE IV*, Gold Coast, Australia, 2013.

[6] G. Karanam, "Interfacing Red/Clear Sensors to ADSP-BF609® Blackfin Processors," Analog Devices, Norwood, Engineer-to-Engineer Note EE-358, Rev 1, May 28, 2013.

[7] Website OpenEXR [Online]. Available: www.openexr.com

[8] J. E. Farrell *et al.*, "Digital camera simulation," in *Applied Optics,* Vol. 51 , issue. 4, pp. A80–A90, 2012.

[9] M. Pharr and G. Humphreys, *Physically Based Rendering, Second Edition: From Theory to Implementation (2nd ed.)*, Morgan Kaufmann Publishers Inc., San Francisco, CA, USA, 2010.

[10] M. Betke *et al.*, "Real-time multiple vehicle detection and tracking from a moving vehicle," *Machine vision and applications* 12.2, 2000, pp. 69-83.

[11] P.F Alcantarill *et al.*, "Night time vehicle detection for driving assistance lightbeam controller," in *Intelligent Vehicles Symposium, 2008* IEEE, pp. 291-296, 4-6 June 2008.

[12] L. Hosek and A. Wilkie, "An analytic model for full spectral sky-dome radiance," in ACM Trans. Graph. 31, 4, Article 95, 2012.

[13] D. Gerónimo *et al.*, "2D–3D-based on-board pedestrian detection system," in *Computer Vision and Image Understanding*, issue 5, vol. 114 pp.583–595, 2010.

[14] M. Vrhel *et al.*, "Measurement and analysis of object reflectance spectra," in *Color Research and Application,* issue 1, vol. 19, pp.4–9, 1994.

[15] M. Mathias *et al.*, "Traffic Sign Recognition - How far are we from the solution?," in *Proceedings of IEEE International Joint Conference on Neural Networks (IJCNN 2013)*, 2013, Available: http://rodrigob.github.io/documents/2013_ijcnn_traffic_signs.pdf.

[16] R.N. Clark *et al.*, "USGS digital spectral library splib06a," U.S. Geological Survey, Digital Data Series 231, 2007.

[17] F.E. Nicodemus *et al*, "Geometrical Considerations and Nomenclature for Reflectance," National Bureau of Standards, U.S. Department of Commerce, 1977.

[18] O.J. Gietelink *et al.*, "Pre-crash system validation with PRESCAN and VEHIL," in *Proc. of the IEEE Intelligent Vehicles Symposium (IV)*, pages 913–918, Parma, Italy, June 14–17, 2004.

Predicting Natural Driving Behavior

Shun Taguchi * and **Takayoshi Yoshimura** *

* *Toyota Central R&D Labs., Inc., 41-1 Yokomichi, Nagakute-shi, Aichi-ken 480-1118, Japan (e-mail: s-taguchi@mosk.tytlabs.co.jp, yoshimura@mosk.tytlabs.co.jp) .*

Abstract: This paper proposes a method that uses a state-space model to predict vehicle behavior. It incorporates a proposed model of a generic driver, who is described by a simple feedback model with various constraints corresponding to general traffic rules and the physical limits of the vehicle. In addition, data assimilation is used to estimate the state and the model parameters on-line. By being able to predict natural driving data in unknown situations, the prediction error of the proposed model is significantly reduced compared to constant prediction, since data assimilation can be used to adapt the model to new situations. The data assimilation makes this model universal and robust against any new road-traffic situations. Furthermore, it is confirmed that this ability to predict can improve the fuel efficiency of adaptive cruise control systems.

Keywords: driver model, data assimilation, autonomous driving

1. INTRODUCTION

Prediction of the behavior of nearby vehicles plays an important role in various driver safety and assistance systems. In particular, with advances in technology, collision safety systems have evolved to operate more quickly. Better prediction of the behavior of the next vehicle in the line of travel (*forward vehicle*) may help to improve fuel consumption by suppressing unnecessary acceleration and deceleration (Luo et al. (2010); Kamal et al. (2013); Kamal et al. (2015)). For these reasons, vehicle behavior prediction is expected to be a key technology for the future driver assistance systems.

On the other hand, with advances in wireless communication, information about the other vehicles will be able to be obtained by vehicle-to-vehicle (V2V) communication systems. Cooperative adaptive cruise control (CACC) is one of the driver assistance systems that uses V2V, and its effectiveness was shown in Arem et al. (2006) and Naus (2009). CACC systems have improved the performance of assistance systems by estimating the behavior of nearby vehicles for up to one second in advance. If future behavior can be estimated for a longer period (say, several seconds to ten seconds), this can be expected to further improve the performance. To accomplish this, it is not sufficient to predict the physical movements of the vehicles; it is also necessary to predict the behavior of the other drivers.

Models that predict future driving behavior have been researched for many years. In early studies, car-following models were actively studied, such as those by Gipps (1981) and Treiber et al. (2000). Currently, researchers are targeting more-complex situations (Levesque et al. (2011); Dagli (2002); Dagli et al. (2003); Gindele et al. (2010); Brechtel et al. (2011); Gindele et al. (2013)); for example, Gindele et al. (2010) modeled basic driving behavior, including overtaking, by using a fully probabilistic approach. However, almost all research has focused on a limited number of situations, such as a overtaking. There are no existing general models that can cope with a wide variety of situations.

Therefore, in this study, we propose a driver model that can respond to a variety of situations, as follows. The proposed driver model is expressed as a model with various constraints, and it is based on a control model that controls the position in order to reach the destination. Physical constraints and traffic rules are introduced as constraints, since by doing this, we can guarantee that the modeled behavior will follow traffic rules. It is possible to ensure that the model is at least trying to obey all traffic rules. To add new conditions or traffic rules, it is only necessary to add the appropriate constraint.

In addition to control-based models, such as the one used in this study, there are also models based on knowledge and on machine learning. However, in order to accommodate different situations, it is necessary to collect data on various human characteristics relating to driving, and this can be difficult to achieve. In addition, it is difficult to apply these other models to the operation support system, which is critical, since it is not possible to guarantee the behavior of them. On the other hand, control-based model is possible to guarantee the behavior of it.

This paper presents a driver model in the framework of cascade feedback control. It incorporates some constraints that correspond to general traffic rules and the physical limits of the vehicle. The model parameters can be tuned on-line through a data assimilation process, and this makes the model universal and robust against any new road-traffic situations. Moreover, by the evaluation eco-driving systems that are based on the predicted driving behavior, we show that this can improve actual fuel economy.
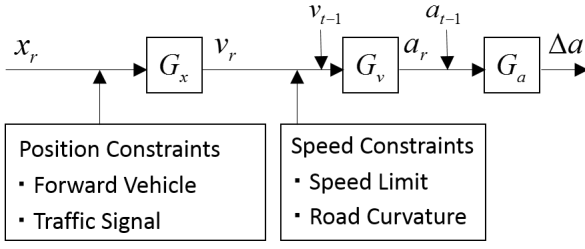
Fig. 1. Proposed driver model.

2. PROPOSED MODEL

2.1 Driver Model

We use a control model for the driver. The objective function J is defined as follows:

$$J = min\,|\boldsymbol{x}_G - \boldsymbol{x}| \tag{1}$$

where $\boldsymbol{x}_G$ is the location of the goal, and $\boldsymbol{x}$ is the current position of the vehicle. This objective function only determines that the vehicle will move to the goal, and for the driver model, we will add various constraints that describe the physical constraints and traffic rules; the model will use the framework of cascade feedback control. The proposed driver model contains four constraints, which are related to the speed limit, the curvature of the road, the forward vehicles, and any traffic signals (see Fig. 1). In Fig. 1, x_r is the distance between the current position and the goal, v_r is the desired velocity, v_{t-1} is the current velocity, a_r is the desired acceleration, a_{t-1} is the current acceleration, and G_x, G_v, and G_a are the mean gain parameters of feedback models.

Next, the four constraints are explained.

Speed Limit Constraint   Speed limits are a basic traffic rule, and we incorporate this as the following constraint:

$$v_r \leq p_n V_{road} \tag{2}$$

where v_r is the desired velocity, V_{road} is the speed limit for the current location, and p_n is a parameter for how well the individual driver keeps within the speed limit.

Curve Constraint   The curve constraint is a physical constraint to avoid slipping in a curve. It is defined by centrifugal force as follows:

$$\left|\frac{mv_t^2}{R}\right| \leq C_1 \tag{3}$$

where m is the weight of the vehicle, R is the radius of curvature, and C_1 is the threshold of the centrifugal force. This equation can be rewritten as follows:

$$v_r \leq p_c \sqrt{\frac{1}{\delta_{t+T}}} \tag{4}$$

where δ_{t+T} is a forecast of the curvature δ_t in T seconds, and p_c is a parameter for each vehicle and is proportional to the threshold of the centrifugal force C_1.

Forward Vehicle Constraint   The forward vehicle constraint is a physical constraint to avoid a collision with the forward vehicle. It uses the car-following model, and here we define it by the headway time, as follows:

$$\frac{x_f - l}{v} \geq C_2 \tag{5}$$

where x_f is the distance to the forward vehicle, l is the length of the car, and C_2 is the threshold of the headway time. This equation can be rewritten as follows:

$$x_r \leq x_{f,t+T} - p_f \tag{6}$$

where $x_{f,t+T}$ is the predicted distance to the forward vehicle $x_{f,t}$ after T seconds, and p_f is a parameter for an individual car and is defined as the sum of the car length l and safety margin.

Traffic Signal Constraint   Traffic signals convey basic traffic rules, and we incorporate this as the following constraint:

$$x_r \leq \begin{cases} x_s & (S_{t-1} = S_{red} \land D_{stop} < p_{signal}) \\ \infty & (otherwise) \end{cases} \tag{7}$$

where x_s is the distance to the stop line corresponding to a given traffic signal, S_{t-1} is the color of a given traffic signal, where S_{red} indicates red, D_{stop} indicates a requirement to decelerate and stop at the stop line, and p_{signal} is a parameter for the decision of an individual driver. We have assumed that the color of the traffic signals are known in advance.

2.2 State Space Model

When predicting the behavior of a vehicle, as well as modeling the driver, the physical capabilities of the vehicle must be considered. Thus, we propose the following state space model:

$$\begin{aligned} \boldsymbol{X}_t &= \boldsymbol{f}_t(\boldsymbol{X}_{t-1}) + \boldsymbol{u}_t \\ \boldsymbol{Y}_t &= \boldsymbol{H}\boldsymbol{X}_t + \boldsymbol{w}_t \\ \boldsymbol{X}_t &= [x_t\ y_t\ \theta_t\ v_t\ a_t\ \delta_t]^T \\ \boldsymbol{Y}_t &= [x_t\ y_t]^T \end{aligned} \tag{8}$$

where $\boldsymbol{X}_t$ is the state vector; $\boldsymbol{Y}_t$ is the observation vector; $\boldsymbol{f}_t$ is the system function; $\boldsymbol{H}$ is the observation matrix; x_t, y_t are the position of the vehicle east and north, respectively, as measured from the origin; θ_t is the orientation of the vehicle; v_t is the velocity of the vehicle; a_t is the acceleration; δ_t is the curvature of the vehicle's trajectory; and $\boldsymbol{u}_t$ and $\boldsymbol{w}_t$ are the system error and observation error, respectively.

Typically, x_t, y_t, θ_t, and v_t are predicted by the vehicle dynamics model, and a_t and δ_t are predicted by the driver model. However, in this study, δ_t is taken as known, so the driver model predicts only a_t.

The vehicle dynamics model predicts vehicle movement from control inputs, as follows:

$$\begin{bmatrix} x_t \\ y_t \\ \theta_t \\ v_t \end{bmatrix} = \begin{bmatrix} x_{t-1} + v_{t-1}\Delta t \sin\theta_{t-1} \\ y_{t-1} + v_{t-1}\Delta t \cos\theta_{t-1} \\ \theta_{t-1} + v_{t-1}\delta_{t-1}\Delta t \\ v_{t-1} + a_{t-1}\Delta t \end{bmatrix} + \boldsymbol{u}_t \tag{9}$$

This model is similar to a kinematic one-track model. For simplicity, our model assumes that a_t and δ_t are directly controlled by the driver.

2.3 Data Assimilation

In the driver model, it is difficult to determine unique parameter values for each driver, and so the characteristics

Fig. 2. Driving route of evaluation data. (Google Earth)

of the drivers must be estimated. In order to estimate the parameters sequentially, we use a technique called data assimilation, which uses observations to determine the parameters, and thus creates more realistic simulations. Data assimilation is used extensively in areas such as weather forecasting, and it uses a filtering technique with the state space model. In the model presented here, we use data assimilation in the driver model; this is done by using the state space model shown in the previous subsection and the extended Kalman filter (EKF) (Chen (2003)). To do this, the state-space vector is expanded as follows:

$$\boldsymbol{X}_t = [x_t \; y_t \; \theta_t \; v_t \; a_t \; \delta_t \; G_x \; G_v \; G_a \; p_n \; p_f \; p_c]^T \qquad (10)$$

By encapsulating the parameters as a state space vector, it is possible to use the EKF to estimate the parameters. There were not sufficient data to estimate the signal constraint parameter p_{signal}, so it was set to $p_{signal} = 4.5$.

Data assimilation is used not only to fit the behavior of the individual drivers but also to fit various situations. By modifying the model parameters sequentially, it is possible to reduce the adverse effects that can occur when forcing the model to fit data for a situation that is not covered by the model.

3. EVALUATION

3.1 Evaluation Data Set

The proposed method was evaluated by using data from actual driving on many kinds of roads (e.g., lanes of various number and width), and with various driving behaviors (e.g., right and left turns). The data were obtained over period of about 30 minutes, following the route shown in Fig. 2.

3.2 Prediction Performance

The profile of the prediction for a short time segment of the data is shown in Fig. 3; this figure shows how the data is fit by the proposed model.

The prediction performance is shown in Fig. 4, and we can see that data assimilation can reduce the proposed prediction error by 53% for a prediction for the behavior in three seconds. In comparison with a prediction based on constant velocity, it can reduce the error by about 25% for a prediction for the behavior in three seconds. In the result shown, the prediction by the proposed model without data
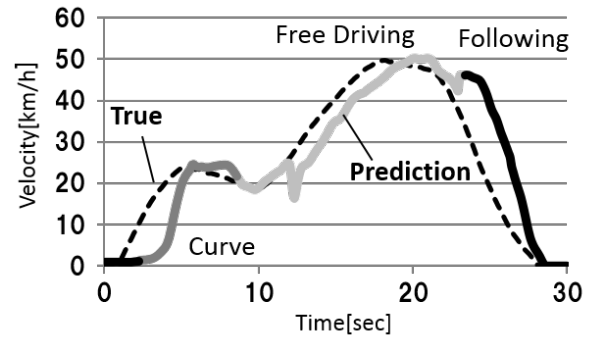
Fig. 3. Prediction time profile.
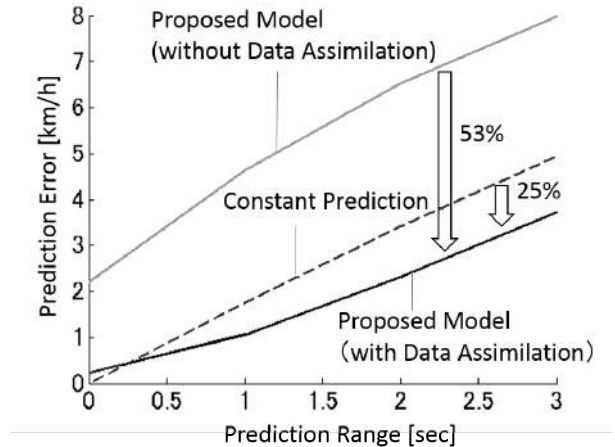
Fig. 4. Vehicle velocity prediction results.

assimilation is not adequate, and this occurs because the proposed model can simulate only the situations have been included in the specifications. Thus, if the vehicle encounters situations outside those modeled, the prediction performance will be worse than that of a constant model. However, when using data assimilation, the model parameters are tuned sequentially, so if a new situation is encountered, the model parameters are tuned for it. From these results, we conclude that data assimilation improves the robustness of the model.
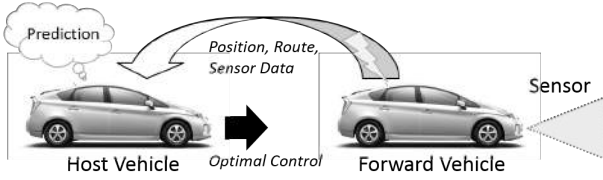
Fig. 5. Eco-driving system.

4. APPLICATION TO ECO-DRIVING SYSTEMS

4.1 Application Overview

One of the major applications of predicting driving behavior is in eco-driving systems, and so we will introduce such a system and use it to evaluate the proposed method. We will assume that the forward vehicle is operated by a human, and the host vehicle is automatically controlled. The host vehicle obtains information about the forward vehicle, and it uses this to predict its behavior while minimizing its own fuel consumption (see Fig. 5).

4.2 Model Predictive Control

Fuel consumption is optimized by using an optimal control technique known as model predictive control (MPC), which uses a prediction model to calculate the control input that optimizes the evaluation function in a certain time range. The evaluation function is defined as sum of the fuel consumed, and the penalty is the distance to the forward vehicle.

$$J(t) = \sum_{\tau=0}^{k} j(t+\tau) \qquad (11)$$

if $x_f < T_{m1}(v_{hv} + L)$ then

$$j(t+\tau) = w_1 \frac{W(a_{hv}, v_{hv})}{v_{hv}} + w_2(x_f - T_{m1}(v_{hv} + L))^2$$

else if $T_{m1} \leq x_f \leq T_{m2}(v_{hv} + L)$ then

$$j(t+\tau) = w_1 \frac{W(a_{hv}, v_{hv})}{v_{hv}}$$

else

$$j(t+\tau) = w_1 \frac{W(a_{hv}, v_{hv})}{v_{hv}} + w_2(x_f - T_{m2}(v_{hv} + L))^2$$

where $J(t)$ is the objective function at time t; h is the range of time for the optimization (*the horizon*); v_{hv} and a_{hv} are the velocity and acceleration of the host vehicle; x_f is the distance between the forward vehicle and the host vehicle; $W(a_{hv}, v_{hv})$ is the rate of fuel consumption [ml/s]; L is the minimum of x_f; T_{m1} and T_{m2} are the minimum and maximum headway times [sec]; and w_1 and w_2 are weight parameters, which are tuned to $w_1 = 0.23$ and $w_2 = 0.20$.

Equation (11) minimizes the fuel consumption, and the penalty function is related to the distance between the forward vehicle and the host vehicle. The penalty function is shown in Fig. 6.

4.3 Eco-driving Performance

We evaluated the performance of our model by simulating an eco-driving system in which a simulated host vehicle followed a forward vehicle for which the behavior was
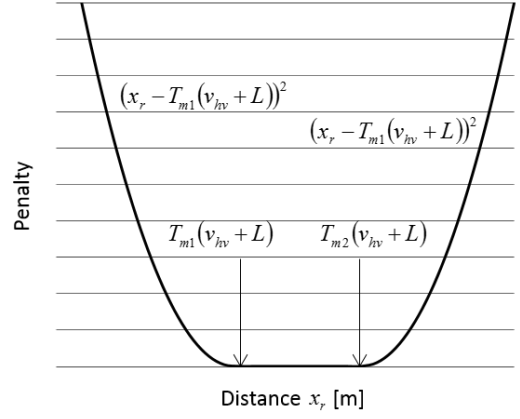
Fig. 6. Penalty function.

based on actual data. We compared its performance to that of two benchmark methods that emulated adaptive cruise control (ACC) and CACC (Arem et al. (2006); Naus (2009)). The ACC and CACC systems are as follows:

ACC:

$$a_{hv} = G_1(x_f - L - T_m v_{hv}) \qquad (12)$$

CACC:

$$a_{hv} = G_1(x_f - L - T_m v_{hv}) + G_2 a_{pv} \qquad (13)$$

where x_f is the distance between the forward vehicle and host vehicle [m]; v_{hv} and a_{hv} are the host vehicle's velocity [m/s] and acceleration [m/s^2], respectively; T_m is the desired headway time [sec]; L is the minimum x_f; and G_1 and G_2 are gain parameters. ACC (12) is a basic autonomous following system that only uses the distance to the forward vehicle, and CACC (13) uses that distance but also the acceleration of the forward vehicle. Both are feedback control systems. For this evaluation, the parameters were set to $T_m = 1.8$, $L = 5$, $G_1 = 0.4$, and $G_2 = 0.1$.

The fuel efficiency results are shown in Fig. 7. These are from a simulation that followed the natural driving data that was used to evaluate the predictions of our model. The three lowest bars show the data for the MPC, which used a different prediction method. Compared with the ACC, the proposed method improved fuel consumption by 4.6%, and compared with the MPC with a predicted constant velocity, it improved fuel consumption by 2.6%. Thus, we confirmed the effectiveness of using the MPC with the proposed prediction method. The time profile of the vehicle speed is shown in Fig. 8, and it can be seen that the vehicle is operated more smoothly by the proposed method than by the ACC. This is why the MPC with the proposed prediction method performs better than do the conventional approaches. Furthermore, from Fig. 7, which compares the prediction when using MPC to the true value, it can be seen that improving the prediction improves the fuel efficiency. Thus, there is worth aiming to further improve the prediction.

5. CONCLUSION

We proposed a driver-vehicle integrated state-space model that incorporates a generic driver and is to be used for predicting the behavior of a vehicle. The driver was modeled by a cascade feedback model with some constraints
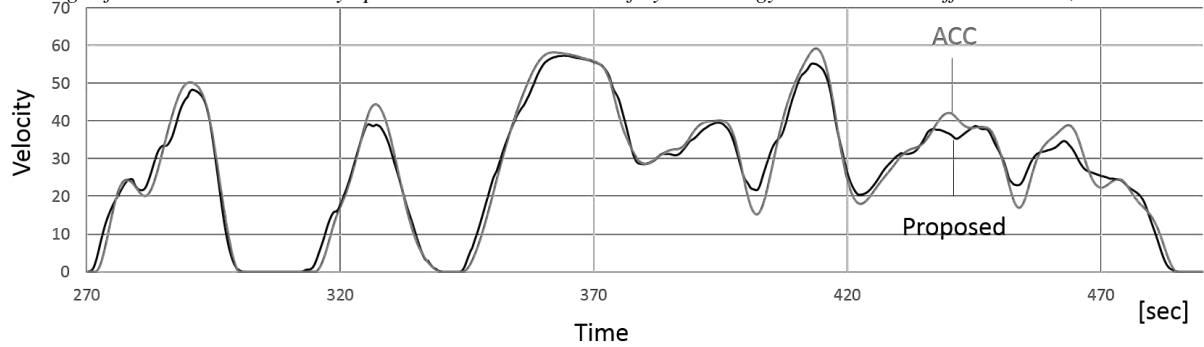
Fig. 8. Time profile of eco-driving with ACC.
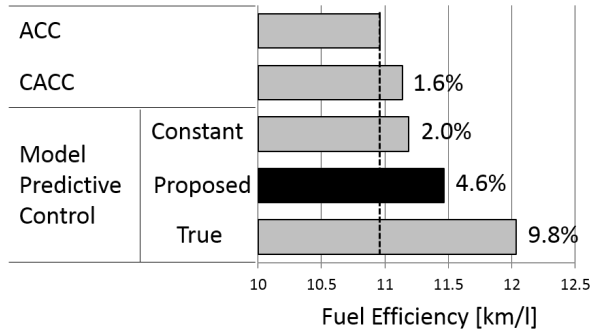
Fig. 7. Improving fuel efficiency.

that mimic physical constraints and traffic rules. Data assimilation was used to estimate sequentially the state and the model parameters. Compared to a prediction based on constant behavior, the proposed model was able to reduce the prediction error by about 25%. We also showed that the use of data assimilation makes our method robust against deviations from the situations initially included in the model. When using our method with a simulated eco-driving system, the fuel efficiency was reduced by about 5%, as compared to the fuel used with ACC. From the results with the MPC using the true values, we confirmed that further improvement of the prediction model can improve fuel efficiency. In our future work, we intend to evaluate the accuracy when using a greater amount of data, and we intend to introduce additional traffic rules into our model.

REFERENCES

Arem, B., Driel, C., and Visser, R. (2006) The Impact of Cooperative Adaptive Cruise Control on Traffic-Flow Characteristics. *IEEE Transaction on Intelligent Transportation Systems*, Vol. 7, No. 4, 429-436.

Brechtel, S., Gindele, T., and Dillmann, R. (2011) Probabilistic MDP-Behavior Planning for Cars. *Intelligent Transportation Systems (ITSC), 2011 14th International IEEE Conference on*, 1537-1542.

Chen, Z. (2003) Bayesian filtering: From Kalman filters to particle filters, and beyond. *Statistics*, Vol. 182, No. 1, 1-69.

Dagli, I., and Reichardt, D. (2002) Motivation-Based Approach To Behavior Prediction. *Intelligent Vehicle Symposium, 2002, IEEE*, Vol. 1, 227-233.

Dagli, I., Brost, M., and Breuel, G. (2003) Action Recognition and Prediction for Driver Assistance Systems Using Dynamic Belief Networks. *Agent Technologies, Infrastructures, Tools, and Applications for E-Services*, Springer Berlin Heidelberg, 179-194.

Gindele, T., Brechtel, S., and Dillmann, R. (2010) A Probabilistic Model for Estimating Driver Behaviors and Vehicle Trajectories in Traffic Environments. *Intelligent Transportation Systems (ITSC), 2010 13th International IEEE Conference on*, 1625-1631.

Gindele, T., Brechtel, S., and Dillmann, R. (2013) Learning Context Sensitive Behavior Models from Observations for Predicting Traffic Situations. *Intelligent Transportation Systems (ITSC), 2013 16th International IEEE Conference on*, 1764-1771.

Gipps, P. (1981) A behavioural car-following model for computer simulation. *Transportation Research Part B: Methodological*, Vol. 15, No. 2, 105-111.

Kamal, M., Mukai, M., Murata, J., and Kawabe, T. (2013) Model predictive control of vehicles on urban roads for improved fuel economy. *Control Systems Technology, IEEE Transactions on*, Vol. 21, No. 3, 831841.

Kamal, M., Taguchi, S., and Yoshimura, T. (2015) Efficient Vehicle Driving on Multi-Lane Roads Using Model Predictive Control under a Connected Vehicle Environment. *Intelligent Vehicle Symposium, 2015, IEEE*.

Luo, L. H., Liu, H., Li, P., and Wang, H. (2010) Model predictive control for adaptive cruise control with multi-objectives: comfort, fuel-economy, safety and car-following. *Journal of Zhejiang University SCIENCE A*, Vol. 11, No.3, 191-201.

Levesque, A., and Johrendt, J. (2011). The State of the Art of Driver Model Development. *SAE Technical Paper*.

Naus, G. (2009) Cooperative Adaptive Cruise Control. *IEEE automotive engineering symposium Eindhoven, The Netherlands*, Vol. 6.

Treiber, M., Hennecke, A., and Helbing, D. (2000) Congested traffic states in empirical observations and microscopic simulations. *Physical Review E*, Vol. 62, No. 2, 1805.

2-D Pedestrian Motion Prediction Modeling in Urban Driving Scenario Based on Potential Field

Kazuhiro Ezawa*, Pongsathorn Raksincharoensak**

**Tokyo University of Agriculture and Technology, 2-24-16 Naka-cho, Koganei,
Tokyo,184-8588, Japan (Tel: +81-42-388-7395; e-mail: 50014833002@st.tuat.ac.jp).
**Tokyo University of Agriculture and Technology, 2-24-16 Naka-cho, Koganei,
Tokyo,184-8588, Japan (Tel: +81-42-388-7397; e-mail: pong@cc.tuat.ac.jp).*

Abstract: This paper presents 2-D pedestrian motion prediction model based on potential field for a hazard-anticipatory collision avoidance braking system to enhance the collision avoidance performance. 1-D pedestrian motion prediction reaches its limit under the situation that a pedestrian walks towards a parked vehicle as the prediction is conducted based on the current position and velocity of pedestrian within a finite time horizon. If the change of pedestrian motion can be predicted, the vehicle maneuver to avoid collision with pedestrian can be executed in advance. 2-D pedestrian motion prediction model based on potential field is constructed. The effectiveness of the proposed prediction model is verified by comparing the measured trajectory with the calculated data based on 1-D prediction and 2-D prediction.

Keywords: Automotive Control, Active Safety, Driver Assistance Systems, Collision Avoidance, Pedestrian Motion Prediction, Path Planning

1. INTRODUCTION

In recent years, the Japan National Police Agency (JNPA) reported that the pedestrian-relevant accident was involved in 36.2 percent (1,584 cases) of traffic fatal accidents in Japan (JNPA, 2013). Most of pedestrian-related fatal accidents were occurred in the case that vehicles are running strait (83.3%, 1,310 people), and the major causes can be categorized into three types: careless driving (35%), inattentive driving (35%) and insufficient safety confirmation (19%) (ITARDA, 2010). Nowadays, there are a number of active safety devices in markets which can activate the autonomous braking (AEB) to avoid collisions with objects in front of the ego-vehicle. Conventional AEB systems avoid collisions with harsh braking in the last second when the collision risk becomes imminent. However, the AEB may not be always powerful enough to cope with any given situation. Suppose that a pedestrian suddenly tries to cross the road from occluded area with short time margin to collision. Then the AEB may fail to prevent the vehicle-pedestrian collision. Against such a background, it is important to predict the risk of accidents in advance in order to be able to cope with unexpected situations which might occur in crowded urban road.

Precise prediction for pedestrian motion is a key point to achieve good collision avoidance performance. Conventional pedestrian motion prediction uses 1-dimensional prediction (Tiemann, 2010) based on the current position and the velocity. There are a number of researches (Shimizu, 2012) (Tsuyuki, 2013) that 2-D pedestrian motion prediction is necessary in traffic situation. Though the 2-D pedestrian motion prediction was constructed in previous study (Ezawa, 2014), it is applicable in only the specific scenario which pedestrian walking around the parked vehicle and it was difficult to generalize the prediction model for other scenes. In this

situation, the proposed scheme can predict that pedestrian would walk out to the center of the road avoiding parked vehicle. Therefore, this research constructed a generalized 2-D pedestrian motion prediction based on potential field which has more versatility to be applicable in various situation.

The rest of the paper is organized as follows. Section 2 describes the experiment to clarify the characteristics in the pedestrian motion trajectory. Section 3 describes the definition of the potential field function which affects pedestrian motion. Section 4 describes the formulation of the 2-D pedestrian motion prediction based on the defined potential field method and the randomized path generation. Section 5 describes the confirmation of the validity of the 2-D pedestrian motion prediction by the simulation. Finally, Section 6 describes the conclusion of this paper.

2. ACQUISITION OF PEDESTRIAN TRAJECTORY

In order to clarify the characteristics in pedestrian trajectory, the experiment for the data collection was conducted. The participants were instructed to walk pass through a parked vehicle naturally. As shown in Fig.1, the pedestrians' trajectory were measured every 0.2 seconds by using a LIDAR equipped at another measurement vehicle vertically. 17 participants were employed in the experiment. The experiment included two scenarios: to walk at a normal pace (2 trials) and at a quick pace (2 trials).

All measured trajectories are shown in Fig. 2. The *X*-axis shows the displacement for x direction, and the *Y*-axis shows the displacement for y direction. The characteristics of the recorded pedestrian motion trajectory when passing the parked vehicle were found as follows. First, the pedestrian walks straight toward the parked vehicle. Next, in order to avoid the parked vehicle blocking pedestrian's way, the pedestrian changes moving direction so as to draw half-egg-shape. When

the pedestrian passed the parked vehicle, the pedestrian walks back to the roadside and starts walking straight again.
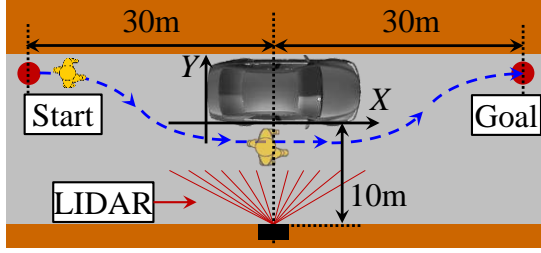
Fig. 1. Pedestrian trajectory measuring experiment.
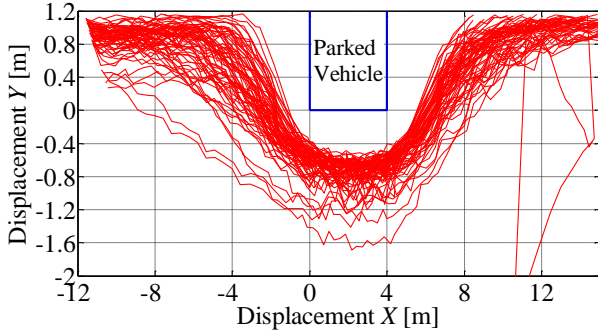
Fig. 2. Measured pedestrian trajectory.
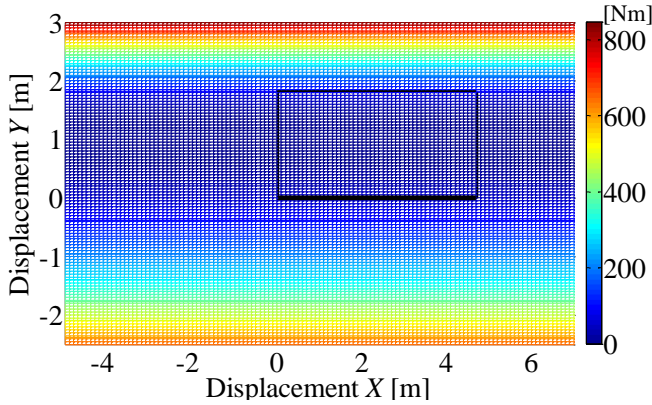
Fig. 3 Contour map of the road potential field.

3. POTENTIAL FIELD FUNCTION

This section describes the definition of potential function based on the characteristics of pedestrian motion trajectory that was shown in Section 2. If there is no parked vehicle, it is assumed that a pedestrian keeps to walk on the roadside. Of course, the pedestrian will walk near the wall on the left hand side so as to avoid the contact with the wall. On the other hand, if there is the parked vehicle, the parked vehicle also affects the pedestrian's trajectory. The pedestrian avoids to contacting with the parked vehicle and then takes a space margin with the parked vehicle. In this paper, the potential field of road boundary U_w and the potential field of the parked vehicle U_c are defined by using a spring elastic potential energy model. The equation of road boundary potential functions U_w is shown in Eq. (1), and the contour map of generated risk field potential U_w is shown in Fig. 3.

$$U_w = \begin{cases} \frac{1}{2}k_{wl}(y-Y_0)^2 & if \quad Y_0 < y \\ \frac{1}{2}k_{wr}(y-Y_0)^2 & if \quad y < Y_0 \end{cases} \quad . (1)$$

where, k_{wl} indicates the virtual spring constant of the road boundary on left hand side of the pedestrian, k_{wr} indicates the virtual spring constant of the center of the road, Y_0 indicates the initial position of the pedestrian, and y indicates the lateral position of the pedestrian.

Next, the definition of the potential U_c for the parked vehicle is described. In the results of data collection that was shown in Section 2, each pedestrian avoided the vehicle keeping different space margin in each area, rear (section *a*), side (section *b*) and front (section *c*) of the vehicle. Therefore, the potential U_c of the parked vehicle is divided into the three sections as shown in Fig. 4. Virtual spring is equipped in the center of the vehicle, and the displacement of the virtual spring is calculated by considering the positional relation between the pedestrian and the parked vehicle. Here, in order to generate seamless potential energy on the boundary of three areas, the difference of the natural length of the virtual spring have to be considered. In Fig. 4, the red solid line denotes the natural length of the egg-shaped potential U_c and the red dotted line denotes the apparent contract d of the virtual spring. The apparent contract d cannot be used for potential calculation and the pedestrian Y_{ped} in the rear area have to be converted into Y_{ped}' by considering the difference of the natural length.

$$Y_{ped}' = (Y_{ped} - Y_c) \cdot \frac{l_{0-Xcr}}{l_{0-Ycs}} \quad . (2)$$

where, l_{0-Xcr} is longitudinal (*X*-axis) natural length of virtual spring for the parked vehicle in the rear area of the vehicle, l_{0-Ycs} is lateral (*Y*-axis) natural length of the virtual spring in the side area of the vehicle, and Y_c is the lateral central position of the vehicle. From the above consideration, the potential functions for the parked vehicle can be calculated as shown in Eq. (3) to Eq. (5), and the contour map of the potential field generated by the parked vehicle is shown in Fig. 5.

Section *a*:

$$U_C = \frac{1}{2}k_c\left(l_{0-Xcr} - \sqrt{(x-X_{cr})^2 + \left\{(y-Y_c)\cdot\frac{l_{0-Xcr}}{l_{0-Ycs}}\right\}^2}\right)^2 \quad . (3)$$

$$if \quad x < X_{cr} \quad or \left(\frac{x-X_{cr}}{l_{0-Xcr}}\right)^2 + \left(\frac{y-Y_c}{l_{0-Ycs}}\right)^2 < 1$$

Section *b*:

$$U_C = \frac{1}{2}k_c\left\{(y-Y_c)\cdot\frac{l_{0-Xcr}}{l_{0-Ycs}}\right\}^2 \quad . (4)$$

$$if \quad X_{cr} < x < X_{cf} \quad or \quad Y_c - l_{0-Ycs} < y < Y_c + l_{0-Ycs}$$

Section *c*:

$$U_C = \frac{1}{2}k_c\left(l_{0-Xcr} - \sqrt{\left\{(x-X_{cf})\cdot\frac{l_{0-Xcr}}{l_{0-Xcf}}\right\}^2 + \left\{(y-Y_c)\cdot\frac{l_{0-Xcr}}{l_{0-Xcf}}\right\}^2}\right)^2 \quad . (5)$$

$$if \quad X_{cf} < x \quad or \left(\frac{x-X_{cf}}{l_{0-Xcf}}\right)^2 + \left(\frac{y-Y_c}{l_{0-Ycs}}\right)^2 < 1$$

where, k_c is the spring constant of the parked vehicle, X_{cr} is longitudinal rear edge position of the vehicle, X_{cf} is longitudinal front edge position of the vehicle and l_{0-Xcf} is longitudinal natural length of the virtual spring in the front area.
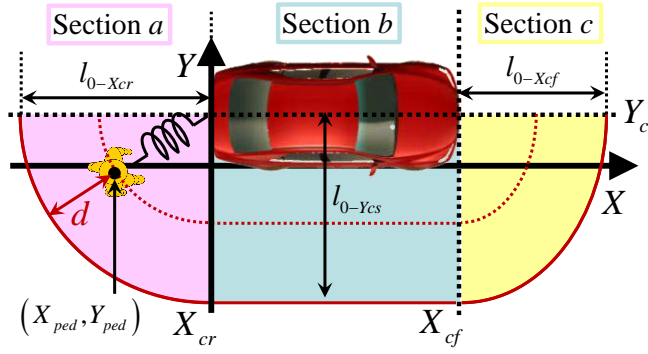
Fig. 4 Displacement conversion by considering flattering.
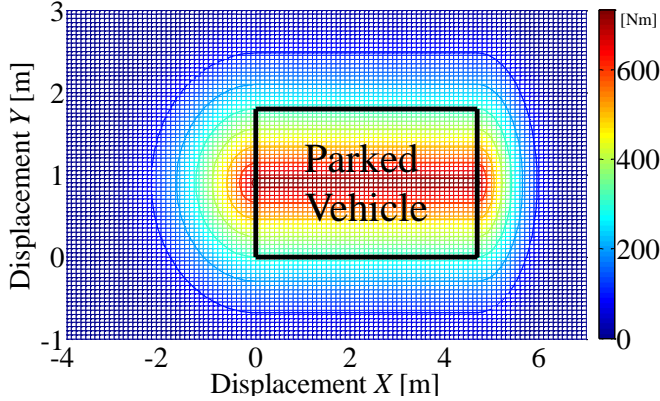
Fig. 5 Contour map of the potential field generated by the parked vehicle.
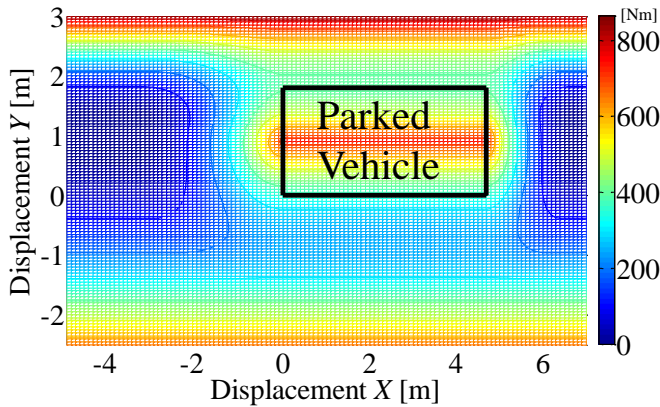
Fig. 6 Contour map of the potential field generated by the road boundary and the parked vehicle.

In the focussed situation, the shape of overall potential field is expressed as Fig. 6. The virtual spring constant k_w and k_c is calculated to be able to adjust the lateral displacement at which the total potential is minimum. The minimum potential position is the displacement that the pedestrian will walk in the side area of the parked vehicle. The pictorial diagram of the potential energy in the side area is shown in Fig. 7. In this area, the total of the potential energy is calculated as Eq. (6).

$$U(y) = U_c(y) + U_w(y)$$
$$= \frac{1}{2} k_c \left\{ (y - Y_c) \cdot \frac{l_{0-Xcr}}{l_{0-Ycs}} \right\}^2 + \frac{1}{2} k_{wr} (y - Y_0)^2 \qquad . (6)$$

The displacement Y_m at which the energy becomes minimum can be calculated by differentiating Eq. (6) with respect to y as shown in Eq. (7).

$$U'(y) = k_c (y - Y_c) \left(\frac{l_{0-Xcr}}{l_{0-Ycs}} \right)^2 + k_{wr} (y - Y_0) \qquad . (7)$$

Here, the displacement Y_m at which the potential U becomes minimum is calculated by

$$Y_m = \frac{l_{0-xcr}^2 \cdot Y_c \cdot k_c + l_{0-ycs}^2 \cdot Y_0 \cdot k_{wr}}{l_{0-xcr}^2 \cdot k_c + l_{0-ycs}^2 \cdot k_{wr}} \qquad . (8)$$

Eq. (8) can be formulated as

$$k_{wr} = \frac{l_{0-xcr}^2 \cdot (Y_m - Y_c)}{l_{0-ycs}^2 (Y_0 - Y_m)} k_c \qquad . (9)$$

From the Eq. (9), the ratio of the virtual spring constant is determined. In addition, l_{0-Ycs} is determined as a double of the distance between Y_c and Y_m in this research. The virtual spring constant k_{wl} is determined in order to the risk on the left hand side of the parked vehicle becomes high enough.
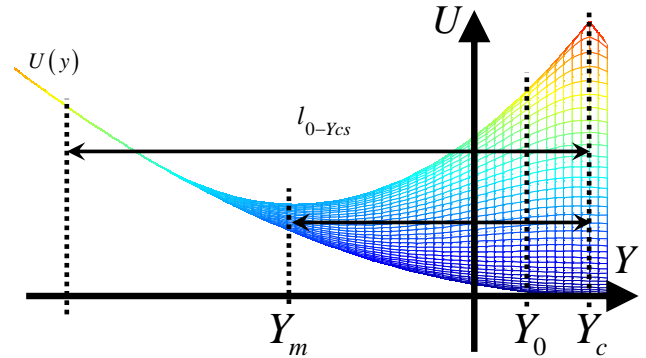
Fig.7 The sum of the lateral potential in the side area.

4. PEDESTRIAN MOTION PREDICTION

Pedestrian motion is predicted based on the optimization of the potential with respect to randomized path generation. If the predictive path is generated under the assumption that the pedestrian changes moving direction every predictive sampling time t_p, the path forms tree diagram. In this case, computation complexity increases exponentially. Therefore, in order to reduce the computation complexity, the path is generated as follows. First, a set of arbitrary path within a finite time horizon is given based on the pedestrian current position as shown in Fig. 8. As shown in Fig. 8, the set of random path is determined under the assumption that the pedestrian changes his/her moving direction randomly based on a normal distribution probabilistic density function at each sampling time Δt_P, and the pedestrian continues changing his/her moving direction till t_p seconds every Δt_P seconds recursively. Here, the standard deviation for the normal distribution probabilistic density function is determined by data analysis of the measured trajectory as shown in Fig. 9. The measured trajectory can be approximated by connecting straight lines,

and the angle when the pedestrian avoids the parked vehicle is calculated. The result of analysis is shown in table 1. In consideration of the analysis, Eq. (10) can be calculated.

$$\theta_{max} < 30 = 3\sigma_\theta \qquad \text{. (10)}$$

As a statistical characteristics of the normal distribution probabilistic density function, the data within the range $\pm 3\sigma_\theta$ includes 99.7% of the whole data. In this case, the maximum angle is 28.3 degrees, and usually the pedestrian moves to the X-axis direction ($\theta = 0$). Therefore, the standard deviation σ_θ of the angle θ_m (n) for generating randomized path is determined as at $\sigma_\theta = 10$.
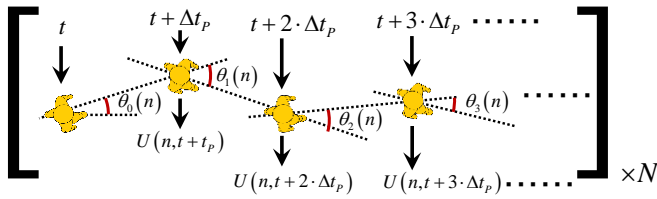
Fig. 8. Pedestrian walking trajectory model for potential field optimization.
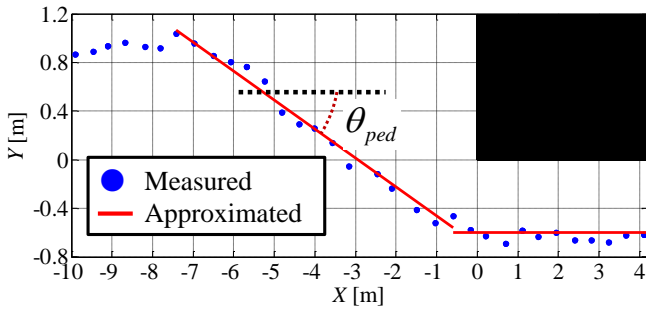
Fig. 9. Relationship between approximated trajectory and θ_{ped}

Table 1. Angle when the pedestrian avoids the parked vehicle

Definition	symbol	value	unit
Mean value of angle	$\bar{\theta}$	16.8	deg
Maximum angle	θ_{max}	28.3	deg
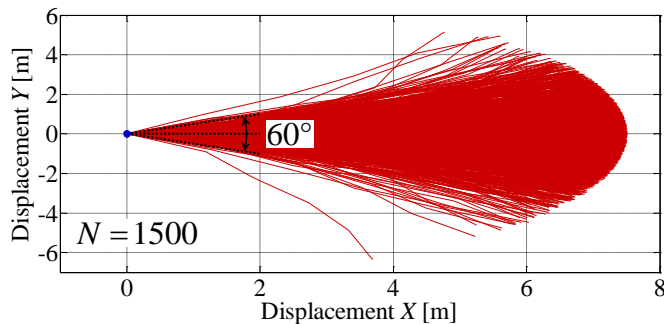
Fig. 10. Generated candidate trajectories from initial pedestrian position.
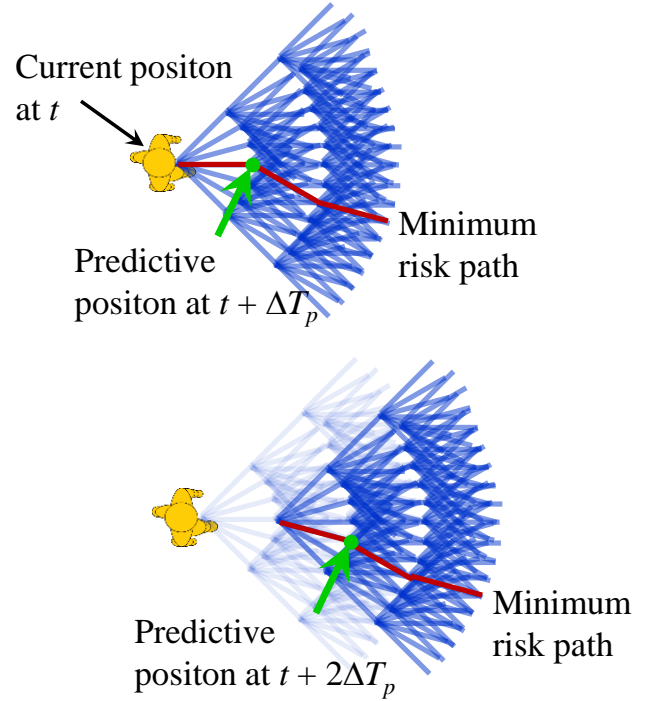
Fig. 11. 2-D motion prediction based on the defined potential and the randomized path generation

A line of path is generated by the above method, and the generated path forms polygonal line as shown in Fig. 10. In Fig. 10, $N = 1500$ lines of path are generated under the condition that pedestrian moves to X-axis direction at 1.5 m/s, the prediction time t_p is 5 seconds and the prediction sampling time Δt_p is 1 second. Based on the set of generated candidate path, the risk is calculated every Δt_p seconds until t_p seconds based on the defined potential in the section 3, and the total risk is evaluated by every path. The probabilistic pedestrian future position is determined by selecting the one that results in minimum potential energy as shown in Fig. 11. Then, new random paths are generated from the point ($t + \Delta T_P$). The pedestrian motion is predicted by repeating this calculation process recursively.

5. EVALUATION OF THE PROPOSED 2-D PEDESTRIAN MOTION PREDICTION

The validity of the proposed 2-D pedestrian motion prediction is confirmed by comparing measured trajectory with the simulated predictive position. The simulation parameters are shown in table 2. In this simulation, measured pedestrian position was used as a current position, and predictive position was calculated based on proposed method every 1 second until 5 seconds. The simulation results are shown in Figs. 12, 13, 14, 15, and 16. In these figures, blue solid lines indicate the measured trajectory, red circles indicate the predictive position simulated by proposed 2-Dprediction, and green squares indicate the predictive position simulated by 1-D prediction. Here, 1-D prediction simulates the pedestrian position by using the moving speed and the moving direction calculated by the past 5 samplings. As can be noticed from Fig. 12, the result of simulation at T_p equals 1 second, both the 1-D and the 2-D predictions can trace measured trajectory. On the other

hand, from Fig. 13 to Fig. 16, the longer prediction time T_p produced the difference between the 1-D and 2-D predictions. In addition, the proposed 2-D pedestrian motion prediction based on potential field can trace actual pedestrian trajectory well.

Table 2. Simulation parameters

Definition	Symbol	Value	Unit
Pedestrian moving speed	V_{ped}	1.4	m/s
Standard deviation for randomized path generation	σ_θ	10	-
The number of path generation	N	1500	-
Displacement X of the rear edge of the vehicle	X_{cr}	0	m
Displacement X of the front edge of the vehicle	X_{cf}	4.7	m
Displacement Y of the center of the vehicle	Y_{cs}	0.9	m
Longitudinal natural length of the virtual spring in the rear area	l_{0-Xcr}	3.2	m
Longitudinal natural length of the virtual spring in the front area	l_{0-Xcf}	2.9	m
Lateral natural length of the virtual length of the virtual spring in the side area	l_{0-Ycs}	2.3	m
Lateral margin between the pedestrian and the parked vehicle	Y_m	0.7	m
Initial displacement Y of the pedestrian	Y_0	0.99	m
Virtual spring constant of the vehicle	k_c	120	N/m
Virtual spring constant of the roadside on the left hand side	k_{wr}	96	N/m
Virtual spring constant of the road center	k_{wl}	1922	N/m
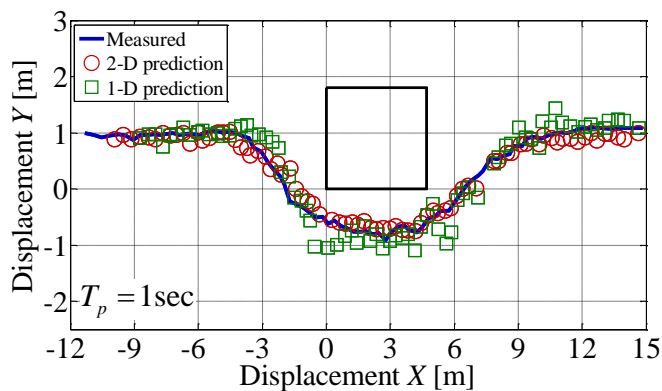
Fig. 12. Comparison of the proposed 2-D prediction and the conventional 1-D prediction at T_p = 1sec.
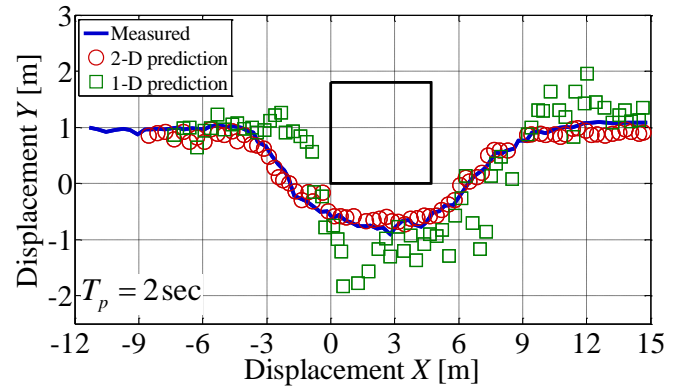
Fig. 13. Comparison of the proposed 2-D prediction and the conventional 1-D prediction at T_p = 2sec.
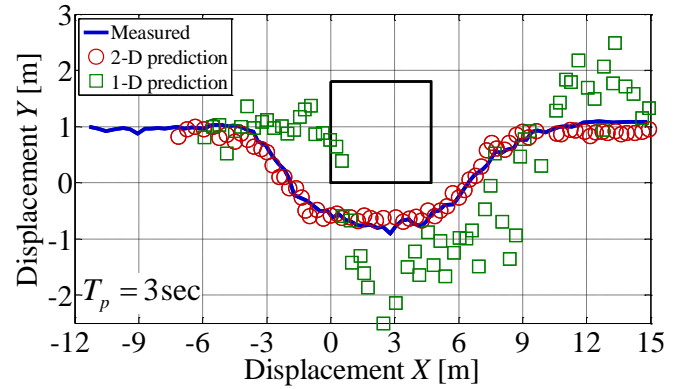
Fig. 14. Comparison of the proposed 2-D prediction and the conventional 1-D prediction at T_p = 3sec.
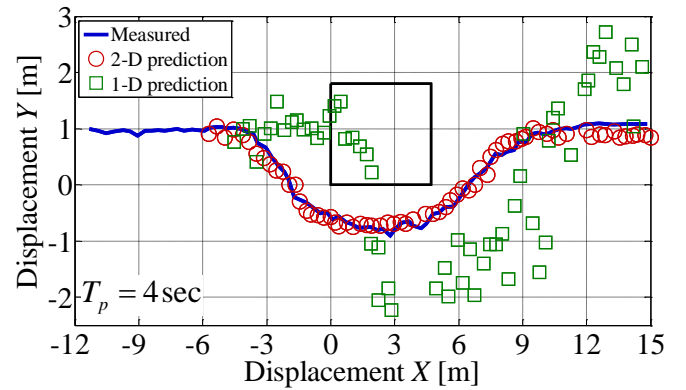
Fig. 15. Comparison of the proposed 2-D prediction and the conventional 1-D prediction at T_p = 4sec.
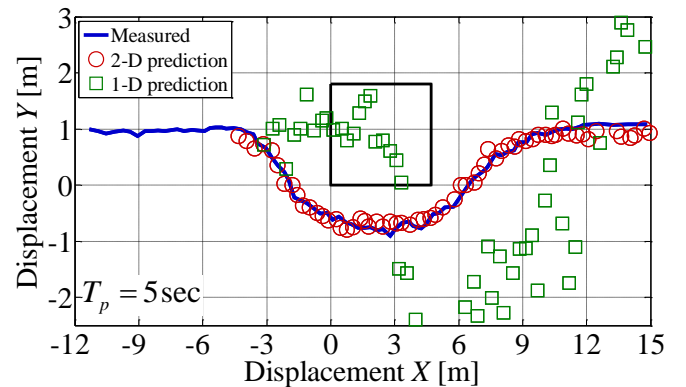
Fig. 16. Comparison of the proposed 2-D prediction and the conventional 1-D prediction at T_p = 5sec.

Next, the error between the measured positions and the predicted positions calculated by the 1-D and 2-D predictions are evaluated, as shown in Fig. 17. The error between the predictive and the actual positions was calculated by Eq. (11) every 1 second until 5 seconds.

$$error = \sqrt{\begin{array}{l}\left(X_{pre}\left(t+\Delta T_p\right)-X_{ped}\left(t+\Delta T_p\right)\right)^2 \\ +\left(Y_{pre}\left(t+\Delta T_p\right)-Y_{ped}\left(t+\Delta T_p\right)\right)^2\end{array}} \quad . (11)$$

The result of calculated error is shown in table 3. Though the proposed 2-D prediction needs to be calibrated every case, the error and the standard deviation of the proposed method were much smaller than conventional 1-D prediction. The accuracy of 1-D prediction was 1.98 ± 2.94 m at the predictive time T_p equals 5 seconds. On the other hand, the proposed 2-D prediction can predict 0.67 ± 0.87. This result indicates that the 1-D prediction reaches the limit in the situation which the pedestrian changes moving direction to avoid something.

From the above results, the proposed 2-D prediction based on the potential field and the randomized path generation was effective to motion prediction in the focused situation that the obstacles exists on the pedestrian's way.
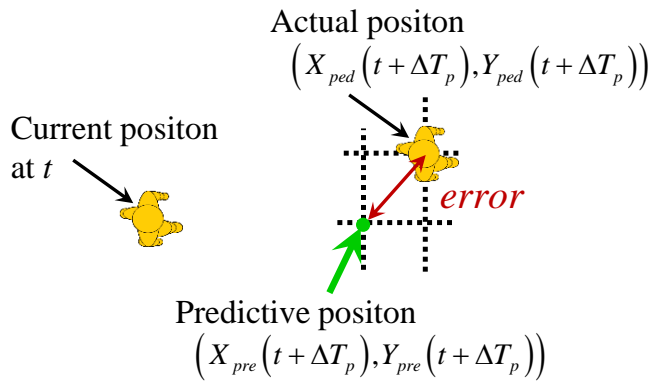
Fig. 17. The error between predictive and actual positions.

Table 3. Calculated error between the actual position and the simulated position

	1sec	2sec	3sec	4sec	5sec
Error of the 2-D prediction [m]	0.27	0.37	0.43	0.55	0.67
Standard deviation of the 2-D prediction	0.15	0.21	0.19	0.24	0.29
Prediction accuracy of the 2-Dprediction [m]	0.27 ± 0.45	0.37 ± 0.63	0.43 ± 0.57	0.55 ± 0.72	0.67 ± 0.87
Error of the 1-D prediction [m]	0.33	0.65	1.03	1.50	1.98
Standard deviation of the 1-D prediction	0.18	0.35	0.52	0.74	0.98
Prediction accuracy of the 1-D prediction[m]	0.33 ± 0.54	0.65 ± 1.05	1.03 ± 1.56	1.50 ± 2.22	1.98 ± 2.94

6. CONCLUSIONS

In the development of ADAS for pedestrian collision avoidance, this research constructed the 2-D pedestrian motion prediction to deal with typical dangerous situations in urban area. First, the potential field based on measured trajectory analysis was defined. In order to reduce computation complexity and realize more precise situational risk assessment in complex driving environments, the motion prediction and the potential evaluation based on the randomized path generation and the potential evaluation was developed. As a result, the effectiveness of the proposed 2-D pedestrian motion prediction is verified by the simulation evaluating the error between the simulated position and the actual position. By installing proposed 2-D prediction system, it is expected that the active safety system could predict the collision risk in advance and avoid the collision without using harsh braking. In addition, these framework for motion prediction can be used for autonomous driving system.

REFERENCES

Japan National Police Agency (2013), Annual report of fatal traffic accidents and status of the violation of the road traffic law enforcement during the year of 2012, pp. 8, Japan

Institute for Traffic Accident Research and Data Analysis (ITARDA) (2010), Car-to-Pedestrian Accidents, *ITARDA Information No.83*, pp. 1-12, Japan

Tiemann, N. et al. (2010), Predictive Pedestrian Protection – Situation Analysis with a Pedestrian Motion Model, *Proceedings of AVEC'10*

Shimizu, T., Ohama, Y., Nagata, S., Sakugawa, J. (2012), A Computational Framework for Estimating Collision Risk against Pedestrians, *R&D Review of Toyota CRDL*, Vol.43 No.1, pp. 33-42

Tsuyuki, H., Hayashi, R., Nagai, M. (2013), Development of Hazard-Anticipative Driving Assistance System at Overtaking a Pedestrian on Narrow Roads, *Proceedings of 2013 JSAE Annual Congress (Autumn)*, No.125-13, pp. 5-8, Japan

Ezawa, K., Raksincharoensak, P., Nagai, M. (2014), Hazard-Anticipatory Collision Avoidance System Based on Two-Dimensional Pedestrian Motion Prediction, *Proceedings of AVEC'14*

Pedestrian detection system while turning at intersection by surround monitor camera

Tokihiko Akita*

*AISIN SEIKI Co., Ltd.
Kariya, Aichi, Japan (e-mail: akita@aisin.co.jp).

Abstract: Recently, demand for active safety systems has been increasing toward zero traffic accident fatality, thus an automated emergency brake system to avoid pedestrian accidents will be commercialized corresponding to Euro-NCAP. However, an effective assistance system for pedestrian accidents while turning at an intersection has not been proposed, though number of the accidents is the second largest after crossing pedestrian accident. We propose the driving assistance system utilizing the surround monitor camera system which is getting popular. Stereo camera configuration utilizing front and side fish eye cameras has been considered to improve detection reliability. However, particular concerns for this configuration are existed, thus we are trying to develop the solution applying machine-learning feature amount in this research. They were preliminarily verified utilizing computer graphics, and then experimented for actual images captured in the real world.

Keywords: Pedestrian detection, Stereo vision, Surround monitor camera, Image recognition

1. INTRODUCTION

Recently, rate of pedestrian accidents is increasing as the population ages. The most common pedestrian accident is an accident by crossing pedestrian on a straight road. These accidents will be solved by pedestrian detection using a front camera or radar. The second most common is the accident of crossing pedestrians at intersection while turning left or right (ITARDA2012). It is known that load of the driving maneuver is high, since attention for through traffic vehicles is necessary (Hagiwara2010). Then, it is also found that it is hard for the pedestrian to recognize the vehicles turning left or right (Hagiwara2012). From the above facts, the countermeasure for these types of accident will become more important in the future.

Radar, Lidar or stereo camera can be adopted as the sensor. However, they have some concerns about cost, mountability and performance to detect the pedestrians at the intersection at present. On the other hand, a surround monitor camera system is becoming popular for parking and low speed manoeuvring assistance. As this system can obtain the view around a vehicle, it is possible to detect the pedestrian while turning left and right by applying image recognition technology and warn the driver. Since this can be realized by utilizing an existing system, there is almost no concern regarding the mountability and cost, which accelerates spread of the assistance system. In this paper, we will propose the driver assistance system to detect crossing pedestrian while turning at an intersection applying this configuration.

2. SYSTEM CONFIGURATION

This system configuration is shown in Fig. 1. Four fish eye cameras with 180 degrees of field of view are installed on front and rear side of a vehicle and under left and right side

mirrors respectively. The system consists of the computer to analyze the images and detect the pedestrian, the display to show the surround images, and the speaker to alert a driver.
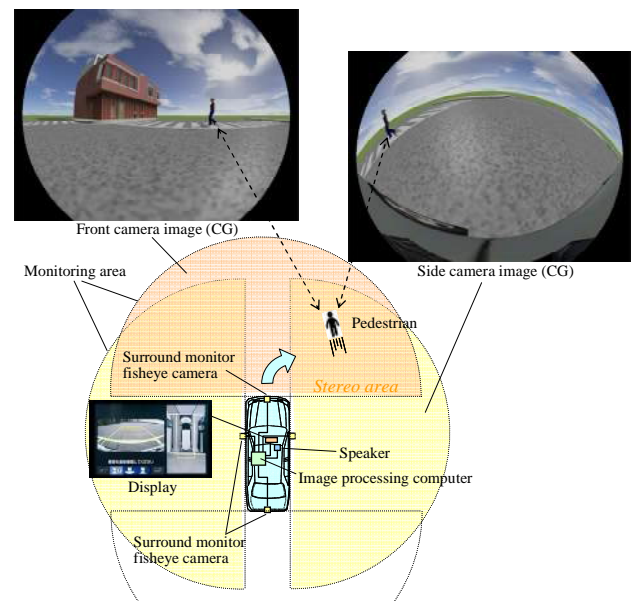
Fig. 1. System configuration
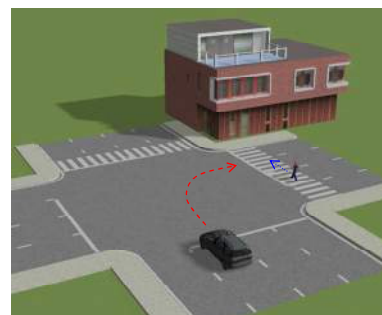
Fig. 2. Simulation scenario

CG images simulating the camera images of a crossing pedestrian while turning right are inserted in Fig. 1. The side camera is tilted 45 degrees downwards since this is mounted under a side mirror. It is found that a same pedestrian is shown in an overlapped area of both camera images. Thus, a pedestrian can be accurately detected by the stereo vision utilizing these cameras.

Fig. 2 shows the CG image of one scene in bird's eye view which reconstructs the traffic accident. This is the scenario that the vehicle turns right and hits the crossing pedestrian on a crosswalk from this side. Left-hand traffic is assumed in this paper.

Feasibility of this system was studied analyzing traffic accident statistics and camera specification. For example, the above pedestrian accidents at less than 20 km/h occupied 88.6 % in Japan, which refers the statistical data on traffic accidents from ITARDA in 2001. Thus the system needs to detect the pedestrian at 16 m ahead or 3 sec. of TTC. This can be realized by the proposed system with the camera resolution of 1920 by 1080 and the baseline of 1.5m.

3. PEDESTRIAN DETECTION ALGORITHM

There are some candidate algorithms to detect pedestrians such as the optical flow-based algorithm (Hariyano2014) and the pattern recognition-based algorithm (Kamijo2010). However, the former one has some disadvantages which are difficulty to detect a pedestrian approaching from around the center of a camera optical axis and estimate the collision risk due to low accuracy of distance measurement to a pedestrian. It is difficult for the latter one to stably detect a pedestrian since appearance of a pedestrian is fluctuated by distortion of the fisheye lens and illumination change. On the other hand, a stereo camera can stably detect pedestrians and distance by disparity in spite of the pedestrian appearance when the stereo correspondence is obtained even partially. However, there are the following concerns to make the surround view cameras into a stereo system. The appearances in both cameras are largely different depending on the coordinate in a camera image due to the fisheye camera. Their luminance is also different due to difference of the image acquisition conditions. As position between the cameras is apart, errors in the camera parameters are occurred and the appearance is also changed by difference of the camera directions to a pedestrian. Thus, since a general area-based stereo cannot be applied, we have considered the feature-based stereo with feature amount applying machine learning to solve these concerns, which may absorb the above fluctuations. In the following sections, the calculation procedure and concrete algorithm are explained.

3.1 Overview

Abstract of pedestrian detection procedure is described. At first, images of the side camera on the side where a vehicle turns and the front camera are captured. The side camera is mounted at a large tilt angle under a side mirror. Thus, slant distortion of the camera image is corrected since bad influence is large if no compensation is applied. However,

distortion caused by the fisheye lens is not rectified because distortion correction error in peripheral area of the fisheye lens is caused by the correction. Overlapped area of both camera images is clipped and set it to the region of interest. The feature points and the feature amounts of image patches around them are calculated in the area. Various feature amounts have been proposed as described later, which is an important part in this proposal. For these correspondences between feature points in each camera image, the calculation cost and accuracy can be improved by minimization of the searching area applying epipolar constraint. However, the relative position between each camera fluctuates due to the structure and the camera external parameters have errors due to limitation of the camera calibration accuracy. Thus, 2-dimentional search around the epipolar lines with margin considering the errors is necessary instead of 1-dimentional search applied by a regular stereo camera. Correlation distances between each candidate patch in these areas are calculated, and the patch pairs with the shortest distance are selected as the stereo correspondence points. 3-dimentional reconstruction is executed by using these correspondence points, and the point cloud can be obtained. Occupancy grid map is calculated by the point cloud. When number of the 3D reconstruction points within the range of pedestrian height in the grid exceeds the preset threshold, it is judged that the pedestrian exists in the grid. After that, tracking the detected grid, the trajectory is estimated when number of the tracking times exceeds the preset value. When the trajectory approaches to the estimated trajectory of an ego-vehicle, it is assumed that the collision risk increases, and a warning is issued. Furthermore, depending on the detection confidence and reaction of a driver, the collision avoidance control by brake or steering can be executed if necessary.

3.2 Feature amount for stereo correspondence

As mentioned above, area-based stereo cannot be applied to this system configuration. Therefore, feature-based stereo is applied. Each appearance of a pedestrian in both cameras is different due to the influence of illumination, image distortion, projection and so on. The feature amount adopted here must be robust for these changes to take the appropriate correspondence. Furthermore, low calculation cost is also necessary because 2-dimensional search of the correspondence is required due to the camera parameter error.

As the feature point, KLT or Harris operator which extract the summits on luminance curved surface is often utilized (Kanazawa2004). In the image patches around these points, the patch pairs at the nearest correlation distance between the 2 camera images are extracted for the stereo disparity. There are various calculation methods regarding the correlation distance. NCC (Normalized Cross Correlation) which normalizes the luminance variation is selected as one of the candidates for the distance calculation. And, SIFT which is often utilized due to advantage for the invariance for scale and rotation is also selected to compare as one of the candidates (Lowe2004). Recently, various machine learning-based feature amounts have been proposed (Fujiyoshi2013). In those feature amounts, D-Brief is also selected to

investigate a possibility which absorbs the above-mentioned image fluctuation (Trzcinski2012). This feature amount has also an advantage that the calculation cost is low due to the binary feature description. FAST with low calculation cost is adopted as the feature point according to the original paper (Rosten2005).

D-Brief is outlined. This binary feature descriptor can be formulated as the following equation (1).

$$\forall_{i \in 1,...,N} \ b_i = \text{sign}(\mathbf{w}_i^T \mathbf{x} + \tau_i) \qquad (1)$$

where, b_i denotes the N bits of descriptor, $\mathbf{w}_i$ the projection matrix, τ_i the threshold vector and $\mathbf{x}$ the image patch vector. In this research, length of the descriptor N is set to 32 in accordance with the original paper.

This binary feature amount is calculated for each image patch around the feature point. Then, the image patch pair at the minimum Hamming distance between them is selected as the stereo correspondence. This projection matrix and threshold vector are calculated from machine learning utilizing the positive sample pairs of corresponding image patches and the negative sample pairs of non-corresponding ones. Furthermore, as this calculation cost is still high, it is reduced by the following equation (2) which is calculated as a linear summation.

$$\mathbf{w}_i = D\mathbf{s}_i \qquad (2)$$

where, D denotes the dictionary such as a rectangular filter and $\mathbf{s}_i$ the coefficient matrix.

This rectangular filter can be calculated at high speed by utilizing integral image. And, $\mathbf{s}_i$ can be obtained by solving the optimization problem so that $\mathbf{s}_i$ becomes sparse as much as possible. This can also make this calculation efficient.

4. EVALUATION

4.1 Fundamental evaluation using CG

4.1.1 Simulation condition

First, evaluation images have been created by computer graphics, and preliminary study has been done. Utilizing the PreScan which is the simulator of environmental recognition sensors, scenarios of traffic accident at the intersection have been reconstructed. Fig. 2 shows a clip of the accident scenario. The right-turn vehicle hits the pedestrian walking from this side on the cross walk at vehicle velocity of 5 m/s and pedestrian velocity of 1 m/s in the scenario. Camera images were created by the simulator, which size is 1440 by 1080. The fish eye lens is simulated with equidistance projection and 180 degree of FOV. Though this specification is different from the experimental cameras, these images were substituted due to constraint of the simulator.

NCC with KLT, SIFT and D-Brief with FAST have been evaluated as the feature amount to match corresponding

points. D-Brief essentially needs to train the classifier by using subject's training images, and the performance depends on them. However, CG was used for the evaluation and enough number of the training images could not be obtained, thus the trained classifier in the original paper has been temporarily utilized. It should be noted that the classifier is not suitable because this was trained by rotated and various-sized image patches in the scenic pictures. The patch sizes for NCC and D-Brief are 32 by 32.

4.1.2 Pedestrian detection results

Corresponding points for each feature amount are shown in Fig. 3 - 5 which include a front and side camera images. Each corresponding point between the cameras is connected with color-coded straight lines in the case of NCC, SIFT and D-Brief, respectively. These side camera images were compensated by converting it to the image at tilt angle of 0 degree so that the image distortion becomes similar to ones of the front camera images. Stereo correspondence seems to be moderately successful in any features though texture on the pedestrian is few due to limitation of the CG. Specially, in the case of SIFT, several wrong corresponding lines appear in the background other than the pedestrian. It is assumed that mis-correspondences were increased by the invariance of SIFT for scale and rotation.
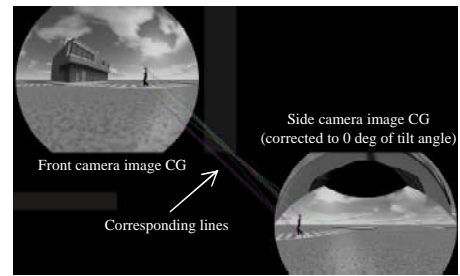
Fig. 3. Result of stereo matching with NCC
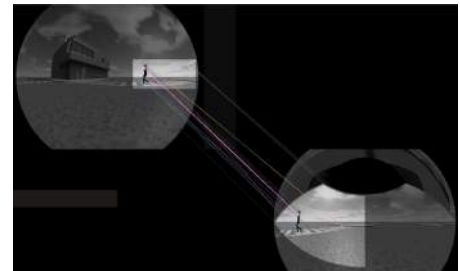
Fig. 4. Result of stereo matching with SIFT

Fig. 5. Result of stereo matching with D-Brief

3D reconstruction was executed by using coordinates of these corresponding points, and they were plotted in 3D coordinate graphs. The results are shown in Fig. 6 - 8. Each figure

corresponds to NCC, SIFT and D-Brief, respectively. Dotted red circles denote correct position of the pedestrian. Scale of the grid is 1m. In the case of NCC, there are a few reconstructed points with large error. In the case of SIFT, there are also a few reconstructed points with large error. From these results, it is difficult to discriminate obstacles from background noise considering characteristics of the reconstructed points. In the case of D-Brief, more reconstructed points around the correct pedestrian position were obtained relatively, though some background noises are also appeared. It is supposed that the pedestrian can be extracted by these points.

3D reconstruction coordinates
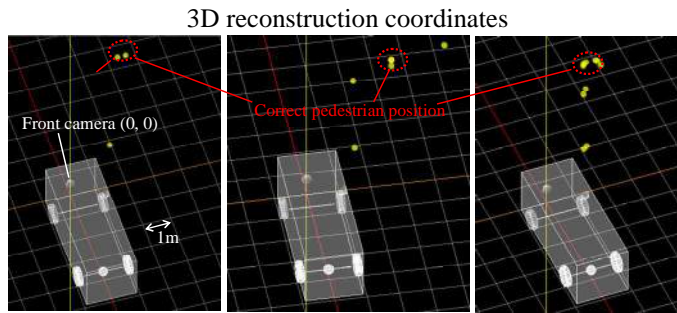
Fig. 6. with KLT   Fig. 7. with SIFT   Fig. 8. with D-Brief

These results have been obtained by a simplified CG image of the pedestrian over the abbreviated background as a preliminary experiment. In the following sections, experimental results and analysis utilizing the actual camera images are explained. In the experiments, SIFT was not evaluated because the performance was not so good in the CG experiments and the invariance for scale and rotation is not necessary and affects the matching adversely for this system.

4.2 Adjustment and evaluation using actual images on public roads
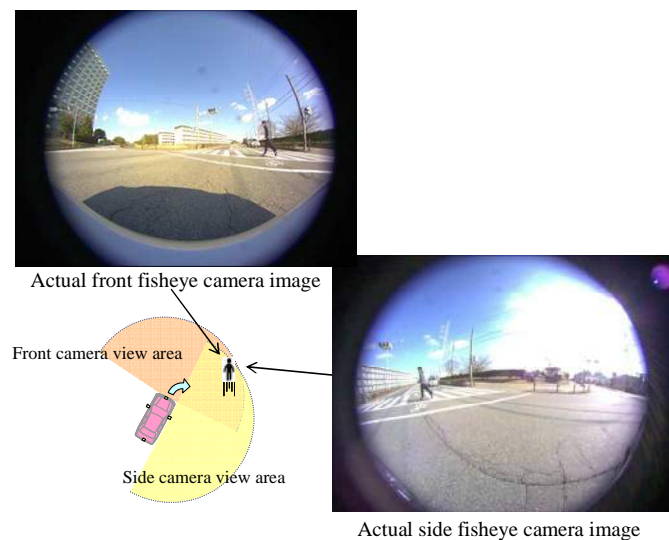
Fig. 9. Fisheye stereo camera images of crossing pedestrian in the actual environment

4.2.1 Pedestrian images for evaluation

Evaluation images were taken on the public roads in order to verify the feasibility in the actual environments. 64 scenes of crossing pedestrians and bicycles when turning right or left at intersections were taken in Kariya city in central Japan, where is a medium-size industrial city. Fig. 9 shows the front and side fisheye camera images of a crossing pedestrian while turning right in the actual environment as the sample scene.

The high-resolution fisheye cameras with 5 Mega pixels (2590x1942) were used here. The field of view of the fisheye cameras is 180 degrees and projection type of the fisheye lens is the Equidistance projection. Optical axis of the front camera was set to almost the vehicle travelling direction. Optical axes of the side cameras were set at right angle to the vehicle driving direction and a tilt angle of -16.6 degree. In the CG image, the tilt angle was set at -45 degree considering installation of the surround view monitor cameras. However, difference of the tilt angle is caused by constraint of mounting on the experimental vehicle. After the installation, the chess boards with known size were arranged correctly around the experimental vehicle, and then external camera parameters were calibrated.

As the training data for the machine learning-typed algorithm,

Fig. 10. Samples of positive image patch pair

Fig. 11. Samples of negative image patch pair

the image patch pairs were collected. Size of the image patches is 32 x 32 corresponding to the original paper. The total number is 3944 including 2520 of positive samples and 1424 of negative samples. These were also utilized to evaluate performance of the stereo correspondence. The positive samples of these image patches are shown in Fig. 10, and the negative samples are shown in Fig. 11. The left side image patch for each image patch pair is one taken by the front camera, and the right side one was taken by the side camera. They include the images which appearances are quite different, which is caused by distortion of the fisheye lens and capturing condition of the cameras.

4.2.2 Adjustment of machine learning algorithm

The parameters of D-Brief were trained by using the collected image patch pairs. And, these were also utilized to adjust the threshold values of NCC. All image patches were divided into 2 sets, which are a training set and an evaluation set. They were randomly assigned so that the training set occupied 3/4 and the evaluation set occupied 1/4 since adequate amount of data is necessary for the training. The results of 2 combination data sets in them are shown Fig. 12 and 13 applying ROC curve. This is the curve plotting correct detection rate of stereo matching versus false positive detection rate for the various thresholds. For the image patch set in Fig. 12, the correct detection rate at 10 % of false positive detection of NCC was better than one of D-Brief by

about 10 %. Appearing further performance difference for the other set in Fig. 13, NCC outperformed D-Brief by about 15 %. This is presumed that generalization performance was degraded by optimizing the training sets too much. And, it is inferred that some bias in appearance features of the patch sets were existed because the performance difference for each set was appeared even for NCC, though the evaluation sets were prepared by random sampling.

Thus, the cases of D-Brief trained by all image patches were tried in order to confirm the ability in case of no bias in training samples. Fig. 14 and 15 show the results of evaluation applying the descriptors trained by all image patches for the previous evaluation sets. They correspond to Fig. 12 and 13 respectively, and the evaluation results by the descriptors trained by all image patches are added in the graphs. For both data sets, the correct detection rates were improved by more than 10 % for NCC and 20 % for D-Brief trained by partial sets. Though they are not fair evaluation since the evaluation sets are included in the training set, these results show the possibility to improve the performance if the training image patches with many variation can be collected. It will be considered including rationalization of an image collection method in the future, though it is difficult to collect the huge amount and variety of image patches due to limitation of the cost to take the images and extract the training image patches. However, actual scenes were evaluated by utilizing this above descriptor trained by all image patches in this paper.
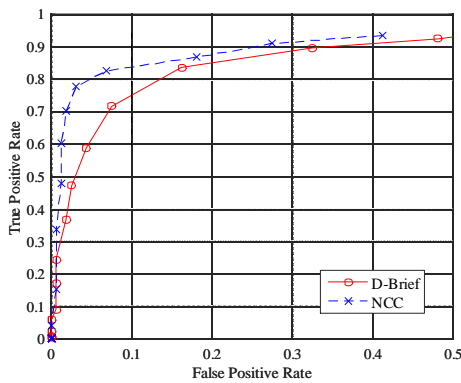
Fig.12. ROC curve of NCC vs. D-Brief (Data set A)

Fig. 14. ROC curve of NCC vs. D-Brief by all patches (Data set A)

Fig. 13. ROC curve of NCC vs. D-Brief (Data set B)
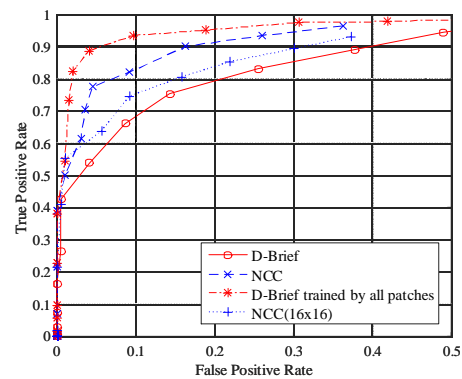
Fig. 15. ROC curve of NCC vs. D-Brief by all patches (Data set B)

As the reference, results by NCC with 16x16 of pixel size are also added in these graphs since 32x32 of size is generally too large as one of NCC. The rates were degraded depending on the data set, especially for data set A.

4.2.3 Pedestrian detection results

Pedestrian detection while turning in actual scenes was tried by NCC and the aforementioned D-Brief. 3-dimentional coordinates were reconstructed for these corresponding feature points, and they were projected on the occupancy grid map of 0.5 by 0.5 m. The cubic objects were simply extracted as the target pedestrians to be detected by count of the points in a cell and the dispersion to the vertical direction. The detection grids are shifted and overlapped by 0.25 m in order to absorb the position offset. The results are shown in Fig. 16 to 19.

Fig. 16 shows the stereo correspondence connected with the colored lines between the front and side camera images in the case of NCC. This graph shows the correspondence seems appropriate globally though it is difficult to confirm in detail. And, Fig. 17 shows the top view for 3D reconstruction coordinates of the corresponding points. The pedestrians can be discriminated from the background since the reconstructed

points concentrate in the cells, though some noises are appeared in the near-field area. The left pedestrian could not be detected though some correct reconstructed points were appeared.

Fig. 18 shows the stereo correspondence by applying D-Brief. This seems appropriate globally as one by NCC. And, Fig. 19 shows the top view for 3D reconstruction coordinates of the corresponding points. The pedestrians can be also discriminated from the background as well as one by NCC, though several noises are appeared in a wide-field area. More mis-correspondences are appeared than ones by NCC. This result corresponds to the discrimination performance of D-Brief caused by lack of amount and quality of the training images as described in the previous section.

Distance to the pedestrians in this scene was about 3 m from the subject vehicle. Other scenes were also evaluated, however the distances were similar because it was difficult to get a chance to capture the images of pedestrians at the far distance in the actual environment due to restriction on the safety and the road environment. We will try to capture more scenes including the images of pedestrians at the far distance to verify the robustness and feasibility as possibility of this system could be confirmed in this research.
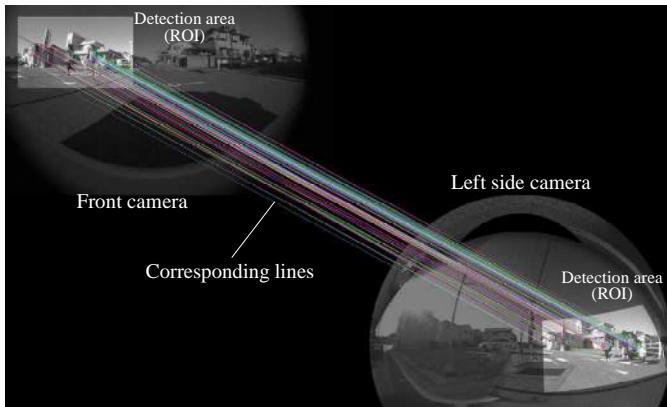
Fig. 16. Stereo correspondence by NCC
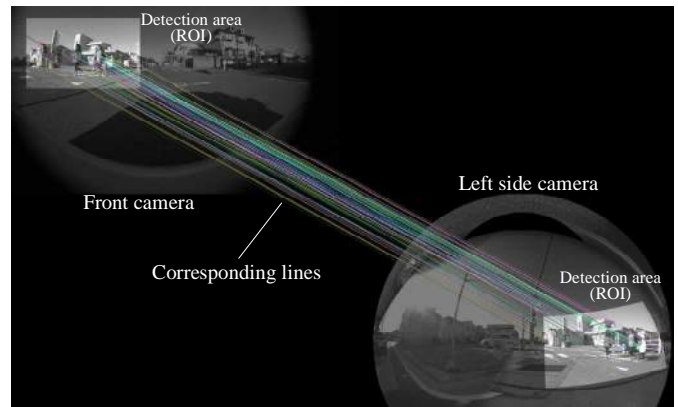
Fig. 18. Stereo correspondence by D-Brief
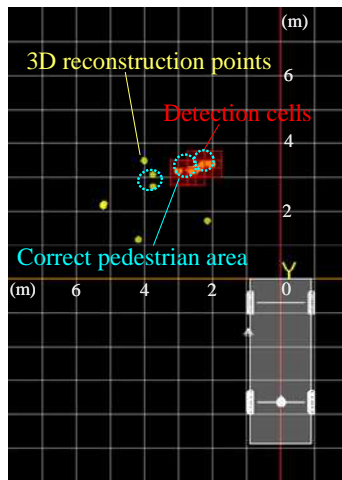
Fig. 17. Top view of 3D reconstruction points
and pedestrian detection by NCC
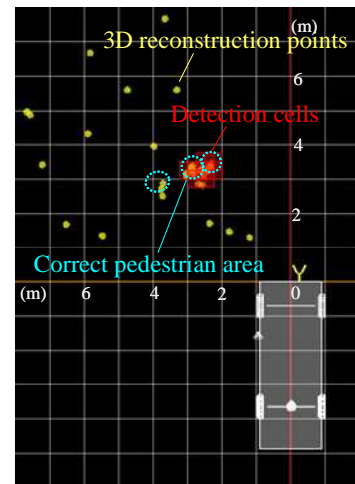
Fig. 19. Top view of 3D reconstruction points
and pedestrian detection by D-Brief

5. SUMMARY AND FUTURE WORK

We have proposed the driver assistant system applying a surround monitor camera system spreading widely as the countermeasure for traffic accidents of crossing pedestrians while turning left or right at the intersection, which will be getting important. This system can improve the recognition reliability by making it into a stereo vision system in overlap areas of the fisheye camera vision. Thus, the function can be realized at low cost since additional expensive sensors such as a radar or LIDAR are not necessary.

Various feature amounts have been tried for the stereo correspondence problem, which is the most important part to realize this system due to the non-rigid mounted stereo camera utilizing fisheye cameras. Possibility of a machine learning-based feature which is a new method as stereo matching has been indicated, though the discrimination performance is not so high compared with NCC that is a conventional method. However, the concern for a machine learning method was also found, which is a necessity of a huge amount and wide variety of training sample images. Preliminary experiments applying CG images were conducted, which could indicate the feasibility. Then, it was verified by the experiments for the actual camera images.

In the future, we will improve the feature amount for stereo correspondence by increasing the training samples or adopting other state-of-the-art feature descriptors. And, robustness of the pedestrian detection performance will be verified under various conditions in the actual environments. Furthermore, we will have to improve the calculation cost towards the practical realization.

REFERENCES

Fujiyoshi, H. (2013). Image Local Feature amount SIFT and subsequent approach, *tutorial in MIRU*2013.

Hagiwara, T., Hamaoka, H., Uchibori, D., Suzuki, K. (2010). Investigation of the Driver's Avoidance Behavior Caused by the conflicts with the Pedestrian/Cyclists at Night at an Urban Signalized Intersection, *Proceedings of JSAE Annual Congresses in spring*, No. 188-20105256.

Hagiwara, T. (2012). Traffic safety countermeasure utilizing ICT the 3rd, *Nikkei electronics* 2012.4.2, pp. 90 - 96.

Hariyono, J., Hoang, V. D., and Jo, K. H. (2014). Moving Object Localization Using Optical Flow for Pedestrian Detection from a Moving Vehicle, *The Scientific World Journal* Volume 2014, Hindawi Publishing Corporation, Article ID 196415.

ITARDA (2012). ITARDA information, No. 94, pp. 3.

Kamijo, S., Fujimura, K., Shibayama, Y. (2010). Pedestrian Detection Algorithm for On-board Cameras of Multi View Angles, *IEEE Intelligent Vehicles Symposium* 2010.

Kanazawa, Y., Kanatani, K. (2004). Detection of Feature Points for Computer Vision, *Journal of the Institute of Electronics*, Information and Communication Engineers, Vol. 87, No. 12, pp. 1043 - 1048.

Lowe, D. G. (2004). Distinctive image features from scale-invariant keypoints, *International Journal of Computer Vision*, 60, 2, pp. 91-110.

Rosten, E. and Drummond, T. (2005). Fusing Points and Lines for High Performance Tracking, *10th IEEE International Conference on Computer Vision* 2005, Vol. 2, pp. 1508-1515.

Trzcinski, T. and Lepetit, V. (2012). Efficient Discriminative Projections for Compact Binary Descriptors, *ECCV* 2012 *Lecture Notes in Computer Science*, Vol. 7572, 2012, pp 228-242.

Investigation of braking timing of drivers for design of pedestrian collision avoidance system

Keisuke Suzuki*, Takuya Kakihara*, Yasutoshi Horii**

*Kagawa University, Takamatsu, Kagawa, Japan
(e-mail: ksuzuki@eng.kagawa-u.ac.jp).
** DENSO SALES SWEDEN AB, Göteborg, Sweden
(e-mail: y.horii@denso.se)

Abstract: The braking behaviors of drivers when a pedestrian steps out from a sidewalk and into the street were analyzed using a driving simulator. Based on drivers' braking behavior, a braking control timing for a system for avoiding collisions with pedestrians was proposed. In this study, the subject drivers started braking at almost the same time in terms of time to collision (TTC), regardless of the velocity of the subject vehicle and the crossing velocity of the pedestrian. The results of our experiments showed that, to minimize the degree of interference between the driver and the system, the optimum timing at which to apply the braking was at a TTC of 1.3 s. Next, the drivers' braking behavior was investigated when the system controlled the braking to avoid a collision with this timing. The drivers did not exhibit any change in their braking behavior, while there was no excessive interference between the braking control system and the drivers when attempting to avoid a collision with a pedestrian, indicating that the drivers were not becoming excessively dependent on the system.

Keywords: Active safety, Collision avoidance, Pedestrian, Braking timing, TTC, Driving simulator

1. INTRODUCTION

The commercial utilization and spread of collision-avoidance braking systems is steadily progressing, with the aim of preventing rear-end collisions when travelling behind another vehicle. Regarding the design of such devices, the sensor fusion algorithm and increasing the accuracy with which obstacles can be detected are important factors affecting user-acceptance of such support systems (Ishida, 2014). It has also been reported a concept integrating several active safety technologies, named the "Integrated Safety Management Concept," would increase user acceptance of the systems (Miichi, 2014). These concepts are being addressed as part of the research activities being undertaken as part of Japan's Advanced Safety Vehicle (ASV) project. In response to the increase in the number of active safety devices being offered on the market, evaluation tests of collision-avoidance braking systems were started in Japan in 2014 as a part of the J-NCAP dynamic vehicle performance tests. Regarding J-NCAP, the details of the methods for evaluating active safety devices such as the autonomous emergency braking system (AEBS) and lane departure warning system (LDWS) have been summarized, allowing us to see that there are slight differences in the evaluation methods used for J-NCAP, Euro-NCAP, and US-NCAP, with these differences originating in the differences between typical traffic accidents in each region (Ujihashi, 2014). Even though there are slight differences in the evaluation test methods, the evaluation of AEBS is progressing because of rapid progress in the systems being brought to market. Among the overseas research projects addressing the system evaluation of the collision

mitigation as enabled by a collision-avoidance braking system, Sweden's City-Safety project is well known (Distner, 2009). For instance, the system was verified using CAE methods and practical tests, with in-depth discussion of the benefits that can be achieved through the application of such systems to real-life safety (Coelingh, 2007; Brannstrom, 2010). In addition to these studies, other studies set out to predict the effects of various collision avoidance support systems, as well as the real world effect of these systems (Ljung, 2015; Isaksson, 2012).

As part of the next phase of popularizing collision-avoidance braking systems, progress is being made in the development of systems capable of avoiding collisions with pedestrians by using millimeter-wave radar and stereo cameras (Inomata, 2014; Coelingh, 2010). In the development of such a system, the improvement in the detection accuracy of a pedestrian's movement vector, so as to predict a collision, is one of the major research items (Raksincharoensak, 2014). In addition, improvement in the accuracy of pedestrian detection, optimization of the human-machine interface, specifically, the interaction between the driver and the system, are crucial issues to be discussed. The optimization of the braking control timing is vital to ensuring that drivers do not become excessively dependent on the system while maintaining trust in the system. For example, when the timing of the braking by the system is extremely late, trust in the braking support system may decrease (Itoh, 2012). On the other hand, if the timing of the braking by the system is extremely early, a driver may become excessively dependent on the system. In a previous study dealing with the design of the control timing for a collision-avoidance braking system intended for

avoiding rear-end collisions, the concept of the system design was reported as part of the efforts of the Japanese ASV projects (Suzuki, 2002, 2003). In this research, braking by drivers to avoid rear-end collisions was analyzed using a driving simulator, as well by experiments performed on a test course. As a result, a braking control timing which does not lead to drivers becoming excessively dependent on the system was proposed. In this study, it was reported that, to minimize the interference between the braking control system and the driver, it is important to prevent the driver becoming dependent on the system. In this study, we set out to devise a method for determining the system braking timing in order to avoid a collision with a pedestrian. First, the braking timing of drivers, when a pedestrian steps out from a sidewalk, was analyzed using a driving simulator. Subsequently, based on the results of this investigation, a method for determining the braking control timing was devised, taking the following two conditions into account.

#1. There is no excessive interference between the braking control system and the driver, and the driver may not become excessively dependent on the system.

#2. The system should apply braking control early rather than at the latest possible timing to avoid a collision, so as to maintain trust in the system.

2. INVESTIGATION OF DRIVERS' BRAKING TIMING

2.1 Experimental conditions

Using the driving simulator at Kagawa University, a situation where a pedestrian steps out from the sidewalk and into the street was set up. This experimental scenario is depicted in Fig. 1. Two conditions for the pedestrian's crossing velocity (Vp), namely, 5 km/h and 8 km/h, were assumed. Three different velocities for the subject vehicle (V) (20 km/h, 40 km/h, and 60 km/h) were set up. The condition whereby a pedestrian steps out from the sidewalk and into the street at a timing of "Time to Collision (TTC; relative distance[m]/relative velocity [m/s]) = 3 s" was set. That is, the timing at which the pedestrian begins to come out into the street was set so that the TTC would be the same under all conditions. In this scenario, when only the risk of a pedestrian stepping out from the sidewalk and into the street was set, the tendency for subject drivers to become sensitive to the risk was observed. For this reason, not only this one risk but also nine fake risks, such as a pedestrian suddenly stopping just before stepping out into the street or suddenly changing his/her direction of movement, but not crossing the street, were included. This means that each subject driver experienced a total of sixty events including six risk events. The experimental sequence is described in Table 1. We focused on these six events and investigated the driver behavior. In a prior experiment, it was observed that subject drivers became sensitive to the presence of the pedestrian, which differs from actual driving behavior. Therefore, numbers were displayed on an LCD display mounted on the

instrument panel every three seconds, and the subject driver was asked to perform mental calculations using these figures, to act as a distraction. In this study, ten males participated as the subject drivers. The average/standard deviation of the age of the subject drivers was 22.4 ± 0.86 years old. Upon starting this experiment, the validity of the contents of experiment was verified by the ethics committee of Kagawa University. In addition, each of the participants was asked to sign an informed consent form by the person in charge of the experiment before the experiment was actually started. In this study, only young male drivers participated in the experiments. Additional studies using female and senior drivers as test subjects should be performed in the future. With this study, we set out to propose a concept for designing the braking onset timing of the system and will verify the validity of this concept which was mentioned in #1 and #2 of a previous section.

V [km/h]	20	20	40	40	60	60
Vp [km/h]	5	8	5	8	5	8
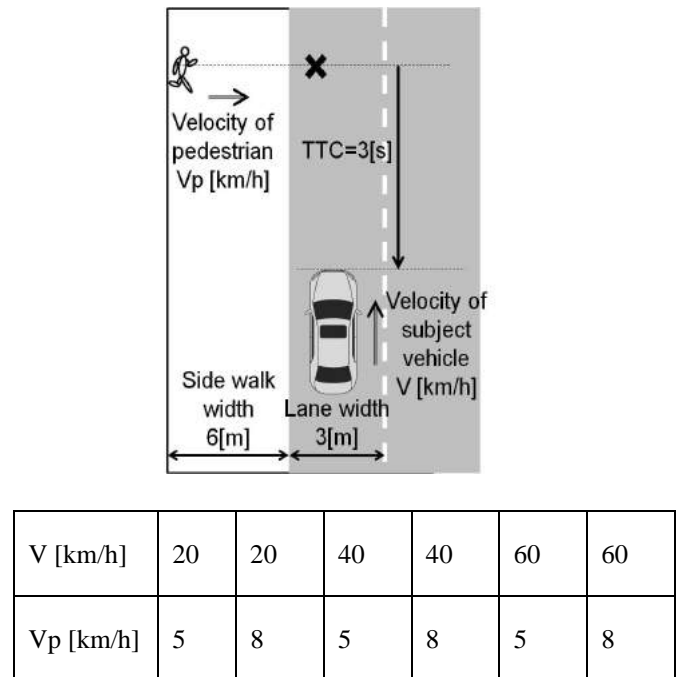
(a) Setup for evaluating braking behavior when avoiding a collision with a pedestrian

(b) View from within driving simulator

Fig.1 Experimental scenario

Table 1 Experimental sequence

Practice run (15minutes)	Investigation of braking timing "each driver experienced sixty events in total including six risk events" (60minutes)	Subjective evaluation for driving using DSQ (15minutes)

(c) ANOVA results among all groups

Source of Variation	SS	df	MS	F	P-value	F crit
Between Groups	0.219872	5	0.043974	0.305237	0.907382	2.408514
within Groups	6.915182	48	0.144066			
Total	7.135054	53				

2.2 Results of investigation of drivers' braking

The average braking start timing of the subject drivers in terms of TTC is shown in Fig. 2 for each velocity of the subject vehicles. An analysis of the variance in the braking timing for each condition based on ANOVA is shown in Table 2. This table shows that there is no great difference in the braking behavior for each driving condition, either in terms of the crossing velocity of the pedestrian or the velocity of the subject vehicle. In this study, it was found that the drivers applied braking approximately 2.1 s before colliding with the pedestrian. This means that the driver braked suddenly after a pedestrian appears 3 s before colliding with the subject vehicle.

In a previous study by Suzuki (2002, 2003), when the velocity of the subject vehicle is higher, a driver brakes earlier to avoid a rear-end collision with the vehicle in front. This means that the driver brakes while taking the total stopping distance needed to avoid a rear-end collision into account. One of the experimental results obtained by Suzuki is shown in Fig. 3. When the velocity of the vehicle is higher, the timing of the braking is earlier. In this figure, the TTC which considers the total stopping distance needed to avoid a rear-end collision with a vehicle in front is also shown. It is possible to say that the start of braking by drivers became earlier with an increase in the TTC, which considers the total stopping distance needed to avoid a collision.

Fig. 2 Braking timing of subject drivers for each vehicle velocity (Appearance timing of pedestrians: TTC = 3 s)
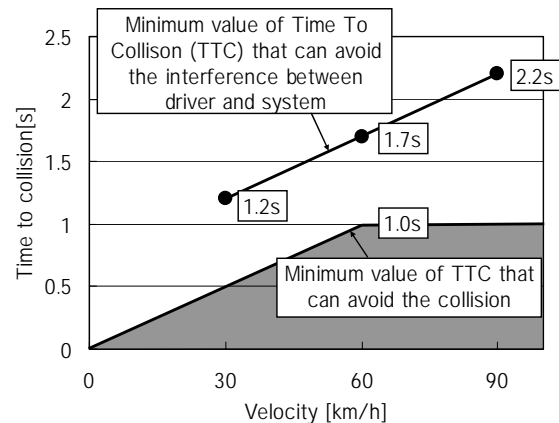
Fig. 3 Drivers' braking timing for avoiding rear-end collision with a vehicle in front (Suzuki (2002, 2003))

Table 2 Variance in braking timing for each condition

(a) ANOVA results when Vp=5km/h

Source of Variation	SS	df	MS	F	P-value	F crit
Between Groups	0.081103	2	0.040551	0.229775	0.79644	3.402826
within Groups	4.235597	24	0.176483			
Total	4.3167	26				

(b) ANOVA results when Vp=8km/h

Source of Variation	SS	df	MS	F	P-value	F crit
Between Groups	0.01924	2	0.00962	0.086162	0.917728	3.402826
within Groups	2.679585	24	0.111649			
Total	2.698825	26				

In the experiment where the driver aimed to avoid a collision with a pedestrian, the results differed from this tendency observed when attempting to avoid a rear-end collision. For example, given the scenario where a pedestrian steps out into the street from the sidewalk, no difference in braking timing depending on the velocity of the subject vehicle ("V" in Fig. 1) or crossing velocity of the pedestrian ("Vp" in Fig. 1) was observed. That is, for the risk scenario in which a pedestrian steps out from the sidewalk and into the street, as soon as the subject driver recognizes that a pedestrian has stepped out into the street at a TTC of 3 s, the subject drivers all braked after approximately the same latency, regardless of the velocity of the subject vehicle or the crossing velocity of the pedestrian.

Next, for all of the subjects' braking timing shown in Fig. 2, above, a cluster analysis of the driving behavior using the driving style questionnaire (DSQ) (Ishibashi, 2008) was

conducted and the drivers were then classified into three groups. The driver characteristics of these three groups, corresponding to eight mental characteristics, are shown in Fig. 4, based on the DSQ evaluation index. Below, we consider the relationship between the characteristics of each driver group and the onset of braking.
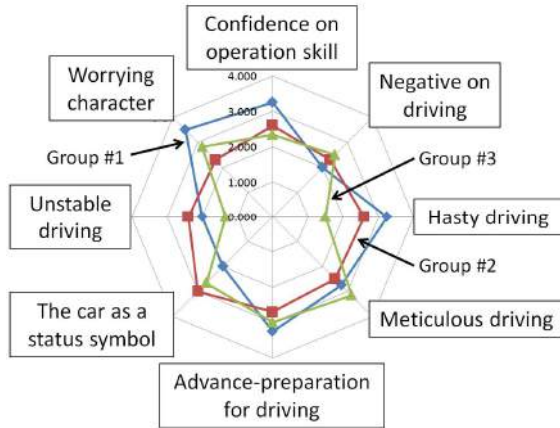
Fig. 4 Results of DSQ analysis of driver characteristics

Three different average braking timings for each subject group in terms of TTC are shown in Fig. 5. Only those subject drivers classified into group #1 exhibit a tendency to greatly delay the start of braking. When we look at the mental characteristics of the subject drivers classified into group #1, we find that they exhibit either a hasty driving characteristic or a worrying character, as shown in Fig. 4. That is, those drivers classified as having a hasty tendency tend to delay their braking such that the TTC at braking is short. Regarding those drivers classified into groups #2 or #3, they do not exhibit a hasty driving characteristic, and hence the braking onset timing is relatively early. Although it is not possible to explain the relationship between the mental characteristics and onset of braking behavior in detail, the DSQ results allow us to roughly understand how they are related.
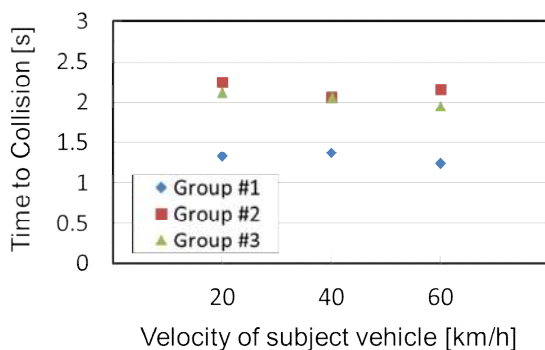
Fig.5 Average value of braking start timing for each driver group

3. METHOD FOR DESIGN OF BRAKING CONTROL TIMING

3.1 Design of braking control timing

For the design of the braking control timing, the following requirements were determined.

(1) The braking control timing of a system should not be dependent on the velocity of the subject vehicles, and should be set up uniformly. This is because no significant difference was observed for the braking start timing of the subject drivers regardless of the velocity.

(2) For every velocity (20 km/h, 40 km/h, and 60 km/h), the system should be able to avoid a collision with a pedestrian.

An example TTC which satisfies the above conditions is 1.3 s, as shown in Fig. 6. For the frequency distribution of the braking initiation timing, a TTC of 1.3 s is equivalent to approximately 5 percentiles of the entire frequency distribution of the brake timing, as shown in Fig. 2, and is equivalent to the average braking timing of group #1, which delayed the braking the most. This means that 95% of the braking initiation timings, in terms of TTC, exceed 1.3 s among all the subject drivers. The braking by the drivers when the control system is implemented is discussed in the following sections.
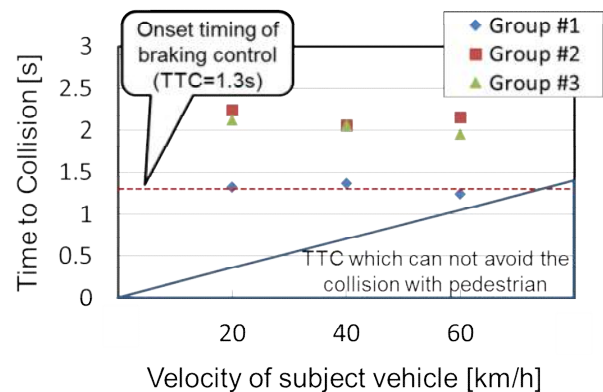
Fig. 6 Average braking start timing for each driver group

3.2 Interference between braking control system and driver

To examine the effect of the velocity of the vehicle being driven by a subject, an experiment was conducted with the vehicle travelling at 20 km/h, 40 km/h, and 60km/h. The braking timing at a TTC of 1.3 s and three different timings (0.45 s for 20 km/h, 0.77 s for 40 km/h, and 1.1 s for 60 km/h) was found to be related to the velocity of subject

vehicle, thus imposing a physical limit on the avoidance of a collision with the vehicle in front. The timing of 1.3 s is equivalent to the above-mentioned timing needed to avoid excessive interference between the system and the driver. The physical limit is the maximum delay possible while still avoiding a collision with the vehicle in front. One risk event and nine fake events were set up, in the same way as in the experiment described above to investigate the drivers' braking timing. Two pedestrian crossing velocities were set up. As a result, the subject driver experienced twenty events, including two risk events. Six subject drivers participated in the experiment.

An example of the time sequences of the braking by a driver and the braking control system is shown in Fig. 7. This figure shows the braking behavior of group #1 for which the braking timing is extremely late. As shown in Fig. 7, the braking timing by the system is not greatly earlier than that of the driver and almost equal to that of the system. Even for a driver who is classified into group #1, and who therefore brakes extremely late, excessive interference between the system and the driver is not observed. Regarding the braking behaviors of groups #2 or #3, who apply braking earlier than group #1, the braking timing by the driver was much earlier than that of the braking control system and there was no interference between the system and the driver. A subjective evaluation showed that it was possible to maintain a high level of trust in the system while simultaneously keeping dependency low, provided the system's braking onset timing is set to a TTC of 1.3 s. We will continue these studies with additional subject drivers to validate these results.

Next, we will consider a subjective evaluation of trust in the system. The results obtained for all of the drivers are shown in Fig. 8. This figure intimates that the drivers' level of trust in the system when braking starts at a TTC of 1.3 s is higher than that when the system starts to brake at the latest possible instant to avoid a collision. We will continue to investigate the relationship between the braking timing by the system and the level of trust in the system.
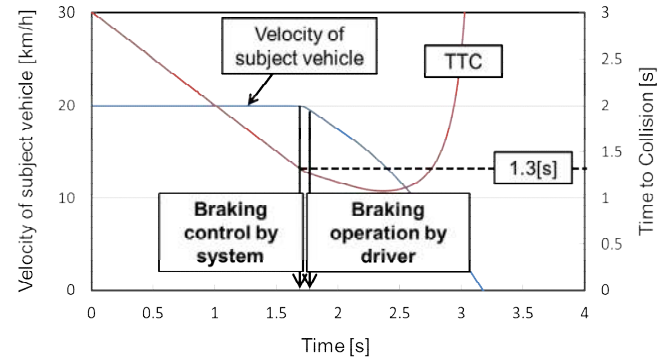
(a) Velocity of subject vehicle: 20 km/h
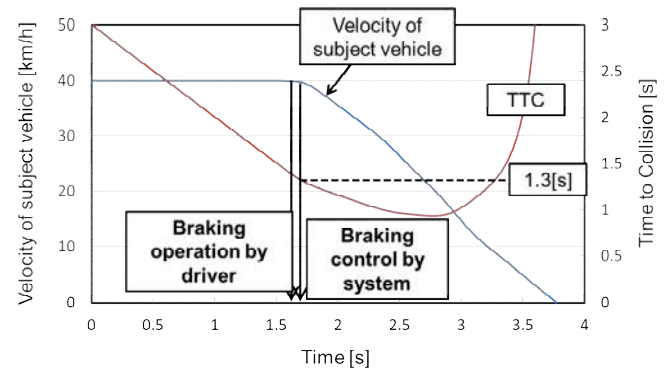
(b) Velocity of subject vehicle: 40 km/h
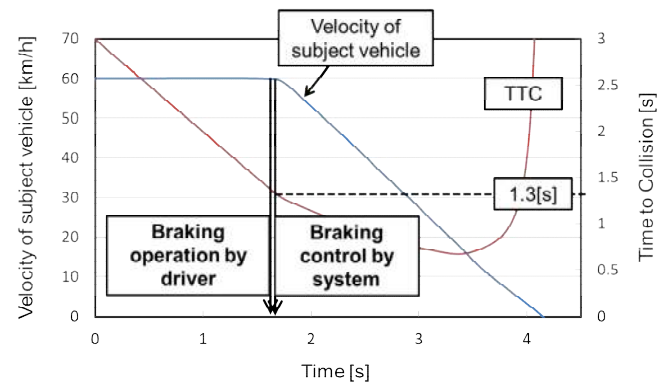
(c) Velocity of subject vehicle: 60 km/h

Fig. 7 Time sequence of braking by driver who tends to brake very late (group #1) and that by the system
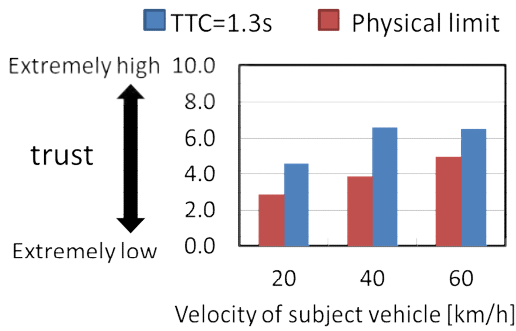
Fig. 8 Subjective evaluation of trust in the system and annoyance with the control applied by the system

Fig. 9 Braking timing of subject drivers for each vehicle velocity (Appearance of pedestrian: TTC = 4.5 s)

4. DISCUSSION

4.1 Major factors affecting the start of braking

In this study, we found that the velocity of the subject vehicle or the crossing velocity of a pedestrian had not effect on the braking timing when attempting to avoid a collision with the pedestrian. This tendency differs from that of avoiding a rear-end collision with a vehicle in front. Therefore, we analyzed the reason why all of the drivers applied braking at almost the same TTC timing. We conducted an additional experiment in which the timing at which the pedestrian appeared varied, such that the TTC was longer. In this additional experiment, the pedestrian appeared such that the TTC was 4.5 s, which is longer than that of the main experiment described above.

In this second experiment, the pedestrian's crossing velocity (Vp) was set to 6 km/h, which was equal to one of the two conditions used in the main experiment. The experiment was set up such that the pedestrian appears at a TTC of 4.5 s, which is 1.5 s earlier than in the main experiment. The pedestrian actually appeared from a sidewalk, further away in the distance. The velocity of the subject vehicle (V) was again set to one of the three values used in the main experiment. Again, fake events were set up for this experiment. That is, a pedestrian appeared at a TTC of 4.5 s and then stopped just before stepping out into the street, again to overcome the simple reaction tendency of the drivers. The results for this condition are shown in Fig. 9.

The timing of the braking by all the drivers was basically the same, even though the velocity of the vehicle was different. This tendency is same as that observed in the main experiment in which the pedestrian appeared at a TTC of 3 s. When the pedestrian appeared at the above-mentioned TTC of 3 s, the median (50th percentile) braking timing was about 2.1 s. When the pedestrian appeared at a TTC of 4.5 s, the median (50th percentile) braking timing was about 2.4 s. When a driver attempted to avoid a pedestrian who had run out from the sidewalk, he actually started braking at almost the same timing regardless of the velocity of subject vehicle. Furthermore, the following tendencies became clear when the results of this experiment were analyzed in detail. When the pedestrian appeared at a TTC of 3 s, the latency in the braking to avoid a collision with a pedestrian was approximately 0.9 s. That is, once a pedestrian is seen, the driver applies the brakes immediately. When the pedestrian appeared at a TTC of 4.5 s in the additional study, the braking latency between the appearance of the pedestrian and the start of braking was approximately 2.1 s. We thus found that the braking latency by a driver when attempting to avoid a collision became longer because the risk of colliding with a pedestrian was lower. We can conclude, therefore, that the timing of the braking is not dependent on the velocity of the subject vehicle, but rather on the TTC related to the risk of colliding with a pedestrian. If the velocity of the subject vehicle increases, the braking distance required until the vehicle comes to a complete stop will be prolonged. But, in a scenario in which a pedestrian runs out from the sidewalk and into the street, it is difficult for a driver to determine the required braking distance. In comparison with the scenario in which the vehicle in front brakes suddenly, the driver's braking behavior is different when a pedestrian steps out into the street, because it is difficult for the driver to estimate the total distance needed to avoid a collision. We believe that when a driver detects a pedestrian in his or her peripheral visual area, it is difficult to estimate the risk of a collision, which would explain the stopping distance of the vehicle, relative to the timing at which the pedestrian appears, in terms of TTC.

4.2 Validation of experiment scenario

In this study, we set up a situation where a pedestrian appeared at a TTC of 3 s and 4.5 s, and investigated the braking latency of the driver. As a result, we concluded that the timing at which braking is applied depends on the timing at which the pedestrian appears, that is, the TTC. This suggests that we should discuss the timing that typifies the appearance of a pedestrian from a sidewalk. In this study, the velocity of the pedestrian was assumed to be 5 km/h and 8 km/h. Therefore, the distance between the lateral position of the pedestrian and that of the subject vehicle is 4.16 m and 6.66 m when the pedestrian appears at a TTC of 3 s. When the pedestrian appears at 4.5 s, this distance is 6.25 m, assuming that the pedestrian's walking velocity is 5 km/h. The distances between the pedestrian and the street on which the subject vehicle is operating are depicted in Fig. 10(a). It would be difficult to determine the distance from the street at which the pedestrian becomes visible to the driver. But, we believe that the condition set up in this study is typical for an urban area. One of the important objectives of this study was to clarify the shortest TTC when a driver starts to brake to avoid a collision with a pedestrians and to clarify the timing at which the system applies braking in order to minimize any interference between the braking by the driver and the braking control applied by the system. We determined that the braking latency of a driver is approximately 0.9 s when a pedestrian appears at a TTC of 3 s. This means that we could set up a high-risk driving situation where the TTC is equal to the braking latency when attempting to avoid a collision with a pedestrian (Fig. 10(b)). Therefore, we can conclude that the results of this study are valid for application to the design of the braking onset timing of a braking control system.
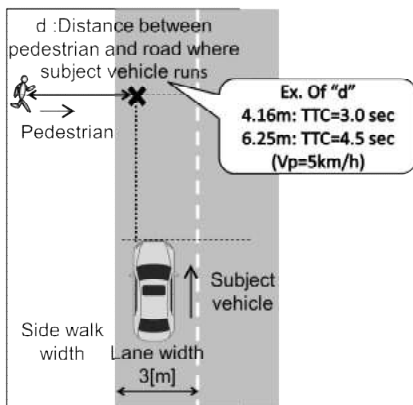
(a) Distance between pedestrian and street on which subject vehicle is operating
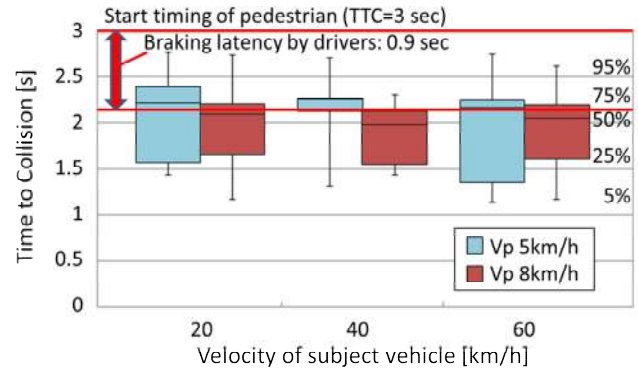
(b) Relationship between start timing of pedestrian and braking timing for three different velocities

Fig. 10 Validation of scenario assumed in this study in terms of set up of a critical situation to a avoid collision with a pedestrian

5. SUMMARY

In this study, we analyzed the timing at which a driver started to brake to avoid a collision with a pedestrian stepping out from the sidewalk and into the street. We noted that the drivers applied braking at approximately the same timing in terms of the TTC, even if the velocity of the subject vehicle and crossing velocity of the pedestrian were different. This tendency differs from that when avoiding a rear-end collision with the vehicle in front. We will next move on to determine the reason for the difference between these two braking behaviors. Regarding the frequency distribution of the braking initiation timing, a TTC of 1.3 s was equivalent to five percentiles of the overall frequency.

Based on the results of an investigation into this braking behavior, the timing of the onset of the braking control at a TTC of 1.3 s was set up for every vehicle velocity and pedestrian crossing velocity. Negative effects, specifically, an excessive dependence on the system, were not observed, provided the system started to apply braking at a TTC of 1.3 s, because there was no excessive interference between the braking control by the system and the braking by the drivers. It was also observed that the drivers' trust in the system does not decrease at this control timing, because the timing at which the system applied braking was not excessively late and was thus acceptable to the drivers.

From the results of this study therefore, we can conclude that the timing at which braking is applied is not dependent on the velocity of the subject vehicle, but rather is dependent on the TTC and the risk of colliding with a pedestrian. This means that the driver does not have sufficient time to draw a mental comparison between the time until a collision with the pedestrian and the time needed to stop the vehicle. This

braking behavior is not the same as that needed to avoid a rear-end collision with a vehicle in front. We will continue to consider why this difference in behaviors is observed. One possibility is that the detection of pedestrians in the peripheral viewing area of the driver incurs a higher mental workload by the driver relative to detecting a sudden deceleration of the vehicle in front, which is in the center of the driver's field of view. Therefore, it is difficult for the driver to control the braking timing, given the relationship between the time until a collision with a pedestrian will occur and the time needed to stop to avoid the collision.

REFERENCES

Brannstrom, M., Coelingh, E., Sjoberg, J. (2010), Model-Based Threat Assessment for Avoiding Arbitrary Vehicle Collisions, Transactions of Intelligent Transportation Systems, IEEE, Volume.11, Issue. 3, DOI: 10.1109/TITS.2010.2048314, pp.658-669

Coelingh, E., Jakobsson, L., Lind, H., Lindman, M. (2007), Collision Warning with Auto Brake, A Real-Life Safety Perspective, Proceedings of the 20th ESV Conference Paper No. 07-0450

Coelingh, E., Eidehall, A., Bengtsson, M. (2010), Collision Warning with Full Auto Brake and Pedestrian Detection - a practical example of Automatic Emergency Braking, Proceedings of Intelligent Transportation Systems (ITSC), 13th International IEEE Conference, DOI: 10.1109/ITSC.2010.5625077, pp.155-160

Distner, M., Bengtsson, M., Broberg, T., Jakobsson, L. (2009), City Safety, A System Addressing Rear-end Collisions at Low Speeds, Proceedings of the 21st ESV Conference Paper No. 09-0371

Inomata, R., Hayashi, H., Fujishiro, R., Ouchi, Y., Nanami, T., Suzuki, K. (2014), Development of Pre-Crash Safety System with Collision Avoidance Assist, Journal of Society of Automotive Engineers of Japan, Vol.68, No.12, pp.25-30

Isaksson-Hellman, I. (2012), The Effect of a Low-Speed Automatic Brake System Estimated From Real Life Data, Transaction of Association for the Advancement of Automotive Medicine, Issue. 2012 Oct; 56, pp.231-240

Ishibashi, M., Okuwa, M., Doi, S., Akamatsu, M. (2008), Characterizing Indices of Driving Style and their Relevance to Car Following Behaviour, Transactions of Society of Automotive Engineers of Japan, Vol.39, No.1, pp.121-126

Ishida, S., Sawamoto, K., Miyagawa, K., Nakanishi. Y., Sasabuchi, Y. (2014), Technical Introduction which Reduces the Traffic Accident by the Data Fusion of a Camera and a Millimeter Wave Sensor, Journal of Society of Automotive Engineers of Japan, Vol.68, No.12, pp.31-37

Itoh,M.,(2012), Toward overtrust-free advanced driver assistance systems, Cognition, technology & work Vol.14, No.1, pp.51-60, Springer-Verlag London

Ljung-Aust, M., Jakobsson, L., Lindman, M., and Coelingh, E. (2015), Collision Avoidance Systems - Advancements and Efficiency, "Collision Avoidance Systems - Advancements and Efficiency," SAE Technical Paper 2015-01-1406, doi:10.4271/2015-01-1406

Miichi, Y., Nakagawa, H. (2014), Approach for Development of Safe Driver Assistance Technology, Journal of Society of Automotive Engineers of Japan, Vol.68, No.12, pp.19-24

Raksincharoensak, P., Sakai, Y., Shimizu, I. (2014), Development of Pedestrian Collision Avoidance System Based on Crosswalk Recognition by an On-Board Camera, Transactions of Society of Automotive Engineers of Japan, Vol.45,No.2, pp.375-380, 2014

Suzuki, K., Marumo, Y. (2002), A Study on the Onset Timing of Collision Avoidance Assistance Systems for Minimizing the Over-reliance on the System, Transactions of the Japan Society of Mechanical Engineers, Vol.69, No.688, C, pp.96-102

Suzuki, K., Marumo Y. (2003), Study on the Control Algorithm of Driving Assistance System to Inhibit the Over-Dependence on the System, Transactions of the Japan Society of Mechanical Engineers, Vol.70, No.699, C, pp.293-299

Ujihashi, S., Kitaoka, T. (2014), Evaluation of Active Safety Performance of Vehicle and Its Introduction to JNCAP, Vol.68, No.12, pp.12-18

5th AdvancedSafety Vehicle Project, http://www.mlit.go.jp/jidosha/anzen/01asv/resourse/data/asv5 pamphlet.pdf

http://www.nasva.go.jp/mamoru/download/JNCAP_2014_active_safety.pdf

Lane Visibility Check Methods based on High Precision Maps and 3D LiDAR for Traffic Prediction

Eijiro Takeuchi * **Yoshiki Ninomiya** * **Shinpei Kato** *

** Nagoya University, Furo-cho, Chikusa-ku, Nagoya 464-8601, Japan
(e-mail: takeuchi@ coi.nagoya-u.ac.jp).*

Abstract: This paper proposes fast lane visibility check methods for traffic prediction using traffic lane information and measurement information given by range sensor. Especially, this paper describes high accurate positioning method using high density point cloud map, competing lane search method, and fast visibility check method using high precision vector map and 3D LiDAR(Light Detection and Ranging). Finally, this paper illustrates experimental results in urban environments. In this experiment, the proposed method can detect occluded traffic lanes at crossing points, behind of vehicle and slopes.

Keywords: Traffic prediction, Blind area, High Precision Map, Vector Map, Localization.

1. INTRODUCTION

Autonomous driving system and advanced driving assistant system detect obstacles by sensors that are mounted on a vehicle to avoid collision and risks. However, it is difficult to detect approaching vehicles in blind spots caused by buildings, vehicles, and slopes.

On the other hand, it is possible to predict other vehicle behavior in short time using traffic lane map information even if the regions are occluded. Moreover, range sensors such as laser scanner, stereo cameras and so on can check the visibility of traffic lanes. Bayes filter base probabilistic prediction methods (Thrun (2005)) are used to predict traffic on lane network. These methods predict near future probability on traffic lanes using stored traffic data and measurement information.

To update prediction information using traffic lane map and sensor information, it is required to solve two problems. The first one is precise positioning on maps because the visible areas are dependent position on lanes. The next one is computation load to estimate broad area traffic network. To reduce computation load, it is important to find competing traffic lanes that crossing with current lane for real-time assist the driving vehicle.

This paper proposes fast 3D visibility check methods using traffic lane information and 3D measurement information given by range sensor for traffic prediction. Especially, this paper describes high accurate positioning method using high density point cloud map, and fast visibility check methods using high precision vector map and 3D LiDAR. Finally, this paper illustrates experimental results in urban environments. In this experiment, the proposed method can detect occluded traffic lanes at crossing points, behind of vehicle and slopes.

Fig. 1. High density point cloud map measured by MMS

2. LOCALIZATION USING HIGH DENSITY MAP

In this research, high density point cloud map and 3D LiDAR are used for localization. This section describes high accuracy positioning method based on high speed point cloud matching.

2.1 High Density Point Cloud Map

Figure 1 is a part of high density point cloud maps that used in this research for localization. This point cloud map is measured by Mobile Mapping System (MMS) that developed by Mitsubishi Electric Corp. . MMS measures environments using high precision laser scanners and generates maps based on estimated position using RTK-GPS and fiber-optic gyros.

The map is measured around Nagoya university, the total run length is about 33km, the total number of points is 1.2 billion.

2.2 NDT scan matching

The measured point cloud consists over one billion points. Therefore, efficient localization methods are required to realize real-time localization.

Currently, so many point cloud base matching methods are proposed. One of the major matching methods is Iterative Crosest Points method (Besl (1992)). The method find matching parameter (transfrom parameter) to find closest points and minimize these distance. The ICP method requires $O(NM)$ to matching with number of measured points N and number of reference (map) points M. The kd-tree algorithm accelerate it to $O(NlogM)$(Greenspan (2003)). Recently, Moothman proposes fast matching method based on ICP (Mootmann (2011)).

In this research, Normal Distributions Transform (NDT) scan-matching method is used for localization (Biber (2003); Takeuchi (2006)). One of characteristics of NDT scan-matching method is matching speed. The computation complexity of the method is $O(N)$ with number of measured points N(Takeuchi (2006)). The matching speed does not depend on map size.

The NDT scan matching process takes the following steps;

(1) Apply NDT to reference scan .
(2) Read an input scan and set initial tentative position that estimated by previous position and speed.
(3) Transform the input scan by 3-D coordinate transformation.
(4) Select a corresponding ND voxel of each input scan point.
(5) Update the matching parameter by newton's method.
(6) If matching parameter is converged, then go to 7, else 3.
(7) Add transformed input scan to reference scan.
(8) Go to 2.

The first process divides point cloud maps into voxel and approximates point cloud in each voxel to normal distributions. Each ND voxel k are updated average $vctp_k$ and covariance matrix $Sigma_k$ with corresponding points $\boldsymbol{x}_{ki}$ $(i = 0 ... M_k-1)$ (M_k is number of points in ND voxel k).

In matching stage(2-5), the method finds corresponding voxels and maximize evaluation function to find transpose parameters. If input point cloud is $\boldsymbol{X} = \boldsymbol{x}_i$ $(i = 0...N-1)$, then transform equation is as follows;

$$\boldsymbol{x'_i} = \boldsymbol{R}\boldsymbol{x_i} + \boldsymbol{t'}, \qquad (1)$$

Here, $\boldsymbol{t} = (t_x, t_y, t_z, t_{roll}, t_{pitch}, t_{yaw})^t$ is transform parameter as sensor position, R is rotation matrix with $t_{roll}, t_{pitch}, t_{yaw}$, and $\boldsymbol{t'}$ is translation vector (t_x, t_y, t_z)

The evaluation function for input points and transform parameters is

$$E(\boldsymbol{X}, \boldsymbol{t}) = \sum_{i}^{N-1} exp \frac{-(\boldsymbol{x'_i} - \boldsymbol{p}_i)^t \Sigma_i^{-1}(\boldsymbol{x'_i} - \boldsymbol{p}_i)}{2}, \qquad (2)$$

. here, $\boldsymbol{p_i}$ and Σ_i is average $\boldsymbol{p}_{k'}$ and $\Sigma_{k'}$ of ND voxel k' that corresponding with point $\boldsymbol{x'_i}$. The NDT scan-matching method maximize the evaluation function $E(\boldsymbol{X}, \boldsymbol{t})$ using
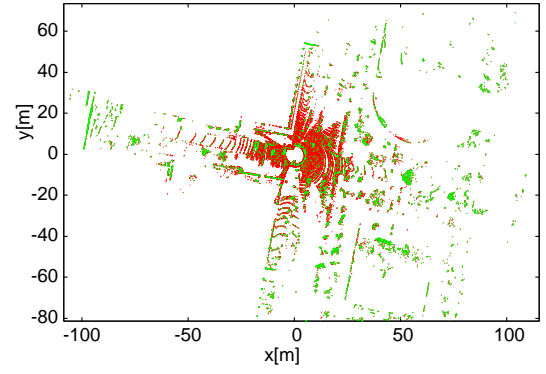
Fig. 2. Points sample results

Newton's method or other non-linear optimization methods.

2.3 Robustness for unknown objects

This section discusses robustness for unknown object In matching process, if the measured data occupied so many unknown objects then the matching process may converge into wrong place. The density of point cloud measured by spinning type laser scanner such as Velodyne HDL 64E-S2 is changed with inverse square distance. Number of points on an object is increased by density of measurement. Therefore, if the sensor measures unknown object in near distance, then the number of unknown points is increase.

One of the solutions to decrease such problems is normalize density of measured points before matching. For example, voxel grid filter normalize density to select one point in each voxel.

This research uses weighting approach to normalize point cloud density. Following equation is normalize weight of point i for matching.

$$w_i = r_i^2(a - e^{\frac{(z_i-h)^2}{\sigma}})$$

here,w_i, r_i, z_i is weight, distance, height of point i, h, σ are mean and variance of height of unknown objects, a is constant value that larger than 1.

Typically, the weight is used in evaluation function. This research uses the weight to sample points to reduce computing speed because the computation speed of NDT scanmatching depends number of input scan points. In this research, input points are sampled by Low variance resamplerThrun (2005) with above weight. This method can select constant number points. Therefore, the computation speed is more stable with environment change than voxel grid filter base point filtering.

Figure 2 and Fig.3 are examples of sampling results. In this figure, red points are measured points and green points are sampled points. In this case, the measured points are reduced in near place(20m), on the other hand, the measured points are remained in far place(100m).

2.4 Localization using pre-measured environment maps

In this research, the environment map is measured by MMS and ego vehicle uses Velodyne HDL64E-S2.

(a) 20m   (b) 100m
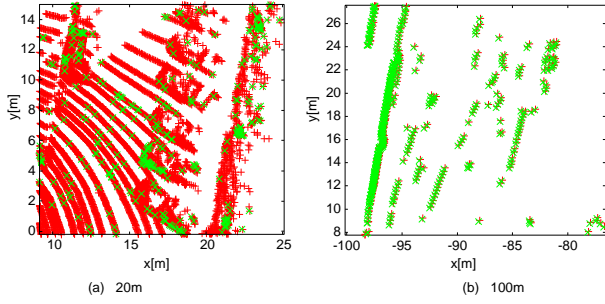
Fig. 3. Points sample results (20m, 100m)
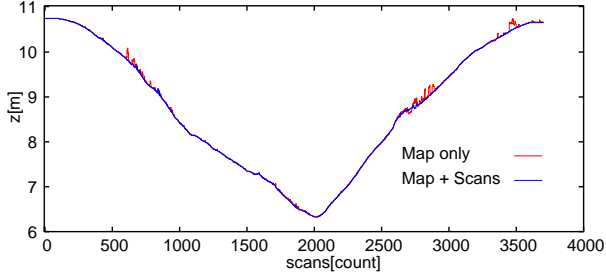
Fig. 4. Estimation error (static map and map with scan data)

Velodyne HDL64E-S2 measures environment by spinning laser scanner. On the other hand, MMS measures environment by fixed laser scanner. Therefore, measured region measured by each sensor are different. Moreover, measured environment is changed with time and measured data includes different objects caused by measured time difference.

This research uses hybrid approach to localize position. Localize position using environment map measured by MMS and mapping measured point by ego vehicle.

When points are added to ND voxel, it is required to calculate mean p_k and covariance matrix Σ_k. Normally, the calculation requires all point information in target ND voxel. This paper uses incremental update method to update ND voxel(Takeuchi (2006)).

Figure 4 illustrates localization results these localized by MMS map only and MMS map and measured points. The lines are estimated height. The experimented environment is smooth slope. The MMS map only case, the height is changed at several places. On the other hand, MMS map and measured points case the height is smooth. This results indicates the map update case decreases position error caused by differences between map and input scan.

2.5 Localization results

Measurement vehicle mounts Velodyne HDL64E-S2 and runs around our university two times about 11km. The measurement is conducted at 7 month after measure environment map. The point cloud map is converted to ND voxel. The voxel size is 1m and total data size is about 2.2GB.

Figure 5 shows localization results(x-y) and Fig. 6 shows height and poses.
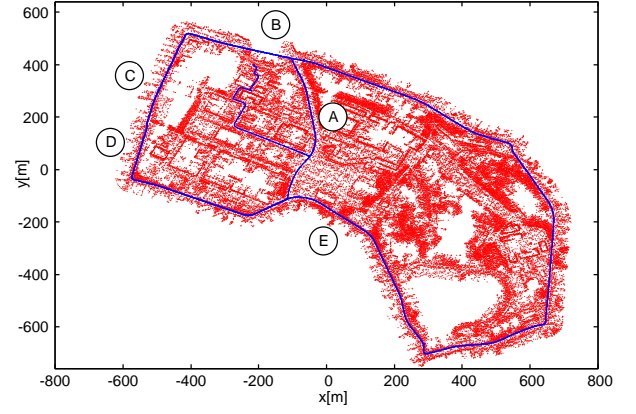
Fig. 5. Estimated results (x,y)
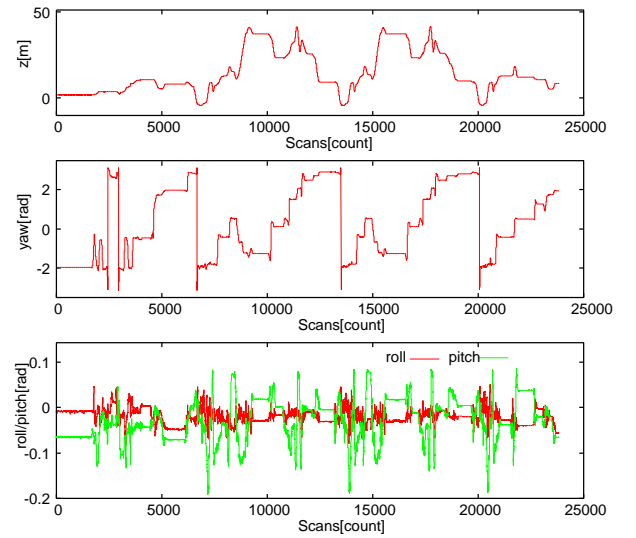
Fig. 6. Estimated results (z,roll,pitch,and yaw)

In this figure, Ⓐ is wide and highly traffic area, Ⓑ is map lack area Ⓒ is residential area   and ⓄⒺ is up-down area. In this case, the localization process is stable. The computation time of scanmatching is under 100ms over all localization. That is enough to compute in real-time with Velodyne HDL64E-S2. As a result, the proposed method in this paper is efficient to localize position in various road.

Figure. 7 is position variance when the vehicle stopped. In this case, the position standard deviation is 0.028, 0.036 on x-y coordinate and angle standard deviation is 0.0004rad. Fig. 8 shows mapping results using localization results. The color is intensity of laser scan. In this case, we can see traffic mark "25". That line width is about 20 cm, therefore, the localization method accuracy is kept with moving.

Figure 9 is zoomed image of Fig. 5Ⓓ. In this figure, the color red, blue, and green is trajectory of each laps. This results shows the accuracy of the localization method is enough to identify the difference of vehicle behavior.
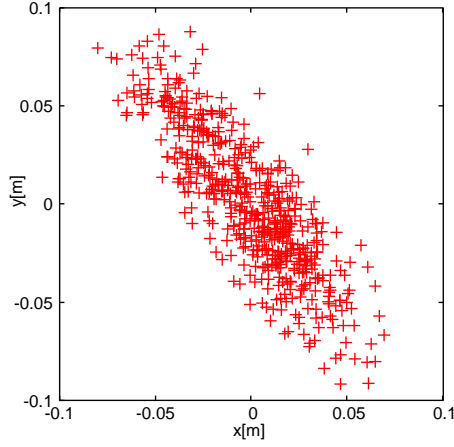
Fig. 7. Estimated position variance
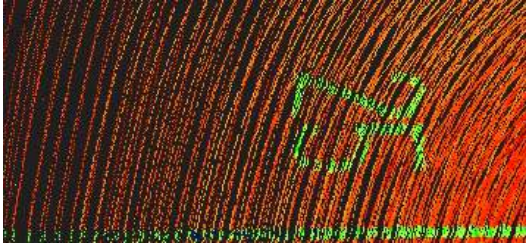
Fig. 8. Intensity image
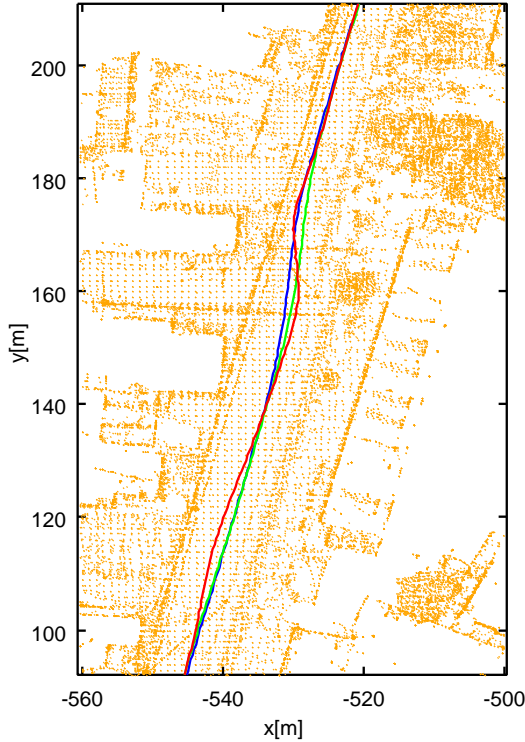
Fig. 9. Trajectories

3. TRAFFIC LANE VISIBILITY CHECK FOR TRAFFIC PREDICTION

This section describes traffic lane visibility check methods for traffic prediction using traffic lane map and range sensors.
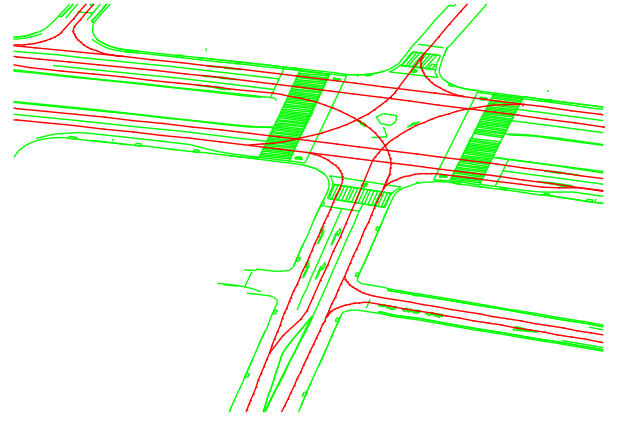
Fig. 10. Vector map (traffic lanes and other line elements)

3.1 Vector maps

Vector maps that describe geometric information and contents are widely used for autonomous driving and advanced driving assist system. The vector map contains traffic lanes, traffic signs, compartment lines, traffic signals and so on. Especially, this research uses traffic lanes information in vector maps.

Figure 10 shows an example of traffic lanes map. The traffic lanes map is directed graph that consists nodes and directed edge.

3.2 Search competing traffic lanes

To reduce unnecessary computation in traffic prediction, the proposed method search competing lanes for the driving car. In this research, competing lanes are lanes that may have vehicles that collide with the ego vehicle in defined time with maximum to minimum speed.

The proposed method searches competing lanes with following method (Fig. 11). At first, the method searches crossing points on current driving lane in length s_e (gray circles in Fig. 11). Next, back trace the crossing lanes in length of ways s_o (black circles in Fig. 11).

The length of ways s_e and s_o are calculated with following collision equations;

$$tv_e = tv_o$$

here, t is collision time, v_e is ego vehicle speed, and v_o is other vehicle speed. The conditions of these parameters are

$$V_{min} < v_e < V_{max}, \quad V_{min} < v_o < V_{max}$$

and

$$0 < t < t_{max}.$$

On the above conditions, the maximum distance of crossing point from current position is $s_e = t_{max}V_{max}$ and the maximum collision time t at crossing points is $t = min(max(s/V_{max}, s/V_{min}), t_{max})$. If the V_{min} is enough small then $t = t_{max}$, and the maximum distance of target lanes is $s_o = tv_{max} = V_{max}t_{max}$. As a result, the search length s_e and back trace length s_o are fixed value.
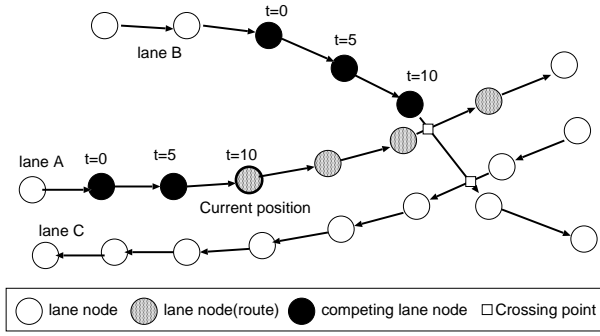
Fig. 11. Target lane search
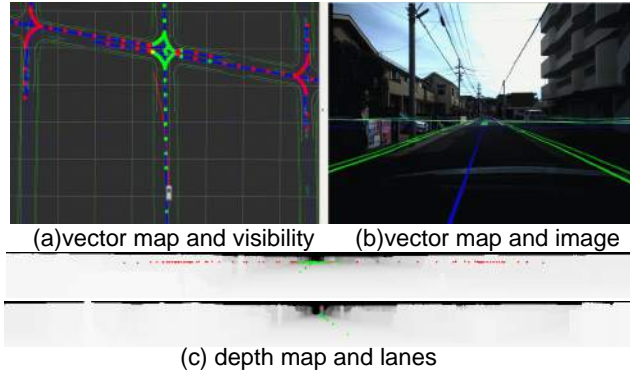
Fig. 12. Visibility update results at near crossing point in residential area.

3.3 Traffic lane visibility check using range sensor

Typically, the visibility check is nearest neighbor search problem between a measurement line and target point, and the computation complexity is $O(LM)$ in pure implementation. However, the number of measurement M and the number of target lane nodes L are large. In this research, depth map is used to check the visibility to improve search time. The check method is as follows;

(1) calculate depth map from velodyne point cloud,
(2) calculate position of target lanes on depth map, and
(3) compare the depth value between target lane and depth map.

If the depth value of target lane is smaller than depth map, then the lane is visible. As a result, the computation complexity is $O(L + N)$ and it is enough to calculate in real-time

In avobe process, created depth map from point cloud that measured by laser scanner lacks some pixels caused by rounding error. In this research, all pixels are filled by minimum distance in upper pixels to fill lacked pixels.

Figure 12 shows example of visibility check. The figure (a) is vector map and visibility and (b) is vector map and camera image. The green lines are vector map, green points are visible lanes, and red points are invisible lanes. The figure (c) is depth map and mapped lane nodes. In this figure, green points indicates the distance is smaller than depth map, and red points are the distance is larger than depth map.
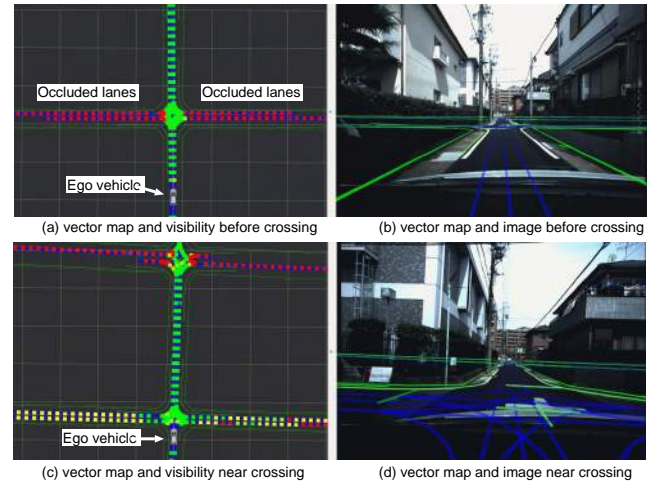
Fig. 13. Lane visibility in residential area.
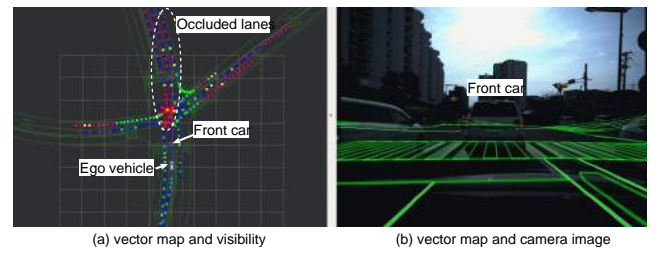
Fig. 14. Lane visibility in crossing with front vehicle.
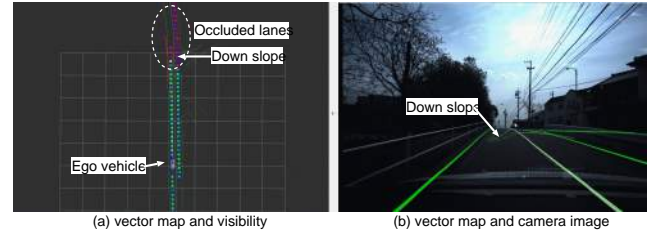
Fig. 15. Lane visibility at up-down slope.

4. EXPERIMENTS

4.1 Visibility at various scenes

Figure 13 shows visibility of lanes at far from crossing and near from crossing point. Fig.13 (a)(c) is vector map and calculated visibility using proposed method. In this figure, green lines are vector map, green points are visible lane, red points are invisible lanes. Fig.13 (a)(b) is visibility at far from crossing. In this case, the crossing lane is almost occluded by buildings and the lanes are estimated "invisible". Fig.13 (c)(d) is visibility at near from crossing. In this case, almost crossing lane is visible.

Next example is occluded by front car. Fig. 14 is case of right turn and opposite lane is occluded by front vehicle. In Fig. 14, occluded lanes are estimated to invisible.

Final examples are updown slope. Fig. 15 is before down slope, and Fig. 16 is approach to down slope. In Fig. 15 case, the front lanes are occluded by road. On the other hand, Fig. 16 case is almost visible.

These results illustrate the proposed method finds risky lanes and detects occluded lanes using laser scanner. The

(a) vector map and visibility   (b) vector map and camera image
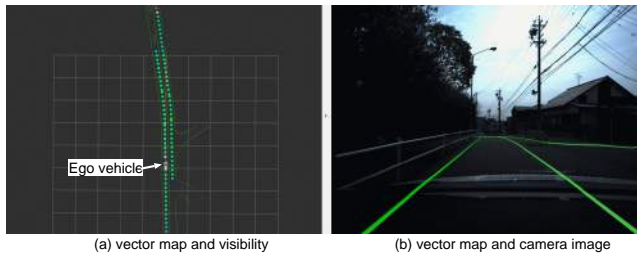
Fig. 16. Lane visibility after up-down slope

(a) far from crossing point   (b) near crossing point
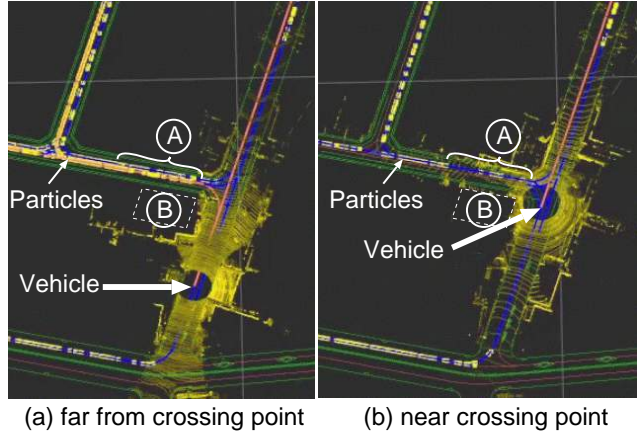
Fig. 17. Visibility update results at near crossing point in residential area.

results can be used for measurement model for traffic prediction.

4.2 Traffic prediction

The proposed method is applied to traffic prediction method using particle filter. The Fig. 17 is one of results of experiments in this research with proposed methods. The experimental environments are residential street and velodyne HDL64E-S2 is used as range sensor. The number of particles was 10000 and updated in real-time. The Fig. 17(a) shows the vehicle is far from crossing point. In this scene, the lane Ⓐ is filled by particles because the vehicle can not see the area that occluded by building Ⓑ. On the other hand, the Fig. 17(a) shows after approaching to crossing point. In this scene, the particles on lane Ⓐ are cleared by measurement.

5. CONCLUSION

This paper proposes fast lane visibility check method using high precision environment maps and LiDAR. To check lane visibility, this paper proposes these three methods. The first one is localization method using NDT scan matching. The localization method can localize position accurately in wide area. The next one is competing lanes finding method. The method finds competing lanes to predict lanes and find crossing lanes. The important point is the method can reduce unnecessary lanes such as opposite lanes. The final one is visibility check method using depth map. The depth map base visibility check enables $O(L+N)$ computation complexity with number of lane nodes L and number of input points N. Finally, this paper conducts experiments in real traffic. These experiments illustrates

the proposed method can find occluded lanes at crossing, right turn scene, and up-down slope;

In future work, we will apply proposed method to probabilistic traffic prediction for safety driving.

REFERENCES

S. Thrun, W. Burgard, D. Fox: "Probabilistic Robotics", Mit Press, 2005.

Paul J.Besl and Neil McKay: "A Method for Registration of 3-D Shapes", IEEE Transactions on Pattern Analysis and Machine Intelligence, Vol.14, pp. 239–256, 1992.

Michael Greenspan and Mike Yurick: "Approximate K-D Tree Search for Efficent ICP", Proceedings of the Fourth International Conference on 3-D Digital Imaging and Modeling, 2003.

Frank Moosmann and Christoph Stiller, "Velodyne SLAM",2011 IEEE Intelligent Vehicles Symposium (IV), pp.393–398, 2011.

Peter Biber and Wolfgang Straßer: "The Normal Distributions Transform:A New Approach to Laser Scan Matching", Proceedings of the 2003 IEEE/RSJ International Conference on Intelligent Robots and Systems, pp. 2743–2748, 2003.

Eijiro Takeuchi, and Takashi Tsubouchi, "A 3-D scan matching using improved 3-D normal distributions transform for mobile robotic mapping", Proceedings of the IEEE International Conference on Intelligent Robots and Systems(IROS), pp. 3068 -3073, 2006.

Alberto Elfes: "Using Occupancy Grids for Mobile Robot Perception and Navigation", Computer,Volume:22,Issue:6,pp.46–57.

A. Hornung,. K.M. Wurm, M. Bennewitz, C. Stachniss, and W. Burgard, "OctoMap: An Efficient Probabilistic 3D Mapping Framework Based on Octrees" Autonomous Robots, 2013.

Acoustic/Lidar Sensor Fusion for Car Tracking in City Traffic Scenarios*

Hamma Tadjine * **Daniel Goehring** **

* IAV GmbH, Carnotstraße 1, Berlin, 10587, Germany (e-mail: Dr.Hadj.Hamma.Tadjine@iav.de).
** Freie Universität Berlin, Arnimallee 7, 14195 Berlin (e-mail: daniel.goehring@fu-berlin.de)

Abstract: In this paper we describe a sound source localization approach which, in combination with data from lidar sensors, can be used for an improved object tracking in the setting of an autonomous car. After explaining the chosen sensor setup we will show how acoustic data from two Kinect cameras, i.e., multiple microphones, which were mounted on top of a car, can be combined to derive an object's direction and distance. Part of this work will focus on a method to handle non-synchronized sensory data between the multiple acoustic sensors. We will describe how the sound localization approach was evaluated using data from lidar sensors.

Keywords: Sound source localization, Autonomous driving, Sensor data fusion.

1. INTRODUCTION

The ability to quickly detect and classify objects, especially other vehicles within the surrounding is crucial for an autonomous car. However, cluttered environments, occlusions and real-time constraints under which autonomous vehicles have to operate let this task remain a key-challenge problem. In recent years, tremendous progress has been made in the field of self-localization, world modeling and object tracking, mainly thanks to lidar, radar, and camera based sensors but also because of algorithmic advances, e.g., how to model uncertainties [Thrun (2005)] and how to apply these methods to sensor fusion [Schnuermacher (2013)], or how to train object classifiers using machine learning techniques [Mitchell (1997)]. In the past, acoustic sensors have played a minor part in robotics, especially in autonomous driving or for outdoor robotics in general only. One reason for this might be the omnipresent noise in most city road traffic and outdoor scenarios and the domination of other sensors like lidar, camera, or radar. In this paper we want to present how an autonomous vehicle can localize other vehicles in a real-world road-traffic environment. For this task we wanted to use low-cost off-the-shelve microphone arrays like the ones provided in a Microsoft Kinect camera. Since it is usually hard to determine the euclidic distance to an object with acoustic data, we will to focus on angular direction approximation. This data can still be very helpful, especially when combined with data from other sensors, e.g., lidar data from laser scanners. One possible scenario, even though not pursued in this work, would be to localize the direction at which an emergency vehicle was detected and then to assign this direction to a tracked object using lidar data. Another challenge in our scenario are the moving sound sources

and comparably high velocities of other vehicles, in addition to temporarily occluded, emerging and disappearing vehicles. The presented solution was implemented on a real autonomous car using the OROCOS realtime robotics framework. For evaluation of the algorithm the acoustic data were synchronized and evaluated with lidar objects from Ibeo Lux sensors.

2. RELATED WORK

A lot of progress for sound source localization has been achieved in the speech and language processing community, as in [Benesty (2007)] on beam-forming methods, or for dialog management [Frechette (2012)].

In the robotics community and especially for indoor robots there are a variety of publications on sound source local-

Fig. 1. Test Car MadeInGermany from Freie Universität Berlin, the Kinect devices were placed on top of the roof, in front of the Velodyne HDL 64 lidar sensor.
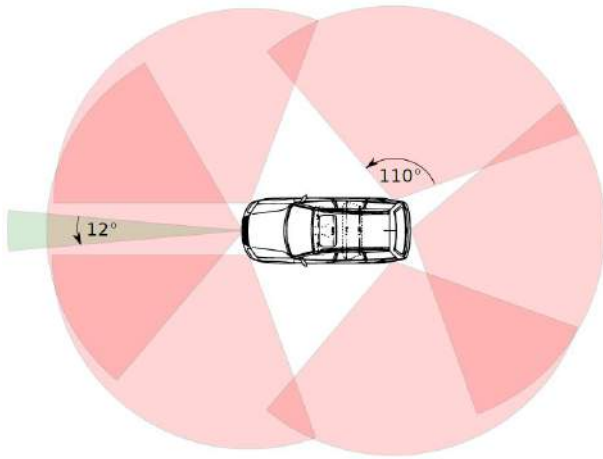
Fig. 2. The six fields of view for the six lidar sensors Lux from Ibeo and one of the radar sensors are shown, facing to the front.

ization available. The interaural time difference method (IDT) has been widely applied, as in [Liua (2010)]. In [Liu (2010)] and in [Li (2012)] the generalized cross-correlation function (GCC) is extended to localize different sound sources using an array of four different microphones. A further approach unsing a four-microphone-array in a room and time-delay estimates is provided by [Pineda (2010)], with focus on a geometric analysis and under optimization criteria. In [Valin (2003)] and in [Valin (2004)], a robot with 8 microphones was used to localize moving sound sources. The work of [Markowitz (2014)] gives a broader perspective on how people can interact with robots by using speech.

This paper is structured as follows: Section 3 will introduce the accoustic sensor setup and setup of lidar sensors, which will be used to evaluate the presented approach. Section 4 will describe the applied and implemented algorithms with an emphasis towards the sensor fusion method in this approach. In Section 5 we will perform experiments and present the results. Section 6 will summarize the approach and will give an outlook for future work.

3. SENSOR SETUP

As a test platform, we used the autonomous car named "MadeInGermany" from Freie Universität Berlin, cf. Fig. 1. The car is fully equipped with a combined lidar system from Ibeo, including 6 laser scanners, as shown in Fig. 2, a second 64 ray lidar sensor from Velodyne, in addition 7 radar sensors for long and short distance perception, at least 5 different cameras for lane marking and traffic light detection, including a stereo camera system for visual 3D algorithms, and a highly precise GPS unit. The car can be operated via a CAN-bus interface, thus, no further actuators are necessary to operate the throttle or brake pedals.

Different configurations were tried for the Kinect camera devices. To be independent from rain or snow and also to avoid wind noise while driving, we would have preferred to put the acoustic sensors inside the car. Unfortunately, the disadvantage of this configuration would have been the weaker signal strengths as well as signal reflections inside

the vehicle. Therefore, we decided to mount both Kinect devices outside on the roof of the test platform, see Fig. 3.

(a)

(b)
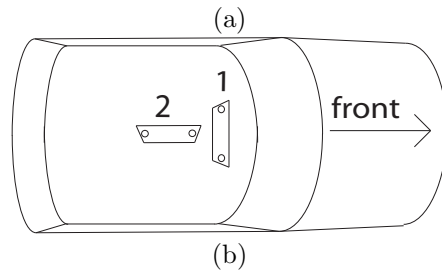
Fig. 3. Kinect sensor setup. (a) the device in the lower left corner is facing to the front of the car, the other one to the left. (b) View from above.

3.1 Kinect Sensor

Each Kinect sensor is equipped with four different, non-equally spaced microphones which are aligned in line, cf. Fig. 4. As a result of this configuration, only pairs of microphones are linearly independent. To achive the highest precision for an angle estimation, we decided to use the two microphones with the largest distance to each other, i.e., the two outer microphones on the left and right side of the Kinect device, depicted in Fig. 4. Another advantage is that the signal strength for those microphones is almost equal. This is not necessarily true for the inner two microphones which are located more inside the kinect case.
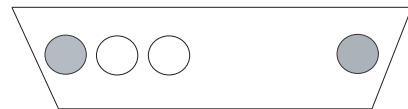
Fig. 4. Kinect microphone configuration, 4 mics are aligned in a line, we used to two outer mics (gray).

In the next section we want to describe how the sound source estimation and sensor fusion of the two Kinect devices was implemented.
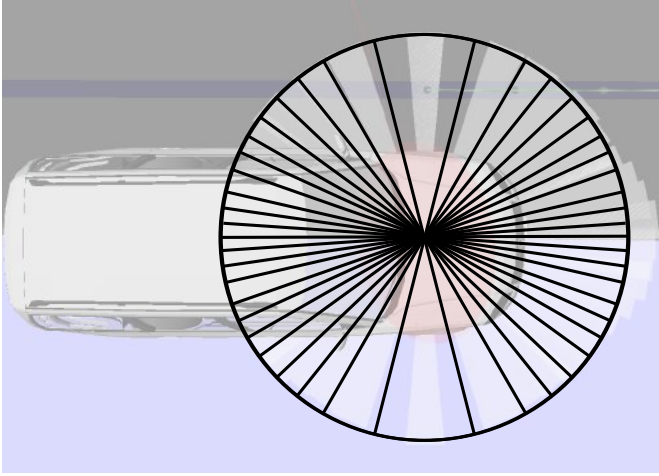
Fig. 5. Each shift between the two microphone signals corresponds to a segment (an interval) of possible angles, given that shifts can take only integer values.

4. SOUND SOURCE LOCALIZATION

In this section we are going to show how to localize an object using two microphones only. Furthermore we will focus on the direction accuracy given all possible directions. In the second part we will show how the resulting angular probabilistic distribution functions of two Kinect devices can be combined. One advantage of this method will be to constrain the set of possible solutions.

4.1 Calculation for one Kinect with two microphones

Estimation of the sound source using two microphones was designed straightforward using a cross-correlation function over the two microphone signals. Given the signal of the left microphone f and the right one g, for a continuous signal the cross-correlation function $f \star g$ with respect to the shift τ can be calculated as:

$$(f \star g)(\tau) = \int_{-\infty}^{\infty} f(t) \cdot g(t + \tau) \ dt \qquad (1)$$

Since we handle digital signals, for discrete functions the cross-correlation is calculated similarly with respect to a given shift n between the two signals f and g:

$$(f \star g)[n] = \sum_{-\infty}^{\infty} f[m] \cdot g[m + n] \qquad (2)$$

Now we want to take a look at the real Kinect audio signals. Both Kinect microphones were sampled with 16800 Hz. For every calculation step we compared 216 data points from the two signals with a shift n ranging from -20 to +20. These 216 data points (provided by a module including the open source libFreenect library) showed to be sufficient for the cross-correlation calculation and allowed us to estimate the sound direction with more than 70 Hz. Each shift between the two signals would result in a certain direction. Regarding the number of possible shifts between the two signals, the two outer microphones of the Kinect are about 22 cm apart, we therefore assumed a base distance of $b = 0.22m$. With the speed of sound at $v_s = 340\frac{m}{s}$ at sea level and with a sampling rate for each microphone of $f_k = 16800Hz$, there is a maximum and a minimum value for possible shifts. These two boundaries

correspond to the sound source being perfectly on the left or on the right side of the device. The maximum and minimum shift can be calculated as:

$$n_{max} = b \cdot f_k \cdot v_s^{-1} \qquad (3)$$

$$= \frac{0.22m \cdot 16.8kHz}{340ms^{-1}} \qquad (4)$$

$$\approx 11 \qquad (5)$$

$$n_{min} = -b \cdot f_k \cdot v_s^{-1} \qquad (6)$$

$$\approx -11 \qquad (7)$$

, resulting in approx. 22 possible values for shifts, making it sufficient to check these 22 possible shifts. As we will see later, on a planar surface with two microphones there are ususaly two solutions for each signal shift (except for $n_{min} = -11$ and $n_{max} = 11$). Thus, we can map each shift n to two angular segments (angular intervals) which are symmetrically located with respect to the connecting line between the two microphones. The angular segments (or intervals) are depicted in Fig. 5.

The calculation of the corresponding angle for a given signal shift is straightforward, too. Given the speed of sound v_s we can translate each shift n into a distance $n \cdot v_s$. Now we have a triangle with a base length of $b = 0.22m$ and a known difference of the two other sides of $n \cdot v_s$ towards each other. Since the real distance to the sound source is unknown, we have to make an assumption, e.g., 25 m (the result of the calculation converges for higher distances) and can solve the angle to the object for each microphone using the Law of Cosines. A geometric sketch of the triangle is shown in Fig. 6.
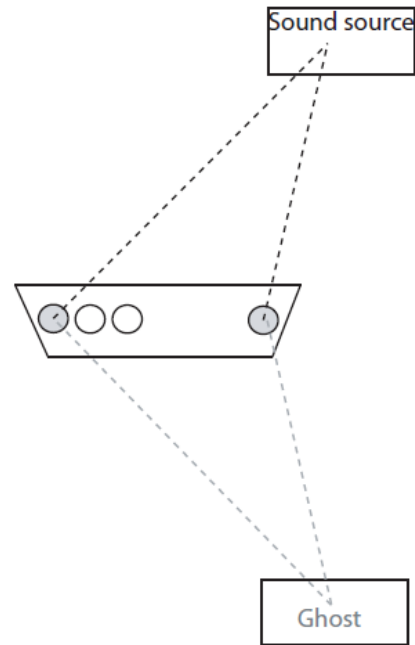
Fig. 6. Given the base distance of the triangle, the difference of the two sides and an assumed far distance (for drawing reasons the distance here is very close) to the object, the angles of the object to each microphone can be calculated - and should converge with increasing distance. Two solutions remain.
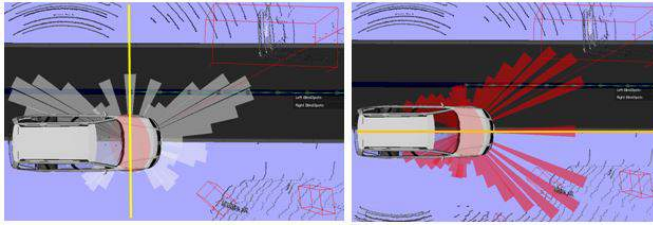
Fig. 7. Symmetry of angular distribution for front facing Kinect (left) and sideways facing Kinect (right). Symmetry axis depicted in yellow.

4.2 Sensor fusion of two Kinect devices

Since the two Kinect devices are not synchronized, we cannot just combine the data of the four outer microphones for triangulation. Moreover, we decided to combine the resulting probability distributions, cf. Fig. 5 of the Kinect devices with each other. As mentioned earlier, the probability of each segment containing the angle to the sound source is calculated from the cross-correlation function. Since both Kinect devices are rotated to each other by 90 degrees, the segment sizes do not match and thus cannot be combined directly. To overcome this problem, we subsample the angular segments for each Kinect with 64 equally-spaced angular segments. In a next step, after we generate the two equally spaced angular segment sets, we can combine them by pairwise multiplication of the probabilities of two corresponding segments, i.e., segments that contain the same angles. As a result of this combination via multiplication, we get a final segment set which represents the resulting probability distribution for both Kinect sensors (belief distribution). While each Kinect device alone cannot distinguish between objects in front and objects behind (see symmetry depictions in Fig. 7), after combination with the second sensor, those symmetries vanish. We show the calculation schematically in Fig. 8 and a step by step calculation with experimental data in a real traffic scenario in Fig. 9.
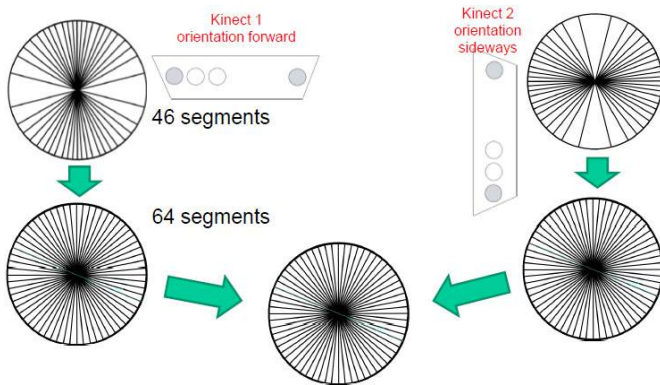
Fig. 8. Schemtatic calculation. The upper two segment sets result from the two different Kinect sensors. Since the segment sizes of the two sets are not equally aligned with respect to each other, we need to subsample them seperately into two segment sets with 64 equally sized segments. In a next step, they can be combined via pair-wise multiplication into a final segment set.

After sensor fusion, the resulting segment set corresponds to a probability distribution (belief distribution) of pos-
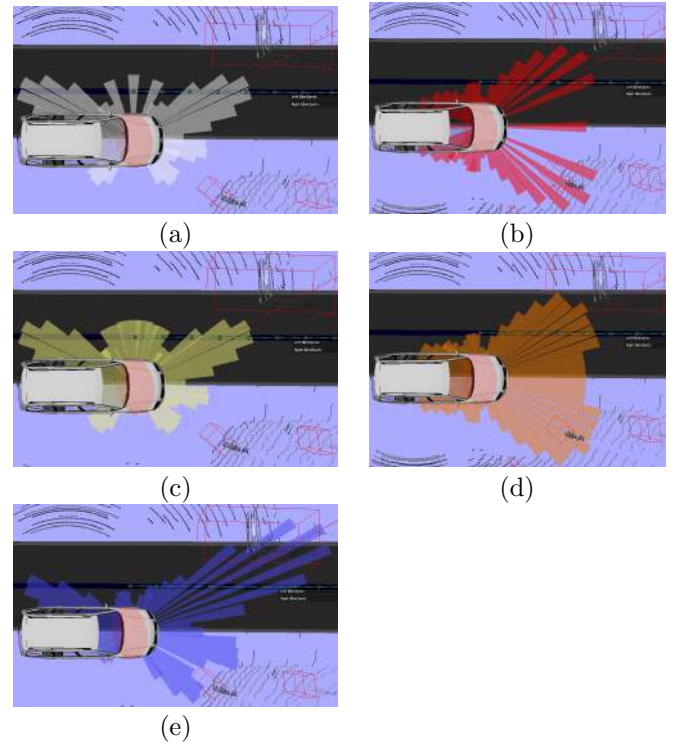
Fig. 9. Illustration of the approach, sound source vehicle in the upper right corner. Segment lengths correspond to cross-correlation amounts of the underlying signal shift and can be interpreted as a probability for the sound source lying in that angular interval. (a) Non-uniform segments for front facing Kinect and (b) left facing Kinect; (c) uniform (equally spaced) segments for front facing Kinect after subsampling, (d) uniform segments for left facing kinect; (e) uniform segments after combining (c) and (d), the resulting probability distribution (belief) for the sound source direction.

sible directions, i.e., where the sound source is located. To calculate a discrete value for the most likely direction, we selected the segment with the highest probability value assigned and took the mean value of that particular segment as the resulting angle. There would have been more sophisticated methods, e.g., integrating over different segments; also we thought about how to calculate directions to multiple sound sources but left this open to future research work.

5. EXPERIMENTAL EVALUATION

As mentioned above, the proposed algorithm was implemented for our autonomous vehicle and tested in a real traffic scenario. The algorithms were tested within a modular robotics framework, the Open Robot Control Software Project Orocos (2011) under an Ubuntu 12.4. 64bit operating system. The data from both Kinect sensors were integrated into our AutoNOMOS software project and time stamped to compare them with our lidar sensory data. The six lidar Lux sensors from Ibeo run with a frequency of 12.5 Hz, the Kinect sensors ran with 70 Hz.

5.1 Test scenario

We tested our approach in a Berlin traffic scenario, close to the campus of the Freie Universität Berlin. Because driving the car was causing a lot of wind noise, we decided to park the car on the road side of the Englerallee, a medium-sized traffic road with trees, parked cars and houses on the side. Vehicles on the street were maintaining a velocity of 50-60 km/h (approx. 35 mph). Since there are trees on the middle strip seperating the two road lanes, cars of the more distant lane were partially occluded by trees while passing. We were interested in the angular accuracy of our approach in comparison to object angles from the lidar sensor. Therefore, data from the lidar sensor (a point cloud) was clustered into 3d-objects and tracked over time, resulting in a position and velocity vector for all clustered lidar objects. Since we were interested in moving (non-static) objects only, we compared the calculated angle from audio data to the closest angle of a moving object (from lidar).

5.2 Experimental results

In Fig. 10 we evaluated the angular error over time. We therefore took more than 5000 measurements, the resulting error-over-time function is depicted in Fig. 10.
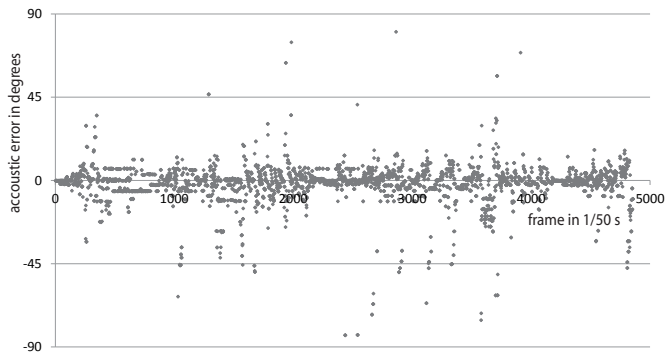
Fig. 10. Experimental evaluation: Difference between the angle from Kinect data to lidar data over time, 5000 data points were recorded. The standard deviation for the difference is $\sigma = 10.3$ degrees.

We also plotted the angular errors over all distances to the objects, as can be seen in Fig. 11. What is interesting, the highest angular errors occurred not for the farest objects but for objects within medium distances. One explanation could be that objects very far away would occupy a very small angular segment in the laser scanner, while objects closer occupy larger angular segments. Since the laser scanner always takes the center point of the detected object as a reference, and since the Kinect sensor will receive the loudest noise from the closest part of the vehicle, which is usually not the center of a car but the approaching front or leaving rear, this might be one reason for an increased detection error. Another reason could be increased reflection of noise on houses or trees for certain distances, which need further analysis.

In Fig. 12 we plotted the standard deviation of the angular error for different distance intervals, which showed the same result in terms that medium distances generated the highest error rates. The calculation time of the algorithm
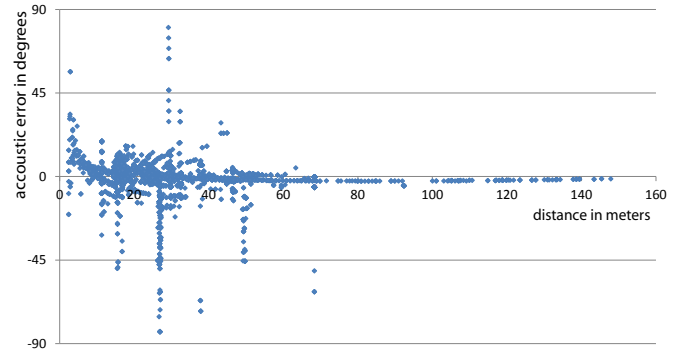
Fig. 11. The angular error over different object distances (measured by lidar). Higher error rates occured for medium distanced objects.

was negligible so that all experiments were performed under realtime constraints
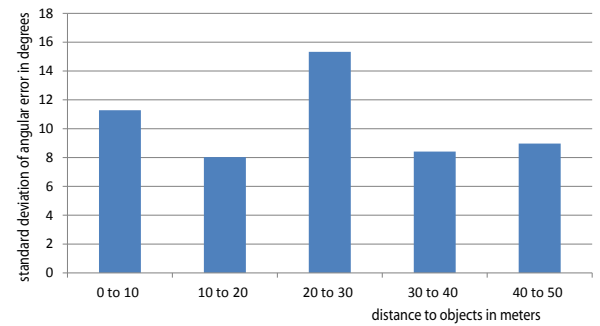
Fig. 12. Angular detection error for different distance intervals. While for high distances the angular error standard deviation was about 9 degrees, for medium distances it was approx. 15 degrees.

6. CONCLUSION

We presented, implemented and tested an approach which allows a road vechicle, equipped with to off-the-shelve Kinect cameras to localize objects in a distance of up to 50 meters and with a velocity of 50-60 km/h. We showed how to combine probabilistic density functions from two Kinect microphone devices using equally spaced angular interval segment sets, which helped to disambiguate possible angular locations while keeping the whole belief distribution. The algorithm can easily perform under real-time constraints with a frequency of 70 Hz. We also showed how the acoustically derived angle to the sound source could be assigned to moving objects from lidar sensors.

6.1 Future work

Future work needs to focus on localization and tracking of multiple objects, since in real traffic scenarios there are usually multiple vehicles in close proximity. Handling wind noise will be a crucial and challenging task for sound localization while in motion. Noise reflections on trees,

buildings and cars provide another challenge. Distance estimation, at least to some extend could support the data fusion problem with objects from other sensors. Band pass filters, e.g., application of Fast Fourier Transformation (FFT) shall be considered in future works. FFT can help to select specific signals, e.g. emergency vehicles with certain signal horn frequencies and signal patterns. Here the detection of alternating sound frequencies, as for emergency horns, would be helpful, too. Another research path worth following could be acoustic object tracking and velocity estimation, taking advantage of the doppler effect, i.e., the change of a frequency spectrum for an approaching or leaving vehicle.

REFERENCES

J. Benesty, J. Chen, Y. Huang, J. Dmochowski: On microphone-array beamforming from a mimo acoustic signal processing perspective. *In: IEEE Transactions on Audio, Speech and Language Processing*, 2007.

M. Frechette, D. Letourneau, J.-M. Valin, F. Michaud: Integration of Sound Source Localization and Separation to Improve Dialog Management on a Robot. *In: Proceedings of the IEEE/RSJ International Conference of Intelligent Robots and Systems (IROS)*, 2012.

Xiaofei Li, Maio Shen, Wenmin Wang, Hong Liu: Real-time Sound Source Localization for a Mobile Robot Based on the Guided Spectral-Temporal Position Method, *In: International Journal of Advanced Robotic Systems*, 2012.

Hong Liu: Continuous sound source localization based on microphone array for mobile robots, *In: Proceedings of the IEEE/RSJ International Conference of Intelligent Robots and Systems (IROS)*, 2010.

Rong Liua and Yongxuan Wanga: Azimuthal source localization using interaural coherence in a robotic dog, *In: modeling and application, Robotica / Volume 28 / Issue 07, Cambridge University Press*, December 2010.

Markowitz: Robots that Talk and Listen, *Technology and Social Impact*, 2014.

Tom Mitchell: Machine Learning, *McGraw Hill*, 1997.

J. Murray, S. Wermter, H. Erwin: Auditory robotic tracking of sound sources using hybrid cross-correlation and recurrent networks, *In: Proceedings of the International Conference on Intelligent Robots and Systems (IROS)*, 2005.

Open Robot Control Software Project *http://www.orocos.org/*, 2011.

Xavier Alameda Pineda, Radu Horaud: A Geometric Approach to Sound Source Localization from Time-Delay Estimates, *In: Robotica*, 12/2010.

M. Schnrmacher, D. Ghring, M. Wang, T. Ganjineh: High level sensor data fusion of radar and lidar for car-following on highways, *In: Recent Advances in Robotics and Automation*, 2013.

S. Thrun, W. Burgard, D. Fox: Probabilistic Robotics, *MIT Press*, 2005.

J.-M. Valin, F. Michaud, J. Rouat, D. Letourneau: Robust Sound Source Localization Using a Microphone Array on a Mobile Robot, *In: Proceedings of the International Conference on Intelligent Robots and Systems (IROS)*, 2003.

J.-M. Valin, F. Michaud, B. Hadjou, J. Rouat: Localization of Simultaneous Moving Sound Sources, *In: Proceedings of the IEEE International Conference on Robotics and Automation (ICRA)*, 2004.

Micro-Scale Traffic Simulator for Analyzing Mutual Interference between Personal Mobility Vehicles and Traffic Flow

Tetsuya Kaneko*, Ichiro Kageyama **,
Yukiyo Kuriyagawa **Tetsunori Haraguchi***

*Department of Mechanical Engineering for Transportation, Faculty of Engineering, Osaka Sangyo University,
3-1-1 Nakagaito, Daito, Osaka, Japan (Tel: +81-72-875-3001; e-mail: kaneko@ tm.osaka-sandai.ac.jp).
**Department of Mechanical Engineering, College of Industrial Technology, Nihon University,
Chiba, Japan (e-mail: kageyama.ichiro@nihon-u.ac.jp) (e-mail: kuriyagawa.yukiyo@nihon-u.ac.jp)
*** Green Mobility Collaborative Research Center, Institute of Innovation for Future Society,, Nagoya University,
Nagoya, Japan, (e-mail: haraguchi@coi.nagoya-u.ac.jp)

Abstract: The personal mobility vehicle (PMV) described in this paper has typical biomimetic characteristics, which incline the vehicle body inside a curve. Because the behavior of this vehicle is similar to that of a two-wheeled vehicle, it is necessary to examine the PMV and the potential for interference with other vehicles in the midst of ordinary road traffic. Therefore, we simulated the vehicle dynamics (including a driver model and a road transportation system) and analyzed the results to ensure the PMV's compatibility with micro-scale traffic flow.

Keywords: Personal mobility vehicle, Traffic simulator, Vehicle dynamics, Risk potential, Modeling

1. INTRODUCTION

In recent years, the ratio of passenger cars to all automobile registrations in Japan has exceeded 74%, and the ratio of owner-driven cars to all passenger cars has exceeded 90%. Although public transportation options, such as trains, buses, and subways, are widely used in Japan, owner-driven cars are one of the most important means of transportation. In addition, the proportion of households in Japan consisting of 1–2 persons has risen to more than 50% of the total households, and this proportion continues to grow. Related to this trend is the gradual decrease in the boarding rate per single vehicle, which is currently approximately 1.3 persons per passenger car.

Furthermore, the number of young Japanese people interested in owning passenger cars is gradually decreasing. It has been noted in the literature that one of the reasons for this decrease is that young people derive little pleasure from driving cars. It appears that the stress of driving is one of the important elements that should be taken into consideration in the design of vehicles for young people.

Given this situation, it is desirable to develop personal mobility vehicles (PMVs) to save both energy and space (i.e., road space and parking space). It is also important to develop personal mobility vehicles for individual users, especially in urban areas.

The PMV we propose in this paper has a large rolling motion, like that of other types of two-wheeled vehicles. This vehicular motion differs from ordinary vehicles, and thus, it is necessary to confirm its applicability for drivers. In this study, we examined the vehicle and its compatibility with drivers using a vehicle dynamics simulation. We also explored the construction of a human–machine system that would be most suitable for this vehicle.

It was also necessary to examine the potential for the PMV to interfere with other vehicles in ordinary road traffic. Therefore, we analyzed it by simulating vehicle dynamics, including a driver model and a road transportation system, to ensure the PMV's compatibility with micro-scale traffic flow.

2. MOTION CHARACTERISTICS OF A PMV

The shape of the PMV examined in this study was designed to have a short wheelbase and short tread base to minimize the space it would occupy in road traffic. Because there is a limit on the height of a vehicle that will ensure the comfort of the driver, the size of the vehicle plane is relatively large value. Thus, the center of gravity is relatively high, and the risk of rollover is assumed to constrain the turning behavior, as with a normal car. Therefore, with respect to turning
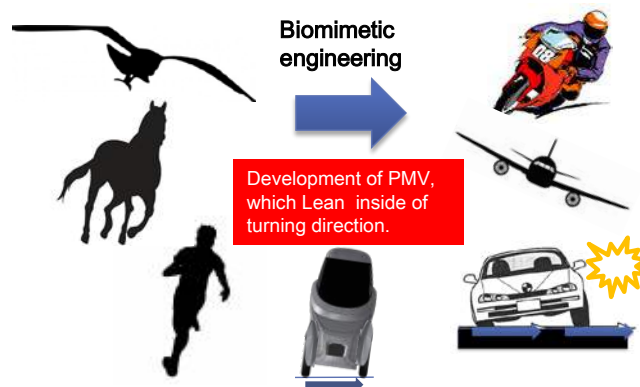
Fig. 1. Biomimetic engineering for vehicles

stability, a vehicle with the motion modality of a motorcycle, which leans dramatically inward during turning, is effective.

Most land-dwelling creatures in motion lean in toward the direction of turning, as shown in Fig. 1. For the vehicle investigated in this study, this biomimetic behavior was taken into consideration, and the motion modality of the vehicle is thought to be appropriate to produce a natural human driving sensation. One of the reasons that two-wheeled vehicles are selected as typical lightweight vehicles is that they provide driving pleasure.

In the motion performance of the vehicle considered in this study, the utilization ratio between the camber thrust and the cornering force is dominant in the tire balance, with the centripetal force being an important element.

In addition, it is necessary to examine the characteristics of both sides of the human–vehicle system because these greatly affect the maneuverability of the driver.

Figure 2 shows a simplified figure of the motion of the vehicle dynamics model with leaning motion. In these vehicles, changing the balancing position of the suspension on the left and right controls the roll angle of the vehicle. Cornering forces and camber forces at the front and rear tires are used on such vehicles for centripetal force.

The relationship between the roll angle of the body and the tire camber angle during roll motion control is illustrated in Fig. 3. In this figure, φ is the roll angle of the vehicle body, and φ_t is the camber angle of the tires. This relationship is an important factor in the vehicle motion performance. The PMV described in this paper has lean-with characteristics.

With respect to direction control of the proposed PMV, roll angle control and steering wheel angle control operations are two inputs to the system. Furthermore, it is necessary for the driver to operate an accelerator and brakes at the same time to control these two input systems independently. This requires very complicated maneuvering and a high load on a general driver. Therefore, we unified these relationships into one input for the steering control, expressed by the following relation.

$$\phi = k(v, \delta_{SW}) \cdot \delta_{SW0} \tag{1}$$

where k is the steering ratio, defined as a function of the vehicle velocity and the steering wheel angle. This function is the most important factor in the maneuverability of the vehicle by the driver. We constructed a driving simulator for the PMV, illustrated in Fig. 4, to explore how to optimize the input parameters.

3. COMPONENTS OF THE TRAFFIC SIMULATOR

3.1 Modeling of PMV Dynamics

An overview of the simulation system developed in this study is shown in Fig. 5. The motion of the PMV and other vehicles in road traffic is described using vehicle dynamics models
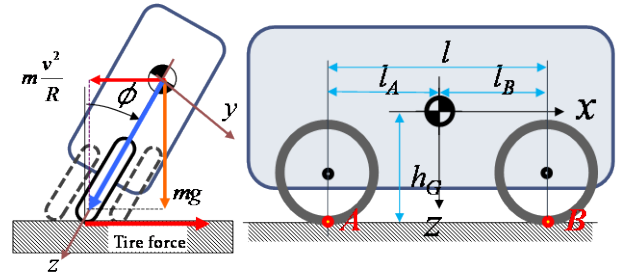
Fig. 2. Simplification of the vehicle dynamics model for the PMV
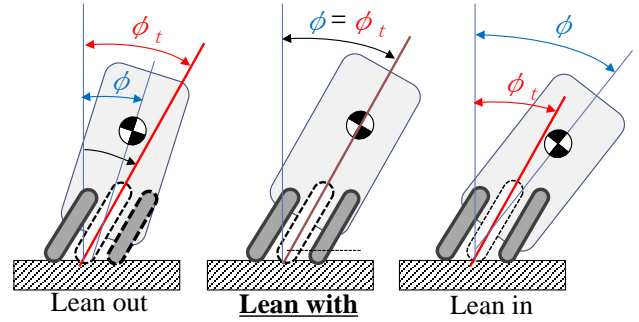
Fig. 3. The definitions of roll states between the vehicle body and the tire camber angle
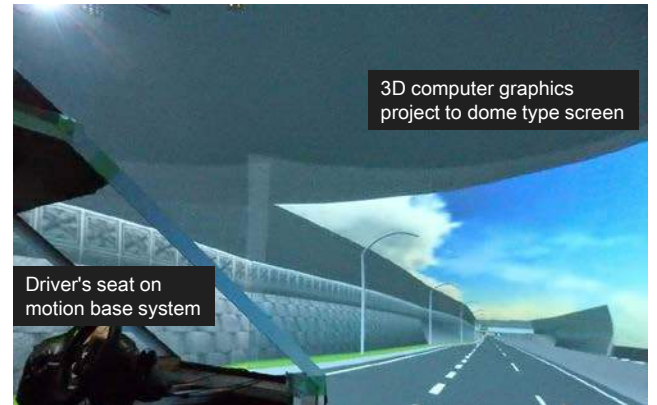
Fig. 4. Driving simulator for the PMV

Table 1. Specifications of the PMV simulation model

Full length	2500mm	Wheel base	1700mm
Full width	850mm	Tread	700mm
Height	1700mm	height of the center of gravity	700mm
Mass	300kg		

with multiple degrees of freedom (CarSim: Mechanical Simulation Co.).

In the PMV dynamics model, the compression displacement of the dampers of the vehicle's right and left sides correspond to the operation selected as an external input variable by the driver model output. These inputs displace the mounting locations of the suspension equivalently and achieve roll motion control of the vehicle body. Table 1 lists the symbols and the main calculation parameters.
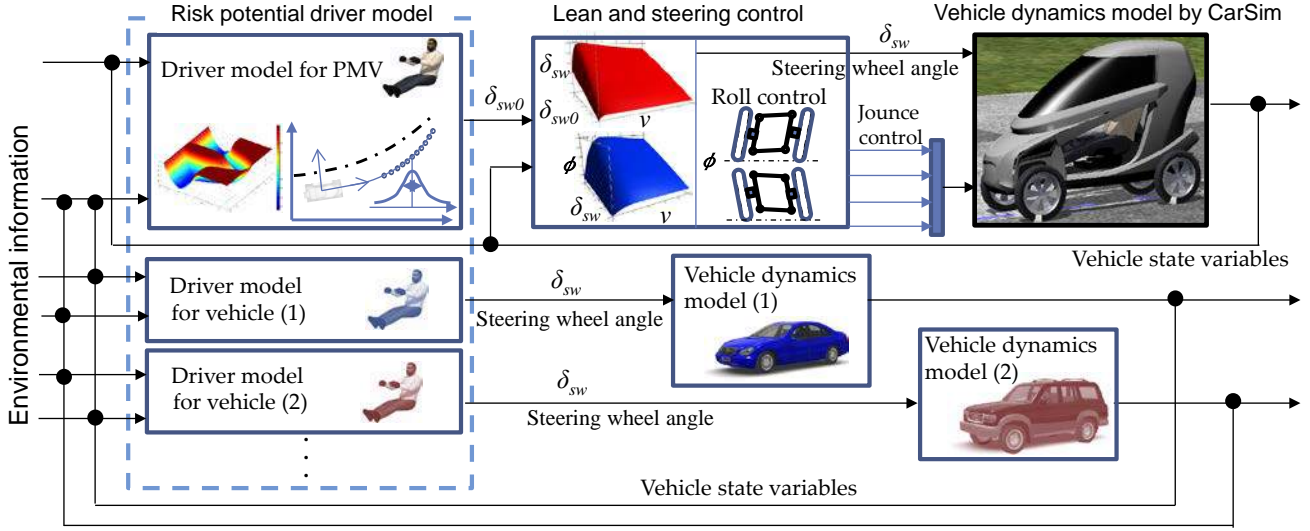
Fig. 5. Driver model and vehicle dynamics model in the simulator

3.2 Driver Models Used in the Simulation

In the simulation system, the driver model converts information on objects and road widths obtained from the surrounding environment, as well as other information, into functional parameters that determine the risk potential for all of the vehicles on the road. When a human driver recognizes a large potential risk presented by an obstacle in his/her forward view, the driver makes every effort to avoid that obstacle. Simultaneously, the risks presented by the lanes on one side and the barrier on the other also lead to conscious driving actions that are typically related to collision avoidance. In other words, the driver estimates the risks presented on all sides and seeks to position his/her vehicle where the risk is lowest.

Figure 6 is an overview of the algorithm for the driver model. The values of the risk potential presented by the right and left sides of a course are expressed using approximations of the derived exponential functions. These functions are allocated to a road map.

When an obstacle on the road is identified, the risk potentials considered when approximating the derived exponential functions include the width of the lane, the lateral position of the obstacle, the front and back ends of the object on the road and the width as shown in Fig. 7. Deviations from the risk potential are provided as feedback, which helps to determine the steering angle and longitudinal inputs. Therefore, by considering the nonlinear factors, input gains with respect to the target deviation are obtained.

Considering the preview points of the driver model, the steering angle is normally determined based on the deviation from one preview point. Nevertheless, a human driver may change the look-ahead distance depending on the operating conditions. In addition, a situation is not considered from a single viewpoint; the target path is also determined from the main preview point. Thus, with the proposed driver model, the preview point is assumed based on a multi-preview-point model, and the steering angle for the simulation vehicle
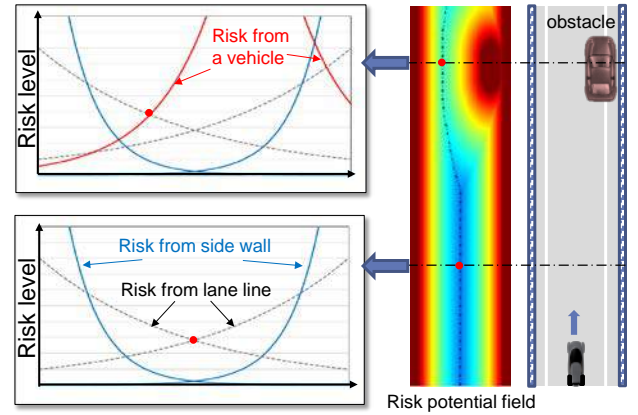
Fig. 6. Risk potential field
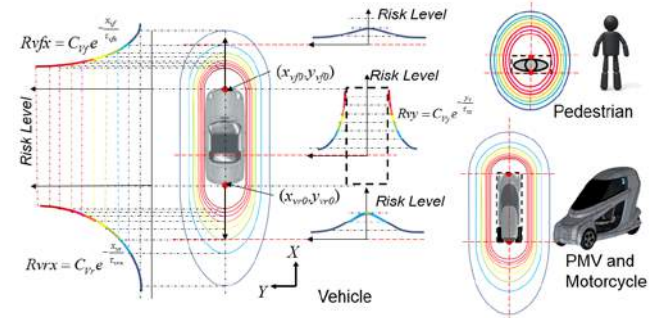
Fig. 7. Schematic of risk potential presented by obstacles

dynamics model is calculated by considering a weighted factor using the standard deviation, as shown in Fig. 8.

The second-order prediction driver model traces the lowest risk potentials as the target course, and the nonlinear steering gain is calculated from the risk potentials at those points where the course deviates from the target on the risk potential map. A preview of the second-order prediction model of the vehicle lateral direction after T_p seconds is given as follows:

$$Y_{pi} = Y_0 + V(\beta + \theta) \cdot T_{pi} + \frac{1}{2}(r + \dot{\beta}) \cdot V \cdot T_{pi}^2 \qquad (2)$$

where Y_0 is the initial lateral position and V is the vehicle velocity.

The preview point $y_{p1\sim11}$ is defined as the total for 11 points with intervals of 0.1 s both before and after a reference preview time $T_{p1\sim11}$. As the weighting function, the normal distribution function of the standard deviation σ is specified for the preview distance $x_{p1\sim11}$ for each preview time, as expressed by the following equation.

$$w(x_i) = \frac{1}{\sqrt{2\pi}\sigma}\exp\left(-\frac{\left(x_{pi} - x_{p6}\right)^2}{2\sigma^2}\right) \quad (3)$$

Furthermore, the mean value of the deviation of the risk feeling potential, ε_{ave}, which considers the weighting function and the steering angle calculated by this multi-preview-point model are given as follows:

$$\varepsilon_{ave} = \frac{1}{11}\sum_{i=1}^{11} w(x_i)\varepsilon_i \qquad \delta = \int K_s \cdot \varepsilon_{ave} \cdot dt \quad (4)$$

where K_s is the steering gain of this driver model.

In our traffic simulation, these driver models were applied to all vehicles in the road traffic, and the range of vehicle behaviors was interpolated by defining the independent parameter for each vehicle.

4. SIMULATION STUDY

As described above, this simulation system can simulate vehicle-to-vehicle mutual interference and road–vehicle interaction by providing the risk potential fields around each vehicle individually. Therefore, it is possible to perform the following:

- Optimization of the relationship between the lean angle and the steering angle of the PMV from the perspective of road traffic safety.

- Optimization and suggestion of traffic rules assuming widespread use of PMVs.

- Creation and reproduction of some accidents related to interference between the PMV and other vehicles.

We describe below an example of an emergency avoidance simulation using this system, as an example of the type of examination mentioned above.

4.1 Simulation Conditions

Figure 9 illustrates the simulation conditions. On a road with two traffic lanes in one direction, a passenger car runs in the right lane and a PMV runs in the left lane, as shown in the figure. Furthermore, a vehicle changes lanes ahead of the passenger car and PMV and then stops. It is assumed that the vehicle velocities are constant. The passenger car running in the right lane avoids the stopped vehicle without slowing
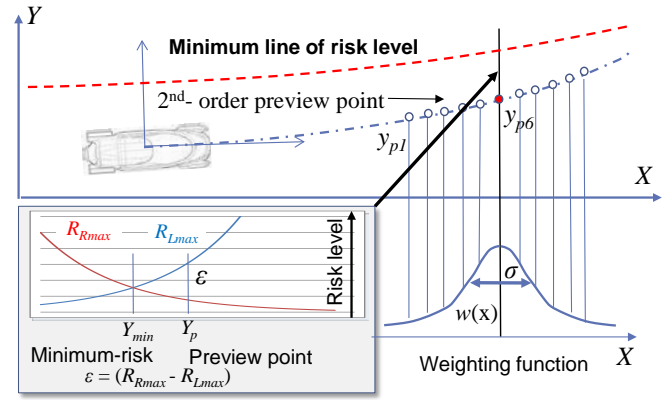
Fig. 8. Driver model with multiple preview points
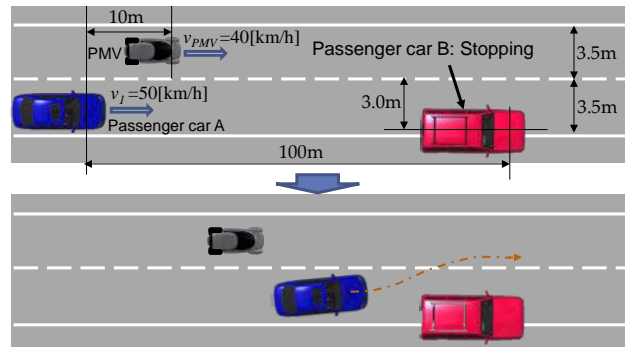
Fig. 9. Condition of the emergency avoidance simulation
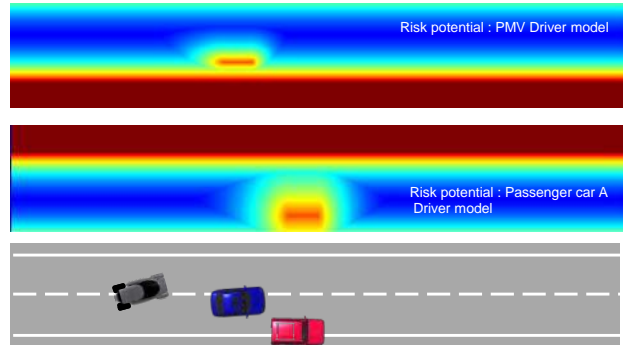
Fig. 10. Risk potential field for the simulation
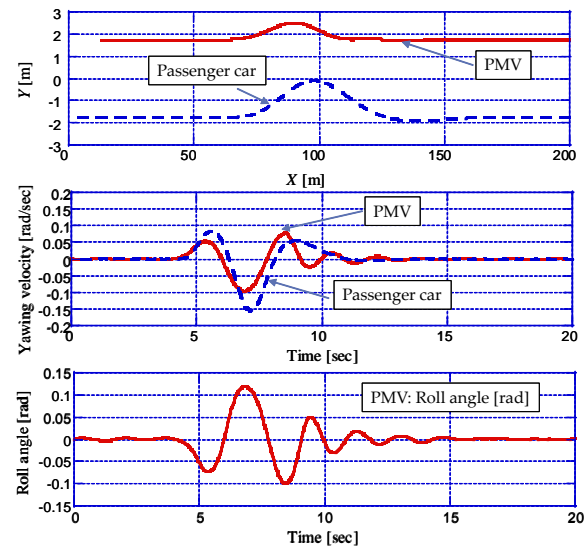
Fig. 11. Time histories of vehicle states in the simulation

down. Under these conditions, the mutual interference between the PMV and the passenger car was simulated.

4.2 Simulation Results

Figure 10 shows the risk potential field of the driver model of each vehicle just before avoiding the stopped vehicle. This figure illustrates the difference in risk sensation of the driver of the passenger vehicle and that of the driver of the PMV. As for the setting of these risk potential parameters, the risk sensation typically received by the driver from a small vehicle such as a motorcycle or PMV is assumed to be higher than that received by drivers of passenger cars and large-scale vehicles.

Figure 11 shows time histories of the vehicle trajectory, along with the lateral deviation, the yawing velocity, and roll angle of the PMV. Figure 12 shows animation images as examples of the simulation results. These results show that vehicle behaviors that occur because of the constantly changing relative relations of the vehicle states are reproduced properly.

5. CONCLUSIONS

We developed a micro-scale traffic simulator to examine the rational compatibility, including the mutual interference, of the motion of a proposed PMV and other vehicles in a specified traffic environment.

The results of a simulation conducted assuming an emergency avoidance situation showed that this simulation system could be used successfully to examine the mutual interference between the PMV and other vehicles in road traffic.

Fig. 12. Animation image of simulation results

REFERENCES

Ichiro Kageyama, and Other, (2013). Study on Fundamental Design for Personal Mobility Vehicle. Proc. of Bicycle and Motorcycle Dynamics 2013.

Ichiro Kageyama, and Other, (1993). On a Driver Model with Feeling of Risk in Forward View. Trans. of JSAE, Vol.24, No.2, (in Japanese)

Tetsuya Kaneko, and Other, (2014). Calculation Algorithm for Motion Control Target for the Platooning of Autonomous Heavy Vehicles. Proc. of 2014 UKACC 10th International Conference on Control

Environment Perception and Event Detection for Object Prediction in Traffic

Adrian Sonka, Louisa Liesner, Torben Pawellek, Florian Krauns,
Dr. Roman Henze, Prof. Dr.-Ing. Ferit Küçükay

Institute for Automotive Engineering, TU Braunschweig, 38106 Braunschweig
Germany (Tel: +49 (0)531 391 2610; e-mail: iffzg@tu-bs.de).

Abstract: Information about the vehicle environment becomes increasingly important as the development of automated driving functions progresses. This paper not only addresses a perception of the current environment, but also an estimation of possible future states. A multi-purpose method for measuring objects, lane markings and road boundaries using a reference sensor system that includes laserscanners is presented. The focus lies on recording a comprehensive environment description that is needed for the examination of vehicle interaction. The results are utilized in the correspondent tool chain for postprocessing, event detection and analysis for object prediction applications. In a final step, different possible applications are introduced.

Keywords: Perception, Sensors, Reference, Surrounding, Objects, Interaction, Behavior, Recognition, Trajectory, Prediction

1. INTRODUCTION

A substantial need for the development of functionality towards the growing field of automated driving is the knowledge about the environment of the automated vehicle [Henze, 2014]. This information includes moving and still standing objects of all kind, lane markings and road boundaries. One part is the representation of the current environment, which is sufficient if there are no moving objects present. However, the other part is an estimation of the paths of moving objects which is needed in order to plan a collision-free ego-vehicle trajectory. The human driver does that subconsciously based on his experience.

Similar to that of the human driver, an experience database of surrounding object behavior considering interaction with other vehicles and infrastructure has to be measured and collected in different traffic situations. This data can be used in different applications. It can act as a knowledge base for an object prediction or reference driving environments for simulation purposes. The former can compare the database with the current environment state and can calculate the possibility of future scenarios which can be used for ego-vehicle motion planning, as shown in figure 1. The overall goal is a sufficiently precise measurement of relevant ego-vehicle, infrastructure and object features in a representative number of real-traffic situations. Unfortunately, object data is much more prone to sensor inaccuracy. The quality of subsequent applications thus strongly depends on the sensor performance [Schlechtriemen et. al, 2014].

While in [Dang et. al, 2013] primarily ego-vehicle data is measured with limited environment sensors, work from [Yao et. al, 2013], although focusing on the ego-vehicle behavior, is obtaining data from surrounding objects through 360° laserscanners. In [Dagli et. al, 2004] a relatively broad

number of characteristics are measured with a narrow field of view using a laserscanner and a mono camera. In [Bahram et. al, 2014] only two attributes are measured for a further use in an object prediction. [Schlechtriemen et. al, 2014] is collecting a wide range of object, lane and infrastructure related data with a stereo camera and multiple radar sensors combining to a 360° field of view. In this work, an environment perception system is presented, combining 360° field of view and lane marking recognition with the series-production sensors radar and camera. The focus lies on online measuring and offline processing ego and object features to get a comprehensive description of object behavior by considering vehicle interaction and infrastructure.
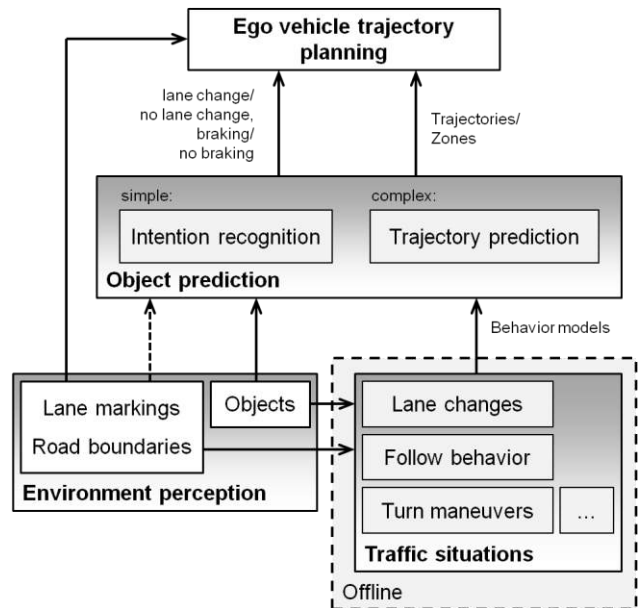
Fig. 1. Use of collected environment data for object prediction and ego-vehicle motion planning.

1

2. TRAFFIC DATA MEASUREMENT

2.1 Experimental Vehicle

The used experimental vehicle in its basic version is equipped with a mid-range radar (MRR) and a mono camera. The latter is used for online lane marking detection to calculate the lateral position of the vehicle in the driving lane. Four laserscanners, each with a multilayer 110° field of view and range up to 200 m are added to the front and rear bumper of the vehicle to get a near 360° field of view. Their primary task is the detection of objects and road boundaries. Additionally, a single layer laserscanner with 180° field of view is mounted on the rear end of the vehicle roof, facing backwards on the road for lane marking detection. This is made possible due to their different character of reflecting infrared laser beams compared to the road. The data can be used afterwards in postprocessing to reconstruct the lanes. Information about basic ego-vehicle features like the velocity or steering wheel angle are obtained by reading the vehicle CAN Bus. A webcam facing in driving direction is installed to get a qualitative visual impression of the measured scenes afterwards. Figure 2 shows a schematic sketch of the vehicle sensors.
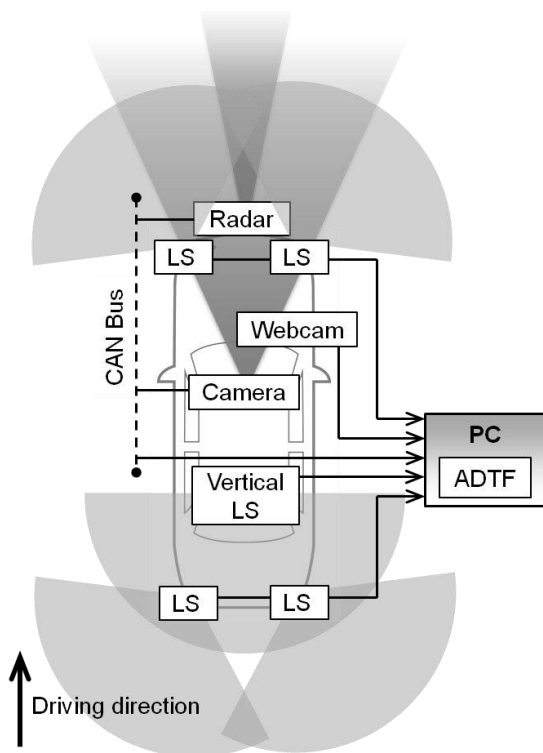
Fig. 2. Schematic top view of the experimental vehicle with laserscanners (LS).

All data is synchronously recorded on a measurement PC in the software ADTF. This environment makes it possible to simultaneously check all available signal traces while having a video of the driving situation for orientation afterwards.

2.2. Measuring Procedure

During a measuring run, environment and ego-data is continuously recorded. Depending on the purpose of use for the data, a method is intended to tag certain driving events. By pressing a button in the center console which is connected to the vehicle CAN Bus, the driver or front seat passenger are able to set a binary signal. This facilitates the data analysis afterwards since only a narrow timeframe has to be examined.

In addition, an optional questionnaire should be filled out by the passenger with a timestamp as an annotation for the marked event. Non measurable features of infrastructure and surrounding conditions like weather or traffic density can be noted and later associated with the recorded tag by comparing the timestamps.

3. TOOL CHAIN

Besides ego-vehicle data, the measurements contain object data, lane marking and road boundary information. Amongst others, object data includes positions, velocities and accelerations of moving and non-moving objects as well as object types and dimensions. Lane markings in front of the vehicle are detected in a limited way by the series-production mono camera. A very comprehensive detection method is provided by the vertical laserscanner on the vehicle roof, which is able to detect all kinds of road markings, including arrows or text. Road boundary information includes the positions of guardrails and curbs. This is possible due to the multilayer laserscanners which allow a vertical resolution of scan points. In order to get consistent environment data and be able to analyze it, a postprocessing step has to be taken.

3.1 Data Postprocessing

The raw laserscanner data goes through a postprocessing step which is done by a software tool of the scanner manufacturer. Missing or insufficient object data is completed by tracing back near objects to the point where they are first indentified. Similarly, the rearward scanned information of lane markings is connected to get a continuous road. The next step is a conversion of the recordings from the chronologic sorted scan data into a more convenient object sorted structure. The results are time-dependent data traces for every scanned object. For the ego lane and adjacent lanes, relevant objects are identified by their types and lateral positions and ordered by growing longitudinal distance to the ego vehicle.

3.2 Event Detection and Analysis

Depending on the future application, the now conditioned data has to be processed further. An example is presented in case the data is used as a basis for an object prediction algorithm that calculates lane change probabilities. This makes an event detection and subsequent analysis necessary. The mentioned manually set tags can be a help to narrow down the time frame which is to be searched. Especially if a large amount of measured data has to be analyzed, they cannot substitute an automatic algorithm to find the exact timestamps of certain events though.

As an example for a possible application, an automated algorithm for searching lane change scenarios is presented. Figure 3 shows an exemplary measurement on this. The dotted line is the lateral position raw data stream of an

2

observed object in front in the right adjacent lane. For better explanation, it corresponds to (I.) in figure 4 and represents the lateral distance of the center of the vehicle with reference to the ego-vehicle. To get ego-vehicle independent values, the own lateral distance to the lane marking is subtracted, (II.) in figure 4. The result is the solid line in figure 3, (III.) in figure 4, which is now the lateral distance between the lane marking and the object. The dashed line in figure 3 shows the tag signal, manually set by the driver. Although it does not perfectly match the lane marking crossing, the tool can now search the lateral position signal for a zero crossing, represented by a circle, in a narrow time window around the tag signal change, which is an application parameter. This reduces calculation time and more important, increases the robustness of the algorithm. Sensor signal errors which frequently result in zero crossings are not taken into consideration and make a complex pattern search with queries on signal conditions unnecessary.
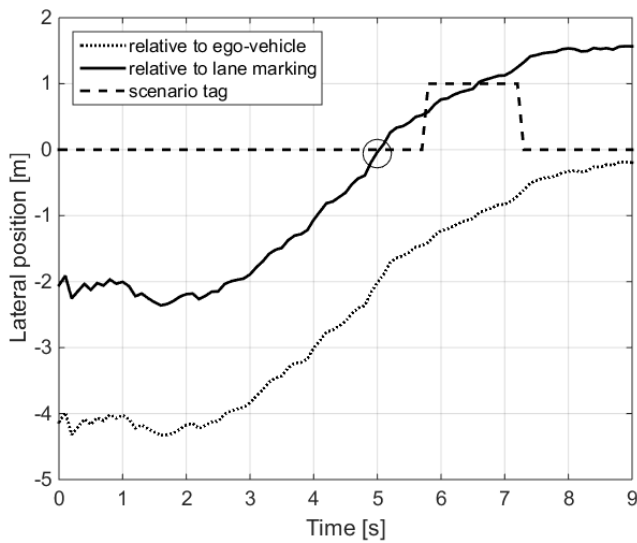
Fig. 3. Lateral object position signals and scenario tags.
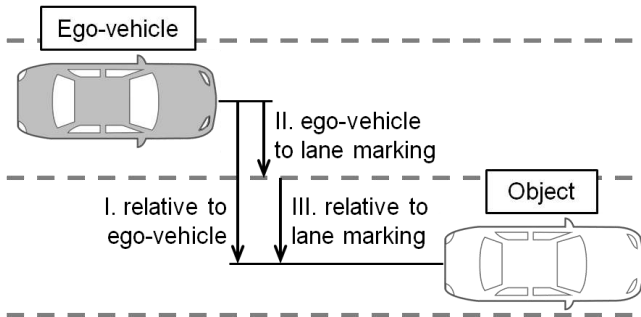
Fig. 4. Overview of used features for figure 3.

The now found exact lane marking crossings of surrounding objects are used as reference points for further data analysis. A variety of characteristic object features can be evaluated at time steps around these points and compared to the same features in non lane changing situations. This is an important step to obtain a training database for probabilistic prediction models. An example is found in figure 5, evaluating the relative longitudinal velocity between the ego-vehicle and an object in front in the right adjacent line. A negative velocity

indicates that the object is slower than the ego-vehicle. For a lane changing situation, drawn in a continuous line, the same scenario and timeframe is depicted as in figure 3. Starting from the lane marking crossing, illustrated by the circle as before, timesteps before and after the event are noted as characterizing values. In this case, similar to [Bahram et. al, 2014], a region of +/- 1.5 seconds is chosen, indicated by the dashed-and-dotted lines. The dashed line represents a different scenario with a lane keeping object which is overtaken by the experimental vehicle maintaining a higher velocity difference. Every value can be taken into consideration as no characteristic event is happening.

The data collecting typically results in two normal distributions for the particular examined feature. The narrower the distributions are and further they are apart, the more powerful is the chosen feature for classifying and predicting purposes. A good example is seen in figure 6, this feature promises good performance when used in a database.
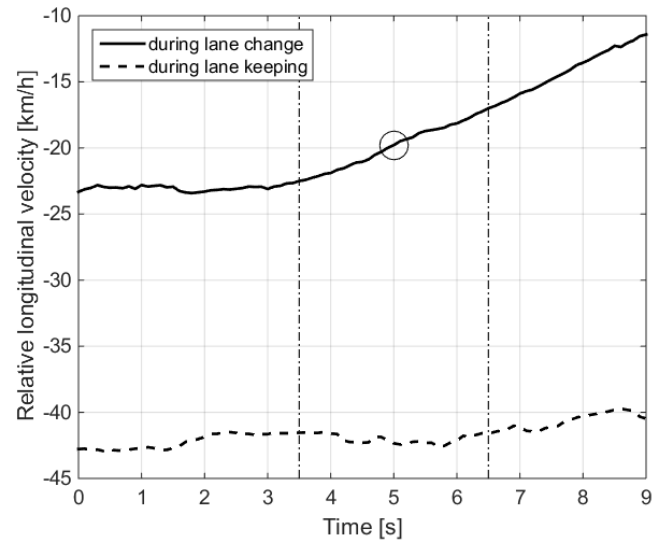
Fig. 5. Signal traces for relative longitudinal velocities in a lane changing and lane keeping scenario.
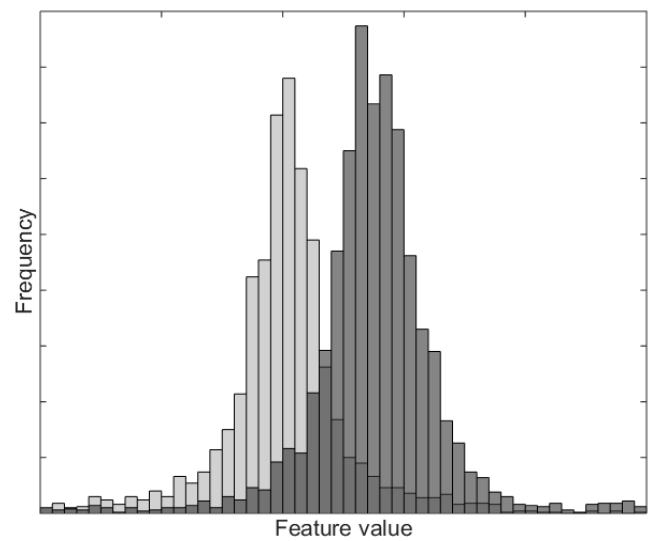
Fig. 6. Schematic resulting frequency distributions for a feature of two evaluated scene types.

3

4. APPLICATION

4.1 Referencing Scenarios

Like mentioned before, one possible application is the use of the environment perception as a system to generate reference measurements. Special event detection steps as described in chapter 3.2 are not necessary in this case, because only postprocessed data is needed. The reference measurements, especially when including detailed maps of lane markings and road boundaries, can be used as input for environment visualization software to generate virtual scenarios for driving simulators with realistic infrastructure information. Object information either is used directly in virtual vehicles to copy their real counterparts or as information for the average prevailing traffic density.

A different use-case is benchmarking series-production sensors by means of accuracy. Laserscanners deliver more accurate data since they are combining the advantages of distance measurement and angular resolution. The system behavior of driver assistance systems working with this reference data can therefore be compared to that of systems working with series-production sensors. By implication, both sensor data can also be compared to get a direct measure of the sensor inaccuracy.

4.2 Object Prediction

The results of the postprocessed and analyzed database can as well be used as training data for object prediction purposes. Probabilistic lane change classificators for example can learn preclassified data to predict the possibility of a lane change [Schlechtriemen et. al, 2014], [Bahram et. al, 2014]. Key factors on the performance of these algorithms are a large radius of observed objects, knowledge about significant features as well as data accuracy, which are all strengths of reference sensors. One cornerstone of motion prediction that is feasible considering those factors is the observation of vehicle interaction, which is necessary for the automation system to make decisions that are human-like. The driver frequently decides based on his experience of the interactions between him and surrounding objects. This makes a global view on traffic much more important than an isolated examination of an object vehicle. Studies show a high predictive power of features that describe interaction between vehicles [Schlechtriemen et. al, 2014]. A common example visualized in figure 7 is an object A in the right lane that is approaching a slower vehicle B in front. A lane change decision is very probable (solid line), but depends strongly on the velocity difference of the faster ego-vehicle that is driving in the left lane. A lane keeping with brake maneuver option for object A remains possible (dashed line).

Object prediction or as an example a lane change recognition is not only useful thinking about highly automated driving, but also in series-production when being integrated in an Adaptive Cruise Control, which still can be improved when it comes to customer acceptance. Current work shows optimization potential for regular maneuvers regarding control behavior and motion characteristics [Liesner et. al, 2015], [Pawellek et. al, 2012]. However intention estimation

can enhance the reaction times of the system and situations can be reduced where the driver is asked to take over the control [Dagli et. al, 2004]. Customer acceptance can be enhanced further by adapting the prediction to the driver preferences and performance, resulting in a more or less sensitive and therefore safety-oriented output [Henze et. al, 2011].
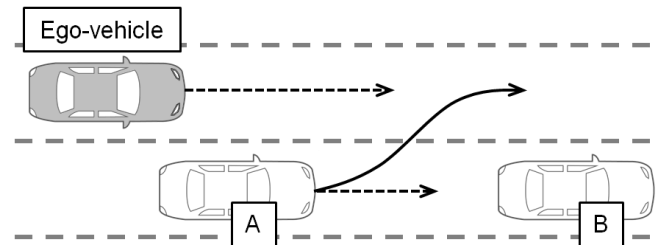
Fig. 7. Schematic figure of object interaction: $v_{Ego} > v_A > v_B$

Another use case is certainly the behavior of rearward objects in case of a stronger deceleration of the ego-vehicle. Knowledge about usual braking maneuvers can be facilitated for Automatic Emergency Brake (AEB) systems that often endanger following vehicles by an unexpected ego-vehicle reaction.

4.3 Online Perception

Environment sensor systems with 360° field of view can not only be used for data collecting but by implication for a highly accurate online perception. This forms a fundamental input for subsequent ego trajectory planning and controlling in automated driving functions and is a precondition for taking advantage of the knowledge mentioned in chapter 4.2, see also figure 1. During operation, all the evaluated features that the database contains have to be observed online with the available sensors. This makes a global approach possible that plans and controls the best possible ego-trajectory for every perceived and predicted vehicle involved in the current scene, regardless if behind or in front of the ego-vehicle.

5. CONCLUSION

This paper presents an experimental vehicle with a laserscanner sensor configuration for precise 360° environment perception with object, lane marking and road boundary detection. Furthermore, a measurement procedure and data postprocessing chain with focus on event detection is introduced. These tools help generating knowledge about specific scenarios which can be utilized for training probabilistic algorithms for object prediction. In the paper, three possible use-cases are shown for the building of reference scenarios, object prediction training and online perception. Further work could concentrate on the development and testing of an object prediction algorithm, which is trained with a database obtained by the presented approach.

4

REFERENCES

Bahram, M., Lohrer, A. and Aeberhard, M. (2014). Generatives Prädiktionsmodell zur frühzeitigen Spurwechselerkennung. In *2014 9. Workshop Fahrerassistenzsysteme FAS2014,* pages 47-54.

Dagli, I., Breuel, G., Schittenhelm, H. and Schanz, A. (2004). Cutting-In Vehicle Recognition for ACC Systems – Towards Feasible Situation Analysis Methologies. In *2004 IEEE Intelligent Vehicles Symposium,* Parma, Italy, June 14th-17h, 2004, pages 925-930.

Dang, R., Zhang, F., Wang, J., Yi, S. and Li, K. (2013). Analysis of Chinese Driver's Lane Change Characteristic based on Real Vehicle Tests in Highway. In *Proceedings of the 16th International IEEE Annual Conference on Intelligent Transportation Systems*, The Hague, Netherlands, October 6th-9th, 2013, p. 1917-1922.

Henze, Dr. R., Kollmer, H., Pion, O., Küçükay, Prof. Dr. F. (2011). Adaptation of ADAS-Functions by Monitoring Driver Characteristics. In *First International Symposium on Future Active Safety Technology toward zero-traffic-accident FAST-zero 11,* Tokyo, September 9th, 2011.

Henze, Dr. R. (2014). Road to Automated Drive – Efficient Function Development – Testing and Optimization. In *12th International Symposium on Advanced Vehicle Control AVEC 14,* Tokyo University of Agriculture and Technology, September 26th, 2014.

Liesner, L., Pawellek, T., Krauns, F., Pan, S., Henze, Dr. R., Küçükay, Prof. Dr. F. (2015). Kundenoptimales Design von längsführenden Komfortsystemen. In *AAET 2015 - Automatisierungssysteme, Assistenzsysteme und eingebettete Systeme für Transportmittel,* February 13th, 2015.

Pawellek, T., Liesner, L., Pan, S., Henze, Dr. R., Küçükay, Prof. Dr. F., Hagerodt, Dr. A., Sochacki, C. and Wonke, M. (2012). Eine Methodik zur Analyse, Bewertung und Auslegung von ACC-Systemen. In *AAET 2012 - Automatisierungssysteme, Assistenzsysteme und eingebettete Systeme für Transportmittel,* February 9th, 2012.

Schlechtriemen, J., Wedel, A.., Hillenbrand, J., Breuel, G. and Kuhnert, K.-D., (2014). A Lane Change Detection Approach using Feature Ranking with Maximized Predictive Power. In *2014 IEEE Intelligent Vehicles Symposium,* Dearborn, Michigan, USA, February 9th, 2012, pages 108-114.

Yao, W., Zhao, H., Bonnifait, P. and Hongbin, Z. (2013). Lane Change Trajectory Prediction by using Recorded Human Driving Data. In *2013 IEEE Intelligent Vehicles Symposium*, Gold Coast, Australia, June 23rd-26th, 2013, pages 430-437.

5

A novel approach to driver behavior prediction using scene context and physical evidence for intelligent Adaptive Cruise Control (i-ACC)

Jens Schmuedderich, *Sven Rebhan, *Thomas Weisswange, *
Marcus Kleinehagenbrock, ** Robert Kastner, **
Morimichi Nishigaki, ** Hiroyuki Kamiya, *** Naoki Mori, ***
Shunsuke Kusuhara, *** Shinnosuke Ishida ***

Honda Research Institute Europe GmbH, Offenbach, Germany
(e-mail: jens.schmuedderich@honda-ri.de).
** *Honda R&D Europe (Deutschland) GmbH, Offenbach, Germany*
*** *Honda R&D Co.,Ltd. Automobile R&D Center, Tochigi, Japan*

Abstract: Conventional driver assistance systems suffer from relatively late reaction timing. Adaptive Cruise Control (ACC) systems, for example, react to vehicles cutting-in from neighboring lanes once these vehicles are at least partly driving on the host vehicle's lane. The improvement by state of the art prediction approaches is limited, because the reliable approaches base on features, which are characteristic for the phenomenological effect of a behavior change. That means they are capable of predicting a behavior once it started. The Honda i-ACC overcomes the above mentioned limitation of delayed reaction by using a novel approach of behavior prediction. This approach combines two prediction methods: A context-based prediction (CBP) and a physical prediction (PP). The CBP evaluates the situational context of a predicted vehicle and does not use any phenomenological feature. It is thus capable of long-term prediction. In contrast, the PP evaluates phenomenological features by accumulating the predicted vehicle's history of recent positions and comparing them to a set of trajectories, which allows for an accurate short-term prediction. In an evaluation on 15000km of driving in Europe we will show that the new prediction approach achieves both, reliable and long-term prediction.

Keywords: Intelligent Adaptive Cruise Control, Prediction, Predictive Driver Assistance System, Prediction Methods, Situation Understanding.

1. INTRODUCTION

Conventional driver assistance systems react to another traffic participant's behavior as soon as it becomes apparent. In other words, they react as soon as the host vehicle's sensors detect the start of another vehicle's change of behavior. ACC systems, for example, react to a vehicle cutting-in from a neighboring lane when the sensors measure a significant lateral motion or displacement. However, a change of behavior is usually the effect of adapting to the current driving situation, i.e. a driver will change lane to overtake a slower vehicle driving ahead of him if the current traffic situation permits. By analyzing the driving situation of other vehicles, attentive drivers are well capable of foreseeing or predicting their behavior before this behavior actually starts. To bridge this gap between technical systems and human capabilities, future active safety technology should therefore base upon prediction to offer what we call assistance beyond sensing. The Honda intelligent Adaptive Cruise Control (i-ACC) is the first implementation of such a predictive system. This system, commercially available in the 2015 model year CR-V behaves like a conventional ACC for free-ride
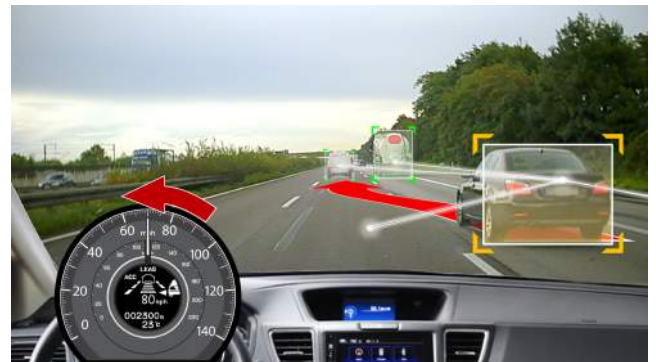
Fig. 1. Visualization of i-ACC function: The host vehicle predicts a cut-in of the vehicle on the neighboring lane and reacts even before the cutting-in vehicle started moving laterally.

or follow- situations. However in cut-in situations it can predict cutting-in maneuvers of vehicles on the adjacent lane and react even before these vehicles start moving laterally, see Fig. 1. In this contribution, we will focus on prediction technology behind this function. A companion
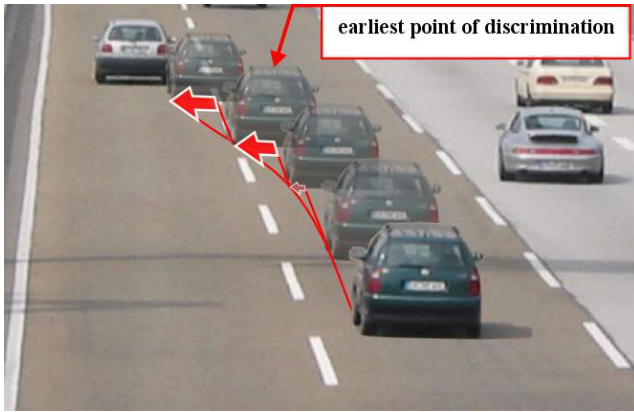
Fig. 2. Earliest point of discrimination: Systems relying on phenomenological features reliably predict a lane change when it has already started.

contribution by Kleinehagenbrock et al. (2015) will detail the system integration and provide a subjective user test.

2. STATE OF THE ART

Various methods for behavior prediction exist. For convenience we will focus here on the prediction of lane changes. A more thorough overview is given by Bonnin et al. (2014). On highway scenarios Bayesian methods are commonly used to estimate the probability of a lane change given a set features, e.g. by Dagli et al. (2004); Kasper et al. (2012); Schlechtriemen et al. (2014). This is usually achieved by estimating models for different behavior classes, consisting of conditional probability distributions over a set of features. Other approaches consider lanes changes as a Markov process, i.e. a future state is considered to depend on one or more previous states. For example Gindele et al. (2010) model such temporal dependency in a Bayesian Network and use if for estimation of future states given one or more recent states and a suited set of discriminative features.

In reasoning based approaches the current situation is compared to a database of known cases in order to determine the future behavior, as reported by Graf et al. (2013).

Behavior prediction can also be understood as classification problem. Similar to the Bayesian approaches the recognition of a situation based on discriminative features can be used to infer how this situation will develop in the future. This idea has been addressed e.g. by Reichel et al. (2010), who use Random Forrest Trees for classification or by Garcia Ortiz et al. (2012) who use Locally-Weighted Projection Regression. In general, model based approaches exhibit a high predictive power especially for long prediction time horizons, however they suffer from a limited application scope. A method to overcome this dilemma by efficiently combining various models is reported by Bonnin et al. (2014, 2013); Graf et al. (2013).

Some of the above approaches use multiple models or decision stages. However, they use a singular prediction method resulting in one singular prediction result. Those approaches achieving reliable results include features that are characteristic for the phenomenological appearance of a lane change, like the lateral velocity or the lateral displacement. Consequently, these approaches can only
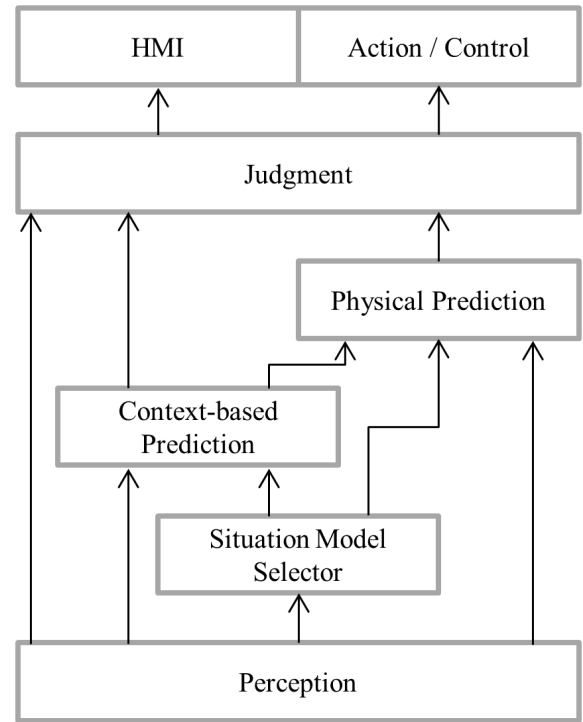
Fig. 3. System Graph: Please refer to the text below for a detailed explanation.

predict lane changes accurately once these lane changes started, which is much later than an attentive driver can do, see Fig. 2. Thus, these approaches are not suited to bridge the gap between the capabilities of an attentive driver and an ADAS. Other approaches, which do not use such phenomenological features, do not yet reach the quality required for commercial ADAS.

3. APPROACH

To overcome the dilemma of choosing between low prediction quality or low prediction horizon, this contribution presents a novel approach for the prediction of other vehicles' behaviors. This approach combines two prediction methods: First, a prediction based on the contextual situation of the predicted vehicle, which we call context-based prediction. Second, a prediction based on physical evidence of the predicted vehicle's movement. The context-based prediction evaluates relations between vehicles and the infrastructure, but it does not use any phenomenological features. This makes it capable of early behavior prediction, before the behavior actually starts. This method will be further detailed in section 3.1. The physical prediction, which will be explained in section 3.2 combines the results of the context-based prediction with observations of recent vehicle positions. These positions are compared with typical trajectories to predict behaviors. This prediction is highly accurate, but only capable of predicting behaviors once they started. To benefit from both, early and reliable prediction, a special system design is used, see Fig. 3:

The system, receives information about the environment and the host vehicle via the perception module. The resulting vehicles and lanes are passed to all following modules. The Situation Model Selector infers one or more fitting situation models for the current traffic situation and passes

them to the context-based and to the physical prediction. Both prediction modules use these situation modules to estimate the future behavior of various traffic participants. The key of this integration is to pass both prediction results to the judgement module, which determines the best fitting action based on the current traffic situation and based on the evidence provided by the prediction methods. This system design allows the judgement module to determine a proper action based on the individual prediction evidence as well as on the combined evidence.

In the current implementation, a high evidence for a cut-in by one of the prediction methods authorizes a mild deceleration, while high evidence from both prediction methods authorizes a strong deceleration.

In the following, we will describe the two prediction methods in more detail.

3.1 Context-based Prediction

The context-based approach considers prediction as a classification problem: The current traffic situation as represented by the perception module is matched against a set of known situation models. Each of these situation models contains information of how this situation will evolve in the future. Thus, a correctly recognized situation model results in a correct prediction. Literally speaking, the context-based prediction answers the question: *Is a vehicle in a situation in which it will change lane to the left?*

This leads to two principal problems: First, how to represent situation models in an efficient way, such that the number of situation models is minimized and at the same time the coverage of situations is maximized? Second, which discriminative features allow for a reliable classification of these situation models?

The problem of efficient situation model representation is handled by so called local relations. The underlying assumption is that driver behavior, especially on European highways, does not primarily require a holistic analysis of the whole scene, but is usually influenced by the traffic participants in the driver's direct vicinity. Which of the neighboring vehicles is relevant obviously depends on the behavior options of the driver – for a lane change left the vehicles on the left are usually more relevant than the vehicles on the right. Consequently the vehicles represented for a lane-change-left-behavior differ from those represented for a lane-change-right-behavior. Fig. 4 visualizes the situation models for both behaviors. The representation of the lane-change-left model contains the vehicle to be predicted, its predecessor on the own lane, as well as the predecessor and successor on its left lane. Equivalently, the lane change-right-model for left-hand driving contains the vehicle to be predicted, its predecessor, as well as the predecessor and successor on its right lane. The situation models are applied separately for each vehicle and each behavior to be predicted.

The second problem, the identification of discriminative features for a correct classification a represented scene, is usually handled by including phenomenological features, such as lateral velocity or lateral offset of the predicted vehicle in its lane. Obviously such features are highly discriminative, but only once the maneuver has already started. A classifier trained with these features would learn to rely on them and consequently only provide high confidence values once the predicted vehicle started its
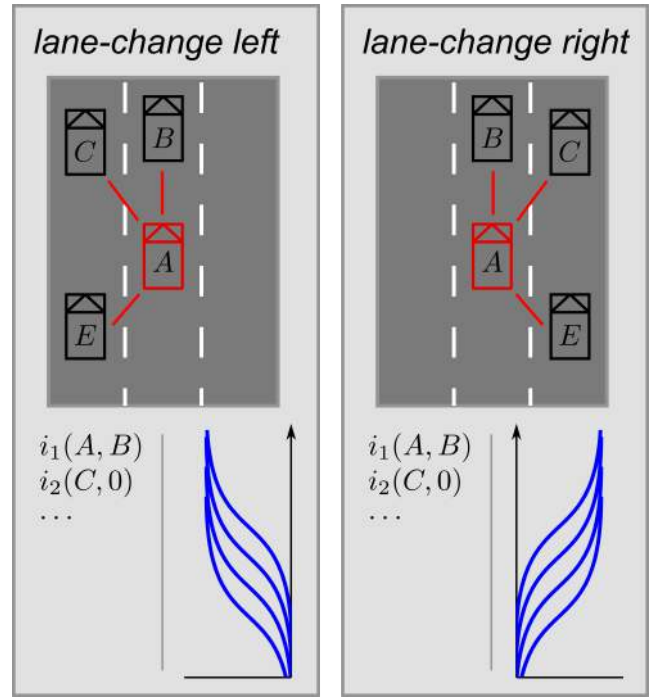
Fig. 4. Situation Models: Two situation models for lane change left and lane change right of vehicle A are shown. Each model consists of set of relevant vehicles (top), a set of indicators i and a set of physical trajectories.
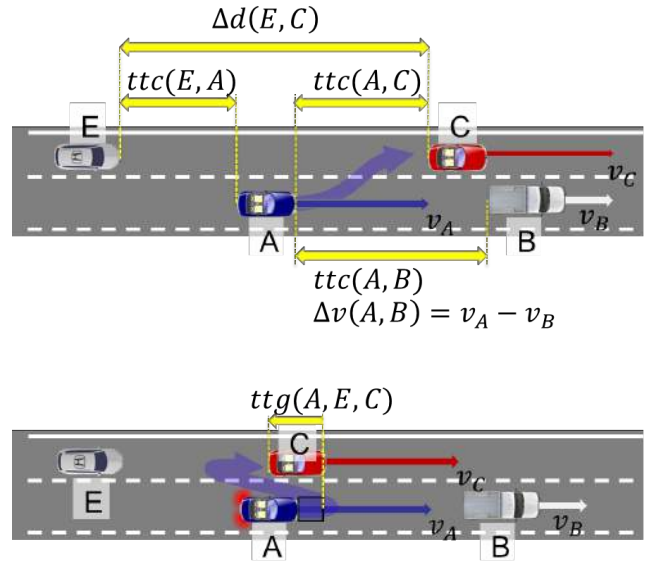
Fig. 5. Features used for context-based prediction: TTC between two vehicles, distances, relative velocities (top) as well as TTG (bottom). For all features only the longitudinal aspect is evaluated, otherwise e.g. the TTC between two vehicles on neighboring lanes would be infinite.

displacement in the lane. Therefore the context-based prediction explicitly excludes any of these phenomenological features.

However, especially in Europe a vehicle typically changes lane if it wants to overtake a slower predecessor and if there

is a fitting gap on the neighboring lane. Thus the context-based prediction evaluates longitudinal aspects of the local relations between vehicles in the situation models. This works in two steps: First the local relations are evaluated to compute features such as the time-to-collision (TTC), the relative velocity and relative acceleration, the distance, the absolute acceleration and the time-to-gap (TTG). TTC is computed by dividing the distance between two vehicles by the relative velocity, whereas TTG is computed by dividing the distance between a vehicle and the next gap by the relative speed between the vehicle and the gap. Compare Fig. 5 for visualization. After computing these feature values, they are recombined to so-called indicators. These indicators are functions which parameterize and combine the features such, that their output values are in $[0,1]$, where 0 indicates that the current scene does not fit to the evaluated situation model and 1 means that it fits perfectly to the situation model. Describing all used indicators in detail would go beyond the scope of this contribution. Therefore we will exemplarily present two of the indicators used to explain the concept. A more thorough list can be found in Schmuedderich and Rebhan (2011); Rebhan (2013); Schmuedderich (2014):

- Approaching and Fitting Left Gap for Situation S_A of vehicle A and its local relations as computed by formula (1):

$$
\varphi_a(S_A) =
\begin{aligned}
&f(\text{TTC} && (A,B), \Theta_1, \Theta_2) \cdot \\
&f(\Delta v && (A,B), \Theta_5, \Theta_6) \cdot \\
&f(\text{TTC} && (E,A), \Theta_3, \Theta_4) \cdot \\
&f(\Delta d && (E,C), \Theta_7, \Theta_8) \cdot \\
&f(\text{TTG} && (A,E,C), \Theta_9, \Theta_{10})
\end{aligned}
\tag{1}
$$

where $\Delta v(A,B)$ is the difference of velocity between two vehicles A and B, $\Delta d(E,C)$ is the distance between two vehicles E and C, $f(.)$ is a non-linear function and Θ_i are parameters to scale the functions output to $[0,1]$ such, that it produces high values ≈ 1.0 if A is approaching B, there is a fitting gap for A between E and C and this gap is soon available.

- Approaching and Accelerate to Gap for Situation S_A of vehicle A and its local relations as computed by formula (2):

$$
\varphi_b(S_A) =
\begin{aligned}
&f(\text{TTC} && (A,B), \Theta_{11}, \Theta_{12}) \cdot \\
&f(\Delta a && (A,E), \Theta_{13}, \Theta_{14}) \cdot \\
&f(\text{TTC} && (E,A), \Theta_{15}, \Theta_{16}) \cdot \\
&f(\Delta d && (E,C), \Theta_{17}, \Theta_{18}) \cdot \\
&f(\text{TTG} && (A,E,C), \Theta_{19}, \Theta_{20}) \cdot \\
&f(a_A, && \Theta_{21}, \Theta_{22})
\end{aligned}
\tag{2}
$$

This function is scaled such, that it produces high values if A is approaching B, if A is accelerating, and if A's acceleration is suited to fit in the gap between E and C.

The parameters Θ_i are estimated by using a CMA-ES algorithm as described by Hansen (2006), an evolutionary optimization algorithm which considers the prediction algorithm as black box and finds the optimal parameters iteratively. The final classification confidence c_i for one situation model M_i for a vehicle A in situation S_A is obtained by maximizing over all indicator values of this classification model by formula (3):
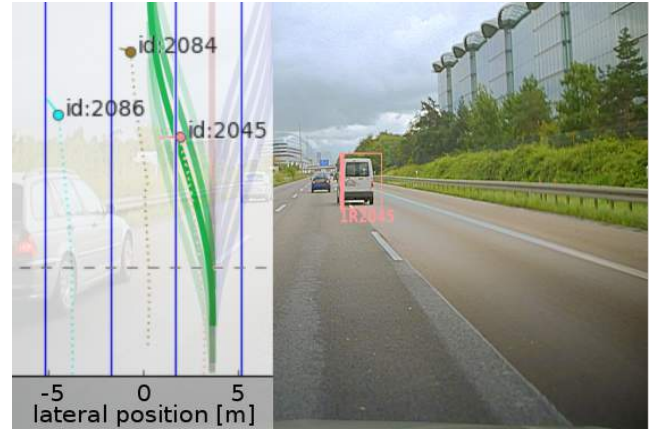
Fig. 6. Physical Prediction: Left side: Accumulated, curve-corrected positions as colored dots, and trajectories fitted for the vehicle on the right lane, where the trajectories' color opacity visualizes the trajectories likelihood fitting. Right: Corresponding scene.

$$
c_i(S_A) = \max_{j \in M_i} \varphi_j(S_A) \ . \tag{3}
$$

3.2 Physical Prediction

The detection of the scene context poses an additional challenge for the sensor system. Furthermore, with increasing prediction horizons the inherent uncertainty of predictions increases. This is due to the fact that, proportionally to the time to a cut-in, the number of options available to the driver of a potential cut-in vehicle increases.

To achieve a reliable estimate of future behaviors in all cases, an additional physical prediction approach is used. This physical prediction compares the history of recently measured vehicle positions to a set of trajectory models, each representative for a set of different behaviors, see Fig. 6. By doing so, the prediction horizon of this type of prediction is inherently limited to a point in time where the cut-in of a vehicle becomes observable.

The physical prediction proposed here uses a pointwise comparison resulting in a likelihood estimate for each possible behavior given the observed positions. In combination with the situation priors determined by the context-based prediction, finally a posterior belief is estimated for the different behavior options. To calculate the physical prediction, the history of positions is compared to a set of trajectory models. For the current system there exist models for 'stay on lane', 'lane change left' and 'lane change right'. A common problem of model-based approaches is to deal with the diversity of the input data. In our case sources for this diversity are:

- sensor noise in the perceived vehicle positions,
- differences in lane change shapes due to driver preferences such as doing a very smooth or very sudden lane change,
- differences in road shape like curved or straight roads.

Whereas the senor noise can be explicitly covered in the model, different models would be required for different lane change shapes (e.g. very smooth or very steep transitions). However, our analyses of real-world lane change data suggest that the majority of lane changes follow one average model, while minimal variations are covered
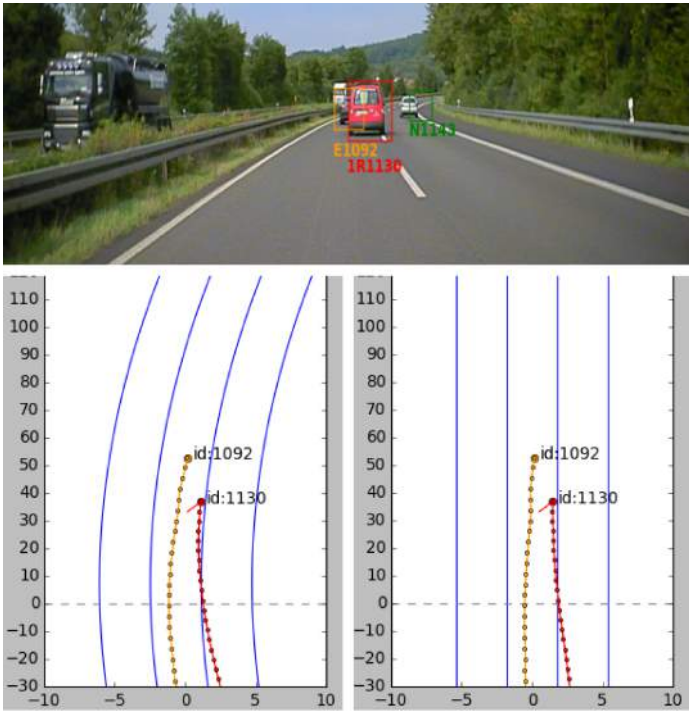
Fig. 7. Position rectification: Left bottom shows perceived history of raw positions for two vehicles, which are a superposition of their trajectory maneuvers and the road curvature. Right bottom shows rectified postions, in which the effect of the road curvature is cancled. Top image shows corresponding scene.

explicitly within this model. These minimal variations are within the range of sensor noise and thus can be handled by the same mechanism. However, the differences in road shapes introduce a large variety when comparing the raw position history with the set of models. This is due to the fact that the observed position history is a superposition of the actual lane change motion and the motion to follow the (curved) road. To eliminate the influence of the road-follow motion, we rectify the history of vehicle positions with respect to the road shape before performing the likelihood calculation minimizing the variance of observed behaviors. Fig. 7 shows the effect of the road-shape rectification. The position history of a vehicle accumulated over time is projected onto the current estimation of the road shape. Thus the position history is transformed such as if it were observed on a straight road. As a consequence, the influence of the road shape on the position history is eliminated and the diversity of behavior models is minimized with respect to the road shape. In a first step, we calculate the Euclidian distance of each position to the closest point of the host-vehicle's lane center. These distances then correspond to the positions that would result from the motion of the vehicle on a straight road. To transform the position history, we simply use the resulting distances as new lateral and the longitudinal values of the closest points as new longitudinal component of the vehicle position history. As a result of using the proposed rectification, only one model for each behavior 'stay on lane', 'lane change left' and 'lane change right' is required.

Fig. 8. Ground-truth reference point: Manually annotated point in time for a cut-in, when the right tire touches the lane marking, see red arrow.

3.3 Judgment, Action, and HMI

The judgement module receives the result of both predictions as well as the current perception data. If any of the prediction methods predicts a lane change for the current situation, the judgment module determines the most relevant vehicle to control on based upon TTC and time gap.

To maximize the effect of an early context-based prediction and a reliable physical prediction, the strength of the control is based on the prediction evidence: If one of the prediction methods predicts a lane change with a confidence higher than a method-specific threshold, the judgment module authorizes a mild-deceleration maneuver. If both prediction methods provide a confidence higher than their respective threshold, a strong deceleration with up to 0.4g is authorized.

It has to be noted, that the judgment module only determines the maximum allowed deceleration force. The actual deceleration force is determined in accordance with the current situation. That means, even if both prediction methods predict a cut-in and thus a strong deceleration is authorized, the vehicle will only brake mildly if the cutting-in vehicle has a high TTC and time gap to the host vehicle.

Whenever the host vehicle brakes for a cutting-in vehicle, a symbol is shown in the meter, as shown in the left corner of Fig. 1.

4. EVALUATION

For a quantitative evaluation of the proposed prediction method, we extracted 15.000km from our recordings of driving with a prototype vehicle equipped with i-ACC on European highways. This subset is a representative sample in terms of varying traffic density from mild to dense traffic, weather conditions from sunny to rainy, day and night, as well as driving style. The prototype vehicle is equipped with the Honda Sensing technology which feeds the system with data of lane markings and vehicles perceived by a sensor fusion of a 74Ghz electric scanning radar and a camera. The longitudinal control was done by the i-ACC system.

For evaluating the Honda intelligent ACC system we use an event-based evaluation as explained by Bonnin et al.
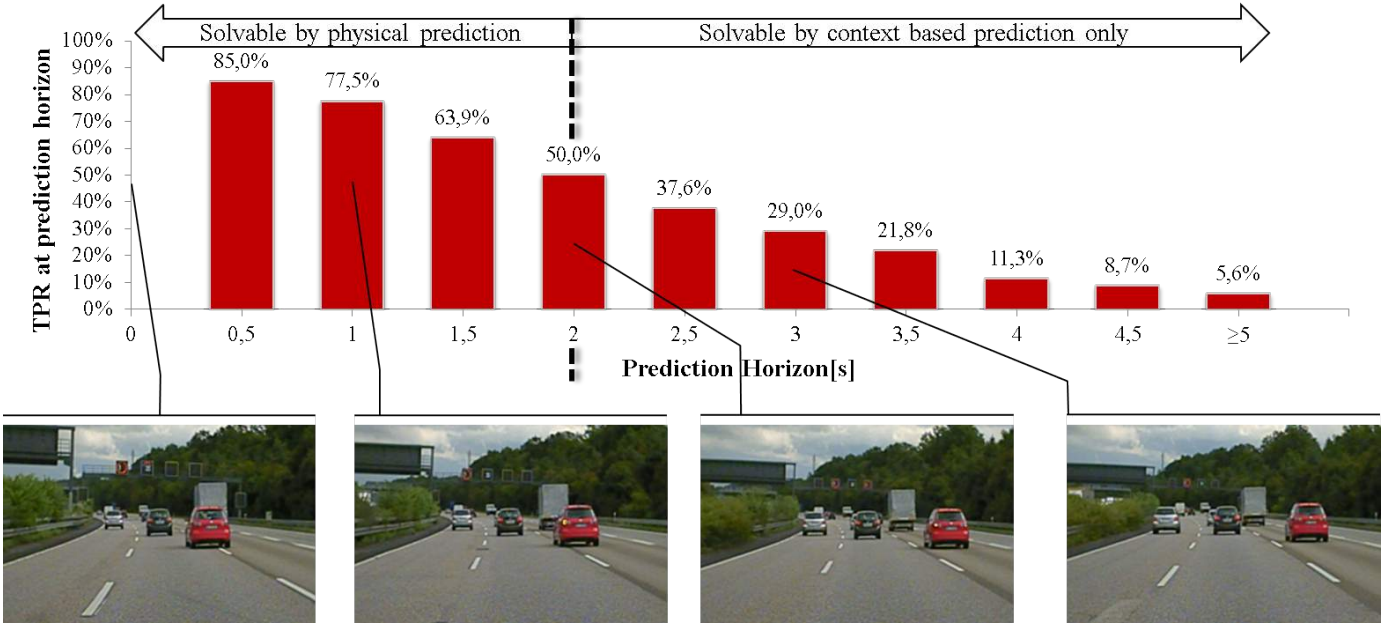
Fig. 9. Prediction Horizon and TPR: Plot of TPR of targeted situations for a given prediction time horizon. For example, 85% of targeted cut-ins are predicted 0.5s before the cut-in and 50% are already predicted 2s before the cut-in (top). For four points in time, the typical corresponding position of a cutting-in vehicle is shown (bottom). As the plot shows, the cutting-in vehicle starts moving laterally at about 2s before the referene point. This is the earliest point in time, where a conventional prediction algorithm can earliest detect a lane-change. With our proposed approach, already 50% of cut-ins are already detected at or before this point.

(2014). This type of evaluation groups successive timesteps of positive prediction to one event, which is especially suited to estimate the effect of a prediction algorithm on an ADAS function. To generate the required ground-truth all targeted cut-in situations are marked: A sitution in which vehicle A cuts-in in front of ego vehicle E is marked as target situation if the following condition is true:

$$(\text{TTC}(E, A) \quad \leq \quad 10[s] \quad (4)$$
$$\vee \Delta d(E, A)/v_E \quad \leq \quad 2[s]) \quad (5)$$
$$\wedge \Delta v(B, A) \quad \geq \quad 2.5[m/s] \ , \quad (6)$$

where v_E is the velocity of the ego vehicle E, $\Delta d(\cdot, \cdot)$ and $\Delta v(\cdot, \cdot)$ are the relative distance and relative velocity respectively. By this definition a cut-in situation is only marked as relevant, if the ego vehicle has to react to the cut-in, either to avoid a collision (4) or to adjust its time gap (5). Additionally the reason for B's cut-in must be a detected slower vehicle A, expressed by a difference speed of at least 2.5m/s (6). The latter restriction is used to limit the system to cases which are also predictable by the driver.

For each of the target cut-in situations a point in time when the cut-in happens is defined. This reference point is shown in Fig. 8. We have chosen the point where the right rear tire first touches the lane marking as reference because at this time conventional ACC systems will take control over the host vehicle. Together with the reference time, the ID of the cutting-in vehicle is stored as ground-truth.

Knowing the manually annotated ground-truth reference, we can classify the predictions of our systems into False-Positives (FP), False-Negatives (FN) and True-Positives (TP). To do so, we apply a threshold to each prediction for each vehicle in the scene individually, where a prediction output above or equal to the threshold will indicate a reaction of our system and a threshold below the threshold will indicate no reaction by our system. A reaction means that our system will take control to adapt the host vehicles velocity and distance to the predicted cut-in vehicle. Contrary to frame-based evaluations, we do not evaluate the TP, FN and FPs for each frame individually, but group successive frames of activation (output above threshold) to one reaction event (see Bonnin et al. (2014) for more details).

A true-positive in our case is defined as at least one frame of activation within 10 seconds before the annotated reference point for the annotated vehicle ID. A false-negative is defined at no frame of activation within 10 seconds before the annotated reference point for the annotated vehicle ID. Finally, a false-positive is defined as one or more successive frames of activation outside a window of 10 seconds before and 4.5 seconds after any annotated cut-in. Please note that the evaluation is vehicle specific, thus both a FP and FN is counted in case our system predicts a cut-in (output above threshold) for one vehicle (FP), but the cut-in is actually performed by another vehicle (FN). Finally, the prediction horizon is defined for TP events as the first frame of activation within the group of successively activated frames.

When discussing the results of our evaluation we use the true-positive rate (TPR) defined by (7)

$$\text{TPR} = \frac{\text{TP}}{\text{TP} + \text{FN}} \quad (7)$$

and the false positives per hour (FP/h) driving time.

To evaluate the prediction accuracy two separate thresholds were chosen, one for the context-based and one for

the physical prediction. If the confidence of the respective prediction method exceeds the corresponding threshold a cut-in is predicted, otherwise no cut-in is predicted. Both thresholds result from a Receiver-Operating-Characteristics (ROC) analysis as introduced by Spackman (1989) and were chosen to optimize the trade-off between true positives and false-positives. In this setting a TPR of 85% of all targeted situations is achieved at 1one false-positive in 10hours. It has to be noted, that all false-positive cases were caused by one of the two prediction algorithms and thus only led to mild braking. No case of simultaneous false-positive prediction by both methods can be found in the data.

Figure 9 visualizes the dependence of TPR and prediction horizon by plotting the TPR of targeted situations for a given prediction time horizon. For example, 85% of targeted cut-ins are predicted 0.5s before the cut-in and 50% are already predicted 2s before the cut-in (the graph does not show the prediction horizon for 0s, because cut-ins which are not predicted *before* this point are considered as FNs). The TPR slowly drops with increasing prediction horizon, however still 5.6% of cut-ins are predicted 5s before the cut-in or earlier.

The reason for the decreasing TPR with inreasing prediction horizon is threefold: First, in general the number of behavioral options dramatically increases with increasing prediction horizon. For example, the driver of a vehicle with a TTC of 10s to its predecessor can choose between braking or changing lane, freely choosing between mild and strong deceleration, shallow or steep lane-change, chaning lane now or later. In contrast, at 1s TTC, the driver can only choose to evade to another lane with a steep emergency trajectory. So in general, prediction with a high prediction horizon is more challenging because there are more alternatives to consider. The second reason for the decrease of TPR with increasing prediction horizon is caused by the physical prediction, because it provides a high confidence for a cut-in maneuver, if the cut-in trajectory significantly differs from the going-straight trajectory - which is at a late state during the cut-in maneuver. Finally, also the confidence of the context-based prediction raises with decreasing prediction horizon, because of the TTC based features used for prediction. These features rise for low TTC values which occur when a vehicle comes close to its predecessor.

Figure 9 additionally shows the typical corresponding position of a cutting-in vehicle at four points in time. At 0s, the vehicle is at the annoted reference point. At 1s, the blinker is activated, the car is in transition of a lane-change and the left tire touches the lane marking. 2s before the cut-in, the vehicle's blinker is active, but only a minimal lateral displacement is observable, whereas at 3s before the cut-in, the vehicle does not show any sign of the upcoming cut-in. Even with highly accurate sensing a conventional prediction algorithm that bases on phenomenological features is not capable of predicting behaviors more than 2s before they happen - simply because they are not yet observable. However, at this point in time, our proposed approach already predicted 50% of the cutting-in vehicles. In other words, context-based prediction is *required* for predicting lane changes more than 2s before they occure, whereas the combination with

physical prediction is required to increase the performance in the interval from $[0, 2[$s.

5. CONCLUSION

This contribution presents a novel approach for predicting other vehicles' behavior by combining a context-based prediction with a physical prediction. In contrast to existing approaches, the context-based prediction evaluates relations between vehicles and does not use any features that are phenomenological for a cut-in. The evaluation shows that the proposed combination of context-based and physical prediction achieves a high accuracy and a high prediction horizon: The context-based prediction is required for predicting maneuvers *before* they become observeable, whereas the physical prediction is required to achieve a high accuracy *once* the behavior becomes observable. The technology has been integrated in to the Honda i-ACC, which is now commercially available in the 2015 Honda CR-V. A companion paper by Kleinehagenbrock et al. (2015) details the system embedding and presents a subjective user test.

REFERENCES

Bonnin, S., Weisswange, T.H., Kummert, F., and Schmüdderich, J. (2013). Accurate behavior prediction on highways based on a systematic combination of classifiers. In *Proc. IEEE Intelligent Vehicles Symposium*, 1803–1808.

Bonnin, S., Weisswange, T., Kummert, F., and Schmuedderich, J. (2014). General behavior prediction by a combination of situation specific models. *IEEE Transactions on Intelligent Transportation Systems*, PP, 1–11.

Dagli, I., Breuel, G., Schittenhelm, H., and Schanz, A. (2004). Cutting-in vehicle recognition for ACC systems- towards feasible situation analysis methodologies. In *Intelligent Vehicles Symposium*, 925–930. doi:10.1109/IVS.2004.1336509.

Garcia Ortiz, M., Kummert, F., and Schmudderich, J. (2012). Prediction of driver behavior on a limited sensory setting. In *Intelligent Transportation Systems (ITSC), 2012 15th International IEEE Conference on*, 638–643. doi:10.1109/ITSC.2012.6338810.

Gindele, T., Brechtel, S., and Dillmann, R. (2010). A Probabilistic Model for Estimating Driver Behaviors and Vehicle Trajectories in Traffic Environments. In *Proc. IEEE Intelligent Transportation Systems*, 1625–1631.

Graf, R., Deusch, H., Fritzsche, M., and Dietmayer, K. (2013). A learning concept for behavior prediction in traffic situations. In *Intelligent Vehicles Symposium (IV), 2013 IEEE*, 672–677. doi:10.1109/IVS.2013.6629544.

Hansen, N. (2006). The cma evolution strategy: a comparing review. In *Towards a new evolutionary computation*, 75–102. Springer.

Kasper, D., Weidl, G., Dang, T., Breuel, G., Tamke, A., Wedel, A., and Rosenstiel, W. (2012). Object-oriented Bayesian networks for detection of lane change maneuvers. 4(3), 19–31. doi:10.1109/MITS.2012.2203229.

Kleinehagenbrock, M., Nishigaki, M., Kastner, R., Schmüdderich, J., Rebhan, S., Weisswange, T., Kamiya,

H., Kusuhara, S., Mori, N., and Ishida, S. (2015). Introduction of intelligent adaptive cruise control (i-acc) – a predictive safety system. In *Future Active Safety Technology Towards zero traffic accidents (FAST-zero)*. FISITA.

Rebhan, S. (2013). Consistent behaviour generation of a predictive advanced driver assistant system. EU Patent EP2840007 A1, Honda Research Institute Europe GmbH.

Reichel, M., Botsch, M., Rauschecker, R., Siedersberger, K.H., and Maurer, M. (2010). Situation Aspect Modelling and Classification Using the Scenario Based Random Forest Algorithm for Convoy Merging Situations. In *Proc. IEEE Intelligent Transportation Systems*, 360–366.

Schlechtriemen, J., Wedel, A., Hillenbrand, J., Breuel, G., and Kuhnert, K.D. (2014). A lane change detection approach using feature ranking with maximized predictive power. In *Intelligent Vehicles Symposium Proceedings, 2014 IEEE*, 108–114. doi:10.1109/IVS.2014.6856491.

Schmuedderich, J. (2014). A method and system for predicting movement behavior of a target traffic object. EU Patent 14 161 248, Honda Research Institute Europe GmbH.

Schmuedderich, J. and Rebhan, S. (2011). A method and system for predicting movement behavior of a target traffic object. EU Patent EP 2562060 B1, Honda Research Institute Europe GmbH.

Spackman, K.A. (1989). Signal detection theory: Valuable tools for evaluating inductive learning. In *Proceedings of the sixth international workshop on Machine learning*, 160–163. Morgan Kaufmann Publishers Inc.

The Foresighted Driver: Future ADAS Based on Generalized Predictive Risk Estimation

Julian Eggert * **Stefan Klingelschmitt** ** **Florian Damerow** **

* *Honda Research Institute (HRI) Europe, Carl-Legien-Str. 30, 63073 Offenbach, Germany (e-mail: julian.eggert@honda-ri.de)*
** *Control Methods and Robotics Lab, Technical University of Darmstadt, 64283 Darmstadt, Germany (e-mail: [stefan.klingelschmitt, florian.damerow]@rmr.tu-darmstadt.de)*

Topics: Driver Behavior Modeling, Vehicle Dynamics Control and Autonomous Driving, Active Safety testing Methods and Tools

Abstract: Separably developed functionality as well as increasing situation complexity poses problems for building, testing, and validating future Advanced Driving Assistance Systems (ADAS). These will have to deal with situations in which several current ADAS domains interplay. We argue that a generalized estimation of the future ADAS functions' benefit is required for efficient testing and evaluations, and propose a quantification based on an estimation of the predicted risk. The approach can be applied to several different types of risks and to such diverse scenarios as longitudinal driving, intersection crossing and lane changes with several traffic participants. Resulting trajectories exhibit a proactive, "foresighted" driver behavior which smoothly avoids potential future risks.

1. INTRODUCTION

We are currently seeing a phase of increased Advanced Driving Assistance Systems (ADAS) functionality for driver support, comprising forward collision warning (FCW), autonomous emergency braking (AEB), traffic jam assist (TJA), cross traffic assist (CTA) and several more. Common to all these is that they have been developed and validated for a specific narrow working domain in terms of context evaluation, operation range and even interfaces and interaction concepts. Future Adaptive Driver Assistance Systems applicable to more complex situations, say, a mixed longitudinal/lateral behavior situation while overtaking on the highway in the presence of multiple other traffic participants, or a multilane crossing with combined frontal and lateral urban traffic, will require (i) a generalization resp. seamless interplay of the concepts used for the existing, specialized ADAS functions, (ii) an extended analysis of the drivers context in terms of larger numbers of interacting traffic participants and road structure information, (iii) a larger prediction horizon for the dynamics of the ego-vehicle and the other traffic participants and (iv) a quantification and validation of the operating system.

On one side, an extended analysis of the drivers context implies capabilities for the automatic interpretation of the current driving situation, as well as the estimation of the consequences a situation interpretation has on the ego-vehicle's behavior options. On the other side, a validation of the future ADAS functions requires new approaches to deal with the combinatorial variety of parameter settings. The rising situation complexity, together with the sparsity of events (e.g. one fatal accident per 127 million driven km, Shladover (2009)) that can be used for a statistical validation of a system in real world operation, leads to prohibitively high testing costs. Common to the extended context analysis and the system validation is that both need a quantification in terms of usefulness for the drivers purpose.

In this work we propose to model the usefulness as a combination between risk and utility. Utility can be measured in a straightforward way as e.g. the time and money required to travel from A to B. On the other hand, general risk is considered as the probability of something happening multiplied by the resulting cost if it does. Since standard risk indicators like Time-to-Contact (TTC) are not sufficient for dealing arbitrary situations, we take an approach for the quantification of general driving risks according to Eggert (2014) and show how it can be used to implement a risk and utility based behavior planning or driver behavior support, for situations of incremental complexity.

The approach comprises the following steps:

- A classification of the current scenario into situation hypotheses as perceived from the ego-vehicle perspective, based on context information and the spatiotemporal pattern of interactions between traffic participants.
- A selection step based on the situation hypotheses and their estimated associated empirical risks. The result is a subset of situation hypotheses considered relevant for the ego-car behavior that apply to the current scenario.
- A prediction step during which we extrapolate the future development of each of the selected situation hypotheses resp. the states of the traffic participants.

- For each situation hypothesis and for a variety of own intended trajectories, an estimation of the future predicted risk and utility. For each situation we then get a risk landscape (*risk map*) which we can use for detecting the future points of high criticality.
- The planning of appropriate ego-car behavior options which cover the space of possible behaviors avoiding points of maximal risk in the risk landscape.
- The evaluation (for ADAS support and warning functions) or selection (for autonomous driving functions) of the most appropriate ego-car behavior according to their overall expected risk and utility.

From a systems perspective, it has been postulated that most ADAS functions rely on the 4 steps of object assessment, situation assessment, risk assessment and decision making, Hall and Llinas (1997). These steps are sufficiently general to be matched to a large variety of systems including the one presented in this paper. However, several components of these 4 steps, as it is the case for appropriate risk metrics and situation prediction technologies, are subject of current research.

In Lefèvre et al. (2013), a difference is made between intentions and expectations of the driver, and risk is assessed by detecting conflicts between the two. It is argued that such an approach is supported by the fact that a large number of accidents is caused by driver errors, see e.g. TRACE project (2008). However, such a model does provide rather a kind of alertness level for an observing driver than a quantifiable risk measure for the ego-vehicle.

In general, *risk estimation* approaches can be divided into 2 major groups. On one side, holistic systems incorporate context information to directly identify the criticality of a traffic situation, extrapolating from previously recorded data or using criticality rules and indicators. Learning systems, knowledge-based systems and systems that rely on risk indicators like TTC (see e.g. van der Horst (1991); Hillenbrand et al. (2006)) fall into this group. Systems that learn from empirical data have been successfully trained to identify potentially dangerous situations based on databases with accident recordings, see Chinea and Parent (2007); Salim et al. (2007). One issue here is that *representative* data is not available to a sufficient extent, neither from real recordings nor from simulations; another drawback is that scalability from simple to more complex situation patterns is difficult.

This first group of approaches involves a strong predictive component, since risk always means *hypothetical future risk*. In the learning approaches, the prediction is implicit, and comes from the mapping between the vehicle states to an accident event or criticality measure some time after. Similary, knowledge and indicator-based systems detect criticality based on sets of heuristics, where a prediction is implicitly comprised in the designed rules and risk indicators, so that e.g. a too high speed before the crossing may imply a risk when the car reaches the intersection.

In the second group, risk estimation approaches are based on internal simulations for predicting the future time course of the entities in the environment. The risk is then calculated as a function of the future states, see e.g. Althoff et al. (2009); Käfer et al. (2010); Rodemerk et al. (2012). Popular are trajectory estimation methods, which use different motion models to predict the possible future states and then check trajectories for mutual collisions. The degree of model complexity of the prediction models varies, ranging from motion models without constraints up to models which incorporate different driving maneuvers and the current road layout, see e.g. Lefèvre et al. (2014) for a review. To consider the uncertainty spread of possible future trajectories, sampling-based methods are frequently used. Popular behavior planning based on grid and potential-field-based context representations also fall into this group.

In this paper, the contribution to active safety systems concentrates on a system with the steps of understanding the current driving situation, efficiently predicting the behavior of the relevant entities in the environment, estimating the level of expected future danger that the situation poses, and planning the most appropriate driving behavior which should be taken in order to lower the danger. Our approach is based on a rigorous foundation of probabilistic risk for traffic scenarios and provides a formal justification why both approaches - holistic risk estimation on one side and detailed state prediction with risk evaluation as function of predicted states on the other side - are needed for an efficient, general-purpose risk estimation.

2. SITUATION-BASED RISK EVALUATION AND BEHAVIOR PLANNING

Figure 1 shows a rough overview of the different components of the general approach for behavior generation, based on risk considerations. Starting from the left-hand side, knowledge $\mathbf{x}_t$ about the scene at time t is acquired using sensor measurements. Since the scene may be composed of several entities (e.g. different traffic participants, infrastructure elements, etc.) with state vectors $\mathbf{x}_t^i$ (ego car state $\mathbf{x}_t^0$), we write $\mathbf{x}_t := \{\mathbf{x}_t^0, \mathbf{x}_t^1, ..., \mathbf{x}_t^n\}$. Using discrete time step indices $t, t+1, ..., t+s$ (time step size Δt), we additionally introduce state vector sequences

$$\mathbf{x}_{t:t+s} := \{\mathbf{x}_t, ..., \mathbf{x}_{t+s}\} \tag{1}$$

which describe e.g. the states of the scene from t (now) until a time $t+s$ (s into the future).

The overall target of the system is to compute a behavior in form of a trajectory over the ego-car states $\mathbf{x}_{t:t+s}^0$ which minimize an expected/predicted risk. Since risk is the probability that a disruptive event (e.g., an accident) happens, multiplied by the cost resp. the damage if it does, we define future risk [1] at $t+s$ as the cost expectation value

$$r(t+s, \mathbf{x}_t) = \int c_{t+s} P(c_{t+s}|\mathbf{x}_t) \, dc_{t+s} \tag{2}$$

where $P(c_{t+s}|\mathbf{x}_t)$ is the probability of a damage c_{t+s} which happens at $t+s$, if we know the states $\mathbf{x}_t$ of the current scene.

An all-situation risk prediction is computationally infeasible, therefore we partition the prediction space into different prototypical situation classes. A situation combines a small subset of interacting entities (usually car-car or car-infrastructure pairs) with a prototypical spatiotemporal behavior pattern $\hat{\mathbf{x}}_{t+1:t+s}$ (with $\hat{\mathbf{x}}_t = \mathbf{x}_t$), like the ego-car braking to give another car right-of-way at an intersection.

---

[1] To be precise, this is the risk *density* over time.
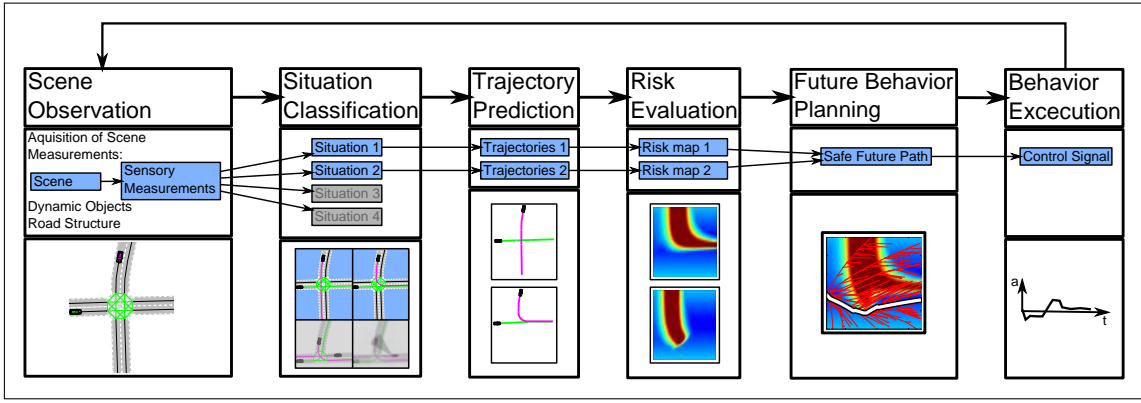
Fig. 1. General approach for situation based risk evaluation and behavior planning.

This results in situation-specific state vector sequences which depend on the situation hypotheses h_t, so that we get

$$P(c_{t+s}|\mathbf{x}_t) = \sum_{h_t} P(c_{t+s}|\mathbf{x}_t, h_t)P(h_t|\mathbf{x}_t) \qquad . \quad (3)$$

The situation hypotheses probabilities $P(h_t|\mathbf{x}_t)$ are calculated at t from the evidence $\mathbf{x}_t$ and are valid during the prediction interval $[t, t+s]$, until their calculation is renewed. In Fig. 1, second box from left, the situation classification component is shown.

The situation-dependent damage probability from (3) can be expanded to

$$P(c_{t+s}|\mathbf{x}_t, h_t) := \int d\mathbf{x}_{t+s} \dots \int d\mathbf{x}_{t+1} \quad (4)$$

$$\sum_{e_{t+s}} P(c_{t+s}|e_{t+s}, \mathbf{x}_{t+s}) \, P(e_{t+s}|\mathbf{x}_{t:t+s}) \, P(\mathbf{x}_{t+1:t+s}|\mathbf{x}_t, h_t)$$

i.e., a combination of (i) a damage probability $P(c_{t+s}|...)$ given that an event e_{t+s} happens at $t+s$ and the states at the event time are known, (ii) a future event triggering probability $P(e_{t+s}|...)$ which depends on the predicted state sequence $\mathbf{x}_{t:t+s}$, and (iii) a prediction probability $P(\mathbf{x}_{t+1:t+s}|...)$ of the state vector sequences $\mathbf{x}_{t+1:t+s}$ for each situation hypothesis h_t, if we start with states $\mathbf{x}_t$.

The discrete variable e_{t+s} describes the event class such as e.g. car-to-car, car-to-pedestrian or car-to-infrastructure collisions or control loss at drivability limits. For each of them, a specific damage probability $P(c_{t+s}|e_{t+s}, \mathbf{x}_{t+s})$ is used, e.g. car-to-car accidents are modeled using a partially inelastic collision approach. In addition, $e_{t+s} = 0$ indicates no event, in this case the costs are given by efficiency, utility and comfort considerations.

The event triggering probability $P(e_{t+s}|\mathbf{x}_{t:t+s})$ can be calculated using a so-called *survival function* as used in this paper (see Eggert (2014)), or by checking physical collision by coincident spatial occupancy (Schreier et al. (2014)). What remains to be calculated is the situation-dependent state prediction $P(\mathbf{x}_{t+1:t+s}|\mathbf{x}_t, h_t)$. A standard way is to use (expensive) stochastic sampling methods in combination with appropriate propagation probabilities $P(\mathbf{x}_{t'+1}|\mathbf{x}_{t'}, h_t)$ from one timestep to the next. However, to reduce the complexity of the integrals in (4) yet appropriately capture the growing prediction uncertainty over time, we approximate the probabistic state vector

sequence by its situation-specific prototypical state vector sequence $\hat{\mathbf{x}}_{t+1:t+s}$,

$$P(\mathbf{x}_{t+1:t+s}|\mathbf{x}_t, h_t) \sim \delta(\mathbf{x}_{t+1:t+s} - \hat{\mathbf{x}}_{t+1:t+s}(\mathbf{x}_t, h_t)) \quad (5)$$

and model the growing uncertainty in the event triggering probability by incorporating explicitly the prediction time s to get $P(e_{t+s}|\mathbf{x}_{t:t+s}, s)$. As a second approximation, for simplification [2] we introduce a deterministic damage calculation for fixed known states $\mathbf{x}_{t+s}$,

$$P(c_{t+s}|e_{t+s}, \mathbf{x}_{t+s}) \sim \delta(c_{t+s} - \hat{c}_{t+s}(e_{t+s}, \mathbf{x}_{t+s})) \quad (6)$$

Taking eqs. (2), (3) and (4) and inserting eqs. (5) and (6), results in the final risk estimation formula

$$r(t+s, \mathbf{x}_t) = \sum_{h_t} r(t+s, \mathbf{x}_t, h_t) \, P(h_t|\mathbf{x}_t) \quad (7)$$

with the situation-dependent risk

$$r(t+s, \mathbf{x}_t, h_t) \sim \sum_{e_{t+s}} \hat{c}_{t+s}(e_{t+s}, \hat{\mathbf{x}}_{t+s}(\mathbf{x}_t, h_t))$$

$$P(e_{t+s}|\hat{\mathbf{x}}_{t+1:t+s}(\mathbf{x}_t, h_t), s) \qquad . \quad (8)$$

The risk calculation therefore contains a damage cost calculation according to $\hat{c}_{t+s}$ for critical events, a future event triggering probability $P(e_{t+s}|...)$ which depends on the predicted prototypical state sequence $\hat{\mathbf{x}}_{t:t+s}(\mathbf{x}_t, h_t)$, and a situation hypothesis probability $P(h_t|\mathbf{x}_t)$.

The prediction of future states $\hat{\mathbf{x}}_{t:t+s}(\mathbf{x}_t, h_t)$ is achieved by a deterministic interactive agent model according to Eggert et al. (2015), however, arbitrary other models with a sufficient behavior complexity can be used here. In Fig. 1, third box, predicted trajectory pairs are shown for 2 different situation hypotheses. In the 4th box, the risk is calculated according to (7) for different ego-car behavior options, yielding so-called *risk maps*. In the 5th box, behaviors are planned by searching for the best trajectories in terms of overall cost. Finally, the 6th box shows the selected behavior execution.

The situation classification and its benefits are explained in section 3. The detailed risk evaluation, behavior planning and execution are extended in section 4. The result is a behavior estimation based on generalized predictive risk estimation.

---

[2] This is however not necessary so that a full probabilistic treatment of the damage can be easily incorporated back again.
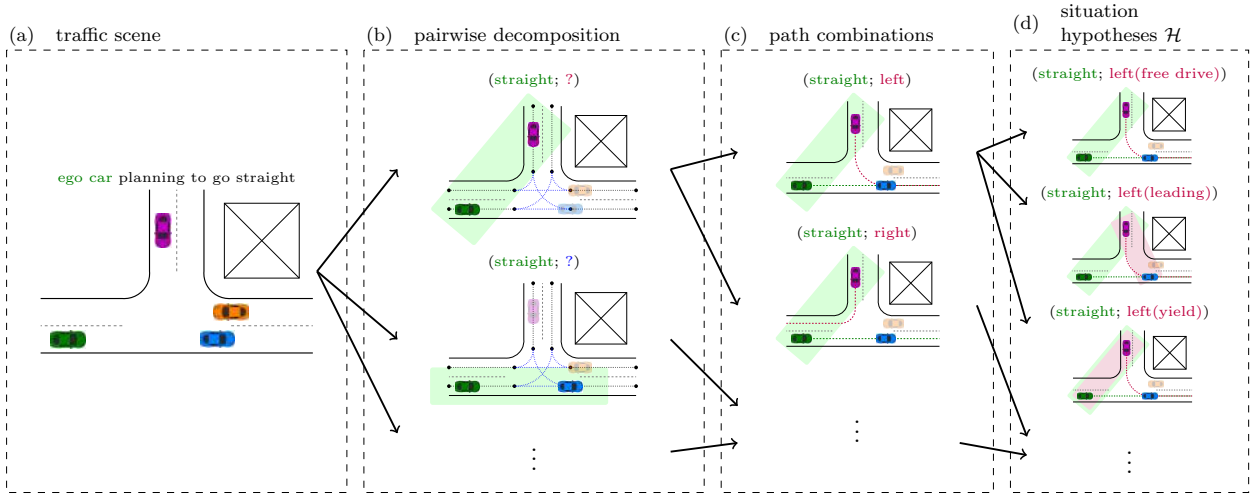
Fig. 2. Hypotheses generation, starting from a complex traffic scene (a). In (b), the scene is decomposed into interacting entity pairs (green boxes), containing the ego-vehicle. In (c), possible path combinations are considered. In (d), for each of the affecting vehicle's potential dynamic behavior patterns a situation hypothesis is created.

3. SITUATION RECOGNITION & SITUATION HYPOTHESES SELECTION
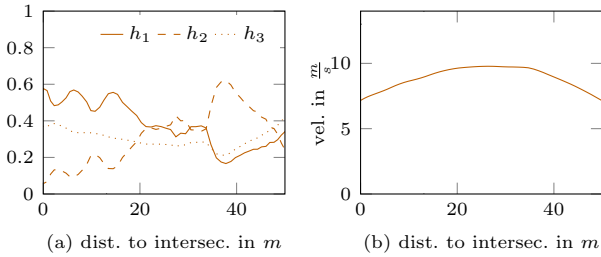
Fig. 3. (a) shows the probability of possible hypotheses (h_1(left; right(free drive)), h_2(left; straight(free drive), h_3(left; straight(yield)) dependent on the distance of the affecting vehicle to the intersection. The vehicle actually performs a right turn. (b) shows the corresponding longitudinal velocity profile.

From (8) we see that in order to reliably asses traffic scenes it is necessary to predict future state vectors $\hat{\mathbf{x}}_{t+1:t+s}$ of traffic participants several seconds into the future. However, inner-city traffic scenes exhibit a high variability and complexity, due to the number of possible occurring scene entities and their interactions, which leads to an overwhelming number of necessary predictions. Therefore, we propose to decompose traffic scenes into discrete situations, as proposed in section 2, with similar occurring spatiotemporal trajectory patterns of interacting scene entities forming a discrete prototypical situation. At the same time, we focus on keeping the number of simultaneously considered interacting traffic participants per situation as low as possible. Situations allow to efficiently partition complex, unseen traffic scenes into patterns with limited interactions and predict *situation-specific* future state vector sequences $\hat{\mathbf{x}}_{t+1:t+s}(\mathbf{x}_t, h_t)$.

3.1 Hypothesis Generation and Validation

Based on the evidence of a traffic scene $\mathbf{x}_t$, comprising infrastructure information, dynamic as well as static scene entities, usually a large set $\mathcal{H}$ of situation hypotheses

h_t applies. Each hypothesis consists of one possible path combination for simultaneously considered scene entities (non ego-vehicles are referred to as affecting entities) Additionally, each affecting entity's path is associated with a characteristic *dynamic behavior pattern* (e.g. differing velocity profiles). Typical patterns comprise e.g. giving right of way, driving behind a vehicle, stopping at a traffic light, etc.

The generation process for hypotheses h_t is exemplarily presented focusing on bilateral situations. The hypotheses generation can be divided into three steps, as illustrated in Figure 2, comprising entity grouping, path combinations and dynamic behavior patterns, to arrive at the full set of situation hypotheses $\mathcal{H}$.

To be able to deal with uncertainties, caused by imperfect sensor perception, unobservable variables (e. g. driving intention, style, ...) and insufficient prediction capabilities, we propose a probabilistic situation hypotheses validation, resulting in a belief $P(h_t|\mathbf{x}_t)$ for each situation hypothesis, as introduced in (3).

For the calculation of the situation hypothesis probability, we use probabilistic classifier methods like proposed in Klingelschmitt et al. (2014). These are fed with different situation indicators based on situation-dependent context information extracted from $\mathbf{x}_t$, which quantify the matches between the entities states with their expected paths and spatiotemporal behavior patterns. The result is $P(h_t|\mathbf{x}_t)$, the probability that a situation h_t will apply to the driving patterns during an upcoming time interval.

Figure 3 shows the result of an exemplary situation hypotheses validation performed on a real-world scenario similar to the one shown in Figure 2 (a), except that the ego-vehicle is planning to make a left turn. In this case, situation hypotheses resulting from the pairwise combination of the ego-vehicle with the orange vehicle are evaluated.

3.2 Hypothesis Selection

Depending on the complexity of the encountered infrastructure and present scene entities, the set of instantiated
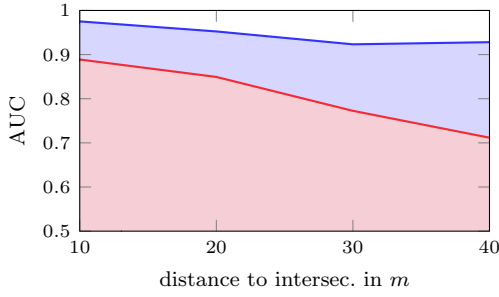
Fig. 4. The AUC curves are based on ROC curves created by adapting the threshold γ for our proposed selection scheme (9) (blue) and a strictly belief-based hypotheses selection ($\gamma < P(h_t|\mathbf{x}_t)$) (red). The *true positive* and *false positive rates* are based on the number of selected situation hypotheses compared to the actually encountered *relevant* situation hypotheses. The data used for the shown quantitative evaluation is obtained from a realistic traffic simulator. A detailed real-world example can be found in Klingelschmitt et al. (2015).

situation hypotheses increases combinatorially. This leads to two main disadvantages. Firstly, the computational costs for predicting and evaluating all hypotheses $h_t \in \mathcal{H}$ several seconds into the future get concomitantly high. Secondly, subsequent risk assessment techniques and behavior planning algorithms also suffer from the amount of hypotheses taken into account. Therefore, we propose a beforehand situation hypotheses selection scheme, with a subsequent concentration on those situations that are relevant for the ego-car's behavior.

The selection is based on combining the situation-specific risk $r(t + s, \mathbf{x}_t, h_t)$ from eq. (8) with the hypothesis belief $P(h_t|\mathbf{x}_t)$ from the validation step in section 3.1 in order to assess if the particular hypothesis h_t needs to be further investigated by subsequent systems. A situation hypothesis is selected, and thus added to the *set of relevant situation hypotheses* $\mathcal{H}'$, if the joint situation-specific risk and hypothesis belief exceed a threshold γ

$$\gamma < r(t + s, \mathbf{x}_t, h_t)P(h_t|\mathbf{x}_t). \tag{9}$$

Since $r(t + s, \mathbf{x}_t, h_t)$ is not yet known at this point and only calculated afterwards as explained in section 2 for the selected situation hypotheses, we proposed to learn situation-specific regression models M_h that estimate expected situation-specific risks from empirical data, as introduced in Klingelschmitt et al. (2015). In order to make conservative and robust estimations, we estimate the situation-specific risk from (9) by using the maximum measured situation-specific risk within the considered time interval $t' \in [t, t+s']$. Hence, we train our situation-specific risk regression models to estimate

$$M_h(\mathbf{x}_t) \sim \max_{s'} r(t + s', \mathbf{x}_t, h_t).$$

Using this approach, the number of superfluously inspected hypotheses can be drastically reduced, as shown by the AUC (**A**rea **U**nder the **C**urve) plots in Figure 4.

4. GENERALIZED PREDICTIVE RISK ESTIMATION

4.1 Predictive Risk Maps

Once we have selected a suitable subset of relevant situation hypotheses which apply to the current ego-car's
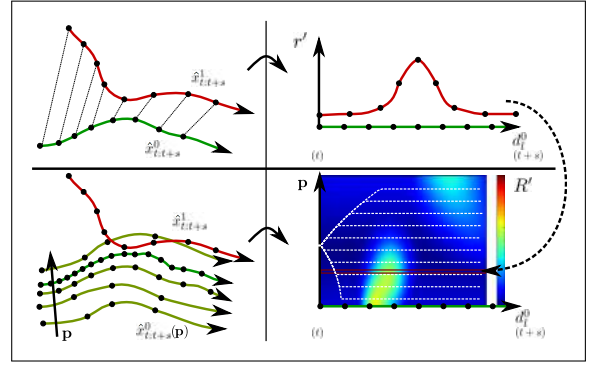
Fig. 5. Predictive Risk Map - Top: evaluation of risk (top right) based on predicted ego car (green) and other car (red) trajectories (top, left) - Bottom: Generation of predictive risk map (bottom, right) based on risk evaluation of a variation of ego car trajectories and other car trajectory (bottom, left).

driving context, the general target of our system is to plan the ego car's future behavior (here future velocity profile) to be safe and of high utility. For this purpose we have to evaluate possible future behavior alternatives in terms of risk and utility. In a first step we concentrate on the behavior evaluation of a single situation. This can be done by building so called Predictive Risk Maps, introduced by Damerow and Eggert (2014), which indicate how risky a certain behavior will be in the future. The trajectory prediction of one situation provides one predicted prototypical trajectory for each involved entity, here $\hat{\mathbf{x}}_{t:t+s}^0$ for the ego and $\hat{\mathbf{x}}_{t:t+s}^1$ for another car. We can now evaluate the risk by comparing the ego car's and one other car's trajectory pairwise at the same moment in predicted time using the situation dependent risk function (8). For illustrative purposes we use the risk over longitudinal distance d_l^0 instead of future time s, as we can equivalently write $r'(d_l^0, \mathbf{x}_t, h_t) = r(t + s(d_l^0), \mathbf{x}_t, h_t)$.

As a result we gain a measure for future risk, illustrated in Fig. 5 (top). If we now build a variation of ego car trajectories $\hat{\mathbf{x}}_{t:t+s}^0(\mathbf{x}_t, h_t, p)$ using a variation parameter p and evaluate the risk for each variation, we gather a predictive risk map $R(t + s, \hat{\mathbf{x}}_{t+s}^0(\mathbf{x}_t, h_t, p), \mathbf{x}_t, h_t)$, or

$$R'(d_l^0, \hat{\mathbf{x}}_d^0(\mathbf{x}_t, h_t, p), \mathbf{x}_t, h_t), \tag{10}$$

as shown in Fig. 5 (bottom).

Here we vary only the ego car longitudinal velocity $v_l^0(\mathbf{x}_t, h_t, v_{l,target}^0)$ using different target velocities $v_{l,target}^0$ and incorporate dynamic constraints in terms of maximal acceleration/deceleration indicated by the dashed white trajectories in Fig. 5 bottom right. As a result we arrive at a predictive risk map in the (d_l^0, v_l^0)-plane for a fixed initial state $\mathbf{x}_t$ and one situation h_t, as $R'(d_l^0, v_l^0)$ [3] (in the following we omit constant parameters in case they are not necessary).

We now search for low-risk paths across the risk map. These will vary from the predicted trajectories $\hat{\mathbf{x}}_d^0(\mathbf{x}_t, h_t, p)$ used for building the risk map (e.g. dashed white lines in Fig. 5 bottom right), leading to distortions in the risk map. For small deviations from the original trajectories,

---

[3] Remark however that risk maps which depend on more complex ego-car behavior parameterization, as e.g. for lateral control, can be treated similarly.
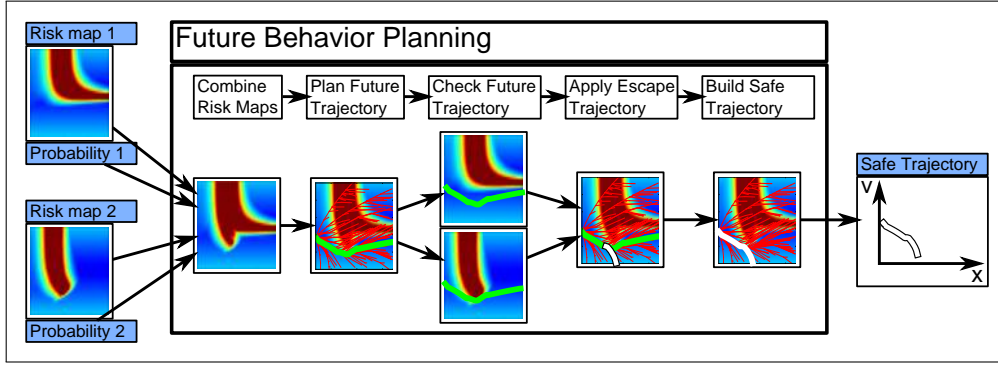
Fig. 6. Planning of safe and efficient future behavior: Scenario with 2 active situations with different probabilities, generating 2 risk maps. Both are then weighted with their situation occurrence probability and combined into one risk map, which is then used to plan the future behavior. The resulting trajectory is then checked for risk threshold violations in each situation and escape trajectories are applied. As a result we get an efficient safe trajectory by using the planned future trajectory with the earliest necessary escape trajectory.
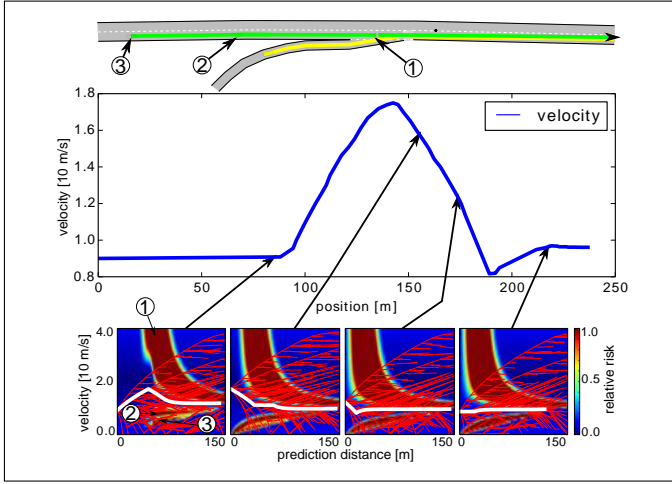
Fig. 7. Highway Accessing.
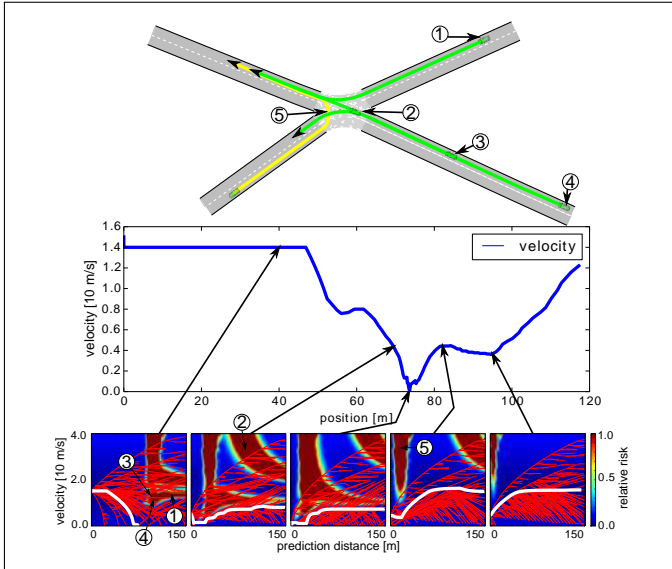
Fig. 8. Complex Turning Behavior: other cars as risk sources (1-4), curve as risk source (5).

however, the risk map topology does not vary substantially and can be used for planning.

4.2 Safe Trajectory Planning in Dynamic Environments

With the predictive risk maps $R'(d_l^0, v_l^0)$ for a certain situation we can now plan the best possible future behavior using e.g. a sampling based trajectory planner such as RRT*. The RRT* is an extension to the general RRT (Rapidly exploring Random Tree) enabling the algorithm to converge to the globally optimal solution minimizing a given cost function. As presented by Damerow and Eggert (2015) we use the algorithm to plan the ego car's future trajectory minimizing the overall costs as a combination of risk and utility normalized by the ego car's driven distance,

$$\text{Cost}(d_l^0, v_l^0) = \frac{1}{d_l^0} \int_0^{d_l^0} [R'(d_l, v_l^0) + \text{TC}(d_l, v_l^0)] \mathrm{d}d_l \ , (11)$$

with the utility / travel costs TC. We employ a cost function which is linearly increasing with the deviation of the ego car's velocity v_l^0 from the desired velocity $v_{l,des}^0$. TC_0 and m define the minimal travel costs and slope of the cost function.

$$\text{TC}(d_l^0, v_l^0) = \text{TC}_0 + m \left| v_{l,des}^0 - v_l^0 \right| \ . \tag{12}$$

The simulation results in Figs. 7 and 8 show, that this approach can be applied to a wide range of different scenarios, starting from highway scenarios with multiple traffic participants (e.g. Fig. 7) up to complex inner city scenarios (e.g. turning left at an unmanaged intersection with multiple other traffic participants involved (see Fig. 8). The turning scenario illustrates that our approach is also able to handle multiple types of risk, here additionally the risk for loosing control in curves due to high lateral acceleration, besides collision risks caused by several other dynamic objects.

4.3 Safe Trajectory Planning under Multiple Situations with Uncertainty

Until now we concentrated on a single, although complex, situation to plan the future behavior, using only one predicted spatiotemporal trajectory for each involved traffic participant. However, the situation classification and selection steps described in section 3.1 are in general not able to provide the one and only occurring situation, but a selection of situation hypotheses h_t. We additionally obtain the occurrence probability $P(h_t|\mathbf{x}_t)$ for each selected

(a) `(straight;left(yield))` Other car (purple) stopping to give way for the ego car (green).

(b) `(straight;left(free))` Other car not stopping due to overlooking the ego car.

(c) Driven velocity profiles.

(d) Situation occurrence probabilities $P(h_t|\mathbf{x}_t)$.

(e) Combined predictive risk maps timeline $t = [0, 2, 4, 6]s$ including planned future trajectory (green) and safe future trajectory (white).

(f) Situation-dependent unweighted predictive risk maps and planned future trajectory including risk threshold violations (white arrow). "other stopping" situation (top) and "other not stopping" situation (bottom).

(g) Comparison of velocity profiles. Check indicates correct situation classification, flash indicates wrong situation classification

Fig. 9. T-Intersection with uncertainty if other car is giving way.

situation and, by the following trajectory prediction step of each situation, one predicted trajectory for each involved entity. The target is now to find a future behavior which is of low risk and high utility in all hypothetical situations, and especially in the situation that will finally occur. The risk evaluation step generates one predictive risk map per

situation using the situation dependent predicted trajectories $\hat{\mathbf{x}}_{t:t+s}(\mathbf{x}_t, h_t)$.

The behavior planning step, consisting of 5 sub-steps, is shown in detail in Fig. 6. It is based on the concept of planning the future behavior with high utility for the most probable situation and additionally keeping an always safe, but possibly inefficient "plan b" for the other situations. By following these steps, we obtain a future behavior which is of high utility for a confident situation classification, but still safe for the case of an unconfident or even wrong situation classification. For this purpose, we first join the predictive risk maps of all possible situation hypotheses in a combined predictive risk map, according to (7) and (8).

$$R'(d_l^0, v_l^0) = \sum_{h_t \in \mathcal{H}'} R'(v_l^0, d_l^0, h_t) \frac{P(h_t|\mathbf{x}_t)}{\max_{h_t' \in \mathcal{H}'} (P(h_t'|\mathbf{x}_t))}. \quad (13)$$

This has the desired effect that the most likely situation is fully taken into account for behavior planning, whereas the other, less likely, situations are still taken into account, but weighted with $P(h_t|x_t)/\max_{h_t'}(P(h_t'|x_t)) \leq 1$. This results in a future behavior that mostly adapts to the best behavior for the most likely situation, but smoothly incorporates less likely situations. A confident situation classification would provide high probability only for one situation and low probability for the other situations. In this case the behavior adapts almost only to the best behavior of the most probable situation. In case of an unconfident situation classification, there are several situations with similar probability, and the resulting behavior would take risk of all those situations similarly into account.

Still we can not ensure an always safe behavior for the case that an unlikely situation suddenly kicks-in. Although the risk of this unlikely situation was partially taken into account and the resulting behavior averts this situation's risk, this might not be sufficient to ensure a safe behavior for this situation.

Thus in a further step we check the planned future trajectory for a risk threshold violation on each situation's risk map. In case of a threshold violation we then apply an escape trajectory (e.g. emergency braking) as late as possible, but as early as necessary to safeguard the situation for the case it actually kicks in. The finally executed safe trajectory consists of two parts, the trajectory of high utility planned using the combined risk map, followed by a possibly necessary escape trajectory. In general / in case of a confident situation classification, situations with low probability and high risk drop even further in probability and are finally discarded by the situation classification step as explained in section 3.2, or drop in risk, as the entities act in a risk aversive manner. As we reevaluate and replan from time to time the escape trajectory will usually never be executed. Only if a risky situation does not drop in risk and/or occurrence probability this escape trajectory will be executed to keep the overall situation safe.

In Fig. 9 we present a scenario, where a car approaches a T-intersection and plans to turn left onto the ego car's way. We analyze how our approach copes with the two hypothetical alternatives that (a) the other car yields to the ego car and (b) the other car violates the left-yields-to-right-rule and drives through. The most common scenario - the other car yielding way of right - is analyzed in detail

using the generalized predictive risk estimation approach. In this case, the situation classification (d) results in a high probability for the correct situation (a) and a low probability for situation (b). The predictive risk maps in (f) for the two situations are calculated and combined (wheighted by their occurrence probabilities) into the overall risk map (e), which is then used by the RRT* planner to calculate the desired future behavior (green line). This is then checked and safeguarded with possibly necessary escape trajectories (white line). The resulting ego-velocity profile (c) for this scenario shows a behavior of low risk and high utility (not significantly slowing down). In Fig. 9 (g), we compare different alternative cases, where the situation classification provides a false or correct classification results for the two situations (that the other car stops or does not stop). A wrong situation classifications deteriorates the resulting trajectories leading to an emergency braking maneuver, however they still are within the low-risk bounds of operation.

Confirmed by the simulation results the approach enables to plan safe and efficient trajectories for the case of a confident and correct situation classification. With lower situation classification confidence we get a less efficient, but still safe future behavior. This holds even for the case that the situation classification favors the wrong situation.

5. SUMMARY

We proposed a general approach for predictive risk estimation and behavior planning in dynamic environments that can be applied to several different scenarios comprising a mixture of risks such as e.g. longitudinal collision risks, risks of passing nearby without collision, risks at intersections and highway entrances and risks in curves.

The predictive risk approach allows to incorporate the inherent uncertainty that is involved when dealing with long-term trajectory predictions and noisy sensor measurements. Risks that are still further away in the future appear broader and more delocalized in space and time, increasing and sharpening as they become more imminent. The results show that different types of risk can be integrated within a single, generalizing model which additionally scales with increasing complexity. The same model results in simulated smooth and low-risk driving trajectories for such diverse situations as unmanaged intersections, lane entrances and lane changes. In the inspected situations with a simulated driver, the resulting behavior mimics that of a "foresighted" driver who is aware of the upcoming risks and reacts proactivley to avoid them. For real-world operation, the approach requires sensor-based estimations of the other traffic participants positions and velocities as well as of the road structure, which will be available in the not-so distant ADAS future.

After the desired types of risks have been selected and parameterized, we can apply the same type of estimation as a measurement for the quality of a performed driving action. E.g., the risk along a driving route can be measured with and without a certain new ADAS function, allowing for an efficient continuous quantification and validation of new ADAS functions by risk in conditions where conventional approaches like TTC are insufficient.

REFERENCES

Althoff, M., Stursberg, O., and Buss, M. (2009). Model-based probabilistic collision detection in autonomous driving. *IEEE Trans. on Int. Transp. Sys.*, 10, 299–310.

Chinea, A. and Parent, M. (2007). Risk assessment algorithms based on recursive neural networks. In *The 2007 International Joint Conference on Neural Networks (IJCNN)*, 1434–1440.

Damerow, F. and Eggert, J. (2014). Predictive risk maps. In *ITSC*, 703–710. IEEE.

Damerow, F. and Eggert, J. (2015). Balancing risk against utility: Behavior planning using predictive risk maps. In *IV*, in press. IEEE.

Eggert, J. (2014). Predictive risk estimation for intelligent adas functions. In *ITSC*, 711–718. IEEE.

Eggert, J., Damerow, F., and Klingelschmitt, S. (2015). The foresighted driver model. In *IV*. IEEE.

Hall, D. and Llinas, J. (1997). An introduction to multisensor data fusion. In *Proc. of the IEEE*, volume 85, 6–23.

Hillenbrand, J., Spieker, A.M., and Kroschel, K. (2006). A multilevel collision mitigation approach - its situation assessment, decision making, and performance tradeoffs. *IEEE Trans. on Int. Transp. Sys.*, 7(4), 528–540.

Käfer, E., Hermes, C., Wöhler, C., and Kummert, F. (2010). Recognition and prediction of situations in urban traffic scenarios. In *ICPR*, 4234 – 4237. IEEE.

Klingelschmitt, S., Damerow, F., and Eggert, J. (2015). Managing the complexity of inner-city scenes: An efficient situation hypotheses selection scheme. In *IV*, 388–393.

Klingelschmitt, S., Platho, M., Gross, H.M., Willert, V., and Eggert, J. (2014). Combining behavior and situation information for reliably estimating multiple intentions. In *IV*, 388–393. doi:10.1109/IVS.2014.6856552.

Lefèvre, S., Laugier, C., and Ibañez-Guzmán, J. (2013). Intention-aware risk estimation for general traffic situations, and application to intersection safety. Research Report RR-8379.

Lefèvre, S., Vasquez, D., and Laugier, C. (2014). A survey on motion prediction and risk assessment for intelligent vehicles. *Robomech Journal*, 1(1).

Rodemerk, C., Habenicht, S., Weitzel, A., Winner, H., and Schmitt, T. (2012). Development of a general criticality criterion for the risk estimation of driving situations and its application to a maneuver-based lane change assistance system. In *IV*, 264–269. IEEE.

Salim, F., Loke, S., Rakotonirainy, A., Srinivasan, B., and Krishnaswamy, S. (2007). Collision pattern modeling and real-time collision detection at road intersections. In *ITSC*, 161–166. IEEE.

Schreier, M., Willert, V., and Adamy, J. (2014). Bayesian, maneuver-based, long-term trajectory prediction and criticality assessment for driver assistance systems. In *ITSC*, 703–710. IEEE.

Shladover, S.E. (2009). Automated driving in progress and prospects. In *ITSC*. IEEE.

TRACE project (2008). Accident causation and pre-accidental driving situations - in-depth accident causation analysis. In *Deliverable D2.2*.

van der Horst, A. (1991). *Vision in Vehicles III*, chapter Time-to-Collision as a cue for decision making in braking, 19–26. Elsevier.

Driver's Judgment Assistance System at Signalized Intersection by Indicating GO/NOGO Indices

Yoshitaka Marumo*. Takashi Nakano**
Hiroyuki Kobayashi**. Yohei Michitsuji***

* College of Industrial Technology, Nihon University, 1-2-1 Izumi-cho, Narashino-shi, Chiba 275-8575, Japan (e-mail: marumo.yoshitaka@nihon-u.ac.jp)
** Graduate School of Nihon University, Chiba, Japan
*** Department of Mechanical Engineering, Ibaraki University, Ibaraki, Japan

Abstract: This study examines the driver assistance system which informs the passage possibility at a signalized intersection ahead. The assistance system indicates the distance which the vehicle can forward by maintaining the present velocity until turning to the red signal using the signal information. If the indicated distance is shorter than the distance to the intersection from the vehicle, the system also indicates a stopping distance by assuming the ordinary deceleration. The driving simulator experiments are conducted to evaluate the proposed assistance system. The assistance system encourages the earlier deceleration before the amber signal and prevents the emergency braking behavior or the risky passage through the intersection.

Keywords: Driver assistance systems, Driver behavior, Active safety, Signalized intersection, Dilemma zone

Topics: Cooperative Driver Assistance Systems, Cooperation between Drivers and Assistance Systems, Human Machine Interface.

1. INTRODUCTION

Many traffic accidents occur not only at unsignalized intersections but also at signalized intersections. "Dilemma zone" may cause traffic accidents at signalized intersections (Papaioannou et al., 2007). The dilemma zone is an area in which it is difficult for a driver to decide to pass through (GO) or stop at (NOGO) the intersection when the green signal turns to the amber signal.

Various technologies have been developed to prevent the traffic accidents at the signalized intersections caused by the dilemma zone (Long et al., 2013). A driver assistance system which informs passage possibility at a signalized intersection ahead through an onboard monitor is examined as field test using the road-vehicle communication (Honda Motor Co., Ltd., 2014). However, the assistance system with the onboard monitor may cause the driver's distraction to be led to unexpected accident such as the rear-end collision to the preceding vehicle.

If the information on passage possibility of the signalized intersection ahead is indicated in the driver's central vision, the assistance system assists the driver's judgment without the driver's distraction. This study examines the driver assistance system which indicates the information on passage possibility on the road ahead virtually assuming the AR (Augmented Reality) technology. The driving simulator experiments are conducted to evaluate the proposed assistance system.

2. ASSISTANCE SYSTEM

This study assumes that the signal information on the signalized intersection ahead is acquired by the road-vehicle communication. The assistance system informs the driver visually of the distance of the following two indices by assuming the HUD (Head-Up Display).

2.1 GO Index

One is "GO" index. This is composed of two distances, the entry possible distance and the passage possible distance. The entry possible distance $d_e(t)$ means that the vehicle can enter the intersection until the signal turns to the red signal by maintaining the present vehicle velocity $v(t)$. This distance is calculated by multiplying the present velocity and the time to the red signal TTR (Time To Red) as follows:

$$d_e(t) = v(t) \cdot \text{TTR} \tag{1}$$

The passage possible distance $d_p(t)$ means that the vehicle can pass through the intersection until the cross road signal turns to the green signal, i.e. the end of all the red signals, by maintaining the present vehicle velocity. This distance is calculated by multiplying the present velocity and the time to green signal of the cross road TTGc (Time To Green Cross) as follows:

$$d_p(t) = v(t) \cdot \text{TTG}_C \tag{2}$$
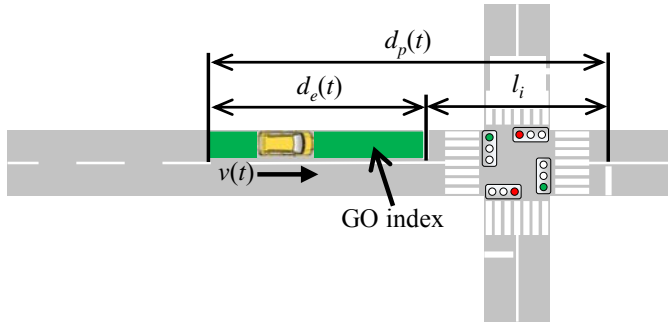
(a) Possible to enter and pass
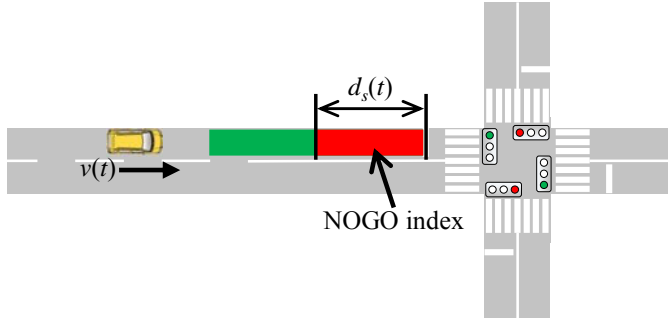
(b) Impossible to enter or pass

Fig. 1. Schematic diagram of indicating GO/NOGO indices

Fig. 2. Overview of fixed-base driving simulator
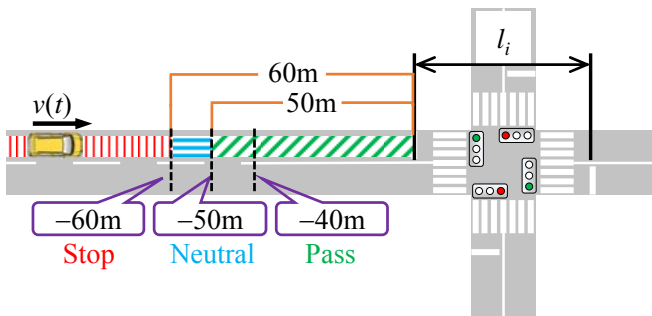
Fig. 3. Experimental condition of signal timing

2.2 NOGO Index

The other is "NOGO" index. This is a stopping distance that the vehicle can stop before the intersection with the moderate deceleration. The stopping distance is calculated by the present velocity, the assumed deceleration a_a (<0), and the driver's reaction time T as follows:

$$d_s(t) = v(t) \cdot T + \frac{v^2(t)}{2(-a_a)} \quad (3)$$

2.3 Indication of GO/NOGO Indices

Figure 1 illustrates the schematic diagram of indicating the two indices. If the distance to the intersection from the vehicle is shorter than that of the GO index, which is colored in green, the vehicle can enter and pass through the intersection as shown in Fig. 1(a). If the distance to the intersection from the vehicle is longer than that of the GO index, the vehicle cannot enter or pass through the intersection and the vehicle should start the deceleration before approaching the NOGO index, which is colored in red, as shown in Fig. 1(b).

3. DRIVING SIMULATOR EXPERIMENTS

3.1 Experimental Method

Driving simulator experiments are examined with seven male participants who travel a straight road through some signalized intersections. This study uses the CarSim DS 8.1.1 (Mechanical Simulation Corporation) as shown in Fig. 2 for the driving simulator experiments. This experiment evaluates the effectiveness when indicating the GO/NOGO indices on the road virtually. The participants are required to drive with and without the proposed assistance system.

Figure 3 illustrates the experimental condition of signal timing. Here, the intersection length l_i is 32m (passage time is about 2s with 60km/h). The duration of the amber signal is set to 3s, and of all the red signals is set to 2s, respectively. The assumed deceleration a_a is -2.94m/s^2 and the driver's reaction time T is 0.75s (Michitsuji, Y. et al., 2013).

If the driver maintains the vehicle speed of 60km/h (16.7m/s), the vehicle moves forward 50m during the amber signal. Therefore, the slash lines as shown in Fig. 3 indicate the area where the vehicle can enter the intersection until the end of the amber signal.

On the other hand, if the driver makes the vehicle stop at the stop line with the vehicle speed of 60km/h, the vehicle needs to start the brake at 60m before with the assumed deceleration a_a and the reaction time T. Therefore the vertical lines as shown in Fig. 3 indicate the area where the vehicle can stop before the stop line.

From the above mentioned two areas, the dilemma zone is defined between 50m and 60m before the intersection. In this area where is indicated by the horizontal lines as shown in Fig. 3, the vehicle can neither enter the intersection with maintaining the speed, nor stop before the stop line with the assumed deceleration and the reaction time.

This experimental condition of signal timing to the amber signal is placed at three positions where the vehicle passes as shown in Fig. 3. These positions are set to -40m, -50m, and -60m, which are referred to as the "Pass," "Neutral," and "Stop" conditions, respectively.
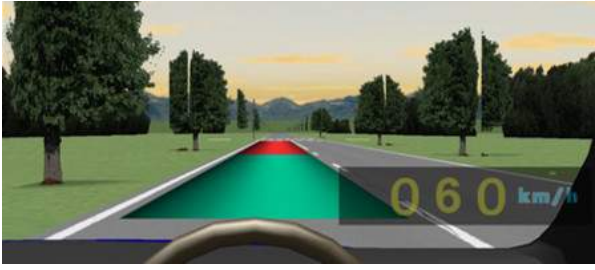
Fig. 4. Indication image of GO/NOGO indices
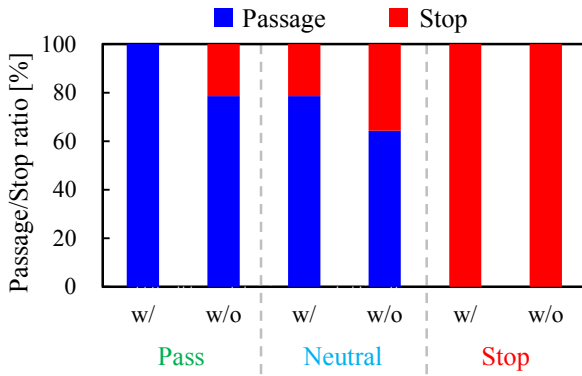
Fig. 5. Ratio of passage and stop (14 trials)

The participants pass through several intersections, which include a dummy condition of a fixed green signal, and cannot expect the event occurred intersection in a random order.

Indication image of the GO/NOGO indices is shown in Fig. 4. The evaluation index is indicated on the road ahead virtually by assuming the HUD, after the vehicle passes through the position of −167m (corresponding to 10s before arriving at the intersection with maintaining the vehicle speed of 60km/h).

The participants accelerate to 60km/h (=16.7m/s) from the stop situation. After the acceleration, the participants are required to keep the velocity 60km/h until the beginning of the indices indication with the assistance system or the changing the signal without the assistance system.

Seven males (Participant A through G) participated in the simulator experiments. All the participants gave their written informed consent before the experiments. The test drive was conducted to familiarize themselves with the simulator driving and the indication of the GO/NOGO indices. The participants are to experience the trials with the GO/NOGO indices assistance before the experiments without the assistant. These two driving conditions, i.e. with and without the assistance system, were repeated twice to make all 12 trials for each participant.

3.2 Experimental Results

The ratio of the passage and the stop is depicted in Fig. 5. This figure shows the 14 running results (total of the two trials for the seven participants). In the Stop condition, all the
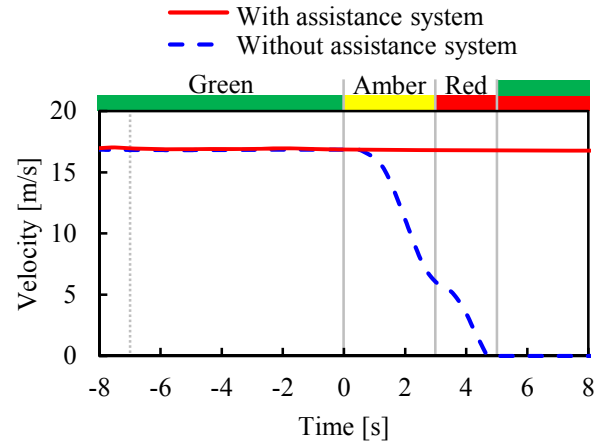
Fig. 6. Vehicle velocity (Neutral condition: 1st trial by Participant A)
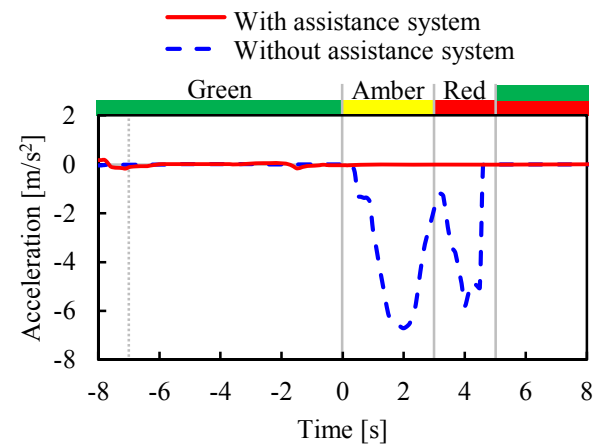
Fig. 7. Vehicle acceleration in Neutral condition (1st trial by Participant A)

participants make the vehicle stop with and without the assistance system. On the other hand, all the participants pass through the intersection with the assistance system, while a few participants stop at the intersection without the assistance system, under the Pass condition.

3.2.1 Driving Behavior

Figure 6 illustrates an example of the vehicle velocity with and without the assistance system (1st trial by Participant A) in the Neutral condition. In this figure, 0s in the horizontal axis means the signal change timing from the green to amber, and −7s corresponds to the start timing of the assistance. The driver with the assistance system (solid line) maintains the vehicle velocity and passes through the intersection, whereas the driver without the assistance system (broken line) makes the vehicle decelerate after turning to the amber signal (0s).

The acceleration (1st trial by Participant A) in the Neutral condition is shown in Fig. 7. The driver with the assistance system passes through the intersection without the deceleration, while the driver without assistance system initiates the braking with large deceleration.
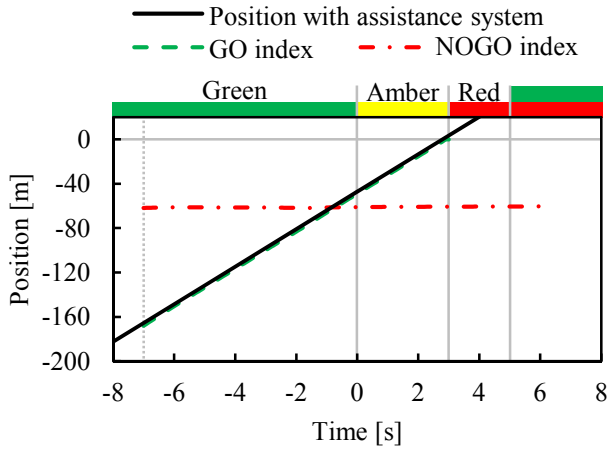
(a) With assistance system
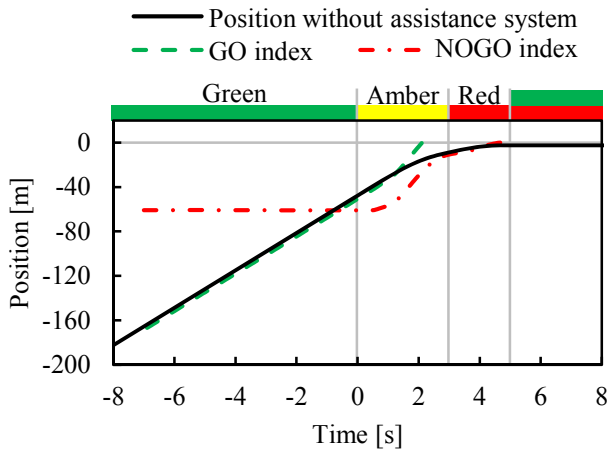
(b) Without assistance system

Fig. 8. Vehicle position in Neutral condition (1st trial by Participant)

Fig. 9. Vehicle velocity in Stop condition (1st trial by Participant B)
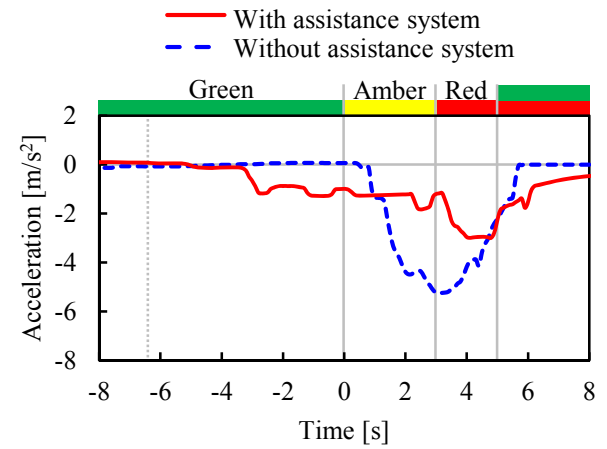
Fig. 10. Vehicle acceleration in Stop condition (1st trial by Participant B)

The vehicle position with and without the assistance system is depicted in Fig. 8. Figure 8(a) shows the position with the assistance system, and Fig. 8(b) is without the assistance system. 0m in the vertical axis means the stop line (entrance of the intersection). In this figure, the solid line indicates the vehicle position, the broken line shows the front end of the GO index, and the dashed line is the front end of the NOGO index. In fact, the evaluation indices are not indicated on the road without the assistance system, so the indices without the assistance system are shown for reference.

The vehicle position changes together with the GO index with and without the assistance system in the early stage. The driver with the assistance system can recognize the possibility to enter and pass through the intersection, and maintains the vehicle velocity. On the other hand, the driver without the assistance system decelerates after turning to the amber signal, even though the vehicle could enter and pass through the intersection. This braking maneuver makes the large deceleration because of the late reaction, which is observed by over vehicle position than the NOGO index (dashed line).

Figure 9 illustrates an example of the vehicle velocity with and without the assistance system (1st trial by Participant B) in the Stop condition. In this figure, −6.4s in the horizontal axis corresponds to the assistance start timing. The driver with the assistance system (solid line) initiates the braking behaviour before changing to the amber signal (0s), whereas the driver without the assistance system (broken line) makes the vehicle decelerate after turning to the amber signal.

The acceleration (1st trial by Participant B) in the Stop condition with and without the assistance system is depicted in Fig. 10. The driver with the assistance system brakes with the ordinary deceleration, while the driver without assistance system applies the strong brake because of the later deceleration.

The vehicle position with and without the assistance system is depicted in Fig. 11. The vehicle position does not reach the GO index (broken line) with and without the assistance system in the early stage. The driver with the assistance system, therefore, can recognize that the vehicle cannot enter nor pass through the intersection, and initiates the braking maneuver before turning to the amber signal. On the other
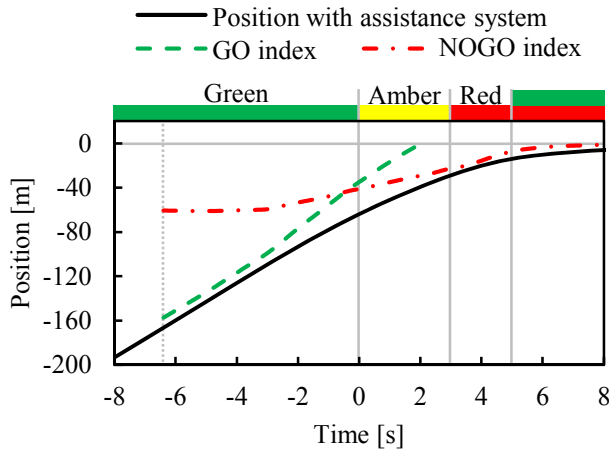
(a) With assistance system
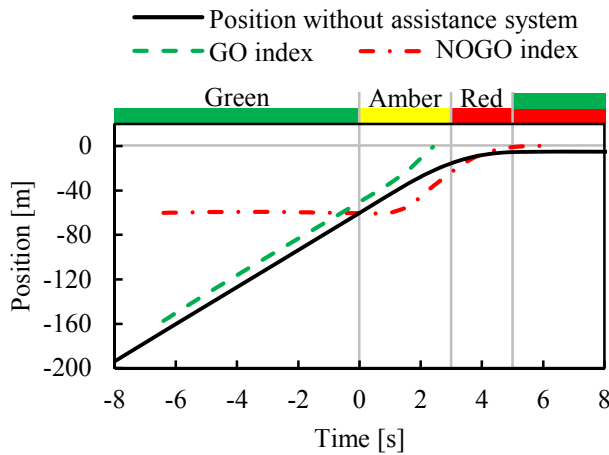
(b) Without assistance system

Fig. 11. Vehicle position in Stop condition (1st trial by Participant B)

(a) Average deceleration

(b) Maximum deceleration

Fig. 12. Averaged deceleration (Neutral and Stop conditions)

hand, the driver without the assistance system decelerates after turning to the amber signal. The vehicle position is over the NOGO index at 0s. This braking maneuver makes the large deceleration because of the late reaction.

The averaged deceleration including the other participants' braking is depicted in Fig. 12. Figure 12(a) shows the average deceleration by the braking distance, and Fig. 12(b) is the maximum deceleration. The assistance system reduces the average and the maximum deceleration.

3.2.2 Evaluation by Driving Indices Concerning Intersections

This section examines the margin to pass through or stop at the intersection using the evaluation indices concerning intersections. These evaluation indices are the Margin To Stop (MTS), Margin To Enter (MTE), and the Margin To Pass (MTP) proposed by Michitsuji (Michitsuji et al., 2013).

The MTS is the margin to make the vehicle stop at the stop line with the assumed deceleration. The MTS is calculated by dividing the distance from the vehicle to stop line $d(t)$ by the stopping distance with the assumed deceleration as follows:

$$\text{MTS} = \frac{d(t)}{v^2(t)/2(-a_a)} \tag{4}$$

If the MTS is lower than 1, the vehicle needs larger deceleration to stop at the stop line.

The MTE is the margin to make the vehicle enter the intersection until turning to the amber signal. The MTE is calculated by dividing the forward distance during the TTA (Time To Amber) by the distance to the stop line as follows:

$$\text{MTE} = \frac{v(t) \cdot \text{TTA}}{d(t)} \tag{5}$$

If the MTE is less than 1, the vehicle cannot enter the intersection with maintaining the vehicle speed until turning to the amber signal.

The MTP means the margin to make the vehicle pass through the intersection until turning to the green signal of the cross road. The MTP is defined by dividing the forward distance during the TTG_C by the distance to the stop line and the intersection length as follows:

$$\text{MTP} = \frac{v(t) \cdot \text{TTG}_C}{d(t) + l_i} \tag{6}$$

If the MTP is below 1, the vehicle cannot pass through the intersection with maintaining the vehicle speed until changing to the green signal of the cross road.
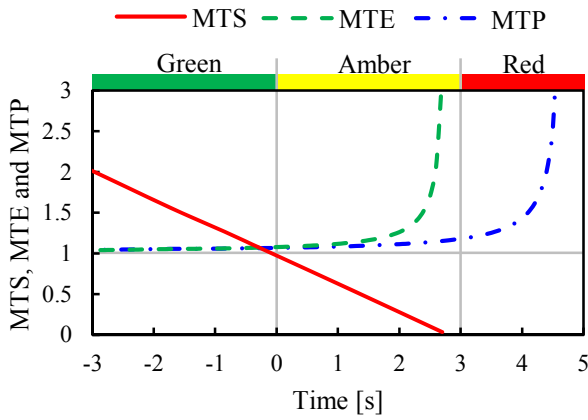
(a) With assistance system
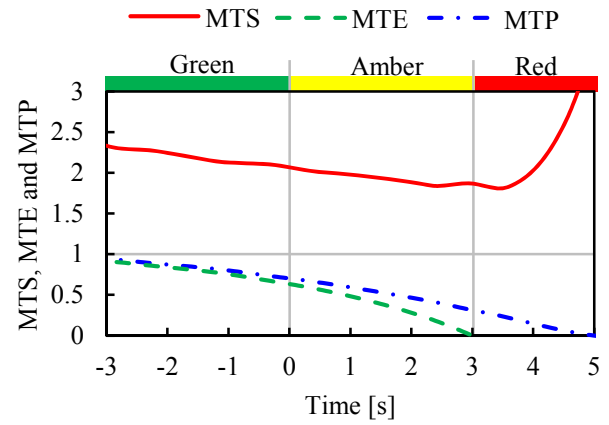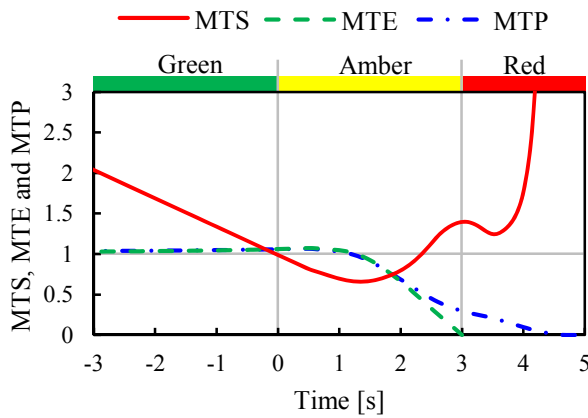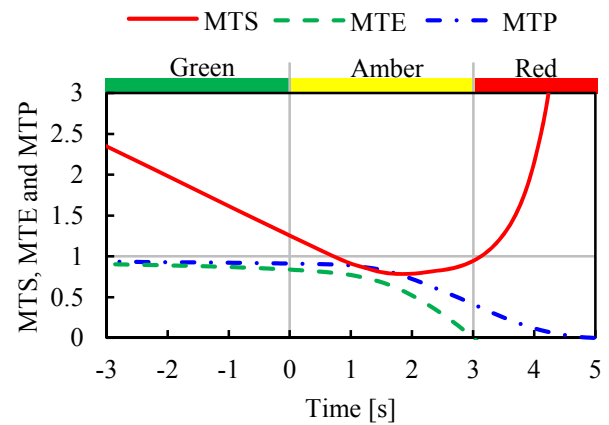
(b) Without assistance system

Fig. 13. Evaluation indices in Neutral condition (1st trial by Participant A)

An example of the evaluation indices (1st trial by Participant A) in the Neutral condition is depicted in Fig. 13. Figure 13(a) shows the indices with the assistance system, and Fig. 13(b) is without the assistance system. The solid line indicates the MTS, the broken line shows the MTE, and the dashed line is the MTP.

The driver with the assistance system passes through the intersection in this condition. The MTE and MTP maintain over 1, and this behavior proves the safe entry and passage of the intersection. The driver without the assistance system, on the other hand, stops at the intersection in this condition. The MTE and MTP is over than 1 especially at 0s, and the driver could enter and pass through the intersection. However, the driver decides to make the vehicle stop. This judgment causes the smaller MTS and the large deceleration.

Figure 14 illustrates an example of the indices (1st trial by Participant B) in the Stop condition. Figure 14(a) shows the indices with the assistance system, and Fig. 14(b) is without the assistance system. The driver with and without the assistance system stops at the intersection in this condition.

(a) With assistance system

(b) Without assistance system

Fig. 14. Evaluation indices in Stop condition (1st trial by Participant B)

The driver without the assistance system maintains the vehicle speed until turning to the amber signal. The MTE and MTP maintain under 1, and this transition implies the impossibility of the safe entry and passage of the intersection. The driver recognizes this fact after changing to the amber signal, and this judgment causes the smaller MTS and the large deceleration. The driver with the assistance system, on the other hand, recognizes the lower possibility of the entry and passage through the intersection by the assistance. Therefore, the driver makes the earlier braking maneuver, and avoids the smaller MTS and large deceleration.

4. CONCLUSION

This study examines the driver assistance system which indicates the information on passage possibility on the road ahead virtually by the driving simulator experiments.

The driving simulator experiments revealed the assistance system realizes the earlier deceleration before the amber signal and prevents the emergency braking behavior. These effects contribute to the reduction of the average and maximum deceleration. In addition, the assistance system improves the margin to pass through or stop at the intersection.

REFERENCES

Honda Motor Co., Ltd., (2014). Honda to Begin Demonstration Testing of Driving Support System on Public Roads Utilizing Traffic Signal Information in April 2014, available at http://world.honda.com/news/2014/c140328Driving-Support-System/index.html (accessed on 10 February, 2015).

Long, K. et al., (2013). Impact of countdown timer on driving maneuvers after the yellow onset at signalized intersections: An empirical study in Changsha, China, *Safety Science*, 54, 8-16.

Michitsuji, Y. et al., (2013). Proposal on driving risk indices for crossing pedestrians at signalized intersection during yellow phase, *Transactions of Society of Automotive Engineers of Japan*, 44(2), 555-560 (in Japanese with English summary).

Papaioannou, P. et al., (2007). Driver behaviour, dilemma zone and safety effects at urban signalised intersections in Greece, *Accident Analysis & Prevention*, 39(1), 147-158.

Evaluation of Post Impact Control Function with Steering and Braking Superposition in High-fidelity Driving Simulator [⋆]

Derong Yang [*] Xiaoli Xie [**] Fredrik Bruzelius [***]
Bruno Augusto [***] Bengt Jacobson [****] Mats Jonasson [*]

[*] *Active Safety and Vehicle Dynamics Functions, Volvo Car Corporation, 405 31, Sweden (e-mail: derong.yang@volvocars.com).*
[**] *Chang'an University, China (e-mail: xiaoli@chd.edu.cn).*
[***] *Vehicle Technology and Simulation, The Swedish National Road and Transport Research Institute, 402 78, Sweden (e-mail: fredrik.bruzelius@vti.se, bruno.augusto@vti.se).*
[****] *Applied Mechanics, Chalmers University of Technology, 412 96, Sweden (e-mail: bengt.jacobson@chalmers.se).*

Abstract: This paper evaluates the effectiveness of an active chassis control function after an initial light impact. The experiment was designed in a high-fidelity driving simulator with motion platform that is adapted to mimic a real-world crash. The post-impact control function here superimposes individual-wheel brake and steering wheel torque in order to minimize the vehicle maximum lateral deviation from its original traveling lane. It is found out that drivers with the function intervention has smaller lateral deviation after the disturbance from an initial impact, and thus less risk of leaving the road which may cause a secondary impact. The driver reaction with and without the function is also found to be different in terms of both braking the steering behaviours.

Keywords: Active safety, collision avoidance, function evaluation, vehicle dynamics control, vehicle simulation, driving simulator, driver response, post impact.

1. INTRODUCTION

Vehicle traffic safety has been attracting considerable attention from all perspectives, given the continuing high numbers of accidents registered in road traffic statistics. One type of accident is gradually increasing according to the recent accident statistics: multiple-event accidents (MEAs) Sander et al. (2009). These are characterized by having at least one vehicle subjected to more than one impact, such as collision with another vehicle or object. Statistics show that MEAs comprise approximately 25% of all passenger vehicle accidents Zhou et al. (2010); Yang et al. (2009); Fay et al. (2001); Langwieder et al. (1999); human injury levels in MEAs are higher than in single-event accidents (SEAs), with more than one third of accidents with severe (i.e. AIS3+) injuries being MEAs Fay et al. (2001); Langwieder et al. (1999). Studies on more recent accident statistics show that MEAs have a three-fold risk for severe and four-fold risk for fatal injury compared to SEAs; on average, 50% of all passenger vehicles suffering MEAs have the severe injuries sustained in one or several subsequent impacts Sander (2013).

To specially tackle the vehicle motion control problem after an initial impact in MEAs, new type of driver assistance systems are now emerging on the market Robert Bosch GmbH (2010.09.21); Bickerstaffe (2012.10.28); NCAP (2012.12.05), which can be generally called Post Impact Control (PIC) system. In Robert Bosch GmbH (2010.09.21); Bickerstaffe (2012.10.28); NCAP (2012.12.05), the function simultaneously apply full or partial braking on all four wheels after initial impacts, i.e. Post Impact Braking (PIB). This function is now in several launched vehicles, such as new Volvo XC90 2015, where it is called "Auto braking after a collision". In Mouatamid et al. (2013), PIB is evaluated for four representative impact scenarios and three typical driving styles in a driving simulator, assuming Anti-lock Brake System (ABS) is functioned or malfunctioned; results show that PIB helps to lower the risk and severity of secondary impacts with respect to reduced displacements and road leaving speed; while it leads to higher risk for possible side and off-road collisions due to increased yaw angle and lateral deviation; the test scenarios were simplified that the host car is disturbed suddenly by "magic hands", i.e. no visualization of a bullet car which imposes the impact. In Häussler et al. (2012), driving tests were carried out on test track, where a rather light side impact was introduced by a steam "cannon" at the vehicle rear axle on low-friction surface; results show that even experienced and prepared drivers could not stabilize the induced lateral force by means of immediate, fast counter-steering. Both Mouatamid et al. (2013) and Häussler et al. (2012) found

that most drivers became disoriented, confused and even panicking after unexpected external disturbance, for instance, acceleration pedals were incorrectly pressed.

In the present paper, we develop and apply the method to evaluate post impact control function *with driver in the loop* and *with both brake and steer torque overlay* in a high-fidelity test environment. Driving simulator with motion platform is adapted in order to best comply with the predefined criteria such as accuracy, repeatability and safety. A test scenario from real-world accident database is reconstructed in the simulator. The PIC function which minimizes the vehicle maximum lateral deviation from its original traveling lane, is implemented in the real-time testing interface. This function uses optimal control theory to calculate the individual-wheel brake torques and front steering angle request, more information about the algorithm can be found in Yang et al. (2014). Driver response and interaction characteristics are revealed at the presence of both individual wheel brake torque superposition and steering wheel torque overlay. The function performance is quantified by comparing the vehicle trajectories with and without the function. It is expected that the method developed in this paper can be further used for a larger scale experiment in the future; the results here can provide invaluable understanding about post-impact driver behaviours and the potential of such active chassis control functions.

2. METHOD

2.1 Experimental set-up

The experiment was set up in a car driving simulator at the Swedish National Road and Transport Research Institute (VTI). It has a hexapod which provides six degrees of freedom (DOF) movements of the cabin above the motion platform, which can move at longitudinal and lateral directions simultaneously; 210° field of forward-facing view is provided in the visual system, plus emulated rear and center mirrors using monitor screens VTI (2013.04.27). The simulator uses a multi-body dynamics vehicle model, with 6-DOF motions for car body together with wheel rotations and vertical travels, plus tyre relaxation with wheel and suspension compliances. The vehicle model is parameterized to mimic one on-market sedan. More information about the model and its validation can be found in Bruzelius et al. (2013). An ABS algorithm is designed, which was calibrated using the measurement data from vehicle tests. It is assumed that the regular Electronic Stability Control (ESC) system is deactivated due to implausible sensor signals during impact.

The road designed in the simulator, as seen in Fig. 1, is a typical 1+1 Swedish country road with approximately 3.5 m lane width and speed limit as 70 km/h, where the road surface is dry with daylight. The drivers recruited here are considered experienced, with at least 10000 km driving distance per year and have held driver license more than 5 years. They are required to respect the traffic legislations. For each driver, he/she was given about 15 minutes to test drive freely, so as to get familiar with the road environment and vehicle dynamic response properties of the simulator. Some accelerating, braking and lane

change manoeuvres are also included in this training period. Before the bullet car is introduced at one specific T-junction, the host car driver will pass several similar T-junctions along the road; this is to let the driver know the existence of junctions on this road and will learn intuitively about possibilities of pulling-out cars from side.

Furthermore, a combination of different physiological measurements together with behavior measurements and a questionnaire were employed to cover both behavior and emotion aspects of driver reactions. For driver physiological evaluation, we measure a set of variables for EEG, EDA and ECG that are commonly believed to have strong relations with emotion arousal level. Cameras were installed in four different views in order to capture the driver's body movements: front, right side, back and feet. The driver's front view of the road, such as seen in Fig. 1, was also recorded from the simulation graphics. At the end of experiment, the driver was interviewed with a number of questions about their reaction and self-evaluation of their driving experience.

2.2 Test scenario

One post-impact scenario from German In-depth Accident Study database is reconstructed here, see Fig. 2 below. The host car (red) is driving on a straight country road at about 70 km/h, it is struck on the side in front of center of gravity (CoG) by the bullet car (gray) which is pulling out from a side road. From accident reconstruction, the impact properties are estimated and abstracted as below: impact amplitude is 45000 N, impact angle is 90 deg, impact position relative to the car CoG is $x = 0.23$ m, $y = -0.6$ m, $z = -0.15$ m, and impact duration is 200 ms. The speed change during impact can be estimated as 16 km/h and is thus approximately at the level of triggering a common airbag system. Fig. 2 illustrates a representative result from the experiment: without the function, the host car saturates its front axle road grip immediately after the 1st impact and leads to large lateral deviation that may cause a secondary impact with road side objects such as trees; with the function, the car trajectory is instead corrected back towards the original lane and the risk of leaving the road is minimized.

Fig. 1. The road designed in the simulator.

(a) without PIC function
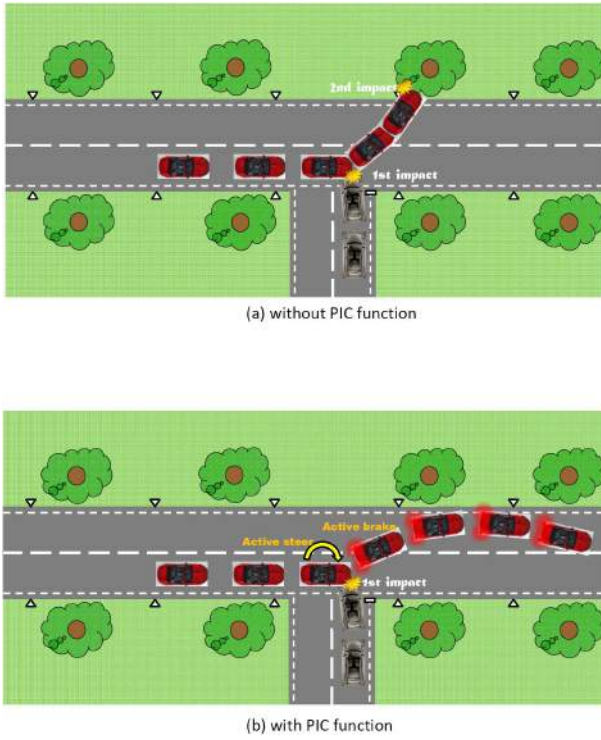
(b) with PIC function

Fig. 2. A post-impact test scenario at T-junction, illustrated with and without PIC function.

3. DRIVER REACTION AFTER IMPACT

The collision rose the arousal level of almost all drivers. Some of the drivers made mistakes because of stress. In Fig. 3 below, one example is shown for the driver pressing down acceleration pedal after the initial impact. Another case without the function is shown in Fig. 4, where the driver did not release the throttle and never pressed the brake pedal.

PIC function did not add extra stress during the intervention, however some braking hesitation is noted by the drivers after the intervention. Interviews after the experiment show that during the intervention, most drivers did not realize PIC, or any function was activated. It was also observed from the videos that some drivers held the steering wheel still for a while during the intervention. Future research is needed to clarify the steering wheel holding behavior.
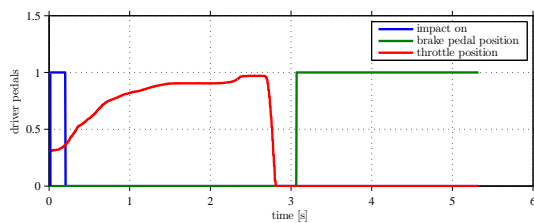
Fig. 3. Driver pedal positions after impact, with PIC. 0: released, 1: 100% pressed.

Fig. 5 below summarizes the reaction time for pedals of all subject drivers. It is interesting to notice that with the PIC function, many drivers tend to delay the throttle release and thus brake pressing action. It may be understood that
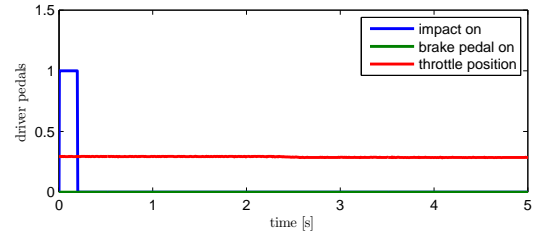
Fig. 4. Driver pedal positions after impact, without PIC. 0: released, 1: 100% pressed.

the instant brake intervention from PIC function reacted much faster than driver braking so that driver did not need to brake. It also shows that driver may be little confused and hesitated to release throttle at the presence of PIC braking. Here it should be noted that throttle input from driver is decoupled if PIC function is triggered.
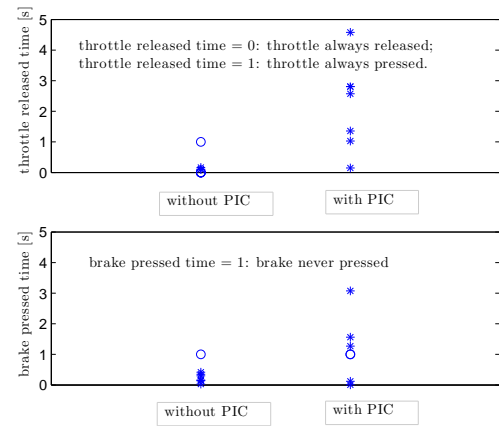
Fig. 5. Driver reaction time in throttle and brake, without/with PIC.

A certain time delay in counter-steering is also well observed for most drivers. Fig. 6 shows the resulting steering wheel angle is approximately 0.1s delay without the help of PIC function. In post-impact situation, even a small time delay in steering will make noticeable difference in path, see paths of all test subjects in Section 4.
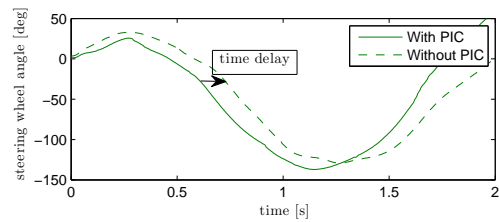
Fig. 6. Steering wheel angle, without/with PIC.

4. DRIVER PERFORMANCE WITHOUT/WITH PIC FUNCTION

Fig. 7 shows the vehicle trajectories recorded for a number of drivers at the experiment with and without the function intervention. Clear pattern differences are noticed: with

PIC assistance, all the drivers could limit their lateral deviation within 4 m (approximately distance from mid lane to road edge) at a relatively small longitudinal displacement; while without the function, nearly all drivers left the road. Fig. 8 shows path and yaw angle for one example with and without PIC.
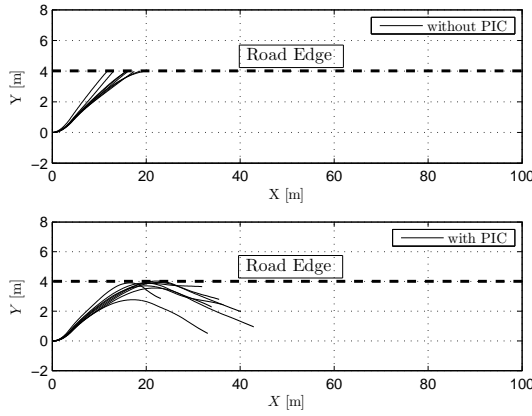
Fig. 7. Post-impact vehicle lateral deviation (Y) without and with PIC function. Impact occurs at $X = 0$ [m]. Vehicle leaves the road if Y exceeds 4 [m].
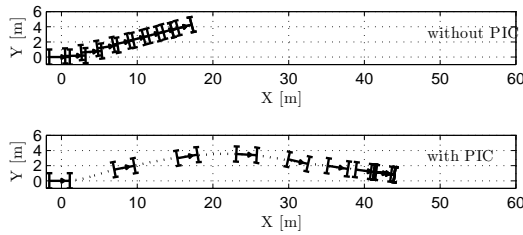
Fig. 8. Post-impact vehicle trajectory without and with PIC function. Impact occurs at $X = 0$ [m]. Vehicle leaves the road if Y exceeds 4 [m]. Note that the path without PIC continues outside the road edge, but it is not drawn.

The optimal brake intervention is designed to minimize the maximum lateral deviation; it depends on a mechanism with best balance between global later force and yaw moment, see details of the optimal control algorithm in Yang et al. (2012). Fig. 9 shows that both rear wheels were braked first to apply optimal control for reducing path lateral deviation. All wheels are thereafter braked as a settling part of the function, i.e. as a PIB function.

Fig. 10 shows steering wheel torque. The driver needs less steering torque with PIC than without the function. The driver follows the PIC steering intervention instead of steering against PIC.

5. CONCLUSIONS

A developed Post Impact Control (PIC) function has been evaluated in a driving simulator. The PIC function, which has been developed to minimize the vehicle's maximum lateral deviation from it's lane, was enabled for a part of the test subjects. The resulted lateral deviation for those drivers is significantly improved. All drivers with the PIC
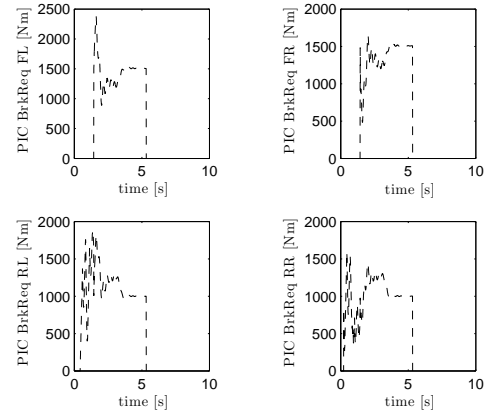
Fig. 9. Post-impact brake intervention from PIC function.
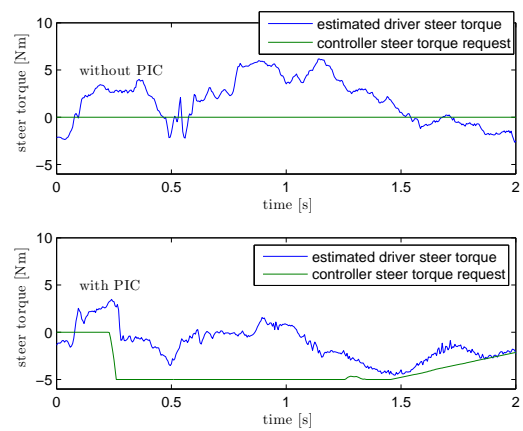
Fig. 10. Post-impact driver steering torque without/with PIC function.

function enabled kept the vehicle at the road, while all other drivers departured.

The collision scenario caused clear emotion unpleasantness for almost all drivers and they made mistakes because of stress. It was evident that some drivers gave inadequate commands e.g. unintentionally pressed two pedals simultaneously. During the intervention, most drivers did not realize that PIC or any function was activated. They follow the guidance from function and no one steers against the steering torque requested by the function.

REFERENCES

Bickerstaffe, S. (2012.10.28). Conti puts the brakes on secondary collisions - Emergency braking function stops the car after the first impact. URL http://ae-plus.com/technology/conti puts the brakes on secondary collisions.

Bruzelius, F., Fernandez, J.G., and Augusto, B. (2013). A basic vehicle dynamics model for driving simulators. *International Journal of Vehicle Systems Modelling and Testing*, 8(4), 364–385.

Fay, P., Sferco, R., and Richard, F. (2001). Multiple Impact Crashes - Consequences for occupant protection measures. In *Proc. IRCOBI Conference*. Isle of Man, UK.

Häussler, A., Schäffler, R., Georgi, A., and Stabrey, S. (2012). Networking of airbag and ESP for prevention of further collisions. *ATZ - Automobiltechnische Zeitschrift*, 114, 22–26.

Langwieder, K., Sporner, A., and Hell, W. (1999). RESICO - Retrospective safety analysis of car collisions resulting in serious injuries.

Mouatamid, F., Kusachov, A., Jacobson, B., and Yang, D. (2013). Towards evaluation of post impact braking function in driving simulator. In *Proc. of the IEEE International Conference on Systems, Man, and Cybernetics*. Manchester, United Kingdom.

NCAP, E. (2012.12.05). Audi secondary collision brake assist. URL `http://www.euroncap.com/rewards/audi secondary collision brake assist`.

Robert Bosch GmbH (2010.09.21). Secondary collision mitigation: Protection against subsequent crashes. URL `http://www.bosch-automotivetechnology.com`.

Sander, U. (2013). *Requirements to occupant restraint systems in multiple impact crashes in-depth analysis of real world accident data*. Master's thesis (june 2009), graz, austria, Technical University in Graz.

Sander, U., Mroz, K., Boström, O., and Fredriksson, R. (2009). The effect of pre-pretensioning in multiple impact crashes.

VTI (2013.04.27). Driving simulator iv in vti. URL `http://www.vti.se`.

Yang, D., Gordon, T.J., Jacobson, B., and Jonasson, M. (2012). Quasi-linear optimal path controller applied to post impact vehicle dynamics. *IEEE Transactions on Intelligent Transportation Systems*, 13(4), 1586–1598.

Yang, D., Jacobson, B., and Lidberg, M. (2009). Benefit prediction of passenger car post impact stability control based on accident statistics and vehicle dynamics simulations. In *Proc. 21st International Symposium on Dynamics of Vehicles on Roads and Tracks*. Stockholm, Sweden.

Yang, D., Jonasson, M., Jacobson, B., and Gordon, T.J. (2014). Closed-loop controller for post-impact vehicle dynamics using individual wheel braking and front axle steering. *International Journal of Vehicle Autonomous Systems*, 12(2), 158–179.

Zhou, J., Lu, J., and Peng, H. (2010). Vehicle stabilisation in response to exogenous impulsive disturbances to the vehicle body. *International Journal of Vehicle Autonomous Systems*, 8(Nos. 2/3/4), 242–262.

Simulation of lane departure accidents in Germany

Nils Lubbe, Maminirina Ranovona

Toyota Motor Europe, Technical Affairs Planning, Hoge Wei 33, 1930 Zaventem, Belgium
(Tel: +32 2 712 3969; e-mail: nils.lubbe@toyota-europe.com)

Abstract: The aim of this paper was to extend an existing simulation environment for lane departure accidents in the USA and Japan to be applicable for Germany. The German situation was described primarily using the German in-depth accident Study (GIDAS) as input to the simulation. Simulation output was validated against accident data. Two changes to the simulation environment were proposed: First, use of weighted empirical cumulative distributions for input variables , and second, use of weighted logistic regression for injury risk curves. Further methodological consideration, should be given to inclusion of non-injury cases, object grouping and treatment of uncertainty.

Keywords: Traffic Simulation, Lane Departure, Collision, Germany, ASSTREET

1. INTRODUCTION

Safety benefits offered by vehicle technology can be studied retrospectively analysing real-world data and the difference in injury outcome, insurance claims, or collision numbers between vehicles fitted with the technology and those that are not fitted. Safety benefits of Electronic Stability Control (Ferguson, 2007; Lie et al., 2006; Farmer, 2004) and recently Automated Emergency Braking for low speed car to car rear end collisions (Rizzi et al., 2014) have been established in such retrospective studies.

Retrospective benefit estimates for systems aiming at preventing or mitigating lane departure accidents are ambiguous (IIHS, 2012). Due to low market penetration of the systems and scarcity of accident data, accurate estimates might not be available for several years to come.

Prospective study on the other hand might employ simulation methods to estimate the effects of technologies that are to be introduced on the current traffic and accident situation, irrespectively of the number of systems installed in the vehicle fleet.

Traffic simulation creates a description of the traffic environment and the paths travelled by vehicles and other traffic participants from traffic or accident data. Replication of accidents with and without the active safety system under study establishes the comparative impact a system has on collisions. The active safety system is usually a simplified model of the real system including sensors, logic and actuation. Employing a simulation approach, safety benefits for lane departure warning systems were estimated for the USA (Kusano et al., 2014).

A traffic simulation environment for lane departure accidents called ASSTREET was developed not only for the USA (Tanaka et al., 2012) but also Japan (Morales Teraoka et al., 2014). Accident characteristics for these regions are obtained from crash databases and driver reactions from Driving Simulator experiments. Lane departure accident

characteristics between the USA and Japan differ (Morales Teraoka et al., 2014).

The aim of this paper was to extend the traffic simulation environment ASSTREET for lane departure accidents to Germany. First, the German situation of lane departure accidents was described as input to the simulation. Second, the simulation environment was validated comparing characteristics of the simulated accidents against the original accident data.

2. METHODS

The primary source of information was the German in-depth accident Study (GIDAS) for the accident years 2003 to 2012. GIDAS is an in-depth accident database collecting data in the regions of Hannover and Dresden (Pfeiffer and Schmidt, 2006). GIDAS data was assumed to be representative for the national accident situation, except for the injury outcome. Thus, all input data in this study was weighted for national injury outcome. Information are given, where applicable, for the first collision object only as the simulation does not handle multiple collisions. Additional information was obtained from the German Pre-Crash Matrix (PCM) (Erbsmehl, 2009) version 2.2 and the statistical federal bureau of Germany (DESTATIS).

2.1 Weighting factors

Risk of minor, severe and fatal injury was calculated per collision object as a function of driving speed. Injury information was obtained from GIDAS using police reported injury severity coded as PVERL. As GIDAS tends to be biased towards higher injury severities, the injury data was weighted to national data obtained from DESTATIS. Probability weights were derived from GIDAS coded car occupant injuries summed for 2003-2012 compared to the national average of injured car occupants from 2003-2012 (table 1). Unknown injury status cases were removed from the analysis. The number of uninjured car occupants cannot

be obtained accurately as uninjured traffic participation is not reported on national level and underreporting must be expected. The number was estimated to be 1'500'000 with below approximation:

Uninjured occupants = Injured occupants * (accidents without injury / accidents with injury)

= 237 223 * (1 990 735 / 321 991) =1 500 000.

The weights were 1.44 for no injury cases, 0.37 for slight injury, 0.24 for severe injury and 0.21 for fatal injury as given in table 1.

Table 1. Weighting factors

	no injury	slight	serious	fatal
GIDAS	16 679	8788	2151	189
	60%	32%	8%	1%
Germany	1500000	201983	32715	2525
	86%	12%	2%	0.1%
Weight	1.44	0.37	0.24	0.21

2.2 Definition of lane departure accidents

Lane departure accidents are not explicitly coded in GIDAS. They were defined by the criteria:

- Complete case with reconstruction (STATUS =4)
- Accident type: Driving error, encounter and sideswipe (UTYP 100-200, 651, and 680-690)
- No skidding (SCHLEU not 2)
- Excluding parking and driveway accidents (STRART not 7 and not 10)
- Passenger car (ARTTEIL = 1)

In order to define the departing vehicle in collisions with multiple vehicles, the participant who was assigned the guilt for the accident was assumed to have departed from the lane. Resulting were 465.4 weighted cases (824 unweighted) with known injury outcome identified as lane departure accidents in GIDAS as given in table 2.

Table 2. Lane departure accidents with in jury outcome

	no injury	slight	serious	fatal
Raw	186	349	260	29
Weighted	267.8	129.1	62.4	6.1

2.3 Definition of lane departure angle and lateral distance to collision object

Lane departure angle and lateral distance to the collision object are not explicitly coded in GIDAS. For cases with road departure, GIDAS information on road departure angle, directional lane width and lane use was used to approximate the lane departure angle. The lane departure angle was assumed to equal road departure angle if the used lane was adjacent to the road departure side. For cases without road departure, such information was not available in GIDAS, thus

PCM data was used. The lane departure angle was extracted from the vehicle trajectory and road marking information (Fig. 1). This led to a reduction of available case information. While 141.7 cases of lane departure without road departure were identified in GIDAS, information from PCM could be obtained only for 28.5 cases. All these cases were lane departures to the left and resulted in collisions with other traffic participants.

Vehicles were assumed to continue travelling in direction of their velocity vector at the time of departure to the first collision object. Consequently, lateral distance to the collision object was calculated by multiplying the shortest distance between road departure and collision object (MABST) with the sinus of the departure angle (ABWINK). For cases where lanes had been crossed before road departure, the distance to cross lanes between the used lane and the road border were added. An assumption for left road side departure was that a road with a single lane in driving direction has collision objects to the left of the road (incl. opposite lanes) while a road with multiple lanes in driving direction has collision objects between the lanes in opposite directions (Fig. 1). For cases without road departure, lateral distance was obtained using shortest distance information extracted from PCM trajectories.

2.4 Injury risk

Injury risk was calculated in weighted logistic regression for no injury, severe injury and fatal injury using Matlab R2013a statistical toolbox. Slight injury was expected to be the least reliable estimation and therefore not calculated by regression but as the missing proportion to equal a total risk of 1. Injury risk was calculated for all vehicle occupants irrespectively of seating position, belt use and other potential influences. Injury outcome and collision speed were known for 667.6 occupants (1166 unweighted) in 442.4 (797 unerighted) accidents

2.5 Other variables

All other variables of interest were obtained from GIDAS directly. Curve radius was taken from the variable KRADIUS, lane width from the division of REBREIT with FSPUR, and driving speed from V0. Collision object type was retrieved from KONOBJ. The reaction after lane departure was taken from the coded driver reactions prior to the first collision in SEQS and SEQA. The accident cause was given from police assessment coded in HURSAU. The share of causes is given in relation to all driver mistakes, not taking into consideration technical defects and causes attributed to the environment.

Empirical cumulative distributions were weighted according to Heeringa et al. (2010) in Equation (1)

$$F(x) = \sum w_i \, I(\, y_i \leq x \,) / \sum w_i \qquad (1)$$

Whereby $I(\, y_i \leq x \,)$ is an indicator equal to 1 if y is less than or equal to a specified value of x, and 0 otherwise and w_i is the weight for case i.
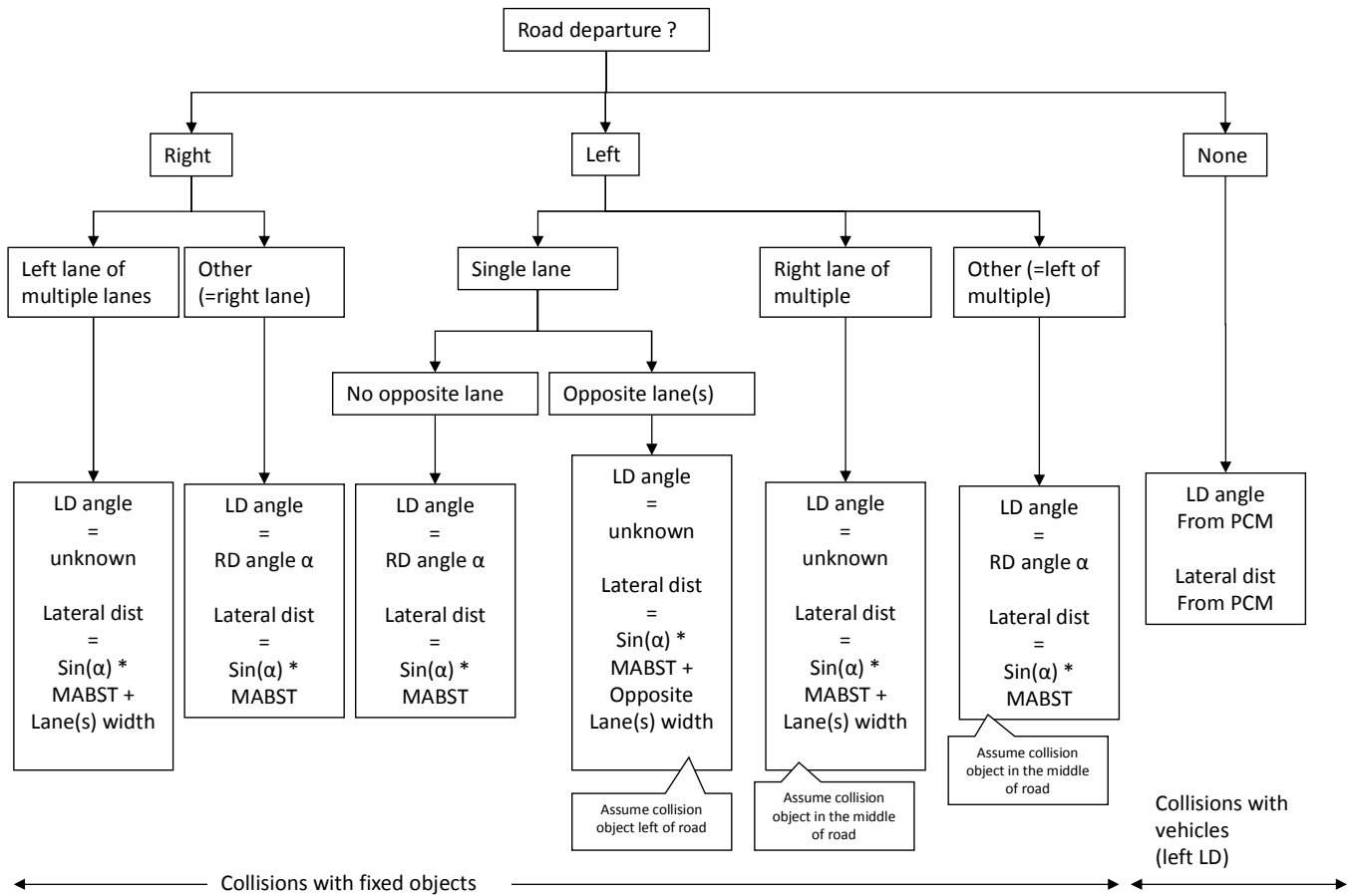
Fig. 1. Definition of lane departure angle and lateral distance to collision object

3. RESULTS

3.1 Road curvature

Out of 465.4 lane departure cases, 438.2 had information on road curvature. 223.2 cases (51% of known radii) occurred on straight roads while the remaining 215 cases occurred on bends with a distribution of inner radii given in Fig. 2. Curve radius, driving speed and lane departure angle were correlated. Curve radius was divided in 3 groups of equidistant cumulative probability (33% and 67%). The number of groups was selected to get a sufficient number of cases per group. Curve radius was grouped into (1) straight road: 223.2 weighted (359 unweighted) cases, (2) radius >0 and <30m: 63.9 weighted (229 unweighted) cases, (3) >=30m and <110m: 79.7 weighted (87.5 unweighted) (4) >110m: 71.4 weighted (90 unweighted) cases. Driving speed and departure angle are given for each group separately in the following sections.

3.2 Lane departure angle

Lane departure angles were known for 121.9 weighted (254 unweighted) cases in total and were calculated for each curve radius group. Small angles were related to large curve radii (Fig. 3). Lane departure angle was also dependent on driving speed, which is discussed in section 3.4. There was little difference between left and right lane departure allowing modelling independent of departure direction.
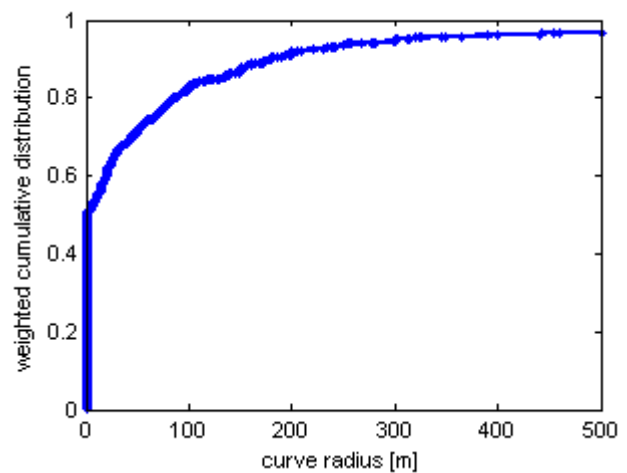
Fig. 2. Curve radius distribution
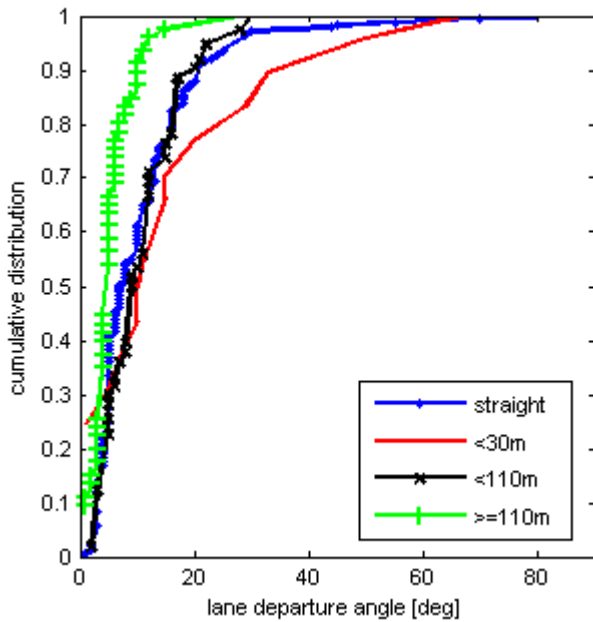
Fig. 3. Lane departure angle distribution

3.3 Driving speed

Driving speed was known in 396.7 cases (698 unweighted) and calculated for each curve radius group (Fig 4). Small radii were related to the lowest driving speed. There was again little difference between left and right lane departure allowing modelling independent of departure direction.
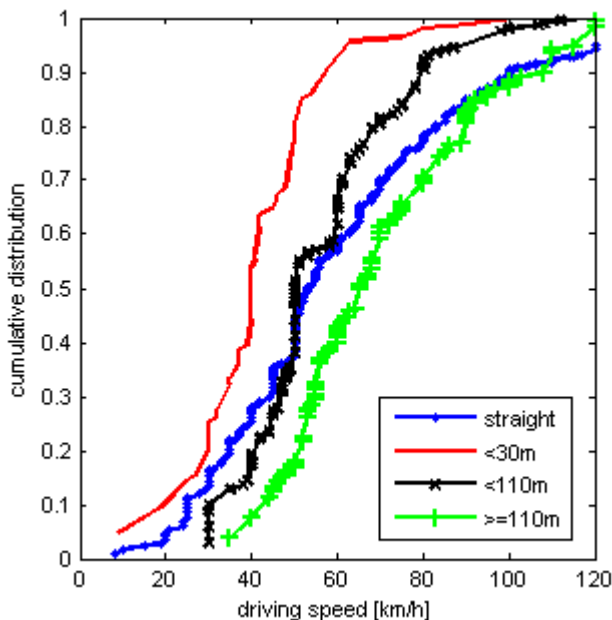
Fig. 4. Driving speed distribution

3.4 Relation between driving speed and lane departure angle

Fig. 5 shows some relation between driving speed and lane departure angle: Combinations of high speed and large angles did not occur, while for low speeds, both large and small angles were observed. The relation was neither linear nor rank-linear. The correlation was modelled using a modification of **restricted pairing** (Cullen and Frey, 1998). First, driving speed and departure angle were independently sampled. An "inappropriate" area was defined as driving speed above 100 km/h and lane departure angle above 30 degrees. If a data point (speed, angle) was generated in this "inappropriate" area, the speed part was exchanged with another data point so that both data points were out of the "inappropriate" area after the exchange.
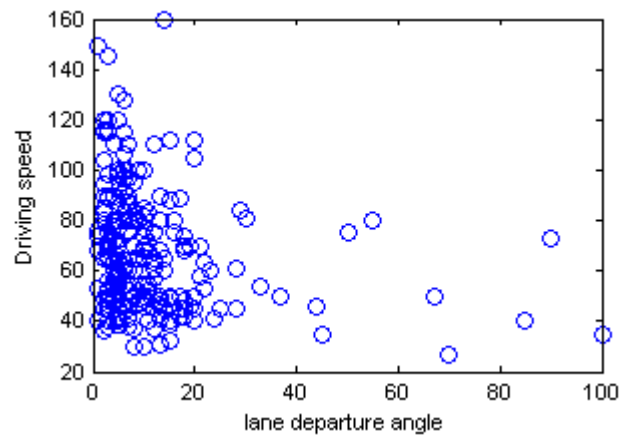
Fig. 5. Driving speed and lane departure angle

3.5 Lane width

There was little evidence for dependency of lane width on other variables, thus it was assumed to be independent. 373.4 weighted cases (658 unweighted) had information on lane width with a cumulative distribution given in Fig 6. Cases with a lane width below 1.8m were assumed to be miscoded and were disregarded.
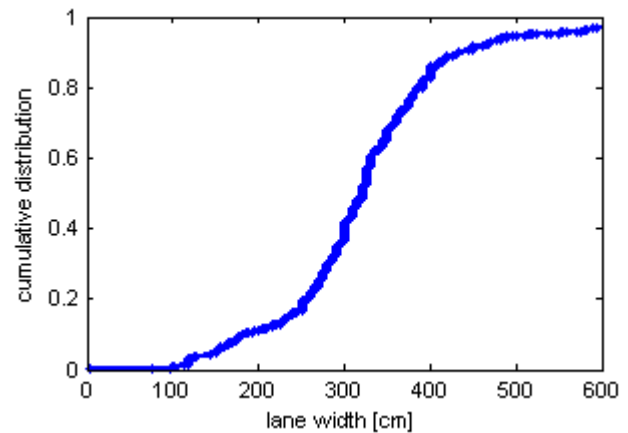
Fig. 6. Distribution of lane width

3.6 Collision objects and location

Lane departure was more frequent to the left side (75%) than to the right side (25%). Collision objects were grouped into (1) pole, post, and tree; (2) Other object; and (3) traffic participant. Group (1) was formed to reflect upon the high injury risk associated with these rigid narrow objects, group (3) was formed as moving and stationary collision partner were assumed to be different. Further grouping was not attempted as case numbers were small. Empirical cumulative distributions for lateral distances to the collision where available are given in Fig. 7.
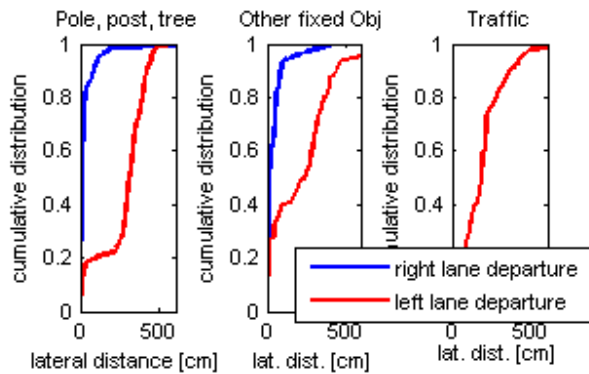
Fig. 7. Lateral distance to collision. Left: Pole, post and tree, center: Other object, right: traffic participant.

The cumulative distribution of lane departure speed is given in Fig. 8. It can be noted that collisions with traffic participants occured at lower lane departure speed.
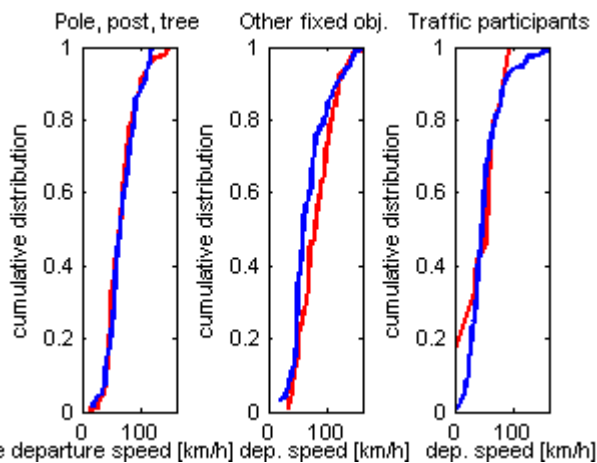
Fig. 8. Lane departure speed by collision object

3.7 Injury risk by collision object

Weighted logistic regression injury risk curves are given in Fig. 9. The probabilities to sustain different severities of injuries increased with collision speed for all objects. Notably, the probability to sustain injuries was higher for collisions with poles, posts and trees than for collisions with other traffic participants. For the pole, post, tree group an average of 1.56 people were involved in a collision, for other objects, an average of 1.69 people were involved, and for traffic participants 1.33 people were involved.
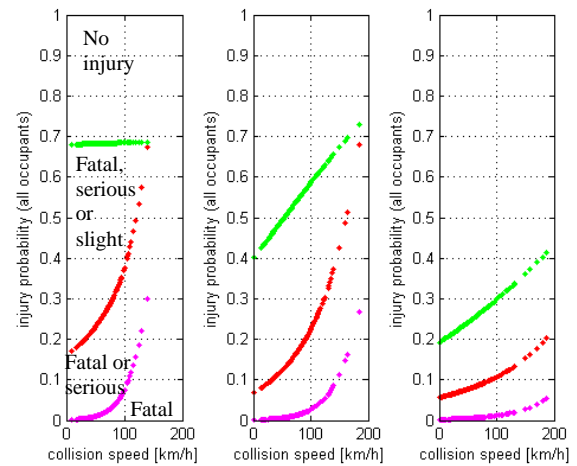
Fig. 9: Injury risk curves. Left: Pole, post and tree, center: Other object, right: traffic participant

3.7 Reaction after lane departure

Driver action prior to the first collision was taken as approximation for lane departure reaction which was not coded in GIDAS. Driver action in the sequence prior to first collision was known for 723 (unweighted) accidents (Fig. 10). A majority of drivers (57%) applied the brakes, either as only reaction (37%) or together with steering (20%). Brake deceleration (weighted) is given in Fig. 11. This brake deceleration applies for the sequence preceding the first collision and does not necessarily coincide with lane departure.
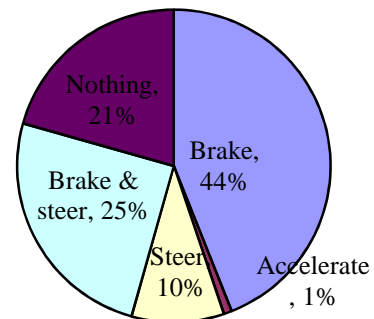
Fig. 10. Reaction after lane departure
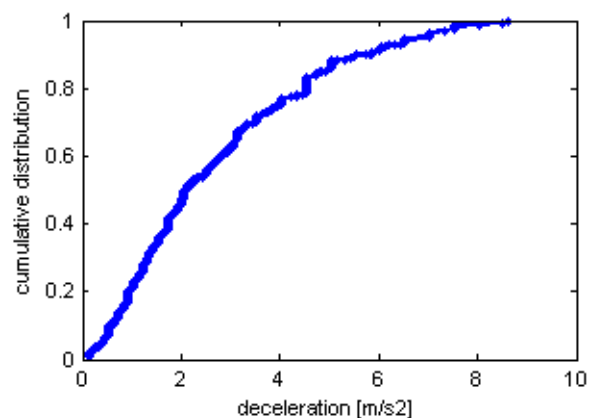
Fig. 11. Brake deceleration levels

When applying a factor of 2 to brake deceleration in Fig. 11, one can compensate for errors introduced by using an estimate for deceleration distance based on lane departure angle and (estimated) lateral position of objects and the difference in brake onset in accident data (any time is possible) and simulation (always at lane departure). Fig. 12 and 13 depict calculated collision speed with and without the correction factor. Dependent calculation means that each case's collision speed was calculated using the case's coded departure speed, lateral distance and sequence deceleration as one combined dataset. Independent calculation resembles ASSTREET simulation, where each case was created by assigning values for departure speed, lateral distance and sequence deceleration independently of each other. Fig. 12 and 13 show that the assumption of independence introduced a bias towards higher collision speeds. Fig. 12 shows as that the error by using sequence deceleration as deceleration at lane departure and the estimation of brake distance using lateral distance and departure angle lead to a bias towards higher collision speeds.
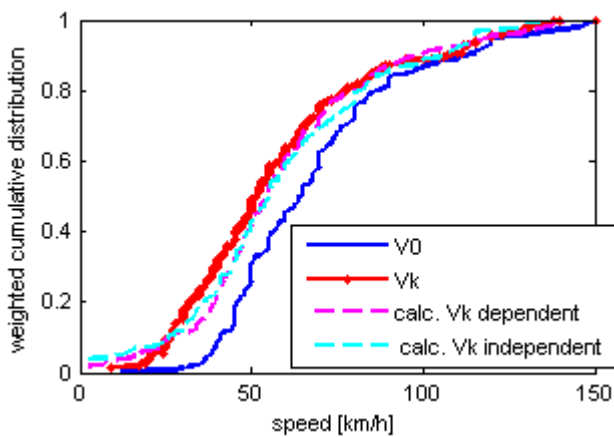
Fig. 12. Collision speed from accident data and calculation
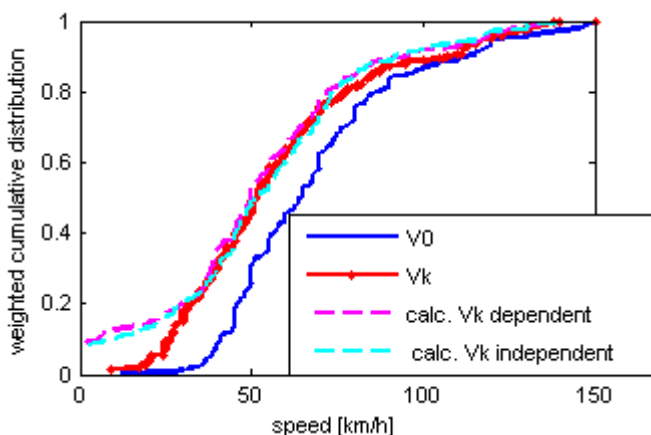
Fig. 13. Correction factor for brake deceleration

3.8 Accident causation

The causes for the lane departure accidents are given in Fig. 14. A majority was attributed to excessive speed (33%). Excessive speed was more frequent for lane departure accidents than for all types of accidents (16%). Drowsiness

(3%), alcohol (9%) and other physical deficiencies (3%) contributed to some extent. A large share of "other driving mistakes" (19%) was observed and was assumed to consist largely of distraction cases that are not coded otherwise.
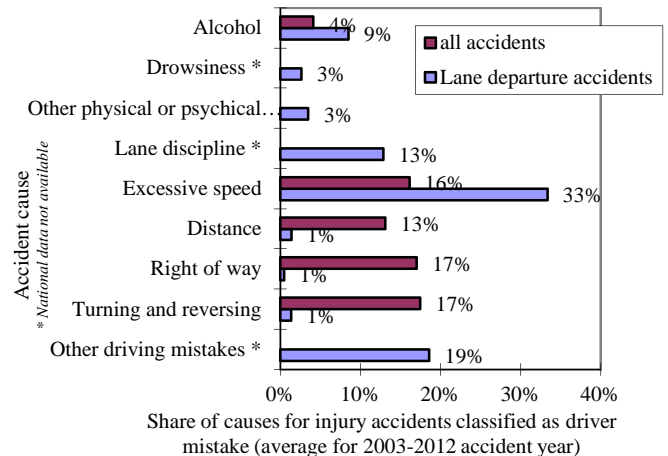
Fig. 14. Lane departure accident causation

4. VALIDATION

The overall injury outcome of lane departure accidents was reproduced in the simulation (Fig. 15).
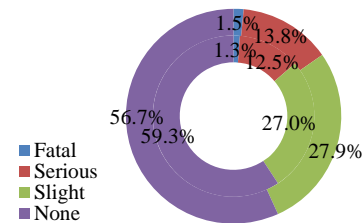
Fig. 15. Injury outcome of simulation (outer ring) compared to accident data (inner ring)

The number of collisions with each object as well as resulting injury outcome of the simulation matched the accident data (Fig. 16). There were slightly more cases of uninjured occupants in collisions with traffic participants in the simulation, while cases of no injury in collisions with other objects were slightly underrepresented. Deviations were below 3%.
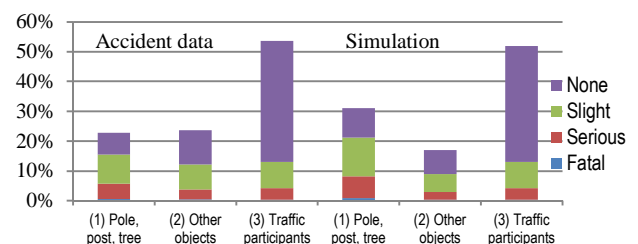
Fig. 16. Collision objects and injury outcome for accident data and simulation

The lane departure speed of the accident data was reproduced by the simulation while collision speeds in the simulation were higher compared to the accident data (Fig. 17). This simulation error is likely to be caused by the restriction of 9.81 m/s^2 for deceleration. Introducing the correction factor

of 2 for brake deceleration coded for the sequence before crash leads to a significant amount of brake deceleration levels above 9.81 m/s², which cannot be modelled in ASSTREET. Thus, the speed reduction in ASSTREET was lower compared to accident data and the collision speed VK was higher. However, as the main driver response of interest for lane departure accidents was steering and the overall injury severity distribution was reproduced, this error was judged to be acceptable. The slightly higher share of fatal and serious injury in the simulation might be explained by the slightly higher collision speeds.
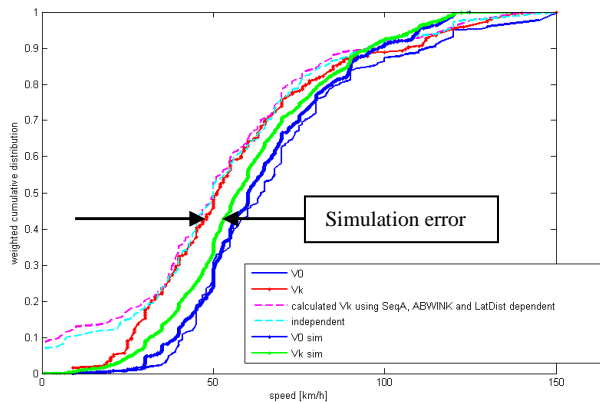
Fig. 17. Departure and collision speed in accident data and simulation

Injury risk curves were reproduced from the simulation data. At first, the simulation output "injury proportions" had to be translated into binary injury outcome. For example, the proportions [0.01, 0.1, 0.5, 0.7] for (fatal, serious, slight, none) has to be translated into [0, 0, 1 ,0] for (fatal, serious, slight, none) using a random number generator and assigning the injury outcome according to injury probability. Logistic regression was performed on the binary injury data and collision speed. Fig. 18 shows the simulation input (as shown already in Fig. 9) in colour dots and the reproduced injury risk curves from simulation output as black crosses. The fit appeared to be reasonable.

5. DISCUSSION

5.1 Inclusion of non-injury cases

The estimation of uninjured car occupants is inaccurate as national data is not available. Other studies have overcome this issue by focusing on fatal, serious and slight injury only and giving effectiveness in terms of fatal and severe injury reduction. The increase in slight injury is then interpreted as a consequence of the model.

This study attempts to highlight also the reduction of slight injury with any given technology and thus requires including non-injury cases as done in previous research (Tanaka et al., 2012; Morales Teraoka et al., 2014). Benefits and drawbacks of inclusion or exclusion of non-injury cases should be further investigated.
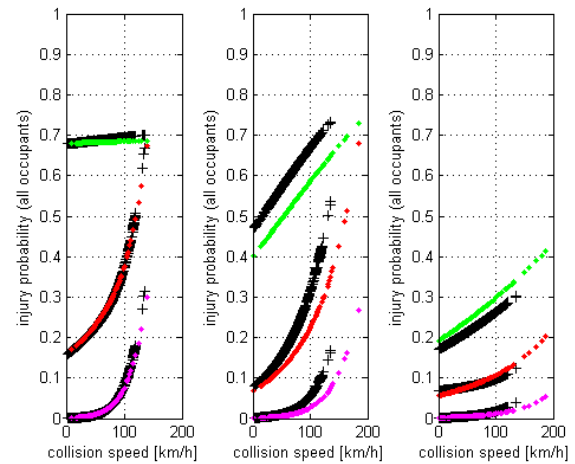
Fig. 18. Injury risk curves as simulation input (from accident data) and output

5.2 Grouping of collision objects

Grouping of collision objects in this paper was based on subjective judgment of similarity, based on injury risk, structural properties and kinetic energy. An objective statistical method **K-means clustering** was investigated as an alternative to get more reliable results (Martinez and Martinez, 2008). K-means clustering was based on distance and injury information. Specifically, the mean distance to the object for both left and right departure and the proportion of fatally injured occupants was defined as the base for clustering. It did not provide meaningful results as clusters were either almost empty or contained similar distributions for distance and injury, irrespectively of pre-selected cluster numbers.

5.3 Weighting of all data for injury outcome

The accident characteristics were weighted to national data for injury outcome. The difference between weighted and unweighted data was small for descriptive variables with little correlation to injury risk: Curve radius, lane width departure angle, and brake deceleration. Thus, it seems not necessarily to be required to weight these variables. For driving speed and injury risk, the difference between weighted and unweighted data is large, thus weighting appears to be essential. Driving speed becomes lower and injury risk is reduced at given collision speed for weighted data.

Parametric formulation of weighted distributions appears to be difficult except for normal distributions (Heeringa et al., 2010). Previous research avoided this difficulty by using national representative data, thus making weighting unnecessary or by using unweighted data besides sampling bias. This study proposed the use of empirical cumulative distributions without any attempt for a parametric formulation. The empirical cumulative distributions showed that normal distribution would have a poor fit to the data.

5.4 Variability and uncertainty

This study, in line with previous research (Tanaka et al., 2012, Morales Teraoka et al., 2014), described the variability in input data, but not the uncertainty (Cullen and Frey, 1998). This means that for each variable the distribution due to natural variation is given, but confidence intervals due to the uncertainty resulting from the (limited) sampling are not given. For the previous research, it might be that variability dominated uncertainty so that treatment of uncertainty was not required.

There is indication for this study that uncertainty was of a similar magnitude as variability. The quantified uncertainty could be processed through the model in 2D simulation, in addition to the established 1D simulation of variability. This would however require major revisions of the programming code and was beyond the scope of this study. Therefore, it should be noted as a limitation of this study that uncertainty was not assessed and confidence intervals for any outcome of interest should not be calculated. Attempting to calculate confidence intervals on output numbers without consideration of uncertainty in the sampling distributions used as input will lead to meaningless confidence intervals converging to zero when simulation runs converge to infinity.

5.4 Comparison with Japan and USA

The injury outcome is comparable between Germany, USA (Morales Teraoka et al., 2014) and Japan (Tanaka et al., 2012) (Fig. 19). Germany has the highest share of severe injuries (13.4%). Furthermore, poles, posts, and trees appears to be closer to the lane in Germany than in Japan or USA. The majority of lane departures occurred at small angles in all countries, but the trend is most pronounced in Germany. Lane departure speed in Germany is higher than in Japan but comparable to the USA.
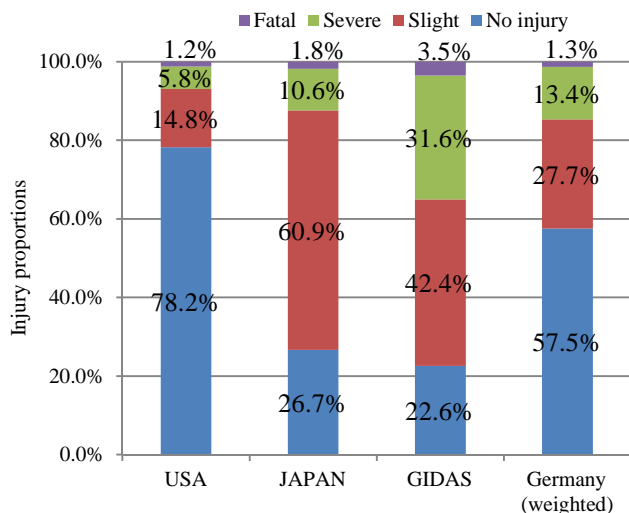
Fig. 19. Injury proportions in lane departure accidents

6. CONCLUSIONS

The situation of German lane departure accidents was described using GIDAS, PCM and DESTATIS data. Simulation results (without safety system) were validated against the original accident data. The simulation environment can be used to estimate the effectiveness of system parameters aiming at preventing or mitigating lane departure accidents.

The methodology of previous research (Tanaka et al., 2012, Morales Teraoka et al., 2014) was generally followed. Two changes were proposed: (1) Use of weighted empirical cumulative distributions for input variables. (2) Use of weighted logistic regression for injury risk curves. Further methodological consideration, even though no changes were made, should be given to inclusion of non-injury cases, object grouping, and treatment of uncertainty.

ACKNOWLEDGEMENTS

REFERENCES

Cullen, A. C., Frey, H. C. (1998) *Probabilistic Techniques in Exposure Asessment. A Handbook for Dealing with Variability and Uncertainty in Models and Inputs*. Plenum Press.

Erbsmehl, C. (2009) Simulation of Real Crashes as a Method for Estimating the Potential Benefits of Advanced Safety Technologies. Proceedings of *21st Enhanced Safety of Vehicles (ESV) conference*, Stuttgart, Germany, paper number 09-0162.

Farmer, C. M. (2004). Effect of Electronic Stability Control on Automobile Crash Risk. Traffic Injury Prevention 5 (4), 317-325.

Ferguson, S. A. (2007). The Effectiveness of Electronic Stability Control in Reducing Real-World Crashes: A Literature Review. Traffic Injury Prevention 8 (4), 329-338.

Heeringa, S. G., West, B. T., Berglund, P. A. (2010) *Applied Survey Data Analysis*. Chapman & Hall.

IIHS (2012). Special Issue: Crash Avoidance. Status Report 47(5).

Kusano, K., Gorman, T. I., Sherony, R., Gabler, H. C. (2014). Potential Occupant Injury Reduction in the U.S. Vehicle Fleet for Lane Departure Warning–Equipped Vehicles in Single-Vehicle Crashes. *Traffic Injury Prevention* 15 (Supp 1), 157-164.

Lie, A., Tingvall, C., Krafft, M., Kullgren, A. (2006). The Effectiveness of Electronic Stability Control (ESC) in Reducing Real Life Crashes and Injuries. *Traffic Injury Prevention* 7 (1) , 38-43.

Martinez, W. L., Martinez, A. R. (2008). *Computational Statistics Handbook with Matlab*. 2nd edition. Chapman & Hall.

Morales Teraoka, E. Y., Tanaka, S., Mochida, T. (2014) Benefit Estimation Method for Lane Departure Warning Systems in the American Traffic Environment. Proceedings of *SAE World Congress*, Detroit, USA, paper 2014-01-0172.

Pfeiffer, M., Schmidt, J. (2006). Statistical and methodological foundations of the GIDAS accident survey system. Proceedings of *2nd International Conference on ESAR*, Hanover, Germany, pp. 81–87

Rizzi, M., Kullgren, A., Tingvall, C. (2014). Injury crash reduction of low-speed Autonomous Emergency Braking (AEB) on passenger cars. Proceedings of *IRCOBI conference*, Berlin, Germany, pp. 656-65

Tanaka, S., Mochida, T., Aga, M., Tajima, J. (2012) Benefit Estimation of a Lane Departure Warning System using ASSTREET. Proceedings of *SAE World Congress*, Detroit, USA, paper 2012-01-0289.

Human-Machine Cooperation principles to support driving automation systems design

Marie-Pierre Pacaux-Lemoine, Philippe Simon, Jean-Christophe Popieul

LAMIH, UVHC-CNRS UMR 8201, University of Valenciennes, France
{marie-pierre.lemoine, philippe.simon, jean-christophe.popieul}@univ-valenciennes.fr)

Abstract: Car manufacturers and automotive suppliers design more and more Advanced Driving Assistance Systems (ADAS) that are quickly installed into cars. Nevertheless, such ADAS address different types of driving activities and driver's behaviors; they might concern longitudinal and lateral controls, lane changes, navigation, and try to take into account driver state and behavior. But what about the complementarity of such different ADAS if they are all together implemented in one car? And what about their interactions with the driver? Interactions have to be defined according to the levels of automation selected by the car manufacturer. In the French national project CoCoVeA (French acronym for Cooperation between Driver and Automated Vehicle), three levels of automation have been studied involving several existing ADAS. And this paper proposes a methodological approach to identify competences and capacities of driver and ADAS in the case of many driving situations in order to check complementarity, function allocation, authority management, as well as cooperative aspects in order to assess reliability of such a Human-machine system and the acceptance and even the attractiveness of highly automated vehicle.

Keywords: Automation, Human-Centered Design, Man-machine systems, Shared control, Automotive control.

1. INTRODUCTION

Systems capabilities are increasing and might provide today safe, efficient and comfortable environment for Humans. But what about the integration of such advanced systems regarding the Human needs, the expectations and the dynamic and complexity of some environments that do not allow room for error? The objective of the paper is to present Human-Machine Cooperation principles and to highlight its contribution to the usual scales used to characterize the level of automation of systems.

The principles of Human-Machine Cooperation (HMC) have been laid down with a focus on Dynamic Task Allocation and generic concepts have been proposed in order to identify all kinds of interactions between one or several Human operators and one or several assistance systems. Human-Machine Cooperation principles have been applied to several domains: air traffic control (Hoc and Lemoine, 1998; Pacaux-Lemoine and Debernard, 2002), robotics (Pacaux-Lemoine et al., 2011), fighter aircraft (Pacaux-Lemoine and Loiselet, 2002) and car driving (Pacaux-Lemoine *et al.*, 2005).

Therefore, an overview of existing scales describing levels of automation/levels of autonomy is provided. Scales have been defined for aeronautics and robotics domains (Sheridan, 1992; Inagaki and Sheridan, 2008; Kaber and Endsley, 2004). Others have been defined more specifically for car driving domain (SAE, 2014; NHTSA, 2013; Marinik *et al.*, 2014). Scales deal with the type of the tasks allocated to the driver

or the assistance system, the type of coordination between the tasks allocated to each other, the criteria used to decide allocation, authority, and responsibility. Several differences between scales have already been highlighted in a previous study conducted in robotics (Pacaux-Lemoine and Vanderhaegen, 2013). The analysis of the differences confirms our hypothesis that Human-Machine Cooperation principles can help at defining more generic scales and then at designing more adapted systems. Following this initial finding, methodological approach, aiming at designing and evaluating Human-Machine Systems (Pacaux-Lemoine & Crévits, 2010), has been improved. The base of this investigation has been the use of the model of a cooperative agent. The agent can be an intelligent artificial one, like an Advanced Driving Assistance System (ADAS) composed by one or several current ADAS functions already used in cars (ACC or LKA for example). But these functions can also be "mixed" with new ADAS functions under development. The agent can be a Human and in this case the model is used as a representation of the driver state and his/her behavior that is provided to the ADAS. The model of a cooperative agent and HMC principles are detailed in the next paragraph.

2. HUMAN-MACHINE COOPERATION PRINCIPLES

Cooperation is one of the kinds of interaction between two agents. More than the collaboration and the co-action, with the cooperation the agents share a common goal (Pelayo et al., 2013). And next definition precises that: "Two agents of a

system are in a situation of cooperation if: (a) each of them strives towards goals although interfering with the goals of the other (at least on the basis of resources or procedures), and (b) they try to manage such interference to make easier the activities of the other" (Hoc and Lemoine, 1998).

So, cooperative agents, in interaction and involved in the control of the same process, perform individual tasks as well as cooperative tasks. The abilities corresponding to each type of task are respectively called the "know-how" and the "know-how-to-cooperate" (Millot and Lemoine, 1998) (cf. Fig. 1).

- **Know-how (KH)**
  - *Internal ability* to solve problems (regarding the process)
    - competences: knowledge, rules, skills / experience, expertise
    - processing abilities: inferences, workload, fatigue…
  - *External ability* to:
    - get information (from the process and the environment)
    - act (on the process)
- **Know-how-to-cooperate (KHC)**
  - *Internal ability* to:
    - build up a model of other agents (KH and KHC)
    - deduce the other agents' intentions
    - analyze the task and identify the cooperative organization
    - produce a common plan regarding tasks and coordination
  - *External ability* to communicate:
    - understanding other agents
    - providing information to other agents

Fig. 1.   Model of a cooperative agent

2.1   Know-How

The know-how of an agent defines the ability this agent has to control the process without taking into account potential communication with other agents. It is split up into two parts, one is called the internal know-know, the other the external know-how. The internal know-how relates agents' competences and capacity to control the process and deals with problem solving (Rasmussen, 1983; Hoc and Amalberti, 1995). The external know-how is associated to the ability to get information from the process and the ability to act on the process. The know-how defines the tasks that can be allocated to agents in order to reach a common goal.

2.2   Know-How-to-cooperate

The know-how-to-cooperate is also split up into two parts, an internal part and an external one. The internal know-how-to-cooperate allows an agent to build up a model of other agents (their know-how and know-how-to-cooperate) in order to make easier the cooperation with them. The external know-how-to-cooperate is the ability to exchange information with others. The know-how-to-cooperate defines the management of the interactions between agents and supports a mutual understanding and control.

Analyzing the design of a Human-Machine System through the use of Know-how and Know-how-to-cooperate allow to scan all possible interactions between agents. For the moment they depend on the availability, the similitude and/or the complementarities of agents' know-how, as well as agents'

know-how-to-cooperate. The forms of cooperation proposed by Schmidt (1991) support such an approach. But in this paper we would like to extend this work by analyzing more in details interactions using each part of the know-how which can be defined as four main activities: information acquisition, information analyzing, decision selection, action implementation (Parasuraman *et al.*, 2000); and we would like to use each part of the know-how-to-cooperate: information gathering and analyzing regarding the activity of other agents, detection and management of interferences between agents' activities in order to define task allocation and coordination (Hoc and Lemoine, 1998). Cooperative activity is supported by a Common Work Space which is a visual, sound and/or haptic interface between agents and provides support tools to control the process but also information about the process analysis conducted by other agents (Pacaux-Lemoine and Debernard, 2002).

3.   FROM THE MODEL TO CAR DRIVING APPLICATION

3.1   Objectives of the project

In this paper we propose to use this model within the framework of a French national project called CoCoVeA (French acronym for Cooperation between Driver and Automated Vehicle) run by academic partners (University of Valenciennes and Caen, INRIA, IFFSTAR) and industrial partners (PSA, Valeo, Continental, AKKA, Spirops). The objective of the project is to define cooperation between driver and automated driving assistance systems at several automation levels provided at the operational, tactical and planning levels of the driving activity. The use of Human-machine cooperation principles might help at designing cooperation between driver and one or several systems inside each level of activity, but also between each level of activity. It is a Human-centered design approach regarding the interaction of systems with driver, but coherence and complementarities between the several systems can also be evaluated. Levels of automation will be especially defined for each level of activity according to the driving situation, systems abilities, driver state, but also according to the levels of automation defined for the other levels of activity.

Three levels have been defined and based on the levels of automation proposed by SAE (Society of Automotive Engineers) and OICA (French acronym for International Organization of Motor Vehicle Manufacturers) (SAE, 2014). They have been mainly defined at the operational and tactical levels, focusing on specific driving situations such as driving on motorway, on an exit lane, in traffic jam, passing a toll, driving on expressway and in a roundabout. Level of automation has been defined for each driving situation and for each transition between driving situations. Level 0 is without assistance except warning systems, the driver has to perform lateral and longitudinal control of the vehicle. Level 1 is the "assisted level", i.e. the ADAS performs the lateral OR the longitudinal control but not both. In the CoCoVeA project, the level 1 allows the ADAS to control the speed and so it can be seen as a driving "without the feet" (Ferron et al.,

2014). At the level 2, called "partial automation", the ADAS can control the lateral AND the longitudinal trajectory. So it can be seen as a driving "without feet and hands".

3.2 Implementation of the model

Fig. 2 proposes a synthesis of the several abilities and supports (Pacaux-Lemoine, 2014).

The Know-How of the driver (KH-D) is decomposed into four main functions (Fig. 2 Driver/N°1): gathering information from the environment (infrastructure, traffic,

weather…), analysing this environment, making a decision regarding the need to modify current trajectory and implementing the selected decision. The Know-How of the ADAS (KH-ADAS) is similar (Fig. 2 ADAS/N°1). It gathers information from the environment thanks to sensors, it analyses information and make a decision thanks to its software, and apply the selected decision using "drive by wire".
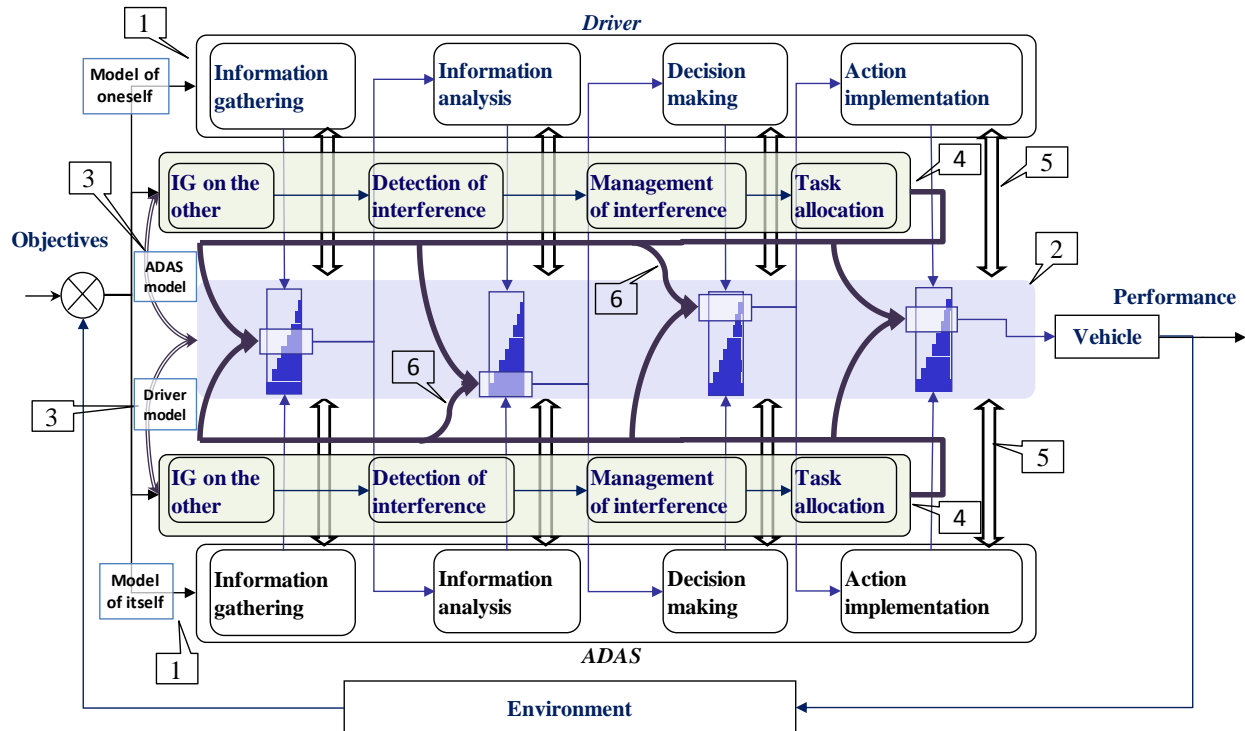
Fig. 2.   Individual and cooperative tasks (1-Know-How; 2-Common Work Space; KHC to build up a model of the other (3); KHC on the current task (4), KHC to provide intention (5), KHC to manage authority (6)).

The main differences between driver and ADAS are: — training and experience lead the driver to anticipate some driving situations in order to adapt the trajectory and the itinerary in order to avoid accident with unexpected events such as aberrant road user behaviour, road works, and diversion for example; — workload, fatigue and distraction lead the driver to be less aware of the driving situation and less ready to implement correctly his/her KH; — weather conditions, system breakdown or error lead the driver to stay in the control loop of the vehicle in order to supervise ADAS functioning for some driving situations.

So, a balance has to be found to combine driver and ADAS KH in order to take advantage of the efficiency of each one and to compensate the temporal or permanent inability of

each one. The Know-How-to-Cooperate (KHC) helps at defining and implementing such a balance.

Communication between driver and ADAS is supported by the Common Work Space (CWS) (Fig. 2 N°2), which can be a visual display as well as a haptic feedback provided through the seat, the steering wheel or the pedals, as well as a sound feedback. But CWS is more than a simple interface; it is also the support of the cooperation. It provides tools to implement and to control the KHC which is now detailed.

The Know-How-to-Cooperate (KHC) consists firstly in having a model of the KH and the KHC of the other (Fig. 2 N°3). This model is used to understand and to assess the other (Fig. 2 N°4). Secondly, it consists in being able to communicate with the other to provide information about him/her/itself (Fig. 2 N°5) and to negotiate, to accept or to

control function allocation (Fig. 2 N°6). If the ADAS use is easy and sufficiently intuitive, the driver has not to learn the ADAS functioning and to train himself/herself with it. So the driver's KHC can be quite light. But the more the ADAS is complicated, the more the driver's KHC (KHC-D) must be important and the more cooperative tasks are difficult to manage; this leads to driver overload and frustration. In order to avoid such situations, the ADAS KHC (KHC-ADAS) must be efficient.

The driver tries to build up a model of the ADAS functioning in order to use it as well as possible (Fig. 2 Driver/N°4. And the ADAS try to build up a model of the driver in order to be the more cooperative as possible (Fig. 2 ADAS/N°4). The driver does not provide information about himself/herself to the ADAS, except perhaps at the first use of the car regarding some preferences in the driving style. On the opposite, ADAS can provide information regarding some parameters it uses to control longitudinal and lateral trajectory such as acceleration/deceleration or time headway. Such parameters can be adapted by the driver by means of the Common Work Space in order to adapt ADAS functioning to the driver habits. In that case, the ADAS is able to build up a model of driver's behaviour, intentions and expectations.

Using the model of the driver, the ADAS is able to assess his/her behaviour (Fig. 2 ADAS/N°3). Using the model of the ADAS, the driver is able to assess its behaviour (Fig. 2 Driver/N°3). KHC-ADAS can evaluate driver state regarding distraction and vigilance, and driver actions regarding driving situation control. It gathers information from the driver (information gathering: IG) thanks to its sensors; it analyses driver state or behaviour (information analysis: IA); it can detect interferences between its analysis of the situation and the one of the driver, or it detects driver distraction or loss of vigilance (interference detection: ID); it manages interferences by making a decision about the driver (interference management: IM). For example, it can communicate with him/her; it decides to control the function (function allocation: FA). KHC-Driver can evaluate ADAS functioning through information provided by the way of the dashboard. But KHC-Driver can also evaluate ADAS through its actions. All these information take place in the CWS. Driver can disagree ADAS analysis and decision making, and so he/she can decide to overtake the control for example.

Nevertheless it is difficult to be sure that the model of the other agent is correct. So, one way to ensure that the model is right is to have direct information from the other (Fig. 2 N°5). By providing or asking explicitly information to the other, inferences are avoided. In car driving, ADAS provide information about its information gathering and analysing, its

decision making and future actions through the visual display. At the operational level, one example is the information provided the ADAS that the speed has to be reduced within 1 kilometre. At the tactical level, regarding the ability of the ADAS to overtake the following vehicle, it can provide its intention to the driver: approaching a slow vehicle, no vehicle arriving in the other lane, overtaking within some seconds, displaying on a visual interface to inform the driver and to avoid his/her surprise to feel or to see the vehicle going on the other lane. At the strategic level, an example is the information provided by the navigation system that the vehicle has to exit the motorway within two kilometres. It is more difficult to imagine the driver providing information to the ADAS regarding his/her intention except when a new destination is given.

The result of the previous cooperative activities is to manage authority and function allocation (Fig. 2 N°6). At each step of the problem solving activity included in the KH, it is possible to allocate the function to the driver or the ADAS. Allocation can be predefined or can be updated according to driver or ADAS decision because of an unexpected and/or a risky driving situation. Levels of automation aim at defining the rules to manage such function allocation but it is mainly at the last stage of problem solving activity, i.e. the action implementation. But we would like to highlight other possibilities to manage interferences between driver and ADAS. It is the objective of the next paragraph which underlines all the possible interactions between driver and ADAS KH and KHC.

3.3 Cooperation inside and between levels of activity
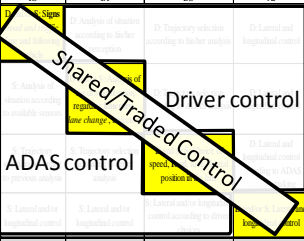
The next table (cf. Table 1) proposes a synthesis of what could be the KH and KHC of the driver and ADAS. They are all crossed in order to extract all interactions. This is one way to identify the competences of each one in the current moment, and what competences must be to reach efficient and accepted (even more requested) cooperation. An increase or an adaptation of competences involves new developments for ADAS, training for the driver. But this last possibility must be limited.

The KH is presented according to the four steps, Information Gathering (IG) from the driving situation, Information Analysis (IA) of the driving situation, Decision Selection (DS) and Action Implementation (AI). The KHC is presented according to Information Gathering (IG) from the other, Interference Detection (ID) about the other, Interference Management (IM) and Function Allocation (FA). Those individual and cooperative functions have been presented in the previous paragraph, but the Table 2 highlights interactions between them.

Table 1.   Driver/ADAS KH and KHC complementarity

(Know-How: IG: Information Gathering; IA: Information analysis; DS: Decision Selection; AI: Action Implementation)

(Know-How-to-cooperate: IG: Information Gathering; ID: Interference Detection; IM: Interference Management; FA: Function Allocation)

Strategic level		Driver							
Tactical level		know-how				know-how-to-cooperate			
Operational level		IG	IA	DS	AI	IG	ID	IM	FA
know-how — IG		D and/or S: **Signs** *road and traffic lane and following vehicle*	D: Analysis of situation according to his/her perception	D: Trajectory selection according to his/her analysis	D: Lateral and longitudinal control	D: Sensors states	D: Sensors are breakdown, unsuited, improperly adjusted	D: Modification of sensors	D: Manual control
know-how — IA		S: Analysis of situation according to available sensors	D and/or S: Analysis of the driving situation regarding **itinerary**, *lane change*, trajectory	D: Trajectory selection according to ADAS analysis	D: Lateral and longitudinal control	D: Perception of ADAS analysis	D: ADAS analysis procedure is wrong or not the best one	D: Modification of drivers' preferences	D: Accept or refuse
know-how — DS		S: Trajectory selection according to previous analysis	S: Trajectory selection according to driver analysis	D and/or S: Choice of speed, **road**, *lane*, lateral position in the lane	D: Lateral and longitudinal control according to ADAS decision making	D: Perception of ADAS decision making	D: ADAS decision making is wrong or not the best one	D: Modification of drivers' preferences, correction of decision	D: Accept, refuse or modify
know-how — AI		S: Lateral and/or longitudinal control	S: Lateral and/or longitudinal control	S: Lateral and/or longitudinal control according to driver choices	D and/or S: Lateral and longitudinal control	D: Perception of ADAS actions	D: ADAS actions are wrong or not the best one	D: Modification of drivers' preferences, correction of action	D: Accept, refuse or modify
know-how-to-cooperate — IG		S: Eyes, head, face, hands perception, steering wheel, pedals state	S: Eyes, head, hands, steering wheel, pedals movement	S: Eyes, head, hands, steering wheel, pedals movement	S: Steering wheel, pedals, HMI use	D & S perceptions are different	ADAS justification of sensors fonctioning…		
know-how-to-cooperate — ID		S: Eyes closed, hands off the steering wheel	S: Driver is distracted, drowsy	S: Driver intention is wrong	S: Driver action is wrong		D & S analysis are different	ADAS justification of its analysis…	
know-how-to-cooperate — IM		S: Alert message, Wakeup procedure	S: Alert message, Wakeup procedure	S: Visual, audio alert message	S: Haptic alert	Driver justification of his/her presence	Driver justification of his/her analysis	D & S decision making is different	ADAS justification of its decision making...
know-how-to-cooperate — FA		S: Stop of the vehicle in the lane or on the hard shoulder	S: Return to the manual control or lower LOA	S: Haptic alert	S: Collision avoidance ?			Driver justification of his/her decision making	D & S action implementations are different

Table 2.   Driver/ADAS zones of interaction

The Table 2 proposes four main parts:

- The upper and left scare deals with the complementarity between the KH-D and the KH-ADAS.
  - The diagonal of this square corresponds to the sharing ("and" operator) or the trading ("or" operator) of all or part of the functions allowing the control of the

vehicle if they are both able to perform them. It is used in the CoCoVeA project at the operational level for Action Implementation functions. The sharing can only concern the longitudinal control: the driver and the ADAS share the control through the gas pedal. The sharing can only concern the lateral control: the driver and the ADAS share the control through the steering wheel. The sharing can concern both controls at the same time; it is the sharing of the trajectory control. At the operational level, the sharing of the other functions (IG, IA and DS) is more difficult because of the time pressure. They would be defined at the tactical and strategic levels. Sharing can be conducted to analyze respectively the possibility to overtake and the possibility to select an itinerary. But those functions sharing, before action implementation, must be sufficiently pertinent to compensate the time spent to the sharing definition. It could be predefined and updated if necessary by the driver. More detailed about shared control are presented in the extension of this concept according to functions and levels of activity (Pacaux-Lemoine and Itoh, 2015).

The traded control proposes to alternate the control between the driver and the ADAS. The criteria of allocation can be driver overload/underload,

confidence into him/herself, into the ADAS, trust/reliance/overreliance, state… Regarding the ADAS point of view, criteria mainly concern its abilities.

o The part above the diagonal deals with driver control. The driver performs one or several functions. The part below the diagonal deals with ADAS control. The first line (for the driver) and the first column (for the ADAS) correspond to a complete automation of the task, all functions are involved. But other lines and columns involve mixing functions. An example is given in the Table 3. The driver fulfills the three first functions and then delegates the implementation of the action to the ADAS. It is for example the case of an overtaking delegated to the ADAS. Nevertheless, the ADAS could also perform the three first functions in order to verify if the driver decision is right and if it is able to perform the implementation (vertical column written in grey).

Table 3. Driver/ADAS KH

- The lower and left scare deals with one part of the KHC-ADAS, which is the ability of the ADAS to assess the state and the behavior of the driver according to the model it built up.

  The Table 2 highlights four columns. The ADAS could assess each function the driver performs, but in fact it is not so easy.

  o The two first columns provide example concerning the driver state and not the driver behavior. In fact, it is difficult to evaluate the analysis conducted by the driver. The ADAS has to be able to deduce his/her analysis from eyes scanning behavior or movement analysis. But ADAS are not efficient enough to do this itself. So, in the CoCoVeA project, only the driver monitoring is implemented. A device developed by Continental is used and provides indicators regarding driver drowsiness and driver distraction (interferences). The indicators allow checking if the driver is able to gather information about the driving environment and the vehicle, and if he/she is able to conduct the analysis of the driving situation. In order to manage interferences, the ADAS can firstly alert the driver and if there is no reply from the driver, the ADAS can decide to stop de vehicle.

o Regarding the two last columns, current ADAS are only able to perform the last one, i.e. the action implementation. In fact, it is very difficult, for the ADAS to have access to the decision making of the driver before the implementation of his/her action. It is mainly the case at the operational level. But it could be imagined at the tactical and strategic levels. In the previous example about the overtaking, the driver specifies his/her intention to overtake through a specific interface and the ADAS assesses the decision. It can refuse if it detects a coming vehicle on the other lane or if speed and headway do not suit with its dynamic abilities and constraints. At the strategic level, continuing to use this example, the ADAS can refuse to overtake because the exit of the motorway is very near. If the three levels are involved, ADAS has to make sure that the results from each level are compatible and do not alert the driver one by one, or in the same time. Priorities must be defined to order ADAS results for the control as well as for the driver alert. This issue is also taken into account in the CoCoVeA project.

- The upper and right square deals with one part of the KHC-D, which is the ability of the driver to assess the functioning of the ADAS according to the model he/she built up. The table 2 highlights four lines. The ADAS could assess each function the ADAS performs. At the opposite of the ADAS, the driver, normally, can follow each function of the ADAS. As explained in the next sub-paragraph, the CWS supports such information. It is a way for the driver to learn ADAS functioning, to adapt some parameters if necessary and to assess its behavior.

  o The first line concerns the state of the ADAS sensors. They can have problem regarding their accuracy, the fitness with the driving situation for example.

  o The second line deals with driving situation analysis performed by the ADAS. At the operational level, the ADAS diagnoses that the current speed is too high (information provided by the navigation system for example). But the driver can disagree the analysis because this information is not updated and wrong regarding current road signs he/she has seen. At the tactical level, ADAS diagnoses that it is not good to stay in the middle of the three lanes.

  o The two last lines deal with ADAS decision making and action implementation. ADAS proposes decision such as reducing the speed, going around the middle of the lane at the operational level; it proposes to change the lane and to go on the lane close to the hard shoulder (as defined in the Highway Code). The driver accepts or refuses the diagnosis of the ADAS. Interference is then managed with the CWS.

- The lower and right scare deals with the use of the CWS that supports the second part of the KHC-D and KHC-ADAS. It is the ability to communicate with the other for negotiation, acceptance or refusal regarding the result of their KH functions. In car driving, the driver has usually no time to negotiate with the ADAS. He/she accepts or

refuses the ADAS decision selection or action implementation. In the CoCoVeA project, the acceptance and refusal are performed by the way of haptic information through the gas pedal and the steering wheel. For example, if the driver wants to overtake when the ADAS prevents him/her to do it because of a vehicle coming on the other lane, the driver feels a pressure point in the steering wheel. But if he/she decides to overtake despite the alert, he/she can turn the steering wheel beyond the "hard point". A similar behavior is implemented for speed control. If the driver wants to go faster than the speed limit, he/she has to press on the gas pedal; he/she can feel a "hard point" in the pedal but he/she can go beyond the "hard point" by continuing to press.

This paragraph explains how to use the Table 1 and provides some examples. To sum up, each square leads the Human-machine system designer to raise questions about each possible interaction between the ADAS and the driver. But for the moment, this table does not implement levels of automation. When interferences appear between the driver and the ADAS function, they can negotiate the solution and the function sharing, or authority can be allocated to the driver or the ADAS according to the type of driving situation. The management of the authority is partly defined with the levels of automation.

4. CONCLUSIONS AND PERSPECTIVES

The paper proposes one generic approach that can support the design of ADAS, but more broadly Human-machine systems for several domains of application. The approach uses Human-machine cooperation principles that are presented and detailed in order to assess all possible interactions between the driver and the ADAS. Some examples are provided in order to explain how models and tables can be used to reach such goals.

This method is like a tool that can be shared at the beginning of a new project between automotive suppliers and car manufacturers, system designers, researchers from different domains like automation, cognitive and social psychology, computer sciences. It provides a support presenting all the steps that must be followed in order to anticipate advantages but also problems can that occur after the implementation of new assistance systems.

The CoCoVeA project is in its second year. ADAS we would like to use are selected regarding some specific driving situations. Next step is now to check our selections with the method in order to highlight the necessary improvements we have to realize in order to combine all selected ADAS actions and their interactions with the driver. The evaluations of the cooperation between driver and ADAS will be realized by the way of experiments. They will be conducted on the SHERPA driving simulator of the LAMIH and also on test tracks with a demonstrator vehicle. The results stemming from the analysis of the experiments will provide also an evaluation

the usefulness of the method. We will especially check if we were able to anticipate problems regarding cooperative functions.

ACKNOWLEGMENTS

REFERENCES

Feron, S., Valaix, P., Benloucif, A., Sentouh, C. (2014). Rapport de présentation des configurations de références et des scénarios d'usages types. Projet ANR-TDM 2103 CoCoVeA (Coopération Conducteur Véhicule Automatisé), France, décembre.

Hoc, J.-M. and Amalberti, R. (1995). Diagnosis: some theoretical questions raised by applied research. Current Psychology of Cognition, 14, 73-100.

Hoc, J.-M., Lemoine, M.-P. (1998) Cognitive evaluation of human-human and human-machine cooperation modes in Air Traffic control, *The International Journal of Aviation Psychology*, Vol. 8, N°1, 1-32.

Inagaki, T. and Sheridan, T.B. (2008) Authority and responsibility in human-machine systems: Is machine-initiated trading of authority permissible in the human-centered automation framework? *Proceeding of Applied Human Factors and Ergonomics.*

Kaber, D. B. and Endsley, M. R. (2004). The effects of level of automation and adaptive automation on human performance, situation awareness and workload in a dynamic control task, *Theoretical Issues in Ergonomics Science*, ISSN 1463–922X.

Marinik, A., Bishop, R., Fitchett, V., Morgan, J. F., Trimble, T. E., & Blanco, M. (2014, July). Human factors evaluation of level 2 and level 3 automated driving concepts: Concepts of operation. (Report No. DOT HS 812 044). Washington, DC: National Highway Traffic Safety Administration.

Millot, P., Lemoine, M.-P. (1998). An attempt for generic concepts toward human-machine cooperation. *IEEE SMC Conference*. San Diego, USA, October.

National Highway Traffic Safety Administration (2013) Preliminary Statement of Policy Concerning Automated Vehicles.

Pacaux-Lemoine, M.-P. (2014). Human-Machine Cooperation Principles to support Life Critical Systems management. In P. Millot, Risk Management in Life critical

Systems, ISTE-Wiley, London, pp. 253-277, ISBN 978-1-84821-480-4

Pacaux-Lemoine, M.-P., Debernard, S., (2002). A Common Work Space to support the Air Traffic Control, Control Engineering Practice, A Journal of IFAC, 10, 571-576,

Pacaux-Lemoine, M.-P., Debernard, S., Godin, A., Rajaonah, B., Anceaux, F. and Vanderhaegen, F. (2011). Levels of automation and human-machine cooperation: Application to human-robot interaction, *IFAC World Conference*, Milano, Italy.

Pacaux-Lemoine M.-P., Crévits I. (2010). Methodological approach for road safety system evaluation. 11th IFAC International Conference on Analysis, Design, and Evaluation of Human-Machine Systems, Valenciennes, France, septembre .

Pacaux-Lemoine, M.-P. and Itoh M. (2015). Towards vertical and horizontal extension of shared control concept. *IEEE SMC Conference*, Hong Kong, October.

Pacaux-Lemoine, M.-P., Loiselet A. (2002). A common workspace to support cooperation in the cockpit of a two seater fighter aircraft. In M. Blay-fornarino, A.M. Pinnadery, K. Schmidt, P. Zaraté (Ed.) *Cooperative systems design: a challenge of mobility age*, IOS Press, Amsterdam, North-Holland, 157-172.

Pacaux-Lemoine M.-P., Ordioni J., Popieul J.-C., Debernard S., Millot P., Cooperating with an assistance tool for safe driving. *Proceedings of 16th IFAC World Congress*, Prague, Czech Republic, 2005 July.

Pacaux-Lemoine, M.-P. and Vanderhaegen, F. (2013). Towards Levels of Cooperation. *IEEE SMC Conference*, Manchester, UK, October.

Parasuraman, R., Sheridan, T., Wickens, C. (2000). A model for types and levels of human interaction with automation. *IEEE Transactions on Systems, Man, and Cybernetics-Part A*, may, 30 (3), 286-297.

Pelayo, S., Anceaux, F., Rogalski, J., Beuscart-Zéphir, M.C. (2013). Impact of CPOE implementation vs. organizational determinants on doctors-nurses communications and cooperation: revisiting the evidence. *International Journal of Medical Informatics*, 82 (12), e321-e330. (ISSN: 1386-5056)

Rasmussen, J. (1983). Skills, rules and knowledge; signals, signs, and symbols, and other distinctions in human performance models, *IEEE Transactions on systems, man and cybernetics,* SMC13, n°3, May-June.

SAE International (2014) SAE J3016: Taxonomy and Definitions for Terms Related to On-Road Motor Vehicle Automated Driving Systems.

Schmidt, K. (1991). Cooperative Work: a conceptual framework, In Rasmussen J., Brehmer B., and Leplat J. (Eds), *Distributed decision making: Cognitive models for cooperative work*, pp 75-110, John Willey and Sons, Chichester, UK.

Sheridan, T.B. (1992) Telerobotics, automation and human supervisory control, The MIT Press.

Join the joyride before it's too late!
Effects of autonomous driving on perceived driving enjoyment

P. Roßner*, S. Scherer**, K. Simon***, M. Jentsch****, A. C. Bullinger*****

TU Chemnitz, Chair for Ergonomics and Innovation Management, 09107 Chemnitz, Germany
* (Tel: 0371-531 39931; e-mail: patrick.rossner@mb.tu-chemnitz.de).
** (e-mail: svenja.scherer@mb.tu-chemnitz.de)
***(e-mail: katharina.simon@mb.tu-chemnitz.de)
****(e-mail: martin.jentsch@mb.tu-chemnitz.de)
***** (e-mail: bullinger-hoffmann@mb.tu-chemnitz.de)}

Abstract: Autonomous driving vehicles will become a key element of mobility in the near future. Although it opens up new opportunities for the individual and increases traffic safety, there is a highly controversial debate about how much this new way of driving is accepted by the driver. In this article, relevant factors and expectations for autonomous driving are investigated. The basic theories on determinants for driving enjoyment will be opposed to different levels of automation for vehicles to predict their possible effect on driving enjoyment. An insight will be given into content analysis and online survey. Results indicate that attitudes towards autonomous driving can vary between situations. Especially situations with a high dynamic aspect such as driving a curved road are rejected, while over 90% of the participants were able to name at least one situation where they could imagine to be driven with an autonomous vehicle. This paper contains a detailed presentation of the results and is completed with the discussion of possible impacts of autonomous driving on the driver, on society, and its potential implication for the automotive industry.

Keywords: Autonomous driving, driving enjoyment, driver attitude, automated driving

1. INTRODUCTION

Autonomous driving will become reality in the not too distant future. Vehicles are already able to participate partially automated in road traffic and possibly soon as autonomous cars (Spiegel, 2014). Although autonomous driving opens up new opportunities for individual mobility such as increasing traffic safety (Kessler et al., 2012), this development is viewed with scepticism by many drivers. Surveys among German drivers show that about 12% of respondents refuse an autonomous driving vehicle as a way of transportation in general (e.g. Autoscout24, 2014; Ernst & Young in Fuß, 2014). Recent studies focus on expected impact of autonomous driving (Simon et al., in press). The aim of this study is to better understand the enjoyment and the attitude of drivers and to identify causes of the negative attitude.

To explore pros and cons of autonomous driving in general, a content analysis of comments was performed on German websites. Subsequently, an online survey was conducted, where various situations of autonomous driving vehicles are mentioned as particularly good or particularly bad. These situations are examined in particular with regard to the expected driving pleasure, comfort and perceived safety.

In the present article, these basic theories on the development of driving pleasure as well as the current state of automation of driving tasks are first shown. Afterwards a description and results of empirical studies will occur, consisting of a content

analysis and an online survey. It concludes with a summary of the findings and the overall practical implications as well as the derived further research needs.

2. THEORETICAL BACKGROUND

2.1 Emergence of driving pleasure

Previous publications dealt with the first definition of "driving pleasure" and a possible distinction to the term "driver comfort". The definition of driving pleasure by Tischler and Renner (2007, p. 109) is: "driving pleasure is a positive emotional state of a person provided through an active involvement, which is understood by a momentary sensual experience of the interaction human-vehicle-environment" (translated). Engelbrecht, Engeln and Arndt (2009) set their focus on individual driving actions. In their model, a distinction is made between fun / fun deficiency and comfort / discomfort. Thereby driving pleasure goes hand in hand with a positive quality of experience and high intensity action. For comfort, although the positive quality of experience remains, however, the action intensity is low. Driving pleasure can thus arise or result from the active confrontation with the vehicle only at active actions. In an online survey the importance of 15 actions for driving pleasure and ride comfort was determined by Engelbrecht (2013). Mostly positive experienced driving actions were inter alia "accelerate the car", "driving at a constant speed,"

"keep the lane while driving and follow the road" and "changing gears". Among predominantly negatively experienced driving actions figure "convoy driving", "stopping" and "deceleration". These individual actions were evaluated dependent on sustainable characteristics of the driver, as motivation for action, gender and age as well as driving experience. Furthermore, it is expected that there are influencing factors for subjectively experienced driving pleasure above particular driving actions. These include the reason for the trip (work vs. leisure rides), traffic conditions (free ride vs. stop-and-go) and the driver's state (fit vs. tired) (Pöschel, Kienast & Spanner-Ulmer, 2011).

The described findings relative to the driving pleasure are based on the assumption of a non-assisted driving task. In order to be able to look at presumed influences of driver assistance systems and autonomous driving on driving pleasure as a further development, the theoretical basic principles concerning driver assistance systems and automation levels are presented.

2.2 Automation of driving task

The range of functions and the complexity of driver assistance systems have changed over the years. At the beginning the functions of the driver assistance systems were limited to the stabilization of the vehicle without having a direct and conscious interaction between assistance systems and drivers. Due to progressive technology, it was possible to warn and inform the driver and in addition to increase the safety of the driver and rise the comfort while driving (Jentsch, 2014).

The next step of the assistance will be an autonomous way of driving with complete takeover of the driving task. Since it is still a long way from assisted driving to autonomous driving, Gasser (2013) defined different levels of automation which are shown in table 1.

Table 1. Definition of levels of automation (Gasser, 2013)

Degree of automation	Definition
5) Autonomy /driverless	The system is able to initiate and execute every required control for driving without limitations.
4) Fully automated	The system takes over lateral and longitudinal control completely. In absence of a takeover, the system will return to minimal risk condition by itself.
3) Highly automated	The system takes over lateral and longitudinal control. The driver doesn't have to permanently monitor the system and is requested to take over control within a certain time buffer.
2) Partially automated	The system takes over lateral and longitudinal control. The driver must permanently monitor the system and be prepared to take over complete control of the vehicle.
1) Assisted	The driver continuously accomplishes either lateral or longitudinal control. The other/remaining task is accomplished by the automating system to a certain level.
0) Driver only	The driver continuously accomplishes lateral and longitudinal control.

Present driver assistance systems are therefore still at the first stage of automation. In current research, the effects of partially and highly automated vehicles on the driver-vehicle interaction will be investigated theoretically (Othersen, Hackenberg, Petermann-Stock & Bendewald, 2013), in driving simulator studies (Damböck, 2013) or in tests with real vehicles (Lange, Maas, Albert, Siedersberger & Bengler, 2014).

According to the existing theory of driving pleasure, it can be assumed that the lack of active control will adversely affect the driving pleasure of the vehicle. To answer these questions, the individual attitudes concerning autonomous driving were considered with a content analysis and an online survey.

3. METHOD

3.1 Content analysis

Readers' comments of five "Zeit" and four "Spiegel" articles as well as two forum discussions dealing with autonomous driving were investigated. 201 out of 852 comments were considered as relevant, because a specific aspect regarding autonomous driving was positively resp. negatively mentioned. A content analysis of these 201 comments was performed.

3.2 Online survey

At the beginning, an introduction to autonomous driving was presented to build a precise and equal knowledge level of that term. The following questionnaire was divided into five sections:

(1) Attitude towards autonomous driving by using nine items of van der Laan et al. (1997) with a five-point Likert-scale.

(2) List of one to five situations where autonomous driving is desired and, subsequently, assessing driving pleasure, comfort and perceived safety on a five-point Likert-scale separately for non-autonomous and autonomous vehicles.

(3) List f one to five situations where autonomous driving is undesired following the structure of (2).

(4) List of scenarios which generate driving pleasure with non-autonomous vehicles and statements to that driving pleasure in an autonomous driving scenario with reasons for decreasing cases.

(5) Sociodemographic data like age, gender, driver's licence duration, owned vehicle model, and kilometres (km) covered during last year.

83 persons (32 female, 51 male) attended the online survey. Age varied from 18 to 64 years (M = 32.2, SD = 10.9). Duration of driver's licence ownership covered values from one to 46 years (M = 14.1, SD = 10.6). The participants drove 13,586 km on average last year (SD = 13,570). To enable

inferential statistics, age, last year's driven km and duration of driver's licence ownership were divided into two (median as cut-off value) resp. three groups (33rd resp. 66th percentile as cut-off value) as shown in table 2.

Table 2. Sample grouping

Cut-off value	age in years	duration of driver's licence ownership	driven km last year
33rd percentile	26.5	7.5	8,000.5
median	29.5	11.5	10,000.5
66th percentile	33.5	26.5	15,000.5

4. RESULTS

4.1 Content analysis

Nine statements representing categories were extracted. Therefore, a comment was able to address several categories. Table 3 delivers an overview differentiated by positive and negative mentions.

Table 3. Number of citations of assumed impact of autonomous driving

category	positive mentions	negative mentions	summed mentions
safety & system reliability	49	33	82
comfort	44	11	55
society & environment	7	24	31
costs	9	10	19
driving pleasure	3	15	18
legal aspects & liability	0	17	17
data integrity	0	11	11
concrete applications	10	0	10
traffic flow	12	0	12
total	**134**	**121**	**255**

The most mentioned categories are "safety and system reliability" and "comfort". Positive comments on "safety and system reliability" include an expected increase of safety by achieving a higher regulatory compliance as well as the elimination of the "risk factor human" in case of autonomous driving.

"Ja, wenn die Leute vernünftig wären, ihre Emotionen im Griff hätten, nicht müde würden, sich nicht ablenken ließen, sich nicht verschätzen würden und so weiter und so weiter. Aber wir haben es nun mal mit dem Faktor Mensch und all seinen Unzulänglichkeiten zu tun. Insofern finde ich die Idee gar nicht schlecht". (Comment on article "Automatisiertes Fahren: Mensch gegen Maschine", Spiegel Online, 2013a)

Critical comments on the safety aspect relate primarily to the expected error rate and a general distrust in the technology.

"Was meinen Sie wohl, weshalb Microsoft und Apple nahezu täglich Software-Updates servieren? Weil die Programme vor Fehlern nur so strotzen! Warum sollte das bei Autos anders sein? Im Leben nicht!" (Comment on article "Autonomes Fahren - Zu kurz gesprungen", ZEIT Online, 2014)

Statements concerning the expected comfort are predominantly positive. Many comments address the possibility to use the time of driving for other activities. Takeover of strenuous and unpleasant driving activities is another relevant aspect of autonomous driving.

"ich [sic!] fahre sehr viel Auto und so etwas wäre echt ein Traum. Dieses stupide rumfahren [sic!] auf der Autobahn oder im Berufsverkehr ist echt langweilig. Da könnte man echt viel bessere Sachen machen. […]". (Comment on article "Roboter-Autos: Deutsche sind offen für autonomes Fahren", Spiegel Online, 2013b)

Negative comments on comfort include mainly the fear of not being able to sit relaxed in an autonomous driving vehicle, as the driver probably continues to monitor all processes. Very critical, each with no mention in a positive sense, the legal aspects and liability as well as data integrity are seen. Hereof, mainly the still not clarified questions of liability in an accident with an autonomous driving vehicle as well as the fear of not being able to demonstrate personal innocence are mentioned. Also data integrity issues are viewed critically. One aspect is the fear of a virus or hacker whose attack could affect the safety of the vehicle. The possibility of personal data collection and abuse from autonomous vehicles is another criticized point. Concrete applications and impact on traffic flow are exclusively positively discussed, the latter primarily in terms of a homogenization of traffic.

"Es sind geringere Abstände zum vorausfahrenden Automatischen möglich. UND höhere Geschwindigkeiten. Dadurch könnte die mögliche Verkehrsdichte/ Transportleistung leicht doppelt [sic!] werden. […]". (Comment on article "Roboter-Autos: Deutsche sind offen für autonomes Fahren", Spiegel Online, 2013b)

Besides, the positive impact that particularly older road users could participate in road traffic in a safer way was stated. In addition, autonomous driving vehicles provide the opportunity to chauffeur physically limited, ill or intoxicated persons. Cost aspects are highly controversial. Possible positive economic effects like cost savings due to higher car sharing rates as a consequence of automation. Increased maintenance costs are seen negative on an individual level.

With regard to the impact on the driving pleasure, the aspect of active driving is considered as an important determinant. Many comments mention the fear that driving would not be applicable as a leisure activity in the age of automation and therefore reject autonomous driving in general. Some comments consider the problem more differential and emphasize the distinction of various driving actions.

"Atuonomes [sic!] Fahren heißt ja nicht, dass der Fahrspaß verloren geht, ich verjage auch gern mit 240 km/h andere Fahrer auf der linken Spur, aber ich kann eben auch in der Stadt mit 50 km/h leise dahinrollen und der Wagen hält den nötigen Abstand. Darum geht es beim autonomen Fahren in meinen Augen: repetitive, ermüdende und langweilige Vorgänge übernimmt der Wagen und wenn man will, nimmt man einfach selbst wieder das Steuer in die Hand". (Comment on article "Roboter-Autos: Deutsche sind offen für autonomes Fahren", Spiegel Online, 2013b)

4.2 Online survey

(1) **Attitude of respondents towards autonomous driving**

Firstly, a total score of all items has been formed. The higher the average, the more negative each item resp. the total score was rated. The calculated centre of the scale was M = 3. The total score shows that men (M = 2.66; SD = 1.12) rated autonomous driving worse than women (M = 2.32; SD = 0.67) in general. The older the driver, the longer they have their driver's license and the more kilometers they drive per year, the worse they estimated autonomous driving (significant correlations, p < .01). Considering the differences between groups using a one-way ANOVA more differentially, results show that mainly the oldest and longest driving licenses owning group are responsible for the significant differences (ANOVA: (F (2,80) = 11.773, p < .01).

(2) **Situations where autonomous driving is desired**

On average, respondents gave in M = 2.37 (SD = 1.48) preferable situations. The demographic variables age, gender, duration of driver's license ownership and km driven per year had no effect on the number of these situations. Overall, these situations could be classified into 15 categories with the help of an inductive category formation. The ones most frequently mentioned are presented in Table 4.

Table 4. Situations where autonomous driving is desired

Category	examples	number of mentions
impaired driving ability	impairment because of age, alcohol, illness, fatigue etc.	49
heavy road traffic	stop & go, traffic jam	26
specific driving situations	parking, rerouting, dangerous situations	21
other activities	reading, working during business trips	19
long driving distances	vacation trips	13
highway	highways with speed restriction	12

Respondents formulated partially complex situation descriptions that contained more than one aspect. These were separated and recorded separately in the category system. For example, the phrase "highway with a lot of traffic" contains the aspects "highway" and "heavy road traffic". Similar multiple answers to a category by an individual were counted once.

(3) **Situations where autonomous driving is not desired**

On average, the respondents mentioned less undesirable (M = 1.35, SD = 0.89) than desirable situations (t-test: t(82) = -6.854; p < .01). The demographic variables age, gender, duration of driver's license ownership and km driven per year again had no effect on the number of stated situations. The situations were divided with regard to content into eleven categories with the help of an inductive category formation. Table 5 illustrates the most common categories.

Table 5. Situations where autonomous driving is not desired

category	examples	number of mentions
situations with dynamic driving style	fast driving, active driving, drifting, curvy routes	31
specific driving situations	dangerous situations, probation, work zones	17
urban regions	urban routes	14
particular route	nice, empty and varying routes	10

Following the extraction of desirable and undesirable situations for autonomous driving differentiating characteristics were investigated. The attributes of safety, comfort and driving pleasure reached from "1 - very low" to "5 - very high". It turns out that the desirable situations are currently evaluated as more unsafe, less comfortable and with a smaller driving pleasure, as situations in which an autonomous driving style is not desired. Means, standard deviations and results of t-tests are shown in Table 6.

Table 6. Comparison of desired and not desired situations without autonomous driving

characteristic	situation	N	M	SD
safety	desired	140	2.51	1.15
	not desired	72	3.04	1.05
	t-test	t(155,316) = -3.340, p < .01		
comfort	desired	140	2.44	0.98
	not desired	72	3.22	1.00
	t-test	t(210) = -5,482, p < .01		
driving pleasure	desired	140	2.17	1.27
	not desired	72	3.65	1.43
	t-test	t(210) = -7,431, p < .01		

The comparison of the anticipated impacts of autonomous driving between the desired and undesired situations shows

that safety, comfort and driving pleasure is estimated higher in the desirable situations than in the undesirable situations. The means, standard deviations and results of t-tests are shown in Table 7.

Table 7. Comparison of desired and not desired situations when driving autonomously

characteristic	situation	N	M	SD
safety	desired	140	4.15	0.90
	not desired	72	3.51	1.32
	t-test	$t(105,609) = 3,672, p < .01$		
comfort	desired	140	4.29	0.78
	not desired	72	3.21	0.98
	t-test	$t(210) = 8,116, p < .01$		
driving pleasure	desired	140	2.49	1.20
	not desired	72	1.68	0.92
	t-test	$t(179,528) = 5,442, p < .01$		

Herefrom it is possible to draw the interim conclusion that drivers particularly prefer autonomous driving when they are in unsafe and uncomfortable situations which pose few driving pleasure. In these situations, safety, comfort and driving pleasure of driving autonomously are higher than in situations without desired autonomous driving style. As this finding is no more surprising as that safety, comfort and driving pleasure increase in the situations where autonomous driving is desired (all t-tests with $p < .042$), investigation focus is to check how these characteristics will change by autonomous driving in not desired situations.

While comfort (t-test: $t(71) = 0.013$, $p = .918$) does not change for these situations, respondents specify that despite the rejection of autonomous driving, safety increases (t-test: $t(71) = -2.437$, $p = .017$). The rejection of autonomous driving is, in principle, caused in the decrease of driving pleasure (t test: $t(71) = 8.919$, $p < .01$) in certain situations.

To analyze conclusively whether the perceived safety, comfort or driving pleasure have an impact on whether the respondents want autonomous driving style in a situation a one-way analysis of variance was performed with the categorized situations as an independent variable.

Regarding the evaluated comfort, despite of a significant overall effect (ANOVA: $F(9.202) = 4.564$, $p < .01$), no differences between the situations in the post-hoc analysis are detectable. Concerning perceived safety (ANOVA: $F(9.202) = 9.032$, $p < .01$) and driving pleasure (ANOVA: $F(9.202) = 11.803$, $p < .01$) there are also differences between the situations in the post-hoc analysis. So, safety of impaired driving ability (M = 1.82, SD = 0.91) is estimated lower than in all other situations, while the situations "particular route" (M = 3.5, SD = 1.08) and "urban regions" (M = 3.64, SD = 0.93) are rated as safer than any other situations. Considering the assessed driving pleasure for these situations it is evident that "heavy road traffic" (M = 1.46, SD = 0.86) is the situation that causes the least driving pleasure, while the situations "particular route" (M = 3.9, SD = 1.37) and

"dynamic driving style" (M = 4.16, SD = 1.28) cause more driving pleasure than any other situations.

These results strengthen the assumption that perceived driving pleasure has a great influence on the attitude towards autonomous driving. Drivers appreciate safety benefits of autonomous driving styles, but only in situations in which they assess safety and driving pleasure to be extremely low, they are ready to be driven autonomously. In contrast, there are reservations about the new technology, if a sufficient degree of (traffic) safety is perceived in the situation and the traffic situation is associated with driving pleasure.

(4) **Driving pleasure with respect to non- or autonomous vehicles**

75 respondents indicated at least one aspect, why they currently feel pleasure while driving cars. The most common dynamic driving aspects were mentioned, such as "fast and curvy driving", "drifting with an all-wheel resp. rear wheel car under wet conditions or in winter" or "shifting quickly". The second most common category was self-determined driving with answers like "to drive the car by him- or herself and decide what needs to be done" or "sense of control and mastery". This was followed by naming comfort aspects, such as "seat heater", "transport qualities" or "music".

When asked whether the driving pleasure would preserve in autonomous driving, 55.4% responded with "no", only 20.5% said "yes" and 24.1% with "do not know". These responses were independent of participants' demographic characteristics. As the most common reasons for the loss of driving pleasure the lack of control and the passivity behind the steering wheel were stated.

5. DISCUSSION AND IMPLICATIONS

That article focused on the expected driving pleasure during autonomous driving and on driver's attitude towards an autonomous vehicle. Due to the fact that these vehicles cannot be experienced yet, the article provides essential insights into attitudes and expectations of German drivers at this time. These findings need to be verified when autonomous driving vehicles are available.

Analysis of online fora shows that numerous reservations about autonomous driving vehicles exist. Especially, safety aspects, both concerning the vehicle itself and the data integrity, are stated very often. If these aspects are ignored and concrete application scenarios are considered, as done in the online survey, results show that the expected lack of driving pleasure plays a major role in the rejection of autonomous driving.

The results confirm previous studies and have to be considered differentiated. Rejection of autonomous driving is particularly large in dynamic driving situations. More than half of respondents expect that driving pleasure providing situations in autonomous vehicles offer no more fun. As the aspect of control to your own vehicle is cherished over all operations, which also turned out to be an important factor for driving pleasure in previous studies, many drivers no

longer consider the sense of autonomous vehicle, but describe that they "in that case [...] also [can] ride Taxi".

In that sample also, similar to the surveys mentioned at the beginning, a general 10%-rate of rejection was found. Nevertheless, particularly interesting is that over 90% of subjects in the online survey name concrete situations in which they desire autonomous driving. Most common these are situations that do not provide driving pleasure currently, are exhausting or are perceived as particularly unsafe. Thus, the category of impaired driving ability is mentioned most frequently, when it comes to desirable situations for autonomous driving. Concerning that drivers already see a tangible and practical benefit, as an autonomous driving system allows driving generally in these cases or make this much safer.

Based on these results, it is recommended not to discuss autonomous driving as a holistic vision of the future. In most cases it leads to rejection if drivers imagine that they could only drive autonomous in the future. To increase acceptance, desired application scenarios found in this investigation, such as driving in heavy traffic or impaired driving ability due to fatigue or illness, should be used for communication with future users.

REFERENCES

AutoScout24 (2014). Unser Auto von morgen 2013/2014 – Was wünschen sich die Europäer vom Auto von morgen? http://ww2.autoscout24.de/autoscout24_-_unser_auto_von_morgen_2013-14_-_klein.pdf.

Damböck, D. (2013). Automatisierungseffekte im Fahrzeug – von der Reaktion zur Übernahme. Dissertation, TU München.

Engelbrecht, A. (2013). Fahrkomfort und Fahrspaß bei Einsatz von Fahrerassistenzsystemen. Berlin, Humboldt-Universität, Dissertation.

Engelbrecht, A., Engeln, A., Arndt, S. (2009). Wie entstehen Fahrkomfort und Fahrspaß? Beschreibung und Bewertung von Fahrkomfort und Fahrspaß aus Expertensicht. In: Verein Deutscher Ingenieure (Hrsg.). Der Fahrer im 21. Jahrhundert. Fahrer, Fahrerunterstützung und Bedienbarkeit, S. 261-268. Düsseldorf: VDI-Verlag.

Fuß, P. (2014). Autonomes Fahren: Spaßbremse oder Erfolgsrezept? http://www.handelsblatt-automobil.de/news/autonomes-fahren-spassbremse-oder-erfolgskonzept. Visited on 21/05/2015.

Gasser, T. M. (2013). Herausforderungen automatischen Fahrens und Forschungsschwerpunkte. In: Tagungsband 6. Tagung Fahrerassistenz. 28.-29.November 2013, München.

Jentsch, M. (2014). Eignung von objektiven und subjektiven Daten im Fahrsimulator am Beispiel der Aktiven Gefahrenbremsung - eine vergleichende Untersuchung. Universitätsverlag Chemnitz, Chemnitz.

Kessler, C., Etemad, A., Alessandretti, G., Heinig, K., Selpi, Brouwer, R., Cserpinszky, A., Hagleitner, W. & Benmimoun, M. (2012). euroFOT - Deliverable D11.3:

Final Report. Ford Forschungszentrum Aachen GmbH, Aachen.

Lange, A., Maas, M., Albert, M., Siedersberger, K.-H., Bengler, K.: Automatisiertes Fahren - So komfortabel wie möglich, so dynamisch wie nötig. In: Tagungsband VDI/VW Gemeinschaftstagung Fahrerassistenz und Integrierte Sicherheit 2014. VDI Verlag, Düsseldorf, 2014.

Othersen, I., Hackenberg, L., Petermann-Stock, I., Bendewald, L. (2013). From Driver to Supervisor - An Analysis of Partly Automated Driving. In: Tagungsband 6. Tagung Fahrerassistenz. 28.-29.November 2013, München.

Pöschel, K., Kienast, H., Spanner-Ulmer, B. (2011). Welche Faktoren bestimmen Fahrspaß? In: Gesellschaft für Arbeitswissenschaft e.V. (Hrsg.), Mensch, Technik. Organisation - Vernetzung im Produktentstehungs- und -herstellungsprozess, Tagungsband GfA-Frühjahrskonferenz 2011, S. 193 - 196. Dortmund: GfA-Press.

Simon, K., Jentsch, M., Bullinger, A. C., Meinicke, E. & Schamber, G. (in press). Sicher aber langweilig? Auswirkungen vollautomatisierten Fahrens auf den erlebten Fahrspaß. Zeitschrift für Arbeitswissenschaft.

Spiegel (2014). Testfahrt in Google Self-Driving Car: Dieses Auto kommt ohne Sie aus. http://www.spiegel.de/auto/aktuell/google-auto-unterwegs-im-selbstfahrenden-auto-a-969532.html Visited on 30/01/2015.

Spiegel Online (2013). Automatisiertes Fahren: Mensch gegen Maschine. Autor: Christoph Stockburger. http://www.spiegel.de/auto/fahrkultur/rechtliche-und-ethische-fragen-zum-automatisierten-fahren-a-905181.html. Published on 14/06/2013. Visited on 30/01/2015, 2013a.

Spiegel Online (2013). Roboter-Autos: Deutsche sind offen für autonomes Fahre. Pressemitteilung rom/reuters. http://www.spiegel.de/auto/aktuell/mobilitaet-der-zukunft-deutsche-sind-offen-fuer-autonomes-fahren-a-920081.html Published on 03/09/2013. Visited on 30/01/2015, 2013b.

Tischler, M.A. & Renner, G. (2007). Ansatz zur Messung von positivem Fahrerleben. Die Messung von Fahrspaß und Ableitungen für die Fahrzeuggestaltung. In Fahrer im 21.Jahrhundert. Human Machine Interface. VDI-Berichte 2015, (S. 105-117), Düsseldorf: VDI-Verlag GmbH.

Van der Laan, J.D., Heino, A., De Waard, D (1997). A simple procedure for the assessment of acceptance of advanced transport telematics. Transportation Research - Part C: Emerging Technologies, 5, 1-10, 1997.

ZEIT Online (2014). Zu kurz gesprungen. Autor: Adrian Lobe. http://www.zeit.de/2014/33/autonomes-fahren-auto-strassenverkehr. Published on 23/08/2014. Visited on 30/01/2015, 2014.

A study of appropriate model complexity
for estimation of car-following behavior

Malin Sundbom * **Jonas Sjöberg** *

* *Chalmers University of Technology, 41296 Gothenburg, Sweden*
(e-mails: malin.sundbom@gmail.com, jonas.sjoberg@chalmers.se).

Abstract: This paper investigates model complexity, or equivalently, necessary model structure, for describing car-following behavior. The recently suggested PrARX modeling framework is systematically investigated and compared with simpler model structures containing less tuning parameters to see to what extent complex models can be motivated. The results indicate that for long prediction horizons there is no gain having a complex model structure. However, one-step ahead prediction of complex models can be useful for classification of whether the driver should be braking or not.

Keywords: Driver behavior modeling, hybrid models, advanced driver assistance systems

1. INTRODUCTION

Advanced Driver Assistance Systems (ADAS) that automatically adapt to the driver's preferences are gaining increased attention. For example, the potential of automatic braking systems for avoiding rear-end accidents can be improved without increased risk for false interventions, if the treshold can be adapted to the individual driver. By estimating a model of the driver's normal behavior, ADAS functionality can be tuned with help of the individual driver model as depicted in Fig. 1 where the system continuously compares the response of the driver model with that of the real driver. If the driver model correctly describes the behavior of an alert and attentive driver, this comparison will detect, for example, when the driver approaches the vehicle in front faster than normally. Based on this, a warning or intervention by the ADAS may be triggered. This automatic tuning is however a delicate issue, especially when safety related functionality rely on it, which motivates further studies on the topic.

A common strategy is to divide the driver model into different modes corresponding to distinct driver maneuvers, e.g. straight driving or lane-changes, so that fairly simple models can be used for each mode in combination with a detection mechanism which monitors the change between the modes. With such an approach, both the parameters describing each mode, and the parameters describing the shift between the modes need to be adapted to the driver. One way of accomplishing this is to use hybrid models, containing both a discrete and a continuous part. This allows capturing the driver's behavior in each mode as well as the switching between the modes, corresponding to the driver's decision making process. For example, in Liu and Pentland (1997) and Oliver and Pentland (2000), Hidden Markov Models (HMMs) were used to cluster the driver behavior into different modes based on vehicle signals.

Suzuki et al. (2005) tried to extend the HMM framework and combine it with dynamical models by letting the behavior in each mode be described by an Auto Regressive model with eXogenous input (ARX model) to create the Stochastic Switched-ARX (SS-ARX) driver model. The SS-ARX model is an example of a hybrid ARX models for driver behavior, which have recently then been the focus of several studies. In the SS-ARX model, the switching betwen modes is stochastic and the output depends only of the mode in which the driver currently is operating. Suzuki et al. (2005) tested this model structure in a driver simulator, achieving good performance in recognizing the lateral driving behavior in a car-following scenario.

Probabilistic ARX (PrARX) models also belong to the family of hybrid ARX models and are particularly suitable for online estimation applications. In such a model structure, the system output is calculated by weighting the outputs of several ARX sub models, each corresponding to one mode. The weights each represent the probability that the system operates in a certain mode. PrARX models have been used e.g. in Taguchi et al. (2009) to model the longitudinal driving behavior in a car-following scenario, while in Mikami et al. (2010) it was combined with a model predictive control (MPC) algorithm to minimize the time spent in modes where the driver had to engage in collision avoidance behavior.
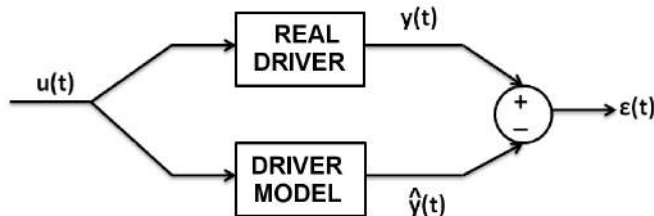
Fig. 1. Possible use of a driver model which describes an alert correct behaiving driver: The driver action is compared to that of the model during driving and if the difference becomes large, this indicates that the driver is not behaiving correctly.

This paper considers the possibility to model the driver's car-following behavior. Dynamic models of different complexity are estimated. For an extensive review of the evolution of car-following models from the 1950s and forward, see Brackstone and McDonald (1999). The input signals to the models are signals related to the distance to the car in front, and the output is the driver's pedal action, either acceleration or braking. In general, to estimate an advanced model, a lot of information is required from the available data. In case the data is not informative enough, a simpler model must be accepted. During routine driving on e.g. a highway, the signals do not excite the system very much, which sets limits on the level of complexity of the estimated models. Therefore, in this paper we study a set of different models with varying degree of flexibility and explore what level of complexity can be motivated for a car-following model. The most flexible model structure studied in this paper is the PrARX modeling framework with two modes and a parameterized switching between them. The less complex models can be seen as simplifications of the PrARX model imposing various degrees of assumptions. For example, one assumption which is explored is that the driver has one behavior when the driver in front is restricting the speed, and another behavior when the driver can decide the speed themselves.

It should be emphazised that this paper investiges possible model structures for describing the driver's behaivor. No driver models are suggested. The investigated model structures can be used to obtain driver models, but for that more driver data is necessary and a thorough validation procedure.

One of the results is that it is not possible to accurately predict the pedal use more than one time step ahead, i.e., the modeled output signal $\hat{y}_{\tilde{t}}$ cannot be predicted well for $\tilde{t} > t+1$. This means that it is not possible to predict that a driver will miss a braking maneuver using these signals and these models. However, the models can detect a missed braking maneuver at t using $\epsilon(t)$. Hence, the models can be used to classify whether the driver is in a situation where they normally prefer to brake or not, and that is enough to be used in an ADAS. These two classes are, here on, called *dangerous mode*, when the driver normally prefer to brake to keep a safe distance, and *safe mode* when braking is not judged necessary. Furthermore, the models are compared once more based on their ability to classify correctly, and their performance is compared with traditional classifiers based on physical modeling of the braking need rather than the driver's preferences.

The paper outline is as follows. In the first section, the data used for estimation and validation of the models are described. This is followed by a section describing a first principle braking model based on a time to collision measure. Section IV gives an overview of ARX and PrARX model structures and compares the prediction performance of different model structures for describing a driver's car-following behavior. In section V, the focus is instead on classifying the driver's car-following behavior and determining whether the driver is going to brake or not. Section VI concludes the paper and gives suggestions on future work.

2. DATA DESCRIPTION

The data used in this study was collected by the Suzuki lab at Nagoya University, Japan, using a simulator with a stereoscopic immersive environment as in Taguchi et al. (2009). In a qualitative study, five drivers, from here on referred to as driver A, B, C, D and E respectively, where asked to perform car-following in the manner they would usually do in real driving. Car-following is defined as situations when there is a vehicle, from here on called *leader vehicle*, in front of the own car, which we have chosen to call *ego car*.

Since there are no critical events in the data set, the models estimated in this study should describe the drivers acting correctly, i.e. brake when it is necessary and accelerate accordingly. The drivers are referred to as *correct drivers* and their output is denoted y_t. The modeled output signal is denoted $\hat{y}_t$. The mean square error (MSE),

$$MSE = \frac{1}{N} \sum_{k=1}^{N} \epsilon^2(k) \qquad (1)$$

is used to measure the quality of the models, where $\epsilon(t) = y_t - \hat{y}_t$, and N is the number of time samples.

For modeling of drivers in car-following scenarios the relative distance between the vehicles, the *range r*, and the respective relative velocity, the *range rate $\dot{r}$*, are commonly used as model inputs, see e.g. Mikami et al. (2010), Burgett et al. (1998). In addition to these inputs, a risk-index signal called KdB index, see Wada et al. (2007), may be added as input to the hybrid model. In Ikami et al. (2011) this signal was found to be important in determining when the driver switch between different operational modes. The index is defined as:

$$\text{KdB} = \begin{cases} -10 \log |-\frac{\dot{r}}{r^3} 4 \cdot 10^7|, & \dot{r} > 0 \\ 10 \log |-\frac{\dot{r}}{r^3} 4 \cdot 10^7|, & \dot{r} \le 0. \end{cases} \qquad (2)$$

It can be understood as a measure similar to the logarithm of the inverse time-to-collision signal and corresponds to the area change of the visual image of the preceding vehicle on the retina. Already in 1976, Lee (1976) proposed a framework for the driver's longitudinal control based on TTC and the optical expansion of the vehicle in front on the retina. In Wada et al. (2007), this concept was extended to create a performance index for approach and alienation, also called the KdB risk index.

In equivalence to Ikami et al. (2011), the range, range rate and KdB are considered as inputs to the driver models in this study, and it is investigated whether some of these signals can be excluded to obtain simpler models. As output the driver's pedal action is used by introducing a signal, y_t, called *pedal operation*, defined as a positive value between 0 and 1 when the gas pedal is pressed and a negative value between 0 and -1 when the brake pedal is pressed. 0 corresponds to no pressure and 1 respectively -1 to maximum pedal pressure.

One assumption which is investigated is whether the dynamics are different when pressing the brake pedal as compared to pressing the gas pedal. Depending on which pedal is pressed, we define two modes,
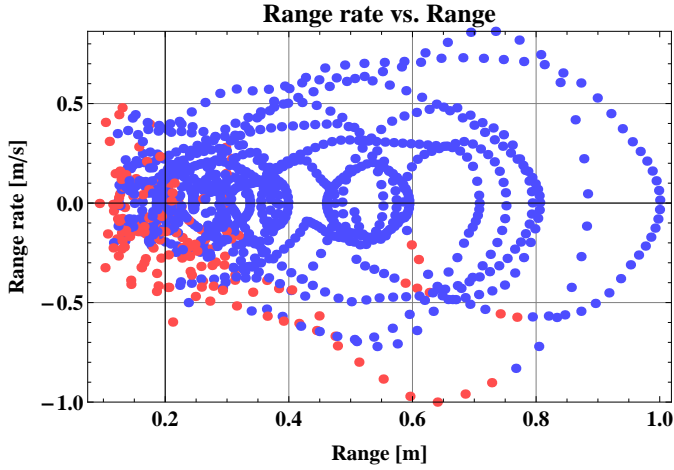
Fig. 2. Acceleration (blue dots) and braking (red dots) behavior in the range, range rate space for driver A.

$$\text{Mode at time } t = \begin{cases} \text{Safe,} & y_t > 0 \\ \text{Dangerous,} & y_t \leq 0. \end{cases} \quad (3)$$

In Fig. 2 the data from driver A is shown in the range rate versus range space. Red dots indicate braking and blue dots acceleration. From the figure it is clear that the two modes cannot be linearly separated using only the range and the range rate, but more signals are necessary.

3. FIRST PRINCIPLE BRAKING MODEL

To benchmark the driver model structures investigated in this paper, a first principle model based on assumed braking capability is derived. It is based on the time-to-collision (TTC) measure, assuming fixed acceleration,

$$TTC(t) = \frac{r(t)}{\dot{r}(t)}, \dot{r} < 0 \quad (4)$$

where $r(t)$ is the range and $\dot{r}(t)$ is the range rate at time t. A car-following situation where $TTC < 4 - 5\ s$ is often judged as critical enough for an automatic emergency braking system to intervene, see e.g. Van der Horst and Hogema (1993) . To calculate when it is appropriate to brake, a TTC threshold of 5 s is therefore chosen in this model, i.e. when $TTC > 5\ s$, the driver is classified to be in the safe mode and when $TTC < 5\ s$ the driver operates in the dangerous mode. For driver A and D, this gives the mode partitions shown in Fig. 3. As can be expected, it is observed that the driver is in the dangerous mode when the range to the car in front is small and decreasing. This was also the case in the previous section when plotting the gas/braking behavior of the driver. It is also observed that the driver is generally braking when operating in the dangerous mode. However, this simple model structure is not satisfactory since it results in many cases where the driver brakes although the model predicts differently, these misclassifications are shown in black in the figure. For these drivers, the two modes are not linearly separable in the range - range rate plane.

4. DYNAMICAL MODELS WITH DIFFERENT LEVELS OF COMPLEXITY

4.1 ARX and PrARX models

In Sundbom et al. (2013), an overview of the fundamentals of ARX and PrARX modeling and their identification is made. This section is a review of the basic concepts. An ARX model calculates the output y_t of system S, at the current time t as

$$y_t = \theta^T \phi_t + e_t, \quad (5)$$

where e_t is an error term and the parameter vector θ and the regression vector ϕ_t are defined as

$$\theta = [c_1, c_2, \ldots, c_n, d_0, d_1, \ldots, d_m]^T, \quad (6)$$

$$\phi_t = [y_{t-1}, y_{t-2}, \ldots, y_{t-n_a}, u_t, u_{t-1}, \ldots, u_{t-n_b}]^T, \quad (7)$$

The orders of the ARX model are denoted n_a and n_b, while $c_1, c_2, \ldots, c_{n_a}$ and $d_0, d_1, \ldots, d_{n_b}$ represent the model parameters. In this paper, a DC-level will be included in
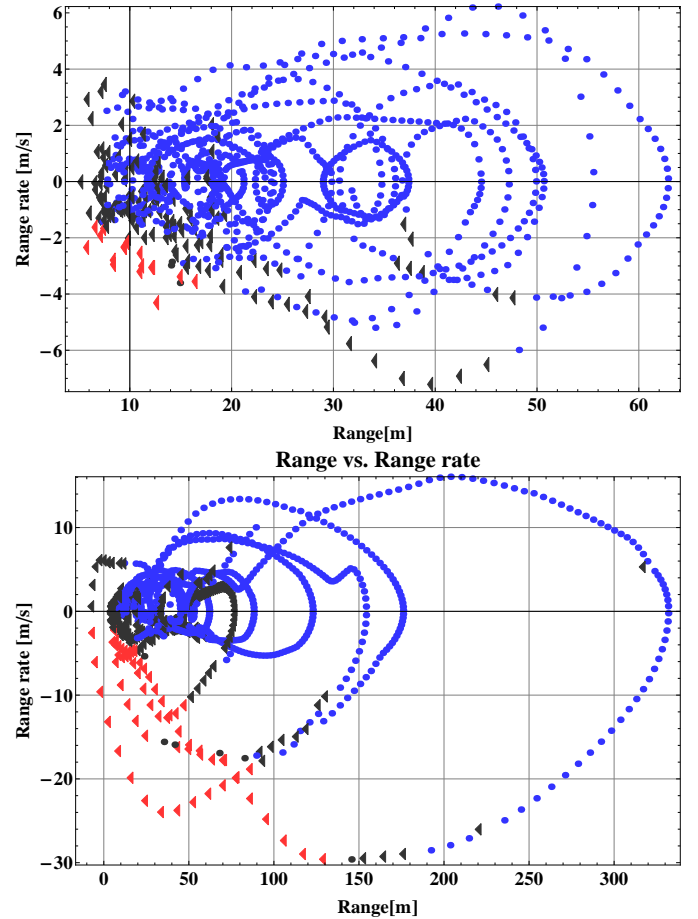
Fig. 3. Mode partition resulting from the TTC-based model applied to data from driver A (upper) and D (lower). Red dots correspond to the driver operating in dangerous mode, blue dots correspond to the safe mode. The triangles represent that the driver is braking, while dots mean that the throttle is pressed. A black triangle or dot means that the sample is incorrectly classified by this model.

the ARX-models to account for bias in the data. This adds a parameter k_0 to the right hand side of (5).

An extension to the ARX models for describing the system S operating in s modes $S_i, \ldots, S_s$, can be made by introducing PrARX models. The PrARX models consist of s ARX models, each describing the system behavior in one mode S_i, and equally many probability functions P_i. Generally, $P_i(\cdot, \phi_t)$ is a function of ϕ_t, but it may also be a function of other variables which are not included in the regressor vector. The notation is simplified by writing $P_i(\phi_t)$ and refer to the case where P_i is a function of the regressor vector only. The output y_t is calculated as a linear combination of the ARX model outputs with the corresponding probability functions P_i,

$$y_t = \sum_{i=1}^{s} P_i(\phi_t)\theta_i^T \phi_t. \tag{8}$$

The probabilistic weighting functions $P_i(\phi_t)$, $i = 1, \ldots, s$ express the probability that the system S is operating in mode i and are defined by a softmax function

$$P_i(\phi_t) = \frac{e^{\eta_i^T \phi_t}}{\sum_{j=1}^{s} e^{\eta_j^T \phi_t}}, \tag{9}$$

where the parameter vectors η_i, $i = 1, \ldots, s-1$ determine the switching between the operating modes.

The regressor space is partitioned by hyperplanes, defined by η_i, $i = 1, \ldots, s-1$, separating the operating modes.

4.2 Parameter estimation

The parameters of the ARX and PrARX models, are calculated based on the Prediction Error Method (PEM). This means that the MSE, eq. (1), is minimized with respect to the parameters θ_i and η_i. Since the PrARX models are nonlinear in the parameters, it is a nonlinear least squares problem. Details on methods for nonlinear modeling and identification can be found in e.g. Ljung (1999) and Sjöberg et al. (1995). For the analysis in this paper, the data from each driver was divided into two sets: one set used for estimation of the parameter values (60%) and one set used for validation (40%). All results presented below are based on the validation data sets. The estimates are computed using the Mathematica software package described in Hjalmarsson and Sjöberg (2012).

4.3 Performance comparison of ARX and PrARX models

To analyze the necessity of using more than one mode for modeling a driver's car-following behavior, the PrARX model is compared to its linear counterpart, an ARX model, with the following inputs:

- KdB risk index, $u_1(t)$
- Range, $u_2(t)$
- Range rate, $u_3(t)$.

The output is the predicted pedal operation signal, $\hat{y}_t$. Both the ARX sub models of the PrARX model and the pure ARX model have the same simple structure, using the regressor $\phi_t = [1 \; \hat{y}_{t-1}, u_{1,t-1}, u_{2,t-1}, u_{3,t-1}]$, where the 1 is included to make it possible to capture a non-zero mean

value. Below, only the results from driver A are presented, however the conclusions hold for the other drivers as well.

Fig. 4 shows the mean square error and its variance for the PrARX and ARX models with different prediction horizons. It is observed that the PrARX model has a lower MSE than the ARX model for one-step-ahead prediction. The difference is small, but significant, which confirms the advantage of having two modes in the model when using it for short term predictions. However, there is no significant difference between the models for longer time horizons, why it is not necessarily a benefit to use the nonlinear model when a longer prediction horizon is needed. This is discussed further in section 4.5. The relative high MSE for the simulation case indicates that disturbances are highly influencing the model. This is likely to be low frequency disturbances.

The next step is to determine whether it is possible to simplify the PrARX model while keeping the two modes. It can be observed that all inputs to the model are functions of range; the range rate is the time derivative of the range and the KdB risk index is a nonlinear combination of the range and range rate. Thus, possibly, the range rate input could be disregarded and its effect accounted for by instead increasing the order of each ARX model. The MSE of this simplified model structure is compared to that of the original PrARX model with three inputs in Fig. 5. It is observed that the output from the two models are very close, but not identical. The difference may arise from the fact that the approximation of the range rate is not exact, it can also be due to the nonlinear estimation algorithm and to numerical issues in the calculations.

To further reduce the complexity of the PrARX model, another PrARX model structure with two inputs is used, this time a model where the KdB risk index signal is omitted. However, in this model the ARX sub models are first order models. The results are compared to the three inputs PrARX-model. Surprisingly, there is no significant
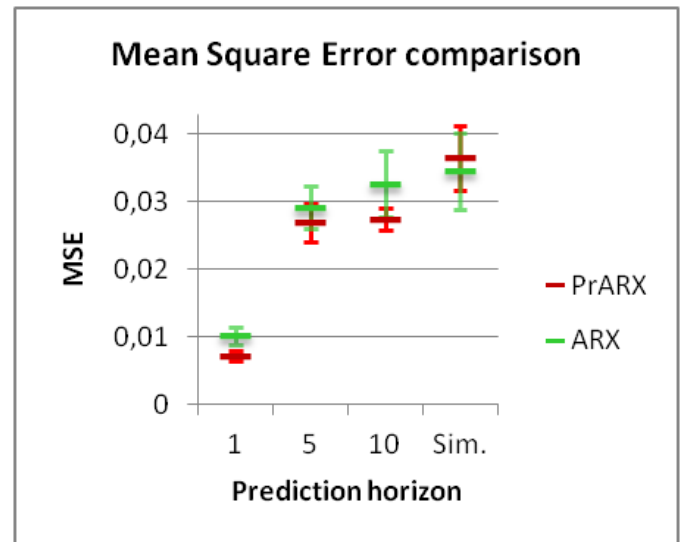
Fig. 4. Mean square error of the PrARX (red) and ARX (green) models for different prediction horizons. The vertical lines represent the variance of the mean square error.
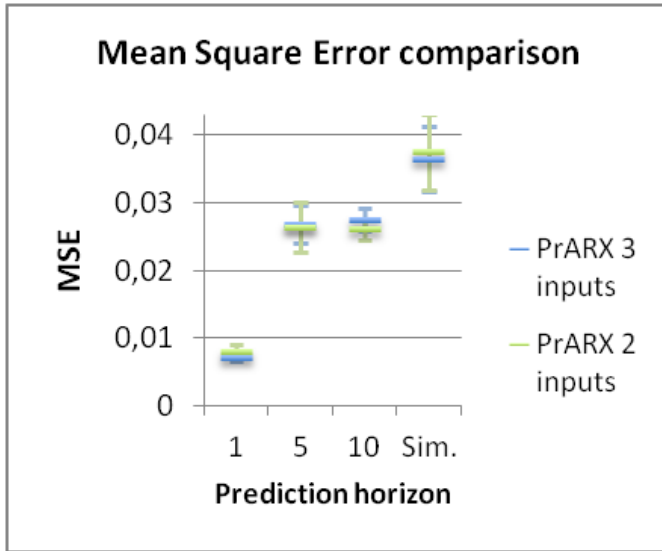
Fig. 5. Mean square error of the PrARX models with three inputs (violet) and two inputs (green) respectively, for different prediction horizons. The vertical lines represent the variance of the mean square error.

difference in the MSE-value for the two models. This indicates that the KdB risk index is not important to fit the pedal operation curve correctly. However, the variance of the MSE of the model with two inputs is larger than the variance of MSE of the model having three inputs. Also, when using first order ARX sub models, the model with two inputs has a significantly higher MSE than the three input PrARX model.

Reducing the number of inputs to only one, the range, and compensating by increasing the order of the ARX sub models, results in numerical problems for longer prediction horizons. This can be due to instability in the system. The results in this section thus suggest that the PrARX model with two inputs, range and range rate, is the least complex model giving the best results. See Fig. 6 for an illustration of the comparison of the three models.

4.4 PrARX model with simplified mode transition

A different way of simplifying the PrARX model is to remove the switching parameters and create a hybrid ARX model, switching modes according to whether the value of an input signal exceeds a certain threshold or not. Fig. 7 shows the pedal operation signal with its corresponding mode partition for the PrARX model with three inputs. The figure suggests that it is reasonable to assume that current operating mode can be determined by having a threshold value on the pedal operation signal. This opens on to a *PrARX model with simplified mode transition*, henceforth called a *PrARX-SMT model*. The structure is similar to the PrARX model structure, but the mode transition is determined solely based on a threshold on the pedal operation signal. The threshold value and the smoothness of the corresponding mode transition is modeled by a sigmoid function with two parameters, α and β. The model structure is as follows

$$y_t = \sum_{i=1}^{s} \sigma(y_{t-1})\theta_i^T \phi_t, \quad \sigma(x) = \frac{1}{1 + \beta e^{x-\alpha}} \quad (10)$$

where $\sigma(x)$ close to 1 corresponds to the driver operating in the safe mode and $\sigma(x)$ close to 0 to the driver operating in the dangerous mode. The parameter α represents the threshold value of the pedal operation signal and β represents the smoothness of the switch, i.e. the steepness of the middle part of the sigmoid curve. The model parameters are estimated as described in section 4.2 and the obtained values are $\alpha = -0.02$ and $\beta = 141$. Since β is large, and α is almost zero, this suggests a steep transition curve and a mode switch at a pedal operation of almost 0. This confirms the hypothesis that the driver uses different dynamics when braking from when accelerating.

To compare the PrARX-SMT model to the PrARX model with three inputs, the MSE was calculated. Fig. 8 shows a comparison of the MSE of the two models for different prediction horizons. The PrARX model performs clearly
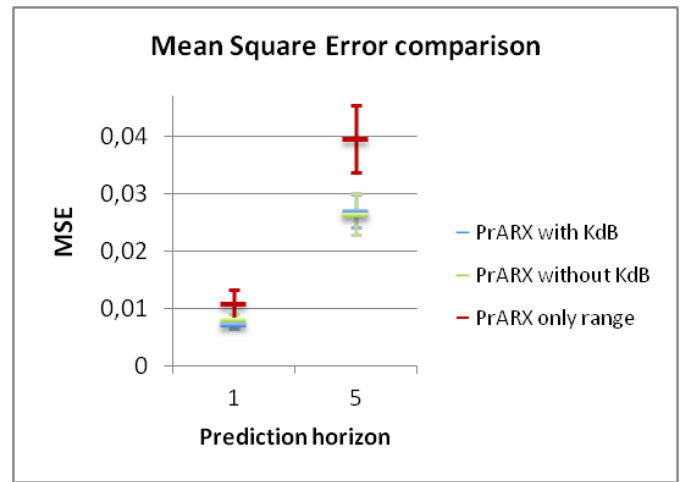
Fig. 6. Mean square error of the PrARX models with three inputs (red), two inputs (green) one input (blue) respectively, for different prediction horizons. The vertical lines represent the variance of the mean square error.
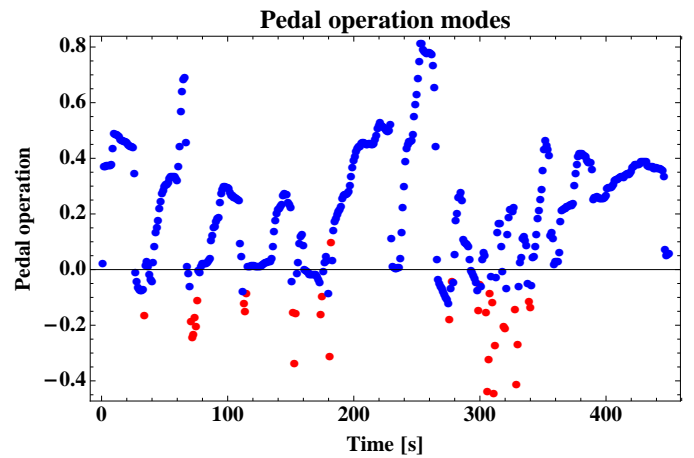
Fig. 7. Pedal operation signal. The predicted modes from the PrARX model with three inputs is indicated by red (dangerous mode) and blue (safe mode) dots.

better than the PrARX-SMT model, except for in the simulation case where the performances are equal.

Hence, there is a significant support for the more complex model, although it is not very large.

4.5 Prediction performance

The results in this section indicate that for five-step-ahead prediction, corresponding to a time horizon of 2 s, the PrARX model is not better than the linear ARX model and thus nothing is gained from using a more complex model structure than the ARX for this time horizon. Fig. 9 shows the five-step-ahead prediction of the PrARX model. From the figure, it is clear that the model is unsatisfactory in the regions around the peaks. The corresponding figure for ARX is very similar and can be used to draw the same conclusion. However, both models give good results in the region around the x-axis, and are hence also good in detecting switches between acceleration and braking. That is, it is not possible to accurately predict the driver's exact pedal operation behavior, all we can do is to predict whether the driver is going to brake or not. This can be done using one-step ahead prediction, where the PrARX model is significantly better than both the PrARX-SMT
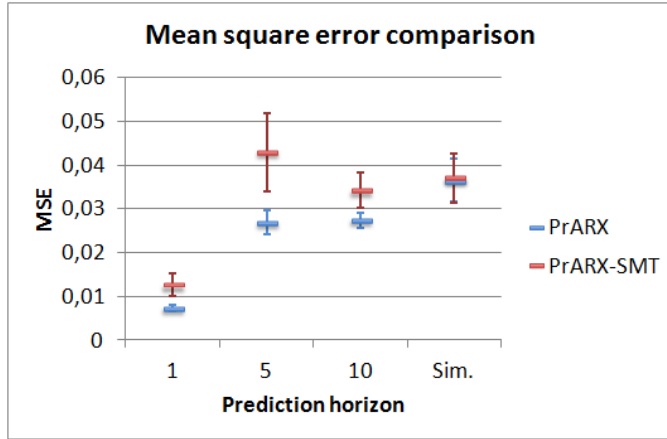
Fig. 8. Mean square error of the PrARX model (blue) and the PrARX-SMT model (red) respectively, for different prediction horizons. The vertical lines represent the variance of the mean square error.
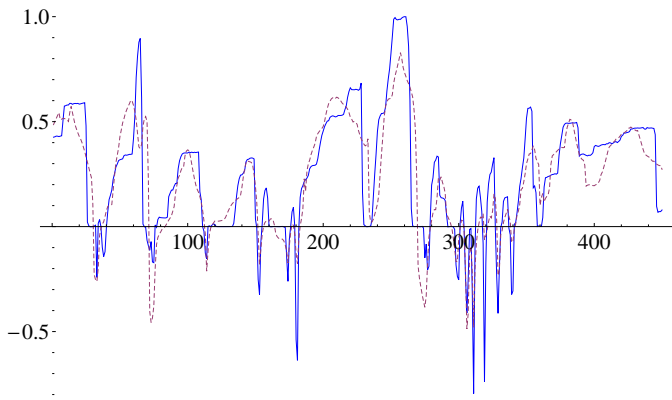
Fig. 9. Five-step-ahead prediction results of the PrARX model. The blue line corresponds to the true output and the dashed purple line is the prediction.

and the ARX models. Predicting whether the driver will brake or not can also be done without using a dynamical model, a topic which is discussed in the next section.

5. CLASSIFICATION MODELS

In this section, the classification performance of a very simple classification method is compared to the classification performance of the dynamical models presented in the previous section.

5.1 Quality measures

The quality of the classification is measured by comparing the model output to the correct driver behavior by using sensitivity and specificity. Sensitivity is a measure on how well the classification performs on data belonging to the dangerous mode and specificity is a measure on how well it does on safe mode data. In addition to this, the method's ability to detect mode switches is evaluated. A mode switch corresponds to that the driver either initiates or ends a braking sequence, i.e. a time sequence where the brake pedal is first pressed and then released. Let n_{true}^i denote the number of cases where the driver initializes a braking sequence and n_{corr}^i correspond to the number of cases where the model correctly estimates that the driver will do so within an interval of 2 s before or after the true initialization moment. Moreover, let n_{est}^i be the number of braking sequences as estimated by the model. The quality measure used is based on the following measures:

- **Correct braking initialization:** $c_i = \frac{n_{corr}^i}{n_{true}^i}$, i.e. the fraction of true braking sequence initializations that are correctly detected by the model.
- **Missed braking initialization:** $m_i = 1 - \frac{n_{true}^i - n_{corr}^i}{n_{true}^i}$, i.e. the fraction of braking sequence initializations that are not detected by the model.
- **False braking initialization:** $f_i = 1 - \frac{n_{est}^i - n_{corr}^i}{n_{est}^i}$, i.e. the fraction of model estimated braking sequence initializations where the driver is actually not braking at all.

Analogous measures c_e, m_e and f_e are used for the case of ending the braking sequence. A more general measure is defined to summarize the above measures into one value and make it more simple to compare the models. The measure is based on the average performance on braking sequence initialization and ending:

$$\textbf{Brake init./end measure} = \frac{c_m + m_m + f_m}{3}, \quad (11)$$

where $c_m = \frac{c_i + c_e}{2}$ $\quad m_m = \frac{m_b + m_i}{2}$ $\quad f_m = \frac{f_i + f_e}{2}$ (12)

All measures, i.e. $c_i, c_e, m_i, m_e, f_i, f_e$ and the brake init./end measure, have values between 0 and 1, where 0 corresponds to a very bad performance and 1 corresponds to a perfect performance.

5.2 Linear classification estimated by a feed forward neural network

A very simple classification model consists of estimating the parameters of a straight line, dividing the data into
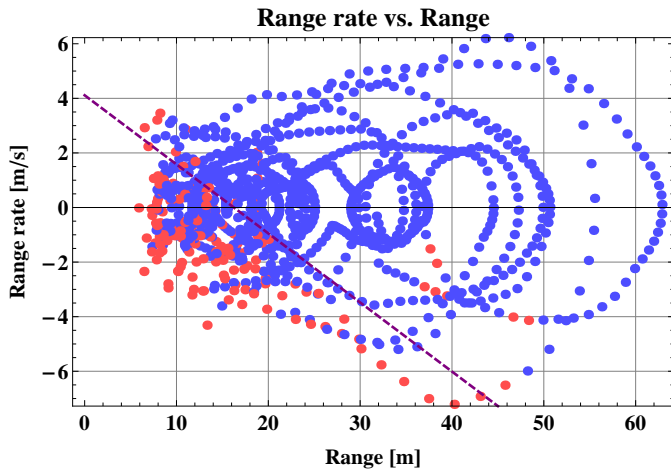
Fig. 10. The data (driver A) is not linearly separable, but a simple classifier can be used for comparison with the performance of other classification methods. The line is estimated using a feed forward neural network.

two modes in a two-dimensional space. Fig. 10 shows such a mode partition in the range-range rate space for driver A. Most of the dangerous mode samples are located in the bottom left of the figure and most safe mode samples in the upper right, which agrees well with the results from the first principle braking model in section 3. However, as was the case for the first principle braking model, the modes are not entirely linearly separable. Estimating a partition line from this data will not result in a perfect classification, but is done as a benchmark for comparing the results with the performance of other classification methods. The parameters of the line are found using a feed forward neural network (FFNN). The model has a sensitivity of 0.72 and a specificity of 0.87. The ability to detect braking sequence initializations and endings has a mean value for the five drivers of only 0.2, which is a very low value. This means that even though the classifier can divide the samples into modes relatively well, it is not reliable enough to determine when it is necessary to start and stop braking.

5.3 Classification based on dynamical models

All the dynamical models presented in the previous section, with the exception of the linear ARX model, are hybrid models with a discrete part that can be used for classification. Since the ARX model lacks a discrete part, the sign of the estimated pedal operation signal is used for dividing the driver behavior into different modes. This procedure is tested on the PrARX-SMT and PrARX model as well, the methods are then named PrARX Output and PrARX-SMT Output method respectively.

It is found that the performance of the models differs depending on the driver. Fig. 11 shows that performance of the PrARX-model for four of the drivers. It gives very good results for driver A and D, but very bad results for driver C and E. A reason for this may be that the model classifies driver C as constantly belonging to the dangerous mode, which gives a perfect specificity but low sensitivity and no correctly detected braking sequence initialization or endings. Driver E is instead classified to constantly operate

in the safe mode, leading to the same kind of problem. Also the linear ARX-model performs different for different drivers.

Despite the differences between drivers for some methods, the overall best classifiers gave good results for the majority of the drivers. The results are illustrated in Fig. 12. It can be observed that several models have good performance for classifying the modes, but worse in detecting braking sequence initializations and endings. Only the PrARX-SMT model performs equally well in both classification and brake detection and is also the model having the best performance overall. From this, it can be concluded that it is not necessary to use the PrARX model to detect when the driver should be braking, but it is enough to use the less complex PrARX-SMT model.

5.4 Dynamical models vs. models with a fixed classification threshold

From Fig. 12 it can be concluded that the ARX model has a relatively bad performance compared to the other dynamical models, but is still better than TTC-model which is a model with a fixed classification threshold for all drivers. This means that a very simple dynamical
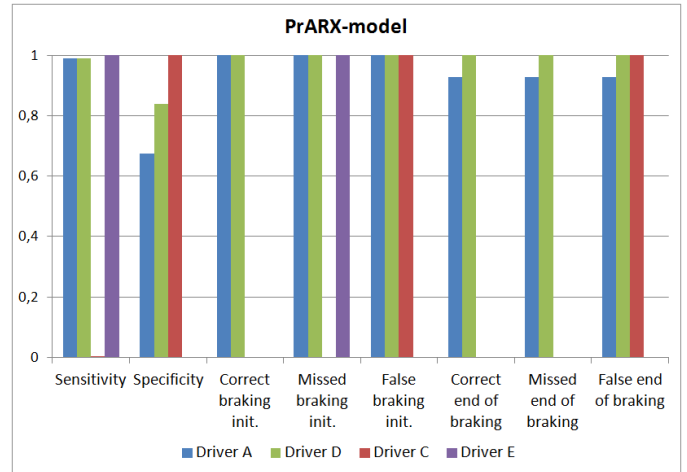
Fig. 11. The performance of the PrARX-model as a classifier, for drivers A, C, D and E.
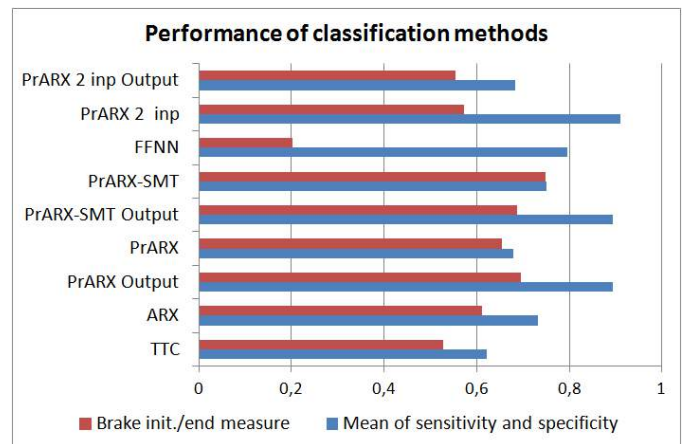
Fig. 12. Comparison of the performance of classification methods, calculated as the mean of five different drivers.

model may give a better performance of a brake assist system than using fixed TTC-threshold for deciding when to intervene. However, Fig. 12 suggests that quite a lot can be gained from using the more complex PrARX-SMT model, which has a brake stop/gas measure and sensitivity/specificity mean of 0.75.

6. CONCLUSIONS

In this paper, the necessary complexity of a dynamical driver model has been analyzed qualitatively on a small set of drivers. Although the number of drivers in this study is very low, the findings are rather consistent for all drivers. The study indicates that for one-step ahead prediction it is enough to use a PrARX-model having range and range rate as inputs. However, since the prediction performance for longer horizons was unsatisfactory all models in this paper, it is concluded that the best approach is to instead use these models to only classify whether the driver is aware of the dangerous situation or not, i.e. whether they is going to brake. The classification performances of the dynamical models were compared to the performance of a fixed classifier, i.e. a classifier that does not adapt to the current driver. It could be observed that too early or too late brake detection was a common problem amongst most classifiers. Several models had extensive problems in detecting that the driver should start or stop braking within a window of 2s, which must be considered as a very long time frame in a critical traffic situation. The best performance was obtained using a PrARX model with simplified mode transition, where the mode partitioning was based on the drivers pedal operation in the previous time step.

The results from this study shows that driver models with simple structures often performs better than the complex ones. To motivate complex driver models, many informative data are necessary.

ACKNOWLEDGEMENTS

REFERENCES

Brackstone, M. and McDonald, M. (1999). Car-following: a historical review. *Transportation Research Part F: Traffic Psychology and Behaviour*, 2(4), 181–196.

Burgett, A.L., Carter, A., Miller, R., W.G., N., and D.L., S. (1998). A collision Warning Algorithm for Rear-End Collisions. In *16th International Technical Conference on Enhanced Safety of Vehicles (ESV)*.

Hjalmarsson, H. and Sjöberg, J. (2012). A Mathematica toolbox for signals, models and identification. In *16th IFAC Symposium on System Identification*, number PART 1 in IFAC Proceedings Volumes (IFAC-PapersOnline), 1541–1546. IFAC.

Ikami, N., Okuda, H., Tazaki, Y., Suzuki, T., and Takeda, K. (2011). Online parameter estimation of driving behavior using probability-weighted ARX models. In *2011 14th International IEEE Conference on Intelligent Transportation Systems (ITSC)*, 1874–1879.

Lee, D.N. (1976). A theory of visual control of braking based on information about time-to-collision. *Perception*, (5), 437–59.

Liu, A. and Pentland, A. (1997). Towards real-time recognition of driver intentions. In *Intelligent Transportation System, 1997. ITSC'97., IEEE Conference on*, 236–241. IEEE.

Ljung, L. (ed.) (1999). *System identification (2nd ed.): theory for the user*. Prentice Hall PTR, Upper Saddle River, NJ, USA.

Mikami, K., Okuda, H., Taguchi, S., Tazaki, Y., and Suzuki, T. (2010). Model predictive assisting control of vehicle following task based on driver model. In *2010 IEEE International Conference on Control Applications*, 890–895.

Oliver, N. and Pentland, A.P. (2000). Driver behavior recognition and prediction in a smartcar. In *AeroSense 2000*, 280–290. International Society for Optics and Photonics.

Sjöberg, J., Zhang, Q., Ljung, L., Benveniste, A., Deylon, B., Glorennec, P., Hjalmarsson, H., and Juditsky, A. (1995). Nonlinear black-box modeling in system identification: a unified overview. *Automatica*, 31, 1691–1724.

Sundbom, M., Falcone, P., and Sjöberg, J. (2013). Online driver behavior classification using probabilistic arx models. In *Intelligent Transportation Systems Conference*.

Suzuki, T., Sekizawa, S., Inagaki, S., Hayakawa, S., Tsuchida, N., Tsuda, T., and Fujinami, H. (2005). Modeling and recognition of human driving behavior based on stochastic switched arx model. In *Decision and Control, 2005 and 2005 European Control Conference. CDC-ECC'05. 44th IEEE Conference on*, 5095–5100. IEEE.

Taguchi, S., Suzuki, T., Hayakawa, S., and Inagaki, S. (2009). Identification of Probability weighted multiple ARX models and its application to behavior analysis. In *Proceedings of the 48h IEEE Conference on Decision and Control (CDC) held jointly with 2009 28th Chinese Control Conference*, 3952–3957. Shanghai, China.

Van der Horst, A. and Hogema, J. (1993). Time-to-collision and collision avoidance systems. In *6th ICTCT workshop Salzburg*.

Wada, T., Doi, S., Imai, K., Tsuru, N., Isaji, K., and Kaneko, H. (2007). Analysis of Drivers Behaviors in Car Following Based on A Performance Index for Approach and Alienation. In *Proceedings of SAE2007 World Congress*.

Augmented Reality Interface Design for Autonomous Driving

Raïssa POKAM*, Christine CHAUVIN**, Serge DEBERNARD***, Sabine LANGLOIS****

*IRT SystemX, Renault,France
(e-mail : raissa.pokam@irt-systemx.fr).
**Lab-STICC UMR CNRS 6285, Université Bretagne Sud, France
(e-mail: christine.chauvin@univ-ubs.fr)
*** LAMIH UMR CNRS 8201, Université de Valenciennes, France
(e-mail: Serge.Debernard@univ-valenciennes.fr}
***Human Factor, Renault, IRT SystemX, France
(e-mail:sabine.langlois@renault.com)

1. INTRODUCTION

Recently, a new kind of vehicles has appeared. These vehicles are called autonomous, self-driving, or driverless vehicles. The most well known is the Google car prototyped by Google Corporation. These autonomous vehicles have changed the traditional driving paradigm. Instead of the usual unilateral configuration where drivers are solely responsible for the driving task, a bilateral configuration where drivers rely totally or partially on the vehicle has emerged. For example, in the Google car, the driver is completely out of the driving loop. As a consequence, these fully automated vehicles are not authorized to drive on the open road because of safety issues.

There are a number of projects working on lower levels of automation in vehicles, such as the LRA (French acronym for Localization and Augmented Reality) project. The LRA project, which involves about 10 partners from the industry and academic worlds, is sponsored by the French government, in an Institute for Technological Research (IRT) SystemX structure. In its automotive part, the project deals with technical and behavioral issues related to the automotive human-machine interface (HMI) design. Our work is related to this task.

The HMI design for autonomous vehicles is an important issue in two particular situations: autonomous mode and handover processing. In the autonomous mode, where drivers can perform a few secondary tasks, they should be able to establish, at any time, a mental representation of the automated system state and the whole context (traffic, infrastructure type, ambient characteristics, etc.). While favoring a trust construct, this representation will enable mutual control, assumptions on how the system works, etc. Before and during the handover processing, drivers should be aware of all the information that will ensure their safety and that of the other road users. Drivers thus need to be reengaged in the control loop. It is possible that they have lost proper situation awareness in the autonomous mode (Endsley, 1995).

Many modern cars (e.g. Audi Q7, BMW M3 Berline) are equipped with Head-Up Display (HUD) technology. This technology enables Augmented Reality (AR) implementation (Tonnis, Sandor, Lange, & Bubb, 2005). Usually, AR is defined as a continuum from real to Virtual Reality (Milgram, 1994). We adapt this definition to introduce what we call "Registrated Augmented Reality". The term means that the AR annotation will match the real objects first, and then adapt itself to the drivers' glance. It is thus a kind of dynamic AR. Generally, AR in cars deals with "the problem of directing a user's attention to a point of interest" (Tonnis et al., 2005). AR can "alert drivers and guide their attention to dangerous situations" (Tonnis et al., 2005). We thus assume that AR can enhance global awareness and local guidance by conveying the right information at the right moment. The issue thus becomes: What if we combine AR and a classical interface to ensure safety on the road during autonomous driving and handover processing?

This summary presents the research questions that arise when defining the problem of interface specifications. It also presents our methodology, namely building an algorithm from a cognitive approach to support the design of the final adaptive interface for autonomous driving in complex environments. Finally, it presents the expected output of this work.

2. RESEARCH QUESTIONS

We consider an autonomous vehicle at level 3 in terms of National Highway Traffic Safety Administration (NHTSA) classification. Vehicles at this level of automation enable the driver "to cede full control of all safety-critical functions under certain traffic or environmental conditions and in those conditions to rely heavily on the vehicle to monitor for changes in those conditions requiring transition back to driver control. The driver is expected to be available for occasional control, but with sufficiently comfortable transition time. The vehicle is designed to ensure safe operations during the automated driving mode" (NHTSA, 2014).

1

In terms of all the previously mentioned factors, we pose three fundamental questions to design the interface:

a. In autonomous mode and in handover processing, which sufficient representation should the drivers maintain or establish? According to the Situation Awareness model defined by Endsley (1995), this question may be subdivided into three sub-questions: (i) What should the drivers perceive? (ii) What should they understand? (iii) Which projection of the external environment and the system should they perform?

b. How should we design the displays? (i) What should be displayed? (ii) How should that information be displayed? (iii) When should it be displayed? With which prioritization?

c. What is the added value of Augmented Reality in the displays?

3. METHODOLOGY

The steps of the method used are shown in *Fig. 1*
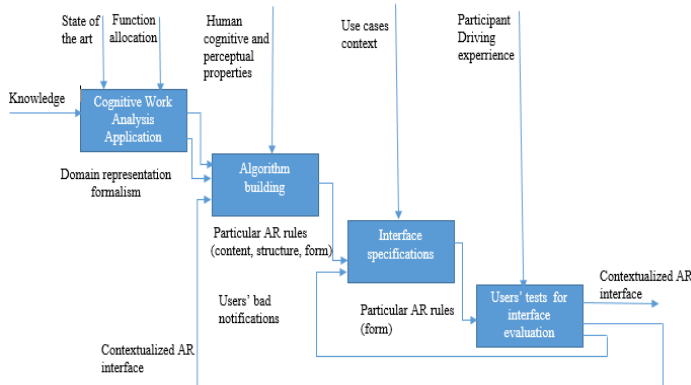
Fig. 1: HMI design methodology

The first step involves modeling tasks and extracting cognitive information. We decided to use a method that considers both technical and human aspects together: cognitive work analysis (CWA) (Rasmussen, 1990). It is an integrated approach that defines the work demands of complex sociotechnical systems in terms of the constraints on actors (Rasmussen, 1986; Rasmussen, Pejtersen, & Goodstein, 1994; Vicente, 1999; Naikar, 2013). CWA also provides information regarding the different possibilities for actions inside the system. This method comprises five steps: work domain analysis, task analysis, strategies analysis, organizational analysis, and skills analysis.

In the second step, we suggest defining general rules to deal with the complexity and dynamics of the driving system. CWA is quite theoretical, although a method is proposed to translate the results obtained in terms of interface specifications (Burns & Hajdukiewicz, 2013). This is why we suggest building a strong structure of prioritized rules of information. Michon (1985) divided the driving task into three levels of skills and control: strategical, tactical, and operational. Parasuraman (2000) identified four classes of functions that can be automated at different levels: information acquisition, information analysis, decision and action selection, and action implementation. Those levels, combined with the extracted CWA information, will allow us to build a matrix of salient information regarding driving

management and the interaction between driver and automated system. This matrix will lead to a set of prioritized AR rules, which will provide the drivers with means to deal with unanticipated and unforeseen events.

The third step consists in specifying the interface practically according to the two use cases we selected: lane change maneuver and handover phase. We will define clusters of information and their modality on the interface.

In the final step, we will evaluate the interface design through user testing on a simulator.

In the full paper, we intend showing the first step of our methodology on our use cases. We will thus focus on the work domain analysis of the systems involved in the cases.

4. CONCLUSION

Our work is significant in two main ways. First, in the application domain, it will lead to the design of an AR interface in autonomous driving with a focus on safety issues. Second, there is a methodological interest, as we will use and enrich an existing method to determine function allocation based on human-machine cooperation (Hoc, 2000) and AR elements to communicate with drivers. We believe that iterative evaluation with different technology elements (HUD, AR glasses) will enable us to improve the whole design.

REFERENCES

Burns, C. M., & Hajdukiewicz, J. (2013). Ecological interface design. CRC Press.

Endsley, M. R. (1995). Toward a theory of situation awareness in dynamic systems. *Human Factors: The Journal of the Human Factors and Ergonomics Society*, *37*(1), 32-64.

Hoc, J. M. (2000). From human–machine interaction to Human–machine cooperation. *Ergonomics*, *43*(7), 833-843.

Michon, J. A. (1985). A critical view of driver behavior models: what do we know, what should we do?. In *Human behavior and traffic safety* (pp. 485-524). Springer US.

Milgram, P., & Kishino, F. (1994). A taxonomy of mixed reality visual displays.*IEICE TRANSACTIONS on Information and Systems*, *77*(12), 1321-1329.Naikar, N. (2013). *Work domain analysis: Concepts, guidelines, and cases*. CRC Press.

NHTSA (2014). Human Factors Evaluation of Level 2 and Level 3 Automated Driving Concepts. US Department of Transportation, DOT HS 812 044

Parasuraman, R., Sheridan, T. B., & Wickens, C. D. (2000). A model for types and levels of human interaction with automation. *Systems, Man and Cybernetics, Part A: Systems and Humans, IEEE Transactions on*, *30*(3), 286-297.

Rasmussen, J. (1986). Information Processing and Human-Machine Interaction: An Approach to Cognitive Engineering. New York: North Holland.

Rasmussen, J., Pejtersen, A. M., & Goodstein, L. P. (1994). *Cognitive systems engineering*. John Wiley & Sons, Inc.

Vicente, K. J. (1999). *Cognitive work analysis: Toward safe, productive, and healthy computer-based work*. CRC Press.

2

Development of Motorcycle-and-bicycle Anti Roll-down System

Daisaku Senoo*, Yoshimi Furukawa**, Kazuaki Takeya***,
Hiroshi Hasegawa****, Toshio Ito*****

*Shibaura Institute of Technology, Saitama, Japan(e-mail: bq12057@shibaura-it.ac.jp)
**Shibaura Institute of Technology, Tokyo, Japan(e-mail:furukawa@shibaura-it.ac.jp)
** Shibaura Institute of Technology, Saitama, Japan(e-mail:bq11054@shibaura-it.ac.jp)
****Shibaura Institute of Technology, Saitama, Japan(e-mail:h-hase@shibaura-it.ac.jp)
***** Shibaura Institute of Technology, Saitama, Japan(e-mail:tosi-ito@shibaura-it.ac.jp)

Abstract: Motorcycle and bicycle Anti-Roll-down System, that controls vehicle roll angle by gyro moment created by the directional changes of flywheel axis, is proposed. Control system is designed by referring the vehicle motion model and effects of gyroscopic torque on vehicle motion. The effects of the proposed system is evaluated and validated by theoretical analysis and vehicle motion simulation.

Keywords: Motion Control, Active Safety, Rider Assistance, Motorcycle, Bicycle

1. Introduction

Bicycles and motorcycles are recognized as vehicles to provide ecological and convenient mobility. However, they are not widely used compared to cars because a rider needs to have certain skills to keep them stand safely. Therefore, statistics on traffic accidents show that roll down accidents account for the largest category of two wheel vehicle accidents.

In this paper, as a solution for the two encountered subjects, penetration and safety, Motorcycle-and-bicycle Anti Roll Down System (MARS) that controls the roll motion of a two wheeled vehicle by utilizing gyroscopic moments is proposed. MARS is designed to be attached posteriorly to a two wheel vehicle in order to improve the safety of existing two wheel vehicles.

MARS can even make an elderly person ride on a two wheel vehicle peacefully and safely, and can provide an appropriate solution for transportation in an aging and low carbon society. In this paper, its system concept, design specification and effects on the anti-roll-down function of MARS is discussed.

2. System Concept

2.1 Functional specifications of MARS.

The two wheel vehicle to which MARS applies was determined as an electric assisted bicycle or light weight motorcycle. MARS was designed to obtain following functional specifications;

(1) to stabilize a two wheel vehicle roll motion near standing postures
(2) not to disturb rider's maneuvering
(3) to be within small compact size and in light weight
(4) to additionally settle to an existing two wheel vehicle
(5) to control horizontal flywheel axis about vertical axis in order to create roll gyroscopic moments as shown in Fig.1

2.2 Dynamics of gyro effects

The gyroscopic system, which has a flywheel rotating around η axis in the rotation speed of ω_η and controls rotation angle θ of axis η about ζ axis as shown in Fig.1, creates a gyroscopic moment T around ξ axis as presented in the formula (1), where $I_{\eta\eta}$ and $I_{\zeta\zeta}$ show the inertia moment of flywheel around η axis and ζ axis respectively. The primarily flywheel axis is parallel to the axis of the rear wheel of the two wheel vehicle. φ is the roll angle of a two wheel vehicle.
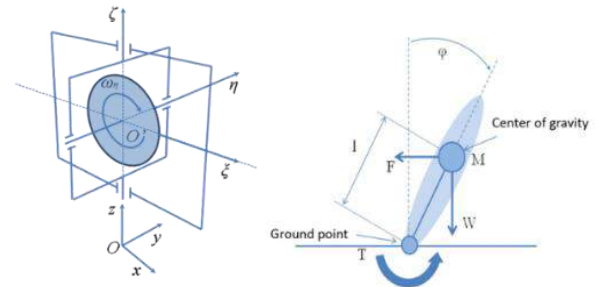
Fig.1　Coordination of Gyro system

$$T = \dot{\theta} \cos\theta \left(I_{\eta\eta}\omega_\eta - I_{\eta\eta}\dot{\varphi}\sin\theta + 2I_{\zeta\zeta}\dot{\varphi}\sin\theta \right) \qquad (1)$$

2.3 Design specification of MARS

The appropriateness of design specifications was analyzed by examining if the design satisfies both conditions: the gyroscopic moment is enough to control vehicle roll motions and that an additional weight increment is within the certain level. The result of the analysis on the design specification is shown in Table 1 and Fig. 2 demonstrates the configuration of the flywheel.

Table.1　Design specification of flywheel

A[mm]	300
B[mm]	255
C[mm]	30
D[mm]	15
E[mm]	5
Density [kg/m^2]	7.8
M[kg]	4.34
I[kg・m^2]	0.0625
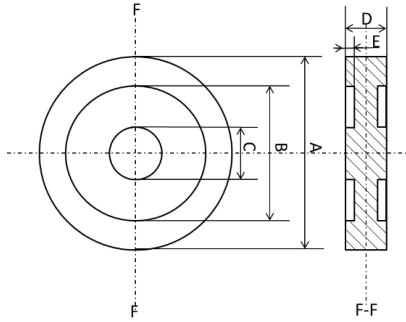
Fig.2　　Configuration of the flywheel

3. Control system design

The control objective of MARS is to maintain a two wheel vehicle roll angle φ near appropriate ideal value φ* that is a function of driving conditions such as a steering angle input by a rider and so on. The controlled roll moment is actuated by the gyroscopic mechanism, by using the flywheel axis control. Sensing variables used for the feedback control are roll angle φ, roll angular velocity φ˙, and steering angle δ. Also the vehicle forward velocity v is referenced for determining feedback control parameters.

Fig.3 shows a block diagram of the control system. Actuating roll moments is proportional to angular velocity of flywheel axix θ˙. Thus, the basic feedback control strategy is shown as Formula (2). Parameters a, b and c , in the reference function that determines the gain from a steer angle δ to appropriate the ideal roll angle φ* , are determined as presented in Formula (2) by the recursive execution of motion simulation of rider- two wheel vehicle system in various conditions.

$$\dot{\theta}=(\varphi^*-\varphi)\times(G_\varphi) \qquad \varphi^*=(av^2+bv+c)\times\delta$$
$$a=0.02286 \quad b=-0.5337 \quad c=4.051 \qquad (2)$$
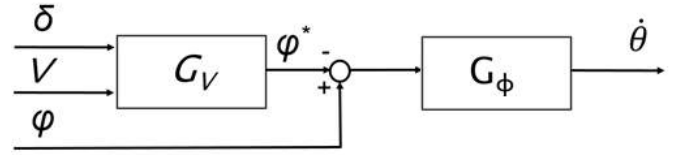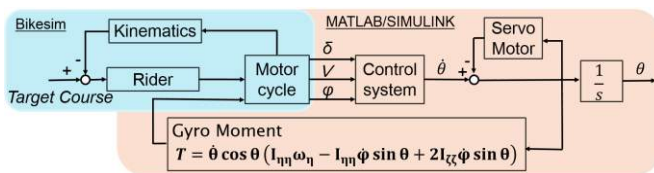
Fig.3 Block diagram of control system

4. Evaluation of MARS

4.1 Methodology

To evaluate the effects of MARS on safety improvement of rider-two wheel vehicle system, rider-two wheel vehicle simulation was executed. Following two conditions of simulation were selected as typical riding conditions that represented the situation resulting roll down accidents.

(1) standing upright during stop

A two wheel vehicle is most unstable in roll motion at stopping. Aged people cannot control bicycles easily at the start of pedalling and they may fail to keep bicycles upstanding often. Moreover roll down accidents while raiding on road are most major type of two wheel vehicle accidents. Consequently, we select the situation of standing upright as one of evaluation conditions. If the function of assisting upright stopping is enough, a rider could conduct brake actuation in emergent colliding situation, and that consequently a rider could successfully avoid the collision.

(2) riding through rough road surface

Another major accident type in two wheel vehicle is rolling down by disturbance from uneven road surface. So, stability on rough road surface was selected as second evaluation item.

Bike Sim software was applied to execute simulation and MARS control algorithm, implemented by Mat Lab, was cooperated with Bike Sim.

4.2 Evaluation of system in standing upright during stop

4.2.1 Initial condition of simulation

In simulation calculating by ideal physical principle in virtual world, initial roll angle of zero results in no roll down motion. So, initial roll angle is settle as a certain value to lead roll down motion. Initial roll angle is selected by experiments that record riders' subjective rating for roll inclination of two wheel vehicle body. 3 subjects feel dangerous situation and leave their foot from the pedal at the certain roll angles as shown in table 2 in stand still condition.

Table.2   Roll angles at the time that riders leave their foot from pedal

Test subject	1st result [deg]	2nd result [deg]	3rd result [deg]
A	5	7	8
B	7	9	6
C	8	10	6

The mean roll angle was identified as 7[deg] from the above-mentioned results.   The initial roll angle of the vehicle body to use for simulation is settled 7 [deg]. In the simulation, the rider controls the lateral position of his center of gravity so as to raise the two wheel vehicle's body from 7[deg] of roll angle to zero [deg], following stepwise target as shown in Fig.4.

Table.3   Stepwise target for roll angle parameter

X axis	Y axis
-1	7
0	7
0.1	0
1	0
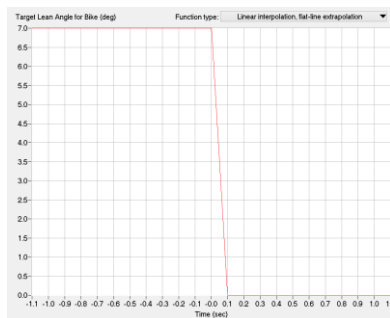
Fig.4   The configuration Stepwise target for roll angle by typing

4.1.2   Simulation result

Fig.5 shows the simulation results.   Red line shows the result with MARS and black line shows without MARS. In the condition without MARS, roll angle suddenly increased to roll down, but in the condition with MARS, roll angle converges to zero.
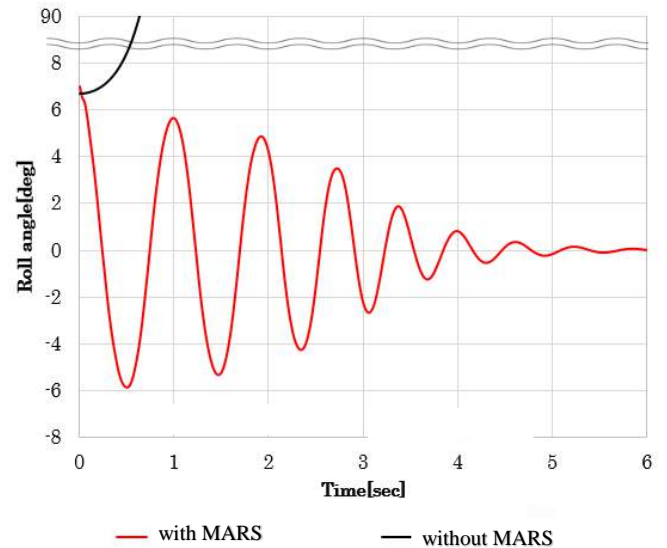
Fig.5.   Change of the body roll angle

MARS was confirmed to have control function of avoiding roll-down accident, even in the initial condition of 7[deg] inclination of roll angle.   Next, effects of feedback gain on control performance was examined.   Fig.6 shows the simulation results, changing feedback gain.   Bigger gain makes convergent characteristics fast.   Further bigger gain need more energy power, so there is still remain the discussion on gain optimization as considering the balance between two conflicted cost function, control performance and energy consumption.
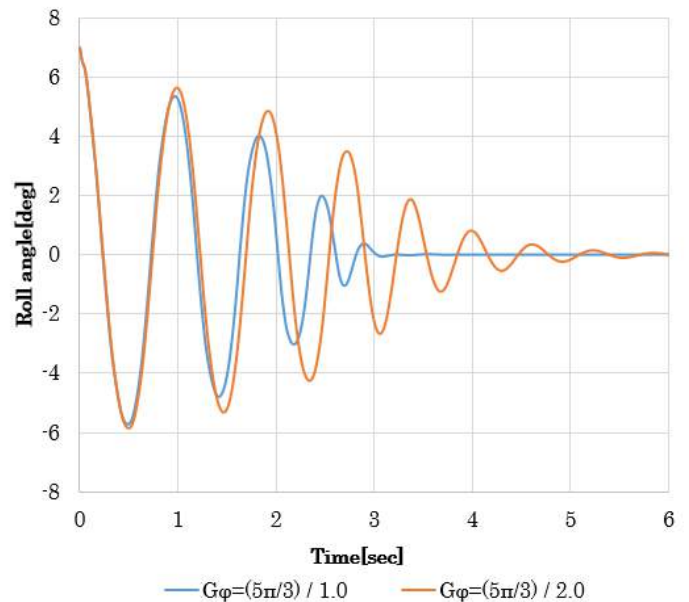
Fig.6   Effect of feedback gain on control performance

Furthermore, even by the bigger gain control, time history of roll angle has high frequency vibration before convergence. Reason of this vibration is considered that feedback control loop has some phase delay in P control. So, PD control was applied to MARS control system.

Fig.7 shows the results of PD control compared with P control. In the case of PD control, time history of roll angle improved drastically and became less vibrating tendency, and converges in short time comparing that in P control.
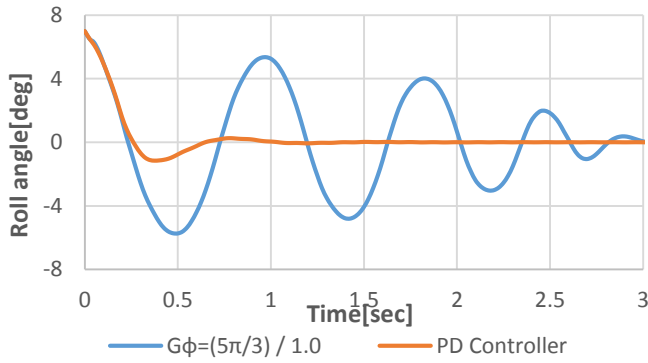
Fig.7　Effect of PD control performance

4.2　Evaluation of system on rough road surface

4.2.1　Riding conditions

The road surface profile was settled as random irregularity with 0.8[m] of maximum height change. Riders negotiate the two wheel vehicles along straight line by using rider model of course tracking as shown in Fig.7. In this condition of simulation, deviations of roll angle change are evaluated.

4.2.2　Rough road run simulation result

Fig.8 shows the roll angle time histories, where red line indicates the result of rider-vehicle system with MARS and black line indicates the result of rider-vehicle system without MARS.
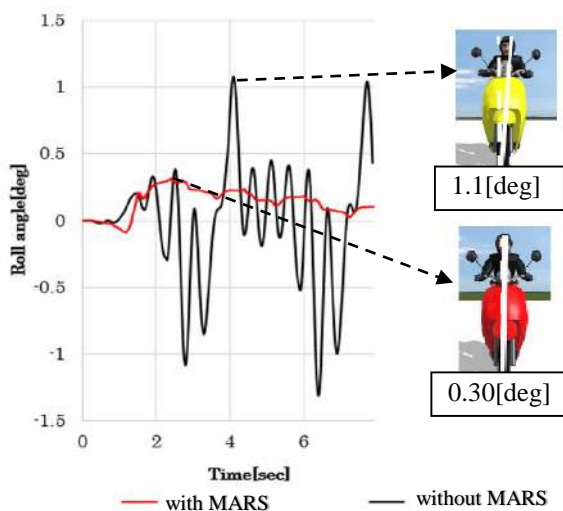
Fig.8　Time histories of roll angles

Roll angle history in the condition of with MARS shows drastically improvement of deviation within ± 0.3[deg], comparing to that over ± 1[m] in the condition of without MARS.

Effects of feedback gain levels on the control performance were examined and the results are shown in Fig.9.
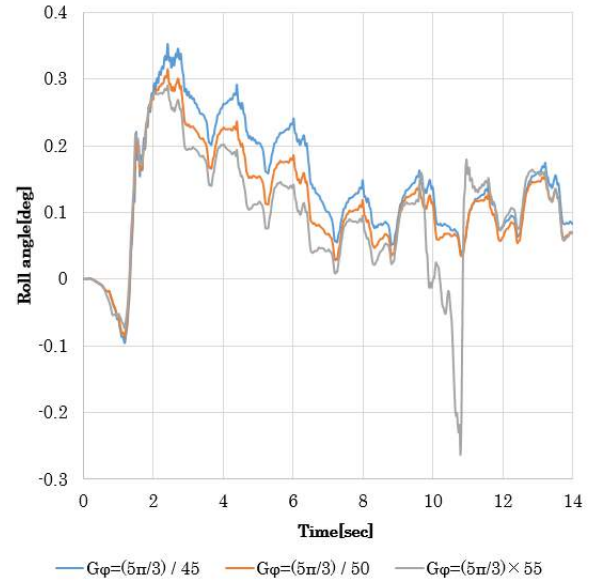
Fig.8　Effects of feedback gain on control performance

This result shows that this system is preferable for a feedback gain level G_φ to be $(5\pi/3)/50$.

5. Conclusion

The new concept of two wheel vehicle Anti-Roll-down System using gyroscopic control was proposed. Proposed system was evaluated by rider-vehicle simulation and following items are concluded;
(1) In the stand still condition, MARS improves standing stability drastically, especially when PD control was applied.
(2) In the rough road riding, MARS improves performance evaluated as roll deviation drastically.
(3) In both condition, effects of feedback gain on control performance were analysed.

6. References

Mitsuhashi, Y. and Furukawa, Y. , "Development of Gyro Mechanism That Controls Posture of Motorcycles", Proc. Of FAST-zero'11 symposium, Tokyo, 2011

New Trends in Automotive Software Design for the Challenges of Active Safety and Autonomous vehicles

Mostafa Anwar Taie

ISAQB, Mannheim, Germany

SAE Active Safety Systems Standards Committee, Detroit, USA

Centre for Informatics Science, Nile University, Cairo, Egypt (e-mail: mostafa.anwar@ieee.org)

Abstract:

The automotive mobility innovative systems like: Advanced Driver Assistance Systems (ADAS), Active Safety Systems, Autonomous Driving and even Connected Vehicles are continuously being developed for more convenient driving and for achieving higher safety standards. Therefore, software and hardware designs have to handle the increasing challenges and complexities introduced by those systems. Interactive distributed automotive real time systems are typically used to implement such complex systems, which have many real-time constraints distributed in several Electronic Control Units (ECUs) and communication bus(es). This requires form OEMs to specify accurate software integration performance requirements for different suppliers, which is very tough task and contains many integration challenges. This talk will discuss the new trends in the embedded systems software design to overcome the challenges introduced by active safety and autonomous driving systems.

The state of the art industrial solutions in software real-time architectural design will be discussed like ATESST2 project and Timm-2-use project. Moreover, the **AUTOSAR timing extension** standard (used to describe timing specifications, real-time constraints and probabilistic timing properties for events and event chains) will be explored as a good practice to provide clear timing requirements for each ECU. It also provides sufficient timing information for real time measurements and for efficient validation of the system real time requirements. A practical example of **BMW** tools (Artime, T1 and Artip), as mentioned in BMW's publications, for AUTOSAR timing extension will be shown.

Moreover, some other advanced real-time architectural design methods shall be discussed like: modeling the timing requirements and real-time constraints, modeling the real-time architectural design (operating systems tasks and interrupts), simulating the real-time architectural design, optimizing & refining the real-time architectural design, verifying the timing requirements and time triggered based real-time Architecture. Recent approaches predict the tasks and ISRs execution times used in the real-time architectural designs at early phases of the development. One of the approaches uses machine learning algorithms and provides good estimates of the tasks' execution times and the overall CPU loads. Afterwards, the complete real-time architectural design simulation and verification is used to be able to refine and optimize the design. Moreover, eVlaue, European project for evaluation of active safety systems, will be explained with its performance testing process and the impact on software design.

Active safety and self-driving systems are increasing the usage of sensors fusion (e.g. fusion between laser scanners, radars, cameras, and ultrasonic sensors) and the usage of high speed buses (e.g. Ethernet, MOST) to exchange data between sensors and their control units. Therefore, combination of some embedded hardware systems are needed (e.g. multi-core, FPGA, DSP processors, High speed automotive buses, etc..). This talk will explain the impact of using those complex hardware systems on software design taking **Audi zFAS** computer, shown in CES 2014 in Las Vegas, as an industrial solution example.

1. INDUSTRAIL STANDARDS TO OVERCOME CHALLENGES OF TOUGH REAL-TIME CONSTRAINTS (AUTOSAR TIMING EXTENSION)

As indicated in Fig. 1, an example of simple control system will be given. The Maximum latency from sensor input to actuator output and the Maximum sampling jitter will be

explained. Moreover, event timing chain in Fig. 2 will be illustrated.
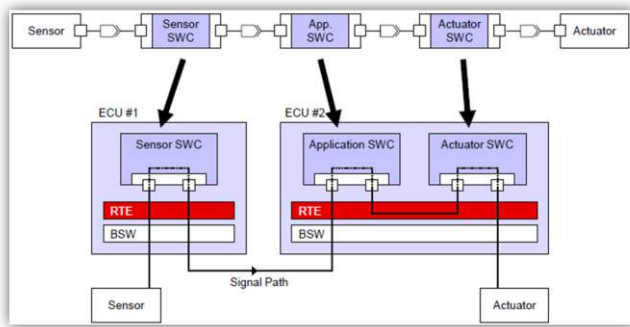
Fig. 1. Control application example, which impose timing requirements to meet control performance requirements.
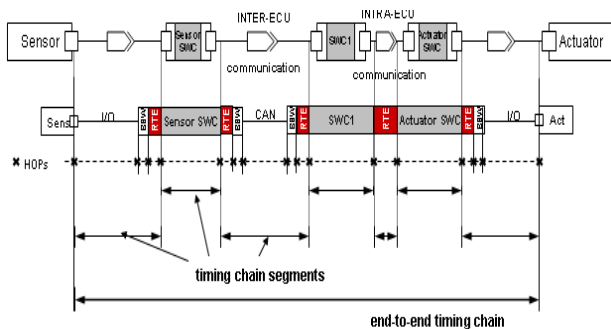
Fig. 2. Timing Description Event Chain is used to specify a causal relationship between timing description events and their occurrences during the runtime of a system.

2. INDUSTRAIL TOOLS FOR AUTOSAR TIMING EXTENSION – BMW EXAMPLE

An example of BMW tools based on AUTOSAR timing extension will be given as indicated
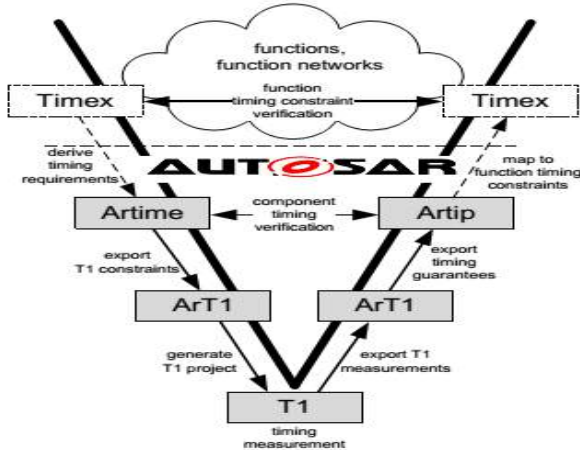
Fig. 3. BMW tools as presented in BMW's paper with title "Tool Support for Seamless System Development based on AUTOSAR Timing Extensions".

3. INDUSTRAIL HARDWARE DESIG SOLUTIONS FOR ADAS CALLENGE

Audi zFAS computer, which is indicated in Fig. 4, will be explained as an example. The impact and challenges on software design for using this hardware will be illustrated. The real-time software architecture based on time triggered operating system versus event triggered operating systems will be explained.

Fig. 4. *Compact and in one place: The central driver assistance control unit from Audi is currently the size of a compact laptop – and is set to become even smaller.*

4. ACTIVE SAFETY EVALUATION STANDARDS AND SOFTWARE DESIG – eVALUE PROJECT EXAMPLE

eVlaue standard will be explained from the software design performance testing point of view, as indicated in Fig. 5. and Fig . 6.
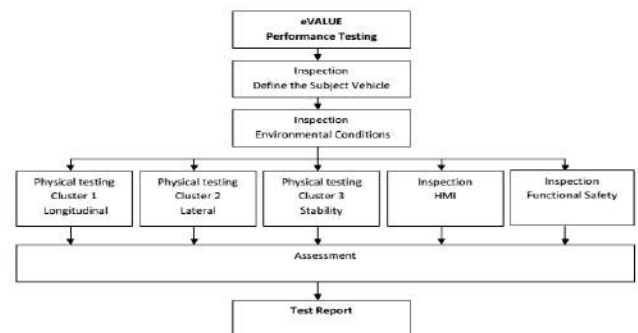
Fig. 5. eVALUE performance testing process
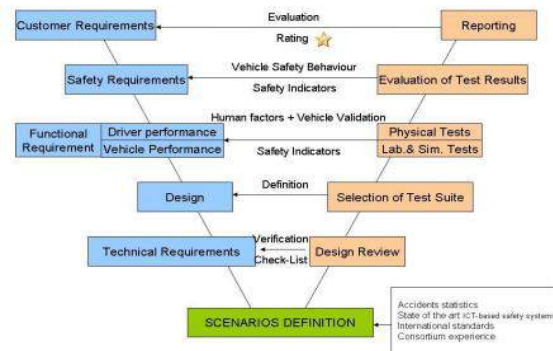
Fig. 6. eVALUE approach V-mode

On Construction of Driver Model for Analysing Driver Characteristics

Ichiro Kageyama*   Yukon Kuriyagawa**

*Nihon University College of Industrial Technology, Narashino, Chiba, 275-8575 Japan
(Tel: +81-47-474-2337; e-mail: kageyama.ichiro@nihon-u.ac.jp).

* *Nihon University College of Industrial Technology, Narashino, Chiba, 275-8575 Japan
(Tel: +81-47-474-2336; e-mail: kageyama.ichiro@nihon-u.ac.jp).

Abstract: This paper deals with a fundamental study to analyze driver characteristics using driver model. At the first stage of this research, we consider a possibility for identification of driver control manner by using a preview driver model. Influence of each term for preview in the model has been considered by using experimental data, and the order of the model has been decided. And it is shown that the model above can describe an ordinary control action of a driver. From these results, it is shown that the driver model constructed in this research is effective for driver's various analyses.

Keywords: Driver models, Vehicle Dynamics, Identification, Driver behavior, Human factors

1. INTRODUCTION

In the field of automotive engineering, normally, research on drivers has been done from two categories, one is from a viewpoint of control engineering, and the other is from a viewpoint of human factors. As for the research from the viewpoint of the control, the driver models for simulation of vehicle dynamics have been constructed from the purpose to clarify the relation between vehicle behaviour and driver characteristics at the first stage for development of several new systems, for example driver support system such as ADAS, ITS and so on. And, various driver models have been proposed, for example, transfer function model, n^{th} order preview and prediction model, expert model such as fuzzy model/ NNS, and so on.

On the other hand, the researches on human factor have been done from the purpose of design for human-machine interface, evaluation for driver's ability, influence of driver condition, for example optimal design of human-machine interface, influence of fatigue, age, skill, mental stress and so on. And, various evaluation methods have been proposed, for example by using vital reactions, subjective rating, interview to panels, and so on.

Mainly, the researches in the two categories have been individually advanced respectively. However, since the researchers in the two categories have different background, it is difficult for each other to share the research results on the other category.

In this paper, we try to understand the driver characteristics by using control algorithm. However, the driver's control algorithm is still on research level, and is not established.

In order to evaluate the driver behaviour by using a driver model, it is necessary to start from construction of the model. Therefore, at the first stage of this research, we need to examine the possibility of construction of the driver model. Next, characteristics of drivers are tried to identify by using the control parameters of the driver model.

2. EXPERIMENT

We organized driver's performance test on ordinary road. Experimental road conditions are as shown in Fig.1, and the experimental vehicle to use this research is standard size SUV as shown in Fig.2.
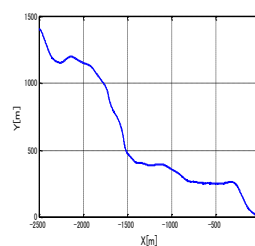
Fig.1 Experimental course   Fig.2 Experimental vehicle

We measured the vehicle data such as vehicle speed, lateral speed, 3 axis acceleration, 3 angler velocity, steering angle, the steering torque, throttle angle, brake-pedal force, forward-view video, RTK-GPS, and so on. Experimental road conditions are as follows: 1) Course length is about 1.4km, 2) Road width is about 5~6.5m, 3) Minimum radius of curvature is 65m, 4) There is no centre-line, 5) Speed limit is 40km/h. An example of

measurement results in this course is described as shown in Fig. 3.
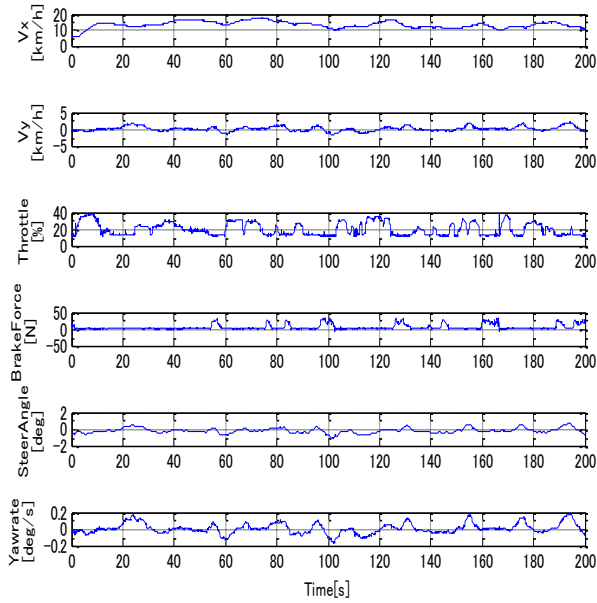
Fig.3 Experimental result

3. DRIVER MODEL

We adopt a nth prediction control algorithm as a driver model. A relation between a vehicle position at present, a target course, and a vehicle position at preview point is described as shown in Fig.4.
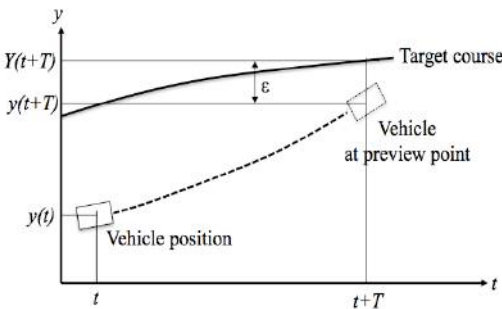
Fig. 4 Vehicle position

Here, since we define steering gain as K and preview time as T respectively, then, the lateral position at preview point is described by following equation using Taylor expansion.

$$y(t+T) = y(t) + \dot{y}(t)T + \frac{1}{2}\ddot{y}(t)T^2 + \cdots + \frac{1}{n!}y^n(t)T^n \quad (1)$$

And, the algorithm of the driver model is described as shown in Fig.5.

4. IDENTIFICATION OF DRIVER

This driver model expresses each characteristics of the driver behavior by steering gain K and preview time T. Therefore, it seems that the driver can be identified by these parameters. However, we need to consider that driver usually change their own parameters by the change of environment.
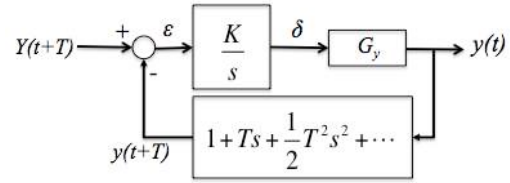
Fig.5 A nth order driver model

Therefore, the system identification is performed for every short time period, because of the description. An example of these analytical results using the 2nd order preview model is shown in Fig. 6. From this figure, it is found that a driver always changes his/her preview time and the steering gain.
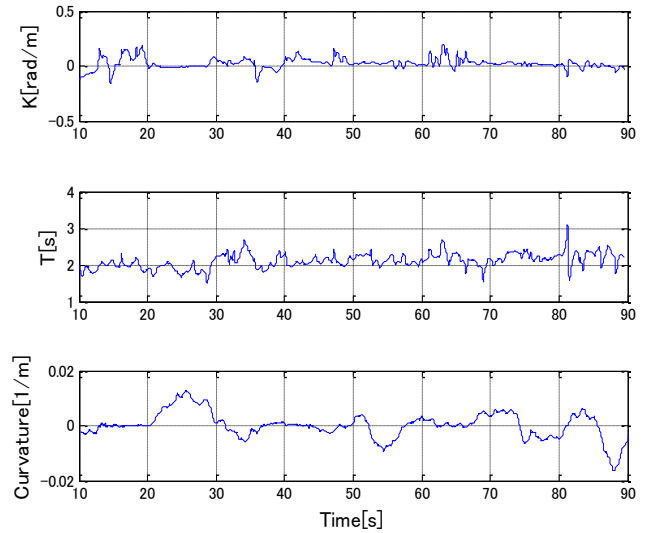
Fig. 6 Parameter variations (2nd order)

5. CONCLUSIONS

This study focuses on change of driver control parameter, and we examined possibility to evaluate driver's control action on ordinary road. And it is shown that parameters identified from the experimental result have possibility to evaluate ordinary drivers. At the next stage, we need to find the relation between environmental change and the driver parameters.

REFERENCES

[1]I.Kageyama: Analysis of driver's steering behavior usin g driver model, Proceedings of JSAE,No.117-06,(2010)
[2]A.Isomura: Human factors in Driver's Steering Operation -Three parameters for evaluating characteristics of driver's steering wheel operations-,Transactions of JSAE, Proceedings of JSAE,No.27(1),(1996)
[3]I.Kageyama: Study on construction of driver model for evaluation of control action, Proceedings of JSAE, No.123-10, (2010)

The Effect of Curve Geometry on Driver Behaviour in Curves by Using Naturalistic Driving Data

Andréa Palmberg*, Jakob Imberg*
Selpi*, Robert Thomson*

** Dept. of Applied Mechanics, Chalmers University of Technology, 412 96 Göteborg, Sweden
(email:{pandrea|imberg}@student.chalmers.se; {selpi|robert.thomson}@chalmers.se)*

Abstract: Traffic accidents are commonly found on horizontal curves. It is therefore important to study how the curve geometry affects the driver behaviour. This paper focuses on analysis of speed and maximal lateral acceleration in seven curves on two-lane rural highways in Sweden. The curve geometry factors studied are radii, presence and length of spiral transitions, tangent lengths and radius of previous curve. Of the studied factors, radii and spiral transitions were found to influence the driver behaviour most. Both larger radii and longer spiral transitions result in higher speeds in curves, and speed variations within curves seemed to be independent on choice of speed entering the curve.

Keywords: Curve geometry, Driver behaviour, Horizontal curves, Naturalistic driving data

1. INTRODUCTION

Traffic safety is regarded as an interaction between human, vehicle and environment (OECD 2008). Many accidents occur on horizontal curves, Zegeer et. (1990) found that the accident rate is up to four times higher for curves compared to tangents. The number and the severity of crashes in curves have been suggested to correlate to geometric factors as well as driver factors. Driver factors include speeding, other speed-related behaviour, and not following the road alignment. Geometric factors include for instance radius, presence and lengths of spiral transitions and tangent lengths.

Driver behaviour must be taken into account in road design in order to decrease accident frequency and severity (Wegman, 2003) ; (Theeuwes, et al., 2012). For already existing roads, it is hard to make geometric changes. Therefore, it is of importance to consider safety already in the planning stage of a new road construction and to develop active safety systems that compensates for insufficient road design.

An understanding of driver behaviour in curves is of importance to both design safe roads and to develop active safety systems, this is also important knowledge for the development of autonomous vehicles. This study therefore analyses how curve geometry influences driver behaviour in curves by using naturalistic driving data from Swedish roads.

Several previous studies have investigated traffic safety and driver behaviour in horizontal curves. Most studies have used driving simulators or instrumented vehicles (Montella, et al., 2015); (Zakowska, et al., 2008); (Altamira, et al., 2014). Only a few studies have used naturalistic driving data to analyse driver behaviour in curves (Othman, et al., 2011). Naturalistic driving data is data collected from everyday driving, and represents continuous driving behaviour under real traffic conditions.

The naturalistic driving data used in this study was collected as part of the EuroFOT project (Europe Field Operational Test). It was the first European large-scale Field Operational Test on Active Safety Systems (EuroFOT, 2012). The data used was collected from 100 Volvo cars in Sweden during 2010 and 2011. Advanced logging equipment was installed in the cars, which included GPS and cameras to record the driver, pedals and the rear and front view. It also comprised can-bus signals about speed, acceleration, lateral acceleration etc.

2. OBJECTIVES

The purpose of this work is to study how curve geometry influences driver behaviour in curves, by using naturalistic driving data. Specifically, the objectives are to:

- Describe the driver behaviour in curves in terms of speed and maximum lateral acceleration based on naturalistic driving data
- Investigate how the driver behaviour in curves is affected by radii, tangent lengths, presence and length of spiral transitions, radius of previous curve and driver

3. METHOD

Naturalistic driving data from euroFOT car data collected in Sweden was used as a data source. The data was collected from everyday driving for the years 2010 to 2011 from 100 cars in the Gothenburg area. The data includes vehicle dynamics data (speed, acceleration, yaw rate etc.), location information, and video inside and outside the vehicle. Compared to using data from simulator studies and other controlled experiments, naturalistic driving data gives the possibilities to study everyday driving, and both the driver and the environmental factors at the same time.

Seven curves on two-lane rural highways with posted speed limit 70 km/h were chosen for the analysis. The curves are

located in Gothenburg and Kungälv, Sweden. The curve geometry was estimated using satellite images.

The radius of the curves varied from 110 to 500 m, and the tangent lengths from 100 to 710 m, see Table 1. Curve numbers 1 to 4 have spiral transitions on both sides, while curve number 5 and 6 have spiral transition only on one side of the circular arc. Curve number 7 is circular.

Table 1. Characteristics of the selected curves

Curve	R [m]	R of curve before [m]	Spiral length in [m]	Spiral length out [m]	Approach tangent length [m]	Exit tangent length [m]
1 inner	110	300	50	50	230	100
1 outer		100	50	50	100	230
2 inner	120	110	25	25	240	100
2 outer		160	25	25	100	240
3 inner	290	800	50	50	100	180
3 outer		385	50	50	180	100
4 inner	300	470	50	25	160	480
4 outer		410	25	50	480	160
5 inner	385	290	80	0	425	180
5 outer		730	0	80	180	425
6 inner	410	450	0	40	130	480
6 outer		300	40	0	480	130
7 inner	500	350	0	0	710	100
7 outer		470	0	0	100	710

For each curve, passages were selected for inner and outer travel direction separately. Only trips with the following prerequisites were selected;

- Free flow conditions during curve passage
- No trailer connected
- Adaptive cruise control off
- Driver accepts the data to be used for future analysis.

Trips in which drivers used mobile phone or had passengers in the car were included in the study, since they represent everyday driving. Trips with all light and weather conditions were included as they represent Swedish road conditions and everyday driving. This choice also resulted in more data to get a statistically significant analysis.

CAN-bus signals were plotted and videos were watched to identify trips a) in which cruise control (not same as adaptive cruise control) was used, b) in which overtaking was performed in the curve, or c) with no free flow conditions due to bicyclists, etc. These trips were then manually removed.

The data includes continuous data for every tenth of a second. However, to connect the data to the curve geometry, it was necessary to select driving data for different positions in the curves. For each trip, speed data was collected for eleven points along each curve, and were based on curve geometry. The points are shown in Figure 1, the different segments of the example curve are tangents (T), spiral transition (SP), circular curve (C), middle point of the tangents (TM), and middle point of the curve (CM). Maximal lateral acceleration was collected from continuous data within the curvature.
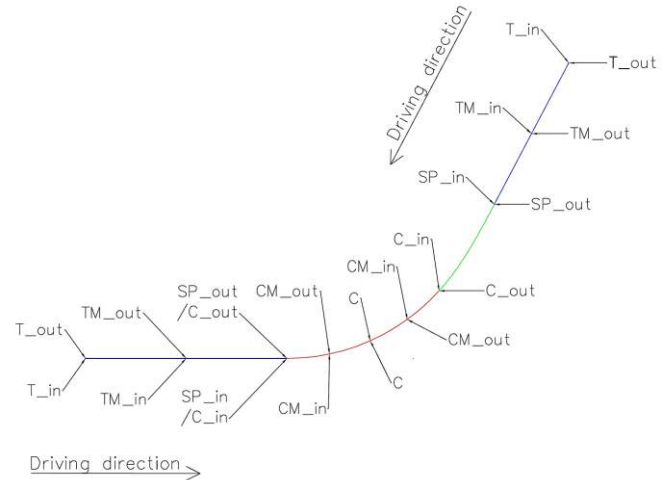
Figure 1. Analysis points along an example curve

Speed profiles for different drivers and speed profiles in the curves were generated to analyse patterns in speed variation. Previous studies have also used speed differentials to describe driver behaviour in curves. The speed differential in, ΔV_in, was calculated by subtracting the lowest speed in the curvature with the highest speed on the two points on the approach tangent. The speed differential out, ΔV_out, was calculated by subtracting the highest speed on the two points on the exit tangent with the lowest speed in the curvature.

Linear regression analyses were performed in SPSS to find factors affecting the speed at the beginning (C_in) and centre (C) of the curve, speed differential and maximum lateral acceleration in the curvature. The stepwise method was chosen, with an entry probability of 0.05, removal probability of 0.10 and a 95 percent confidence interval. The regression analysis was made excluding driver A, since the driver mainly drove in curve number 3 and 5 and showed a different behaviour than other drivers in terms of very high speeds.

4. DRIVER BEHAVIOUR AND CURVE GEOMETRY

The most common methods used by previous research studying driver behaviour and curve geometry are driving simulators and controlled field study with instrumented vehicles. However, naturalistic driving data has also been used to study driver behaviour in curves. Most previous studies about driver behaviour are based on data collected under favourable weather conditions and during daytime.

4.1. Speed

Speed is a common investigated parameter in the reviewed literature. The choice of speed when travelling in a curve is complex, and is influenced by vehicle-, driver-, weather- and

road factors which provide information about the comfort and safety to travel at a certain speed (Ritchie, 1972).

Several studies have pointed out radius as a parameter strongly affecting the choice of speed in curves. In the simulator studies by Montella et al (2015) and Helmers & Törnros (2006), and in the study of naturalistic driving data by Othman (2011), the speed was found to decrease with small radii. However, the radius of the curve does not only affect the speed in the curve, but also the speed at the tangents. According to Montella et al (2015), the speed at the exit tangent is decreased with smaller radius.

The simulator studies by Helmers & Törnros (2006) and Zakowska et al (2008) found spiral transitions increasing the speeds in curves and on the approach tangent.

4.2. Longitudinal acceleration and deceleration

The acceleration and deceleration rate is affected by radius, gradient and tangent lengths (Altamira, et al., 2014); (Montella, et al., 2015). Small radii lead to high deceleration values when approaching curves, according to both Altmira et al (2014) and Hu & Donnell (2010). High speed at approach tangents can occur if the tangent is long, and therefore long tangents lead to increased deceleration at the curve entrance.

The radius of the previous curve also affects the deceleration (Hu & Donnell, 2010). For a curve with larger radius than the upstream curve, the deceleration is lower than if the curve would have a smaller radius. The study by Hu and Donnell (2010) also found that higher deceleration when entering a curve resulted in lower speed in the curve.

Pérez-Zuriaga et al (2013) found high deceleration for small spiral parameters. According to Altmira et al (2014), the deceleration is higher on the approach tangent than in the curvature. Also, the deceleration at the end of the tangent was more affected by radius than by speed. The deceleration length was found to vary between 50 and 230 meters.

Hu and Donnell (2010) found that acceleration rates when leaving curves were higher for curves with small radii. In curves with small radii, the acceleration also begins closer to the end of the curve (Montella, et al., 2015). In curves with larger radii, the acceleration starts earlier in the curve. Acceleration lengths have been seen to vary between 150 and 270 meters, in the study performed by Altmira et al (2014).

Hu and Donnell (2010) found lower rates of acceleration when drivers depart curves with large radii, which can be related to higher speeds in the curve. The length of the exit tangent also affects the acceleration at the end of a curve. In the study by Hu and Donnell (2010), drivers accelerated less in curves with long exit tangents.

The previous studies by Nie (2006) and Pérez-Zuriaga et al (2013) have used speed differentials to analyse driver behaviour in curves. Individual speed differential is calculated by subtracting each individual's speed on the curve with the speed on the preceding tangent. Pérez-Zuriaga et al (2013) found that the speed differential was high for sharp curves, and flattened out for larger radii curves.

4.3. Lateral acceleration

Lateral acceleration has been named as a key factor in the choice of speed when approaching a curve (Ritchie, 1972). Lateral acceleration is dependent on speed squared, and is higher for small radii curves than on curves with large radii (Othman, 2011). In order to minimize the lateral acceleration when travelling in a curve, the speed has to be lowered or the driver has to choose a trajectory with the highest possible radius (Boer, 1996).

In a study by Helmers & Törnros (2006) it was found that the maximum lateral acceleration was unaffected of spiral transition length.

5. RESULTS AND DISCUSSION

The study was limited to the car data collected, mainly in Gothenburg area, as part of the euroFOT project. Therefore, only curves close to Gothenburg were selected to get a large number of passes. This has limited the number of curves that could be used, and the amount of data. Another limitation with using naturalistic driving data is that the curve geometry cannot be affected, which resulted in difficulties to find comparable curves with specific characteristics. Using simulator instead of naturalistic driving data would make it possible to both influence the curve geometry and the prerequisites of the participants. This would make it possible to control and design the curve geometry. However, the main advantage with the naturalistic driving data is that it represents natural driving behaviour, compared to data from simulators studies and controlled field studies with instrumented vehicles.

The result shows that most drivers choose speeds higher than the posted speed limit when travelling in the curves. This was found for all curves except for curve number 1. Since data for all weather conditions is used in the study, the speeds are most probably even higher if the study would include only favourable weather conditions. Curves are designed to provide safe and comfortable driving. Driving at higher speeds than the designed speed causes longer stopping distance and higher lateral acceleration. The fact that drivers keep higher speeds in the curves than the speed they are designed for results in safety problems.

5.1. Speed profiles

The speed profile for curve number 1 represents a typical behaviour for a small radii curve, see Figure 2. In such curves, drivers decrease their speed when anticipating the curvature and accelerate first towards the end of the curvature. This result is consistent with previous studies by Helmers & Törnros (2006), Montella et al (2015) and Othman (2011). For these three curves, the inner and outer speed profiles appear mirrored, which indicates a similar behaviour regardless of travel direction. The different behaviours on the tangents are probably due to different tangent lengths, and different radii of previous and following curves.
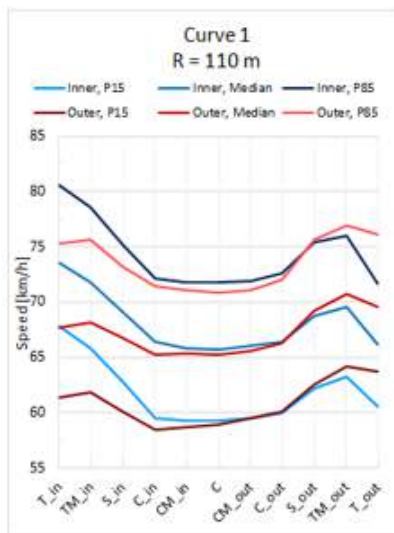
Figure 2. Speed profile for curve number 1
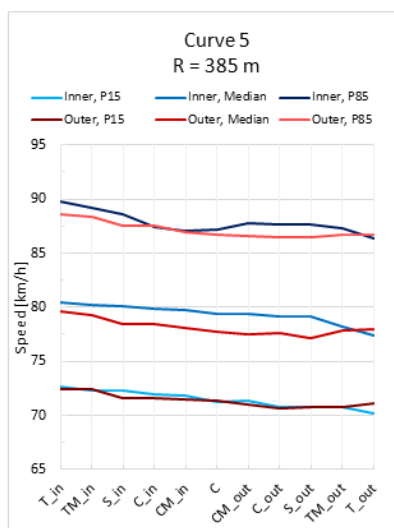
Figure 3. Speed profile for curve number 5
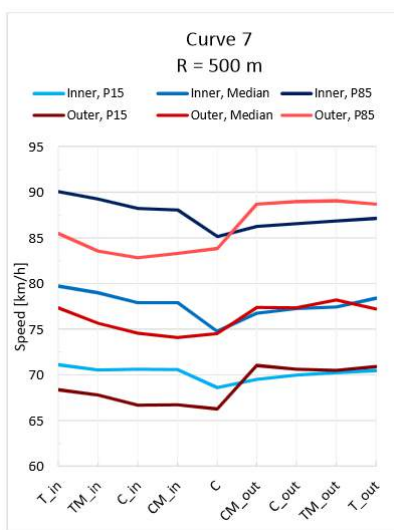
Figure 4. Speed profile for curve number 7

For the larger radii curves, number 4, 6 and 7, the speed patterns between inner and outer differs. The speed profile for curve number 7 can be seen in Figure 4. In one direction the speed increases, and in the other direction the speed decreases instead. By studying the vertical grade of the road it could be seen that there are gradients. The speed profiles for each curve direction seemed to correlate well to the gradient.

Curve number 5 shows a smooth speed profile which is almost identical for both travel directions, see Figure 3. The tangents are of different lengths, and the speed slightly decreases between the approach and exit tangent for both directions. Therefore, the tangent length does not influence the speed profile in this curve.

By studying speed profiles for different drivers driving in the same curve and in the same direction, it could be seen that the speed patterns were similar. However; different drivers choose different speeds. Figure 5 shows an example of speed profiles for different drivers in the same curve and travel direction. Driver A chose higher speed than driver B, even though the speed patterns are similar. This indicates that the choice of speed is not only dependent on the road geometry, but also on other factors such as personality. The rather large difference in choice of operating speed between drivers should be taken into account for the development of personalised active safety systems such as curve speed warning system.
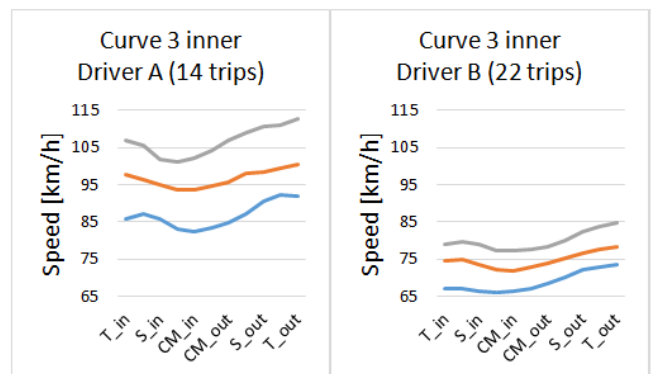
Figure 5. Speed profiles for driver A and driver B for curve number 3 inner.

It was found that in trips where driver A drove slower than normal the driver was influenced by factors such as child in the car or use of mobile phone. Therefore, this driver obviously desires to drive at high speeds but changes behaviour during certain circumstances.

It is interesting that driver A can manage to drive through the curve at over 100 km/h, and still shows similar speed reduction when driving at 70 km/h. Why does not the driver keep constant speed when driving slower? The speed reduction when driving slower is consequently not necessarily connected to difficulties in driving at the current speed. One possible reason could be that the speed reduction is a learned behaviour that is triggered when approaching a curve, regardless of speed. If drivers and passengers expect the speed to be reduced in curves, it is important to take this into consideration in the development of autonomous

vehicles as this could affect the acceptance of such vehicles. However, how autonomous vehicles should behave in curves has to be studied further.

Another possible reason for the speed reduction could be that the driver's driving abilities gets reduced during certain circumstances, like having a child in the car or using a mobile phone. Driving in curves demands more concentration compare to driving on tangents. In order to manage both the distraction and the curve, the driver needs to decrease the speed.

5.1. Regression analysis

The result from the regression analysis is shown in Table 2. The dependent variables are speed at point C_in and C, speed differentials in and out respective maximum lateral acceleration.

Table 2. Result from regression analysis

	Speed at C_in [km/h]	Speed at C [km/h]	ΔV_in [km/h]	ΔV_ut [km/h]	Max lateral acceleration [m/s²]
Constant	63.787	62.874	-7.430	6.229	3.062
Radius of previous curve	Not significant	-0.004	-0.004	Not included	-0.001
Approach tangent length	0.002	-0.003	-0.006	Not included	0.000
Approach spiral length	Not significant	0.050	0.055	Not included	Not significant
Curve radius	0.039	0.046	0.016	-0.012	-0.003
Exit spiral length	Not included	Not included	Not included	-0.006	Not included
Exit tangent length	Not included	Not included	Not included	0.004	Not included

5.1.1. Radius

The curve radius is the factor that influences the driver behaviour in curves most. The regression analysis showed increased speed with larger radii, both at C_in and at C. This result is consistent to previous studies by Helmers & Törnros (2006), Montella et al (2015) and Othman (2011).

The speed differential between the approach tangent and the curvature was found to be smaller with increasing radius, meaning that drivers do not decrease their speed as much when approaching large radii curves. This result corresponds well to previous studies by both Altmira (2014) and Hu & Donnell (2010).

The speed differential out was also affected by radius. Larger radius decreased the speed differential, meaning that drivers accelerate less out from large radii curves. Since drivers were found to keep a higher speed in large radii curves, they probably do not have to accelerate as much to reach their desirable speed after the curvature. This result is also consistent to previous studies. Hu & Donnell (2010) found for instance that acceleration rates when exiting curves were higher for small radii curves than for large radii curves.

Radius also has a major influence on maximum lateral acceleration. The maximum lateral acceleration decreases with increased radius, which corresponds to the result in the study by Helmers & Törnros (2006).

5.1.2. Radius of previous curve

Previous studies have found the radius of previous curves to also affect the driver behaviour. This was also found in the regression analysis. However, the result indicates that the influence is low compared to other parameters such as curve radius and approach spiral length.

Higher speed reduction was found for curves with a previous curve having large radius. A large previous curve allows the driver to drive faster within the curvature, and therefore accelerate to high speeds on the tangent. This could be an explanation for why drivers decelerate more. The radius of the previous curve did not affect the speed at C_in, but the speed at C decreased with larger radius of previous curve.

The radius of the previous curve affects the maximum lateral acceleration. Larger radius of previous curve results in a decrease of the maximum lateral acceleration within the curvature. This is probably a result of that larger radius of previous curve also causes lower speed at C.

5.1.3. Tangent lengths

The regression analysis showed that a longer approach tangent resulted in higher speed at C_in. However; at the centre point, C, longer approach tangent resulted in lower speed instead. The influence is low compared to other parameters in the regression analysis.

The higher speed at C_in for longer tangents is probably due to that there is a longer distance to accelerate on, and therefore higher speeds are possible. This result agrees with the study by Hu & Donnell (2010), in which they found that high speeds can occur at the approach tangents if they are long. This could also explain the result that longer approach tangent resulted in larger speed differential. When driving at high speeds on a long approach tangent, the driver would have to decelerate more to reach an appropriate speed in the curvature.

The speed differential out of the curve was found to increase with longer exit tangent length. Therefore, the length of the exit tangent affects how much drivers accelerate when departing from curves. This is in contrast to a previous study made by Hu & Donnell (2010). They found that drivers accelerate less when departing from curves with long exit tangents. The reason why drivers would accelerate less could for instance be that they have a long stretch to accelerate on, and therefore they do not have to accelerate as much. An explanation for the result found in the regression analysis could be that drivers desire to drive at higher speeds at long tangents and therefore accelerate more. This therefore has to be studied further.

5.1.4. Length of spiral transitions

A simulator study by Zakowska et al (2008) found higher speeds in curves with spiral transitions. The simulator study by Helmers & Törnros (2006) also found higher speeds at the

approach tangent and at the centre point, increasing with the length of the spiral transition. The regression analysis agreed that the speed at the centre point increases with longer spiral transition. However, the speed at C_in was found to be independent on the spiral transition length. Since C_in is the point where the spiral transition transfers into the circular curve, this result indicates that drivers keep the same speed at a spiral transition as they would have on a tangent.

Since the spiral transition length affect the speed at the centre point of the curve, even though it does not change the speed at the entrance of the constant curvature, it most probably changes the trajectory. According to Boer (1996), the speed has to be decreased or the drivers have to choose a trajectory with larger radius if the lateral acceleration is to be decreased. Therefore, in order to maintain the same lateral acceleration for a higher speed, the trajectory has to be changed. This could be a reason for drivers to keep a higher speed at the centre point in curves with spiral transitions. A better lateral position in the curve would allow for higher speeds for the same lateral acceleration. This reasoning is strengthen by the result that the maximum lateral acceleration within the curvature is unaffected by the length of the spiral transition, and that a previous study by Helmers & Törnros (2006) have found that spiral transitions only affect the maximum lateral acceleration in curves with small radii.

Pérez-Zuriaga et al (2013) found higher deceleration values for smaller spiral parameters (small parameters result in shorter spiral transition length). The same result was found in this study. Longer spiral transitions were found to result in lower speed reduction when approaching a curve. This result is related to that drivers keep higher speed in the centre of the curve if the spiral transition is long. Since drivers keep higher speeds in the curve, they do not have to decelerate as much when approaching the curve. The speed differential when leaving a curve decreased with increased length of the exit spiral transition. However, the influence of exit spiral length is low compared to other factors.

6. CONCLUSIONS

The majority of drivers drove faster than the posted speed limit in the curves, which could result in safety problems. The speed patterns seem to be dependent on the curve geometry, and do not seem to be affected by the choice of speed. In small radii curves, the speed is reduced significantly within the curvature.

The rather large difference in terms of operating speed chosen by different drivers when negotiating curves could potentially be used for development of personalised active safety systems such as curve speed warning system.

All studied factors affected the driver behaviour in curves. Of these, radius was the most influencing factor. Larger radius results in higher speeds, lower speed differentials and decreased maximum lateral acceleration. The second most influencing factor was length of approach spiral transitions. Longer transition results in higher speeds at the centre of the curve, and do not affect the maximum lateral acceleration – indicating a changed trajectory. The length of the exit spiral,

radius of the previous curve and tangent lengths had less influence on the driver behaviour.

REFERENCES

Altamira, A., García, Y., Echaveguren, T. & Marcet, J., (2014). Acceleration and deceleration patterns on horizontal curves and their tangents on two-lane rural roads, Universidad Nacional de San Juan.

Boer, E. R., (1996). Tangent Point Oriented Curve Negotiation. Cambridge, MA, USA, Nissan Cambridge Basic Research.

EuroFOT, (2012). EuroFOT - Bringing intellegent vehicles to the road. www.eurofot-ip.eu, (2015-04-13)

Helmers, G. & Törnros, J., (2006). Effekt av övergångskurvor på förares säkerhetsmarginal samt inverkan av träning - ettförsök i körsimulator, VTI.

Hu, W. & Donnell, E. T., (2010). Models of acceleration and deceleration rates on a complex two-lane rural highway: Results from a nighttime driving experiment. *Transportation Research Part F: Traffic Psychology and Behaviour,* 13(6), p. 397–408.

Montella, A., Galante, F., Mauriello, F. & Aria, M., (2015). Continous Speed Profiles to Investigate Drivers' Behaviour on Two-Lane Rural Highways. *Transportation Research Record: Journal of Transportation Research Board.*

Nie, B., (2006). Effect of Horizontal Alignment on Driver Speed Behaviour on Different Road Classifications, University of Ottawa.

OECD, (2008). Towards zero - Ambitious Road Safety Targets and the Safe System Approach, OECD.

Othman, S., (2011). Safety Evaluation of Road Characteristics - Addressing a Road, Vehicle and Driver System by Exploiting Diverse Data Sources, Gothenburg, Sweden: Chalmers University of Technology.

Pérez-Zuriaga, A. M., Camacho-Torregrosa, F. J. & García, A., (2013). Tangent-to-curve transition on two-lane rural. *Journal of transportation engineering,* pp. 1048-1057.

Ritchie, M. L., (1972). Choice of Speed in Driving Through Curves as a Function of Advisory Speed and Curve Signs. *Human Factors,* 14(6), pp. 533-538.

Theeuwes, J., Van Der Horst, R. & Kuiken, M., (2012). Designing Safe Road Systems. Ashgate Publishing Limited.

Wegman, F., (2003). Fewer crashes and fewer casualties by safer roads, SWOV Institute for Road Safety Research.

Zakowska, L., Benedetto, A., Calvi, A. & D'Amico, F., (2008). The Effect of Curve Characteristics on Driving Behaviour: a Driving Simulator Study. Transportation Research Board.

Zegeer, C., Reinfurt, D., Neuman, T., Stewart, R., Council, F., (1990). Safety improvements on horizontal curves for two-lane rural roads - Informational guide. University of North Carolina, Highway Safety Research Center.

What Determines Where Drivers Press the Gas Pedal When Crossing an Unsignalized Intersection?

Toru Kumagai*

** National Institute of Advanced Industrial Science and Technology, Tsukuba, Ibaraki 3058566
Japan (Tel: +81-29-861-6674; e-mail: kumagai@ toru.aist.go.jp).*

Abstract: We investigated factors determining the *start position*, defined as the point where a driver presses the gas pedal immediately prior to entering an intersection. Start positions are highly important for safety, because they mark the point where drivers complete their safety confirmation and begin accelerating to enter an intersection. Drivers' intersection crossing behavior, without right-of-way, was recorded at six unsignalized intersections in a residential area of Tsukuba, Japan. A total of 8 subjects drove the vehicle, at each intersection, 36 times. We analysed only the first three and last three trials because our previous study showed that start positions changed over repeated trials. We used linear regression analysis to identify significant explanatory variables. For the last three trials, own-road width ($p < 0.01$), crossroad sidewalk width ($p < 0.01$), and driver properties such as the start position alteration pattern ($p < 0.01$) were significant. The adjusted R-squared was 0.60, and the root mean square error was 0.80. The distance from the nearest edge of the crossroad to the start position typically increased when the crossroad sidewalk width and/or own-road width were broad, and was roughly equal to or less than the crossroad sidewalk width. For the first three trials, however, only own-road width ($p < 0.01$) was significant, and crossroad sidewalk width and the start position alteration pattern were not significant. The R-squared was 0.48, and the root mean square error was 1.29. These results suggest that subjects did not grasp the dimensions of the intersections sufficiently, in approaching the crossing, to drive as effectively as they otherwise would. Through repeated trials, they learned these dimensions, and drove more effectively as a result. This suggests that drivers should be better informed of intersection dimensions, for improved safety. The statistical significance of the start position alteration pattern indicated that individual drivers tended to maintain their characteristic driving behavior when crossing the intersections, which clearly demonstrated the importance of driver behavior properties as explanatory variables. It seems important, then, to consider this pronounced tendency when seeking to provide suitable assistance to individual drivers, with the aim of improving driver safety.

Keywords: unsignalized intersection, driving behavior, human factor, linear regression analysis.

1. INTRODUCTION

Collisions at intersections account for more than 50 percent of total traffic accidents in Japan (ITARDA, 2005), and the most common cause of these incidents is human error; thus, understanding the nature of driving behavior at intersections is essential for developing and implementing accident prevention measures.

In this study, we investigated factors determining the *start position*, defined as the point where a driver presses the gas pedal immediately prior to entering an intersection. Start positions are highly important for safety, because they mark the point where drivers complete their safety confirmation and begin accelerating to enter the intersection.

We applied linear regression analysis to identify significant factors. In addition to intersection properties and driver behavior properties, *start position alteration patterns* were used as explanatory variables, because our previous study showed that start positions changed over repeated trials, and alteration patterns differed among subjects (Kumagai, 2013).

2. METHODS

2.1 Data Measurement

Drivers' intersection crossing behavior, without right-of-way, was recorded at 6 unsignalized intersections in a residential area of Tsukuba, Japan (Takahashi, 2013). A vehicle equipped with sensing devices (Akamatsu, 2002) was used to measure driving behavior. Devices included instruments that sensed a driver's operational behavior (such as steering wheel operation), and instruments designed to detect vehicle performance (such as traveling speed). Data from sensors attached to the pedals indicated pedal presses for both acceleration and braking, while speed data was obtained by sensors on the front wheels.

First, subjects received an outline of the experiment, and their consent was obtained. Next, a total of 10 subjects drove the vehicle, at each intersection, 6 times a day, for 6 successive weekdays. The ethics committee of the National Institute of Advanced Industrial Science and Technology (AIST) approved this experiment.

Table 1. Intersection properties

	Visibility		Road width [m]		Distance from the nearest edge of the crossroad [m]	Crossroad sidewalk width [m]
	Left	Right	Own	Cross		
I1	Bad	Some	5.0	6.4	3.8	1.9
I2	Some	Bad	5.0	6.4	2.7	1.9
I3	Bad	Bad	5.0	6.4	3.0	3.7
I4	Bad	Bad	5.0	6.4	4.6	1.9
I5	Some	Bad	5.0	6.4	4.7	1.9
I6	Some	Some	6.4	6.4	10.8	1.9
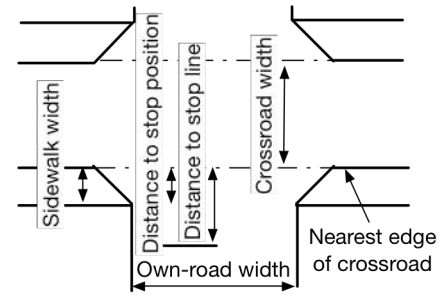
Fig. 1 Definition of intersection properties.

Eight out of 10 subjects' data were used in the following analysis. The reason was because the start positions of one subject were much larger in dispersion than those of the other subjects, and another subject stopped at stop lines in most cases and his or her start positions were highly influenced by this habit that the other subjects did not have.

Figure 1 and Table 1 illustrate the respective properties of the intersections. All the intersections were crossroads. There was little traffic in these intersections. In table 1, 'Some visibility' (left or right) means that drivers had some visibility, as the buildings on the left (or right) corners were set back from the road.

Figure 2 shows a sample intersection from the viewpoint of an approaching driver. On the left side of the intersection, a stop sign (red inverted triangle) clearly indicates the presence of the intersection. However, the exact position of the edge of the crossroad and the width of the crossroad sidewalk are not easily identified.

In the measurement experiment, the position of the vehicle in the intersections was determined as follows. The time at which the stop line was crossed was detected by video cameras attached to the right and left door mirrors, and the relevant traveling distance of the vehicle was calculated using speed data (with time stamp) obtained by sensors on the front wheels. Based on the above information and the geometry of intersections, the position of the vehicle (especially the start position) was calculated, with the edge of the crossroad regarded as the origin.

In the following analysis, we used data that were not influenced by other traffic; that is, though there were cases where other traffic came into the subjects' view and influenced their intersection crossing behavior, we only considered cases where other traffic did not come into their view, and thus did not directly influence their driving behavior.

2.2 Start Position

Intersection crossing behavior consists of *deceleration*, *safety confirmation*, and *acceleration* (Kumagai, 2006). Drivers

Fig.2 Typical intersection in a residential area.

sometimes do not actually enter the intersection when they first accelerate, but briefly decelerate again to confirm safety. Thus, in this study, the *start position* was defined as the point where a driver presses the gas pedal immediately before actually entering the intersection, and was measured as the distance from the car (more specifically, from the driver's door mirror) to the nearest edge of the crossroad.

We used the first three measured values, and the last three measured values, at each intersection, in the following linear regression analysis, because our previous study (Kumagai, 2013) showed that start positions changed over repeated trials, likely due to adaptation. This was intended to clarify the difference between the first part and last part of the trials.

2.2 Explanatory Variables

Intersection properties and driver behavior properties were used as explanatory variables.

The intersection properties included right and left visibility, own-road width, distance from the nearest edge of the crossroad to the stop line, and crossroad sidewalk width.

The behavior properties included the *start position alteration patterns*. Three pattern types were defined, based on the

correlation coefficients of start positions and number of crossings: subjects whose correlation coefficients were greater than 0.6 at some intersections were categorized as IE (Increase with experience); those whose coefficients were less than -0.6 at some intersections, as DE (Decrease with experience); and the other subjects, as NC (No change).

2.3 Linear Regression Analysis

We applied linear regression analysis, with the following Backward Elimination procedure, to identify factors influencing the start positions.

1. Start with all the explanatory variables.

2. Calculate the regression coefficients and their p-values.

3. Remove the variables with the highest p-value greater than 0.2 and go to 2, or stop when all the variables' p-values are less than 0.2.

For verification, we used the Forward Selection procedure.

3. RESULTS

Table 2 shows the average start position of the first three trials. Table 3 shows the average start position of the last three trials. Table 4 shows the correlation coefficients of start positions and number of intersection crossings by a given driver over the course of the study (only coefficients of 0.6 or more are shown). Table 5 shows the start position alteration patterns.

Table 6 shows the regression coefficients of the linear regression models for the last three trials. The M1 row shows the results of the Backward Elimination procedure. The Forward Selection procedure yielded the same results. The M2 results were obtained using the same procedure, but with a p-value threshold of 0.25 instead of 0.20.

Table 7 shows the regression coefficients of the linear regression models for the first three trials. The N1 row shows the results of the Backward Elimination procedure. The Forward Selection procedure yielded the same results.

4. DISCUSSION

The results of linear regression analysis showed that, for the last three trials, own-road width ($p < 0.01$), crossroad sidewalk width ($p < 0.01$), and the start position alteration pattern ($p < 0.01$) were significant, whereas the stop line position was not significant. For the first three trials, however, only own-road width ($p < 0.01$) was significant, and sidewalk width, the start position alteration pattern, and stop line position were not significant.

These results suggest that subjects had a tendency to insufficiently grasp the dimensions of unfamiliar intersections, especially the position of the edge of the crossroad and the crossroad sidewalk width, and thus were not driving as effectively as they otherwise would. It was considered that, through repeated trials, they learned the configuration of the respective intersections, and drove as effectively more as a result. This suggests that drivers should be better informed of intersection dimensions for improved safety.

Table 2. Average start position of the first three trials

Subject	Intersection					
	I1	I2	I3	I4	I5	I6
S1	n/a	0.0	0.0	1.6	2.4	4.1
S2	0.5	0.0	1.0	2.9	-0.3	4.1
S3	0.8	0.7	2.0	0.6	1.0	3.1
S4	0.1	1.7	2.3	1.3	-1.0	6.1
S5	2.1	1.4	0.3	0.3	1.0	3.5
S6	1.1	1.4	1.7	1.6	2.7	4.8
S7	2.8	0.7	1.7	0.3	1.1	8.5
S8	-0.2	0.7	1.3	0.6	-0.3	0.4

Table 3. Average start position of last three trials

Subject	Intersection					
	I1	I2	I3	I4	I5	I6
S1	n/a	1.3	2.7	2.3	2.7	3.8
S2	0.8	0.0	1.6	0.9	0.4	2.8
S3	-0.2	0.0	1.0	0.3	-0.6	1.1
S4	0.1	-0.1	0.7	-0.7	-06	2.8
S5	2.1	1.0	3.0	1.3	1.7	4.5
S6	2.1	0.7	3.0	0.9	1.0	2.8
S7	0.8	1.0	1.0	0.9	1.0	4.8
S8	1.5	2.0	2.0	0.9	1.0	1.8

The significance of the start position alteration pattern means that intersection crossing behavior was different depending on drivers and drivers tended to maintain their characteristic driving behavior tendencies when crossing intersections, and clearly demonstrates the importance of driver behavior properties as explanatory variables. It seems important, then, to consider this pronounced tendency when seeking to provide suitable assistance to individual drivers, with the aim of improving driver safety.

Among the significant variables, own-road width and sidewalk width have a direct relationship to crossroad visibility. For example, when the distance from the nearest edge of the crossroad to the vehicle is less than the crossroad sidewalk width, drivers have a broader view of the crossroad. Therefore a broad sidewalk width tended to result in increased distance from the nearest edge of the crossroad to the start position. Broad own-road width also tended to result

in increased distance to the start position, because it increased the viewing angle.

These observations are reflected in the notable result that all the start positions were roughly equal to or less than the crossroad sidewalk width, suggesting that drivers typically only began to accelerate when they had gained an adequate view of the crossroad.

The stop line position was not significant for the first and last part of the trials, namely the stop line position did not influence start positions. This was because stop lines did not have a relationship to the viewing angle of crossroads and did not indicate the configuration of intersections although they could show the presence of intersections.

Neither right nor left visibility was significant in M1 and N1. In M2, left visibility showed a weak significance (Table 2), likely because 'some visibility,' as defined in this experiment, was not sufficient for safety confirmation.

5. CONCLUSIONS

Factors determining the start position, defined as the point where a driver presses the gas pedal immediately prior to entering an intersection, were investigated by linear regression analysis.

For the last part of the trials, own-road width, the position of the nearest edge of the crossroad, and crossroad sidewalk width were statistically significant, presumably because these factors determined where drivers gained a view of the crossroad sufficient for safe crossing.

The start position alteration pattern was also significant, meaning that intersection crossing behavior was different depending on drivers and individual drivers tended to maintain their characteristic driving behavior when crossing the intersections.

For the first part of the trials, only own-road width was significant, suggesting that drivers tended not to adequately

Table 4. Overall correlation coefficients of start positions and number of intersection crossings by individual drivers (only coefficients of 0.6 or more are shown.)

Subject	Intersection					
	I1	I2	I3	I4	I5	I6
S1	--	0.9	0.8	--	--	--
S2	--	--	--	--	--	--
S3	--	--	--	--	--	--
S4	--	-0.8	--	-0.7	--	--
S5	--	--	0.7	--	0.8	--
S6	0.6	-0.6	--	--	-0.7	--
S7	-0.6	--	--	--	--	--
S8	--	--	--	--	--	--

Table 5. Start position alteration patterns

Distance from the nearest edge of the crossroad to the start position	Subject
Increase with Experience (IE)	S5, S1
No Change (NC)	S2, S7, S3, S8
Decrease with Experience (DE)	S4, S6

Table 6. Regression coefficients of linear regression models for the last three trials

Linear regression model	Intercept	Own-road width	Visibility		Distance from the crossroad edge to stop line	Crossroad sidewalk width	Start position alteration patterns (1 for IE, 0 for NC or DE)	Root mean squared error	Adjusted R squared
			Left	Right					
M1	-8.1 $p < 0.01$	1.5 $p < 0.01$	--	--	--	0.54 $p < 0.01$	1.2 $p < 0.01$	0.80	0.60
M2	-8.4 $p < 0.01$	1.7 $p < 0.01$	0.36 $p = 0.21$	---	---	0.43 $p < 0.05$	1.3 $p < 0.01$	0.79	0.60

Table 7. Regression coefficients of linear regression models for the first three trials

Linear regression model	Intercept	Own-road width	Visibility		Distance from the crossroad edge to stop line	Crossroad sidewalk width	Start position alteration patterns (1 for IE, 0 for NC or DE)	Root mean squared error	Adjusted R squared
			Left	Right					
N1	-10.9 $p < 0.01$	2.4 $p < 0.01$	--	--	--	--	--	1.29	0.48

grasp the dimensions of unfamiliar intersections, especially the position of the nearest edge of the crossroad and the crossroad sidewalk width, as they assessed the intersection on their approach. This suggests that more effectively informing drivers of the dimensions of intersections could contribute to traffic safety.

6. ACKNOWLEDGEMENTS

REFERENCES

Akamatsu, M. (2002) Measuring driving behavior, detecting unusual behavior for Driving Assistance, in *SICE Annual Conf. 2002*, Osaka, P170.

ITARDA (2005). Analysis of human factors in crossing collisions, *ITARDA Information*, (56).

Kumagai, T., and Akamatsu, M. (2006) Prediction of human driving behavior using dynamic Bayesian networks, *IEICE Trans. Inf. & Syst.*, E89D-2, pp. 857-860.

Kumagai, T., and Takahashi, A. (2013) Influence of repeated experience without right-of-way, in *HCI International 2013*, Las Vegas, Part II, pp. 323-326.

Takahashi, A., Kumagai, T., Tanaka, S., Teraoka, E.Y.M., Mochida, T., and Kurahashi, T. (2013) Naturalistic driving analysis of crossing non-signalized intersections without right-of-way, *Trans. of JSAE*, 44(6).

Parameters Optimization Using Genetic Algorithm Technique for Vestibulo-ocular Reflex model

Le Anh Son[*], **Hirofumi Aoki**[**], **Hiroto Hamada**[***], **and Tatsuya Suzuki**[*]

[*]*Department of Mechanical Science and Engineering, Nagoya University*
Furo-cho, Chikusa-ku, Nagoya 464-8603, JAPAN; Phone: (+81-52) 789-5583; E-mail: leanhsonvn@gmail.com
[**]*Institute of Innovation for Future Society, Nagoya University*
Furo-cho, Chikusa-ku, Nagoya 464-8603, JAPAN; Phone: (+81-52) 789-5585; E-mail: hiro.aoki@nagoya-u.ac.jp
[***]*Human System Integration Group, Vehicle Engineering Development Div., Toyota Motor Corporation*
1 Toyota-cho, Toyota, Aichi, 471-8572, JAPAN; Phone: (+81-565) 72-5563; E-mail: hiroto_hamada@mail.toyota.co.jp

ABSTRACT: The Vestibulo-ocular reflex (VOR) model proposed by Merfeld and Zupan (2002) has been used in a wide number of medical applications as well as the driver behavior model. This model is one of the reflex eye movements. It can deal with the interaction between the otolith and the semicircular canal with four parameters to compensate for the individual difference of the VOR characteristics and two parameters to compensate for that of the eye muscle characteristics. In order to increase the reliability, exact ability of this model, by using genetic algorithm (GA) the parameters were identified base on the result of experiment and simulation. We conducted 12 experiments with the motion capture and the eye movement equipment. The new parameters identified by the new GA technique improved simulation results compares with Merfeld parameters and the previous GA method by applying the generating near optimal initial population and changing fitness function. The range of each parameter on VOR model was identified with main purpose to choose the best parameters for each model application. We developed a Matlab toolbox for identifying parameter base on Matlab Graphical User Interfaces.

Keywords: Parameter identification, Genetic Algorithm, Vestibule-Ocular Reflex, Matlab toolbox, Driver behavior

1. INTRODUCTION

The vestibular system, which contributes to balance in the most mammals and to the sense of spatial orientation, plays a very important role for driving. This system is the sensory system that provides the leading contribution about movement include gaze stabilization, spatial navigation, spatial perception, and so on. According to previous research, the eye movement can be estimated base on the head movement (Merfeld & Zupan 2002) (Robinson 1981). When you turn your head to the left, the eyes will be moved oppositely in order to stabilize the visual world based on the input to the vestibular organ.

This vestibule-ocular reflex (VOR) is one of the reflex eye movements. Using the VOR models, eye movements were simulated base on the angular velocity and the linear accelerator of the head. The VOR models have been proposed by a number of researchers and applied to various applications. In this research, we use a VOR model proposed by Merfeld and Zupan (Zupan & Merfeld 2003). This model has been used by other researches that included a driver behavior aspect. For example, Omura et al. (2014) used the VOR model to find out the relationships between the measured eye movement with the subjective evaluation of simulated brake motion. In this research, the passenger's comfort was measured by comparing the observed eye movement with the simulated one by using VOR model. However, the number of subject was not good enough for making a decision. In addition, the parameter identification using hybrid genetic algorithm still had a gap between simulation and measurement.

Obinata et al. also used the VOR model to evaluate the mental workload (Obinata et al. 2009) and driver distraction of memory decision workload (Obinata et al. 2008).

On the other hand, there are several methods to find out the good parameters for each model such as Brute Force search, Nelder-Mead simplex, Trust region method, Gauss-Newton (Munster 2009), and so on. One of the successful methods is a Genetic algorithm (GA) which is founded on Darwinian evolutionary principles – mechanics of natural genetics (Goldberg n.d.). This method has been applied to a variety of areas especially for parameter estimation (Angeles 2001), (Wang et al. 2004), (Petcu & Leonida-dragomir 2010), (El-mihoub et al. 2006). The GA is suitable for optimization of non-linear problem by finding out the global optimal solution bases on natural selection and genetics.

Koljonen and Alander presented the effects of population size and the relative elitism on optimization speed and reliability of genetic algorithms (Koljonen & Alander 2006). They showed that the initial parameters had a strong effect on the optimization speed and reliability. Kuczapski and Micea showed a method to enhance GA by generating near optimal initial populations (Kuczapski et al. 2010).

This paper aims to show a new generation by using GA method and MATLAB (graphical user interface) with main ideal to increase the reliability and exact ability. To enhance the VOR parameters, we apply the generating near optimal initial population and change the fitness

function.

2. METHOD

2.1. VOR model

To find out the best model for eye movement which can be deal with the influence of rotational cues on the neural representation of gravity, the resolution of gravitoinertial force and the neural representation of the dynamic of the semicircular canals are important (Merfeld & Zupan 2002). Here we use a VOR model by Merfeld and Zupan (2002). The output of this model represents only the eye movement to stabilize the view which does not consider such as the physical conditions, the state of arousal and the visual. On the other hand, the model shows the interaction between the otolith and the semicircular canal with input is the head movement (linear acceleration and the angular velocity). However, there is the first order lag characteristic in the eye muscle. In this case, we apply the final common path that is a part of Robinson's model (Robinson 1981).

VOR model proposed by Merfeld and Zupan (2002)

Final Common path part proposed by Robinson (1981)
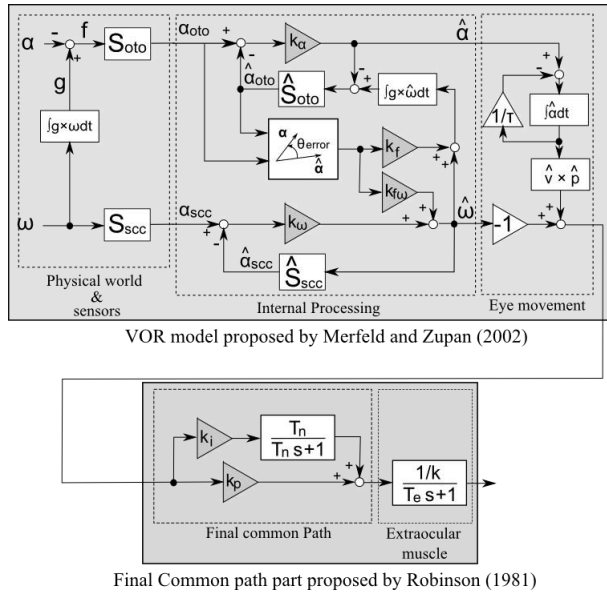
Figure 1: VOR model

Figure 1 shows the detail blocks of the VOR model. The semicircular canals (measure the angular velocity of the head (ω)) and the otolith organs (measure linear accelerator of the head (a) and gravity (g)) sense the proprioceptive information to the surrounding world; this is the first step to calculate the sensory information from the measurements (α_{oto}, α_{scc}). In the next step, the measurements are compared with the sensory information predicted by the internal model. This model combines four free parameters (k_ω, $k_{f\omega}$, k_f and k_a). The parameter values were determined by the feedback of this error.

After calculating the eye movement, the final common path proposed by Robinson (Robinson 1981) will be applied. In this part, two parameters (k_i, k_p) will be used to represent the different types of muscle fibers in eye muscles.

2.2. Experimental setup

The overview of experiment is shown in Figure 2. The motion capture (Optitrack Prime 17W) was installed with six cameras around an automobile seat with a caster placed on the guide rail. The seat can be moved by a lever by another person behind shown in Figure 3. The cameras capture the motion of the subject's head and the seat. In addition, T.K.K.2930a (Takei Scientific Instruments Co., Ltd.) was used for measure eye movement by limbus tracking method.
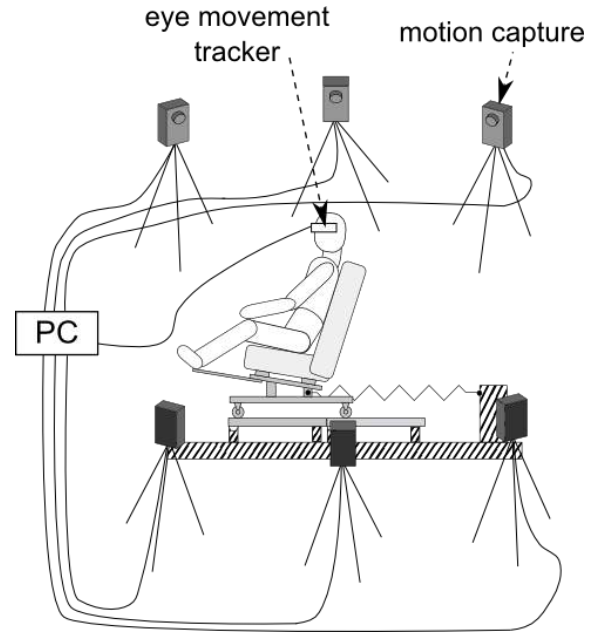
Figure 2: Overview of the experiment

In this experiment, subjects who sit in the seat are given the pitching vibration while gazing at a target placed in front of the seat during that time. We measured the eyeball rotations, head movement and seat movement during that time. All data were imported to MATLAB with Data Acquisition Toolbox and processed.
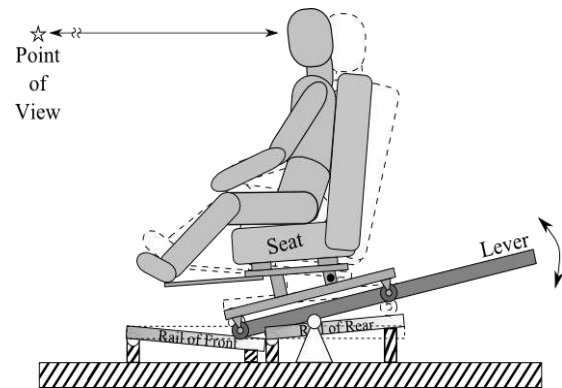
Figure 3: Parameter identification

The head movement is obtained by using an optical motion capture software (Motive software). Then, the data

from Motive software live streaming markers are used to build the rigid body through Natnet SDK to Matlab (Figures 4 and 5). On the other hand, the eye movement is collected by Takei Scientific Instruments 2930a. Because this device has analog output, a high-precision analog I/O terminal PCI (AOI-160802AY-USB, Interface Co. Ltd.) is used. By using Data Acquisition Toolbox, both data from the eye and head movements are synchronized and directly imported to Matlab software. This synchronization is an important point to obtain better input values for the VOR model.
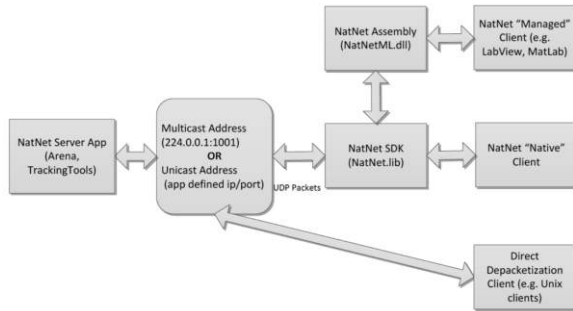
Figure 4: Natnet Component Overview
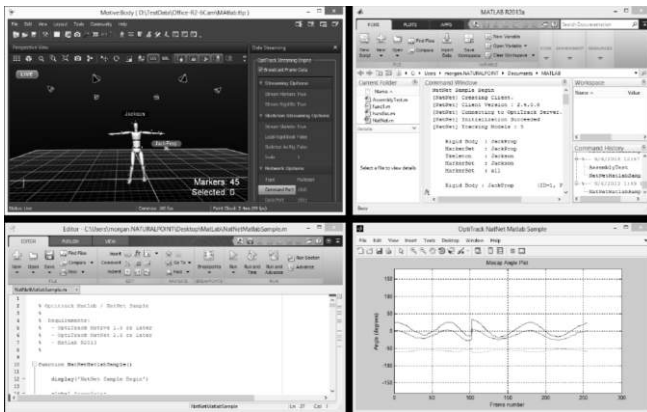
Figure 5: Real-time streaming Mocap data from Motive into Matlab

2.3. Genetic Algorithm

The Genetic Algorithm (GA) is one of the optimization techniques by using fitness value. GA belongs to the larger class of evolutionary algorithms and its application in various fields such as bioinformatics, computer science, engineering chemistry, mathematics. Due to the aspects or the people who apply, GA can be used in different ways.

Figure 6 shows the comparison of the measurement and the simulation by applying original parameters proposed by Merfeld and Zupan. The result shows that there are big gaps between them. To deal with this problem, Genetic Algorithm (GA) will be applied with main purpose to find out better parameter for VOR models.
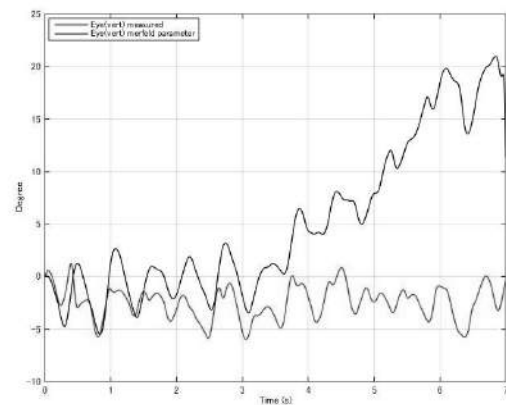
Figure 6: VOR model using Merfeld and Zupan parameters
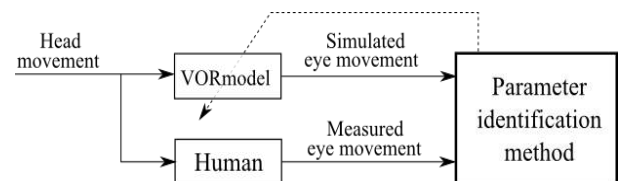
Figure 7: Data flow of the parameter identification

Figure 7 shows the flow of parameter identification. By comparing the simulated eye movement and the measured one, the parameter can be found out base on GA.

Based on the GA method of Beasley et al. (1993), GA provides a method to solve complex optimization problem with global search technique that searches multiple points. In this research, GA method is used for five steps (Figure 8): Initial population, evaluation, fitness value, reproduction cross-over and mutation, and stop − display result.

Initial population: The initial values of the estimate parameters are randomly assigned. On this research we use simple estimation base on fitness function value to find out the parameter have better results by comparing with the measurement.
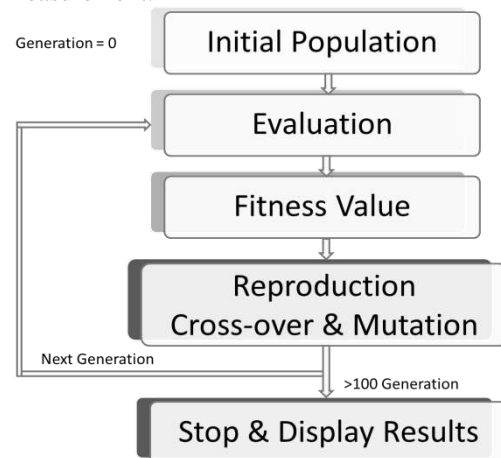
Figure 8: Genetic Algorithm

In their series of research, Obinata et al. used a hybrid

– GA method for the VOR parameter identification (Usui et al. 2007), (Obinata & Tokuda 2008), (Omura et al. 2014). In these cases, 8 parameters from Merfeld and Robinson were identified at same time with initial value as Merfeld and Zupan parameters. However, due to the big range of each parameter, the result after 100 generations still had a small gap with the measurement. Based on this research, we found out the range of each parameter and ran a simple estimation. The results of estimation were used as the initial value for this time. The parameter also divided into two sets for estimation: the first 4 parameters are from the VOR model proposed by Merfeld and the second 4 parameters are in the final common path proposed by Robinson.

Evaluation: By using MATLAB/SIMULINK, the VOR model was created based on the study by Merfeld and Zupan. The input signal was the head movement; with initial parameters from Merfeld, the output from the VOR model was compared with the actual eye movement.

Fitness value: In this research, we used fitness function of GA combine with mean square error. The duration of the mean square error was 6 seconds. The equation shows below:

$$MSE = 1/n \left(\sum (\text{eye simulation }_i - \text{eye measurement }_i)^2 \right.$$

Cross-over and mutation: this step is for preparing the next generation that selects genes from parent chromosomes and creates a new offspring. Then, mutation randomly changes the new offspring.

After 100 generations, the program stops and chooses the best result as a minimum of fitness value. As a result the figures and the parameters are displayed.

2.4. Identification of parameters

The parameters can be found out by using minimum of fitness value. The parameters are used for the VOR model, and the result of simulation and measurements are shown in the figure. The mean square error value shows the difference of simulation and measurement.

3. RESULTS AND DISCUSSION

3.1. Comparison the results from the VOR model using Merfeld and GA parameters

The difference of the simulation by this method and the measurement is shown as the value of mean square error. Table 1 shows the value of mean square error of each subject.

In total 12 subjects, all of the results from this GA method show better performance compared with the VOR model using Merfeld's parameters. The minimum mean square error of this method is 6.54E-5 and the maximum is 4.40E-3. On the other hand, by applying Merfeld's parameters for each subjects, we found higher error in the results. The maximum of mean square error is 3.80; it is higher than GA method more than 14837 times. However, in some case, the parameters of Merfeld are also

acceptable with mean square error around 1.12E-3. It means that the higher errors are not due to the model but the parameter identification. Each individual has different parameters for the VOR model. To find out the parameters that can be acceptable for any case or the rules of changing parameters of person needs to make more experiments with larger subjects and different characteristics.

Table 1: Mean square error of Merfeld and GA method

Subjects	MSE of Merfeld	MSE of GA	Merfeld/GA
Subject 1	1.05E-01	3.04E-04	346.87
Subject 2	1.24E+00	2.90E-03	427.97
Subject 3	1.12E-03	8.40E-04	1.33
Subject 4	3.80E+00	2.56E-04	14837.86
Subject 5	1.65E-01	1.58E-03	104.67
Subject 6	3.68E-01	6.54E-05	5623.42
Subject 7	5.22E-03	1.40E-03	3.73
Subject 8	3.19E-01	1.20E-03	266.03
Subject 9	8.11E-02	1.30E-03	62.38
Subject 10	5.89E-01	5.87E-04	1002.90
Subject 11	6.26E-01	2.86E-04	2189.74
Subject 12	4.33E-01	4.40E-03	98.45

Table 2: Mean square error hybrid and genetic algorithm

Subjects	HGA	GA	HGA/GA
Subject 1	4.0E-04	3.0E-04	1.31
Subject 2	3.3E-03	2.9E-03	1.14
Subject 3	8.5E-04	8.4E-04	1.01
Subject 4	3.2E-04	2.6E-04	1.25
Subject 5	1.6E-03	1.6E-03	1.01
Subject 6	6.9E-05	6.5E-05	1.06
Subject 7	2.1E-02	1.4E-03	14.86
Subject 8	1.5E-03	1.2E-03	1.25
Subject 9	1.7E-03	1.3E-03	1.31
Subject 10	1.0E-03	5.9E-04	1.70
Subject 11	2.9E-04	2.9E-04	1.01
Subject 12	2.0E-02	4.4E-03	4.43

Table 2 shows the comparison of the previous method that uses the hybrid GA with Merfeld and Zupan parameters as the initial values and this new GA method with simple estimation as the initial. The result of the new method shows better performance. In some cases, two methods present the same mean square error. In other cases, however, the new method shows much better results such as Subject 12 and 7 (4 times and 14 times, respectively). Figure 9 presents the measurement and simulation of two subjects (the left side is the vertical and the right side is the horizontal eye movement) from the VOR model using both parameters.
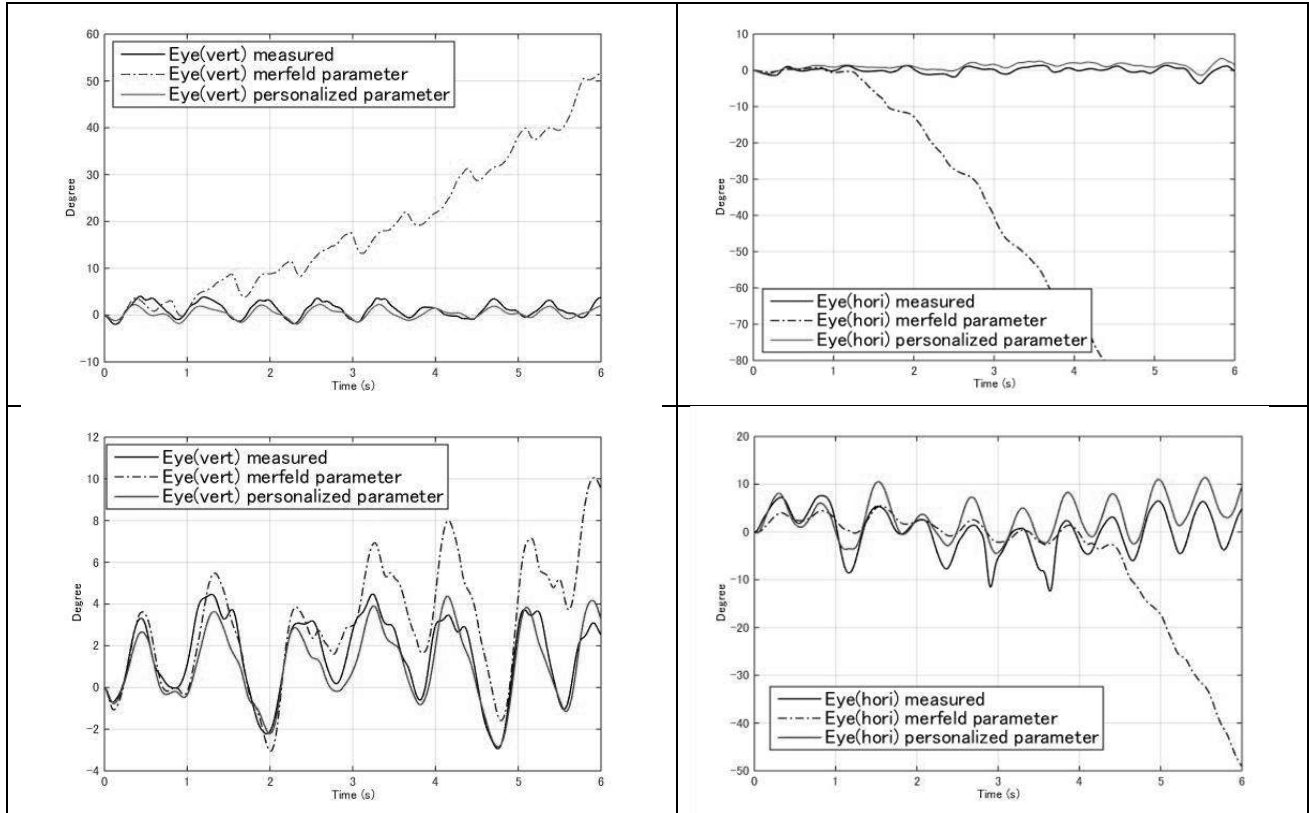
Figure 9: Results of the experiment and VOR model simulation

As same with MSE error, the result for running the VOR model using GA (personal) method show better performance compared with using Merfeld parameters. Both trend and value of the result using new method to identify parameter are almost same as the measurement.

3.2. Parameter for each subject using GA method

Table 3 shows the parameters of each subject. In total, we conducted 12 experiments with 12 different people. The parameters of each person are different, which may represent the individual characteristics. The range of each parameter is based on choosing the initial of GA method. All parameters have positive number

except k_a. The minimum of k_a is around -13. On the other hand, other parameters are positive and maximum around 8. This is also a suggestion for other researches want to apply GA to identify parameter for VOR model can be easy to choose the initial parameters.

In the experiment, we tried to shake the chair only in pitch. Besides that, the people who shook the chair tried to make the frequency and amplitude as the same with all subjects. However, it was very difficult to keep the same frequency and amplitude by hand and thus, the input had some errors, which would also be the main reason for some bad parameters.

Table 3: Parameters of each subject

Parameters	S1	S2	S3	S4	S5	S6	S7	S8	S9	S10	S11	S12
k_a	-6.4	-12.7	-12.7	-12.7	-9.4	-9.4	-12.7	-7.7	-7	-9.8	-6.4	-11.8
k_f	0.1	0.1	0.1	0.1	0.3	0.4	**6.3**	0.4	0.1	0.1	0.1	0.1
k_{fw}	**4.9**	0.1	0.1	1.5	1.9	2.4	0.1	1.5	1.8	2	0.1	**4.2**
k_w	6.3	3.2	3.2	2.2	2.9	3.2	5.9	2	6.4	2.7	4.8	2.6
k_{iv}	0.5	1.6	1.2	0.8	0.8	0.5	0.5	0.1	0.1	0.7	0.8	1.2
k_{ih}	0.7	2	2.4	1.5	2.7	0.3	**0**	0.9	0.8	**0**	**0**	**0**
k_{pv}	1.4	**0.1**	5.4	2.3	3.2	2.3	4.7	1.7	1.5	2.1	2.3	7.5
k_{ph}	3.1	2.8	5.2	0.8	4.7	6.1	2.5	4.3	4.8	6.3	3.1	**0**

Focusing more on the details about the identified parameters, the value of k_f of Subject 7 is 6.3, which is more than 10 times higher than others. By checking the input data, we found that there was a big error from the head and eye movement inputs. In the middle of the experiment, the subject moved his head and eye down and made the horizon of eye and head movement change suddenly (Figure 10) which is the main reason for increasing k_f. It also implies that k_f has strong effect on the horizontal eye movement.

In case of k_{fw}, Subject 1 and 12 have quite bigger values compared with others. The reason is that the values of vertical eye movement increased by the time. It may be the effect by the people who controlled the movement of the chair (Figure 11).
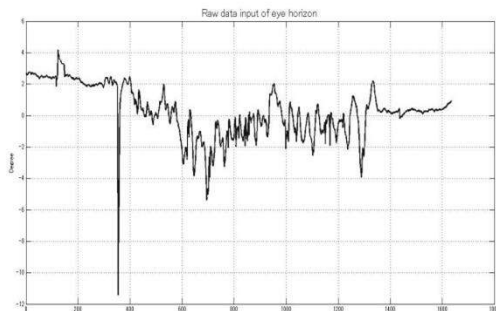
Figure 10: Raw data input of eye horizon
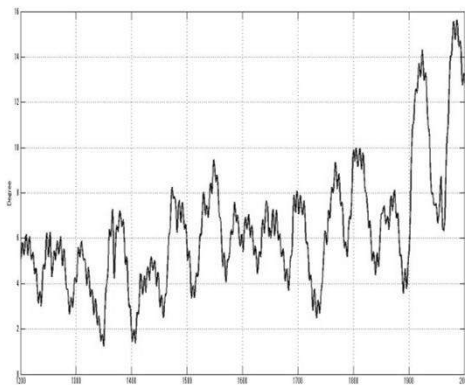
Figure 11: Raw data input of eye vertical

On the other hand, the four parameters (k_{ih}, k_{iv}, k_{pv}, and k_{ph}) from the Robinson model work mainly as gains for the signal output. k_{ph} and k_{ih} are gains of the horizontal eye movement. Those values of some subject are equal to zero because in this experiment, the experimenter shook the seat only in pitch. The error would occur when the seat is also moved in yaw.

3.3. Matlab toobox for identifying parameters

The Matlab graphical user interface is used to create an application. The steps to build the program are shown in Figure 9. This toolbox consists of 3 steps. In the first step, the toolbox supports two kinds of hardware as the input data for each movement (head

movement: Motive or Polhemus hardware; eye movement: Takei or Smarteye hardware). In the next step, the input data are shown in figures that help users choose the area for identifying parameters (Figure 12).
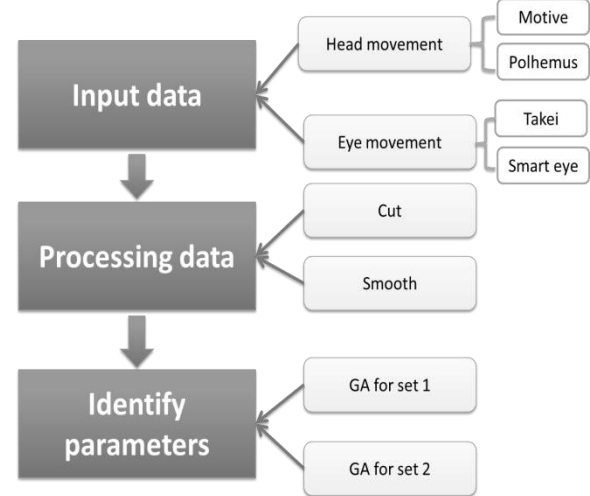
Figure 12: Step for identifying parameters

In the input and processing data steps, the tool shows with the menu bar that includes joint head marker (Figure 13). In this window, by choosing hardware, raw data of the eye and head movement are selected using a dialog box. The head and eye movements are shown in the figure by pressing on "View on Figure" button which helps people choose the best area to identify parameters. With one click on "Generate Data," two files consist of all information of the head and eye after cutting, transferring and smoothing are created as input of next step.
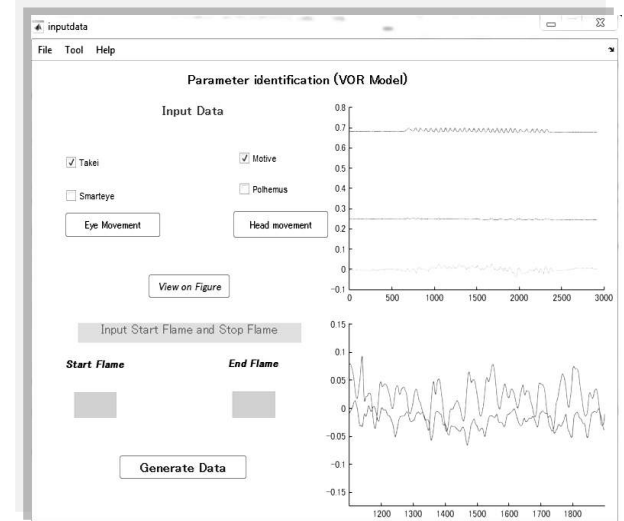
Figure 13: Input and processing data

In case of using old version of the motion capture which has only data for each marker, this tool supports to combine all markers become one which is used as the head movement input data.
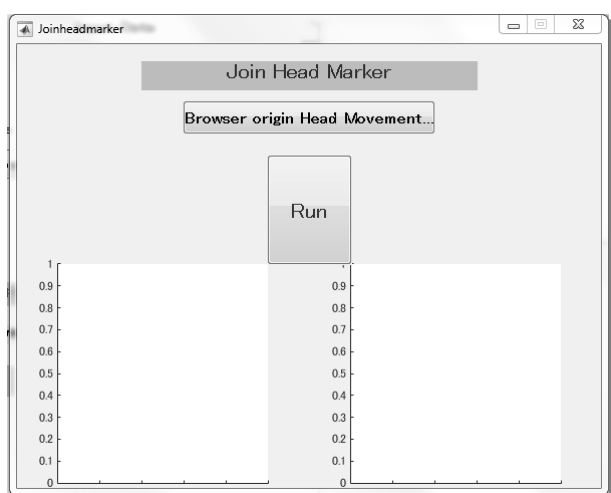
Figure 14: Join head marker

After generating data, the results of this tool are used for the parameter identification in the next step (Figure 15). All parameters after identification are shown in the windows and other information is saved in files under the same directory as the input data. Similarly, all of the parameters after identification are also shown in the main program and saved in the same directory with the mean square error.
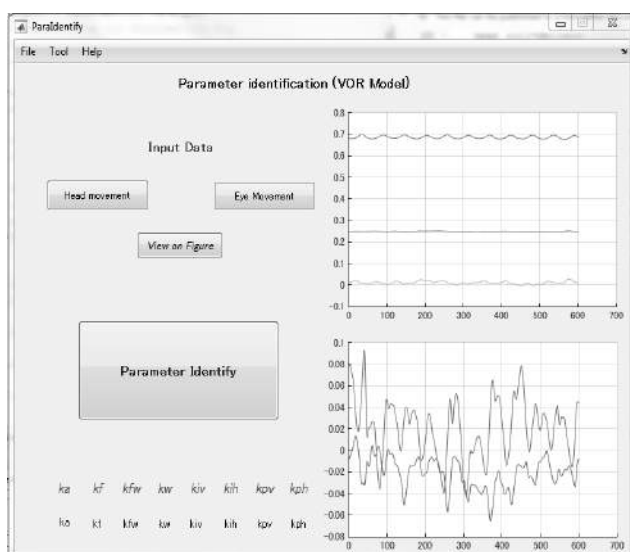
Figure 15: Parameter identification

4. CONCLUSIONS

Genetic algorithm applying to identify parameter of the VOR model shows better performance compared with using Merfeld and Zupan parameters and the previous hybrid GA.

The parameters of individuals depend on characteristic of each person. One individual have one set of parameters. To find the relationship between parameter and individual information, we need to continue more experiments.

The ranges of each parameter shown in Table 2

would make researches want to use GA method to find out the parameters of the VOR model.

Based on this experiment, there are some errors that made the parameters change, due to the seat movement by hand. We need to use an apparatus mechanically controlled in order to reduce errors for much precise parameter identification.

Successful creation of a toolbox can be identified parameters for the VOR model with more exact ability and reliability. This toolbox supports for various kinds of eye and head tracking devices.

By improving the exact ability for identifying parameters of VOR model, it may be possible to apply VOR model for evaluate driver distraction as well as to change vehicle dynamic base on simulation brake motion:

For evaluating driver distraction, Obinata et al. also used the VOR model to evaluate the mental workload (Obinata et al. 2009) and driver distraction of memory decision workload (Obinata et al. 2008). However, their research was not applied for changing gaze direction. By improving the exact ability of parameters identification, we will conduct other experiments with changing the gaze direction in naturalistic driving behavior to evaluate the driver's distraction based on the VOR model. In addition, there are several researches that apply the VOR to predict of drowsiness (e.g., Shirakata et al. 2010). By increase the exact ability, we hope that this method can also be applied to evaluate such effect as sleeping, alcohol, music, mobile phone, and texting on driver distraction base on the VOR model. Similarly, Omura et al (Omura et al. 2014) evaluated the passenger's comfort using the difference of the observed eye movement with the simulated one by using VOR model. By improve the exact ability, we also hope that this method can be more applicable and better performance with previous one.

REFERENCES

Angeles, L., 2001. Parameter Identi cation : A New Perspective (Second Draft) 1 Introduction and Preliminary Terminology : , 1(January), pp.1–19.

Beasley, D., Bull, D.R. & Martin, R.R., 1993. An Overview of Genetic Algorithms : Part 1, Fundamentals. *University Computing*, 2(15), pp.1–16. Available at: http://www.geocities.ws/francorbusetti/gabeasley 1.pdf.

El-mihoub, T.A. et al., 2006. Hybrid Genetic Algorithms : A Review. *Engineering Letters*, 11(August).

Goldberg, D.E., Genetic Algorithms in Search ,

Optimization , and Machine Learning.

Koljonen, J. & Alander, J.T., 2006. Effects of population size and relative elitism on optimization speed and reliability of genetic algorithms. *New Developments in Artificial Intelligence and the Semantic Web*.

Kuczapski, A.M. et al., 2010. Efficient generation of near optimal initial populations to enhance genetic algorithms for job-shop scheduling. *Infomation technology and control*, 39(1), pp.32–37.

Merfeld, D.M. & Zupan, L.H., 2002. Neural processing of gravitoinertial cues in humans. III. Modeling tilt and translation responses. *Journal of neurophysiology*, 87, pp.819–833.

Munster, D., 2009. Parameter Identification : A Comparison of Methods.

Nishiyama, J., Kinoshita, S. & Hirata, Y., 2010. Prediction of drowsiness by the Vestibulo-Ocular Reflex. *Transactions of Japanese Society for Medical and Biological Engineering*, 48(1), pp.1–10.

Obinata, G. et al., 2009. Quantitative Evaluation of Mental Workload by Using Model of Involuntary Eye Movement. In D. Harris, ed. *Engineering Psychology and Cognitive Ergonomics SE - 24*. Lecture Notes in Computer Science. Springer Berlin Heidelberg, pp. 223–232. Available at: http://dx.doi.org/10.1007/978-3-642-02728-4_24.

Obinata, G. & Tokuda, S., 2008. Mental Workloads Can Be Objectively Quantified in Real-time Using VOR (Vestibulo-Ocular Reflex). *The International Federation of Automatic Control*, 17, pp.15094–15099.

Obinata, G., Usui, T. & Shibata, N., 2008. On-line Method for Evaluating Driver Distraction of Memory-decision Workload Based on Dynamics of Vestibulo-ocular Reflex. *Review of Automotive Engineering*, 29(4), pp.627–632. Available at: http://ci.nii.ac.jp/naid/130004544409/en/ [Accessed January 5, 2015].

Omura, K., Aoki, H. & Obinata, G., 2014. Objective evaluation of the brake motion by means of passenger's reflex eye movements. *International symposium on Future active safety teachnology*, 13.

Petcu, F. & Leonida-dragomir, T., 2010. Solar Cell Parameter Identification Using Genetic Algorithms. *CEAI*, 12(1), pp.30–37.

Robinson, D.A., 1981. The use of control systems analysis in the neurophysiology of eye movements. *Annual review of neuroscience*, 4, pp.463–503.

Usui, T., Obinata, G. & Shibata, N., 2007. On-line method for evaluating the driver distractions of memory-decision work load based on dynamics of vestibulo-ocular reflex. *Proceedings of International Symposium on EcoTopia Science*, 07, pp.1132–1136.

Wang, G.S., Huang, F.K. & Lin, H.H., 2004. Application of genetic algorithm to structural dynamic parameter identification. *13 th World Conference on Earthquake Engineering*, (3227).

Zupan, L.H. & Merfeld, D.M., 2003. Neural processing of gravito-inertial cues in humans. IV. Influence of visual rotational cues during roll optokinetic stimuli. *Journal of neurophysiology*, 89, pp.390–400.

A physiological based Driver Model for longitudinal Vehicle Guidance and its Challenges in Validation

M. Mai*, T. Tüschen**
G. Prokop***

Dresden Institute of Automobile Engineering – IAD,
Dresden University of Technology
Dresden, 01062 Germany
*(Tel: +49-351-463-34058; e-mail: marcus.mai@tu-dresden.de)
**(e-mail: thomas.tueschen@tu-dresden.de)
***(e-mail: guenther.prokop@tu-dresden.de)

Abstract: In this paper, a numerical driver behaviour model is presented in terms of how drivers possibly regulate their deceleration in braking tasks. It is based on David N. Lee's τ-theory, which describes how drivers can perceive values of relative motion like *time to collision* or *headway*. This physiological model provides more universal application possibilities than purely empirical models, but its validation within critical traffic situations constitutes great issues. Therefore, a highly dynamic driving simulator providing all the requirements needed is currently under development at the Dresden University of Technology.

Keywords: Driver Behaviour Modelling, Driving Simulators.

1. INTRODUCTION

The longitudinal guidance of vehicles by the driver constitutes a central topic in regarding the whole driving task. Especially under the increasing amount of advanced driver assistance systems and autonomous driving functions, the understanding of driver behaviour demands considerations in a more detailed manner.

There are numerous evidences (e.g. Bubb, 1977) that humans' capabilities of estimation for distance and velocity are too limited and considered with a too large effort of cognition, for realizing safe vehicle guidance based on those estimations. Hence, the traffic related driving task must be accomplished by much more low-level cognitive mechanisms. David N. Lee developed his τ-theory according to those considerations, whereby the coordination of visual-motoric tasks is strictly based on the temporal changes in retinal projections.

In this paper, the fundamentals from Lee (1976) are recapitulated in chapter 2 to explain, how drivers can perceive time related values of relative motion. Their applications within a numerical driver behaviour model are explained subsequently in chapter 3. A mechanism is introduced, how drivers possibly regulate the vehicle's deceleration in a target braking task. This approach provides more universal application possibilities through the underlying physiological mechanisms.

However, the validation of such models constitutes great issues, especially within critical traffic situations. Therefore, a highly dynamic driving simulator, which is currently under development at the Dresden University of Technology, provides all the requirements needed and is shortly introduced in chapter 4.

2. FUNDAMENTALS OF THE T-THEORY

Lee (1976) regards the monocular optical projection of environmental objects on the retina as projections through a pinhole (pupil) on the inside of a sphere (retina) with unit radius. This constitutes the following simplifications:

- The projection occurs through the centre of the lens.
- The retina depicts a sphere and its radius is negligibly small compared to the distance from the object.

For modelling purposes, the retinal projection of a real world object must be simplified and can be considered by two arbitrary points on the object's surface. The object's outlines provide that information in general, which can be further simplified and described by the object's width or height. The geometrical relations by means of an environmental object E of width w_E along the visual axes x_v are shown in Fig. 1.
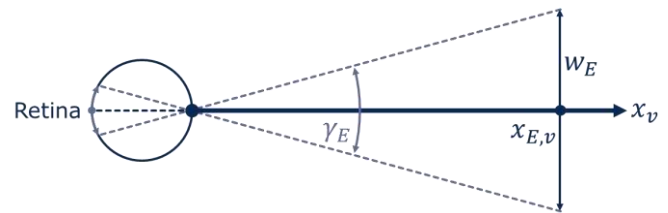
Fig. 1: Retinal projection of an environmental object E of width w_E along the visual axes x_v (according to Lee, 1976)

γ_E constitutes the retinal size of the projection of E in terms of its real width w_E. It can be expressed by the angular relations of the two right-angled triangles:

$$\gamma_E = 2 \cdot \operatorname{atan} \frac{w_E}{2 \cdot x_{E,v}} \qquad (1)$$

Declaring that w_E is much smaller than the relative distance $x_{E,v}$ to the object E, (1) can be simplified to:

$$\gamma_E \approx \frac{w_E}{x_{E,v}} \qquad (2)$$

In case of a relative motion between eye and object E, the relative distance $x_{E,v}$ changes by the relative velocity $x_{E,v,d}$, while the object's real size w_E remains constant. The angular change $\gamma_{E,d}$ of the retinal size γ_E is given by the time derivative of (2):

$$\gamma_{E,d} \approx -\frac{w_E \cdot x_{E,v,d}}{x_{E,v}^{\,2}} \qquad (3)$$

(2) converted to w_E and substituted into (3) reveals:

$$\gamma_{E,d} \approx -\frac{\gamma_E \cdot x_{E,v,d}}{x_{E,v}}$$

$$\tau = \frac{\gamma_E}{\gamma_{E,d}} \approx -\frac{x_{E,v}}{x_{E,v,d}} = TTC \qquad (4)$$

The right side of (4) complies with the definition of the time-to-collision *TTC*. Therefore, the human eye can most likely perceive the *TTC* to an object E from simply detecting the kinematical changes of its retinal projection. Lee defined the left side of (4) as the optical variable τ.

However, the *TTC* is an incomplete value to describe a relative motion, because it does not consider the possible existence of a relative acceleration $x_{E,v,dd}$. Lee postulates that the eye also uses the time derivative τ_d of the optical variable τ for that matter. τ_d can be concatenated with the values of relative motion by deriving (4) with respect to time:

$$\tau_d = -\left(1 - \frac{x_{E,v} \cdot x_{E,v,dd}}{x_{E,v,d}^{\,2}}\right) \qquad (5)$$

3. APPLICATION OF THE T-THEORY

A numerical driver behaviour model for the simulation of scenarios in the field of Active Safety is currently under development at the Dresden University of Technology (see Prokop et al., 2014 and Mai, 2013). The schematic structure of this model is shown in Fig. 2.
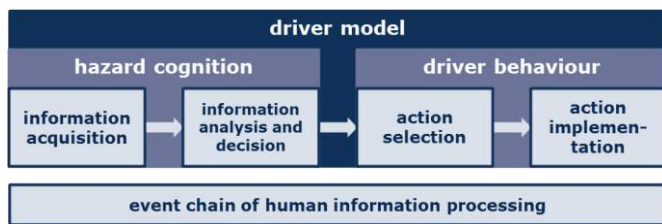
Fig. 2: Schematic structure of the driver behaviour model of the Dresden University of Technology

Besides numerous other mechanisms and theories, the aspects of the τ-theory are included in each of the four submodels: *Information acquisition* provides the optical values explained in chapter 2 and considers thresholds in perception by the visual system. *Information analysis and decision* processes the perceived optical values for the detection of a collision course and the assessment of urgency. Both criteria are essential for the decision making process, which usually leads to the choice of a braking reaction in *action selection*. The execution of this braking reaction by operating the vehicle controls is part of *action implementation*.

The Subject of the present paper is the regulation of the vehicle's deceleration during a braking reaction based on the τ-theory. The scenario considers a target braking task in front of a stationary object E, so the vehicle's deceleration is equal the relative acceleration $x_{E,v,dd}$. The theoretical background emerging from Lee (1976) is given in chapter 3.1 first. Chapter 3.2 presents a verification on real driver behaviour accomplished by Yilmaz and Warren (1995) and derives the algorithm of *action selection*, which regulates the relative acceleration $x_{E,v,dd}$ based on optical values. The second part of the human controller in *action implementation* is introduced in chapter 3.3 for the sake of completeness. It translates the command variable $x_{E,v,dd}$ into the actuating variable p_b (normalized brake pedal position) and is inspired by the phenomenology of Donges' two-level model of driver steering behaviour (see Donges, 1976 or Donges, 1978). A scheme of the overall control loop and a demonstration of its abilities, qualitatively compared to a real driver are finally given in chapter 3.4.

3.1 Knowledge emerging from Lee

Lee (1976) does not explicitly explain how the driver regulates a braking reaction after its initiation from *information analysis and decision*. However, he derives the minimum relative acceleration $x_{E,v,dd}$ needed to prevent a collision in kinematical terms for decision making purposes, considering an uniformly accelerated motion:

$a(t)$ be the predicted course of the relative acceleration. As acceleration remains constant, $a(t)$ can simply be described by the current relative acceleration $x_{E,v,dd}$:

$$a(t) = x_{E,v,dd} \qquad (6)$$

The predicted course of the relative velocity $v(t)$ can be determined by integrating (6) with respect to time under the initial condition of current relative velocity $x_{E,v,d}$:

$$v(t) = x_{E,v,dd} \cdot t + x_{E,v,d} \qquad (7)$$

The predicted course of the relative distance $s(t)$ can finally be determined by integrating (7) with respect to time under the initial condition of current relative distance $x_{E,v}$:

$$s(t) = \frac{x_{E,v,dd}}{2} \cdot t^2 + x_{E,v,d} \cdot t + x_{E,v} \qquad (8)$$

A stop time t_S is introduced to determine the minimum value of the relative acceleration $x_{E,v,dd}$, which still prevents a collision under the considerations above. The following constraints are associated with t_S:

$$v(t_s) = 0 \qquad (9)$$

$$s(t_s) > 0 \qquad (10)$$

(9) substituted into (7) reveals the following definition for t_S:

$$0 = x_{E,v,dd} \cdot t_s + x_{E,v,d} \rightarrow t_s = -\frac{x_{E,v,d}}{x_{E,v,dd}} \qquad (11)$$

(10) and (11) applied on (8) reveal the following expression for the minimum value of the relative acceleration $x_{E,v,dd}$, which is needed to prevent a collision:

$$x_{E,v,dd} > \frac{x_{E,v,d}{}^2}{2 \cdot x_{E,v}} \qquad (12)$$

In case of equality in (12), the vehicle stops directly in front of the object E with a relative distance $x_{E,v}$ equal to zero. The consequences for the perception of τ_d can be determined by substituting (12) in its equal form into (5):

$$\tau_d = -\left(1 - \frac{x_{E,v} \cdot x_{E,v,d}{}^2}{2 \cdot x_{E,v} \cdot x_{E,v,d}{}^2}\right) = -0.5 \qquad (13)$$

It becomes evident from those considerations that an adequate braking reaction consists in a regulation of τ_d. In case of a target braking, τ_d must be kept equal to –0.5 and in case of a stop in front of a static object, τ_d must be kept greater than –0.5. The manipulated variable, which is therefore available to the driver, is the relative acceleration $x_{E,v,dd}$, because he can directly manipulate it through the braking pedal. The mathematical connection behind that consideration can be derived from (4) and (5):

$$\tau_d = -\left(1 + \frac{\tau \cdot x_{E,v,dd}}{x_{E,v,d}}\right) = -1 - \frac{\tau \cdot x_{E,v,dd}}{x_{E,v,d}}$$

$$x_{E,v,dd} = -\frac{x_{E,v,d}}{\tau} \cdot (\tau_d + 1) \qquad (14)$$

(14) reveals the controller's transfer function in time domain:

$$x_{E,v,dd,set} = -\frac{x_{E,v,d,act}}{\tau_{act}} \cdot (\tau_{d,set} + 1) \qquad (15)$$

$\tau_{d,set}$ is the value of τ_d set by the driver, which can vary according to the situation or the driver itself. $x_{E,v,dd,set}$ is the target value of the relative acceleration $x_{E,v,dd}$ derived by the driver, which serves as the command variable for the downstream control loop of the brake pedal position (see chapter 3.3). The other variables are subscripted by *act* to characterize them as state variables.

As the internal command variable $\tau_{d,set}$ is directly implemented in (15) and is not compared against the real value $\tau_{d,act}$ of τ_d, this transfer function constitutes an open-loop control.

3.2 Considering real driver behaviour

Yilmaz and Warren (1995) investigated the control strategy presented in chapter 3.1 within a laboratory survey amongst other strategies, which were advancements or adaptations of the τ-theory or were based on completely other approaches. The results of this survey revealed that the application of a τ_d-constant-strategy is possible in general, but the real driver is also not able to use τ_d as an intrinsic command variable for the continuous regulation according to (15). Yilmaz and Warren found a discrete control mechanism instead.

The experiments revealed, that the test subjects did not continuously regulate the relative acceleration $x_{E,v,dd,set}$, but hold it constant over short periods of time. At the beginning of each period, they corrected the previous value of the relative acceleration $x_{E,v,dd,set}$ about a value $\Delta x_{E,v,dd,set}$, which was always proportional to the necessary difference $\Delta \tau_d$ at the end of the previous period, for regulating τ_d back to –0.5. This relation already indicates that τ_d is also determined by a closed-loop control. Yilmaz and Warren (1995) specified the period length t_{adj} between the control interventions (periods of constant relative acceleration $x_{E,v,dd,set}$) as $0.71\ s \pm 0.61\ s$. They also declared a value of 0.20 s for t_{adj} as the minimum processing time of the control mechanism.

Yilmaz and Warren also found a relation between the level of control intervention and the actual value $\tau_{d,act}$ of τ_d at the beginning of control intervention. The level of intervention can therefor be characterised by the difference $\Delta x_{E,v,dd,set}$ of the relative acceleration $x_{E,v,dd,set}$ or by the difference $\Delta \tau_d$ of τ_d. From the survey results, Yilmaz and Warren (1995) ascertained a regression line for the latter case:

$$\Delta \tau_d = -0.54 - 1.04 \cdot \tau_{d,act} \qquad (16)$$

(16) reveals that the level of intervention expressed by $\Delta \tau_d$ is almost linear related to the actual value of $\tau_{d,act}$ (slope ≈ 1). There are no significant scaling effects between the two variables. Furthermore, the root of (16) is at $\tau_{d,act} \approx -0.52$, what illustrates again that the testing subjects tried to maintain values of τ_d equal to –0.5.

To derive the real value of the command variable $x_{E,v,dd,set}$ form the intended level of intervention $\Delta \tau_d$, (15) can be used again. Thereby, the proportionality criterion between the adjustments $\Delta \tau_d$ and $\Delta x_{E,v,dd,set}$ has to be considered. Assuming, that the relative velocity $x_{E,v,d,act}$ and the optical variable τ_{act} stay almost constant over the step of control adjustment and the adjustments $\Delta \tau_d$ and $\Delta x_{E,v,dd,set}$ are defined as the differences of states *after adjustment* (index 2) and *before adjustment* (index 1), the necessary adjustment $\Delta x_{E,v,dd,set}$ can be described by:

$$x_{E,v,dd,set,1/2} = -\frac{x_{E,v,d,act}}{\tau_{act}} \cdot (\tau_{d,set,1/2} + 1)$$

$$x_{E,v,dd,set,1/2} = -\frac{x_{E,v,d,act}}{\tau_{act}} \cdot \tau_{d,set,1/2} - \frac{x_{E,v,d,act}}{\tau_{act}}$$

$$x_{E,v,dd,set,1} + \frac{x_{E,v,d,act}}{\tau_{act}} \cdot \tau_{d,set,1} = -\frac{x_{E,v,d,act}}{\tau_{act}}$$

$$= x_{E,v,dd,set,2} + \frac{x_{E,v,d,act}}{\tau_{act}} \cdot \tau_{d,set,2}$$

$$x_{E,v,dd,set,1} - x_{E,v,dd,set,2} = \frac{x_{E,v,d,act}}{\tau_{act}} \cdot (\tau_{d,set,2} - \tau_{d,set,1})$$

$$\Delta x_{E,v,dd,set} = -\frac{x_{E,v,d,act}}{\tau_{act}} \cdot \Delta \tau_d \qquad (17)$$

Within the target braking algorithm of *action selection*, the necessary adjustment $\Delta x_{E,v,dd,set}$ is calculated by means of (16) and (17) in discrete time periods of t_{adj}. $\Delta x_{E,v,dd,set}$ is than added to the current value $x_{E,v,dd,act}$ of the relative acceleration $x_{E,v,dd}$ to generate the new value of $x_{E,v,dd,set}$, which serves as the command variable for the control loop in the next chapter.

3.3 Translating deceleration into brake pedal position

The outer control loop presented in the chapters above is suitable for most simulations considering macro- or microscopic traffic scenarios, whereat the interface port between driver and vehicle is defined by the vehicle's longitudinal acceleration $x_{E,v,dd}$ itself. In sub-microscopic simulations or even real hardware tests, the driver input to the car regulating $x_{E,v,dd}$ is defined by the brake and accelerator pedal position. A second (inner) control loop, which regulates the acceleration $x_{E,v,dd,set}$ from the visual controller by manipulating a normalized brake pedal position p_b is therefore presented in the current chapter.

The layout of the vestibular controller is inspired by the concept of Donges' two-level model of driver steering behaviour (see Donges, 1976 or Donges, 1978), which was further developed into the more general, phenomenological three-level hierarchy of driving task (see Donges, 1982 or Donges, 1999). The two-level model distinguishes between behaviour on the *Guidance level* and the *Stabilization level*.

Besides the path planning task by means of a chain of discrete driving manoeuvres, the *Guidance level* involves vehicle control in an anticipatory way. Unless they are absolute novices at their first driving lesson, drivers have a particular knowledge about how their vehicle will behave when they turn the steering wheel about a specific angle or move the brake pedal to a specific position. They use this knowledge for accomplishing the pre-planned driving manoeuvres in the way of an open-loop controller. For instance, Donges (1976) used a first-order transfer function to derive a steering angle fraction λ_S from the street's curvature κ_S at a foresight time T_A, which underlines the anticipatory character of the *Guidance level*.

The *Stabilization level* serves as an underlying compensatory part of behaviour, because the anticipation abilities of most drivers are limited to more simple control mechanisms. Also as typical for an open-loop controller, the *Guidance level* is not able to *react* on disturbance variables like crosswind or slope, because it does not verify its own impact on the system's behaviour. The *Stabilization level* compensates the vehicle guidance errors, which cannot be addressed by the anticipation of the *Guidance level* and therefore must behave like a closed-loop controller. For instance, Donges (1976) used three P-controllers to derive a steering angle fraction λ_R from the curvature error κ_Δ, the heading angle error ψ_Δ and the lateral deviation y_Δ by a time delay τ_H, which is necessary to perceive these guidance errors. The overall steering angle consists of the summation of λ_S and λ_R. Donges (1976) developed and validated his two-level model of driver steering behaviour be means of a human subject study.

Translating Donges' explanations above into the domain of longitudinal guidance for a braking task, the anticipatory open-loop control of the *Guidance level* consists in the calculation of a needed fraction $p_{b,olc}$ of the normalized brake pedal position p_b to adjust a certain acceleration $x_{E,v,dd,set}$ based on the driver's knowledge about his vehicle. For modelling purposes of normal drivers, a point mass approach is considered as suitable enough.

The acceleration $x_{E,v,dd,set}$ of the vehicle mass m has to be created by an overall braking force $F_{bra,set}$ within the wheel contact patches:

$$F_{bra,set} = m \cdot x_{E,v,dd,set} \qquad (18)$$

For the inversion of the point mass model, a very simple mental model of the vehicle's brake system by the driver is declared subsequently:

- No brake pedal actuation produces no braking force.
- Full brake pedal actuation produces the maximum possible braking force $F_{bra,max}$.
- The relation between brake pedal position and braking force is purely linear.

This mental model can be expressed by (19) ($p_b \in [0,1]$):

$$F_{bra} = p_b \cdot F_{bra,max} \qquad (19)$$

By means of (18) and (19), the steady part of the anticipatory open-loop control can be constituted as followed:

$$p_{b,olc,ste} = \frac{m \cdot x_{E,v,dd,set}}{F_{bra,max}} \qquad (20)$$

According to Donges (1976), (20) constitutes the input signal for a first-order transfer Function producing the fraction $p_{b,olc}$ of the normalized brake pedal position p_b to adjust a certain acceleration $x_{E,v,dd,set}$:

$$T_{olc} \cdot \dot{p}_{b,olc} + p_{b,olc} = \frac{m \cdot x_{E,v,dd,set}}{F_{bra,max}} \qquad (21)$$

T_{olc} is the time constant of the anticipatory open-loop part of the vestibular controller expressed by (21). A foresight time is not considered here, because the acceleration $x_{E,v,dd,set}$ is calculated internally and is not driven bottom-up like the street's curvature κ_S in Donges' two-level model.

The compensatory closed-loop control of the *Stabilization level* in longitudinal guidance tasks generally serves for regulating the vehicle's velocity, because this state variable cannot be manipulated directly by the pedals. It is possible to apply two different controllers for acceleration and velocity regulation or just apply one for the latter case and manipulate its control difference. For the current model, a P-controller in accordance to Donges (1976) is applied, which compensates the difference between the command variable $x_{E,v,d,set}$ and the current relative velocity $x_{E,v,d,act}$. $x_{E,v,d,set}$ can be obtained by integrating $x_{E,v,dd,set}$ with respect to time:

$$p_{b,clc}\big|_t = P_{clc} \cdot \left(x_{E,v,d,set} - x_{E,v,d,act}\right)\big|_{t-T_{clc}} \qquad (22)$$

P_{clc} is the gain of the compensatory closed-loop part of the vestibular controller expressed by (22) and T_{clc} is time delay, which is necessary to perceive the control difference between $x_{E,v,d,set}$ and $x_{E,v,d,act}$.

With (21) and (22), the vestibular controller for the braking task is completely defined. The overall brake pedal position p_b is produced by the summation of $p_{b,olc}$ and $p_{b,clc}$.

3.4 Concluding the overall braking model

The overall control loop of the target braking task is finally shown in Fig. 3. The visual controller serves as a generator of command variables for the vestibular controller of the relative acceleration $x_{E,v,dd,act}$ and is based on the structures explained in chapter 3.1 and 3.2. The human vestibular perception is therefore simplified and presented as a continuous controller according to chapter 3.3. The regulation of the brake pedal position p_b based on τ_d can therefor be described as a closed-loop two-level cascade controller.
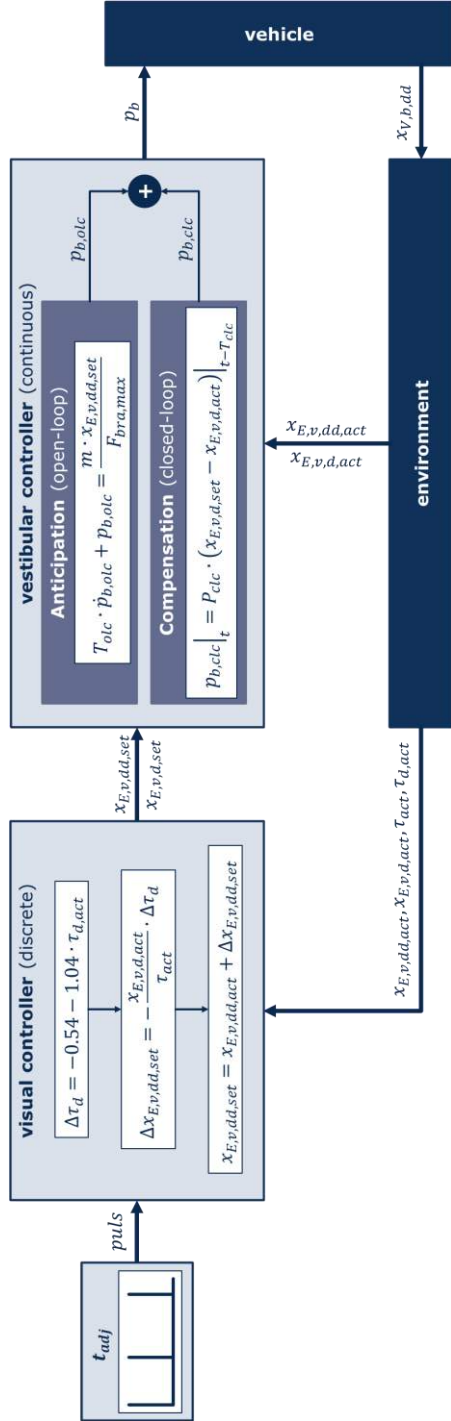
Fig. 3: Overall control loop of the target braking task ($x_{V,b,dd}$ = vehicle longitudinal acceleration)

A demonstration of the braking model's abilities is given in conclusion by an emergency braking scenario: The driver is confronted with a stationary obstacle 20 m ahead, while driving with a velocity of 50 km/h. Therefore, the *TTC* at the start of the simulation is about 1.44 s. The simulated vehicle is a full one-lane model of a premium class sedan and the driver parameters mentioned above are shown in Tab. 1.

Tab. 1: Driver parameters used for the simulations

Driver parameter	Value
t_{adj}	μ = 0.71 s σ = 0.61 s Min. = 0.20 s
m	1850 kg
$F_{bra,max}$	22.3 kN
T_{olc}	0.05 s
T_{clc}	0.1 s
P_{clc}	0.5 s/m

The adjustment time t_{adj} is the only random variable in the overall braking model and is realized by a lognormal distribution according to the parameters found by Yilmaz and Warren (1995). Therefore, the behaviour of the driver model presented here varies only due to the random length of the acceleration plateaus and the differing kinematical circumstances at the discrete acceleration adjustments. Fig. 4 and Fig. 5 show the simulation results in the kinematical terms of relative motion for two different drivers, whereas driver 1 prevents a collision and driver 2 does not.
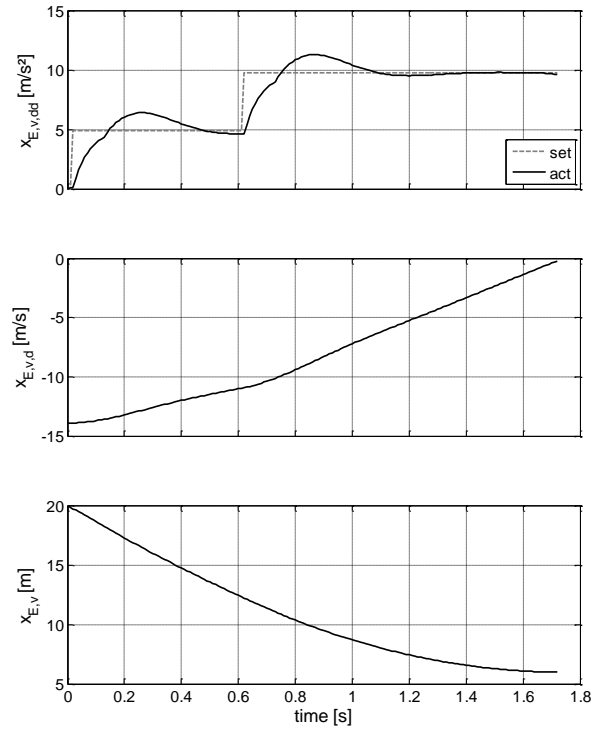
Fig. 4: Emergency braking situation – Simulation results for driver 1 (no collision)
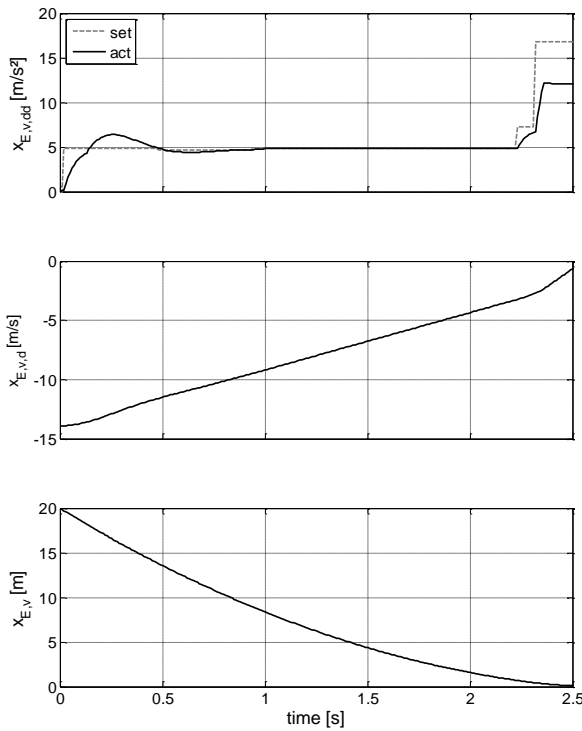
Fig. 5: Emergency braking situation – Simulation results for driver 2 (collision)

The upper plots of Fig. 4 and Fig. 5 show the acceleration $x_{E,v,dd,set}$ planned by the visual controller and the acceleration $x_{E,v,dd,act}$ realized by the vestibular controller. Comparing the latter qualitatively with the measured vehicle acceleration from a human subject study in Fig. 6, the simulated patterns appear to show real human driver behaviour.
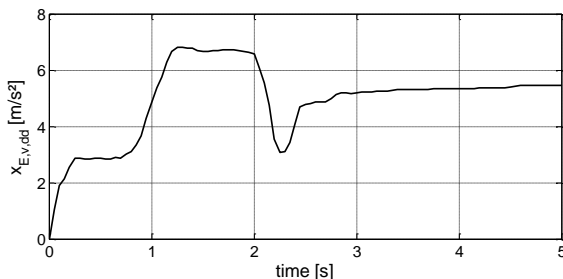
Fig. 6: Emergency braking situation – measured acceleration from human subject study

The validation of a combined visual-vestibular-controller like shown in Fig. 3 constitutes great issues. For the range of normal driving, human subject studies in real cars are suitable, but for critical situations like the simulation examples in Fig. 4 and Fig. 5, there is almost no alternative to driving simulator studies. However, most of the currently existing driving simulators suffer from a more or less low immersion of the simulation on the human subjects. Especially a highly integrated accuracy in the combined simulation of visual and vestibular feedback to the driver, which is required for the validation of the shown model, is not sufficient in most driving simulators today. Therefore, a new highly dynamic driving simulator is currently under

development at the Dresden University of Technology, which is shortly introduced in the next chapter.

4. HIGHLY DYNAMIC DRIVING SIMULATOR

As mentioned above, the majority of the state-of-the-art driving simulators, which are used in the development of driver assistance systems, do not meet the requirements that result from the driving simulator studies. Due to the fact that current state-of-the-art driving simulators are sharing a very similar design and motion strategy, they all suffer from the same limitations, which are determined by their motion concept. The most commonly used motion concept of driving simulators is a parallel kinematic mechanism, usually in form of a hexapod (Stewart platform) with an attached visualization dome (e.g. Stöbe, 2006). Regarding the very limited horizontal working space of a hexapod, most of the acceleration is presented via Tilt-Coordination[1], which leads to a misperception in the simulator and a low immersion. Since the presentation of the vehicle motion by using only a hexapod is not sufficient enough, the parallel kinematics with its visualization dome are often mounted additionally on a single or double slide (e.g. Zeeb, 2010). Depending on the concept, it is thereby possible to realize an additional longitudinal / lateral motion. These simulators have two inherent disadvantages:

1. They are limited in their travel space by their parallel kinematics and slide system.
2. They have a great moving mass due to their complexity.

Regarding point 2, Betz (2015, pp. 20-22) showed that the slide system would need to have a motion space of about 495 m and a Tilt-Coordination system to ensure a motion presentation without frequency gaps. An improvement of the travel space would increase the dimensions of the simulator and lead to a higher mass. Furthermore, the visualization dome often contains a complete vehicle, which increases the weight of the simulator additionally. However, this in turn means that the driving simulator has a lower motion dynamic and is no longer able to present highly dynamic driving manoeuvres, as it is required.

To meet the required dynamics of driving manoeuvres, as well as the presentation of long lasting accelerations, a light and highly dynamic driving simulator with a virtually unlimited working space is necessary.

The new highly dynamic driving simulator concept of the Dresden University of Technology eliminates the travel restriction, without affecting the dynamics of the system. The main feature, which will vastly improve the immersion of the simulation, is that the simulator is based on wheels, which will allow the generation of accelerations up to 10 m/s² with almost no restrictions due to frequencies, except the simulator independent available plane dimensions for movement.

The highly dynamic driving simulator, shown in Fig. 7, consists of two main parts: The inner subsystem (containing a tripod, a driven ring bearing and the simulation dome for the

---

[1] Tilt-Coordination: Tilting a subject in relation to the gravity vector to create a longitudinal / lateral acceleration impression.

cockpit mock-up) allows the presentation of yaw, pitch, roll, and vertical movements. Contrary to the inner subsystem, which is very similar to current simulator concepts, the outer subsystem is the key difference to the standard concepts in particular. It is constructed as a wheel based self-moving motion system with four steerable wheel pairs. Each of those wheel pairs has two separately driven wheels. The energy for the driven wheels, the steering, and the auxiliary devices is supplied by an accumulator, which is installed inside the outer subsystem. Thereby, the simulator is able to travel freely (depending on the available driving area) and represent highly dynamic driving manoeuvres. According to the requirements of a simulator study, it is possible to use the highly dynamic driving simulator on any sufficient plain surface and expand its limits of possible motion presentation.
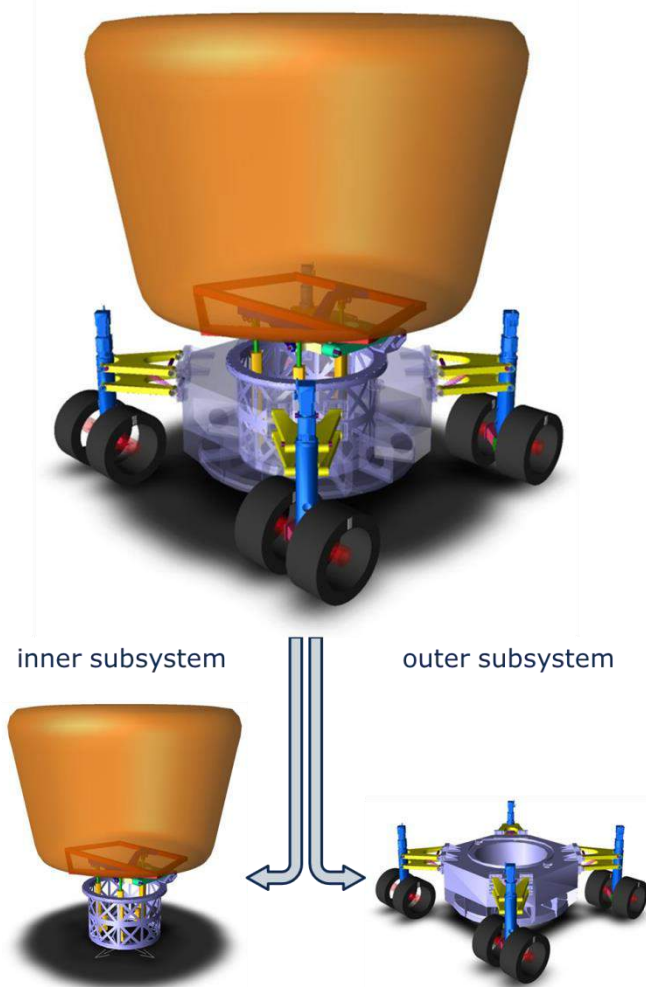
Fig. 7: MBS model of the highly dynamic driving simulator of the Dresden University of Technology

Due to the fact that a tire is a non-holonomic constraint, which means that it cannot actively build up a lateral acceleration while standing still, the tires of the simulator must not stand still. This problem is solved by a continuous rotation of the outer subsystem and a counter-rotation of the inner subsystem while the simulator's horizontal speed is under a certain border. Thereby, it is possible to build up forces in any direction anytime.

A Motion Cueing system is responsible for the simulator never leaving the given driving area. It is exemplary demonstrated in Fig. 8, how the Motion Cueing works. Based on the simulated vehicle manoeuver, it calculates a trajectory for the simulator, optimized for the giving driving area and without harming the human perception thresholds. Due to the fact that humans perceive speed only by their visual system, it is possible for the Motion Cueing to lead the simulator back to its initial or an alternative defined position, while the simulated vehicle moves with a constant speed or stands still. Thereby, the size of driving area can be reduced and the requirements of the simulator studies can be met.
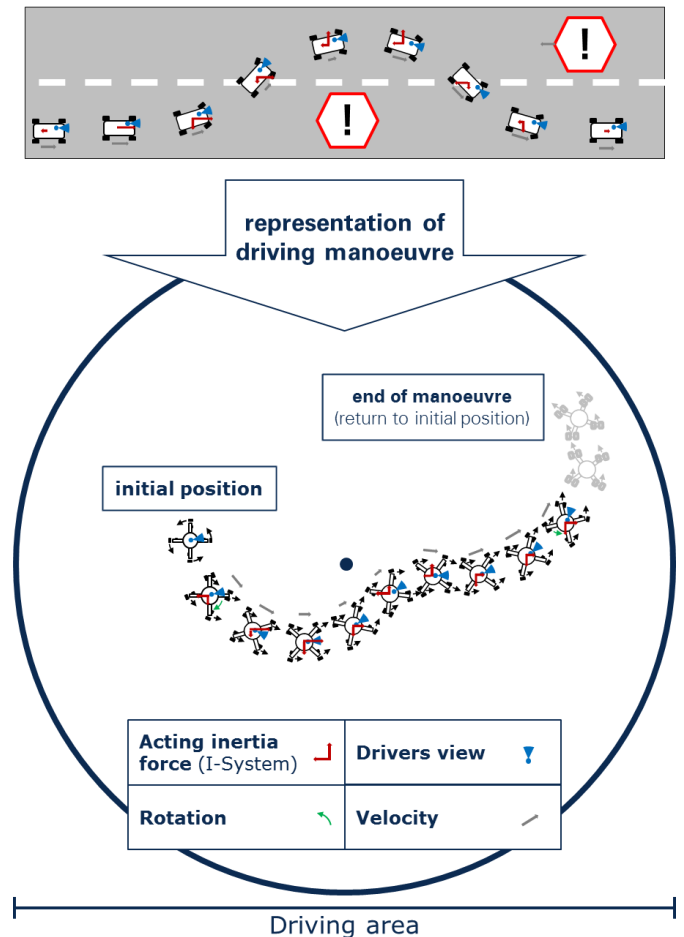
Fig. 8: Motion space of the highly dynamic driving simulator

5. CONCLUSIONS

An essential part of the prevention of road traffic accidents is the understanding of how drivers control their vehicles. This knowledge provides the opportunity to develop driver models, which really represent the human driver behaviour. Such models are necessary tools for the development and validation of all kinds of technology regarding road traffic safety. The model presented in chapter 3 addresses this demand, because it simulates driver behaviour through simulating the underlying physiological mechanisms with all their imperfections, rather than simply reproduce empirical data obtained by a single group of human subjects.

However, driver behaviour models are pretty much useless, if they are not properly validated themselves. The analysis of real human driver behaviour, especially in critical situations, requires high performance tools like the highly dynamic driving simulator presented in chapter 4, for the safety of the human subjects, but also for a high immersion of the simulation to stimulate real human driving behaviour.

The presented methodology thereby contributes an indispensable part of work towards *Vision Zero*.

REFERENCES

Betz, A. (2015). *Feasibility Analysis and Design of Wheeled Mobile Driving Simulator for Urban Traffic Simulation*. PhD Thesis, Technische Universität Darmstadt

Bubb, H. (1977). Analyse der Geschwindigkeitswahrnehmung im Kraftfahrzeug. *Zeitschrift für Arbeitswissenschaft*, 31 (2), pp. 103-111.

Donges, E. (1976). *Experimentelle Untersuchung und regelungstechnische Modellierung des Lenkverhaltens von Kraftfahrern bei simulierter Straßenfahrt*. PhD Thesis, Technische Hochschule Darmstadt.

Donges, E. (1978). A Two-Level Model of Driver Steering Behavior. *Human Factors: The Journal of the Human Factors and Ergonomics Society*, 20 (6), pp. 691-707.

Donges, E. (1982). Aspekte der Aktiven Sicherheit bei der Führung von Personenkraftwagen. *Automobil-Industrie*, 27 (2), pp. 183-190.

Donges, E. (1999). A Conceptual Framework for Active Safety in Road Traffic. *Vehicle System Dynamics*, 32 (2-3), pp. 113–128.

Lee, D. N. (1976). A theory of visual control of braking based on information about time-to-collision. *Perception*, 5, pp. 437-459.

Mai, M. (2013). Simulation der sensorischen Wahrnehmung des Fahrers als Teil eines Fahrerverhaltensmodells zur Entwicklung und Bewertung warnender Fahrerassistenzsysteme. In: *Proceedings of the 9. VDI-Tagung 'Fahrzeugsicherheit'*, pp. 285-300. VDI-Verlag, Düsseldorf.

Prokop, G., Mai, M., Weller, G. & Heyne, F. (2014). Fahrerverhaltensmodell zur prospektiven Effektivitätsbewertung der aktiven Sicherheit. In: *Proceedings of the 16. VDA Technischen Kongress,* pp. 209-240. Verband der Automobilindustrie, Berlin.

Stöbe, M. (2006). Die Fahrsimulation des DLR – Funktionen und Anwendungsmöglichkeiten. *Presentation at the ZVB-Kolloquium*, Braunschweig.

Yilmaz, E.H. and Warren, W.H. (1995). Visual Control of Braking: A Test of the Tau-dot Hypothesis. *Journal of Experimental Psychology: Human Perception and Performance*, 21 (5), pp. 996-1014.

Zeeb, E. (2010). Daimler's New Full Scale High-dynamic Driving Simulator – A technical Overview. In: *Proceedings of the Driving Simulator Conference (DSC)*, pp. 157-165. Paris.

Driving Signature Extraction

Ekim Yurtsever*, Chiyomi Miyajima*, Selpi** and Kazuya Takeda*

** Graduate School of Information Science, Nagoya University, Furo-cho, Chikusa-ku, Nagoya, 464-8603, JAPAN (e-mail:
{yurtsever.ekim, miyajima, takeda}@g.sp.m.is.nagoya-u.ac.jp)*

** Dept. of Applied Mechanics, Chalmers University of Technology, 412 96 Goteborg, SWEDEN (e-mail: selpi@chalmers.se)

Abstract: This study proposes a method to extract the unique driving signatures of individual drivers. We assume that each driver has a unique driving signature that can be represented in a *k* dimensional principal driving component (PDC) space. We propose a method to extract this signature from sensor data. Furthermore, we suggest that drivers with similar driving signatures can be categorized into driving style classes such as aggressive or careful driving. In our experiments, 122 different drivers have driven the same path on Nagoya city express highway with the same instrumented car. GPS, speed, acceleration, steering wheel position and pedal operations have been recorded. Clustering methods have been used to identify driving signatures.

Keywords: Driving style recognition, driver identification, driver modeling

1. INTRODUCTION

Understanding the distribution of driver behaviour is very important for traffic analysis. Especially identifying aggressive or dangerous drivers is crucial as many researchers such as [1], [2], [3] and [4] showed the relationship between aggressiveness of drivers and car accidents. Even though recent developments in road safety and driver assisting systems improved vehicle safety, they did not eliminated human factors in traffic incidents.

Previous researches introduced various approaches on driver classification and driving style recognition. [5] utilized inertial sensors and used braking, acceleration and turning as three main driving events for driver classification with support vector machine (SVM) and k-mean clustering algorithms. [6] divided driving style into two categories as typical (non-aggressive) and aggressive. Dynamic time warping (DTW) has been used for recognizing aggressive driving and a smartphone as a sensor device. [7] developed Gaussian mixture models (GMM) for car following and pedal operation modelling. Driver identification with these models has been done for evaluation. [8] suggested and categorized drivers into five driving categories: flow conformist, extremist, hunter/tailgater, planner, and ultraconservative. Drivers has been categorized according to the distance they keep with the proceeding vehicle and their velocity. [9] investigated driving behaviours at a roundabout. Speed and acceleration models have been developed using Bayesian inference methods. A detailed survey for driving style recognition has been made by [10].

Driving style recognition and observing the changes of the driving style classes' populations could lead to better road design in terms of safety. For example, if population of aggressive driving style increases for a given amount of drivers on a particular highway turn, it will indicate that turn stimulates aggressive driving.

Finding dangerous driving patterns and tracking the history of these patterns could manifest reasons and show patterns for risky behaviour; evaluating of these information could lead to the design of better safety systems. However before achieving such demanding goals, data mining and feature extraction processes should be done. In this study we focus on this aspect. The driving features will be extracted from sensor data first, then these features will be evaluated and meaningful relationships between drivers and features will be established.

This study aims to develop a method to recognize driving styles and extract driving signatures. We believe that driving behaviour of a human driver is a complex structure which has many sub features. We call these sub features principal driving components (PDC). Each driver behaviour is a unique combination of these PDC. Instead of predetermining driving behaviour classes as aggressive, dangerous or safe and categorizing drivers into these classes, we propose to group drivers which shows similar PDC distributions together. This paper explains the PDC extraction out of driving data.

2. EXPERIMENTAL SETUP

122 drivers' driving data on Nagoya city highway in Japan has been obtained in a one year period. Each driver followed the same path during the experiment and each driving session lasted approximately ten minutes. All of the data has been collected with the same vehicle, a Toyota Estima. The intra city highway area where the experiment was held is shown on Google Earth in Fig. 1. 122 different drivers followed this route. 52 of the drivers were female and 70 of them were male. Seven driving signals obtained from this experiment have been used in this study. These signals are: GPS, speed, longitudinal and lateral acceleration, steering wheel position, force on the brake pedal and the gas pedal. Units of these signals are shown in Table 1. Sampling rate of the GPS is 1 Hz while the original sampling rates of the other signals were 16 kHz. However, in our study those signals are downsampled at 10 Hz. Histograms

Fig. 1. Google Earth image of the highway area
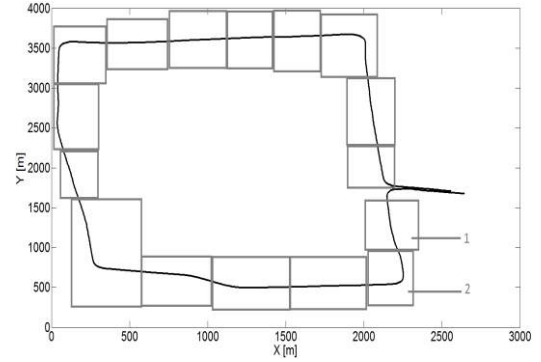
Fig. 2. Sections of the highway. Section 2 and Section 1 are shown. (Traffic is clockwise)

of driving signals are shown in Fig. 3. and driving signal examples are shown in Fig. 4. In Fig 3. x axis represents normalised (z score) values and y axis represents data count. Detailed information about the corpus can be found in [11].

3. EXTRACTION OF DRIVING SIGNATURE

We assume that each driver has a unique driving signature. Categorizing drivers without a complete driving analysis into predetermined driving style classes such as aggressive or normal may lead to wrong categorization. Further, we assume that each driver's unique driving signature (v) is a vector in a k dimensional `principal driving component` (PDC) space. We propose a method to determine the dimension of this space and construct the driving signature vector.

$$v = \begin{pmatrix} a_1 \\ a_2 \\ : \\ a_k \end{pmatrix} \quad (1)$$

After each drivers v have been extracted, these vectors can be clustered. The final clusters can represent the driving styles.

3.1 PDC space

It is assumed that driving on a straight section and on a curved section of a highway is different for the driver. Because of this, the road network, the highway loop in our case, has been divided into sections. In this paper, the Nagoya highway loop is divided into 16 sections, as shown in Fig. 2.

PDC extraction has been done separately section by section. It should be noted that if PDC extraction would have been done without sectioning, the clusters (PDC's) would have been influenced by the road shape. For example, all of the drivers increase their lateral acceleration and rotate their steering wheel on a turn while most of them would drive straight on a straight section of the road. Therefore, without sectioning, the drive vectors of all drivers on a turn would have been clustered together. Then, differences between particular drivers' driving styles could not be recognized.

The collected driving signals have been also divided into corresponding sections for each driver. GPS data has been used to divide the signals with respect to location after time stamps of GPS have been synchronized with other signals. There are 16 sections and 122 drivers in total. s is used for representing the sections and i for the drivers.

$$\begin{aligned} s&: 1,2, \dots, S \\ i&: 1, 2, \dots, D \\ n&: 1, 2, \dots, N \end{aligned} \quad (2)$$

n is the time stamp. N is the sample count of a particular driver at a particular section. A faster driver will have a lower N value than a slower driver at the same section.

Derivative values of each signal were calculated. Then, the driving signals of each driver at each section was vectorised to create drive vector. In our study, there are 12 signals used (see Table 1).
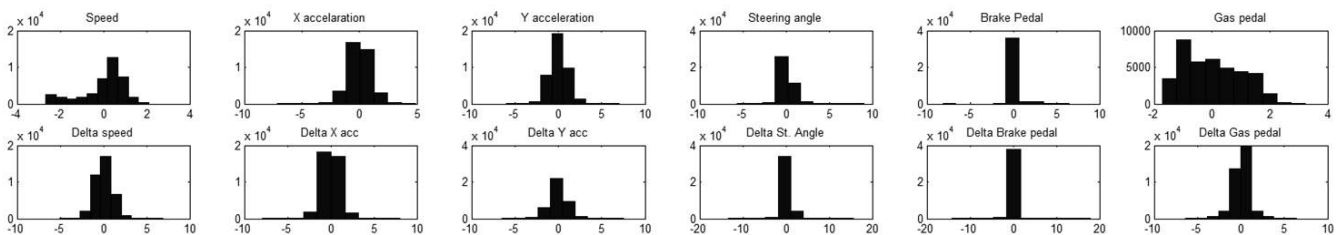
Fig. 3. Histograms of the driving signals at Section 2
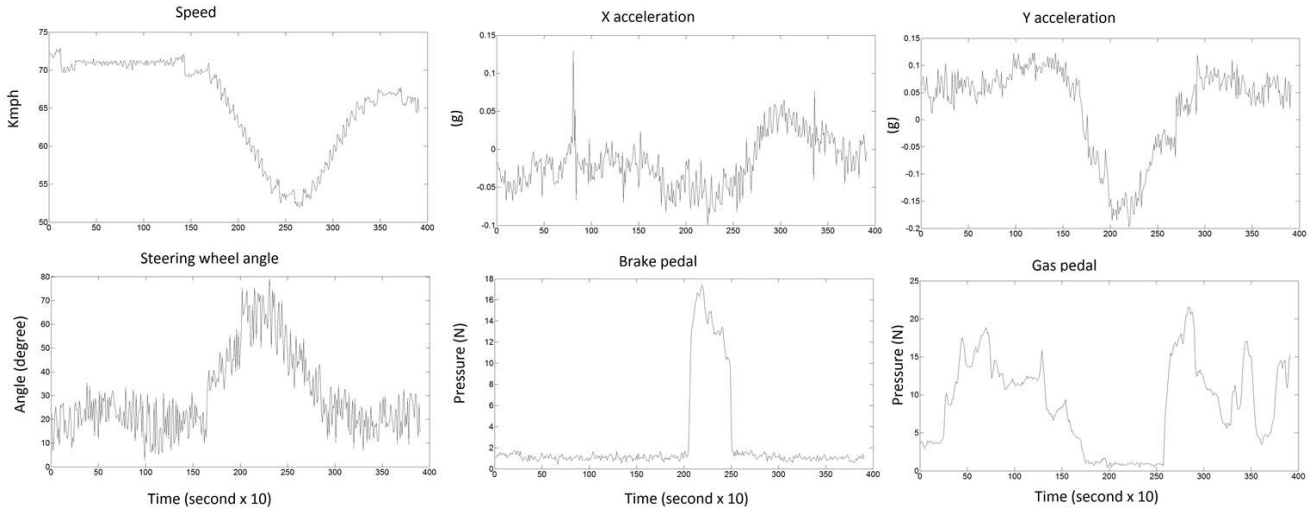
Fig. 4. Drive signal examples

$$\Delta x[m] = \frac{\sum_{k=-K}^{K} kx[m+k]}{\sum_{k=-K}^{K} k^2} \qquad (3)$$

The 12 dimensional drive vector (x) at a particular section (s) for a particular driver (i) with a particular time stamp (n) is as follows.

$$x(i,s,n) = \begin{pmatrix} x_1(i,s,n) \\ x_2(i,s,n) \\ . \\ . \\ x_{12}(i,s,n) \end{pmatrix} \qquad (4)$$

Table 1. Variables

Variable	Physical quantities	unit
x_1	speed	Km/h
x_2	longitudinal acceleration	G
x_3	lateral acceleration	G
x_4	steering wheel angular position	degree
x_5	Force on brake pedal	Newton
x_6	Force on gas pedal	Newton
x_7	Δx_1	
x_8	Δx_2	
x_9	Δx_3	
x_{10}	Δx_4	
x_{11}	Δx_5	
x_{12}	Δx_6	

All drive vectors on the same section were used to create various number of drive clusters. K means clustering method was used for this purpose. With observations *(O₁, O₂, ..., On)* and *k (≤n)* sets Q = *{Q₁, Q₂, ..., Qₖ}* :

$$\text{argmin}_Q \sum_{i=1}^{k} \sum_{O \in Q_i} \|O - \mu_i\|^2 \qquad (5)$$

Dimension of the PDC space is equal to the meaningful number of clusters, k. An empirical approach has been followed to determine k.

k was selected as 2 at first, then increased incrementally to 15. Average of sums of point to cluster centroid, distortion has been calculated for each number of clusters. The relationship between number of clusters and average distortion in our experiment is shown in Fig.5. Different curves represent different sections.

The `elbow` point, where the curve bends and starts to show linear behaviour is selected as the meaningful number of clusters, dimension of the PDC space. It is selected as 6 in our experiments.

Unit vectors (*e₁, …, eₖ*) of the PDC space represents the clusters.

$$e_1 = \begin{pmatrix} 1 \\ 0 \\ : \\ 0 \end{pmatrix}_{kx1} , e_2 = \begin{pmatrix} 0 \\ 1 \\ : \\ 0 \end{pmatrix}_{kx1} \dots e_k = \begin{pmatrix} 0 \\ 0 \\ : \\ 1 \end{pmatrix}_{kx1} \qquad (6)$$

3.2 Driver signature

The drive vectors of driver *i* at section *s* is as follows

185
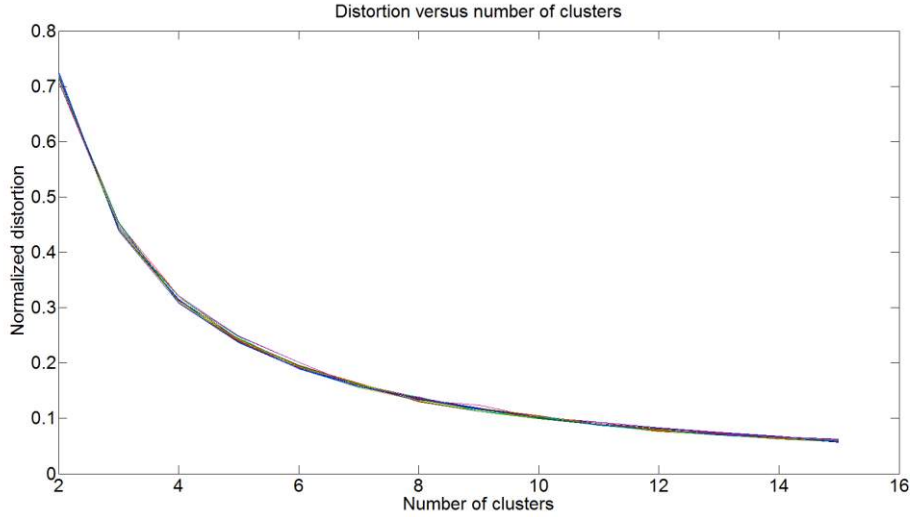
Fig. 5. Distortion versus number of clusters.

$$\boldsymbol{x}(i,s,1),\dots,\boldsymbol{x}(i,s,N) = \overbrace{\begin{pmatrix} x_1(i,s,1) \\ x_2(i,s,1) \\ . \\ . \\ x_{12}(i,s,1) \end{pmatrix}}^{IDX_1},\dots,\overbrace{\begin{pmatrix} x_1(i,s,N) \\ x_2(i,s,N) \\ . \\ . \\ x_{12}(i,s,N) \end{pmatrix}}^{IDX_N} \quad (7)$$

$$\underbrace{\hspace{6cm}}_{N}$$

where N is sample count of the driver at a particular section and IDX is the cluster index for the corresponding vector.

After k has been selected and all of the drive vectors have been clustered accordingly, the indexes (IDX) of each drive vector (index shows which cluster the particular drive vector belongs to) of one driver at a particular section were summed up and divided to N. N depends on the driver, a faster driver will have a lower N value than a slower driver at the same section. Then, a driver index function (f) was constructed for each driver. For driver i at section s, f is as follows:

$$f(i,s) = p_1\boldsymbol{e_1} + p_2\boldsymbol{e_2} + \dots + p_k\boldsymbol{e_k} \quad (8)$$

$$p_m = \frac{\sum IDX(m)}{N} \quad (9)$$

Driver signature vector ($\boldsymbol{v}$) is constructed after this with driver index functions. $\boldsymbol{v}$ for driver i is as follows:

$$\boldsymbol{v}(i) = \begin{pmatrix} a_1(i) \\ a_2(i) \\ \vdots \\ a_k(i) \end{pmatrix} \quad (10)$$

Where a_m is:

$$a_m = \frac{\sum_{s=1}^{S} p_m(i,s)}{S} \quad (11)$$

Coefficients of f, p_m, of three random drivers from our experiments are shown in Fig. 6. Each driver has a unique coefficient distribution as can be seen in this figure.

Each driver has a unique $\boldsymbol{v}$. We propose that K means can be used again to cluster these vectors. These final clusters will represent the driving styles. In this study we focused on driving signature extraction. Categorization of drivers based on driving styles will be investigated in our future works.

4. CONCLUSIONS

The behaviour of drivers, their driving signatures are mathematically represented within a PDC space in our proposed method. However, the meaning of PDC's have not been identified and driving styles (for example aggressive driving or careful) have not been categorized yet.

We would like to utilize this method for driver identification also. In our future works we will work on these issues.

ACKNOWLEDGMENT

REFERENCES

[1] González-Iglesias, B., Gómez-Fraguela, J. A., & Luengo-Martín, M. Á. (2012). Driving anger and traffic violations: Gender differences. Transportation research part F: traffic psychology and behaviour, 15(4), 404-412.

[2] Chliaoutakis, J. E., Demakakos, P., Tzamalouka, G., Bakou, V., Koumaki, M., & Darviri, C. (2002). Aggressive behavior while driving as predictor of self-reported car crashes. Journal of safety Research, 33(4), 431-443

[3] Shinar, D. (1998). Aggressive driving: the contribution of the drivers and the situation. Transportation Research Part F: Traffic Psychology and Behaviour, 1(2), 137-160.

[4] Deffenbacher, J. L., Deffenbacher, D. M., Lynch, R. S., & Richards, T. L. (2003). Anger, aggression, and risky behavior: a comparison of high and low anger drivers. Behaviour research and therapy, 41(6), 701-718.

[5] Van Ly, M., Martin, S., & Trivedi, M. M. (2013, June). Driver classification and driving style recognition using inertial sensors. In Intelligent Vehicles Symposium (IV), 2013 IEEE (pp. 1040-1045). IEEE.

[6] Johnson, D., & Trivedi, M. M. (2011, October). Driving style recognition using a smartphone as a sensor platform. In Intelligent Transportation Systems (ITSC), 2011 14th International IEEE Conference on (pp. 1609-1615). IEEE.
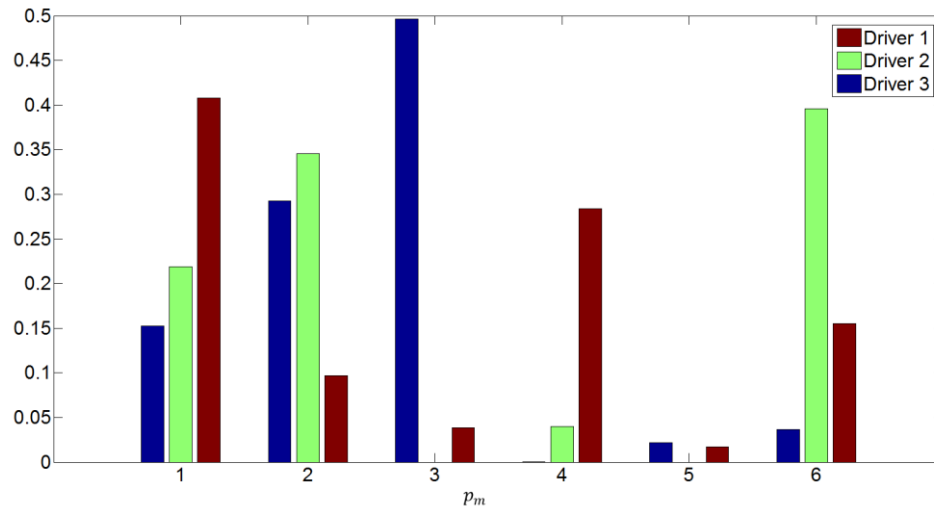
Fig. 6. Coefficients of driver index function for three random drivers from our data

[7] Miyajima, C., Nishiwaki, Y., Ozawa, K., Wakita, T., Itou, K., Takeda, K., & Itakura, F. (2007). Driver modeling based on driving behavior and its evaluation in driver identification. Proceedings of the IEEE, 95(2), 427-437.

[8] Fancher, P. (1998). Intelligent cruise control field operational test (No. UMTRI-98-17).

[9] Mudgal, A., Hallmark, S., Carriquiry, A., & Gkritza, K. (2014). Driving behavior at a roundabout: A hierarchical Bayesian regression analysis. Transportation research part D: transport and environment, 26, 20-26.

[10] Bolovinou, A., Amditis, A., Bellotti, F., & Tarkiainen, M. (2014). driving style recognition for co-operative driving: A survey. In ADAPTIVE 2014, the sixth international conference on adaptive and self-adaptive systems and applications (pp. 73-78).

[11] Takeda, K., Hansen, J. H., Boyraz, P., Malta, L., Miyajima, C., & Abut, H. (2011). International large-scale vehicle corpora for research on driver behavior on the road. Intelligent Transportation Systems, IEEE Transactions on, 12(4), 1609-1623.

AstaZero – an Open Facility for Active Safety Research

Henrik Eriksson*, Josef Nilsson*, and Jan Jacobson*
Peter Janevik** and Håkan Andersson**

*SP Technical Research Institute of Sweden, Box 857, SE-501 15 Borås, Sweden
(Tel: +46-10-516{5716, 5317, 5697}; e-mail: {Henrik.Eriksson, Josef.Nilsson, Jan.Jacobson}@sp.se).
**AstaZero, Box 8077, SE-402 78 Göteborg, Sweden
(e-mail:{Peter.Janevik, Hakan.Andersson}@astazero.com)

Abstract: The AstaZero proving ground for testing of vehicle active safety systems was inaugurated in August 2014. Since then, several research projects have already been active on the proving ground. This paper will introduce the test track, give examples of such research activities, and show the benefits of an open facility for active safety research.

Keywords: active safety, ADAS, test track, proving ground, open facility, road traffic safety, V2X.

Symposium keywords: Active Safety Testing Methods and Tools.

1. INTRODUCTION

Although the trend is promising, a staggering 26000 people were killed on European roads in 2013 (EU, 2015). The goal set by the EU is to reduce the number of fatalities to 15750 in the year 2020 (EU, 2015). This reduction is a tough challenge, and a significant part of the reduction is expected to come from larger penetration as well as newly developed active safety systems. An open research facility specifically designed for testing active safety systems, is a key enabler to design, test, verify, and certify these systems. AstaZero is a recently inaugurated test area of this kind. AstaZero is owned by a university and a research institute which guarantees an open environment and a continuous and sustained supply of competent personnel as well as state-of-the art equipment.

2. ASTAZERO OVERVIEW

AstaZero consists of four track parts and a proving ground centre where workshops are located together with a calibration area. There are ten car workshops and two workshops for trucks and buses. The four parts are: rural road, city area, high-speed area, and multilane road, see Fig. 1.

Fig. 1. AstaZero test track, aerial view.

2.1 Rural Road

The rural road is approximately 5.7 km long. Half is designed for 70 km/h and half for 90 km/h, see Fig. 2. In several places there is scrub or broadleaf trees growing near the track, which make it possible to conceal obstacles before they cross the road in front of the test vehicles. The rural road is specially designed for tests of driver behavior and is well-suited for the use of hidden or suddenly appearing obstacles. There are also two T-junctions and a crossroad as well as bus stops/lay-bys at two locations. The road is not designed for advanced driving maneuvers at high speed. It may be used for bi-directional traffic, but the normal setup is one-way traffic driving on the right-hand side of the road. There are some hills at the road, but the maximum incline is 4.5%. Communication links via optical fibers are prepared around the track, and it is ready to be populated with road-side units for ITS-applications.

Fig. 2. Rural road track.

2.2 City Area

The city area consists of 4 building blocks (40 x 25 x 4 m) and covers a number of different sub-areas such as: town center with varying street widths and lanes, bus stops, pavements, street lighting and building backdrops. Ground-

work is made for another five blocks. The road system in the area includes environments such as: roundabouts, T-junction, lab area (100x30 m) and return-loop. Connections to the rural road occur in two places, allowing vehicles to pass through the city area and continue on the rural road. The city area is based on a relatively flat surface and has dummy structures that resemble buildings both to the human eye and to technical equipment such as radar. The city area is lit up by normal street lighting, which can be switched off by section. Streets have a 2.0% incline for good drainage into sewage drains, and there are acceleration roads, longer than 150 m, before the intersection in the city center. The main street is equipped with "portals" with traffic signs. One block contains the control room and warehouse for dummies.

Fig. 3. Aerial view of the city area.

2.3 High-Speed Area

The high-speed area is connected to the multilane road and consists of a circle, 240 metres in diameter, with "drop add-ons". It slopes laterally to achieve water run-off and is completely flat in the longitudinal direction. The high-speed area has two acceleration roads. The main acceleration road is approximately 1 km long. This will provide sufficient distance also for accelerating heavy trucks to high speed. In addition, it is also possible to use the multilane road for acceleration, which means vehicles can enter the high-speed area from three different directions. This gives the possibility for complex high-speed test scenarios. In this area, focus will primarily be on vehicle dynamics like avoidance maneuvers at high speeds, but also "near misses" for active safety systems at high speeds. A large open asphalt area like the high-speed area is also useful for cases when virtual reality is combined with driving a real vehicle.

The high-speed area slopes 1% in the lateral direction, but is completely flat in the longitudinal direction, (flatness 1.0 acc. to IRI). Asphalt is provided according to the specification SN75-80. There is a turning loop for long vehicles (25.25m) at the end of, as well as halfway into the acceleration road. It has a width of 7 meters. A calibration area (for gyros) is provided at the first turning loop.

A separate control tower is overlooking the area. The tower is two stories high for good visibility, and it provides a platform on the roof for visitors. Remote control of targets, balloon cars and driving robots is performed from the control tower.

Fig. 4. High-speed area.

2.4 Multi-Lane Road

The multilane area is 700 m long, has four lanes, and is connected to the high-speed area. Additionally, it has an acceleration road that is approximately 300 meters long, 7 meters wide, and a turning loop for long vehicles. Several different scenarios can be tested on the multilane road, such as lane changes and departures, different collision scenarios, as well as crossing scenarios. It is possible to change the direction of travel in different lanes, as well as to build a temporary central barrier and different types of traffic barrier railings. The whole area is lit to the normal standard for road lighting. The lighting is designed in four sections that can be individually switched on and off so that one can easily vary between lit and unlit environments. There is a small intersection with the possibility to create intersection scenarios.
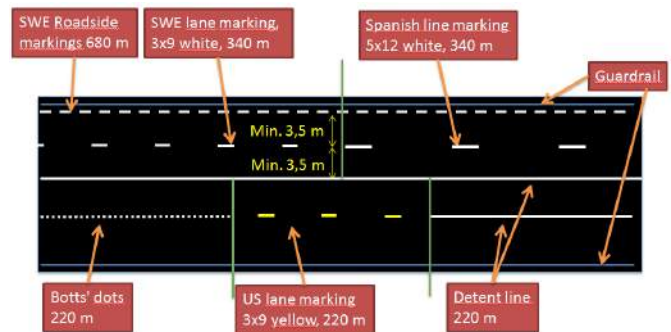
Fig. 5. Lane markings available on the multi-lane road.

2.5 Equipment

At AstaZero there is a lot of equipment available for research as well as production and rating tests. The track has its own RTK base station and state of the art positioning systems (OXTS, 2015) are available. A number of driving robots (steering, throttle, and brake) (ABD, 2015) are also available. The test track can provide cars as well as two trucks and a bus for use in testing.

Both in-house developed and commercially available targets are provided. An in-house developed stationary target can be seen in Fig. 6, and a commercially available target (DRI, 2015) can be seen in Fig. 7. Besides these targets, also the EuroNCAP rear-end rating target, a pedestrian target, and a bicycle target are available.

Fig. 6. In-house developed stationary target.

Fig. 7. Commercially available soft target.

3. EXAMPLES OF RESEARCH

3.1 Seamless Test Methods for Active Safety

In a national project with several OEMs, universities, institutes and a tier one supplier, a seamless tool-chain has been developed for testing of active safety systems, ranging from desktop simulators to tests on a proving ground. In this tool-chain, techniques based on augmented (Blissing, et al., 2013) and virtual reality have been introduced, see Fig. 8.

Fig. 8. Driving with augmented reality.

The large open area which the high-speed area represents is suitable for tests and evaluation of techniques based on augmented or virtual reality. Future work is planned for research on the use of mixed reality techniques on the test track.

3.2 Education of Emergency Vehicle Drivers

Another project has studied the potential use of driving simulators and test track drives for education of emergency vehicle drivers. Critical scenarios were arranged in the simulator and on the test track (Fig. 9), and the drivers were monitored and evaluated using eye-tracking equipment and trained inspectors in the passenger seat. One such scenario included a hidden child (dummy) which suddenly ran out into the middle of the road. The drivers were impressed by the rural road track, which they believe looked and felt like a conventional rural road in Sweden. They also report that it was easy to forget that they were driving on a test track and being part in an experiment.

Fig. 9. An ambulance driving in the city area.

3.3 Platooning

Antenna placement and the reliability of communication links in platooning applications (K. Karlsson, et al, 2015) have been studied in a project involving two Swedish truck companies, several research organizations, and a supplier of communication equipment. The rural road was used to perform measurements, and evaluate the standards proposed by ETSI (ETSI, 2015), see Fig. 10. As one of the project results, a revised version of the solution for vehicle to vehicle communication for platooning in the ETSI standard has been proposed.

Fig. 10. Platooning on the rural road.

3.4 Road Friction Measurement

Active safety and road friction are key ingredients in a research project which wants to develop test methods and simulation models with respect to grip. The project has visited AstaZero and established a "friction map" of the high-speed area (Fig. 11), which can be used in research and future tests.

Fig. 11. Friction measurements on the high-speed area.

3.5 "Soft" Asphalt

"Soft" asphalt has been added on a track segment within the area. The goal of this research is to evaluate if soft asphalt is a viable solution to reduce the resulting injuries of vulnerable road user single accidents; mainly cyclists.

3.6 New Test Methods and Tools

New test methods, tools, and equipment are needed to establish new rating methods and develop new active safety functions. A number of intersection scenarios and scenarios involving vulnerable road-users have been studied and preliminary methods and tools have been researched.

Fig. 12. An intersection scenario in the city environment.

3.7 Rain and fog conditions

The performance of sensors used by active safety and automated driving systems (e.g., radar, camera, and lidar) are affected by adverse weather conditions. A project has been initiated to develop methods and tools for testing the sensor-based systems in controlled rain and fog conditions on the test track.

3.8 Researchers Day

Twice during its first year in operation AstaZero has gathered researchers at the test facility to share and discuss ongoing and future work related to test tracks. The events have been visited by researchers from OEMs, tier ones, academia, and institutes who have presented their work and discussed the future needs for test track testing of active safety and automated driving. Besides participants from Sweden, the researchers day have had visitors from China, USA, Canada, and Germany.

3.9 Chalmers Engineering Education

Students taking a vehicle dynamics course at Chalmers University of Technology have had one of their laboratories at the high-speed area. The laboratory provided the students with a unique opportunity to perceive vehicle handling and stability performance during on-track manoeuvres as well as acquire testing and data collection experience.

Fig. 13. Student laboratory at the high-speed area [photo from Vehicle Dynamics, Chalmers].

4. FUTURE RESEARCH

Coming projects will continue the research on virtual and augmented reality test methods as well as develop new methods, tools, and equipment for testing of active safety systems and automated driving. Other projects will research affordable/crushable accurate positioning systems and detailed digital mapping of the AstaZero premises. There will also be projects related to ITS, e.g. development and testing of comfort and safety systems based on cooperative ITS.

5. CONCLUSIONS

Less than a year after its inauguration, the AstaZero test track has experienced a lot of research-related activities on all its parts, and a lot of novel research is up-coming. This shows that the track was well-specified and suitable for various kinds of research related to active safety, automated driving, and V2X communication.

REFERENCES

ABD. (2015) http://www.abd.uk.com/.

Blissing, B., Bruzelius, F. & Ölvander, J. (2013). Augmented and Mixed Reality as a Tool for Evaluation of Vehicle Active Safety Systems. In *Proceedings of the International Conference Road Safety and Simulation*.

CASTT (2015) http://www.ltu.se/centres/Centre-for-Automotive-Systems-Technologies-and-Testing?l=en

DRI. (2015) http://www.dynres.com/.

ETSI. (2015) http://www.etsi.org/technologies-clusters/technologies/intelligent-transport/cooperative-its/.

EU. (2015). http://ec.europa.eu/transport/road_safety/.

K. Karlsson et al. (2015). On the Effect of Vertical Spatial Diversity on V2V Communication for Three Different Platooning Scenarios. Accepted for presentation at Antennas and Propagation (EuCAP).

OXTS. (2015) http://www.oxts.com/.

Modelling and experimental evaluation of driver behaviour during single wheel hub motor failures

D. Wanner [*], **L. Drugge** [*], **J. Edrén** [*] **and A. Stensson Trigell** [*]

[*] *Department of Aeronautical and Vehicle Engineering,*
KTH Royal Institute of Technology, SE-100 44 Stockholm, Sweden, and
SHC Swedish Hybrid Vehicle Centre
(e-mail: {dwanner, larsd, edren, annika}@kth.se).

Abstract: A failure-sensitive driver model has been developed in the research study presented in this paper. The model is based on measurements of human responses to different failure conditions influencing the vehicle directional stability in a moving-base driving simulator. The measurements were made in a previous experimental study where test subjects were exposed to three sudden failure conditions that required adequate corrective measures to maintain the vehicle control and regain the planned trajectory. A common driver model and a failure-sensitive driver model have been compared, and results for the latter agree well with the measured data. The proposed failure-sensitive driver model is capable of maintaining the vehicle control and regaining the planned trajectory similarly to the way in which humans achieved this during a wheel hub motor failure in one of the rear wheels.

Keywords: Driver model, human behaviour, wheel hub motor failure, driving simulator, vehicle dynamics.

1. INTRODUCTION

The complexity of electrified vehicle components and subsystems has been increasing in recent years due to the possibilities of enhanced vehicle behaviour, and this is a development which at present seems to be continuing in the same manner. One consequence of this complexity is that a larger amount of faults can occur in a vehicle, leading to the increased probability of a failure occurring. Specifically, there is a greater risk of failures affecting the dynamic behaviour of vehicles and endangering traffic safety. In order to gain knowledge of the driver-vehicle interaction during a failure, human driving behaviour was investigated for different failure conditions in an experimental driving simulator study within the ERA-NET Electromobility+ project entitled "EVERSAFE", Cocron et al. (2014). In this simulator study, the test subjects were exposed to three sudden failure conditions in one of the rear wheels, leading to a loss of yaw equilibrium and requiring the drivers to compensate by counter-steering in order to maintain the vehicle control and regain the planned trajectory.

Today driver models are an important tool in the development of vehicles and are a substitute for experimental tests to a greater extent. In combination with appropriate vehicle simulation models, driver models can be used to analyse, adapt and validate the vehicle dynamic behaviour prior to and during the prototype phase. Various types of driver models have been presented and have shown their potential for several applications in the field of vehicle dynamics, Plöchl and Edelmann (2007). A review of different driver models based on human sensory dynamics is pro-

vided in Bigler and Cole (2011). Hereby, the driver model is modelled and characterised according several sensory tasks that are relevant for steering a vehicle. MacAdam (2003) analysed human driving behaviour and described several driver models that were in agreement with his findings. One of the suggested driver models was tested in a simulation of a tyre blowout during a double lane change, i.e. a highly dynamic manoeuvre, in order to show the capabilities of this driver model and its broad application area. The driver model reacted immediately to the tyre blowout without any reaction time, but such a reaction would not be natural human behaviour. Weir and McRuer (1973) analysed simulator experiments and described the driver behaviour as a function of the lateral position and heading error. Sharp et al. (2000) developed a driver steering model employing an optical lever arm as a preview vector. The model's accurate path-following properties and robustness against changes in the vehicle dynamics were demonstrated. Erséus et al. (2011) developed a path-tracking driver model emulating different driving skills. This model enables the analysis of distinct high or low driving skills in vehicle dynamic simulations. Markkula et al. (2014) analysed and compared several models of driver steering behaviour and their suitability for collision avoidance and vehicle stabilisation. Among others, the driver models of MacAdam and Sharp were analysed and found suitable for evasive manoeuvres.

Driver models have been widely investigated in an endeavour to model realistic human behaviour during driving. Most driver models are applicable for a wide variety of regular driving conditions, and even highly dynamic vehicle manoeuvres can be analysed. However, existing driver

models have not been evaluated on their capability to handle an unexpected event, such as a failure of a wheel hub motor, in the same manner as a human and at the same time is based on real driver data. The performance of humans depends on the driving situation and changes if an external disturbance like a wheel hub motor failure affects the vehicle. The number of situations that can be analysed with driver models can be extended with a driver model that can change its behaviour during such an external disturbance. The possibility of adapting such a driver model to real driver data generalises its validity.

The goal of this research study was to develop a failure-sensitive driver model (FSDM) based on measured data from a previous experimental study performed during different failure conditions. The behaviour of the developed model was to resemble the corresponding driver behaviour in the same conditions. This driver model could then be used in a simulation environment to analyse the influence which various failures during different manoeuvres exert on the driver-vehicle interaction. This would enable to gain knowledge about driver-vehicle interaction prior to costly experimental tests.

In Section 2, the developed driver model and the corresponding high-fidelity vehicle model are presented. Furthermore, the analysed failure conditions with their corresponding driving manoeuvres, as well as the previously conducted experimental study, are described. In Section 3, the results for the FSDM are analysed. The conclusions drawn from the findings of the study are summarised in Section 4.

2. METHOD

This section presents the applied vehicle model and its vehicle parameters. Moreover, the underlying experimental study is described and the analysed failure conditions are presented. Finally, the proposed FSDM, including its parameterisation, is described.

2.1 Vehicle model

The vehicle model applied in the present study is the same as the model utilised in the experimental study by Cocron et al. (2014), which was performed in a moving-base driving simulator. This vehicle model is a high-fidelity vehicle dynamics model with non-linear tyre behaviour and non-linear suspension kinematics Bruzelius et al. (2013). It represents a small city car and is parameterised according to the electric vehicle Mitsubishi iMiev, as seen in Table 1. A co-simulation environment with Dymola and Matlab/Simulink is used where the vehicle dynamics model is implemented in the former, and the failure model and the FSDM are implemented in the latter.

2.2 Failure conditions

The failure conditions are based on an experimental study which was conducted as part of the European project EVERSAFE, Cocron et al. (2014). The goal of this experimental study was to analyse the driver-vehicle behaviour during different failure conditions during the normal operation of an electric passenger car. Therefore, the test subjects were exposed to three sudden failures in one of the rear wheels which required driver corrections to maintain the vehicle control and regain the planned trajectory. This experimental study was conducted in a moving-base driving simulator at the Swedish National Road and Transport Research Institute (VTI). The experimental tests and the data acquisition were conducted by VTI in cooperation with Technische Universität Chemnitz (TUC). The definition of the failures and the analysis of the driver-vehicle response, as well as the fault classification, were carried out by KTH Vehicle Dynamics in cooperation with VTI and TUC.

Three failure conditions were analysed, each of them consisting of a wheel hub motor failure and a driving manoeuvre. The failure was based on an inverter shutdown in the field weakening range, as described in Wanner et al. (2014). The driving manoeuvres were divided into cornering and straight-line driving at a speed of 110 km/h. The studied left-hand curve of the cornering manoeuvre had a radius of 450 m, and hence the test subjects achieved an approximate lateral acceleration of $2 \, \text{m/s}^2$ for the given speed. The first failure condition (S) was defined as a straight-line driving manoeuvre with a failure on the left rear wheel. For the cornering manoeuvre, the failure was introduced on the left or right rear wheel, leading to a curve-inward (CI) or a curve-outward (CO) failure condition.

The wheel hub motor failure was implemented as a suddenly applied brake torque of 540 Nm on the affected wheel, resulting in a deceleration of $1.75 \, \text{m/s}^2$ for the vehicle. The failure was implemented as a filtered step function with time constant $\tau = 0.04 \, \text{s}$. The brake torque was held for 3 s and linearly ramped down to zero within another 3 s. Simultaneously, the potential propulsion and hydraulic brake torques on the affected wheel that could have been demanded by the driver were set to zero and subsequently ramped to their original value after another 3 s. Hence, the failure affected the vehicle for 9 s, see Fig. 1.

2.3 Failure-sensitive driver model

The FSDM consists of a longitudinal speed controller and a lateral steering controller, which are described separately below. The longitudinal speed controller regulates the deviation of the actual longitudinal speed from the desired longitudinal speed, v_x and v_x^{ref}, respectively, by means of a PI-controller. The accelerator pedal position ϵ is determined to be

Table 1. Vehicle specifications.

Parameter	Value
Curb weight	1192 kg
Body roll moment of inertia	404 kgm^2
Body pitch moment of inertia	1501 kgm^2
Body yaw moment of inertia	1841 kgm^2
Wheel base	2.55 m
Distance from centre of gravity to front axle	1.173 m
Track width, front	1.31 m
Track width, rear	1.27 m
Drive system	RWD
Motor type	PMSM
Maximum power	49 kW
Maximum torque	180 Nm
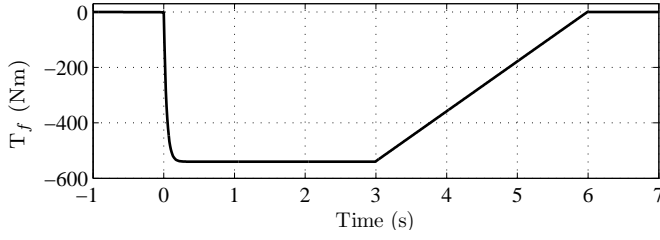
Fig. 1. Brake torque characteristics on the affected wheel with failure activation at t = 0 s.

$$\epsilon = k_{xp}(v_x^{\mathrm{ref}} - v_x) + \int k_{xi}(v_x^{\mathrm{ref}} - v_x)dt \qquad (1)$$

with the proportional and integral gain being k_{xp} and k_{xi}, respectively.

As an extension of the longitudinal speed controller, additional failure-sensitive parameters that describe the driving behaviour during a failure condition are introduced (Fig. 2). Therefore, the human behaviour during a failure condition is modelled with an additional time delay function, incorporating the average reaction time t_r as determined in the previously described moving-base driving simulator experiments, Cocron et al. (2014). For the longitudinal speed controller, the accelerator pedal reaction $t_r = t_\epsilon$ is considered and shown in Table 2. The accelerator pedal movement is continued in the same manner after failure activation as before the failure activation for the time period of the accelerator pedal reaction time. Therefore, the gradient of the longitudinal speed difference $\Delta\dot{v}_x$ is kept constant, starting from the failure activation t_0, and its estimated values is defined according to

$$\Delta\dot{v}_x(t) = \Delta\dot{v}_x(t_0) \quad t_0 \leq t < (t_0 + t_\epsilon). \qquad (2)$$

A transition between this estimated longitudinal speed difference with fixed gradient and the actual longitudinal speed difference has been designed as a continuous switch-over function which is similar to a fuzzy logic block and where both signals are smoothed with a first-order time delay with the time constant τ_ϵ for all failure conditions. The transition period is time-based and further referred to as the synchronisation time, t_s.

The lateral steering controller is based on the multiple-preview-point steering angle controller presented in Sharp et al. (2000). In the presented study, one single preview point was chosen for the lateral steering controller. A basic schematic diagram is provided in Fig. 3. The model consists of three input parameters: the lateral offset Δy_1 between the vehicle position and the road, the heading error $\Delta\psi$ between the vehicle yaw angle ψ_v and the road-heading angle ψ_r, and an optical lever that points from the centre of gravity in the direction of travel. The optical lever represents the preview distance of the driver on the path ahead. Its length, l, is set by the preview time t_p and is a function of the longitudinal speed v_x according to

$$l = t_p \cdot v_x. \qquad (3)$$

A lateral offset, Δy_2, is determined between the tip of the optical lever and the road coordinates normal to the end point of the optical lever. Each of the input parameters is
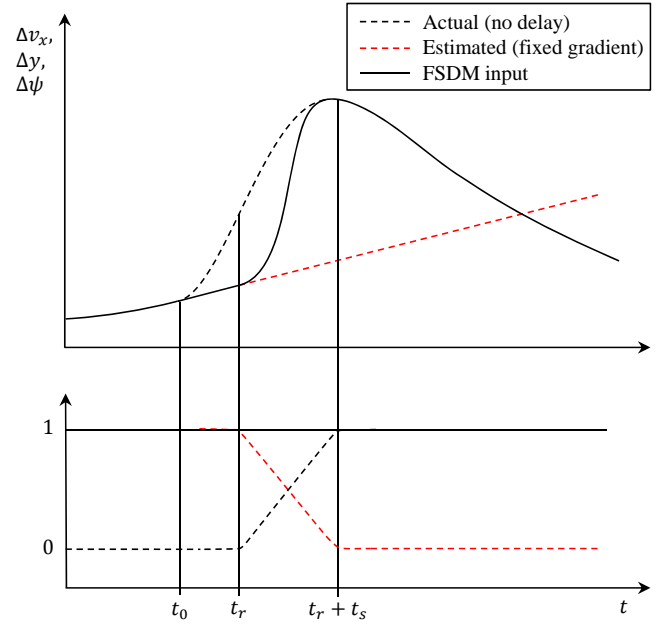
Fig. 2. Schematic diagram of time delay function including fixed gradient and synchronisation time.
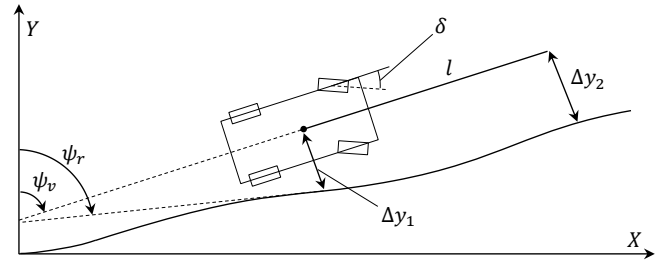
Fig. 3. The lateral steering controller and its parameters, based on Sharp et al. (2000).

provided with a control gain, k_y, k_l and k_ψ. The steering angle δ is determined as the sum of the control inputs

$$\delta = k_y \cdot \Delta y_1 + k_\psi \cdot \Delta\psi + k_l \cdot \Delta y_2. \qquad (4)$$

Additional failure-sensitive parameters for the lateral steering controller are introduced which are similar to the ones utilised in the longitudinal speed controller. Note that the reaction time in Fig. 2 is expressed as $t_r = t_\delta$ for the lateral steering controller. The gradient of the heading error $\Delta\dot{\psi}$ is kept constant during the steering reaction time t_δ according to

$$\Delta\dot{\psi}(t) = \Delta\dot{\psi}(t_0) \quad t_0 \leq t < (t_0 + t_\delta). \qquad (5)$$

The gradients of the lateral offsets $\Delta\dot{y}_1$ and $\Delta\dot{y}_2$ are fixed likewise. The steering reaction time t_δ is based on the minimum steering reaction time for each analysed failure condition in the experimental simulator study, and they were found suitable for the fixed gradient time period. Signal transitions after the reaction period are likewise modelled with a continuous switch-over function including the time constant τ_δ and the synchronisation time t_s. The synchronisation time of the lateral steering controller can be described as the time which the driver needs to adjust to

the new situation. After the initial intuitive driver reaction at t_δ, in which the driver realises the mismatch between the planned and the actual trajectory, the synchronisation time represents the time for planning and finding an alternative path to recover the planned trajectory. Individual saturation levels for the lateral offset, the heading offset and a total saturation level for the steering angle output are further introduced.

All the parameters of the longitudinal speed controller and lateral steering controller of the FSDM are presented for normal driving manoeuvres in Tables 2 and 3. Measured data from the presented experimental driving simulator study were used to tune the FSDM parameters. The longitudinal speed controller is tuned to failure condition S and then evaluated for the other two failure conditions. Its parameters were identical for baseline driving and the three failure conditions, except for the varying accelerator pedal reaction times, see Table 2. The lateral steering controller was tuned for a regular manoeuvre without a failure. The parameters during a failure were derived from the experimental results for N=13 participants for failure condition S, N=15 for CI and N=13 for CO. The average vehicle states of all the measurements for a specific failure condition were utilised to find a suitable fit for the model parameters. The adapted FSDM models were named according to the failure conditions, FSDM-S, FSDM-CI and FSDM-CO, and are presented in Table 3. The standard parameter configuration, FSDM, was applicable for the curve-outwards parameter set, FSDM-CO, while the parameters of the straight-line driving and the curve-inwards failure conditions, FSDM-S and FSDM-CI, had to be adapted during an active failure to achieve a better fit of the measured data. For FSDM-S, the control gain of the optical lever k_l was reduced to zero degrees. This could be justified by the fact that the influence of the optical lever on straight-line driving would have a strong influence on any type of lateral or heading error, and drivers primarily focus on vehicle stabilisation. For FSDM-CI, the preview time t_p was increased, resulting in a longer optical lever. Furthermore, the time constant τ_ϵ was enlarged in order to smooth the adjustment of the optical lever. The steering reaction time t_δ varied for each failure condition.

Besides an analysis of the FSDM parameters for the average vehicle states, an analysis of the parameters for the individual test subjects was conducted for failure condition S, as shown in Table 4. Accordingly, the measured data for each test subject were fed into a parameter estimation of the FSDM. The estimated control gains for all the drivers for failure condition S (N=13) range from 0.65–

Table 3. Parameters of the FSDM lateral steering controller for normal driving and the three analysed failure conditions.

Parameter	FSDM	FSDM-S	FSDM-CI	FSDM-CO
k_y (°/m)	1	1	1	1
k_ψ (°/rad)	18	18	18	18
k_l (°/m)	0.75	0	0.75	0.75
t_p (s)	1	1	2.1	1
t_δ (s)	-	0.45	0 35	0.40
t_s (s)	-	0.67	0.67	0.67
τ_δ (s)	0.02	0.02	0.2	0.02
sat_y (°)	±5	±5	±5	±5
sat_ψ (°)	±5	±5	±5	±5
sat_{tot} (°)	±25	±25	±25	±25

1.52 °/m and 6.52–24.57 °/m for the lateral offset k_y and the heading error k_ψ, respectively. The synchronisation times have a range of 0.2–0.94 s. With these 13 parameter sets, the human behaviour of each individual driver could be analysed during a failure condition in addition to the averaged FSDM parameters. Three parameter sets that cover different aspects of the driver behaviour are shown in Table 4 as examples.

3. RESULTS

The presented driver model FSDM was analysed for a regular manoeuvre with no failure and the three different failure conditions, S, CI and CO. The results of the analysis were compared to the measured data from the experimental study. The longitudinal speed controller and the lateral steering controller are discussed separately below. Further, the individual parameter sets of FSDM-S during failure condition S are presented. Note that the road path and the point of failure activation were identical for the simulation and the experiment.

The comparison of the results for the simulation with those for the experimental study shows that, for regular driving, FSDM follows the road path well at various speeds and curvatures. In Fig. 4, the resulting states of the steering wheel angle, lateral acceleration and yaw rate for the simulated FSDM lay comfortably within the measured vehicle states for the test subjects. These measured data are shown for the test subjects for a cornering manoeuvre and are framed within the overall maximum and minimum values marked with the bold grey lines.

In the case of a failure occurring, FSDM adapts to this new situation in order to handle the failure. The desired path is thereby recovered in a similar manner as human drivers would regain it. Consequently, the previously mentioned gains are adjusted and an additional time delay function

Table 2. Parameters of the FSDM longitudinal speed controller for normal driving and the three analysed failure conditions.

Parameter	FSDM	FSDM-S	FSDM-CI	FSDM-CO
k_{xp} (s/m)	0.05	0.05	0.05	0.05
k_{xi} (m^{-1})	0.002	0.002	0.002	0.002
t_ϵ (s)	-	1.26	2.76	0.74
t_s (s)	2	2	2	2
τ_ϵ (s)	0.2	0.2	0.2	0.2
sat_{xp} (-)	±1	±1	±1	±1
sat_{xi} (-)	±1	±1	±1	±1

Table 4. FSDM parameter analysis for individual drivers for failure condition S.

Parameter	k_y (°/m)	k_ψ (°/m)	t_s (s)
Min	0.65	6.52	0.20
Mean	0.96	15.64	0.52
Max	1.52	24.57	0.94
SD	0.25	6.38	0.21
Test subject 4	0.73	13.89	0.40
Test subject 7	0.89	17.78	0.94
Test subject 12	1.22	23.34	0.51

is implemented, which reflects the measured behaviour of humans, including their reaction times.

The results for failure condition S are presented in Figs. 5–7. The longitudinal speed controller results are displayed in Fig. 5, where the impact of the faulty brake torque is clearly visible and leads to a drop in the longitudinal acceleration and vehicle speed. The accelerator pedal position of FSDM-S increases similarly to the way in which the pooled trend for the drivers increases.
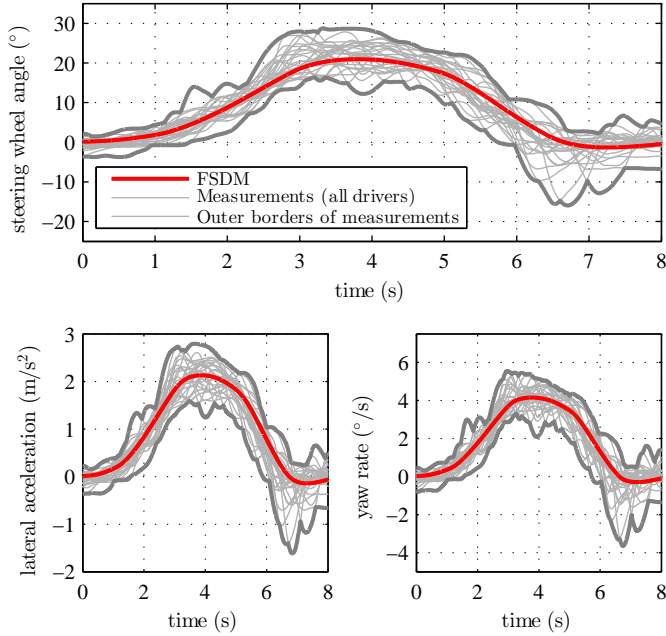
Fig. 4. Vehicle states for a cornering manoeuvre without a failure mode for different drivers of the vehicle and for the FSDM.
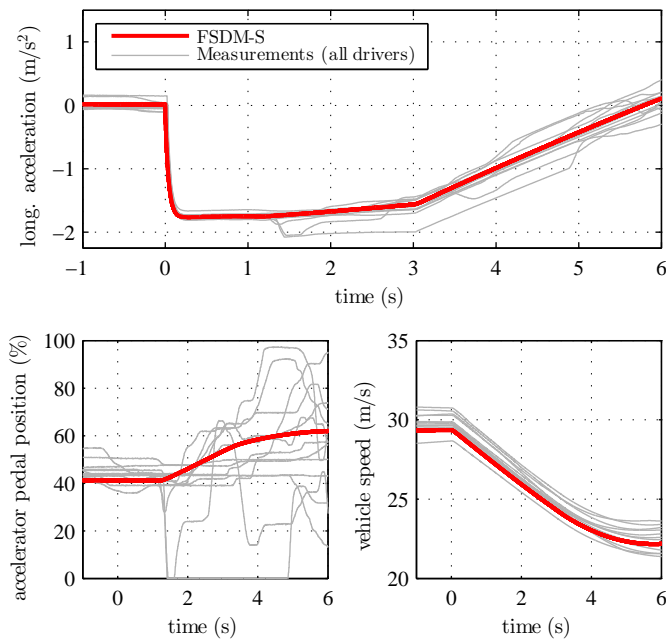
Fig. 5. Longitudinal acceleration and speed, as well as accelerator pedal position, for failure condition S.
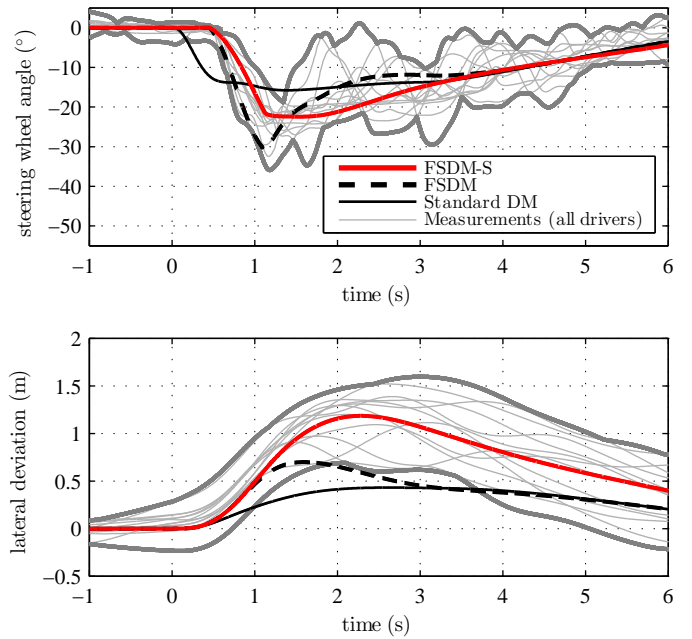
Fig. 6. Steering wheel angle and lateral offset for failure condition S.

Fig. 6 shows a comparison of different driver models. The steering wheel angle and lateral deviation are illustrated for the measured data, the standard driver model (standard DM), and the failure-sensitive driver model for normal driving manoeuvres (FSDM) and its adaptation to failure condition S (FSDM-S). The individual driver data represent various types of driver reactions, from a very responsive and wobbly behaviour with high fluctuations to a rather slow and smooth one. The standard DM without a time delay function and with no adaptation to failure condition S shows an instant reaction to the failure, which leads to a better compensation for the lateral deviation and a lower steering wheel angle compared to the measurements. However, this reaction is not comparable to human behaviour, as the reaction time and the synchronisation time are ignored. FSDM for normal driving situations shows a more human-like behaviour, lying close to the framing borders of the measured data. FSDM-S shows that the adaptation of FSDM to failure condition S fits the average of the measured data well.

The vehicle states for failure condition S are shown in Fig. 7, where the measured data are compared with the results from FSDM and FSDM-S. The yaw motion and the lateral acceleration match the average measured characteristics for FSDM-S, whereas FSDM rather represents the behaviour of a responsive individual driver.

The behaviour of the individual drivers was also analysed and FSDM-S parameter sets were found, as shown in Table 4. Measured and individually modelled steering wheel angles are shown for three selected test subjects in Fig. 8. Test subjects 4 and 12 show responsive steering behaviour by applying counter-steering during the failure condition and slowly reducing it when the failure is ramped down. An unsteady steering behaviour with high fluctuations due to over-compensation for the failure is found for test subject 7. Here the modelled result is limited in the am-
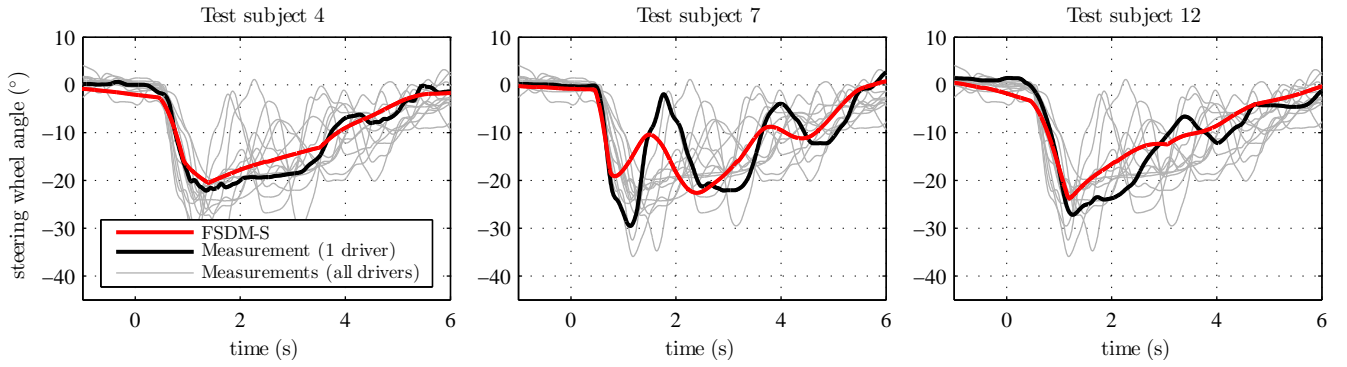
Fig. 8. Steering wheel angles of three selected individual parameter sets.

Fig. 7. Lateral acceleration and yaw motion for failure condition S.

Fig. 9. Longitudinal acceleration and speed, as well as accelerator pedal position, for failure condition CI.
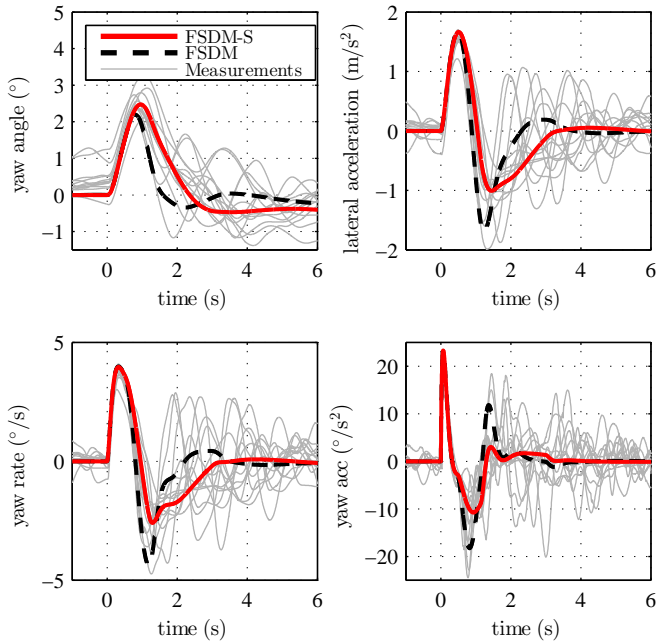
plitude of the fluctuation, although a reasonable solution is achieved. Hence, the developed model is suitable for mimicking not only an average driver, but also individual drivers who differ in their responses.

The vehicle states for failure conditions CI and CO, representing failures during cornering manoeuvres, are illustrated in Figs. 9–12. As is seen in Figs. 9 and 10, the longitudinal speed controller works well for both failure conditions, increasing the accelerator pedal position similarly to the way in which most of the drivers increased the pedal position. The resulting longitudinal acceleration and velocity correspond with the measured data.

Accordingly, FSDM-CI, the driver model for the curve-inwards failure, follows the measured average vehicle states, see Fig. 11. It can be observed that the failure is activated in the transient part of the curve at time $t = 0$ s, i.e. the steering wheel angle and the vehicle states are not constant at failure activation. The steering behaviour of FSDM-CI, i.e. the counter-steering characteristics and the steering wheel angle gradients of the model, matches the measured data of the experimental study well. The vehicle
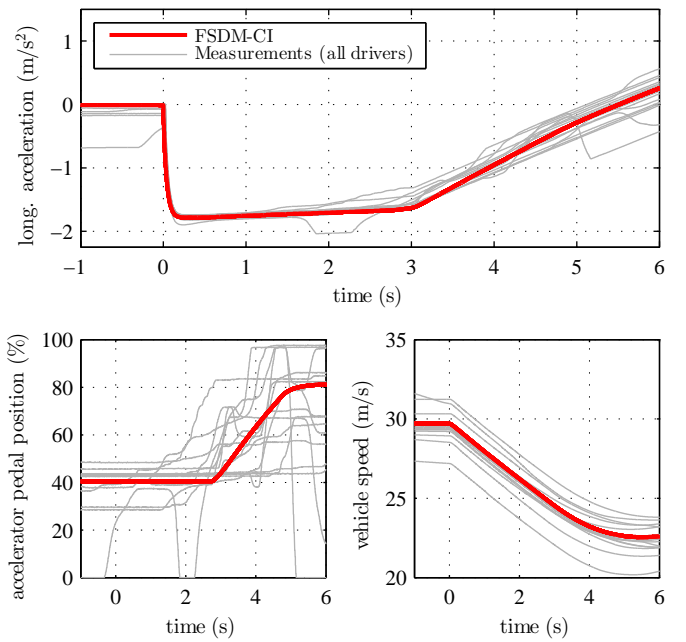
states fit equally well. FSDM (which has no adaptation to failure condition CI) produces results for failure condition CI representing more responsive drivers with vehicle states close to the border of the measured data. This model produces more overshooting, which in turn leads to higher fluctuations of the yaw motion. The results for the adapted driver model FSDM-CI resemble the measured data well, and thus the model has been evaluated for transient road segments.

The curve-outwards failure was activated on the same transient road segment, see Fig. 12. Except for the steering wheel reaction time, no modification of the FSDM specific to failure condition CO was necessary. FSDM-CO and FSDM are identical, and therefore the results for FSDM are not illustrated in Fig. 12. The steering wheel angle characteristics of FSDM-CO fit the measured data well and is characterised by a short and fast increase, followed by a sharp return at the peak value and a rather constant decrease. The vehicle states match the measurements for this failure condition equally well.
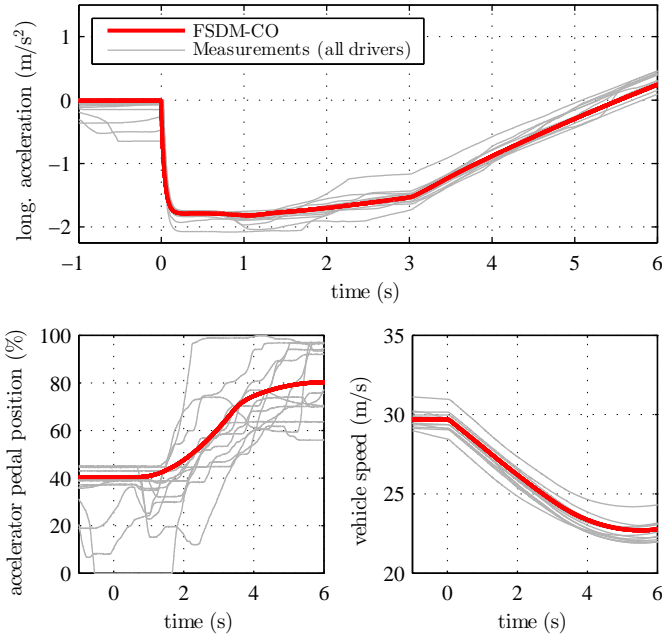
Fig. 10. Longitudinal acceleration and speed, as well as accelerator pedal position, for failure condition CO.
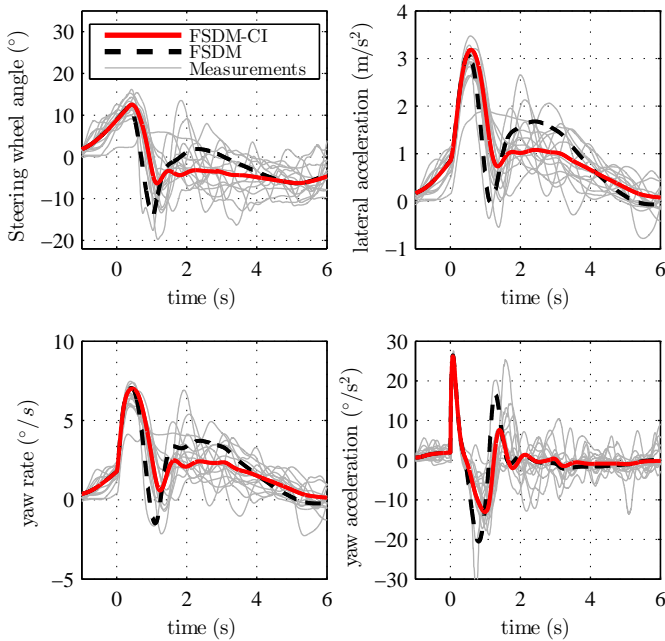
Fig. 11. Steering wheel angle, lateral acceleration and yaw motion for failure condition CI.

4. CONCLUSIONS

In this study, a failure-sensitive driver model based on measurements of human responses during three different failure conditions has been developed and validated. The purpose of the model is to analyse the influence of different failure modes on the driver-vehicle behaviour in a simulation environment, without the necessity of costly and time-consuming experimental tests. Fault-tolerant vehicle dynamic control strategies and alternative traffic scenarios or driving manoeuvres can be evaluated correspondingly.
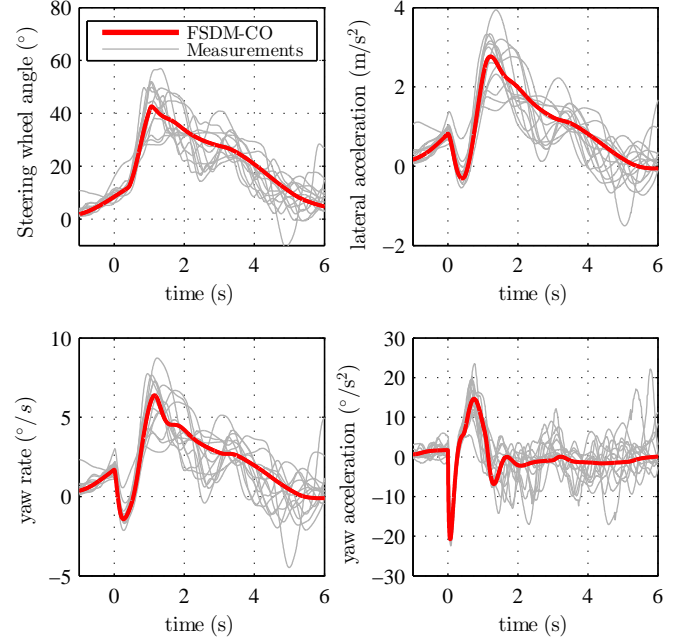
Fig. 12. Steering wheel angle, lateral acceleration and yaw motion for failure condition CO.

The results show that the proposed failure-sensitive driver model is capable of maintaining the vehicle control and regaining the planned trajectory similarly to the way in which humans achieve this during a wheel hub motor failure in one of the rear wheels. Modelling parameters for three different failure conditions, as well as for normal driving conditions without a failure, have been proposed.

This study is limited to the analysed manoeuvres performed on a wide country road without other traffic participants and with the described vehicle. The human reactions may be more distinct with opposing traffic or in other driving situations, e.g. in an urban environment, and this could be analysed in the future development of the model. An automated selection of the adequate parameter sets, depending on the failure condition, could be handled by a failure detection and isolation strategy. Measured data from similar experiments could also be used to generalise the model further.

REFERENCES

P. Cocron, I. Neumann, M. Kreußlein, M. Pereira, D. Wanner, L. Drugge, M. Bierbach and B. Augusto. Driver and vehicle behaviour to power train failures in electric vehicles experimental results of field and simulator studies. *Technical report, EVERSAFE Electromobility+ project.*

M. Plöchl and J. Edelmann. Driver models in automobile dynamics application. *Vehicle System Dynamics*, vol. 45, no. 8, pp. 699–741, 2007.

C.C. MacAdam. Understanding and modeling the human driver. *Vehicle System Dynamics*, vol. 40, no. 1–3, pp. 101–134, 2003.

D.H. Weir and D.T. McRuer. Measurement and interpretation of driver/vehicle system dynamic response. *Human Factors*, vol. 15, no. 4, pp. 367–378, 1973.

R.S. Sharp, D. Casanova and P. Symonds. A mathematical model for driver steering control, with design, tuning

and performance results. *Vehicle System Dynamics*, vol. 33, no. 5, pp. 289–326, 2000.

A. Erséus, L. Drugge and A. Stensson Trigell. A path tracking driver model with representation of driving skill. *Int. J. Vehicle Systems Modelling and Testing*, vol. 6, no. 2, pp. 145-185, 2011.

G. Markkula, O. Benderius and M. Wahde. Comparing and validating models of driver steering behaviour in collision avoidance and vehicle stabilization. *Vehicle System Dynamics*, vol. 52, no. 12, pp. 1658-1680, 2014.

R.S. Bigler and D.J. Cole. A review of mathematical models of human sensory dynamics relevant to the steering task. *Proc. 22nd IAVSD Symposium on the Dynamics of Vehicles on Roads and Tracks*, Manchester, UK, August 2011.

F. Bruzelius, J. Gomez Fernandez and B. Augusto. A basic vehicle dynamics model for driving simulators. *Int. J. Vehicle Systems Modelling and Testing*, vol. 8, no. 4, pp. 364–385, 2013.

D. Wanner, L. Drugge and A. Stensson Trigell. Fault classification method for the driving safety of electrified vehicles. *Vehicle System Dynamics*, vol. 52, no. 5, pp. 704-732, 2014.

Study on Difference of the Traveling Trajectory with Change in Vehicle Response Characteristics in the Lane Change Situation

Shohei Kitazawa*, Tetsuya Kaneko**

* Osaka Sangyo University, 3-1-1, Nakagaito, Daito-city, Osaka, Japan,
(e-mail: kitazawa@ojc.osaka-sandai.ac.jp).
** Osaka Sangyo University, 3-1-1, Nakagaito, Daito-city, Osaka, Japan,
(e-mail:kaneko@tm.osaka-sandai.ac.jp)

Abstract: We believe that a driver's operation and vehicle's motion characteristics during a lane change differ depending on the driver. In this study, we examined a driver's acceptance and operation in relation to a change in the response of a four-wheel steering vehicle. We varied the frequency response characteristics of the yaw rate for the steering wheel operation by changing the control parameters of the four-wheel steering system. We conducted experiments using this experimental vehicle. Based on the results, the vehicle response acceptable to the driver was characterized, and the driver behavior in relation to the vehicle response was determined.

Keywords: Driver behavior, Acceptability, Frequency response characteristics, Four-wheel steering, Yaw rate, Vehicle dynamics, Traveling trajectory

1. INTRODUCTION

In recent years, by-wire technology has improved the flexibility of a vehicle's design characteristics. A vehicle's characteristics can be easily modified by changing a specific control parameter. In other words, it is possible to change a vehicle's characteristics for a given running situation, environment, etc. to provide driving support. It is important that the changes in the vehicle's characteristics and any control intervention related to the provided driving support are acceptable to the driver. Even if the characteristics of the vehicle change, the driver can always change maneuvers to compensate in order to achieve the target control. Drivers show significant individual differences in terms of their sensitivity and discrimination characteristics. Therefore, to build a driving support system that can work in conjunction with the driver, it is important to fully consider the discrimination and acceptance of each driver.

We believe that a driver's operation and the maneuverable vehicle characteristics differ depending on the driver in a lane change situation. The traveling trajectory also varies for each driver. In this study, we investigated a driver's acceptance and operation in relation to a change in the vehicle response by using a modified small electric vehicle with four-wheel steering. We investigated the acceptance and driving behavior in relation to a change in a vehicle's transient response characteristics for a yaw motion by using the experimental vehicle. By using the characteristics of the traveling trajectory during a lane change, we tried to classify different driver attributes.

2. EXPERIMENTAL DEVICES AND CONDITION

2.1. Experimental Vehicle and Yaw Rate Response

We varied the frequency response characteristics of the yaw rate for steering wheel operation by changing the control parameters of the four-wheel steering system. The control parameters were the natural frequency and damping ratio of the yaw rate response. We conducted experiments using this experimental vehicle. The reference vehicle response for the experiment was the simulation of a small car with neutral steering. Fig. 1 shows a planar two-wheel model. The transfer function of this vehicle's dynamic characteristics is given by (1) and (2):
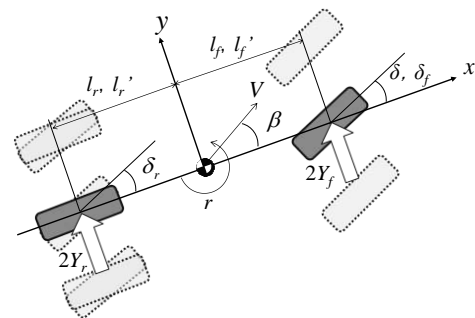
Fig. 1. Vehicle dynamics model.

$$\frac{\beta(s)}{\delta(s)} = G_\delta^\beta(0) \frac{1+T_\beta s}{1+\dfrac{2\zeta s}{\omega_n}+\dfrac{s^2}{\omega_n^2}} \tag{1}$$

$$\frac{r(s)}{\delta(s)} = G_\delta^r(0) \frac{1+T_r s}{1+\dfrac{2\zeta s}{\omega_n}+\dfrac{s^2}{\omega_n^2}}, \tag{2}$$

where the above notation is defined as follows:

$$A = -\frac{m}{2l^2}\frac{l_f K_f - l_r K_r}{K_f K_r}$$

$$\omega_n = \frac{2}{V}\sqrt{\frac{K_f K_r}{mI}}\sqrt{1+AV^2} \qquad \zeta = \frac{m(l_f^2 K_f + l_r^2 K_r)+I(K_f+K_r)}{2l\sqrt{mIK_f K_r(1+AV^2)}}$$

$$G_\delta^\beta(0) = \frac{1-\dfrac{m}{2l}\dfrac{l_f}{l_r K_r}V^2}{1+AV^2}\frac{l_r}{l} \qquad T_\beta = \frac{IV}{2ll_r K_r}\frac{1}{1-\dfrac{m}{2l}\dfrac{l_f}{l_r K_r}V^2}$$

$$G_\delta^r(0) = \frac{1}{1+AV^2}\frac{V}{l} \qquad T_r = \frac{ml_f V}{2lK_r}$$

Here, ω_n refers to the natural frequency, and ζ is the damping ratio. Then, ω_n' and ζ' are defined as changes in the vehicle response properties and are given by (3) and (4):

$$\omega_n' = K_\omega \omega_n \tag{3}$$

$$\zeta' = K_\zeta \zeta. \tag{4}$$

We defined parameters K_ω and K_ζ to denote changes in the vehicle response. K_ω and K_ζ had three patterns (0.6, 1, and 1.4), and ω_n' and ζ' were varied independently. We let the driver feel the response from multiplying K_ω and K_ζ by ω_n and ζ. Therefore, the vehicle's responses r' and β' are expressed by (5) and (6):

$$\frac{\beta'(s)}{\delta(s)} = G_\delta^\beta(0) \frac{1+T_\beta s}{1+\dfrac{2\zeta' s}{\omega_n'}+\dfrac{s^2}{\omega_n'^2}} \tag{5}$$

$$\frac{r'(s)}{\delta(s)} = G_\delta^r(0) \frac{1+T_r s}{1+\dfrac{2\zeta' s}{\omega_n'}+\dfrac{s^2}{\omega_n'^2}} \tag{6}$$

Fig. 2 shows a Bode diagram of the vehicle response. We modified the small electric vehicle into a four-wheel steering vehicle for the experiment, as shown in Figs. 3 and 4. We reproduced this response by using the experimental vehicle.

Fig. 3. Experimental vehicle.

Fig. 4. Diagram of four-wheel steering of experimental vehicle.

We calculated the steer angles δ_f and δ_r for the vehicle response with four-wheel steering, as given in (7) and (8):

$$\frac{\delta_f(s)}{\delta(s)} = \frac{m'l_r'Vs+2l'K_f'}{2l'K_f'}\frac{\beta'(s)}{\delta(s)} + \frac{I's+m'l_r'V+\dfrac{2l_f'l'K_f'}{V}}{2l'K_f'}\frac{r'(s)}{\delta(s)} \tag{7}$$

$$\frac{\delta_r(s)}{\delta(s)} = \frac{m'l_f'Vs+2l'K_r'}{2l'K_r'}\frac{\beta'(s)}{\delta(s)} - \frac{I's-m'l_f'V+\dfrac{2l_r'l'K_r'}{V}}{2l'K_r'}\frac{r'(s)}{\delta(s)} \tag{8}$$

The vehicle motion was controlled in a feedforward function by the given front and rear steer angles. We confirmed the vehicle response by a sweep examination under the following conditions: vehicle speed = 15 km/h, steering wheel angle = 90°, $K_\omega = 1.0$, and $K_\zeta = 1.0$. Fig. 5 shows the results. We confirmed that the real yaw rate followed the calculated yaw rate with the vehicle model well for about 7 s. This is equivalent to steering of less than 1 Hz. When the yaw rate response was over 1 Hz, the phase was delayed, and the gain became small. Based on this, the experimental conditions were set to ensure a sufficient response.

Fig. 2. Comparison of yaw rate frequency responses.
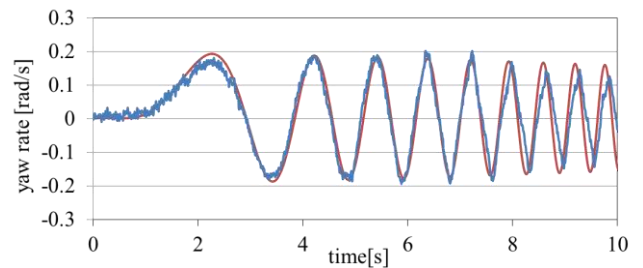
Fig. 5. Comparison of yaw rates of assumed vehicle model and experimental vehicle.
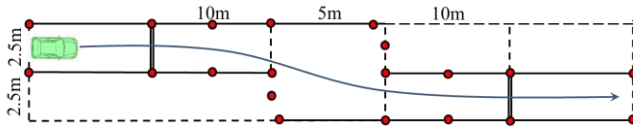
Fig. 6. Experimental course.

Table 1 Experimental subjects

Subject	Driving experience	Frequency of driving	Car class
A	22 years	Every day	sporty
B	4 years	Several days per week	1BOX
C	4 years	Several days per week	sedan
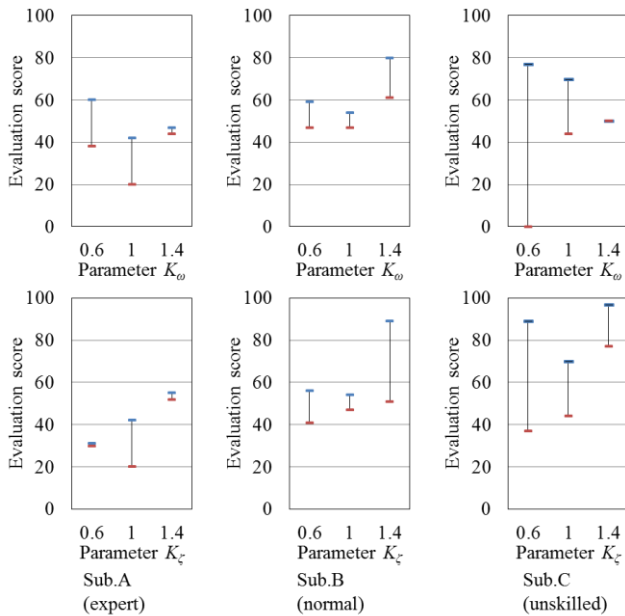
Fig. 7. Subjective evaluations.

2.2. Experimental Conditions

We examined the difference in the driver's characteristics based on vehicle state quantification and subjective evaluations when the driver drove the vehicle under different response conditions. We received permission from the study plan screening committee for humans of our affiliated institution before carrying out the experiment. The experiment utilized a lane change situation, as shown in Fig. 6. We instructed the subjects to drive at a vehicle speed of 15 km/h, and each driver was free to change lanes while traveling over a specified interval. The steering frequency under this condition was about 0–0.3 Hz. Table 1 lists the subjects who were three men. The subjects drove each set of characteristics twice in random order for a total of 10 times. Before the experiment, we described the failsafe mechanism of the experimental vehicle. In addition, each subject was given sufficient time to practice. After each trial, an oral survey was conducted to determine the ease of maneuvering with the vehicle characteristics on a scale.

3. EXPERIMENTAL RESULTS AND CONSIDERATIONS

3.1 Acceptability of Change in Vehicle Response

Fig. 7 shows the subjective evaluation of the ease of maneuvering. All of the subjects felt that the vehicle was easy to operate when $K_\omega = 1.4$. Compared to $K_\zeta = 0.6$, the phase response was similar, but the response of the yaw rate gain was different. Therefore, we believe that the ease of maneuvering was affected by the characteristics of the yaw rate gain. Moreover, the drivers felt that they could maneuver better when the yaw rate gain was appropriately reduced. They also evaluated the vehicle response favorably when $K_\zeta = 1.4$. Compared to $K_\omega = 0.6$, the yaw rate gain was similar, and the phase response was slightly different. The results of the subjective evaluation were about the same when $K_\omega = 0.6$. From these results, the phase delay was found to be acceptable to the drivers under this condition.

3.2. Factors of Subjective Evaluation

Then, we examined the factors that affected the subjective evaluation of the driver. Fig. 8 shows the correlation between various state quantities and the subjective evaluation. Based on the results, the quantities of specific states were found to correlate to the ease of maneuvering. Specifically, significant correlations were confirmed for the maximum yaw rate, steering angle, lateral acceleration in the latter half of a lane change, maximum yaw angle, and lateral deviation from the traffic line center at the end of the maneuver. Fig. 9 shows the transition of these state quantities during the ten experimental trials of each subject's runs. The maximum yaw angle and maximum yaw rate of the latter half converged to a constant value for all subjects.

The traveling trajectory was approximately symmetric in the first and second halves of the lane change. However, the influence of the maximum yaw rate in the latter half on the subjective evaluation differed from that of the maximum yaw rate in the first half. Therefore, we considered the differences in these state quantities. Fig. 10 shows the correlation between the subjective evaluation and the maximum yaw rates of the first and latter halves and their ratio for all subjects. The ratio of the yaw rate and the subjective evaluation showed a correlation, as did the maximum yaw rate of the latter half. From this, the subjects were found to change the maximum yaw rate and operation time in the first and latter halves consciously. Fig. 11 shows the ratio of the yaw rate of the first and latter halves during the ten experimental trials of each subject. Subject A was an expert driver and showed a small unevenness in the ratio of yaw rates. With the better subjective evaluation, the ratio of the yaw rate tended to be small. Therefore, subject A changed the direction of the vehicle for large yaw rates quickly during the first half and changed the direction slowly during the latter half. A similar tendency was shown by all subjects.
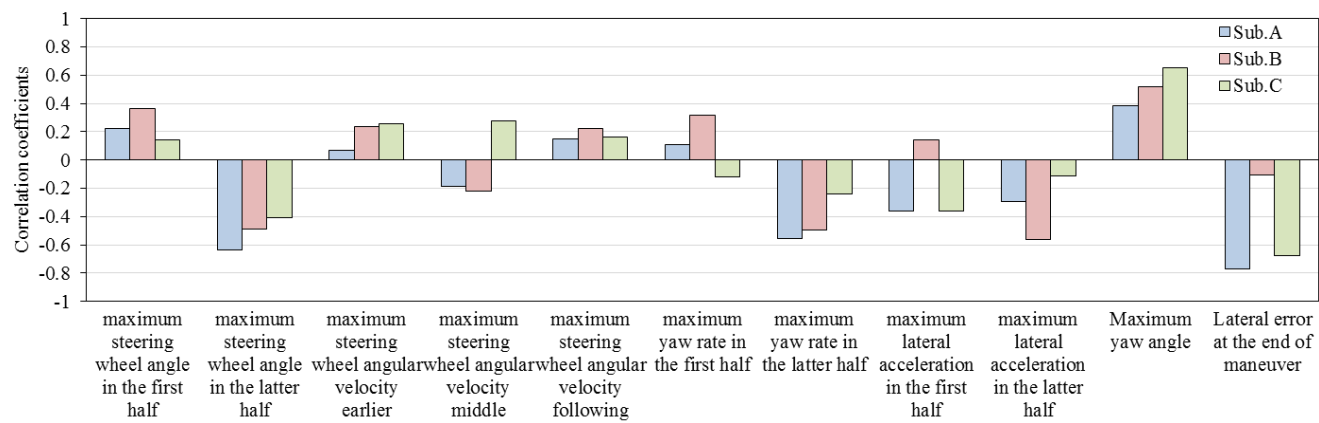
Fig. 8. Correlation between subjective evaluation and each state quantity.
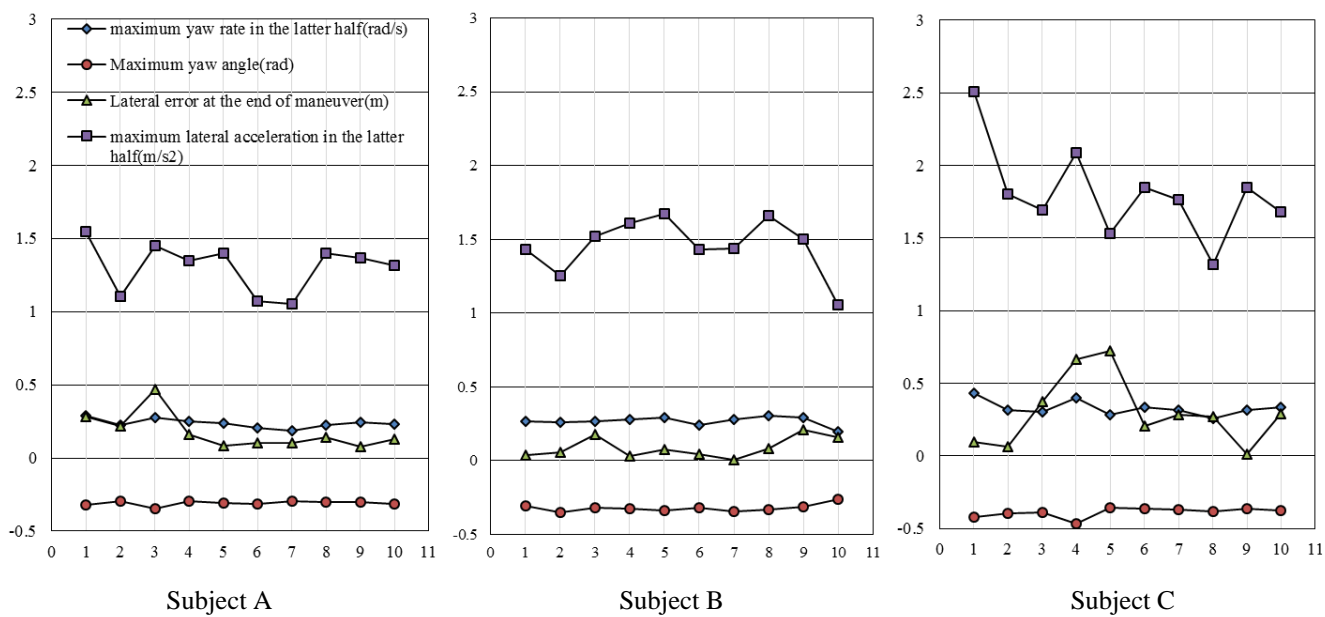
Fig. 9. Transition of some state quantities during ten experimental trials of each subject.
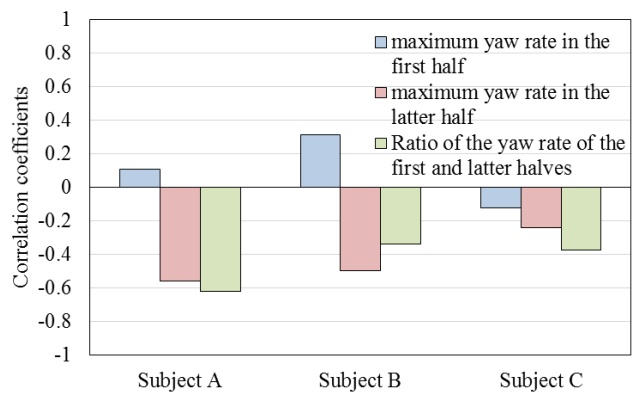
Fig. 10. Correlation between subjective evaluation and maximum values for the yaw rate of the first half, the latter half, and ratio for each subject.
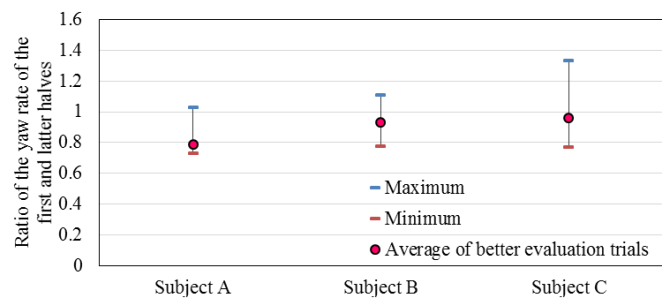
Fig. 11. Ratio of yaw rate of first and latter halves for ten experimental trials of each subject.

Fig. 12 shows the relationships between the relative yaw angle and the subjective assessments of all the subjects. The yaw angle was found to vary for each subject. Despite the different response characteristics, the subjects operated the vehicle to approach the target yaw angle. Therefore, the target yaw angle was considered to be different for each subject, and the traveling trajectory could be characterized.

3.3. Target trajectory during Lane Change

The trace of a lane change is often similar to a sigmoidal curve. Therefore, we defined the traveling trajectory during a lane change by using a tanh function in the coordinate system of the fig. 13 as follows:

$$y(x) = \frac{D}{2} \tanh(w(x) \bullet x) \tag{9}$$

Here, D is the lateral displacement, and $w(x)$ is a weighting function. The slip angle of the vehicle should be 0 for simplification. The weighting function $w(x)$ was assumed to

be a first-order function. The yaw angle θ and yaw rate r can be expressed as follows:

$$w(x) = ax + b \tag{10}$$

$$\theta = \tan^{-1} \frac{\Delta y(x)}{\Delta x} \tag{11}$$

$$r = \frac{d\theta}{dt} \tag{12}$$

Based on this, the maximum yaw angle and ratio of the maximum yaw rates of the first and latter halves demand coefficients a and b for the weighting function to match the experimental results. We found that the mean of three trials of the better subjective evaluation expressed the characteristics of the subject and referred to this value. Table 2 gives the reference value and the calculated coefficients a and b of each subject. Fig. 14 compares the experimental results and model of subject A. Despite being a simple weighting function, the model agreed with the experiment result wells, and the differences in the travel trajectory of each driver could be determined. Therefore, we believe that we can extract the driving maneuver characteristics of each driver to accumulate the quantities of vehicle states during daily driving to calculate the coefficients a and b.

4. CONCLUSIONS

We examined the acceptance of drivers based on a subjective evaluation and the vehicle state during a lane change under different vehicle response conditions. Using the characteristics of the traveling trajectory during a lane change, we classified the attributes of different drivers. We obtained the following conclusions:

1. The drivers felt that they could maneuver better when the yaw rate gain was appropriately reduced.

2. The target yaw angle and the ratio of the yaw rates of the first and latter halves were considered to differ by subject and could be used to characterize the traveling trajectory during a lane change.

3. We suggested a numerical formula to characterize the trajectory during a lane change.

4. The coefficients of the weighting function calculated from the maximum yaw angle and the ratio of the yaw rates of the first and latter halves differed for

Fig. 12. Relationship between relative yaw angle and subjective assessments of each subject.

Table 2 Referred value of yaw angle, ratio of yaw rate, and calculated coefficients a, b

	Sub.A	Sub.B	Sub.C
Average yaw angle of better evaluation trial	-0.3028 (rad)	-0.3026 (rad)	-0.3802 (rad)
Average ratio of yaw rates of first and latter halves of better evaluation trial	0.7896	0.9334	0.9608
Coefficient a	-0.009	-0.002	-0.002
Coefficient b	0.249	0.249	0.319

Fig. 13. Coordinate system of the target trajectory.

Fig .14. Comparison between experiment results and model of subject A.

each driver.

Based on our results, we demonstrated that our approach can potentially be used to classify drivers through the accumulation of daily driving data.

REFERENCES

Aoki, Y. et al. (2011). A study on relation between fundamental vehicle response parameters and handling quality evaluation, *JSAE Annual Congress Proceedings*, No. 20115817. JSAE, Sapporo.

Abe, M. (2012). *Automotive Vehicle Dynamics – Theory and Applications*, pp. 88–102. Tokyo Denki University Press, Tokyo.

Ishio, J. et al. (2007). Vehicle handling quality evaluation through model based driver steering behavior, *Proceedings of the 20th IAVSD Symposium*, Berkeley.

Driving support systems to encourage safe driving in complex situations: providing information to the driver in a less distracting manner

Satoru Takenaka* Sayaka Nogami** Yukiyo Kuriyagawa** Haruhiko Nakatsuji*** Yosuke Tate*** Hiroki Seto***

*Nihon University Graduate School, 1-2-1 Izumi-cho, Narashino-shi, Chiba, 275-8575, Japan
*JPN (Tel: 047-474-9879; e-mail: cisa14017@g.nihon-u.ac.jp)
**Nihon University, 1-2-1 Izumi-cho, Narashino-shi, Chiba, 275-8575, Japan
*** Alpine Electronics, Inc., 1-7 Yukigayaotsuka-machi Ota-ku Tokyo, 145-0067, Japan

Abstract: The premise of driving support systems is to reduce a driver's load and traffic accidents as a whole. However, we feared that such systems can degenerate a driver's ability by causing an overreliance on driving assistance systems consciously and/or unconsciously. Therefore, we produced a pre-reminder system that reduces encounters with accident factors by helping the driver turn their attention back to safe driving methods. We installed the system in a driving simulator and conducted an experiment to assess the system. As a result, the pre-reminder system did work as intended, and the driver's behaviour was focused more on the road, lessening overreliance on road safety systems.

Keywords: Man/machine systems, Human factors, Driver behaviour

1. INTRODUCTION

Recently, various driving assistance systems which reduce traffic accidents, human error and driver load have been developed. Drivers can use these systems for increased safety in various situations. However, traffic accidents still result in over 4,000 fatalities per year. In recent years, fatal traffic accident incidences are often the result of aimless driving. Table 1 shows the main violations. In response to this problem, studies have been conducted to actively estimate the driver's state in operation based on physiological reaction and driver behaviour. However, a technique for detecting the state of aimless drivers in real time and with high accuracy has not yet been established. In addition, as one of the driving support issues includes overconfidence and distrust, there is concern that a driver's ability will be negatively impacted if they rely on these systems too much. For example, if the driver uses a front of the obstacle detection alarm, he or she is more likely to neglect attention to the front.

Table 1 Main violations of fatal accidents in Japan

Main violations	No.	%
Aimless driving	687	16.1
Inattentive driving	542	12.7
Failure of operation	504	11.8
Failure to drive safely	432	10.1
Pedestrian interference, etc.	248	5.8

Therefore, we suggest a driver assistance system in an attempt to avoid dangerous situations in advance. ure 1 shows the driver assistance system in regards to our concept. Here, conventional driver assistant systems consist of the warning system and the vehicle control system, so when a driver cannot cope alone in a particular situation, these systems will be activated. On the other hand, our system gives drivers a pre-reminder for a potentially hazardous situation. This pre-reminder promotes safe driving, and can expect resultant effect of drivers avoiding encounters with accident factors, or even if an accident factor occurs, reacting instantly and smoothly to warnings. We then expect that drivers will maintain and improve their driving ability because they are not over-relying on present safety systems.
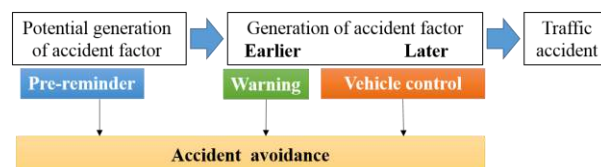
.1 Concept of proposed driver assistance system

Some existent systems of driver support against potential hazardous situations include warning signboards and paintings of roads and walls to reduce highway speeds. However, these require enormous provisions for all roads, and will provide information in the same way to all drivers. On the other hand, a pre-reminder can be provided at a low-cost, and respond flexibly to changes and newly created roads and temporal traffic situations. In addition, it is possible that a pre-reminder could structure individual assistance in accordance with the characteristics of drivers; for example, the elderly may be supported with earlier responses, while beginners may be supported with more frequent responses.

Furthermore, this pre-reminder is expected to develop into a more advanced support via progressing information technology such as cloud technology.

In this study, we checked the pre-reminder system in a complex environment using a driving simulator. We examined whether this system can increase a driver's attention and lower the possibility of an accident.

2. PERSONAL FIT OF THE PRE-REMINDER

2.1 Drivers acceptant of the pre-reminder

Existing warnings or vehicle controlling devices are effective at decreasing accident factors. Therefore, we think that the system would readily be accepted by the driver even if the system is somewhat irritating. However, the driver may have difficulty with the effects of the pre-reminder because the situation may have already been made less dangerous by the support offered through additional driver safety systems. As a result, the driver may have a greater tendency to ignore a pre-reminder which can be irritating. Therefore, the pre-reminder is aimed to be as non-irritating as possible, whilst still having the desired effect. From this, the drivers were adjusted to the pre-reminder in order to accept it positively before assessment of the system.

2.2 Traffic scenes and scenarios

We prepared a traffic situation that simulates a city, consisting of complex environments aimed to increase the possibility of generating higher accident factors using a driving simulator (DS). The complex environment consists of two situations which simulate crowded sidewalks or many parked vehicles. When approaching this section, the DS provides support beforehand by using the pre-reminder system.   ure 2 shows one traffic scene.
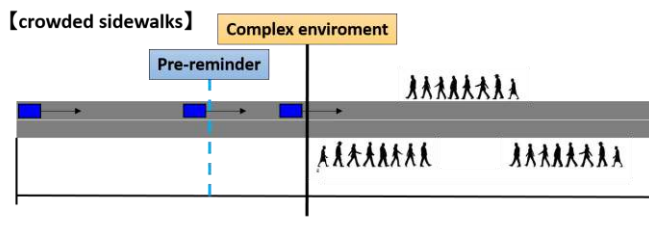
.2 Traffic scene of crowded sidewalks

2.3 Pre-reminder of high risk potential system

The useful information differs among the level of the individual driver's driving skill. The reasoning behind this approach is that it considers different margins in driving abilities. Thus, the pre-reminder should change the methods of support according to the skills of the driver in order to ensure personal fit. Contents of the pre-reminder are summarised in Table 2.

Table 2 Two types of the pre-reminder

Pre-reminder	Driving skills	Contents of the pre-reminder		
		Sound	Display	Announce
alpha	High	ON	ON	OFF
beta	Low	ON	ON	ON

The pre-reminder is designed to initially play a sound to alert the driver to a potential hazard. Then, both text and an image denoting either high pedestrian concentrations or parked vehicles are displayed. This image is illustrated in ure 3.The pre-reminder audio announces 'attention to speed' by voice at the same time as the image appears on the screen. The reason for the presence or absence of the announcement is as follows. The highly skilled driver that can be judged of their own accord felt discomfort when instructed by the announcement. The low-skilled driver, however, whose skills are inadequate to judge their own driving abilities, felt grateful for the announced instruction.

. 3 The displayed illustration

2.4 Participants

In this experiment, we have selected 12 participants by carrying out a pre-questionnaire distributed to about 60 people. The pre-questionnaire prompted participants to respond on their driving experience and driving frequency, for example. In addition, participants were asked to respond as to whether or not they would use two types of pre-reminders in a situation where several aimless states are present (see Table 2). Experimental participants chose the following people: 'people with high skills who responded that they use alpha' and 'the people with low skills who responded that they use beta'. There were six participants each in the high skills and low skills categories. The 12 paid participants all had a driver's license and drive frequently. The average participant age was 41.3±12.6 years. Participants gave written informed consent to participate in this experiment.

All experiments reported in this paper were executed by permission of the president of College of Industrial Technology, Nihon University in accordance with the report of the Ethics Committee (Approval No. S2014-4).

2.5 Personal fit of the pre-reminder

In this pre-reminder, the following four factors were applied for personal fit: timing, type of sound, loudness, and screen position. Experimental participants were personally fit while experiencing the actual system. The timing was controlled at a distance from the complex environment. As a result, the overall average timing became -120 ± 44.2 [m]. Kind of the sounds they select the most like one individually from among the three types. As a result, they were divided into three to five members according to each sound. As to the position of the screen, due to the constraints of the

experiment, the two options given were in the centre console or in the instrument panel position. As a result, 10 participants selected the dashboard position. In addition, after the personal fit, experiment participants experienced both the alpha and beta of the pre-reminder. As a result, 9 out of 12 participants evaluated the beta as more useful.

3. EVALUATION OF THE PRE-REMINDER SYSTEM

The pre-reminder was made to provide basic personal fit within certain parameters, but the following preferences were common among participants: the display set in the dashboard position, and the use of beta support exclusively.

3.1 Traffic scenes and scenarios

Observation of the exclusive use of the pre-reminder has been conducted several times. Thereafter, the DS provided the pedestrian detection warning with a generated pedestrian designed to rush out in front of the driver. To confirm the effects of the pre-reminder to an unexpected pedestrian rushing into traffic, participants were divided into two groups; one being the 'group that receives the pedestrian warning after the pre-reminder' (group A) and the other being the 'group that receives the pedestrian warning turned off the pre-reminder' (group B). This scenario is indicated in   ure 4 and Table 3.
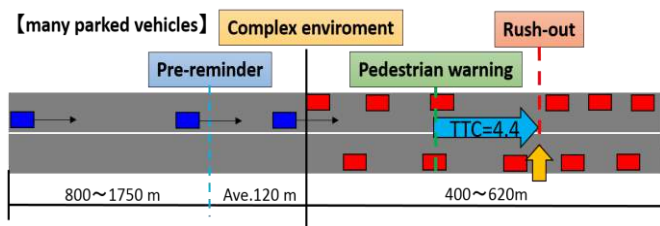
.4 Simulated scenarios

3.2 Pedestrian detection warning system

The pedestrian warning is raised 4.4 seconds before the vehicle reaches the pedestrian hazard (Time To Collision: TTC=4.4). In addition, when the driver cannot see the pedestrian, a warning is raised. An alarm sounds a beeping noise along with voice guidance lasting 1.5 seconds.

3.3 Experimental procedure

First, we taught the participants to use the pre-reminder system for the first time. We produced the initial systems training to not include generating hazards, such as pedestrians rushing into the road. Next, we asked participants to drive using the system as intended. The drivers then experienced pedestrians rushing into the road after running the simulation 17 times.

Table 3 Experimental order

No.	Pre-reminder	Driver condition	Rush-out
1	ON	Usual	-
2	ON	Aimless	-
3	ON	Usual	-
4	ON	Aimless	-
5	ON	Usual	-
6	ON	Aimless	-
7	ON	Usual	-
8	ON	Aimless	-
9	ON	Usual	-
10	ON	Usual	**Occur**
11	ON	Usual	-
	Recess		
	Pre-reminder	Driver condition	Rush-out
12	ON	Usual	-
13	OFF	Usual	-
14	ON	Usual	-
15	OFF	Usual	-
16	ON(A) or OFF(B)	Usual	**Occur**
17	ON	Usual	-

3.4 Measuring items

We measured three types of data: the subjective ratings of participants, driver operations, and gaze behaviour. The subjective rating could be scored from a range of zero to 100, zero meaning 'Disagree totally' and 100 meaning 'Agree totally'. The driver operations consisted of vehicle speed, pedal operation, and the x, y and z positions of the vehicle by the DS.

4. INFLUENCE ON THE EVALUATION BY THE DRIVERS' EXPERIENCE

We confirmed that the average speed was deceleration average 63 ± 4.4 [km / h] from 57.0 ± 0.6 [km / h] in the target section by the pre-reminder.

ure 5 shows the results of the subjective ratings regarding 4 conditions. From this   ure, many drivers positively evaluated the system as less irritating and useful. By increasing the variation of pedestrians rushing out, it seems that the pre-reminder systems influenced the effect of the pedestrian warnings. Therefore, in the next section, we consider focusing on the evaluation and effects of the pedestrian warning when pedestrians rush out into the road.
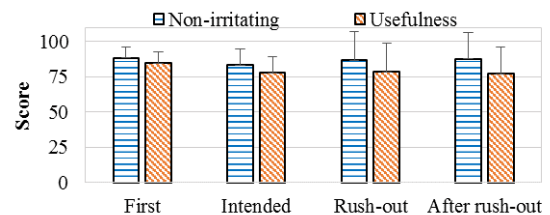
.5 The subjective ratings for non-irritating and usefulness

5. INFLUENCE ON THE DRIVER BY RUSH-OUTS

We consider the results of 8 drivers, who had the same rush-out hazard scenarios in the DS.

5.1 Subjective ratings of the pedestrian warning

ure 6 shows the results of the subjective ratings regarding group A and group B. From this   ure, group A evaluated a high score of suitable timing. It seems that group A paid attention when the warning was raised by the pre-reminder system. Therefore, the driver detected the pedestrian quickly and proceeded with smooth operation of the vehicle after the warning was raised.
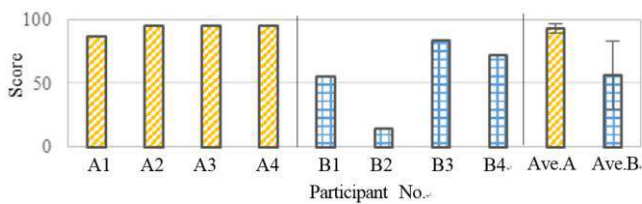
.6 Subjective ratings regarding suitable timing

5.2 Driver behaviour

We calculated the corresponding time of recognition, judgement, and operation in 4 sections consisting of 5 points in regards to the coping behaviour process after the warning was raised. Specifically, these were 'raised the warning', 'released the accelerator', 'started stepping on brake', 'maximised brake pedal force', and 'stopped the car'. We also calculated time when the driver 'found the pedestrian'.
ure 7 shows the results of drivers' coping behaviour.
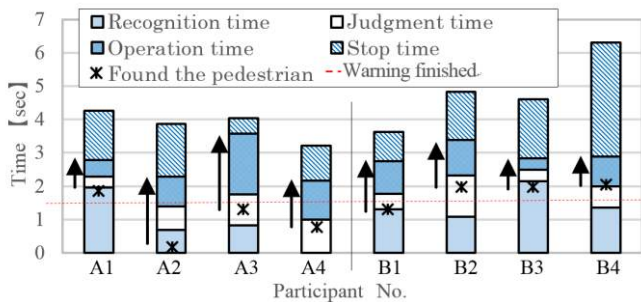
.7 Time course of drivers' coping behaviour

Note: Arrow in   .7 denotes time from finding the pedestrian to applying maximum force to the brake pedal.

From this   ure, group A has a longer time between the point of 'maximised the brake pedal force' and the time they 'found the pedestrian' as compared to group B, showing that with the warning, group A drivers typically spotted the hazard earlier, and stopped the vehicle in a more controlled manner. Without the pre-reminder system group B drivers reaction times were stressed, causing rapid 'maximised brake pedal force' times. This resulted in a slower response, and a less controlled stop of the vehicle for group B participants. Drivers that gained a better score with the warning system found the pedestrian early, so it seems that the driver soon adapted the system into their coping behaviour. The drivers evaluated the system highly despite the sudden changes they were required to make. For this reason, we think that the drivers will highly benefit from the effects of pre-reminder systems.

6. CONCLUSIONS

In complex situations when generating accident factors, the driver can find the hazard earlier, resulting in smooth operation and better judgement of the vehicle courtesy of the new pre-reminder system. The drivers appreciated the effects of the pre-reminder system before the hazard manifested, and fared better than those only given a standard sudden action announcement by the system. Pre-reminder systems therefore show good potential in regards to further cutting the number of potential accidents.

In future studies, the pre-reminder must be evaluated in several other driving scenarios to address the limitation of few participants in this paper.

REFERENCES

Ayumi Han et al., '"Optical Dot System" as Assistance for Drivers to Visualize Affordance of Road Environment – Development and the Result of Four Years Empirical Analysis', *Seisan Kenkyu,* Vol.66, No.2, p.p.147-154, (2014).

Cabinet Office, Government of Japan, 'White Paper on Traffic Safety', 2013 edition: (2013).

Hiroshi Takahashi, Hirohiko Honda, 'A Proposal of Driver Assistant System with Subliminal Visual Mark', *Proc. of Jpn.Soc. Mech. Eng.*, Vol.2010 No.7, p.p.155-156, (2010).

Hiroshi Uno et al., Study on Communication of Criticality and Urgency Using Physical Qualities of Visual and Auditory Displays, *Proceedings of JSAE*, Vol.31, No.4, p.p.73-78, (2000).

Issei Ichikawa, 'Construct and Evaluation of Reminder System for Driver Assistant Systems', *Nihon University Graduate school of Industrial Technology Master's thesis*, (2013).

Kouichi Kuroda et al., 'Study of Useful Information for Driver Assistance (Second Report) -Composition of the Providing Information Rules to Increase Benefit of the Information', *Transactions of JSAE*, Vol.43, No.1, p.p.141-146, (2012).

Analysis of Drviers' Behavior
at Non-signalized Intersection Without Right-of-Way
Using a Developed Simulation Program

Kei Sato*, **Hiroshi Mouri***, **Masao Nagai****

** Tokyo University of Agriculture and Technology, Tokyo, 184-8588
JAPAN (Tel: +81-42-388-7419; e-mail: keimsato@ cc.tuat.ac.jp).
**Japan Automobile Research Institute, Tokyo, 105-0012, JAPAN (e-mail:
mnagai@jari.or.jp*

Abstract: In Japan, many head-on collisions occur on subsidiary roads at non signalized intersections and elderly drivers tend to cause this type of accidents. Therefore, to clarify the principal accident causation of head-on collisions is strongly required in our country which is an aging society. In the current study a simulation program was established based on the experimental data and the driving behavior of expert drivers and elderly drivers were compared with focusing on the collisions with crossing bicycles, drivers' confirming safety behavior and their foot positions.

Keywords: **Non signalized intersection, Driver behavior, Simulation**

1. INTRODUCTION

Currently, approximately 50 thousands of fatal and heavily injured accidents occur per year in Japan. Of all the types of accidents, head-on collisions, which are the most frequent type of accidents, account for around 30% of the total number of accidents [1]. Therefore, various studies have been performed which aim at reducing this type of collisions. We also gathered the data of elderly drivers and expert drivers and reported the detail of their behavior at non signalized intersections focused on the change of velocity and the confirmation the safety [2].

In this study a simulation program was developed based on experimental data and the crossing bicycles with various velocities were set up to clarify the causalities between head on collisions and elderly drivers' behaviour.

2. EXPERIMENTAL PROCEDURE

The experiment was conducted on the test course of Japan Automobile Research Institute. A non signalized intersection was constructed by using an array of containers. Seven expert male drivers and a total of 10 healthy elderly drivers in their seventies and eighties were included in the study. All participants gave written informed consent to all aspects of this study to participate in this study. The participants were instructed to perform their usual drive at approximately 40 km/h and drive 10 times. The experimental vehicle which was equipped with a continuous logging drive recorder and 7 cameras was used. The driver's face angle was recorded by the 3D yaw motion sensor which was attached to a cap. The velocity of experimental vehicle, acceleration, images of the front of the vehicle (center, right and left), the rear of the vehicle, drivers' foot position and face were recorded by drive recorder.

This experiment was conducted as a blind test and all procedures were approved by the ethical committee of Tokyo University of Agriculture and Technology.

3. CONSTRUCTION OF SIMULATION PROGRAM

The vehicle and drivers' behavior when passing through the intersection were emulated based on experimental data, e.g., the velocity of vehicle and drivers' face angle. The positional relation of bicycle and host vehicle is shown in Fig. 1.
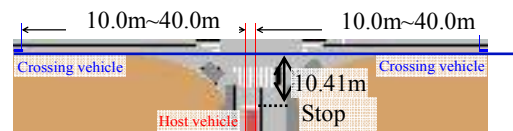
Fig.1 The positional relation of bicycle and host vehicle

Drivers' view The drivers' view was set up based on their recorded face angle. The range of view is sector form and its radius is 100 [m]. The maximum range of view was fixed as 35 [deg] for the right and left sides.

Host vehicle When the bicycle enters into the driver's view the host vehicle starts deceleration after the elapse of a certain period of time. This time depends on the position of driver's foot. The time was set as 0.30 [s] when driver's foot is on the brake pedal and when it is on the accelerator pedal it was fixed as 0.77 [s] for expert drivers. For elderly drivers it was set based on obtained experimental data using driving simulator (Table 1).

Bicycle The bicycle which crosses in the front of host vehicle was set for the simulation. It drives on the line which is lined 10.41 m from the stop line and starts at various positions (Y_{Bike} [m]; 10.0, 11.0, … 39.0, 40.0) with various velocities (V_{Bike} [km/h]; 5.0, 6.0, … 29.0, 30.0) from the right

and left side. The total patterns of crossing bicycle is 1612 for both sides.

Table 1. Reaction time

Driver	Foot position	Time [s]
Expert	0.0: Treadle accelerator pedal	0.77
	-1.0: Set accelerator pedal	
	-2.0: Middle	
	-3.0: Set brake pedal	0.30
	-4.0: Treadle brake pedal	
Elderly	0.0: Treadle accelerator pedal	0.93
	-1.0: Set accelerator pedal	0.77
	-2.0: Middle	0.77
	-3.0: Set brake pedal	0.41
	-4.0: Treadle brake pedal	0.37

As described above when the bicycle enters into the driver's view the host vehicle starts deceleration. As shown in Fig. 2, only between the timing of detection of bicycle and the start of deceleration is simulated section.
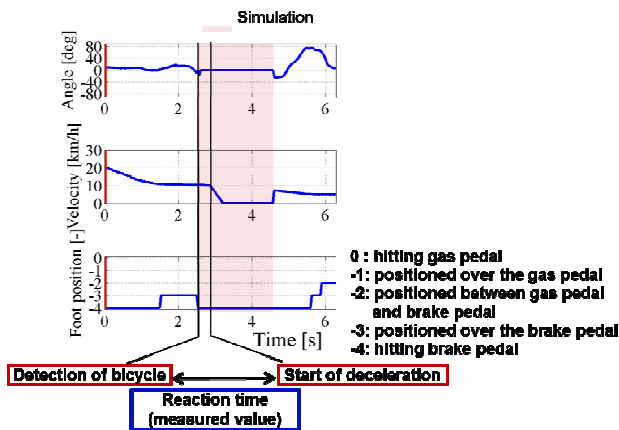
Fig. 2. Drivers' view

4. RESULTS

Because of space of limitations the data of elderly driver S1 (1st lap) is shown as an example. In Fig. 3 the collisions with bicycle and host vehicle are displayed. The x axis indicated the position of bicycle and the y axis shows the velocity of bicycle. The triangle symbol indicates the case the vehicle collided with bicycles even though driver detected them. The square mark means the collision with no detection of bicycles. S1 collided with 124 bicycles on the left side. With bicycle from the right side, 162 collisions occurred.

The face angle and the velocity of host vehicle are shown in Fig. 4. The x axis indicates distance from the vehicle side. The degree of face angle is 0 [deg] when driver faces to the front of the vehicle, the positive value indicates the angle of left side and the negative value means the right side.

S1 did not stop at the stop line and entered into the intersection with high velocity and tended to confirm the safety of the right side, therefore, the detection of bicycle from the left side was delayed. Thus, high velocity near the intersection and partial confirmation behavior induced collisions with bicycles.

Left side   Right side
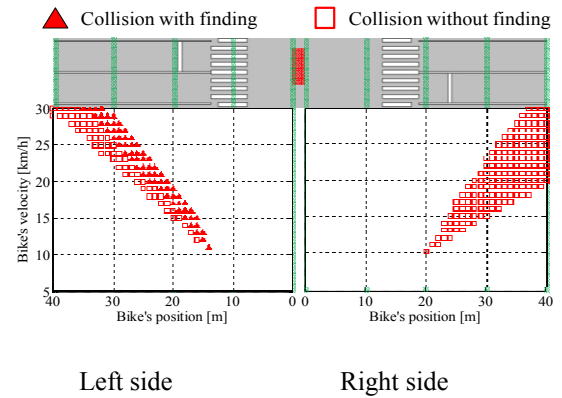
Fig. 3. Collision with bicycle

Left side   Right side
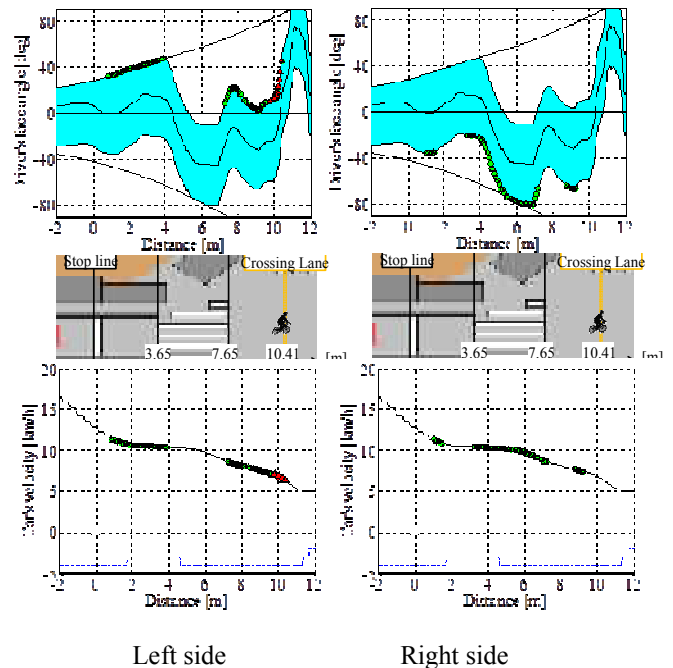
Fig.4. Driver's face angle and velocity profile

5. CONCLUSION

The simulation program was constructed based on experimental data and the elderly drivers' driving behavior was evaluated. The data of expert drivers and the rest of elderly drivers were also analysed.

REFERENCES

ITARDA INFORMTATION. (2007). Collision at intersection from point of view road environment. Institute for Traffic Accident Research and Data Analysis, No.69.

K. Sato et al. (2014) Analysis of Driver Behavior at Unsignalized Intersections of Urban Area - Comparison of Expert and Elderly Drivers-, Journal of Automotive Engineering, Vol. 45, No. 2, pp.425-430

i

Automatic Parking System for Electrified Vehicles Using Sonar Sensors

Michitoshi Azuma*, Kazuto Yokoyama**, Yukiyasu Akemi**, Toshihide Satake*, Ryotaro Suzuki***

** Automotive Electronics Development Center, Mitsubishi Electric Corporation,
840, Chiyodamachi, Himeji-shi, Hyogo 670-8677, Japan (e-mail: Azuma.Michitoshi@dc.MitsubishiElectric.co.jp)
** Advanced Technology R&D Center , Mitsubishi Electric Corporation, 8-1-1, Tsukaguchi-Honmachi, Amagasaki City,
Hyogo 661-8661, Japan (Tel: +81-6-6497-7698; e-mail: Yokoyama.Kazuto@ab.MitsubishiElectric.co.jp).
*** Sanda Works, Mitsubishi Electric Corporation,
2-3-33, Miwa, Sanda-shi, Hyogo 669-1513, Japan (e-mail: Suzuki.Ryotaro@ce.MitsubishiElectric.co.jp)*

Abstract: Mitsubishi Electric has been developing an automatic parking system. The main part in the system is provisionally named e-Park controller. It executes PSM (parking slot measurement) using our sonar sensors to find a parking slot available. Simultaneously, the controller estimates states of the vehicle and calculates an optimal path to the parking slot. After the path planning, reference signals for our electric power steering and driving motor control systems are generated to track the path automatically. The parking can be executed externally using our device for the keyless entry system. For safety, the parking system also has an emergency braking function based on the sonar sensors and operation of the driver. This paper mainly focuses on the design of the path planning algorithm and the vehicle speed controller. The automatic parking system is verified in experiments.

Keywords: Automatic Parking, Electrified Vehicle, Sonar, Path Planning, Optimization, Vehicle Speed Control, Feedforward Control.

1. INTRODUCTION

Various driving assist systems that relieve burden of drivers and enhance safety of vehicles have been put into practice in the world. Mitsubishi Electric has been developing several technologies to realize the systems. One of them is the automatic parking system. The system consists of our products such as a sonar sensor (ultrasonic sensor), an electric power steering (EPS), a motor, an inverter, and a keyless entry system. In the automatic parking system, a main controller provisionally named e-Park (easy park) plays an important role. First, the e-Park controller processes signals
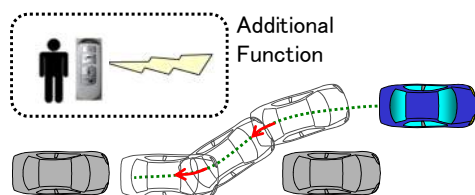
Fig. 1. Automatic parking.
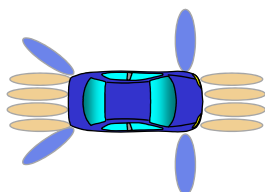
Fig. 2. Configuration of the sonar sensors.

from the sonar sensors and find an available parking slot simultaneously estimating the position and the attitude of the vehicle. Second, an optimal path to park is calculated considering physical constraints of the vehicle and its surroundings. Third, the e-Park controller commands reference signals for the driving systems such as the EPS and the motor while the driver gives an execution signal through an interface as shown in Fig. 1. The signal can be transmitted with our device of the keyless entry system from the outside of the car. Finally, the vehicle automatically tracks the desired path. This paper mainly focuses on the design of the path planning algorithm and the vehicle speed controller. The automatic parking system is verified in experiments.

2. AUTOMATIC PARKING SYSTEM

2.1 Overview of Automatic Parking System

In the automatic parking system, the vehicle is equipped with 12 sonar sensors as shown in Fig. 2. A block diagram of the system is shown in Fig. 3. The main part of the system is the e-Park controller. It consists of the PSM (parking slot measurement), the vehicle state estimator, the obstacle detector, and the path planner. Outputs of the controller are the reference signals to the drive systems of the vehicle.

2.2 Sonar Sensor System

Two front side sensors are used for the PSM. Four bumper sensors are attached each in front and rear. They are used to detect obstacles around the vehicle. Two rear side sensors
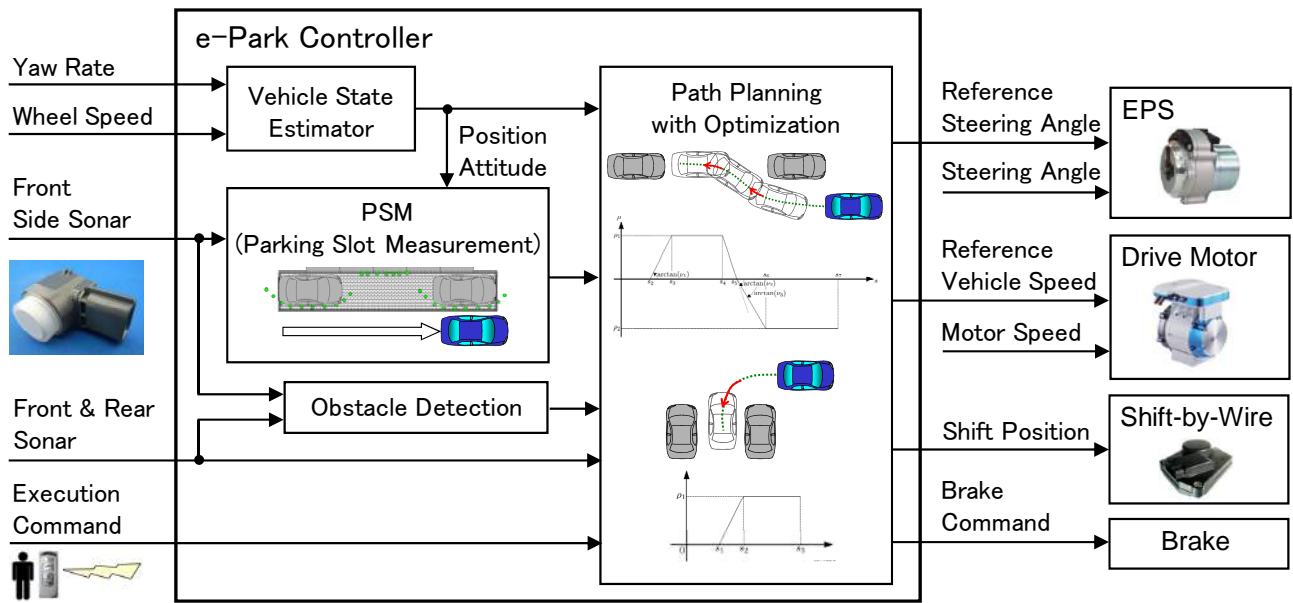
Fig. 3. Block diagram of the automatic parking system.

detect the corner of the cars next to the target parking slot. The information of the corner is also used to compensate the position of the vehicle for the perpendicular parking in real time.

2.3 e-Park Controller

The PSM takes a major role in the e-Park controller. The slot length, depth, presence or absence of curbs, and the road width (the space margin to swing the front end of the vehicle in parking motion) are detected with the PSM. It also judges a level of difficulty to park the vehicle to the detected slot.

After the parking slot is found, the e-Park controller calculates a feasible parking path considering physical constraints to drive the vehicle smoothly and avoid collision with environments. The path consists of straight lines, arcs, and clothoid curves. An optimization technique is used to minimize the position error from a reference line which passes a goal position. Fig. 4 shows a problem setting of the path planning for perpendicular parking. The planned optimal path is given as a relationship between the travel distance and the path curvature that is converted to the steering angle. The planning algorithm supports both the perpendicular and the parallel parking. The detailed design is described in the next section. The e-Park controller automatically changes the shift depending of the surroundings, the position and the attitude of the vehicle to reach the desired position.

In the process of the PSM and the parking motion, the position and the attitude of the vehicle is estimated with dead reckoning using wheel sensors and a Kalman filter. The e-Park controller has a failsafe mechanism that stops the vehicle when a mismatch of the vehicle position between the results from the dead reckoning and the sonar sensing occurs.

In the automatic parking mode, the vehicle is allowed to move while the driver commands the execution signal through an interface. It can be a push button on the device for the keyless entry system, which enables us to park the vehicle externally. The e-Park controller also has a function to stop the vehicle in an emergency. When an obstacle which is closed to the vehicle is detected with the sonar sensors, the controller immediately commands a brake signal to avoid collision.

2.4 EPS Controller

The steering angle is controlled to track the planned path from the e-Park controller. A block diagram of the EPS controller is shown in Fig. 5. In the automatic parking mode, the steering angle controller is mainly activated. In the case the driver try to operate the steering by his/her self, the EPS system stops the steering angle control and activate the standard EPS controller to put the steering control into the driver's hand. This makes the automatic parking system flexible to the driver's judgement.

2.5 Vehicle Speed Controller

The vehicle speed controller is designed for electrified vehicles to drive the motor and track the reference speed from the e-Park controller. A block diagram of the speed controller is shown in Fig. 6. The controller realizes accurate motion of the vehicle taking advantages of motors: quick response and precise and large torque even at a low speed. However, the speed of the response cannot be made arbitrarily fast because the powertrain is not an ideal rigid body. In our previous work, dynamics of the powertrain are considered in the derivation of the controller not to excite vibration (Yokoyama et al. 2015a, b). In our present system, a feedforward controller has been added to improve the

(a) Problem setting of perpendicular parking.

(b) Path for perpendicular parking.
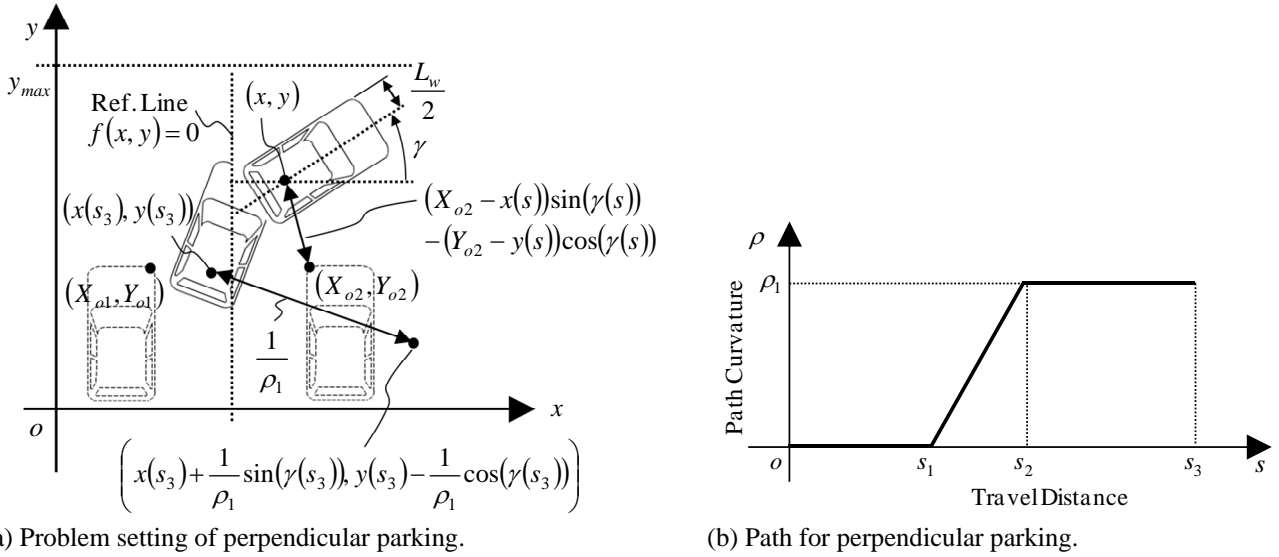
Fig. 4. Optimal path planning.
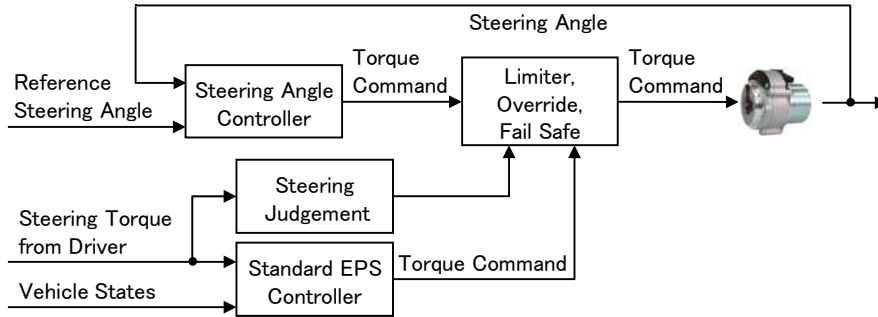
Fig. 5. Block diagram of the EPS controller.
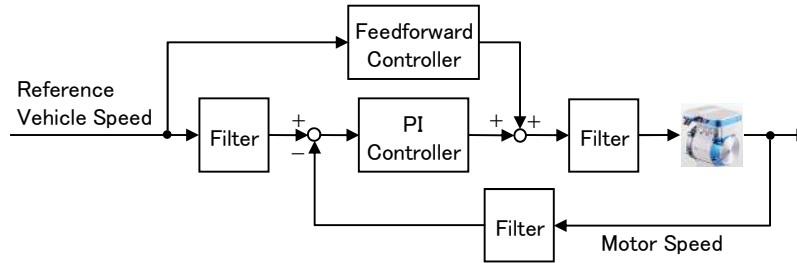
Fig. 6. Block diagram of the vehicle speed controller.

response further. The direction of the travel is automatically controlled on the basis of the commands from the e-Park controller without the driver operating the shift.

3. PATH PLANNING ALGORITHM AND VEHICLE SPEED CONTROLLER DESIGN

This paper mainly focuses on the path planning algorithm and the vehicle speed controller. The design procedures are shown in the followings.

3.1 Path Planning

Our path planning algorithm is divided into two steps, which is a feature of our parking assist system. In the first step, a path from the start point of the parking motion to the first turning back position is planned. The calculation is based on an optimization to minimize the position error from a reference line which passes the goal position. The first step has a merit to guide the vehicle to the neighbourhood of the goal position efficiently. In the second step, the path is planned in a feedback manner to compensate the detection error of the parking slot obtained from the initial PSM.

The vehicle model used for the path planning is

$$\frac{dx}{ds}(s) = \mathrm{sgn}(v_x)\cos(\gamma(s))$$

$$\frac{dy}{ds}(s) = \mathrm{sgn}(v_x)\sin(\gamma(s)) \tag{1}$$

$$\frac{d\gamma}{ds}(s) = \rho(s)$$
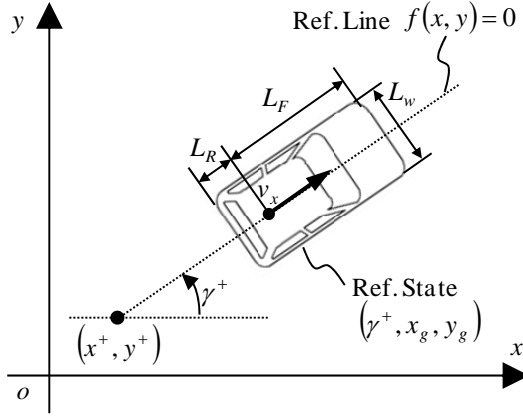
Fig. 7. Reference line and reference state.

$$0 < s_1 \leq s_2 \leq s_3$$

$$0 < \rho_1 \leq \rho_{max}$$

$$0 < v_1 \leq v_{max}$$

$$\max_{s \in [0, s_3]} y(s) + L_F \sin(\gamma(s)) + \frac{L_w}{2} \cos(\gamma(s)) \leq y_{max}$$

$$\max_{s \in [0, s_3]} (X_{o2} - x(s)) \sin(\gamma(s)) - (Y_{o2} - y(s)) \cos(\gamma(s)) \geq \frac{L_w}{2} \quad (5)$$

$$\gamma(s_3) = \gamma^+$$

$$f(x_3, y_3) \leq 0$$

$$\left\{ X_{o1} - x(s_3) - \frac{1}{\rho_1} \sin(\gamma(s_3)) \right\}^2 - \left\{ Y_{o1} - y(s_3) + \frac{1}{\rho_1} \cos(\gamma(s_3)) \right\}^2 > \frac{1}{\rho_1^2}$$

(X_{o1}, Y_{o1}) and (X_{o2}, Y_{o2}) are the positions of the corners of the parked vehicles detected with the PSM.

where $v_x \neq 0$. It is assumed that the vehicle moves slowly and there is not side slip of the tires. x and y are positions of the center of the rear axle. γ is the vehicle attitude with respect to the x axis. ρ is the curvature of the vehicle trajectory which can be converted to the steering angle. We also define L_w as the width, L_F and L_R as the length between the center of the rear axle and the front and rear bumpers of the vehicle respectively.

Let us consider to guide the vehicle at an arbitrary initial state (γ_0, x_0, y_0) to a reference state $(\gamma^+, x_g, y_g) \in \{\gamma^+\} \times S$. γ^+ is the final reference value of the vehicle attitude. The set S is defined as

$$S = \{(x_g, y_g) \in \mathbb{R}^2 | f(x_g, y_g) = 0\} \quad (2)$$

where $f(x, y) = 0$ is a reference line which passes the goal position (x^+, y^+) as shown in Fig. 7.

In this paper, the path planning algorithm for the perpendicular parking is described. In the case of parallel parking, the same way of thinking can be applied.

In the first step of the path planning, the general shape of the path is predefined which is shown in Fig. 4 (b). The path consists of a straight line, a clothoid curve, and a arc.

$$\rho(s) = \begin{cases} 0 & (s \in [0, s_1]) \\ v_1(s - s_1) & (s \in (s_1, s_2]) \\ \rho_1 & (s \in (s_2, s_3]) \end{cases} \quad (3)$$

s_1, s_2, and s_3 are travel distances where the steering maneuver changes. v_1 is the rate of change of the path curvature with respect to the travel distance.

As a result, the problem of the path planning comes down to the determination of the four parameters of (ρ_1, s_1, s_2, s_3). Considering the physical conditions for the path as shown in Fig. 4 (a), the optimal parameters are calculated numerically solving the following problem:

$$\min_{(\rho_1, s_1, s_2, s_3)} f(x(s_3), y(s_3))^2 \quad (4)$$

subject to

After the vehicle reaches the turning back point, the second step of the path planning based on a feedback method is applied. It drives the vehicle to the reference line $f(x, y) = 0$ simultaneously constraining $\gamma(x, y)$ to a reference attitude $\gamma^* \in T$, where

$$T = \{ \gamma^* \in \mathcal{C}^1(\mathbb{R}^2) | \text{sgn}(\sin(\gamma^+ - \gamma^*(x, y))) = -\text{sgn}(v_x)\text{sgn}(f(x, y))$$
$$\text{for } ^\forall (x, y) \in \mathbb{R}^2 \} \quad (6)$$

As a result, the vehicle state converges to (γ^+, x_g, y_g). The planning algorithm is basically inspired by a previous method which controls the vehicle to a reference point using path-generating regulator (Takashima et al. 2004). In our paper, it has been extended to control the vehicle to a reference line.

A Candidate of a Lyapunov function is set as

$$V(s) = \frac{1}{2} \{ k_1 e_1(s)^2 + e_2(s)^2 \}, \quad k_1 > 0 \quad (7)$$

$$e_1(s) = f(x(s), y(s)) \quad (8)$$

$$e_2(s) = \gamma^*(x(s), y(s)) - \gamma(s) \quad (9)$$

where $k_1 > 0$ is a controller parameter. Differentiating V with respect to s along the dynamics of the vehicle (1), we have

$$\frac{dV}{ds}(s) = k_1 \text{sgn}(v_x) e_1(s) \sin(\gamma^+ - \gamma(s))$$
$$- e_2(s) \left\{ \frac{d\gamma^*}{ds}(x(s), y(s)) - \rho(s) \right\} \quad (10)$$

To make V negative definite and guarantee stability, $\rho(s)$ is designed as

$$\rho(s) = \frac{d\gamma^*}{ds}(x(s), y(s))$$
$$+ k_1 \text{sgn}(v_x) e_1(s) \frac{\sin(\gamma^+ - \gamma(s)) - \sin(\gamma^+ - \gamma^*(x(s), y(s)))}{e_2(s)} \quad (11)$$
$$+ k_2 e_2(s)$$

where $k_2 > 0$ is a controller parameter. Although the denominator of the second term contains $e_2(s)$ which can be zero, $\rho(s)$ is continuous because it can be represented as
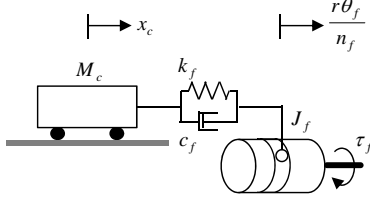
Fig. 8. Vehicle model considering the dynamics of the powertrain.
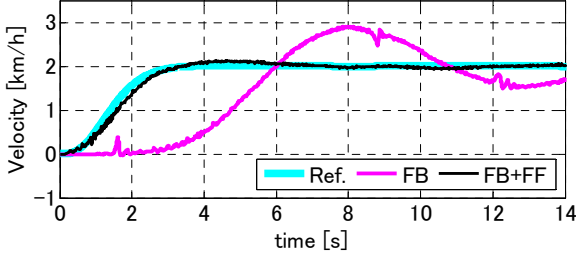
Fig. 9. Experimental results of the vehicle speed control.

$$\rho(s) = \frac{d\gamma^*}{ds}(x(s), y(s))$$
$$+ k_1 \operatorname{sgn}(v_x) e_1(s) \cos\left(\gamma^+ - \frac{\gamma^*(x(s), y(s)) + \gamma(s)}{2}\right) \operatorname{sinc}\left(\frac{e_2(s)}{2}\right) \quad (12)$$
$$+ k_2 e_2(s)$$

Substituting $\rho(s)$ to dV/ds,

$$\frac{dV}{ds}(s) = k_1 \operatorname{sgn}(v_x) e_1(s) \sin(\gamma^+ - \gamma^*(x(s), y(s))) - k_2 e_2(s)^2$$
$$= -k_1 |e_1(s)| |\sin(\gamma^+ - \gamma^*(x(s), y(s)))| - k_2 e_2(s)^2 < 0 \quad (13)$$
$$\text{for } ^\forall(e_1(s), e_2(s)) \neq (0,0)$$

Therefore, V becomes a Lyapunov function and the vehicle is controlled to the reference state (γ^+, x_g, y_g) maneuvering the steering angle along the planned curvature $\rho(s)$ of (12).

3.2 Vehicle Speed Control

In electrified vehicles, the driving motor torque is transmitted to the wheels through mechanical elements such as a reduction gear, a differential gear, and a drive shaft. However, the elements are not ideal rigid bodies and can be modeled as springs and dampers. These are obstacles to make the response of the vehicle arbitrarily fast. The problem gets worse when the sampling time of the speed controller is long. In our previous work, the dynamics of the powertrain are considered in the derivation of the controller not to excite vibration (Yokoyama et al. 2015a, b). In our present system, a feedforward controller has been added to improve the response speed further. A S-shape filter which achieves smooth vehicle motion is also introduced for a reference velocity.

To derive the speed controller, the elasticity and the viscosity are taken into account. Fig. 8 represents a dynamical model of the vehicle. The equations of motion are as follows:

$$J_f \ddot{\theta}_f = \tau_f - k_f'(\theta_f - \theta_c) - c_f'(\dot{\theta}_f - \dot{\theta}_c) - c_{mf}\dot{\theta}_f \quad (14)$$

$$J_t \ddot{\theta}_c = -k_f'(\theta_c - \theta_f) - c_f'(\dot{\theta}_c - \dot{\theta}_f) - c_c'\dot{\theta}_c \quad (15)$$

$$x_c = \frac{r\theta_c}{n_f} \quad (16)$$

$$J_t = \frac{M_t r^2}{n_f^2} \quad (17)$$

$$M_t = M_c + 4 \cdot \frac{J_w}{r^2} \quad (18)$$

$$k_f' = \frac{r^2}{n_f^2} k_f \quad (19)$$

$$c_f' = \frac{r^2}{n_f^2} c_f \quad (20)$$

The dynamics are so-called two-mass system. θ_f is the angle of the rotor and x_c is the displacement of the body. J_f and J_w are the inertia of the rotor and the wheel, respectively. M_c is the mass of the body, k_f and c_f are the stiffness and the viscosity between the front motor and the body, respectively. τ_f is the motor torque. r is the radius of the wheel and n_f is the reduction ratio. The transfer function from the motor torque to the vehicle speed is

$$G_{cf}(s) = \frac{N_{cf}(s)}{D_{cf}(s)} \quad (21)$$

$$N_{cf}(s) = c_f' s + k_f' \quad (22)$$

$$D_{cf}(s) = J_t J_f s^3 + \{(J_t + J_f)c_f' + J_t c_{mf} + J_f c_c'\}s^2$$
$$+ \{(J_t + J_f)k_f' + c_c'c_f' + c_f'c_{mf} + c_{mf}c_c'\}s \quad (23)$$
$$+ (c_c' + c_{mf})k_f'$$

A block diagram of the speed controller is shown in Fig. 6. The feedforward controller $C_{FF}(s)$ is derived using a transfer function of the S-filter $G_S(s)$.

$$C_{FF}(s) = \frac{G_S(s)}{G_{cf}(s)} \quad (24)$$

PI controller with an anti-windup algorithm is used as a feedback method in our system.

4. EXPERIMENTAL VERIFICATION

4.1 Vehicle Speed Control

Fig. 9 shows the experimental results of the speed controller. The reference velocity smoothly rises with S-shape. Without the feedfoward controller, the response of the vehicle speed is slow. This is because the PI gains cannot be set large due to low resonance frequency of the powertrain and sampling time of the speed controller. In the experiments, the vibration occurred when the gains are increased. In the case of the two-degrees of freedom control, the vehicle speed tracks the reference closely. This leads to smooth vehicle motion of automatic parking.
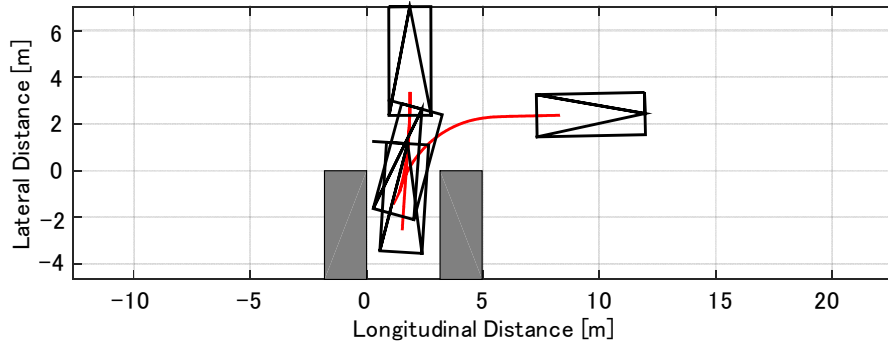
(a) Trajectory of the whole parking motion.
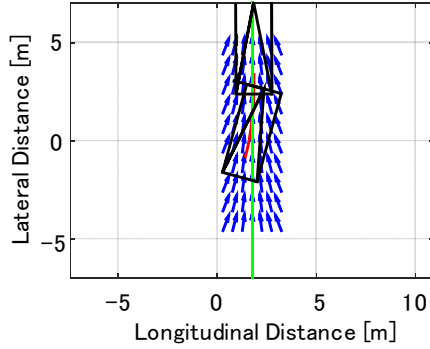
(b) Parking motion after the first turning back.
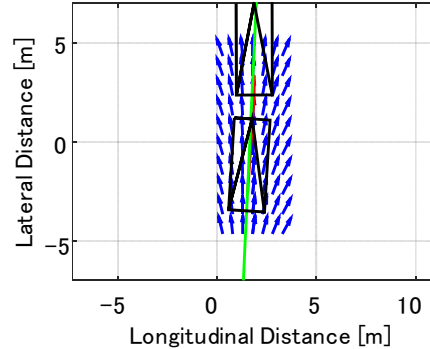
(c) Parking motion after the second turning back.
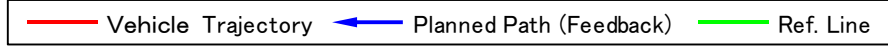
Fig. 10. Experimental verification of perpendicular parking.
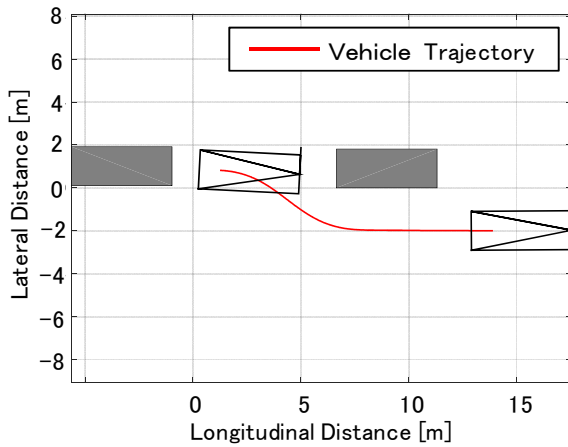
(a) Case of large parking slot.
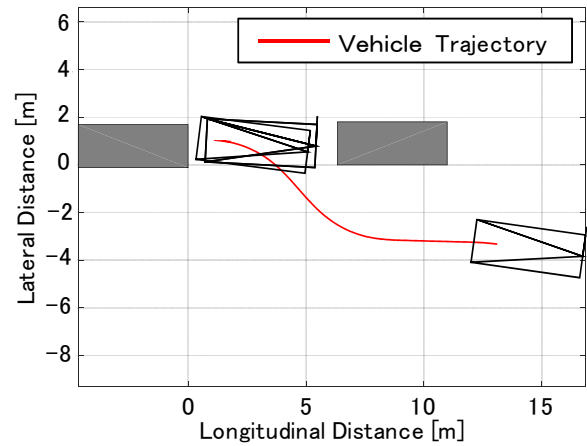
(b) Case of small parking slot.

Fig. 11. Experimental verification of parallel parking.

4.2 Automatic Parking

Perpendicular and parallel automatic parking was verified in the experiments. The trajectories of the vehicle after the PSM is finished and the automatic parking is started with the reverse mode are shown in Fig. 10 and Fig. 11. The vehicle position is recorded with KGPS (Kinematic Global Positioning) system.

Fig. 10 (a) represents the whole trajectory of perpendicular parking motion. First, the vehicle was guided to the parking slot without collision along the planned path calculated using the optimization in the e-Park controller. However, the vehicle could not go into the slot enough and changed the shift. Second, after the turning back, the e-Park controller used the path planning based on feedback method. In Fig. 10 (b), the arrows represents the reference attitude $\gamma^*(x, y)$. The green vertical line is the reference one where the vehicle is controlled to converge. In our system, the line is modified using the rear side sonar sensors every time the vehicle turned back. As the vehicle went forward, the steering angle is maneuvered along the arrows. When the vehicle state came close to (γ^+, x_g, y_g) or the front bumper of the vehicle

(a) PSM (Parking Slot Measurement) with manual drive.

(b) Start of the automatic parking.

(c) Control along the optimal path (The 1st step).

(d) End of the 1st step and automatic turning back.

(e) Control along the path with feedback (The 2nd step).

(f) Finish of the automatic parking.

Fig. 12. Successive pictures of parallel parking with the automatic parking system.

approached to an obstacle, The e-Park controller automatically changed the shift again. Finally, in Fig. 10 (c), the vehicle went backward adjusting the position and attitudes on the basis of the planned path with the feedback method. Although it is not shown in Fig. 10 (c), the parking system is automatically finished when the vehicle enters the slot enough. Our system achieves precision of parking with errors of the position and attitude less than 0.3 m and 3 deg, respectively.

Fig. 11 (a) shows the experiment of the parallel parking with large parking slot. Parking was completed without turning back. In this case, only the first step of the planning algorithm based on the optimization was used. Fig. 11 (b) shows the case where the parking slot was small. The vehicle turned back once and parking was successfully achieved. In both cases, the precision of the parking is the same as the case of the perpendicular parking.

Successive pictures of the experiment of the parallel parking are shown in Fig. 12. In Fig. 12 (a), the driver manually operated the vehicle executing the PSM. After the PSM was finished and an optimal path to the parking slot was found, the driver could get off the vehicle as shown in Fig. 12 (b). While the driver kept pressing the button of the device for keyless entry system, the vehicle was driven with the speed control and the steering angle was controlled along the optimal path in Fig. 12 (c). When the rear bumper approaches to the next vehicle, turning back is automatically executed in Fig. 12 (d). In the next phase, the vehicle went forward being guided along the path based on the feedback method to modify the vehicle position and attitude as shown in Fig. 12 (e). Finally, Fig. 12 (f) shows the finish of the automatic parking.

5. CONCLUSIONS

Mitsubishi Electric has been developing the automatic parking system. The main controller in the system is called e-

Park. It executes the PSM using signals from the sonar sensors simultaneously estimating the states of the vehicle. The optimal path to park the vehicle is calculated considering physical constraints and the e-Park controller finally commands the reference signals to the EPS and the motor control systems. After finding the path, the vehicle automatically tracks the desired path. The parking motion can be executed externally using our device of the keyless entry system. This paper mainly focuses on the vehicle speed controller with the driving motor and the path planning algorithm. The feature of the former technology is the smooth motion control considering vibration characteristics of the vehicle powertrain using the two degrees of freedom controller. The feature of the path planning algorithm is the two-step structure. The first step plans a path on the basis of optimization which guides the vehicle close to the parking slot efficiently. The second step uses feedback algorithm to compensate detection errors of the PSM and improves the precision of the parking. The whole system has been verified in the experiments and achieved parking accurate enough. For future works, the system is going to be verified in various situations and modified to enhance robustness.

REFERENCES

Yokoyama, K., Iezawa, M., Tanaka, H., and Enoki, K. (2015a). Development of three-motor electric vehicle "EMIRAI 2 xEV. *SAE International Journal of Commercial Vehicles*, 8 (1).

Yokoyama, K., Iezawa, M., Akashi, Y., Satake, T., Akemi, Y., Inoue, S., and Ryotaro, S. (2015b). Speed control of parking assist system for electrified vehicle. *SAE Technical Paper*, 2015-01-0316.

Takashima, A., Hashimoto, Y., Hori, K., Hanajima, N., Hikita, H., and Yamashita, M. (2004). Feedback control of non-holonomic mobile robots by path-generating regulator. *Transactions of the Japan Society of Mechanical Engineers. C*, 70 (689), 120-126.

Detection of Drowsy Driving via a Dual Control Theoretic Driver Assistance

Yuichi Saito*, Makoto Itoh**, Toshiyuki Inagaki**

** Tokyo University of Agriculture and Technology, 2-24-16 Naka-cho, Koganei,
Tokyo, 184-8588, Japan (Tel: +81-42-388-7395; e-mail: y-saito@cc.tuat.ac.jp).
** University of Tsukuba, 1-1-1 Tennoudai, Tsukuba, Ibaraki, 305-8573,
Japan (Tel: +81-29-853-5011; e-mail: {itoh.makoto.ge, inagaki.toshiyuki.gb}@u.tsukuba.ac.jp).*

Abstract: Driver drowsiness is one of major causes of fatal traffic accidents. We proposed a driver assistance system with a dual control theoretic scheme, which tries to perform safety control of a vehicle as well as identification of a driver's state (e.g., low arousal, degradation of mental and physical states) simultaneously. The dual control theoretic driver assistance works in a situation-adaptive manner, and it takes into account sleepy driver characteristics and circumstantial contexts. This paper gives an analysis of driver behavior when the driver assistance is active, and discusses the type of assist that is effective for prevention of sleep-related vehicle accidents.

Keywords: Safety, driver assistance, dual control, adaptive automation, driver behavior monitoring

1. INTRODUCTION

In order to reduce the number of sleep-related vehicle accidents, it is important to develop proactive safety technologies that detect driver drowsiness and provide a driver with an appropriate assist. Technologies for detecting driver drowsiness can be classified into four methods: (1) physiological indices based scheme (e.g., Ingre et al., 2006), (2) driver body movement based scheme (e.g., Itoh et al., 2006), (3) driving performance based scheme (e.g., Krajewski et al., 2009), and (4) facial expression based scheme (e.g., Åkerstedt et al., 1990). However, most of these methods tend to be unreliable. For example, with physiological indices, ensuring correct judgment is difficult due to individual differences in physiological properties. Similarly, the evaluation of driver body movement is affected by individual differences. A facial expression may not be useful when a driver wears sunglasses. Therefore, many researchers have attempted to develop a reliable method for monitoring driver drowsiness based on driver and vehicle data fusion (e.g., Omidyeganeh et al., 2011).

Today, a common approach to prevent a sleep-related vehicle accident is that a system suggests taking a break through an alert when symptoms of sleepiness or fatigue are observed. However, a driver who is aware of his/her drowsiness may still try to continue driving. In such a case, the warning type support may fail to assure the driver safety. What type of assist is necessary or effective for prevention of sleep-related vehicle accidents from occurring?

In vehicle safety control domain, some driver assistance systems have already been put into practical use. Lane Departure Warning Systems (LDWS) assist in maintaining safety by alerting drivers using visual, auditory or haptic modality when the system anticipates the lane departure (Navarro et al., 2007). Warnings are expected to assist the driver's action selection. However, when a driver's mental

and physical states are degraded and/or a driver falls asleep, it is hard to expect the driver to take a proper steering action. Humans may not always be powerful enough to cope with any given situation. On the other hand, although Lane Keeping Assistance Systems (LKA) that assist driver's action implementation by relieving his/her workload and maintain the vehicle at the center of the lane also have been put into practical use, the current LKA do not take into account sleepy driver characteristics and circumstantial contexts.

We proposed a driver assistance system with a dual control theoretic scheme, which tries to perform safety control of a vehicle as well as identification of a driver's state (e.g., low arousal, degradation of mental and physical states) simultaneously (Saito et al., 2014). The dual control theoretic driver assistance works in a situation-adaptive manner (Inagaki, 2006), and it takes into account sleepy driver characteristics and circumstantial contexts. This paper gives an analysis of driver behavior when the proposed system is active, and discusses the type of assist that is effective for prevention of sleep-related vehicle accidents.

2. DRIVER ASSISTANCE SYSTEM

Suppose a vehicle is going to deviate from the driving lane at a speed of V km/h and deviation angle of ψ degree. When the system anticipates that the lane departure will occur in t_d seconds, the system implements partial control (α %) as the control of first stage to prevent the lane departure (Fig. 1).
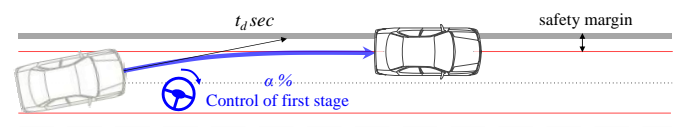
Fig. 1 Control of the first stage to prevent the lane departure

The control of the first stage is powerful enough to keep the vehicle in the lane but not to bring the vehicle back to the

center of the lane. In other words, (100 - α) % of the control is left without being implemented. Normally, the driver feels uncomfortable with the situation that the vehicle runs near the lane boundary if his/her situation awareness is appropriate. If the driver implements himself/herself the remaining control within the time period of t_i seconds, the system judges that "the driver is in a normal cognitive state" (Fig. 2).
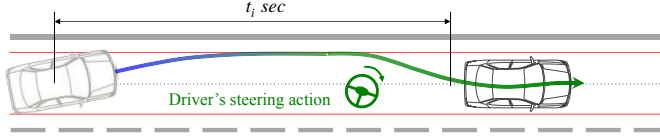
Fig. 2 Driver's action to lead the vehicle to the center of lane

If the driver does not implement himself/herself the remaining control within the time period of t_i seconds, the system judges that "the driver is in an off-normal cognitive state", and thus implements the remaining control as the control of the second stage (Fig. 3).
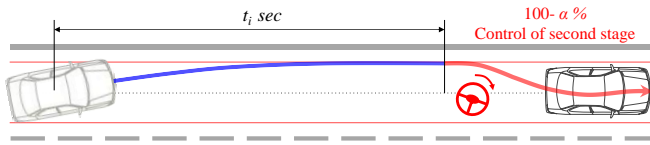
Fig. 3 Control of the second stage

2.1 Judgment for Lane Departure Prevention

Judgment lines for the lane departure are set at 0.5 m inside the lane markers on the right and left sides. Lane departure is defined as a state that the lateral position $y(t)$ exceeds the judgment line. Let $d(t)$ be the distance between the lateral position $y(t)$ and the judgment line. The predicted value of the time margin, $t_d(t)$, to reach the judgment line is

$$t_d(t) = d(t)/\{v(t) \cdot \sin \psi(t)\}. \tag{1}$$

The system initiates control of the first stage at time t^* when $t_d(t)$ becomes less than 1 second for the first time.

2.2 First- and Second-stage Controls

Fig. 4 shows the system's overall structure using steering torque control. Both the driver's input torque T_h and the system's assistance torque T_a are input on the steering wheel. In this study, the controller is designed using a state feedback (Saito et al., 2014), and the state vector x are yaw rate $\dot{\psi}$, yaw angle ψ, lateral velocity $\dot{y}_c$, lateral displacement y_c, steering angle velocity $\dot{\theta}$, and steering angle θ. The feedback gain is switched according to controls of the first and the second stages. When $t_d(t)$ becomes less than 1 second, the system's target position y_s^* is set at the judgment line, and the system performs the steering control that the vehicle is parallel to the lane maker at the judgment line. If the driver's steering action is not detected within t_i seconds, the system's target position y_s^* is set at the center of the driving lane at time $t^* + t_i$, and the system performs the second-stage control.
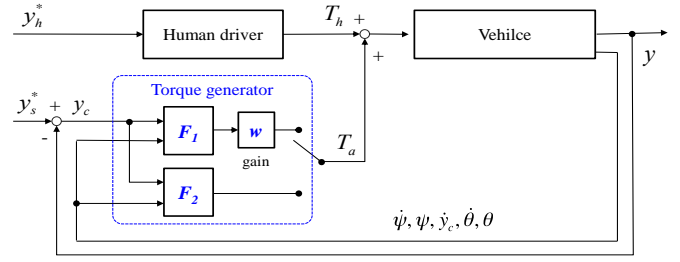
Fig. 4 Block diagram of the driver assistance system

Based on the state feedback, T_a is calculated as follows:

$$T_a(t) = \begin{cases} -w F_1 x(t), & t \in \left[t^*, t^* + t_i\right) \\ -F_2 x(t), & t \in \left[t^* + t_i, t^* + t_i + 5\right] \end{cases} \tag{2}$$

Assuming that the driver takes the proper steering action within 5 seconds from initiating the first-stage control if he/she is in a normal cognitive state, we designed the time length t_i for 5 seconds. Also, after 5 seconds from initiating the second-stage control, the system finishes the control. In the proposed system, an optimum control technique is applied to determine the assistance torque, and the state feedback gains were designed to obtain good control performance through numerical simulations using a general two-wheel vehicle model (Saito et al., 2014).

2.3 Detection of Driver's Steering Action

The system monitors driver behaviour within t_i seconds. If the driver takes steering action while the system is implementing control of the first stage, it is necessary to reduce the assisting torque in order to minimize conflicts between the driver and the system. As can be seen in *Eqs.* (2), (3), this study introduces a gain w into the state feedback controller in order to reduce the assistance torque.

$$w = \begin{cases} 1/\{1 + 0.001 \cdot \exp[-15 \cdot \psi(t)]\} & if \ \psi(t^*) > 0 \\ 1/\{1 + 0.001 \cdot \exp[15 \cdot \psi(t)]\} & if \ \psi(t^*) < 0 \end{cases} \tag{3}$$

The gain w between 1 and 0 is designed as a sigmoid function of the yaw angle, where $w=1$ denotes full assist and $w=0$ denotes no assist. As can be seen in the *Eq.* (3), as the vehicle direction turns toward the center of the driving lane, the gain w is reduced gradually from 1 to 0. When the driver takes steering action to lead the vehicle back to the center of the driving lane, the gain w is reduced from 1 to 0 so as to draw a sigmoid curve and the assistance torque is also reduced gradually. Also, if the driver takes unconsciously or reflexively steering action to lead the vehicle to the lane boundary, the system provides assistance torque to recover the target line for the first-stage control because the gain w remains at 1. Furthermore, when the gain w is less than 0.5 for 0.5 seconds, the system judges that "the driver took the steering action to lead the vehicle back to the center of the driving lane". When the driver takes the proper steering action, the controls by the system and the driver are coupled. In this way, the system judges whether or not the driver took the steering action by monitoring only the gain w while reducing the assisting torque.

3. DRIVING SIMULATOR EXPERIMENT

We collected data of driver behaviour when the dual control theoretic driver assistance system is active in order to investigate its functionality and effectiveness on safety control and driver state identification.

3.1 Apparatus

The experiment was conducted with a fixed-based driving simulator equipped with the driver assistance system. A 50 km expressway course consisting of straight lines was used. In addition, the Smart Eye system was installed to measure the degree of opening of the eyelids.

3.2 Participants and Driving Tasks

Twenty students (15 males and 5 females between the ages of 20-24) who drive daily participated in this experiment. Each participant held a valid driver's license.

The task imposed was to maintain the vehicle at the center of the lane. In this experiment, an adaptive cruise control that maintains the speed of the vehicle automatically at 100 km/h was used while a participant was driving in order to make the monotonous driving environment and to induce a driver's drowsiness. Thus, participants were required to maintain only lateral control of the vehicle. In addition, the participants were required to take proper steering actions to return the vehicle to the center of the lane when he/she recognized the system's first-stage control.

3.3 Procedure

The experiment was conducted in one day for each participant. First, each participant read and signed a written consent forms, and informed consent was obtained from all participants. Next, the participants were completed practice drives to familiarize themselves with the simulator. In the training trials, the participants drove freely the driving simulator equipped with proposed system. Thus, all participants have experienced the operation of the dual control theoretic driver assistance. In addition, the participants were asked "please take a lunch from at 12:00 to at 12:50 if acceptable and do not intake caffeine as much as possible" in order to induce their drowsiness. The driving was scheduled as follows: (1) trial 1 is from at 13:00 to at 13:30, (2) trial 2 is from at 14:00 to at 14:30, and (3) trial 3 was from at 15:00 to at 15:30.

3.4 Hypothesis

This study included two hypotheses as follows:

(1) If a participant fell asleep while driving, it is difficult for a participant to implement the steering action to lead the vehicle to the center of the lane after the system's first stage control because of his/her loss of situation awareness.

(2) It is difficult for a participant to implement the corrective steering in order to maintain the center of the lane after

the system implements the control of the second stage. Thus, the system implements both the first- and second-stage controls repeatedly.

3.5 Measures

The following measures were collected at a frequency of 120 Hz: speed [km/h], lateral position [m], yaw angle [degrees], steering angle [degrees], gain *w*, driver's torque [Nm], system's assisting torque [Nm], the initiated times of the controls of the first and the second stages, degree of opening of eyelids [mm], and facial image at 30 frame per 1 second. In addition, the evaluation of facial expressions (Kitajima et al., 1997) was carried out every 20 seconds by three evaluators of our laboratory using the criteria listed in Table 1. The sleepiness levels evaluated by the three evaluators were averaged out at every rating and were rounded off.

Table 1 Scales of sleepiness level (Kitajima et al., 1997)

Level 1	**Not Drowsy:** Eye movement is rapid, and the time between blinks remains stable.
Level 2	**Slightly Drowsy:** Eye movement is slow.
Level 3	**Moderately Drowsy:** Blinks are slowly, the mouth moves, or the driver touches his/her face.
Level 4	**Significantly Drowsy:** Number of blinks increases noticeably, motions unnecessary for driving are seen, yawns are frequent, deep breathing is detected.
Level 5	**Extremely Drowsy:** Eyelids are almost closed, or the driver's head inclines to the front or rear.

4. RESULTS

4.1 Distribution of Sleepiness Levels

Fig. 5 shows the distribution of the subjective ratings for the sleepiness level based on facial expression.
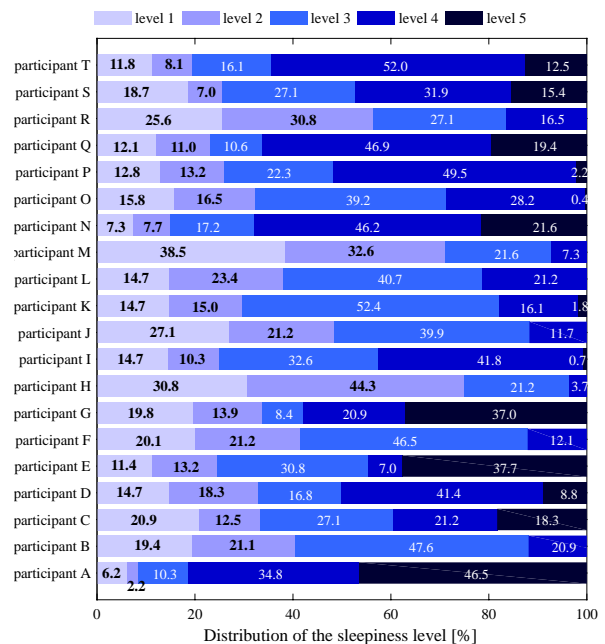
Fig. 5 Distribution of Sleepiness Levels

Even though individual differences were observed in terms of the tendency to be drowsy, thirteen participants (A, C, D, E, G, I, K, N, O, P, Q, S, T) were rated as "extremely drowsy (level 5)" at least once. Moreover, there were four participants (A, C, E, S) who fell asleep completely. In other words, the number of the trials in which a participant fell asleep was 6 trials for a total of 60 trials. On the other hand, in 15 trials of five participants (F, J, L, M, R) who were not rated as "extremely drowsy", the system was not activated even once.

4.2 Driving Performances

Fig. 6 illustrates the relationships (a) between the sleepiness level based on facial expression and the standard deviation of the lateral position, (b) between the sleepiness level and the standard deviation of the steering angle, (c) between the sleepiness level and the number of blinks. A single-factor ANOVA with the sleepiness level on the standard deviation of the lateral position showed that the main effect of the sleepiness level was statistically significant ($F_{(4, 5335)} = 721.96$, $p < 0.01$). Tukey's HSD test has found statistically significant differences between levels 1 and 3, 1 and 4, 1 and 5, between levels 2 and 3, 2 and 4, 2 and 5, and between levels 3 and 4, and 3 and 5, between levels 4 and 5 ($p<0.01$).

A single-factor ANOVA with the sleepiness level on the standard deviation of the steering angle showed that the main effect of the sleepiness level was statistically significant ($F_{(4, 5335)} = 519.55$, $p < 0.01$). Tukey's HSD test has found statistically significant differences between levels 1 and 3, 1 and 4, 1 and 5, between levels 2 and 3, 2 and 4, 2 and 5, and between levels 3 and 4, and 3 and 5, levels 4 and 5 ($p<0.01$).

A single-factor ANOVA with the sleepiness level on the number of the blinks showed that the main effect of the sleepiness level was statistically significant ($F_{(4, 5068)} = 145.29$, $p < 0.01$). Tukey's HSD test has found statistically significant differences between levels 1 and 3, 1 and 4, 1 and 5, between levels 2 and 3, 2 and 5, and between levels 3 and 4, and 3 and 5, between levels 4 and 5 ($p<0.01$).

For each measure, we performed a single-factor ANOVA with five sleepiness levels. These results are consistent with previous studies for detecting driver drowsiness (e.g., Ingre et al., 2006; Krajewski et al., 2009). As the degree of sleepiness becomes larger, the lane keeping performance to maintain the vehicle at the center of the lane was degraded. In general, the driver's corrective maneuver to compensate the lateral error between target and actual vehicle positions is delayed when the driver feels sleepy, because longer eye blink durations as a visual occlusion are often occurred (Ingre et al., 2006).
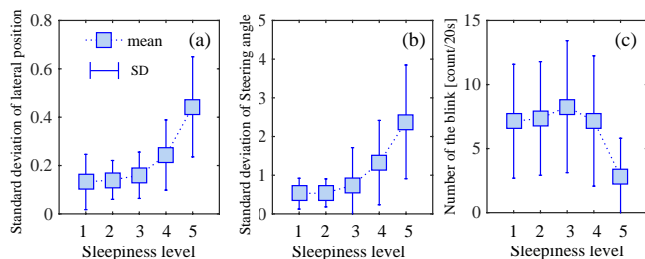
Fig. 6 Means and standard deviations of the measures

The results of detailed analysis are described with analysis for safety control performance of the proposed assistance in the next subsection.

4.3 Safety Control Performances and Driver's Actions

In this experiment, among 709 times of control of the first stage implemented, 678 times (95.6%) was implemented the control at the time point when a participant was at level 4 or 5 of sleepiness. In addition, 695 times (98%) was implemented the control of first stage when the driver's eyelids are going to be closed or were closed. Also, among 253 times of control of the second stage implemented, 248 times (98.4%) was implemented the control at the time point when a participant was at level 4 or 5 of sleepiness.

(a) Time-series data of 1800 seconds

(b) Relative frequency for lateral position
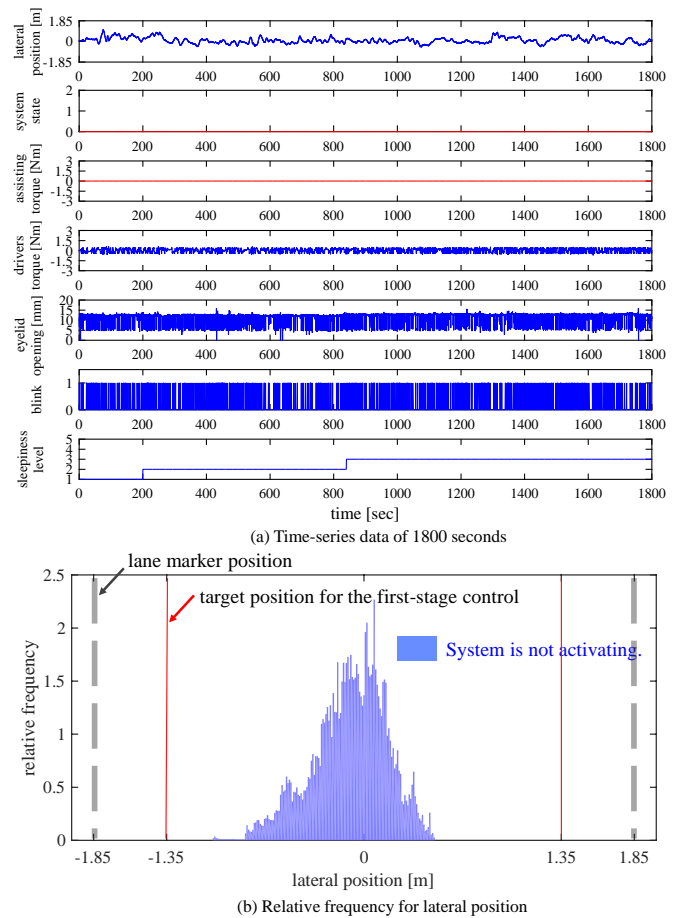
Fig. 7 Trial 3 of participant L

There were various situations that the system was activated or not activated according to the participant's state. Figs. 7 and 8 illustrate the time-series data of 1800 seconds during each trial. Fig. 7 shows the measurement data that the system was not activated even once, and Fig. 8 shows the measurement data that the participant fell asleep completely.

The measures are lateral position [m], system states [1; implementing the first-stage control, 2; implementing the second-stage control], assisting torque [Nm], driver's input torque [Nm], eyelid opening [mm], blink [1; to blink, 0; other], and sleepiness level [1; Not Drowsy ~ 5; Extremely Drowsy]. In the eyelid opening, approximately 5 mm denotes that the driver's eyelids were closed. In addition, the relative

frequency of lateral position was evaluated as the safety control performances of the proposed system. The blue color denotes the lateral position when the system is not activating and the red color denotes the lateral position when the system is activating.

As can be seen from Fig. 7 (a), we can confirm that participant L was going to blink frequently during the trial, and the vehicle was maintained within the driving lane by the driver's steering action. The system was not activated even once. It is clear from Fig. 7 (b) that participant L implemented the steering action to maintain the vehicle at the center of the lane. On the other hand, in the trial 1 of participant E (Fig. 8), approximately 62 % of the trial time was at level 5 of sleepiness. Participant E fell asleep while driving. It is clear from the system state, eye opening, blink, and sleepiness level of Fig. 8 (a) that the system implemented the first- and second-stage controls when the participant's eyelid were almost closed and/or sleepiness level reached at level 5. The system implemented the first-stage control sixty-one times and implemented the second-stage control forty-four times during 30 minutes. It is clear from Fig. 8 (b) that the vehicle's lateral position was maintained within the driving lane by the system's control. The driver assistance system assisted the driver only when almost really needed. The proposed assistance was useful for attaining driver safety.

In this experiment, after the system implemented the control of first stage, three types of driver's action were observed: (a) the driver took the proper steering action after he/she opened the eyelids, (b) although the driver opened the eyelids, he/she could not take the proper steering action, and (c) neither the driver opened the eyelids nor took the proper steering action. Fig. 8 (c) shows the distribution of the driver's actions after the system implemented the control of first stage. When the sleepiness level of participant E was at level 5, the cases of approximately 74% were that they could not take the proper steering action to lead the vehicle to the center of the lane after the system's first-stage control. In addition, the cases of approximately 56% were that neither the driver opened the eyelids nor took the proper steering action. The results suggest that it is difficult for a participant to implement steering action that returns the vehicle to the center of the driving lane if he/she falls asleep while driving (off-normal cognitive state). Moreover, Fig. 8 is typical example of the results which the system implements both the first- and second-stage controls repeatedly when the participant falls asleep while driving. The system state shows that the system implemented the controls of the first and the second stages repeatedly after the sleepiness level of the driver reached at level 5. This tendency was common to participants (A, C, E, S) who fell asleep completely. It is apparent from this typical example that it is difficult for a participant to implement corrective steering to remain in the center of the lane after the system's second-stage control when he/she fell asleep. These results support hypotheses that was made in Section III.

5. DISCUSSIONS

In the lane departure situation, the proposed system implements the partial control for preventing the lane departure that can be satisfied with the minimum. The system

(a) Time-series data of 1800 seconds

(b) Relative frequency for lateral position

(c) Driver's steering action
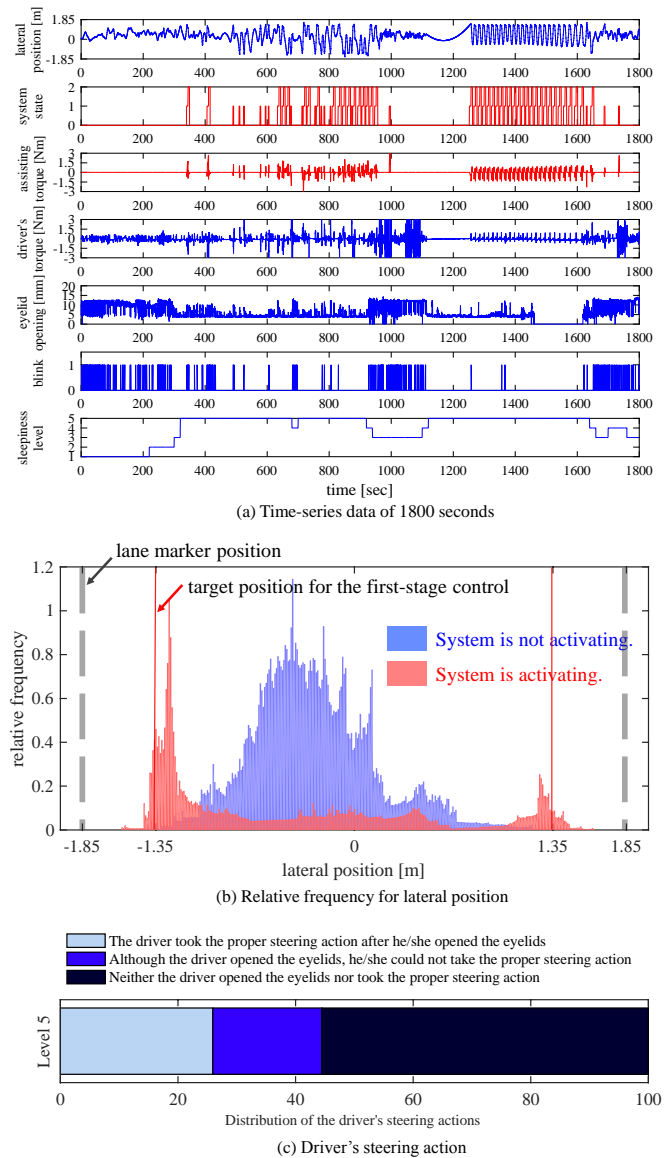
Fig. 8 Trial 1 of participant E

extends the time to lane-closing and gives the driver a chance to voluntarily take the action needed. If the driver failed to implement the steering action needed within a limited time, the system determines the "the driver is in an off-normal cognitive state" and executes the remaining control on behalf of the driver. The experimental results suggested that the system implements both the first and second stage control repeatedly when the driver falls asleep while driving. When a driver's mental and physical states are degraded and/or a driver falls asleep, the system should lead to stop the vehicle as soon as possible. In the situation in which the system implements controls of the first and second stages repeatedly, when should the system determine that "the driver cannot continue driving", and/or when should the system initiate a control for leading to stop the vehicle?

Fig. 9 shows the time intervals between two consecutive controls when the sleepiness level of the participant was at level 5. The time interval was evaluated by using all measured data. There were many cases in which the time interval between two consecutive controls of the second stage is within 30 seconds.
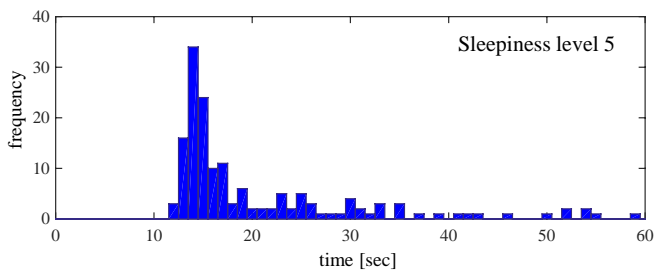
Fig. 9 Time intervals between two consecutive controls

Based on the results, we developed the following scheme for determining the driver state: The system judges that "the driver is in a state which cannot continue driving" when the second-stage control is implemented two times per 30 seconds. Fig. 10 shows that the time elapsed before the system judged that "the driver cannot continue driving" after the sleepiness level reached at level 5 for the first time. The six trials are cases in which the participant fell asleep while driving. The time elapsed were different according to the participant's state because he/she is making effort to wake up or to keep arousal level. In the other hand, the sleepiness level was at level 5 when the system judged that "the driver cannot continue driving" in the six cases. In this way, the proposed system can be identified the driver state (low arousal) by monitoring the driver's action while implementing the first-stage control. Further study will be necessary to improve the algorithm of the driver state identification to be able to identify the driver state earlier.
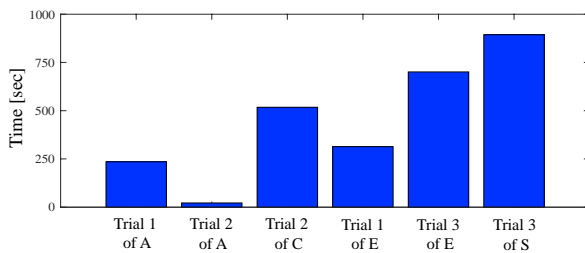
Fig. 10 Time elapsed before the system determined the driver state after the sleepiness level reached at level 5

In the experiment, the dual control theoretic driver assistance system assisted the driver only when almost really needed. However, there were the situations that a sleepy driver continues driving with the assist of first-stage control. This situation is not preferable. The driver should stop driving as soon as possible. What type of assist is necessary or effective for prevention of sleep-related vehicle accidents from occurring? This paper proposes a multi-layered assist via the dual control theoretic driver assistance: (a) when the system implemented the first-stage control three times, the system suggests the driver to take a break with an alert, and (b) when the system implemented the second-stage control two times per 30 seconds, the system judges that "the driver cannot continue driving", and thus performs deceleration and lane centering controls to slowly stop the vehicle. However, the system's decision-making may not be always right. If the driver stepped on the accelerator while implementing the control for stopping the vehicle, the deceleration and lane centering controls is canceled. Execution of the first-stage

control means symptoms of driver's sleepiness or fatigue. When the driver takes the proper steering action after the system executed the first-stage control, it is assumed that the driver is aware of their lowering arousal. The driver may make effort to wake up. Although the proposed system can be useful for attaining driver safety, it will be necessary to design the human-machine interface to encourage a break along with the assist.

6. CONCLUSIONS

To investigate its functionality and effectiveness on safety control and driver state identification, we collected data of driver behaviour with a driving simulator having the driver assistance system. The system assisted the driver only when almost really needed in lane departure situations. In addition, the results showed that the system implemented both the first- and second-stage controls repeatedly when a participant falls asleep. From these results, the hypothesis was supported. Moreover, these experimental results suggested that the dual control theoretic driver assistance that takes into account sleepy driver characteristics and circumstantial contexts can be effective for attaining the driver safety and identifying the driver state.

Future works are described. There are some ways for leading to stop the vehicle after the system determined that "the driver cannot continue driving". One is to stop the vehicle on the driving lane in which the vehicle is moving. The other is to pull over and to stop on the side of the road. In the latter case, a lane change may be required to stop the vehicle. Then, it will be necessary to notify the surrounding to be the emergency stop. Further studies are necessary to investigate whether or not drivers accept the system's behavior in a more realistic driving context when the drivers do not have the prior experience of interacting with the system.

REFERENCES

Åkerstedt, T. & Gilberg, M. (1990). Subjective and Objective Sleepiness in the Active Individual. International Journal of Neuroscience, Vol. 52, No. 1, pp. 29-37.

Inagaki, T. (2006). Design of Human-machine Interactions in Light of Domain-dependence of Human-centered Automation, Cognition, Technology & Work, Vol. 8, No. 3, pp. 161-167.

Ingre, M. et al. (2006). Subjective Sleepiness, Simulated Driving Performance and Blink Duration. Journal of Sleep Research, Vol. 15, No. 1, pp. 47-63.

Itoh, M. et al. (2006). Analyses of Driver's Body Movement for Detection of Hypovigilance due to Non-driving Cognitive Task. Proc. IFAC-CTS, 6 pages.

Kitajima, H. et al. (1997). Prediction of Automobile Driver Sleepiness: Rating of Sleepiness based on Facial Expression and Examination of Effective Predictor Indexes of Sleepiness. Journal of The Japan Society of Mechanical Engineers, Vol. 63, No. 613, pp. 3059-3066.

Krajewski, J. et al. (2009). Steering Wheel Behavior Based Estimation of Fatigue. Proc. 5th International Driving Symposium on Human Factors in Driver Assessment and Design, pp. 118-124.

Navarro, J., Mars F. & Hoc, JM. (2007). Lateral Control Assistance for Car Drivers: A Comparison of Motor Priming and Warning Systems, Human Factors, Vol. 49, No. 5, pp. 950-60.

Omidyeganeh, M., Javadtalab, A. & Shirmohammadi, S. (2011). Intelligent Driver Drowsiness Detection through Fusion of Yawning and Eye Closure, Proc. IEEE International Conference on Virtual Environments Human-Computer Interfaces and Measurement Systems, 6pages.

Saito, Y. et al. (2014). Dual Control Theoretic Driver Assistance -Dynamic Characteristics of Steering Torque Control based on Linear Quadratic Regulator-. Proc. IEEE SMC, pp. 1753-1758.

Vehicle Motion Control for Integrated Risk Management of Automated Vehicle

Kyuwon Kim*, Beomjun Kim*, Kyoungjun Lee**, Hyokjin Chong**, Bongchul Ko** and Kyongsu Yi*

*Mechanical and Aerospace Engineering Department, , Seoul National University,
Seoul, Korea, (e-mail: kyi@snu.ac.kr)}
**Hyundai Kia Motors R&D Center, Hwaseong, Korea

Abstract: This paper describes an approach to vehicle motion control algorithm for application of an automated vehicle. A full recognition of environment is achieved by data fusion and data interpretation based on the dynamic measurements from the environmental sensors such as radar and vision. The recognition of environment is transformed into an artificial risk potential representation, which is collision probability. In order to guarantee lateral stability in the high speed maneuver, constraints of the vehicle motion based on vehicle dynamics have been considered. Probabilistic predictions of surrounding vehicles are included into the risk potential function for represent the predicted collision risk based on the estimated motion of the subject vehicle and the surrounding vehicles. The potential field interpretation has been proposed to represent the risk potential to the surrounding vehicles based on the predicted motion of the vehicles. The proposed motion control algorithm has been investigated via closed-loop simulation.

*Keywords: **Automated vehicle, Motion control, Potential field, Motion prediction, Risk management***

1. INTRODUCTION

In recent years, global passenger vehicle sales exceed 60milion units per year. With the increasing number of vehicles on the road, safety has become a focal issue. In order to deal with the safety issue, a number of active safety systems have been developed in passenger vehicles, such as brae assist system (BAS), adaptive cruise control(ACC), lane keeping control(LKS), and collision mitigation(CM)[1]. The functionalities of the systems include the assistance in recognizing hazards on roadway e.g. forward vehicles, obstacles, the unexpected lane departure. Beyond the development of each independent safety system, the integrated safety system has been considered nowadays. An Artificial potential field approach has been successfully implemented for robot motion planning and path tracking so far[2], and the concept has been applied on an integrated safety system and automated vehicle navigation[3],[4].

A state prediction methods have been studied for threat assessment and decision-making function[5],[6]. However, the conventional method is insufficient to ensure the future path of a vehicle, and may cause wrong threat assessment and decision-making. To ensure the future path of the vehicle, states extension and uncertainty evaluation, a sensor fusion based probabilistic prediction method for holistic vehicle states is developed. A vehicle filter and road geometry filter have been used to establish the vehicle predictor which presents future vehicle states by maximum likelihood filtering method. The collision probability based on the predicted vehicle states is defined to represent the collision risk between a subject and surround vehicles.

This paper presents the risk management strategy using a risk potential field approach based on a probabilistic states prediction focusing on the data relevant to the subject vehicle

interacting with the surround vehicles. Dynamic constraints due to steering behavior, side slip and rollover have been considered as the limitation of the desired motion for safety control and lane keeping in the high speed driving. The performance of the proposed collision avoidance algorithm has been investigated via closed-loop simulation with the vehicle simulation software, Carsim.

2. PROBABILISTIC STATE PREDICTION ALGORITHM

A probabilistic state prediction presents the predicted potential states of the subject vehicle and the surrounding vehicles in finite time horizon. The probabilistic state prediction algorithm yields a time-series of predicts for vehicle position and corresponding likely ellipses. The state prediction algorithm consists of 2 parts as: 1) prediction and 2) probabilistic risk assessment as shown in Fig.1[7].
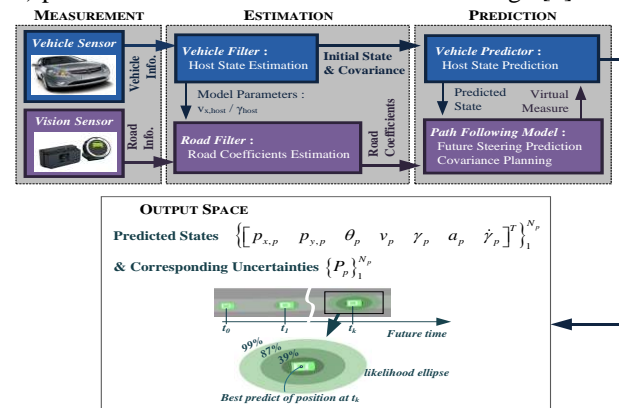
Fig. 1. Schematic Description of Probabilistic Prediction

2.1 Vehicle Predictor

The Kalman filter is widely used to estimate the states represented in a state space equation. In order to establish a state prediction, the vehicle state estimation method such as longitudinal velocity, yaw rate, longitudinal acceleration and yaw acceleration has been developed[7].

A road geometry estimation has been established with the measurements from a vision sensor. The road geometry can be described by a 2nd order polynomial[8]. Likewise with the vehicle states estimation, the Kalman filter is used for the estimation of road geometry coefficients of the polynomial.

The state prediction of the vehicle has been established under the assumptions that a subject and surround vehicles maintain current behavior in the finite time horizon. The vehicle position in the finite time horizon is represented as follows[7]:

$$x_p[i+1] = f_p\left(x_p[i]\right) + w_p[i], \qquad i = 0,\cdots,N_p - 1$$
$$= \begin{bmatrix} f_{1,p} & f_{2,p} & f_{3,p} & f_{4,p} & f_{5,p} & f_{6,p} & f_{7,p} \end{bmatrix} + w_p[i] \tag{1}$$

where,

$$x_p = \begin{bmatrix} p_{x,p} & p_{y,p} & \theta_p & v_p & \gamma_p & a_p & \dot{\gamma}_p \end{bmatrix}^T$$

$$f_{1,p} = p_{x,p} + \left(v_p\cos\theta_p\right)\Delta t + \left(a_p\cos\theta_p + \gamma_p v_p\sin\theta_p\right)\frac{\Delta t^2}{2}$$

$$f_{2,p} = p_{y,p} + \left(v_p\sin\theta_p\right)\Delta t + \left(a_p\sin\theta_p + \gamma_p v_p\cos\theta_p\right)\frac{\Delta t^2}{2}$$

$$f_{3,p} = \theta_p + \left(\gamma_p\right)\Delta t + \left(\dot{\gamma}_p\right)\frac{\Delta t^2}{2} \qquad f_{4,p} = v_p + \left(a_p\right)\Delta t + \left(-k_a a_p\right)\frac{\Delta t^2}{2}$$

$$f_{5,p} = \gamma_p + \left(\dot{\gamma}_p\right)\Delta t + \left(-k_{\dot\gamma}\dot{\gamma}_p\right)\frac{\Delta t^2}{2}$$

$$f_{6,p} = a_p + \left(-k_a a_p\right)\Delta t + \left(k_a^2 a_p\right)\frac{\Delta t^2}{2}$$

$$f_{7,p} = \dot{\gamma}_p + \left(-k_{\dot\gamma}\dot{\gamma}_p\right)\Delta t + \left(k_{\dot\gamma}^2\dot{\gamma}_p\right)\frac{\Delta t^2}{2}$$

$$w_p[i] \sim \left(0, W_p[i]\right)$$

$$W_p[i] = \left(B_p\Delta t + F_p[i]B_p\frac{\Delta t^2}{2}\right)Q_p\left(B_p\Delta t + F_p[i]B_p\frac{\Delta t^2}{2}\right)^T$$

$$F_p[i] = \left.\frac{\partial f_p}{\partial x_p}\right|_{x_p=\hat{x}_p[i]} \qquad B_p = \begin{bmatrix} 0 & 0 & 0 & 0 & 0 & 0 & 1 \\ 0 & 0 & 0 & 0 & 0 & 1 & 0 \end{bmatrix}^T$$

The subscript 'p' in (1) denotes 'predictive'. A prediction procedure at the first future time step is depicted as Fig.2. The desired yaw rate for lane keeping is supposed to be a virtual measurement as shown in the following equation.

$$z_p[i] = H_p\cdot x_p[i] + v_p[i], \qquad i = 0,\cdots,N_p$$
$$= \begin{bmatrix} 0 & 0 & 0 & 0 & 1 & 0 & 0 \end{bmatrix}\cdot x_p[i] + v_p[i]$$
$$= \bar{\gamma}_{des,p}[i] \tag{2}$$
$$= -C\cdot\bar{x}_{e,p}[i] + \gamma_{ff,p}[i]$$

where,

$$\bar{x}_{e,p}[i] = f_e\left(\bar{x}_p[i],\hat{x}_r[0]\right)$$
$$= \begin{bmatrix} \bar{e}_y[i] & \bar{e}_\theta[i] & \bar{\gamma}_p[i] \end{bmatrix}^T$$
$$= \begin{bmatrix} \bar{p}_{y,p}[i] - \left\{\hat{a}_2\cdot\bar{p}_{x,p}[i]^2 + \hat{a}_1\cdot\bar{p}_{x,p}[i] + \hat{a}_0 + \hat{w}_{road}\cdot N[i]\right\} \\ \bar{\theta}_p[i] - \tan^{-1}\left(2\hat{a}_2\cdot\bar{p}_{x,p}[i] + \hat{a}_1\right) \\ \bar{\gamma}_p[i] \end{bmatrix}$$

$$v_p[i] \sim \left(0, V_p[i]\right)$$

$$V_p[i] = V_{p,const} + \begin{bmatrix} \bar{e}_y[i] & \bar{e}_\theta[i] \end{bmatrix}^T w_{correct}\begin{bmatrix} \bar{e}_y[i] \\ \bar{e}_\theta[i] \end{bmatrix}$$
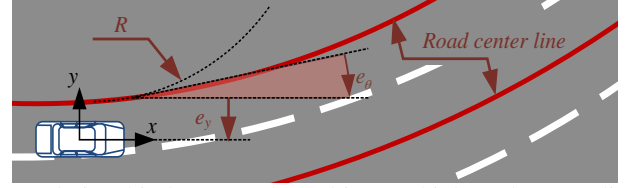
(a) Relationship between the Subject Vehicle and Center line of road
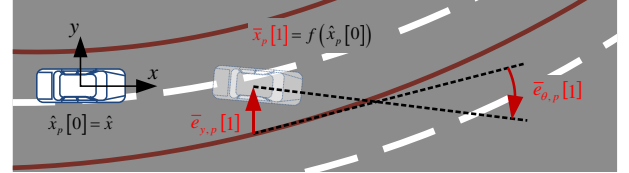
(b) Time-update of Subject Vehicle States and the Relative Error States to Road Geometry
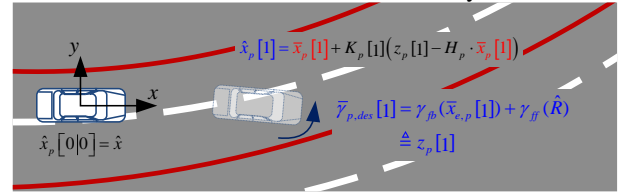
(c) Measurement-update of Subject Vehicle States with Predicted Yaw Rate for Lane Keeping as Virtual Measurement

Fig. 2. Procedure of State Prediction

2.2 Probabilistic risk assessment

The potential collision risk between a subject vehicle and surrounding vehicles is represented by the predicted vehicle motions the under the assumptions on their decoupled states. The collision probability is defined as shown in (3). The possibility for collision is represented as the surface integral form of the cross product of each probability which means the existence of each vehicle on the pre-defined domain.

$$CP_i(k) =$$
$$\int_{-\infty}^{\infty}\int_{-\infty}^{\infty}\left\{P\left(X_{i,p,k}\in D_{X_{p,k}}\right)\cdot f_k\left(X_{p,k}\right)\right\}dp_{x,p,k}dp_{y,p,k} \tag{3}$$

where,

$$P\left(X_{i,p,k}\in D_{X_{p,k}}\right) = \iint_{DX_{p,k}} f_{i,k}\left(X_{i,p,k}\right)dp_{i,x,p,k}dp_{i,y,p,k}$$
$$D_{X_{p,k}} = \{(x,y)\big| \|x - p_{x,p,k}\| \le \varepsilon_x \cap \|x - p_{y,p,k}\| \le \varepsilon_y\}$$
$$X_{p,k} = \begin{bmatrix} p_{x,p,k} & p_{y,p,k} \end{bmatrix}^T$$

3. DESIRED MOTION DETERMINTATION FOR AUTOMATED DRIVING

This section describes the desired motion determination for safety control and lane keeping. An artificial potential field approach has been considered to represent the potential risk of surrounding vehicles. The desired motions derived from the potential function are bounded by the dynamic limitation of the vehicle.

3.1 Potential field definetion

Typical path planning using potential field consists of two different types of energy functions which are an attractive

potential and repulsive potential. The attractive potential generates the attractive force between the subject and the pre-defined goal point. The repulsive potential generates the force which prevents the subject to get close to the obstacles and keeps the marginal distance. The first step of the potential field approach is calculating the gradient of the summation of each pre-defined potential energy function which is a resultant force as follows:

$$F_{result} = -\nabla\left(U_a(q) + U_r(q)\right) \qquad (4)$$

The following step is to find the desired path based on the resultant force. A gradient descent algorithm is the most popular method which has been widely used for path planning using a potential field approach as shown in (5).

$$q_{i+1} = q_i + f\left(F_{result}(q_i)\right) \qquad (5)$$

The function of resultant force in (5) is usually represented as the production of unit vector of the resultant force and a fixed step size. This kind of approach may cause a local minimum problem which makes the calculated path remain around the local solution of the path, not a global goal point. In order to deal with this kind of local minimum problem, various approaches have been developed so far[9].

For an automated vehicle, which has pre-defined way points using GPS/INS, the potential field approach can be adopted to find the path for safe driving with local obstacle by the desired motion from repulsive potential. Furthermore, in order to guarantee the real time performance of the motion planning, the algorithm should be confirmed with computational efficiency.

The risk potential in driving situation can be represented in Fig. 3. The collision risks are assessed by predicted motion of the surrounding vehicles in various driving conditions.
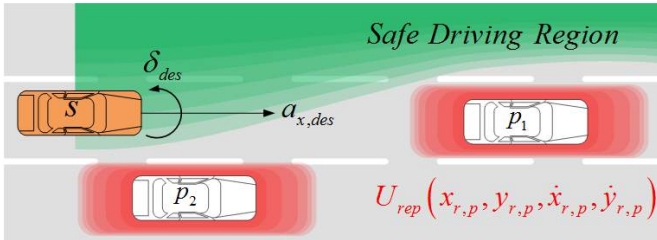
Fig. 3. Risk Potential to Surrounding Vehicles

In order to determine the desired motion for safety control, the repulsive potential energy function has been designed as follows:

$$U_{rep} = \begin{cases} k \cdot f(CP_i) \cdot \exp\left(-\left(\dfrac{x_{r,p}}{\dot{x}_{r,p}}\right)^2 - \dfrac{y_{r,p}^2}{w_y^2}\right) & if \ \|\rho(x_{r,p}, y_{r,p})\| \le \rho_{long} \\ 0 & else \end{cases} \quad (6)$$

where, $x/y_{r,p}$ and $\dot{x}/\dot{y}_{r,p}$ denote the longitudinal/lateral distance between the subject vehicle and target vehicle, and relative longitudinal/lateral velocity, respectively. k represents the stiffness of the repulsive energy. $f(CP_i)$ denotes the i-th normalized collision probability representing the normalized probability between 0 to 1. The magnitude of the risk potential increases when the subject vehicle approaches the obstacle near the safety margin, or the subject vehicle is getting closer to the obstacle with high relative speed.

The desired motions for automated driving control are determined with longitudinal / lateral candidate motions as shown in the Fig. 4. The boundaries of the candidate motion are determined from the collision risks around the subject vehicle, i.e., the vehicles in left-lane, right-lane and in-lane. The candidate motions for longitudinal and lateral safety are discretized within the predicted time horizon[10].

(a) Desired Yawrate Candidates for Lateral Safety Control

(b) Desired Acceleration Candidates for Longitudinal Safety Control
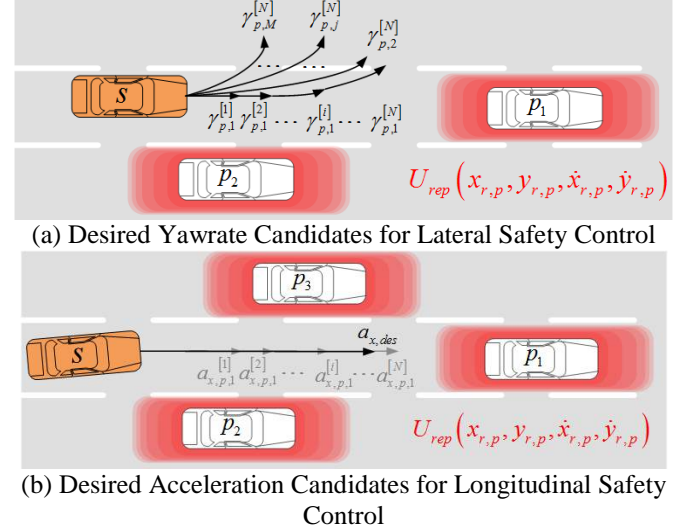
Fig. 4. Desired Motion Validation via Test Result

Cost functions for the desired longitudinal and lateral motion are defined with the potential energy function of predicted motions of the subject and object vehicles, and control input limitations such as the norm of control input, and the rate of control input as shown in (7), (8). The desired motions can be determined from the pre-defined cost functions to be minimized within control input boundaries.

$$J_{lat}(j) = \sum_{i=1}^{N}\left(\begin{array}{l} w_1 \cdot U_{rep}\left(x_{r,p}(j), y_{r,p}(j), \dot{x}_{r,p}(j), \dot{y}_{r,p}(j)\right) \\ + w_{lat,1} \cdot \left(\gamma_{p,j}^{[i]}\right)^2 \end{array}\right)$$
$$+ w_{lat,2} \sum_{i=0}^{N-2}\left(\gamma_{p,j}^{[i+1]} - \gamma_{p,j}^{[i+1]}\right)^2 \qquad (7)$$

$$J_{long}(j) = \sum_{i=1}^{N}\left(\begin{array}{l} w_1 \cdot \left(U_{rep}\left(x_{r,p}(j), y_{r,p}(j), \dot{x}_{r,p}(j), \dot{y}_{r,p}(j)\right)\right) \\ + w_{long,1} \cdot \left(a_{x,p,j}^{[i]}\right)^2 \end{array}\right)$$
$$+ w_{long,2} \sum_{i=0}^{N-2}\left(a_{x,p,j}^{[i+1]} - a_{x,p,j}^{[i]}\right)^2 \qquad (8)$$

$$u_{k,des} = \underset{u_{k,min} \le u_k \le u_{k,max}}{\arg\min}\left(J_k(j)\right), \ k \in [long \ lat] \qquad (9)$$

A potential field approach can be applied for lane keeping situation[11]. The previous research proposed a potential energy function including the heading angle of the vehicle to the lane, which is provided a vision sensor with low reliability. A proposed risk potential includes the relative distance and velocity to the center lane which can be calculated with the measured lane information from vision sensor such as distance-to-line crossing(DLC) and time-to-line crossing(TLC) represented as:

$$\hat{v}_y = v_x \cdot \psi \approx \frac{d(DLC)}{dt} \quad where, \ \psi : vehicle \ heading \ angle \qquad (10)$$

$$TLC = \frac{DLC}{\hat{v}_y} \qquad (11)$$

The artificial risk potential is assessed around the center lane as shown in Fig. 5 with the same concept of safety margin represented in Fig. 4.
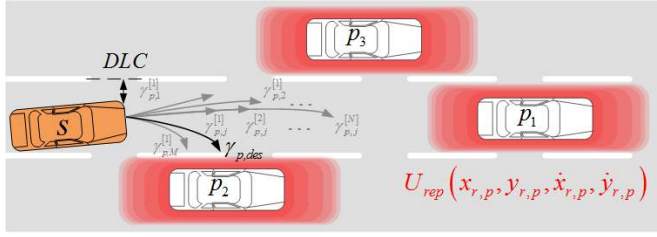
Fig. 5. Description of Line Crossing

$$J_{lane}(j) = \sum_{i=1}^{N}\left(w_1 \cdot U_{rep,lane}\left(DLC, \psi_{heading}\right) + w_{lane,1} \cdot \left(\gamma_{p,j}^{[i]}\right)^2\right)$$
$$+ w_{lane,2}\sum_{i=0}^{N-2}\left(u_{lat}^{[i+1]} - u_{lat}^{[i]}\right)^2 \qquad (12)$$

$$\gamma_{des} = \underset{u_{min} \le \gamma \le u_{max}}{\arg\min}\left(J_{lane}(j)\right) \qquad (13)$$

A driving mode of automated driving is determined as the following procedure represented in Fig. 6. A subject vehicle drives with pre-defined set speed with lane keeping control in the low collision risk situation with front vehicle. If the collision risk of the front vehicle increases, the control algorithm should determine the driving mode for collision avoidance with lane change or lane keeping with speed control under the consideration of the collision risks of the vehicle in left land and right lane.
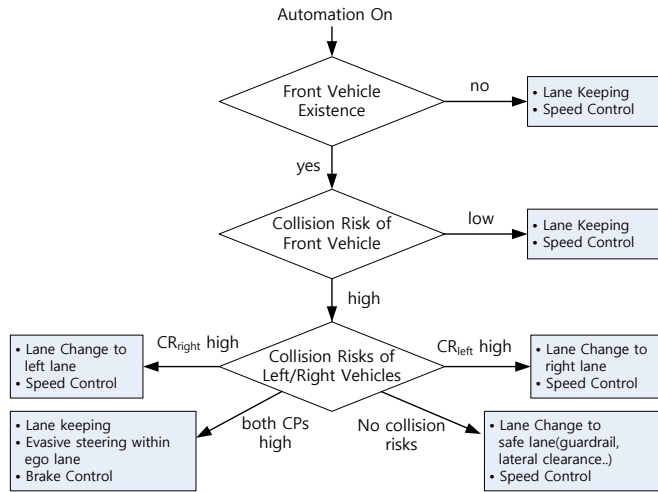
Fig. 6. Driving Mode Decision Procedure

3.2 Dynamic constraints

Several constraints between the vehicle and ground are considered to ensure vehicle dynamic stability along the path. The constraints treated in this paper include: 1) limits on tire force, and limits on the lateral motion which includes 2) limits on steering characteristics, 3) limits on side slip behavior, and 4) limits on rollover characteristics. Each longitudinal and lateral motion of the vehicle should be bounded with the physical constraint and dynamic constraint corresponding with the vehicle speed.

a. Tire force constraint

The braking pressure produces the friction force tangent to the path at the contact patch. Normally the friction force is proportional to the measured brake pressure. The friction force is represented with the normal load on the tire, the friction coefficient of the tire-road interface, and the slip ratio defined as follows:

$$\lambda = \frac{r_{eff}\,\omega_w - v_x}{v_x}, \text{during braking}$$

$$\lambda = \frac{r_{eff}\,\omega_w - v_x}{r_{eff}\,\omega_w}, \text{during acceleration} \qquad (14)$$

where, r_{eff} = *effective radius of the tire*

ω_w = *rotational velocity of the wheel*

When the longitudinal slip ratio is small(less than 0.1 on dry asphalt), the friction force is found to be proportional to the slip ratio with longitudinal tire stiffness. The maximum tire friction force for passenger cars can be determined tire characteristics, and the driving force is directly related with the maximum engine force. These limitations are assumed to be constant and independent of speed. Equation (15) yields the feasible deceleration range due to constraints on the tire friction force.

$$-\frac{F_{x,max}}{m} \le a \le F_{engine} \qquad (15)$$

b. Limits on the lateral motion

Limits on the lateral motion of the vehicle are represented with the steering constraint, side slip constraint, and rollover constraint. The states within the area denote the stable condition in the current driving situation, and the boundary around the area represents the marginal states guaranteeing the stable condition. Equation (16) represents the relationship between the lateral acceleration, yaw rate and longitudinal velocity in steady-state case [12]

$$a_y = \dot{v}_y + v_x \cdot \gamma \approx v_x \cdot \gamma \qquad (16)$$

A steering constraint represents the limitation on the lateral acceleration by maximum steering angle attainable with dynamic handling properties of a vehicle. The dynamic handling properties are obtained from a 2-DOF bicycle model represented as:

$$m \cdot a_y = 2C_f \cdot \alpha_f \cdot \cos\delta_f + 2C_r \cdot \alpha_r$$
$$I_z \cdot \dot{\gamma} = 2l_f \cdot C_f \cdot \alpha_f \cdot \cos\delta_f - 2l_r \cdot C_r \cdot \alpha_r \approx 0 \qquad (17)$$

Where, α_f and α_r represent the wheel slip angle at front and rear wheel. From the definition of the slip angle, the following relationship can be derived with the understeer gradient K_{steer}:

$$\delta_f = K_{steer} \cdot a_y + \left(l_f + l_r\right)\frac{\gamma}{v_x}$$

$$K_{steer} = \frac{m \cdot l_r}{2C_f \cdot \left(l_f + l_r\right) \cdot \cos\delta_f} - \frac{m \cdot l_f}{2C_r \cdot \left(l_f + l_r\right)} \qquad (18)$$

From (16) and (18), the steering constraint in the current states is represented as shown in (19) with the maximum steering angle, which is near 540deg in a passenger car, current front steering angle, and vehicle speed.

$$|\gamma| \le \frac{\delta_{max} \cdot v_x}{Ksteer \cdot v_x^2 + (l_f + l_r)} \qquad (19)$$

A side slip constraint represents the maximum yaw rate of a vehicle within the boundary of lateral stability. A vehicle shows the skid maneuvering when a magnitude of the lateral force exceeds the physical limit of tire-road friction. The slip constraint is derived from the tire-road friction including road friction coefficient, μ, as following equation:

$$m \cdot |a_y| \le \mu \cdot m \cdot g \qquad (20)$$

Equation(20) can be rewritten by substituting (16) into (19) as shown in (22). A side slip constraint is represented with the tire-road friction and current speed of a vehicle.

$$|\gamma| \le \frac{\mu \cdot g}{v_x} \qquad (21)$$

A rollover constraint which represent the limit of lateral acceleration for rollover prevention can be obtained from rollover index[13]. A rollover risk can be determined with the following factors: 1) roll angle and roll rate, 2) lateral acceleration, and 3) time to wheel lift of a vehicle. The rollover index(RI) is calculated by using the lateral acceleration which can be measured from electronic stability control(ESC) module, the estimated roll angle, the estimated roll rate, and their critical values as following equation:

$$RI =$$

$$\begin{cases} C_1 \dfrac{|\phi(t)| \cdot \dot{\phi}_{th} + |\dot{\phi}(t)| \cdot \phi_{th}}{\phi_{th} \cdot \dot{\phi}_{th}} + C_2 \dfrac{|a_y|}{a_{yc}} + C_3 \dfrac{|\phi(t)|}{\sqrt{\phi(t)^2 + \dot{\phi}(t)^2}}, & K_r > 0 \\ \\ 0 \quad , K_r \le 0 \end{cases} \qquad (22)$$

$$where, \ K_r = \phi \cdot (\dot{\phi} - k_1 \phi)$$

where, $C_1 + C_2 + C_3 = 1$. C_1, C_2, C_3 and k_1 are positive constants. The subscript *th* represents the critical value of each state. The maximum lateral acceleration which keeps the rollover index below the critical value can be represented as follows:

$$a_{y,roll,max} =$$

$$\frac{a_{y,c}}{C_2}\left(RI_{tar} - C_3 \cdot \frac{|\phi(t)|}{\sqrt{\phi(t)^2 + \dot{\phi}(t)^2}} - C_1 \cdot \frac{|\phi(t)|\dot{\phi}_{th} + |\dot{\phi}(t)|\phi_{th}}{\phi_{th}\dot{\phi}_{th}} \right) \qquad (23)$$

$$where, \ RI_{tar} = Target \ Rollover \ Index$$

$$a_{y,c} = Critical \ Acceleration$$

RI_{max} denotes the maximum rollover index. The maximum yaw rate considering rollover prevention can be represented by substituting (23) into (16) as shown in (24).

$$|\gamma| \le \frac{a_{y,roll,max}}{v_x} \qquad (24)$$

A steering constraint, side slip, and rollover constraints are subspaces of the drivable area, which included the set of vehicle longitudinal speed and yaw rate which are attainable at a given instant as shown in Fig. 7.
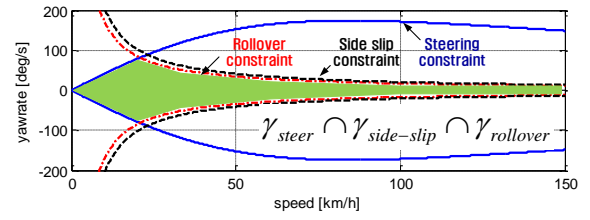
Fig. 7. Drivable Area

The desired motions for collision avoidance derived by the risk potential function should be bounded within the drivable area. In consequence, the desired steering angle with desired yaw rate can be represented as follows:

$$\delta_{des} = \frac{v_x \cdot C_f \cdot C_r \cdot L}{C_f \cdot C_r \cdot L^2 + m \cdot v_x^2 (C_r \cdot l_r - C_f \cdot l_f)} \gamma_{des} \qquad (25)$$

4. SIMULATION RESULTS

The simulation results indicating the time history of the vehicle behavior are depicted as shown in Fig. 8. The preceding vehicle drives at 80km/h keeping its lane with 70m of initial clearance to the subject vehicle, which cruises at 105km/h set speed. The risk potential function assesses the desired motion of the subject vehicle for collision avoidance with proceeding vehicle. The first step for the desired motion determination is to assess whether the current collision risk is avoidable without braking. If the current collision risk can be avoidable without braking, then the lateral acceleration profile is calculated to satisfy both avoiding the collision with the preceding vehicle and preventing the lateral collision with adjacent vehicle. Fig. 8 depicts the avoiding motion of the subject vehicle.

(a) Lane keeping and speed control (b) Starting Lane change

(c) Finishing Lane change and lane keeping (d) Lane keeping and speed control

Fig. 8. Lane Keeping and Lane Change Animation

(a) Driving Mode Transition

(b) Desired Steering Wheel Angle

(c) Velocity Profile of a Subject Vehicle

(d) Collision Probability of Inlane Target (Target1)
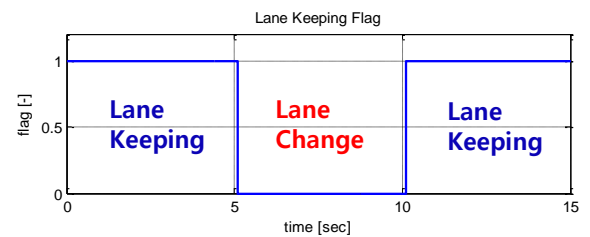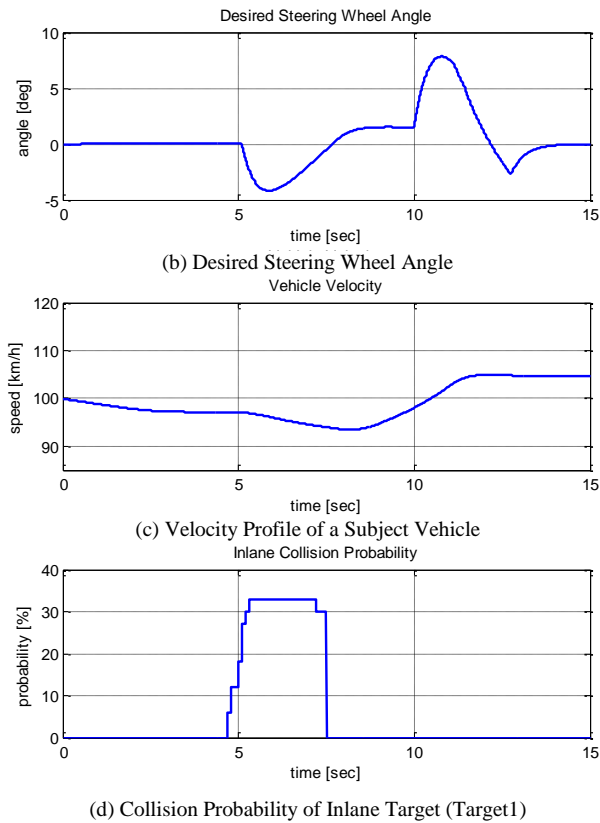
Fig. 9. Simulation Results

CONCLUSIONS

An automated driving control algorithm for safety management has been developed in this paper. The probabilistic prediction method has been adopted to represent the future collision risk between a subject and surrounding vehicles, and the collision probability has been defined using the predicted motions of the vehicles. A risk potential function has been investigated considering the predictive relative position and velocity between the subject and the obstacles. The desired motion for lane keeping, or lane change for safety has been determined with the predictive motion of the subject and object vehicles considering with its collision risk. In order to guarantee the lateral stability in high-speed driving, the desired motion of the subject vehicle is bounded by the dynamic constraints classified as the steering constraint, side slip constraint and rollover constraint. The performance of the proposed algorithm has been investigated via computer simulation. The simulation results revealed that the proposed collision avoidance algorithm prevents the collision with the surrounding vehicles by changing its lane considering the collision risk around the subject vehicle.

ACKNOWLEDGEMENT

REFERENCES

[1] Rolf Isermannn, Roman Mannale, Ken Schmitt. "Collision-avoidance systems PRORETA: Situation analysis and intervention control", Control Engineering Practice, Vol.20, 2012, pp. 1236-1246.

[2] S. Ge and Y. Cui, "Dynamic Motion Planning for Mobile Robots Using Potential Field Method," Autonomous Robots, Vol. 13, 2002, pp.207-222

[3] Ryosuke Matsumi, Pongsathorn Raksincharoensak, Masao Nagai, "Autonomous Braking Control System for Pedestrian Collision Avoidance by Using Potential Field", Proceedings of the 7TH IFAC Symposium on Advances in Automotive Control, 2013

[4] Shingo Shimoda, Yoji Kuroda and Karl Iagnemma, "Potential Field Navigation of High Speed Unmanned Ground Vehicles on Uneven Terrain", Proceedings of the 2005 IEEE International Conference on Robotics and Automation, 2005

[5] Polychronopoulos, A. Tsogas, M., Amditis. A.J., Andreone, L., "Sensor Fusion for Predicting Vehicles' Path for Collision Avoidance Systems," Intelligent Transportation Systems, IEEE Transactions on , vol.8, no.3, pp.549-562, Sept. 2007.

[6] Kyongsu Yi, Il-Ki Moon, "A driver-adaptive stop-and-go Cruise control strategy," Proceedings of the 2004 IEEE International Conference on Networking, Sensing and Control, 2004

[7] Beomjun Kim and Kyongsu Yi, "Probabilistic States Prediction Algorithm using Multi-sensor Fusion and Application to Smart Cruise Control System", Proceedings of the 2013 IEEE Intelligent Vehicles Symposium, 2013

[8] Schwartz, D.A., "Clothoid road geometry unsuitable for sensor fusion clothoid parameter sloshing," , Proceedings of the 2003 IEEE Intelligent Vehicles Symposium, 2003

[9] Liu Chengqing, Marcel0 H Ang Jr, Hariharan Krishnan, Lim Ser Yong, "Virtual Obstacle Concept for Local-minimum-recovery in Potential-field Based Navigation", Proceedings of 2000 IEEE International Conference on Robotics & Automation, 2000

[10] Takahiro Hasegawa, Pongsathorn Raksincharoensak and Masao Nagai, "Risk-Potential Based Motion Planning and Control of Proactive Driving Intelligence System for Enhancing Active Safety", Proceedings of the AVEC'14, 2014

[11] Eric J. Rossetter and J. Christian Gerdes, "Lyapunov Based Performance Guarantees for the Potential Field Lane-keeping Assistance System", Journal of dynamic systems, measurement and control, 128(3), pp. 510-522, 2005

[12] Matthew Spenko, Yoji Kuroda, Steven Dubowsky and Karl Iagnemma, "Hazard avoidance for high-speed mobile robots in rough terrain", Journal of Field Robotics, Vol. 23, pp. 311–331, 2006

[13] Jangyeol Yoon, Dongshin Kim and Kyongsu Yi, "Design of a rollover index-based vehicle stability control scheme", Vehicle System Dynamics, Vol. 45, pp. 459-475, 2007

Probabilistic Threat Assessment of Vehicle States Using Wireless Communications for Application to Integrated Risk Management System

Donghoon Shin*, Beomjun Kim* and Kyongsu Yi*

**Department of Mechanical and Aerospace Engineering, Seoul National University,
Seoul, Korea, (e-mail: kyi@snu.ac.kr)}*

Abstract: This paper presents a probabilistic threat assessment of vehicle states using wireless communications for application to integrated risk management system. Since one of the main concerns in risk assessment is an assessment of collision risk, it is necessary to estimate the probability of collision occurrence of the ego vehicle which expresses driver sensitivity. Recent developments in vehicle onboard computers and wireless communications devices, also known as dedicated short-range communication (V2V) devices allow the exchange of information between vehicles (V2V communications). The prediction performance of the proposed method, which integrates V2V communications to conventional advanced driver assistant systems (ADAS), has been investigated via simulations using the commercial vehicle software Carsim and Matlab/Simulink. It is shown the threat assessment performance for the given driving situations can be significantly enhanced by the proposed algorithm. This leads to improvement of conventional driver assistance functions of ADASs.

Keywords: Cooperative Driver Assistance Systems, Risk Assessment, V2V Communications

1. INTRODUCTION

In recent years lots of research efforts are underway with the goal of enhancing the safety, efficiency and comfort of highway/urban traffic with the aid of Vehicle-2-Vehicle communications. Roeckl et al. (2008) addresses future driver assistance system which aims to a complete and accurate target prediction performance because using an inaccurate information of a single vehicle may result in a hazardous situation. Most traffic accidents occur due to a human false estimation of the current traffic situation which is the consequence of misinterpretation or a limited amount and accuracy of information. Thus numerous advanced driver assistant systems (ADAS) have been developed and commercialized for the driver's safety and handling enhancement (Pilutti 1998). In the same context, the automotive safety concerns has to be addressed with an integrated risk management system (IRMS) approach. In order to interact with V2V communications, current ADASs and wireless communications should become integrated and merging with each other.

The current stages of risk metrics are mainly based on the predicted time when some predefined risky event occurs. The typical predicted time indices include the time to collision or time to impact. According to a number of literature reviews, an assessment of collision risk which corresponds with driver behavior which also can be applied to many complex situations is discussed. A proposed risk assessment algorithm cover a range of all requirements by focusing on collision probability.

As is known to all, automotive radar is the best fitted vehicular sensing technology for the target state estimation problem. However, in an application of automotive radars, one of the most significant problems is an uncertain measurement model problem which is wandering on the target's physical boundary. And the data obtained is limited to the relative information such as position, speed and acceleration measurements, as well as an approximate shape. Object detection is also restricted by object occlusion and it heavily depends on the sensor coverage area. Since many heuristics are applied to the target detection, a compromise between sensitivity and false positive rates always exists. Furthermore it is really hard to reliably detect static objects and objects in far distances. To overcome this issue, more accurate target vehicle's information such as yaw rate, absolute velocity and acceleration needs to be transmitted using the V2V communications.

We consider the V2V communications which allow the enhancement of already existing driver assistance system. Once the target vehicle information is transmitted to ego-vehicle, it can be used for instance in driver assistance systems to improve safety, efficiency and comfort of driving.

However, the V2V communication experiences random power fluctuations over time due to changing reflections and attenuations. These power fluctuations cause time-varying data rates and intermittent connectivity. Thus, wireless communication networks inevitably introduce time delay and packet loss.

Despite the shortcomings in both technologies, it is found that radar and V2V are complimentary to each other. Since radar is able to provide a constant passive scanning of the surrounding by catching all detection candidates. Therefore it provides good relative positioning measurements. If those candidates happen to be wireless communications equipped,
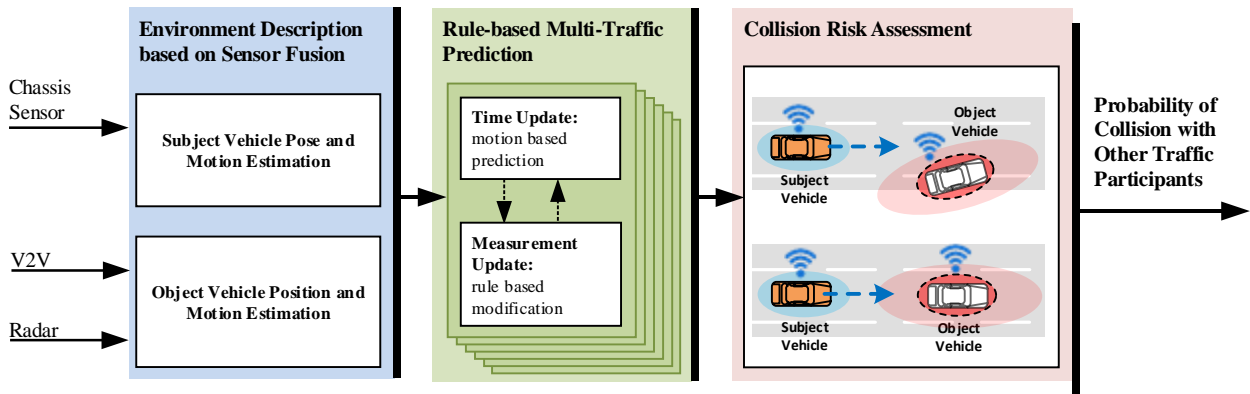
Fig. 1. Architecture of a probabilistic risk assessment algorithm

the information from their V2V communications messages can help to eliminate most uncertainties and enrich those candidates with more additional information. In this sense, drops in V2V message reception is not such a big issue. The integrated or fused target information can be regarded as more reliable than each individual source. Once the information from V2V is fused to radar detected objects, shortcomings of both systems can be eliminated. Hence, the environment perception capability can be greatly enhanced, in terms of sensing reliability and detection range. Therefore, improvements to existing driver assistance systems or even new features are possible.

Recently, several researchers have focused their research on development of new concept of risk index and elaboration of estimation and prediction steps with consideration of uncertainties. Some approaches calculate the probability of a collision based on the joint predicted probability density function of the host and the object vehicle (Jansson 2004), (Lambert 2008). The probability density function is obtained by a Kalman filter, and its prediction is based on the same simple motion models used in the Kalman filter. As there is no analytical solution to the integral over the joint probability density function, Monte Carlo approximations are performed. For the second demand, the improvement by an integrated particle filter approach is presented by Karlsson et al. (2004). Schubert et al. (2012) proposed a direct link between the Bayes filters used by the tracking modules and the situation assessment based on Bayesian networks. Broadhurst et al. presented a prediction and planning framework for analyzing the safety and interaction of moving objects in complex road scenes (Broadhurst 2005).

The contributions of this paper are as follows. The V2V communication concept and the radar system are discussed with the explanation of data fusion concept. The V2V message delay compensation method based on state augmented Kalman filters (AKF) is also explained. Environment description based on sensor fusion and rule-based vehicle state prediction is presented in the following section. A numerical approximation method of collision probability is derived in Section *5*. And the proposed algorithm is evaluated and validated via simulations using the commercial vehicle software Carsim and Matlab/Simulink. Finally, conclusions drawn.

The overall architecture of the proposed automated driving control algorithm is shown in Fig. 1. The probable behaviors of the surrounding vehicles over a finite prediction horizon are predicted using the information of current states of surrounding vehicles. The controller is designed to determine the desired longitudinal acceleration and the desired steering angle separately.

2. COMMUNICATION CONCEPT AND RADAR SYSTEM

2.1 Key Wireless Communication Concepts

To facilitate the exchange of control information, vehicles are equipped with wireless communications devices, also known as dedicated short-range communication (V2V) devices. Each vehicle is equipped with an IEEE 802.11p (V2V) transceiver (Challita 2009). The typical message update rate is 20ms, depending on the configuration and the wireless channel load. For example the Basic Safety Message (BSM) contains three categories of information about the hosting vehicle (DSRC Committee 2009): 1) position information 2) vehicle parameters and real-time vehicle behavior status, from the on-board sensors via the CAN bus interface 3) history information, such as a waypoint history of its past trajectory produced by the internal software. The range of transmission depends on the power settings and path-loss over distance. Simulations and tests show that good reception can be achieved within 800m (Breu 2014) in line-of sight scenarios. But a certain amount of messages transmitted by others might be missed due to packet collisions at high channel load (Chen 2011). The message delay, dominated by the channel access delay, is generally less than 0.2ms in moderate channel load scenarios (Alimohammadi & Puoyan). Once a message is received, the information about the sender becomes known to the host vehicle. The vehicle behavior status information is highly precise, because they are direct readings at the sender side. The following further assumptions were made for the communication system: (Challita 2009), (Zhou 2012).

a) For each vehicle, messages are sent every   time steps from time 0.

b) After each message is sent, it takes τ_0 seconds for encoding and decoding the message.
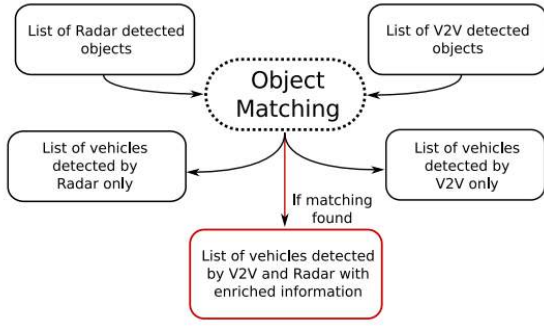
Fig. 2. Generalized process overview for radar and V2V fusion

c) When one message is sent, it is received by each vehicle independently with probability 1 − ρ, where ρ is the message loss rate. This rate ρ was assumed to be a constant for all sender–receiver pairs and for all time.

2.2 Radar System

Radar sends out wave beams to scan its surroundings and collect the reflected signals. Based on the wave traveling time, distance can be computed in high accuracy. Reflected signals are registered as points in the vehicle coordinate system. Point clouds are grouped and tracked by filters, to form the detection candidates. Those with high confidence are output by the radar system as a list of detected objects. Usually each object contains an internal tracking ID, distance, speed measurements and acceleration estimates based on the Doppler Effect. Advanced radar systems can even give rough dimension estimations based on the L-shape reflecting points. However, radar usually only sees a side or a corner of a vehicle, thus object dimension estimation is not very consistent. The classification of objects types can also be difficult. The vehicle's behavioral status, such as the intention to make a turn or brake, is even harder to determine by a radar system. Those intentions cannot effectively be detected until the vehicle dynamics have undergone a noticeable change for some period of time.

2.3 Wireless Communication and Radar Data Fusion Concept

When a vehicle is equipped with both V2V and radar systems, a list of detected objects from radar and a list of object vehicle which can be known via V2V is available for data fusion. The purpose of the fusion concept, as shown in Fig. 2, is to 1) synchronize two sources of information 2) associate V2V object vehicles to radar objects 3) append the rich information from V2V to the radar objects 4) forward fused data to advanced driver assistant applications. To associate two sets of data, certain common information shall be picked to serve as data linkage cues, such as position, velocity, acceleration or a combination of those values. We pick position as the data linkage cue and use the algorithm described in Section 3 find associations between V2V data and radar detected objects.

2.4 Communication Delay Compensation

In order to compensate delayed state variable using delayed measurements, state variable is augmented to incorporate previous state variable. Thus the process model is transformed to as below.

$$\begin{bmatrix} x(k+1) \\ x(k) \end{bmatrix} = \begin{bmatrix} F \cdot x(k) + v(k) \\ x(k) \end{bmatrix}$$
(1)

3. ENVIRONMENT DESCRIPTION BASED ON SENSOR FUSION

As shown in Fig. 3 a rule-based object-vehicle, a rule-based object-vehicle prediction and a collision risk assessment utilize an environment description based on multi-sensor (V2V/Radar) fusion [19, 20].

3.1 Host Vehicle Pose and Motion Estimation

An estimation of host vehicle's pose and motion is achieved using measurements of an onboard chassis sensors such as wheel speeds, yaw rate, and longitudinal acceleration.

The host vehicle's state vector is defined as follows:

$$\mathbf{x}_{host} = \begin{bmatrix} p_x & p_y & \theta & v_x & \gamma & a_x & \dot{\gamma} \end{bmatrix}^T$$
(2)
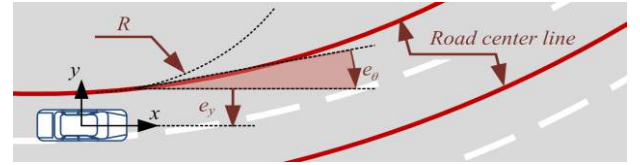
(a) The relationship between the subject vehicle and the road center line of each lane
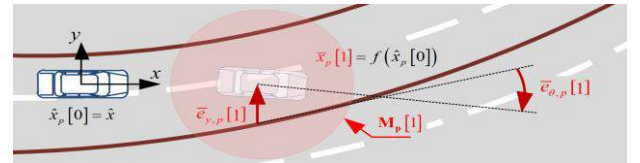
(b) The time-update-predicted host vehicle states and the relative error states with respect to road geometry defined on current body coordinate
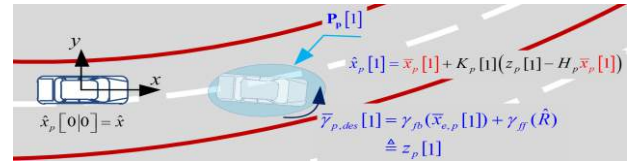
(c) The measurement-update-predicted subject vehicle states where the predicted desired yaw-rate to keep the lane is defined as virtual measurement
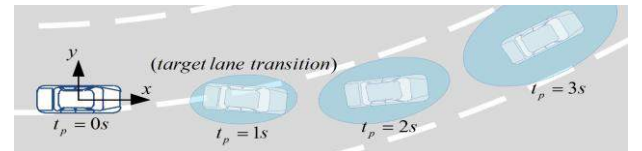
(d) Prediction results for 1s, 2s, and 3s of prediction time, t_p, at a lane-changing instant

Fig. 3. Procedure and Concept of Traffic Behavior Prediction

where p_x is the vehicle's longitudinal position, is the vehicle's lateral position θ is the orientation, v is the velocity, γ is the yaw rate, a is the acceleration, and $\dot{\gamma}$ is the yaw acceleration.

3.2 Object Vehicle State Estimation

The object vehicle is detected, tracked and estimated. To describe motion of target vehicles, the state vector of object vehicle are defined as follows:

$$\mathbf{x}_{obj} = \begin{bmatrix} p_{obj,x} & p_{obj,y} & \theta_{obj} & v_{obj,x} & \gamma_{obj} & a_{obj,x} & \dot{\gamma}_{obj} \end{bmatrix}^T \quad (3)$$

where subscript obj denotes object vehicle, note that p_{objx}, p_{objy} and θ_{obj} are defined on the subject vehicle's body-fixed moving frame and other elements are defined on the ground-based fixed frame. A detailed description of the environment description can be found in (Kim 2015, 2014)

4. RULE-BASED VEHICLE STATES PREDICTION

In order to compute reachable set for traffic participant, stochastic process of object-vehicle is modelled by Markov chains. It is assumed that the driver may maintain the current behavior in the near future and keep the relevant lane in the far-off future. To implement this assumption, a path-following model and a vehicle-state predictor keep interacting with each other during one cycle of the prediction process. This concept is summarized and presented in Fig. 3 (Kim 2015, 2014).

4.1 Traffic Behavior Model

The objective of the traffic behavior model is to develop a yaw control system for human-like lane keeping. To achieve this goal, it is useful to utilize a dynamic model in which the state variables are in terms of position and orientation error with respect to the given road. The error state is defined in terms of fixed coordinates under the assumption of traveling with constant longitudinal velocity on a road of constant radius. The error state is defined in inertial fixed coordinates rather than body-fixed moving coordinates. Assume that the human drivers determine the desired yaw rate γ_{des} by a state feedback and a feed-forward term that attempts to compensate for the road curvature.

4.2 Stochastic-filtering-like Traffic Behavior Prediction

The ellipses around the vehicles in Fig. 3 depict the reachable area of the vehicle. Because the proposed prediction algorithm is based on a stochastic filtering method, the covariance of the prediction error can be evaluated at each time step. Furthermore, the eigenvalue and eigenvectors of the 2nd leading principal minor of the covariance determine the likelihood ellipse around the predictive position. Using the square root of the eigenvalues as semi-axes measured

along the eigenvectors, we can sketch the 39% likelihood ellipse with the center at the most likely predictive position. This analysis is very useful to compute the probability of collision occurrence and assess the risk of current driving scene.

5. Risk Assessment Algorithm

This Section describes the algorithm for estimating the probability of collision occurrence of the ego vehicle. As following the basic idea of the particle filtering, the collision probability is numerically implemented and calculated.

(a) A collision case example of the generated N particles and its two vehicle-body-shaped-polygons. Intersection between two polygons.

(b) A non-collision case example of the generated N particles and its two vehicle-body-shaped-polygons.

Fig. 4. Procedure and concept of approximation of collision probability

Input
  Predicted states and its covariance within a pre-defined prediction horizon for all tracked traffic participants.

For all tracked traffic participants, $n = 1, \cdots, N_{target}$

For every predictive time step, $p = 0, \cdots, N_p$

- Initialize collision count with participant n at predictive time step p, $C.P.cnt_n^i = 0$.
- From the given predicted state and covariance, randomly generate N particles, $\mathbf{x}_n^i[p]$.

  For every particle, $i = 1, \cdots, N$

  - Generate two vehicle-body-shaped-polygons.
  - Check if the vehicle bodies can be possibly intersected.
  - If intersection is detected, $C.P.cnt_n^i = C.P.cnt_n^i + 1$
  - Else, $C.P.cnt_n^i = C.P.cnt_n^i$.

  End

- Approximate collision probability with participant n at predictive time step p.
- $C.P._n^i = C.P.cnt_n^i / N$.

End
End

Fig. 5. Algorithm for collision probability calculation

5.1 Collision Probability

The conceptual visualization of probabilistic collision risk is summarized and presented in Fig.4. Details of the algorithm are presented in Fig.5. As the beginning of the collision probability estimation, we randomly generate a given number N state vectors based on the initial probability density function which is known (from prediction algorithm). The parameter N could be chosen by the user as a trade-off between computational effort and collision probability approximation accuracy. The state vectors are called particles and are denoted as:

$$\mathbf{x}_n^i[p] = \begin{bmatrix} \hat{\mathbf{x}}_{host}[p] \\ \hat{\mathbf{x}}_n[p] \end{bmatrix} + \left(\sqrt{\begin{bmatrix} \hat{\mathbf{P}}_{host}[p] & \\ & \hat{\mathbf{P}}_n[p] \end{bmatrix}} \right) \cdot \tilde{\mathbf{r}}^i \qquad (i = 1, \cdots, N)$$

(3)

where p is the predictive time step, $\hat{\mathbf{x}}_{host}$ is the predicted position and orientation state of the host vehicle, $\hat{\mathbf{x}}_n$ is the predicted pose state of nth traffic participant, $\hat{\mathbf{P}}$ denotes proper size of covariance matrix of each predicted state, and $\tilde{\mathbf{r}}$ *is a white noise* random vector of proper size. For every possible pair of host and one of traffic participants, we investigate whether the vehicle bodies of the traffic participant can intersect the host vehicle at each predicted time step. To determine the body intersection, a body-shaped-polygon is introduced.

6. SIMULATION SCENARIOS

6.1 Parked Vehicle Cut-in (PVC)

For the PVC simulations in Fig. 5-(a), initially the subject vehicle is cruising at certain speed of 35kph on the urban-road. Then a parked vehicle in adjacent lane, object vehicle, suddenly cuts in. In this scenario, the object vehicle accelerates from 0kph to 30kph.

With the aid of V2V communication system, the cut-in vehicle transmits the exact information such as yaw rate,
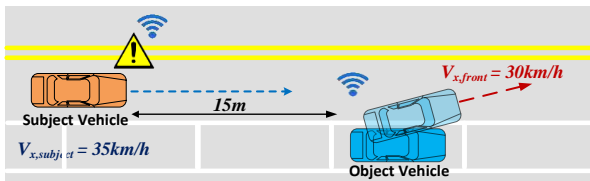
(a) Parked Vehicle Cut-in (PVC)
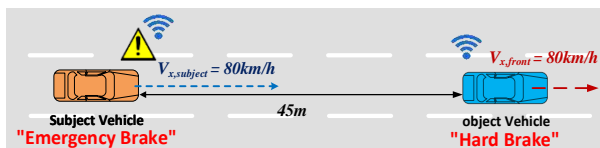
(b) Highway Acceleration and Deceleration

Fig. 5. Simulation Scenario

longitudinal velocity and acceleration to the subject vehicle at the instant it starts to cut in from the center of the of the adjacent parking space. The V2V communication system allows the subject vehicle to have 2-3seconds to slow down and to change the lane by making space for the cut-in vehicle.

With respect to wireless communication environment, it is to simulate vehicles driving at a normal state, with only a few disruptions in the wireless channel. Therefor $K_s = 2$, meaning that messages are sent every 0.1 s. The message loss rate is set at $\rho = 0.1$, which means that 10% of the messages are lost during one transmission (Zhou 2012). In this the maximum time delay is about 140ms.

6.2 Highway Acceleration and Deceleration (HAD)

The other simulation scenario in Fig. 5-(b) is constructed by unexpected deceleration and acceleration of the preceding (object). In this scenario, initially subject and object vehicle are cruising at 80kph with the clearance of 45m. Then the object vehicle applies hard brake with the break pressure of 2MPa from 4 to 7 seconds and accelerates again right after then. Without V2V communication, the radar only using vehicle would recognize the cut-in vehicle's hard brake with the estimation of acceleration based on the Doppler Effect.

With the aid of V2V communication system, the sudden decelerating vehicle transmits the exact information such as yaw rate, longitudinal velocity and acceleration to the subject vehicle at the instant it starts to apply hard brake.

With respect to wireless communication environment, it is to simulate vehicles driving at a normal state, with only a few disruptions in the wireless channel. Therefore $K_s = 2$, meaning that messages are sent every 0.1 s. The message loss rate is set at $\rho = 0.1$, which means that 10% of the messages are lost during one transmission [22]. In this the maximum time delay is about 140ms.

7. SIMULATION RESULTS

7.1 Parked Vehicle Cut-in (PVC)

Error! Reference source not found. 6 presents a case example of the proposed algorithm at the moment that the object vehicle is coming out from the parking spot. **Error! Reference source not found.** 7 shows the predicted positions and its uncertainties of each traffic participant.

Table 1. Simulation Results Analysis

Phase0	Normal Driving Situation
Phase1	Dangerous Situation (Human Perception Fail)
Phase2	Warning Detection/Collision Prevention Control
Phase3	Re-enter to Safety Region/Spacing

the object vehicle's motion information such as yaw rate and acceleration, is directly transmitted to subject vehicle, the

(a) V2V/Radar Fusion   (b) Radar only
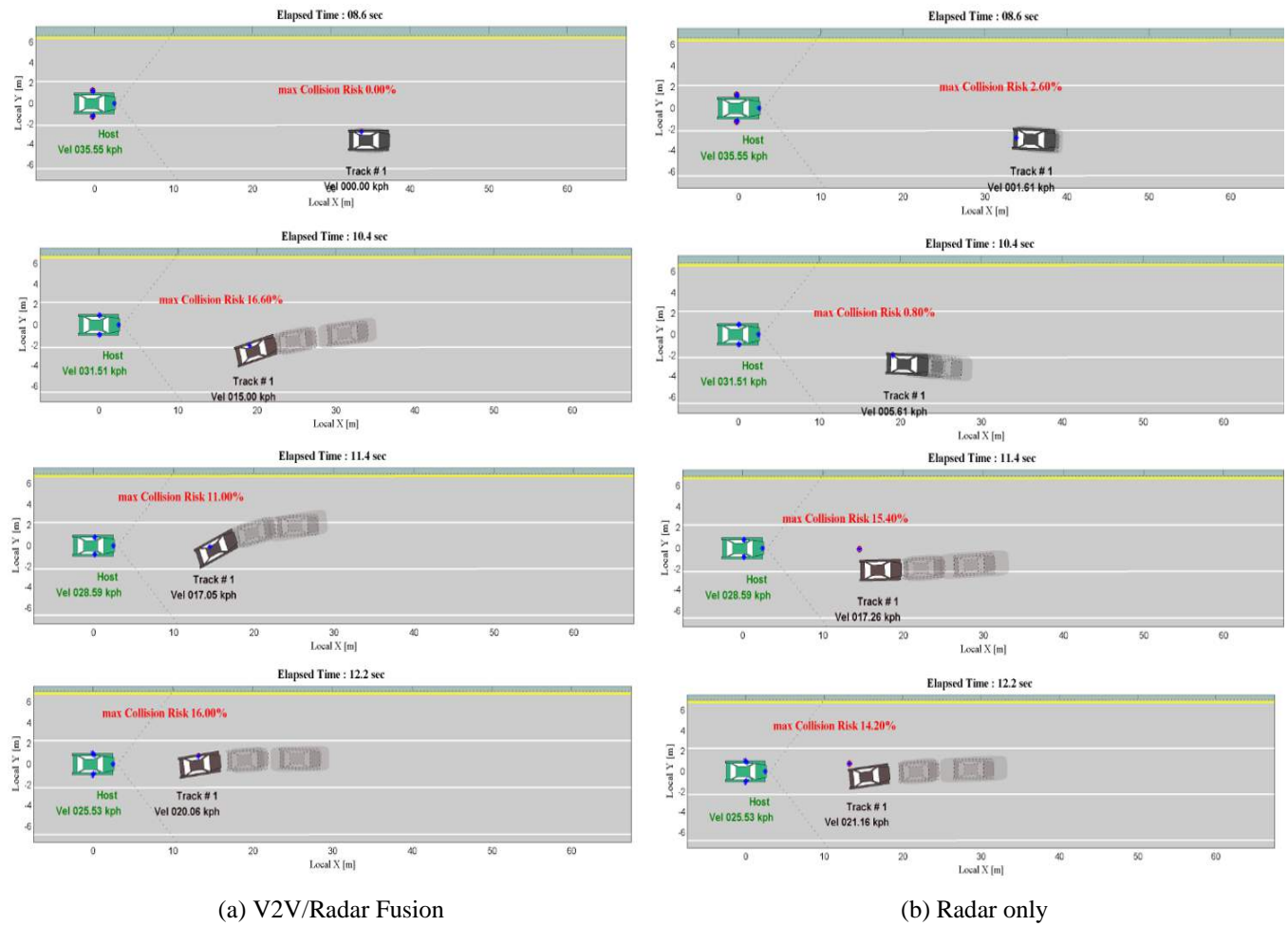
Fig. 6. Simulation Results for Parked Vehicle Cut-in Scenario

Table 1 shows the analysis method of simulation results based on Integrated Risk Management System (IRMS). As shown in Fig. 6, the subject (host) vehicle is described by green and the cut in vehicle (Track #1) is expressed by grey. The predictions for reachable set are described by the vehicle with the dotted-line and the color continuously changes for every 1s of the time interval depending on the collision risk. The total range of prediction time horizon is given by 2s.

Since more accurate and additional object vehicle information is sent to subject vehicle, V2V/Radar fusion algorithm shows smaller likelihood ellipsoid because of the lower prediction uncertainty level than radar only case. This means that more reliable collision risks can be described by V2V/Radar fusion.

In terms of collision risk assessment, the peak collision risk probabilities addressed by V2V/Radar fusion stay low during the given prediction time horizon compared to radar only. Since

subject vehicle is more likely to increase the accuracy of perception performance. Therefore the collision probability with the Radar only vehicle has shown the peak value of 18% at 3s of peak predicted time, which is 3% more than that of V2V/Radar fusion. This results demonstrate that the proposed V2V/Radar fusion algorithm allows automated vehicle to

Fig. 7. Peak collision Risk during given prediction time horizon

(a) V2V/Radar Fusion   (b) Radar only
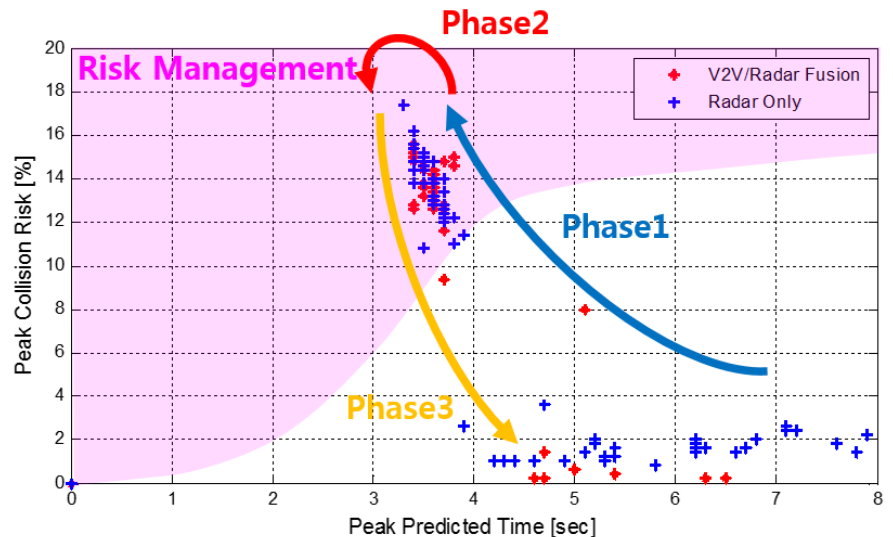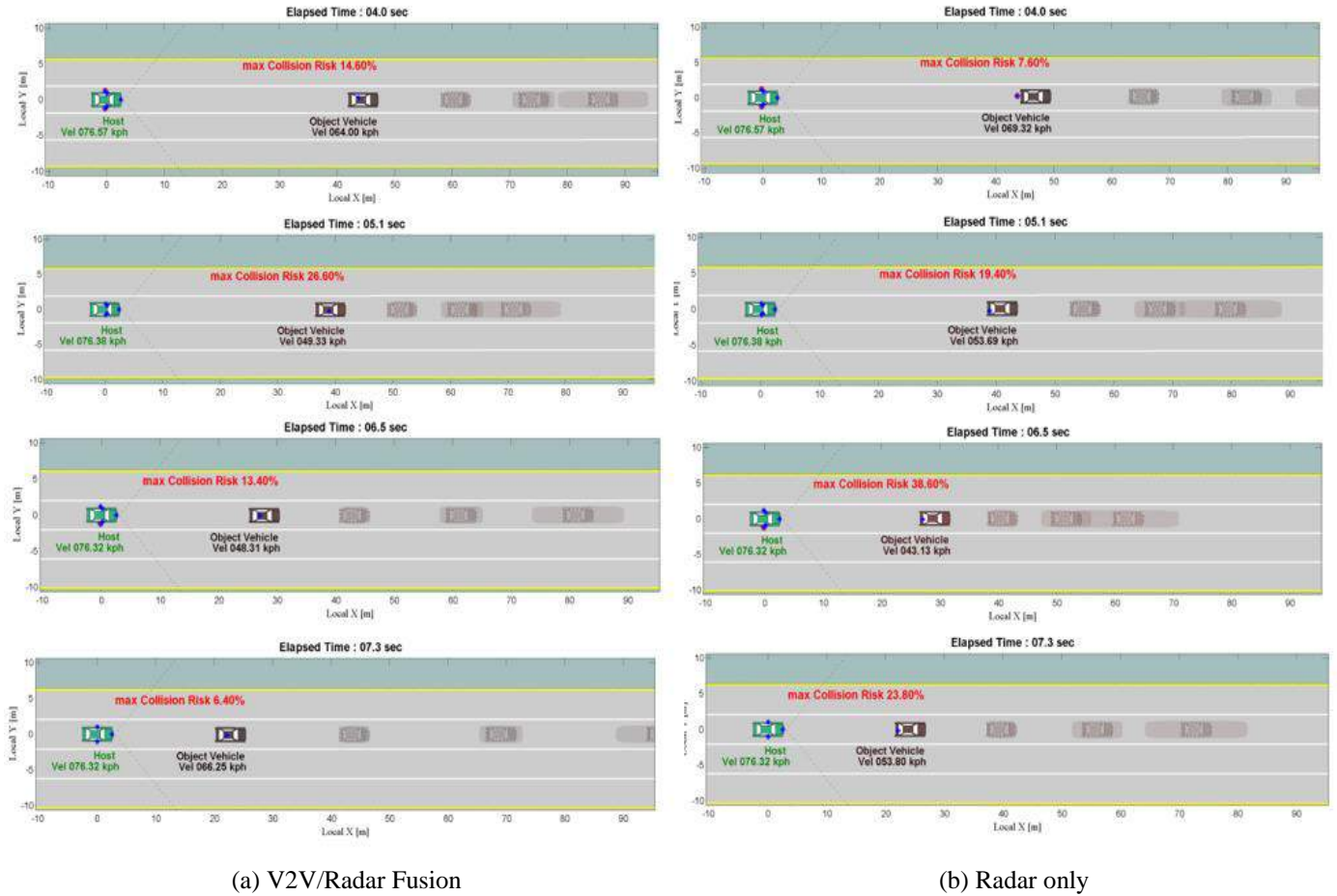
Fig. 8. Simulation Results for Parked Vehicle Cut-in Scenario

respond and recover much faster from the dangerous situation.

7.2 Highway Acceleration and Deceleration (HAD)

Likewise, the subject vehicle is described by green and the cut in object vehicle is expressed by grey in Fig. 8. And the predictions for reachable set are described by the vehicle with the dotted-line and its color continuously changes for every 1s of the time interval depending on the severity of collision risk. The total range of prediction time horizon is set to be 3s. Fig. 8 demonstrates that the V2V/Radar fusion algorithm shows smaller likelihood ellipsoid because of the lower prediction uncertainty level than radar only case. Since more accurate and additional object vehicle information is sent to subject vehicle, more reliable collision risks can be described by V2V/Radar fusion.

Based on the analysis method based on Integrated Risk Management System (IRMS) in Table 1, the peak collision risk probabilities addressed by V2V/Radar fusion stay low for the prediction time horizon compared to Radar only. Since the object vehicle's

acceleration information is directly sent to subject vehicle, subject vehicle's response is much faster than radar only, which reduces the chances of misperception of the object vehicle. Therefore the collision probability with the radar only vehicle has shown the peak value of 40% at 2.5s of peak predicted time, which is 8% more than that of V2V/Radar fusion. This result demonstrates that the proposed V2V/Radar fusion algorithm allows much faster recovery from dangerous situation.
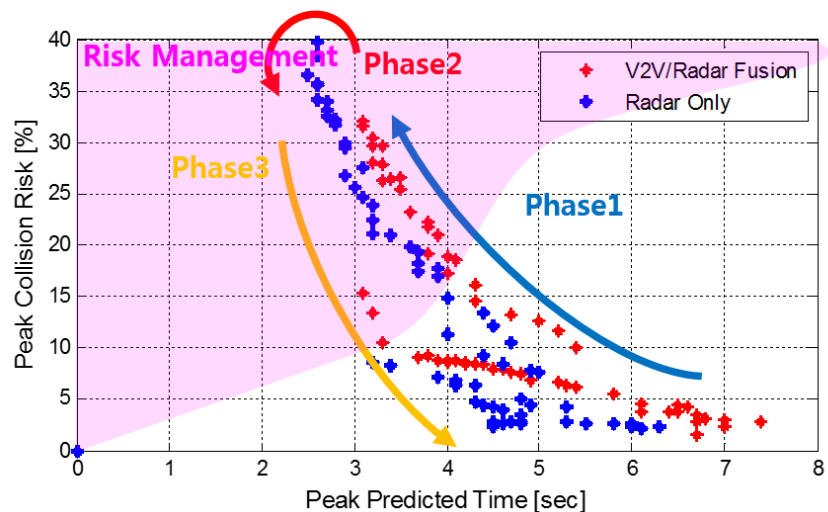
Fig. 9. Peak collision Risk during given prediction time horizon

7. CONCLUSION

This paper presents a probabilistic threat assessment of vehicle states using wireless communications for application to integrated risk management system. The concept is integrating/fusing V2V and radar data in a complimentary way by matching detected objects. Hence driver assistance systems can keep on using the position measurements from radar and use additional vehicle status information from V2V communications.

A rule-based object-vehicle prediction and a collision risk assessment utilize an environment description based on multi-sensor (V2V/Radar) fusion. The proposed algorithm for estimating the probability of collision occurrence of the subject vehicle follows the basic idea of the particle filtering and the collision probability can be numerically implemented and calculated for each of the V2V/Radar fusion and Radar only case.
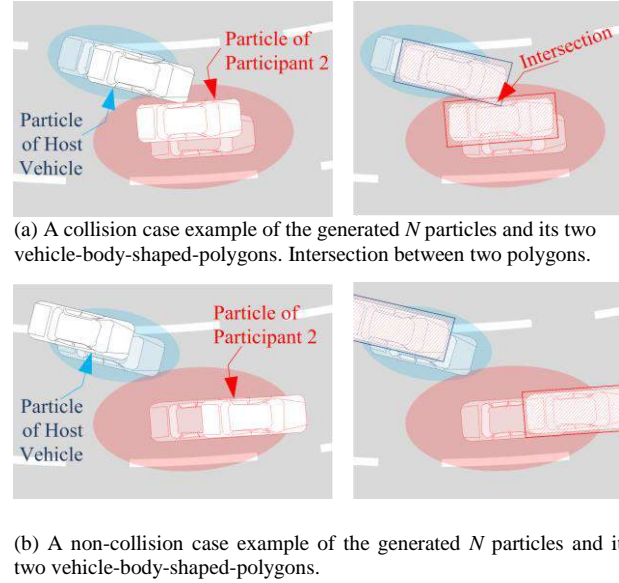
The overall performance of the proposed V2V/radar fusion algorithm is verified via simulation studies. It has been shown that the V2V/Radar fusion algorithm shows smaller likelihood ellipsoid because of the lower prediction uncertainty level than radar only case. This means that the proposed algorithm stays low level of peak collision probabilities compared to radar only case during the given prediction time horizon. And the proposed algorithm allows better perception performance compared to radar only case. According to the probabilistic risk assessment, it has been shown that the proposed V2V/Radar fusion algorithm enables faster and smoother response when the vehicle enters the dangerous situation

REFERENCES

Roeckl, M., Gacnik, J., Schomerus, J., Strang, T., & Kranz, M. (2008, June). Sensing the environment for future driver assistance combining autonomous and cooperative appliances. In *Fourth International Workshop on Vehicle-to-Vehicle Communications (V2VCOM)* (pp. 45-56).

Pilutti, T., Ulsoy, G., & Hrovat, D. (1998). Vehicle steering intervention through differential braking. *Journal of dynamic systems, measurement, and control*,*120*(3), 314-321.

Kaempchen, N., Schiele, B., & Dietmayer, K. (2009). Situation assessment of an autonomous emergency brake for arbitrary vehicle-to-vehicle collision scenarios. *Intelligent Transportation Systems, IEEE Transactions on*, *10*(4), 678-687.

Jansson, J. (2004). Dealing with uncertainty in automotive collision avoidance. In *Advanced Microsystems for Automotive Applications 2004* (pp. 165-180). Springer Berlin Heidelberg.

Lambert, A., Gruyer, D., Pierre, G. S., & Ndjeng, A. N. (2008, October). Collision probability assessment for speed control. In *Intelligent Transportation Systems, 2008. ITSC 2008. 11th International IEEE Conference on* (pp. 1043-1048). IEEE.

Karlsson, R., Jansson, J., & Gustafsson, F. (2004, June). Model-based statistical tracking and decision making for collision avoidance application. In *American Control Conference, 2004. Proceedings of the 2004* (Vol. 4, pp. 3435-3440). IEEE.

Schubert, R. (2012). Evaluating the utility of driving: Toward automated decision making under uncertainty. *Intelligent Transportation Systems, IEEE Transactions on*, *13*(1), 354-364.

Broadhurst, A., Baker, S., & Kanade, T. (2005, June). Monte carlo road safety reasoning. In *Intelligent Vehicles Symposium, 2005. Proceedings. IEEE* (pp. 319-324). IEEE.

Challita, G., Mousset, S., Nashashibi, F., & Bensrhair, A. (2009, October). An application of V2V communications: Cooperation of vehicles for a better car tracking using GPS and vision systems. In *Vehicular Networking Conference (VNC), 2009 IEEE* (pp. 1-6). IEEE.

DSRC Committee. (2009). Dedicated Short Range Communications (DSRC) Message Set Dictionary.

Breu, J., Brakemeier, A., & Menth, M. (2014). A quantitative study of Cooperative Awareness Messages in production VANETs. *EURASIP Journal on Wireless Communications and Networking*, *2014*(1), 1-18.

Chen, Q., Jiang, D., Tielert, T., & Delgrossi, L. (2011, September). Mathematical modeling of channel load in vehicle safety communications. In*Vehicular Technology Conference (VTC Fall), 2011 IEEE* (pp. 1-5). IEEE.

Alimohammadi, M., & Pouyan, A. A. Vehicular Ad Hoc Networks: Introduction and a proposal for vehicle positioning.

Challita, G., Mousset, S., Nashashibi, F., & Bensrhair, A. (2009, October). An application of V2V communications: Cooperation of vehicles for a better car tracking using GPS and vision systems. In *Vehicular Networking Conference (VNC), 2009 IEEE* (pp. 1-6). IEEE.

Zhou, H., Saigal, R., Dion, F., & Yang, L. (2012). Vehicle Platoon Control in High-Latency Wireless Communications Environment: Model Predictive Control Method. *Transportation Research Record: Journal of the Transportation Research Board*, (2324), 81-90.

Kim, B., Yi, K., Yoo, H. J., Chong, H. J., & Ko, B. (2015). An IMM/EKF Approach for Enhanced Multitarget State Estimation for Application to Integrated Risk Management System. *Vehicular Technology, IEEE Transactions on*, *64*(3), 876-889.

Kim, Beomjun, and Kyongsu Yi. "Probabilistic and Holistic Prediction of Vehicle States Using Sensor Fusion for Application to Integrated Vehicle Safety Systems." *Intelligent Transportation Systems, IEEE Transactions on*15.5 (2014): 2178-2190.

Zhou, H., Saigal, R., Dion, F., & Yang, L. (2012). Vehicle Platoon Control in High-Latency Wireless Communications Environment: Model Predictive Control Method. *Transportation Research Record: Journal of the Transportation Research Board*, (2324), 81-90.

The Influence of Roadway Features
on Observed Lane Departure Warning Response in a Simulator

John M. Sullivan*, Rini Sheroni**
Shan Bao***

*The University of Michigan Transportation Research Institute, Ann Arbor, MI 48109
USA (Tel: 734-764-8560; e-mail: jsully@umich.edu).
** Collaborative Safety Research Center, Toyota Engineering and Manufacturing
Ann Arbor, MI 48176 USA (e-mail:rini.sheroni@tema.toyota.com)
*** The University of Michigan Transportation Research Institute,
Ann Arbor, MI 48109 (e-mail: shanbao@umich.edu)

Abstract: A simulator study was conducted to characterize driver steering responses to lane departure warnings. Drivers were asked to perform a distracting secondary task while their vehicles were occasionally pushed to the side of the roadway to encourage lane departures. Three lane departure warning treatments were investigated: no warning, an auditory warning, and a tactile warning using steering wheel vibration. Overall drivers' corrective steering responses suggested that both the presence of a lane departure warning and characteristics of the roadway environment influenced the magnitude of the steering corrections observed.

Keywords: lane departure warning, distracted driving, driver steering correction

1. INTRODUCTION

The current collision avoidance new car assessment program (CA-NCAP) confirmation test for lane departure warnings (LDW) is a pass/fail procedure that assesses LDW detection performance for left and right departures on straight roads with three types of lane boundary markings (Fokenbrock & Barickman, 2009; United States Department of Transportation, 2010). In these tests, a lateral road departure speed of between 0.1 and 0.6 m/s at the time of the LDW are prescribed, although some suggest that departure rates of 3.5 to 5.1 m/s are more representative of actual road departure crash scenarios where LDW is expected to be most helpful. This scenario has been called the "no-manoeuvre scenario" where there is little evidence that the driver intervened prior to the crash (Kusano & Gabler, 2012). Assuming a 3.6 m wide travel lane, a 1.7 m wide vehicle, and an initial vehicle lane position at the centre of a lane, there would be less than 1.3 m distance from the edge of the vehicle to the latest warning line proposed for LDW (International Organization for Standardization, 2007; Society of Automotive Engineers, 2007). This presents an implementation challenge for LDW systems that seek to design early warnings that allow up to 1.5 s advanced notice to drivers of an imminent departure. The reported lateral departure speeds involved in road departure crashes leave little time for a driver to respond to a warning before the vehicle leaves the road. Indeed, it is unclear that the design intent of most LDWs is to prompt a sleeping or otherwise incapacitated driver into action.

In the present study, we examined a driver's response to LDW in the context of an in-vehicle distraction task in which a driver's eyes are momentarily diverted from the roadway. While this scenario may share fewer characteristics of the road departure crashes noted earlier, it may resemble more commonplace circumstances of lane departures. For each induced lane departure, we examined the characteristics of the departure (e.g., lateral speed, maximum excursion), and the driver's response to the LDW (e.g., peak corrective steering velocity, driver reaction time to LDW) as a function of two LDW implementations and one no-LDW condition, driver age, gender, roadway configuration, and departure direction.

We expect that more detailed data about a driver's response to LDWs might contribute to the evaluation of the performance of a lane departure warning system by allowing characteristics of driver-responsiveness to be factored into an overall LDW response model. This would allow refinement of the current evaluation procedures to permit a more discriminating test. For example, data on driver response latency and steering control might help estimate the likely extent of lane excursion after an LDW is triggered. This study was conceived as a step toward such a refinement.

2. METHODS

Measures of driver control responses to various lane departure warnings were collected in a fixed-base medium-fidelity simulator. To help instigate a lane departure, drivers were asked to perform a secondary task that distracted them momentarily from the roadway. During some of these distraction intervals, a rotational force was applied to the simulator vehicle (much like a wind-gust) in order to increase the likelihood that a lane departure would occur. Not all

observed lane departures in this study required such an intervention.

2.1 Participants

Thirty-seven licensed drivers (19 male, 18 female) participated in the LDW simulator study. Drivers were recruited from two distinct age groups. There were 22 younger drivers (25 to 35 years—mean age = 30.5), and 15 older drivers (55 to 65 years—mean age = 60).

2.2 Simulator/Driving Environment

Driving behaviour was studied in the UMTRI fixed-base driving simulator equipped with a fully functional Nissan Versa sedan chassis. The driving scene was projected onto three forward screens that spanned a 120-deg field of view, and one rear-view screen spanning a 40-deg field of view. The simulator roadway was a 10-mile (16 km) rural two-lane roadway with a posted limit of about 55 mph (89 km/h). The roadway contained an equal number (6) of left turning curves, right turning curves, straight road segments, and straight road segments that were fenced near the right road edge. This latter condition was included to determine whether drivers were sensitive to the presence of a fixed object adjacent to the roadway. Roadway lane widths were 3.5 m; curved road segments had a centreline radius of about 300 m. No opposing traffic was present in the adjacent lane throughout the drives.

2.3 Secondary Task

The secondary task was modelled after a task used by Horrey, Wickins, and Consalus (2006) and involved glancing at a low-mounted 7-inch LCD display in which a 7-digit numeric string was displayed for 8 seconds. Drivers were given an auditory alert each time the numeric string was displayed. The driver was asked to judge whether there were more odd or even digits in the string, indicating their judgment by a button-press within an 8-second time limit. In all cases, the odd/even count was constrained to never differ by more than one digit. The task was designed to divert the driver's gaze off the roadway momentarily in order to make the judgement. To perform this task accurately, participants would need to review at least four or more digits on the display.

2.4 LDW implementation:

Two forms of LDW were examined in this study: an audible LDW that indicated the lateral direction of the departure (LDA), and a tactile non-directional vibration of the steering wheel (LDV). Trigger conditions for the LDA and LDV treatments were identical and occurred when the lateral edge of the subject vehicle crossed within 0.2 meters of the lane boundary on either the left or right side.

The LDA sound was presented in two bursts constructed of five 50-ms 400 Hz square waves separated by 100 ms of silence. Bursts were separated by 250 ms. After initial triggering, a 5-second refractory period was applied before an LDA was repeated. The LDA sound was lateralized using the in-vehicle stereo system speakers mounted in the doors to indicate the direction of departure.

The LDV used a 20 Hz square wave steering wheel vibration delivered in 250 ms bursts followed by 250 ms of no vibration. These vibration bursts were repeated a maximum of 4 times; steering torque amplitude was approximately 1.1 N·m, centred on a zero-output point. Both the LDA and LDV warnings were terminated when the vehicle returned to the roadway.

2.5 Procedure

Overall, the simulator session involved one initial practice drive in which the different LDW treatments were demonstrated. This was followed by three, 12-minute experimental drives over the same 10-mile segment of roadway. Within each drive, a different LDW treatment condition was investigated: a baseline drive with no active LDW (labelled LDX); a drive with the audible LDW (LDA); and a drive with a tactile non-directional steering vibration LDW (LDV). The order of these three LDW treatment conditions was counterbalanced across participants.

Within each drive, three experimental conditions were randomly assigned to two of the six road segments within each of the four road types (straight, fence, left curve, right curve). These conditions were defined as follows: 1) No distraction (no secondary task or lateral force pushing the vehicle off the road); 2) Secondary task presentation (no lateral force); and 3) Secondary task presentation with lateral force on the vehicle. These conditions are tabulated in Table 1.

On road segments in which a secondary task was scheduled, as the driver entered the segment an alerting beep occurred signalling the driver to perform the secondary task as a 7-digit numeric string was displayed on the head-down display. On half of the secondary task trials, drivers were also induced to depart from their lane by a brief lateral push resembling a wind gust, directing the vehicle off the roadway. Note that this induction was not always successful.

Table 1. Conditions within each 10-mile drive.

Road Type	Secondary Task	Lateral Push	Observations
Left Curve	Yes	No	2
	Yes	Yes	2
	No	No	2
Right Curve	Yes	No	2
	Yes	Yes	2
	No	No	2
Straight	Yes	No	2
	Yes	Yes	2
	No	No	2
Straight with Fence	Yes	No	2
	Yes	Yes	2
	No	No	2
		Total	24

The likelihood of a lane departure occurrence was evaluated with respect to several experimental conditions that included: road type, presence of a secondary task, lateral push, LDW type, departure direction, and driver age and gender. For each occurrence of a lane departure, drivers' corrective steering responses were also measured with respect to when the response was initiated (reaction time) and the peak angular velocity of the steering correction. Other measures recorded, but not reported here, included the maximum angular steering wheel deflection, the peak steering torque applied, and the peak change in steering torque.

3. RESULTS

Results will be presented in two parts. The first part describes the characteristics of the lane departures induced in the vehicle simulator. The second section describes driver corrective responses to regain position on the roadway after a departure.

3.1 Characteristics of induced departures

Within each drive, 24 road segments were monitored for the occurrence of a road departure. Lane departures to the left occurred in 27% of the road segments; departures to the right occurred on 16% of the segments (Fig. 1). A total of 1460 lane departures were observed in this study.
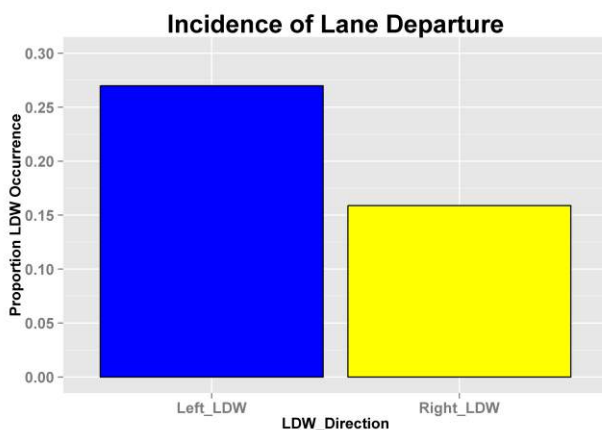
Fig. 1. Proportion of left and right road departures.

A generalized mixed model analysis incorporating driver as a random effect was used to examine the influence of LDW Treatment (LDA, LDV, LDX), Secondary Task/Push (Task with Push, Task without Push, No Task or Push), Road Type (Left Curve, Right Curve, Straight, Fence), Age Group (Older, Younger), and Gender (Male, Female) on the odds that a left or right lane departure would occur during a trial. Separate analyses were conducted for each departure direction. Several main effects were found to influence the odds of a left lane departure, including LDW Treatment, Secondary Task/Push condition, and Road Type. These effects can be seen in Fig. 2 for left lane departures. For the LDA and LDV treatments, the odds of a lane departure are smaller (0.68 and 0.75, respectively) than that of a lane departure for the LDX treatment (Odds Ratio [OR] = 0.68,

$p = 0.001$, CI: 0.55, 0.84; OR: 0.75, $p = 0.02$, CI: 0.60, 0.93). Likewise, compared to no secondary task conditions, the presence of a secondary task with and without a push makes a left-side lane departure about 7-8 times more likely (OR = 7.9, $p < 0.001$, CI: 6, 10.3; OR = 6.7, $p < 0.001$, CI: 5.1, 8.8, respectively). Pairwise comparisons of the roadway types also revealed differences between the odds of a left departure on left and right curves—participants were nearly twice as likely to make left departure along a left curve (OR = 1.95, $p < 0.001$, CI: 1.5, 2.6) compared to a right curve.
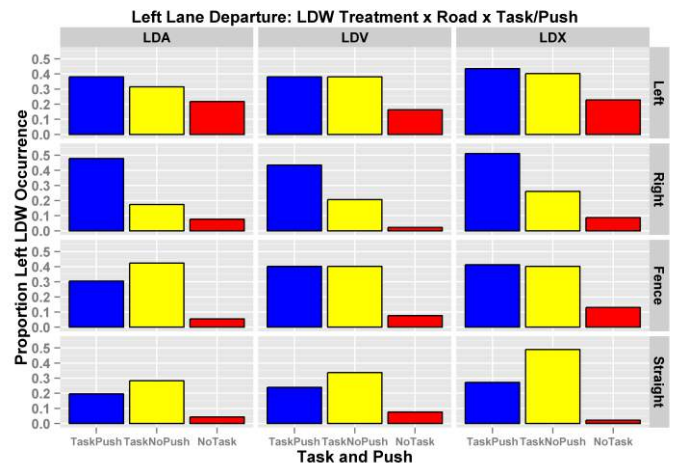
Fig. 2. Proportion of left lane departures by treatment, road type, and task.

A similar analysis, conducted for the right lane departures, revealed main effects of road type and secondary task/push combination. For comparison, Fig. 3 shows the same main effects breakdown presented for left lane departures. Unlike the left departure analysis, there seems to be less influence of LDW Treatment on proportion of right departures. However, there are robust effects of task/push combination on right departures (as expected)—a secondary task accompanied by a push is 14.9 times as likely to result in a right lane departure than when no secondary task or push occurs (OR = 14.9, $p < 0.001$, CI: 9.7, 22.7). Likewise, performing a secondary task alone made right lane departures about 3.4 times as likely than when there were no secondary tasks or pushes (OR = 3.4, $p < 0.001$, CI: 2.4, 5.8). Secondary tasks accompanied by a push were also 4 times more likely to result in a right lane departure than performing the secondary task alone (OR: 4.0, $p < 0.001$, CI: 3.0, 5.3). Thus, most of the time, a push increases the likelihood of a right lane departure. One exception to this appears to be the LDA condition on right curves. On this roadway segment, the push is actually to the left side of the road, so it is expected to reduce a participant's inclination to depart on the right. This is not observed in either the LDV or LDX treatment conditions.

Overall, it appears that left-side lane departures occurred more frequently than right-side lane departures, perhaps because drivers were mindful that no opposing traffic was present in that lane. Departures on the left side of the road were more frequent when performing a secondary task,

regardless of whether a lateral push was present, compared to when no secondary task was performed. Departures on the right side of the road, however, appeared to occur most often when a lateral push was used to induce a departure. This seems to suggest that drivers were more casual about left departures, in which the vehicle crosses into a generally unoccupied lane, compared to a right departure where the vehicle could leave the roadway.

It is also noteworthy that the odds of a lane departure to the right side of a straight road were smaller when a fence was present along the roadway (Fence) than when there was no fence (Straight; OR = 0.63, p < 0.05, CI: 0.46, 0.87). This can be seen in Fig. 3 comparing the Fence to the Straight road types. Drivers seemed especially resistant to leave the road on the right when a fence was present, compared to when no fence was present.
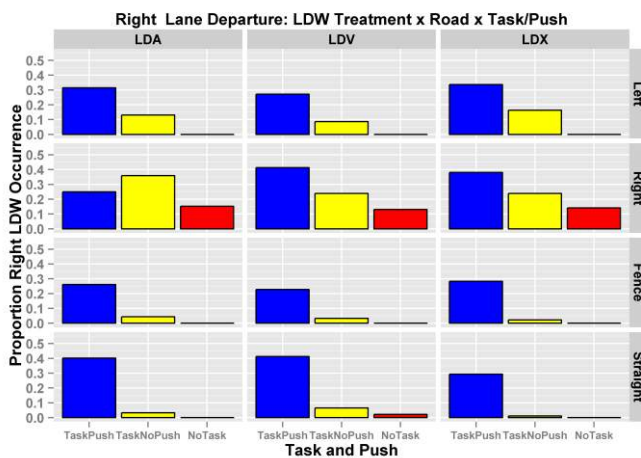
Fig. 3. Proportion of right lane departures by treatment, road type, and task.

3.2 Characteristics of drivers' corrective responses

Reaction time to LDW. Both braking and steering responses were examined to determine driver reaction time to an LDW. Out of all the lane departures, braking occurred on 6 of the trials. Consequently, the response analysis focused on steering. To determine the start of a steering correction, we began by finding the peak lateral departure velocity, i.e. the point at which the rate of departure began to decline. The preceding 2 s of steering was then examined to determine the peak angular acceleration of steering in the corrective direction. This differs from other response metrics such as response completion time (Eriksson et al., 2013). It likely also differs from steering responses reported variously as the moment when drivers begin to turn the wheel (e.g., Navarro, Mars, & Hoc, 2007), or steering latency (Suzuki & Jansson, 2003) which may assume that a static steering angle immediately precedes a corrective steering response. It is, however, similar to methods that assume more variable steering occurs before correction is made and determines the onset of a corrective manoeuvre by examining steering angle acceleration preceding maximum steering angle velocity (e.g., Tijerina et al., 2010). The time between the start of

LDW and the start of the steering correction was defined as the reaction time.

Using the above definition of reaction time, driver's responses were found to often precede the onset of the LDW. This is shown in Fig. 4. Average steering response time measured across drivers occurred between 0.4 to 0.5 s before the LDW was initiated. This result suggests that in the simulator, drivers were able to anticipate a likely road departure and perhaps began remedial action before being alerted by the LDW system.
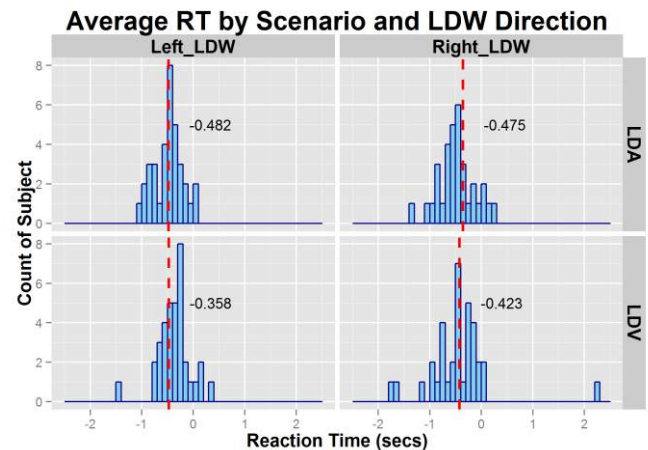
Fig. 4. Distribution of average LDW reaction time for each driver by condition and departure direction. Negative offsets indicate steering responses that occur before LDW onset.

Peak angular steering velocity. After the onset of the steering response to a lane departure, the peak angular corrective steering velocity was determined over the following 4 s interval. This measure was collected for both the LDA and LDV conditions as well as the LDX (no-LDW) condition. Peak corrective steering velocities were analyzed separately with respect to direction of departure in a mixed model analysis in which driver was modelled as a random effect. For both left and right departures, main effects were observed for LDW Treatment and Road Type. In left departures, peak angular steering velocities observed for the LDV condition were about 11 deg/s greater than for LDA conditions (t = -3.69, p < 0.001) and 15 deg/s greater than corrections observed for the LDX condition (t = 5.38, p < 0.001). Similar (albeit statistically marginal) effects were observed in right departures—LDV peak velocities were 8 deg/s greater than LDA (t = 1.61, p = 0.11) while LDV velocity was about 20 deg/s greater than LDX (t = 5.38, p < 0.001). These effects are shown in Fig. 5.
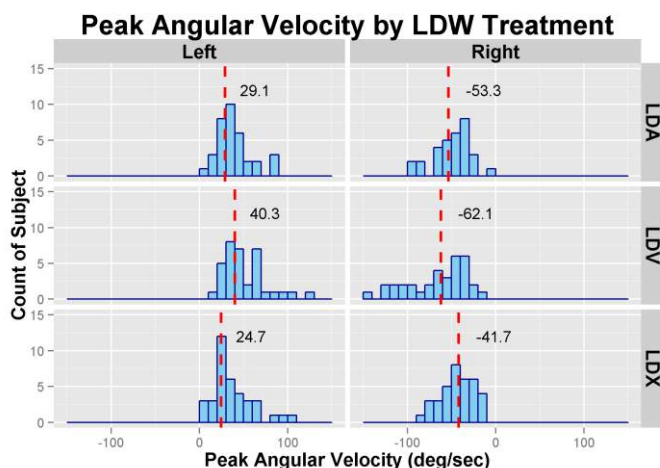
Fig. 5. Distribution of peak angular steering velocities by LDW condition.

Road types were also related to the observed peak corrective steering velocity—the two straight roads (Straight and Fence) did not differ from each other nor did the two curved roads (Left and Right) in left lane departures. In right lane departures, the effects were less regular. The peak corrective steering velocity differed between the two types of straight roads. The peak angular velocity of the Fence condition is about 16.4 deg/sec greater than the straight (t = - 2.5, p = 0.01) possibly because a right departure could result in a collision with the fence—something drivers may want to avoid. Curved roadway conditions also differ in right departures. Right departures on left-curving roads appear to result in a peak corrective steering velocity that is about 32 deg/sec greater than on a right curved roadway (t = -5.11, p < 0.001). These effects can be seen in Fig. 6. These observed effects may be related to differences in the driver's perception of the severity of the departure—departing on the right side of a left-curving roadway would quickly result in a significant departure off the roadway; a departure on the right of a right-curving roadway may not seem so severe since the roadway is travelling in the direction of the departure and might be perceived to result in a less significant departure.
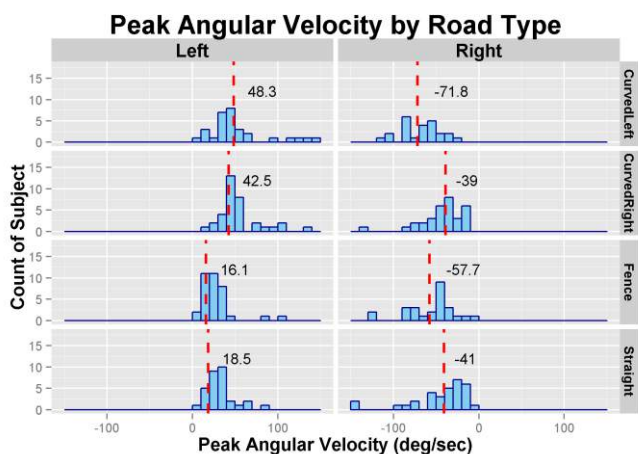
Fig. 6. Peak angular corrective steering velocities among drivers as a function of departure direction and road type.

4. DISCUSSION

In this simulator study, drivers clearly anticipated road departures and were not likely surprised by the occurrence of any of the lane departures. Indeed, any multi-trial simulator study of LDW is unlikely to replicate conditions in which a drowsy or inattentive driver is surprised by a lane departure. However, the observed departures might arguably resemble departures that result from a driver's conscious engagement in a secondary task that redirects the eyes off the roadway. While lane departures in these circumstances are likely to be less catastrophic, they may be more common and resemble the low lateral departure speeds that LDW may be most suited to address. In this study, drivers most frequently departed the left lane, perhaps choosing to risk a lane departure over a less forgiving road departure.

Although the LDWs did not appear to trigger the driver's corrective steering, since steering reactions often appeared to precede the LDW, the LDWs did seem to increase the strength of the driver's corrective response resulting in higher peak steering velocities than when no LDW was present. Perhaps the presence of an LDW helps prompt a driver to make more assertive steering corrections.

It also appears that drivers were influenced by the characteristics of the roadway environment. As a class, rightward lane departures seemed more successfully avoided by drivers; left lane departures were far more frequent. When a right lane departure occurred, drivers addressed them with corrective steering responses that were generally greater in peak angular velocity than the left lane departures. Perhaps this is also related to the difference in perceived hazard of a crossing a centreline versus departing the roadway.

Similarly, drivers also appeared to be influenced by the presence of a fence on the roadside. Maximum corrective steering angle velocity was greater when a fence was located on the right side of the road compared to a similar non-fenced straight roadway segment.

5. CONCLUSION

This study represents the response one might observe from a relatively alert, but momentarily distracted, driver when a lane departure warning occurs. The results suggest that even though a driver's attention may be diverted from the roadway, the driver appears to remain generally mindful of the roadway environment and adjusts corrective actions with respect to the roadway and the presence of a LDW. Corrective responses appear to be generally boosted by LDW presence, with the wheel-vibration LDW (LDV) resulting in somewhat greater response than a directional audio LDW (LDA). These effects are modulated by both the direction of the road departure and the presence of a fixed object on the roadside.

6. ACKNOWLEDGEMENTS

7. REFERENCES

Eriksson, L., Bolling, A., Alm, T., Andersson, A., Ahlstrom, C., Blissing, B., et al. (2013). *Driver acceptance and performance with LDW and rumble strips assistance in unintentional lane departures.* (ViP publication No. 2013-4). Linkoping, Sweden: Center of Excellence at VTI.

Fokenbrock, G., & Barickman, F. (2009). *Lane departure warning (LDW) performance evaluation.* Paper presented at the 21st International Technical Conference on the Enhanced Safety of Vehicles.

Horrey, W. J., Wickens, C. D., & Consalus, K. P. (2006). Modeling drivers' visual attention allocation while interacting with in-vehicle technologies. *Journal of Experimental Psychology-Applied, 12*(2), 67-78.

International Organization for Standardization. (2007). *ISO 17361:2007 Intelligent transport systems -- Lane departure warning systems -- Performance requirements and test procedures.* (Standard No. ISO/DIS 17361). Geneva, Switzerland: International Organization for Standardization (ISO).

Kusano, K. D., & Gabler, H. C. (2012). Field Relevance of the New Car Assessment Program Lane Departure Warning Confirmation Test. *SAE International Journal of Passenger Cars - Mechanical Systems, 5*(1), 253-264.

Navarro, J., Mars, F., & Hoc, J. M. (2007). Lateral control assistance for car drivers: A comparison of motor priming and warning systems. *Human Factors, 49*(5), 950-960.

Society of Automotive Engineers. (2007). *J2808: Road/Lane Departure Warning Systems: Information for the Human Interface.*

Suzuki, K., & Jansson, H. (2003). An analysis of driver's steering behaviour during auditory or haptic warnings for the designing of lane departure warning system. *JSAE Review, 24*(1), 65-70.

Tijerina, L., Blommer, M., Curry, R., Greenberg, J., Kochhar, D., Simonds, C., et al. (2010). Effects of Adaptive Lane Departure Warning System on Driver Response to a Surprise Event. *Transportation Research Record*(2185), 1-7.

United States Department of Transportation. (2010). *Lane Departure Warning System Confirmation Test.* Washington, D.C.: U.S. Department of Transportation, National Highway Traffic Safety Administration.

Free Space Grid for Automotive Radar Sensors

Maryam Foroughi*, Uri Iurgel*, Alexander Ioffe*, Wolfgang Doerr*

**Delphi Deutschland GmbH, Delphiplatz 1, 42119 Wuppertal, Germany*
(e-mail: maryam.foroughi@delphi.com, uri.iurgel@delphi.com,
alexander.ioffe@delphi.com, wolfgang.doerr@delphi.com)

Abstract: A new method for generating a separate two-dimensional free space grid map for ADAS based on data from radar sensors is presented in this paper. We introduce a free space model based on an inverse sensor model to compute the Gaussian-based free space probability for each cell of the free space grid map. A Bayesian approach is used for free space probability estimation independently from the occupancy probability, which enables increased amount of information for environment description. For this purpose, two free space grid maps are generated: The instantaneous free space map is generated in each measuring cycle and the accumulated free space map is generated once and updated in each measuring cycle. We describe how the free space grid maps are generated and updated by new observations. In contrast to other approaches, the detection accuracy is taken into account in the free space model. Finally we present the experimental results obtained from real world environments.

Keywords: Free Space Grid, Mapping, Radar, Sensors, Advanced Driver Assistance Systems, Automotive

1. INTRODUCTION

In recent decades Advanced Driver Assistance Systems (ADAS) have been developed to help and assist drivers and prevent accidents. ADAS provide a more comfortable and safer driving experience by supporting human awareness and actions with exact machine tasks and warnings. These reduce significantly the amount of accidents caused by driver errors.

ADAS are usually based on Proximity Sensors (e.g. Radar, Laser and Ultrasound), Camera Systems, GPS, Car-to-Car and Car-to-Infrastructure systems. Proximity sensors are used to develop systems such as Adaptive Cruise Control (ACC), Automatic Parking, Lane Change Assistance, Blind Spot Detection (BSD) systems, Emergency Brake Assist (EBA), etc. Simulation of a precise world model is among the essential requirements of a successful implementation of the ADAS, which would significantly reduce the complication of tasks such as navigation, path planning, and obstacle avoidance. The Occupancy Grid Map and the Free Space Grid Map are two world models of real-world environment.

This paper proposes a new method for constructing a two-dimensional free space grid map for ADAS based on data from proximity sensors. A free space grid map is used in scenarios like automatic parking etc., because of the essential role of drivable free spaces within these systems.

Free space grid maps are maps which are generated based on noisy sensor data to represent empty vs. occupied spaces in any given environment. Similar to a Bayesian occupancy grid map, the implementation of a free space map is based on the concept of probability. The basic idea is the initial assumption that the space between a proximity sensor and its detection is empty. This space and its associated probability is calculated and then updated in real time using "Bresenham Line-Drawing Algorithm" (Bresenham 1965) methods. We also consider the angular accuracy of a detection for the free space model.

A separate grid map is implemented based on Delphi 77 GHz Short Range Radar. In addition, the detection's angular accuracy is taken into account so as to retrieve more accurate results. In this paper, we present both the method and the promising experimental results obtained from real world environments.

This paper is organized as follows: Section 2 introduces related works, Section 3 describes an algorithm for generating occupancy and free space grids. Section 4 is devoted to the description of the proposed work and section 5 presents the conclusions.

2. RELATED WORKS

In this section we describe existing approaches for free space detection and description for ADAS and autonomous vehicles in a 2D environment.

A widely used approach for identification of free space is to use an occupancy grid, and represent the area between a sensor reflection and the, sensor with a low probability of occupancy (Vu et al. 2008, Garcia et al. 2008). Thus, occupancy and free space are modeled in the same grid.

An occupancy grid is also the base for other approaches to identify the free space.

2.1 Segmentation based on an occupancy grid

For example, the method by Schmid (Schmid 2012) intends to identify parking spaces next to the ego vehicle. It is based on a static hierarchical occupancy grid. Starting from the ego vehicle, rectangular segments are increased perpendicularly until reaching occupied cells in the grid. The set of all segments describes the free space. In the publication, this approach is used to determine free parking slots.

2.2 Morphological Image Processing

Another occupancy-grid based approach is presented in (Schreier and Willert 2012, 2013). First, a local occupancy grid map is built. Starting with a median filtering step for the partial removal of mapping errors, a pixel-based segmentation is performed in by thresholding. Afterwards, morphological erosion is applied in order to reduce the size of the free space firstly in a way that free space segments the vehicle does not fit into are removed, and secondly that larger free space areas that are only joined together by narrow, impassable connections are separated from each other. Finally, the arbitrarily shaped free space around ego vehicle is modeled and tracked using B-spline contours.

Other methods model the free space independently of an occupancy grid, either directly, or implicitly.

2.3 Interval-based Free Space Model

The method by Bouzouraa (Bouzouraa 2011) models free space in front of the ego vehicle as a series of rectangular intervals. Each rectangle is described by its left and right boundary position and speed, where its longitudinal dimension (length) is typically constant for all rectangles. Their orientation is linked to the current orientation of the ego vehicle. On each processing cycle, the free space rectangles are bounded by radar detections. The dimension and speed of the rectangles are estimated over time by a Kalman filter.

2.4 Vehicle classification for identification of parking slots

Other approaches model the free space implicitly. For example, (Zhou et al. 2012) detect L-shaped bumpers of parked vehicles using an AdaBoost-based classifier. A spatial analysis determines the structure of a parking lot, and free parking slots are identified based on the identified position of bumpers.

3. PREVIOUS WORK

In this section we present an algorithm for generating an occupancy grid. A similar approach is part of the generation of the free space map (as discussed below). The occupancy grid map represents the occupied spaces in any given environment based on sensor data. Each cell of the occupancy map covers an area of 10×10 cm in the environment of the host vehicle (Khlifi et al. 2014).
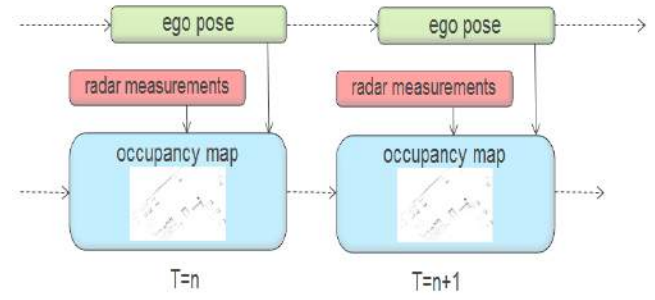
Fig. 1. Data flow for creation of an occupancy map.

As shown in Fig. 1, in each measuring cycle the ego vehicle data and the detections which are received by the sensors are taken and the occupancy probability of each occupied cell is updated using a recursive Bayes filter (Vu et al. 2008):

$$Logit_k(x) = log \frac{p(x|y_k)}{1-p(x|y_k)} + Logit_{k-1}(x) - Logit_0 \qquad (1)$$

In the equation (1), the term $p(x)$ is the occupancy probability of the map cell. It is initialized to 0.5, representing an unknown state:

$$p_0 = 0.5 \, , \; Logit_0 = log \frac{p_0}{1-p_0} \, , \; \rightarrow Logit_0 = 0 \qquad (2)$$

The probability $p(x|y_k)$ is called the inverse sensor model. It specifies the probability that a grid cell x is occupied given a sensor measurement y_k. The term $Logit_{k-1}(x)$ is the recursive term, describing the occupancy map in the previous time step.

Fig. 2 visualizes an example of an occupancy grid map computed with short range radars in an urban scenario. The rectangle shows the host vehicle in the occupancy grid. The parked vehicles are clearly visible.
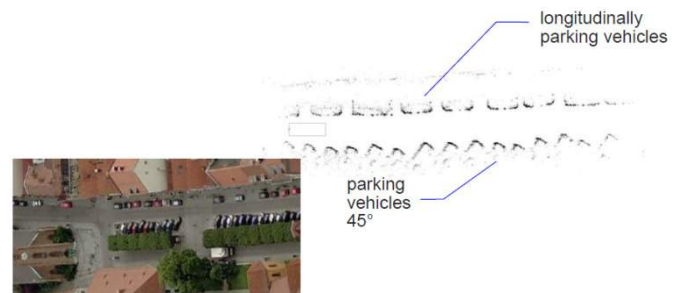
Fig. 2. Example for an occupancy grid map computed with radars.

4. PROPOSED WORK

As discussed in Section 2, in existing approaches, free spaces are often detected using an occupancy grid map. This paper proposes a method to implement a separate free space grid map based on short range radars, which is outlined in this Section. The free space generation method presented in this paper is based on the free space grid mapping approach proposed in (Foroughi 2015).

The Bayesian approach used in this paper is competitive to the Dempster Shafer approach (Dempster 1967, Shafer 1976) which introduces an additional "unknown" state to the "occupied" and "free" states. In the Bayesian approach, these two states are always complementary and sum up to 1 (or 100%). We introduce the use of separated probabilistic occupancy grid and probabilistic free space grid, where (for every grid cell) the probability of "occupied" in the occupancy grid and the free probability in the free space grid (usually) do not sum to 100%.

In our approach, probabilities for free cells are kept separately from the probability of occupancy. Thus, during time, these two pieces of information do not influence each other. For example, the free space information from a far detection does not reduce the probability of a nearer occupied cell lying on the same beam. As a consequence, we have a free space grid that has more accurate information about probability of free spaces, for example the free probability of the points which are in front of the short obstacle is more than the free probability of the points which are behind that obstacle.
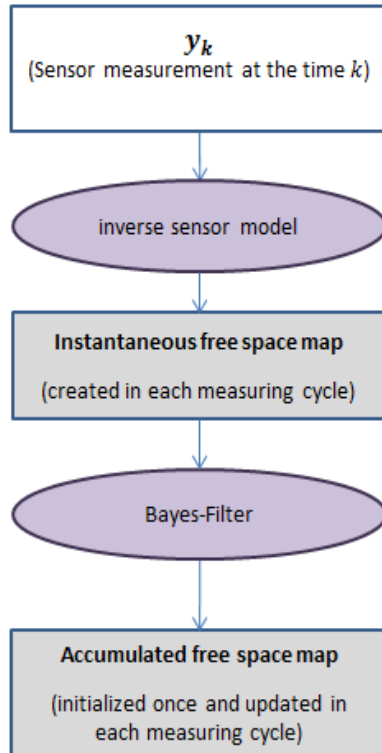
Fig. 3. Two free space maps are created: The instantaneous free space map and the accumulated free space map.

As shown in Fig. 3, two free space maps are created: The "instantaneous free space map" is generated in each measurement cycle (according to Section 4.1) -1in order to find the free grid cells and their free probability in each measuring cycle. An "accumulated free space map" is updated in each measuring cycle using the "instantaneous free space map" (according to Section 4.2).

4.1 Instantaneous Free Space Map
4.1.1 Inverse Sensor Model for Free Space Grid

Similar to the occupancy map, an inverse sensor model is used as a measurement model to calculate the probabilities in the free space grid. It describes the probability for a cell being free, given a sensor's measurement.

In this model, we interpret the space between a sensor and a detection as empty (Garcia et al. 2008). In contrast to other approaches, we consider the angular accuracy of a detection for the free space model, assuming a Gaussian distribution. Usually, the angular accuracy of a sensor measurement is only considered for the part of the inverse sensor model that describes the occupancy.

4.1.1.1 Free Space Model

Due to measurement inaccuracies, the reported position of a sensor's detection is not exact. Let $(\pm \frac{\alpha}{2})^{\circ}$ be the angular accuracy of a detection. Fig. 4 depicts the effect of angular accuracy of two detections with different ranges. The tangential inaccuracy of the position of a far detection (in Cartesian coordinates) is greater than the inaccuracy of the position of a closer detection.

This accuracy information can be used for the identification of the free cells between a detection and the sensor. As mentioned above, the space between the sensor and a detection is considered as free. The idea is that not only the beam between the sensor and the detection's cell itself are used, but also the beams between the sensor and the cells adjacent to the detection's cell, which are covered by the angular accuracy model.
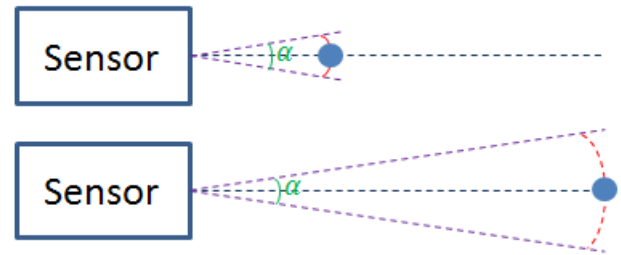
Fig. 4. The effect of angular accuracy of two detections with different ranges.
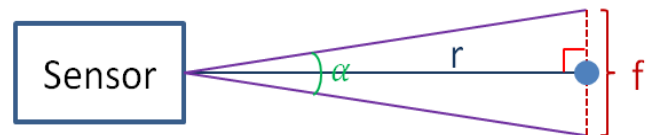
Fig. 5. The tangential accuracy of a detection.

In Fig. 5 the whole angular accuracy of the detection is shown with α and the range between the sensor and the detection is shown with r. The effect of angular accuracy in

tangential direction f is approximated by the following equation (conversion from polar to Cartesian coordinates with linearization)

$$\tan\frac{\alpha}{2} = \frac{\frac{1}{2}f}{r} \;\rightarrow\; f = 2\,r\tan\frac{\alpha}{2} \tag{3}$$

As shown in equation (3) the effect of tangential accuracy f depends on both the range r and the angular accuracy α. Thus, only the range r influences f for a given α.

Since f is small for low ranges r, the angular accuracy has limited influence for near detections. In order to reduce computational effort, angular accuracy is ignored for ranges less than a threshold L.

Each cell of the free space map covers an area of **10x10 cm**. As a result, for example for f = 50 cm, five cells in in the map are covered by the angular accuracy model (see Fig. 6).
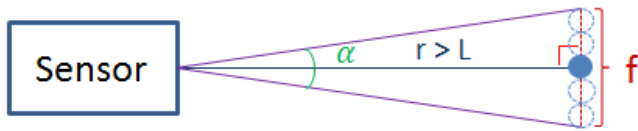
Fig. 6. Considering the effect of angular accuracy: five cells are affected by the model for angular accuracies of a detection (for ranges $r > L$ from the sensor).

Hence both the estimated position of detection and the area f should be considered. For this purpose first the area f is determined by the equation (3). Then the cells between the sensor and all the cells in area f are determined using the well-known Bresenham algorithm (Bresenham 1965). This process can be seen in Fig. 7. The rectangle shows the host vehicle, which has a sensor mounted on its upper right corner. The free spaces between the host vehicle and the detection are white. The range of detection is less than L in Fig. 7(a), whereas it is more than L in Fig. 7(b).
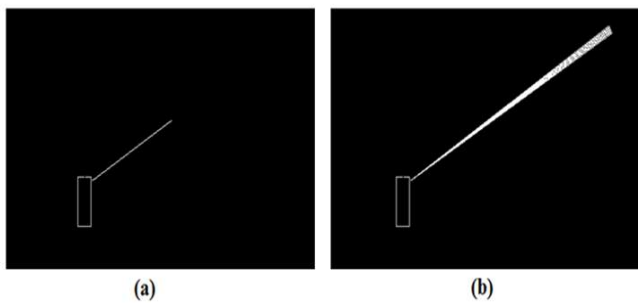
Fig. 7. Free spaces between the right sensor of the host vehicle and the detection: (a) the range of detection is less than L; (b) this range is more than L.

4.1.1.2 Gaussian-based Free Space Probability

The previous Section described how the free space cells are determined. This Section presents how the free probability of

these cells is calculated to create the "instantaneous free space map" in each measurement cycle.

First, an "instantaneous free space map" is created in each measuring cycle with the initial value 0% for all cells, which means that there are no free cells:

$$p(x_f) = 0 \tag{4}$$

Then, for all determined free cells (Section 4.1.1.1) the free-probability is calculated as follows: if the range of detection is less than L, a constant value is added to each cell between the sensor and the detection. In this paper we assume a free space probability γ for each cell.

If the range of detection is more than L, first the effect of the angular accuracy is taken into account and the cells in the f area ($\bar{f}$) are determined. The normal distribution is a good approximation for the angular accuracy of the sensor. Therefore in this paper the angular accuracy is modeled with a one-dimensional normal distribution. As shown in Fig. 8 the standard deviation of the normal distribution (σ) is $\frac{\bar{f}}{2}$ defined, such that the result of the mean of the normal distribution (μ) can be derived.
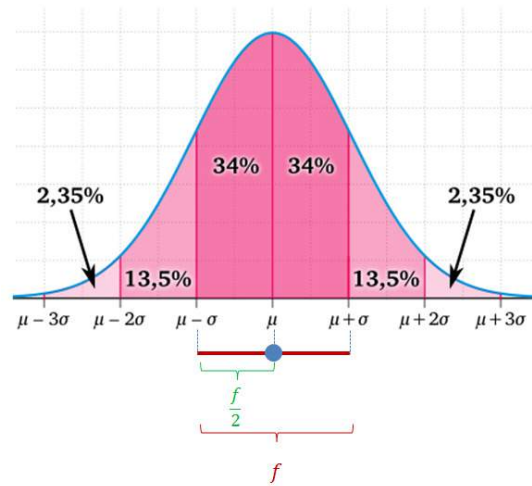
Fig. 8. Using the normal distribution to model the effect of angular accuracy

Afterwards the corresponding values of the normal distribution z_i, $i \in f$ in the f area ($\bar{f}$) are discretized. Finally, the free probability of each cell in $\bar{f}$ is calculated by

$$p(z_i|y_k) = \frac{z_i}{0.68} * \gamma \tag{5}$$

This value $p(z_i|y_k)$ is also used for all cells between the sensor and the cells in $\bar{f}$. In other words, $p(z_i|y_k)$ is the free probability for the cells lying on the beam between the sensor and the *i*-th cell covered by the angular/tangential accuracy model. Fig. 9 depicts how the cells of the free space grid are modeled using the normal distribution ($p(z_i)$ is used instead of $p(z_i|y_k)$ in this figure).
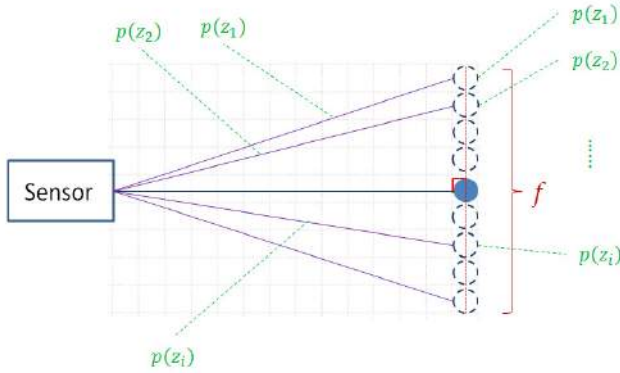
Fig. 9. Using the normal distribution to model the effect of angular accuracy in free space grid.

The individual $p(z_i|y_k)$ are used as the inverse sensor model $p(x_f|y_k)$ to fill the values of the cells of the instantaneous free space map.

4.2 Accumulated Free Space Map

As mentioned above, the individual free space map is created from scratch in each cycle. Their data is used to update the accumulated free space map (using an approach equivalent to (1)), which integrates the information on free cells over time. One design goal for the accumulated free space map was to be compatible to an occupancy map. This is not the case for the instantaneous free space map, which has increasing values describing higher *free* probabilities, whereas higher values of an occupancy maps describe a higher probability of *occupancy*.

This section describes how the accumulated free space map is compatible with the Bayesian occupancy map and how the accumulated free space map is updated with the aid of free probability of cells.

As shown in Fig. 10 the occupancy grid is set to an initial value of 0.5 which means that the free probability and probability of occupancy of all cells are the same.

Occupied cells have a probability >0.5, whereas the occupancy probability of a cell that is assumed to be free is <0.5.
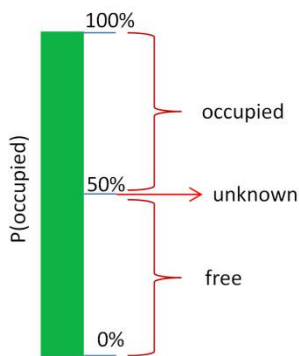
Fig. 10. Determining the status of a cell in the occupancy map.

In the previous section we described how inverse sensor model for the free space map is calculated. A conditional free probability for each cell $p(x_f|y_k)$ is computed. As described above, the occupancy probability for a free cell in the occupancy map, $(occupied)$, is less than 50%. Therefore we define the occupancy probability of free cells $\tilde{p}(x)$ in the accumulated free space map as:

$$\tilde{p}(x|y_k) = \frac{1 - p(x_f|y_k)}{2} \tag{7}$$

which specifies the occupancy probability of the grid cell x conditioned on the measurement y_k. As mentioned, the free probability $p(x_f|y_k)$ takes on a value between 0 and 1. Therefore $\tilde{p}(x)$ takes a value between 0 and 0.5, which means the occupancy probability of free cells is less than 50%.

Like a Bayesian occupancy grid map, the free space map is updated in each measuring cycle using Bayes filter:

$$L_k(x) = log\frac{\tilde{p}(x|y_k)}{1 - \tilde{p}(x|y_k)} + L_{k-1}(x) - L_0 \tag{8}$$

with the initialization

$$L_0 = log\frac{p_0}{1 - p_0}, \ p_0 = 0.5 \rightarrow L_0(x) = 0 \tag{9}$$

where $L_k(x)$ is the log-odds ratio and $L_{k-1}(x)$ is the previous log-odds ratio.

As discussed above, in every measurement cycle, the inverse sensor model and the Bayes filter are used to update the cell's probability for the current cycle.

4.3 Visualization

This section is dedicated to the visualization approach of both the instantaneous free space map and the accumulated free space map in a two-dimensional view.

The host vehicle is represented as a rectangle in the maps. Fig. 11 shows an example of an instantaneous free space map, which is created in one measuring cycle. As illustrated on Fig. 12, two sensors are equipped in front of the ego vehicle. The free spaces between the sensors and the corresponding detection are shown as white.
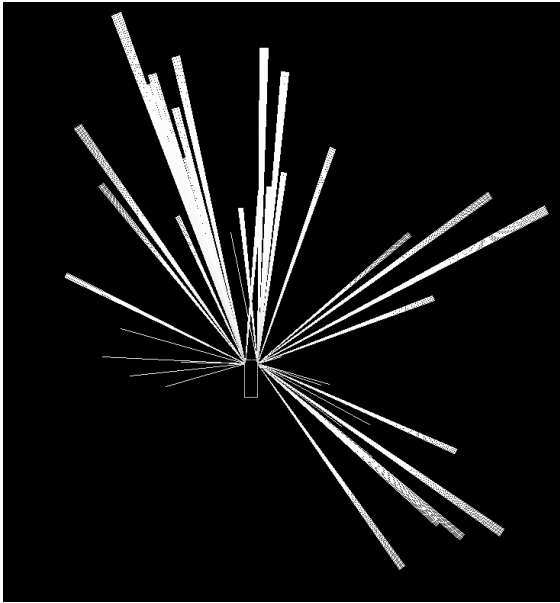
Fig. 13. Instantaneous free space map: the free spaces between the sensors and the corresponding detection are shown as white.

Fig. 14 and Fig. 15 depict two examples of our grid maps, respectively occupancy grid map, free space grid map and the combination of both maps simulated by our vehicle driving in an urban scenario. The free spaces in (b) and (c) are shown with green. The occupied cells are illustrated with black in (a) and with red in (c). The probability is shown with darker and lighter colors (darker means more probable). For example dark green means more probable free, etc.
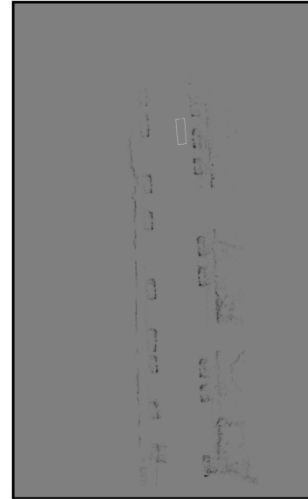
(a)
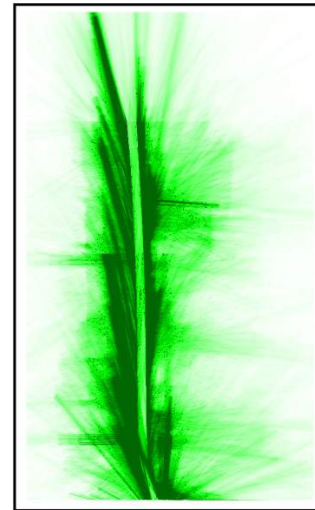
(b)
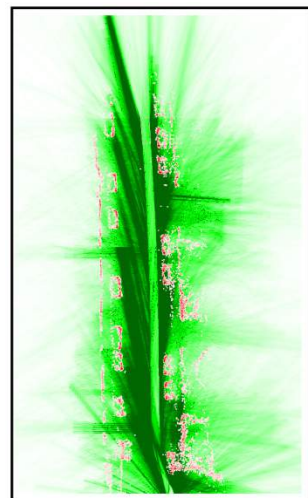
(c)

Fig. 14. (a) An occupancy grid (b) the accumulated free space map (c) the combination of two maps.

(a)

(b)

(c)

Fig. 15. (a) An occupancy grid (b) the accumulated free space map (c) the combination of two maps.

5. CONCLUSION

The presented paper introduces a new method for constructing a two-dimensional free space grid map – the so-called accumulated free space map – based on data from radar sensors. In contrast to other (Bayesian) approaches, we do not integrate the free space and the occupancy information into one single map. Thus, the free probability in the free space grid map and the probability of "occupied" in the occupancy grid map are not complementary (which is also the case for Dempster-Shafer based approaches).

To model the free space, the initial assumption is that the space between a sensor and its detection is empty. In every measurement cycle, these spaces – the so-called free spaces – are determined, a conditional free probability for each grid cell in this space is computed, and stored in an Instantaneous Free Space Map. A novel contribution is the fact that the detection's tangential accuracy is taken into account into the free space model.

The accumulated Free Space Map is updated in every measurement cycle using Instantaneous Free Space Map and Bayes filter. This accumulated Free Space Map is trajectory independent and represents all free spaces by a free probability.

The resulting high quality Free Space Map created from Delphi 77 GHz Short Range Radars was shown, next to an occupancy map and the integrated occupancy and free space map.

The accumulated Free Space Map can be used in scenarios like automatic parking etc., because of the essential role of the drivable free spaces in these systems.

REFERENCES

Bouzouraa, M. E. (2011). Belegungskartenbasierte Umfeldwahrnehmung in Kombination mit objektbasierten Ansätzen für Fahrerassistenzsysteme. Ph.D thesis, Technische Universität München.

Bresenham, J. E. (1965). Algorithm for computer control of a digital plotter. Paper presented at the *IBM Systems Journa,* IBM, P. 25 – 30.

Dempster, A. P. (1967). Upper and lower probabilities induced by a multivalued mapping. The Annals of Mathematical Statistics *38 (2): 325-339.*

Foroughi, M. (2015). Erweiterung einer Belegungskartierung durch eine Freiraum-basierte Überfahrbarkeitserkennung im Rahmen eines radargestützten Automotivsystems. Unpublished Master thesis, Bergische Universität Wuppertal.

Garcia, R., Aycard, O., Vu, T. (2008). High Level Sensor Data Fusion for Automotive Applications using Occupancy Grids. Paper presented at *the IEEE 10th Intl. Conf. on Control, Automation, Robotics and Vision,* IEEE*,* Hanoi. P. 530 – 535.

Khlifi, R., Wurth, M., Ioffe, A., Iurgel, U. and Doerr, W. (2014). 360° Radar based parking. Paper presented at *the IQPC International Conference "The Road to Automated Drive 2014" and "Chassis Sensors & 360° Sensing"*, Stuttgart.

Schmid, M. R. (2012). Umgebungserfassung für Fahrerassistenzsysteme mit hierarchischen Belegungskarten. Ph.D thesis, Universität der Bundeswehr München.

Schreier, M. and Willert V. (2012). Robust free space detection in Occupancy Grid Maps by methods of image analysis and dynamic B-Spline contour tracking. Paper presented at *the IEEE Intelligent Transportation Systems,* IEEE, Anchorage, AK. P. 514 – 521.

Schreier, M. and Willert V. (2013). From grid maps to parametric free space maps - a highly compact, generic environment representation for ADAS. Paper presented at *the IEEE Intelligent Vehicles Symposium (IV),* IEEE, Gold Coast, QLD. P. 938 - 944.

Shafer, G. (1976). *A Mathematical Theory of Evidence*, Princeton University Press.

Vu, T., Burlet, J., Aycard, O. (2008). Grid-based localization and local mapping with moving object detection and tracking.

Paper presented at *the Intelligent Vehicles Symposium,* IEEE, Eindhoven. P. 684-689.

Zhou, J., Navarro-Serment L. E., and Hebert M. (2012). Detection of parking spots using 2D range data. Paper presented at *the IEEE Intelligent Transportation Systems,* IEEE, Anchorage, AK. P. 1280 – 1287.

,

Simultaneous localization and mapping (SLAM) for automotive using forward looking radar

Johan Degerman [*] **Klas Alenljung** [**] **Yoshihiro Abe** [***]

[*] *Qamcom Research and Technology, Falkenbergsgatan 3, SE-412 85 Gothenburg (e-mail: johan.degerman@qamcom.se).*
[**] *DENSO Sales Sweden AB, Gotaverksgatan 6A, SE-41755 Gothenburg (e-mail: k.alenljung@denso.se).*
[***] *DENSO CORPORATION, 1-1 Showa-cho Kariya, Aichi 448-8661, Japan, (e-mail: yoshihiro_a_abe@denso.co.jp)*

Abstract:
Localization is the process of finding ones relation to the surrounding stationary objects, and mapping is the process of determining the relation between the stationary objects. Mapping requires a sensing technique, and in addition to that a known (or estimated) location. If we neglect the possibility of external support such as GPS or street maps and instead consider localization using ranging sensors, we are facing two strongly interconnected problems that needs to be solved simultaneously. We have investigated the possibility to perform SLAM (simultaneous localization and mapping) in automotive using a forward-looking radar, primarily designed for ACC (adaptive cruise control) and PCS (pre-crash safety). Our positioning is not only relying on the inertial measurements speed and yaw-rate from the vehicle, but also incorporates radar measurements and performs extended Kalman filter SLAM (EKF-SLAM). Using collected data from a single forward-looking radar, we have shown that it is possible to enhance the positioning performance without support from GPS. The heading of the vehicle was drifting as yaw-rate error accumulated, but when adding EKF-SLAM we mitigated this problem. However, this system was very sensitive to parameter settings, as well as radar misalignment, and needs a thorough on-line calibration. Robustness can be achieved by increasing the field of view or having side-looking radars.

Keywords: Signal processing, Tracking filters, Positioning systems, SLAM, Autonomous vehicles

1. INTRODUCTION

The localization and mapping without support from infrastructure or prior maps is regarded as a very difficult problem since it contains an inherent chicken-or-the-egg dilemma where one depend on the other. This problem has been studied extensively within the robotics field for in-door navigation, where fire-fighting robots is one application using the technology. In this paper we present our work of applying Extended Kalman filter (EKF) SLAM for positioning a vehicle. The growing interest for SLAM in automotive emerges from the rapid development towards autonomous vehicles, combined with the shortcomings of the GPS. Those are mainly insufficient accuracy (due to highly correlated noise) and the demand for line-of-sight to several satellites. The last issue makes it difficult to rely on GPS data in urban environment, since occlusion and multi-path are widely occurring, especially in tunnels and parking garages. When losing the update of reference position, vehicles are referred to dead reckoning of wheel speed and yaw-rate sensors supported by a street map - unless we employ SLAM by sensing the stationary environment around the vehicle.

However, SLAM is accompanied with two major problems, of which association ambiguity is the most crucial one. Incorrect measurement-to-landmark assignment causes error in the position relative to the previously acquired map. The other side of the coin is that the map is being distorted. The second problem with SLAM is the rapid growth in computational complexity as the number of detected stationary objects increase. Those problems were targeted by Montemerlo et al. (2002) as FastSLAM was introduced as an alternative to the standard EKF-SLAM. To avoid having full covariance matrix, containing vehicle state and all landmarks, FastSLAM factorizes the problem into many sub-problems, as estimation of ego-position and estimation of all the landmarks is handled separately. This approach helps reduce matrix inversion computations and make FastSLAM scale linearly with the number of landmarks. However, the particle filter implementation adds some computational load as all particles carry their own version of landmark estimates. Many researchers have circumvented the association problem by pre-processing raw measurements into high-level objects, which occur more sparsely in the environment. Although this is possible for laser scanners and cameras, it is very difficult for a radar sensor. The reason for that is that the resolution
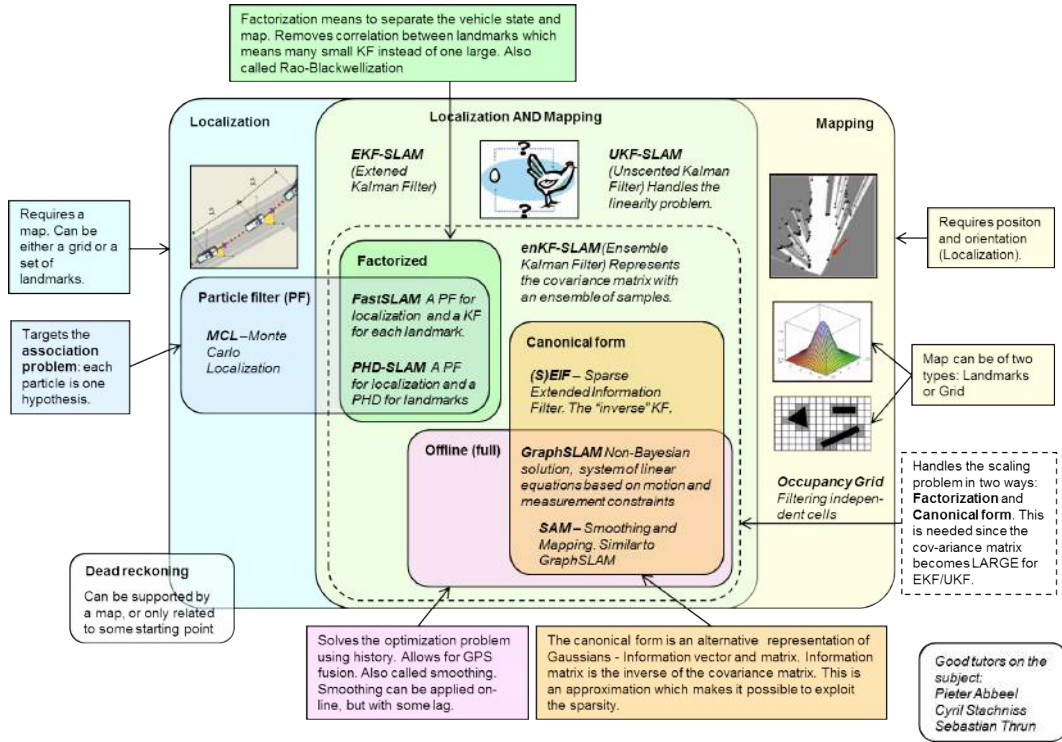
Fig. 1. An overview of localization and mapping. The left part concerns localization (with known map) and the right part is about mapping (with known position). The intersection in the middle constitutes the Gordian knot which we call SLAM, both on-line (which we cover here) and off-line. For SLAM, the representation of the environment is landmarks, that is points in state-space. For the mapping, one usually uses another representation called grid maps, but that is not relevant here.

for todays radars are lower and the interference between different scatterers causes the signal to fluctuate substantially. However, the next generation radars operating on 79 GHz, increased resolution is offered and this problem will be mitigated.

The factorization of landmarks can be achieved in another way, namely by solving the problem in information space. This is employed by many methods, including Graph-SLAM by Thrun and Montemerlo (2005). The information form is the reciprocal of the state space and the information matrix is the inverse of the covariance matrix. Here, we can view the problem as an optimization problem where the goal is to optimize the whole trajectory by using measurements and inertial data as constraints. This may be the biggest motivation for using GraphSLAM; instead of solving the online SLAM problem by recursively updating, we can effectively solve the offline SLAM problem using least squares techniques for optimization. In the GraphSLAM framework, GPS measurements can be integrated naturally as global constraints, see Carlson (2010). In Figure 1 we try to picture the whole field and categorized EKF-SLAM, FastSLAM, and graphSLAM. Worth mentioning in this context is that there are other ways of solving the position involving communication and off-line processing of large amounts of data, which is the backbone of Google's solution.

Also, one could relieve the Gordian knot by having a few reference vehicles equipped with differential GPS record ranging sensor data. The data will serve as "virtual landmarks" for the other vehicles equipped with the same

ranging sensor, which aim to follow the same route as the reference vehicle. This will remove the S from SLAM, but require off-line data support in order to work. A promising version of this approach to (S)LAM is to pre-process the data into occupancy grid maps (OGM), and then have the maps for positioning as in Moritz and Pettersson (2014). OGM uses pixel maps instead of discrete landmarks as representation of the stationary object. Each pixel gets a probability of a object being there.

Despite the significant difficulties with on-line SLAM in it's generic EKF-form, we have chosen to investigate the possibility to employ the method for a forward looking radar. To begin with, FastSLAM is still quite computationally intense, and to avoid the scaling problem, we make some approximations regarding the correlation between landmarks and vehicle state. Instead of using conditional independence and factorize the probability density, which is the trick behind FastSLAM (called Rao-Blackwellization), we assume complete independence between vehicle and landmarks.

$$p\left(\mathbf{x}_k|\mathbf{z}_k\right) = p\left(\mathbf{x}_k^{\mathrm{LM}}|\mathbf{x}_k^{\mathrm{EGO}}, \mathbf{z}_k\right) p\left(\mathbf{x}_k^{\mathrm{EGO}}|\mathbf{z}_k\right) \approx$$
$$p\left(\mathbf{x}_k^{\mathrm{EGO}}|\mathbf{z}_k\right) \prod_i p\left(\mathbf{x}_k^{\mathrm{LM}_i}|\mathbf{z}_k\right) \qquad (1)$$

The localization is contained in the EGO part of the state and the mapping is in the LM (landmark) part. This is a coarse approximation but it enables for computation of likelihood and Kalman gain when the computational resource is limited. Moreover, it increases robustness since it

removes a lot of off-diagonal elements from the full covariance matrix. The approximation is a heuristic approach and has been verified through extensive simulations.

In the next section we describe how we employed EKF-SLAM for the automotive application. Although this is not novel, we believe that this is of common interest, particularly as the computations of the Jacobian matrices becomes unexpectedly complicated. After that we present our result using collected real data.

2. EKF-SLAM

In a standard EKF-SLAM all the estimated quantities are put in the state vector. Thus, concatenating the vehicle state and landmarks into

$$
\mathbf{x}_t = \left[\underbrace{x\ y\ \alpha\ s\ \omega}_{\text{vehicle}}\ \underbrace{m_x^1\ m_y^1\ m_x^2\ m_y^2\ \dots\ m_x^N\ m_y^N}_{\text{landmarks}} \right]^{\text{T}} \quad (2)
$$

The state is considered as stochastic with covariance

$$
\mathbf{P} = E\left[(\mathbf{x} - E\left[\mathbf{x}\right])(\mathbf{x} - E\left[\mathbf{x}\right])^{\text{T}} \right] \quad (3)
$$

We use a coordinated turn vehicle model, where the position x, y is defined as the location of the pivot center of the vehicle around which is turns, in a ground fixed coordinate frame. This is about the same as the midpoint of the rear axis. This should not be confused with the location of the sensor, which we will come back to later. The variable α is the heading of the vehicle, where we use radians (zero is east). The last two quantities are speed s and yaw-rate ω. The yaw-rate is simply the time derivative of the heading $\omega = \frac{d\alpha}{dt}$. The extended Kalman filter contains four major steps, prediction, likelihood computation, association, and update. Our methods are described in the next four subsections.

2.1 Prediction

For the prediction we need a model of the dynamics, which is done by forming the time-derivative of the state $\dot{\mathbf{x}}_t$. The predicted state is then extrapolated from the last upated state to some time in the future, similarly as the state uncertainty.

$$
\mathbf{x}_{k+1|k} = f\left(\mathbf{x}_{k|k}, T\right) \quad (4)
$$
$$
\mathbf{P}_{k|+1k} = \mathbf{F}_k \mathbf{P}_{k|k} \mathbf{F}_k^{\text{T}} + \mathbf{Q}_k \quad (5)
$$

To put this in time-discrete form for EKF we can either do what is called discretized linearization, or linearized discretization. Since we are expecting a high sampling rate (relative to the dynamics of the vehicles) we can choose any of the two. The most common method is discretized linearization and this is the one we will use. The prediction is is written as

$$
f\left(\mathbf{x}, T\right) = \begin{bmatrix} x + sT\cos\alpha \\ y + sT\sin\alpha \\ \alpha + T\omega \\ s \\ \omega \\ m_x^1 \\ m_y^1 \\ \vdots \\ m_x^N \\ m_y^N \end{bmatrix} \quad (6)
$$

and the Jacobian $\mathbf{F}_k$ and state covariance $\mathbf{Q}_k$ is defined in section A.1. From now on the discrete-time index will always be k, but sometimes omitted.

2.2 Likelihood

The likelihood is a measure of goodness for the assignment between measurement of range, bearing, and range-rate

$$
\mathbf{z}_j = \begin{bmatrix} R_j \\ \theta_j \\ \dot{R}_j \end{bmatrix} \quad (7)
$$

and the landmark m_x^i, m_y^i. We will use index i for a landmark. The index for a measurements is j, and the variable i_j to indicate which landmark which is assigned to measurement j. To compute the likelihood we need to project the state to the measurement space. We will use an intermediate step, which we call sensor-state

$$
\mathbf{x}_s = \left[\underbrace{x_s\ y_s\ \alpha_s\ \dot{x}_s\ \dot{y}_s}_{\text{sensor}}\ \underbrace{m_x^1\ m_y^1\ m_x^2\ m_y^2\ \dots\ m_x^N\ m_y^N}_{\text{landmarks}} \right]^{\text{T}} \quad (8)
$$

which is the sensor state in ground-fixed Cartesian coordinate system. The measurement equation is written as

$$
h_i(\mathbf{x}_s) = \begin{bmatrix} \sqrt{(\Delta_x^i)^2 + (\Delta_y^i)^2} \\ \tan^{-1}\left(\dfrac{\Delta_y^i}{\Delta_x^i}\right) - \alpha_s \\ \dfrac{-\dot{x}_s\Delta_x^i - \dot{y}_s\Delta_y^i}{\sqrt{(\Delta_x^i)^2 + (\Delta_y^i)^2}} \end{bmatrix} \quad (9)
$$

where

$$
\begin{aligned} \Delta_x^i &= m_x^i - x_s \\ \Delta_y^i &= m_y^i - y_s \end{aligned} \quad (10)
$$

The conversion from state-space to sensor state-space is simply

$$
\mathbf{x}_s(\mathbf{x}) = \begin{bmatrix} x_s \\ y_s \\ \alpha_s \\ \dot{x}_s \\ \dot{y}_s \end{bmatrix} = \begin{bmatrix} \begin{bmatrix} x \\ y \end{bmatrix} + R_\alpha \begin{bmatrix} d_1 \\ d_2 \end{bmatrix} \\ \alpha + \alpha_d \\ R_\alpha\left(\begin{bmatrix} s \\ 0 \end{bmatrix} + \omega \begin{bmatrix} -d_2 \\ d_1 \end{bmatrix}\right) \end{bmatrix} \quad (11)
$$

where

$$
R_\alpha = \begin{bmatrix} \cos\alpha & -\sin\alpha \\ \sin\alpha & \cos\alpha \end{bmatrix} \quad (12)
$$

and d_1 and d_2 is the longitudinal and lateral displacement (from vehicle centre), respectively. α_d is the mounting angle of the sensor.

Using 9 to 12 we can form the Jacobian for the measurement equation by using the chain rule

$$\mathbf{H} = \frac{\partial h}{\partial \mathbf{x}_s} \frac{\partial \mathbf{x}_s}{\partial \mathbf{x}} \tag{13}$$

where the landmarks-to-sensor part is

$$\frac{\partial h}{\partial \mathbf{x}_s} = \begin{bmatrix} \mathbf{H}_1^{\mathrm{EGO}} & \mathbf{H}_1^{\mathrm{LM}} & 0 & \cdots & 0 \\ \mathbf{H}_2^{\mathrm{EGO}} & 0 & \mathbf{H}_2^{\mathrm{LM}} & & \vdots \\ \vdots & \vdots & & \ddots & 0 \\ \mathbf{H}_N^{\mathrm{EGO}} & 0 & \cdots & 0 & \mathbf{H}_N^{\mathrm{LM}} \end{bmatrix} \tag{14}$$

and the sensor-to-vehicle part is

$$\frac{\partial \mathbf{x}_s}{\partial \mathbf{x}} = \begin{bmatrix} \mathbf{H}^{\mathrm{S}} & 0 & \cdots & 0 \\ 0 & 1 & & \vdots \\ \vdots & & \ddots & 0 \\ 0 & \cdots & 0 & 1 \end{bmatrix} \tag{15}$$

See Section A.2 for how $\mathbf{H}_j^{\mathrm{EGO}}$, $\mathbf{H}_j^{\mathrm{LM}}$, and $\mathbf{H}^{\mathrm{S}}$ are computed. Now we can compute the residual between measurement j and its assigned landmark i_j

$$\mathbf{y}_k = \begin{bmatrix} \mathbf{z}_1 - h_{i_1}(\mathbf{x}_{k|k-1}) \\ \mathbf{z}_2 - h_{i_2}(\mathbf{x}_{k|k-1}) \\ \vdots \\ \mathbf{z}_M - h_{i_M}(\mathbf{x}_{k|k-1}) \end{bmatrix} \tag{16}$$

and its covariance

$$\mathbf{S}_k = \mathbf{H}_k \mathbf{P}_{k|k-1} \mathbf{H}_k^T + \mathbf{I}_M \otimes \mathbf{R}_k \tag{17}$$

where

$$\mathbf{R}_k = \begin{bmatrix} \sigma_R^2 & 0 & 0 \\ 0 & \sigma_\theta^2 & 0 \\ 0 & 0 & \sigma_{\dot{R}}^2 \end{bmatrix} \tag{18}$$

Up to this stage all is the same as the standard EKF-SLAM, however we will need to make some simplifications in order to reduce the computational complexity. To avoid computing the likelihood for every reasonable combination of i_j and inverting the corresponding and possibly large matrices, we assume at this stage that the vehicle is independent from the landmarks (which are also independent from each other). Thus we approximate the residual covariance for any assignment i_j as

$$\tilde{\mathbf{S}}_k^{i_j} = \mathbf{H}_j^{\mathrm{EGO}} \mathbf{H}^{\mathrm{S}} \mathbf{P}_{k|k-1}^{\mathrm{EGO}} \left(\mathbf{H}^{\mathrm{S}}\right)^T \left(\mathbf{H}_j^{\mathrm{EGO}}\right)^T + \tag{19}$$

$$\mathbf{H}_j^{\mathrm{LM}} \mathbf{P}_i^{\mathrm{LM}} \left(\mathbf{H}_j^{\mathrm{LM}}\right)^T + \mathbf{R}_k \tag{20}$$

where $\mathbf{P}_{k|k-1}^{\mathrm{EGO}}$ is the 5-by-5 vehicle covariance matrix and $\mathbf{P}_j^{\mathrm{LM}}$ is the 2-by-2 landmark j covariance matrix. This way, we can approximate the likelihood for the i_j assignment. Usually the log-likelihood is used instead, which is written as

$$L_{ij} \approx -\log\left(2\pi \left|\tilde{\mathbf{S}}_k^{i_j}\right|\right) - \tag{21}$$

$$\frac{1}{2} \left(\mathbf{z}_j - h_{i_j}(\mathbf{x})\right)^{\mathrm{T}} \left(\tilde{\mathbf{S}}_k^{i_j}\right)^{-1} \left(\mathbf{z}_j - h_{i_j}(\mathbf{x})\right) \tag{22}$$

and we only need to invert M 3-by-3 matrices, where M is the number of measurements.

2.3 Association

The association of measurement-to-landmark is made using the approximated log-likelihood from the previous subsection. The assignment of a measurement j to the null landmark $i = 0$, i.e. not assigning the measurement to any track needs some measure of goodness, as well as the assignment of a landmark i to the null measurement $j = 0$,

$$L_{0j} = L_{\mathrm{new}} \ \forall j \tag{23}$$
$$L_{i0} = L_{\mathrm{lost}} \ \forall i \tag{24}$$

The fixed parameters act as a gate when assigning measurements to landmarks, and they were set to $L_{\mathrm{new}} = L_{\mathrm{lost}} = -6$. The Association matrix will look like

$$\mathbf{D} = \begin{bmatrix} \times & L_{\mathrm{new}} & L_{\mathrm{new}} & \cdots & L_{\mathrm{new}} \\ L_{\mathrm{lost}} & L_{11} & L_{12} & \cdots & L_{1M} \\ L_{\mathrm{lost}} & L_{21} & L_{22} & & L_{2M} \\ L_{\mathrm{lost}} & \vdots & & \ddots & \vdots \\ L_{\mathrm{lost}} & L_{N1} & L_{N2} & \cdots & L_{NM} \end{bmatrix} \tag{25}$$

The global hypothesis contains the M measurement to landmark associations which is the set $\Omega_M = \{i_1, i_2, \ldots, i_M\}$. For clarity we change the notation from i_j indexing to the binary association matrix $\chi_{ij} \iff \Omega_M$

$$\chi_{ij} = \begin{cases} 1 & \text{landmark } i \text{ is assigned to measurement } j \\ 0 & \text{landmark } i \text{ is NOT assigned to measurement } j \end{cases} \tag{26}$$

We want to minimize the sum of all distances

$$\min_{\chi_{ij}} \left(\sum_{i=0}^{N} \sum_{j=0}^{M} \mathbf{D}_{ij} \chi_{ij} \right) \tag{27}$$

with constraint

$$\sum_{j=0}^{M} \chi_{1j} = 1, \sum_{j=0}^{M} \chi_{2j} = 1, \ldots, \sum_{j=0}^{M} \chi_{nj} = 1 \tag{28}$$

$$\sum_{i=0}^{N} \chi_{i1} = 1, \sum_{i=0}^{N} \chi_{i2} = 1, \ldots, \sum_{i=0}^{N} \chi_{im} = 1 \tag{29}$$

This means that each landmark can only be assigned to one measurement and vice versa. The null landmark and null measurement may get several assignments. For all $\chi_{0j} = 1$ we initiate new landmarks and for every $\chi_{i0} = 1$ we decrease some counter so that we can remove landmarks that have not been seen for a while. This discrete linear optimization problem is solved using the modified auction algorithm by Bertsekas (1991). Once we have the association matrix $\chi_{ij} = \Omega_M$ we can compute the residual $\mathbf{y}_k$ and residual covariance $\mathbf{S}_k$ and update the vehicle state and landmarks.

2.4 Update

For the vehicle update we have added two things, a gating step and inclusion of speed and yaw-rate. The additional gating step is due to the fact that the vehicle state update is extremely sensitive to incorrect associations. False associations will distort the map by changing the heading of the vehicle and must be avoided at all cost. If no measurement is inside gate, which may happen during a turn, we still have the speed and yaw-rate as a fall-back. Since the radar is assumed to have good measurement accuracy and thus each assignment will get a significant Kalman gain, it is better to exclude assignments if there exists any doubts.

From the assigned plots we narrow it down to include only measurements within $\pm 0.5°$ the predicted bearing and within $\pm 1 \frac{m}{s}$ of the predicted radial velocity

$$j^* = \forall j : i_j \neq \text{null} \wedge \left| \mathbf{z}_j - h_{i_j}(\mathbf{x}) \right| < \begin{bmatrix} \infty \\ 0.5° \\ 1\frac{m}{s} \end{bmatrix} \qquad (30)$$

which yields a new set of measurements of size M^* for the vehicle update. In the next section we show in Figure 5 the number of plats, the assigned plot, and the narrow selection for vehicle update.

It is common to include speed in the prediction as a control signal and not have it as an estimated quantity. But since both speed and yaw-rate are measurements it makes sense to treat them as such. The speed and yaw-rate are added by concatenating the residual of the selected plots j^*

$$\mathbf{y}_k^* = \begin{bmatrix} \mathbf{z}_{j^*} - h_{i_{j^*}}(\mathbf{x}_{k|k-1}) \\ \vdots \\ \text{speed}_k - s_{k|k-1} \\ \text{yaw-rate}_k - \omega_{k|k-1} \end{bmatrix} \qquad (31)$$

and altering the Jacobian $\mathbf{H}_k$ accordingly. Again, we will approximate the residual covariance by assuming independence between vehicle state and landmarks

$$\mathbf{S}_k^* = \begin{bmatrix} \mathbf{H}_{j^*}^{\text{EGO}}\mathbf{H}^{\text{S}} \\ \vdots \\ 0\ 0\ 0\ 1\ 0 \\ 0\ 0\ 0\ 0\ 1 \end{bmatrix} \mathbf{P}_{k|k-1}^{\text{EGO}} \begin{bmatrix} \mathbf{H}_{j^*}^{\text{EGO}}\mathbf{H}^{\text{S}} \\ \vdots \\ 0\ 0\ 0\ 1\ 0 \\ 0\ 0\ 0\ 0\ 1 \end{bmatrix}^{\text{T}} + \mathbf{R}^* +$$

$$\begin{bmatrix} \mathbf{H}_{j^*}^{\text{LM}}\mathbf{P}_{i_{j^*}}^{\text{LM}} \left(\mathbf{H}_{j^*}^{\text{LM}} \right)^{\text{T}} \\ \ddots \end{bmatrix} \qquad (32)$$

and the Kalman gain for the vehicle update is approximated as (the approximation is since all correlation between vehicle and landmarks is omitted)

$$\mathbf{K}_k^* \approx \mathbf{P}_{k|k-1}\mathbf{H}^{\text{T}} \left(\mathbf{S}_k^* \right)^{-1} \qquad (33)$$

and used in the update as follows

$$\mathbf{x}_{k|k}^{\text{EGO}} \approx \mathbf{x}_{k|k-1}^{\text{EGO}} + \mathbf{K}_k^* \mathbf{y}_k^* \qquad (34)$$

$$\mathbf{P}_{k|k}^{\text{EGO}} \approx \left(\mathbf{I} - \mathbf{K}_k^* \mathbf{H}_k \right) \mathbf{P}_{k|k-1}^{\text{EGO}} \qquad (35)$$

The landmarks are updated with all the selected assignments i_j and not only the subset i_j^*. Following the independence assumption we treat them individually using the innovation noise $\tilde{\mathbf{S}}_k^{i_j}$ computed for the likelihood. The approximated Kalman gains for both the vehicle and landmarks which are treated separately are found using heuristics, and not through modeling. We have used extensive simulations to make sure that the approximations are acceptable for our application.

3. RESULTS RECORDED DATA

We omit the part where we describe our simulation environment and the results from simulated data. Instead we move on to describe our work with collected data from an off-the-shelf DENSO front-looking medium range radar (MRR), designed for ACC (adaptive cruise control) and PCS (pre-crash safety). We have used the default signal processing for this particular application, however we record raw data and produce measurements $[R_j, \theta_j, \dot{R}_j]$ offline, to be able to study different parameterization and configurations of our EKF-SLAM. This means that the signal processing is designed to track objects in a narrow field of view in front of the vehicle $\pm 15 - 20°$. The radar is mounted on a Volvo S60 test vehicle, see Figure 2, equipped with differential GPS.

Fig. 2. The DENSO test vehicle with front-looking radar

The narrow field of view and the signal processing is optimized for ACC and PCS which make EGO-motion estimation a non-trivial task. Particularly, estimation of the rotational motion is cumbersome. We selected a nearby parking lot where we drive in a closed loop, see Figure 9. However, in this paper we do not try to "close the loop" in the SLAM algorithm, we are only considering EGO-motion.

We start at the red X-mark and drive counter-clockwise for one and a half lap, ending at the blue X-mark. The heading during the driving is plotted in Figure 3, and the speed in Figure 4.

The number of measurements used in radar EKF-SLAM is shown in Figure 5. We observe that the selected measurements for vehicle update drops significantly in the turns, which is due to the narrow field of view. This is unfortunate since it is when they are needed the most, to compensate for the drift in yaw-rate.
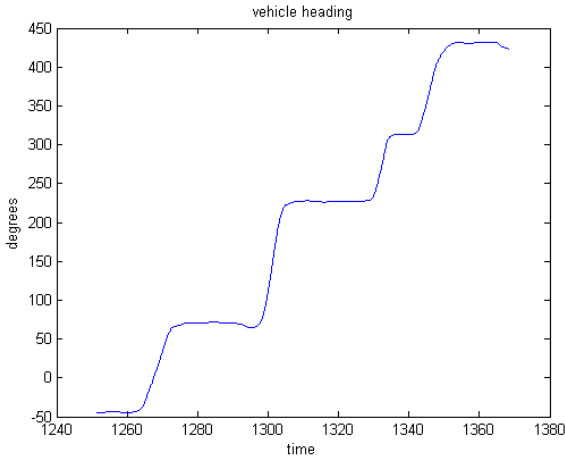
Fig. 3. The heading during the recorded scenario, where zero degrees is east and 90 degrees is north. We see four left turns, where the fourth turn is the same as the first.
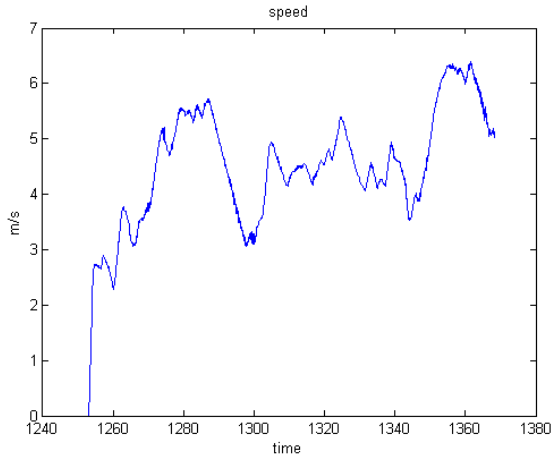
Fig. 4. The relatively low speed during the recorded scenario, taken from the DGPS system.

To test the performance of the EGO-position using EKF-SLAM (including yaw-rate and speed), we run the algorithm twice, first with no radar measurements and then with radar on. We call the method with no radar "dead reckoning" since we are only integrating the speed and yaw-rate. The comparison between dead reckoning and EKF-SLAM is made by plotting the error in heading, the longitudinal and lateral error (as compared to the ground truth). Here longitudinal offset means the offset of the position in the driving direction of the vehicle, and lateral offset is the offset in position perpendicular to the driving direction (left is positive).

We see that the heading error for the dead reckoning is accumulating and constantly increasing, but for EKF-SLAM there is no such drift, see Figure 6. The longitudinal error in figure 7 shows that the estimated position using dead reckoning falls up to ten meters behind due to the drift in heading, which is not the case for EKF-SLAM. The lateral error keeps alternating side, which is a direct result of the drift in heading and the sharp turns. However, we see that the offset is much smaller when we have support of radar measurements, see Figure 8.
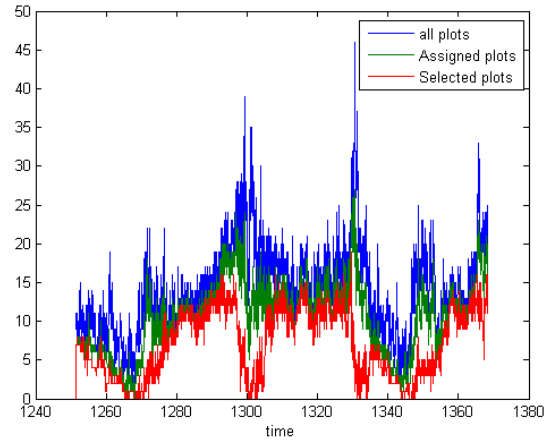
Fig. 5. The number of measurements M at each time instance, in blue. The number of plots used for updating landmarks in green, and the exclusive selection of plots, using gating, for the vehicle update in red.
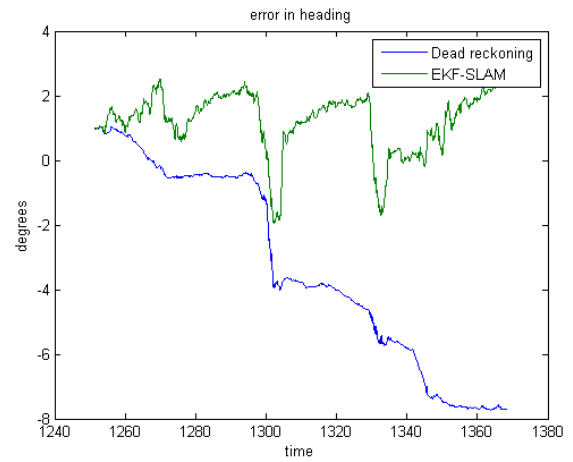
Fig. 6. The error in heading, which is constantly accumulating for the dead reckoning case, but not for radar EKF-SLAM.
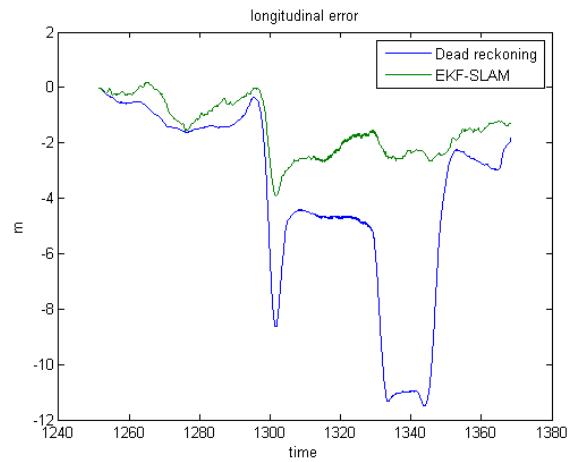
Fig. 7. The longitudinal error, which illustrates the offset in the driving direction
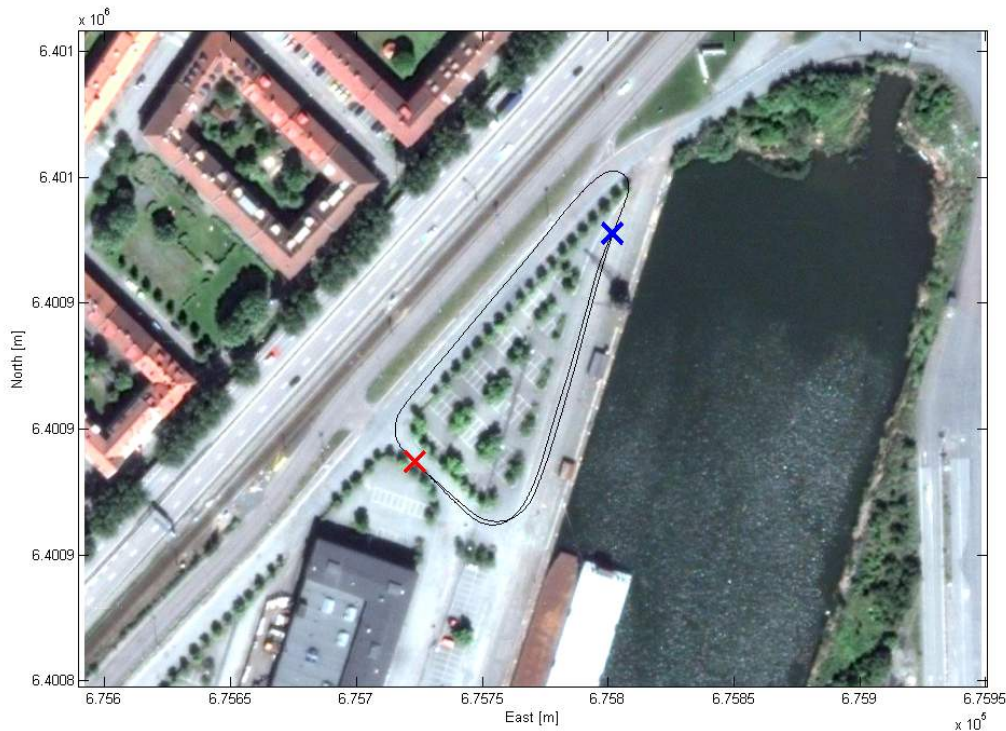
Fig. 9. The parking lot used for testing the performance of EKF-SLAM. We drove counter-clockwise for one and a half lap, starting at the red corss and ending at the blue.
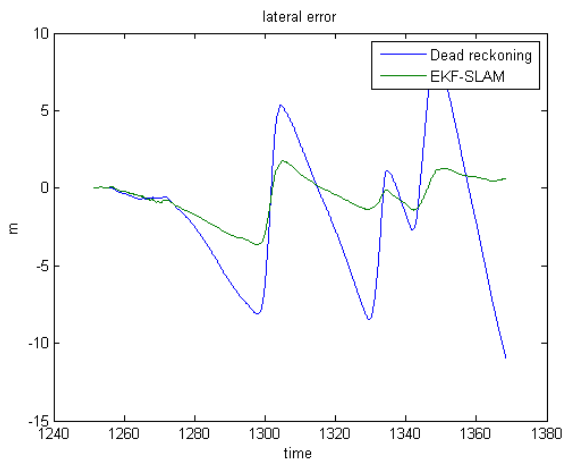
Fig. 8. The lateral error, which illustrates the sideways offset.

4. CONCLUSIONS

In this paper we show how EKF-SLAM using radar can be utilized to enhance positioning, but it is important to point out that inertial measurements were also involved. The SLAM should be viewed upon as a complement to the speed and yaw-rate since the inertial measurements works (although poorly) without EKF-SLAM but the opposite does not old. We believe that having a much wider field of view will improve the situation significantly. This is because we will then have radial velocity to objects not only in bore-sight, but also to objects to the left and right side of the vehicle. This will help when estimating the rotational motion of the vehicle, which is what is important. The speed is already well-known from the inertial sensors. Thus, the next step would be to mount two side-looking radars in each front-corner of the vehicle instead.

The second point is that rather than trying to untie the Gordian knot we should cut it by using reference vehicles and off-line processing. Clearly, using this approach the mapping issues with SLAM will be solved. That is, by creating "virtual landmarks" off-line for a specific sensor, we avoid the middle section in Figure 1. Now localization is the only problem, and it is essentially a much smaller one. To make the map less sensor-specific we should convert the sensor readings into occupancy maps.

REFERENCES

Bertsekas, D. (1991). *Auction algorithms, in Linear Network Optimization: Algorithms and Codes, 1ed.* The MIT Press.

Carlson, J.D. (2010). *Mapping Large, Urban Environments with GPS-Aided SLAM.* Ph.D. thesis, Robotics Institute, Carnegie Mellon University, Pittsburgh, PA.

Montemerlo, M., Thrun, S., Koller, D., and Wegbreit, B. (2002). Fastslam: A factored solution to the simultaneous localization and mapping problem. In *In Proceedings of the AAAI National Conference on Artificial Intelligence*, 593–598. AAAI.

Moritz, M. and Pettersson, A. (2014). *Estimation of Local Map from Radar Data.* Master's thesis, Linkping UniversityLinkping University, Automatic Control, The Institute of Technology.

Thrun, S. and Montemerlo, M. (2005). The GraphSLAM algorithm with applications to large-scale mapping of urban structures. *International Journal on Robotics Research*, 25(5/6), 403–430.

Appendix A. JACOBIANS

In this section we write in detail how all the EKF Jacobians are computed. While not novel, it is still non-trivial task even for very simple geometries.

A.1 EKF prediction

The prediction is very simple, we predict the vehicle using a standard coordinated turn model and the Jacobian is

$$
\mathbf{F}_k =
\begin{bmatrix}
1 & 0 & -sT\sin\alpha & T\cos\alpha & -s\dfrac{T^2}{2}\sin\alpha & & & \\
0 & 1 & sT\cos\alpha & T\sin\alpha & s\dfrac{T^2}{2}\cos\alpha & & \mathbf{0}_{5\times 2N} & \\
0 & 0 & 1 & 0 & T & & & \\
0 & 0 & 0 & 1 & 0 & & & \\
0 & 0 & 0 & 0 & 1 & & & \\
& & & & & 1 & & \\
& \mathbf{0}_{2N\times 5} & & & & & \ddots & \\
& & & & & & & 1
\end{bmatrix}
\tag{A.1}
$$

The process noise is written as

$$
\mathbf{Q}_k = \mathbf{G}_k
\begin{bmatrix}
0 & & & & & & & \\
& 0 & & & & \mathbf{0} & & \\
& & \sigma_\alpha^2 & & & & & \\
& & & \sigma_s^2 & & & & \\
& & & & \sigma_\omega^2 & & & \\
& & & & & 0 & & \\
& \mathbf{0} & & & & & \ddots & \\
& & & & & & & 0
\end{bmatrix}
\mathbf{G}_k^{\mathrm{T}}
\tag{A.2}
$$

and

$$
\mathbf{G}_k =
\begin{bmatrix}
T & 0 & -s\dfrac{T^2}{2}\sin\alpha & \dfrac{T^2}{2}\cos\alpha & -s\dfrac{T^3}{6}\sin\alpha & & & \\
0 & T & s\dfrac{T^2}{2}\cos\alpha & \dfrac{T^2}{2}\sin\alpha & s\dfrac{T^3}{6}\cos\alpha & & \mathbf{0}_{5\times 2N} & \\
0 & 0 & T & 0 & \dfrac{T^2}{2} & & & \\
0 & 0 & 0 & T & 0 & & & \\
0 & 0 & 0 & 0 & T & & & \\
& & & & & T & & \\
& \mathbf{0}_{2N\times 5} & & & & & \ddots & \\
& & & & & & & T
\end{bmatrix}
\tag{A.3}
$$

where the parameters used are $\sigma_\alpha = 0$, $\sigma_s = 3m/s$, and $\sigma_\omega = 87$mrad.

A.2 Likelihood computation and EKF Update

The Jacobian for the sensor-to-vehicle is

$$
\mathbf{H}_i^{\mathrm{EGO}} =
\begin{bmatrix}
\dfrac{-\Delta_x^i}{r_i} & \dfrac{-\Delta_y^i}{r_i} & 0 & 0 & 0 \\
\dfrac{\Delta_y^i}{r_i^2} & \dfrac{-\Delta_x^i}{r_i^2} & -1 & 0 & 0 \\
\dfrac{\Delta_y^i\left(\dot{y}_s\Delta_y^i - \dot{y}_s\Delta_x^i\right)}{r_i^3} & \dfrac{-\Delta_x^i\left(\dot{y}_s\Delta_y^i - \dot{y}_s\Delta_x^i\right)}{r_i^3} & 0 & \dfrac{-\Delta_x^i}{r_i} & \dfrac{-\Delta_y^i}{r_i}
\end{bmatrix}
\tag{A.4}
$$

where

$$
\begin{aligned}
\Delta_x^i &= m_x^i - x_s \\
\Delta_y^i &= m_y^i - y_s \\
r_i &= \sqrt{(\Delta_x^i)^2 + (\Delta_y^i)^2}
\end{aligned}
\tag{A.5}
$$

and the vehicle-to-sensor is

$$
\mathbf{H}_i^{\mathrm{S}} =
\begin{bmatrix}
\mathbf{I}_{2x2} & R'(\alpha)\begin{bmatrix} d_1 \\ d_2 \end{bmatrix} & \mathbf{0}_{2x1} & \mathbf{0}_{2x1} \\
\mathbf{0}_{1x2} & 1 & 0 & 0 \\
\mathbf{0}_{2x2} & R'(\alpha)\begin{bmatrix} s - \omega d_2 \\ d_1 \end{bmatrix} & R(\alpha)\begin{bmatrix} 1 \\ 0 \end{bmatrix} & R(\alpha)\begin{bmatrix} d_1 \\ d_2 \end{bmatrix}
\end{bmatrix}
\tag{A.6}
$$

where

$$
R'_\alpha =
\begin{bmatrix}
-\sin\alpha & -\cos\alpha \\
\cos\alpha & -\sin\alpha
\end{bmatrix}
\tag{A.7}
$$

The Jacobian for the landmarks are similar to the the sensor-to-landmark, but with a different sign,

$$
\mathbf{H}_i^{\mathrm{LM}} =
\begin{bmatrix}
\dfrac{\Delta_x^i}{r_i} & \dfrac{\Delta_y^i}{r_i} \\
\dfrac{-\Delta_y^i}{r_i^2} & \dfrac{\Delta_x^i}{r_i^2} \\
\dfrac{-\Delta_y^i\left(\dot{y}_s\Delta_y^i - \dot{y}_s\Delta_x^i\right)}{r_i^3} & \dfrac{\Delta_x^i\left(\dot{y}_s\Delta_y^i - \dot{y}_s\Delta_x^i\right)}{r_i^3}
\end{bmatrix}
\tag{A.8}
$$

The Jacobians $\mathbf{H}_i^{\mathrm{EGO}}$ and $\mathbf{H}_i^{\mathrm{S}}$ is a nice way of using the chain rule to write the derivative of the mesurements with respect to state when we are not tracking objects in a sensor coordinate system, but in a vehicle coordinate system where the middle rear axis is the centre coordinate.

Evaluating Body Movements of a Drowsy Driver with Pressure Distribution Sensors

Makoto Itoh*. Ryo Ishikawa**
Toshiyuki Inagaki*

*Faculty of Engineering, Information and Systems, University of Tsukuba, Tsukuba, Ibaraki 305-8573
JAPAN (Tel: +81-29-853-5502; e-mail:{itoh,inagaki} @risk.tsukuba.ac.jp).
**Department of Risk Engineering, University of Tsukuba, Tsukuba, Ibaraki 305-8573 JAPAN[1]

Abstract: The purpose of this research is to develop a method to detect driver drowsiness with pressure distribution sensors on the driver seat. Use of such sensors has an advantage that the measurement can be done in a non-intrusive manner, and that sensing data can always be obtained while driving. We conducted an experiment with a fixed-base driving simulator. The results suggested that driver body movement increases when driver drowsiness begins to increase.

Keywords: Drowsiness, Driver monitoring, Safety, Prevention.

1. INTRODUCTION

Automated or autonomous driving systems are becoming real on the basis of today's rapid development of sensing, inference and controlling technologies. According to today's legal systems (e.g., Convention of Road Traffic (1968)), however, a person behind the steering wheel (or on the driving seat) has to bear the final responsibility as the "driver" for attaining safety. It is the driver responsibility to be awake while driving.

There are many discussions on levels of autonomous driving (e.g., Gasser and Westhoff, 2012; NHTSA 2013, SAE 2014). The law or social systems may change in terms of the driver responsibility in a future, and thus there is a possibility that it is not necessary for a driver to have the responsibility (i.e., the system or another body bears the responsibility on behalf of the driver). Still, a driver has to keep awake or smoothly recover from drowsiness in order to survive in a sudden emergency. In any way, it is/will be a vital issue for a driver to keep awake.

The necessity for a driver to be awake in a self-driving car is due to an assumption that all the machines, including autonomous driving systems, have limited capability or reliability. That is, such "imperfect" autonomous driving systems depend on human driver. However, humans also have limited capability or reliability. In particular, humans may become drowsy when the workload is very low. A driver monitoring system to detect driver drowsiness would be needed in order to ensure the driver is awake.

A driver monitoring system should be highly reliable for attaining safety. It is ironical in this context that the necessity of driver monitoring systems comes from imperfectness of autonomous driving systems. If an autonomous driving system can handle every situation safely, such driver monitoring is not necessary because human intervention in emergency is not needed.

Which is better to establish a perfect autonomous driving system (thus it does not require any driver monitoring system), or to develop "imperfect" autonomous driving system that may rely on a driver monitoring system? We believe the latter might be realistic.

The final goal of our study is to propose a novel method to detect driver drowsiness while driving. Such methods should be applicable to the situations where an automated driving system is working as well as the manual driving situations. Along this context, methods for detecting driver drowsiness based on driving performance (Fukui et al., 1993; Krajewski et al., 2009; Saito et al. 2015; Wierwille and Ellsworth, 1994) are not enough.

Other than the approach based on driving performance, driver drowsiness or too low workload can be detected by physiological indices (e.g., Brookhuis and de Waard, 2010; Roman et al., 2001; Fijita et al., 2005; Tsuchida et al., 2009). In particular, indices related to driver's eyes, such as eye blinking (Aoki et al., 2009), PERCLOS (Dinges and Grace, 1998) and eye movement or EOG (Planque et al., 1991) are useful. Facial expressions can also be used to evaluate driver drowsiness. Kitajima et al. (1997) proposed a sleepiness rating scale based on the driver's facial expression for external evaluation. In this paper, we call it Kitajima's scale. Osuga et al. (2011) modified the Kitajima's scale by taking into account the driver's resistance to sleepiness. Ishida et al. (2011) suggested using facial muscular activities in a drowsy facial expression to automatically estimate driver drowsiness in real time.

---

[1] Ryo Ishikawa is currently working for Hitachi, Ltd. Infrastructure Systems Company.

However, most of these methods are not reliable enough to be used alone in the real world. In order to make a drowsiness detection system highly reliable, it is important to increase types of drowsy detection.

Our idea is to use pressure distribution sensors on a driving seat in order to count driver activities that result in body movements. When a driver becomes drowsy, he/she may perform some activities in order to reduce his/her drowsiness. Itoh et al. (2010) suggested that such activities could be detected with pressure distribution sensors. However, it has not been clarified how the body movements change according to drowsiness.

In this paper, we conduct an experiment with a driving simulator in order to collect the driver behaviour data when the drivers are drowsy. Based on the data, we investigate the relationship between drowsiness levels and body movements. The main purpose of this study is to understand the interrelationships between the effects of driver drowsiness on physiological indices, driving performance, and subjective evaluations, such as the above-mentioned self-evaluation and external evaluation.

2. METHOD

2.1 Apparatus

A fixed-base driving simulator was used in this study (Fig. 1). The driving course is a two-lane expressway consisting of straight lines and gentle curves.

Fig. 1. A fixed-base driving simulator.

2.2 Participants

Four male drivers (A, B, C, and D) between the ages of 20-25 participated in this experiment. Their driving experiences ranged from 5 months to 6 years. Each participant had a valid driver's license and drove more than three days a week.

2.3 Task

In each trial, the participants were requested to drive along the expressway of the driving simulator for forty minutes.

The driving task of the participants was to follow the lead vehicle running in the left cruising lane. The lead vehicle neither accelerated nor decelerated, and ran at a constant speed, 100km/h. In the passing lane on the right hand, some cars are running at 120km/h with constant time headway to their forward vehicle. Passing the lead vehicle was prohibited to make the driving monotonous.

2.4 Procedure

Each participant took part in the experiment for three days. On each day, each participant did two forty-minute drives, and so the participants undertook six drives in total. The procedure is shown in Table 1.

We explained the procedure to each participant and obtained informed consent on the first day. After placing sensors on the participant, we let the participant do a simple practice drive on the driving simulator to familiarize him with the simulator. Then two drives with data collection drives were undertaken. Between these two trials, each driver took a break of 30 minutes. After the second trial, each driver filled in a questionnaire.

Table 1. Procedure of the experiment for each day

	Procedure	Time length
1	Explanation of the experiment (Obtain informed consent on the first day only)	10 min
2	Setting the experimental devices & Calibration	10 min
3	Practice drive	10 min
4	First trial	40 min
5	Break	30 min
6	Setting the experimental devices & Calibration	10 min
7	Second trial	40 min
8	Questionnaire	5 min

2.5 Measures

(1) Number of blinks
  We used an EMR-9 eye mark recorder, made by Nac Image Technology to record eyelid movement, and counted the number of blinks every minute

(2) R-R interval
 We put a wireless physiological analysis sensor made by CCI on the chest of the participants before the experiment to record electrocardiograms (ECG). We measured the average R-R interval every minute.

(3) The number of body movements
Pressure distribution sensor sheets, made by NITTA were placed on the seat cushion as well as the backrest of the driving seat. Each sensor sheet has 44×48 measurement points. Itoh et al. (2010) showed that the number of body movements is related to driver drowsiness. Let f_{xy} denote the measured value of the load at point (x, y). The load center position (LCP_x, LCP_y) is calculated as follows:

$$LCP_x = \frac{\sum\limits_{x,y} x f_{xy}}{\sum\limits_{x,y} f_{xy}} \quad LCP_y = \frac{\sum\limits_{x,y} y f_{xy}}{\sum\limits_{x,y} f_{xy}} \qquad (1)$$

When the driver's body moves, the load center position also changes. If the load center position moves more than a certain threshold within two consecutive sampling time points, this is regarded as a body movement occurred. In the experiment by Itoh et al. (2010), the sampling rate was set at 2Hz, and the threshold value was set at 0.3 inches for the seat cushion and 0.4 inches for the backrest. This study adopted their method of detecting body movements, and counted the number of body movements every minute.

(4) Driving performance

To evaluate driving performances, we measured lateral position of the vehicle (m), the steering angle (deg), and the distance to the lead vehicle (m). Their standard deviations were calculated every minute.

(5) External subjective rating of drowsiness

The subjective evaluation based on facial expression was carried out using the five level sleepiness scale proposed by Kitajima et al. (Table 2). The evaluation was carried out every 20 seconds by three trained evaluators. The three evaluators were members of our laboratory, but they did not receive any information on the participants except the video images of the drivers' facial expressions. The sleepiness levels evaluated by the three evaluators were averaged out at every rating. The average of the sleepiness levels was computed every three ratings (i.e, every minute) and were rounded off.

Table 2. Sleepiness scale based on the facial expression for external evaluation (Kitajima et al., 1997)

Sleepiness scale	Features of behavior
1	**Not Drowsy**: Eye movement is rapid, the time between blinks remains stable.
2	**Slightly Drowsy**: Eye movement is slow.
3	**Moderately Drowsy**: Blinks are slowly, the mouth moves, or the driver touches his/her face .
4	**Significantly Drowsy**: The number of blinks increases noticeably, motions unnecessary for driving are seen, yawns are frequent, deep breathing is detected.
5	**Extremely Drowsy**: The eyelids are almost closed, or the driver's head inclines to the front or rear.

A Japanese version of the Stanford Sleepiness Scale (SSS) (Hoddes E et al., 1973) (Table 3) developed by Ota et al. (1999) was used for the self-evaluation. A beeping sound was played to each participant every two minutes as a reminder to the participant to answer the sleepiness level.

Table 3 was shown to the driver in an A3 size sheet on the right-hand side of the driver's seat so that the participant could give his level easily while driving.

Table 3. The Stanford Sleepiness Scale (SSS) for self-evaluation (Hoddes E et al., 1973)

1 - Feeling active and visual alert; wide awake.
2 - Functioning at a high level, but not at peak; able to concentrate.
3 - Relaxed; awake; not at full alertness ; responsive.
4 - A little foggy; not at peak ; let down.
5 - Fogginess; beginning to lose interest in remaining awake ; slowed down.
6 - Sleepiness; Prefer to be lying down; fighting sleep ; woozy.
7 - Almost in reverie; sleep onset soon; lost struggle to remain awake.

3. RESULTS AND DISCUSSIONS

3.1 Result of subjective ratings of sleepiness scale

Fig. 2 shows the results of subjective ratings of the sleepiness scale based on facial expression. Even though individual differences were observed in terms of the tendency to be drowsy, every participant was rated as "extremely drowsy" at least once. Moreover, there was no participant who was completely drowsy from the beginning of a trial.
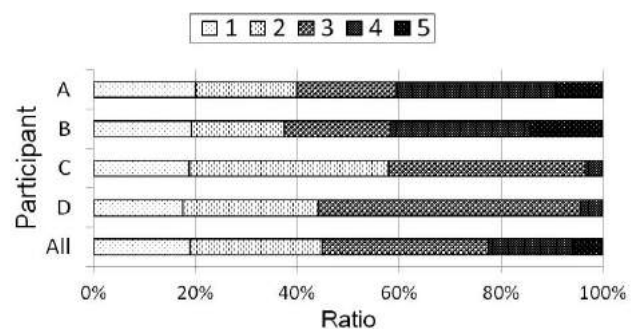
Fig 1. External subjective ratings *of* sleepiness

3.2 Correlation between the self-evaluation and the external evaluation

In order to investigate the relationship between the self evaluations and the external evaluations of sleepiness, their correlation coefficient was calculated. Fig. 3 shows data for

all participants. The size of the point represents the number of points which overlap.

A positive correlation was found between the self and the external evaluations (coefficient of correlation r = 0.782). A statistical test showed a highly significant correlation between SSS and Kitajima's scale (p < 0.01).

In the remaining part of this paper, the value of the external evaluation is regarded as the true degree of the driver's sleepiness, and relations are analyzed between the degree of sleepiness and physiological indices, as well as between the degree of sleepiness and driving performance.
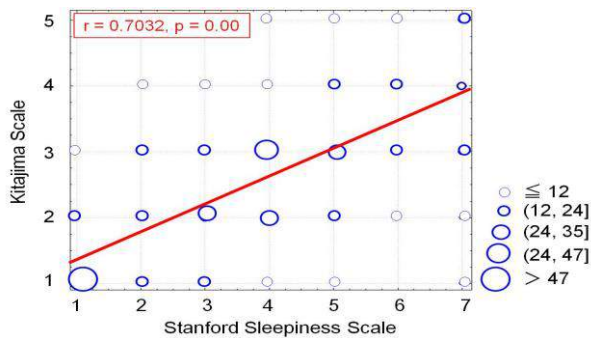
Fig 2. Correlation between SSS and the Kitajima's sleepiness Scale based on the facial expression

3.3 Physiological indices

Fig. 4 depicts the relationship between the degree of sleepiness and the number of blinks. A single-factor ANOVA with the degree of sleepiness (Kitajima's scale) on the number of blinks showed that the main effect of the degree of sleepiness was statistically significant $(F(4,955)=6.0589, p<0.01)$. Tukey's HSD test has found statiscally significant differences between levels 1 and 3, 1 and 4, 1 and 5, and between levels 2 and 3, 2 and 4, and 2 and 5 (p<0.01). In other words, as the degree of sleepiness became larger, the number of blinks tended to become smaller. In particular, the difference between levels 2 and 3 was large.
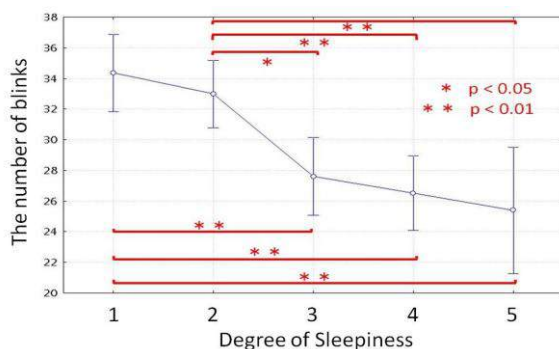
Fig 3. Relationship between the degree of sleepiness and the number of blinks

Fig. 5 illustrates the relationship between the degree of sleepiness and the average R-R interval every minute. A single-factor ANOVA with the degree of sleepiness on the average R-R interval showed that the main effect of the degree of sleepiness was not statistically significant $(F(4,955)=2.2789, p<0.05909)$.
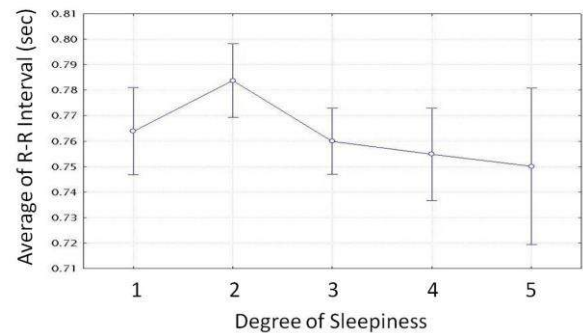
Fig 4. Relationship between the degree of sleepiness and the average R-R interval

Fig. 6 shows the relationship between the degree of sleepiness and the number of body movements. In the case of the seat cushion, a single-factor ANOVA with the degree of sleepiness showed that the main effect of the degree of sleepiness was statistically significant $(F(4,955)=18.802, p<0.01)$. Tukey's HSD test has found a statistically significant difference between levels 1 and 3, 1 and 4, 1 and 5, and between levels 2 and 3, and 2 and 4. Similary, in the case of the backrest, a single-factor ANOVA with the degree of sleepiness showed that the main effect of degree of sleepiness was statistically significant $(F(4,955)=32.245, p<0.01)$. Tukey's HSD test has also found a statistically significant difference between levels 1 and 3, 1 and 4, and 1 and 5, and between levels 2 and 3, and 2 and 4. Therefore, as the degress of sleepiness become larger, the number of body movements tends to increase. However, there is one thing to note here. Even though a significant difference was not shown, the data suggests that the number of movements in level 5 might be smaller than those in levels 3 and 4. It is thought that as the driver finds it harder to fight off the urge to sleep, his body movements decrease.
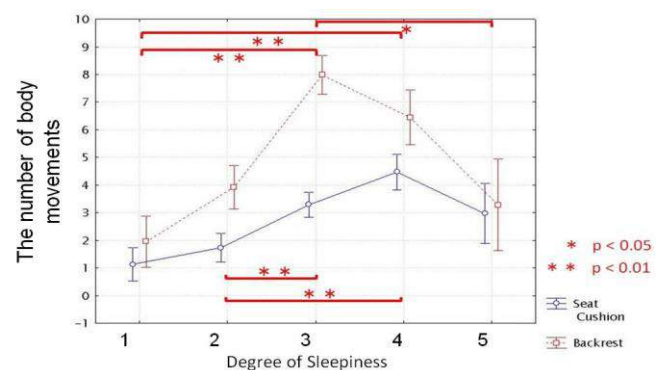
Fig 5. Relationship between the degree of sleepiness and the number of body movements

3.4 Driving performances

Fig. 7 illustrates the relationship between the degree of sleepiness and the lateral fluctuation of the vehicle. A single-factor ANOVA with the degree of sleepiness on the lateral fluctuation of the vehicle showed that the main effect of the degree of sleepiness was statistically significant ($F(4,955)=114.41$, $p<0.01$). Tukey's HSD test has found statistically significant differences between levels 1 and 3, 1 and 4, 1 and 5, between levels 2 and 4, 2 and 5, and between level 3 and 4, and 3 and 5 ($p<0.01$). Therefore, as the degree of sleepiness becomes larger, the lateral fluctuation of the vehicle tends to become bigger.

Fig. 8 illustrates the relationship between the degree of sleepiness and the standard deviation of the steering angle. A single-factor ANOVA with the degree of sleepiness on the standard deviation of the steering angle showed that the main effect of the degree of sleepiness was statistically significant ($F(4,955)=114.41$, $p<0.01$). Tukey's HSD test has found statistically significant differences between levels 1 and 3, 1 and 4, 1 and 5, between levels 2 and 4, 2 and 5, and between levels 3 and 4 ($p<0.05$). Therefore, as the degree of sleepiness becomes larger, the standard deviation of the steering angle tends to become bigger. On the other hand, the standard deviation of the steering angle in level 5 was smaller than that in level 4. It is thought that drivers found it hard to fight off the urge to sleep.

Fig. 9 illustrates the relationship between the degree of sleepiness and the standard deviation of the distance to the lead vehicle. A single-factor ANOVA with the degree of sleepiness on the standard deviation of the distance to the lead vehicle shows that the main effects of the degree of sleepiness were statistically significant ($F(4,955)=33.124$, $p<0.01$). Tukey's HSD test has found statistically significant differences between levels 1 and 3, 1 and 4, and 1 and 5 and between level 2 and 4, and 2 and 5 ($p<0.01$). Therefore, as the degree of sleepiness becomes larger, the standard deviation of the distance to the lead vehicle tends to become bigger.
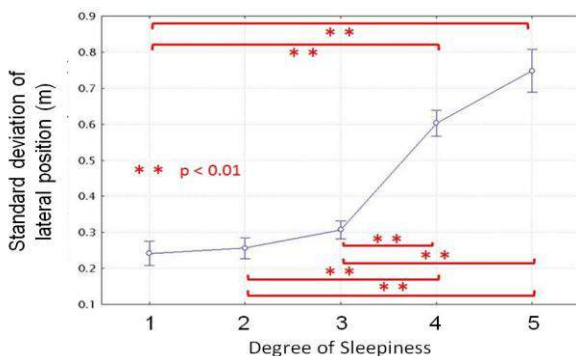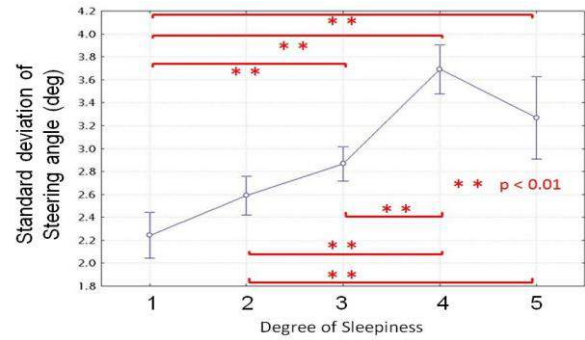
Fig 7. Relationship between the degree of sleepiness and the standard deviation of the steering angle
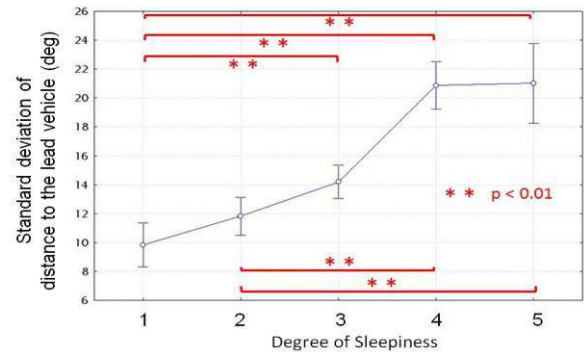
Fig 8. Relationship between the degree of sleepiness and the standard deviation of the distance to the lead vehicle

The above results show that the driving performance degrades when the degree of sleepiness is greater than level 3. There was a significant difference between levels 2 and 3 in the number of blinks and the number of body movements, which suggests that the number of blinks and body movements could be used to detect driver drowsiness earlier, before driving performance degrades significantly.

4. CONCLUSIONS

This study investigated the effects of driver drowsiness on various physiological indices, namely the number of blinks, R-R interval, and the number of body movements, indices of driving performance, namely lateral fluctuation of the vehicle, steering angle, and distance from the lead vehicle, and subjective evaluations namely the self-evaluation and the external evaluation and their relationships.

The results show that driver drowsiness is closely related to the number of blinks and body movements, and to driving performance. The results also suggest the possibility that the number of blinks and the body movements could be used to predict driver drowsiness. However, the relationship between the number of blinks and the number of body movements are still unclear. Further study is necessary to clarify the relationship in order to develop reliable drowsiness detection method.

Fig 6. Relationship between the degree of sleepiness and the lateral fluctuation of the vehicle

Another future issue to be addressed is the data analysis by shortening the time interval. In this study, the analyses were carried out for the data of each index every one minute, but it is necessary to examine what kind of results would be obtained when they are analyzed at shorter intervals. Futhermore, based on the findings obtained from the results of our study, it is important to develop an algorithm to integrate the indices to establish systems which can reliably detect drowsiness.

ACKNOWLEDGMENT

REFERENCES

Aoki, H., Yoshida, K., Suzuki, K., & Minakami, Y. (2009). Detection of the low wakefulness level with a view to the eye blinking behavior, *Journal of The Japan Society of Mechanical Engineers*, 7, 385-386. (in Japanese)

Brookhuis, K. A., & de Waard, D. (2010). Monitoring drivers' mental workload in driving simulators using physiological measures. *Accident Analysis & Prevention*, 42(3), 898-903.

Convention on Road Traffic (1968). http://www.unece.org/fileadmin/DAM/trans/conventn/crt1968e.pdf

Dinges, D. F., & Grace, R. (1998). *PERCLOS: A valid psychophysiological measure of alertness as assessed by psychomotor vigilance.* US Department of Transportation, Federal Highway Administration, Publication Number FHWA-MCRT-98-006.

Fukui, K., Hayashi, Y., & Asakura, Y. (1993). Study of the driver's fatigue assessment by steering maneuver, *Transactions of Society of Automotive Engineers of Japan*, 24(1), 135-139. (in Japanese)

Fujita, E., Ogura, Y., Ochiai, N., Miao, T., Shimizu, T., Murata, K., Kamei, T., Ueno, Y., & Kaneko, S. (2005). Experimental study on prediction of sleep during wakefulness, *Proc. VSTech 2005*, 282-287.

Gasser, T.M., & Westhoff, D. (2012). BASt-study, definitions of automation and legal issues in Germany, 2012 Road Vehicle Automation Workshop, Transportation Research Board, July 25

Hoddes, E., Zarcone, E., Smythe, H., Philips, R., & Dement, WC. (1973). Quantification of sleepiness: a new approach, *Psychophysiology*, 10, 431-436.

Ishida, K., Ichimura, A., & Kamijo M. (2010). A study of facial muscular activities in drowsy expression, *Kansei Engineering International Journal*, 9(2), 57-66.

Itoh, M., Iitsuka, K., & Inagaki, T. (2010). Effects of drowsiness on load center position of the pressure distribution on driving seat, Journal of *The Japanese Council of Traffic Science*, 10(1), 3-10. (in Japanese)

Kitajima, H., Numata, N., Yamamoto, K., & Goi, Y. (1997). Prediction of automobile driver sleepiness (1st Report, rating of sleepiness based on facial expression and examination of effective predictor indexes of sleepiness), *Journal of The Japan Society of Mechanical Engineers*, 63(613), 3059-3066. (in Japanese)

Krajewski, J., Sommer, D., Trutschel, U., Edwards, D., & Golz, M. (2009). Steering wheel behavior based estimation of fatigue, *Proc. the Fifth International Driving Symposium on Human Factor in Driver Assesment, Training and Vehicle Design*, 118-124.

NHTSA (2013). Preliminary statement of policy concerning automated vehicles

Osuga, M., Kamakura, Y., Inoue, Y., Noguchi, Y., Shimada, K., & Mishiro, M. (2011). Estimation of driver's arousal state using multi-demential physiological indices, Engineering Psychology and Cognitive Ergonomics - 9th International Conference, EPCE 2011, Held as Part of HCI International 2011, Orlando, FL, USA, July 9-14, 2011.

Planque, S., Chaput, D, Petit, C., and Tarriere, C. (1991). Analysis of EOG and EEG signals to detect lapses of alertness in car simulation driving. Proc. the 13th ESV Conference, Paris, France

Roman, B., Pavel, S., Miroslav, P., Petr, V., & Lubomír, P. (2001). Fatigue indicators of drowsy drivers based on analysis of physiological signals. In *Medical Data Analysis* (pp. 62-68). Springer Berlin Heidelberg.

SAE International (2014). Taxonomy and definitions for terms related to on-road motor vehicle automated driving systems, Surface Vehicle Information Report, J3016.

Saito, Y., Itoh, M., & Inagaki, T. (2015). Detection of Drowsy Driving via a Dual Control Theoretic Driver Assistance, Prof. FAST-Zero 2015. (to appear).

Tsuchida, A., Bhuiyan, M. S., & Oguri, K. (2009). Estimation of drowsiness level based on eyelid closure and heart rate variability, Proc. Engineering in Medicine and Biology Society, 2543-2546.

Wierwille, W. W., & Ellsworth, L. A. (1994). Evaluation of driver drowsiness by trained raters, *Accident Analysis and Prevention*, 26(5), 571-581.

The Development of High-Sensitivity Uncooled Infrared Night-Vision Sensors for Use in Driver-Assistance Systems

K. Miyazaki*, M. Suzuki*, K. Shibuya**, A. Sawa**, J. Fujita***, and T. Iwaki*

*DENSO CORPORATION, DENSO Research Laboratories, 500-1 Minamiyama, Komenoki-cho, Nishin-shi, Nagoya, Aichi, Japan (Tel: +81-561-75-1137; e-mail: megumi.suzuki@denso.co.jp).
**National Institute of Advanced Industrial Science and Technology (AIST), Tsukuba, 305-8562, Japan
*** University of Tsukuba, Tsukuba, 305-8573, Japan

Abstract: Uncooled sensors for use in night vision are a promising technology for use in active driver-assistance systems (ADAS) in combination with active-type sensors. However, the sensitivity of conventional uncooled sensors is low because attempts to achieve high sensitivity with conventional sensors are hampered by their high resistivity, which increases thermal noise. To overcome this problem, we have developed new uncooled sensors that have a low resistivity and high sensitivity. This was achieved by improving the crystal quality of the detector materials. Consequently, the sensitivity of the developed sensors was about five times higher than that of conventional low-resistivity sensors. This result could expand the range of use of such sensors and might improve object-recognition accuracy in forward-facing ADAS.

Keywords: automotive control, infrared detectors, temperature measurement, thermal noise

1. INTRODUCTION

The market for applications relating to active driver-assistance system (ADAS) for automotive use is growing rapidly as a result of the decrease in the cost of sensors and the recent rise in safety awareness among users (SBD, 2014a). The concept of ADAS involves the use of various sensors in various combinations that extend their functionalities to improve road safety and to enhance the driving experience. The functionality associated with safe driving is the improvement of the accuracy of information relating to sensed objects by the use of multiple sensors that cover the same field of view, for example, in adaptive cruise control, autonomous emergency braking (AEB), forward collision warning, lane-departure warning, and the like. According to a report (SBD, 2014b), most sensor functionalities that are available are focused on implementing forward-facing ADAS. This is because most traffic accidents happen in the direction of movement while driving. However, suitable combinations

Forward facing ADAS   Detectable objects

Fig. 1. Forward-facing ADAS and detectable objects such as forward vehicles, pedestrians, animals, and other obstacles.

of sensors for implementing forward-facing ADAS have not yet been established because the various sensor combinations have particular advantages and disadvantages. One such difficulty is in developing sensors that are capable of dealing with all weathers, day and night. For example, automobile manufacturers and suppliers currently use about ten different combinations of sensors to implement AEB. Therefore, combinations of sensors that are capable of improving road safety in all weathers, day and night, are desirable.

Night-vision sensors are one of the most promising technologies for ADAS because they permit the detection of pedestrian or animals in darkness without sunlight (Fig. 1). In Japan, although less than one third of all traffic accidents occur at night, transportation fatalities during this period account for more than half the total transportation fatalities. Similar tendencies are also observed in the US, EU, and other countries. Therefore incorporating night-vision sensors into ADAS systems such as AEB would improve their capacity to detect obstacles, resulting in a reduction in traffic accidents involving pedestrians, not only during the daytime, but also at night. Furthermore, the European New Car Assessment Programme (Euro NCAP) will be promoting the use of night-vision sensors by the inclusion of night-time pedestrian collision-mitigation solutions in its testing program from 2018. In the future, automatic driving systems might also use night-vision sensors among their monitoring components.

Several methods are under development for the detection of objects when driving at night. These include as 24 or 77 GHz radar, near-infrared cameras, laser intensity direction and ranging (LIDAR) systems, and far-infrared (FIR) cameras. Other than FIR cameras, these systems require an active beam, such as a millimeter-wave beam, near-infrared source, or a laser. Active-type sensors can accurately measure the
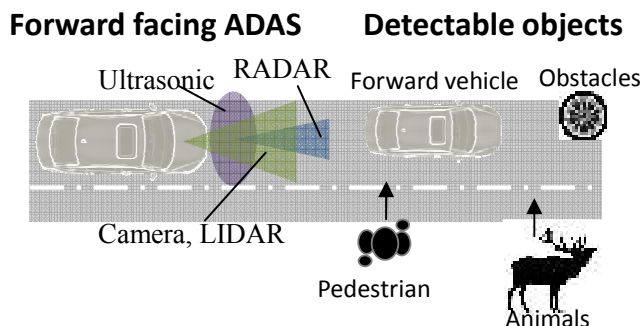
distances between distant objects and the current position, because they use the time-of-flight method. However, it is difficult for these sensors to distinguish accurately between obstacles, pedestrian, and animals. Because object recognition by these sensors involves pattern-matching techniques or the evaluation of differences in intensity between objects and their background, ADAS using active-type sensors exclusively for night vision might identify objects such as dolls or thin rods as pedestrians. Therefore, active-type sensors need to be used in combination with other types of sensors to improve the overall identification accuracy. An FIR camera is a passive-type sensor that detects the infrared radiation emitted from objects and it is therefore capable of distinguishing pedestrian from obstacles by the differences in their temperatures. Passive sensors can detect over longer ranges (about 300 m) than can active-type sensors. This is because passive sensors directly detect radiation from objects, whereas the detection range of active-type sensors depends on the power of the active beam, sensed by the detector, the intensity of which is influenced by the optical-path distance, which is twice that of a passive-type sensor. Therefore, an ADAS systems that combines active- and passive-type sensors would be ideal, as each type of sensor could compensate for the disadvantages of the other. However, there are two obstacles to the widespread adoption of such sensor combinations: their high price and the restriction on their use to night-time only. To overcome these two challenges, we are developing high-sensitivity uncooled FIR sensors by manipulating the materials for the detectors of the sensors with the aim of developing sensors capable of both night-time and daytime use by expanding their ranges to include the high ambient temperatures found in the daytime at an appropriate cost.

Table 1. Comparison of 77 GHz radar, camera, LIDAR, and the FIR camera in terms of their detection distances, detection methods, and detectable objects.

		77GHz RADAR	Camera	LIDAR	FIR camera
Detection distance @ night		200m	100m	50-80m	300m
Detection methods		active	active	active	passive
		reflection	reflection	reflection	temperature
objects	car	O	O	O	O
	Pedestrian animals	△	O	△	O
	obstacles	O	O	O	△

For use in automobiles, uncooled night-vision sensors are more suitable than cooled sensors, because uncooled sensors work at ambient temperatures without liquid-nitrogen, cooling, leading to lower costs and smaller sizes of sensor equipment. Uncooled sensors operate by means of thermal sensitivity. The sensors detect changes in temperature by absorbing FIR radiation from target and converting it into an electrical output signal. There are three main types of FIR thermal sensors: the resistivity-change type, the

thermoelectric type, and the pyroelectric type. In these thermal sensors, a bolometer using a resistivity change has the highest sensitivity, because a bolometer has the best insulation structure for retaining the heat generated by radiation from the target. We therefore used bolometer-type sensors. The sensitivity of a bolometer is determined by the temperature coefficient of resistance (TCR) defined as $(1 \cdot \rho^{-1})(d\rho \cdot dT^{-1})|$, where ρ is the resistivity or the resistance and T is the temperature of the material. Oxide-deficient vanadium oxide (VO_x), amorphous Si (a-Si), or Si diodes are all widely used as bolometer materials. However, the TCRs of these conventional materials are about $1–3\% \cdot K^{-1}$. These low values hamper the expansion of the ranges of use of such sensors. Because the TCR value affects the identification performance and the pedestrian-detection distance for automotive use in various detection situations, materials with higher TCR values are desirable. However, it is difficult to enhance the TCR values of these materials because of the poor reproducibility of their properties as a result of the deposition process and the thermal noise arising from the high resistivity present in regions of higher TCR. Crystalline vanadium dioxide (VO_2) with a temperature-driven metal–insulator transition (MIT) has a high TCR value ($>70\% \cdot K^{-1}$) near its MIT temperature (340 K). In this respect, thin films of VO_2 are suitable materials for bolometers. However, VO_2 films have a large thermal hysteresis, caused by the MIT and its accompanying structural change, which causes deterioration in the performance of the bolometer. One solution to this problem would be to enhance the TCR and to lower the resistivity without thermal hysteresis. Recently, Nishikawa et al. (2011) demonstrated that thermal hysteresis and resistivity in VO_2 can be decreased by doping with Ti or Nb. However, metal-ion doping in VO_2 decreases the TCR values to as low as $1–5\% \cdot K^{-1}$. This suggests that it is difficult to suppress thermal hysteresis in VO_2 by metal-ion doping while maintaining a high TCR.

To realize a high-TCR thermal sensor with a low resistivity, we investigated the effects of co-ion doping on the TCR and the resistivity of Cr- and Nb-doped VO_2 films. Previous studies have shown that as the level of single-ion doping in VO_2 is increased, the TCR values and the resistivity decrease (Miyazaki, 2014). We found that doping with a co-ion could produce a different relationship between the TCR and the resistivity. The effect enhanced the TCR by more than $10\% \cdot K^{-1}$ while maintaining a low resistivity.

2. EXPERIMENTS

Films of $V_{1-x-y}Cr_xNb_yO_2$ were deposited on Si(001) single crystal with a 200-nm coating of SiO_2 as a buffer layer between the doped VO_2 and the Si substrate. The films were deposed by pulsed-laser deposition using a KrF excimer laser (λ = 248 nm). Mixed ceramic pellets consisting of V_2O_5, Cr_2O_3, and Nb_2O_5 were used as targets. The deposited films were examined by means of X-ray diffraction to determine their crystal structure and quality. The resistivity of the films was measured by a conventional four-probe method, using Au/Ti layered electrodes to ensure a good electrical contact with the films. Transport properties were examined by means of a physical-property-measurement system (PPMS;

Quantum Design), and the temperature-sweep rate was set to $0.3 \text{ K} \cdot \text{min}^{-1}$.

3. RESULTS AND DISCUSSION

Figure 2 shows the TCR values for VO_x, a-Si, doped VO_2, and co-doped VO_2 as a function of their resistivity. These results show that the TCR of VO_x, a-Si, and single-doped VO_2 increase with increasing resistivity, whereas the TCR of co-doped VO_2 is $11.3\% \cdot \text{K}^{-1}$, a very high value compared with that of the other materials. These characteristics are very useful for practical use, providing a high sensitivity coupled with low thermal noise. The TCR of co-doped VO_2 is about five times higher than that of conventional VO_x (about $2\% \cdot \text{K}^{-1}$). Detailed discussions will be presented at the conference.

4. CONCLUSION

We have developed high-sensitivity bolometer material with a low resistivity by doping Cr and Nb in VO_2 films on a buffer/Si substrate. The TCR value of $11.3\% \cdot \text{K}^{-1}$ is five times higher than that of conventional materials. This result might expand the range of use and improve the object-recognition accuracy of forward-facing ADAS.

Fig. 2. Temperature coefficient of resistivity (TCR) of vanadium oxide (VO_x), amorphous Si, single-ion-doped vanadium dioxide (doped VO_2) and co-doped vanadium dioxide (co-doped VO_2) as a function of their resistivity.

REFERENCES

Miyazaki K., Shibuya K., Suzuki M., Wado H., and Sawa A. (2014). Correlation between thermal hysteresis width and broadening of metal–insulator transition in Cr- and Nb-doped VO_2 films, *Jpn. J. App. Phys.* 53, 071102.

Nishikawa M., Nakajima T., Kumagai T., Okutani T., and Tsuchiya T. (2011). Adjustment of thermal hysteresis in epitaxial VO_2 films by doping metal ions. *J. Ceram. Soc. Jpn.* 119(1391), 577–580.

SBD (2014a), *ADAS Forecast–EU/USA/China (SAF/538).* SBD, Milton Keynes, UK.

SBD (2014b), *Safe Car: Sensor Fusion Vs Single Sensor Systems (SAF/561).* SBD, Milton Keynes, UK.

Localization Method Based on Road Boundary Detection

Keisuke Kazama* Kei Sato* Yasuhiro Akagi*
Pongsathorn Raksincharoensak* Hiroshi Mouri*

* Department of Mechanical Systems Engineering, Tokyo University of Agriculture and Technology, Tokyo, Japan (Tel: +81-42-388-7419; e-mail: {50014833801, keimsato, akagi-y, pong, h-mouri} @st.tuat.ac.jp).

Abstract: We tried to develop the new localization method by simple 2D-plane map without deterioration of estimation accuracy. The boundary line has a lot of features e.g. changes of height, color and brightness, but they are sensitive for noises. From the robustness point of view, it is difficult to match the road boundary line with the boundary line on 2D map. The localization method using 3D point cloud matching or texture matching are so accurate, but these have disadvantage in adaptation to the change of environment. So, we decide to make the classifier to classify as road area or the other area, and propose the new localization method that has advantage in robustness by matching the identified shape of road area with the shape of the road on 2D plane map. First, we calculate the HOG features from the range data acquired by 3D LiDAR. Then, we make the road plane classifier applying SVM.

Keywords: Autonomous vehicle, Histograms, Gradients, Machine Learning, Active safety

1. INTRODUCTION

The localization for autonomous driving is to estimate the self-vehicle position and altitude on the global map. 3D map is often used for localization in many studies, however it takes a lot of effort to make it and it is hard to maintain to keep it its newest state. In addition, 3D states such as the state of leaves of trees are easy to be varied, and these factors make difference between 3D map and real world configurations. On the other hand, 2D-plane map which is widely spread is easy to be obtained and convenient to use as an on-board map. The 2D plane map consists of boundary lines of roads, foot pavements and buildings. In comparison with 3D-map, 2D-plane map has less information of the road features. As a result, deterioration of the estimation performance might be caused by using 2D map. We tried to develop the new localization method by simple 2D-plane map without such deterioration of estimation accuracy.

It is general localization method to make matching boundary lines on the 2D map and boundary on the real world. The representative road boundary line is the lane marker. A lot of methods of lane marker detection are studied. Yamaguchi et al. proposed to use the sobel filter based on first order differential of brightness. Muramatsu et al. studied the canny edge filter which enhances the continuity of edges. Haramiishi et al. investigated the use of the summation of dot product of brightness gradient vector. In this way, it is necessary to make differential process in order to detect the changes of state in above methods. But if they try to detect small changes, the misrecognition increases by enhanced noise, and if they try to reduce the effect of noise, the non-detection of boundary lines occurs.

There are several methods not using the change of state of the road plane but using state itself. State of the road plane has less information than the changes of state around the boundary lines. But these methods can make up for small amount of information because the number of state data of plane is large. The representative localization method using state itself is 3D point cloud matching with the highly precise 3D map (Yoneda, K. et al., 2014). It is possible to estimate self-vehicle position with about 0.5m errors in real time. But, this method spends a great cost in making map and the calculation. And it cannot support a change in the environment by wind, snow and other factors. Another method is texture matching using high-resolution infrared reflectivity road map and intensity of 3D LiDAR (Suganuma, N. et al., 2014). This method shows very accurate estimation results, and localization error is about 0.1m. But it is difficult to adapt to the change of intensity with rain, pool and fallen leaves and to make the high-resolution infrared reflectivity map.

The boundary line has a lot of features e.g. changes of height, colour and brightness, but these features are sensitive for noises. From the robustness point of view, it is difficult to match the road boundary line with the boundary line on 2D map. The localization method using 3D point cloud matching or texture matching show very accurate estimation performance, but these methods have disadvantage in adaptation to the change of environment.

Hereupon, we decide to make the classifier to classify as road area or the other area, and propose the new localization method that has advantage in robustness by matching the identified shape of road area with the real road area shape on the 2D plane map. First, we calculate the HOG (Histogram of Oriented Gradient) features from the range data acquired by 3D LiDAR. Then, we make the road plane classifier employing SVM (Support Vector Machine). This paper describes the road area detection portion of the new localization method.

2. PROPOSED METHOD

This chapter describes the algorithm of road plane detection. Figure 1 shows the raw measurement data of 3D LiDAR in real world. When the 3D LiDAR is set vertically and detects horizontal plane, the range data changes in the layer direction and does not change in the rotation direction. The beam range data which hit the road surface shows this tendency, and the beam data on the other area changes in the both direction. So, we find that the road plane can be detected by gradient direction of the range data, and employ HOG features of the range data. HOG features which are obtained by LiDAR data are classified as the road area or the other areas by SVM.

(a) Camera Image

(b) 3D LiDAR range data
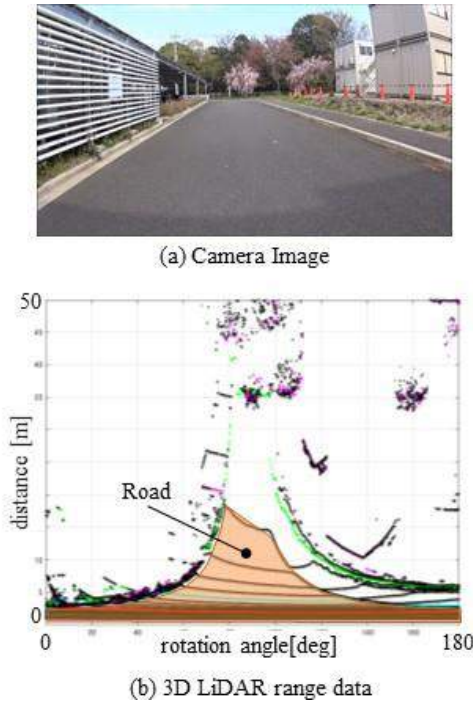
Fig.1 Raw measurements data of 3D LiDAR

2.1 About the 3D LiDAR

We use the Velodyne, HDL-32E. This 3D LiDAR outputs the range data which has 32 layers from -30degrees to +10degrees per 1.667degrees in vertical direction and 2160 data from 0degree to 360degrees per 0.167degrees in rotation direction per a scan. To detect the road plane in front of vehicle, the range data from 0degree to 180degrees in rotation direction are used. The number of used range data becomes 32x1080.

We studied the height of the position where the LiDAR is set. This value affect the detection performance and we find that the detection performance is deteriorate when the LiDAR is set near the road surface.

2.2 The calculation of HOG features

The HOG features are one of the image processing technique used for the pedestrian detection. This is the method to express the direction and intensity of brightness gradient in local area using histogram (Dalal, N. et al., 2005). We replace the brightness with the range data and calculate the HOG features. First, we make two difference range data dD_x, dD_y in layer direction and rotation direction from range data D as

shown in equation (1). The range data D is normalized in advance.

$$\begin{cases} dD_x(x, y) = D(:, x+1) - D(:, x-1) \\ dD_y(x, y) = D(y+1, :) - D(y-1, :) \end{cases} \quad (1)$$

Second, a gradient magnitude *Mag* and direction *Dir* are calculated in equation (2).

$$\begin{cases} Mag(x, y) = \sqrt{dD_x(x, y)^2 + dD_y(x, y)^2} \\ Dir(x, y) = \tan^{-1}\left(\dfrac{dD_y(x, y)}{dD_x(x, y)}\right) \end{cases} \quad (2)$$

Next, we make the histogram. We determine the area to make histogram per 3x30 data in the layer direction and rotation direction and shift them in the both direction. This area is called cell. We make the 10 histogram data in layer direction and 35 data in rotational direction, and 350 histograms in the total per a scan. The number of bin of histogram is 9 from 0degree to 180degrees per 20degrees. We vote the gradient magnitude for the bin that corresponds to the gradient direction. Finally, we conduct the normalization of histogram for each cell.

2.3 Making the classifier by SVM

We make the classifier by using SVM (Vapnik, V. N., 1995). The dimension of a feature vector used in SVM is 11. 9 units of the vector are provided from histogram made in the previous section *2.2*. Remaining 2 units are average height and its standard deviation of each cell. We used the function "fitcsvm" of Statistics Toolbox, MATLAB, Mathworks, Inc. for making the classifier.

2.4 The confirmation of the classifier performance in simulation

In order to confirm the performance of classifier, we make simulation. We make observation model of 3D LiDAR, and calculate the range data which would be acquired in 3D environment. Noises are added to the range data depending on the distance to express the performance like an actual sensor. Figure 2 shows the range data acquired by observation model, and figure 3 shows 3D point cloud data calculated by its range data. Figure 4 and 5 shows area segmentation of road plane and other areas in figure 2 and 3. The road plane are indicated by navy blue lines, and the other areas are shown by black lines.
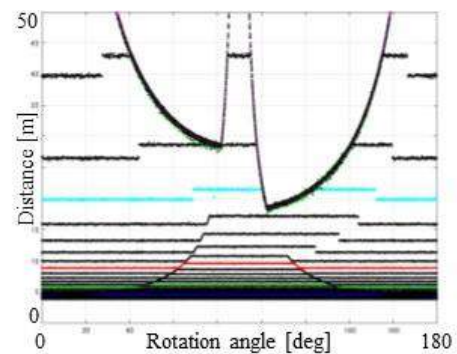
Fig.2 Range data of 3D LiDAR model
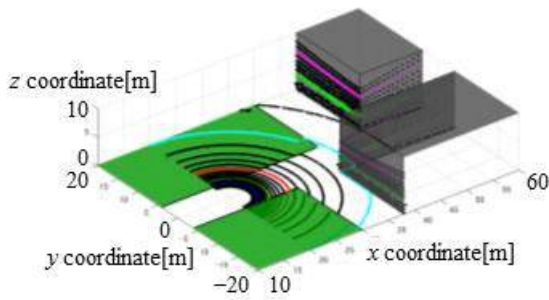
Fig.3 3D point cloud data of 3D LiDAR model
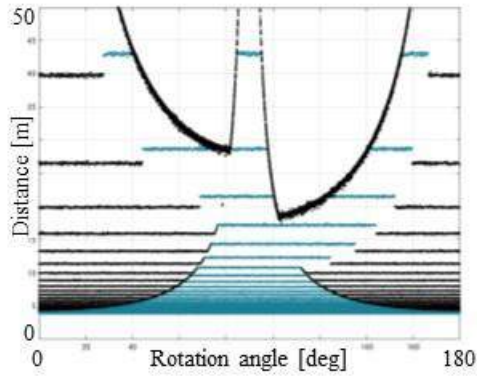
Fig.4 Area segmentation of above range data
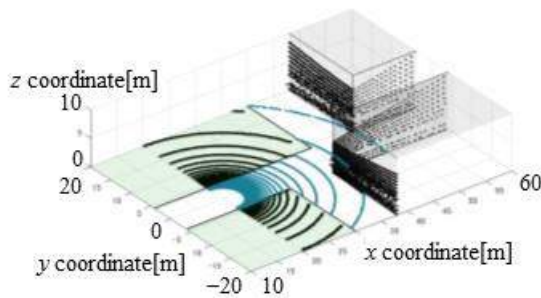
Fig.5 Area segmentation of above 3D point cloud data

Figure 6 shows the difference of histogram between the road plane and other area. In the histogram of the road plane, the gradient appeared only in the bin 5 (80-100deg direction) as expected. At the other areas, the gradients are seen in several directions.

As described above, we make the SVM classifier from acquired range data. The number of training data is 3500 (road: 1218 (34.8%), non-road: 2282 (65.2%)), and validation data is 700 data (road: 146 (20.8%), non-road: 554 (79.2%)). Error rate of classifier is 5.14% (36 data / 700 data). Figure 7 shows the labelled range data, and figure 8 shows its 3D point cloud data as validation data. The orange lines indicate the area of road plane.

Figure 9 and 10 shows the identification result of range data and 3D point cloud data. Green line indicates road, and black line indicates non-road. We confirm that the road plane is extracted accurately.
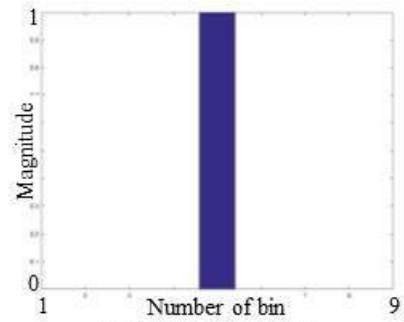
(a) Histogram on road
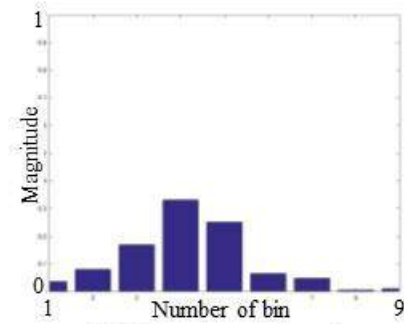
(b) Histogram on not-road

Fig.6 Difference of histogram
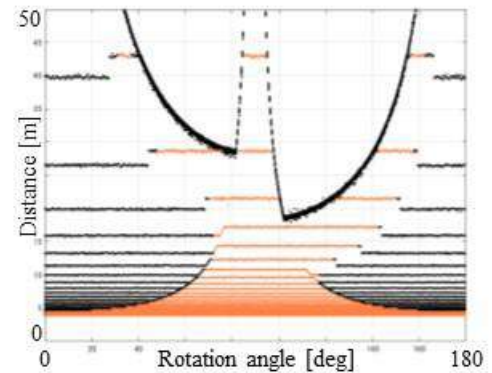
Fig.7 Labelled range data as the validation data
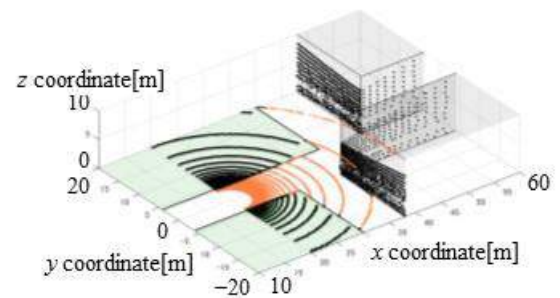
Fig.8 Labelled 3D point cloud data as validation data
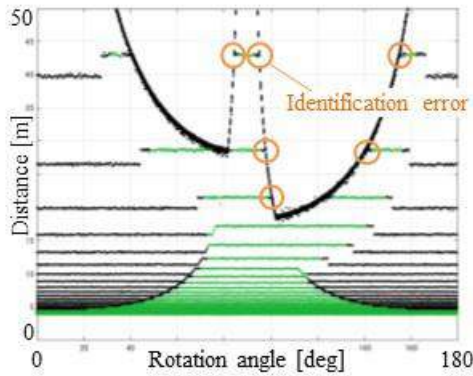
Fig.9 Identification result of range data
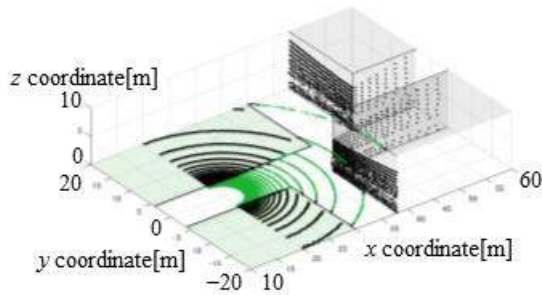
Fig.10 Identification result of 3D point cloud data

3. EXPERIMENTAL RESULT

We confirmed the availability of our proposed algorithm by simulation. Then, we validated whether the road plane can be detected properly in the real world using 3D LiDAR. We conducted the experiment using small-scale electric vehicle (Toyota Auto Body, COMS, figure 11). This vehicle is equipped with the 3D LiDAR in front of the vehicle. We drove this vehicle with manual operation in the campus of Tokyo University of Agriculture and Technology and acquired 3D point clouds data. Figure 12(b) shows the range data, and figure 13 shows the 3D point cloud data corresponding to Figure 12(b).
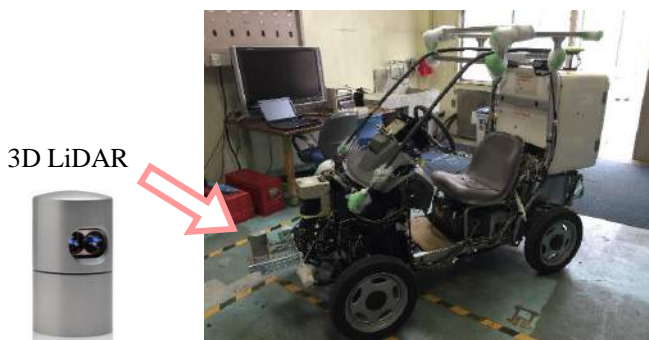
Fig.11 Experimental small-scale electric vehicle

(a) Camera image
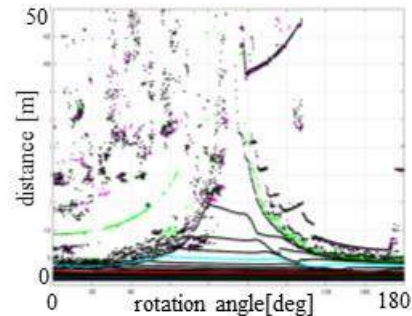
(b) 3D LiDAR data

Fig.12 Raw measurement data of 3D LiDAR
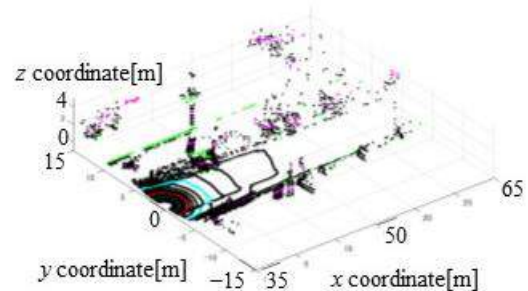
Fig.13 3D point cloud of 3D LiDAR

Figure 14 shows the difference of histogram between the road plane and other area in real world. In the histogram of the road plane, the gradient appeared only in the bin 5 (80-100deg direction) like the observation model of simulation. At the other area, the gradients are seen in several directions.

We make the classifier from the acquired range data. Training data which are used for the making of classifier is 2100 data (road: 824 (39.2%), no road: 1276 (60.8%)), and validation data is 700 data (road: 314 (44.9%), non-road: 386 (55.1%)). Error rate of classifier is 8.00% (56 data / 700 data). Figure 15 and 16 shows the Identification results at certain places. Green line indicates road, and black line indicates non-road. The road plane in front of the vehicle up to 10m ahead can be identified correctly. But exceeding 10m, the road plane cannot be identified well, because the beam of 3D LiDAR did not hit the road surface. The left side curbs were identified as the other area correctly in spite of the existence of leaves, petals and pool around these curbs.

Although the road surface where the data in figure 16(a) is obtained is rough, the road area 10m ahead is identified as road area correctly. But the right side foot pavements was misidentified because of the effect of vehicle roll motion. From these result described above, we confirmed that it is possible to identify the road plane and other areas.

(a) Histogram on road

(b) Histogram on not-road

Fig.14 Difference of histogram

(a) Camera image

(b) Identified range data

(c) Identified 3D point cloud
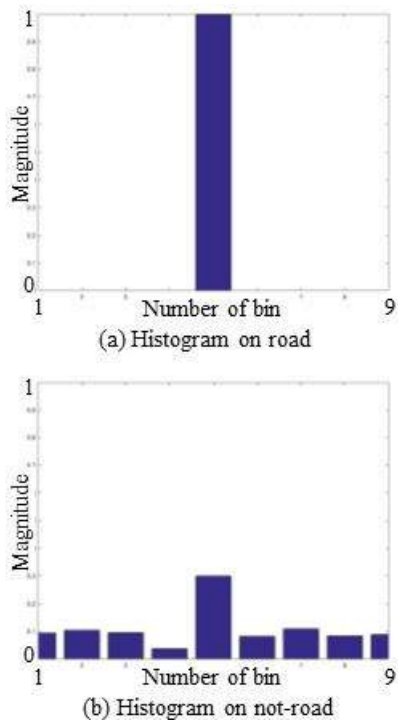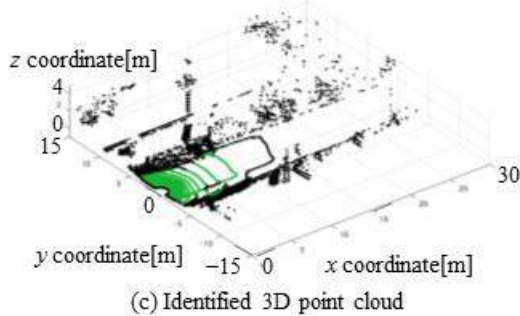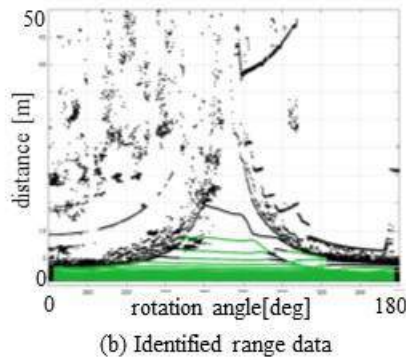
Fig.15 Identification result 1

(a) Camera image

(b) Identified range data

(c) Identified 3D point cloud
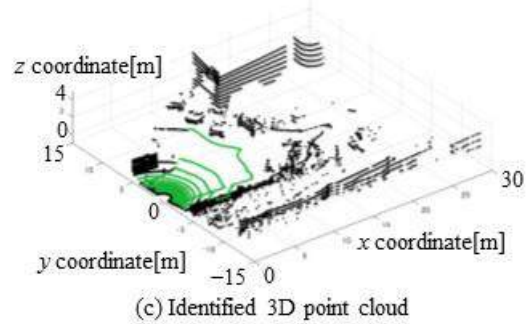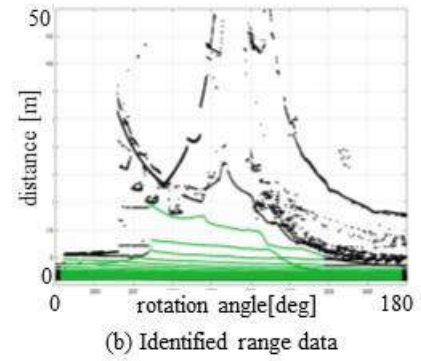
Fig.16 Identification result 2

4. CONCLUSIONS

In order to develop the new localization method by using simple 2D plane map, we made the simulation model and confirmed the followings.

・The range data of 3D LiDAR which hit the road surface changes in the layer direction and doesn't change in the rotational direction

・As a results, the HOG features of the road area concentrate in the same bin (80-100deg). On the other hand, HOG features of non-road area distribute in the several bins of directions.

・In this way, there are large difference between the histograms of the road planes and that of other areas.

・The road plane and other area can be identified by SVM with error rate 5.14% in simulation model.

We applied the road area identification method validated its availability in simulation to the real world data, and obtained the result mentioned below.

・The HOG features shows the same tendency with the result of simulation in road planes and other areas.

・It is possible to identify whether the road plane or other areas with error rate 8%.by using SVM.

・The area in front of own vehicle 10m ahead can be identified correctly. But it is difficult to identify whether road area or not over 10m.

We will improve the identification accuracy and realize the new localization method using map matching.

ACKNOWLEDGMENT

REFERENCES

Dalal, N. and Triggs, B., Histograms of Oriented Gradients for Human Detections, *Computer Vision and Pattern Recognition, 2005. CVPR 2005. IEEE Computer Society Conference on*, vol.1, p.886-893.

Date, H., Ohkawa, M., Takita, Y. and Kikuchi, J. (2013). High Precision Localization of Mobile Robot Using LIDAR Intensity of Surface, *TRANSACTIONS OF THE JAPAN SOCIETY OF MECHANICAL ENGINEERS Series C*, vol. 79 (No. 806), p. 3389-p.3398. (in Japanese).

Haramiishi, Y., Kazama, K., Hioki, T., Furusho, H. and Mouri, H. (2014). Study on the Edge Detection Algorithm Using Brightness Gradient Vector Applied to the Forward Road Image of the Vehicle, *Transactions of the Society of Automative Engineers of Japan*, Vol.45 (No.5), p.865-p.870. (in Japanese).

Muramatsu, M., Kawata, T. and Kubo, F. (1998). Traffic Lane Recognition by Image Segmentation and Object Recognition based on Rules, *Technical report of IEICE. PRMU*, Vol.98 (No.334), p.1-p.8. (in Japanese)

Omae, M. and Fujioka, T. (1999). Differential GPS-Based Position Measurement and Steering Control for Automatic Driving, *Journal of JSME,* vol.65 (No.634), p.211-p.218. (in Japanese).

Saneyoshi, K. (2013). Drive Assist System of a Car by means of Stereo Vision, *Technical report of IEICE. PRMU*, vol.2013-CVIM-185 (No.20), p.129-p.134. (in Japanese).

Suganuma, N. (2015). Trend and Example of Autonomous Vehicle, *The Journal of the Institute of Electronics, Information, and Communication Engineers*, vol.98 (No.1), p.48-p.53. (in Japanese).

Suganuma, N., Hayashi, Y. and Nagata, D. (2014). Path planning for intersection driving by autonomous vehicle, *Proceedings of JSME TRANSLOG2014,* p.293-p.296. (in Japanese).

Yamaguchi, N., Tamori, N. and Shiomi, A. (2005). A Lane Detection Method Using Adaptive Edge Preservative Smoothing, *The transactions of the Institute of Electronics, Information and Communication Engineers. D-II*, Vol.J88-D-II (No.8), p.1421-p.1431. (in Japanese)

Yoneda, K., Mita, S., Chenxi Y., Quoc, H.D., Hossein, T. and Muto, K. (2014). Virtual Automated Vehicle System for Urban Driving Experiment, *Proceeding of JSME TRANSLOG2014,* p.289-p.292. (in Japanese).

Yoneda, K., Tehrani, H., Ogawa, T., Hukuyama, N. and Mita, S. (2014). Laser Scan Feature for Localization with Highly Precise 3-D Map, Proceedings of 2014 IEEE Intelligent Vehicles Symposium, p.1345-p.1350. (in Japanese).

Vapnik, V. N. (1995). The nature of statistical learning theory, *Springer*.

Smart Traffic Cone - Dynamic detection and localization of traffic disruptions

René Schönrock. Franziska Wolf.
Tim Russ

{ rene.schoenrock | franziska.wolf | tim.russ }@ifak.eu

Institut für Automation und Kommunikation e.V., Magdeburg, CO 39106
Germany (Tel: +49 391 9901457):

Abstract: Suddenly occurring disruptions on the road and especially at intersections – such as accidents, disabilities by vehicles and objects – may cause significant adverse effects on the traffic flow and in turn lead themselves to potentially dangerous situations. By using its integrated GNSS receiver and its mobile communication device the smart traffic cone provides timely and spatially accurate information about local disruptions in the road environment. It is a tool for police, rescue, recovery and service staff for detecting hazard areas that could not be detected so far.

Keywords: Cooperative Systems, V2X, GNSS, Low-Cost-RTK

1. INTRODUCTION AND MOTIVATION

In 2013 3355 accidents involving personal injury occurred at construction sites. 44 persons were killed and 677 seriously injured (DESTATIS (2014) cited in ADAC (2015)). This fact shows that even today accidents at construction areas are likely to occur.

In order to improve the overall traffic safety it is needed to improve near-field and broadcast information concerning short-term traffic disruptions. Information concerning theses disruptions, such as closures due to accidents, roadwork or construction sites has to be high-precise and timed in order to avoid new crashes or injured or killed persons.

Dangers arising from street closures and construction sites are for example:

- Limited view

- Slow moving or blocking construction vehicles

- Crashed vehicles, injured people

The aim of the Cooperative Protection System (CPS) including a Smart Traffic Cone (STC) is to enhance distinct temporal and local traffic information availability for traffic participants and traffic staff. Information concerning road closure such as time, place, area and cause are automatically captured by CPS during activation. The information is transferred to traffic participants (near-field) and to traffic management centers. When the smart traffic cone is de-activated and put back by the service staff, the information about the de-activation is also communicated. The whole process of information capture and data communication is embedded in the standard operating procedures of the service and emergency staff.

STC combines a simple and intuitively usable application with the efficient acquisition of information. Especially when used in traffic zones of high risk it can offer a significant contribution to road safety.

The protective function of an ordanary traffic cone is based exclusively on direct visual perception by road users. This perception may be affected by sensitive weather conditions (fog, rain, and snow), lighting (glare, backlit) or topographical features (curves, slopes). The STC offers self-positioning and automated transfer of position and positioning-causes to control centers or directly to vehicles in the environment. Therefore a better self-protection of road users and more reliable warnings to the environment can be offerd by widening the perception horizon from the direct visual line of sight between the driver and traffic cones to a digital horizon. If used by appropriate driver assistance systems in vehicles (navigation system, board computer, etc.), traffic reports, applications on mobile devices or other roadside transport facilities (dynamic text panels) the warning messages can be used whereever needed.

The collected information shall be used for real-time warnings at sites of accidents (on driver assistance systems, Car2X, Navi, broadcast messages) or also for strategic traffic management applications. For now approaches of warnings based on digital warning (e.g. by smartphone apps) collides with prescribed procedures for internal and external security and to priority saving lives and infrastructure by paramedics or police officers. The STC fits transparently into the processes and does not generate any additional human or organizational effort. The hardware used is resistant to

mechanical and climatic influences, maintenance and reliable.

The cones shall be used by rescue and emergency services such as firedepartment, police. The additional information collected automatically by setting up (geographic location, time, etc.) are transmitted in real time, and evaluated for example for driver assistance or navigation systems. In times of fog, rain, darkness, curves and mountains a timely and efficient warning application can be received by this system.

The STC therefore combines state of the art information and communication technology with proven safety technology for traffic applications. The acquisition of important real-time traffic data in the area of accident or road works is embedded into the well-established usage of traffic cones in general. Therefore the standing operating procedures are warranted.

2. SAFETY ENHANCEMENT

2.1 Safety enhancement for traffic participants

A timed communication of specific traffic warnings can be crucial for the personal safety of traffic participants. It can offer a specific added value for all road users. By using suitable technology for safety-critical near-field messaging such as Wireless LAN IEEE 802.11p future driver assistance systems and their actuators can be given useful warnings facing arising dangerous situations.

2.2 Safety enhancement and information for service staff

The smart traffic cone can also enhance safety of service staff at constructions sites or accident locations distinctively. Traffic participants can be informed to pay attention concerning rescue staff or blocking vehicles. Traffic participants can e.g. adapt their speed at danger areas. The operational safety for emergency services can therefore benefit. The timed communication of data concerning time, place and cause to coordination centers can furthermore lead to enhanced optimization of operations e.g. rescue routes. By using the automatically captured outline data of the case work of operational staff can be improved and optimized e.g. by using positioning data for georeferencing.

2. 3 Safety enhancement due to traffic avoidance

Apart from providing near-field communication of time- and space-critical data also long term optimization can arise by using CPS. Information provided by the internet, radio Traffic Message Cannel (TMC), control centers about closed areas and roads can be used by traffic participants or navigation systems on-trip or pre-trip in order to plan or adapt their destination routes. Traffic and fleet management systems may also use information gathered by the CPS in order to optimize their operations because they are able to react to dangerous and critical situations more quickly. Similarly, urban traffic management centers can optimize traffic light systems or public transport strategies based on more distinct traffic information.

These overall improvements can enhance safety for traffic participants, service staff and can reduce stress and enhance in the end the acceptance of the future traffic management strategies.

3. COOPERATIVE PROTECTION SYSTEM

3.1 System description

The CPS is a distributed system, which can be generally divided in four main components. The first component, the smart traffic cone, is the front end device of the CPS and will be described in general later in this paper. Another component is the hard- and software of the configuration- and charging terminal, which is located on the service vehicle, ensuring the data- and energy supply for the STCs. The actual CPS-software application executed on the STC-Server, manages all STCs and generates and distributes the temporary disruption information. The Road Side Unit (RSU), the 4th component, takes information from the STC-server, decodes, evaluates and distributes these by radio to traffic participants. An overview of the involved components of the KSE is given in Fig. 1.
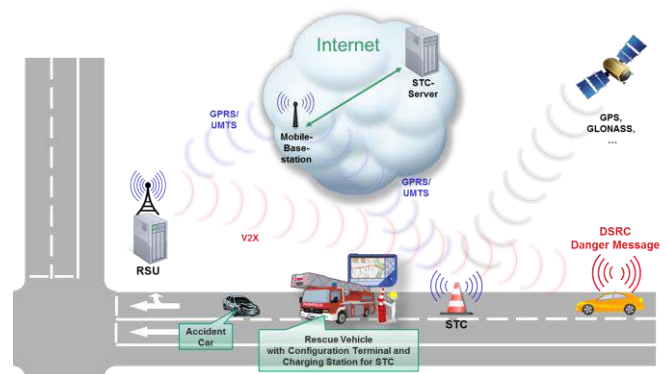
Fig. 1. System components of the CPS.

The operation of the CPS is described as follows. In the configuration phase, data regarding the cause of disruption can be keyed in by the service staff via a robust and intuitive Human Machine Interface (HMI). Right after installing, the STC is automatically enabled and begins to record location-based information such as position, lanes and so on. This information is transmitted along with information giving the cause of disruption and degree of impairment over a cellular connection to the STC- Server. A software application on STC-Server evaluates the received information from one or more STC, generates a disruption information message and transmits these to the appropriate RSU. The RSU generates collective danger messages from the disruption information and provides it to the traffic participants over Dedicated Short Range Communication (DSRC) radio link. For this purpose, the automotive radio Wi-Fi ITS-G5 as described in Car2Car (2015) will be used. The deactivation of the CPS in turn informs all participating applications and traffic participants about the revocation of the temporary disruption. After deactivation, sending of danger messages will also be

set and the road or intersection goes back to its initial configuration. The individual interfaces and the communication scheme of the CPS are shown in Fig. 2.
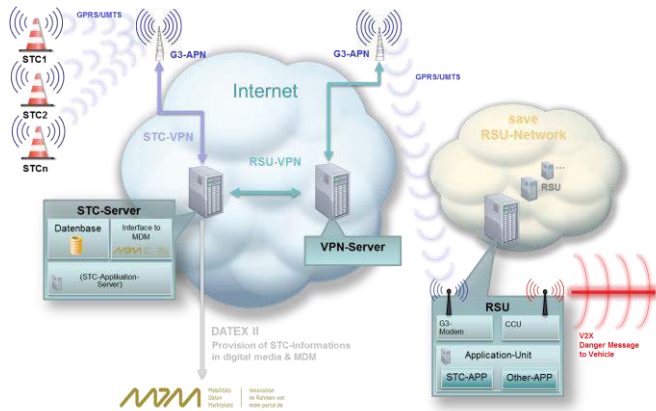
Fig. 2. Interfaces and communication scheme of the CPS.

3.2 STC-Server

The STC-Server in combination with the STC application on the RSU is the core component of the CPS. The most important tasks that covered by the STC-Servers, are:

- Provision of a Virtual Private Network (VPN) for the STCs (VPN-Server)

- Management of the STCs in a MySQL database,

- Allows remote access, maintenance and status check of the STCs,

- Generates disruption events from the raw data of one or more individual STCs (Fig. 3),

- establishes the VPN-connection to the RSU-network (as VPN-client)

- Initiates remote access to that RSU, which is responsible for the disruption event,

- Manages the dataexchange with the RSU (Upload of the disruptiondata),

- receives optional GNSS-correction data from the RSU and distributes these to the STCs (see also section 3.3),

- Transmits the disruption information to MDM via a https connection in DATEX II format (see section 4.2)
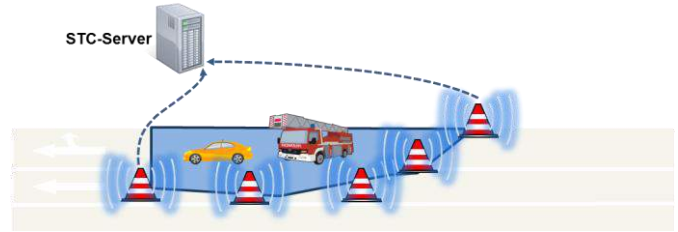
Fig. 3. STC-Server generates disruption information by combination of two ore more STCs

The STC-Server is a Java Enterpise Edition (Java EE) application installed and running on an Apache Tomcat Application Server. The communication between the STCs and the STC-server is realized by a special Java servlet. The individual STCs and their data are organized in a MySQL database.

3.2 Smart Traffic Cone

In Germany Traffic cones are transport facilities reffered to in road traffic regulations according to § 43 Straßen Verkehrsordnung (StVO) i. V. m. Appendix 4. Basically, the traffic cone consists of a stable base plate and a rising conically shaped body. The base plate is noticeably wider and heavier than the rising body. Through this lower center of mass, the risk is reduced that the cone is tilting or shifting. From the administrative regulation StVO a proviso is given that they must be carried out fully retroreflecting. Within the scope of road traffic regulations, in the guidelines for securing secure jobs on roads and the technical delivery for traffic cones only traffic cones are used, in which both colors (red and white) are made retroreflective in order to ensure the necessary day/night equality.

A modified traffic cone, the Smart Traffic Cone, is the key component and the main data provider of the CPS. The block diagram of the STC internals is illustrated in Fig. 4.
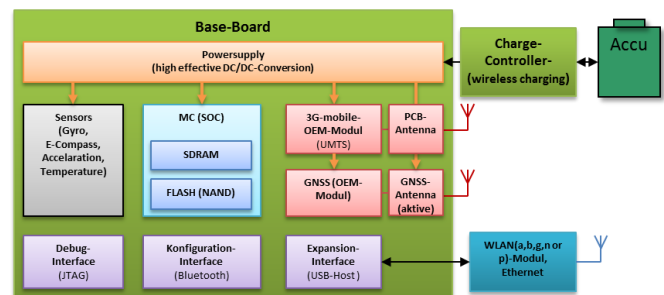
Fig. 4. Block diagram of the STC internals.

The main part of the STC is a microcontroller based computer system, on which an embedded Linux operating system is running. Various internal sensors, like gyro- and accelarationsensor, realize the movement and orientation detection of the STC. During setting up and collecting the STC, these sensors can generate trigger signals for an automated activation and deactivation of the system. Even

the collision of an STC by a vehicle can be detected by the internal sensors and reported to central control, which further increases the safety of operations. For communication with the central server the IL has a cellular modem for bidirectional data exchange according to the UMTS standard. This interface can also be used to report the status of the IL to the central server or to make firmware update over the air (OTA). The energy for short-term use of the STC is provided by a lithium-ion accumulator, which is charged wirelessly after each use. The wirelessly charging via a coil system has many advantages for this application. Prevention of soiled contacts, enhancement of safety protection and the overall simple handling of the device show their advantages. As configuration and service interface in the field, the STC has a Bluetooth module that can be easily accessed using handheld, tablet or smartphone devices. For test-, debug- and development purposes an expansion interface is also available, which can be used with various modules such as Wi-Fi or Ethernet. Constraints such as low power consumption, shock resistance, thermal stability and not least cost reduction for the entire system, represented further challenges in the development of the STC.
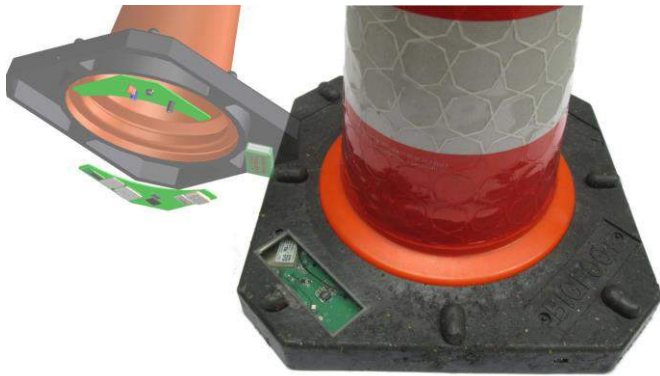
Fig 5: Prototyp of the STC

In Fig. 5 the STC with a conically shaped body and the base plate for accommodating the electronic and mechanical components is shown. The foot plate is an advantageously recessed to accommodate the components and modules suitable for wireless communication, for the energy supply, for the positioning as well as for additional sensors. The components or modules are electrically connected to another. In order to ensure the necessary resistance to weather and environmental influences in the transport area, the gaps at the base plate are closed water- and dust-tight.

More environmental sensors can be integrated in further stages, in order to improve the data acquisition capability of the STCs. With the integrated temperature sensor, it is for example, possible to detect the risk of freezing of the roads. Highly accurate position and orientation detection data of whole areas, described by two or more STCs, can also be used to get a more precise view. The self-monitoring of the cone recognizes displacing or removing from the areas of accidents and may send alerts to the emergency services.

3.3 Global Navigation Satellite System (GNSS) modules and precise localisation

One of the major functions of the STC is the automated self-localisation in the road environment. The exact geographical location, along with added information, is the base for correct description of a temporary disruption. Lanes-fine localization with submeter accuracy is currently still a main challenge. Even the urban use of the STC, e.g. at intersections, sets high demands on the positioning module. The reason for this are often effects like shadowing and multipath propagation of the rf-signals from the satellite.

Multi-GNSS modules are able to receive and evaluate at least 2 independent satellite systems in parallel. This leads to an improvement in positional accuracy and position availability. Modern GNSS modules can receive the currently existing satellite systems such as GPS, GLONASS and SBAS. In addition, there are already modules that can take into account the satellite systems that are currently in preparation such as Galileo and Beidou and thus provide a further improvement in position determination.

Low-cost Real-Time-Kinematic (RTK) and Precise Point Positioning (PPP) methods, as described in Piotraschke (2013) and Stempfhuber and Buchholz (2011), are predestined for the presented system. Because the position of the STC does not change after setting up in road space, the required accuracy can be achieved by using post-processing methods. Such methods are described in Takasu and Yasuda (2009). The required raw data are provided by some GNSS modules, which in turn represent another important criterion for the selection of a suitable GNSS module.

Suitable technologies for communication and highly accurate positioning already exist or are constantly being developed. But geodetic multifrequency receivers for highly accurate positioning are very expensive, making it unusable for the presented system. The technological challenge is primarily in the fine track position determination in the transport area, by means of low-cost single frequency GNSS receiver. Such low-cost modules, as shown in Figure 6, cost about 40 euros. Unlike cheaper modules, the modules depicted, offer the possibility of issuing the code- and phase data directly as raw data stream, which is a prerequisite for the PPP method described in section 3.3 and makes them of particular interest for the presented system.

The rapidly progressing development in the field of GNSS positioning modules, driven by the cell phone and smart phone market, is of particular interest for the STC, because new and more powerful tracking devices are introduced nearly every six months. The modular design of the system is in this case particularly advantageous, as this allows to adequately respond to new developments. Thus, new and better modules, for example new positioning modulses, can be integrated into the system at a later point in time.
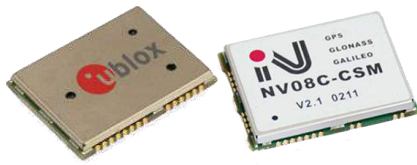
Fig. 6. Suitable gnss-modules for STC, Ublox Neo7p and NVS-Technologies MVS08CSM

Differential Global Navigation Satellite System (DGNSS) with RSU as base station

With the DGNSS-Method, code measurements will be corrected, leading to an accuracy of 50 cm to 1 meter, depending on the precision of the GNSS receiver hardware. In the RTK in addition the significantly more accurate phase measurements are corrected, making an accuracy of about 2 cm possible in real time. The idea is, the RSU, whose position is known very accurately, is used as gnss base station for the positioning of the STC. To this end, the RSU, which is now equipped with a gnss receiver, sends correction data to the STC. The STC uses these date, to calculate its own position. Since the data connection required for the sending of the correction data already exists for transmission of alarm signals to the RSU, this approach is a good alternative to slower PPP-approach. Various tests with this approach yielded very positive results and enabled a positioning accuracy in the centimeter range after just a few minutes. A disadvantage is the relatively high volume of data in the transmission of the correction data. This critical point has to be considered, since it may result in higher costs for the mobile communication. With favorable mobile phone tariffs or data flat rates, this approach could be considered.

DGNSS with comercial correction data

Different vendors, such as Axio-Net or Satellitenpositionierungsdienst der deutschen Landes-vermessung (SAPOS), operate commercial reference station networks and calculate tailor correction data. These data are provided in different services. Disadvantages are also here the additional costs for the operation. In addition to the higher cost of correcting data transmission via mobile radio, additional ongoing costs for the use of correction data services are necessary.

Positioning with the static PPP-method

PPP is a GNSS evaluation technology for precise positioning, which works without correction data from a reference station or a reference station network. However, this process requires not only the consideration of numerous corrections, introducing precise satellite orbits and clock data. For PPP numerous applications are possible. It can be used for the precise static point determination, as in the case of the STC, or for kinematic positioning of moving objects such as satellite, aircraft, ships and buoys as described in Hesselbarth (2009). Precise Ephemeris and clock correction data are required for positioning with the PPP method. These products are provided free of charge by the International GNSS Service (IGS) and the various Analytical Centers (ACs) of the IGS. With the code- and phase observation data, provided

by some low-cost single frequency receiver in raw data mode, the precise satellite orbits and clock data, and different, necessary corrections, calculations with cm-accuracy are possible. In the STC the free softwarelibrary rtklib is used for the position calculation with the PPP-method. A typical positioning result, sowing cm-level accuracy, is shown in Fig. 7. The real position of the STC was given by a highly accurately measured reference point.
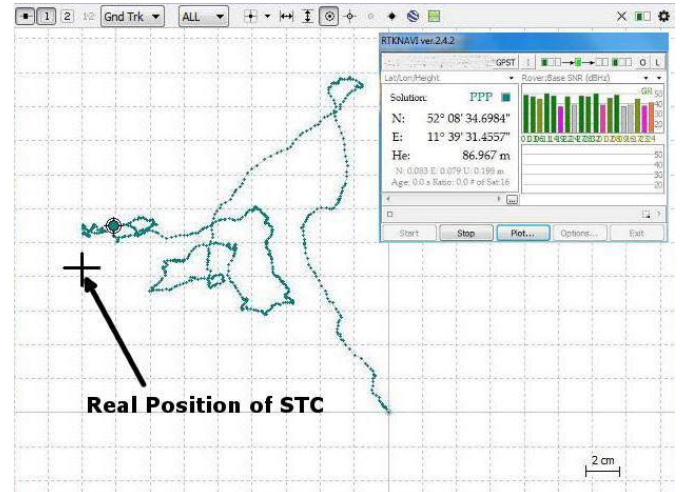
Fig. 7. Positioning accuracy in the cm-range with the free softwarelibrary rtklib. The solution was calculated by the STC using the program rtknavi in Static PPP mode and displayed graphically with the program rtkplot. The measurement time was 15 minutes at very good reception conditions.

4 DISSAMINATION OF CPS INFROMATION TO THE ROAD USER

The distribution of the generated CPS information to the affected road users is an important aspect. The feasible range, the timeliness of the data and the delay from the activation untill processing and displaying in the vehicle, are important parameters that have a direct influence on the safety enhancement by the CPS. When using the information provided by the CPS, it must be differentiated, whether the providing of the informations is time-critical or not. When a vehicles is moving in short distance (<1km) to the disruption location this case is a time-criticalal one. Here a safe warning with little delay must be transmitted, so that there is enough time for an adequate response by the vehicles driver. For this, the DSRC radio is predestined, because this technique offers a very low latency.

Uncritical dissemination scenarios in the context of the CPS are those cases where the data of the CPS have more informative Charcter. Such applications are, for example, the traffic situation-dependent route guidance described in Schade (2015). Either before departure or dynamically when the message appears, the routing can eventually be adjusted so, that the relevant road users can bypass the disrupted lane (see also section 2.3). The distribution of disruption

informations over the WEB or via broadcast media, such as the TMC radio, are further examples of an time-uncritical dissemination of the CPS data. For such cases, the distribution over the MDM and standardized interfaces should be used, as described in section 4.2.

4.1 Dissemination and usage of CPS information over 802.11p DSRC-radio

In a first approach, the RSU was used as radio relay, for the dissemination of the CPS-danger messages via DSRC. This had mainly practical reasons. The RSU as fixed infrastructure component has special antennas that are installed at some height on a mast, thus allowing optimal coverage. Depending on structural conditions, ranges of up to 1km are possible. A STC placed on the ground, with a simple, round radiating antenna, would achieve significantly less coverage here. The dissemination of information on geonetwork mechanisms (forwarding) could, in case of a sufficiently large number of equipped vehicles, provide a remedy. Nevertheless, the problem remains that the first vehicles may not be warned in time, if the radio range is too low. Another important aspect that has spoken for the RSU as radio relay was the fact, that at the time of development, there were no suitable radio modules, which would have allowed a meaningful integration into the STC. In the near future it will also be possible to equip intelligent infrastructure components, such as the STC, with 802.11p DSRC radio modules. With DSRC modules, like the MK5 module from Cohda Wireless, the integration in smaller embedded systems can be done, as can be seen in Cohda Wireless (2014). Thus, the STC, for the dissemination of its data via DSRC, would no longer be limited to intersection areas and the presence of an RSU. Also scenarios and application areas such as highways or on motorways could be covered hence.

The specification of the Decentralized Environmental Notification Message (DENM), which is transmitted from the CPS application via the RSU as danger message to the road users, was based on the protocoll spezification described in simTD Consortium (2009). In the near future here the ETSI standard ITS-G5 will be applied. In the specification phase of the CPS-DENM, it was first necessary to consider, whether all required information will be covered by the appropriate message format. Starting from an analysis of requirements with the project partners, a preliminary list of requirements was drawn up, from which the following required information could be derived, which must be encoded in the CPS-DENM:

- reason/cause of hindrance,

- position of the STC as World Geodetic System (WGS) coordinates,

- Information regarding the accuracy and reliability of STC-position,

- appropriate operators (police, fire department, …)

- direction or lane precise localization of hindrance,

- type of hindrance (Narrowed lanes, locked lanes, number of affected lanes, full closure of lanes, ...),

- length and extent of the hindrance,

- distance to the stop line at intersections,

- range of the DENM (Destination-Area) for Geonetworking and DENM-forwarding

For the encoding of information such as appropriate operator, type of hindrance or cause of hindrance, the Transport Protocol Experts Group (TPEG)–Traffic Event Compact (TEC)-standard in TPEG TEC (2006) was used.

The information coded in the DENM, is received by the vehicle applications, evaluated and converted into corresponding warnings or action recommendations. In the simplest case, one such indication may be, that the traffic disruption is displayed in a HMI with the measured distance. An appropriate recommendation for action could be, that a timely threading is proposed, in the case of lane closure. Moreover, the information of the CPS system can provide important input parameters for different assistance system. Mentioned may be here the "Kreuzungslotse", which will be actually developed in the project "UR:BAN", URBAN (2015). Even the partial- and highly automated driving, can benefit from the very precise and current CPS-information.

In the integration- and test phase, see also section 5, the dissemination of the CPS data via DSRC-radio was successfully tested. For this, some car manufacturers, such as VW and Opel, has implemented the UseCase, display of warning message with distance information, in its own vehicle-HMI.

4.2 Dissemination and usage of CPS information over the Mobility Data Marketplace (MDM)

Only by offering merged traffic data to a wider scope including communication structures, data flows and authenticated user management the overall usage of STC can be persuasive in order to realize intelligent mobility services.

Necessary prerequisite for this is a comprehensive data base in conjunction with the possibility of a simple and standardized data access. Potential mobiliy service providers have great interest in gaining this heterogeneous traffic information simply. Therefore a national project and data platform has been launched offering the Mobility Data Marketplace (MDM) in order to simplify and improve access and availability of current traffic data in order to realize new applications on the field of mobile information and services, as described in Mobilitäts Daten Marktplatz (2015). The possibility of standardized access to traffic data as well as simple connectability widens the opportunities for offering a variety of new, intelligent mobility services. The use of

standardized data access is crutial in this context. Therefore the EU-wide standard DATEX II described in Directorate General for Mobility and Transport (2013) is used, which includes varios application data – varying from detector data on parking information to construction site reports. Figure 8 shows the relationship between data providers, data consumers and the broker system of MDM as a central platform for the exchange of information.
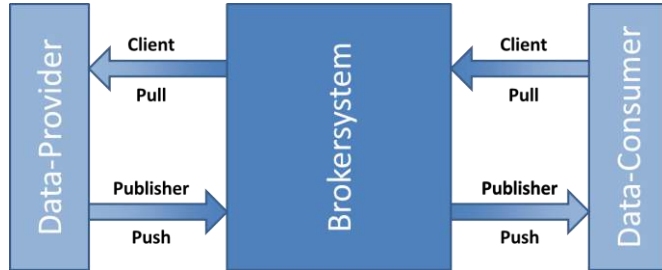
Fig. 8. MDM interfaces connecting data provider, brokersystem and data consumer

The service presented in Schade (2015), regarding a traffic-dependent navigation with dynamic traffic data from the MDM, demonstrates the possibilities for the development of mobility services, which arise from the availability of a centralized data exchange platform like the MDM with standardized access mechanisms.

Other possible moblity services based on CPS as data provider are:

- premium navigation service with offline routing functions,

- current traffic states and information for service centres and control units e.g. for fleet coordination,

- up-to-date information for traffic management centres,

- improved arrival time prediction for public transport

5 FIELD TEST AND RESULTS

Varios field tests have been a part of the research project "UR:BAN" where the CPS has been researched on. The "Anwendungsplattform Intelligente Mobilität" (AIM) test field in Braunschweig offers various intersections equipped with state of the Art and DSRC communication technology making them an ideal platform for the test of new technologies.

As an important milestone in the realization and implementation of the applications at the smart junction the testing of the CPS has been fulfilled. Here, the applications were tested under real world conditions, various interacting applications communicated to each other and their interfaces were tested. Several testing days were prepared in the AIM-test field and the ifak participated successfully in October 2014.

The integration tests were also carried out in the AIM test field in Braunschweig. All the necessary infrastructure and software components were provided by the project partner and the organizer of the AIM testfield, the DLR. Other involved Project partners such as VW, Opel, Continetal successfully received the DENM of the CPS and displayed the information in their HMIs.
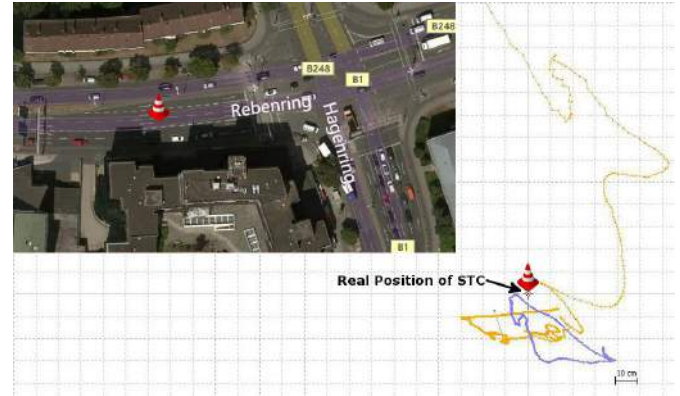
Fig. 9. Psitioning of the STC in the driveway Rebenring in Braunschweig after 10 minutes of observation (yellow: real "RTK" position, calculated in the STC; blue: PPP-position wit the post-processing method, based on raw- and correction data).

The main results of the field tests durging the function- and integration tests are:

- downloading and decoding of intersection topology message for high-precise track matching was sufficiently implemented,

- the generation of a corresponding CPS-DENM by the CPS server works (with one ore more STC),

- the coding of the CPS-DENM was correct in all cases,

- the automated activation/deactivation of the CPS workes sufficiently,

- the positioning accuracy of the STC was sufficiently correct for lanes fine localization in all tested cases,

- all necessary information about the disruptions have been correctly encoded and sent,

- the hardware workes even under difficult conditions in the real application scenario,

- the entire communication chain with all the provided and required interfaces was successfully tested,

- the reception and presentation of the CPS-information in the vehicles, with enough time for appropriate reaction, was guaranteed in all cases

Figure 9 shows a typical positioning result which has been achieved in the field tests. For this purpose, the STC has been positioned in a driveway of the appropriate test intersection.

After two minutes of observation the position accuracy was in the sub-meter range, wich garantes the lanes fine localisation. In this szenario the real position of the STC was given by a referenz measurement with a geodetic GNSS-receiver of type JAVAD Delta-G3T

Fig. 10. Picture taken during the field test in the AIM-test field in Braunschweig, showing the STC-prototype on a building site

6. CONCLUSION

Currently traffic information is given using broadcast media such as radio or TMC technology. Actualy, this information offers only limited temporal and local distinction. Very often no warning is given at all, especially at one-day construction sites, small crashes or traffic holdups in urban areas. As a consequence traffic participants can hardly connect their routes with occurring traffic disruptions and usually no or insufficient recommended course of action are given. Due to the temporal shift, very often the information is received too late.

By communicating high-precise, distinct and precise traffic information and warning messages, traffic safety of the staff and all traffic participants can be enhanced decisively and offers an important contribution to road safety enhancement.

The greatest potential lies in the saving of additional positioning technique as well as the indirect avoidance of accident-costs. The methods for detecting and logging of danger zones are through the automation of processes with the help of the CPS significantly faster, more reliable and more cost-effective.

Neverless current practical challenges for the overall launch of these technologies remain. First the relevant stakeholders such as service staff (police, fire department, etc.) have to be persuaded of the additional benefit of using these new tchnologies. Therefore a seamless integration of the technological use in the workflow of the service staff is essential. This entails also wide aspects of data protection in order to address user concerns, such as the feeling of "Big Brother is watching you". Then the whole data pipeline from data collectors, users and processors for future services must be established and integrated in the work flows.

The success on the market depends largely on financial constraints of the governmental and public parties. Here attractive prices and proactive service structure has to be offered in order to realize a "work culture of trust".

Furthermore Sscientific challenges of the current system remain. The main current challenge lies in the submeter-precise location enableb with low-cost single frequency GNSS modules. The static porting of the PPP algorithm on low-cost, low-power microcontroller is such a main future challenge.

REFERENCES

ADAC (2015). Statistiken Tabelle 9.2. Baustellenunfälle Online Available 01.29.2015: http://www.adac.de.

AIM (2015). Online Available 06.15.2015: http://www.dlr.de/ts/desktopdefault.aspx/tabid-6422/#gallery/25304.

Car 2 Car Communication Consortium (2015). Online Available 01.29.2015: http://www.car-to-car.org/

Cohda Wireless (2014). CohdaMobility MK5 Module Datasheet. version: V1.0.0.

DESTATIS (2014). - German Statistic Federal Bureau Traffic and Transport Division 8, Series 7. Wiesbaden, http://www.destatis.de.

Directorate General for Mobility and Transport (2013). DATEX II User Guide. document version 2.2.

Hesselbarth, A. (2009). GNSS-Auswertung mittels Precise Point Positioning (PPP). Zeitschrift für Geodäsie, Geoinformation und Landmanagement 5/2009.

Mobilitäts Daten Marktplatz (2015). Online Available 06.15.2015: http://www.mdm-portal.de/.

Mobilitäts Daten Marktplatz (2012). Technische Schnittstellenbeschreibung. version 2.3, S.15.

Piotraschke, H. F. (2013). RTK für Arme - Hochpräzise GNSS-Anwendungen mit den kostengünstigsten Trägerphasen-Rohdatenempfängern. Jahrestagung der Gesellschaft für Informatik in der Land-, Forst- und Ernährungswirtschaft e.V.

Schade, J. (2015). Routing service in consideration of traffic situation with data from MDM. Conference: AmE 2015 – Automotive meets Electronics - Beiträge der 6. GMM-Fachtagung.

simTD Consortium (2009). Spezifikation der Kommunikationsprotokolle. öffentliches Deliverable D21.4.

Stempfhuber, W. and Buchholz, M. (2011). A PRECISE, LOW-COST RTK GNSS SYSTEM FOR UAV APPLICATIONS. Conference on Unmanned Aerial Vehicle in Geomatics, Zurich, Switzerland.

Takasu, T. and Yasuda, A. (2009). Development of the low-cost RTK-GPS receiver with an open source program package RTKLIB. International Symposium on GPS/GNSS, Jeju.

TPEG TEC (2006). Application Specification. version 1.0.

URBAN (2015). Online Available 06.15.2015: http://www.urban-online.org.

Lessons Learnt in Non-supervised Record of Real Crossings

Araceli Sánchez*, Licesio J. Rodriguez-Aragón**, Isaac Martín de Diego***,
Cristina Conde***, Enrique Cabello***

*Universidad de Salamanca, Departamento de Informática y Automática, Plaza de la Merced s/n,
Salamanca, Spain (e-mail: maraceli@usal.es).
**Escuela de Ingeniería Industrial de Toledo Avda. Carlos III s/n
Toledo, Spain (e-mail: L.RodriguezAragon@uclm.es)
*** Universidad Rey Juan Carlos, ETSII, C/ Tulipán s/n,
Mostoles Spain, (e-mail: isaac.martin, cristina.conde, enrique.cabello@urjc.es)}

Abstract: This paper presents an artificial vision based video-sensor designed to detect pedestrian-vehicle conflicts at crossing points. This video sensor detects moving objects by isolating them from the background. Then the speed and trajectories are estimated using a Kalman filter. Potential conflicts are then predicted. This system has been tested at two real crossing points at the city of Salamanca (Spain).

Keywords: Include a list of 5-10 keywords, preferably taken from the IFAC keyword list.

1. INTRODUCTION

A vast number of reports and statistics state the vulnerable role played by pedestrians in traffic accidents, especially in those who take place in areas considered safe for them (zebra and traffic light controlled crossings). Walking is recognized as a healthy exercise with almost non-existing negative consequences except for those caused by road traffic.

In the last decades numerous projects have focused their efforts to study and improve the conditions of pedestrians crossing points in their multiple variations. Evaluations of pedestrian risks (L. Leden 2002), studies about drivers' speed behaviour at zebra crossings (A. Várhelyi 1998) or analysis of particular situations as adult-child pairs at pedestrians crossings (M. S. Zeedyk and L. Kelly 2003) are recent approaches to improve the safety of the weakest part. Most of these studies have as their data source on databases from pedestrian accidents, which are considered as one of the most important building blocks in setting up a strategy for the development of intelligent integrated road safety systems (eSafety 2002). Others use punctual observations carried out by trained observers who measure, categorize and register the situations they witness. Accidents at zebra or traffic lights fortunately seldom occur, and whenever take place the data collected from the scene appear obscure not to erase or avoid responsibilities but to show evidence or preventing them from happening again. In order to provide proactive safety, a tool capable of performing a preventive analysis of every pedestrian crossing point should be available.

2. TRAFFIC CONFLICTS

Pedestrians and drivers perception has been used as this proactive safety tool comparing perceived risk locations with police-reported crashes (R. J. Schneider et al. 2004) or studying drivers behaviour (T. Lajunen et al. 2004). Other approaches have focused their efforts on the concept of "conflict" defined as those situations involving one or more pedestrians or vehicles in which danger of collision or overrun is present (S.J. Older and B. R. Spicer 1976). Conflicts frequency is much higher than that of accidents and avoiding risky situations certainly would increase safety.

Depending on the observer location and point of view, we can identify a conflict from the position of the parts involved in it, their type, trajectories, speed and other subjective properties that a trained observer may include in his notes. In previous works, trained observers (G. Tiwari et al. 1998) and materials as measuring tape, chalk, sprays and laptops to gather the data (D. Lord 1996) have been used for the recording of those conflicts.

Our objective was the development of an artificial vision based on automatic conflict recorder and analyzer, which provided us with a vast database of pedestrian-vehicle conflicts as well as with the technical data, such as position and speed of all the parts involved. We also record the images and store the precise time when possible conflicts have taken place so that trained observers can pass up routinely crossing situations and center their attention on precise situations. Therefore observations length can be increased without rising significantly, surprisingly even reducing, the time and the resources needed for the treatment of the data.

3. DATA COLLECTION

In collaboration with the DGT (General Traffic Directorate, Spain) two different crossing points were selected in the town of Salamanca (Spain), a middle size town in the north-west of Spain with a population of 140,000. The historical city center is devoted to pedestrians so that vehicles have to drive around it. As reported by local police, about 1000 accidents are reported each year, 100 of them imply overruns involving about 120 pedestrians. The data available of these accidents are, age, gender and injures (4 people killed, 36 seriously injured, 80 with minor injuries). The two crossing points

were endowed with specific characteristics (Fig. 1) as described below.
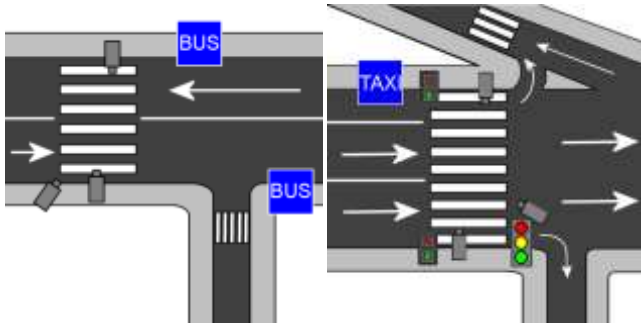
Fig. 1. Schemes of the two crossing points selected and the precise situation of the cameras.

The first one is located at a zebra crossing in a two-way street with a bus stop closely situated to the crossing point. It is not regulated by traffic lights and both directions are allowed for vehicles; therefore pedestrians have to stop and be aware that both directions are free of cars before crossing. Parking is allowed in both sides of the street. The bus stop is placed before the pedestrian crossing, in front of the camera placement. When the bus stops, it is an obstacle for vehicles moving from right to left.

The other was at a traffic light controlled crossing point in a one-way street and with a taxi stand at one side of the street. Vehicles have two lanes, and another one is devoted to the taxi stand which is just before the pedestrian crossing. The first taxi is waiting just at the border of the zebra crossing. The configuration of this crossing point had recently been changed from two to one way due to the high traffic density of the area. Even though the number of accidents reported at the point are not significant, local police had the feeling its configuration was not the most adequate.

These points were selected between thousands of other possible candidates in order to study the influence of the bus stop and the taxi stand in the behavior of pedestrians and vehicles, so that information for other possible alternatives for these services could be provided.

A computer and three cameras were closely and strategically situated at the crossing points as to cause minimum alterations to the environment. Two cameras were situated at both sides capturing a front view of the crossing point, each at one side of the street. The other was about 10 meters above the crossing point capturing a high and overlooking view. Thus, pedestrians behavior and trajectory could be followed before, during and after they have crossed the street. Images were recorded and stored in gray levels and with a resolution of 240×180 pixels, enough for the treatment to be carried out. The recording periods were from January the 18th to February the 14th and from April the 9th to March the 30th during the year 2013 respectively. Day and night situations were recorded, artificial street illumination at night time proved good enough to let the system perform properly. This experiment contrasts with previous attempts to analyze periods of days, fractions of days or a limited number of pedestrians.

4. IMAGE ANALYSIS

The process and analysis took place once the images were captured and stored. To exactly distinguish movement from static objects is essentially required to evaluate and track the moving objects. Therefore, a background subtraction was performed (N. Papanikolopoulos 2000; N. Obolensky et al. 2002) in order to undertake this task. To obtain a continuously updated background image, a consecutive set of images organized in a FIFO queue is selected and processed. Two methods were initially considered: evaluation of either the mean or the mode of every pixel grey level. The number of images forming this set was also a variable that had to be chosen. Tests were done with sets from 5 to 20 images. Experience lead us to make the choice of a 10 images set and mode evaluation of every pixel grey level to carry out a most adequate calculation of the background.

However, a precise study of the particular crossing point where the system may be installed may lead us to other best fitting choices for the situation. After obtaining the images of the moving objects on a white background, the following step was to delimit those objects, which will be hereafter referred to as components. The calculation of the convex hull of these components was finally established through a sequential labeling, based on neighborhood properties, while a matricial labeling algorithm was put aside due to the high computational cost and the little improvement reached (R. Jain 1995; R. C. Gonzalez and R. E. Woods 1993).

Through a consecutive coverage of every pixel in the image, checking and labeling each active pixel in correspondence with their neighbors, a labeled image is obtained, where each component is identified. Once the components were labeled, a filter was applied to ignore those components which did not reach a minimum amount of pixels, and that were considered as noise produced in the subtraction process. Then each component is extracted as a separated image. Vehicles and pedestrians were clearly distinguished due to their different size and orthogonal trajectories, and the tracking and the recording process of the characteristics of every component then began.

5. TRACKING OF THE COMPONENTS

Kalman filter is an iterative technique designed to forecast in time series models (R. E. Kalman 1960). Each pedestrian and vehicle trajectories have been therefore modeled as a Linear Dynamical Systems subjected to Gaussian noise. A modified Kalman filter was implemented (N. Obolensky et al. 2002; P. J. Hargrave 1989). The algorithm adapts its model at each step to improve the movement estimation of every component. Position, speed and values of the acceleration at different steps are used to predict the future object localization.

The tracking process can be defined as follows, for modelling smooth trajectories a state vector providing information of every component at time t is given: $(p_t, v_t, a_t, a_{t-1}, a_{t-2})^t$, where p, v and a represent the position, velocity and acceleration at step described by its subindex. States vectors provided by Kalman estimations will be denoted as x_t while real state

vectors obtained through observations in the images will be denoted as y_t.

The iterative model forecasts state vectors trough a transition matrix A that relates the state vector at a previous time step k−1 to the state at the current step k. C is the coefficient matrix that relates the predicted state to the measurement y_k. The process and the measurement noise, q_k and r_k, are assumed to be independent of each other, white and with normal probability distributions, mean 0 and covariance matrices Q and R respectively.

$$x_k = Ax_{k-1} + q_k \quad q \sim N(0,Q)$$

$$y_k = Cx_k + r_k \quad r \sim N(0,R)$$

The Kalman filter is essentially a set of mathematical equations implementing a predictor-corrector type estimator that minimizes the estimated error covariance. The way it works is trough a feedback process, the filter estimates the state vector at some time and obtains feedback in the form of noisy measurements. Therefore the Kalman equations can be classified in two sets, prior estimations and posterior corrections. The prior part is formed by a predicted state vector, $\widetilde{x_k}$, and a predicted error covariance, S_k^- , both at future time k.

$$\widetilde{x_k} = A\, x_{k-1}$$

$$S_k^- = AS_{k-1}A^t + Q$$

Then, at time k, when the correct measurement y_k is obtained, the Kalman Gain, K, is calculated and the prior estimation updated, $\widetilde{x_k}$, proportionally to the prior error obtained. Also the prior error covariance leads to the updated error covariance, S_k.

$$K_k = S_k^- C^t (CS_k^- C^t + R)^{-1}$$

$$\widetilde{x_k} = \widetilde{x_k} + K_k(y_k - C\widetilde{x_k})$$

$$S_k = (I - K_kC)S_k^-$$

At the end of each iteration prior error, $e_k^- = (y_k - \widetilde{x_k})$, and posteriori error, $e_k = (y_k - \widetilde{x_k})$ are obtained. The transition matrix A and C, process noise covariance Q and measurement noise covariance R are important parameters of the Kalman filter. Its performance is largely determined by how well the parameters are tuned according to the problem. At our system, a one step Kalman filter is used. That means that no more than one step ahead in time is requested as prediction, using as input state vector of each iteration the measurement y_k obtained previously the transition matrix trivially becomes C = Id. Transition matrix A is calculated using classical physical considerations of position, velocity and acceleration.

Transition matrix A is calculated using classical physical considerations of position, velocity and acceleration.

$$\begin{pmatrix} p_k \\ v_k \\ a_k \\ a_{k-1} \\ a_{k-2} \end{pmatrix} = \begin{pmatrix} 1 & t & t^2w_1/2 & t^2w_2/2 & t^2w_3/2 \\ 0 & 1 & tw_1 & tw_2 & tw_3 \\ 0 & 0 & w_1 & w_2 & w_{31} \\ 0 & 0 & 1 & 0 & 0 \\ 0 & 0 & 0 & 1 & 0 \end{pmatrix} \begin{pmatrix} p_{k-1} \\ v_{k-1} \\ a_{k-1} \\ a_{k-2} \\ a_{k-3} \end{pmatrix}$$

The weights (w_1, w_2, w_3), are positive and verify $\sum_i w_i = 1$. Obtaining a weighted acceleration mean.

As a spatial movement is being explained trough bidimensional information provided by the cameras, parameter A is then corrected in terms of Kalman gain, K_k, and posterior error, e_k.

$$A_{k+1} = A_k + \eta(K_k, e_k)$$

When the components have been labeled and filtered, the prediction of future trajectories through Kalman filter provides the system with crucial information to predict possible conflicts and to match the moving objects in the next instant of time. That allows us to follow the trajectory of every component while is present at the crossing point. (Fig. 2)
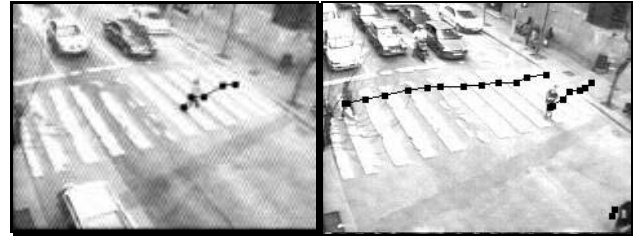
Fig. 2. Tracking of pedestrians in one of the selected zebra crossing.

6. CONFLICT PREDICTION

Once the system had registered and stored trajectory, speed and distinction between vehicles and pedestrians, analysis of these data was automatically performed. The objective was to detect possible conflicts (crashes) between pedestrians and vehicles if their trajectories and speeds were not to change (Fig. 3).

Fig. 3. Conflict prediction between a pedestrian and a vehicle.

To perform these estimations a mean value of the last stored trajectory and speed values were calculated. In this way we are considering a rectilinear and uniform movement along the crossing point for both vehicles and pedestrians. Then a simulation is performed for a number of future instants specified and the distance between the components is measured. If this distance is lower than a specified parameter, specified then the conflict is classified as a potential one and time and frame of occurrence are recorded for the later analysis.

7. EXPERIMENTAL RESULTS

The aim of this project was to test if computer vision systems are robust enough to work in real situations towards detection of traffic conflicts. This result has been achieved, a computer vision system has been built and real sequences have been processed. Computer vision system can help a trained human operator to estimate conflicts, by processing huge amounts of video and labeling only those sequences in which a conflict can be observed.

Once the video has been processed, the situations containing possible conflicts are labeled and a trained operator can then estimates and analyze them. This approach represents an enormous time earning. The trained operator task is reduced to label and analyze potential conflicts and situations. The amount of time processed by a single trained observer is seriously increased. Results are based in a long time observation of the pedestrian crossing (huge part in automatic way and interesting sequences in a human supervised overview).

The computer vision system can help the user by increasing its performance as only significant elements require his attention. Once sequences were labeled a preliminary study of the conflicts detected was done. As a result, changes in the configuration of both pedestrians' crossings were proposed and accepted by the traffic department.

For the first situation, the bus stop appeared clearly to be an important obstacle for both pedestrians and vehicles, so it was moved after the zebra crossing. Conflicts in this pedestrian crossing were motivated by pedestrians moving in front of the bus or by cars trying to avoid the bus with reduced visibility of the traffic way. The new configuration made pedestrians to cross the street behind the bus, so they become clearly visible for vehicles approaching the zebra crossing.

For the second situation the taxi stand is responsible for the highest amount of conflicts. When the first taxi departures the scenario abruptly changes, the street configuration is transformed from a two lanes to a three lanes. This sudden change may affect pedestrians waiting or approaching to the crossing point. The taxi stand was then moved away from the crossing point and parking was allowed at the place where the taxi stand used to be.

The computer vision system has been also applied to images provided by Lund University (Almost an Accident). Five video sequences containing conflicts were studied (Fig. 4). Only small parameter adjustments were required to adapt the system to the new images. No changes in the implementation were done, and the five conflicts were correctly labeled. This is a promising result even though more experiments have to be done in order to test algorithms.

Fig. 4. Conflict prediction in new situations.

Descriptive statistics about the conflicts are now an easy task to be performed. Once the conflicts have been determined and specified through its occurrence time, a trained observer can then easily check the images and determine whether the pedestrian or the vehicle is responsible for the accident.

8. CONCLUSIONS

Automatic detection and categorization through artificial vision tools has proved to be a powerful and valuable way of analyzing the occurrence of vehicle-pedestrians conflicts. Centering our efforts on proactive safety and not on the analysis of accidents databases, the complexity of the problem increases so greatly as to become unattainable without an automated process.

Results show in a general overview, that the specific conditions of each crossing point are responsible in a crucial way for the kind of conflicts that take place in its surroundings. In summary, the tool here developed can be adapted and installed at different crossing points with different geometry and characteristics providing us with clear and trustful tips in order to make concrete decisions for the improvement of safety.

ACKNOWLEDGEMENTS

REFERENCES

[L. Leden 2002] L. Leden, Pedestrian risk decrease with pedestrian flow. A case study based on data from signalised intersections, Accid. Anal. And Prev., 34, pp.457-464, 2002.

[A. V´arhelyi 1998] A. V´arhelyi, Drivers speed behaviour at a zebra crossing: a case study, Accid. Anal. and Prev., 30, pp. 731-743, 1998.

[M. S. Zeedyk and L. Kelly 2003] M. S. Zeedyk and L. Kelly, Behavioural observations of adult-child pairs at pedestrian crossings, Accid. Anal. And Prev., 35, 771-776, 2003.

[eSaefty 2002] eSaeftey, Final Report of the eSaefty Working Group on Road Saefty, Final Report, European Commision, November 2002.

[R. J. Schneider et al. 2004] R. J. Schneider, R. M. Ryznar and A. J. Khattak, An accident waiting to happen: a spatial approach to proactive pedestrian planning, Accid. Anal. and Prev., 36, pp. 193-211, 2004.

[T. Lajunen et al. 2004] T. Lajunen, D. Parker and H. Summala, The Manchester driver behaviour questionnaire: a cross-cultural study, Accid. Anal. and Prev., 36, pp. 231-238, 2004.

[S.J. Older and B. R. Spicer 1976] S.J. Older and B. R. Spicer, Traffic conflicts: a development in accident research, Human Factors, 18, pp. 335- 350, 1976.

[G. Tiwari et al. 1998] G. Tiwari, D. Mohan and J. Fazio, Conflict analysis for prediction of fatal crash locations in mixed traffic streams, Accid. Anal. and Prev., 1998.

[D. Lord 1996] D. Lord, Analysis of pedestrian conflicts with left-turning traffic, Transportation Research Record 1538, University of Toronto, 1996.

[N. Papanikolopoulos 2000] N. Papanikolopoulos, Pedestrian Control at Intersections, Intelligent transportation Systems Institute, University of Minnesota, 2000.

[N. Obolensky et al. 2002] N. Obolensky, D. Erdogmus and J. C. Principe, An Time-Varing Kalman Filter to Moving Target Tracking, Proc. of CONTROLO'02, pp. 418-422. 2002.

[R. Jain 1995] R. Jain, R. Kasturi and B. G. Schunck, Machine Vision, McGraw-Hill, 1995.

[R. C. Gonzalez and R. E. Woods 1993] R. C. Gonzalez and R. E. Woods, Digital Image Processing, Addison-Wesley, 1993.

[R. E. Kalman 1960] R. E. Kalman, A New Approach to Linear Filtering and Prediction Problems, Trans. of the ASME-Journal of Basic Engineering, vol. 82, Series D, pp. 35-45, 1960.

[P. J. Hargrave 1989] P. J. Hargrave, A tutorial Introduction to Kalman Filtering, IEEE Colloquium on Kalman Filters: Introduction, Applications and Future Developments (Digest No.27), 1989.

Avoiding collisions between pedestrians/cyclists and vehicles at signal controlled intersections using V2X

Tim Ruß * **Sebastian Naumann** **

* ifak e.V. Magdeburg, Germany (e-mail: tim.russ@)ifak.eu)
** ifak e.V. Magdeburg, Germany (e-mail: sebastian.naumann@ifak.eu)

Abstract: Especially at intersections, pedestrians and cyclists are endangered by crossing vehicles. Modern sensor and radio communication technologies offer the possibility to detect dangerous situations and to prevent accidents. In the joint research project UR:BAN, the following is being researched and implemented prototypically: At intersections, so called *vulnerable road users* are being detected by radar, as well as their mobile devices, like smartphones. After the upcoming introduction of the new communication technology *V2X*, vehicles can distribute information gathered by their internal sensors. All these data sources serve a so called *cyclist and pedestrian protection system*. It calculates trajectories and predicts possible collisions. V2X and mobile devices with Wi-Fi offer a return channel to warn all road users in time and in an appropriate way.

Keywords: V2X Communication, Cyclist Protection, Mobile Applications, Data Glasses, Radar Detection, Improvement of Position Measurement

1. MOTIVATION AND INNOVATION

There are many intersections where motorized vehicles, as well as pedestrians and cyclist have a green traffic light at the same time. The latter can be summarized as *vulnerable road users* (VRUs). When they pass the crossing, they are endangered by turning vehicles. Though more road users can pass an intersection with this simultaneous green phase, solutions must be found for the accompanied higher accident rate. Until now, vehicles were equipped with sensors to analyze their environment themselves and to feed driver assistance systems. E.g., the driver can be informed via optical or acoustic alarms. Or, an assistance system for braking or steering can react.

But such detection systems only rely on the data that can be gathered from their point of view. Cooperative systems offer additional benefits: Sensor data can be gathered from several road users and shared among them. Applications that offer information services as well as to improve safety are possible. Also, all affected road users can be warned, including endangered cyclists and pedestrians. Appropriate solutions are still in development. One example is the communication between cars and a special bicycle helmet, developed by Volvo, POC and Ericsson (Elfstroem, 2014). Volvo cars and the helmet are connected via internet. They share position data and warn each other when a collision is possible: Drivers via their head-up display, cyclists through a helmet-mounted alert light. The main problem with such proprietary solutions is always the equipment rate. Cyclists must want to wear a bicycle helmet in general. Then, they need this new model with networking and warning abilities. Last but not least, only some new Volvo models offer the necessary networking and warning features that work with this helmet. Such a

cooperative systems that is meant to save lives particularly needs a high equipment rate. Because of the low market share of single manufacturers it is necessary that several companies agree on a standard and apply it. Because of licensing and reputation it is not very likely that other manufacturers just apply Volvo's implementation. Rather an open standard is needed that is developed by several companies from the start to fit everyone's needs.

The standardization of a new traffic related communication called V2X represents such a development. Several european manufacturers and research institutes gathered in the so called *CAR 2 CAR Communication Consortium* (C2C-CC). They work on a non-commercial basis to improve traffic safety by cooperative intelligent transport systems. The key technology is the vehicle to vehicle and vehicle to infrastructure communication, in short V2X. Is uses the 5.9 GHz band and special protocols to share data between equipped road users. The IEEE has standardized it as IEEE 802.11p as an extension of the WiFi standard. The European Telecommunications Standards Institute (ETSI) reserved the frequency band for applications of intelligent traffic systems (ITS) within Europe. Within the C2CCC, a reservation of the same band is also projected for the USA and Japan. Several applications are under development to share data between equipped vehicles and infrastructure. Because of the high amount of participating manufacturers all over the world and already succeeded standardization it is very likely that V2X becomes a standard feature in vehicles, like the airbag did.

But still it must be found out how vulnerable road users can participate and be equipped, too. Possible solutions are being researched at the ifak e.V. in Magdeburg, Germany. This done within the joint research project UR:BAN
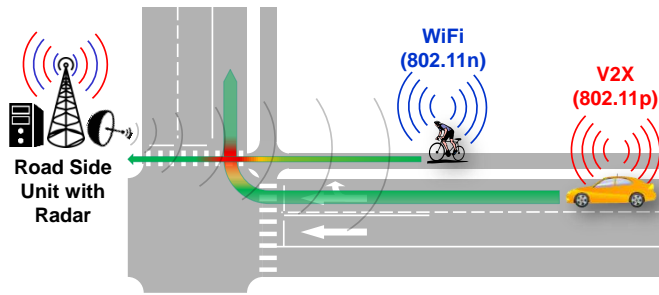
Fig. 1. Overview of an intersection where a vehicle and a cyclist could collide, with the predicted conflict area in red.

(UR:BAN Consortium (2013)): Here, several companies, cities and research institutes gathered to develop driver assistance and management systems for the city. One field of research is the smart intersection with several cooperative applications that use V2X communication. One is the so called *cyclist and pedestrian protection system*: These vulnerable road users shall take part in V2X communication via suitable devices. They share data with vehicles and infrastructure at dangerous intersections to predict and prevent collisions. One idea is to use existing hardware and devices of the vulnerable road users to achieve a high penetration rate from the start: Smartphones can share data and receive warnings via WiFi. The interface between V2X and WiFi can be implemented on infrastructure side.

All associated devices and applications that are incorporated or have been developed especially for the protection of these road users compose the protection system. This paper describes details of the research as well as a developed demonstrator.

2. USE CASES AND GENERAL ARCHITECTURE

There are many traffic situations that can serve as possible use case for a protection system. In general they can be found everywhere where a collision between vehicles and vulnerable road users is possible. According to (Forester, 1993), the most car-bike collisions happen at turnings and crossings. Within the UR:BAN project, especially those intersections with a traffic signal timing that gives vehicles and vulnerable road users green at the same time are considered especially dangerous and therefore represent a typical use case.

In particular, two traffic situations shall be considered: The driver of a motorized vehicle wants to turn right at an intersection which also has a bicycle path crossing. In the first scenario, a cyclist also approaches the intersection from the same direction and want's to cross it. In the second scenario the cyclist comes from the opposite direction, but on the same bike path.

The aim is to detect road users, predict collisions and prevent them via suitable warnings. This shall be achieved via sensors, networking and available human to machine interfaces. V2X communication can be the appropriate technology to link motorized vehicles: Because of the defined standard, a protection system can use the defined message formats for status and warning messages. This is described in section 4.

The best solution would be to equip all cyclists and pedestrians with V2X transceivers. But the willingness to buy and carry extra devices would be too low and therefore also the penetration rate. The idea is to use hardware that is already in use for other reasons: smarthphones, and also the upcoming wearables like smartwatches. Developing and supplying applications for them has the potential to achieve a much greater penetration rate. Section 5 lists some possibilities on how to collect status data this way.

Mobile devices like smartphones have transceivers for WiFi in the 2.4 or 5.2 GHz band, while V2X communicates in 5.9 band. Because of this physical difference, an interface is needed as a kind mediator. Because intersections are the main areas of application, an infrastructure solution is suitable: In connection with other V2X applications, special application units shall be connected to V2X transceivers. They shall be installed as *Road Side Units* (RSUs) at appropriate intersections. The protection system shall be one application among other V2X related ones that can be installed on every of these RSUs. Figure 1 gives a simplified overview of the whole system and its components.

The following message formats are standardized and can be utilized for the protection system:

- Cooperative Awareness Message (CAM): Generally for cyclic status data *from* equipped road users, e.g. with position and speed. In the protection system this message type can be used to detect approaching vehicles that pose a thread to vulnerable road users.
- Decentralized Environmental Notification Message (DENM): Generally for non-cyclic information *to* equipped road users. Can be used to send warnings in the case of a predicted collision.
- Signal Phasing and Time (SPAT): Information about the current status and phases of traffic lights. Could be used to only predict collisions when both vehicles and VRUs have a green light at the same time.
- Topology Message (TOPO): At an intersection this gives position information about the approaches and its lanes. It could be used to save positions of bike paths and vehicle lanes to verify position data.

In addition to collecting data from the road users themselves, sensors on the infrastructure side can improve their detection. For the present protection system, a special radar sensor is used - see section 6. Last but not least the RSU shall take over the task of calculating collision probabilities, which is described in section 7.

The protection system shall warn vehicles, pedestrians and cyclists about each other if they are about to cross an intersection at the same time. Figure 1 gives an overview of a possible conflict situation and with which technologies data is gathered. In the first step, sensors are needed to detect the presence and route to calculate the possibility of a collision. Second, status data and warnings must be transferred via a communication channel. Vehicles are equipped more and more with sensors for satellite navigation (GNSS), thus they are able to provide their position. And just recently, V2X communication has been standardized and is about to be equipped as standard in many vehicles (e.g. see CAR 2 CAR Communication Consortium (2015)). Different message types have been

defined to send status data cyclically, as well as to receive event messages. For a high benefit by cooperative systems like the protection system, a certain rate of equipped V2X transceivers will be needed.

Vulnerable road users also need to measure and tell their position and heading, as well as receive notifications. Nowadays it is quite common to carry mobile smart devices. They can be smartphones, smartwatches or even smart glasses. They offer adequate sensors like GNSS, compass and gyroscope to track their route. Also, important traffic information can be given via display, sound or vibration. The problem is that such mobile devices do not possess chips to use V2X communication. Instead, they can communicate via Wi-Fi.

Eventually, the traffic infrastructure shall be used as a third party to connect vehicles and vulnerable road users. A *road side unit* (RSU) is equipped with V2X, as well as Wi-Fi modules to communicate with all kinds of road users. In addition to that, a radar shall help to detect even unequipped objects.

3. ROAD SIDE INFRASTRUCTURE

Because vehicles and vulnerable road users cannot communicate directly, an infrastructure solution is added. The installation is called *Road Side Unit* (RSU): First, it consists of an *Application Unit* (AU). This computer runs several applications and manages data from connected interfaces and sensors. One interface is a *V2X Communication Unit (CCU)*. It has a transceiver for the 5.9 GHz band and a software protocol stack to decode V2X messages. Within the UR:BAN project, a special application on the AU saves received V2X messages in an own format. Thus the contained data can be accessed by other applications on the AU. Another interface is a WiFi transceiver. With it the communication to vulnerable road users with WiFi capable devices can be established.

Topographical information about an intersection can be stored in a file and distributed cyclically via the RSU and topology (TOPO) messages to all V2X users in the vicinity. Thereby the coordinates of all lanes with connections to each other are available for correspondent applications. For a protection system, this message type could be used for two reasons.

The first is identifying road user types by their position. Vulnerable road users are most likely to be on sidewalks and bike paths. But currently, the communication medium (V2X or WiFi) alone indicates the status as vehicle or vulnerable road user, assuming that only vehicles are equipped with V2X. Additionally, the vehicle type must be given in the list of tagged values of a CAM. This helps identifying road users, even when vulnerable road users are equipped with V2X technology in the future. Last but not least, bike paths must be recorded within TOPOs. Currently, rather only road lanes are encoded, because just vehicles are the planned to be the message receivers for day one V2X applications. It would cost additional effort to extend the TOPO information just for the protection system.

The second reason to use TOPOs could be to identify crossings of road lanes, sidewalks and bike paths, respec-

tively. But even when bike path coordinates are recorded, the lane positions typically end at the intersection's stop lines. Just from TOPOs, the intersection of lanes and bike paths behind stop lines cannot calculated automatically. Because of the problems with these two reasons, TOPO messages are currently not considered for being used in combination with the protection system.

Another information that RSUs can deliver via V2X are the signal phases of the intersection's traffic lights. Via an extra connection, their signal states can be read and distributed via Signal Phasing and Time (SPAT) messages. Also, a prediction of signal changes is possible. But this and the certainty depends on the type of the phase control and if it can be changed dynamically, e.g. by preemption of ambulance vehicles or public transport. Acceptance by the user of a new safety related application is a key attribute for its success. The higher the correct collision prediction and dissemination of warnings that are comprehensible, the higher is the acceptance. If a vehicle and a cyclist approach the intersection and would collide by just regarding their trajectories, they still could have red lights. Only when both have green lights in addition to their predicted crossing at the same time, affected road users should be warned. Therefore, processing SPAT messages is not mandatory for a protection system but can improve collision certainty and therefore user acceptance.

4. DETECTION OF VEHICLES VIA V2X

The data exchange with motorized vehicles is done via V2X (also: Car2X) communication. A vehicle must be equipped with a V2X CCU. This way it can send and receive standardized messages. Sharing its status data occurs by sending *Cooperative Awareness Messages* (CAMs) cyclically. These broadcast messages can be received and decoded Road Side Units running the protection system application. Among many others, a CAM contains the following mandatory parameters which can be utilized for the protection system:

- Position (latitude and longitude in the WGS 84 coordinate system)
- Speed, longitudinal acceleration and heading
- If the left or right turn signal is on

For position measurement, the vehicle itself or the V2X CCU have a built-in sensor for the *Global Navigation Satellite System* (GNSS). Though the American service GPS is mostly used as synonym, these sensors usually also use other services, e.g. the Russian GLONASS. An advantage is the refinement by using other sensor data, e.g. the wheel speed. Therefore, the protection system can expect already improved position and movement data from CAMs.

With position, speed, acceleration and heading, the current trajectory can be calculated. This gives the information, at which time the intersection will be reached. For this, the intersection's topology can be used: By knowing the position and course of all lanes, the position of the vehicle can be matched against a single lane. This geometry data is decoded within V2X *topology* (TOPO) messages which can be provided by the road side unit.

Because only turning vehicles pose a danger, this must be predicted, too. If there is a lane that is solely for turning vehicles and a vehicle is matched against it, it can be assumed that it will turn if it stays on this lane. Another possibility is to use the turn signal status flags within a CAM.

5. DETECTION OF VULNERABLE ROAD USERS

Cyclists and pedestrians don't own V2X hardware, but most of them carry a smartphone these days. And all of them are equipped with a Wi-Fi transceiver. Therefore, one part of the protection system is an application for such mobile devices, e.g. an Android app. It is assumed that a user has installed the app and has it running in the background. Also he has added the RSU Wi-Fi network with name and key once. If he approaches the intersection and the signal gets strong enough, the device automatically logs into the network and the app starts transmitting status data cyclically. As an alternative, the use of data glasses is also being researched. They extend the smartphone app by being able to display a warning directly in the field of view. An arrow can indicate the direction where a danger is ahead.

Theoretically, the V2X formats for CAM and DENM could be used to structure the data. But the overhead would be quite large when just a few values are needed. Eventually, just these data are currently transmitted cyclically from the mobile device:

- Position (latitude, longitude)
- Speed, longitudinal acceleration and heading

The source of the position data is the satellite navigation system (GNSS), like GPS. To improve its accuracy, filters and the data of other sensors are applied. E.g. the acceleration sensor helps to detect a periodic movement. Steps of pedestrians are one example. By knowing the step size, the device carrier's velocity can be calculated via the step frequency. This can correct or even replace missing GNSS data.

6. RADARS FOR POSITION IMPROVEMENT AND ADDITIONAL ROAD USER DETECTION

Like stated before, the equipment rate is a critical point for the success of such a protection system. If a road user is equipped with an appropriate device to get warned mainly depends on two factors: First of all, his will to invest into such a device, like buying a car with V2X capabilities or installing the application on his mobile phone. Secondly, legal regulations could force road users to use such protection features. This could come true one day for V2X communication to be equipped in every new car when this technique proves itself. But it can be doubted for vulnerable road users where equipment like bicycle helmets is not dictated.

But the plain detection of road users can be improved by installing additional sensors and connecting them to the application unit. This offers two advantages: Firstly, detect those road users that are not capable to tell their position via any wireless communication. And secondly, GNSS position data of equipped road users can be improved.

Cameras are one possibility. But firstly, procession of video data needs quite some computing power which would raise the costs of an appropriate and powerful RSU. Secondly, such optical sensors can get dirty quite easily and therefore need regular maintenance. And thirdly, the acceptance of cameras in public space can be quite low, for privacy reasons. Therefore, radar sensors have been evaluated as an alternative. Because only approaching road users matter for a collision detection, one sensor for each intersection approach suffices.

For the presented project, an *UMRR sensor* from Smart-micro (Smart Microwave Sensors GmbH, 2015) has been chosen and installed at some research intersections. In fact, this device consists of several sensors in one housing to measure different parameters of obstacles, like their speed. It combines the measurements and supplies them in an already interpreted form. The protection application does not need to compute image data or the like. By connecting the sensors to the application unit via CAN or Ethernet and setting up a TCP server, all UMRR radars connect automatically and send their object detection data cyclically. Thus the protection application on the AU can work with the following values:

- Object ID: The radar already tracks individual objects when they come in sight and reassigns this ID not before the object has left the field of view.
- Range: Distance from the radar installation point.
- Speed
- Acceleration

Initially, all detected objects are saved as independent road users. In a new collision prediction cycle, these radar objects are compared separately to vehicles and vulnerable road users (GNSS objects) which where detected via wireless communication. Now, three cases are possible, which are also presented in figure 2:

- Within a certain radius to a GNSS object, there is *only one* radar object.
- Within a certain radius to a GNSS object, there is *more than one* radar object.
- Within a certain radius to a radar object, there is no GNSS object.

When there is only one object within a certain radius, they are probably the same physical objects (case 1). The GNSS position can be corrected with the radar position, according to a reliability factor. This determines which position determination method is more reliable. For a first implementation, 0.5 was chosen to set the new position right between the two old ones. Alternatively, it could be something like 0.9 if the radar was far more reliable than the GNSS position measurement.

When there are several radar objects near a GNSS object it is difficult to determine which belong together (case 2). In this case, no correction occurs. It couldn't be determined in which direction and with which factor these points should be weighted.

After all GNSS positions have been corrected by available radar data, there still can be radar objects with no corresponding GNSS object (case 3). Probably these are unequipped road users. The position determines if they
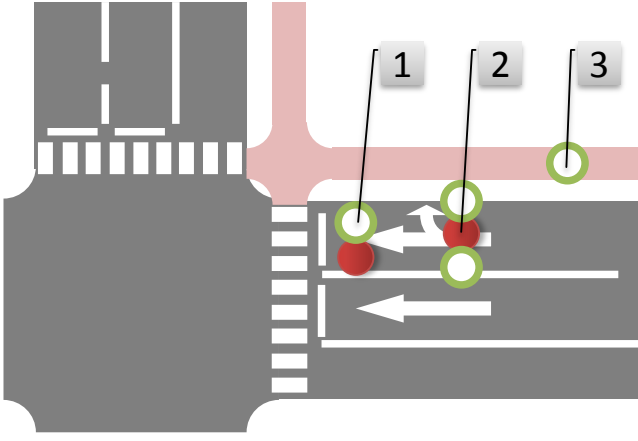
Fig. 2. Overview of an intersection where objects have been detected by V2X communication (full red circles) and a radar (green hollow circles). In the displayed three cases a correction is possible (1), not possible (2) or unequipped road users can be detected additionally (3).

are on the road or the bike path and therefore their type. These objects will be added to the list of vehicles or vulnerable road users, respectively. In the collision detection algorithm their positions can be still used to predict collisions and to warn equipped road users. E.g. in figure 2 for case 3, the radar has probably detected a cyclist on the bike path. A disadvantage is that only speed and acceleration data are directly available via radar. Acceleration and heading must be calculated by the application unit, if needed.

7. COLLISION PREDICTION

With the gathered data, the protection system's application on the infrastructure's application unit can predict possible collisions. The following data is available:

- At least position and speed of detected road users
- Topology of the intersection - at least crossings of street lanes and bike/pedestrian paths
- Traffic light status, if SPaT messages are available, decoded and supplied for the protection system application

Only collisions between different road user types shall be predicted. Therefore, all vehicles are compared to all vulnerable road users. For such a pairing, the *time-to-collision* (TTC) can be calculated. This is the time a road user needs to get to the point where a collision is possible. In this case, this is the crossing between the bike/pedestrian path and the lane where turning cars would drive into the next approach, like depicted in figure 1. For the both cases where a turning car could come from the same or the opposite direction as a vulnerable road user, this crossing area is the same. If there are several lanes in the next approach, the crossing area could again be divided. But for simplification and normal sized urban intersections, one crossing area for one approach should suffice. It can again be approximated as one point. This can be written once in a configuration file that the protection application loads at start-up.

The next issue is the positions of the different types of road users. They are gained from different measurement systems: Status data from vehicles and mobile devices like smartphones supply latitude and longitude of the global WGS 84 coordinate system. But each radar sensor has its own local Cartesian coordinate system. To make them comparable, positions are converted to a reference system. Its origin is the reference point of the intersection. This is also given in TOPO messages, if at hand.

For a first and prototypical solution, just the momentary positions, speed, acceleration and heading can be used to calculate the time an object needs to reach a crossing. For an advanced development, an object's history could be recorded to filter movement data and to get a more accurate trajectory. But the tracking of individual moving objects over time is quite difficult. When a radar loses an object for a short time, finds it again and labels it with a new ID, this object has probably a new position and even another velocity. Vehicles don't even send an Id via V2X communication for privacy reasons. For these objects it would be hard to determine if different data sets belong together. Therefore, the protection system shall rely on the built-in correction: The radar has an own tracking mechanism. The mobile application for vulnerable road users uses a low-pass filter. And vehicles correct their data via other sensors like wheel speed.

A problem that can be incorporated is tailback. If the traffic light is red and several vehicles wait in line, they will need some time to accelerate when the light turns green. This increases their individual TTCs, according to their position in the queue. This can be detected by the radar. According to (Forschungsgesellschaft fr Straenund Verkehrswesen, 2001), approximately two seconds pass for the start-up of every vehicle. With the distance to the stop line d_{SL}, the length of a vehicle l_V and the distance between two vehicles d_V, the delay Δt (in seconds) for the start-up of a certain vehicle can be estimated:

$$\Delta t = \frac{d_{SL} \cdot 2s}{l_V + d_V}$$

When the time-to-collision for a specific pairing has been determined, the difference is calculated. If it is above a predefined threshold, a collision is considered as very likely. A good threshold still needs to be determined experimentally. A value of about a few seconds seems to be probable.

This boolean result of a probable collision can be combined with the traffic light phases, if they are at hand. Both the turning vehicle and the vulnerable road user must have a green light at the time of the predicted collision. This time point t_C must be between the switching time to green t_{SG} and back to red t_{SR}:

$$(t_{SG} < t_C) \wedge (t_{SR} > t_C)$$

8. WARNING OF VEHICLES VIA V2X

Assuming that a collision has been predicted for a certain pairing, both road users shall be warned via their wireless communication. While V2X CAMs from vehicles are emitted cyclically, events like warning messages are only sent for a specific period of time. They are encoded

within *Decentralized Environmental Notification Messages* (DENMs). An advantage of V2X is the standardized message format: Any application just has to fill in its parameters according to the standard. A V2X capable vehicle can decode and interpret it without being programmed for this specific application. This way, the protection system can send a DENM to warn of people on the road in some distance. How this is being presented is totally up the vehicle's manufacturer.

The following parameters can be used for a warning from the protection system:

- Cause code and (optionally) sub cause
- Severity
- Location Reference
- Destination Area

With the cause code, 'people on the road' can be given as a reason of the event. The advantage is that the V2X system of a vehicle does not need to know about the protection system. The understanding of the general warning does not require a further implementation. If a manufacturer adds a warning handling for people on the road, maybe by displaying a message, this will work for all applications sending out these DENMs. Because vehicles can't by identified by an unique ID, DENMs are sent as broadcast. The vehicle's computer system decides for itself if a received message is relevant. This is mainly done by two things: Firstly, the *location reference*. This is the danger's location, in this case the crossing with the vulnerable road user in the middle of the lane. Secondly, the *destination area*. This is the area where the sending application thinks that the DENM is valid. In this case it could be a rectangle which marks a lane where vehicles that could endanger cyclists are approaching. Unfortunately, only one area can be given. When several lanes from several approaches can be the destination area, the whole intersection should be marked.

The vehicle's manufacturer can decide for himself what to do with the warning. Most probably it will be displayed in the instrument cluster or any other kind of HMI (human machine interface). Also, vibration in the steering wheel is possible. But for a first evaluation of the protection system, a tablet computer has been utilized. One single mobile application has been developed for mobile devices of vulnerable road users, as well as the vehicle's tablet. By using the *Qt* framework (The Qt Company, 2015), this even happens platform independent: The C++ source code can be compiled for different operating systems like Android, iOS and Windows Phone. First, the user chooses his role, i.e. if he's a cyclist, pedestrian or travels with a motorized vehicle. This determines mainly if status data is send and the warnings being displayed. For the protection system demonstration, an additional application has been installed on a test vehicle's V2X CCU. If the protection system's road side unit broadcasts a DENM to warn of a cyclist at the next intersection, it is received by this. The additional application reads the DENM, extracts the most important parameters and sends them via WiFi to the tablet. Here, a warning of the cyclist is shown. Such an additional warning via smart devices could complement existing systems like the built-in HMI some day in the future.

Fig. 3. Screenshot of the developed smartphone app, showing a warning.

9. WARNING OF VULNERABLE ROAD USERS

Vulnerable road users can be warned via the same devices that collected and shared the status data. For the prototypical protection system, WiFi is also utilized as the return channel. Because the road side unit will emit warnings as long as the collision is probable, several messages will be sent for one event. Within a UDP data packet, these information will be encoded amongst others:

- Event ID
- Cause code (e.g. blocked road or turning vehicle)
- Location of the event
- Distance to and direction of danger

The same application as the one for the vehicle's mobile device can be used. Figure 3 shows a screenshot of a warning for a cyclist.

Receiving devices like smartphones offer several ways to alert the wearer:

- Display
- Vibration
- Audio

Displaying a warning only makes sense when the user can see the display. Of course it cannot be demanded from a user to hold the smartphone in his hands and watching it the whole time for being able to be warned in dangerous situations. The only possibility is to mount it on the bicycle's handlebar, like done for navigation purposes. Furthermore, a warning message on the smartphone's display should be as simple and intuitive as possible. The amount of text must be at a minimum. Pictograms in different colors are a better method signalize events. Common color codes should be used: Yellow for normal warnings, e.g. a predicated collision on a crossing that is still far enough away. Or of a closed bike path, known through other services. Red is used for severe warnings that suggest a stop, like known from traffic lights. In the demonstration app, a red warning triangle has been implemented. In addition, an arrow can indicate the direction of the danger. The user shall be instructed to look over his shoulder to identify the cause of the warning and react accordingly. But still,

the user cannot watch the display the whole time while being in traffic. Therefore, displaying warning messages must be considered not very reliable and should always be accompanied by another warning method.

One further method is *vibration*. The advantage is that the wearer can have the device in his pockets and can still be notified. But first, the vibration of a smartphone is often not strong enough to be felt every time and while riding a bike. Second, it can be easily misunderstood as an incoming call. Last but not least, the direction of the danger cannot be indicated. Therefore, this kind of warning is also not very reliable when used alone. But it also shouldn't be used when mounted to a handlebar, because this could loosen the fixation.

The third possibility is to use *sound*. In addition to a warning sound, a voice output can be used to inform about the type and direction of the danger. The problem of this warning type is the possibility to use sound while being in traffic: When using the loudspeaker, it could be drowned by traffic noise, especially when worn in a pocket. And waring headphones can be dangerous and even be forbidden for cyclists.

All in all, warning users via their smartphone may sound like a good idea because of the high penetration rate. But no type of warning fits all needs of being save and noticeable at the same time. Mounting a smartphone to a bicycle's handlebar and using audio output via loudspeaker at the same time seems to be the best solution.

Apart from smartphones, any smart device a vulnerable road users is willing to wear additionally or is wearing already can be utilized. They can also be called *wearables*. In connection with the presented project, these warning methods have been reviewed and tested:

- Commercial data glasses
- Home-made glasses with LEDs
- Vibration wristband

Within the UR:BAN project, the warning via novel data glasses has been researched. A research for available devices has shown that many manufacturers like Google, Epson and Sony have already launched a product for end customers or are about to do so around the year 2015. While the Google Glass may have caught most of the media's attention, it lacks a main requirement for augmented reality and safety applications in traffic: Being able to display information in a relatively large field of view, including both sides. Google Glass projects an image only to the right lens, so that an application can't display information like a warning on the left side. But to produce an intuitive reaction of the wearer it is advised to show a warning on the side where a potential danger is coming from - e.g. an approaching car.

Considering this and other requirements like a good development kit and product availability, the *Epson Moverio BT-200* has been chosen. It was included into the protection system's demonstrator and a proband test to evaluate the acceptance of different warning devices. It has a prisma build into every lens. Thus a projected image appears to be like a computer screen, floating in some distance. An additional mobile device with battery, sensors for GNSS

Fig. 4. Example of what a user with data glasses sees when warned of a danger from the left.

and acceleration and a touch surface is attached to the glasses. It runs an Android operating system, so that every Android app can be used and viewed with the glasses. Also, the application for the vulnerable road user can be implemented as an Android app. Theoretically, the existing smartphone app could be extended for the glasses. But because it requires its Android-only development kit, it was easier for development to separate the two application: One is portable and can be installed on smartphones and the glasses mobile device for collecting and sending status data. The second can just be installed on the glasses mobile device to receive and display warnings.

It is possible to disable the projection so that a cyclist could wear the device without being distracted by any unnecessary information or even just a black background. Only in the case of an imminent danger an arrow indicates its direction. This information can be used to let the user look over his shoulder to really see the cause and to react accordingly. Also, by not displaying something in the middle of his field of view, the user still can see the road and his environment. While the color red seems to be a good color for such warnings, the human eye can recognize much less red on the outer field of view (Utesch, 2014). This is due to the different distribution of cone cells which are responsible for color vision. In the peripheral view, blue and white can be see much easier than red and green. Therefore, a white warning arrow has been implemented. As (Utesch, 2014) also states, the peripheral view is preferred over the center view in information processing. The human brain suppresses the center perception when it detects a moving object in the peripheral view to lead attention to it. Therefore, the warning arrow has been implemented with a movement animation. An example is shown in figure 4.

Other appropriate devices could be smartwatches and Volvo's bicycle helmet. The problem is always how they can be connected to the cooperative infrastructure. If V2X proves itself successful in the next years, the integration of appropriate transceivers into wearables will gain importance.

10. CONCLUSION AND OUTLOOK

There is always a demand for traffic solutions that lower accident rates. To warn turning vehicles and vulnerable road users at dangerous intersections, a network communication can be utilized to share presence information. The upcoming V2X technology has just been standardized and may offer an ideal way to link motorized vehicles. The main challenge is to communicate with cyclists and pedes-

trians to incorporate them into the network. This paper presented a possible solution that has been researched along with the UR:BAN project and has already been tested with a demonstrator. And apart from the presented protection application the collected data of cyclists and pedestrians can easily be used for similar applications.

Because the V2X message formats have been normalized, status data from equipped vehicles as well as warnings to them can be send. One big advantage of the presented protection system is that it does not need the implementation of additional hardware or software. It is only one among many V2X applications so that vehicle manufacturers can realize reaction handling in general which will work with all kinds of applications that send a warning of people on the road.

To overcome the problem that vehicles and vulnerable road users can't communicate with each other directly, a road side unit complements the cooperative system and creates an intelligent intersection. Radars as additional sensors have been evaluates and tested successfully to correct position data and even detect unequipped road users. This helps to raise the effectiveness of such an application in the first years after its market launch.

To communicate with vulnerable road users it is proposed to use existing devices and wearables. The most reasonable solution is to offer a special application for smartphones. By using Qt as a platform independent framework, the app can be compiled for different mobile operating systems. This also helps to increase the penetration rate. The app collects and sends status data to the road side unit. In return, warnings can be received and be represented via the display, audio output and vibration. A smartphone fixated on the handlebar of a cyclist that gives visual output and a phone in the pocket of a pedestrian that vibrates belong to the best solutions to warn such road users nowadays. For future applications, the Epson Moverio as an example for data glasses has been evaluated. It is another example of smart devices that a vulnerable road user may carry anyway and therefore can easily be incorporated into a cooperative traffic system.

One main challenge of such cooperative systems is the penetration rate. If a road user is not equipped with appropriate wireless technology he cannot be warned. At least, the detection is possible via sensors at the infrastructure. Vehicles have quite a long lifetime, so that new features like V2X need some time to raise in equipment rate. According to (U.S. Department of Transportation, 2011) it could take 13 years before 90% of the population is equipped.

Last but not least, the development, verification test and maintenance can be highly supported by automated testing methods and tools. At the ifak, an own tool chain has been developed to test such distributed traffic system. E.g. the network communication of V2X or WiFi can be checked automatically against a targeted behavior to identify problems. Some descriptions can be found in (Russ, 2014) and (Krause, 2013).

REFERENCES

CAR 2 CAR Communication Consortium (2015). URL www.car-2-car.org.

Elfstroem, S. (2014). Volvo cars, poc and ericsson demonstrate cloud-based wearable cycling tech concept. URL www.media.volvocars.com.

Forester, J. (1993). Effective cycling. URL www.borealisoutdoor.com.

Forschungsgesellschaft fr Straenund Verkehrswesen (2001). *Handbuch fuer die Bemessung von Straenverkehrsanlagen (hbs)*.

Krause, J. (2013). Secure traffic networks - a method for model based security tests in the field of its. In *20th World Congress on Intelligent Transport Systems*.

Russ, T. (2014). Neuartige diagnosemethode fuer netzwerke der smart city. In *VDE-Kongress 2014 Smart Cities*.

Smart Microwave Sensors GmbH (2015). URL www.smartmicro.de.

The Qt Company (2015). URL www.qt.io.

UR:BAN Consortium (2013). Urban space: User oriented assistance systems and network management. URL urban-online.org/en/urban.html.

U.S. Department of Transportation (2011). Aashto connected vehicle infrastructure deployment analysis. URL www.car-2-car.org.

Utesch, F. (2014). *Unscharfe Warnungen im Kraftfahrzeug. Eignet sich eine LED-Leiste als Anzeige fuer Fahrerassistenzsysteme?* Ph.D. thesis, TU Braunschweig.

Safety in Pedestrian Navigation: Road Crossing Habits and Route Quality Needs

S. Schwarz, D. Sellitsch, M. Tscheligi and C. Olaverri-Monreal

AIT Austrian Institute of Technology GmbH, Innovation Systems Department, Business Unit Technology Experience, Vienna, Austria (e-mail: {Stephanie.Schwarz, David.Sellitsch, Manfred.Tscheligi, Cristina.Olaverri}@ait.ac.at).

Abstract: Still most commercial navigation tools used by pedestrians fail to encompass a comprehensive organization and prioritization of safety-related route qualities and accordant information in the user interface. To support pedestrian route choices to minimize potential dangers, we study in this paper user requirements for an enhanced pedestrian navigation system that considers safety related route quality parameters. Besides effectiveness, related factors of distance and time, safety was highly prioritized to become an explicit requirement for the conceptual design. The acquired data from an online survey provides the basis for pedestrian's classifications and requirements regarding user friendly interfaces for mobile routing and navigation that enhance road safety.

Keywords: Pedestrian Navigation, User Requirements, Road Crossing, Safety.

1. INTRODUCTION

As members of the digital age, pedestrians have come to rely more heavily on mobile navigation as a means to find ones way throughout varying contexts of foot travel. Perhaps the individual is intent upon finding the fastest walking route to work, or a more scenic route to a place of interest, or simply as a means of familiarizing oneself with new surroundings. As a prominent example, in 2013, Google Maps was the most used app worldwide, providing valuable information for pedestrians (Hedencrona 2013). However, available maps often provide rather general information, not tailored to the actual needs of the pedestrian. Still most commercial navigation tools used by pedestrians fail to encompass a comprehensive organization and prioritization of safety-related route qualities and accordant information in the user interface.

It has been stated that poorly designed user interfaces can affect visual attention from the road and decrease road safety. Additionally, cognitively demanding interaction indicates a reduction in the traffic situation awareness (Olaverri-Monreal and Bengler 2011). In a vehicular context, proper in-vehicle warnings and function location that enhances visibility and reduces the distraction potential has been the focus of design by automotive manufacturers (Olaverri-Monreal et al. 2014). However, this has not been extended to mobile devices that are increasingly being used in a road context. As usability is one of the factors to be considered in an ergonomic design, it is crucial to determine the needs of the pedestrians through a user centered approach.

To support pedestrian route choices to minimize potential dangers, route qualities such as e.g. safety (including safe crossing facilities, motor traffic volume and speeds) need to be considered in the design of pedestrian navigation systems (Czogalla and Hermann 2011).

The use of mobile phones by pedestrians (for talking, texting, reading), affects their awareness of the surrounding environment, hence augmenting the risk of incidents. Moreover, it has been stated that pedestrian behavior varies at road crossing (Thompson et al. 2013). Observing pedestrians crossing streets has shown that mobile phone users exhibited more unsafe behavior than other pedestrians. Moreover, mobile phone users are far less likely to recognize crossing opportunities, which results in slower crossing times (Neider et al. 2010). Hence, pedestrian distraction associated with mobile phone usage is a very prominent, contemporary safety issue, particularly relevant in urban environments with high traffic density. However, most mobile solutions rather neglect the risks related to the influence of mobile phone usage in a situation where traffic needs to be considered.

Particularly, pedestrian navigation and routing systems need to be developed in a user friendly manner that enhances road safety and provides an optimal user experience. Additionally, persuasive technologies should be applied into the development of mobile applications to promote more desirable pedestrian behavior and motivate pedestrians to adopt less risky behavior by providing specific information regarding road conditions and possible disturbances on a route (Fogg 2009) such as for example accurate information regarding available access conditions, location and type of near crosswalks.

In this work, we study user requirements for an enhanced pedestrian navigation system that considers safety related route quality parameters:

(1) We determine pedestrians usage routines in relation with existing navigation and route planning tools in urban environments on a daily basis.

(2) Relying on studies of route quality including route safety, comfort, attractiveness and accessibility (Czo-

galla and Hermann 2011), we collected information related to preferences of routes to dissociate between main characteristics of route quality and preferences, and thus allowing for the definition of corresponding pedestrian user groups.

(3) As part of a user centered design process (UCD) consisting of a multi-disciplinary design approach based on the early and continuous involvement of end users we sought a more clear understanding of user requirements relying on related studies (Vredenburg et al. 2001).

Although previous works have targeted the classification of users of pedestrian navigation tools (i.e. Wen et al. 2013), there is still an important need to elaborate a comprehensive typology that aligns user preferences to different route quality parameters provided by todays navigation tools. Therefore, this work focuses on the assessment of self-reported habits toward different types of road-crossing behavior (i.e. optimal, distractive, risky) in Austria, to uncover less visible attitudes and routines related to the use of mobile tools in traffic related areas.

2. RELATED WORK

According to a study from Thompson et al. 2013, 29.8% of 1102 pedestrians performed a distracting activity while crossing the road. The specific activities were distributed in the following way: 11.2% listened to music, 6.2% were involved in a phone conversation holding the phone and 7.3% were texting. The crossing time was longer during the texting activity and the eyes were also diverted from the road, indicating these results that texting was the most dangerous activity compared to the other two.

These results were confirmed by the authors in Schwebel et al. 2012 that also compared the same dual task situations: crossing while talking on the phone, crossing while texting, crossing while listening to a personal music device, with crossing without performing other tasks. Their results suggested that although all three situations caused attention to deviate from the road, texting and listening to music while crossing were considered to be more dangerous than talking on the phone.

In Neider et al. 2010, results from several simulator tests showed that pedestrians are less likely to cross a road without being involved in a road accident when talking on a phone (in a hands free situation) than when listening to music. Phone users are also less likely to recognize crossing opportunities. These dual task situations seem to be especially challenging for older people (Neider et al. 2011, Hatfield and Murphy 2007).

Furthermore, other works intended to improve safety for pedestrians in situations where they were particularly exposed to danger while crossing, due to simultaneous tasks that deviated attention from the road. For example, the Android application WalkSafe (Wang et al. 2012), aims to improve safety by using the phone's back-camera in order to detect approaching vehicles and alerting the user in case of an unsafe situation.

In the same context the authors in Chen et al. 2012 notified users via a smart phone app when they were about to cross a potentially dangerous street. They conducted tests in a simulated environment and found out that users were more careful and waited longer before crossing when they received a warning.

An additional work tackled crime related safety issues for pedestrians focusing on assessing the safety of sidewalks by using light sensors for the generation of safety efficient routes (Matsuda and Arai 2014). In accordance with the Japan Security Systems Association the authors stated that brightness of street lights may improve safety. They also suggested including information from crime reports for generating routes.

Illumination was also the target of the work by Miura et al. 2011. Relying on the deployment of a network of sensors, the authors gathered information about road illumination conditions to incorporate them in pedestrian navigation systems.

3. DATA ACQUISITION

As part of UCD process, we designed and developed an online survey that we later deployed among potential subjects within Austria, addressing them directly and attaching the link to the questionnaire. The survey was organized according to the following thematic categories:

3.1 Mobility Routines

The first part of the survey dealt with the collection of mobile users daily walking routines regarding typical ways and routes to reach specific destinations that for example included ways to work, duties (running errands or attending appointments (i.e. visiting public authorities, going to special events, kids school, etc.), as well as leisure activities (e.g. meeting friends, sports, cinema, theater, etc.).

3.2 Experience with Routing and Navigation Tools

In relation with mobility patterns we investigated whether pedestrians make use of (public) transportation means to effectuate their daily routes. Previous experience with (pedestrian) navigation/ routing systems was addressed, i.e. users were asked to report type and use frequency of their preferred (mobile) navigation tools.

We particularly focused on the use of navigation tools for specific route sections in combination with some mean of transportation and specifically asked to enter information related to origin destination matrices such as: from the origin to a public transportation station or from a point of transfer to the destination.

3.3 Road Crossing Behavior

To gather further insight on road crossing behavior, we presented selected statements to respondents which exemplified certain road crossing situations such as texting or reading text on the smartphone or scampering among traffic to cross a road. To this end, we asked participants to complete a modified 10-item version of the Self-Report Habit Index (SRHI), self-report instrument to measure habit strength, which collects data from the features which display a history of repetitive behaviors, the difficulty of controlling behavior, the lack of awareness, efficiency, and the identity element (Verplanken and Orbell 2003). Respondents had to indicate to what extent they agreed to

a certain behavior on a 5-point-Likert scale, by which low scores denoted a more frequent behavior and high scores a less frequent behavior. Based on this, we calculated the mean scores of the SRHI.

3.4 Sense of Direction

Spatial abilities are involved in most of our daily orientation tasks in two and three dimensional surroundings (e.g. reading maps, using navigation tools). Beside psychometric approaches such as mental rotation tests, self-assessed sense of direction such as the Santa Barbara sense of direction scale (SBSOD) (Hegarty et al. 2002), has shown to provide valuable insights to a person's spatial skills. We relied on the SBSOD scale in order to determine the environmental spatial ability of our subjects and investigated possible relationships between individual sense of direction, gender and safety.

3.5 Pedestrian Route Quality Criteria

Previous work on pedestrian quality needs (Methorst 2010) stated the existence of different route quality criteria that influence route choices in pedestrian navigation. In order to determine the factors influencing route selection, we additionally investigated the prioritization of quality parameters based on the classification in Czogalla and Hermann 2011. Furthermore, we asked in our survey to select the main reasons for not using a certain route.

4. RESULTS

4.1 Sample

175 participants correctly completed the survey. The final sample was nearly equally distributed in terms of gender (90 female (51,4%), 85 male (48,57%)). The youngest participant was 19 years; the oldest was 64 years old, while the average age was 37,2 +/- 11 years. The majority of respondents (84%) lived in cities with more than one hundred thousand inhabitants. 101 respondents (57,7%) were fully employed, 29 (4,6%) partly employed, and 21 (12%) currently at university.

Regarding experience with mobile phones and navigation tools the sample turned out to be homogeneous: 171 respondents (97,7%) were experienced in using digital maps, route planning or navigation systems, while 148 users (84,6%) answered to use mobile internet services on a regular basis (at least once a day). One participant used a wheelchair. No other participant stated to use any walking aid.

4.2 Mobility Routines

According to the results regarding the mean of transport (multiple answers allowed) people used regularly, 157 (89,7%) named public transport and 103 (58,8%) selected private cars. Private bicycles (72; 41,14%) seem to be also quite popular. Fig. 1 depicts the means of transportation by number of respondents.

Regarding the daily use of the different mean of transport, results showed the choice strongly depended on the nature of the trip. 59,5% of the respondents said they used
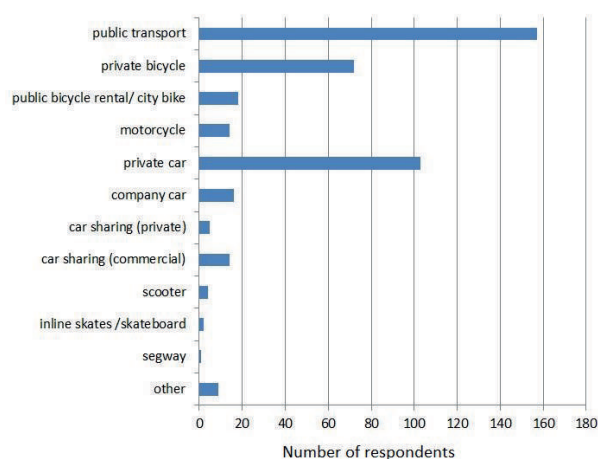
Fig. 1. Preferred mean of transport by number of survey participants
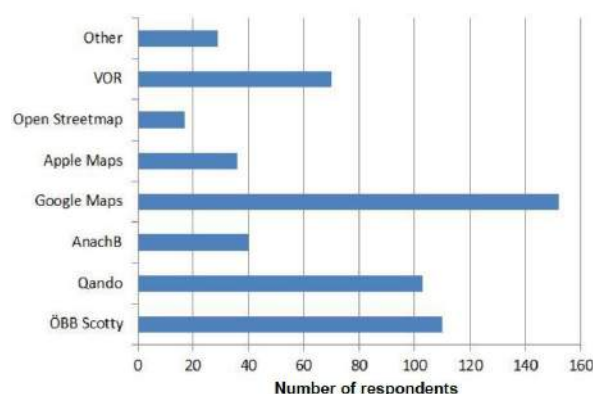
Fig. 2. Preferred navigation apps by number of survey participants

public transportation to go to work, while only 15,8% preferred their car. When asked about duties such as running errands or attending appointments, the results were similar: 50% used public transportation while 37,5% walked and 125% used their private vehicle. According to the results of our survey, 60,7% of the participants preferred go shopping by foot. In their free time, 44,1% of the respondents stated to regularly walk to their target destination and 44,1% indicated to use public transport.

4.3 Experience with Routing and Navigation Tools

The most used navigation apps indicated by the survey participants are depicted in Fig. 2. Google Maps was with 81,7% the most popular, followed by the services provided by the national railway company "ÖBB Scotty" (57,1%) and the local public transport routing assistant named "Qando" (53,7%). Also mentioned but not included in the figure were brands such as "TomTom" (by 5 respondents) and "Garmin" (by 2 respondents), as well as further services from public transportation providers in Austria (i.e. "Wiener Linien" (by 4 respondents)).

Regarding trips in which public transportation was used in combination with navigation tools, our results showed that people use navigation tools mostly to find their way from their starting point to the bus or railway station or from the latter to their final destination (outdoor navigation).
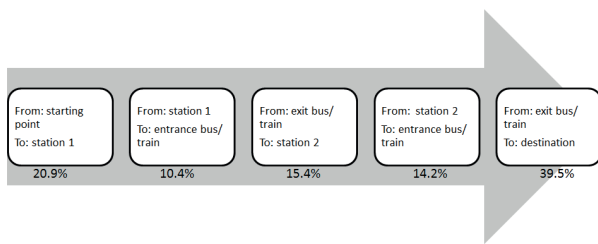
Fig. 3. Transition while traveling using public transport and walking
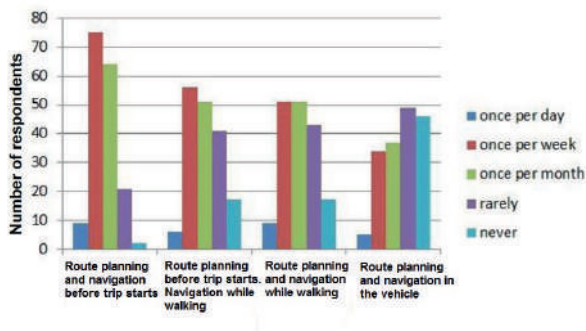
Fig. 4. Route planning strategy by number of respondents

Using navigation to find the way to the train transfer is far less common. Only a small number of people use their navigation system to find their way within a train station, to find out where the train stops (Fig. 3). With regard to the planning of trips, we found that not all the users plan their trips spontaneously while traveling even though 84,6% of the respondents affirmed to use mobile data connection on a daily basis. As a result, planning a route in advance is still very popular (Fig. 4).

4.4 Road Crossing and Pedestrian Behavior

With respect to self-assessed risky behavior, low scores in the SRHI index reflect a strong habit and high scores represent a less frequent behavior. Results indicated that respondents very often crossed the road while vehicles were approaching (M = 2,2; SD = 0,7), while crossing the road at crosswalks was not a strong habit (M = 3,5; SD = 0,9). Finally, respondents indicated to usually avoid texting or reading text on the mobile device during road crossing ($M = 4,0$; $SD = 0,9$), and being consequently not exposed to distraction sources that could jeopardize their safety.

However, looking closely at the data, we could examine differences related to age and habits. According to the Spearman's rank correlation coefficient, there was a significant relationship between age and distractive behavior at road crossings (P = -.333; p<.001), revealing that younger pedestrians were more often exposed to distraction sources such as texting or reading on the mobile device while crossing a road than older pedestrians (Fig. 5).

4.5 Pedestrian Route Quality Criteria and Needs

Results regarding the prioritization of quality parameters based on the classification in Czogalla and Hermann 2011 are depicted in Fig. 6. The figure shows the ranking of the quality criteria and needs from most important (1) to less
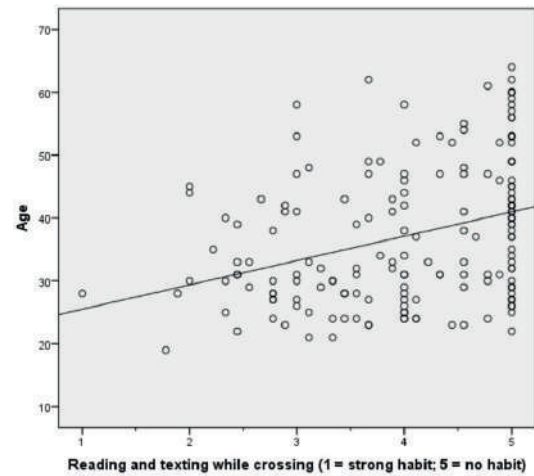
Fig. 5. Relationship between age and distractive behavior at road crossings.
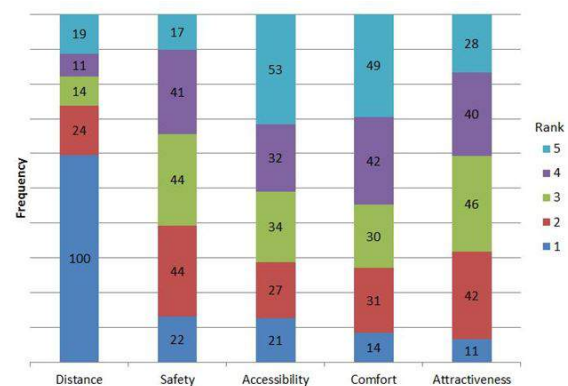
Fig. 6. Prioritization of route quality parameters for pedestrians route choice (1 more important, 5 less important)

important (5).

Furthermore, Table 1, shows the factors influencing pedestrian route selection and behavior and its relationship to the quality criteria in Czogalla and Hermann 2011. As the main reason for a decision to not use a certain route, 100 respondents (72%) classified long distance as the leading quality factor for route choice. The second most relevant criteria was being in a hurry, which is directly related to the distance. More than 40% of the respondents ranked safety as the third factor, parameters included insufficient illumination of the environment or record of criminality, decisive for the selection. Less participants but a still considerable amount of users (36,6%) named overly crowded streets as a parameter to select one or another route. Comfort was not a decisive parameter for routing.

4.6 Sense of direction

Our results showed that there were statistically significant differences in the perceived sense of direction between genders (t(173) = -3,1, p = 0.002), being the mean Santa Barbara-score for men 5,12, SD = 0,8 and for women 4,69, SD = 0,9. Regarding the relationship between safe or risky crossing habits and sense of direction no statistically significant differences could be found.

Factor	Selections#	%	Category
Long distance	126	72,00%	Distance
Short of time /hurry	108	61,71%	Distance
Unsafe route (crime)	87	49,71%	Safety
Poor street lighting	71	40,57%	Safety
Too crowded	64	36,57%	Comfort/Safety
Pavement	41	23,43%	Accessibility
Habits	37	21,14%	Other
Unfamiliarity	28	16,00%	Other
Illegible signage	21	12,00%	Accessibility
Missing guidance	17	9,71%	Accessibility
Missing shelter	16	9,14%	Comfort
Poor infrastructure	15	8,57%	Comfort
Stairs existence	15	8,57%	Accessibility
Steep ramp	13	7,43%	Accessibility
Lacking experience	13	7,43%	Attractiveness
Other	6	3,43%	Other

Table 1. Factors influencing pedestrian route selection

5. DISCUSSION

The survey presented in this work depicted early investigation of mobility and safety related aspects in pedestrian navigation as part of a user-centered design process. We investigated usage routines with pedestrian navigation tools, self-reported habits in relation with road crossing behaviors as well as criteria and barriers for route choice decision.

Overall the results of our survey provided useful insights into pedestrians routines in urban areas regarding the use of navigation tools. As the final sample turned out to be rather homogeneous in terms of the main characteristics (e.g. frequency of use of public transportation, pedestrian usage of navigation tools) certain limitations must be considered in the interpretation of the data from a methodological point of view. As a consequence, the results of the conducted survey are not to be generalized for all pedestrians. However, the sample serves to elaborate on the requirements and design concepts of future safety-enhancing navigation systems.

The study was conducted in metropolitan areas in Austria. As the public transportation in these areas is very good, results regarding the combination of public transportation with walking over using a personal vehicle are not surprising.

Continuous advancements of mobile navigation aids in general aim at enhancing overall effectiveness and comfort in pedestrian mobility. However the use of such mobile technologies in the streets might be a compromising thread for pedestrian safety. Our survey results show that despite all the new technological advances regarding internet connection on smart devices, pedestrian routes are calculated in advance, before leaving the starting point, which hamper safety measures and lead to potentially distracting situations while the navigation tool is being employed. In the case pedestrians were still need to spontaneously check the route several times while walking in traffic areas, future navigation systems could incorporate strategies to motivate the users to calculate routes in advance to foster awareness toward navigation behavior.

Results on road crossing habits showed a higher tendency of younger adults to adopt risky and distractive behavior (i.e. texting during road crossing) than older respondents. Whereas not reflected in our data, previous research identified the effect of age as predictors of unsafe crossings, considering factors such as walking speed, start-up delay, safety margins and subjective walking time estimation of the pedestrians (Holland and Hill 2010). Hence it is assumed that the likelihood of unsafe crossing increases with age. The mentioned work also uncovered the effect of gender on unsafe road crossing decisions in adult pedestrians. With increasing age, women were shown to make more unsafe crossing decisions, to leave small safety margins and to become poorer at estimating their walking speed. However, our results did not reveal any significant effect of gender in reported road crossing habits.

Mobile navigation systems could be used to support users in their appraisal of a crossing situation by e.g. providing alerts for using larger safety margins, planning more accurate walking time for the road crossing etc. Users need to become aware of potential dangers related to their own behavior. Raising the awareness regarding unsafe crossing behavior might reveal better risk perception and behavior change towards a safer crossing.

The Table 1 showing the factors influencing pedestrian route selection and behavior includes a mapping to the quality criteria in Czogalla and Hermann 2011. This mapping is a first ad hoc approximation, that needs to be further tested. Particularly the quality factors "too crowded" and "poor street lighting" are relevant factor for user experience in terms of perceived safety and decisive to select one or another way.

6. CONCLUSION AND FUTURE WORK

The acquired data from the online questionnaire provides the basis for pedestrian's classifications and requirements regarding user friendly interfaces for mobile routing and navigation that enhance road safety.

Beside effectiveness related factors of distance and time, safety was highly prioritized to become an explicit requirement for the conceptual design. Accessibility (and comfort) were not decisive parameters for selecting a route. This can be explained by the fact that except one respondent only people without mobility related aids completed the survey. Furthermore, being that most of the respondents were employed fulltime, their main activity of on foot navigation was arriving at their respective place of work, comfort along the route was of low priority.

Further research will focus on the elaboration of concrete design concepts and development and testing of prototypes relying on the acquired knowledge, focusing on raising pedestrian users awareness of risky crossing situations in order to reduce risky behavior. It is through this end, that pedestrian users will be steered toward less distraction and safer navigation in the streets.

ACKNOWLEDGEMENTS

REFERENCES

Chen, X., Zhu, Y., and Wang, G. (2012). Evaluating a mobile pedestrian safety application in a virtual urban environment. In *Proceedings of the 11th ACM SIGGRAPH International Conference on Virtual-Reality Continuum and its Applications in Industry*, 175–180. ACM.

Czogalla, O. and Hermann, A. (2011). Parameters determining route choice in pedestrian networks. In *Transportation Research Board Annual Meeting*. Washington, DC, USA.

Fogg, B.J. (2009). A behavior model for persuasive design. In *Proceedings of the 4th international Conference on Persuasive Technology*, 40. ACM.

Hatfield, J. and Murphy, S. (2007). The effects of mobile phone use on pedestrian crossing behaviour at signalised and unsignalised intersections. *Accident Analysis & Prevention*, 39(1), 197–205.

Hedencrona, S. (2013). Q3 gwi launch: Video and images dominate mobile app growth. `http://www.globalwebindex.net/blog/mobile-app-usage/`. [Online; accessed 26-January-2015].

Hegarty, M., Richardson, A.E., Montello, D.R., Lovelace, K., and Subbiah, I. (2002). Development of a self-report measure of environmental spatial ability. *Intelligence*, 30(5), 425–447.

Holland, C. and Hill, R. (2010). Gender differences in factors predicting unsafe crossing decisions in adult pedestrians across the lifespan: a simulation study. *Accident Analysis & Prevention*, 42(4), 1097–1106.

Matsuda, Y. and Arai, I. (2014). A safety assessment system for sidewalks at night utilizing smartphones' light sensors. In *Proceedings of the 2014 ACM International Joint Conference on Pervasive and Ubiquitous Computing: Adjunct Publication*, 115–118. ACM.

Methorst, R. (2010). Policy process. *Pedestrians' Quality Needs*, 19.

Miura, H., Takeshima, S., Matsuda, N., and Taki, H. (2011). A study on navigation system for pedestrians based on street illuminations. In *Knowledge-Based and Intelligent Information and Engineering Systems*, 49–55. Springer.

Neider, M.B., Gaspar, J.G., McCarley, J.S., Crowell, J.A., Kaczmarski, H., and Kramer, A.F. (2011). Walking and talking: dual-task effects on street crossing behavior in older adults. *Psychology and aging*, 26(2), 260.

Neider, M.B., McCarley, J.S., Crowell, J.A., Kaczmarski, H., and Kramer, A.F. (2010). Pedestrians, vehicles, and cell phones. *Accident Analysis & Prevention*, 42(2), 589–594.

Olaverri-Monreal, C. and Bengler, K.J. (2011). Impact of cultural diversity on the menu structure design of driver information systems: a cross-cultural study. In *Intelligent Vehicles Symposium (IV), 2011*, 107–112. IEEE.

Olaverri-Monreal, C., Hasan, A.E., Bulut, J., Körber, M., and Bengler, K. (2014). Impact of in-vehicle displays location preferences on drivers' performance and gaze. *IEEE Transactions on Intelligent Transportations Systems*, 15, 1770–1780.

Schwebel, D.C., Stavrinos, D., Byington, K.W., Davis, T., ONeal, E.E., and de Jong, D. (2012). Distraction and pedestrian safety: how talking on the phone, texting, and listening to music impact crossing the street. *Accident Analysis & Prevention*, 45, 266–271.

Thompson, L.L., Rivara, F.P., Ayyagari, R.C., and Ebel, B.E. (2013). Impact of social and technological distraction on pedestrian crossing behaviour: an observational study. *Injury prevention*, 19(4), 232–237.

Verplanken, B. and Orbell, S. (2003). Reflections on past behavior: A self-report index of habit strength. *Journal of Applied Social Psychology*, 33(6), 1313–1330.

Vredenburg, K., Isensee, S., and Righi, C. (2001). *User-Centered Design: An Integrated Approach*. Prentice Hall.

Wang, T., Cardone, G., Corradi, A., Torresani, L., and Campbell, A.T. (2012). Walksafe: a pedestrian safety app for mobile phone users who walk and talk while crossing roads. In *Proceedings of the Twelfth Workshop on Mobile Computing Systems & Applications*, 5. ACM.

Wen, J., Helton, W.S., and Billinghurst, M. (2013). Classifying users of mobile pedestrian navigation tools. In *Proceedings of the 25th Australian Computer-Human Interaction Conference: Augmentation, Application, Innovation, Collaboration*, OzCHI '13, 13–16. ACM, New York, NY, USA.

A Safety Index for Road Crossing [*]

Sebastian Naumann [*] **Olaf Czogalla** [**] **Felix Kühner** [***]

[*] *Institut f. Automation und Kommunikation e.V. Magdeburg,*
Germany (e-mail: sebastian.naumann@ifak.eu).
[**] *Institut f. Automation und Kommunikation e.V. Magdeburg,*
Germany (e-mail: olaf.czogalla@ifak.eu)
[***] *Institut f. Automation und Kommunikation e.V. Magdeburg,*
Germany, (e-mail: felix.kuehner93@gmx.de)

Abstract: Normally, pedestrians do not walk on streets but on sidewalks. Thereby, crossing the road is often necessary. Particularly in peripheral areas, dedicated crosswalks are rare and pedestrians are forced to cross roads apart from them. In order to integrate road crossing into a routing and navigation system for pedestrians a decision of where to cross the road is needed. In order to express how safe it is to cross the road at a certain location we suggest an index. Among others, the value of the index depends on various criteria as the roads' geometries, the traffic volume and the speed of the vehicles. In order to safely cross a road, a free gap with a certain length between two consecutive vehicles on a lane is required. The calculation of the index is mainly based on the probability of the availability of such a gap. All criteria are directly extracted from OpenStreetMap or derived from them.

Keywords: Safety in Crossings, Pedestrian, Road Crossing, Safety Index, Pedestrian Routing, Pedestrian Navigation

1. INTRODUCTION

Nowadays, routing and navigation systems for all types of road users are very common. However, some years ago they have been primarily used by car drivers due to the available digital map data limited to streets as well as the artificial degradation of the GPS signal and the lack of mobile devices. Current trends concerning health and environmental protection in conjunction with a widespread usage of powerful smart phones and much more detailed digital maps bring mobility support for pedestrians more and more into focus.

Normally, pedestrians do not walk on streets. They walk on sidewalks if available or on special ways where cars are not allowed. Thereby, crossing the road is often necessary for pedestrians. In the inner city, pedestrians usually find dedicated crosswalks (zebra crossings and signal controlled crossings). In peripheral areas, dedicated crosswalks are rare and pedestrians are forced to cross roads apart from them.

In order to integrate road crossing into a routing and navigation system for pedestrians a decision of where to cross the road is needed. Safety should be the main criterion here. In order to express how safe it is to cross the road at a certain location we suggest an index. Among

others, the value of the index depends on various criteria as the roads' geometries, the driving speed of the vehicles and the road width. Within the paper we explain how the index is calculated and how far the criteria can be automatically extracted from map data.

1.1 Causes of Accidents

According to IRTAD (2011) cited in Ritter (2014), in 2011 614 pedestrians died in road traffic in Germany, 1,408 in Poland and even 4,432 in the U.S. According to the German Statistic Federal Bureau (2013), in Germany 520 pedestrians died in road traffic in 2012. 388 (75%) of them died in towns and villages. These values correspond to all deaths caused by road traffic at 18% in Germany and 17% in the U.S. and, however, 33% in Poland.

Wrong Behavior Wrong behavior of road users is a main reason for accidents. Table 1 presents common accident scenarios with participation of pedestrians. It is notable that 75% of the accidents happens when the pedestrian crosses the road while the vehicle goes straight.

Table 1. Common scenarios of accidents from GIDAS (German In-Depth Accident Study Database) (2012) cited in Ritter (2014)

Share	Cause
75%	Vehicle goes straight, pedestrian crosses the road
10%	Vehicle moves backward
8%	Vehicle turns left
3%	Vehicle turns right
3%	Vehicle goes straight, pedestrian moves on the road
1%	Other

Following GIDAS (German In-Depth Accident Study Database) (2012) cited in Ritter (2014), a visual concealment was reasonable for 42.7% of all accidents. In 70% of these cases, the pedestrians were covered by another vehicle.

Structural Deficits   A second important reason for accidents with pedestrians are deficits concerning the crossing facilities like missing middle islands and poor visible zebra crossings as stated in Hänel (2014) and of Schreiber (2013, 2014). A major problem too is the sometimes poor visibility of the pedestrians combined with the maximum allowed vehicle speed of 50 km/h in cities in Germany which is too high.

Zebra Crossings and Traffic Light Controlled Intersections
The accident statistics of the German Statistic Federal Bureau (2013) reveal accidents at zebra crossings and traffic light controlled intersections and even 33 dead pedestrians there in 2012 in Germany. At traffic lights, a major problem is a simultaneously green light for the pedestrians as well as for turning cars.

Unfortunately, there are no statistics or studies available concerning road crossing apart from zebra crossings and signal controlled crossings. How often roads are crossed and how often no accident happens would be interesting values. Nevertheless, what can we learn for the intended index for road crossing? Of course, wrong behavior as the most important cause of accidents cannot be compensated by a routing algorithm directly. Though, what could be done is to prevent pedestrians trying to cross a road at an unsafe location by offering them a more safe location from the outset.

1.2 Legal Situation

The German Road Traffic Act (2013) describes in §25 how pedestrians have to behave: ”*(1) Who goes on foot, must use the sidewalks. Pedestrians must go on the road only when there is neither a sidewalk nor has a hard shoulder.*

3) In general, who goes on foot has to cross roadways in compliance with the road traffic quickly by the shortest route across the direction of traffic. If it is required by the traffic situation, crossing the road is allowed at intersections, junctions, traffic lights or pedestrian crossings (sign 293) only. If the road is crossed at intersections or junctions, existing pedestrian crossings or markings shall always be used.”

In Austria, the §76 of the Austrian Road Traffic Act (2015), section (6) ”*If protected paths or certain underpasses or overpasses are available for pedestrians, then pedestrians must use these facilities for crossing the road. However, if there is no facility available or more than 25 meters away, then in principle pedestrians are allowed to cross the road within towns and villages at intersections only. If the traffic situation allows to cross the road safely without any doubt, the road may be crossed at other locations too.*”

We can constitute that crossing the road is not forbidden following the Road Traffic Acts of Germany and Austria. For Austria, we can memorize the value of 25 m, where dedicated crossings must be used.

1.3 Related Work

The only known work dealing with road crossing approximately in the sense of the safety index is the calculation of the green interval at traffic light controlled intersections resp. light controlled crossings. The ideas of how the green interval for pedestrians should considered and signaled calculated are similar in general but may differ in detail from state to state. Here, we would like to exemplary mention the provisions of the Federal Highway Administration of the U.S. Department of Transportation (2013) only.

There, the phase of crossing is divided into the walk interval followed by the pedestrian clearance interval. The walk interval duration should be sufficient to depart the curb. The pedestrian clearance interval then should be sufficient for pedestrians to complete crossing. The pedestrian clearance time PCT is calculated by

$$PCT = \frac{D_c}{v_p} \qquad (1)$$

where

D_c pedestrian crossing distance [feet]
v_p pedestrian walking speed [feet/s]

Table 2 provides PCT values at various crossing distances and various walking speeds.

Table 2. Pedestrian clearance times PCT at light controlled crossings by Federal Highway Administration of the U.S. Department of Transportation (2013)

Pedestrian crossing distance	Walking speed [ft/s]		
	3.0	3.5	4.0
	PCT [s]		
40	13	11	10
60	20	17	15
80	27	23	20
100	33	29	25

2. CRITERIA

The value of the safety index depends on several factors which are described in the following.

Road Width   The road width describes the distance of the way to be covered by the pedestrian when he crosses the road. The road width influences the time for crossing the street. A road may consist of several lanes. The longer the way the pedestrian has to cover the lesser is the safety or the higher is the distance to the approaching vehicles.

Field of Vision   If a road has a strong curvature, the field of vision of the pedestrian may be covered by trees and bushes, walls and buildings and therefore limits the range of vision to the vehicles. As stated in 1.1, coverage of pedestrians by standing vehicles is often reasonable for accidents with pedestrians. Unfortunately, collecting these data is practically impossible. Therefore, this issue is not regarded during this paper.

Vehicle Speed   The speed of the vehicles do not influence the time for crossing the street but the length of the gap required by the pedestrian. The higher the speed the wider is the dimension of the needed gap.

Fig. 1. Idea of the safety index
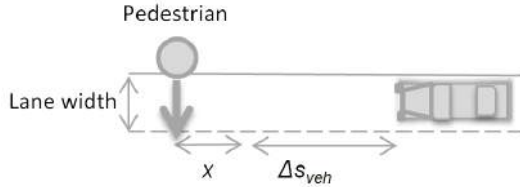
Fig. 2. Safety zone

Traffic Volume The traffic volume is a hint to the time a pedestrian has to wait for a gap for crossing the road. A time dependent distribution of the traffic volume would be beneficial.

Zebra Crossings and Traffic Lights The accident statistics of the German Statistic Federal Bureau (2013) reveal accidents on these crossing locations and even 33 dead pedestrians in 2012 in Germany. At traffic lights the main problem is a simultaneously green light for the pedestrians as well as for turning cars. Nevertheless, for the first time we consider them to have a safety index value of 1 because in our opinion people sense them as safe.

3. SAFETY INDEX

This section describes how the safety index is defined and calculated based on the mentioned criteria.

3.1 Definition

The safety index SI is a value which expresses how safe it is to cross the road at a certain location. It is indicated on a scale from 0 to 1. A value of 0 means the location is very unsafe to cross the street there. A value of 1 stands for the safest location. Fig. 1 provides an example of the idea of the safety index.

3.2 Safety Zone

When a pedestrian is going to cross the road we assume a safety zone. It can be imagined as a distance to the left or to the ride side from the viewpoint of the pedestrian which must be free of any oncoming vehicle so that the pedestrian feels to safely cross the road. The length of the safety zone may be individually and is highly influenced by the speed of the vehicle. We assume a constant speed of the vehicle. Furthermore, we assume that no driver of a vehicle must be forced to decelerate or to brake fearing a collision with the pedestrian.
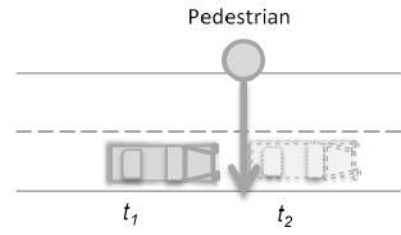
Fig. 3. Consideration of lane (t_1) vs. road (t_2)

The period of time Δt the pedestrian needs to cross one lane of the road with the lane width Δs is calculated by

$$\Delta t = \frac{\Delta s}{v_{ped}} \qquad (2)$$

The walking speed of the pedestrian v_{ped} may differ individually depending of the pedestrian's constitution. When the maximum allowed speed on the road is given by v_{veh}, during the period of time Δt a vehicle covers the distance of

$$\Delta s_{veh} = v_{veh} \cdot \Delta t \qquad (3)$$

Implementing the distance s_{veh} would cause a braking or deceleration action of the vehicle's driver as well as a running action of the pedestrian because both would fear a collision. Therefore an additional buffer x is needed such that the total length of the safety zone l for one lane is calculated by

$$l = \Delta s_{car} + x \qquad (4)$$

Instead of considering the lanes individually, the total width of the road could be chosen for calculating the length of the safety zone. However, this simpler approach seems to us less realistic not taking into account the dynamic aspects of crossing a road with several lanes adequately. In general, crossing the road cannot be started as long as the safety zone is not free of any vehicle. In real, pedestrians start crossing even when the current lane is free but the next lane is not yet free. Fig. 3 shows a sample situation. At the lane based approach, the pedestrian could start crossing at time t_1. At the road based approach, crossing could started at time t_2 only. Therefore, the total length of the safety zone must be greater in the road based approach.

The availability of the length of the safety zone must be guaranteed in any case. Near intersections, the safety zone is expanded to the connecting roads which may have other properties.

3.3 Filtering

According to the legal situation, the safety index for all locations with a distance to a dedicated crossing facility shorter than 25 meters is set to 0. The safety index is also set to 0 for all locations with a field of vision lower than the length of the safety zone.

3.4 Probability of an Available Safety Zone

A strong indicator for the safety of a certain location for road crossing is the probability of an available safety

zone. Availability means, that the length of the safety zone depending on the lane widths, the vehicle speeds and the pedestrian's constitution should be available as a gap between two consecutive vehicles. If a road has several lanes, the traffic volume is distributed to them.

At first, the traffic density k on the considered road section is calculated by the traffic volume q and the speed v:

$$k = \frac{q}{v} \tag{5}$$

The expectation value μ is calculated by the traffic density k and the length of the safety zone l:

$$\mu = k \cdot l \tag{6}$$

We assume a standard normal distribution of the vehicles on the road section with the density function

$$f_n(x|\mu,\sigma^2) = \frac{1}{\sigma\sqrt{2\pi}} e^{-\frac{1}{2}(\frac{x-\mu}{\sigma})^2} \tag{7}$$

The distribution function is the integral of the density function from 0 to $-\infty$:

$$F_n(x|\mu,\sigma^2) = \frac{1}{\sigma\sqrt{2\pi}} \int_{-\infty}^{x} e^{-\frac{1}{2}(\frac{x-\mu}{\sigma})^2} dt \tag{8}$$

The probability is given by the function value of the distribution function:

$$P(X \le x) = F_n(0|\mu,\sigma^2) \tag{9}$$

The value of the safety index SI is equal to the probability:

$$SI = P(X \le x) \tag{10}$$

4. DATA ACQUISITION

OpenStreetMap (OSM) is a crowd retrieved map with much more degree of detail than other (commercial) maps. OSM data are described in XML structures. Main elements are nodes. Ways are lists composed of nodes. Ways can have several attributes.

Our aim is to bring the approach of road crossing and route calculation based on the network of pavements to practice. Other data sources may be available in particular cases but at the moment the data of OpenStreetMap is the only uniform data source available for the whole world. Therefore, we have to lower our sights with respect to the factors described in the former sections.

4.1 Data Directly Available from OSM

Road Network   The geometry of the roads is given by the tag `Way` as a list of `Node` whereby the location of each `Node` is described by its latitude and longitude value. The Number of lanes of a road is available from the `lanes` attribute of a `Way`. The number of drives of an intersection can be retrieved by analyzing the roads connected at an intersection.

Crossing Facilities   Zebra crossings and traffic lights are directly available from OSM. The `highway` attribute of a `Way` is set to `traffic_signals` or to `crossing`. In the second variant the type of the `crossing` attribute is set to `marked` for zebra crossings or set to `traffic_signals` for traffic lights.

Field of Vision   The field of vision can be calculated from the curves of the roads and from buildings or other obstacles which are available from the map data as well.

Lane Width   Lane widths are available from OSM by the `width:lanes` attribute. However, mostly they are not collected comprehensively. Therefore, we suggest a method to conclude to the lane width from the road class provided by the `highway` attribute if no lane width is given. The values provided in table 3 has been taken from the German standard regulation RASt by Baier (2008). For roads in residential areas without road marking in the middle, the recommended values has been divided by 2.

Table 3. Linkage between the OSM `highway` attribute of a `Way` and the lane width based on recommendations of Baier (2008)

highway=	Lane width [m]
trunk	4.00
primary	4.00
secondary	3.75
tertiary	3.50
residential	3.25
living_street	2.25

Vehicle Speed   The `maxspeed` attribute of a `Way` provides the allowed maximum speed on a road.

4.2 Traffic Volume

Although most cities and other road operators periodically collect traffic volume data of their roads, traffic volume data are neither available in OSM nor exists a standardized open data interface to request the data – at least in Germany and Austria. At most, the Open Communication Interface for Road Traffic Control Systems (OCIT) by the OCIT Developer Group (1999) could be considered as a quasi standard. However, it cannot be used by third parties free of charge.

Even though local available traffic volume data could be used, we propose a unique approach here with simplified assumptions. As a unique assumption, the total traffic volumes for a complete day have been collected for Magdeburg, Germany, by ECO AKUSTIK Engineering office for noise protection (2007, 2012) as part of a noise measurement campaign and have been taken from the German standard regulation RASt by Baier (2008). Three periods of daytime were used for the noise measurement campaign: (a) day 6-18 clock, (b) evening 18-22 clock and (c) night 22-6 clock. The total traffic volume was distributed on average as follows: (a) day 74.7%, (b) evening 18.8% and (c) night 8.8%. From these values the share of each period of time in [*vehicles/hour*] has been calculated. Table 4 shows the results.

4.3 Length of the Safety Zone

As mentioned above, the length of the safety zone and particularly the value of x in equation (4) strongly depends on the individual physical and mental constitution. A big field campaign with a representative set of test persons would be neccessary in order to retrieve reliable values. Although this was no subject of our work, we collected

some non-representative values in order to get a better understanding of the issue.

Table 5 provides some values collected (a) at a street with a lane width of 3.00 m and a maximum allowed speed of 30 km/h and (b) at a street with a lane width of 3.75 m and a maximum allowed speed of 50 km/h. The test person had to look at the oncoming vehicle and to decide up to which distance to the vehicle he would cross the road. There were no exact measurement of the vehicles' speeds. Instead we assumed the maximum allowed speed on the road. The test person was a well constituted young person with an age of 22 years. So we assumed a walking speed of 4.0 ft/s resp. 1.22 m/s.

Table 6 then provides for both lane types (a) and (b) the walking durations Δt for different walking speeds and the distances Δs_{veh} covered by the vehicles during the period of time Δt. Since our test person could only estimate the length of the safety zone for its own physical and mental constitution, the column x provides values for a walking speed of 4.0 ft/s resp. 1.22 m/s. Despite the thin data base, the big difference of x at a vehicle speed of 30 km/h and a vehicle speed of 50 km/h is obviously.

Table 4. Linkage between the OSM `highway` attribute of a `Way` and traffic volumes from [1]ECO AKUSTIK Engineering office for noise protection (2007, 2012) and [2]Baier (2008)

highway=	Lane width	Traffic volume total and per hour			
		Total	6-18	18-22	22-6
trunk	4	50,000[1]	3,100	2,100	550
primary	4	24,000[1]	1,488	1,008	264
secondary	3.75	20,000[1]	1,240	840	220
tertiary	3.5	14,400[2]	893	605	158
residential	3.25	7,200[2]	446	302	79
living_street	2.25	3,600[2]	223	151	40

Table 5. Experimental acquisition of the length of the safety zone at different vehicle speeds and lane widths

$v_{veh} = 30 km/h$ $\Delta s = 3.00m$	$v_{veh} = 50\ km/h$ $\Delta s = 3.75m$
31	72
35	76
31	68
36	71
-	75
-	67
-	79
$\varnothing 33$	$\varnothing 73$

Table 6. Experimental acquisition of the length of the safety zone assuming

v_{veh} [km/h]	Δs [m]	v_{ped} [ft/s]	[m/s]	Δt [s]	Δs_{veh} [m]	x [m]
30	3.00	3.0	0.91	3.30	27.50	-
30	3.00	3.5	1.07	2.80	23.33	-
30	3.00	4.0	1.22	2.46	20.50	12.50
50	3.75	3.0	0.91	4.12	57.22	-
50	3.75	3.5	1.07	3.50	48.61	-
50	3.75	4.0	1.22	3.07	42.64	30.36

Fig. 4. Sample area in Magdeburg, Germany (OSM)

5. RESULTS

Fig. 5 shows the result of a sample area in Magdeburg, Germany, shown in Fig. 4. A red color means a low value of the safety index, a green color means a high value. The values of the safety index are almost all low due to the high traffic volume derived from the street categories. At the two drives in the north and the northwest, the values of the safety index become higher the more the distance to the roundabout. These two streets belongs to minor road categories with a lower traffic volume. Near the roundabout, the higher traffic volume of the roundabout which belongs to a higher road category is responsible for the bad values of the safety index. The good index values near the roundabout result from marked crossings.

6. FUTURE WORK

6.1 Routing

As mentioned in the introduction, the safety index will be integrated into a routing algorithm intended for pedestrians. Here, the routing graph is not build up of streets but of sidewalks and dedicated pedestrian ways where no vehicles are allowed, e.g. in parks. Connections between these ways available from the map data are only zebra crossings and traffic lights. Considering this network, routing may work well in the city center with a high presence of zebra crossings and traffic lights. However, in the outskirts this is not the case. This would cause long ways round, or the routing algorithm does not find a route at all because start location and destination location are not connected. Therefore, the calculated safety indexes of the locations must be integrated into the network in order to make it denser. Nevertheless, generating a lot of additional nodes and edges might be adversely for the performance of the routing algorithm. A sophisticated idea is needed in order to combine both.

6.2 Number of Drives

So far, the number of drives are only included when the probability of the safety zone is calculated. However from
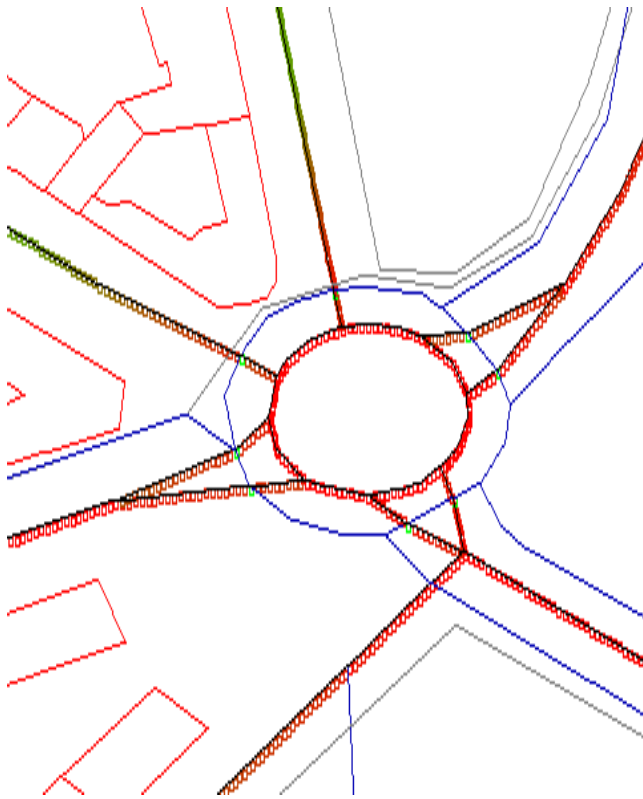
Fig. 5. Result of the sample area

our individual experience, the more directions with potentially oncoming vehicles the pedestrian has to observe the harder it is for him and the more unsafe is the location. The cognitive process of recognizing a vehicle and estimating its speed becomes more complex and more time-consuming. The simplest variant is a one way street. Here the pedestrian only have to take care to one direction with potentially oncoming vehicles. The next variant is the normal street with two driving directions. It becomes rather difficult near intersections, because at a standard intersection there are already four directions. Non-linear vehicle movements near intersections (e.g. when a vehicle is decelerating, turning and finally accelerating) also complicate the matter. Therefore, we would like to include the number of drives more adequately in the future.

REFERENCES

Austrian Road Traffic Act (2015). `http://www.jusline.at/76_Verhalten_der_Fu%C3%9Fg%C3%A4nger_StVO.html`. State of legislation 01/02/2015.

Baier, R. (2008). Guidelines for city streets (original: Richtlinien für die Anlage von Straßen, RASt 06, FGSV R1). Regulations volume 200, FGSV publishing house Köln.

ECO AKUSTIK Engineering office for noise protection (2007). Noise mapping of Magdeburg under 34. BlmSchV type of noise: noise from the street (original: Lärmkartierung der Landeshauptstadt Magdeburg gemäß 34. BlmSchV Lärmart: Straßenlärm).

ECO AKUSTIK Engineering office for noise protection (2012). 2. stage of noise mapping of Magdeburg under 34. BlmSchV type of noise: noise from the street (original: Lärmkartierung der Landeshauptstadt Magdeburg gemäß 34. BlmSchV Lärmart: Straßenlärm).

Federal Highway Administration of the U.S. Department of Transportation (2013). Traffic signal timing manual. `http://ops.fhwa.dot.gov/publications/fhwahop08024/chapter5.htm`.

German Road Traffic Act (2013). `http://www.stvo.de/strassenverkehrsordnung`.

German Statistic Federal Bureau (2013). Traffic and Transport 2012, Division 8, Series 7., Wiesbaden. `http://www.destatis.de`.

GIDAS (German In-Depth Accident Study Database) (2012).

Hänel, A. (2014). VCD Cities Check 2014. Safety of pedestrians (original: VCD Städtecheck 2014. Sicherheit von Fußgängerinnen und Fußgängern). `http://www.vcd.org/fileadmin/user_upload/redakteure_2010/projekte/vcdstaedtecheck/staedtecheck_2014/Hintergrund_VCD_Staedtecheck_2014_komprimiert.pdf`.

IRTAD (2011). `http://internationaltransportforum.org/irtadpublic/group.html`.

OCIT Developer Group (1999). Open Communication Interface for Road Traffic Control Systems. `http://www.ocit.org/`.

Ritter, S. (2014). Active pedestrian protection development of a standardised performance test (original: Aktiver Fußgängerschutz - Entwicklung eines einheitlichen Performancetests). *ZVS - Journal for traffic safety (original: Zeitschrift für Verkehrssicherheit)*, 1/2014, 38–43.

Schreiber, M. (2013). Accidents involving pedestrians and cyclists in cities (original: Innerörtliche Unfälle mit Fußgängern und Radfahrern). *Accident research compact (original: Unfallforschung Kompakt)*, 39.

Schreiber, M. (2014). Typical dangers for pedestrians and cyclists in urban traffic (original: Typische gefahren fr fugnger und radfahrer im innerstdtischen verkehr). *ZVS - Journal for traffic safety (original: Zeitschrift für Verkehrssicherheit)*, 60/4, 221–227.

MobileUTDrive: An Android Portable Device Platform for In-vehicle Driving Data Collection and Display

Yang Zheng, John H.L. Hansen*

*CRSS: Center for Robust Speech Systems – UTDrive Lab
The University of Texas at Dallas, Richardson TX 75080
(e-mail: {yxz131331, john.hansen}@utdallas.edu)

Abstract: Smart portable device used in car provides a cost effective approach to obtain driving dynamic signals and location information by utilizing its inertial sensors. MobileUTDrive is an Android App that we developed for in-vehicle data collection. This paper first describes motivation of using portable device for driving record, and then discuss the system design in hardware and software aspects. Finally, and details of software implementation is presented.

Keywords: Portable device, Android App, In-vehicle data collection

1. INTRODUCTION

Smart portable device use in cars makes a double-sided effect in driving. It may result in distracted driving in some circumstances, whereas on the other side, smart devices could also provide driving assistance, as well as traffic support from network. Therefore, it is beneficial to discover the advantages of smart devices and help improve driving safety.

There are generally two main branches to utilize smart devices within vehicles. The first branch is to employ their ability of connection to the network, thus changing a vehicle into a mobile terminal. For example, traffic notification [1], remote diagnostics [2], vehicle-to-vehicle (V2V) connectivity [3], and other applications in Intelligent Transportation System (ITS) area. The other branch, which focuses on the driving events, contains driver monitoring [4], distraction or drowsy alert [5], driver behavior estimation [6], and so on.

This paper propose to present a smart device App – MobileUTDrive – for in-vehicle driving data collection. As shown in Fig. 1, when mounting a smart device against the windshield, MobileUTDrive would be able to obtain vehicle kinetic signals, location information, as well as driving record video. The App would also include data display function to give a quick review. All collected data would be stored within the device for offline post processing, which will be applied for driving maneuver detection or driver behavior modeling [7, 8].

The remaining part of this paper is organized as follows. Section 2 describes the background and motivation of developing the portable device driving data collection platform. Section 3 discusses the system design in the view of requirement analysis, hardware resource, and software architecture. In Section 4, the details about software implementation is presented. Finally, Section 5 concludes the paper.

Fig. 1. Mount a Samsung tablet within a car, and use the App MobileUTDrive for data collection.

2. BACKGROUND AND MOTIVATION

With the increasingly development of smartphone use in daily life, automobile manufacturers are introducing more and more smartphone applications into their infotainment systems. For example, Android Auto [9] integrates media entertainments and message service with vehicle console system, providing a simplified interface for apps that can be used in a car. At the same time, a large amount of smartphone software that related with driving and traffic come into the market, such as "Car Home Ultra" [10] and "Car Dashboard" [11]. These software usually contain voice control, map navigation, weather forecast, and music player functions, helping drivers get useful information and easy operating their smartphone. In all, smartphone is changing driving into an informative event.

Besides convenient driving assistance, smart device could also act as a driving data collection platform. Modern smart device is equipped with front and back camera, which could be used to monitor and record driving route or driver's face. S. Singh used the back camera for lane keeping [12], and N. Li used the front camera to track driver's eye movements

[13]. C.W. You employed the dual cameras to alert drowsy and distracted driving [14]. Once a smart device is mounted in car, its inertial sensors such as gyroscope and accelerometer could also be exploited to mimic vehicle kinetics. With the collected vehicle signals, M.V. Ly used them for driver classification [15] and A. Sathyanarayana used them for driving maneuver recognition [16]. The collected in-vehicle signals are valuable to understand driver's behavior, and therefore helpful in the development of personalized driving assistance systems, or driver evaluation in insurance companies.

MobileUTDrive is a smart device Android App that we developed for in-vehicle driving data collection. In the previous version of this App [7, 16], we designed the collection of video and inertial sensor signals. Data is saved in the smart device for post processing, but cannot be viewed on device. This paper will present an upgraded version, in which location information is gathered and displayed on Google Map. Users could also review the recorded video and data plots within the App.

3. SYSTEM DESIGN

3.1 Hardware Resource

To make full use of portable device resources, MobileUTDrive acquire all information from its inertial sensors. These information includes media stream, kinetic signal, and location and environment information, which are summarized in Table 1. Since CAN-Bus data is the direct approach to reflect vehicle running status, we add CAN-Bus acquisition option by utilizing the Bluetooth resource of portable device to connect with OBD-II scan tool (ELM327). More details on vehicle diagnostics, CAN-Bus and OBD-II ports can be found in protocols ISO15765-4 [17], ISO14229-3 [18], and ISO9141-3 [19]. A close related work also implements the OBD-Bluetooth connector in [20].

3.2 Software Architecture

MobileUTDrive is intentionally designed for in-vehicle driving data collection and display. Therefore, we propose to develop two main function modules – data recording module and data display module. The block diagram of software architecture is illustrated in Fig. 2. Data recording module is designed to collect multi-channel signals synchronously, it should also shows the camera preview and current location on a map. All collected data is stored in portable device, and can be read for display. Data display should provide a file explorer for users to select collected data, and then use media player, signal plotting, or route drawing for appropriate data files. Additionally, the Setting functionality provides options for user, to set recording length, Bluetooth connectivity, GPS enable, and so on.

Table 1. Signals to be collected from portable device and their resource sensor

Information	Signal	Sensor
Media	Video Audio	Camera (Front & Back)
Kinetic	3-way Acceleration	Accelerometer
	3-way Rotation	Gyroscope
Location	Coordinates Bearing Speed	GPS
Environment	Temperature	Thermometer
	Brightness	Light
Connection	CAN-Bus	Bluetooth
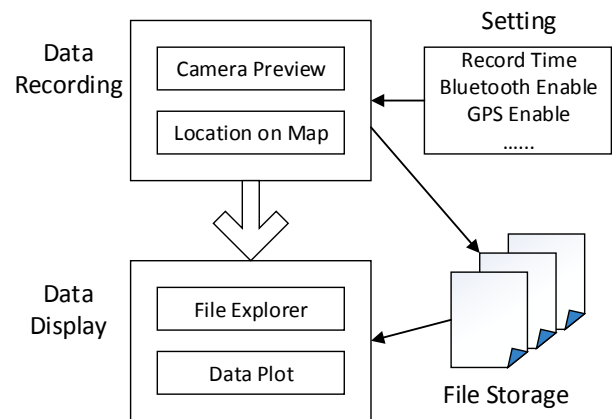
Fig. 2. Block diagram of MobileUTDrive software architecture.

4. SOFTWARE IMPLEMENTATION

Software is programed within the environment of Java Eclipse IDE, with the portable device application support of Android Development Tools (ADT) [21] and map support from Google Location Service – Google Maps Android API [22].

4.1 Data Recording Module

Fig. 3 illustrates the flow diagram of data recording module. Data recording module starts as soon as MobileUTDrive is launched. According to the pipeline of Android activity lifecycle, two threads are started once the main activity is created – recording thread and timer thread. Since the main activity is primarily used for Graphic User Interface (GUI), data acquiring and storing tasks are executed in recording thread. Timer thread is used for handle the recording time length, i.e. every 5 minutes or unlimited length. In the meanwhile of "onCreate" method, the activity also send requests for Google Map displayed on device. The method of "onResume" initiates the camera hardware and "onPause" releases it, this is intent to use the camera resource in an effective way.
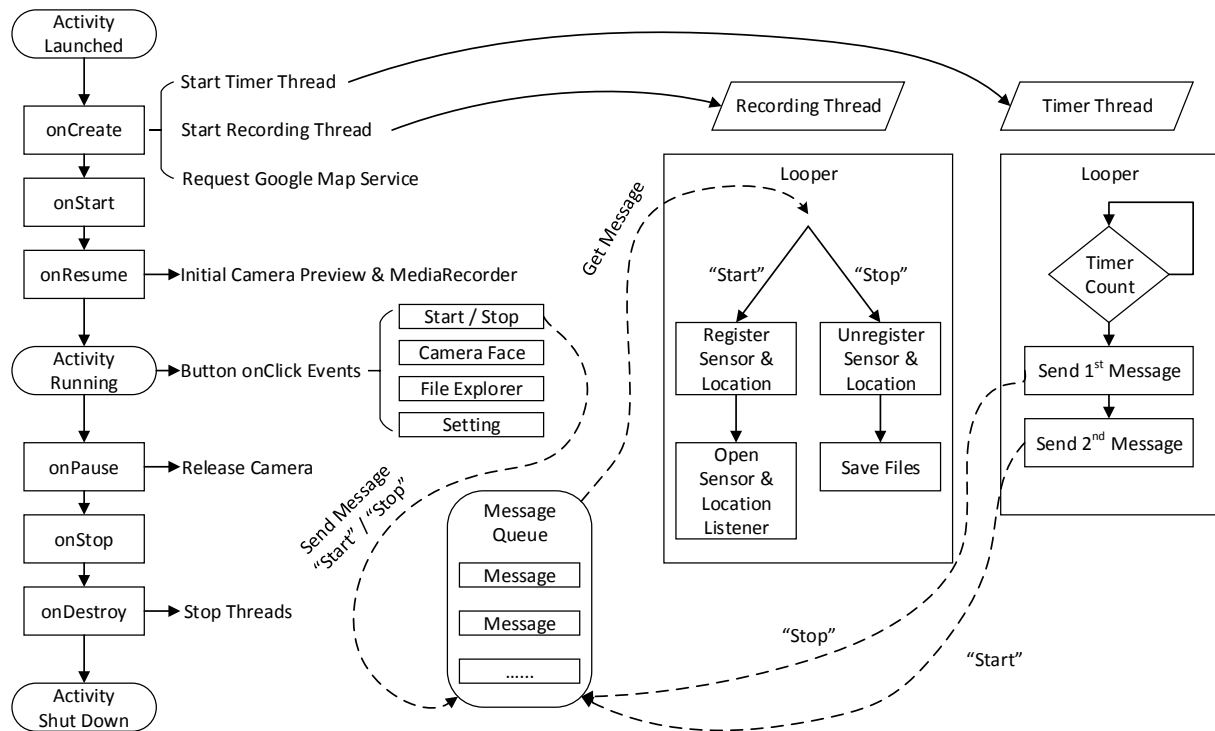
Fig. 3. Flow diagram of data recording module.

Table 2. Button functions in the GUI of MobileUTDrive

Button	Event
Start /Stop	Start or stop recording
Camera Face	Choose front camera or back camera
File Explorer	Open data display activity page
Setting	Open setting dialog

When the main activity is running, it previews the camera and map, and is ready to respond functional button "onClick" events, which are listed in Table 2. The communication channel between the three threads is through message queue mechanism. The main thread send "Start" or "Stop" messages into message queue, and the recording thread is always running to handle messages obtained from the queue. If the message is "Start", it registers sensors and location hardware, and open their listeners to get data. Whereas if a "Stop" message obtained, it unregisters sensors and save all recorded data into files. The timer thread also send messages into the same queue. Once timer count reaches the set length, it sends a "Stop" and then followed with a "Start".

Fig. 4 shows the snapshots of MobileUTDrive on its recording page. The left half screen displays the camera preview and the right half screen displays the current location on Google Map. Recording time is also shown on the top

right corner of camera preview. Four functional buttons are placed on the top of the screen.
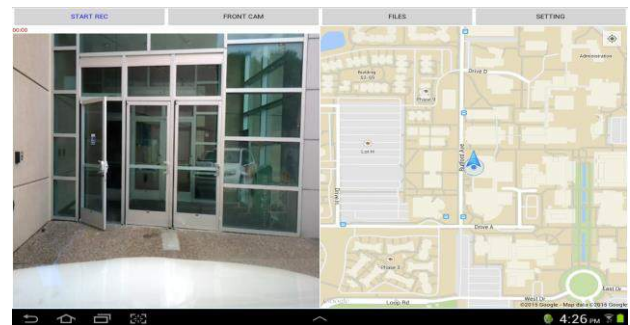
Fig. 4. Snapshot of MobileUTDrive – Data recording page.

4.2 Data Display Module

The data display module is relatively simple, it is opened once the "File Explorer" button is clicked. As Fig. 5 illustrates, this activity creates a "File ListView" and a "Data Preview" on screen (see Fig. 6). The "File ListView" lists all save folders by their collection time, and all files within the folder by the signal types. The "Data Preview" layout could be changed to display appropriate data types, 3x1 canvas for

3-channel accelerometer or gyroscope, isolate canvas for drawing driving route, and media player for playing video.
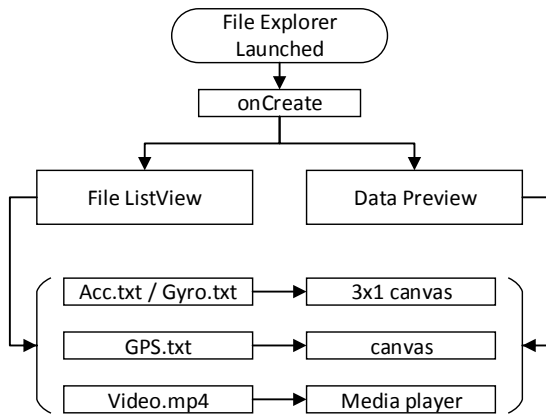
Fig. 5. Flow diagram of data display module.

4.3 Setting Options

Fig. 7 displays the snapshot of setting dialog, which provides the options of setting record duration, Bluetooth enable and GPS enable. Once the "Save" button is clicked, the dialog will disappear and the main activity will implement the returned interface to start using the updated options.
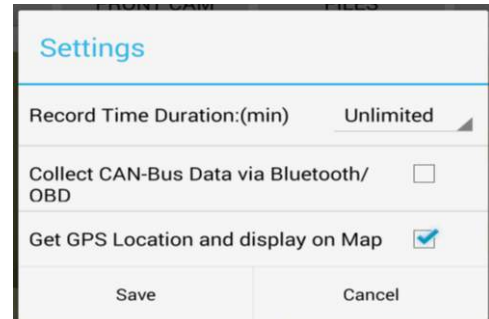
Fig. 7. Snapshot of MobileUTDrive – Setting dialog.
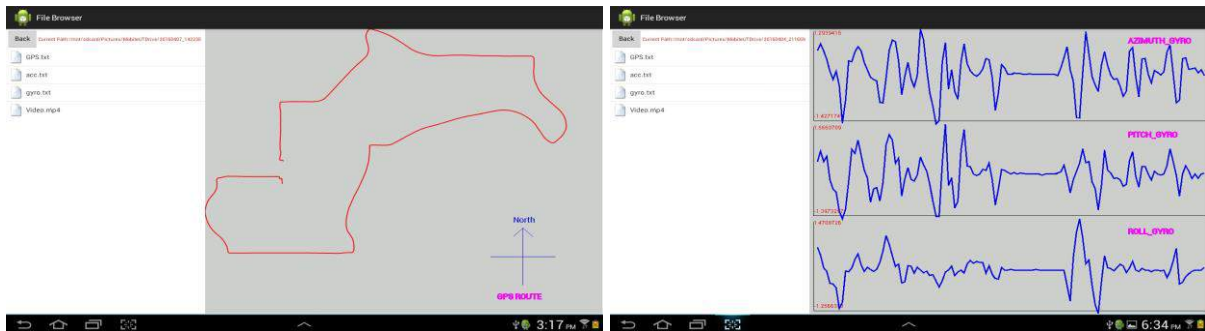
Fig. 6. Snapshots of MobileUTDrive – Data display page, with (a) driving route and (b) gyroscope signals.

5. CONCLUSION

To discover more applications of smart device use in vehicle, we developed an Android App – MobileUTDrive – for driving data collection. This App collects multi-channel signals including video, sensors, location, and so on. Its software architecture is composed of two main modules – data recording module and data display module. Recording task is executed in a background thread and recorded files are stored in device.

REFERENCES

[1] C. Campolo, A. Iera, A. Molinaro, S.Y. Paratore, and G. Ruggeri, "SMaRRCaR: An integrated smartphone-based platform to support traffic management app", *1st Int. workshop on vehicular traffic management for smart cities*, 2012.

[2] J. Wideberg, P. Luque, and D. Mantaras, "A smartphone application to extract safety and environmental related information from the OBD-II interface of a car", *Int. Journal of Vehicle Systems Modelling and Testing*, 2012, 7(1), pp. 1-11.

[3] K.-C. Su, H.-M. Wu, W.-L. Chang, and Y.-H. Chou, "Vehicle-to-vehicle communication system through wi-fi network using android smartphone," *IEEE International Conference on Connected Vehicles and Expo (ICCVE)*, Beijing, China, Dec 2012, pp. 191-196.

[4] J. Hong, B. Margines, and A.K. Dey, "A Smartphone-based Sensing Platform to Model Aggressive Driving Behaviors", *In Proc. of the SIGCHI Conference on Human Factors in Computing Systems*, 2014, pp. 4047-4056.

[5] C.W. You, M. Montes-de-Oca, T.J. Bao, N.D. Lane, H. Lu, G. Cardone, L. Torresani, and A.T. Campbell, "CarSafe: a driver safety app that detects dangerous driving behavior using dual-cameras on smartphones." *In Proc. of the 2012 ACM Conference on Ubiquitous Computing,* 2012, pp.671-672.

[6] H. Eren, S. Makinist, H. Akin, and A. Yilmaz, "Estimating driver behavior by a smartphone", *in Proc. IEEE IV, 2012*, pp.234-239

[7] A. Sathyanarayana, S. O. Sadjadi, and J.H.L. Hansen, "Automatic driving maneuver recognition and analysis using cost effective portable devices," *SAE Int. J.*

Passeng. Cars – Electron. Electr. Syst. 6(2), 467-477, 2013.

[8] D.A. Johnson, and M.M. Trivedi, "Driving style recognition using a smartphone as a sensor platform," *In Proc. IEEE Intelligent Transportation Systems Conference (ITSC),* Washington, DC, Oct. 2011, pp. 1609-1615.

[9] https://developer.android.com/auto/index.html

[10] https://play.google.com/store/apps/details?id=spinninghead.carhome

[11] https://play.google.com/store/apps/details?id=com.nezdroid.cardashdroid

[12] S. Singh, S. Nelakuditi, R. R. Choudhury, and Y. Tong. Your smartphone can watch the road and you: mobile assistant for inattentive drivers. In Proceedings of ACM MobiHoc, 2012, pages 261-262.

[13] N. Li and C. Busso, "Analysis of facial features of drivers under cognitive and visual distractions," in Proc. IEEE Int. Conf. Multimedia Expo (ICME), San Jose, CA, USA, Jul. 2013, pp. 1-6.

[14] C.W. You, N.D. Lane, F. Chen, etc., "CarSafe App: Alerting Drowsy and Distracted Drivers using Dual Cameras on Smartphones", *MobiSys'13*, June 25-28, 2013, Taipei, Taiwan, pp. 13-26.

[15] M.V. Ly, S. Martin, and M.M. Trivedi, "Driver Classification and Driving Style Recognition using Inertial Sensors", *In Proc. IEEE Intelligent Vehicles Symposium (IV),* Gold Coast, Australia, June 23-26, 2013, pp. 1040-1045.

[16] A. Sathyanarayana, S. O. Sadjadi, and J. H. L. Hansen, "Leveraging sensor information from portable devices towards automatic driving maneuver recognition," *in Proc. International IEEE Conference on Intelligent Transportation Systems*, Anchorage, AK, Sept. 2012, pp. 660–665.

[17] Road vehicles -- Diagnostic communication over Controller Area Network (DoCAN) -- Part 4: Requirements for emissions-related systems, ISO 15765-4:2011.

[18] Road vehicles -- Unified diagnostic services (UDS) -- Part 3: Unified diagnostic services on CAN implementation (UDSonCAN), ISO 14229-3:2012

[19] Road vehicles -- Diagnostic systems -- Part 3: Verification of the communication between vehicle and OBD II scan tool, ISO 9141-3:1998

[20] J. Zaldivar, C.T. Calafate, J.C. Cano, and P. Manzoni, "Providing Accident Detection in Vehicular Networks Through OBD-II Devices and Android-based Smartphones," *5th IEEE Workshop On User Mobility and VEhicular Networks*, Bonn, Germany. 4-7 October 2011.

[21] http://developer.android.com/index.html

[22] https://developers.google.com/maps/documentation/android/

Estimation Methods of the Number of Accidents Considering Quality of Active and Passive Safety Performance

Hisashi Imanaga*. Shigeru Kashima**

*Japan Automobile Research Institute, Tsukuba, Japan
(e-mail: hima@jari.or.jp).
**Department of Civil Engineering, Chuo University, Tokyo, Japan
(e-mail: kashima@civil.chuo-u.ac.jp)

Abstract: This study proposes a model to estimate the number of accidents using two parameters. One parameter expresses quality of active safety, and the other one expresses quality of passive safety. This model uses data on accident occurrence from 1999 to 2009. The estimated parameters indicate that during this period the quality of active safety did not increase, whereas the quality of passive safety did increase.

Keywords: Statistical analysis, Road traffic, Mathematical models

1. INTRODUCTION

The number of traffic accident victims is affected by two factors: passive safety and active safety. Passive safety is measured by the number of victims per accident, and active safety is determined by the number of accidents per mile. The number of accidents is measured by the product of these two qualities. However, measuring each quality separately would provide a useful index for traffic accident analysis. This study seeks to measure the index of these two qualities using macroscopic traffic accident data.

2. IDEA OF MODELLING

2.1 Japanese National Accident Statistics

The number of traffic accidents in Japan can be derived from accident data managed by the Institute for Traffic Accident Research and Data Analysis (ITARDA), based on police reports (hereafter, ITARDA data). ITARDA data include all traffic accidents involving at least one fatality or injury.

For each accident included in this data, the primary party (the person who is most responsible for the accident) is determined. Some accidents involve only the primary party or more than three parties; however, most involve two parties, a primary party and a secondary party. This study focuses on the accidents which have more than two parties. However it does consider only primary and secondary parties.

In the present study, parties are aggregated by vehicle type: bus, ordinary passenger vehicle, Kei[*1] passenger vehicle, large commercial vehicle, ordinary commercial vehicle, Kei[*1] commercial vehicle, and non-four-wheel vehicle (e.g., motorcycle, small motorcycle, or bicycle).

2.2 Modelling Accident

It is assumed that an accident between primary party i and secondary party j ($i,j \in$ vehicle type) occurs as follows.

Primary party i creates a dangerous situation with probability p_i. A dangerous situation is defined as a situation that requires avoidance action. If avoidance efforts fail, there is an accident; if the efforts are successful, there is not an accident or much slight accident. Here, parameter p_i is determined by the rate of dangerous situation occurrence (DSO) and is proportional to u_i, which denotes the mileage of all parties i. Thus, all dangerous situations involving primary party i is

---

*[*1]Kei size is defined as a vehicle whose body is 3.4[m] long, 1.48[m] wide, and 2.0[m] tall or less, with displacement of 0.66[l] or less.

calculated by

$$d_i = p_i \cdot u_i, \quad (1)$$

where d_i denotes the number of dangerous situations caused by primary party i.

Secondary party j encounters a dangerous situation with probability r_j. This probability is proportional to account for mileage of secondary party j

$$r_j = \frac{u_j}{\sum_j u_j}. \quad (2)$$

Thus, the number of dangerous situations that secondary party j *involving* and are caused by primary party i (D_{ij}) is calculated as

$$D_{ij} = d_i \cdot r_j = p_i \cdot u_i \cdot \frac{u_j}{\sum_j u_j}. \quad (3)$$

In such a situation, secondary party j tries to avoid an accident. If the avoidance attempt is successful, the result is r_S; if it fails, the result is r_F. In this situation, the secondary party fails to avoid with probability q_j. Here, this probability q_j determined by the rate of failing to avoid a dangerous situation (FDA).

Using this probability, the number of accidents between primary party i and secondary party j is calculated as

$$A_{ij} = D_{ij} \cdot q_j = p_i \cdot q_j \cdot \frac{u_i \cdot u_j}{\sum_j u_j}, \quad (4)$$

where A_{ij} is the number of accidents related to primary party i and secondary party j.

Parameter p_i can be interpreted as the index of active safety quality, and q_j can be interpreted as the index of passive safety quality.

3. PARAMETER ESTIMATION

3.1 Parameter Estimation using Constrained Optimization Problem

Parameters p_i and q_j can be estimated by solving the constrained optimization problem:

$$Z = \sum_i \sum_j \left[A_{ij} - p_i \cdot q_j \cdot \frac{u_i \cdot u_j}{u} \right] \rightarrow \min$$

$$\begin{aligned} \text{s.t.} \quad & 0 \leq p_i, \\ & 0 \leq q_j \leq 1, \\ & \sum_i A_{ij} = \sum_i p_i \cdot q_j \cdot \frac{u_i \cdot u_j}{u} \\ & \sum_j A_{ij} = \sum_j p_i \cdot q_j \cdot \frac{u_i \cdot u_j}{u} \\ & \sum_i p_i \cdot u_i = \sum_i (r_{Si} + r_{Fi}) = \sum_i d_i, \end{aligned} \quad (5)$$

where $\widehat{A}_{ij}$ is the actual number of accident types r_{Fi} involving primary party i and secondary party j, and r_{Si} is the number of r_S involving secondary party j. The first two constrained conditions are related to the range of probability. The next two conditions involve conforming marginal distribution between real data and an estimation matrix. The last condition is related to defining a dangerous situation. In this model, the number of dangerous situations is the total number of fatal accidents and injury accidents.

Fig. 1. Concept of the constrained optimization problem.

3.2 Modelling Case

A four-wheel vehicle fatal accident model is used in this study, because of the availability of

Table 1. Number of fatal accidents (2009)

primary party / secondary party		Four-wheel vehicle						Two-wheel vehicle			Total
		Bus	Ordinary passenger	Kei passenger	Large commercial	Ordinary commercial	Kei commercial	Motor cycle	Small motor cycle	Bicycle	
Four-wheel vehicle	Bus	0	4	5	0	3	0	5	1	2	20
	Ordinary passenger	0	125	57	22	1	62	50	43	50	410
	Kei passenger	1	53	17	10	5	12	21	22	22	163
	Large commercial	0	114	85	47	21	64	32	33	21	417
	Ordinary commercial	0	18	12	6	2	13	9	18	26	104
	Kei commercial	0	31	11	12	4	9	7	19	14	107
Two-wheel vehicle	Motor cycle	2	101	38	32	21	17	6	6	11	234
	Small motor cycle	0	58	25	22	11	18	0	2	1	137
	Bicycle	8	150	79	84	56	54	9	4	5	449
Total		11	654	329	235	124	249	139	148	152	2,041

source:ITARDA

Table 2. Number of fatal and injury accidents (2009)

primary party / secondary party		Four-wheel vehicle						Two-wheel vehicle			Total
		Bus	Ordinary passenger	Kei passenger	Large commercial	Ordinary commercial	Kei commercial	Motor cycle	Small motor cycle	Bicycle	
Four-wheel vehicle	Bus	20	594	209	73	100	90	44	75	100	1,305
	Ordinary passenger	656	114,282	47,664	8,488	14,790	15,265	2,792	5,045	6,435	215,417
	Kei passenger	224	58,022	30,702	3,479	6,929	10,028	995	2,523	2,945	115,847
	Large commercial	45	3,046	1,442	1,703	688	693	216	303	214	8,350
	Ordinary commercial	75	10,682	4,261	1,521	2,307	1,753	294	644	839	22,376
	Kei commercial	76	15,768	7,631	1,382	2,515	3,213	355	840	1,084	32,864
Two-wheel vehicle	Motor cycle	124	22,755	7,027	1,187	2,571	3,168	937	1,244	687	39,700
	Small motor cycle	143	29,265	11,663	1,272	3,661	5,403	809	2,009	952	55,177
	Bicycle	563	69,624	25,182	2,827	8,294	11,648	2,831	5,424	3,881	130,274
Total		1,926	324,038	135,781	21,932	41,855	51,261	9,273	18,107	17,137	621,310

source:ITARDA

utilizable mileage data. This model provides two parameters, DSO p_i and FDA q_j. A dangerous situation is defined as the occurrence of a fatal accident or an injury accident. Thus, DSO is equal to the rate of encountering accidents by mileage unit. Accident avoidance means avoiding a fatal accident. In other words, if the secondary party's avoidance effort fails, the result is a fatal accident; if it is successful, the result is an injury accident. Thus, FDA is equal to account for fatal accidents by all accidents (fatal accidents plus injury accidents).

source: statistics from ministry of Land, Infrastructure, Transport and Tourism

Fig. 2. Mileage of each party

3.3 Accuracy of Estimation

Parameters are estimated for each year from 1999 to 2009, using accident and mileage data for each year. Table 1 lists the number of fatal accidents involving each party in 2009, and Table 2 lists the number of fatal and injury accidents in the same year. Figure 2 plots the mileage of each party. Figure 3 plots the accuracy of estimation in 2009, illustrating that the number of accidents involving each party can be estimated accurately. The same level of accuracy is derived in estimations for each year.

Fig. 3. Accuracy of the estimated number of fatality accidents in 2009.

3.4 Estimated Parameters

Figures 4 and 5 plot estimated parameters p_i and q_j for each party. The trend of parameter p_i changes little during this period. However, that of q_j decreases. This result indicates development of the quality of passive safety.
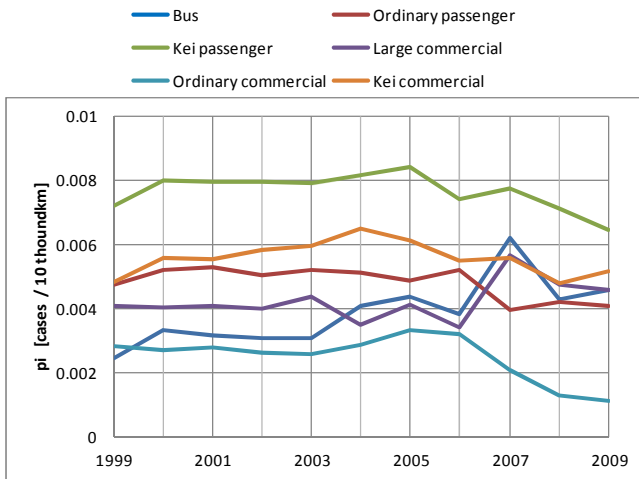
Fig. 4. Trend of estimated parameter p_i.
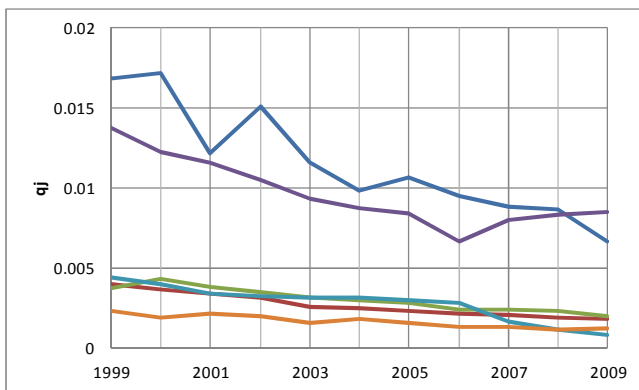
Fig. 5. Trend of estimated parameter q_j.

4. EXTENSION TO TWO-WHEEL VEHICLES

In this section, types of party are extended to two-wheel vehicles (e.g., motorcycles, small motorcycles, and bicycles; four- and two-wheel

Table 3. Average mileage of two-wheel vehicles.

Vehicle type	average mileage	source
Motor vehicle	4,273 [km/year]	JAMA statistics[*2]
Small motor vehicle	2,507 [km/year]	
Bicycle	272 [km/year]	Cabinet Office, Government of Japan report[*3]

*2 Surveys were conducted in 1993, 1995, 1997, 1999, 2001, 2003, and 2005. Average mileage of each vehicle type did not change significantly. Thus, the average value of each survey is used as the estimated value.
*3 Estimated mileage of 2009 in the report
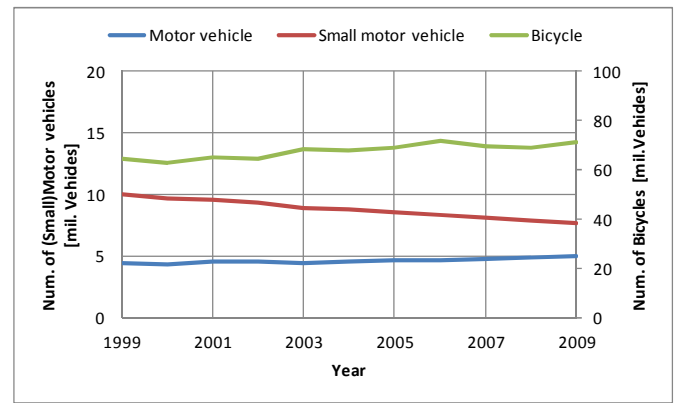
source: JAMA statistics[*4]
*4 Non-surveyed year's values are estimated from the values before and after surveyed years one.

Fig. 6. Number of two-wheel vehicles.
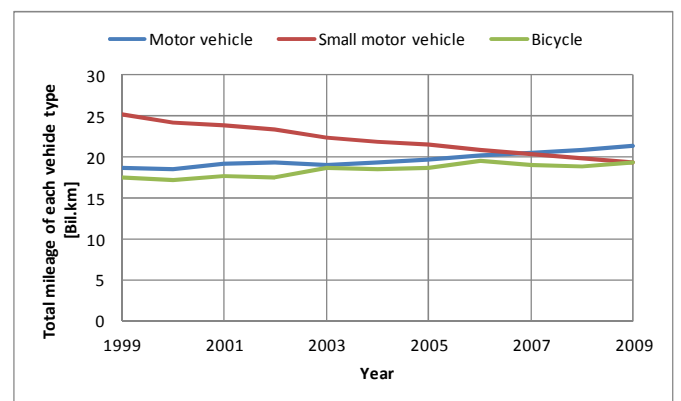
Fig. 7. Estimated total mileage of two-wheel vehicles.

vehicle fatal accident model). No data on the mileage of these vehicle types are available. Thus, these parties' mileage is estimated using the number of vehicles of each type, and average mileage of these vehicles is based on a sampling survey.

Figure 8 and 9 plot trends of estimated parameters p_i and q_j. ??The trend of each parameter is different from four wheels vehicle model (Figure 4 and 5). Parameter p_i of motor vehicles, small motor vehicles, and bicycles exhibits the trend of reducing more than that of other four-wheel vehicles.

However, parameter q_j maintains the same level, with no reducing trend for four-wheel vehicles. This result may be due to the passive safety qualities of two-wheel vehicles, which do not increase during this period.
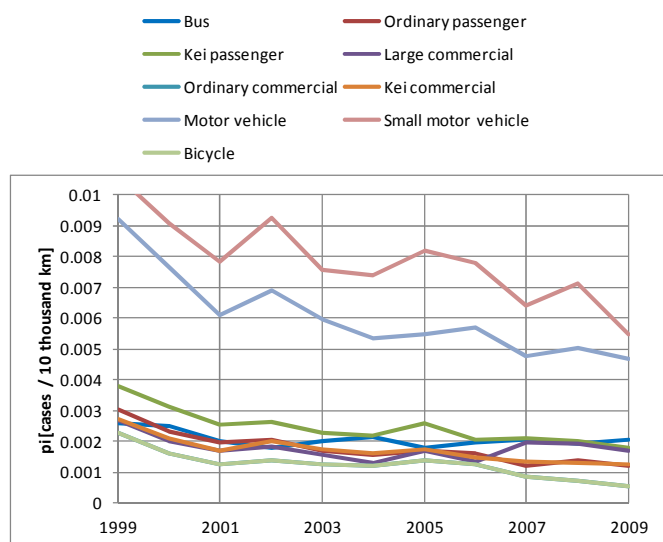
Fig. 8. Trend of estimated parameter p_i (four-wheel plus two-wheel vehicles).
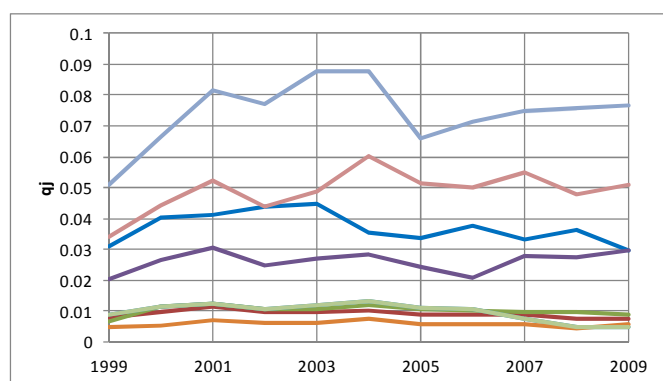
Fig. 9. Trend of estimated parameter q_j (four-wheel plus two-wheel vehicles).

5. CONCLUSION

This study proposes a method to estimate parameters p_i (quality of active safety) and q_j (quality of passive safety) using real accident data. The four-wheel vehicle model indicates a trend of increasing passive safety quality. However, the four-wheel plus two-wheel model does not indicate such a trend. The parameters of this model mixing the four-wheel quality increase and two-wheel compatibility problem. The parameter of this model considers all accidents against to all types of vehicles in the model. To overcome this problem, the parameter of party i must discriminate between vehicle types as party j.

This model uses fatal accidents plus injury accidents as dangerous situations. If data on types of accident (e.g., non-injury and near-accident) were available, a much more interesting estimation could be developed using this method.

REFERENCES

Institute for Traffic Accident Research and Data Analysis (1999), Statistics of Traffic Accident

Japan Automobile Manufacturers Association (2001), A survey of motorcycle market in Japan, http://release.jama.or.jp/sys/news/detail.pl?item _id=49(2014.5.21)

Japan Automobile Manufacturers Association (2014), Number of owned motorcycle in Japan, http://www.jama.or.jp/industry/two_wheeled/tw o_wheeled_3t1.html(2014.5.21)

Cabinet Office, Government of Japan (2010), A survey about safety development of bicycle transportation, http://www8.cao.go.jp/koutu/chouken/h22/houkoku. html(2014.5.13)

Modeling Driver's Skill of Merging Operation toward Its Assistance System

Shohei Ueda [*] **Takahiro Wada** [**]

[*] *School of Information Science and Engineering, Ritsumeikan University, Shiga, Japan, (e-mail: is0055rx@ed.ritsumei.ac.jp)*
[**] *School of Information Science and Engineering, Ritsumeikan University, Shiga, Japan, (e-mail: twada@fc.ritsumei.ac.jp)*

Abstract: Merging into the traffic flow on an expressway is a challenging driving task. We aim to develop a driver assistance system for such a demanding driving task. Our previous study revealed that a driver's decision making of the merging space in the oncoming traffic skill can be inferred by the driver's behaviors after the driver was able to see the environment of the main lane. In addition, the study suggested that the merging behaviors were different among drivers and it seemed to depend on driver's skill. Thus, the present paper proposed a method to characterize driver's skill in merging operation based on the driver model and driver's active longitudinal control toward a driver assistance system for merging.

Keywords: Driver behavior, Driver models, Human factors, Prediction method, Regression analysis

1. INTRODUCTION

The advanced driver assistance systems (ADASs) realize safe and/or comfortable driving. It is believed that applying the ADAS during demanding situations for drivers is more effective to reduce driver's workload and improve driving environment. Merging operation into the flow of high-speed traffic on roadways such as expressways is one of the demanding and challenging driving tasks (e.g. See de Waard et al. (2010) or Baumann et al. (2011)). To achieve safe and smooth merge, some driving skills are required. It is thought that the merging behavior is constructed by continuous and parallel execution of cognition, decision making, and operation. Therefore, it is important to understand driving behaviors by considering these drivers' tasks. Regarding to research studies on driving behavior, there are many studies on the car-following behaviors (Gipps (1981)) and (Herman and Rothery (1961)), deceleration behaviors (Lee (1976)), (Wada et al. (2010)) and (Goodrich et al. (1999)), and steering behaviors (Markkula et al. (2012)). Further, a few research studies have investigated driving behaviors with regard to merging into expressway. de Waard et al. (2009) investigated the merging behaviors of young and elderly drivers and revealed that the slow-speed driving styles of elderly drivers can result in adverse situations during merging. Another study Baumann et al. (2011) indicated that the gap where a driver merges into approaching traffic varies depending on the traffic velocity and the distance between the ego vehicle and the approaching vehicles. Yamanaka et al. (2012) developed a mathematical model for the merging operation for automated driving vehicles. However, there are no research studies that consider differences in driver's behaviors based on driver's skills in merging operation, though it is important when understanding the difficulties associated with merging and constructing its assistance method.

Yamanaka et al. (2012) postulated that merging behavior can be divided into three phases:

(1) Decision making of the merging space in the traffic flow
(2) Velocity control
(3) Final merging decision

The first phase is considered to be the most important because drivers have to make their decision for the merging space at the beginning of whole merging behavior. In our previous study (Ueda and Wada (2015)), we focused this phase and proposed a decision making model of merging space by a logistic regression method. In addition, the same study suggested that a driver's behaviors in merging operations were different among individuals and the difference could reflect driver's skill.

Therefore the purpose of the present paper is to propose a method to characterize driver's skill in merging operation. We try to characterize the driver's merging behaviors from the viewpoint of their active longitudinal control that is thought to be related to their decision making. First, we focus on the fact that the data sets separate into two groups in the phase space of variables of vehicle motions by the final merging spaces. We hypothesize that the degree of the separation reflects driver's skill of merging behavior. The amount of the separation is quantified by the distance between each driving data point and the separator line of these two data sets, which is determined by support vector machine (SVM). These results are interpreted with the analysis results of initiation timing of driver's active longitudinal control that is investigated using the jerk.
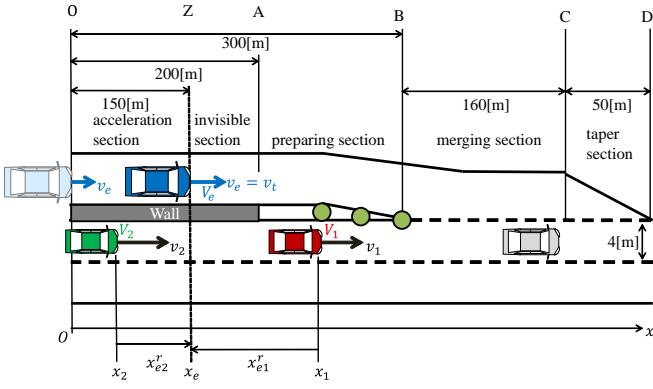
Fig. 1. Scenario assumed: merging into main lanes on the express way.

2. PROBLEM DESCRIPTION

Fig. 1 shows the scenario assumed in this paper: merging into main lanes on the express way. The x-coordinate was taken to the driving direction along the main road as shown in Fig. 1. The ego vehicle V_e was initially located at point O on the merging lane and its position of the front bumper was represent to x_e, and its velocity was written as v_e. The merging behavior was divided into five sections by the road geometry and the section boundaries, which were named points Z, A, B, C, and D, as shown in Fig. 1.

There were two other vehicles labeled V_i on the main lane whose positions of the front bumper and velocity were given by x_i and v_i ($i = \{1, 2\}$), respectively. The velocities v_i were set to $v_i = v_e$ until the ego vehicle passed point Z; then, they were changed to the predetermined velocities v_i. In addition, two other vehicles 60 m ahead of V_1 and 60 m behind V_2 were located to prevent unrealistic behavior of the ego vehicle such as very fast driving or very slow driving before merging.

x_{ei} denotes the relative distance of the ego vehicle and a vehicle V_i, which is defined as $x_{ei} = x_e - x_i$. v_{ei} denotes the relative velocity of the ego vehicle and a vehicle V_i, which is defined as $v_{ei} = v_e - v_i$. In the same way, $x_{ij} = x_i - x_j$ and $v_{ij} = v_i - v_j$ are defined. The driver of the ego vehicle were unable to see the main lane until they passed point A because there was a wall between the merging lane and the main lane.

3. DECISION MAKING MODEL OF MERGING SPACE

The decision making model of merging space predicts the probability of merging in front of vehicle V_i through logistic regression as eq. (1).

$$\text{logit}\,(p_i) = \sum_{k=1}^{K} \beta_k^i x_k^i \qquad (1)$$

where β are coefficients, x_k^i are explanatory variables, $x_0^i = 1$ and subscript i takes $i = 1$ and 2 in accordance with the assumed scenario. K denotes the number of explanatory variables. The logit p_i denotes eq. (2).

$$\text{logit}\,(p_i) = \log\left(\frac{p_i}{1 - p_i}\right). \qquad (2)$$

The relative distance x_{ei} and relative velocity v_{ei} were used for explanatory variables of the model because it has been shown that these are important factors for the model from our previous study (see Ueda and Wada (2015)). $K = 2$ was chosen in the present study. Algorithm 1 describes the method to predict the merging space using the regression model.

Algorithm 1 Method to predict the merging space.

if $p_1 > 0.5$ **then**
    merging space is predicted as **in front of** V_1
else if $p_2 > 0.5$ **then**
    merging space is predicted as **between** V_1 **and** V_2
else
    merging space is predicted as **behind** V_2
end if

---

4. EXPERIMENT

The experiments were performed to gather data on merging behaviors of drivers by the fixed-base driving simulator(DS). The simulator reproduced a merging scenario as shown in Fig. 1.

4.1 Apparatus

Hardware   Fig.2 shows the DS used to investigate merging behaviors of drivers during the task of merging. The

Fig. 2. The driving simulator used in the experiment.

DS has four 40-inch LCDs, which display a driving environment to participants. Three displays were placed on the right hand side of participants because, in this study, we assumed that merging into the main lanes was to be performed on the right hand side; accordingly, visual information in that direction was required. The computer graphics of the DS for each of the four LCDs I, II, III and IV are shown in Fig.3. The distance of the center LCD in front of the driver from his/her viewpoint was about 0.9 m. As shown in the figure, participants were also able to see the rear-view mirror and side mirrors. A 250 W brushless DC motor (Maxon Corporation) was attached to the steering shaft to generate self-alignment torques.
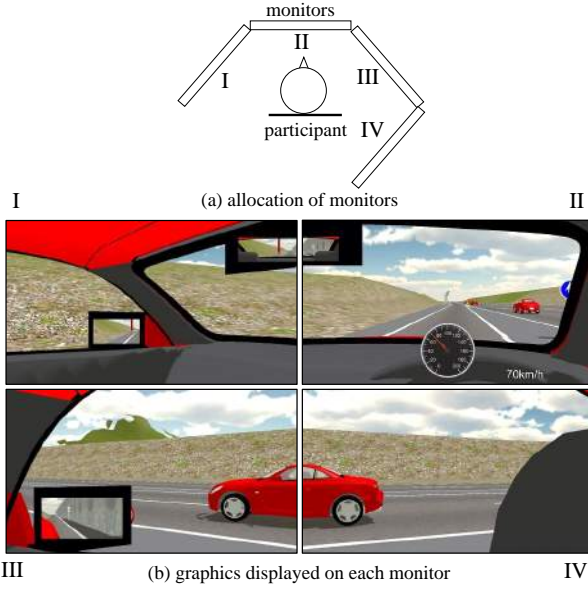
Fig. 3. Graphics displayed to participants: (a) The location of the four LCD monitors. (b) The computer graphics on each monitor.
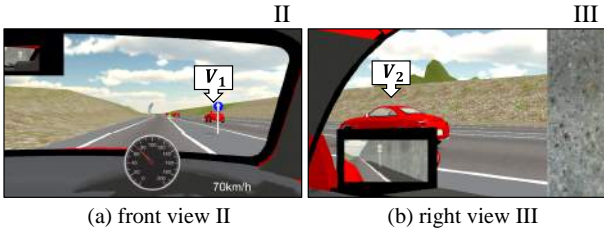
Fig. 4. Computer graphics for a participant when the ego vehicle has just passed point A: (a) LCD II; front view, and (b) LCD III; right view of the participant. The labels of each panel in the figure correspond to those in Fig.3.

Software   The vehicle dynamics were calculated using CarSim (Mechanical Simulation Corp.) software with 1000Hz updating rate. To generate visual image, Unity 3D (Unity technologies) was used, its updating rate was 30Hz. Fig.4 shows an example of the computer graphics of LCDs II and III when the ego vehicle has just passed point A of the merging scenario.

4.2 Participants

Four individuals with a driver's license participated in the experiment. Their ages ranged from 21 to 24 (mean=22.8, sd=1.5), 3 males and 1 female. They were not given any special incentives in this experiment. The attributes of the participants are shown in Table.1.

Table 1. Attributes of the Participants.

Participant	Age	Sex	Driving frequency
P1	22	female	1/week
P2	23	male	1/week
P3	24	male	8/year
P4	22	male	1/week

4.3 Design

Protocol   The participants were instructed to merge into the main lane as usual. There were no instruction on steering, accelerating, and braking behaviors. However, the participants were instructed to control the velocity of the ego vehicle v_e close to the target velocity v_t until the ego vehicle passed point Z. The target velocity v_t was displayed on the right hand side of the dashboard for the participants (see Fig.3). The participants drove 108 trials in total, 36 trials per day for three days. In addition, the participants practiced on the DS for some time to be accustomed to it before starting the experiment each day.

Conditions   In order to generate variety of situations of merging, condition vector $\boldsymbol{C_i} = [x_{ei} \ x_{12} \ v_i]^T$ was determined by the following range from eq. (3) to eq. (4) .

$$\boldsymbol{C_i^{min}} = [-40[\text{m}] \ \ 20[\text{m}] \ \ 65[\text{km/h}]]^T \quad (3)$$

$$\boldsymbol{C_i^{max}} = [20[\text{m}] \ \ 60[\text{m}] \ \ 85[\text{km/h}]]^T \quad (4)$$

where subscript i denotes variables regarding vehicles V_i. Either $\boldsymbol{C_1}$ or $\boldsymbol{C_2}$ is selected randomly for each trial. In addition, v_t was randomly selected from 60, 70, and 80 km/h. The velocity v_j ($j = \{1, 2\}$) was determined by eq. (5).

$$v_j = v_i + \alpha \quad (5)$$

where $\alpha \in [-3, 3]$ was set for $j \neq i$.

5. RESULTS

5.1 Accuracy of Decision making model

The prediction accuracies of the decision making model, which is matching rate of prediction and measured data about merging space, was defined as eq. (6) by K-fold cross-validation method.

$$\frac{1}{K} \sum_{k=1}^{K} \frac{\sum_{i=1}^{N_k} \delta_{i,k}}{N_k}. \quad (6)$$

This method divides a sets of data to K groups. In eq. (6), N_k denotes the number of trials in the group k and function $\delta_{i,k} = 1$ is satisfied when the output of the model with the parameters identified through the learning data set of the remaining $k - 1$ groups coincides the observed results in the group k. Otherwise, $\delta_{i,k} = 0$ is satisfied. In this study, $K = 5$ was chosen.

The prediction accuracy at each position along the path of the ego vehicle of all the participants are shown in Fig. 5. As shown in the figure, The high accuracy in predicting merging space of the model was indicated. In addition, the prediction accuracies of all participants were not very high at point A. At point B, the accuracy of participants P3 and P4 reached 100 % while those of participants P1 and P2 were relatively smaller.

5.2 Distribution of driving data of explanatory variable plane

Figs. 6 and 7 illustrate the final merging spaces with regard to the explanatory variables plane for participants P1 and
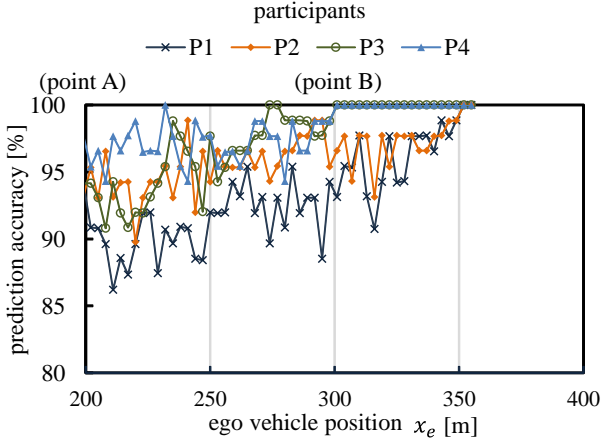
Fig. 5. Prediction accuracy of decision making model for every participants.
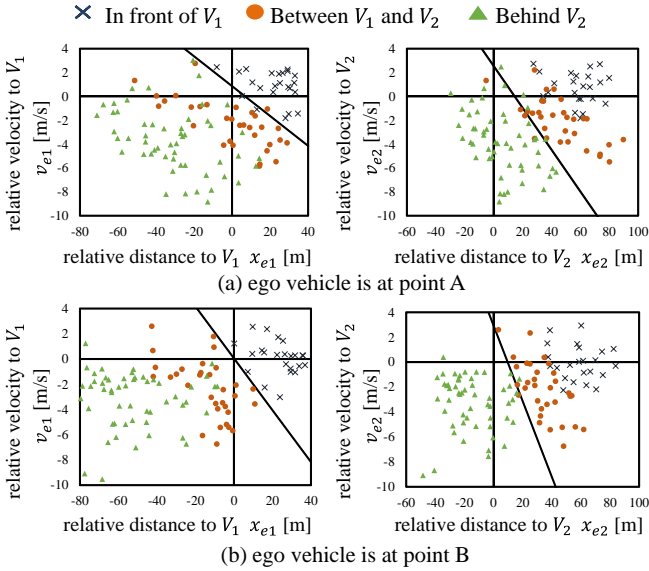
Fig. 6. Driving data of participant P1 at a certain position of ego vehicle, labeled by final merging space. A line on the explanatory variables plane illustrates $p = 0.5$ of decision making model.

P4 at points A and B. The line in each figure denotes $p_i = 0.5$ calculated by the logistic regression model that was used to predict the merging space . From these figures, the plots at point B are distributed farther from the $p_i = 0.5$ line than that at point A for both participants P1 and P4. This tendency was more significant for participant P4 than participant P1. It can be interpreted that the participants are facing difficulty in making their decision on the merging space when the plotted data is closer to the $p_i = 0.5$ line. From this interpretation, it is thought that the participant P4 may control the ego vehicle so as to be farther away from the line to avoid such a difficult situation. This reflects the fact that the model accuracies were different among participants P1 and P4 at point B. It is suggested that the driver's behaviors in merging operations could reflect driver's skill.
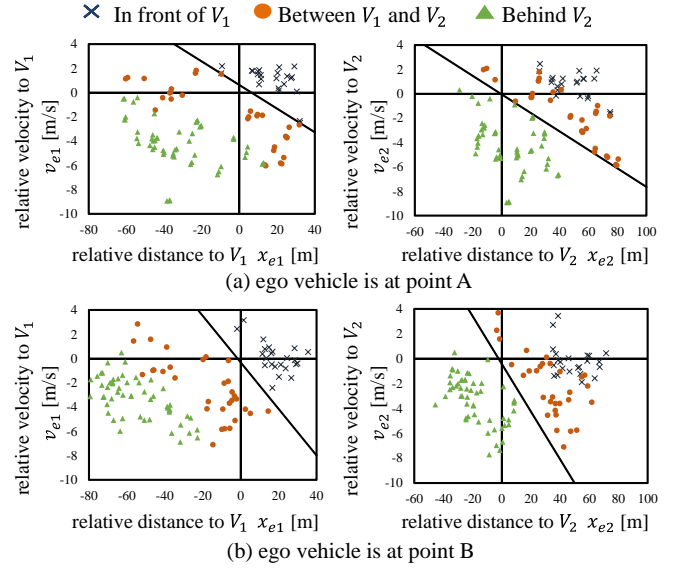
Fig. 7. Driving data of participant P4 at a certain position of ego vehicle, labeled by final merging space. A line on the explanatory variables plane illustrates $p = 0.5$ of decision making model.

6. CHARACTERIZATION OF DRIVER'S SKILL IN MERGING BEHAVIOR

In the previous section, it was observed that the points on the explanatory variable plane formed two groups according to the final merging position with the decision making model. In this section, we try to characterize the driver's merging behaviors from the viewpoint of their active longitudinal control using the forming process of these groups because the process is thought to reflect driver's active control.

6.1 Separation by final merging space

The behaviors of data points on the plane are investigated as follows. A separator line that divides the data points on the plane by the final merging space is calculated by the support vector machine (SVM) with a soft margin. The SVM was used after normalizing data. Fig. 8 shows the calculated results of the separator line by SVM for vehicle V_1 of participant P4 at $x_e = 200$ and 300 as an example. The types of plots in the figure denote the final merging space: cross is in front of V_1, circle is between V_1 and V_2, and triangle depicts behind V_2. It is found that the separator line by SVM separates data sets by the final merging space well.

Degree of separation of the two groups is quantified using the distance between the separator line and each data point. The separator line obtained by SVM for V_i is given by eq. (7).

$$\boldsymbol{w_i^T} \boldsymbol{x} + b_i = 0 \tag{7}$$

where x denotes the explanatory variables, w_i is its coefficient vector, and b_i denotes an intercept. Then, the distance between each data point $\boldsymbol{x_k}$ and the separator line $D_i(\boldsymbol{x_k})$ is determined by eq. (8).

$$D_i(\boldsymbol{x_k}) := \frac{\boldsymbol{w_i^T} \boldsymbol{x_k} + b_i}{||\boldsymbol{w_i}||} \tag{8}$$
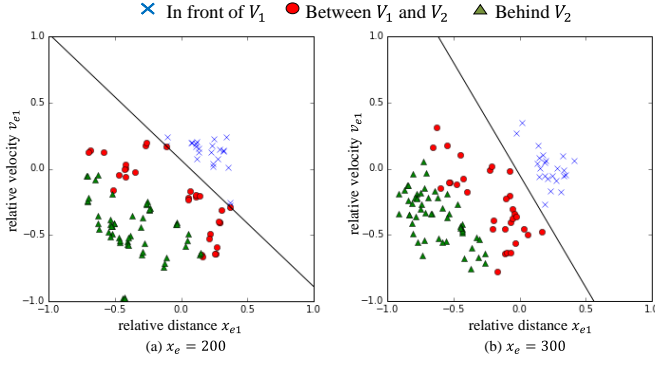
Fig. 8. A separator line between driving data merged in front of V_1 and the others determined by SVM.

where subscript i denotes vehicle V_i.

To quantify the degree of the separation of the two data sets, the frequency of the experimental trials where the data was far away from the separator line for vehicle V_i was defined as eq. (9).

$$f_i = \sum_{k \in S_i^F} \delta(D_i(\boldsymbol{x_k})) + \sum_{k \in S \setminus S_i^F} \delta'(D_i(\boldsymbol{x_k})) \qquad (9)$$

where S denotes the labels of all trials, and it was defined as $S = \{1, 2, \cdots, 108\}$. S_i^F denotes the labels of trials when the participant merged in front of vehicle V_i in S. The functions $\delta(D_i(\boldsymbol{x_k}))$ and $\delta'(D_i(\boldsymbol{x_k}))$ are defined as eq. (10) and eq. (11).

$$\delta(D_i(\boldsymbol{x_k})) := \begin{cases} 1 & (D_i(\boldsymbol{x_k}) > D_0) \\ 0 & (otherwise) \end{cases} \qquad (10)$$

$$\delta'(D_i(\boldsymbol{x_k})) := \begin{cases} 1 & (-D_i(\boldsymbol{x_k}) > D_0) \\ 0 & (otherwise) \end{cases} \qquad (11)$$

where D_0 is a threshold and $D_0 = 0.1$ is used. Fig 9 (a) and (b) show the transition of this frequency by the ego vehicle position for vehicle V_1 and V_2, respectively.

As shown in this figure, the frequencies of data that was far away from the separator line increases by ego vehicles position for all participants. The frequencies for participants P3 and P4 are greater than those for participants P1 and P2 for throughout the travel to V_1 and at the final stage for V_2. It demonstrates that participants P3 and P4 drove their vehicle differently according to the final merging position from the earlier stage of the merging preparation than other two participants. This tendency suggests that their skills of merging behavior were relatively high.

6.2 Activeness in longitudinal control

In order to investigate when drivers started to actively control their longitudinal direction, frequency of their jerk exceeding a given threshold is calculated based on the assumption that drivers accelerates or decelerates after they make their decisions for merging position. The number of trials in which jerk j [m/s³] satisfies inequality (12) is counted for each position after point A.

$$|j| > j_0 \qquad (12)$$

where j_0 denotes a threshold and $j_0 = 0.5$ is used in the present paper. The ego vehicle position that the jerk
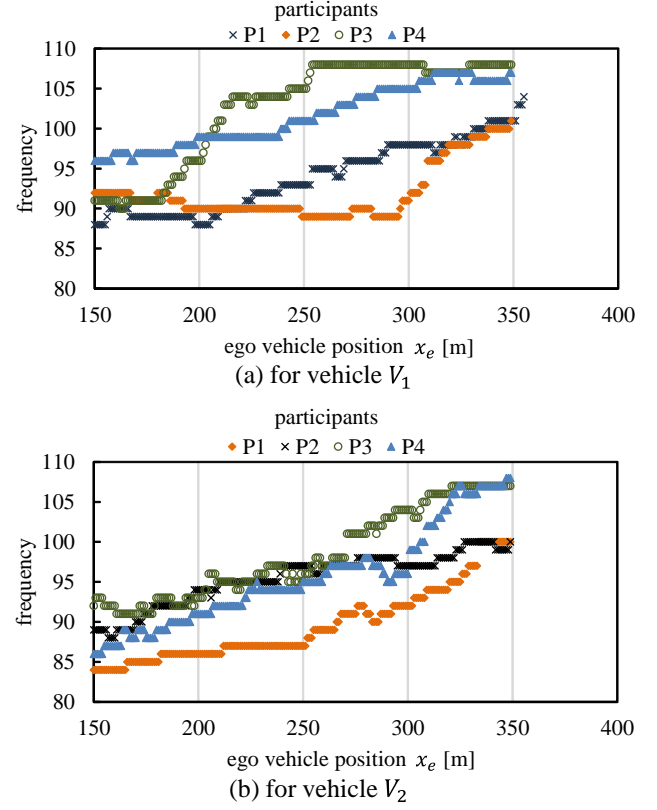
Fig. 9. Number of experimental trials where data was far away from a separator line.

firstly satisfies inequality (12) is referred to as action timing in the present paper. Fig. 10 shows the histogram of action timing of all participants. In this figure, the
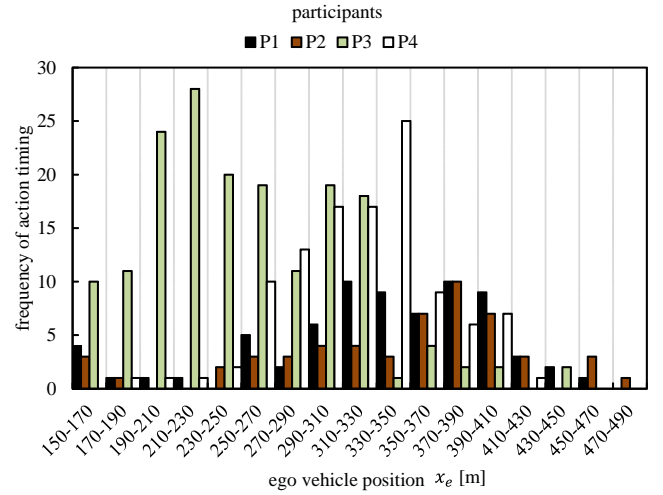
Fig. 10. Action timing.

bin was divided by ego vehicle position and the width is 20 [m]. Vertical axis indicates the frequency of action timing of all 108 trials of the experiment. As shown in this figure, action timing of participants P3 and P4 are greater than participants P1 and P2. This indicates that the participants P3 and P4 behaved more actively for merging than the others. Regarding ego vehicle position, it is shown that the participant P3 took action earlier than others. In addition, action timing of other participants

increased gradually as the ego vehicle approached merging point. In particular, the result of participant P4 shows this tendency clearly.

Given this result, the results of their longitudinal control on the phase plane suggests that the driver with high activeness leads to clear behavior for merging, and they are though to be skilled driver for merging. Therefore, it is suggested that the driver's skill can be characterized by the relationship of action timing and separating ability on the phase plane or clear distinction according to different final merging position.

7. CONCLUSION

This paper aimed to propose a method to characterize driver's merging behavior for quantifying driver's skill. The decision making model of the merging space suggest that the driver's behaviors in merging operations were different among individuals and the difference reflected driver's skill. On the basis of this suggestion, we tried to characterize the driver's merging behaviors from the viewpoint of their active longitudinal control. The degree of separation of driving data sets of the different final merging position is quantified by the distance between the separator line and each data point by the final merging space. The analysis results showed that the degree of the separation increased according to the ego vehicle position in the merging preparation lane. In addition, the degree of the separation was different among participants. Action timings in the longitudinal control that were detected by the vehicle jerk were different among drivers. It was found that the participants with larger separation degree had larger amount of active longitudinal control. These results demonstrated that the driver with activeness lead to clear behavior for merging. Therefore, it was indicated that the driver's skill can be characterized by process of clear distinction of the driving behavior sets with different final merging position.

A method to quantify the degree of driver's skill should be developed for applying it for advanced driving assistance systems to improve driving performance in merging operations.

REFERENCES

Baumann, M., Steenken, R., Kassner, A., Weber, L., and Ludtke, A. (2011). Merge into heavy motorway traffic by young and elderly drivers. In P. Cacciabue, M. Hjalmdahl, A. Ludtke, and C. Riccioli (eds.), *Human Modelling in Assisted Transportation*, volume II, 343–351. Springer-Verlag, New York, 3rd edition.

de Waard, D., Dijksterhuis, C., and Brookhuis, K. (2009). Merge into heavy motorway traffic by young and elderly drivers. *Accident Analysis and Prevention*, 41, 588–597.

de Waard, D., Thigri, G., Bold, V.D., and Lewis-Evans, B. (2010). Driver hand position on the steering wheel while merging into motorway traffic. *Transportation Research Part F: Traffic Psychology and Behavior*, 13, 129–140.

Gipps, P. (1981). A behavioural car-following model for computer simulation. *Transportation Research Part B: Methodological*, 15, 105–111.

Goodrich, M., Boer, E., and Inoue, H. (1999). A characterization of dynamic human braking behavior with implications for acc design. *Proceedings of IEEE/IEEJ/JSAI Conference on Intelligent Transportation Systems*, 964–969.

Herman, D.G.R. and Rothery, R. (1961). Nonlinear follow the-leader models of traffic flow. *Operations Research*, 9, 545–567.

Lee, D. (1976). A theory of visual control of braking based on information about time-to-collision. *Perception*, 5, 437–459.

Markkula, G., Benderius, O., Wolff, K., and M.Wahde (2012). A review of near-collision driver behavior models. *Human Factors*, 54, 1117–1143.

Ueda, S. and Wada, T. (2015). Modeling of drivers' decision making of merging space on expressways. *Proceedings of 41st Annual Conference of the IEEE Industrial Electronics Society(to be submitted)*.

Wada, T., Doi, S., Tsuru, N., Isaji, K., and Kaneko, H. (2010). Characterization of expert drivers' last-second braking and its application to a collision avoidance system. *IEEE Transactions on Intelligent Transportation Systems*, 11, 413–422.

Yamanaka, N., Kuriyagawa, Y., Kaneko, T., Momiyama, F., and Kageyama, I. (2012). Study on construction of decision making at junctions of highway. *Proceedings of JSAE*, 87-12, 1–4.

An Experimental Study on the Effect of Sequential Transverse and Lateral Markings on Perceived Speed in Curved Road

Hirofumi Yotsutsuji*. Takahide Matsumoto**. Keiichiro Yonemura***. Hideyuki Kita****.

*Organization of Advanced Science and Technology, Kobe University,
1-1 Rokkodai, Nada-ku, Kobe, Hyogo 657-8501, Japan, (e-mail: yotsutsuji@people.kobe-u.ac.jp).
**Katahira & Engineers Inc., Osaka Branch Office,
2-14-14 Miyahara, Yodogawa-ku, Osaka, Osaka 532-0003, Japan, (e-mail: tak@katahira.co.jp).
***Katahira & Engineers Inc., Tokyo Head Office,
2-22-2 Koishikawa, Bunkyo-ku, Tokyo 112-0002, Japan, (e-mail: yonemura@katahira.co.jp).
****Department of Civil Engineering, Graduate School of Engineering, Kobe University,
1-1 Rokkodai, Nada-ku, Kobe, Hyogo 657-8501, Japan, (e-mail: kita@crystal.kobe-u.ac.jp).

Abstract: For the purpose of enhancing road markings to prevent speeding on curved road, we focused on the vehicle speed inducement effect of sequence patterns of sequential transverse and lateral markings on a straight section of roadway leading into a transition section of the curved road. We tested the effectiveness of several sequence patterns through a driving simulation experiment with a driving simulator (DS) and a driver perception experiment with recorded moving pictures (MPs). The sequence patterns were characterised by patterns of progressively and concurrently reduced spacing of transverse lines on the lane surface and lateral poles on both the shoulder edge and the median strip. While estimating trends in spot speed that was perceived by a driver (test subject) who went into the curve entrance under the influence of sequence patterns, we examined a discrepancy between the perceived speed transition and the vehicle speed transition, by using hidden Markov model (HMM) on the estimation. We prepared four types of the sequence patterns including the types which had greater decrease rates of the intervals of spacing in the beginning, middle, and end sections than in the remaining sections among all the sections consisting of the pattern. The experimental results concluded that the sequence pattern type which had greater decrease rates in the end section than in remaining sections might be encouraged to be laid on the curved road, in terms of a safe vehicle speed inducement effect.

Keywords: road markings, sequence pattern, vehicle speed inducement effect, speed perception, hidden Markov model, driving simulator, in-house experiment

1. INTRODUCTION

In order to realise active safety on expressways, enhancing safety equipment such as road markings is required in addition to both improving vehicle technology and educating driving technique. As for road surface markings inducing a driver to decelerate, it is known that, while driving a vehicle on the markings with a pattern of progressively reduced spacing after having adapted to a constant speed, the driver decelerates due to an illusion that the speed is increasing (Denton, 1966). Recently on the road surfaces and tunnel walls in Japanese expressways, not only the markings producing the deceleration inducement effect but also those with progressively increased spacing producing the acceleration inducement effect have been reported by traffic administratours (Adachi et al., 2010, Han et al., 2013). However, a mechanism by which these markings develop the vehicle speed inducement effects has not been clear yet.

As for the vehicle speed inducement mechanism, we focus on driver's perception of speed, and we hypothesise that the change of flow speed at which the markings flow relative to the vehicle speed may trigger either the decelerating or accelerating behaviours in the driver via visual perception (Yotsutsuji et al., 2010). If a correlation between the change of flow speed of the markings and the change of the speed perceived by the driver can be discovered on the basis of validations on predetermined alignment patterns of the markings, a reasonable alignment that puts both the vehicle speed and the driver-perceived speed within safety zone will be determined. The reasonable intervals of spacing in the markings will then be able to be designed to realise active safety because of not only the vehicle speed but also the driver-perceived speed lower than a safety speed. However, the relationship among the vehicle speed transitions, the driver-perceived speed transitions, and the alignment patterns has not been clear so far.

Yotsutsuji et al. (2015) proposed sequential transverse and lateral markings that produce the deceleration inducement effect on a single-lane straight road. Through a driving simulation experiment with a driving simulator (DS) and a driver perception experiment with recorded moving pictures (MPs), they tested the effectiveness of several sequence patterns of the markings displayed on one lane of a two-lane bi-directional intercity expressway typical of Japan. They

referred to "sequential transverse and lateral markings" as road markings which are characterised by a sequence pattern of progressively and concurrently reduced spacing of transverse lines on the lane surface and lateral poles on both the shoulder edge and the median strip, a "sequence pattern" as an alignment pattern which is composed by the intervals of spacing of the sequential transverse and lateral markings, and a "sequence effect" as a vehicle speed inducement effect which has been produced by the sequence pattern. As for the alignment of the intervals of spacing in the sequence pattern, they proposed to divide the markings into a number of sections. Although the intervals were equally spaced in each section, the degree of the equally spaced intervals in an arbitrary section was decreasing at a rate greater than that in the previous section. Hence, by comparison with two adjacent sections, the degree of spacing in each section was decreasing in the direction of vehicle forward movement, although the equally spaced intervals were within the limits of each section. By the way, since even without the sequential transverse and lateral markings the drivers seem to decelerate on the straight section leading into the curve, the sequence patterns on the curved road should consider the impact of deceleration behaviour of the drivers who face with the curve.

We focus on the sequence patterns aligned on the straight section leading into the curve, although Yotsutsuji et al. (2015) focused on those aligned on the straight road only. Through the driving simulation experiment and the driver perception experiment, we test the effectiveness of several sequence patterns on the curved road with several curvatures, while displaying the patterns on one lane of a two-lane bi-directional intercity expressway typical of Japan. The purpose of this study is to examine a discrepancy in transition between the vehicle speed and driver-perceived speed while estimating trends in spot speed that is perceived by a driver (test subject) who goes into the curve entrance under the influence of several sequence patterns, by using hidden Markov model (HMM) on the estimation.

2. METHODS

2.1 Procedure

We adopt the following procedure of study in the almost same manner as Yotsutsuji et al. (2015) although considering a few distinctions.

We first conduct the driving simulation experiment in which the vehicle speed transitions are investigated in relation to several types of the sequence patterns on the curved road. As we employed a commercial-release DS in this experiment, UC-win/Road 9.1 Driving Sim from FORUM 8 was put into use and a main monitor screen mounted around the driving seat was hi-vison display of 138 cm times 84 cm, in addition to two sub monitors on both sides of the driving seat. In this experiment, we can figure out only the relationship between a vehicle speed transition obtained from the experiment and a given sequence pattern. With regard to a driver-perceived speed transition based on a given vehicle speed transition under a given pattern, we estimate it by using the HMM. The

HMM requires the initial state probabilities of latent variables expressed by the perceived speed, which can be represented by the conditional probabilities of the vehicle speed.

We then conduct the driver perception experiment to identify the initial state probabilities of the driver-perceived speed under a given equally-spaced interval on the straight road. The reason why it is on the straight road is because the beginning road section leading into the curve becomes straight. We prepare three types of MPs in order to raise more accuracy of investigation in our study than it in Yotsutsuji et al. (2015). The first is a reference MP in which the sequence patterns are displayed at a constant speed on the DS screen. The second is a comparison MP of which the sequence pattern types and the MP playback speeds differ from those of the reference MP. Both the pattern type and the playback speed of the comparison MP are constant regardless of number of trials. The third is a random MP in which a combination of the pattern type and the playback speed changes in random order through trials. Three MPs are simultaneously displayed on a large screen of 260 cm times 90 cm. A group of the test subjects concurrently takes part in the experiment, looking at the screen all together. Comparing a difference in flow speed between the comparison and reference MPs with one between the random and reference MPs, the subjects choose which difference is larger. We examine a difference in flow speed between the comparison MP and the random MP in the case that the choice probability is 0.5. We consider it as a discrepancy between the MP playback speed and the subject-perceived speed under the given interval.

Finally, we use the HMM to estimate the driver-perceived speed transition under the given vehicle speed transition in the case of each of the sequence patterns and each of the curvature radii. The driver perception experiment easily analyses correspondence relationships, but not transitioning. In contrast, the driving simulation experiment easily measures the vehicle speed, but not continuous data related to the driver-perceived speed. For these reasons, we estimate transitions of the perceived speed using the HMM. In this study, the change rate of the perceived speed is a discrete latent variable of the HMM and the transition of change rate of the vehicle speed observed under each sequence pattern is supervised data of the HMM.

2.2 Experiments

2.2.1 Driving simulation experiment

Fig. 1 shows a snapshot of the DS screen. Although the roadway displayed on the screen was a two-lane bi-directional expressway, a driver (test subject) drove on one lane of the expressway. In the same manner as Yotsutsuji et al. (2015), total width of the roadway was 13 m, comprising two 3.5 m lanes, a 1.5 m median strip, two 1.75 m left shoulders, and two 0.5 m right shoulders. In the sequential transverse and lateral markings illustrated in Fig. 1, the width of each transverse line in the direction of vehicle movement was 45 cm, and the length of each transverse line

perpendicular to the lane was 3.5 m. The height of each lateral pole on both the left shoulder edge and the median strip was 2.5 m. In contrast to Yotsutsuji et al. (2015), the curvature radii varied with a distance of 100 m between 200 m and 1000 m on the lane equipped with an arbitrary sequence pattern.

The test subjects were 10 fourth year students at Kobe University, each of whom was an unskilled driver with an AT-car-only license. No speedometer was displayed on the DS screen when the test subjects drove on lane sections with the markings. The speedometer, on the other hand, was displayed when they drove on a run-up section in which they accelerated from speed zero. Taking a look at the speedometer in the run-up section preceding the marking sections, they held the feeling of adjusting the driving speed.

We experimented on a high-speed driving and a low-speed one, because there was the experience in which the vehicle speed chosen by the subjects eventually tended to be high in the experiment in Yotsutsuji et al. (2015). In our study, the experimenter instructed each subject to adjust the driving speed to be the high and low levels in the run-up section in the high-speed and low-speed driving tests, respectively. In the high-speed test, the length of the run-up section was 600 m and the target speed when driving in the run-up section was 80 km/h, while a 200m length and a 40 km/h target speed in the low-speed test.

The tests were run three times for an arbitrary combination of the sequence patterns, the run-up target speeds, and the curvature radii. The experimenter instructed each subject to enter the curve in safety while the subject drove looking into the far distance along the marking sections in the DS screen. Two trial tests with the speedometer without the markings were done before all three times run. In all run, conditions of the lane surface and the weather in the DS were dry and serene, respectively.

Table 1 shows four sequence patterns labelled A, B, C, and D, which were provided to the test subjects. Each of sections involving section Z was aligned with equally spaced interval, but the intervals decreased in two adjacent sections. We here define a decrease rate (DR) of the equally spaced intervals in two adjacent sections, as the indicator that can be calculated to divide the value of an arbitrary section interval minus the previous section interval by the value of the previous section interval. Types A, B, and C had respectively greater DRs in the beginning, middle, and end sections than in the remaining sections. Concerning the DRs, any of 5%, 10%, or 15% was applied to the rates, except type D. Type D had a zero DR because of its equally spaced intervals.

Five sections labelled I-V in Table 1 were preceded by the run-up section, in the same manner as Yotsutsuji et al. (2015). The length of each section I-V was 100 m. The run-up section had the markings with 12 m intervals, the last 100 m in which was labelled as Z.

2.2.2 Driver perception experiment

Fig. 1. A snapshot of screen display in the DS. (Keeping to the left).

Table 1. The four sequence patterns.

	Section	Z	I	II	III	IV	V
	Length [m]	100	100	100	100	100	100
A	Interval [m]	12.00	10.20	9.18	8.72	8.28	7.87
	DR [%]	0	15	10	5	5	5
B	Interval [m]	12.00	11.40	10.26	8.72	7.85	7.46
	DR [%]	0	5	10	15	10	5
C	Interval [m]	12.00	11.40	10.83	10.29	9.26	7.87
	DR [%]	0	5	5	5	10	15
D	Interval [m]	12.00	12.00	12.00	12.00	12.00	12.00
	DR [%]	0	0	0	0	0	0

Fig. 2. A snapshot of motion pictures displayed in large screen.

Fig. 2 shows a snapshot in the MP comparisons, which was watched by a group of the subjects. In order from the left to the right of Fig. 2, the comparison MP, the reference MP, and the random MP are located in the left, the middle, and the right, respectively. Every time all MPs were simultaneously played back, the sequence pattern type and playback speed were randomly changed in the random MP located on the far right in Fig. 2. We experimented on a high-speed test and a low-speed one just like the driving simulation experiment. In both tests, the comparison and reference MPs had 12 m intervals being the same as the type D sequence pattern. In the high-speed test, the playback speed of the comparison MP and that of the reference MP were 65 km/h and 75 km/h, respectively. In the low-speed test, on the other hand, the playback speed of the comparison MP and that of the reference MP were 25 km/h and 35 km/h, respectively.

We prepared several random MPs displaying the markings at four cases of the intervals and displayed at eight cases of the playback speeds for six cases consisting of the transverse-only, the lateral-only, and the transverse and lateral markings in both the high-speed and low-speed tests. In short, the experimenter showed a test subject 192 cases of random MPs

Table 2. Random MP comparisons. (High-speed test).

Case	1	2	3	4	5	6	7	8
Interval [m]	12.0	12.0	12.0	12.0	12.0	12.0	12.0	12.0
Speed [km/h]	75	72	70	69	67	65	60	55
Case	9	10	11	12	13	14	15	16
Interval [m]	11.4	11.4	11.4	11.4	11.4	11.4	11.4	11.4
Speed [km/h]	75	72	70	69	67	65	60	55
Case	17	18	19	20	21	22	23	24
Interval [m]	10.8	10.8	10.8	10.8	10.8	10.8	10.8	10.8
Speed [km/h]	75	72	70	69	67	65	60	55
Case	25	26	27	28	29	30	31	32
Interval [m]	10.2	10.2	10.2	10.2	10.2	10.2	10.2	10.2
Speed [km/h]	75	72	70	69	67	65	60	55

Table 3. Random MP comparisons. (Low-speed test).

Case	1	2	3	4	5	6	7	8
Interval [m]	12.0	12.0	12.0	12.0	12.0	12.0	12.0	12.0
Speed [km/h]	35	32	30	29	27	25	20	15
Case	9	10	11	12	13	14	15	16
Interval [m]	11.4	11.4	11.4	11.4	11.4	11.4	11.4	11.4
Speed [km/h]	35	32	30	29	27	25	20	15
Case	17	18	19	20	21	22	23	24
Interval [m]	10.8	10.8	10.8	10.8	10.8	10.8	10.8	10.8
Speed [km/h]	35	32	30	29	27	25	20	15
Case	25	26	27	28	29	30	31	32
Interval [m]	10.2	10.2	10.2	10.2	10.2	10.2	10.2	10.2
Speed [km/h]	35	32	30	29	27	25	20	15

in random order, which calculated as 32 cases times 6 cases. Table 2 and Table 3 show the 32 cases of the high-speed test and those of the low-speed test, respectively.

The test subjects were 44 people, a part of whom was publicly recruited, consisting of fourteen unskilled young drivers, eleven unskilled old drivers, eight skilled young drivers, and eleven skilled old drivers. If a subject has held a driving licence more than three years and has driven more than two times a week, we considered him/her as a "skilled" driver, otherwise an "unskilled" driver. Moreover, we considered the over 50s as an "old" driver, otherwise a "young" driver. Immediately after the experimenter played one of the cases shown in Table 2 or 3 during 30 seconds, the subject compared a difference in playback speed between the comparison and reference MPs with one between the random and reference MPs, while the experimenter forcibly let the subject choose which difference was larger, within 7 seconds. Each of the subjects repeatedly made such choice total of 192 times, based on 32 cases shown in Table 2 or 3.

2.3 Models

2.3.1 Hidden Markov model

For readers' convenience, we briefly explain here part of our models which relates to the HMM (with regard to all the details of our models including the HMM, see also Yotsutsuji

et al., 2015; with regard to solution algorithms of the HMM, see for example Zucchini et al., 2009).

A HMM is, in general, a Markov chain of each discrete latent variable in combination with some discrete observed variables, and it requires both the number of the latent and observed variables and the initial probability distribution regarding the latent variable (Zucchini et al., 2009). In our study, the latent variable and the observed variable correspond to the driver-perceived speed and the vehicle speed, respectively. As for how to determine the number of both variables, we propose discretising the change rate of speed to partitions by "class". Before explaining the "class", we begin to define a "change rate" of speed as the indicator that can be calculated to divide the value of the average speed in an arbitrary section minus that in the previous section by the value of the average speed in the previous section. The term "class" means a partition of the change rate of speed over a common range regardless of section, sequence pattern, driver, and drive frequency. Yotsutsuji et al. (2015) proposed to divide the change rate of speed into seven parts, each of which had the upper and lower limits, and tested the goodness-of-fit regarding these limits. According to this result, our study adopts seven parts as the number of class.

We now define Δ_{S}^{dq} as a change rate of the driver-perceived speed representative of all drivers in section $d \in D$ with sequence pattern $q \in Q$. When Δ_{S}^{dq} belongs to the k-th class, we let the class be C_{Sk}^{dq}, where $k \in K$. Concerning the vehicle speed, the same applies to C_{Ok}^{dq}, where $k \in K$. The upper and lower limits of C_{Sk}^{dq} are the same as those of C_{Ok}^{dq}. Since C_{Sk}^{dq} represents that the change rate of the driver-perceived speed belongs to class k, the changed driver-perceived speed can be estimated through multiplying C_{Sk}^{dq} by the driver-perceived speed in section $d-1$. Suppose that $\{C_{O}^{1q}, \cdots, C_{O}^{d-1,q}, C_{O}^{dq}, \cdots, C_{O}^{Dq}\}$ representing a series of C_{Ok}^{dq} has been observed from section 1 to D. We premise the Markov property for transitions of C_{Sk}^{dq}. A transition probability p_{lk} is defined as the probability that the class of the driver-perceived speed homogeneously transitions from $C_{Sl}^{d-1,q}$ to C_{Sk}^{dq}. An outcome probability $\Pr(C_{Sl}^{d-1,q} \mid C_{Oh}^{d-1,q})$ is defined as the probability that $C_{Sl}^{d-1,q}$ occurs subject to $C_{Oh}^{d-1,q}$. We then define $\hat{p}(C_{Sk}^{dq})$ as the maximum among the probabilities that the series from section 1 to d, $\{C_{O}^{1q}, \cdots, C_{O}^{dq}\}$, have been observed when the driver-perceived speed belongs to C_{Sk}^{dq} in section d. Based on the Viterbi algorithm in the HMM, $\hat{p}(C_{Sk}^{dq})$ is calculated by the following recursive equation.

$$\hat{p}(C_{Sk}^{dq}) = \max_{l} \left\{ \hat{p}(C_{Sl}^{d-1,q}) p_{lk} \Pr(C_{Sl}^{d-1,q} \mid C_{Oh}^{d-1,q}) \right\}. \tag{1}$$

Based on the Baum-Welch algorithm in the HMM, the transition probability p_{lk} can be calculated as follows. Focusing on $\{C_{Sl}^{d-1,q}, C_{Sk}^{dq}\}$ and $\{C_{Oj}^{d-2,q}, C_{Oh}^{d-1,q}, C_{Om}^{dq}, C_{On}^{d+1,q}\}$ from section $d-1$ to d, we define $f(C_{Sl}^{d-1,q})$ as the summation of the probabilities that the forward series from section 1 to $d-1$, that is $\{C_{O}^{1q}, \cdots, C_{O}^{d-1,q}\}$, have been observed when the driver-perceived speed belongs to $C_{Sl}^{d-1,q}$

in section $d-1$, $g(C_{Sk}^{dq})$ as the summation of the probabilities that the backward series from section D to d, $\{C_O^{dq}, \cdots, C_O^{Dq}\}$, have been observed when the driver-perceived speed belongs to C_{Sk}^{dq} in section d. The forward indicator $f(C_{Sl}^{d-1,q})$ and the backward indicator $g(C_{Sk}^{dq})$ are defined by the following recursive equations.

$$f(C_{Sl}^{d-1,q}) = \sum_{i \in K} f(C_{Si}^{d-2,q}) p_{il} \Pr(C_{Si}^{d-2,q} \mid C_{Oj}^{d-2,q}), \quad (2)$$

$$g(C_{Sk}^{dq}) = \sum_{i \in K} g(C_{Si}^{d+1,q}) p_{ki} \Pr(C_{Si}^{d+1,q} \mid C_{On}^{d+1,q}). \quad (3)$$

A transition probability at section $d-1$, γ_{lk}^{d-1}, is defined as the following equation using $f(C_{Sl}^{d-1,q})$ and $g(C_{Sk}^{dq})$.

$$\gamma_{lk}^{d-1} = \frac{f(C_{Sl}^{d-1,q}) p_{lk} \Pr(C_{Sk}^{dq} \mid C_{Om}^{dq}) g(C_{Sk}^{dq})}{\sum_{a \in K} \sum_{b \in K} f(C_{Sa}^{d-1,q}) p_{ab} \Pr(C_{Sb}^{dq} \mid C_{Om}^{dq}) g(C_{Sb}^{dq})}. \quad (4)$$

Accordingly, p_{lk} is calculated as the value that divides the expectation of γ_{lk}^{d-1} transitioning from class l to k by the expectation of $\gamma_{l\bullet}^{d-1}$ transitioning from class l to any class. $\Pr(C_{Sk}^{dq} \mid C_{Om}^{dq})$ is calculated as the value that divides the expectation of $\gamma_{k\bullet}^d$ when observing class m by the expectation of $\gamma_{k\bullet}^d$ when observing any class. Then, p_{lk} and $\Pr(C_{Sk}^{dq} \mid C_{Om}^{dq})$ are represented by the following equations.

$$p_{lk} = \frac{\sum_{d-1 \in D} \gamma_{lk}^{d-1}}{\sum_{c \in K} \sum_{d-1 \in D} \gamma_{lc}^{d-1}}, \quad (5)$$

$$\Pr(C_{Sk}^{dq} \mid C_{Om}^{dq}) = \frac{\sum_{m \in K} \sum_{c \in K} \gamma_{kc}^d}{\sum_{d \in D} \sum_{c \in K} \gamma_{kc}^d}. \quad (6)$$

There exist p_{lk} and $\Pr(C_{Sk}^{dq} \mid C_{Om}^{dq})$ inside γ_{lk}^{d-1} in equation (4), so that equation (5) and (6) are solved with iterative convergence computation via the EM algorithm (Zucchini et al., 2009).

By the way, the HMM requires the initial distribution of latent variables corresponding to that of observed variables. As for the observed variables, the initial distribution of those can be obtained from the initial vehicle speed in section Z shown in Table 1. In contrast, as for the latent variables, we estimate the initial distribution of those by using a binary logit model which belongs to the discrete choice models, based on the results of the driver perception experiment (with regard to more details of discrete choice models, see for example Train, 2003).

2.3.2 Binary logit model

For readers' convenience, we briefly explain here the binary logit model in our study. In the case that a difference in playback speed between the random and reference MPs is larger than one between the comparison and reference MPs, we let $P_{\text{random}}(\theta)$, where $0 \leq P_{\text{random}}(\theta) \leq 1$, as a probability that the test subject chooses the former rather than the latter, and θ as a characteristic vector which is a column vector representing the difference between the characteristics of the former and those of the latter. If the subject feels that the former is absolutely identical to the latter, $P_{\text{random}}(\theta)$ is 0.5. We now assume that θ meets $\theta = (\theta_{\text{speed}}, \theta_{\text{interval}}, \theta_{\text{frequency}}, 1)$, where θ_{speed}, θ_{interval}, and $\theta_{\text{frequency}}$ represent a speed difference between the former and the latter, an interval difference between them, and a driving frequency of the subject, respectively. The units of θ_{speed}, θ_{interval}, and $\theta_{\text{frequency}}$ are kilometre per hour, metre, and times a week.

We then define an "odds" ratio and a "logit" as the following equations, where $\beta' = (\beta_{\text{speed}}, \beta_{\text{interval}}, \beta_{\text{frequency}}, \beta_0)'$ is the transposed vector of parameters.

$$logit = \ln odds = \ln \frac{P_{\text{random}}(\theta)}{1 - P_{\text{random}}(\theta)} = \beta' \cdot \theta, \quad (7)$$

$$P_{\text{random}}(\theta) = \frac{1}{1 + \exp[-\beta' \cdot \theta]}. \quad (8)$$

The parameter values of β are estimated by maximising the log-likelihood function using the maximum-likelihood method. Accordingly, $P_{\text{random}}(\theta)$ equal to 0.5 derives the following equation from equation (8).

$$\beta_0 + \beta_{\text{speed}}\theta_{\text{speed}} + \beta_{\text{interval}}\theta_{\text{interval}} + \beta_{\text{frequency}}\theta_{\text{frequency}} = 0. \quad (9)$$

Because θ_{speed} calculated from equation (9) is equivalent to the difference between the vehicle speed and the driver-perceived speed, we assume that the initial vehicle speed in section Z minus θ_{speed} meets the initial value of the driver-perceived speed.

3. RESULTS

Table 4 shows the results of parameter estimation on the binary logit model with explanatory variables θ, based on the driver perception experiment. In general, the goodness-of-fit of a logit model is considered to be strong when a McFadden's pseudo ρ^2 and a hit rate are more than about 0.2 and more than 70%, respectively, although 0.2 of the pseudo ρ^2 corresponds approximately to 0.5 of determination coefficient R^2 of an ordinary least square method. We therefore conclude that the goodness-of-fits illustrated in Table 4 are not very weak in terms of the common model for all the cases, on the basis of the results of the McFadden's pseudo ρ^2 and the hit rate.

No matter how playback speed is high or low in the driver perception experiment, the speeds and intervals of both the comparison and random MPs were as well or slower and shorter than those of the reference MP. Accordingly, when the random MP is compared with the comparison MP,

Table 4. Estimation results for binary logit model.

		High-speed test			Low-speed test		
		T/L	L	T	T/L	L	T
β_{speed}	[t-value]	0.161 [14.58**]	0.107 [9.72**]	0.124 [11.95**]	0.335 [19.04**]	0.219 [17.04**]	0.319 [18.58**]
$\beta_{interval}$	[t-value]	-0.422 [-4.70**]	-0.495 [-5.56**]	-0.482 [-5.58**]	-0.471 [-4.12**]	-0.378 [-3.96**]	-0.462 [-4.29**]
$\beta_{frequency}$	[t-value]	-0.146 [-2.14*]	0.132 [1.96*]	0.141 [2.14*]	-0.163 [-1.89]	0.016 [0.22]	0.071 [0.87]
β_0	[t-value]	0.588 [4.62**]	1.206 [9.25**]	0.578 [4.72**]	0.391 [2.46*]	0.041 [3.04**]	0.485 [3.18**]
McFadden's pseudo ρ^2		0.155	0.144	0.103	0.427	0.236	0.371
Hit rate		75.2	40.5	67.7	74.7	74.1	71.6

T/L : the transverse and lateral markings, L : the lateral-only markings, T : the transverse-only markings.
* p < .05, ** p < .01.   Sample size : 1,408.
McFadden's pseudo ρ^2 : the likelihood ratio index defined as "(beginning log-likelihood – final log-likelihood) / beginning log-likelihood".
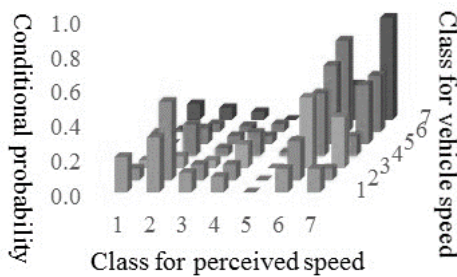Hit rate : the percentage of choices predicted correctly in the consequences of choice.

Fig. 3. Conditional probability of class for perceived speed based on class for vehicle speed corresponding to class for section speed in section Z in type D pattern.

Table 5. Class settings. (Yotsutsuji et al., 2015)

Class	1	2	3	4	5	6	7
UL [%]	-100	-8	-4	-2	-1	0	3
LL [%]	-8	-4	-2	-1	0	3	100

UU : the upper limit, LL : the lower limit.

$P_{random}(\boldsymbol{\theta})$ means the probability that the random MP is chosen by the test subject who has felt the random MP moving as well or slower than the comparison MP, although there are cases when the speed of the random MP is faster than that of the comparison MP as described in Table 2 and 3.

Parameter signs in Table 4 show that β_{speed}, $\beta_{interval}$, and β_0 are positive, negative, and positive, respectively, for all the cases. Because β_{speed} is positive, an extra unit of θ_{speed} produces the increase of $P_{random}(\boldsymbol{\theta})$. This means that, "ceteris paribus", the random MP is chosen if the speed of it is slower than that of the comparison MP. Because $\beta_{interval}$ is negative, an extra unit of $\theta_{interval}$ produces the decrease of $P_{random}(\boldsymbol{\theta})$. This means that, ceteris paribus, the random MP is not chosen if the interval of it is shorter than that of the comparison MP. In short, the shorter the equally spaced intervals are, the faster the subject feels. Because β_0 is positive, $P_{random}(\boldsymbol{\theta})$ is positive if $\boldsymbol{\theta}$ is zero. In addition, equation (9) derives $\theta_{speed} = -\beta_0 / \beta_{speed} < 0$ if $\theta_{interval}$ and

$\theta_{frequency}$ are zeros and $P_{random}(\boldsymbol{\theta})$ is 0.5. This means that, in the case that the intervals of both the comparison and random MPs are equal as 12 m, even if the test subject feels the speeds of both MPs equal, the speed of the random MP is actually faster than that of the comparison MP. In short, there is a systematic discrepancy by which the perceived speed is faster than the actual speed in both the high-speed and low-speed tests. This means that, for example, a driver estimates a vehicle speed at 80 km/h in contrast with 70 km/h of the actual vehicle speed. We here regard this as a propensity to overestimate the vehicle speed.

Fig. 3 shows a conditional probability distribution of the perceived speed class based on the vehicle speed class in the type D sequence pattern, which becomes the distribution of initial state of the HMM. As the DS has measured a spot speed per about 0.02 second for each section and the test subject has run three times on the section, we consider an average of the three average spot speeds as a "section speed" of the vehicle. The interval of the markings was 12 m in section Z in which the initial vehicle speed was obtained, so we estimated the conditional probability of the perceived speed class by employing the results of driver perception experiment in the case of 12 m intervals of the random MP.

As shown in Table 5, we used the seven classes. We determined the upper and lower limits for each class, in the same manner as Yotsutsuji et al. (2015). The subject-perceived speed corresponding to the section speed for each section can be estimated by using the upper or lower limit. The perceived speed in an arbitrary section, namely, was obtained to multiply the value in which the upper limit of the class in the arbitrary section plus one by the value of the perceived speed in the previous section.

Fig. 4 shows the results of estimating the discrepancy between the driver-perceived speed and the vehicle speed for each curvature radius in the case of the high-speed and low-speed areas under a given sequence pattern, based on the driving simulation experiment. In this regard, however, each perceived speed for each curvature radius in Fig. 4 is shown
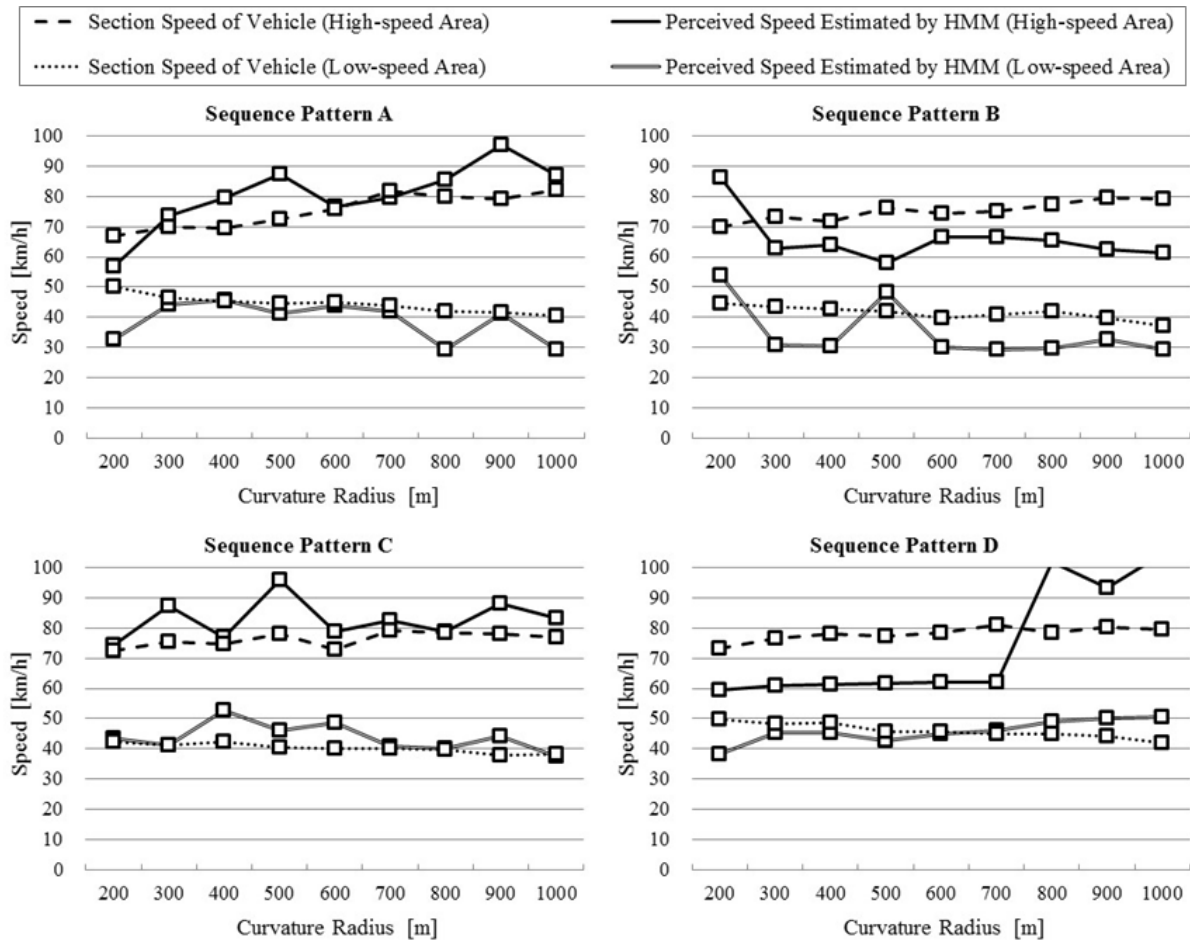
Fig. 4. Discrepancy between driver-perceived speed and vehicle speed for each curvature radius in the case of the high-speed and low-speed areas under a given sequence pattern.

as the average of the section IV and V perceived speeds. The same applied to each vehicle speed for each curvature radius shown in Fig. 4. As we figured out that the subjects had a propensity to overestimate the actual speed in both the high-speed and low-speed areas in section Z as the results of the driver perception experiment, we were therefore interested in whether or not the subjects had the same propensity in the sections near the curve. This is the reason why we used an average of the section speeds in section IV and V.

We regard a propensity to underestimate a driving speed as dangerous in the curved road. An "underestimation" of the speed here gives expression to the case of the perceived speed transition located below the vehicle speed transition, otherwise an "overestimation". Let us now consider which sequence pattern is best for among types A, B, C, and D for a given curvature radius, from the viewpoint of the vehicle speed inducement effect. Suppose the overestimation of speed occurs on the beginning sections of the sequence pattern. When any one of the sequence pattern types is laid on the last sections near the curve, it may as well not cause the speed change due to the underestimation. Accordingly, the curvature radius under which the perceived speed is

located above the vehicle speed in Fig. 4 is considered not to be dangerous.

Among the sequence pattern types shown in Fig. 4, the high-speed area of type A, the high-speed area of type D, and the low-speed area of type D show a tendency to shift from the underestimation to the overestimation while the curvature radii change from 200 m and 1000 m. We can find thresholds of the curvature radii existing 200 to 300 m, 700 to 800 m, and 600 to 700 m in the high-speed area of type A, the high-speed area of type D, and the low-speed area of type D, respectively. In contrast, the high-speed and low-speed areas of type B show a tendency to shift from the overestimation to the underestimation while the curvature radii change from 200 m to 1000 m. We can also find threshold of the curvature radius existing 200 to 300 m in the high-speed and low-speed areas of type B. As for the rest, the high-speed and low-speed areas of type C show a tendency to remain at the overestimation, and the low-speed area of type A show a tendency to remain at the underestimation.

Type B should be discouraged because of existing the underestimation of speed in almost all curvature radii in both

the high-speed and low-speed areas. Type A should be also discouraged because of remaining at the underestimation in the low-speed area. Type D may be conditionally encouraged in both the high-speed and low-speed areas if the curvature radius is more than 800 m.

We conclude that type C may be encouraged for the reason set forth above.

4. CONCLUSION

Our experiments resulted in the following main findings:

- The driver perception experiment regarding the markings on the straight road showed that (1) the shorter the equally-spaced intervals were, the faster the test subjects felt, and (2) with regard to the equally spaced intervals, there was a systematic discrepancy by which the subjects had a propensity to overestimate vehicle speed in both the high-speed and low-speed areas.

- The driving simulation experiment regarding the markings on the curved road showed that (1) the sequence pattern types which had greater decrease rates of the intervals in the beginning and middle sections than in the remaining sections should be discouraged, and (2) the sequence pattern type which had a zero decrease rate because of equally spaced intervals may be conditionally encouraged in more than 800 m of the curvature radius.

This study thus concludes that a sequence pattern type which had greater decrease rates in the end section than in remaining sections may be encouraged to be laid on the curved road, in terms of a safe vehicle speed inducement effect. Some issues remain. We have to analyse which marking is more effective between the transverse lines and the lateral poles in the curved road. We also have to develop a new HMM with consideration for the delays in speed perception. Finally, we need to study the impact of rapid deceleration of a lead vehicle on following vehicles leading into the curve after the lead vehicle encounters the markings, and whether a resulting accident is a concern in the curve.

ACKNOWLEDGEMENTS

REFERENCES

Adachi, Y., Fujii, Y., Tamagawa, D., Iwasato, Y., Yamada, K., and Nakamura, Y. (2010). Experimental study on speed reduction effect by sequence design. *Journal of the Japan Society of Civil Engineering: Part D*, 66, 27-39.

Denton, G.G. (1966). A subjective scale of speed when driving a motor vehicle. *Ergonomics*, 9, 203-210.

Han, A., Ono, S., Ikeuchi, K., Suda, Y., and Sasaki, M. (2013). Road marking 'Optical Dot System' for controlling the speed: development and four years empirical analysis. *Proc. of the 20th ITS World Congress*.

Train, K.E. (2003). *Discrete Choice Models with Simulation*. Cambridge University Press, Cambridge.

Yotsutsuji, H., Kita, H. (2010). Self-motion speed perception of visual information in driving. *Traffic and Transportation Studies*, 7, 1029-1045.

Yotsutsuji, H., Kitamura, K., and Kita, H. (2015). An experimental study on the effect of sequential transverse and lateral markings on perceived speed on a single-lane straight road. *Journal of Ergonomics*, S3:010, 1-7.

Zucchini, W., and MacDonald, I.L. (2009). *Hidden Markov models for time series: an introduction using R*. Chapman & Hall CRC Press, London.

Lane-level Localization using Around View Monitoring Camera for Automated Urban Driving

Dongwook Kim*. Taeyoung Chung**,
Kyoungsu Yi*

* Seoul National University, Gwanak 599, Gwanak-Ro, Seoul, Korea
(Tel: 82-2-880-1942; e-mail: mechar04@snu.ac.kr)
** Hyundai Mobis, 80-9, Mabook-dong, Hiheung-gu, Yongin-si, Gyeonggi
(e-mail: inxskick@mobis.co.kr)

Abstract: This paper describes a method of lane-level localization for automated driving using around view monitoring (AVM) camera. Today's on-board sensors such as radar or camera do not reach a satisfying level of development from the point of view of robustness and availability. Thus, map data is often used as an additional data input to support these systems. A digital map is used as a powerful additional sensor. So we propose a lane map-based localization using an AVM camera. The maps are created beforehand using an AVM camera and RTK GPS. A pose estimation of vehicle was derived from a low-cost GPS and an iterative closest point(ICP) match of real-time sensor data to lane map. And the estimated pose was used as an observation inside a Kalman filter framework. The performance of the proposed localization algorithm is verified via vehicle tests in ITS proving ground. It has been shown through vehicle tests that good localization performance can be obtained. The proposed algorithm will be useful in the implementation of automated driving.

Keywords: Lane-level Localization, Lane-level Map, Automated Driving, Lane Detection, Around View Monitoring Camera.

1. INTRODUCTION

In recent years, interests on map-based vehicle localization are rapidly increasing due to the availability of accurate digital navigation maps. Vehicle location tasks can be broken down into three level scales according to the required accuracy: Macroscale, Mesoscale and Microscale (J. Du et al., 2004). Advanced driving assistant systems(ADAS) including automated driving require different scales of map according to their driving tasks.

Macro scale map is used for widespread navigation system based on digital road network data. Macroscale navigation usually consists of finding a particular path between two nodes in the network. And its accuracy is about 10m. The mesoscale level is a level in-between the micro- and macro-scales. This is equivalent to lane-level accuracy for a digital map. Many researchers considered building lane-level maps (D. Betaille et al., 2010), (A. Chen et al., 2010). And this map was very useful in the implementation of ADAS for lane-level localization. The microscale level typically considers navigation at the vehicle level and is concerned with tasks such as lane-keeping, as well as detecting and avoiding obstacles. And the required resolution accuracy is at the decimeter-level.

To localize a vehicle with decimeter-level accuracy for a microscale task in real-time is a major challenge. A highly accurate GPS cannot guarantee the required accuracy during the whole driving task, due to insufficient number of visible satellites or multi-path reflections of the signal.

To overcome this problem, map-matching algorithms are then proposed, where a prior road map is used as either additional motion constraint or observation to update the localization estimation (El Najjar et al., 2005), (Guivant et al., 2007). Map-aided localization algorithms are proposed for high precision localization using local features. In (Jabbour et al., 2006), single side curb features are extracted by a vertical LIDAR to build a boundary map to improve vehicle localization. This map is learned beforehand in the form of line segments. In (Langerwisch et al., 2010), a novel "Virtual 2D Scans" method is proposed by making use of the building outlines as features. A simplified 2D line feature map is generated beforehand as prior knowledge. However, possible lack of these features limits its effectiveness.

In this paper, lane markers are used as local features, which are extracted from images of AVM camera. A digital lane marker map is used as prior. Lane markings have similar properties with road center-lines both are clothoids. They can be simplified to polylines with a limit number of shape points. In this paper, we integrate lane information obtained by AVM camera into digital maps based on these characteristics. And digital maps are applied to improve performance of vehicle localization.

The rest of the paper is organized in the following manner. Section II introduces the method of lane detection using AVM camera. Section III describes the mobile mapping process for building a digital map of the lane markings that is to be used as source of map matching. Section IV describes the map based localization algorithm. Vehicle test results for the

evaluation of the proposed algorithm are conducted in Section V. Finally, Section VI concludes the paper.

2. LANE AND STOP LINE DETECTION

In this paper, we use commercial AVM module consisted of four fisheye cameras to obtain bird-view image. Four fisheye cameras are installed on center of front/rear bumpers and under the side view mirrors as shown in Fig. 1.
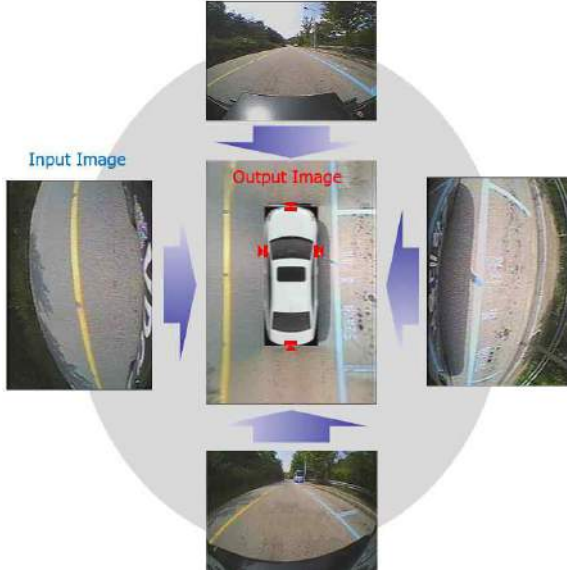

Fig. 1. Configuration of Commercial AVM Module and its Input and Output Images.
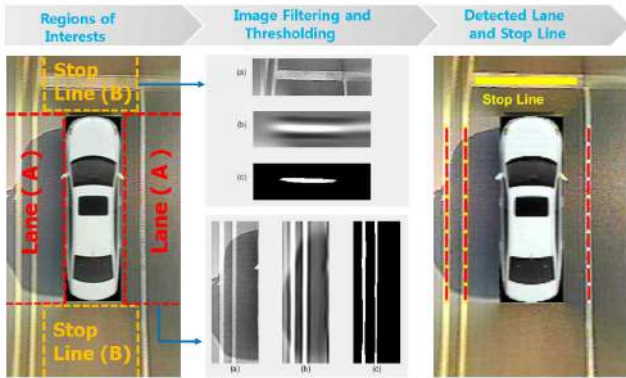

Fig 2 Schematic Diagram of the Lane and Stop Line Detection; (a) Grayscale Image (b) Image after Filtering (c) Image after Thresholding

In order to detect the lane and stop line, regions of interest (ROI) was set as shown on the right of Fig.2. Red and orange dash boxes(*A,B*) indicate the ROI in order to detect lanes and stop lines. And each region images are filtered by a two dimensional Gaussian kernel. The vertical direction of image *A* and the horizontal direction of image *B* are smoothing Gaussians, whose $\sigma_{y,A}$ $\sigma_{x,B}$ are adjusted according to the required height of lane and stop lines to be detected.

$$f_{v,A}(y_A) = \exp\left(-\frac{y_A^2}{2\sigma_{y,A}^2}\right)$$

$$f_{h,B}(x_B) = \exp\left(-\frac{x_B^2}{2\sigma_{x,B}^2}\right) \quad (1)$$

Horizontal direction of image *A* and vertical direction of image *B* are second-derivative of Gaussians, whose $\sigma_{x,A}, \sigma_{y,B}$ is adjusted according to the expected width of the lane and stop line.

$$f_{h,A}(x_A) = \frac{1}{\sigma_{x,A}^2}\exp\left(-\frac{x_A^2}{2\sigma_{x,A}^2}\right)\left(1-\frac{x_A^2}{2\sigma_{x,A}^2}\right)$$

$$f_{v,B}(x_B) = \frac{1}{\sigma_{y,B}^2}\exp\left(-\frac{y_B^2}{2\sigma_{y,B}^2}\right)\left(1-\frac{y_B^2}{2\sigma_{y,B}^2}\right) \quad (2)$$

Each filter *A* and *B* are tuned specifically for vertical bright lines and horizontal bright lines on dark background of specific width, which is our assumption. And these filter can also handle quasi-vertical and quasi-horizontal lines which produce considerable output after the thresholding process (Aly et al., 2008).

Fig. 2 shows the original image (left), (a) grayscale image, (b) filtered image. As shown in Fig.2(b), areas where lanes exist have high response, and so we only retain the highest values. The threshold value was determined by selecting the q% quantile value from the filtered image. And then filtered image was binarized by this threshold value. In this paper, q is set to 95%. Fig. 2(c) shows the result after thresholding.

Next pixels exceeding threshold value are reprojected in the vehicle coordinates system. To find a polyline expression that best approximates the lane data, RANSAC algorithm was used. Lanes in the AVM images can be sufficiently represented by second order polynomial. So we use second order polyline for expressing the lane. Two thresholds are necessary for RANSAC algorithm; the first one indicates the expected outliers rate in the points set, which is directly related to the iterations number, and the second one specifies the distance above which a point is considered as an outlier. The result of lane detection is shown at Fig. 3. Red dash lines represent the extracted lane marker using the RANSAC algorithm. It can be seen that the various lane markers are well extracted.
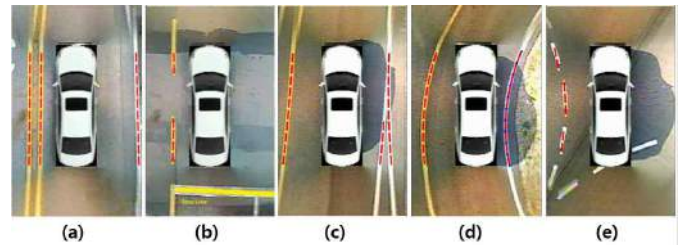

Fig 3 Result of Various Lines Detection; (a) Straight Double and Single Line (b) Dashed Line (c) Merged Line (d) Curved Line (e) Curved and Dashed Line

3. LANE MAP BUILDING

Our localization algorithm was based on the lane map includes geo-localized lane markings providing a lateral constraint. For real-time application, a limited number of parameters must represent the map line segments. However, it is very difficult to extract simplified lane data by processing the whole lane marking data at once. As we said at start, lane markings have similar properties with road center-lines. This is the starting point of our algorithm. First we find a polyline expression that best approximates the road center-lines. The road center-lines are surveyed by driving as close as possible to center of road using a high-precision DGPS. Based on these polylines, we divide global lane marking data into local segment for easier lane searching. From segmented lane data, polylines of lane are approximated using Radon transform. In the following, we describe the detailed processes that are involved in the map building.

3.1 Road Center-line Segmentation

We need to find the simplified poly-lines of road center-lines. In other words, we need to determine the segments. The Douglas–Peucker's algorithm (Douglas et al., 1973) is used to find the shape points which divide the road center-lines into parts with different headings. This algorithm is a well-known algorithm for reducing the number of points in a curve that is approximated by a series of points. In this algorithm, the accuracy is determined by choosing suitable tolerance which is the maximal Euclidean distance allowed between simplified segments and the origin points. If we choose a very small tolerance, the segments in a polyline can be too short, and there can be too many shape points in the polyline. For this reason, we propose to choose a tolerance of decimeter-level.

In order to further improve the accuracy of the polylines by reducing the errors effects due to the segmentation process, a least-squares algorithm is performed with every point between two adjacent shape points of the segmented polyline(Tao et al., 2013).
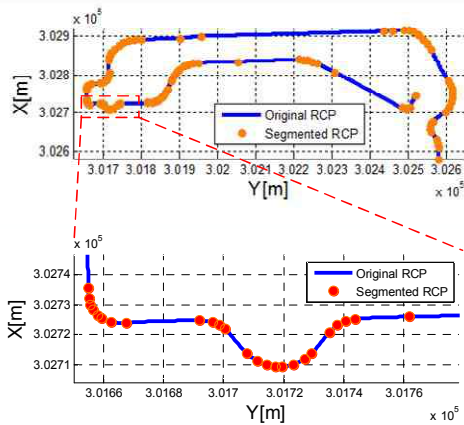

Fig 4. Illustration of Road Center-line Segmentation. The tolerance is 0.1m

3.2 Lane Approximation

For each segment determined by lateral offset distance from the road center-line as shown in Fig. 5, lanes are detected by applying the radon transform to segmented lane data. The Radon transform was proved to be robust against occlusions, noise and outliers. Compared to the Hough transform, the Radon transforms exhibits the advantage of a calculation time independent of the numbers of lane markers and the capability to handle grayscale images efficiently and without thresholding(Kammel et al., 2008).
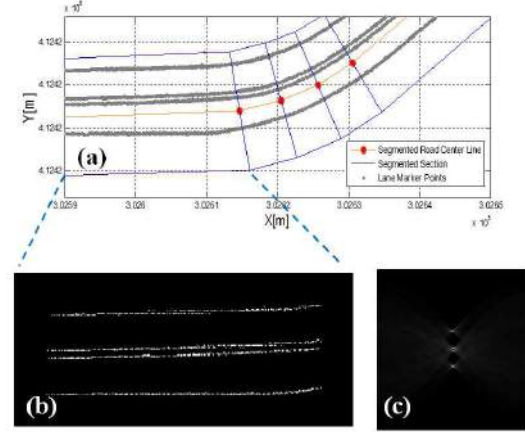
Fig 5. Lane Extraction (a) Global lane data, (b) Segmented lane data, (c) Radon transform of (b)

The Radon transform of segmented lane data *f(x,y)*; denoted as *g(s,θ)*; is defined as its line integral along a line inclined at an angle θ from the y-axis and at a distance s from the origin. Mathematically, it is written as

$$g(s,\theta) = \int_{-\infty}^{\infty} \int_{-\infty}^{\infty} f(x,y)\delta(x\cos\theta + y\cos\theta - s)\,dx\,dy \tag{3}$$

where $-\infty < s < \infty, 0 \le \theta < \pi$. The Radon transform is the one-dimensional projection of *f(x,y)* at an angle θ. The maxima in the Radon image are considered as candidates for lane. To improve the performance of the algorithm, the number of points contributing to this possible lane determined.

4. LANE-LEVEL LOCALIZATION

In this section, we present the key stages of the localization system that uses GPS loosely coupled with proprioceptive sensors and lane marking detections map-matching with a previously built map. Fig. 6 shows the structure of lane map based localization.
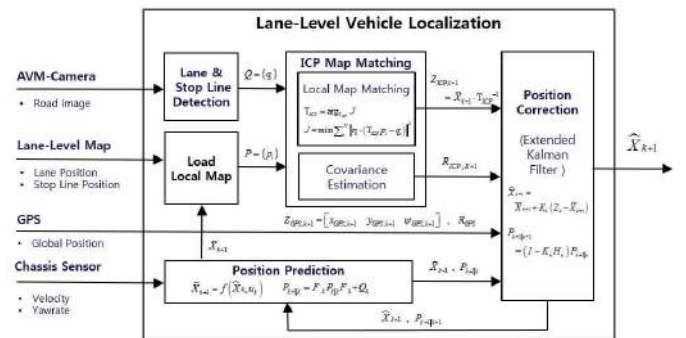
Fig 6. Structure of Lane Map based Localization

4.1 Prediction

The state vector *X* is defined as following in order to represent vehicle's planar behaviour:

$$X = \begin{bmatrix} x & y & \psi \end{bmatrix}^T \tag{4}$$

where x, y, ψ is the vehicle's global position. By integrating using the Euler approximation and assuming that the control signals, v and $\dot{\psi}$ are approximately constant over the sample period, the nominal discrete process model equations can be written as

$$X_{k+1} = f(X_k, u_k) + w_k \quad , \quad w_k \sim N(0, W)$$
$$\bar{X}_{k+1} = f(\hat{X}_k, u_k)$$
$$= \begin{bmatrix} \hat{x}_k + v_k \cdot \Delta t \cdot \cos(\hat{\psi}_k + \Delta t \cdot \dot{\psi}_k) \\ \hat{y}_k + v_k \cdot \Delta t \cdot \sin(\hat{\psi}_k + \Delta t \cdot \dot{\psi}_k) \\ \hat{\psi}_k + \Delta t \cdot \dot{\psi}_k \end{bmatrix} \tag{5}$$

where k is the time index of discrete model, and w_k describes the process noise. The process noise is assumed to be a white noise with associated covariance matrix, W. And v and $\dot{\psi}$ are obtained by proprioceptive sensors. The covariance of the predicted state is described as,

$$M_{k+1} = F_k \cdot P_k \cdot F_k^T + W$$
$$F_k = \frac{\partial f}{\partial x}\Big|_{x=\hat{x}_k}, \tag{6}$$
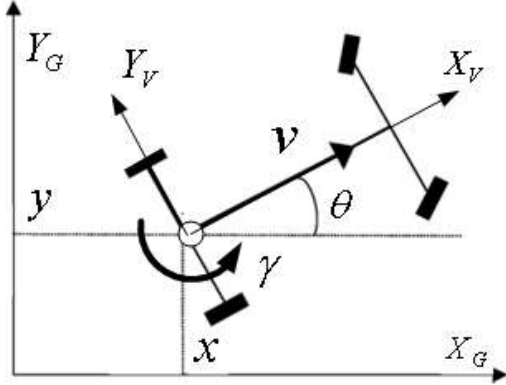

Figure 7. Vehicle Model

4.2 Map-Matching

A lane map is previously generated and stored in the system. Localization can be achieved by matching the global lane map with the local lane map accumulated by AVM camera in a short distance. A robust matching algorithm should be used to guarantee the reliability. Considering that the local map is composed of points and global map is composed of polyline, so the map matching can be viewed as a point to plane matching, which are related by a rotation and a translation. The Point to Plane ICP algorithm(Segal et al., 2010) is a useful method to solve this kind of problems. ICP selects the closest point as the corresponding polyline and estimates the matching

result by minimizing the value of an error function as shown below.

$$E = \sum_i \left\{ w_i \left\| \eta_i \cdot (T \cdot b_i - m_i) \right\|^2 \right\} \tag{7}$$

Where η is the surface normal at mi.. These two steps are iteratively implemented to obtain high accuracy. Every point in the local map searches its corresponding point in the global map. The algorithm 2 resumes this process. A challenge in the ICP is how to reduce the search area in the global map. Large search area will increase the computation considerably and make the result get into local minimum. In this paper, odometry data is utilized to address this problem. According to equation(4), the prior estimation of vehicle pose can be calculated and we can search in a small area just around the estimated pose. The size of the area is relevant to the uncertainty of odometry data ang GPS.

Algorithm Point to Plane ICP
Input: Two point clouds: Map:A = {ai}; Data: B ={bi} An initial transformation: T_0
Output: The correct transformation, *T*, which aligns A and B
1) $T \leftarrow T_0$;
2) **While** not converged do
3)   **For** i ← 1 to N do
4) m_i ← Find Closest Point In A(T·b_i);
5)   If $\| m_i - T \cdot b_i \| < d$max then
6) $w_i \leftarrow 1$;
7)   Else
8) $w_i \leftarrow 0$;
9)   End if
10)   End for
11) $T \leftarrow$ argmin{ $\sum_i w_i \| \eta_i \cdot (m_i - T \cdot b_i) \|^2$ }
12) End while

T is the matching result, which represents the rotation (R_r) and translation (T_t) between the local map and the corresponding submap in the global reference map. This result can be used to localize the intelligent vehicle. Let X_v, ψ express the current vehicle pose obtained by equation (5). Let b_i represent a lane marker point in the local map. Its global and local coordinates (i.e.vehicle coordinates) are represented by X_G and X_L. Let ai be the corresponding point of bi in the global map. Its global and local coordinates are represented by MX_G and MX_L. Because the ICP algorithm is carried out in the local coordinate system, we can obtain the following equations:

$$X_{L,ICP} = R_r X_L + T_t$$
$$X_{G,ICP} = R_\theta M X_{L,ICP} + X_v$$
$$= R_\theta R_r X_{L,ICP} + R_\theta T_t + X_v \tag{8}$$

$$where \quad R_\theta = \begin{bmatrix} \cos(\psi) & -\sin(\psi) \\ \sin(\psi) & \cos(\psi) \end{bmatrix}, R_r = \begin{bmatrix} \cos(r) & -\sin(r) \\ \sin(r) & \cos(r) \end{bmatrix}$$

The corrected vehicle pose can be derived as:

$$Z_{map} = \begin{bmatrix} \hat{P}_{icp} \\ \hat{\theta}_{icp} \end{bmatrix} = \begin{bmatrix} R_{\theta}T_t + X_v \\ \theta + r \end{bmatrix} \ where \ \hat{P}_{icp} = \begin{bmatrix} \hat{x}_{icp} \\ \hat{y}_{icp} \end{bmatrix}$$

(9)

4.3 GPS and MAP Correction

The extended Kalman filter is used to correct the vehicle position using GPS and result of map-matching. The measurement model are given by following form:

$$Z_{k,GPS} = \begin{bmatrix} x \\ y \\ \psi \end{bmatrix} = \begin{bmatrix} 1 & 0 & 0 \\ 0 & 1 & 0 \\ 0 & 0 & 1 \end{bmatrix} x_k + v_{k,GPS}$$

$$Z_{k,Map} = \begin{bmatrix} x \\ y \\ \psi \end{bmatrix} = \begin{bmatrix} 1 & 0 & 0 \\ 0 & 1 & 0 \\ 0 & 0 & 1 \end{bmatrix} x_k + v_{k,Map}$$

(10)

The measurement noise is assumed to be a white noise with associated covariance, V. With above measurement model, vehicle states are corrected by measurement update of the extended Kalman filter as following specific equations:

$$\hat{x}_{k+1} = \overline{x}_{k+1} + K_k \cdot (z_k - H \cdot \overline{x}_{k+1})$$
$$S_k = HM_{k+1}H^T + V_k$$
$$K_k = M_k H^T \cdot S_k^{-1}$$
$$P_k = (I - K_k H) \cdot M_k$$

(11)

The rate of time update is same as the sampling rate of proprioceptive sensors 100 Hz, and the rate of measurement update is same as GPS sensor and LiDAR sensor update rate. (GPS: 1 Hz, LiDAR: 10 Hz)

4.4 Validation Gate

A validation gate is set up to eliminate the fault of the GPS and map correction. The validation gate represents a threshold that is associated with the acceptability of the measurements. Only measurements inside of the validation gate are used to update the filter (BAR-SHALOM et al., 2010). The validation gate can be obtained as following:

$$e^2 = (z_k - H\overline{x}_k)^T S_k^{-1}(z_k - H\overline{x}_k)$$
$$V_k = \{z : e^2 < g^2\}$$

(12)

where g^2 is chosen to for a confidence level. Normalized error e^2 varies as a Chi-Squared distribution with number of measurements degrees of freedom.

5. TEST RESULTS

Tests were carried out at the ITS proving ground as show in Fig.7. The ITS Proving Ground simulates an urban environment with faithfully replicated roads and traffic signals. The length of the path is about 2.6 km. The vehicle passed nine crossroads and two access roads. The experimental vehicle was equipped with a OXFORD RTK-GPS receiver coupled with a IMU running at 100Hz. The system received RTCM corrections through radio modem from a GPS base station. This high accuracy system(few centimeter) was used during the mobile mapping process. It also provided ground truth data for the localization method. A CAN-bus gateway was used to access to wheel speed sensors and to a yaw rate sensor. The

low-cost GPS was a U-blox EVK-6T with a patch antenna. Specifications of sensor used in the tests were described in table1,2.

Table 1. Noise Specifications of Proprioceptive Sensors

Sensors	Specifications			
	Range	*Resolution*	*Noise(RMS)*	*Unit*
Yaw rate	± 120	0.0625	0.5	Deg/s
Wheel speed	0-130	0.035	0.3	m/s

Table 2. Specification of GPS Receivers

GPS receivers		RTK GPS	Low-cost GPS
Accuracy (RMS)	Position	*2cm*	*5m*
	Velocity	*0.03m/s*	*0.05m/s*
Data rate		*100 Hz*	*1Hz*
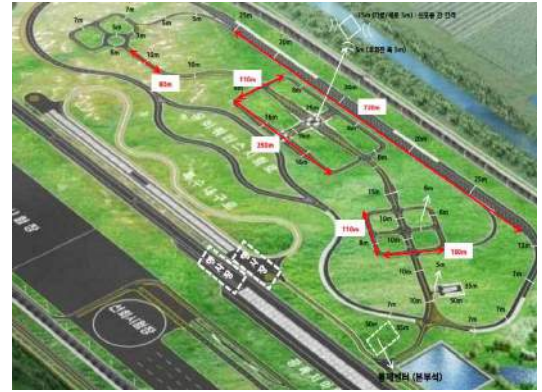
Figure. 8. ITS Proving Ground

The proposed localization algorithm described in section IV has been tested by using data replay. Fig. 8 b),c),d) show changes of localization errors on X and Y over time, plotted with ±3σ bounds (red lines) to show how the filter is well tuned. And Fig. 9 e),f) show changes of localization errors respect to vehicle coordinate(Xv, Yv). The performance of proposed localization algorithm(esp. lateral and yaw error) allows a lateral control precise enough to be applicable. At the moment (generally crossroads), the localization error is accumulated slightly.

a) Vehicle Trajectory

b) X Position Estimation Error

c) Y Position Estimation Error

d) Yaw Angle Estimation Error

e) Longitudinal Error

f) Lateral Error
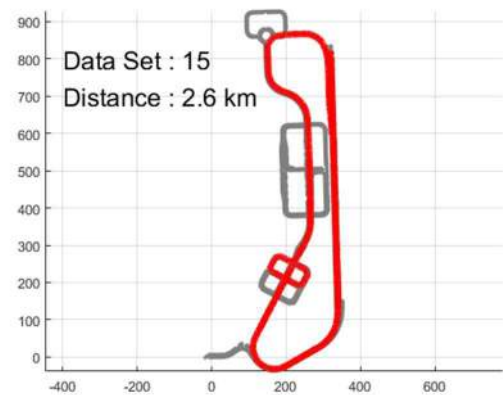
Fig. 9. Localization Result

6. CONCLUSION

Lane map based Localization algorithm for Automated Driving has been presented. It is based on the point to plane ICP algorithm using the lane map consisted of polylines. The uniqueness of our solution is that it exploits information from detected lane markings from a AVM camera. This information is matched to the lane maps and then used to assist the estimations of a low-cost-GPS receiver together with vehicle proprioceptive data. Test results have shown the good performance.

REFERENCES

J. Du, J. Masters, and M. Barth, "Lane-level positioning for in-vehicle navigation and automated vehicle location (avl) systems," Proc IEEE Int. Transp. Systems, pp. 35–40, 2004.

D. Betaille and R. Toledo-Moreo, "Creating enhanced maps for lane -level vehicle navigation," IEEE Transactions on Int. Transp. Systems, vol. 11, pp. 786–798, 2010.

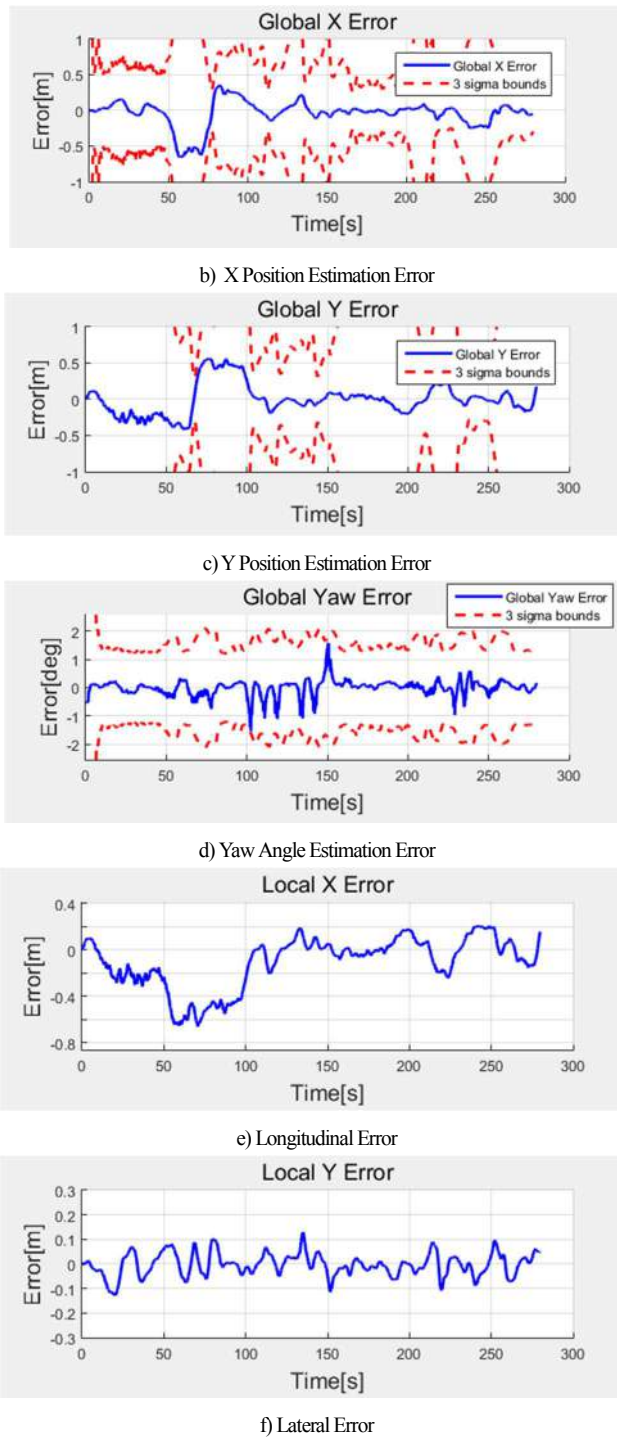A. Chen, A. Ramanandan, and J. A. Farrell, "High-precision lane-level road map building for vehicle navigation," Position Location and Navigation Symp., pp. 1035–1042, 2010.

El Najjar, Maan E., and Philippe Bonnifait. "A road-matching method for precise vehicle localization using belief theory and Kalman filtering." Autonomous Robots 19.2 (2005): 173-191.

Guivant, Jose, and Roman Katz. "Global urban localization based on road maps." Intelligent Robots and Systems, 2007. IROS 2007. IEEE/RSJ International Conference on. IEEE, 2007.

Jabbour, Maged, and Philippe Bonnifait. "Global localization robust to GPS outages using a vertical ladar." Control, Automation, Robotics and Vision, 2006. ICARCV'06. 9th International Conference on. IEEE, 2006.

Langerwisch, Marco, and Bernardo Wagner. "Registration of Indoor 3D Range Images using Virtual 2D Scans." ICINCO (2). 2010.

Aly, Mohamed. "Real time detection of lane markers in urban streets."Intelligent Vehicles Symposium, 2008 IEEE. IEEE, 2008.

Kammel, Sören, and Benjamin Pitzer. "Lidar-based lane marker detection and mapping." Intelligent Vehicles Symposium, 2008 IEEE. IEEE, 2008..

Douglas, David H., and Thomas K. Peucker. "Algorithms for the reduction of the number of points required to represent a digitized line or its caricature."Cartographica: The International Journal for Geographic Information and Geovisualization 10.2 (1973): 112-122.

Tao, Zui, et al. "Lane marking aided vehicle localization." Proceedings of the 16th International IEEE Annual Conference on Intelligent Transportation Systems (ITSC 2013). 2013.

Segal, Aleksandr, Dirk Haehnel, and Sebastian Thrun."Generalized-ICP. "Robotics : Science and Systems. Vol. 2. No. 4. 2009.

BAR-SHALOM, Y. & FORTMANN, T. E. 1987. Tracking and data association, Wiley-Interscience.

Suganuma, Naoki, and Takahiro Uozumi. "Precise position estimation of autonomous vehicle based on map-matching." Intelligent Vehicles Symposium (IV), 2011 IEEE. IEEE, 2011.

Automatic Vehicle Following of Personal Mobility Vehicles for Autonomous Platooning

Jeffrey Too Chuan Tan*. Yoshihiro Suda*

** Institute of Industrial Science, The University of Tokyo,
Tokyo, Japan. (e-mail: jeffrey@iis.u-tokyo.ac.jp)*

Abstract: The motivation of this work is to enhance personal mobility vehicles (PMV) with autonomous vehicle technologies, such as autonomous vehicle platooning to realize new potentials and possibilities for future urban transportation system. This paper reports our development on the automatic vehicle following system building for autonomous platooning of PMV. We have developed a 3D sensing system for both object (front vehicle) detection and longitudinal distance sensing. We have conducted straight and curve paths vehicle following experiments using the automatic vehicle following system to fine-tune the control parameters. We have furthered our investigation to evaluate the performance of the developed system in autonomous platooning of two automatic following PMVs with a leading human-driven PMV. The experimental results have proven the effectiveness of the developed vehicle following system to achieve autonomous platooning of PMV.

Keywords: Automatic Vehicle Following, Autonomous Platooning, Personal Mobility Vehicles

1. INTRODUCTION

Recently, autonomous vehicle technologies are in great blooming, creating a new horizon in road vehicle developments. For example, the advancement of autonomous platooning has made successfully several well-known automated platooning projects in commercial vehicles, such as a European project led by Volvo called Safe Road Trains for the Environment (Sartre) (Dávila et al. (2010)), a project at RWTH Aachen University in Germany (Ramakers et al. (2009)), research at the University of California, Berkeley, in US and Scania Transport Laboratory in Sweden (Scania (2012)), and the Energy ITS project (Yoshida et al. (2010)) under NEDO (New Energy and Industrial Technology Development Organization) in Japan.

On the other hand, personal mobility vehicles (PMV) comprise of a wide range of personal level vehicles including electric bicycle, senior car, electric wheelchair, inverted pendulum type vehicle (e.g. Segway), etc. that can be used on footpaths, bike ways, and also normal road in low and medium travel speeds. Emerging as the next generation of urban mobility, however, the usages of current available PMV are still very limited due to the lack of practical applications, and the readiness of traffic policies and support infrastructures.

The motivation of this work is to enhance PMV with autonomous vehicle technologies, such as autonomous vehicle platooning to realize new potentials and possibilities for future urban transportation system. In this paper, we will introduce a development of a 3D perception system that enables front vehicle following (Section 2). The system is implemented to conduct straight and curve paths vehicle following experiments to fine-tune the control parameters (Section 3.1). Further experimental investigation is conducted

to evaluate the autonomous platooning performance by lining up two automatic following PMVs with a leading human-driven PMV (Section 3.2).

2. AUTOMATIC VEHICLE FOLLOWING

2.1 PMV with Environment Perception

There are several developmental stages for the different level of automations in autonomous vehicle development. Before jumping straight into the Level 4 – Full Self Driving Automation, this paper reports our preliminary development on the perception system building for the next generation PMV.

With the perception capability, the PMV will be able to sense the surroundings, makes it possible to track the vehicle ahead to achieve adaptive cruise control, obstacle detection for safety improvement, and vehicle platooning by lining up several PMV in series. The following sections of this paper will further explain the developed 3D sensing system with the approach of front vehicle detection in lateral lane keeping and longitudinal distance sensing, and the experiments of vehicle tracking and PMV platooning.

2.2 3D Perception System for Front Vehicle Following

In this work, the maximum traveling speed of the PMV is set to below 15 km/h. Under such relatively low operating speed as compared to the normal vehicle, the sensing system specification requirements will be relatively lower too. Hence, an off-the-shelf low cost motion sensor (Microsoft Kinect (Kinect (2014))) is selected to develop the 3D sensing system for front vehicle tracking (Fig. 1).

The Kinect sensor consists of a RGB color VGA video camera, a depth sensor, and a multi-array microphone. The depth sensor is an infrared projector and a monochrome CMOS (complementary metal-oxide semiconductor) sensor work together to sense in 3D regardless of the lighting conditions. Both the video and depth sensor cameras have a 640 x 480 pixel resolution and run at 30 FPS (frames per second). The Kinect sensor horizontal and vertical Field of View in default range (MSDN (2015)), taken from the official documentation as shown in Fig. 2 and Fig. 3 respectively.

The Kinect sensor is attached on a PMV with the 3D sensor data visualization as shown in Fig. 1. During the operation, the output data of the sensor is acquired by a controller laptop for online processing of front vehicle tracking.

2.3 Automatic Vehicle Following System

The point cloud (Kinect (2015)) of the depth data from the Kinect consist of values in 3 dimensions, which are x-axis, y-axis and z-axis (Fig. 4). x-axis represents the horizontal (lateral) axis, y-axis represents the vertical axis while z-axis represents the depth (longitudinal) axis.

A 3D virtual box is defined as the space of interest within the Kinect sensing range (Fig. 5) for the front vehicle detection. The dimension of the virtual box is adjusted according to the shape of the front vehicle and the sensitivity of the detection. Six parameters are available for this adjustment: min_y, max_y, min_x, max_x, max_z, $goal\_z$.

In order to track the vehicle in front, the Kinect will look for the front vehicle through the virtual box in front of it. From the Kinect sensing data, the PMV will seek to keep the centroid of the observed front vehicle directly in front of it (align in lateral) and a fixed longitudinal distance. If the centroid of the vehicle is too far away, it will drive forward, too close backward, and if offset to the side, it will turn toward the centroid.

The calculation of the detected object centroid is based on the following equations (Eq. (1)-(2)), when n points are detected within the virtual box.

Fig. 2. Kinect horizontal Field of View in default range (MSDN (2015)).
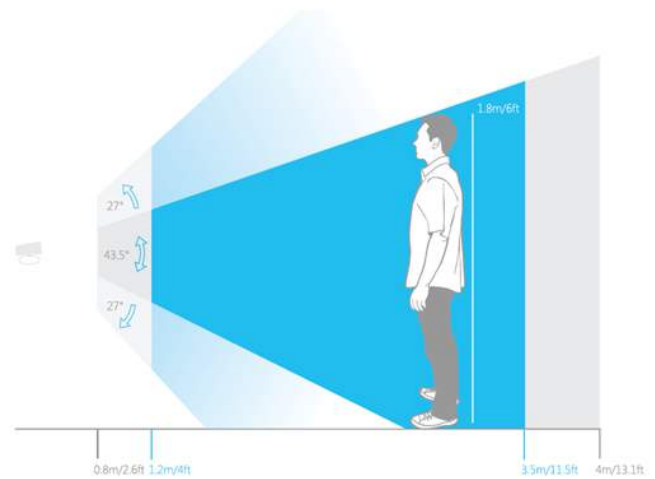
Fig. 3. Kinect vertical Field of View in default range (MSDN (2015)).

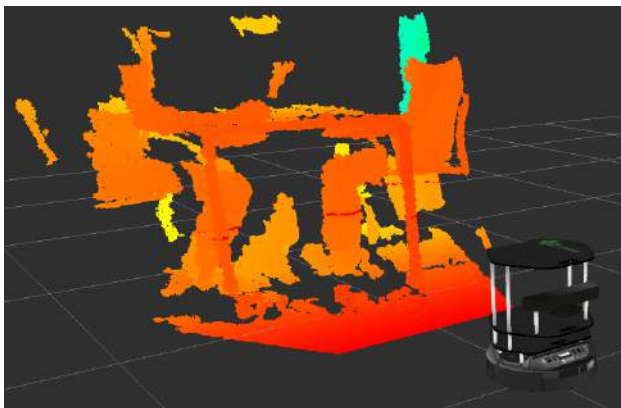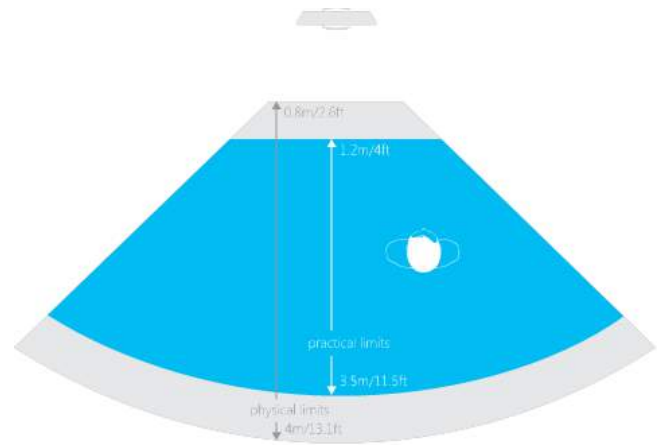

Fig. 1. The 3D sensor data visualization of Kinect, different color represents different depth values.

Fig. 4. Kinect coordinate system (Kinect (2015)).

In lateral direction,
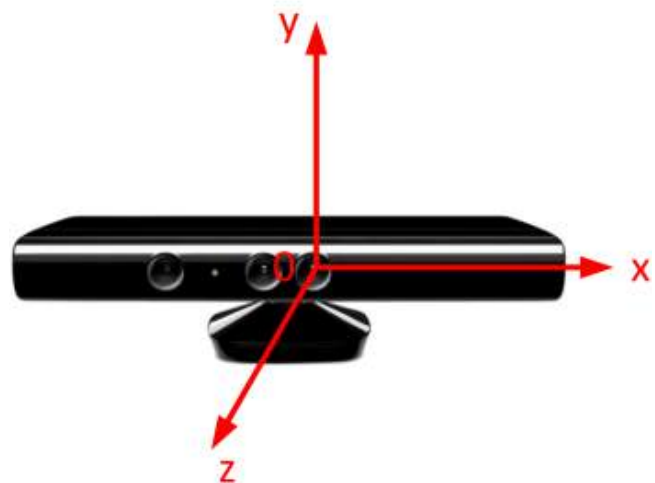
$$X_{centroid} = \frac{\sum_{i=1}^{n} x_i}{n} \quad (1)$$

In longitudinal direction,

$$Z_{centroid} = \frac{\sum_{i=1}^{n} z_i}{n} \quad (2)$$

Refer to Fig. 5, if an object is detected on the left hand side of the PMV, positive $X_{centroid}$ value will be obtained from Eq. (1). Using the following Eq. (3) to control the angular rotation of the PMV, negative ω_{PMV} will result to turn the PMV in anti-clockwise direction, and hence, rotating the PMV towards the front object. The parameter *x_scale* is available for the adjustment of the rotational response.

$$\omega_{PMV} = -X_{centroid} \times x\_scale \quad (3)$$

Similarly in longitudinal direction, when the front object is further from the PMV ($Z_{centroid}$ is larger than *goal_z*), Eq. (4) below can be used to calculate the forward speed of the PMV, v_{PMV}. The parameter *z_scale* is available for the adjustment of the forward response.

$$v_{PMV} = (Z_{centroid} - goal\_z) \times z\_scale \quad (4)$$

By continuous sensing the front vehicle with centroid calculations to control the rotational and forward speed of the PMV, we are able to achieve automatic vehicle following with the proposed system.

3. VEHICLE FOLLOWING AND AUTONOMOUS PLATOONING EXPERIMENTS

3.1 Automatic Vehicle Following Experiment

In this work, a compact inverted pendulum type PMV (Robstep Robin M1 (Robstep (2014))) is referred as the leading PMV. Open source mobile robotics platforms (TurtleBot2 (Willow (2008))) are used to simulate the following PMV, where both PMV systems are having similar non-holonomic differential drive mobile base (Fig. 6).

The Kinect sensor is assembled on the mobile base and the vehicle following algorithm is implemented on the autonomous system. The eight parameters in the automatic vehicle following algorithm listed in Table 1 are determined empirically based on the experiment system.
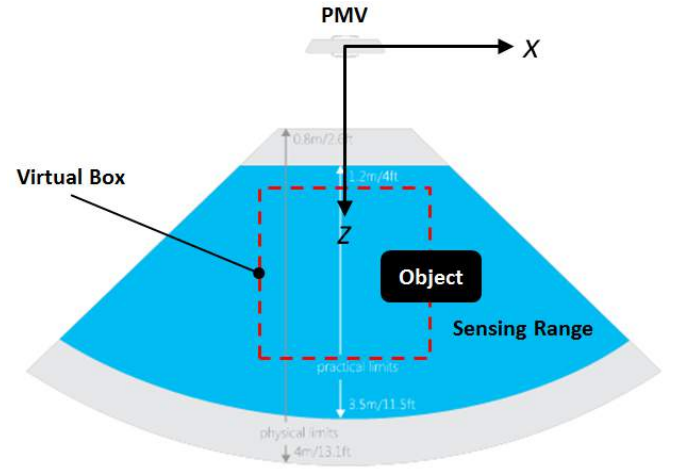
Fig. 5. A 3D virtual box is defined as the space of interest to detect the presence of the object within the box.
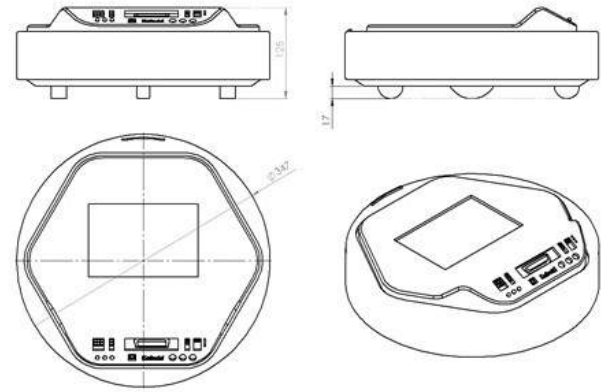
Fig. 6. The specifications of the mobile base (Willow (2008)).

Table 1. Experimental values of the parameters in the automatic vehicle following algorithm

Parameter	Value
min_y	0.1 [m]
max_y	0.5 [m]
min_x	-0.35 [m]
max_x	0.35 [m]
max_z	1.2 [m]
goal_z	0.6 [m]
x_scale	3.0
z_scale	2.0

Vehicle following experiments in straight (Fig. 7) and curve (Fig. 8) paths were conducted in various traveling speeds and vehicle distances, to validate the developed algorithm.

In the vehicle following experiments, there was one PMV leading which will be followed by another identical PMV. A 1.0 m width travel path was prepared with a 90 degree curve at the end. The leading PMV was manually remote control by an operator, while the following PMV was using the proposed vehicle following algorithm. The observation results are summarized in Table 2.

Fig. 7. Vehicle following experiment (straight path).

Fig. 8. Vehicle following experiment (curve path).

Table 2. Vehicle following experiment observations

Speed of leading vehicle (m/s)	Clearance in between two vehicles (m)	Performance
0.20	0.20	◎
	0.30	◎
	0.40	◎
0.35	0.20	△
	0.30	○
	0.40	○
0.50	0.20	△
	0.30	○
	0.40	○

◎ Following smoothly

○ Following smoothly, with overshoot when sudden stop

△ Following smoothly, with overshoot when sudden stop, and almost collide

3.2 Autonomous Platooning Experiment

Based on the safe traveling speed (approximately 0.2 m/s) and vehicle distance (0.6 m distance between two vehicles) in the vehicle following experiment above, vehicle platooning experiment were conducted by lining up two automatic following PMVs with a leading PMV driven by human driver (Fig. 9). The first PMV that followed immediately after the leading PMV was PMV1 and the second PMV that followed behind it was PMV2. The straight and curve paths were similar to the previous experiment. The positions (*x*, *y* coordinates) of the following PMVs along the travel were computed and recorded based on the vehicle odometry.

Fig. 9. Autonomous platooning experiment.

The motion trajectories of PMV1 and PMV2 are plotted as in Fig. 10 for straight path and Fig. 13 for curve path experiments. To further investigate on the following performance, the longitudinal and lateral positions of PMV1 and PMV2 are plotted against travel time in Fig. 11, Fig. 12 and Fig. 14, Fig. 15 for straight and curve paths respectively.

Fig. 10 and Fig. 13 showing that the PMVs following well the leading PMV in traveling straight and right turning paths. Fig. 11 and Fig. 14 display similar S curves with almost constant longitudinal gap in between PMV1 and PMV2. This proven that the vehicle following system is effectively maintaining a constant longitudinal distance in between the two vehicles while platooning in straight and also cornering movements. From the lateral positions plots of Fig. 12 and Fig. 15, the vehicle following system is also functioning in keeping the lateral distance to within 0.1 m range.

4. CONCLUSION AND FUTURE WORK

The objective of this work is to enhance PMV by developing a vehicle following system with environment perception and control algorithm, in order to realize autonomous platooning of PMV.

In this work, we have developed a 3D sensing system with control algorithm that enables front vehicle following. The system is implemented to conduct straight and curve paths vehicle following experiments to fine-tune the control parameters.
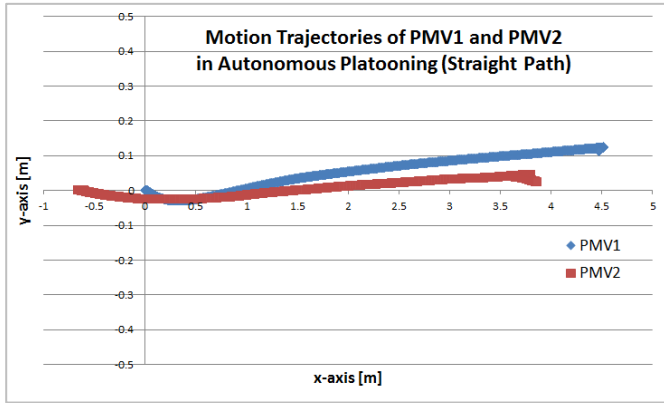
Fig. 10. Motion trajectories of PMV1 and PMV2 in autonomous platooning (straight path).

Fig. 13. Motion trajectories of PMV1 and PMV2 in autonomous platooning (curve path).

Fig. 11. Longitudinal positions of PMV1 and PMV2 in autonomous platooning (straight path).

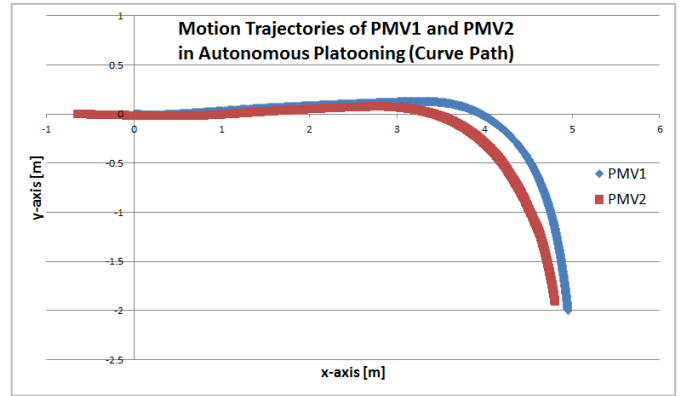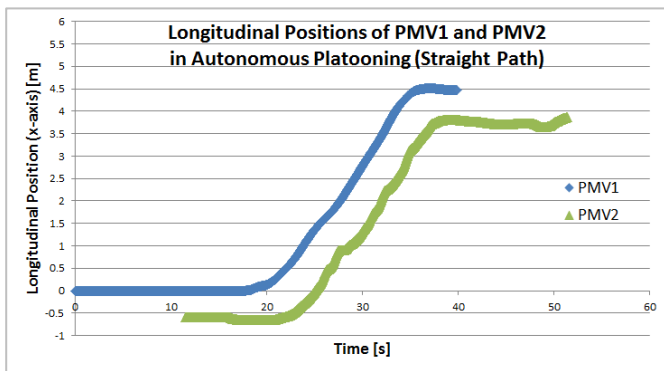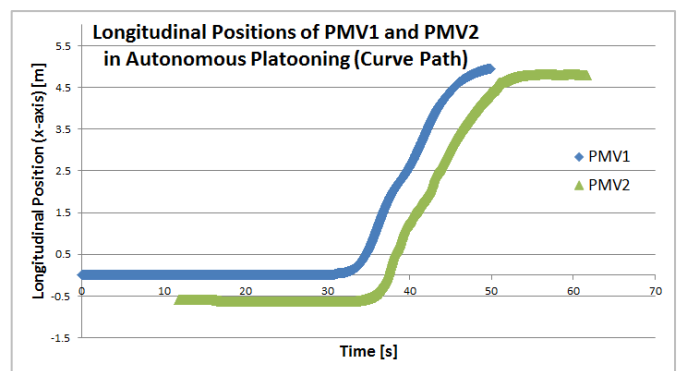Fig. 14. Longitudinal positions of PMV1 and PMV2 in autonomous platooning (curve path).
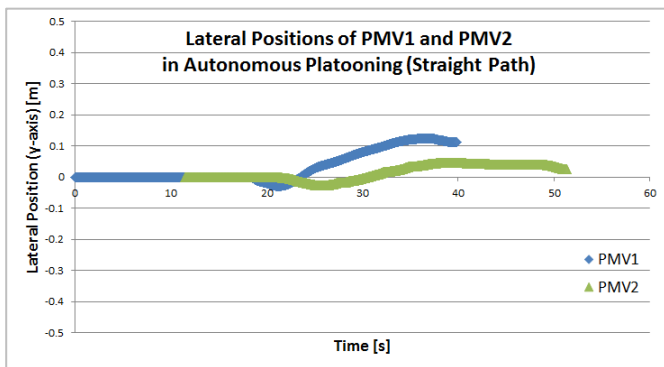
Fig. 12. Lateral positions of PMV1 and PMV2 in autonomous platooning (straight path).
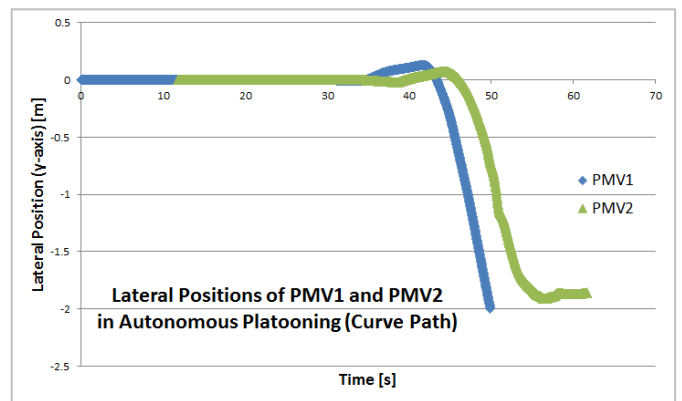
Fig. 15. Lateral positions of PMV1 and PMV2 in autonomous platooning (curve path).

We have furthered our investigation to evaluate the performance of the developed system in autonomous platooning of two automatic following PMVs with a leading human-driven PMV. From the experimental results, we have achieved safe constant longitudinal distance between the vehicles when traveling in straight and curve paths. The system is able to keep lateral distance within 0.1 m range in the same traveling conditions.

However, there are a lot more research and development can be done in order improve the system. Modeling of the platooning system can help to optimize the control parameters in order to allow high speed travel and better response. Adding color identification or object recognition to the system may help to separate target vehicle from other obstacles. Another future work suggestion will be adding vehicle-to-vehicle (V2V) communication to develop cooperative cruise control for better platooning operation.

REFERENCES

Dávila, A. and Nombela, M. (2010). Sartre: Safe road trains for the environment. In *Conference on Personal Rapid Transit PRT@ LHR*, vol. 3, pp. 2-3.

Kinect for Xbox One (2014). http://www.xbox.com/en-US/xbox-one/accessories/kinect-for-xbox-one.

Kinect SDK C++ Tutorials – 3 (2015). Kinect Point Clouds. http://www.cs.princeton.edu/~edwardz/tutorials/kinect/kinect3.html.

MSDN Microsoft (2015). Skeletal Tracking. https://msdn.microsoft.com/en-us/library/hh973074.aspx.

Ramakers, R., Henning, K., Gies, S., Abel, D. and Max, H. (2009). Electronically coupled truck platoons on German highways. In *IEEE International Conference on Systems, Man and Cybernetics, 2009*, pp. 2409-2414.

Robstep (2014). Robin M1. http://www.robstep.co.uk/robin.html.

Scania lines up for platooning trials (2012). http://newsroom.scania.com/en-group/2012/04/04/scania-lines-up-for-platooning-trials/.

Willow Garage (2008). Turtlebot. http://www.willowgarage.com/turtlebot.

Yoshida, J., Sugimachi, T., Fukao, T., Suzuki, Y. and Aoki, K. (2010). Autonomous Driving of a Truck Based on Path Following Control. In *Proc. 10th Int. Symposium on Advanced Vehicle Control* (CD-ROM).

Vehicle Platoon Formation using Interpolating Control with Integral Action [*]

Alon Tuchner [*] **Jack Haddad** [**]

[*] *Technion Autonomous Systems Program (TASP), Technion - Israel Institute of Technology, Haifa 32000, Israel (e-mail: alontu@campus.technion.ac.il)*
[**] *Technion Sustainable Mobility and Robust Transportation (T-SMART) Laboratory, Haifa 32000, Israel (e-mail: jh@technion.ac.il)*

Abstract: In this paper, a control design approach known as interpolating control is used for cooperative vehicle longitudinal control in order to form vehicle platoons. The objective is to regulate the vehicles' speeds and the spacings between the vehicles, from their initial conditions into a shared consensus. A discrete state space formulation is used to model the system, in which constraints are enforced. The interpolating control approach is implemented and compared with other methods such as MPC. The paper presents an implementation of the interpolating controller that includes integral action, for the purpose of improving the steady state performance in the presence of a disturbance. We show that this controller can indeed eliminate the steady state error, defined as the output of the system, if the disturbance is a bounded step function and the initial conditions are feasible.

Keywords: Platoon Formation, Interpolating Control, Autonomous Vehicles.

1. INTRODUCTION

Platooning of vehicles, i.e. grouping cars, buses, or trucks into a road train, can improve the traffic flow performances of transportation systems. The main idea is that the throughput of vehicles on freeways may potentially increase by forming vehicle platoons with small inter-vehicle spacings, which might allow more vehicles to fit on a road segment, Van Arem et al. (2006). Vehicle platooning can also improve traffic emission and fuel consumption by creating better group aerodynamics, especially if the vehicle leader is a truck or a bus.

Recent research works, e.g. in Schakel et al. (2010); Rajamani and Zhu (2002); Brinon Arranz et al. (2014), have shown that creating platoons with small inter-vehicle spacings is feasible with the use of cooperative multi-agent technology, such as Cooperative Adaptive Cruise Control (CACC). CACC requires vehicle to vehicle communication capability, e.g. VANET - vehicular ad-hoc network, which enables vehicles to transmit real-time data such as their individual accelerations, absolute positions, and speeds to other vehicles in the shared network. The acquisition of this data in real-time can improve the control performance of the platoon, and can enable vehicles to maintain small inter-vehicle spacings while keeping the vehicle-string stable, Schakel et al. (2010); Rajamani and Zhu (2002). The string stability of a platoon of vehicles has several definitions in the literature, e.g. refer to Rajamani and Zhu (2002). Simply put, a string is called stable if an interference that is created downstream is not amplified as it

propagates upstream. CACC evaluation and experimental results can be found, e.g. in Ploeg et al. (2011).

Recently, in Tuchner and Haddad (2015) the task of forming platoons is addressed by utilizing a novel approach called interpolating control (also known as improved vertex control), presented in Nguyen et al. (2013, 2014). This approach aims at regulating to the origin uncertain and/or time-varying linear discrete-time systems, with state and control constraints. The current paper presents an implementation of the interpolating controller that includes *integral action*, for a system subject to a bounded, unmeasured disturbance. The transient and steady state performance of this controller is simulated and analyzed.

2. SYSTEM MODEL DESCRIPTION AND PROBLEM FORMULATION

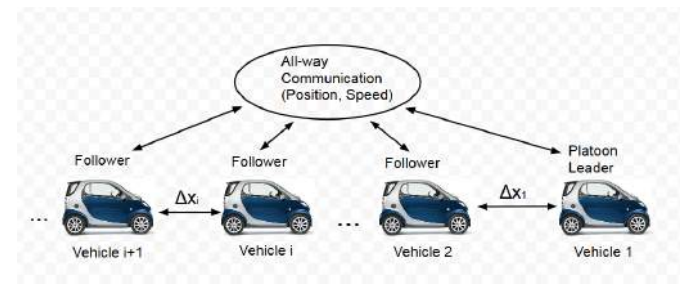Let us consider a group of n vehicles traveling in a road section, as schematically shown in Fig. 1. The position

Fig. 1. Problem description for vehicle platoon formation.

and speed for vehicle i are respectively denoted as $x_i(t)$

(m) and $v_i(t)$ (m/s), where $v_i(t) = \dot{x}_i(t)$. The spacing or distance between vehicle i and its follower, $i + 1$, is denoted as $\Delta x_i(t) = x_i(t) - x_{i+1}(t)$. At t_0 the vehicles are in their initial conditions $v_i(t_0) = v_{i,0}$, $i = 1, \ldots, n$, and $\Delta x_i(t_0) = \Delta x_{i,0}$, $i = 1, \ldots, n-1$. The *platoon leader vehicle* has the subscript $i = 1$.

In order to derive a platoon formation model, we first focus on the dynamics of a single vehicle. Several vehicle models with different levels of detail and accuracy have been suggested in literature, see e.g. Corona and De Schutter (2008); Naus et al. (2009). In this paper, a typical model is used in which vehicle i has a mass m_i (kg) subjected to an input force bu_i (N), where b (N) is a constant force and u_i $(-)$ is a normalized control input. In a discretized formulation, assuming constant input force at the duration of a single time step, the dynamic equations for vehicle i are given as follows:

$$x_i(k+1) = x_i(k) + Tv_i(k) + \frac{T^2}{2m_i}bu_i(k), \quad (1)$$

$$v_i(k+1) = v_i(k) + \frac{T}{m_i}bu_i(k), \quad (2)$$

where k $(-)$ is the time step, and T (s) is the time step duration. The vehicle spacing is then calculated as follows:

$$\Delta x_i(k+1) = \Delta x_i(k) + Tv_i(k) - Tv_{i+1}(k) + \frac{T^2}{2m_i}bu_i(k)$$
$$- \frac{T^2}{2m_{i+1}}bu_{i+1}(k). \quad (3)$$

The aim of the controller is to group the vehicles together into a platoon with steady-state speed and spacing, denoted by v_e and Δx_e, respectively. The steady-state spacing can be chosen as $\Delta x_e = \Delta x_{\min} + hv_e$, where h (s) is a constant time headway and $\Delta x_{\min}$ (m) is the minimum gap at zero speed. This spacing policy is commonly used in traffic flow theory for car following models, Treiber and Kesting (2013). The steady-state speed v_e is assumed to be a priori known.

In order to get a stable and collision-free platoon, constraints are enforced on the spacing between vehicles, i.e. $\Delta x_{\min} \leq \Delta x_i(k) \leq \Delta x_{\max}$ for all k. Speed limitations are also postulated as $v_{\min} \leq v_i(k) \leq v_{\max}$ for all k. Moreover, due to limitations on engine torques and break forces, the normalized control inputs should operate within a certain range, formulated as $u_{\min} \leq u_i(k) \leq u_{\max}$ for all k.

The control problem is defined as follows: given the dynamics in (2) and (3), manipulate the control inputs $u_i(k)$, $i = 1, \ldots, n$, to bring all vehicle speeds $v_i(k)$ and spacings $\Delta x_i(k)$ to the common steady-state speed v_e and spacing Δx_e, while satisfying the aforementioned state and control constraints.

Let us now define the control input as $\boldsymbol{u}(k) = [u_1(k), \ldots, u_i(k), \ldots, u_n(k)]^T$, introduce new state variables as $\tilde{v}_i(k) = v_i(k) - v_e$, $\Delta \tilde{x}_i(k) = \Delta x_i(k) - \Delta x_e$, and denote $\boldsymbol{x}(k) = [\tilde{v}_1(k), \ldots, \tilde{v}_n(k), \Delta \tilde{x}_1(k), \ldots, \Delta \tilde{x}_{n-1}(k)]^T$. This selection of state variables transforms the control problem into a regulation to the origin problem, since at steady-state one gets $\Delta \tilde{x}_{i,ss} = 0$ and $\tilde{v}_{i,ss} = 0$. Using (2) and (3), one gets the following state space model for a system of n vehicles:

$$\boldsymbol{x}(k+1) = A\boldsymbol{x}(k) + B\boldsymbol{u}(k), \quad (4)$$

where

$$A = \begin{bmatrix} 1 & 0 & \ldots & 0 & 0 & \ldots & 0 \\ 0 & 1 & \ldots & 0 & 0 & \ldots & 0 \\ \vdots & & \ddots & & & & \vdots \\ 0 & 0 & \ldots & 1 & 0 & \ldots & 0 \\ T & -T & 0 & 1 & 0 & \ldots & 0 \\ 0 & T & -T & 0 & 1 & \ldots & 0 \\ \vdots & & \ddots & \ddots & & \ddots & \vdots \\ 0 & \ldots & 0 & T & -T & 0 & 1 \end{bmatrix},$$

$$B = \begin{bmatrix} b\frac{T}{m_1} & 0 & \ldots & & 0 \\ 0 & b\frac{T}{m_2} & 0 & \ldots & 0 \\ \vdots & & \ddots & \ddots & \\ 0 & \ldots & & 0 & b\frac{T}{m_n} \\ b\frac{T^2}{2m_1} & -b\frac{T^2}{2m_2} & 0 & \ldots & 0 \\ \vdots & & \ddots & \ddots & \vdots \\ 0 & \ldots & 0 & b\frac{T^2}{2m_{n-1}} & -b\frac{T^2}{2m_n} \end{bmatrix}.$$

The system (4) has the initial condition $\boldsymbol{x}(t_0) = \boldsymbol{x}_0$ and the following state and control constraint sets:

$$v_{\min} - v_e \leq \tilde{v}_i(k) \leq v_{\max} - v_e,$$
$$\Delta x_{\min} - \Delta x_e \leq \Delta \tilde{x}_i(k) \leq \Delta x_{\max} - \Delta x_e, \quad (5)$$
$$u_{\min} \leq u_i(k) \leq u_{\max},$$

for $i = 1, \ldots, n$. Note that the constraints (5) can be formulated as polytopes in a half-space representation, i.e. $F_x \boldsymbol{x} \leq g_x$, $F_u \boldsymbol{u} \leq g_u$ which will be utilized in the interpolating control design in Section 4. The formulation of F_x, g_x, F_u, and g_u is a straightforward and not shown in this paper.

3. INTERPOLATING CONTROL APPROACH

In the following, we first describe the interpolating control approach in subsection 3.1, while subsection 3.2 describes the improved interpolating control.

3.1 Interpolating control

Interpolating control is a recently introduced approach designed for discrete-time linear time-varying systems with model uncertainties and state and control constraints. It provides improvements in optimality and performance compared with a previously introduced control approach for constrained systems, known as Vertex Control, Gutman and Cwikel (1986). In the following, a brief description for interpolating control is given. For a thorough description, the reader can refer to Nguyen et al. (2013).

In the Interpolating Control (IC) scheme, at each time step k the state space $\boldsymbol{x}(k)$ is decomposed as $\boldsymbol{x}(k) = c(k)\boldsymbol{x}_v(k) + (1 - c(k))\boldsymbol{x}_0(k)$, and the corresponding control input is decomposed as $\boldsymbol{u}(k) = c(k)\boldsymbol{u}_v(k) + (1 - c(k))\boldsymbol{u}_0(k)$, where $\boldsymbol{u}_v(k)$ is the control action of a vertex controller at $\boldsymbol{x}_v(k)$ and $\boldsymbol{u}_0(k)$ is the control action of a local controller at $\boldsymbol{x}_0(k)$. The variable $c(k)$, $0 \leq c(k) \leq 1$, represents a Lyapunov function that is minimized to let $\boldsymbol{u}(k)$ be as close as possible to the local controller. The state space $\boldsymbol{x}(k)$ is decomposed such that $\boldsymbol{x}_0(k)$ belongs to a set Ω, called the Maximal Admissible Set (MAS), which is calculated for a specific unconstrained local controller

that can be designed off-line using any control method, as long as it is asymptotically stabilizing. The set Ω includes the origin $\boldsymbol{x} = 0$ in its interior and has the properties of: (i) satisfying constraints for all $\boldsymbol{x}(k) \in \Omega$, and (ii) $\boldsymbol{x}(k) \in \Omega \Rightarrow \boldsymbol{x}(k+i) \in \Omega \, \forall i \geq 1$. The local controller $\boldsymbol{u}_0(k)$ at $\boldsymbol{x}_0(k)$ is designed off-line and can be, e.g., a proportional control $\boldsymbol{u}_0(k) = K\boldsymbol{x}_0(k)$ where K is the off-line calculated matrix of gains. $\boldsymbol{x}_v(k)$ is chosen such that $\boldsymbol{x}_v(k) \in C_N/\Omega$ where C_N is an N-step controlled invariant set of Ω. A controlled invariant set of a target set Ω is the set of all $\boldsymbol{x}$, that satisfy the constraints and for which there *exists* a control sequence that drives the state space $\boldsymbol{x}$ into Ω in no more than N steps. Calculation of the variables c, $\boldsymbol{x}_0$, $\boldsymbol{x}_v$, and $\boldsymbol{u}_v$ involves the solution of two on-line LP problems at each time step (i) decomposition of the state space $\boldsymbol{x}(k)$ which generates $c, \boldsymbol{x}_v$ and $\boldsymbol{x}_0$, and (ii) generating the vertex controller $\boldsymbol{u}_v$.

3.2 Improved interpolating control

Calculating the control invariant set C_N in the interpolating control scheme, which generally involves the polyhedral set projection operation, is computationally expensive especially for high-order systems. Therefore, an Improved Interpolating Control (IIC) scheme has been proposed in Nguyen et al. (2014) that renders the explicit calculation of C_N redundant. The IIC scheme guarantees recursive feasibility and asymptotic stability for all feasible initial conditions.

In the ICC scheme, two (or more) unconstrained local controllers are designed off-line: (i) an inner high gain local controller, denoted $\boldsymbol{u}_0$, which generates good performance when the state is close to the origin, and (ii) an outer low gain local controller which is designed so that it has a large MAS. The MAS of the latter controller is computed implicitly by solving only one on-line LP problem, which produces the state decomposition $\boldsymbol{x}(k) = \boldsymbol{x}_v(k) + \boldsymbol{x}_0(k)$ and the vertex controller $\boldsymbol{u}_v(k)$ at each time step. An interpolation between the inner local controller and the on-line computed vertex controller is used to calculate the control input $\boldsymbol{u}(k) = \boldsymbol{u}_v(k) + \boldsymbol{u}_0(k)$. The local controllers are typically chosen as proportional state feedback, although any asymptotically stabilizing controllers whose MAS can be calculated are also valid. For a comprehensive description of IIC, the reader can refer to Nguyen et al. (2014).

4. NUMERICAL EXAMPLES

4.1 Interpolating control design for a two-vehicle system

We first implement the IC to a system of two vehicles, i.e. $n = 2$ in (2) and (3). The system parameters are defined in Table 1, where the mass and engine parameters are taken from the SMART vehicle model presented in Corona and De Schutter (2008), while the speed limitations are in accordance with typical urban environments. Note that a maximum spacing constraint is imposed on the system. Although it is unnecessary from the point of view of traffic and platoon management, the addition of this constraint helps to produce faster and more robust invariant set calculations. Incorporating the parameter values from Table 1 into the two-vehicle system, we get

Table 1. List of Parameters

Parameter	Description	Value
m_1	Mass of vehicle 1	800 $[Kg]$
m_2	Mass of vehicle 2	800 $[Kg]$
b	Constant force	3700 $[N]$
$u_{\min}$	Minimum input (brake)	-1
$u_{\max}$	Maximum input	0.9
$v_{\min}$	Minimum speed	$0 \left[\frac{m}{s}\right]$
$v_{\max}$	Maximum speed	$17 \left[\frac{m}{s}\right]$
v_e	Steady-state speed	$15 \left[\frac{m}{s}\right]$
$\Delta x_{\min}$	Minimum spacing	$3[m]$
$\Delta x_{\max}$	Maximum spacing	$30[m]$
h	Time headway	$0.2[s]$
T	Integration time interval	$0.2[s]$

a state space system $\boldsymbol{x}(k+1) = A\boldsymbol{x}(k) + B\boldsymbol{u}(k)$ where $\boldsymbol{x}(k) = [\tilde{v}_1(k) \ \tilde{v}_2(k) \ \Delta\tilde{x}_1(k)]^T$ and

$$A = \begin{bmatrix} 1 & 0 & 0 \\ 0 & 1 & 0 \\ 0.2 & -0.2 & 1 \end{bmatrix}, B = \begin{bmatrix} 0.925 & 0 \\ 0 & 0.925 \\ 0.0925 & -0.0925 \end{bmatrix},$$

subjects to the constraint sets, in a half-space representation, $F_x\boldsymbol{x} \leq g_x$, $F_u\boldsymbol{u} \leq g_u$ where

$$F_x = \begin{bmatrix} 1 & 0 & 0 \\ 0 & 1 & 0 \\ -1 & 0 & 0 \\ 0 & -1 & 0 \\ 0 & 0 & -1 \\ 0 & 0 & 1 \end{bmatrix}, F_u = \begin{bmatrix} 1 & 0 \\ 0 & 1 \\ -1 & 0 \\ 0 & -1 \end{bmatrix},$$

$g_x = [10 \ 10 \ 20 \ 20 \ 4 \ 24]^T$, $g_u = [0.9 \ 0.9 \ 1 \ 1]^T$.

Designing the local unconstrained controller The local controller for the IC method has been designed according to (discrete) Linear Quadratic Regulator (LQR). The objective function is chosen as

$$J(\boldsymbol{u}) = \sum_{k=0}^{\infty} \left[\boldsymbol{x}(k)^T Q\boldsymbol{x}(k) + \boldsymbol{u}(k)^T R\boldsymbol{u}(k) \right], \quad (6)$$

where $Q = 0.1\text{diag}([1 \ 1 \ 1])$ and $R = \text{diag}([1 \ 1])$. The objective function (6) offers a trade-off between performance and control effort, according to weighting matrices Q and R. Other objective functions can be selected. Note that in this selection of Q, an equal weight has been given to velocity regulation and spacing regulation (equal values in the matrix diagonal elements). Solving the infinite horizon discrete time Riccati equation yields the local controller $\boldsymbol{u}_0(k) = K\boldsymbol{x}_0(k)$, where

$$K = \begin{bmatrix} -0.3665 & 0.0932 & -0.1742 \\ 0.0932 & -0.3665 & 0.1742 \end{bmatrix}. \quad (7)$$

Calculation of the MAS and the N-step controlled invariant set Once the local controller has been designed, its MAS is calculated. The methods for constructing the exact MAS or polyhedral approximations are available in the literature, Blanchini and Miani (2008); Gilbert and Tan (1991). The MAS is then used as the target set in the construction of the N-step controlled invariant set (C_N), which is constructed using methods presented in Bemporad et al. (2003). The results for the MAS and $C_{22} = C_\infty$ are shown in Fig. 2, where the MAS is the small polyhedron object in the figure, and C_∞ is the large

polyhedron object for the two-vehicle system with local proportional feedback controller and gain matrix K in (7).
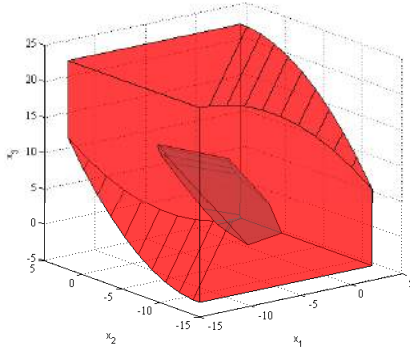

Fig. 2. MAS (small polyhedron object), and C_∞ (large polyhedron object) for the two-vehicle system with local proportional feedback controller and gain matrix K in (7).

Comparison results with other control approaches The results of IC are compared with results obtained from two other approaches: (i) model predictive control (MPC), and (ii) input-saturated LQR solutions. The MPC is implemented with the objective function (6) and the same weighting matrices Q and R. The prediction and control horizons for the MPC, denoted as N_p and N_c, are chosen as $N_p = N_c = 10$. The selection of these values was found to be suitable for the platoon formation system, as longer horizons produced negligible differences in the control inputs and state responses of the system. The unconstrained LQR is constructed with an input saturation to make sure that the control input, $\boldsymbol{u}(k)$, stays within its limits. Simulation results, for the initial conditions $v_1(0) = 5$, $v_2(0) = 13$ and $\Delta x_1(0) = 9$, are shown in Fig. 3. It can be observed from these figures that a set of initial conditions exists such that the input-saturated LQR might produce a state trajectory that violates (at least one of) the state constraints, e.g. spacing between vehicles exceeds the minimum limit, while the IC and MPC do not.
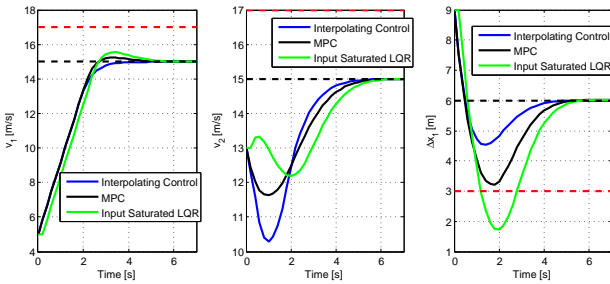

Fig. 3. State trajectories for the initial conditions $v_1(0) = 5$, $v_2(0) = 13$ and $\Delta x_1(0) = 9$. Dashed black - the desired reference. Dashed red - the constraints limits.

4.2 Improved interpolating control design for a three-vehicle system

Let us now consider a three-vehicle system, i.e. $n = 3$ in (2) and (3), with the same parameter values from Table 1 and

the mass of the additional vehicle is $m_3 = 800$ [kg]. Due to the high order of the system, i.e. a state order of five and an input order of three, constructing the controlled invariant set, C_N, is too demanding for the solvers [1]. Therefore, instead of using IC, the IIC approach is utilized for control design in the three-vehicle system.

The state space formulation model for the three-vehicle system is $\boldsymbol{x}(k+1) = A\boldsymbol{x}(k) + B\boldsymbol{u}(k)$ where $\boldsymbol{x}(k) = [\,\tilde{v}_1(k)\ \tilde{v}_2(k)\ \tilde{v}_3(k)\ \Delta\tilde{x}_1(k)\ \Delta\tilde{x}_2(k)\,]^T$ and

$$A = \begin{bmatrix} 1 & 0 & 0 & 0 & 0 \\ 0 & 1 & 0 & 0 & 0 \\ 0 & 0 & 1 & 0 & 0 \\ 0.2 & -0.2 & 0 & 1 & 0 \\ 0 & 0.2 & -0.2 & 0 & 1 \end{bmatrix} B = \begin{bmatrix} 0.925 & 0 & 0 \\ 0 & 0.925 & 0 \\ 0 & 0 & 0.925 \\ 0.092 & -0.092 & 0 \\ 0 & 0.092 & -0.092 \end{bmatrix}$$

where the constraints (5) can be formulated as polytopes, $F_x \boldsymbol{x} \leq g_x$ and $F_u \boldsymbol{u} \leq g_u$. The local optimal controller is chosen as an LQ control law with the following weight matrices, $Q = \mathrm{diag}([\,0.25\ 0.25\ 0.25\ 1\ 1\,])$, $R = \mathrm{diag}([\,1\ 1\ 1\,])$. Note that in this selection of Q, a higher weight is given to the spacings regulation, i.e. the values on the diagonal corresponding to $\Delta\tilde{x}_1(k)$, $\Delta\tilde{x}_2(k)$ are 1, while the values corresponding to $\tilde{v}_1(k)$, $\tilde{v}_2(k)$, $\tilde{v}_3(k)$ are 0.25. Hence, the vehicles should exhibit behavior that aims at settling the spacings faster and the velocities slower, in comparison with a uniform weight selection of Q.

Main results of the IIC design are presented in the following. The designed inner and outer controller gains, according to the IIC, are given as follows:

$$K_1 = \begin{bmatrix} -0.694 & 0.12 & 0.061 & -0.669 & -0.206 \\ 0.12 & -0.753 & 0.12 & 0.463 & -0.463 \\ 0.061 & 0.12 & -0.964 & 0.206 & 0.669 \end{bmatrix},$$

$$K_2 = \begin{bmatrix} -0.058 & 0.03 & 0.02 & -0.01 & -0.003 \\ 0.031 & -0.069 & 0.031 & 0.008 & -0.008 \\ 0.019 & 0.031 & -0.058 & 0.003 & 0.001 \end{bmatrix}.$$

The comparison simulation results of IIC, MPC, and input-saturated LQR for the three-vehicle system are shown in Figs. 4–6. The results in Fig. 4 and Fig. 5 show respectively the velocity and inter-vehicle spacing trajectories for the initial conditions $v_1 = v_2 = v_3 = 10$, $\Delta x_1 = \Delta x_2 = 20$. The desired steady-state speed and distance are respectively $v_e = 15$ and $\Delta x_e = 6$, and shown in dashed black lines, while the upper and lower bounds for state and control constraints, see Table 1, are shown in dashed red lines. Fig. 4 shows that for the given initial states the input-saturated LQR controller produces a state response that violates one of the constraints, see v_3, while the trajectories obtained from IIC and MPC satisfy all constraints. Fig. 5 shows that the MPC controller exhibits better settling time performance compared with IIC, and Fig. 6 shows that for the given set of initial conditions, the IIC and MPC controllers produce smoother control inputs compared with a saturated LQR.

---

[1] The maximal admissible sets and controlled invariant sets are calculated using known iterative algorithms, and implemented with Matlab and the Multi Parametric Toolbox (MPT).
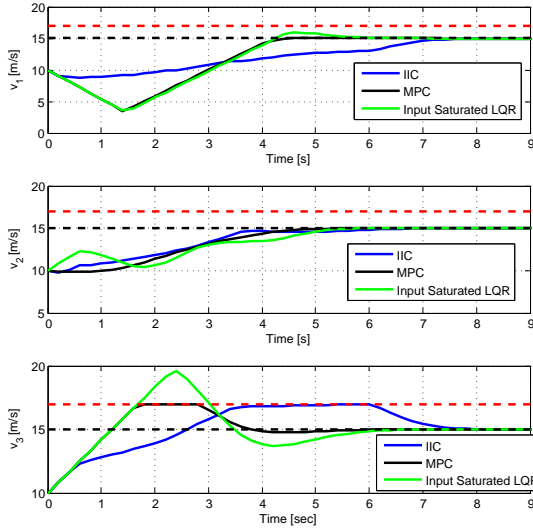
Fig. 4. System velocity trajectories for the initial conditions $v_1 = v_2 = v_3 = 10$, $\Delta x_1 = \Delta x_2 = 20$. Dashed black and red lines are respectively the desired reference and the constraints limits.
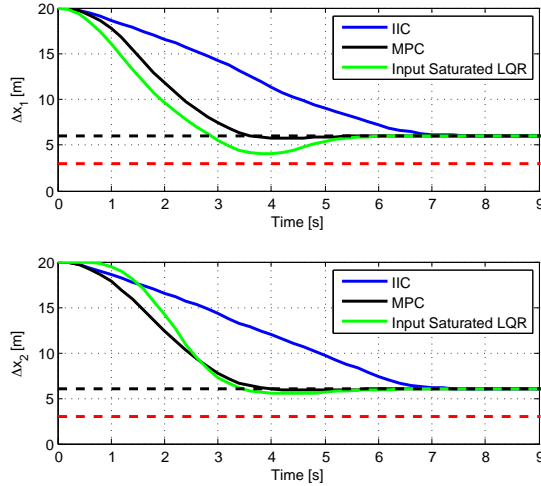

Fig. 5. Inter-vehicle spacing trajectories for the initial conditions of Fig. 4. Dashed black and red lines are respectively the desired reference and the constraints limits.

5. INTERPOLATING CONTROL WITH INTEGRAL ACTION

5.1 System model

In order to improve steady state performance, it is sometimes useful to incorporate integral action in the controller, as presented in this section to address the platooning problem. Suppose that the vehicles are travelling on a sloped road. A gravitational force $f_{g,i}(k)$ (N) is applied on vehicle i at time k, i.e. $f_{g,i}(k) = m_i g \sin(\alpha_i(k))$, where g (m/s^2) is the gravitational acceleration constant and $\alpha_i(k)$ is the slope angle for vehicle i at time k. The state space model for this system can be written as:

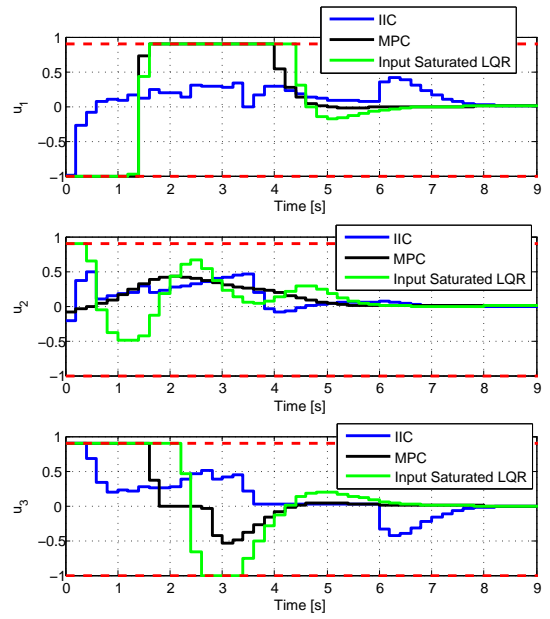$$\boldsymbol{x}(k+1) = A\boldsymbol{x}(k) + B\boldsymbol{u}(k) + E\boldsymbol{d}(k) \qquad (8)$$

Fig. 6. System control action for the initial conditions of Fig. 4. Dashed red - the constraints limits.

where

$$E = \begin{bmatrix} -Tg & 0 & \dots & & & 0 \\ 0 & -Tg & 0 & \dots & & 0 \\ \vdots & & \ddots & \ddots & & \\ 0 & \dots & & & 0 & -Tg \\ \frac{-T^2}{2}g & \frac{T^2}{2}g & 0 & & \dots & 0 \\ 0 & \frac{-T^2}{2}g & \frac{T^2}{2}g & 0 & \dots & 0 \\ \vdots & & \ddots & \ddots & & \vdots \\ 0 & \dots & & 0 & \frac{-T^2}{2}g & \frac{T^2}{2}g \end{bmatrix}.$$

and $\boldsymbol{d}(k) = [\sin(\alpha_1(k)), \sin(\alpha_2(k)), \dots, \sin(\alpha_n(k))]^T$

Here, $\boldsymbol{d}(k)$ can be considered as a disturbance input. The matrices A and B are given in section 2. The slope is bounded by maximum and minimum angle values, hence the disturbance is bounded at all times. These bounds can be formulated in a half-space representation as $F_e \boldsymbol{d}(k) \leq g_e$ for all k. In the IC methodology, the local controller can incorporate integral action in addition to other control actions such as proportional state feedback. This addition adds one or more state variables to the local controller, while the number of state variables used to produce the vertex controller remains the same. The integral action should eliminate steady-state errors, defined as $\boldsymbol{y}(k) = C\boldsymbol{x}(k)$, if the disturbance is a bounded step function. The integrator equation can be formulated as $\boldsymbol{e}(k+1) = T\boldsymbol{y}(k) + \boldsymbol{e}(k) = S\boldsymbol{x}(k) + \boldsymbol{e}(k)$, where T is the sampling period of the system and $S = TC$. Adding the integral action to the local controller with proportional state feedback yields $\boldsymbol{u}_0(k) = K\boldsymbol{x}(k) + L\boldsymbol{e}(k)$. An extended state space system is then formulated as:

$$\begin{bmatrix} \boldsymbol{x}(k+1) \\ \boldsymbol{e}(k+1) \end{bmatrix} = \begin{bmatrix} (A+BK) & BL \\ S & I \end{bmatrix} \begin{bmatrix} \boldsymbol{x}(k) \\ \boldsymbol{e}(k) \end{bmatrix} + \begin{bmatrix} E \\ 0 \end{bmatrix} \boldsymbol{d}(k),$$
$$(9)$$

where the gain matrices of the proportional and integral parts of the local controller, namely K and L, are computed off-line. The procedures used to construct the

MAS and the N-step controlled invariant set, C_N, are then applied to the extended state space system (9).

5.2 Numerical example

As an example, a two vehicle system is considered. The matrices A and B are taken from Section 4, and the system output is chosen as $y(k) = C\boldsymbol{x}(k)$ where $C = [\,0\ 0\ 1\,]$. This selection of the matrix C, states that the output $y(k)$ is a scalar defined as the spacing $\Delta x_1(k)$ between the two vehicles. Utilizing the LQR approach to tune the local controller, yields the parameters $K = \begin{bmatrix} -1.03 & 0.13 & -1.12 \\ 0.13 & -1.03 & 1.12 \end{bmatrix}$ and $L = \begin{bmatrix} -0.71 \\ 0.71 \end{bmatrix}$. Asymptotic stability of the local controller is verified by checking that the magnitudes of the eigenvalues of the extended state space matrix $\tilde{A} = \begin{bmatrix} (A+BK) & BL \\ S & I \end{bmatrix}$ are less than unity. Utilizing an algorithm to calculate the robust MAS, which takes into account the worst case scenario of the disturbance in the calculation, refer to Nguyen et al. (2013), and solving the on-line improved interpolating control problem with integrator, we get the simulation results, as shown in Fig. 7. In this simulation, a constant step disturbance is added to the system and the output is compared with a control law without integral action. It can be observed that the steady state error equals zero with integral action, and a non zero constant value without integral action, as expected. However, it can be observed that a controller with integral action produces a response with a longer settling time and a larger over-shoot. That is also expected since integral action usually negatively effects the performance of the transient response.
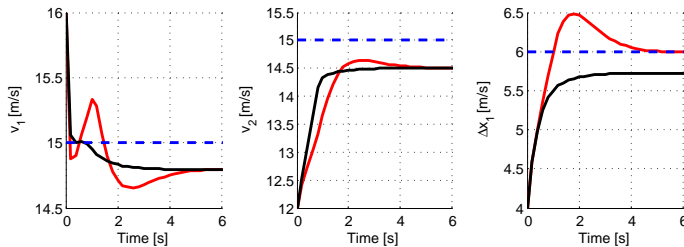

Fig. 7. Velocity and spacing trajectories as a function of time, for a two vehicle system with the initial conditions $v_{1,0} = 16(\text{m/s})$, $v_{2,0} = 12(\text{m/s})$, $\Delta x_{1,0} = 4(\text{m})$, and step disturbance input $\mathbf{d}(k) = [\,0.15\ 0\,]^T$. Red - control with integral action. Black - control without integral action. Dashed blue - desired steady-state values.

6. CONCLUSIONS

In this paper, the vehicle platoon formation problem is presented and addressed using a new control approach known as interpolating control. The control and state responses of the interpolation based approach are compared with other methods for constrained MIMO systems, such as the MPC. Moreover, an interpolating controller with integral is designed for a plant with a bounded disturbance. We conclude that the IIC scheme can be used as an alternative for the MPC approach, and show here that it can

incorporate integral action in a similar fashion to the MPC with integral action.

REFERENCES

Bemporad, A., Borrelli, F., and Morari, M. (2003). Min-max control of constrained uncertain discrete-time linear systems. *Automatic Control, IEEE Transactions on*, 48(9), 1600–1606.

Blanchini, F. and Miani, S. (2008). *Set-theoretic methods in control*. Springer.

Brinon Arranz, L., Seurect, A., and Canudas De Wit, C. (2014). Cooperative control design for time-varying formations of multi-agent systems. *IEEE Transactions on Automatic Control*, 59(8), 2283–2288.

Corona, D. and De Schutter, B. (2008). Adaptive cruise control for a smart car: A comparison benchmark for mpc-pwa control methods. *Control Systems Technology, IEEE Transactions on*, 16(2), 365–372.

Gilbert, E.G. and Tan, K.T. (1991). Linear systems with state and control constraints: The theory and application of maximal output admissible sets. *Automatic Control, IEEE Transactions on*, 36(9), 1008–1020.

Gutman, P.O. and Cwikel, M. (1986). Admissible sets and feedback control for discrete-time linear dynamical systems with bounded controls and states.

Naus, G., Vugts, R., Vd Molengraft, R., Steinbuch, M., and Ploeg, J. (2009). Towards on-the-road implementation of cooperative adaptive cruise control. In *16th ITS World Congress and Exhibition on Intelligent Transport Systems and Services*.

Nguyen, H.N., Gutman, P.O., and Bourdais, R. (2014). More efficient interpolating control. In *Control Conference (ECC), 2014 European*, 2158–2163. IEEE.

Nguyen, H.N., Gutman, P.O., Olaru, S., and Hovd, M. (2013). Implicit improved vertex control for uncertain, time-varying linear discrete-time systems with state and control constraints. *Automatica*, 49(9), 2754–2759.

Ploeg, J., Scheepers, B.T., van Nunen, E., van de Wouw, N., and Nijmeijer, H. (2011). Design and experimental evaluation of cooperative adaptive cruise control. In *Intelligent Transportation Systems (ITSC), 2011 14th International IEEE Conference on*, 260–265. IEEE.

Rajamani, R. and Zhu, C. (2002). Semi-autonomous adaptive cruise control systems. *Vehicular Technology, IEEE Transactions on*, 51(5), 1186–1192.

Schakel, W.J., van Arem, B., and Netten, B.D. (2010). Effects of cooperative adaptive cruise control on traffic flow stability. In *Intelligent Transportation Systems (ITSC), 2010 13th International IEEE Conference on*, 759–764. IEEE.

Treiber, M. and Kesting, A. (2013). Traffic flow dynamics. *Traffic Flow Dynamics: Data, Models and Simulation, ISBN 978-3-642-32459-8. Springer-Verlag Berlin Heidelberg, 2013*.

Tuchner, A. and Haddad, J. (2015). Vehicle platoon formation using interpolating control. In *the 8th IFAC Symposium on Robust Control Design (ROCOND15)*. Bratislava, Slovakia.

Van Arem, B., van Driel, C.J., and Visser, R. (2006). The impact of cooperative adaptive cruise control on traffic-flow characteristics. *Intelligent Transportation Systems, IEEE Transactions on*, 7(4), 429–436.

Novel Map Platform Based on Primitive Elements of Traffic Environments for Automated Driving Technologies

Takuma Ito*, Masahiro Mio**, Kyoichi Tohriyama**, Minoru Kamata*

*The University of Tokyo, Kashiwanoha, Kashiwa, Chiba, 277-8589, Japan
(Tel: +81-4-7136-6683; e-mail: ito@iog.u-tokyo.ac.jp).
**Toyota Motor Corporation

Abstract: To realize driver assistance systems based on automated driving technologies, intelligent vehicles need to recognize surrounding driving environments. On this point, sensing technologies with high-cost sensors have several problems for future popularization. Therefore, this research aimed at developing automated driving technologies with lean sensors via the enhancement of existing ADAS Horizon.

Keywords: Vehicle Dynamics Control and autonomous driving, Vehicular Sensors and Environment Perception, Digital map

1. INTRODUCTION

Since public transportation systems are declining in country areas according to the growth of aged society in Japan, we need new technologies to support the elderly in country areas for their daily travels. To this end, our research group (Inoue 2014) considered making automobiles intelligent as the solution for safe daily travels; further, we have been developing intelligence for automated vehicles. Although we need a large amount of discussion regarding to what degree the machine intelligence controls the vehicle instead of human drivers, we need the technologies that enable the vehicle complete the fully automated driving, at first and at least. In regard to this point, the advanced driver assistance system based on automated driving technologies are more difficult than simple autonomous driving because the former has the difficulty involving a human driver. Thus, we need to start from fully automated driving for our final goal.

Unlike to existing automatic emergency braking systems, what our research group aim to develop is a highly matured driving intelligence based on the techniques of matured drivers that enable proactive driving without approaching surrounding risks. To realize such systems, it is necessary for intelligent vehicles to recognise the surrounding situations enough far. However, we have problems regarding such long-range sensing only by the vehicular sensors because such high-spec sensors cost too much to be practically used. On the contrary, although technologies of virtual long-range sensing based on communication technologies with roadside infrastructures have been developed, such systems focus not on the community roads of country areas but on the highways of urban areas. Thus, currently we cannot apply such technologies to driver assistance systems for elderly drivers of country areas, though we have the possibility of applying them in future.

Given these motivations, we focus on the technologies regarding digital maps to realize proactive vehicle controls only by using lean components of a system platform. Since existing technologies regarding maps focus only on navigation of a driving route and providing information, we need to discuss the requirement of digital maps for automated driving in this research. Furthermore, on the assumption of the lean components of a system platform, we need to complementally combine the vehicular sensors with digital maps. Thus, in this research, we will design the system platform of sensing based on above limitations.

2. SENSING PLATFORM COMPLEMENTALLY COMBINED WITH DIGITAL MAP

2.1 Usages of digital map

In general, usages of digital map are roughly classified into two categories, namely route navigation and road information. Although we need both to realize the autonomous driving, technologies regarding the former has been developed enough to date; thus, we focus on the latter.

Similarly, usages of road information are also roughly classified as follows:

- Localization: Based on the information of digital maps and detected landmarks by vehicular sensors, intelligent vehicle grasps the current position on the map.

- Long-range sensing: Based on the information of digital maps and current position of the vehicle on the map, intelligent vehicle grasps the elements of traffic environments in front of the vehicle, such as crossings, crosswalks, stop lines, curvature of the road, and so on.

Regarding above technologies, although various approaches have been developed to date, requirements of technologies depend on the goal and limitations; thus, we need to discuss the requirements based on our goals and our limitations.

2.2 Requirement of localization

In regard to localization on a digital map, technologies based on GPS, such as car-navigation systems, has been developed. However, since precision of localization for car-navigation based on common GPS is approximately several meters order, much more precise localization is necessary for autonomous driving. On this point, when we assumes the example of turning left on the crossing with the error of localization more than 1.0 m, some parts of the vehicle body may enter into the opposite lane after finishing the left turn. Thus, precision of less than 0.5 m is necessary for autonomous driving.

To this requirement of localization precision, although an existing research (Omae 2004) realized autonomous driving by RTK-GPS, such sensors have the problems of the cost for our purpose. In addition, although we need digital data of waypoint map for autonomous driving, we have the problems of the size of data on the assumption that RTK-GPS is simply used and waypoint map is simply combined with GPS coordination system on the precision of RTK-GPS. Even though such approaches with the in-vehicle data storage can be applied for autonomous driving in the limited areas, such as parking areas, it is difficult for us to store such large amount of data for all community roads of country areas in the in-vehicle storage. On the contrary, although some exiting research proposed on-demand acquisition of digital map via high-speed communication network, such approaches can be applied only on the urban areas where the infrastructures of wireless network are well constructed, and not on the country areas. Furthermore, though some researches (Kummerle 2009) proposed a localization method utilizing the simultaneous localization and mapping (SLAM) methods, they have problems of high-cost sensors and too much amount of digital data for general use of autonomous driving on community roads similar to the case of RTK-GPS.

Considering the approaches for our problems based on the above discussions, since using sensors specialized only for the localization causes a problem of the cost, simple sensors used for various functions of advanced driver assistance systems (ADAS), such as common GPS, cameras, and so on, have the possibility of solving the cost problem. On the other hand, regarding too much amount of data for a digital map, preliminarily preparing the precise landmark map on the global coordination system causes the problem. For solving this problem, dynamically reconstructing landmark map based on the primitive elements of traffic environments on the local coordination system, such as stop lines, crosswalks, and so on, has the possibility of solving the problem of data size. Furthermore, since we need to complementally utilize the digital map and vehicular sensors for both approaches, we need to focus not only on developing the individual sensing technologies, but also on developing the system platform.

2.3 Requirement of long-range sensing

Regarding the usage of digital maps as a long-range sensor, researches around PReVENT project (Blervaque 2006) proposed ADAS Horizon system. ADAS Horizon defines a map as the combination of main path and sub path. Sub path

is divaricated from main path at the node which is called as stub. The position of self-vehicle and various elements of traffic environments is defined as "Offset," which is a distance measured from the origin stub of main path. Fig. 1 shows the schematic of concept regarding path and stub. Orange line in the figure indicates main path, while blue lines indicate sub path. In addition, green circles, which indicate the divaricated points of sub path, indicate stub. The position of the self-vehicle, stubs, and elements of traffic environments on main path are expressed as the offset, which are shown in the figure.
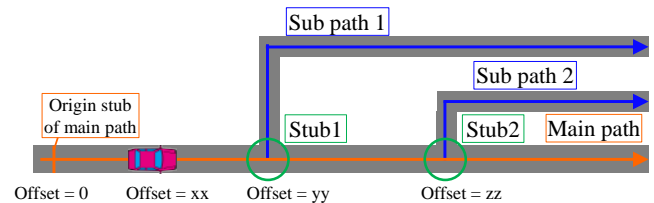

Fig. 1. Schematic of concept regarding path and stub

ADASIS v2 protocol, which has been already published as a protocol of ADAS Horizon, defines the various information, such as the limitation of velocity, lane information, slope of the road, and so on. Since it assumes the ADAS providing the information to the drivers and ones simply controlling the vehicle, such as eco-drive, ADASIS v2 protocol does not directly assume the autonomous driving; thus, information necessary for autonomous driving on community roads of country areas, such as position of stop lines, and so on, is not defined. In addition, ADASIS v2 protocol defines the value of offset as integer numbers because ADASIS v2 protocol does not assume precise vehicle controls unlike to our purpose. Therefore, since we cannot use the precise offset of various information, it is hard for us to use the ADAS Horizon via current protocol as the long-range sensor for our target situations.

However, the expression of offset defined in the ADAS Horizon is very useful for our problem that we need to dynamically reconstruct the digital map on local coordination system based on primitive elements of traffic environments, because definition of offset is relative one based on the assumption that origin point of map information changes in accordance with the situations. Fig. 2 shows the conceptual schematic of digital map via global coordinate system. For global one, we need precision of relative position of various elements of traffic environments and waypoint map for the large area. On the other hand, Fig. 3 show the conceptual schematic of digital map via local coordinate system. For local one, we assumed many origin stub of each path and define the offset information of various information based on position of the origin stubs. Thus, we need precision of relative position of various objects only within each path, and connectivity between an end point of previous path and a stub of next path. For the latter one, we have a merit that we can easily measure and prepare the data of digital map due to numerical expressions of map data with relatively low-precision of position information. In addition, relatively low-precision of position information can realize the reduction of
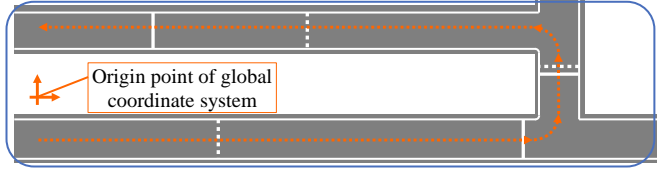
data size. In this way, the reason of referring ADAS horizon is that offset can easily achieve these merits of managing digital maps.

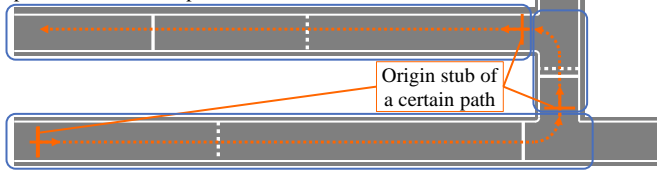Fig. 2. Conceptual schematic of digital map via global coordinate system

Fig. 3. Conceptual schematic of digital map via local coordinate system

Thus, we decide to enhance the existing protocol of ADAS Horizon to realize the small-sized digital map that fulfil both functions of localization and long-range sensing. In this paper, to contrastingly discuss the function of long-range sensing with waypoint map and landmark map, we call the digital map regarding long-range sensing as control target map from now on.

2.4 Enhancement of ADAS horizon

ADAS Horizon assumes the combined use of ADAS Horizon provider, which provides the information of digital maps, and ADAS applications, which use the provided information. Although there are various types of ADAS applications, such as warning systems, eco-drive systems, and so on, we focus on the dynamic reconstructor of three kinds of digital maps which are used for autonomous driving, namely waypoint map, landmark map, and control target map. These maps have common elements of traffic environments. For example, information of stop line is used as both landmark for localization and control target for deceleration. These commonality is the key of reducing the data size. Thus, we need to discuss the enhancement of the protocol with considering the common use of primitive elements of traffic environments.

Since the existing protocol assumes the CAN bus I/F as the connection between the provider and the applications, the maximum size of every message is limited to less than 8 bytes. Furthermore, the exiting protocol defined the bit assign of message header and message container according to the types of message. Since the existing protocol defines the type "Profile Long," which is defined as universal use for

enhancements, aside from the existing types of message, we discussed the enhancement of existing protocol based on "Profile Long." The former 4 bytes of "Profile Long" is assigned as the message header, while the latter is assigned as a data container. Difficult point is how we define the necessary information via only the latter 4 bytes.

2.5 Waypoint map

Since ADAS Horizon manages the discontinuous information with discrete values of offset, information regarding the state change is more important than information regarding the constant state. Thus, information of curves is more important than information of straight roads to dynamically reconstruct waypoint map. Although there are many methods to define information of curves, usable ones are as follows:

- Definition as simple arcs: This definition is enough simple to summarize necessary information into one message. In addition, it is easy to apply this information to the reconstruction of the control target maps. However, it is difficult to versatilely express gradual curving roads.

- Definition as spline curves: This definition has the merit to easily express various curves including gradual curving roads. On the other hand, this definition has the demerits that numerical expression is complex so that relatively large amount of information is necessary for one information.

Although above methods have both merits and demerits respectively, we selected the former as the first step. Table 1 shows the detailed expression. Since data size of expression shown in the table is 25 bits, we can put necessary information into one message, of which size of data container is 32 bits. The important point is that we add first decimal place of offset expression into enhanced protocol because expression of offset based on existing protocol manages only integer number, which is expressed in the header part.

Table 1. Expression of curve information

Contents	bit type	Num. of bit	LSB
First declimal palce of offset for start point of simple arc	Unsigned	4	0.1 m
Angle of the curve	Unsigned	4	15 degree
Radius of curvature	Unsigned	8	0.1 m
Various Flags		Totally 9	

When the reconstructor of waypoint map receives the curve information from ADAS Horizon provider, the reconstructor considers the corresponding areas as curve roads while the reconstructor considers other areas as straight roads. Based on these information, the reconstructor dynamically make the waypoint map at the necessary density. In this research, we reconstructs the waypoint on the density of 0.02 m. Fig. 4 shows the conceptual schematic of reconstructing the waypoint map. For the situations of upper row in the figure, the system alternately reconstructs the waypoint of straight part and curve part based on the information of curves, as shown in the lower row of the figure.
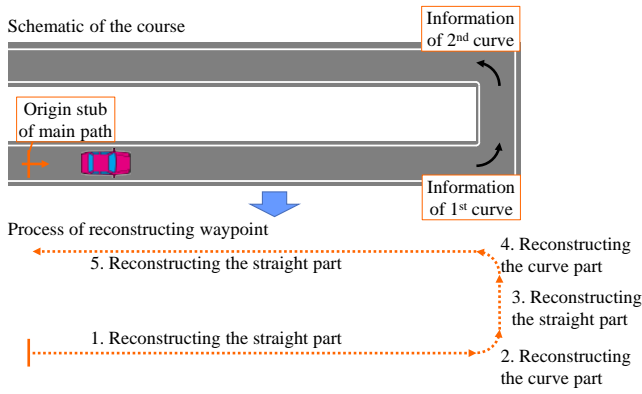
Fig. 4. Conceptual schematic of reconstructing waypoint map

Regarding the data size, the size of preliminary prepared waypoint map and dynamically reconstructed one is defined as follows. As is shown below, our proposal achieves the reduction of data size for usual cases.

- Total data size of preliminary prepared waypoint map = (Size of a way point) × (Density of waypoint map) × (Length of the curse)

- Total data size of dynamically reconstructed waypoint map = 8 byte × (Number of curves)

2.6 Landmark map

To grasp the current position of the self-vehicle, the vehicle need the information regarding position of unmoving elements of traffic environments. In addition, to realize the localization via a lean sensing platform, we had better to target on the landmark that are detected only by common sensors, such as cameras and simple LIDARs, and so on. Although there are many candidates of landmarks that meet above requirements on the community roads, we focus on the stop line and guardrail at the T-junction as the first step. Figs. 5 and 6 show the schematic of parameters of landmarks, while table 2 and Table 3 show the detailed expressions of corresponding landmarks. For guardrails, since sometimes there is no stop line in front of the curve, we define the virtual stop line at the point where a stop line need to be drawn. If there is a real stop line in front of the guardrail, we use the offset information of the real stop line.
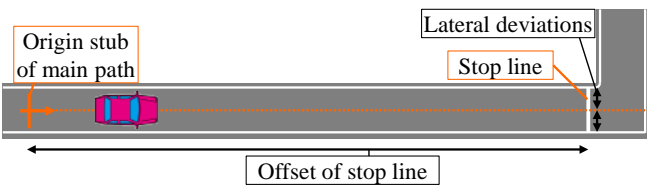

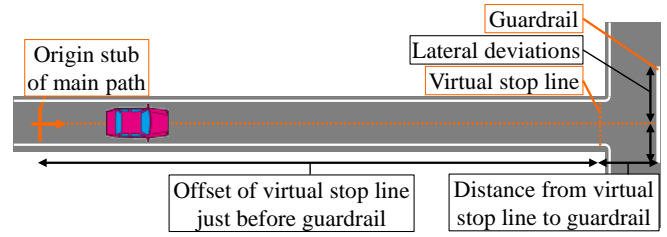Fig. 5. Schematic of parameters of stop line as a landmark

Fig. 6. Schematic of parameters of guardrail as a landmark

Table 2. Expression of stop line

Contents	bit type	Num. of bit	LSB
Lateral deviation from left side of stop line to the center of thr road	Signed	8	0.1 m
Lateral deviation from right side of stop line to the center of thr road	Signed	8	0.1 m
First declimal palce of offset of stop line	Unsigned	4	0.1 m

Table 3. Expression of guardrail

Contents	bit type	Num. of bit	LSB
Lateral deviation from left side of guardrail to the center of thr road	Signed	8	0.1 m
Lateral deviation from right side of guardrail to the center of thr road	Signed	8	0.1 m
Distance from virtual stop line to the guard rail	Unsigned	8	0.1 m
First decimal palce of offset of virtual stop line	Unsigned	4	0.1 m

Although what we mainly focus on is information regarding position of landmarks for localization, we add the definition regarding the size of landmarks as the support information of landmark detection to effectively utilize the limited size of the data container. In addition, though we use other definition of enhanced messages for the experiment, which will be described in the next chapter, we skip the other definitions except for above-mentioned main landmarks.

2.7 Control target map

To realize the autonomous driving, first of all, we need to consider the basic elements of driving, namely acceleration, steering, and deceleration. In regard to the steering, waypoint map can provide necessary information. For rest ones, constant driving with acceleration to the limited speed is the regular state, while deceleration is irregular state of driving. Thus, we need simple information for acceleration such as limited speed of current roads. On the other hand, regarding the deceleration, we need detailed information, namely target velocity of deceleration and offset information on the point that the self-vehicle need to complete the preliminary deceleration, such as deceleration for stopping in front of stop line, deceleration before the curves, and so on.

Regarding the former limited speed of the current road, existing protocol defined partly as the traffic regulations. For other part, such as speed limit based on the radius curvature, we can commonly use the curve information for the waypoint map. On the contrary, in regard to deceleration, target velocity of deceleration and the offset of deceleration point can be determined by the information of landmark map, such

as stop line. Based on above discussions, since information of waypoint map and landmark map can enough provide common necessary information, we do not need any additional definitions of enhanced protocol for reconstructing control target map.

2.8 Prototype implementation

Based on the design of enhanced ADAS Horizon discussed in the previous sections, we implemented prototypes of recognition platform complementally combined with digital maps and vehicular sensors. Fig. 7 shows the appearance of experimental vehicle. Table 4 shows the main sensors equipped with the experimental vehicle. The driving distance of the vehicle is calculated via the rotation pulse of additional sensor in the rear wheels. As we aim to develop the technologies of autonomous driving via lean sensors, we select the vehicular sensors that is currently lean, or ones that will become lean in near future. In addition, we develop a microcomputer-based prototype of provider of enhanced ADAS Horizon.

Fig. 7. Appearance of experimental vehicle

Table 4. Sensors of experimental vehicle

Sensor	Model	Purpose
Monocular Camera	Point Grey Research GRAS-14S5C-C	Stop line Detection
Monocular Camera	Mobileye 560	Lane Detection
LIDAR	IBEO LUX	Guardrail Detection
GPS	Hemisphere A100	Rough Localization
IMU	TAMAGAWA SEIKI AU7428	Estimating Vehicle Dynamics

Fig. 8 show the conceptual schematic of perception platform developed in this research. To implement this platform, we used ROS (ROS.org), which is the middleware for developing robots.
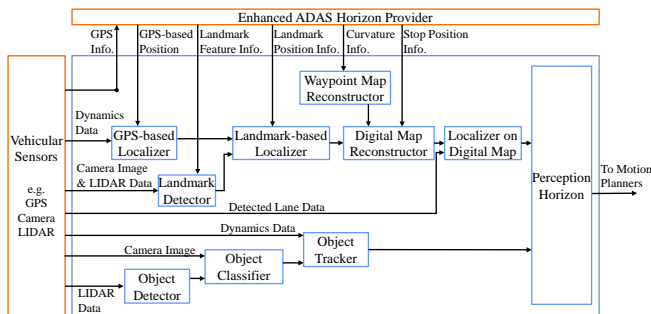

Fig. 8. Conceptual schematic of perception platform

First, the system sends the GPS information to the enhanced ADAS Horizon provider, and GPS-based localizer receives a roughly estimated offset information via ADAS Horizon provider. At the same time, landmark-based detector receives feature information of the nearest landmark, and detects the landmark based on the provided information by cameras and LIDARs. Then, landmark-based localizer receives the detected information from the landmark detector, and position information of landmark from enhanced ADAS Horizon provider. Based on the comparison of these information, landmark-based localizer updates the precise offset information of the self-vehicle.

On the other hand, waypoint map reconstructor receives the curve information from enhanced ADAS Horizon provider, and dynamically makes the waypoint map. In addition, waypoint map reconstructor classifies the situation of each waypoint into three categories, namely straight part, curve entrance part, and curve part. Fig. 9 shows the schematic of this classification. Based on this classification, the system changes the parameters of vehicle controls, such as target velocity for acceleration control, preview time for steering control, and so on. After that, digital map reconstructor add information of stop line, which is received from enhanced ADAS Horizon provider, and then dynamically integrates the three kinds of map, namely waypoint map, landmark map, and control target map.
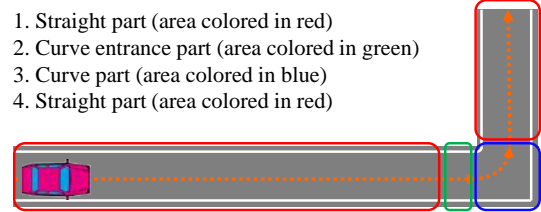

Fig. 9. Conceptual schematic of classifying the situation categories based on the map information

Based on the offset information and lateral position in the lane, which is measured by lane detection camera, localizer updates the position of the self-vehicle on the integrated digital map. Regarding the information of lateral position for steering control, we do not directly use the result of lane detection but indirectly use the result of localized position on integrated digital maps because indirect use of lateral information has the merit of easily calculating the lateral deviation between a preview point, which is used for preview control, and the nearest waypoint. In addition, indirect use of lateral information has another merit that the system can easily estimate the preview lateral deviation based on the information of dynamics via IMU even though the camera cannot detect the lane marks during curves.

Separately from above topics of digital maps, each sensor detects, recognizes, and tracks the surrounding traffic participants. Perception horizon integrates the result of these processes with digital maps. The integrated results are transmitted to the motion planner. Regarding the algorithms for vehicle controls, we implement relatively simple ones. For lateral controls, we adopt a preview driver model based

on risk potential, which our collaborators developed and described some parts in the previous paper (Hasegawa 2014). On the other hand, for the longitudinal control, we adopt the following algorithms:

1. The system set the target velocity of acceleration based on the information of speed limit and curves via enhanced ADAS Horizon.

2. The system set the target velocity of deceleration and the offset where the self-vehicle complete the deceleration based on the nearest control target regarding deceleration such as stop lines, curves, and so on.

3. The system calculate the necessary distance for deceleration on the assumption of a certain deceleration rate, such as 0.1 G.

4. If rest distance to the control target is less than the necessary distance for deceleration, the system starts to decelerate. Otherwise, the system accelerates to the target velocity of acceleration.

Because the main focus of this paper is usage of digital maps, we skip the more details of vehicle controls.

3. FEASIBILITY TEST OF AUTONOMOUS DRIVING ON TEST COURSE

3.1 Test course

To confirm the feasibility of our concept of automated driving via enhanced ADAS Horizon, we conducted the experiments of autonomous driving on test course. Fig. 10 shows a schematic of test course. This course contains seven left turns, which we call as C1 to C7 respectively. The total distance of this course is approximately 450 m. In this course, since four left turns at C1, C4, C6, and C7 is ones from non-priority road to priority road, we need to stop the vehicle before turning left. For other curves, we need to decelerate until approximately 10 km/h as the preparation for left turn.
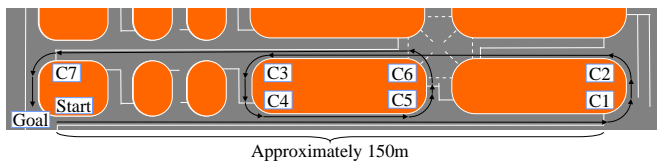

Fig. 10. Schematic of test course

Fig. 11 shows the appearance of landmarks used for localization in this course. There are stop lines at C1 and C7, while there is a guardrail at the opposite side of C4.

Fig. 11. Appearance of landmarks

Regarding the target velocity of acceleration, we set 30 km/h for the straight course, while we set 10 km/h during left turns. In addition, for the short straight road such as a straight road between C4 and C5, we set 20 km/h as the target velocity of acceleration because the self-vehicle starts to decelerate before completing the acceleration for the target velocity of 30 km/h.

As for the stub, original ADAS Horizon assumes an update of stub at the crossing. However, since we aimed at confirming the feasibility of our concept of enhanced ADAS Horizon in this research, we skipped the implementation of stub as the first step. Thus, we simply assumed the single path course although the test course actually have many crossings. For such assumed single path, we measured the test course and prepared the data of enhanced ADAS Horizon, which was stored into the prototype provider of enhanced ADAS Horizon.

3.2 Results

As we focus on the usage of digital maps in this research, primal point of this experiment is whether or not the vehicle set adequate values of the control target based on the provided information of enhanced ADAS Horizon. Thus, we focus on the abstracts of whole driving, and skip the details of dynamics data of the vehicle controls.

Fig. 12 shows the time series offset and its adjustment. Horizontal axis indicates time. Vertical axis of the upper row indicates the offset of the self-vehicle while vertical axis of the lower row indicates the adjustment values. Rectangles colored in orange indicate the offset adjustment at the curves. At the curves of C1 and C7, the system updates its offset by detecting the stop lines. On the contrary, at the curve of C4, the system updates its offset by detecting guardrail. Regarding the adjustment values, we simply added the offset values at that time. At each curve, though the initial values of offset adjustment are relatively large, the values after initial one are almost equivalent to 0. Based on this tendency, we can confirm that offset values were well adjusted.
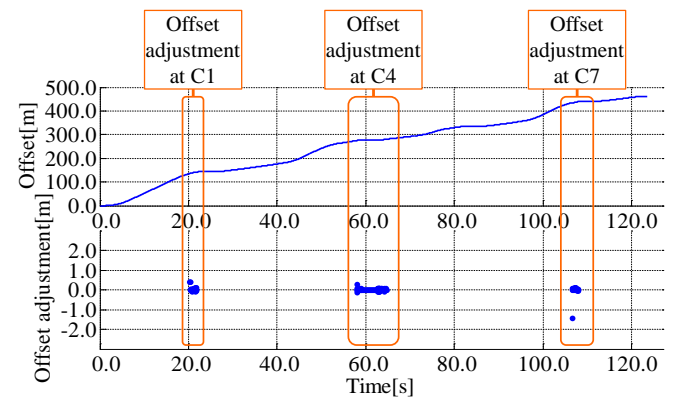

Fig. 12. Time series offset and its adjustment

Regarding the errors of offset, not only the factors caused by the vehicle dynamics, such as slips of tires during acceleration and deceleration, but also the factors of precision

of digital maps are the reasons. Important point is that our complementary combined system of vehicular sensors and digital maps can equally manage these factors of offset errors. In addition, since the concept of ADAS Horizon manages various information of road within each path between stubs, we need the relative precision of offset for various information only within each path between stubs. Thus, since global precision of offset is not necessary, we have another merit that we do not need excessively high precision for globally measuring and preparing the data of digital map.

Fig. 13 shows the time series target velocity based on map information and lane detection state. First row indicates the time series map information regarding the curve based on the provided curve information and current offset of the self-vehicle. The numbers of the curve with orange rectangles above the graph indicate durations for the corresponding situations. At first, the vehicle moves on the straight course from the start point. Then, the self-vehicle approaches the curve of C1, and enters into the curve. After that, the vehicle approaches the curve of C2. As is observable in the figure, the self-vehicle well recognises the state of the road based on the provided information.

The second row in Fig. 13 shows the time series state of lane detection via the monocular camera. Line in red indicates the state based only on the map information, and the system does not rely on the result of lane detection during left turns. On the other hand, line in blue indicate the state based on both map information and the sensor. Because the monocular camera cannot detect the lane mark just after the finishing left turns, the system does not rely on the result of lane detection just after the left turn.

The third row in Fig. 13 shows the time series target velocity of acceleration and deceleration. Line in red indicates the acceleration target, and the system selects the appropriate velocity based on both map information and state of lane detection. On the contrary, line in blue indicates the deceleration target, and the system selects the appropriate velocity based on the provided information of the nearest control target. As is observable in the figure, the self-vehicle well selects the target velocities based on the provided information.
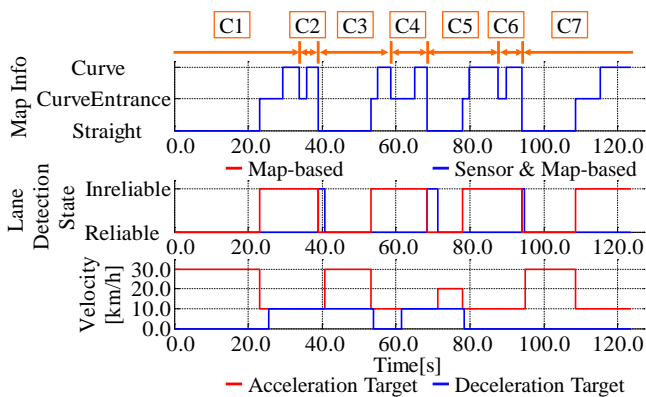
Fig. 14 shows the example of the time series velocity and rest distance to the nearest deceleration position from start to the curve of C1. The first row in the figure indicate the time series rest distance to the nearest control target for deceleration. On the other hand, lines in black, red, and blue of the second row indicate the current velocity, target velocity for acceleration, and target velocity for deceleration, respectively.

At first, the self-vehicle accelerates to the target velocity for acceleration from start point. Then, the self-vehicle keeps the velocity around upper limit. At approximately 17 s, necessary distance for deceleration towards the nearest control target become less than the actual rest distance to the control target, that is stop line at C1 in this case, and the self-vehicle starts to decelerate. After the self-vehicle keeps stopping in front of the stop line of C1 for approximately 2 s, the self-vehicle updates the control target from C1 to C2. Since the curve of C2 does not demand temporary stop before the curve, the system sets 10 km/h as the target velocity for deceleration. Similarly, since the road between C1 and C2 is a curve, the system sets 10 km/h as the target velocity for acceleration. Then, the vehicle restarts with accelerating towards the next curve of C2. This is an example of velocity control based on the information provided via enhanced ADAS Horizon.
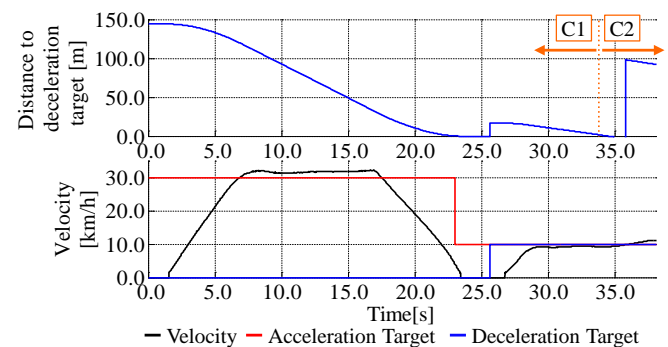
Fig. 14. Time series velocity and rest distance to nearest control target for deceleration form start to C1

Fig. 15 shows the time series velocity and distances to the nearest control targets from start point to the goal point. As is observable in the figure, the self-vehicle stops at the curves of C1, C4, C6, and C7 where temporary stop of the vehicle is necessary, while the self-vehicle turns left with decelerating to 10 km/h at the other curves. For other parts, the self-vehicle accelerates to the speed limit appropriately.

Fig. 13. Time series target velocity based on map information and lane detection state
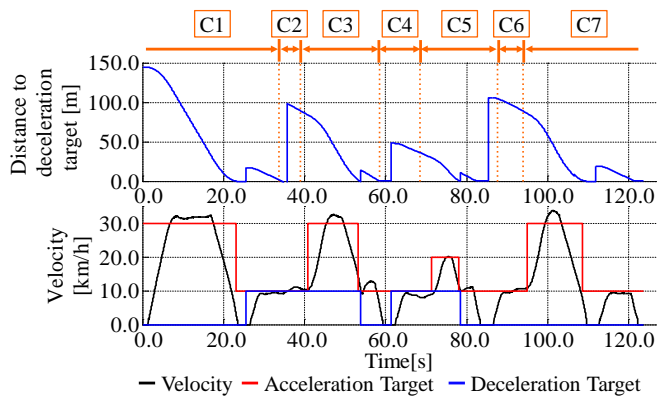
Fig. 15. Time series velocity and rest distance to nearest deceleration position from start to goal

Fig. 16 shows the times series result of lateral control. The first and second rows in the figure indicate the times series deviation angle for the waypoint map and the times series lateral deviation, respectively. For both rows, line in blue indicates the result on the straight road while line in red indicates the one during turning left. The system calculates the risk potential based on the reconstructed waypoint map and these values. Further, the system calculates the necessary lateral force based on the risk potential, and then the system calculates the necessary steering angle, which is the control value of the experimental vehicle, for achieving the necessary lateral force. The third row and fourth rows in the figure indicate time series steering wheel angle and yaw rate, respectively. As is observable in the figure, the self-vehicle appropriately controls the steering with referring the reconstructed waypoint map.
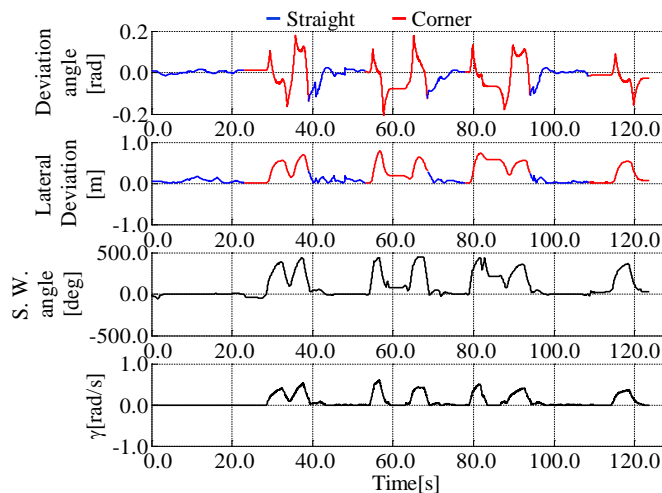

Fig. 16. Time series result of lateral control

4. CONCLUSIONS

To support the daily travels of the elderly in country areas, we aimed to develop the technologies of autonomous driving with a lean system platform for various types of driver assistance systems. To this end, we focused on the problems of excessively high-spec sensors and large amount of digital maps; further, we focused on enhancing the ADAS Horizon to realize the complementally combined platform with lean vehicular sensors and small-sized digital maps. Moreover, we developed the prototypes of proposed systems, and confirmed the feasibility of our concept through the experiment of autonomous driving on the test course.

As the next step, we have many topics to develop for realizing the autonomous driving on public roads in country areas. First, since we focused only on the stop lines and guardrails for localization in this research, we need to focus on other landmarks for localization, such as crosswalks, diamond marks, and so on. Second, since we aimed at confirming the feasibility of our concept, we skipped the implementation of stub. As there are many crossings in the real world, we need to try implementation of stub. Third, though the focus of this research was how to realize basic autonomous driving in the country areas, we need other types of autonomous driving, such as proactive driving and emergency driving. For totally supporting elderly drivers, we need to integrate such technologies with basic driving developed in this research.

REFERENCES

Inoue, H. (2014), "Research into ADAS with Driving Intelligence for Future Innovation", *2014 IEEE International Electron Devices Meeting*, pp. 1.3.1-1.3.7.

Omae, M., Shimizu, H., and Fujioka, T. (2004), "GPS-based Automatic Driving Control in Local Area with Course of Large Curvature and Parking Space", *Vehicle System Dynamics,* Vol.42, pp.59-73.

Kummerle, R., Hahnel, D., Dolgov, D., Thrun, S., and Burgard, W. (2009), "Autonomous Driving in a Multi-level Parking Structure", *IEEE International Conference on Robotics and Automation*, pp.3395-3400.

Blervaque, V., Mezger, K., Beuk, L., Loewenau, J. (2006), "ADAS Horizon — How Digital Maps can contribute to Road Safety", *Advanced Microsystems for Automotive Applications 2006*, pp.427-436.

ROS.org, http://wiki.ros.org (accessed on May 22th).

Hasegawa, T., Raksincharoensak, P., and Nagai, M. (2014), "Risk-Potential Based Motion Planning and Control of Proactive Driving Intelligence System for Enhancing Active Safety", *12th International Symposium on Advanced Vehicle Control.*

The Study on the Risk Proactive Cooperative Cruise Control System with Different Market Penetration Rate Scenarios

S. Tak*, H. Yeo. **, †

**Department of Civil and Environmental Engineering, Korea Advanced Institute of Science and Technology, Daejeon, Korea,
(e-mail: taksehyun@kaist.ac.kr)*

***Department of Civil and Environmental Engineering, Korea Advanced Institute of Science and Technology, Daejeon, Korea,
(e-mail: hwasoo@kaist.ac.kr)*

Abstract: Based on an analysis of collision risk propagation, a vehicle Traffic Predictive Cruise Control (TPCC) system, responding to the change of downstream traffic situation, is proposed in this study to improve traffic operation, safety, and fuel efficiency of vehicle. The proposed TPCC system consists of four parts: (1) Collision risk calculator of a subject vehicle, which represent the state of the subject vehicle. (2) Vehicle Control algorithm only based on the collision risk of the subject vehicle, (3) Cooperative measure for representing downstream traffic state, which is based on the results of an analysis of collision risk propagation, (4) TPCC algorithm, which controls the vehicle by using both collision risk of the subject vehicle and cooperative measure. By using both collision risk of subject vehicle and cooperative measure, which represent the integrated collision risk of leader vehicles, TPCC is designed to proactively determine actuation of vehicle by adjusting parameters of vehicle control algorithm before high collision risk arisen from leader vehicles reaches to the subject vehicle. A simulation using the real vehicle trajectories from the NGSIM data validates the performance of TPCC algorithm with various market penetration rates. It is found that the proposed TPCC system can contribute to CO_2 emission reduction, traffic flow stability, and safety improvement. Such results are due to the effects of suppression of the high collision risk generated from downstream traffic and removal of unnecessary fluctuation of speed.

Keywords: Adaptive Cruise Control, Risk Proactive, Market Penetration Rate

1. INTRODUCTION & MOTIVATION

Cooperative Adaptive Cruise Control (CACC) is a further development of Adaptive Cruise Control (ACC) with recently developing vehicle-to-vehicle (V2V) communication technology. Various types of communication structure have been proposed such as "everybody knows everything", designated platoon leader, bi-directional, N-vehicle look-ahead, and unidirectional (Ioannou & Chien 1993; Peppard 1974; Swaroop & Hedrick 1999; Stankovic 1998; Stanković, Srdjan S., Milorad J. Stanojevic 2000). With these various communication structures, many CACC have been proposed and validated based on field tests and/or simulation studies. CACC vehicles generally show good performances in terms of string stability and road use. Especially, CACC with designated platoon leader, N-vehicles look-ahead, and everybody knows everything communication structure show high string stability. However, these communication structures have a risk of communication failure and a communication delay due to the long communication distance, so small size of platoon is recommended by some researchers (Swaroop & Hedrick 1999; Vugts 2010).

CACC with bi-directional and unidirectional communication structure can overcome this communication related problem of designated platoon leader, N-vehicles look-ahead, and everybody knows everything communication structure by reducing the distance of vehicles for a communication. CACC with bi-directional and unidirectional communication also can guarantee the string stability and improve the road efficiency by increasing the road capacity. However, the autonomous vehicles with these communication structures lose opportunity to further improve the efficiency of autonomous vehicle by only using the information from the preceding vehicle.

Due to these technical problems such as communication delay and risk of communication failure, many previous algorithms control the vehicle based on the information from the neighboring autonomous vehicles and previous studies on autonomous vehicle mainly focus on improving string stability and road efficiency with this information from limited range. However, the control method with this limited range of communication constrains the efficiency of autonomous vehicle from further improving by a lack of information on future state of vehicle. For example, in a road, information from the downstream such as congestion and accident is highly related to the future state of vehicle because the shockwave generated from the congested area propagates to the upstream. In this situation, the information on congested traffic state of downstream can be utilized to improve the traffic flow stability, efficiency, and safety of vehicle if the autonomous vehicle proactively reduces the speed to react to upcoming

shockwave. However, due to the limited range of communication or lack of method that can transmit the downstream information to the autonomous vehicle located in upstream, the current autonomous vehicle mainly determines control actuation based on the information from few preceding vehicles, so CACC vehicle can only reactively determines control actuation after the shockwave arrived at preceding vehicle.

To overcome the limitations of the current advanced ACC and CACC, we develop a new Cooperative Cruise Control System, which can proactively apply the collision risk in downstream to a vehicle control and is called a Traffic Predictive Cruise Control (TPCC) in this study. The proposed TPCC only shares the front vehicle's information such as collision risk, preferred maximum braking rate, and jerk rate and proactively adjusts parameters for vehicle control based on the collision risk of preceding vehicle. For the risk proactive vehicle control, the propagation of collision risk in the platooned vehicles is analysed in the following section. Based on the analysis of risk propagation, the framework for TPCC is provided in section 3. In the section 3, the TPCC is designed to improve safety performance, traffic flow stability, and user comfort based on the unidirectional communication technology with relatively short communication range. The data used in this study and evaluation method are explained in section 4. Section 5 explains the effects of proposed TPCC on the vehicle performance such as safety, CO_2 emission, and traffic flow stability with different market penetration rates. In the section 5, the performance is evaluated with different ratio of TPCC to isolated vehicle, which doesn't transmit the information on downstream traffic state. This paper is then finalized with brief concluding remarks in section 6.

2. COLLISION RISK PROPAGATION

To analyse the propagation pattern of collision risk in platooned vehicles, we estimate the collision risk of vehicles by using Deceleration-based Surrogate Safety Measure (DSSM) (Tak et al. 2015). The DSSM shows more balanced accuracy in both acceleration phase and deceleration phase compared to other surrogate safety measures, which generally focus on the estimation of collision risk during deceleration phase, such as Time-To-Collision (TTC) and Stopping Headway Distance (SHD). DSSM is expressed as the function of maximum braking performance of a vehicle and required deceleration rate to avoid an accident as follows :

$$
\begin{aligned}
K &= [x_n(t) - x_{n-1}(t) + s_{n-1}] + [2 \cdot v_n(t) + a_n(t) \cdot \tau] \cdot \frac{\tau}{2} \\
&\quad - \left[v_{n-1}(t)/2 + \frac{(a_{n-1}(t) + b_{max,n-1})}{4} \cdot \frac{(a_{n-1}(t) - b_{max,n-1})}{L_{n-1}} \right] \\
&\quad \cdot \frac{(a_{n-1}(t) - b_{max,n-1})}{L_{n-1}} \\
&\quad + \left[v_n(t)/2 + a_n(t) \cdot \tau + \frac{(a_n(t) + b_{max,n})}{4} \cdot \frac{(a_n(t) - b_{max,n})}{L_n} \right] \\
&\quad \cdot \frac{(a_n(t) - b_{max,n})}{L_n}
\end{aligned}
\tag{1}
$$

$$
\begin{aligned}
b_n(t) &= b_{max,n-1}(t) \cdot \frac{[v_n(t) + a_n(t) \cdot \tau]^2}{[2 \cdot K \cdot b_{max,n-1}(t) + v_{n-1}(t)^2]}
\end{aligned}
\tag{2}
$$

$$
DSSM_{Sub,n}(t) = \frac{b_n(t)}{b_{max.n}}
\tag{3}
$$

where $a_n(t)$ is the acceleration rate of following vehicle at time t, $a_{n-1}(t)$ is the acceleration rate of leader vehicle at time t, $b_{max,n-1}$ is the maximum braking rate of leader vehicle, which represents the vehicle's mechanical deceleration performance, $b_n(t)$ is the needed deceleration rate of following vehicle to avoid the accident at time t, $b_{max.n}$ is the maximum braking rate of following vehicle, $v_{n-1}(t)$ is the speed of leader vehicle at time t, $v_n(t)$ is the speed of following vehicle at time t, L_{n-1} is the maximum variation of acceleration of leader vehicle, L_n is the maximum variation of acceleration of following vehicle, $v_n(t+\tau)$ is the expected speed of following vehicle after τ, $x_{n-1}(t)$ is the location of leader vehicle at time t, $x_n(t)$ is the location of following vehicle at time t, τ is the perception reaction time, and s_{n-1} is the length of leader vehicle.

DSSM represents the collision risk with a ratio of a maximum braking performance of subject vehicle to a required deceleration rate to avoid an accident when leader vehicle abruptly reduces its speed with maximum braking performance. DSSM value larger than one represents a more risky situation. Compared to other surrogate safety measures, DSSM additionally considers the transition time, which is the minimum time to changes a state of vehicle from acceleration state to deceleration state. DSSM has three strengths to be used in the analysis of collision risk of platooned vehicles. Frist, the DSSM can analyse the collision risk pattern during not only deceleration phase but also acceleration phase. Second, the DSSM can well represent the personalized collision risk by utilizing the each vehicle's mechanical performance. Third, the DSSM well capture a deceleration behaviour of human driver when the driver exposes to the high collision risk.

In the platooned vehicles, the collision risk propagates backward, which is the direction from downstream to upstream with certain propagation rate. For example, in the situation of five platooned vehicles, the high collision risk of the 1st leader vehicle at time t propagates to other following vehicles with different time interval (τ), which varies depending on the traffic state of each following vehicle. The collision risk of following vehicles at time ($t+\tau$) highly depends on the collision risk of the 1st leader vehicle at time t. However, the collision risk of following vehicles may not only depend on the collision risk of the 1st leader vehicle at time t. The collision risk of following vehicles at time t can also affects the collision risk of following vehicles at time ($t+\tau$).

To identify the variables that significantly affect the propagation of collision risk, a linear regression analysis is used. Regression analysis shows the relationship between dependent variable and explanatory variables and shows the statistical properties of the resulting estimators. Based on the statistical properties of regression model, the explanatory power of independent variables can be identified. Furthermore, regression analysis quantifies the strength of the

relationship between collision risk of following vehicle after certain period of time and explanatory variables. The strength of relationship can be used to improve the safety of platooned vehicles by controlling a dependent variable, which has high strength.

With different variables, three regression models are analysed for representing the propagation of collision risk. The variables for three regression models are graphically illustrated in Fig. 3 and each model is demonstrated by :

$$DSSM_{i+2}(t + \tau) = \alpha \cdot DSSM_{i+2}(t) \qquad (4)$$

$$DSSM_{i+2}(t + \tau) = \alpha \cdot DSSM_{i+1}(t) \qquad (5)$$

$$DSSM_{i+2}(t + \tau)$$
$$= \alpha \cdot DSSM_{i+1}(t) + \beta \cdot DSSM_{i+2}(t) \qquad (6)$$

where $DSSM_{i+1}(t)$ is the collision risk of preceding vehicle (i+1) of following vehicle (i+2) at time t, $DSSM_{i+2}(t)$ is the collision risk of following vehicle (i+2) at time t, $DSSM_{i+2}(t + \tau)$ is the collision risk of following vehicle after time τ from time t.

The 1st regression model, which is demonstrated by equation (4), represents that the collision risk of following vehicle at time $(t + \tau)$ is explained by the collision risk of following vehicle at time t. The 2nd regression model, which is demonstrated by equation (5), represents that the collision of following vehicle at time $(t + \tau)$ is explained by the collision risk of leader vehicle at time t. This 2nd regression model shows whether the leader vehicle affects the following vehicle when the shockwave is transmitted from leader vehicle to following vehicles. The 3rd regression model, which is demonstrated by equation (6), represents that the collision risk of following vehicle at time $(t + \tau)$ is explained by the combination of the collision risks of leader vehicle and following vehicle at time t. By comparing the results of the three regression models, the better way to estimate the collision risk of following vehicle at time $(t + \tau)$ is selected. In regression analysis, significance levels are set at P < 0.05.
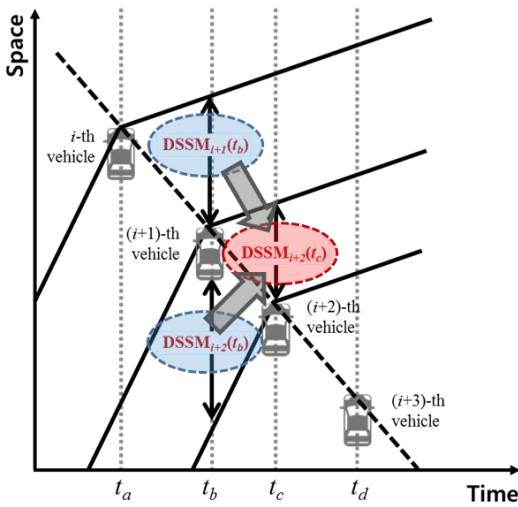

Fig. 1. Variables for three regression models

Fig. 2, 3, and 4 show the results of the three regression models over the time interval τ. By evaluating the regression models with different time interval (τ), the changes in the accuracy of each regression model over time interval τ is observed, and the effective time horizon of regression model to describe the propagation of collision risk is also analyzed.

Fig. 2 shows the results of the 1st regression model (equation 4) varying over the time interval τ. As shown in the figure, when the time interval τ is small, this regression model shows high R-squared value. As the time interval τ is increased, the R-squared value is significantly decreased. These decreasing trend is also observed in the trend of the coefficient value. When the time interval τ is small, the coefficient of dependent variable ($DSSM_{i+2}(t)$) is high as shown in the figure. However, as the time interval τ is increased, the coefficient is dramatically reduced. Especially, when the time interval τ is larger than 1 second, the coefficient of dependent variable is lower than 0.5. These results represent that the collision risk of following vehicle after time interval τ can be explained by the collision risk of following vehicle at time t only when the time interval τ is small (below 0.2). As the time interval τ is increased, the explanatory power of the 1st regression model is dramatically reduced, so, the 1st regression model is not as much as effective when only the time interval τ is small.

Fig. 3 shows the results of 2nd regression model (equation 5) varying over time interval τ. As shown in the figure, the 2nd regression model shows the low R-squared value across all time interval τ and the coefficient of dependent variable ($DSSM_{i+1}(t)$) is also mainly lower than 0.5. The trend of coefficient of the 2nd regression model is similar to that of 1st regression model with low value of coefficient. This result represents that the 2nd regression model relatively well represents the collision risk when τ is small. As τ is increased, the relationship between the collision risk of the leader vehicle and the collision risk of the following vehicle is decreased. In general, compared to the 1st regression mode, the explanatory power of the 2nd regression model is much lower than that of the 1st regression, so, it is also not feasible to represent the collision risk of following vehicle after time τ by only using the collision risk of the leader vehicle at time t.

Fig. 4 shows the results of the 3rd regression model (equation 5) varying over time interval τ. As shown in the figure, this regression model shows higher R-squared value than the 1st and 2nd regression models in all time interval τ. The R-squared value of the 3rd regression model is larger than 0.8 when the time interval τ is smaller than 4.1 second. This result represents that the collision risk of following vehicle after time interval τ can be explained by the combination of collision risks of leader and following vehicles with higher explanatory power compared to other regression models. The trend of coefficient of dependent variables ($DSSM_{i+1}(t)$, $DSSM_{i+2}(t)$) is similar with that of other regression models. The coefficient of $DSSM_{i+2}(t)$, which is the collision risk of following vehicle at time t, is high when the time interval τ is small. As the time interval (τ) is increased, the coefficient of $DSSM_{i+2}(t)$ is decreased. On the other hand, the coefficient of $DSSM_{i+2}(t)$, which is the collision risk of leader vehicle at time t, is increased from 0.09 to 0.58 when the time interval τ is smaller

than 3.2 second. As the time interval τ is further increased, the coefficient of $DSSM_{i+2}(t)$ is decreased. By considering the trends of coefficients of these two dependent variables, when the time interval τ is near 1 second, the coefficient of the two dependent variables is 0.5. This result shows that the collision risk of following vehicle after time interval 1 second is similarly affected by the both dependent variables.

The results show that the future collision risk of following vehicle after certain period of time is highly influenced by both collision risk of the leader vehicle and following vehicle at current state. In this relation, the high collision risk of leader vehicle is transferred to the following vehicle in a form of a weighted average of collision risk of leader vehicle and that of following vehicle. Especially, when the time interval is between 1 and 2 second, the collision risk of leader vehicle and that of following vehicle equivalently affects the future collision risk of following vehicle.
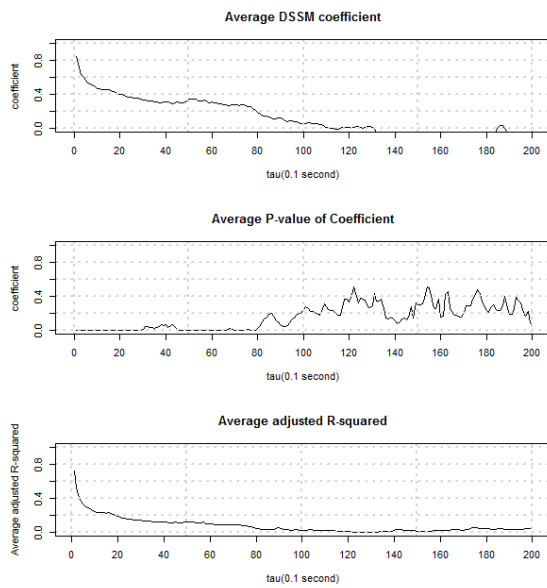

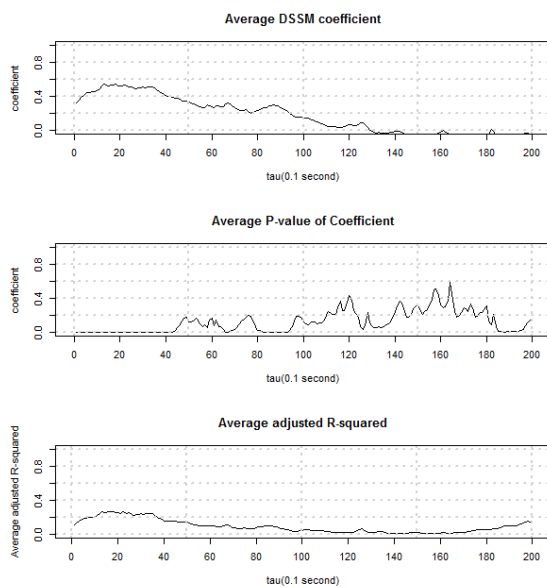Fig. 2. Results of 1st regression model (Equation 4) varying over time interval τ

Fig. 3. Results of 2nd regression model (Equation 5) varying over time interval τ
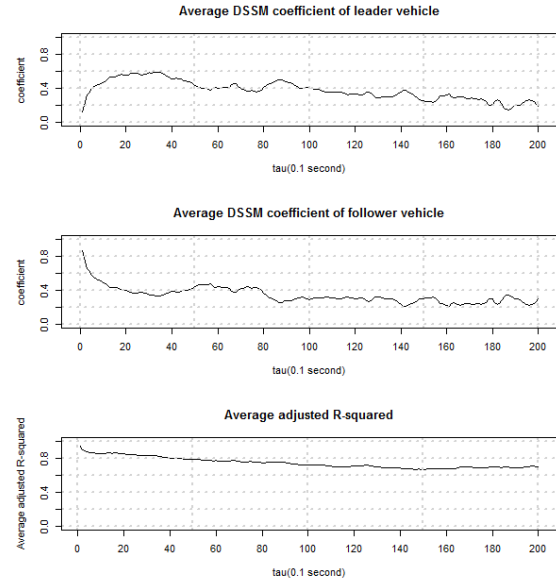

Fig. 4. Results of 3rd regression model (Equation 6) varying over time interval τ

3. TRAFFIC PREDICTIVE CRUISE CONTROL

Based on the results of analysis of collision risk propagation, we propose Traffic Predictive Cruise Control (TPCC) system, which can proactively react to the collision risk arisen from downstream. The proposed TPCC system consists of four parts: (1) Collision risk calculator of a subject vehicle, which represent the state of the subject vehicle. (2) Vehicle Control algorithm only based on the collision risk of the subject vehicle, (3) Cooperative measure for representing downstream traffic state, which is based on the results of analysis of collision risk propagation, (4) Traffic Predictive Cruise Control (TPCC) algorithm, which controls the vehicle by using both collision risk of the subject vehicle and cooperative measure.

2.1 Collision risk-based Spacing Policy for Vehicle Control

In the TPCC system, the collision risk of subject vehicle is estimated by using the DSSM shown in equation 1-3 (Tak et al. 2015). By using a calculated DSSM, the TPCC system controls the vehicle based on the Asymmetric Collision Risk-based spacing policy (ACR spacing policy). ACR spacing policy determines the acceleration and deceleration actions of vehicle based on the calculated DSSM as follows:

$$a_{des,n}(t) \qquad\qquad (7)$$
$$= \begin{cases} a_{max}(t) \cdot \dfrac{(TH_{acc} - DSSM_{Sub,n}(t))}{Std_{up}}, & DSSM_{Sub,n}(t) < TH \\ 0, & TH_{dec} \le DSSM_{Sub,n}(t) \le TH_a \\ -b_{max.n} \cdot \dfrac{(TH_{dec} - DSSM_{Sub,n}(t))}{1.2 - TH_{dec}}, & DSSM_{Sub,n}(t) > TH \end{cases}$$

where $a_{des,n}(t)$ is the desired acceleration at time t, $a_{max}(t)$ is the maximum acceleration of the subject vehicle at time t with 0.1 time interval, $DSSM_{Sub,n}(\ )$ is the collision risk of subject vehicle at time t, TH_{acc} is a threshold value for

acceleration actuation, and TH_{dec} is a threshold value for deceleration actuation.

Cooperative DSSM

$$CoDSSM_i(t) = W_1 \cdot DSSM_{i-1}(t-1) + W_2 \cdot CoDSSM_{i-1}(t-1)$$
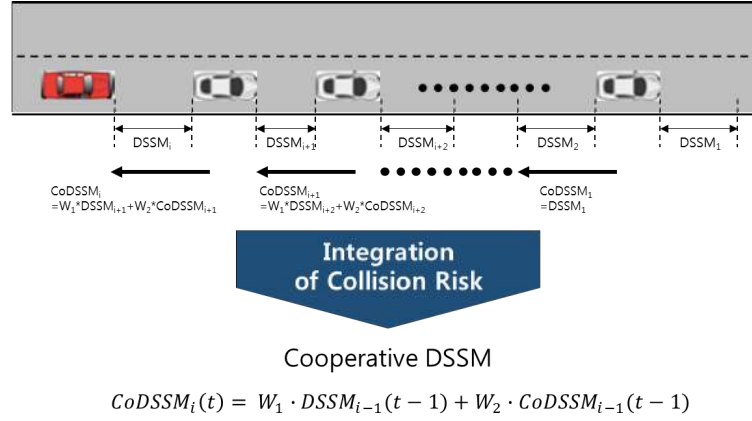
$DSSM_{i-1}(t)$: Collision risk of vehicle i at time t
$CoDSSM_{i-1}(t)$: Cooperative Collision risk of vehicle i at time t

Fig. 5. The Calculation and transmission method of Cooperative DSSM (CoDSSM) in the unidirectional communication structure

As shown in the equation (7), ACR spacing policy controls a traction and braking torques to maintains the collision risk in a safe range, which is between TH_{dec} and TH_{acc}. When calculated DSSM is greater than a threshold value (TH_{dec}) which represents the high collision risk situation, the vehicle with ACR spacing policy decelerates. When calculated DSSM is smaller than a threshold value (TH_{acc}), which represents normal driving situation or low collision risk situation, the vehicle with ACR spacing policy accelerates. Lastly, if the DSSM is between TH_{dec} and TH_{acc}, the vehicle with ACR spacing policy maintains the speeds without any acceleration and deceleration actions.

2.2 Cooperative measure for representing downstream traffic state

In the above section, the future collision risk of following vehicle can be estimated by using a weighted average value of collision risk of leader vehicle and that of following vehicle at current time. By using the weighted average of collision risk of leader vehicle and that of following vehicle at current time with a same weight of 0.5, the collision risk of following vehicle can be accurately estimated with 1~2 second prediction horizon. By applying this propagation pattern to car-following process of multiple-vehicles, the effect of a collision risk arisen from several leading vehicles on a collision risk of the subject vehicle can be evaluated. For example, in the Fig. 5, the collision risk of vehicle *i* at time *t* can be estimated by using a collision risks of vehicle *i* and (*i+1*) at time (*t-1*). At the same time, the collision risk of vehicle (*i+1*) at time (*t-1*) can be also estimated by using a collision risks of vehicle (*i+1*) and (*i+2*) at time (*t-2*). By repeating this process from 1st leader vehicle to last following vehicle in the platoon, the effect of integrated collision risk of leading vehicles on following vehicle can be estimated.

Based on this relationship of collision risks of following vehicle and leader vehicle, CoDSSM is proposed as shown in Fig. 5 to transfer the collision risk arisen from downstream

with unidirectional communication structure. As shown in Fig. 5, the front vehicle sends its own DSSM information to the right next following vehicle. The following vehicle produces the cooperative DSSM by integrating the DSSM of the leader vehicle and its own DSSM value. By repeating this process, cooperative DSSM smoothly reflects the downstream traffic situation even when the subject vehicle communicates only with the nearest front vehicle. In this method, the location information of all leader vehicles is not required to estimate the risk of upcoming traffic situation. So, it can significantly reduce the packets for communication and efforts to reduce the delivery delay of connected vehicles.

2.3 Traffic Predictive Cruise Control

Based on the transmitted CoDSSM from leader vehicles and DSSM of subject vehicle, TPCC algorithm adjusts the threshold values of the ACR spacing policy to proactively react to the arisen collision risk from leader vehicles. For example, when the CoDSSM is higher than the DSSM of subject vehicle, the TPCC algorithm reduces the threshold values for acceleration (TH_{acc}) and deceleration (TH_{dec}) of ACR spacing policy because upcoming traffic situation renders the subject vehicle decelerates. On the other hand, when the CoDSSM is lower than the DSSM of subject vehicle, the TPCC algorithm increase the threshold value for acceleration (TH_{acc}) and deceleration (TH_{dec}) of ACR spacing policy because upcoming traffic situation renders the subject vehicle accelerates. Following equations are the adjusting method of the threshold value for acceleration (TH_{acc}) and deceleration (TH_{dec}) of ACR spacing policy in the TPCC algorithm:

$$TH_{acc,new}(t)$$
$$= \begin{cases} TH_{acc} + \alpha \cdot (DSSM_{sub}(t) - DSSM_{co}(t)), & DSSM_{sub}(t) < DSSM_{co}(t) \\ TH_{acc} + \beta \cdot (DSSM_{sub}(t) - DSSM_{co}(t)), & DSSM_{sub}(t) \geq DSSM_{co}(t) \end{cases} \quad (6)$$

$$TH_{dec,new}(t)$$
$$= \begin{cases} TH_{dec} + \alpha \cdot (DSSM_{sub}(t) - DSSM_{co}(t)), & DSSM_{sub}(t) < DSSM_{co}(t) \\ TH_{dec} + \beta \cdot (DSSM_{sub}(t) - DSSM_{co}(t)), & DSSM_{sub}(t) < DSSM_{co}(t) \end{cases} \quad (7)$$

where α and β are coefficient, which represent sensitivity to difference between $DSSM_{co,n}(t)$ and $DSSM_{sub,n}$. To more sensitively react to the oncoming high collision risk from downstream, α and β are set to 1/2 and 1/4, respectively.

4. CASE STUDY

To evaluate the performance of proposed TPCC algorithm in the mixed environment of manual vehicle and autonomous vehicle, this study uses the Next Generation Simulation (NGSIM) trajectory data collected from a highway site called I-80 in California USA (Anon 2006). The NGSIM data provides microscopic information of human driver, so it is useful to evaluation of performance improvement of autonomous vehicle compared to human drivers. Furthermore, it is good for evaluating the safety of autonomous vehicle because the NGSIM trajectory data contains the congested traffic situation that the high collision risk frequently occurs.

To show the effect of market penetration rate of the proposed TPCC algorithm, we simulated the proposed algorithm in the total 18 car-following cases with different number of communicated vehicles. The 18 car-following cases have more than eight consecutive vehicles. Fig. 6 shows the five different scenarios for the simulation varying the number of connected vehicles, which share the collision risk information. ACR vehicle, which controls the vehicle only based on its collision risk without any downstream traffic information from preceding vehicles. ACR vehicle is marked by the green vehicle in the Fig. 6. TPCC, which controls the vehicle with downstream traffic information by using unidirectional communication. TPCC vehicle is marked by blue vehicle in the Fig. 6.
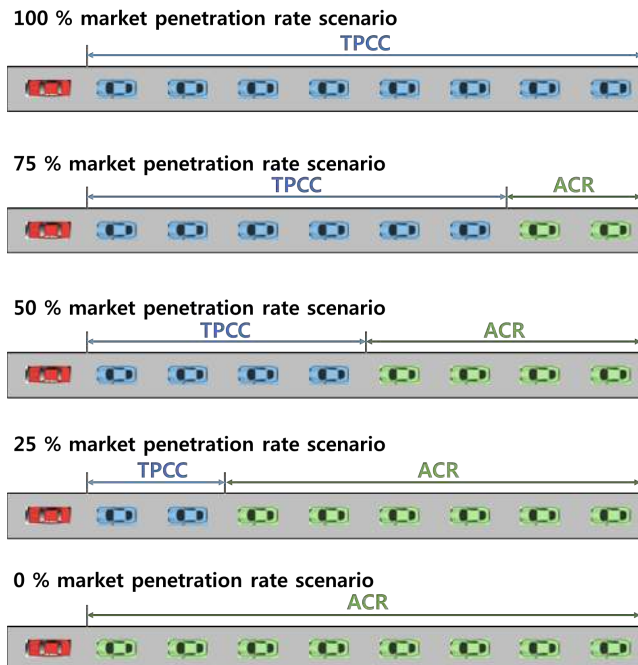

Fig. 6. Five scenarios for simulation

The performance improvement of the proposed TPCC algorithm to human driver is evaluated with various market penetration rates in terms of safety, CO_2 emission, and traffic flow stability. The safety of vehicle is estimated by the frequency of the high collision risk, which is estimated by the

DSSM, and the higher DSSM than 1.0 is used for the threshold to determine the high collision risk. CO_2 emission of human driver, ACR, and TPCC vehicle is estimated by VT-Micro model (Rakha et al. 2004; El-Shawarby et al. 2005). The traffic flow stability is estimated by the standard deviation of speed. In the simulated cases, the human drivers meet the shockwave and the situation that driver must reduce the speed. In this cases, the standard deviation of speed represents a degree of speed fluctuation when it passes through the shockwave. A lower standard deviation of speed means that the vehicle can supress the shockwave and the traffic flow stability is improved.

5. SIMULATION RESULTS

Fig. 7-10 show results of performance evaluation of proposed TPCC algorithm in various market penetration rates. Fig. 7 shows the reduction of frequency of high collision risk and the reduction amount is calculated by subtracting the frequency of high collision risk of proposed TPCC from that of human driver. As shown in the Fig. 7, proposed TPCC algorithm can significantly reduce the frequency of high collision risk as the market penetration rate increases. Compared to human drivers, the frequency of high collision risk is reduced in all scenarios. Considering that average frequency of high collision risk of human driver is approximately 75, more than 50% of high collision risk situations can be reduced by the TPCC when the market penetration rate is 100%. Comparing the 0% market penetration rate case and the 100% market penetration rate case, 28% improvement of safety is achieved. Consequently, the proposed TPCC algorithm can improve the safety of vehicles by transmitting the collision risk of leader vehicles.
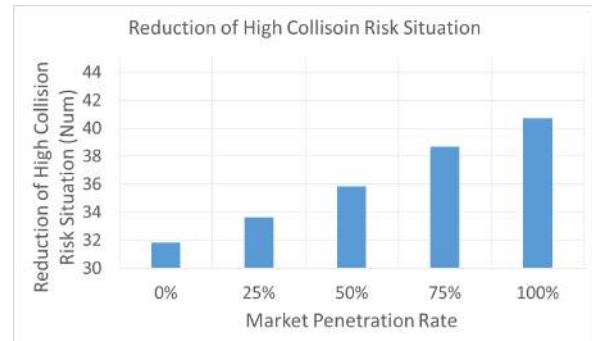

Fig. 7. Reduced amount of frequency of high collision risk situation compared to human drivers with various market penetration rate.
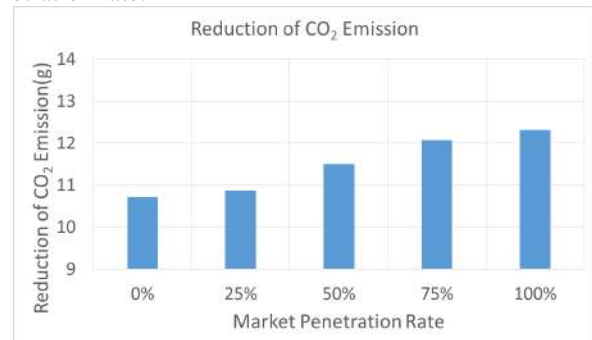

Fig. 8. Reduced amount of CO_2 emission compared to human drivers with various market penetration rate.

We estimate the CO_2 emissions for human drivers, and proposed TPCC vehicles in various market penetration rates by using Virginia Tech microscopic (VT-Micro) model. Then, we subtract the CO_2 emission of TPCC from the emission of human drivers. Fig. 8 shows the reduced amount of CO_2 emission for TPCC compared to the human drivers. In terms of CO_2 emissions, TPCC vehicles show better performance than human drivers and the reduction amount is also increases as the market penetration rate increases. However, the effect of market penetration rate on reduction of CO_2 emission is lower than reduction of frequency of high collision risk.

Fig. 9 shows the reduction of standard deviation of speed. Compared to human driver the standard deviation of speed is reduced in all market penetration rates and the reduction amount of standard deviation of speed is increases as the market penetration rate increases. Less standard deviation of speed means less fluctuation of vehicle speed and this render the trajectory of vehicle smooth by suppressing the shockwave. By considering that shockwave adversely affects the CO_2 emission and safety on the road, the performance improvement of proposed TPCC is partially due to effect of smoothed vehicle trajectory.
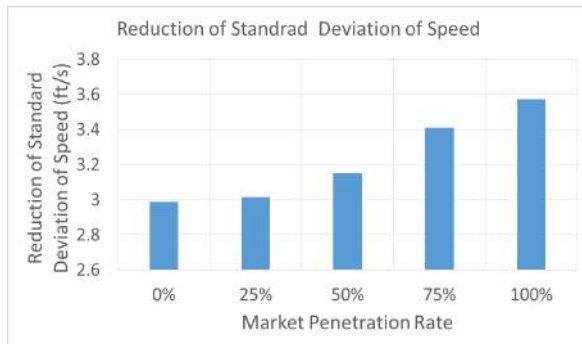

Fig. 9. Reduced amount of standard deviation of speed compared to human drivers with various market penetration rate.

Fig. 10-13 explain reasons that TPCC can improve the performance with downstream traffic information by simulating algorithm in a hypothetical situation. Fig. 10-13 show the vehicles' reactions on intended speed changes based on ACR and TPCC, respectively. The leader vehicle reduces the speed from 60ft/s to below 32ft/s, and it recovers the speed to 60ft/s. As the reaction, the nine following vehicle reduce their speeds with different reduction pattern depending on the algorithm type. For the ACR vehicles shown in Fig. 10, each of the following vehicle shows speed reduction once. The amount of speed reduction decreases as the order of the vehicle in the platoon (1st follower, 2nd follower, ..) gets higher, but the reduction amount becomes almost the same after 8th following vehicle. Then, they accelerate again as the leader recovers its speed to 60ft/s. As the speed of ACR vehicle is fluctuated by the speed change of leader vehicle, the collision risk of following vehicles also fluctuated as shown in Fig. 11. Abrupt deceleration action of leader vehicle increases the collision risk of following vehicles. The highest collision risk is occurred in the 1st following vehicle and is higher than 1.1. Then the highest collision risk of following vehicle decreases

as the order of the vehicle in the platoon (1st follower, 2nd follower, ..) gets higher similar to the propagation pattern of speed reduction.
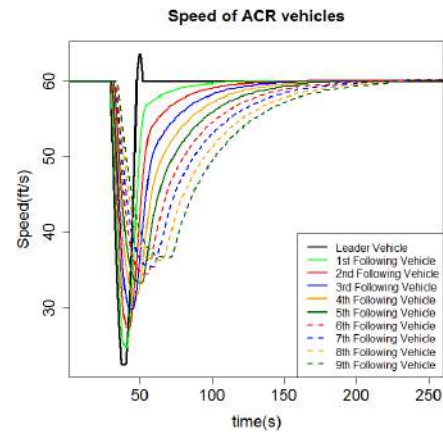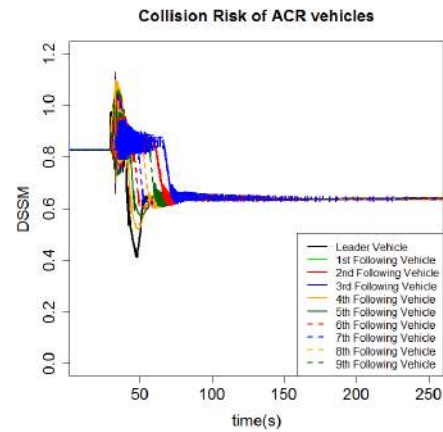

Fig. 10. Speed-time plot of ACR vehicles

Fig. 11. Collision risk(DSSM)-time plot of ACR vehicles

Similarly with the ACR case, for the TPCC vehicles in Fig. 12, the amount of speed reduction decreases as the order of the vehicle in the platoon gets higher. However, some of the following vehicles show speed reduction more than once. There are secondary speed reductions from the 7th following vehicle to the last following vehicle. The 7th follower reduces the speed to 48ft/s and it again reduces the speed to 39 ft/s approximately two seconds later. The following vehicles with the higher order in the platoon show the same behaviour, but with different amounts of speed reduction. The secondary speed reduction is due to proactive reaction to downstream traffic situation of the TPCC algorithm. ACR algorithm controls the vehicle only based on the collision risk of subject vehicle, so the vehicle reduces the speed when the subject vehicle is in danger. However, TPCC algorithm controls the vehicle by considering both collision risk of subject vehicle and integrated collision risk of leader vehicles. By detecting an upcoming high collision risk, TPCC algorithm reduces the speed in advanced when the collision risks of leader vehicles are arisen. The first speed reduction is mainly occurred due to the proactive behaviour of TPCC vehicle, and the secondary speed reduction is occurred due to reactive behaviour to the closest leading vehicle's speed change.

Due to the predictive control of TPCC vehicle, the collision risk of platooned vehicles are also generally reduced as shown in Fig. 13. In the TPCC vehicles, higher collision risk than 1.0 is not occurred in all vehicles, so unsafe situation is not observed. Furthermore, the fluctuation of collision risk induced by the leader vehicle is also gradually reduced in the TPCC algorithm faster than ACR vehicles. Consequently, the proposed TPCC algorithm reduces the speed reduction amount and high collision risk by reflecting the collision risk of leader vehicles in the control algorithm.
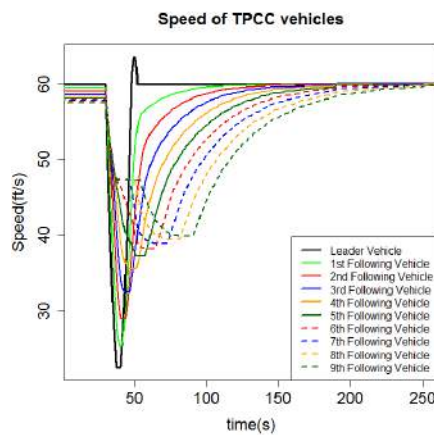

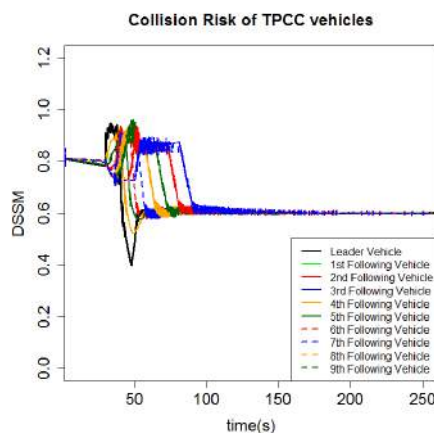
Fig. 12. Speed-time plot of TPCC vehicles

Fig. 13. Collision risk (DSSM)-time plot of TPCC vehicles

6. CONCLUSION

In this paper, Traffic Predictive Cruise Control (TPCC), which can proactively react to the collision risk in downstream, is proposed based on the unidirectional communication structure. TPCC algorithm adjusts control parameters such as threshold for acceleration and deceleration actuation based on the relationship between collision risk of subject vehicle and the integrated collision risk of leader vehicles. The comparison results shows the proposed TPCC can not only reduce CO_2 emission but also improve the safety of vehicle and traffic flow stability, which is estimated by the standard deviation of speed. The positive effect of TPCC on safety, CO_2 emission, and traffic flow stability increases as the market penetration rate increases.

The simulation results in a hypothetical situation show that TPCC algorithm can suppress the occurrence of high collision risk by reducing the speed before closest leader vehicle reduces the speed. The positive effect of TPCC algorithm comes from the "anticipation effect". TPCC vehicle is able to detect the high collision risk arisen by leader vehicles by transmitting the collision risk of each vehicle to each vehicle's following vehicle and mitigate the negative effect of high collision risk on subject vehicle by reducing or increasing the speed in advance.

7. ACKNOWLEDGEMENTS

8. REFERENCES

Anon, 2006. NGSIM - Next Generation Simulation. Available at: http://ngsim-community.org/.

El-Shawarby, I., Ahn, K. & Rakha, H., 2005. Comparative field evaluation of vehicle cruise speed and acceleration level impacts on hot stabilized emissions. Transportation Research Part D: Transport and Environment, 10(1), pp.13–30.

Ioannou, P. & Chien, C., 1993. Autonomous intelligent cruise control. Vehicular Technology, IEEE Transactions on, 42(4), pp.657–672.

Peppard, L., 1974. String stability of relative-motion PID vehicle control systems. Automatic Control, IEEE Transactions on..

Rakha, H., Ahn, K. & Trani, A., 2004. Development of VT-Micro model for estimating hot stabilized light duty vehicle and truck emissions. Transportation Research Part D: Transport and Environment, 9(1), pp.49–74.

Stankovic, S., 1998. Headway control of a platoon of vehicles: inclusion principle and LQ optimization. In IEEE, ed. Decision and Control, 1998. Proceedings of the 37th IEEE Conference on. IEEE..

Stanković, Srdjan S., Milorad J. Stanojevic, and D.D.S., 2000. Decentralized overlapping control of a platoon of vehicles. Control Systems Technology, IEEE Transactions on, 8(5), pp.816–832..

Swaroop, D. & Hedrick, J., 1999. Constant spacing strategies for platooning in automated highway systems. Journal of dynamic systems, measurement, and control, 121(3), pp.462–470..

Tak, S., Kim, S. & Yeo, H., 2015. Development of a Deceleration-Based Surrogate Safety Measure for Rear-End Collision Risk. IEEE Transactions on Intelligent Transportation Systems, In press.

Vugts, R., 2010. String-stable cacc design and experimental validation. Diss. Technische Universiteit Eindhoven..

On the Potential of Accelerating an Electrified Lead Vehicle to Mitigate Rear-End Collisions

Adithya Arikere *,** **Christian-Nils Boda** ** **Jona Olafsdottir** **
Marco Dozza ** **Mats Svensson** ** **Mathias Lidberg** **

* *American Axle & Manufacturing, Nohabgatan 18E, SE-461 53*
Trollhättan, Sweden (e-mail: adithya.arikere@aam.com)
** *Applied Mechanics, Chalmers University of Technology, SE-412 96*
Göteborg, Sweden (e-mail: <first name>.<last name>@chalmers.se)

Abstract: This paper analyzes the potential safety benefit from autonomous acceleration of an electrified lead vehicle to mitigate or prevent being struck from behind. Safety benefit was estimated based on the expected reduction in relative velocity at impact in combination with injury risk curves. Potential issues and safety concerns with the operation and implementation of such a system in the real world are discussed from an engineering and human factors stand point. In particular, the effect of the pre-collision acceleration in reducing whiplash injury risk due to change in head posture and reduction of crash severity is also discussed. In general, this study found that autonomously accelerating an electrified lead vehicle can mitigate and prevent rear-end collisions and significantly increase the safety benefits from existing systems such as autonomous emergency braking.

Keywords: Rear-end collisions, collision avoidance and mitigation, electrified vehicle acceleration, active safety

1. INTRODUCTION

1.1 Background

The rear-end collision is one of the most frequently occuring accident types in most countries accounting for nearly a third of all accidents in the US [Singh (2003)] and a fourth of all accidents in Germany [Unger and Sandner (2013)]. The single most common injury sustained in these accidents are whiplash injuries which have been reported to account for up to 90% of all injuries [Watanabe et al. (2000)]. Compared to other injuries whiplash injuries have the highest risk of leading to permanent medical impairment [Gustafsson et al. (2015); Malm et al. (2008)] and in the US the associated cost of whiplash injuries sustained in rear-end collisions has been estimated to be $2.7 billion annually [NHTSA (2010)]. Reducing the number of whiplash injuries from rear-end collisions can therefore be expected to have high socio-economic impact.

While the Autonomous Emergency Braking (AEB) system (already available on the market from several manufacturers) is estimated to be able to completely avoid 35% and mitigate 53% of all rear-end collisions [Schittenhelm (2013)], the remaining cases still account for a large number of accidents which could potentially be improved by a novel active safety function.

A possible way to do so is to make the lead vehicle speed up in order to reduce the relative speed at impact. To perform such an intervention however, quick response is required in the propulsion actuator which is why a traditional internal combustion engine (ICE) cannot be used whose response can vary significantly depending on the speed, transmission type, gear, turbo lag, etc. Electric drives, on the other hand, have very fast response in the order of tens of milliseconds [Hori et al. (1997)] and can be used to perform this intervention. Therefore, the lead vehicle is assumed to be electrified (fully electric or hybrid) in this paper in order to be able to perform the intervention.

In order to evaluate the potential of such an intervention to mitigate or avoid rear-end collisions, a hypothetical active safety system that uses acceleration on the lead vehicle is envisioned and used for analysis. This system, which works analogously to the AEB, is termed the Automatic Emergency Acceleration (AEA) system further on in this paper.

1.2 Objective

The objective in this paper is to evaluate the potential of an Automatic Emergency Acceleration (AEA) system which accelerates an electrified lead vehicle to avoid or mitigate rear end collisions.

1.3 Assumptions

A few simplifying assumptions have been made in order to limit the scope of this paper, which are detailed below along with the motivation.

(1) *Acceleration capability is limited by friction, not by motor size*

Since electric motors deliver their peak torques at low speeds and can, for short periods of time, deliver torques several times that of their rated torques, it would be reasonable to assume that at low speeds, the acceleration possible is limited by the tyre friction limit rather than the motor size. Furthermore, since 70% of rear-end collisions involve stationary lead vehicles [Knipling et al. (1993)], the acceleration capability of the lead vehicle is assumed to be limited by the grip at the driven axle (since the electric motor typically drives only one axle).

(2) *The lead vehicle has the capability to detect following vehicles behind it*

The lead vehicle is assumed to be able to reliably detect following vehicles behind it. This detection can be done either using sensors or using connected systems (vehicle-to-vehicle or vehicle-to-infrastructure) or by any other method. Due to the advent of advanced driver assistance and autonomous systems, such capabilities are likely to make their way into vehicles of the future.

(3) *It is safe to accelerate*

The lead vehicle is assumed to have the ability to detect threats ahead and that it would be safe to accelerate. While vehicles equipped with AEB have the ability to detect obstacles ahead, the lead vehicle in this work also needs to have the ability to ensure that there is no cross-traffic, that it is not at a traffic signal, etc. Once again, with the advent of cooperative functions in cars, such capabilities could probably be available in cars of the future. While acceleration may not always be possible nor even possible to ensure that such an intervention would be safe, in this work, we assume that the intervention can be safely performed and in later sections discuss alternatives which can help overcome some of these issues.

2. MANOEUVRE KINEMATICS

In order to predict the safety benefit that can be expected from AEA and put the same into context, kinematics of the scenario with a lead vehicle equipped with AEA and a following vehicle equipped with AEB are analysed. From the resulting analysis, expected relative velocity reductions for different cases are predicted which are in turn used to predict expected injury reduction and safety benefit.

In the following subsections, basic actuator and vehicle models similar to those used in Coelingh et al. (2010) are used to derive activation timings for the AEA and AEB system which are then used in a simulation environment to evaluate their performance.

2.1 Actuator modelling

Figure 1 shows the parameterization of the actuator dynamics that is used in the simulation model and, with additional simplifications as needed, in deriving the activation timings for the AEB and the AEA as well. Note that parameterization of steering is also shown since evasive steering has to be considered as a potential option for collision avoidance while determining the window of opportunity for activation of AEB and AEA.
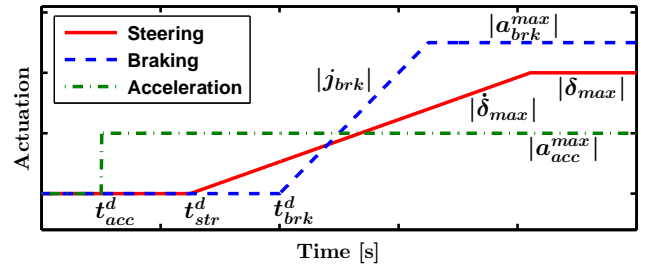

Fig. 1. Parameterization of different actuator dynamics.

The steering and brakes have been modelled with a pure delay, a ramp and a saturation to capture the relatively slow response and dynamics of these actuators. While the delays are mainly determined by the actuator response times, the saturation values are determined by the dynamic limits of the vehicle and the ramp rates by a combination of the two.

The motor on the other hand has been modelled with just a pure delay and a saturation, but no ramp since the dynamics of the motor are much faster. The saturation value here is determined by the grip at the axle driven by the motor. While this can vary significantly depending on the vehicle properties and which axle is being driven, a middle-ground approach is taken in this paper and it is assumed that each axle has half the grip of the entire vehicle.

2.2 AEA timing calculation

Since AEA involves speeding up which is inherently riskier, a conservative approach is taken here wherein AEA is not activated until the last point in time where the following vehicle could have avoided the collision by braking or steering. These activation timings are calculated by taking the minimum of three minimum Time-To-Collision (TTC) values at which: the following vehicle can avoid the collision by braking, by steering or the lead vehicle can avoid the collision by acceleration.

Since collision avoidance by braking or steering is done on the following vehicle about which the lead has limited information, the actuators on the following vehicle are assumed to have ideal performance. Even if the lead vehicle does have some information about the following vehicle actuators or can make some reasonable assumptions regarding the same, they cannot be used by the AEA algorithm. This is because, in a non-cooperative environment, the lead vehicle cannot reliably detect the state of the actuators on the following vehicle (whether they are in the ramp-up stage, operating at peak performance, etc) and therefore cannot count on their response times while estimating the minimum time required for the following vehicle to avoid a collision. As a result, the lead vehicle has to assume best performance of the actuators (no actuator dynamics) while estimating the time required for the following vehicle to avoid a collision. While such an approach reduces window of opportunity available for the AEA system and therefore reduces its effectiveness, it also minimizes the likelihood of a false intervention. Such a conservative timing approach also ensures that there is no detrimental interaction between the AEB and AEA.
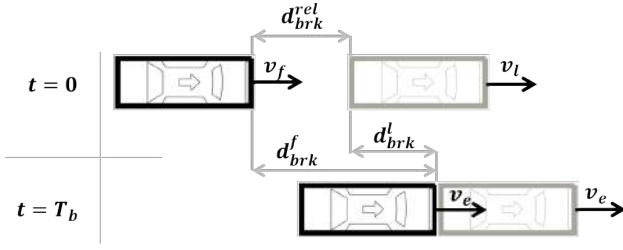
Fig. 2. Collision avoidance by braking

A collision can be avoided by following vehicle braking when the following vehicle can slow down to a speed equal or lower than that of the lead vehicle. Figure 2 shows this case with $t = 0$ representing the final time instant at which the collision can be avoided by following vehicle braking. Assuming that the initial following and lead vehicle speeds are v_f and v_l respectively and that the lead vehicle has an acceleration a_l, the time T_b required for the following vehicle to slow down to a speed equal to that of the lead with deceleration from maximum braking a_{brk}^{max} can be calculated as follows.

$$v_l + a_l T_b = v_f + a_{brk}^{max} T_b \qquad (1)$$

$$T_b = \frac{v_l - v_f}{a_{brk}^{max} - a_l} \qquad (2)$$

The minimum TTC at which the collision can still be avoided (henceforth simply called the minimum TTC) can then be calculated from the relative distance and speed between the two vehicles at the start of the intervention ($t = 0$). The relative distance at the beginning can in turn be calculated from the distance travelled by the two vehicles (d_{brk}^f and d_{brk}^l) during the intervention (see Fig. 2).

$$d_{brk}^f = v_f T_b + a_{brk}^{max} \frac{T_b^2}{2} \qquad (3)$$

$$d_{brk}^l = v_l T_b + a_l \frac{T_b^2}{2} \qquad (4)$$

$$TTC_{brk}^{min} = \frac{d_{brk}^{rel}}{v_{brk}^{rel}} \qquad (5)$$

$$= \frac{d_{brk}^f - d_{brk}^l}{v_f - v_l} \qquad (6)$$

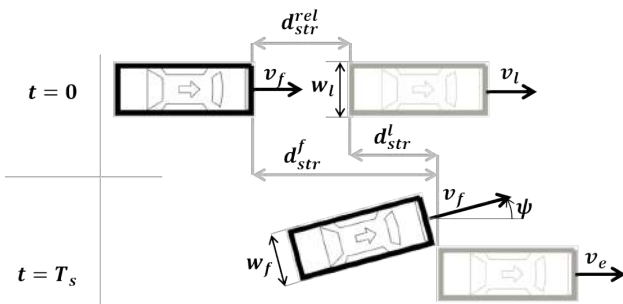$$= \frac{v_f - v_l}{2(a_l - a_{brk}^{max})} \qquad (7)$$

Fig. 3. Collision avoidance by steering

For the case of steering, assuming the following vehicle steers left (the problem is symmetric for turning the other way) and at constant speed v_f, the collision can be avoided

when the front right corner of the following vehicle clears a lateral distance equivalent to the left edge of the lead vehicle. This case is shown in Fig. 3 with $t = 0$ representing the final time instant at which the collision can be avoided by evasive steering of the following vehicle. The condition for collision avoidance by steering can be expressed as (small yaw angle and zero side slip angle assumptions have been made):

$$Y_{fr} \approx Y_c + l_{fe}\psi - \frac{w_f}{2} = \frac{w_l}{2} \qquad (8)$$

where l_{fe} is the distance from the center of gravity to the front edge of the vehicle and the yaw angle (ψ) and lateral center of gravity positions (Y_c) are given by:

$$\psi(t) = \omega_z t \qquad (9)$$

$$\omega_z = \min\left(\frac{\delta_{max}v_f}{L + K_u^f v_f^2}, \frac{a_{lat}^{max}}{v_f}\right) \qquad (10)$$

$$Y_c \approx \int_0^t (v_f\psi(t') + v_{y0})\mathrm{d}t' = v_f\omega_z\frac{t^2}{2} + v_{y0}t \qquad (11)$$

Note that zero initial heading angle for the following vehicle has been assumed since it would be difficult for the lead vehicle to detect the same. It would be easier instead to augment the expression for the following vehicle lateral center of gravity position Y_c, with the intial lateral velocity of the following vehicle v_{y0}, which could possibly be detected by the lead vehicle sensors.

Note also that while the side slip angle is unlikely to be zero in such a manoeuvre, determination of the same requires even more information about the following vehicle which the lead vehicle is unlikely to have. However, since these calculations involve almost exclusively a single type of manoeuvre (manoeuvres which push the vehicle to the limit), it is easier to account for the discrepancy by choosing an appropriate value of the understeer gradient for the following vehicle (K_u^f).

Substituting the expressions in Eq. (8) and solving for time gives:

$$Y_{fr} \approx v_f\omega_z\frac{T_s^2}{2} + (l_{fe}\omega_z + v_{y0})T_s - \frac{w_f}{2} \qquad (12)$$

$$T_s = \frac{-(l_{fe}\omega_z + v_{y0}) + \sqrt{(l_{fe}\omega_z + v_{y0})^2 + v_f\omega_z(w_f + w_l)}}{v_f\omega_z} \qquad (13)$$

The distances travelled by the two vehicles (d_{str}^f and d_{str}^l) and the minimum TTC for evasive steering can be calculated as:

$$d_{str}^f = v_f T_s \qquad (14)$$

$$d_{str}^l = v_l T_s + a_l\frac{T_s^2}{2} \qquad (15)$$

$$TTC_{str}^{min} = \frac{d_{str}^{rel}}{v_{str}^{rel}} \qquad (16)$$

$$= \frac{d_{str}^f - d_{str}^l}{v_f - v_l} \qquad (17)$$

$$= T_s + \frac{a_l}{v_l - v_f}\frac{T_s^2}{2} \qquad (18)$$

For collision avoidance by acceleration, a similar treatment as done in case of braking is done except that the motor
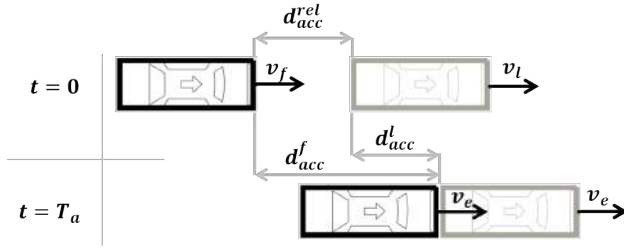
Fig. 4. Collision avoidance by acceleration

dynamics are taken into account. Figure 5 shows this case with $t = 0$ representing the final time instant at which the collision can be avoided by lead vehicle acceleration. Once again the collision is avoided when the lead vehicle velocity equals or is higher than that of the following vehicle.

$$v_f + a_{brk}^{max} T_a = v_l + a_{acc}^{max} \left(T_a - t_{acc}^d\right) \quad (19)$$

$$T_a = \frac{(v_f - v_l) + t_{acc}^d a_{acc}^{max}}{a_{acc}^{max} - a_{brk}^{max}} \quad (20)$$

The minimum TTC is then calculated from the relative distance travelled by the two vehicles and their relative velocities at the start of the intervention.

$$d_{acc}^l = v_l T_a + a_{acc}^{max} \frac{\left(T_a - t_{acc}^d\right)^2}{2} \quad (21)$$

$$d_{acc}^f = v_f T_a + a_{brk}^{max} \frac{T_a^2}{2} \quad (22)$$

$$TTC_{acc}^{min} = \frac{d_{acc}^{rel}}{v_{acc}^{rel}} \quad (23)$$

$$= \frac{d_{acc}^f - d_{acc}^l}{v_f - v_l} \quad (24)$$

$$= T_a + \frac{a_{brk}^{max} T_a^2 - a_{acc}^{max}(T_a - t_{acc}^d)^2}{2(v_f - v_l)} \quad (25)$$

As noted in Coelingh et al. (2010), use of the calculated TTC timings result in unncessarily late interventions and therefore a safety margin has been added which is expressed as:

$$t_{margin} = \max\left(\frac{d_{min}}{v_f - v_l}, t_{min}\right) \quad (26)$$

where d_{min} and t_{min} are the minimum safety margin distance and time respectively.

The activation timings so derived is expressed below and shown in Fig. 5.

$$TTC_{AEA} = \min\left(TTC_{brk}^{min}, TTC_{str}^{min}, TTC_{acc}^{min}\right) + t_{margin} \quad (27)$$

2.3 AEB timing calculation

For the determination of AEB activation timings, a similar method as detailed in Brännström et al. (2010) has been used and is hence not described in detail here. The primary differences here are that small sideslip angle assumption has been made, all manoeuvres start from steady state and straight ahead driving and that we also include a pure delay in the actuator response models. The first two result in a simplification of the method developed in Brännström et al. (2010). The pure delay on the other hand can be accounted for by simply adding a time duration equivalent
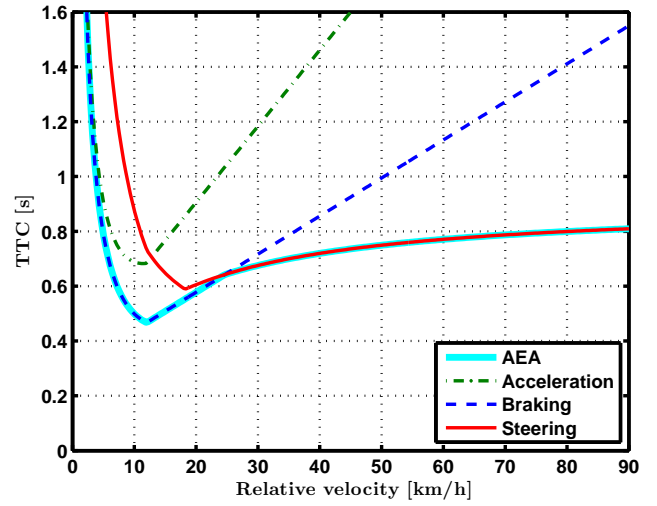

Fig. 5. Critical TTC for collision avoidance by braking, acceleration and steering manoeuvres and the activation timing for AEA. Brake and steering actuator limitations are not considered.

to the corresponding time delay to the TTCs so determined. This is made possible due to the fact that all manoeuvres are assumed to start from steady state and straight ahead driving.

Finally, just as in the case of AEA, a safety margin (Eq. (26)) is added to the TTC timings. The minimum of these two timings for braking and steering is taken as the activation timing for AEB. These timings are shown in Fig. 6 for reference.

$$TTC_{AEB} = \min\left(TTC_{brk}, TTC_{str}\right) + t_{margin} \quad (28)$$
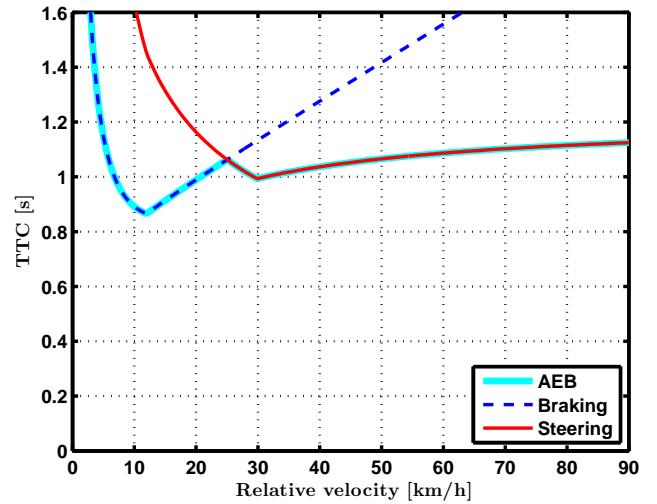
Fig. 6. Critical TTC for collision avoidance by braking and steering manoeuvres and the activation timing for AEB. Brake and steering actuator limitations are considered.

2.4 Expected relative velocity reductions

In order to evaluate the performance of the AEA system and its interaction with an AEB, a simple 1-D kinematic model was built with an AEB on the following and a AEA on the lead vehicles respectively. The actuators (brakes

and motor) are modeled as shown in Fig. 1. The activation timings for the AEB and AEA are determined as detailed in Sections 2.2 and 2.3 and Figs. 5 and 6. Simulations are then carried out with a range of initial velocities until either a collision occurs or is avoided which are determined as follows:

$$X_f(t) \geq X_l(t) \quad \rightarrow \quad \text{Collision occurs} \quad (29)$$
$$v_f(t) \leq v_l(t) \quad \rightarrow \quad \text{Collision avoided} \quad (30)$$

The velocity reductions achieved by the two systems and their combination is shown in Fig. 7. The data used is shown in Table 1. Comparing the relative velocity reduction curve for the AEB to the experimentally validated one presented in Coelingh et al. (2010) shows that they match remarkably well which supports the choice of method and the data used.

Table 1. Data used

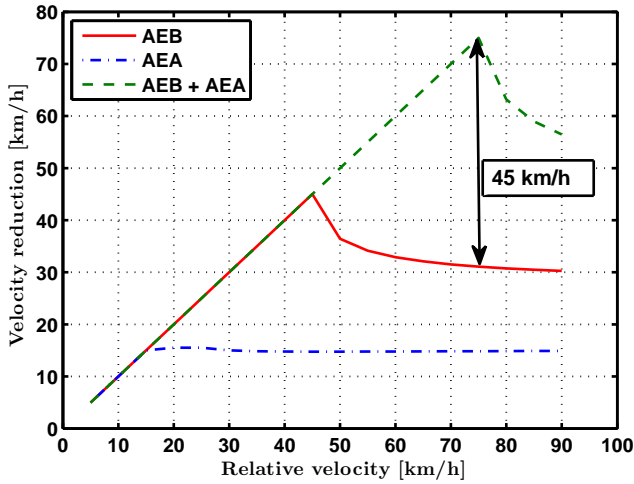| Vehicle and actuator parameters							
L	2.75 m	t_{brk}^d	0.18 s	j_{brk}^{max}	-20 m/s^3	a_{brk}^{max}	-10 m/s^2
w_l	1.5 m	t_{str}^d	0.02 s	δ_{sw}^{max}	720 °	a_{lat}^{max}	7 m/s^2
w_f	1.5 m	t_{acc}^d	0.05 s	$\dot{\delta}_{sw}^{max}$	400 °/s	a_{acc}^{max}	5 m/s^2
n	16.25	v_l	0 m/s	d_{min}	1 m	K_u^f	0.003
l_{fe}	2.4 m	a_l	0 m/s^2	t_{min}	0.3 s	v_{y0}	0 m/s

Fig. 7. Estimated velocity reduction capabilities for AEB on following vehicle, an autonomous acceleration system on the lead vehicle and a combination of the two.

As can be seen, even with conservative activation timings, the AEA system alone can achieve velocity reductions of up to 15 km/h when the following vehicle does not brake at all. When used in conjunction with AEB on the following vehicle, rear-end collisions with relative speeds up to 75 km/h can be completely avoided which represents a 45 km/h improvement over the outcome for the same case when AEB alone is used. These large velocity reductions achieved when the following vehicle brakes as well is in large part due to the fact that acceleration now not only reduces the relative speed, but also increases the distance available to the following vehicle for braking. Consequently, this benefit is obtained with relatively low increase in lead vehicle speed and distance travelled.

This fact is illustrated in Fig. 8 which shows the velocity increase and displacement for the lead vehicle (from standstill) when the AEA is used for a range of initial following vehicle velocities. As can be seen, on average, a velocity increase and displacement of approximately 15 km/h and 2 m respectively can be seen. The peak speed increase is seen to be roughly 25 km/h in order to achieve a velocity reduction of 75 km/h. The corresponding peak displacement is approximately 5 m which is roughly equivalent to the length of a large car.
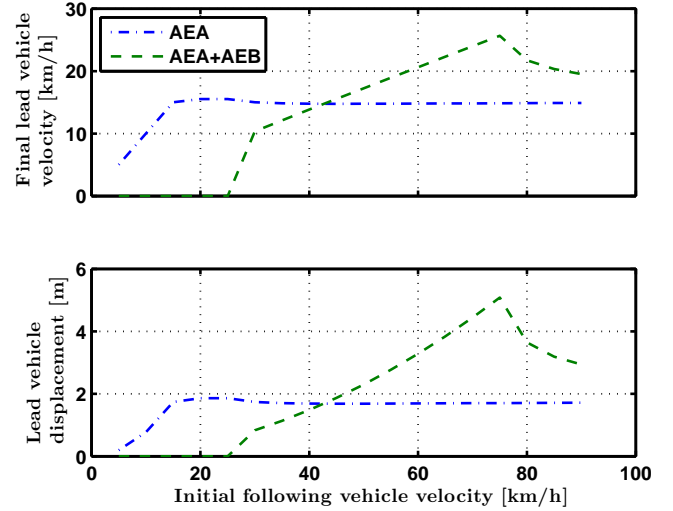

Fig. 8. Estimated increase in lead vehicle velocity and resulting displacement when the AEA is activated. Lead vehicle is stationary at the start of the intervention.

At low following vehicle speeds (less than roughly 30 km/h), when AEB is available on the following vehicle, it can be seen that there is no speed increase or displacement in the lead vehicle. This is because, at such low following vehicle speeds, the AEB is sufficient to prevent the collision and hence the AEA is not activated. While from Fig. 7 it can be seen that the AEB should be able to do so for speeds up to 45 km/h, after about 30 km/h, it is not able to prevent the collision with the required safety margin to spare and as a result, the AEA gets activated.

As noted, since just forward displacement of the lead vehicle can result in a safety benefit and since acceleration of the lead vehicle may not always be possible or advisable, a case of just moving the lead vehicle forward by a fixed distance without significantly increasing the final velocity is investigated.

Since such an intervention is less risky compared to hard acceleration, it can be done significantly earlier and as a result, the forward displacement can be achieved with relatively small or no increase in final velocity. An example use case for such a function could be when the lead vehicle is at a standstill at a traffic junction with a car length's gap in front and there is an imminent collision from a following vehicle behind. In such a case, this function could accelerate the vehicle forward and then decelerate so as to move it forward but also bring it back to standstill when the required lateral displacement has been achieved. This would allow increased braking distance for the following

vehicle and thereby help in preventing or mitigate being struck from behind.
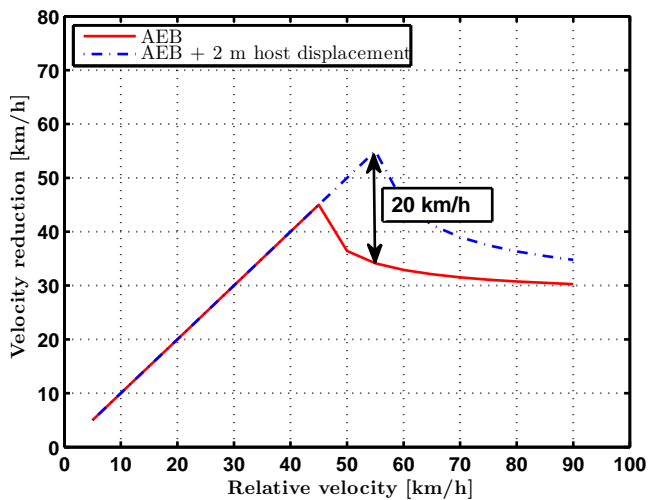

Fig. 9. Estimated velocity reduction capabilities for AEB on following vehicle, when lead vehicle moves forward by 2 m without a net speed increase.

The expected velocity reduction from such an intervention when the lead is moved forward by 2 m (approximately half the length of a small car) is shown in Fig. 9. As can be seen, up to a 20 km/h speed reduction over that of AEB alone can be achieved which represents over a 50 % improvement.

3. SAFETY BENEFIT

Whiplash injury is the most frequently sustained injury type in rear-end crashes [Watanabe et al. (2000)]. Several factors can influence the whiplash injury risk in these crashes, among them impact severity and occupant sitting position [Carlsson (2012)]. In an AEA equipped lead vehicle, impact severity may be reduced by considerably reducing the relative velocity between the colliding vehicles in a rear-end crash (up to 15 km/h, Fig. 7). Studies on whiplash injury risk based on data from real life crashes estimate that a reduction in change of velocity of 5 km/h for the struck vehicle can decrease the risk of sustaining whiplash symptoms lasting for more than one month by up to 65% [Krafft et al. (2005)]. In terms of initial symptoms the same amount of reduction in change of velocity could decrease the risk by up to 40% [Krafft et al. (2005)]. A reduction of change of velocity will also benefit the occupants of the striking vehicle. As an example, Kullgren et al. (2003b) concluded that the neck injury risk decreased from 33% to 27% in frontal impacts with a change of velocity reduction from 20 km/h to 10 km/h. From Krafft et al. (2009), it is known that a 10 % speed reduction before impact results in a 30 % reduction in fatality risk for the occupants of both vehicles. The potential injury risk reduction from a relatively small decrease in velocity change with AEA is therefore large.

Another potential contribution to the safety benefit could be the influence of the pre-collision acceleration on head posture. Occupant head posture with respect to the head restraint has been investigated in the past and several

studies have suggested that increased distance between the head and head restraint is associated with increased risk of a whiplash injury [Jakobsson (2004); Farmer et al. (1999); Deutscher (1996); Olsson (1990); Nygren et al. (1985); Carlsson et al. (1985)]. Numerical simulations of the head-neck motion in a rear-end impact indicated that limiting the head-to-head restraint distance to 6 cm or less could minimize the risk of sustaining a whiplash injury by restricting head retraction and neck extension during impact [Stemper et al. (2006)]. Although it remains unknown how much rearward head motion would be induced by the acceleration of the AEA system, the resulting head repositioning has the prospective safety benefit of reducing whiplash injury risk by decreasing head-to-head restraint distance before impact. This benefit, however, should be evaluated in combination with other influencing factors such as head restraint geometry, height of the head restraint and car seat properties [Carlsson (2012)].

A safety system influencing the neuromuscular response of the occupant has been proposed as a potential way to mitigate whiplash injuries in rear-end impacts [Siegmund (2011); Mang et al. (2012, 2015)]. The system was suggested based on results from neck muscle activity measurements in volunteers subject to replicated rear-end impacts. The suggested system consisted of a loud tone pre-stimulus inducing neck muscle activity to inhibit potentially injury exacerbating startle reflexes during the impact. Startle reflex can be provoked by sudden forward acceleration [Blouin et al. (2006)] indicating that the acceleration from the AEA system could possibly serve as a protective pre-stimulus in a similar fashion as the loud tone. However, it is not clear what characteristics of the pre-collision acceleration pulse are necessary to elicit a sufficient startle response. An alternative would be to include a loud tone as a part of a rear-end collision warning system (see section 4). According to [Siegmund (2011); Mang et al. (2012, 2015)] the tone should be delivered 250 ms before impact and would therefore be the last resort action of the warning system.

Whiplash injuries can occur at relatively low velocity changes of the struck vehicle [Krafft et al. (2005); Kullgren et al. (2003a)], lower than can be achieved with the AEA system. However due to the low acceleration level of the pre-collision acceleration (0.5 g) the AEA intervention is not expected to evoke whiplash symptoms [Krafft et al. (2005, 2002)].

4. DESIGN CHALLENGES AND SAFETY CONCERNS

One other possible way to prevent being struck from behind is to steer away from the threat. However, as seen in Figs. 5 and 6, steering is not very effective at low speeds which is typically the case for the lead vehicle in such scenarios. Another possiblity is to use both steering and acceleration for avoidance. However, not only is it unclear whether it would provide significantly higher benefit, but such an intervention involving vehicle control at the limit using both steering and acceleration/braking brings with it an increased risk of loss of control accidents.

On the other hand, if steering is already turned at the start of an intervention and is deemed undesirable by the

function, one way to correct for it would be to use the Electric Power Steering (EPS) to apply a corrective steering angle (for e.g., like in Active Lane Keeping assist). However, this is only possible if the steering angle is sufficiently small and if the vehicle is equipped with an EPS. Another possible way to correct for small steering angles could be to use differential braking. The disadvantage in this case is that it could potentially reduce the acceleration level that can be achieved. When the steering angle is large on the other hand (for e.g., lead vehicle stopped at a junction in preparation to make a turn), it would propbably be safest to not perform any intervention.

As mentioned in Section 1.3, it may not always be possible to detect if it is safe to accelerate due to difficulty in detecting cross traffic or even liability issues. One way to get around these issues is to warn the driver of an impending rear-end collision and use the driver's response as input to the system. Since typically, autonomous interventions are also preceded by a warning phase wherein the driver has an opportunity to intervene, the detection needs to be done equally early (approximately) in both cases. However, when the system has to just detect and warn the driver and not perform any autonomous intervention, the sensor requirements may be reduced as it offloads part of the liability to the driver.

One could envision simpler versions of the AEA which use the driver response to determine the required response. For e.g., similar to the Emergency Brake Assist (EBA) and Forward Collision Warning (FCW) functions (collectively called the brake assist functions along with the AEB), Emergency Acceleration Assist (EAA) and Rear-end Collision Warning (RCW) functions (collectively called the acceleration assist functions along with the AEA) could be devised. EAA would warn the driver and if the driver tries to accelerate would amplify their input and deliver maximum acceleration that it can achieve. RCW warning on the other hand would simply warn the driver and let the driver perform any intervention.

In Kusano and Gabler (2012), a study comparing the effectiveness of collision warning, brake assist and autonomous braking, it was found that up to 70 % and 50 % effectiveness of a fully autonomous system can be expected with assistance and warning systems respectively. With acceleration systems, similar or potentially even higher benefits can be expected compared to their brake-based counterparts due to the much shorter delays and much quicker response of electric drives.

Furthermore, if a rear-end collision can be detected, it would be easy to warn the following vehicle of an imminent collision by flashing the brake lights of the lead and thereby serve as a rudimentary "collision warning" system as has been speculated in Anderson and Baldock (2008). Additionally, in a cooperative environment the FCW and AEB of a following vehicle could be used to issue RCW and AEA or vice versa.

However, the design of an EAA or a RCW is not as straightforward as the design of EBA and FCW and presents new challenges from a human factors, engineering, and liability standpoint. Accelerating is not an obvious reaction or a standard evasive manoeuvre in rear-end collision scenarios. As a consequence, a warning to trigger such reaction may not be intuitive and require a driver to be trained to appropriately react. FCW guides a driver's attention to the threat (forward roadway), it may be harder for a RCW to guide a driver's attention to the rear-view mirror and, while looking at the rear-view mirror, it could be hard for a driver to deem whether it is safe to accelerate. EAA may surprise the driver who may react in an impulsive way, which may be unsafe. Further, when the acceleration of the lead vehicle is fully autonomous, the transition back to manual driving may be a concern. In fact, it may not be acceptable to assume that the driver is in the loop and able to control a vehicle that is suddenly moving at 15 km/h, and if any collision would happen shortly after the intervention of the AEA the vehicle manufacturer may still be liable. It might therefore be necessary to have supporting functions that bring the vehicle to a safe halt or state after an AEA intervention.

Although in this paper, the AEA activation timings are such that if brake assist functions were to be present on the following vehicle, they would always be activated before the AEA, ensuring a synergetic interaction between the two is still a crucial challenge. In fact, the brake assist algorithms are influenced by TTC and a sudden acceleration of the lead vehicle may abort the brake assist interventions and potentially aggravate the rear-end collision. In a non-cooperative environment, the AEA system would need to perfectly predict the behavior of the brake assist systems in the following vehicle and vice versa to have a safety impact. The potential interaction between autonomous systems in the lead and following vehicle also creates new liability challenges. Even if the AEA and AEB system activity would be logged, the lack of synchronization may prevent from reconstructing the actual crash dynamics.

5. CONCLUSION

An analysis on the potential of AEA in an electrified lead vehicle to mitigate rear-end collisions is presented. It is found that when used in conjunction with AEB, even collisions with high relative speed (up to 75 km/h) can be prevented with low increases in lead vehicle speed and distance travelled (on average ≈15 km/h and ≈2 m respectively). An brief investigation into the injury reduction potential offered by such a system shows that it can have a large safety benefit.

Further development of the AEA concept presented in this paper should address several human factors issues (such as acceptance and the extent of driver in the loop required at different times of intervention), engineering challenges (such as potential interaction between AEA and FCW/AEB in a following vehicle), and liability issues.

REFERENCES

Anderson, R. and Baldock, M. (2008). *Vehicle improvements to reduce the number and severity of rear end crashes.* Centre for Automotive Safety Research.

Blouin, J.S., Inglis, J.T., and Siegmund, G.P. (2006). Startle responses elicited by whiplash perturbations. *The Journal of Physiology*, 573(3), 857–867. doi: 10.1113/jphysiol.2006.108274.

Brännström, M., Coelingh, E., and Sjöberg, J. (2010). Model-Based Threat Assessment for Avoiding Arbi-

trary Vehicle Collisions. *IEEE Transactions on Intelligent Transportation Systems*, 11(3), 658–669. doi: 10.1109/TITS.2010.2048314.

Carlsson, A. (2012). *Addressing Female Whiplash Injury Protection - A Step Towards 50th Percentile Female Rear Impact Occupant Models.* Doctoral thesis, Chalmers University of Technology.

Carlsson, G., Nilsson, S., Nilsson-Ehle, A., Norin, H., Ysander, L., and Örtengren, R. (1985). Neck injuries in rear end car collisions - biomechanical considerations to improve head restraints.

Coelingh, E., Eidehall, A., and Bengtsson, M. (2010). Collision Warning with Full Auto Brake and Pedestrian Detection - a practical example of Automatic Emergency Braking. In *2010 13th International IEEE Conference on Intelligent Transportation Systems (ITSC)*, 155–160. doi:10.1109/ITSC.2010.5625077.

Deutscher, C. (1996). Movement of Car Occupants in Rear-End Accidents, Paper No. 96a5016. In *Int. Conf."Active and Passive Automobile Safety", Capri, Italy.*

Farmer, C.M., Wells, J.K., and Werner, J.V. (1999). Relationship of head restraint positioning to driver neck injury in rear-end crashes. *Accident Analysis & Prevention*, 31(6), 719–728. doi:10.1016/S0001-4575(99)00035-4.

Gustafsson, M., Stigson, H., Krafft, M., and Kullgren, A. (2015). Risk of Permanent Medical Impairment (RPMI) in Car Crashes Correlated to Age and Gender. *Traffic Injury Prevention*, 16(4), 353–361. doi: 10.1080/15389588.2014.940459.

Hori, Y., Toyoda, Y., and Tsuruoka, Y. (1997). Traction control of electric vehicle based on the estimation of road surface condition-basic experimental results using the test EV "UOT Electric March". In *Power Conversion Conference-Nagaoka 1997., Proceedings of the*, volume 1, 1–8.

Jakobsson, L. (2004). Field Analysis of AIS1 Neck Injuries in Rear-End Car Impacts. *Journal of Whiplash & Related Disorders*, 3(2), 37–53. doi:10.3109/J180v03n02_04.

Knipling, R.R., Wang, J.S., and Yin, H.M. (1993). *Rear-end Crashes: Problem Size Assessment and Statistical Decsription.* National Highway Traffic Safety Administration.

Krafft, M., Kullgren, A., Lie, A., Strandroth, J., and Tingvall, C. (2009). The effects of automatic emergency braking on fatal and serious injuries. In *21st International Conference on Enhanced Safety of Vehicles.*

Krafft, M., Kullgren, A., Malm, S., and Ydenius, A. (2005). Influence of crash severity on various whiplash injury symptoms: A study based on real-life rear-end crashes with recorded crash pulses. In *Proceedings 19th ESV Conf*, volume 5, 0363.

Krafft, M., Kullgren, A., Ydenius, A., and Tingvall, C. (2002). Influence of Crash Pulse Characteristics on Whiplash Associated Disorders in Rear Impacts–Crash Recording in Real Life Crashes. *Traffic Injury Prevention*, 3(2), 141–149. doi:10.1080/15389580212001.

Kullgren, A., Eriksson, L., Boström, O., and Krafft, M. (2003a). Validation of neck injury criteria using reconstructed real-life rear-end crashes with recorded crash pulses. In *Proc. 18th ESV Conf*, 1–13.

Kullgren, A., Krafft, M., Tingvall, C., and Lie, A. (2003b). Combining crash recorder and paired comparison technique: Injury risk functions in frontal and rear impacts

with special reference to neck injuries. In *Proc. of the 18th Techn. Conf. on ESV, Paper.*

Kusano, K. and Gabler, H. (2012). Safety Benefits of Forward Collision Warning, Brake Assist, and Autonomous Braking Systems in Rear-End Collisions. *IEEE Transactions on Intelligent Transportation Systems*, 13(4), 1546–1555. doi:10.1109/TITS.2012.2191542.

Malm, S., Krafft, M., Kullgren, A., Ydenius, A., and Tingvall, C. (2008). Risk of Permanent Medical Impairment (RPMI) in Road Traffic Accidents. *Annals of Advances in Automotive Medicine / Annual Scientific Conference*, 52, 93–100.

Mang, D.W.H., Siegmund, G.P., Inglis, J.T., and Blouin, J.S. (2012). The startle response during whiplash: a protective or harmful response? *Journal of Applied Physiology (Bethesda, Md.: 1985)*, 113(4), 532–540. doi: 10.1152/japplphysiol.00100.2012.

Mang, D., Siegmund, G., Brown, H., Goonetilleke, S., and Blouin, J.S. (2015). Loud preimpact tones reduce the cervical multifidus muscle response during rear-end collisions: A potential method for reducing whiplash injuries. *Spine Journal*, 15(1), 153–161. doi: 10.1016/j.spinee.2014.08.002.

NHTSA (2010). Federal Register | Federal Motor Vehicle Safety Standards; Head Restraints.

Nygren, A., Gustafsson, H., and Tingvall, C. (1985). Effects of Different Types of Headrests in Rear-End Collisions. SAE Technical Paper 856023, SAE International, Warrendale, PA.

Olsson, I. (1990). An in-depth study of neck injuries in rear end collisions. In *1990 International IRCOBI conference on the biomechanics of impacts: Proceedings, September 12-13-14, Bron-Lyon (France)/International Research Council On Biokinetics of Impacts.*

Schittenhelm, H. (2013). Advanced Brake Assist–Real World effectiveness of current implementations and next generation enlargements by Mercedes-Benz. In *Proceedings of the 23rd International Technical Conference on the Enhanced Safety of Vehicles (ESV)*. Seoul, South Korea.

Siegmund, G.P. (2011). What occupant kinematics and neuromuscular responses tell us about whiplash injury. *Spine*, 36(25 Suppl), S175–179. doi: 10.1097/BRS.0b013e3182387d71.

Singh, S. (2003). Driver attributes and rear-end crash involvement propensity. Technical report DOT HS 809 540, NHTSA.

Stemper, B.D., Yoganandan, N., and Pintar, F.A. (2006). Effect of head restraint backset on head–neck kinematics in whiplash. *Accident Analysis & Prevention*, 38(2), 317–323. doi:10.1016/j.aap.2005.10.005.

Unger, T. and Sandner, V. (2013). The ADAC advanced emergency brake system test-a real life based approach for a better primary safety. *Berichte der Bundesanstalt fuer Strassenwesen. Unterreihe Fahrzeugtechnik*, (87).

Watanabe, Y., Ichikawa, H., Kayama, O., Ono, K., Kaneoka, K., and Inami, S. (2000). Influence of seat characteristics on occupant motion in low-speed rear impacts. *Accident Analysis & Prevention*, 32(2), 243–250. doi: 10.1016/S0001-4575(99)00082-2.

Analysis of Vehicle Accident Involving Bicycle at Non-signalized Intersection by Near-Crash Incident Database

Shigeyoshi Tsutsumi *. Kei Sato *. Masao Nagai **.

*Tokyo University of Agriculture and Technology, Tokyo, Japan,
(Tel: +81-42-388-7176; e-mail: s_tsutsu@ cc.tuat.ac.jp).
** Japan Automobile Research Institute, Tokyo, Japan

Abstract: This paper describes the factor of crossing collision involving bicycle at non-signalized intersection by analyzing near-crash incident. In recent years, the traffic accident shows gradual decreasing in the number of fatalities, whereas slowly decreasing the total number of accidents and injuries in Japan. In order to decrease the total number of accident, it is necessary to investigate the factors of accident. So the feature of crossing collision involving bicycle at non-signalized intersection was analyzed by traffic accident data and near-crash incident database collected with the drive recorders.

Keywords: Database, Data recorder, Near-crash incident, Bicycle accident, Drive recorder

1. INTRODUCTION

In recent years, the number of accident is decreasing in the fatal accidents, and the total number of accidents and injuries in Japan. In order to decrease the total number of accident aiming at zero traffic accident, it is necessary to investigate what kind of accident has happened.

In this paper, we analyze the crossing collision accident involving bicycle, from multiple points of view firstly.

Then from the Near-Crash Database collected with the drive recorder mounted on a taxi vehicle, the type of risk feature is analyzed in accident and near crash case about with or without temporary stop sign in non-signalized intersection.

Specifically, we describe the feature like vehicle speed at the sudden brake, driver's pedal operation before sudden braking and so on. Furthermore we introduce of some representative examples, and clarify the traffic environment factors delayed to notice the bicycles.

2. ANALYSIS OF ACCIDENT DATA

By Japan National Police Agency (2014) the outbreak situation of the traffic accident in 2013, there are about 630,000 incidents, and 4373 fatalities (shown in Fig.1). It is a downward trend from 1990's, but there are still a lot of accidents.

In addition, there are about 110000 incidents and casualties (includes minor injuries) and 540 fatalities in the accident at the time of bicycle riding. The number of encountered collision accident with car is many even among them. So the measures are necessary to decreasing that of accidents.

By prevention safety technology developments, vehicle accident is considering to be reduced, but it is not taken enough measures against accidents involving elderly people or bicycle. Although there are various research on the accident involving elderly people, but bicycle accident is some exist in Japan. Therefore we consider a factor of bicycle accidents from near crash database.

In Japan, exceptionally, it is permitted the bicycle running in sidewalk on slowing down condition. It was originally the purpose of reducing the accident of the vehicle, but it is thought that there is also an accident which occurs in this environmental reason.

Bicycle has attracted attention in Japan because of ecorogy, so it may increase bicycle riders now. Moreover the road only for the bicycle is being maintained. But Japan has also many narrow roads, blinds and obstacles. It is thought decreasing accidents rapidly is difficult from these environmental factors.

Therefore, it is necessary to investigate how the accident and incident types of patterns occurred toward to decrease traffic accidents. So we analyze the near-crash incident data in order to perform a detailed analysis than accidents data.
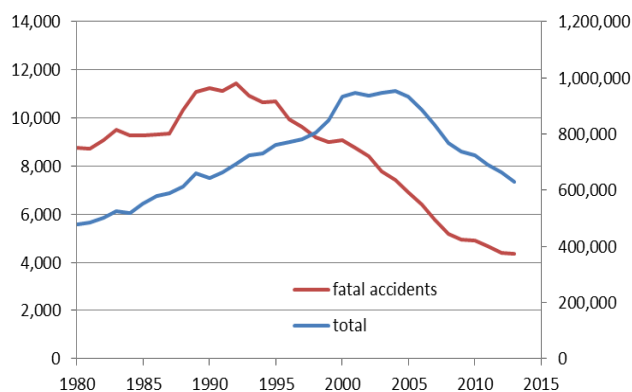

Fig. 1. Fatal accident and total accident number in Japan

3. ANALYSIS OF NEAR-CRASH INCIDENT DATA

3.1 Target Data for Analysis

The near miss incident database (including accident case) was collected by the drive recorder equipped with a taxi vehicle e.g. Minoru Kamata et al. (2006), Masao Nagai et al. (2006). In this paper, near crash situation between vehicle and bicycle were collected even among those databases at non-signal intersection. And that was analysed by distinguish with and without temporary stop sign.

Details of analysis target data are written in Table 1. In this database, there are collected data like date and time, GPS position data, Vehicle speed, vehicle acceleration, brake pedal operation, camera movie of front view when taxi drivers' slam on the brake timing.

Table 1. Number of near-miss incident data

	non-signalized intersection	
	with temporary stop sign	w/o temporary stop sign
Accidents	3	6
Near-crash incidents	67	146
Total	70	152

3.2 Analysis result of road environment characteristic

The analysis about road environmental data from target data in near incident database is shown in Fig.2. In the intersection with temporary stop sign, the ratio of road type about lane numbers is 67.1% in one-way road, and 25.7% in two way single lane without centreline. So near crash incidents are happened in narrow road more than 90% with temporary stop sign intersection.

In the intersection without temporary stop sign, the ratio of road type is 50% in one-way road, and 19.1% in single lane without centreline . So near crash incidents involving bicycle are happened higher in narrow road near the intersection.
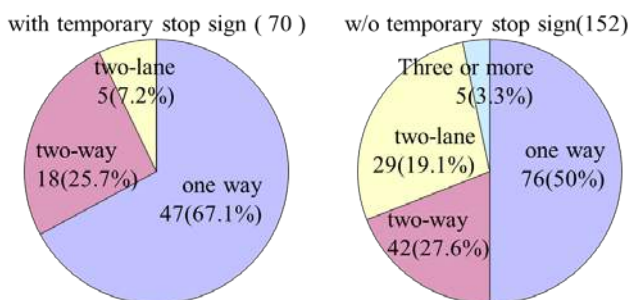

Fig. 2. Analysis results on the road environment

3.3 Analysis result about direction of approached bicycle

The analysis of position relationship and direction about vehicle and approached bicycle is shown in Fig.3.

In the case of with temporary stop sign intersection, the ratio of the bicycle crossing vehicle path from right side was the highest at 44.3% and from left side at 34.3%, bicycle into forward or backward from left side at 12.8% and from right side at 7.2%. In the case of without temporary stop sign intersection was closely same distribution.
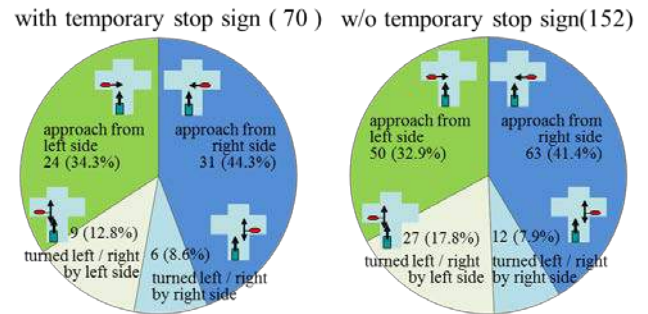

Fig. 3. Analysis results about the relation to the bicycle

3.4 Relative position relation between bicycle and vehicle after near-crash incident

The analysis of relative position relationship between bicycle and vehicle after near-crash incident is shown in Table2. Here, the analysis target data classified as five type shown in table2 from the situation of bicycle crossing vehicle path (N= 55+113). In the case of with temporary stop sign intersection, the case of vehicle stopping (type I, II, III) is more than vehicle passing. Even among those, vehicle stopping and bicycle passing case is most numerous. In the case of without temporary stop sign intersection, the case of vehicle passing is more than vehicle stopping, but there are stopping case, so different distribution from with temporary stop sign case

Table2 Type classification of near-miss incident data

Type classification of near-miss incident data		With stop regulation	No stop regulation
I		6 (10.9%)	11 (9.7%)
II		12 (21.8%)	18 (15.9%)
III		24 (43.6%)	11 (9.7%)
IV		5 (9.1%)	41 (36.3%)
V		8 (14.5%)	32 (28.3%)
■ Vehicle ○ Vehicle stop point ━ Bicycle ● Bicycle stop point		55 (100%)	113 (100%)

3.5 Result of vehicle speed at sudden brake timing

The analysis of the vehicle speed in sudden brake that means the timing of slamming on the brake depended on near-crash factor is shown in Fig.4. The vehicle speed at sudden braking was defined by the time of longitudinal acceleration rise suddenly by brake operation.

In the case of without temporary stop sign intersection, the ratio of the running speed classified as 25 to 29.9km/h was the highest at 19.1%. Average speed is also in this speed range.

On the other hand, in the case of with temporary stop sign intersection, the ratio of the running speed classified as 5 to 9.9km/h is highest at 34.3%. The ratio of speed less than 20km/h was about 70 %.

Vehicle speed range without temporary stop sign is higher than that of with sign. Distribution of vehicle speed in the presence or absence of temporary stop signs is greatly different.
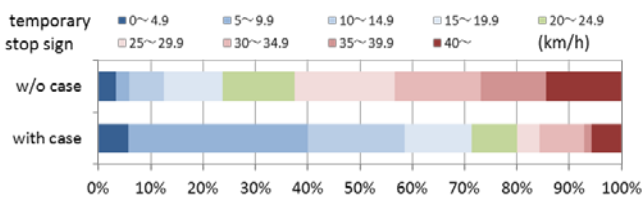

Fig. 4. Distribution of vehicle speed in sudden braking

3.6 Result of driver's pedal operation in sudden braking

Driver's pedal operation just before the slamming on the brake was analyzed by driver's brake operation, vehicle speed, and vehicle longitudinal acceleration in database. Analysis result is shown in Fig.5. The no pedal operation state (no operation) is defined as the state of accel and brake pedal separated.

In the case of without temporary stop sign intersection, there are overwhelmingly many cases which stepped on an accel pedal. In the case of with temporary stop sign intersection, stepping on the brake pedal case is the most numerous pattern.
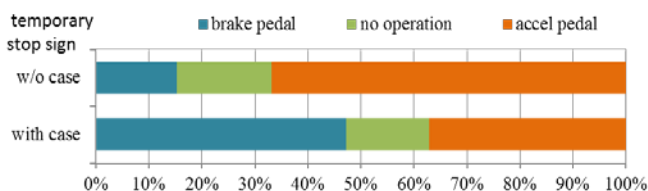

Fig. 5. Driver's foot and pedal position at sudden braking

3.7 Braking distance simulation

Here, we examine the relation between vehicle speed and stopping distance at the braking timing. Simulation was calculated under the conditions below.

-Stamping time from the accelerator to brake pedal is 0.7[s]
-Braking deceleration is a square wave of 0.7 [G]

The calculation of relationship between vehicle speed and stopping distance at the braking timing was shown in Figure 7. The overall stopping distance was the sum of the braking distance by brake (S1) and the idle traveling distance caused by pedal stamping time (S2).

Traveling distance S2 is higher proportion compared with the braking distance S1 as the vehicle speed lower, from Fig.6. So, when the vehicle speed at sudden braking is lower case, it is thought the driver's foot position before sudden braking influenced the stopping distance.
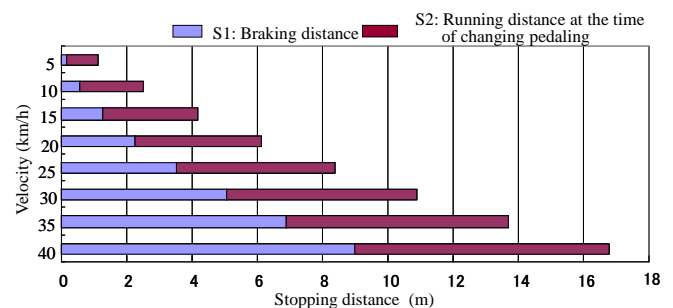

Fig.6. Relationship of stopping distance and running speed

4. DETAILED ANALYSIS OF NEAR-CRASH INCIDENT

4.1 Pattern Classification Analysis

In addition, each near-crash incidents was classified the typical pattern to further analyze the incident factor from the driving conditions and driver behaviours around the sudden braking.

It was described the state of the traffic environment, vehicle motion states and bicycle entry path at the intersection, by conducting detailed analysis of incidents from each picked up typical patterns.

In this paper it was divided into three patterns, and analyzed in detail by picking up the typical 1 case of each patterns.

Also, the distance that positional relationship between the vehicle and the bicycle at sudden braking was calculated using trigonometry software from the front camera pictures.

We divided each incidents into two typical patterns by the behaviour at the around of the stopline with temporary stop sign situation and one typical pattern without temporary stop sign situation.

4.2 With Temporary Stop Sign Case(Pattern A)

Pattern A is a case to slam the brake on short of stopline shown in Fig.7. It accounted for 47 % of the temporary stop sign existence case.

In pattern A, it is assumed running toward to the intersection with temporary stop sign, and driver discovers the bicycle and slam on the brakes.

In this pattern, there were divided two cases that case I is stop case after sudden braking, case II is re-acceleration case. Case I accounted for 79 % of this pattern.
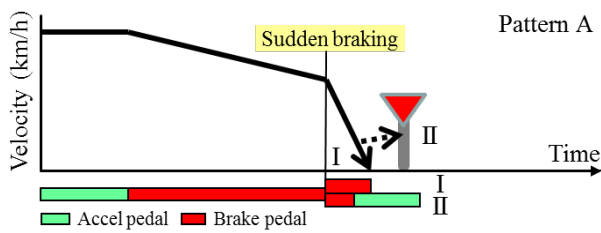

Fig.7 Typical patterns with temporary stop sign (Pattern A)

Here, we will introduce a typical near-crash case of pattern A. The forward image from video, time waveform about vehicle speed and acceleration, and positional relationship of bicycle at sudden braking is shown in Fig.8.

Fig.8. Introduction of image and vehicle data (Pattern A)

4.3 With Temporary Stop Sign Case(Pattern B)

Pattern B is a case to slam the brake on after stopline shown in Fig.9. Drive slam on the brake after decelerating at the stop line and re-acceleration for the passage of the intersection. It accounted for 37 % of the temporary stop sign existence case.

In this pattern, there were divided two cases that case I is stop case after sudden braking, case II is re-acceleration case. Case I accounted for 73 % of this pattern.

Fig.9 Typical patterns with temporary stop sign (Pattern B)

Here, we will introduce a typical near-crash case of pattern B The forward image from video, time waveform about vehicle speed and acceleration, and positional relationship of bicycle at sudden braking is shown in Fig.10.
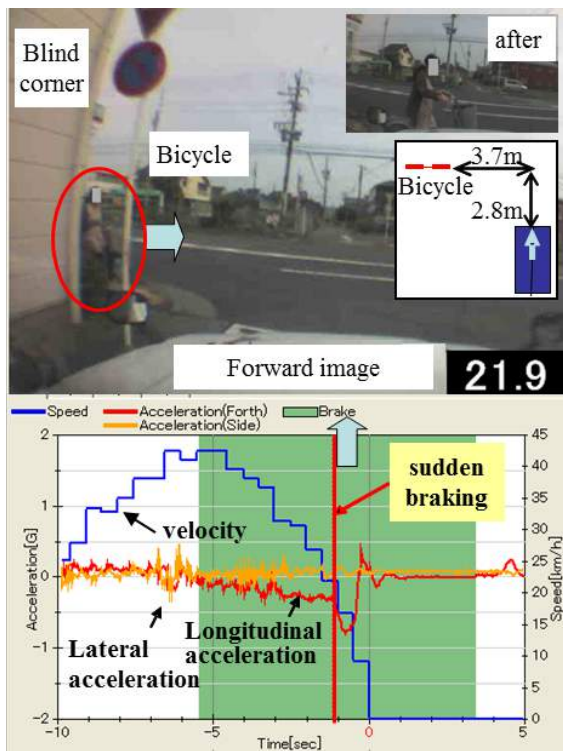

Fig.10. Introduction of image and vehicle data (Pattern B)

4.4 Without Temporary Stop Sign Case(Pattern C)

Pattern C case of without temporary stop sign is shown in Fig.11. It accounted for 67 % of the non-temporary stop sign case.

In pattern C, it is assumed running at during acceleration or constant speed and approaching the intersection without temporary stop sign, and driver discovers the bicycle and slam on the brakes at the intersection.

In this pattern, there were divided two cases that case I is stop case after sudden braking, case II is re-acceleration case. Case II accounted for 73 % of this pattern.
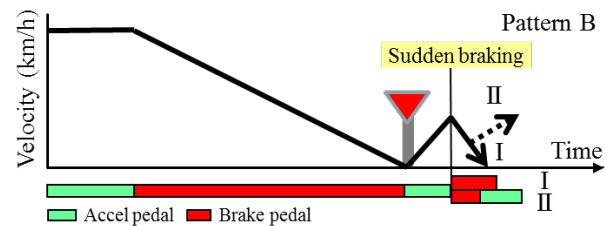

Fig.11. Typical patterns without temporary stop sign (Pattern C)

Here, we will introduce a typical near-crash case of pattern C. The forward image from video, time waveform about vehicle speed and acceleration, and positional relationship of bicycle at sudden braking is shown in Fig.12.
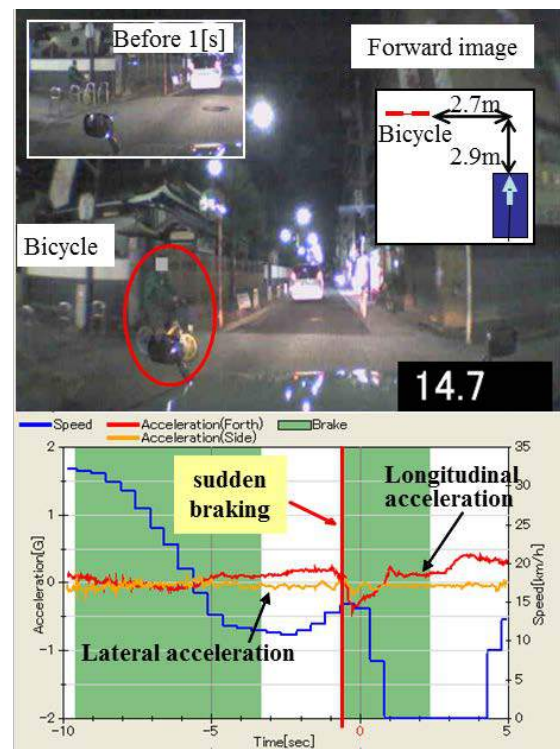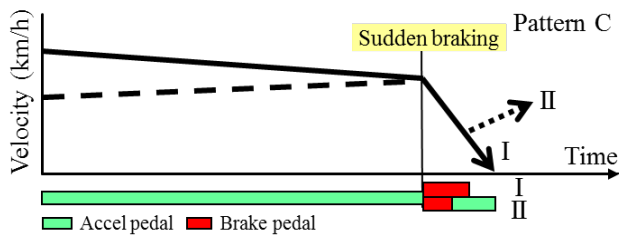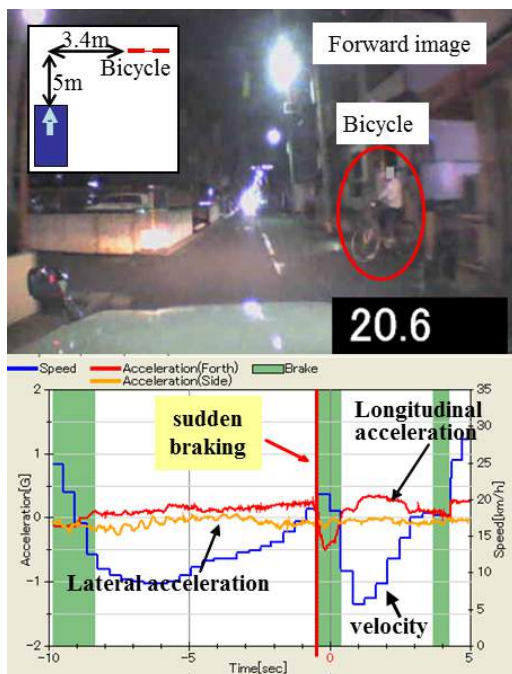

Fig.12. Introduction of image and vehicle data (Pattern C)

5. CONCLUSIONS

This paper is focused on crossing collision accident involving bicycle at non-signalized intersections in order to investigate the actual condition of crossing collision in the intersection.

Analysis of the near-crash data by drive recorder equipped taxi vehicles, and revealed its features. And we elucidate the accident factors from analyzing the vehicle accident involving the bicycle. It referred to the revealed items below.

1）It was able to be clarified situation that could not understand only by the traffic accident data like a behavior when discover bicycle approaching the intersection, vehicle speed, vehicle state and driver's pedal operation at sudden braking,

2）The pattern of a typical near-crash incident was clarified according to the state of existence temporary stop sign in the crossing collision vehicle accident involving bicycle at non-signalized intersection from the driver's pedal operation and vehicle state immediately before sudden braking.

3）Each near-crash incidents was classified the typical pattern to further analyze the incident factor from the driving conditions and driver behaviours.

This paper describes to clarify the vehicle accident factors of the crossing collision involving the bicycle at non-signalized intersection. The method for decreasing such factors will be devised in future woks.

REFERENCES

National Police Agency (2014), The outbreak situation of traffic accident in 2013, http://www.npa.go.jp/toukei/ koutuu48/ toukei.htm, (in Japanese)

Minoru Kamata, Mitsunobu Fujita, Motoki Shino, Masao Nagai, Yohei Michitsuji and Kozo Maeda (2006). Research on incident analysis using drive recorder part 1：Toward database construction, *Proceedings of the FISITA World Congress*. 22 (27). F2006V203

Masao Nagai, Yohei Michitsuji, Minoru Kamata, Mitsunobu Fujita, Motoki Shino, and Kozo Maeda (2006). Research on incident analysis using drive recorder part 2：Toward active safety assessment. *Proceedings of the FISITA World Congress*. 22 (27). F2006V202

Effect of Driving Context on Time to Collision at Brake Application during Car Following[*]

Kristofer D. Kusano[*] **Rong Chen**[*] **Hampton C. Gabler**[*]

[*] *Virginia Polytechnic Institute and State University*

Abstract: Collision Warning (FCW) systems that have customizable warning delivery settings may improve driver acceptance, thus increasing the benefits of such systems. In order to design FCW warning thresholds that match a driver's expectations, system designers need to characterize when the brakes are normally applied. However, a driver's normal braking behavior may vary with the driving context, e.g., traffic congestion or daylight conditions. This study examined over 2.6 million brake applications from the 100-Car naturalistic driving study to determine the effect of driver demographics (age group and gender) and driving context (day of week, time of day, travel speed, and traffic congestion) on brake application time. The results showed that both demographics and driving context were statistically significant indicators of the time to collision (TTC) that drivers applied the brakes during car following.

Keywords: Driver Behavior Modeling, Vehicular Sensors and Environment Perception, Naturalistic Driving

1. INTRODUCTION

The success of active safety systems that warn drivers, e.g., Forward Collision Warning (FCW), is highly dependent on driver acceptance. Drivers who experience warnings they deem unnecessary, i.e., nuisance alarms, may lose trust in and eventually disable the systems (Bliss and Acton, 2003). Therefore, developers of FCW systems need to design warnings such that they are delivered near to or after drivers would normally brake. Complicating this decision is the concern that a driver's normal braking behavior may vary with the driving context, e.g., traffic congestion or daylight conditions.

An emerging data source for collecting driver braking behavior data are naturalistic driving studies (NDS). NDS are longitudinal studies where all normal driving of participants is recorded. The result is thousands of hours of fully instrumented driving available for analysis. Analyzing large scale NDS in order to produce aggregate summaries of driver behavior, however, is difficult. Driver demographics such as age and gender have been shown to affect driver braking behavior (Montgomery et al., 2014). Driving context factors, e.g., road type, congestion level, time of day, can also affect driving behavior (Ellison et al., 2015, 2014). This driving context data is normally not collected directly during NDS and must be derived after the study by linking roadway and other data stets or inferred using the instrumentation data.

The objective of this study is to develop a methodology for inferring driving context using vehicle instrumentation and use this methodology to determine the effects of driving context on time to collision (TTC) when drivers apply the brakes.

2. METHODOLOGY

2.1 Data Source

The data source for this study was the 100-Car NDS (Dingus et al., 2006). The 100-Car study was a landmark NDS that was collected between 2002 and 2004 in the Washington D.C. metropolitan area. Approximately 100 vehicles were instrumented for a period of approximately 1 year.

The 100-Car study oversampled younger drivers by design. To make the estimates in this study representative of the U.S. driving population, we analyzed the data using post stratification weighting. The age and gender of those drivers recruited for the study were compared to the demographics of all registered drivers in the U.S. (Federal Highway Administration, 2012). The post stratification weight of each age and gender combination, w, was calculated as

$$w = \frac{p_{registered}}{p_{sample}}, \tag{1}$$

where $p_{registered}$ is the proportion of drivers with a given age and gender in the U.S. driving population and p_{sample} is the proportion of drivers in the 100-Car sample. The post stratification weights derived for the sample are included in Appendix A. In general, younger drivers had lower weights than the other age groups because they were oversampled.

2.2 Identifying Driving Context

Current and near-production vehicles have an increasing number of sensors relating to safety and infotainment

systems. Vehicles are often equipped with forward facing radar and cameras for detecting objects ahead, light sensors for detecting ambient light, and have reference to time of day and date through navigation systems. Although connected vehicle and infrastructure technology is progressing, their wide adoption is still years away. Therefore, current active safety systems must sense their surroundings using only available outward looking sensors.

In this study, driving context was characterized by vehicle speed, time of day (daylight or nighttime), day of week (weekend or weekday), and traffic conditions. Vehicle speed was recorded by the vehicle instrumentation equipped for the study. The date was recorded by the data acquisition system, which was used to determine the day of the week. The time of day was determined by manual examination of the video data from each trip. The cameras in the study sometimes failed or were dislodged from their mounts, making it impossible to determine the time of day. Another possible reason for not being able to determine the time of day was if the entire trip occurred in a covered structure, such as a parking garage. Any trips where the time of day or day of week was unable to be determined were excluded from further analysis.

The traffic conditions were measured indirectly during the study. For this study, we estimated traffic conditions using the density of objects detected by the front facing radar instrumentation. Each trip was divided into 20 second segments and the number of new objects tracked by the radar system was counted. Only objects with a ground speed in the same direction as the equipped vehicle were counted to avoid including fixed roadside objects, such as road signs or overpasses. From observation of the forward facing video, moderate to heavy congestion had at least 5 new radar objects detected per 20 seconds.

To aggregate the behavior of each driver, the minimum TTC at brake application was computed for all combinations of time of day, day of week, vehicle speed (grouped in 10 mph bins), and the presence of traffic congestion. For example, a minimum TTC was computed for the scenario of the vehicle traveling between 40 and 50 mph during daylight on a weekday in congested traffic. The driver age group was divided into groups of "Novice" 18–20 years, "Young" 21–30 years, "Middle" 31–50 years, and "Mature" 51+ years. The age group and gender were included as covariates for TTC in the statistical models discussed in the next section.

2.3 Statistical Modeling of Driver Car Following Behavior

TTC is the ratio of the instantaneous range, x, to range rate between the equipped vehicle and an object, $\dot{x}$:

$$TTC = \frac{x}{\dot{x}} \qquad (2)$$

TTC gives the amount of time two objects would take to collide if they continued at their current speeds. The TTC metric has been a popular choice for activation thresholds for FCW systems because it relates to a driver's perception of risk of a collision occurring (Lee, 1976). TTC is the metric that is used for the U.S. New Car Assessment Program (NCAP) assessment for FCW systems.

The radar instrumentation in the study was able to track up to seven objects at each time step. Each object that was tracked by the radar had a range, range rate, and azimuth with respect to the instrumented vehicle. For this study, however, driver behavior was characterized by the TTC to the lead vehicle at the time when the brakes were applied. This raw radar data did not include which tracked vehicle was closest in the same lane as the instrumented vehicle, i.e., the lead vehicle.

In order to determine the lead vehicle from the raw radar data, we developed a heuristic algorithm to determine the lead vehicle during brake applications (Kusano et al., 2014). The algorithm picked the lead vehicle as the object that was within 2 m of the vehicle's path for a majority of the braking period that also had a headway of less than 3 s. The 3 s headway requirement was chosen to match the definition of car following commonly used in traffic engineering. We validated the algorithm to determine the lead vehicle by comparing it to 8402 brake applications where the lead vehicle was manually identified by human observers. This validation found that the algorithm matched the human observer in over 92% of brake applications (Kusano et al., 2014).

In order to determine the effect of driver demographics and driving context, linear mixed effects models were constructed (Pinheiro et al., 2015). Linear mixed effects models are similar to ordinary linear models, but can include random effects variables along with traditional fixed effects. In this study, the driver was treated as a random intercept and the remaining independent variables were modeled as fixed effects. This methodology allowed for the models to take into account between subject variability that an ordinary linear model would not account for. To examine the interaction effects, pairwise contrasts were constructed. To test for statistical significance, a Tukey Honestly Significant Difference (HSD) adjustment was made for multiple comparisons (Lenth and Hervé, 2015).

3. RESULTS

3.1 Selected Trips

All trips involving primary drivers, i.e., the owners or lessees of the vehicle, were extracted from the 100-Car study. In order to be included in this study, the drivers had to be operating the vehicle with all required sensors (radar, speed, and yaw rate) for at least 60% of trips traveled during the study. The final dataset included 64 drivers that recorded 19,810 hours of driving resulting in 980,956 km (609,538 miles) traveled. During this driving, the drivers applied the brakes 2.6 million times, of which 37% had a lead vehicle present and closing with the equipped vehicle.

3.2 Distribution of Driving Context Scenarios

Table 1 lists the proportion of travel time and distance under the levels of time of day, driver seatbelt use, and day of week for the 58,239 trips in the dataset. Any trips that had an unknown day of week or time of day were excluded from the analysis, leaving 57,848 trips. Driving on weekdays (78.3% of time and 76.4% of distance) and

during the day (76.4% of time and 74.2% of distance) were most frequent. In particular, the scenario of driving on the weekend, at night, and with congested conditions was extremely infrequent, making up just over 1% of time and distance traveled.

Table 1. Time and Distance Traveled under Driving Context Conditions

Driving Context	% Time	% Distance
Weekday, Day, Uncongested	39.0%	32.6%
Weekday, Day, Congested	22.0%	25.1%
Weekday, Night, Uncongested	12.9%	13.3%
Weekday, Night, Congested	4.4%	5.4%
Weekend, Day, Uncongested	11.1%	11.1%
Weekend, Day, Congested	4.3%	5.4%
Weekend, Night, Uncongested	5.2%	5.6%
Weekend, Night, Congested	1.1%	1.5%

Not all drivers enrolled in the study drove frequently during all driving context levels examined for this study. If a driver had very few braking applications at a given driving context level, it is unlikely they had adequate exposure to exhibit a minimum TTC that is representative of their normal behavior. Any driving context level, e.g., weekday, during the day, uncongested at 30–40 mph, that had less than 5 brake applications for a driver were excluded from the analysis. In addition, braking during trips at night, during weekends, and under congested conditions were excluded from analysis because these scenarios represented just over 1% of driving during the study. Scenarios with less than 5 brake applications occurred 125 times and the weekend/night/congestion scenario occurred 320 times. In total, either of these exclusion criteria was present in 364 out of the 2560 possible driving context levels (2 days of week × 2 times of day × 2 congestion levels × 5 speed ranges × 64 drivers = 2560 possible levels). The resulting dataset was composed of 750,277 brake applications.

3.3 Effect of Driving Context on TTC at Brake Application

Table 2 shows an analysis of variance (ANOVA) for the linear mixed effects model of minimum TTC experienced during the study in each driving context scenario. For the main effects, all of the driving context variables (speed range, time of day, seatbelt status, day of week, and congestion), were significant to the $\alpha = 0.05$ confidence level. Age group was statistically significant to the $\alpha = 0.05$ level and gender was marginally significant at an $\alpha = 0.10$ level. Several of the interaction effects were also significant, which will be explored further in the following section.

Table 3 lists the least squared mean estimate of the minimum TTC for each of the main effect variables. The least squared mean estimates of TTC were produced by the regression model averaged across all other factors. TTC decreased as age increased, with mature drivers applying the brakes almost 1.5 s earlier than novice drivers. Females applied the brakes earlier than males. As vehicle speed increased, TTC also increased. Drivers applied the brakes earlier during the night and on weekends compared to during the day and on weekdays. The presence of congestion caused drivers to apply the brakes slightly earlier than in uncongested conditions.

Table 2. Analysis of Variance for Linear Mixed Effects Model for Minimum TTC

Effect	F value	Pr(>F)	
(Intercept)	1199.04	p<0.0001	***
Age Group	5.85	0.0015	**
Gender	3.38	0.0713	*
Speed Range	276.11	p<0.0001	***
Time of Day	281.92	p<0.0001	***
Day of Week	270.28	p<0.0001	***
Congestion	29.57	p<0.0001	***
(Age Group)*(Gender)	0.92	0.4365	
(Age Group)*(Speed Range)	3.96	p<0.0001	***
(Age Group)*(Time of Day)	13.20	p<0.0001	***
(Age Group)*(Day of Week)	3.73	0.0110	**
(Age Group)*(Congestion)	1.76	0.1523	
(Gender)*(Speed Range)	6.21	p<0.0001	***
(Gender)*(Time of Day)	30.45	p<0.0001	***
(Gender)*(Day of Week)	1.42	0.2328	
(Gender)*(Congestion)	0.34	0.5607	
(Speed Range)*(Time of Day)	14.61	p<0.0001	***
(Speed Range)*(Day of Week)	8.64	p<0.0001	***
(Speed Range)*(Congestion)	3.79	0.0045	**
(Time of Day)*(Day of Week)	1.47	0.2247	
(Time of Day)*(Congestion)	2.19	0.1388	
(Day of Week)*(Congestion)	3.57	0.0590	*

Note: *** = p <0.0001, ** = p <0.05, * = p <0.10

Table 3. Least Squared (LS) Means for Main Effects Variables

Variable	Level	LS Mean TTC (s)
Age Group	Novice (18-20)	2.78
	Young (21-30)	3.21
	Middle (31-50)	3.88
	Mature (51+)	4.26
Gender	Female	3.77
	Male	3.29
Speed (mph)	10-20	2.55
	20-30	2.59
	30-40	3.25
	40-50	4.03
	50-60	5.25
Time of Day	Day	2.89
	Night	4.18
Day of Week	Weekday	2.94
	Weekend	4.12
Congestion	Congested	3.79
	Uncongested	3.28

3.4 Minimum TTC by Interactions of Driving Context Factors

Figure 1 shows the least squared mean estimate for TTC generated from the linear model by travel speed and presence of congestion. The difference was significant at the lower speeds but not the 40–50 and 50–60 mph speed ranges. This result shows that lower TTC occurred when there was no congestion. One possible explanation for this observation is that drivers are more likely to be attentive to other vehicles if they are driving on roads with congestion.

The least squared mean estimate for TTC by time of day and gender is shown in Figure 2. There was no significant difference between gender groups during daytime driving. Females, however, applied the brakes significantly earlier than males during night driving.
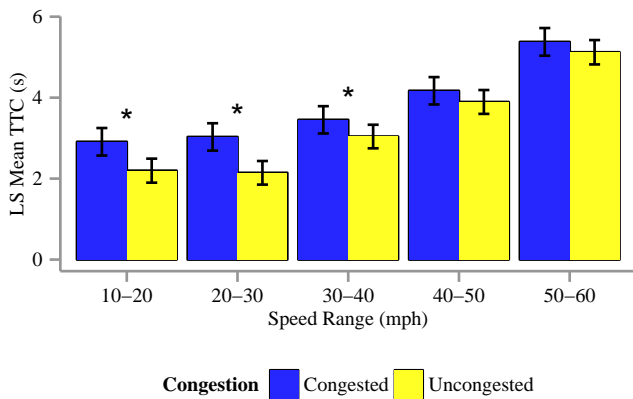
Fig. 1. Least Squared Mean Estimate of Minimum TTC by Travel Speed and Presence of Congestion
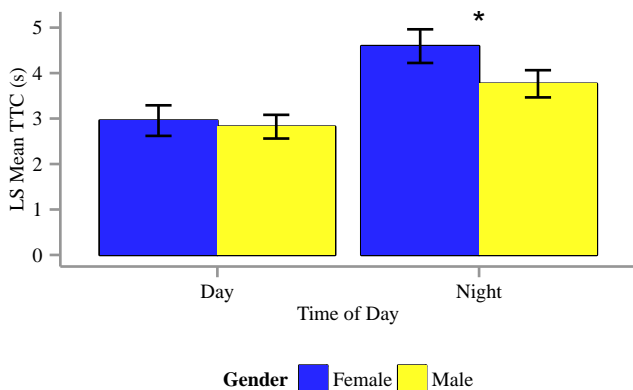

Fig. 2. Least Squared Mean Estimate of Minimum TTC by Time of Day and Gender

4. DISCUSSION

The results of this study show how driving context significantly affects driver braking behavior during car following. Forward crash avoidance systems such as FCW may better match a driver's expectations if it adapts its warning times to the driver and driving context. This adaptation may be accomplished by current on-vehicle sensors, such as navigations systems, ambient light sensors, radar, cameras, and vehicle speed sensors.

This study has several important limitations. First, the 100-Car NDS data was not linked to roadway data. Therefore, traffic and road conditions were only inferred using forward facing radar and vehicle speed. Previous characterization driving behavior using NDS data have found that speeding is a significant indicator of crash risk (Ellison et al., 2015). This study did not have access to the speed limits on the roads and thus could not assess driver speeding behavior. The analysis in this study could be improved if NDS data with linked roadway data were available.

Second, the statistical methodology used for this study aggregated all brake applications during driving context scenarios and took the minimum TTC during each scenario. This aggregation assumes a true minimum that is characteristic of the driver's normal behavior was experienced during each scenario. We observed that if very few brake applications were collected at a given scenario that large variability could be introduced into the results. Typically these scenarios with few brake applications had extremely high TTC, i.e., greater than 20 s. Scenarios with less than 5 brake applications were excluded to attempt to minimize this variability but at the expense of potentially biasing the results. A possible solution to this challenge would be to use a statistical methodology that uses all the recorded braking data instead of aggregating by scenario.

5. CONCLUSION

In addition to driver demographics, driving context factors can affect when drivers apply the brakes during car following. This study showed that driving context can be detected using only vehicle based sensors, such as speed and radar. These results can be used to design adaptive FCW delivery strategies that could reduce nuisance alarms.

ACKNOWLEDGEMENTS

REFERENCES

Bliss, J.P. and Acton, S.A. (2003). Alarm mistrust in automobiles: how collision alarm reliability affects driving. *Appl Ergon*, 34(6), 499–509. doi:10.1016/j.apergo.2003.07.003.

Dingus, T.A., Klauer, S.G., Neale, V.L., Petersen, A., Lee, S.E., Sudweeks, J., Perez, M.A., Hankey, J.M., Ramsey, D., Gupta, S., Bucher, C., Doerzaph, Z.R., Jermeland, J., and Knipling, R.R. (2006). The 100-car naturalistic driving study - phase II results of the 100-car field experiment. Technical report, Department of Transportation, Washington, D.C.

Ellison, A.B., Greaves, S.P., and Bliemer, M.C.J. (2014). Examining heterogeneity of driver behavior with temporal and spatial factors. *Transportation Research Record: Journal of the Transportation Research Board*, 2386, 158–167. doi:10.3141/2386-18.

Ellison, A.B., Greaves, S.P., and Bliemer, M.C.J. (2015). Driver behaviour profiles for road safety analysis. *Accident analysis and prevention*, 76C, 118–132. doi:10.1016/j.aap.2015.01.009.

Federal Highway Administration (2012). Distribution of licensed drivers – 2012 by sex and percentage in each age group and relation to population. URL http://www.fhwa.dot.gov/policyinformation/statistics/2012/dl20.cfm. Accessed 20 March 2015.

Kusano, K.D., Montgomery, J., and Gabler, H.C. (2014). Methodology for identifying car following events from naturalistic data. In *2014 IEEE Intelligent Vehicles Symposium Proceedings*, 281–285. IEEE. doi:10.1109/IVS.2014.6856406.

Lee, D.N. (1976). A theory of visual control of braking based on information about time-to-collision. *Perception*, 5, 437–459.

Lenth, R.V. and Hervé, M. (2015). *lsmeans: Least-Squares Means*. URL `http://CRAN.R-project.org/package=lsmeans`. R package version 2.15.

Montgomery, J., Kusano, K.D., and Gabler, H.C. (2014). Age and gender differences in time to collision at braking from the 100-car naturalistic driving study. *Traffic injury prevention*, 15 Suppl 1(sup1), S15–20. doi:10.1080/15389588.2014.928703.

Pinheiro, J., Bates, D., DebRoy, S., Sarkar, D., and R Core Team (2015). *nlme: Linear and Nonlinear Mixed Effects Models*. URL `http://CRAN.R-project.org/package=nlme`. R package version 3.1-119.

Appendix A. POST STRATIFICATION WEIGHTS

Table A.1 lists the proportion of registered drivers in the entire U.S. (Federal Highway Administration, 2012) and in the 64-driver group of 100-Car drivers examined for this study. The final column lists the post stratification weight used for all analyses in this study.

Table A.1. Post Stratification Weights for Age Group and Gender

Age Group and Gender	% Drivers	% Sample	Weight
Novice, Female	2.8%	9.4%	0.30
Novice, Male	2.9%	9.4%	0.31
Young, Female	7.7%	7.8%	0.98
Young, Male	7.7%	23.4%	0.33
Middle, Female	17.7%	4.7%	3.78
Middle, Male	17.6%	21.9%	0.80
Mature, Female	22.3%	10.9%	2.03
Mature, Male	21.4%	12.5%	1.71

Evaluation of Car-2-X Scenarios for Automated Driving

Marc Bechler*, Amira Horozovic*, Robert Kastner*

* Honda R&D Europe (Deutschland) GmbH
Germany, Europe (e-mail: :{Marc_Bechler | Amira_Horozovic | Robert_Kastner}@de.hrdeu.com).

Abstract: Car-to-X technology enables vehicles to directly exchange information with other vehicles or with roadside infrastructure components using standardized communication and message protocols. Such a communication technology is necessary to deploy cooperative intelligent transport systems (ITS), which make driving safer, more efficient and more convenient. Therefore, several cooperative Car-to-X use cases were defined to improve road safety and traffic efficiency, which will be introduced in different stages. In this paper, we are evaluating major use cases of the early deployment phase – such as electronic emergency brake lights, traffic jam ahead, or weather warning – with respect to their suitability to automated driving. We will see that their current specification only have minor contributions for improving automated driving scenarios. However, we will also see that by improving these use cases we may achieve a significant impact on automated driving technology. Moreover, our evaluation shows that Car-to-X needs to be considered as an essential base technology for cooperative automated driving scenarios.

Keywords: Car-to-X Communication, Automated Driving, Cooperative ITS.

1. INTRODUCTION

Car-to-X technology enables vehicles to directly exchange information with other vehicles or with roadside infrastructure components, as illustrated in Fig. 1. Therefore, vehicles communicate with each other using particular communication technology, such as the ITS G5 communication technology in Europe [Kosch et al (2012)]. The original goal of Car-to-X technology was to improve both road safety and traffic efficiency by several cooperative services. However, cooperation in this sense means that such a standardized system has to work independent of vehicle types, vehicle brands, or manufacturers of infrastructure components. However, standardization – and global harmonization –among so many stakeholders is a rather complex task. Therefore, cooperative use cases based on Car-to-X technology will be introduced in different stages: in the early deployment phase, warning systems like the electronic emergency brake lights, hazard warnings, green light optimal speed advisory or road works warning will be introduced. At a later stage, more complex and assisting cooperation functionality will follow.

Car-to-X communication is based on exchanging messages among vehicles or between vehicles and infrastructure components. Therefore, two message types are specified for Car-to-X communication [Kosch et al (2012)]:

- Cooperative Awareness Messages (CAM) are exchanged periodically among all entities in order to distribute basic vehicle and infrastructure information such as the current position, vehicle type, speed, acceleration, and other information.

- Decentralized Environment Notification Messages (DENM) are sent only in case of special events, such as a warning for other entities in the vicinity.
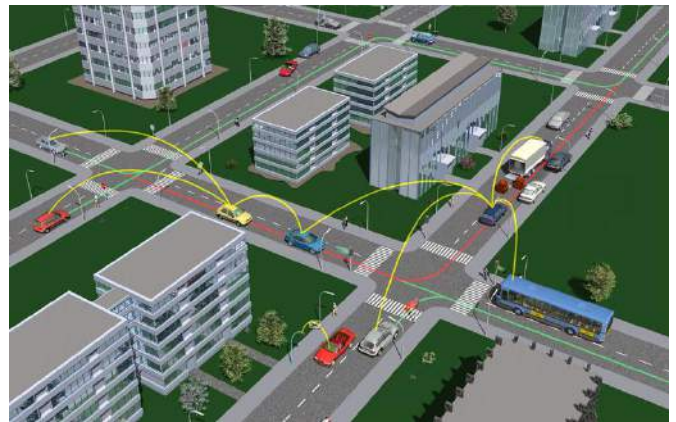

Fig. 1. Car-to-X scenario according to ETSI (and Car-to-Car Communication Consortium) [Car-to-Car (2015)].

In the past years, the rapid development in information technology, data processing and automotive-grade computation capabilities paved the road for automated driving scenarios, which requires complex algorithms, lots of sensor information, as well as environmental and context information. This way, automated driving is definitely one the most challenging future vision in automotive technology. It will be also introduced in different stages with different feature sets: today, we already have systems on the market that allow to park a car automatically ("park assistance") or to follow another car driving in front automatically ("traffic jam assistance"); but the final vision would be a car, which is able to drive completely autonomously without any driver

interaction. So far, several car manufacturers and other companies showed prototypes for automated driving, such as Google, Mercedes, BMW, Audi, or Honda. These prototypes are already able to drive in an automated way in defined conditions or on specially prepared tours. The basic algorithms being used typically rely on sensors sensing their environment as well as the availability of a huge amount of information about the environment.

In this paper, we will examine the early Car-to-X use cases with respect to their contribution to automated driving. Therefore, we will first discuss in section 2 some important sensing technologies necessary for automated driving. We will also see how Car-to-X systems will be integrated in such a technology framework. Section 3 then discusses selected (but important) Car-to-X uses cases from the early deployment phase with respect to their contribution to automated driving. We therefore will focus on both the weaknesses as well as the potential of the use cases, and we will also show what would be needed in order to improve their contribution to automated driving scenarios. Finally, section 4 evaluates the results from a more global perspective and concludes this paper.

2. CAR-TO-X FOR AUTOMATED DRIVING

Before we are actually able to evaluate existing Car-to-X use cases with respect to their usefulness for automated driving, we first have to take a closer look on how Car-to-X will be integrated into the framework for automated driving.

2.1 Basic Technology for Automated Driving

In general, the most important part for automated driving is the sensing and interpretation of the environment around the vehicle. Current state-of-the-art vehicles therefore rely on several sources, which provide information about the environment of the vehicle. These sources have different sensing characteristics and capabilities, as illustrated by the following examples, which are illustrated in Fig. 2 (see also [Australian Communications Authority (2001)]):

- Sensor systems based on radar technology or lidar technology typically scan the near range and midrange of the vehicle for relevant. Such sensing technologies are nowadays used for various driver assistance systems. Examples include front radar for adaptive cruise control (ACC) or Honda's iACC (intelligent ACC), or for emergency braking. Radar technology is also used for sensing the area behind a car, which can be used for park distance control available in many cars today, or for Honda's Cross Traffic Alert, which warns the driver for crossing cars while driving backwards out of a parking lot. Finally, radar sensors on both sides of a car are typically used for blind spot detection, which is also available in many cars today.

- Camera-based systems are typically used for sensing the front area of the car. Systems could be based on infrared cameras, common mono cameras, or stereo cameras. Powerful image processing algorithms thereby scan the

camera information for relevant information, such as traffic signs, persons on the road, other vehicles (or obstacles) in front of the car, or (in case of stereo cameras) they are able to scan the surface of the roads. This information is typically used by different driver assistance systems, such as traffic sign recognition, or (together with radar-based information) for realizing City Break Assistance system. Road surface scanning by stereo camera is nowadays used for the Magic Body Control system by Mercedes-Benz, which adapts the damper setup based on the detected road surface condition. Moreover, camera-systems typically are used to identify markings on the road. Such information can be used for lane keeping assistance, where the car notifies the driver (or even automatically keeps the car within the lane) when leaving the current lane without activating the turning lights.

- Using cellular communications, the car also has access to environmental information provided by third party service providers. Examples include traffic flow information (or congestions on the road) provided by suppliers like, e.g., INRIX, TomTom ore HERE, or it may even provide information within an ecosystem of other vehicles, such as the Mercedes-Benz Drive Kit Plus, which sends events marked by the driver of a Mercedes-Benz to other Mercedes-Benz cars in the vicinity of the event.
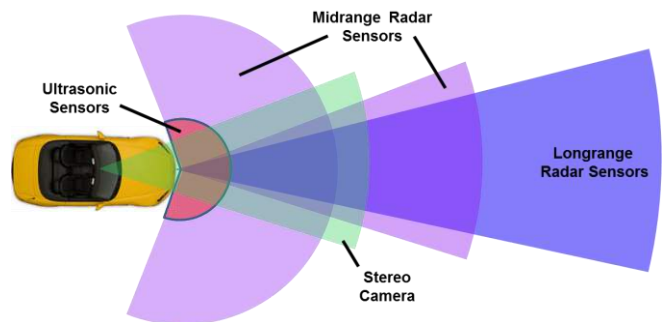

Fig. 2. Typical sensing technology used in current cars (for front detection).

From this point of view, a Car-to-X communication system is considered as an additional sensor technology, which provides further information about the environment of the car. Car-to-X technology therefore provides information from other Car-to-X-enabled vehicles in the vicinity, which typically cover short range to midrange area around the vehicle. Examples for information provided by Car-to-X communication are periodically transmitted information about positions, speeds, turn indicators, vehicle type, accelerations etc. of other Car-to-X-enabled vehicles in the vicinity, or events like hard braking vehicles, vehicles having an accident, or information from road infrastructure such as traffic lights information, traffic signs, or construction sites on the road. Warnings, however, are typically "multi-hopped", i.e. this information is forwarded by the entities to a certain degree, resulting in a larger coverage area.

This information is used to interpret the situation around the vehicle. The information is partially redundant. Hence, it

needs to be fused by each vehicle with the available sensors' information. For example, information about other vehicles in front detected by both the radar system and the camera of the car must be consolidated to improve the quality of the situation interpretation in order to avoid misinterpretations. The result of this interpretation is typically reflected in the electronic horizon of the advanced driver assistance system (ADAS) deployed in the vehicle.
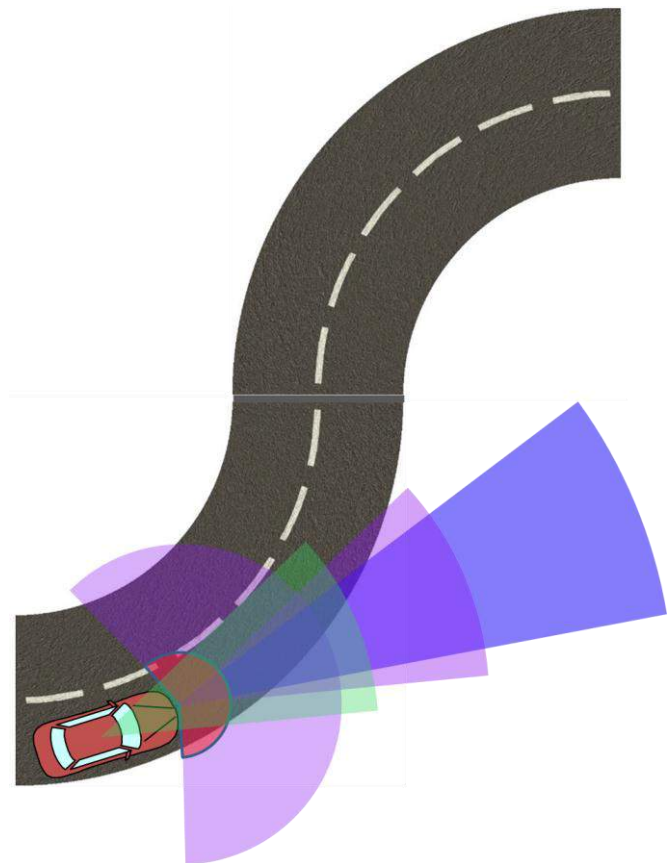

Fig. 3. Example: sensor detection on curvy roads.

Another important technology for automated driving is the availability of high-definition maps (HD maps). Such maps not only provide precise information about the streets and their properties, they also have to support detailed information about lanes, lane markings, and landmarks. Respective map-matching algorithms, which map a vehicle's current position onto the current street in the map, also must be able to map the vehicle onto the lane it is currently driving. Therefore, positioning also has to take into account other vehicle parameters (such as wheel speeds, steering angle) to improve the accuracy of the vehicle's own position. Obviously, this position must be precise enough to map the vehicle onto the lane it currently drives – probably in combination with information coming from other sensors like, e.g., the front camera system. HD maps are important for automated driving, because they are the basis for planning trajectories. Such a planning algorithm is one of the most important aspects for the convenience of automated driving: it avoids dangerous situations on curvy roads, where an automated driving car has to adapt its speed in time before a dangerous curve, which is out of sight of the car's sensors.

Thus, the automated driving car does not have to brake hard before the curve. This scenario is illustrated in Fig. 3, where sensor systems only "see" a very small area of the road ahead, and thus cannot directly recognize that this will be a dangerous curve.

Another very important requirement for Car-to-X-based systems being used for automated driving is the automatic detection of obstacles. Obstacles have to be detected automatically by the car – and not triggered by the driver as this is realised, e.g., for the Drive Kit Plus by Mercedes-Benz. A system where the driver manually has to trigger events (like lost goods, pedestrians or animals on the road, or wrong-way drivers) is of no use for automated driving, and may even be dangerous: the information is highly unreliable, because drivers often do not trigger the events while driving, they may play around with the system and generate false messages, and it may be even dangerous because using the system may distract the driver especially in dangerous situations. This way, it is very important that the information for automated driving is generated automatically by a reliable algorithm in order to ensure a suitable quality of the information. It is worth mentioning that this reliability is of importance not only for the own vehicle, but also for the other vehicles in the vicinity, which will receive this information by Car-to-X communication.

3. CAR-TO-X USE CASE EVALUATION

In this section, we will closely investigate selected early Car-to-X use cases with respect to their suitability for automated driving. We therefore will briefly describe each use case and its characteristics, and we will outline the shortcomings and potentials for automated driving. In the early deployment, Car-to-X-based system will provide both Car-to-Car and Car-to-Infrastructure use cases. We will take our focus on the electronic emergency brake light, approaching emergency vehicle, weather warning, traffic jam ahead, hazard warning, and road works warning in our evaluation.

3.1 Car-to-X Technology for Automated Driving

Before we evaluate the use cases, we first discuss some common features of Car-to-X technology, which need to be considered. In general, there are three characteristics that are of relevance for automated driving:

1. *Positioning.* Car-to-X technology was originally developed without mandatory deployment of map information. This way, positioning is basically achieved by standard positioning systems such as GPS, GLONASS or the upcoming GALILEO system. This positioning can be improved by using vehicle sensor data, achieving high position accuracy. However, Car-to-X technology provides neither map matching nor a sufficient accuracy to determine which lane a vehicle is driving. This way, neither roads, the course of roads, nor lanes are supported.

2. *Imprecise Information.* The information generated by Car-to-X use cases is often not very accurate. For example weather information is typically very coarse (e.g., "storms in southern Germany"). Thus, it does not reflect the current real situation around the vehicle.

3. *Partial Deployment of Car-to-X Technology.* Even with a shipping rate of 100% of all new vehicles, it will not be possible that all vehicles driving on the road will be equipped with Car-to-X technology in the next 20 years. This way, there will still be several vehicles on the road, which will not support cooperative ITS. Also, other traffic participants like, e.g. bicyclists may not be considered by Car-to-X technology.

This way, it is important to mention that Car-to-X technology does not provide information in the accurate and reliable way required for automated driving. Consequently, an automated driving vehicle must be able to sense its environment autonomously with its own sensor systems to generate the environment model with the accuracy required for automated driving.

3.2 Electronic Emergency Brake Light (EEBL)

In this use case, a hard braking vehicle sends a respective Car-to-X message about the strong deceleration to other vehicles in its vicinity. This way, drivers of following vehicles are warned right in time about the hard brake and, thus, can adapt their speed accordingly.

In its current specification, EEBL does not have any real benefit for automated driving. This is due to the fact the trigger condition basically relies on the speed reduction due to braking, which first needs to be measured, before in can be communicated. It also requires that both vehicles – the braking vehicle and the following vehicle – are equipped with Car-to-X technology. Furthermore, since EEBL is based on positions only – which may be highly imprecise due to the location technology being used – it is often difficult to determine the relevancy of this information: the information is typically of relevance for a following vehicle only if it drives on the same lane. However, the inaccuracy of positioning does not allow for lane-based mapping of the vehicles, which may result in false warnings.

Finally, the advances in sensor and data fusion technology in the past years resulted in automated breaking vehicles based on information from radar and camera systems. This way, EEBL in its current specification does not have any additional value to automated driving. However, it could be useful for the validation of the existing sensor system used to identify braking vehicles in front. An enhanced version of EEBL also can be beneficial if it is possible to detect or even predict hard braking scenarios earlier, e.g. based on a vehicle's own radar and camera system. This way, the information about a hard braking would be available in subsequent cars earlier than these cars are able to detect the braking by their autonomous sensors. Such a solution would be also highly valuable for a cooperative adaptive cruise control (ACC), because it allows a proactive control of the ACC algorithms. Current ACC systems are controlled reactively, which may cause an inconvenient driving

behaviour, if the ACC shows knock-on braking effects if several cars follow each other using the same ACC system. For such purposes the positioning of the system of the cars must be highly accurate, since a lane-matching of the position onto the HD map has to be available.

3.3 Emergency Vehicle Warning (EVW)

If an emergency vehicle approaches, EVW notifies about this potentially dangerous situation by indicating the direction in which the emergency vehicle is driving. Therefore, the emergency vehicle sends an emergency vehicle message in case it activates its light bar.

Although the relevance of an emergency vehicle warning depends on precise position information combined with street information EVW is very useful for automated driving, because it may have an effect on the automated driving strategy. Especially on motorways, drivers are urged to give way to approaching emergency vehicles; and in case of a traffic jam, drivers are urged to give way by forming a corridor for the emergency vehicle. This behaviour has to be implemented in the automated driving algorithm of the car, or the automated driving system has to give back the control about the car to driver in case of an approaching emergency vehicle. Even a warning about an emergency vehicle on a neighbouring lane (which has no relevance for the own vehicle) can be useful because the driver typically will realize the blue light bar or the siren of the emergency vehicle and, thus, may be warned about this distraction in advance.

3.4 Weather Warning (WW)

C2X-based weather warning functionality informs a vehicle about potentially dangerous weather situations, such as fog, heavy rain, snow, or black ice on the roads. The information about weather conditions may be generated either from another vehicle using the on-board sensor systems, or respective road conditions may be generated by road sensors or third party weather information providers, which are transferred to the vehicle using road-side stations. This way, weather warning could be both, a Car-to-Car use case as well as a Car-to-Infrastructure use case.

Road conditions in general are highly useful for automated driving, because it has an impact on the driving strategy for the automated driving system. For the example of slippery roads or restricted sight due to heavy rain, snow or fog, an automated driving car may have to reduce its speed, or the driver even has to take over the control of the car, because sensors and/or camera will not work as required under these conditions. However, it is important that such information must be highly reliable, and vehicles (or road sensors) must be able to detect respective situations highly accurate. Moreover, the automated driving functionality of a car must not rely on this information exclusively, because it cannot be guaranteed that this information is available for the route the car drives in an automated way, so an automated driving car must be able to detect road conditions in order to react in an appropriate way.

The contribution of weather warning to automated driving is two-fold. For pure car-to-car functionality, it is rather worthless since the trigger conditions for dangerous road situations do not meet the reliability requirements: Fog needs to be detected automatically and reliably (e.g., by a camera-based system) and not by activated fog lights, and slippery roads require sophisticated friction value estimators, which are currently not available in many cars. Moreover, to improve the quality of this information, respective crowd sourcing mechanisms may be deployed to validate and verify the road conditions in a backend system. This way, the information generated by other cars is almost worthless for automated driving. On the other side, current sensor systems for road condition surveillance (e.g., ice detectors, water level detectors) are nowadays able to provide reliable information or estimations about dangerous road conditions using Car-to-Infrastructure communications, which can be highly useful for the automated driving systems. This enables the car to return the control of the car to the driver in advance, so the driver has enough time to get back into the driving context and can take over the control of the car seamlessly and safely.

In contrast, third party weather information, such as heavy storms, snow, rain, etc. is almost useless for the automated driving. This is due to the fact that the information does not reflect the road conditions, and a mapping from weather information to precise road conditions is not possible in a reliable way.

As a result, WW in its current specification is not very useful for the automated driving system of car. However, with an improved specification of the system together with suitable sensors in mass market vehicles providing reliable information about road conditions, such a system is highly useful for improving the automated driving functionality of a car – although the car always has to be able to drive automated without relying on this information.

3.5 Road Works Warning (RWW)

Road works warnings are typically generated in case of construction sites, which could be of static (e.g., renewing the road surface) and of dynamic nature (e.g., mowing the grass besides the street). Such construction sites are highly challenging for automated driving cars in several ways:

- Entering/Leaving the construction site is very confusing for sensor detection and motion planning – even for experienced drivers it is sometimes difficult to identify the traffic routing in a construction site.

- Lanes are often narrow, vehicles from other lanes may drive onto neighbouring lanes, lane markings may have different colours or may even be rubbed away partially. Moreover, there may be "strange" signs in the construction site, e.g. indicating shifted driving on two lanes without overtaking.

- The boundaries of lanes are "marked" different, e.g. by using plastic pylons or high boundaries made of concrete or metal, which cannot be run over by the cars. This makes it difficult for the car's sensor systems to predict the lane markings in a reliable way.

Moreover, construction sites themselves are hard to detect by a vehicle's sensor system; construction sites do not have typical characteristics, they always look different in different countries and may have to follow different regulations. This way, detection is basically limited to camera systems only.

For automated driving cars, RWW is an important use case for several reasons. On the one hand, passing a construction site has a significant impact on the car's automated driving strategy. On the other hand, construction sites often use "modified" lanes, which often do not match with the available HD map material. This way, the driving strategy must not rely on HD map material (for motion planning) exclusively, but the vehicle also must be able to drive in an automated way completely by its own sensor information. If this is not possible, RWW will support automated driving by indicating the algorithms to give back the driving control back to the driver right in time, before the car reaches the construction site. To overcome this limitation, RWW needs to provide highly precise information about the construction site, its routing lane characteristics, and ideally the traffic flows on each lane. This way, an automated passing of the construction site can be realized efficient and comfortable, e.g. by choosing the quickest and safest lane.

3.6 Hazard Warning (HW)

Hazard warning use cases basically comprise two scenarios: in the breakdown vehicle scenario, a vehicle having a defect or an accident notifies following vehicles about the dangerous situation. This is triggered when the vehicle does not move and has activated its hazard lights, or if the vehicle system detected a crash. In the second scenario, a vehicle warns about dangerous situations on the road caused by obstacles (e.g., lost goods), pedestrians, or animals on the road. In contrast to the breakdown vehicle scenario, the message generation has to be triggered by the driver manually, because an automatic detection basically requires camera systems which will not be available in cheaper cars.

HW also may comprise infrastructure support. For example, if a traffic management centre realizes a hazardous situation on the road, it may generate a respective HW message in the traffic management centre, transfers this message to related roadside stations in the vicinity of the hazard, where it is sent to the passing vehicles.

Like EEBL, the HW use case does not have a significant benefit for automated driving, because it is almost impossible to determine the relevance of the hazard being received. This is due to the fact that no lane-specific (or street-specific) positioning of the own vehicle and the hazard is possible: often, obstacles or defect cars are located at the side of the road, which has no effect on the passing vehicles, whereas an accident typically occurs on the road and sometimes may result in a blocked lane. This way, many false alarms about hazards may be generated, which is of no real benefit for automated driving. However, a more accurate positioning as well as an automatic detection of the obstacles, pedestrians or animals on the road may help to validate the detected information by the autonomous sensor systems of the car, making them more reliable.

3.7 Traffic Jam Ahead (TJA)

The detection of traffic jams is very important for automated driving, because it is a typical and common situation for driving on motorways in many countries, where automated driving will play an important role. It is also a highly challenging situation, because it requires stopping the car from potentially very high speeds. As a result, TJA using Car-to-X technology is a highly useful functionality for automated driving. Although an automated driving car must be able to detect the tail of a traffic jam by its own sensor systems, the car requires a rather long distance to slow down in time. For example, in case of 120 km/h an emergency brake on wet grounds requires a minimum of 80m to stop the car. However, such emergency brakes are neither comfortable nor convenient for the driver. If the car gets a TJA warning before the sensor systems can detect the end of the traffic jam, the autonomous driving strategy can react accordingly, e.g. to preventively reduce speed in order to approach to the traffic jam very smoothly. Therefore, it is not that important to know the exact position of the last car in the traffic jam; it is basically sufficient to know that there is a traffic jam ahead.

As a result, we consider TJA as a highly useful functionality for automated driving, which is important information to smoothen the autonomous driving strategy. Nevertheless, a good prediction of the exact end of the traffic jam may improve this further on. Also, a street dependent matching of this event could be very useful in order to determine if the TJA is relevant for the automated driving car or if it is on a different (and not relevant) street.

4. EVALUATION & CONCLUSION

Our examination shows that the early Car-to-X use cases being deployed will not provide a significant contribution to automated driving technology. In particular, this is due to the fact that the partial deployment in both vehicles and infrastructure components, positioning and information accuracy do not meet the precision requirements for automated driving. As a result, a vehicle must be able to detect all these situations by its own sensor systems autonomously, from which one may deduce that Car-to-X technology is of no use for automated driving. This is certainly true for the basic automated driving algorithms implemented in the cars. However, in the mid term, Car-to-X will become an important technology to make automated driving more comfortable, more efficient and, thus, more convenient for the driver. This factor will be very important for the driver acceptance of automated driving cars, as illustrated by the following examples:

- *Smooth Braking.* Since relevant information may be available in time, a car can adjust its speed in a comfortable way without the need for hard braking. For example, in case of a traffic jam ahead warning, the automated driving car can reduce its speed very early to stop right in time at the end of the traffic jam. In case the traffic jam needs to be detected by the car's sensors very late, the car needs to break hard, which makes traveling very inconvenient (and unacceptable) for the passengers. A driver would likely not like the system if his coffee permanently spills over his cup due to hard braking.

- *Efficient Driving.* For the example of traffic jam ahead or road works warning, the automated driving strategy can be adapted to the situation to approach to the end of the traffic jam very efficiently. This may include utilization of the optimal strategy for powertrain configuration, but also, e.g. to switch of the engine very early in order to save fuel.

- *Safe Driving.* Since relevant information will be available at the time it may be relevant, safety is also increased. For example, in case the traffic or environment situation is not suitable for automated driving (e.g., highly complicated and confusing road works), the driving control must be given back to the driver right in time, which is typically hundreds of meters before the event occurs. Therefore, the driver has sufficient time to get back into the driving context in order to take over the control. Car-to-X technology will help to provide such information very early, whereas autonomous sensing of the cars may be able to detect the event at the time it occurs, potentially resulting in a "recovery mode" to stop the car in case the driver is not able to immediately take back the control about the car.

Of course, such events will not always be available by Car-to-X technology; hence, Car-to-X technology will not be able to avoid such situations like an emergency brake completely. But even if an 80% availability of such information is possible, this highly improves comfortable and efficient automated driving and, thus, helps to significantly improve the acceptance by the drivers.

However, for the future vision of cooperative automated driving, Car-to-X is an important and indispensable technology, because it enables cooperative scenarios among vehicles. For example, imagine the following typical situation: a car enters the acceleration lane of a motorway and now has to decide if it will filter in behind or in front of an automated car driving on the motorway. This typical and frequent situation cannot be solved with autonomously sensing cars: without cooperation both cars may accelerate (or slow down) at the same time, resulting in strange, uncomfortable and even dangerous automated driving behaviours of the cars. This way, a quick deployment of Car-to-X technology is an important precondition for future cooperative automated driving scenarios.

REFERENCES

Australian Communications Authority (2001). *A Review of Automotive Radar Systems – Devices and Regulatory Frameworks.*

Car-to-Car Communication Consortium (2015). *http://car-to-car.org.*

Kosch, T., Schroth, C., Straßberger, M., Bechler, M. (2012). *Automotive Internetworking.* Wiley.

Improvement of Elderly Drivers' Acceptability for Proactive Collision Avoidance Using Passive Information Sharing

Takuma Ito*, Tatsuya Shino*, Minoru Kamata*

*The University of Tokyo, Kashiwanoha, Kashiwa, Chiba, 277-8589, Japan
(Tel: +81-4-7136-6683; e-mail: ito@iog.u-tokyo.ac.jp).

Abstract: In this research, we focus on improving acceptability of proactive collision avoidance systems to elderly drives by using passive information sharing with drivers. In this paper, the information sharing mainly consists of visual contents. As a result of the evaluation experiment by a driving simulator to investigate the effectiveness of the information sharing, we confirmed that passive information sharing were able to improve the acceptability.

Keywords: Cooperation between Drivers and Assistance Systems, Human Machine Interface, Driving Simulators

1. INTRODUCTION

In spite of various development of safety systems for preventing traffic accidents, traffic accidents caused by elderly drivers remain a major issue. Since elderly drivers' physical and cognitive abilities are declined due to aging, their risk of causing traffic accidents and their mortality rate are higher than those of young drivers. Thus, more advanced safety technologies focusing on their features are required.

To this end, our research group is trying to develop an intelligence for automated vehicles by constructing functions that parallel those of human drivers to fully support elderly drivers(Inoue 2014). As discussed in our previous research(Shino 2014a), we proposed the proactive collision avoidance systems, which softly intervene to the vehicle controls several seconds before a driver enters into a dangerous situations. Although our final goal is to realize a proactive collision avoidance system based on "shared control" that actively change their contributions in accordance with the perceived risks of the surrounding situation, as the first step, we focus on a proactive collision avoidance system based on "switching control" that is triggered by some kind of risk index. Fig. 1 shows a conceptual schematic of proactive collision avoidance system by switching control between human driver and intelligence for automated vehicle. One of characteristics of proactive collision avoidance systems based on such intelligence is that the vehicle proactively intervenes operations of the drivers for the purpose of not approaching the risky situations. Thus, we call such systems as "proactive intervention systems" in our researches.

Further, to utilize such proactive intervention systems, investigations of acceptability are important as well as technological developments because drivers do not use unacceptable safety devices. Thus, we previously focused on the acceptability of proactive intervention systems to elderly drivers; further, we conducted driving simulator experiments for the initial investigation of the acceptability of two kinds of proactive intervention systems: namely proactive braking intervention and proactive steering intervention.

As a result of the initial experiment, we confirmed that more than half of elderly drivers who took part in our initial experiment accepted the proactive braking intervention system while many elderly drivers did not accept the proactive steering intervention system. In addition, to improve the acceptability of both systems much more, we proposed some approaches regarding technological and non-technological ways.

Based on the results of initial investigation, in our other researches(Ito 2014) (Shino 2014b), we proposed "information sharing" that provides some kinds of visual contents of internal data of the systems to the drivers. In contrast to existing warning systems, which aim at making drivers behave appropriately, information sharing aims at providing the drivers with the information to let drivers accept the behaviors of the proactive intervention systems. In addition, we implemented prototype contents for information sharing by using visual modality, and conducted the investigation of the basic characteristics of information sharing for proactive intervention systems. As a result of experiments, we confirmed what kinds of visual contents are necessary, and proposed the way of improving the previous implementation of information sharing.

Fig. 2 shows a schematic of the research flow regarding improvement of acceptability of proactive intervention systems and the position of this paper. As shown in Fig. 2, in this paper, we focus on modification of the visual contents implemented in our previous research; further, we aim at investigating the effectiveness of them for improving acceptability to elderly drivers.
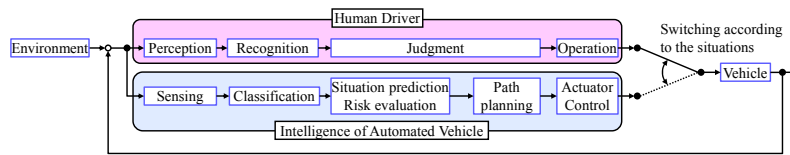
Fig. 1. Conceptual schematic of a proactive collision avoidance systems based on switching control
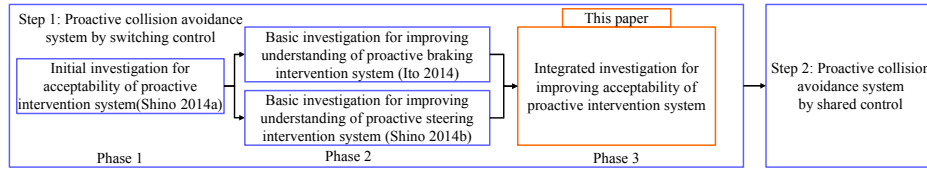

Fig. 2. Research flow regarding improvement of acceptability of proactive intervention systems

2. IMPROVEMENT OF VISUAL CONTETS FOR INFORMATION SHARING

2.1 Proactive Collision Avoidance Systems by Switching Control

Fig. 3 shows a schematic of overhead view of a situation of a proactive braking intervention. Unlike in many other countries, vehicles are driven on the left side of the road in Japan. Thus, as shown in Fig. 3, the self-vehicle drives on the left side. In this situation, the self-vehicle detects the blind spot by the parked truck, and predicts a pedestrian walking into its path. Then the self-vehicle proactively intervenes to the braking with soft deceleration. In contrast to the existing automatic emergency braking systems, our proactive collision avoidance systems aim at avoiding risky situations owing to the prediction of surrounding traffic situations. Regarding the technological development, since our collaborator(Hasegawa 2014) was attempting to develop details of vehicle controls for similar situations simultaneously with our trials, we conducted this research by using the simplified vehicle controls imitating the proactive concept, which are described in the following section.
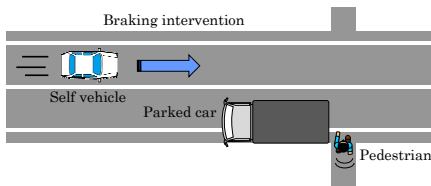
Fig. 3. Overhead view of a situation of proactive braking intervention

On the other hand, Fig. 4 shows a schematic of overhead view of a situation of a proactive steering intervention. In this situation, the self-vehicle detects a cyclist and a parked car, and predicts a lane change of a cyclist. Then the self-vehicle proactively intervenes to the steering with soft yawing motion. Similar to the case of proactive braking intervention, we used simplified controls of steering intervention, which are described in the following section.
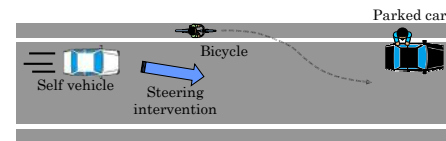

Fig. 4. Overhead view of a situation of proactive steering intervention

2.2 Information Sharing for Improving the Acceptability to the Elderly Drivers

Because intelligent vehicles with various sensors are sometimes able to recognize surrounding situations that elderly drivers would not observe because of their decreased abilities, elderly drivers sometimes may not accept the behaviors of proactive collision avoidance systems because of not understanding when, where, why, and how the systems avoid the risky situations. Thus, it is important to provide the elderly drivers with information regarding the behaviors of intelligence of automated vehicle.

Fig. 5 shows a conceptual schematic of information sharing. Based on the internal numerical data of intelligence of automated vehicle, some kinds of information provision HMI device provide the contents of information. In this paper, for avoiding confusing discussion, we use the term of "information" for the abstract discussion while we use the term of "contents" for the discussion of implementation.
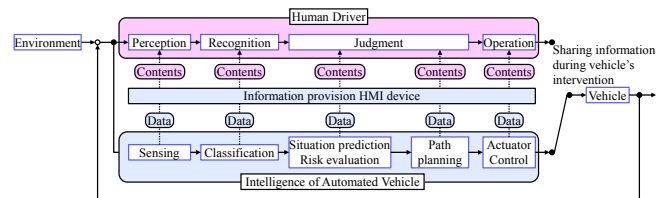

Fig. 5. Conceptual schematic of proactive intervention with information sharing

Information sharing is apparently similar to the existing warning systems on the point that both of them provide

information to the drivers. Although an existing research(Satomi 2009) pointed out that some kinds of existing warning systems had limitations of providing information to the elderly drivers in emergent situations, purpose and concept of information sharing are different from those of existing warning systems.

For example, an existing automatic emergent braking system activates the alert for warning drivers at first. Then, the system starts to assist driver's operation. When the situations become critical, the system starts to avoid collision automatically with indicating the system activation. In this case, since the purpose of the alert is to warn the drivers for make them behave appropriately, precise understanding of provided information is necessary. On the other hand, regarding the proactive intervention systems with information sharing, before the situations become critical, the system starts to intervene the driver's operations. At the same time, HMIs start to provide various kinds of information for sharing states of various functions of the intelligent vehicle. In this case, since the purpose of information sharing is to let the drivers accept the proactive systems by gradual understanding of the status of the proactive systems with corresponding occurrence of feeling the benefit and the trust, precise understanding of provided information is not necessary. In addition, the drivers do not need to behave appropriately because proactive systems control the vehicle appropriately during interventions. Thus, important point is not how the elderly drivers change their behaviours by the provision of visual contents, but how the elderly drivers feel the intervention of the proactive systems by the provision of visual contents.

Based on the above-mentioned discussions, we constructed prototypes of visual contents for information sharing. Regarding the modality of HMI devices, since one of characteristics of information sharing is to provide various kinds of information with enough time, we considered that using visual modality as main resources and auditory modality as sub ones seemed beneficial. Thus, we assumed a head up display (HUD) as the HMI device.

2.3 Basic Investigation of Information Sharing in our Previous Research

In our previous research, main focus point was to investigate what kinds of visual contents were necessary, and what kinds of visual contents we could reduce. Thus, we prepared various kinds of elemental visual contents. In addition, we assumed relatively strong visual stimulation of provided visual contents, which had the possibility of annoyance and disturbance, since we aimed at making elderly drivers forcibly perceive the provided visual stimulation. Based on these assumptions, we compared the effectiveness of single visual contents with those of combination use of multiple visual contents.

Based on the experimental results, we confirmed following ways of improving the visual contents for each proactive intervention system.

- Although almost all of our previous visual contents could tell the intended meaning, some visual contents were needed to be redesigned.

- Combination use of multiple visual contents had the possibility of improving the feeling of the benefits and the trust on the assumption of redesigning some components of previous visual contents.

- Combination use of multiple visual contents might result in the disturbance of driving due to complexity of visual stimulation.

Regarding the necessity of redesigning the previous visual contents, because we designed them without adjusting moderately for actually confirming the potential problems, we need to brush up them in this research from the viewpoint of integrating elemental components moderately with reducing the annoyance. Fig. 6 shows our stances of phase 2 and phase 3 of our researches. Based on the results of brushing up of previous visual contents, we need to confirm the result of modification regarding whether or not the modified visual contents can appropriately tell the meaning of provided visual contents, and whether or not the modified visual contents can appropriately let elderly drivers feel the benefits and the trust of the proactive intervention systems. Furthermore, we need to investigate the effectiveness of information sharing to improve the acceptability of proactive intervention systems to the elderly drivers.
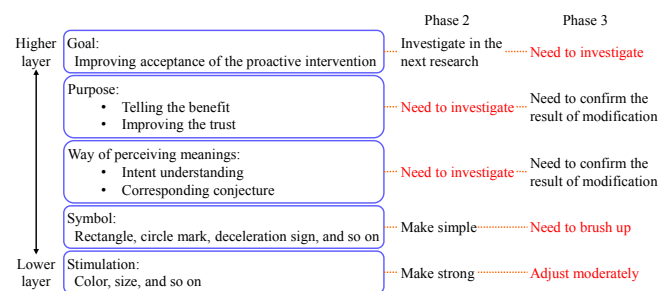

Fig. 6. Research stances regarding the elements of visual contents

2.4 Improvement of Visual Contents

Based on the results of previous experiments, we modified visual contents. Fig. 7 shows a schematic of time flow of proactive braking intervention with information sharing by modified visual contents. Horizontal axis indicates the time, and 0.0 s means the time when the vehicle pass through the conflict point of crossing pedestrian. The schematics above the timeline illustrates the corresponding situations and examples of visual contents over time. In this proactive braking intervention, we assumed that the vehicle had started to decelerate 5.0 s before the vehicle passed through the conflict point. Regarding information sharing of proactive braking intervention, we designed three kinds of visual contents: namely notification of detected risky traffic participants as an advanced notification of proactive braking intervention, notification of activating the systems and

remaining time of intervention, and complete notification of it. For the reference, Fig. 8 shows a schematic of time flow of proactive braking intervention with information sharing by previous visual contents. In contrast to the previous visual contents, we reduced the notification of all detected traffic participants, change the symbol of complete notification of breaking intervention, and weakened the stimulation of some visual contents.
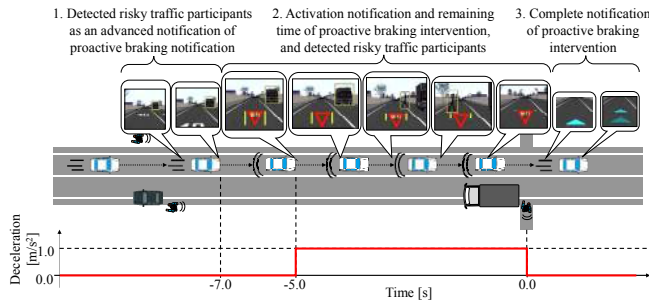

Fig. 7. Time flow of proactive braking intervention with information sharing by modified visual contents
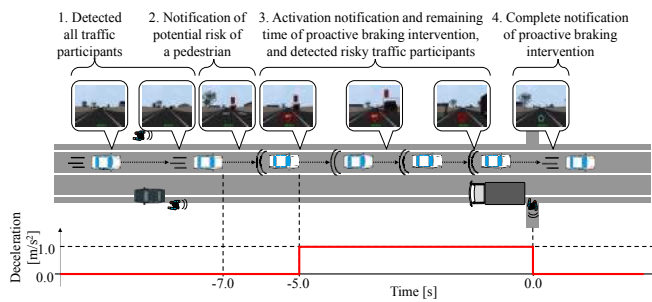
Fig. 8. Time flow of proactive braking intervention with information sharing by previous visual contents

On the other hand, Fig. 9 shows a schematic of time flow of proactive steering intervention with information sharing by modified visual contents. Similar to the case of proactive braking intervention, 0.0 s means the time when the vehicle pass through the point just beside the parked car. In this proactive steering intervention, we assumed that the vehicle had started to steer 5.0 s before the vehicle completed the steering intervention. Regarding information sharing of proactive steering intervention, we designed five kinds of visual contents: namely notification of a detected risky traffic participant, notification of the risk of collision to the parked car, notification of safety confirmation, advanced notification of activating the steering intervention, and planning path of steering intervention. For the reference, Fig. 10 shows a schematic of time flow of proactive steering intervention with information sharing by previous visual contents. In contrast to the previous visual contents, we reduced the notification of system status about the activation of intervention, adjusted the layout of displaying visual contents, and weakened the stimulation of some visual contents.
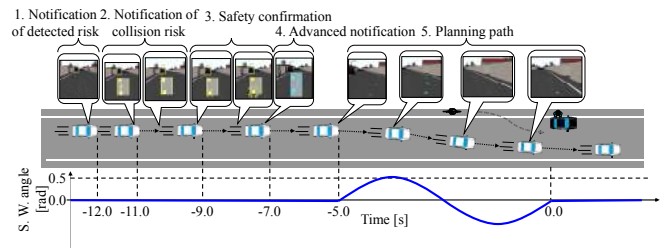

Fig. 9. Time flow of proactive steering intervention with information sharing by modified visual contents
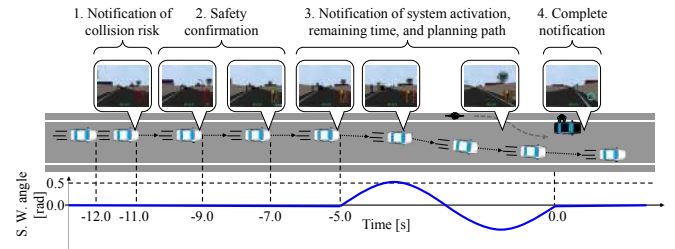

Fig. 10. Time flow of proactive steering intervention with information sharing by previous visual contents

3. EXPERIMENT

To investigate the effectiveness of information sharing to the elderly drivers, we conducted driving simulator experiments. The following protocols were approved by the School of Engineering at the University of Tokyo IRB for human studies. Written informed consent was obtained from all participants.

3.1 Experimental Participants

In our research, we recruited 12 healthy elderly drivers who were 65 to 75 years old (M = 70 yrs; SD = 3 yrs) as experimental participants. They had taken part in our previous experiments.

3.2 Driving simulator

Fig. 11 shows the appearance of driving simulator used in this experiment. This simulator had the following features:

- Three front screens for which the field of view was approximately 120° from the position of the driver,

- Two small displays for right and room mirrors,

- Motion platform via a Stewart link,

- Steering wheel with a servomotor that reproduced reactive torque, and

- Speaker systems that reproduced the sounds of surrounding simulated situations and of the vehicle's engine.

Regarding the motion platform, we set it to reproduce only the longitudinal and lateral accelerations for preventing motion sickness. In addition, we assigned 0.1 to the scale

factor of both accelerations for reproducing only the initial motion cues of braking intervention.

Fig. 11. Appearance of driving simulator

3.3 Experimental Scenarios

To investigate the effectiveness of modified visual contents, we set up two kinds of visual contents for each situation: namely modified visual contents and simply mixture of all visual contents which had been used in the previous experiments.

Fig. 12 shows the overhead view of whole experimental course for proactive braking intervention. This course contains four times of the situation of proactive braking intervention, as shown in Fig. 3. Experimental participants were told to drive the vehicle at 40.0 km/h. When the vehicle arrived at the position where the time to collision (TTC) to the unobservable crossing pedestrian was 5.0 s, vehicle started to intervene the braking proactively. The deceleration rate due to the proactive braking systems was set to 1.0 m/s^2. For setting up the basis of evaluations and reducing the order effect, visual contents were not displayed on 1st and 3rd situations, while they were displayed on 2nd and 4th situations.
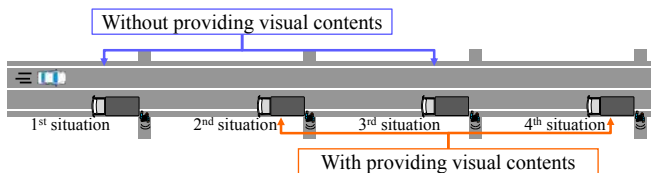

Fig. 12. Overhead view of whole experimental course for proactive braking intervention

Regarding the proactive steering intervention, we set up the similar experimental course which contains four times of the situation of proactive steering intervention, as shown in Fig. 4. Experimental participants were told to drive the vehicle at 30.0 km/h on this course. When the vehicle arrived at the position where the time to collision (TTC) to the parked car was 5.0 s, vehicle started to intervene the steering proactively. The maximum angle of sin-wave shaped steering input was approximately 0.52 rad. As a result of the steering intervention, self-vehicle moves approximately 2.6 m to the right side.

3.4 Evaluation Method

Similar to our previous research, most behavioural data, such as reaction time, operation amount, and so on, were not evaluated quantitatively because driver operations were largely invalidated by the switching control as shown in Fig. 1 during the given interventions. Thus, subjective evaluations are our main resources for analysis and discussion.

For the subjective evaluations, after each trial performed on the driving simulator had been completed, the experimental participants filled out questionnaires to evaluate the systems that they had experienced at that time. Based on the results of our previous research, we asked the following topics.

● Perception of the meaning of provided visual contents: "Compared to the condition without information, how much did you feel to better notice the following topics?"

For both proactive interventions

1. Reason of system activation

2. Surrounding risky traffic participants

3. Start timing of the system

4. Whether the systems is activated or not

5. End timing of the system

For proactive braking intervention

6. Activation of automated deceleration

For proactive steering intervention

7. Activation of automated steering

8. Planning path

9. Advanced safety confirmation

● Feeling of the benefit by information sharing: "Compared to the condition without information, how much did you feel that the system can realize followings?"

1. Avoid dangerous situations.

2. Reduce the number of traffic accidents.

● Feeling of disturbance by information sharing: "Compared to the condition without information, how much did you feel that the system disturbed you in your driving?"

● Feeling of the trust by information sharing: "Compared to the condition without information, how much did you feel distrust of the vehicle control of the system?"

● Acceptability W/O and with information sharing

For the condition W/O information sharing: "How much do you want to introduce the system into your own car?"

For the condition with information sharing: "On the condition that the information is always displayed, how much do you want to introduce the system into your own car?"

Every questionnaire was asked by 9-grade answer sheet. Regarding the feeling of disturbance, grades of answers indicate as following degrees:

Grade 9: They did not feel any disturbance.

Grade 7: They did not feel disturbance so much and they did not have any difficulty in driving.

Grade 5: They felt disturbance a little, but they did not have any difficulty in driving.

Grade 3: They felt disturbance so much that they had some troubles in driving.

Grade 1: They felt disturbance very much so that they had difficulty in driving.

Because sensitivity of evaluation results of each participant is different, the results of this evaluation do not have precise quantitative meaning. Important point is whether they felt difficulty in driving by the provided visual contents or not. In other words, whether the evaluation results are less than grade 5 or not, is the important point.

On the other hand, as for the other questionnaires, grades of answers indicate as following degrees:

Grade 9: They felt very much.

Grade 7: They felt modestly.

Grade 5: They felt same as the condition without any information.

Grade 3: They did not feel so much.

Grade 1: They did not feel at all.

As for the feeling of disturbance, since we used reversal grade, grade 9 was the best similarly to other evaluations. In regard to the results of these evaluations, whether they felt positively, neutrally, or negatively is important. In other words, whether the evaluation results are more than, equal to, or less than grade 5, is the important point.

4. RESULT

4.1 Perceiving the Meaning of Provided Visual Contents

Table 1 shows the evaluation results of understanding of intended meaning of provided visual contents during proactive braking intervention. Larger value indicates the better evaluations. Cells colored in blue, green, and red indicate respectively negative, neutral, and positive evaluations. Regarding the proactive braking intervention, modified visual contents keeps high evaluations although decrease of some evaluations results are confirmed, as is observable in table 1. Important point is that modification of visual contents in this research do not decrease the evaluation results to the negative level.

Table 1. Understanding of intended meaning of visual contents during proactive braking intervention

Intended meaning	Visual contents	1	2	3	4	5	6	7	8	9	10	11	12
Reason of system activation	Previous	9	9	7	8	9	8	9	9	9	9	8	9
	Modified	9	9	7	9	9	9	9	9	9	9	8	9
Surrounding risky traffic paticipants	Previous	8	9	9	9	9	8	9	9	9	9	8	9
	Modified	8	9	8	9	9	9	9	9	9	8	8	9
Start timing of the system	Previous	9	7	7	8	7	8	8	8	9	8	9	9
	Modified	9	9	8	9	9	9	8	9	9	9	7	9
Whether the system is activated or not	Previous	9	7	8	8	9	8	9	8	9	9	8	9
	Modified	9	9	7	9	9	9	9	8	9	8	9	9
End timing of the syste	Previous	9	9	7	9	9	9	7	8	9	9	8	9
	Modified	9	9	7	9	9	9	8	9	8	8	8	9
Activation of automated	Previous	5	9	8	7	9	9	8	8	8	8	8	9
	Modified	7	9	7	8	9	9	8	9	9	9	8	9

Similarly, table 2 shows the corresponding results during proactive steering intervention. Regarding the proactive steering intervention, modified visual contents improved the some evaluation results, especially those of participant 4. Based on the comments of participant 4, moderate adjustment of visual stimulation and layout of visual contents may had improved these evaluations. However, as for the evaluation results regarding planning path of steering intervention, evaluation result still remains negative level. On this point, participant 4 commented that he could not understand the meaning well due to rapid transition of visual contents over time. Thus, we need to improve implementation on this point. For other parts, we confirmed that modification of visual contents in this research does not decrease the evaluation results to the negative level.

Table 2. Understanding of intended meaning of visual contents during proactive steering intervention

Intended meaning	Visual contents	1	2	3	4	5	6	7	8	9	10	11	12
Reason of system activation	Previous	7	9	7	4	9	9	9	8	8	9	7	9
	Modified	8	9	7	9	9	9	9	9	9	9	7	9
Surrounding risky traffic paticipants	Previous	8	9	8	3	9	8	9	8	8	8	7	9
	Modified	7	9	7	9	9	9	9	8	9	9	7	9
Start timing of the system	Previous	9	9	8	3	7	9	8	8	7	9	7	9
	Modified	9	9	8	9	8	9	9	9	9	9	7	9
Whether the system is activated or not	Previous	9	9	7	3	9	9	8	8	8	9	7	9
	Modified	9	7	7	9	9	9	9	8	9	9	7	9
End timing of the syste	Previous	8	9	8	4	7	9	7	7	8	8	7	9
	Modified	8	9	7	9	9	9	9	8	9	9	7	9
Activation of automated steering	Previous	5	9	7	3	8	9	9	8	8	9	7	9
	Modified	7	9	7	8	9	8	9	9	9	9	7	9
Planning path	Previous	9	7	7	3	8	9	9	9	8	9	7	9
	Modified	8	9	6	3	9	9	9	9	9	9	7	9
Advanced safety confirmation	Previous	7	7	7	4	8	8	8	8	8	9	7	9
	Modified	8	9	7	9	9	9	8	9	9	9	7	9

4.2 Feeling of Disturbance

Table 3 shows the evaluation results of interference of driving by visual contents during proactive braking intervention. Larger value indicate better evaluations. Cells colored in blue, green, and red indicate respectively evaluations lower than, equal to, and higher than grade 5. As is observable in Table 3, although we confirmed negative evaluations of simple mixture of previous contents, modified visual contents improved those evaluations at least medium evaluations which gives no difficulty of driving to the elderly drivers. We consider that modification in this research achieved this improvement.

Table 3. Interference of driving during proactive braking intervention

Interference of the driving	Participants ID											
	1	2	3	4	5	6	7	8	9	10	11	12
Previous Contents	4	9	7	5	5	9	8	7	9	9	7	9
Modified Contents	5	9	8	7	5	9	8	8	8	9	7	9

On the other hand, Table 4 shows the corresponding results during proactive steering intervention. Similar to the results of proactive steering intervention, we can confirm the improvement of all evaluation results to the higher level. Especially, regarding the evaluations results of participant 4, modified visual contents improved his evaluations dramatically. This seems that modified visual contents solved the problem of information overload.

Table 4. Interference of driving during proactive steering intervention

Interference of the driving	Participants ID											
	1	2	3	4	5	6	7	8	9	10	11	12
Previous Contents	5	9	7	2	5	9	7	8	7	9	7	9
Modified Contents	7	9	8	8	7	9	7	8	8	9	7	9

4.3 Feeling of the Benefits

Table 5 shows the evaluation results of feeling of the benefit of proactive braking intervention. In this experiment, we investigated two kinds of benefits: namely benefit of avoiding the danger, and that of reducing the number of traffic accidents. The values of upper stage in each cell indicates the evaluation results for visual contents. Left value indicate the evaluation results of previous visual contents while right values indicates those of modified visual contents. Larger value indicates better evaluations. The value of lower stage in each cell indicates the deviation of both evaluations. Regarding the results of proactive braking intervention, we can confirm improvements of some evaluations although we can also confirm negative changes of evaluations. Important point is that modified visual contents of proactive braking intervention still keep good evaluations on high standards.

Table 5. Feeling of the benefits of proactive braking intervention

Benefits	Participants ID											
	1	2	3	4	5	6	7	8	9	10	11	12
Avoiding danger	7→7	9→9	7→7	8→9	7→9	8→8	8→9	8→8	9→9	9→9	8→8	9→9
	0	0	0	+1	+2	0	+1	0	0	0	0	0
Reducing the number of traffic accidents	7→7	9→9	8→7	9→9	9→9	9→9	8→9	8→9	9→9	9→9	9→8	9→9
	0	0	-1	0	0	0	+1	+1	0	0	-1	0

On the other hand, table 6 shows the corresponding results of proactive steering interventions. Regarding proactive steering intervention, modified visual contents improved some evaluation results without reducing any evaluations. Similar to the evaluations regarding the disturbance, modified visual contents dramatically improved the evaluation results of participant 4.

Table 6. Feeling of the benefits of proactive steering intervention

Benefits	Participants ID											
	1	2	3	4	5	6	7	8	9	10	11	12
Avoiding danger	6→8	9→9	7→7	2→8	7→9	8→8	9→9	9→9	8→9	9→9	7→7	9→9
	+2	0	0	+6	+2	0	0	0	+1	0	0	0
Reducing the number of traffic accidents	7→7	9→9	7→7	7→9	7→9	8→9	9→9	8→9	8→9	9→9	7→7	9→9
	0	0	0	+2	+2	+1	0	+1	+1	0	0	0

4.4 Feeling of the trust

Table 7 shows the evaluation results of feeling of the trust for proactive braking intervention. The meaning of the values in each cell indicates evaluation results similarly to the results of feeling of benefits. Regarding the proactive braking intervention, although previous visual contents originally have a good evaluation results, modified visual contents improved some of evaluations of feeling of the trust.

Table 7. Feeling of the trust for proactive braking intervention

	Participants ID											
	1	2	3	4	5	6	7	8	9	10	11	12
The degree of the trust	7→7	9→9	7→7	8→9	7→9	9→9	8→9	7→8	9→9	7→7	7→9	9→9
	0	0	0	+1	0	0	+1	+1	0	0	0	0

Similarly, table 8 shows the corresponding results for proactive steering intervention. Similar to the results of feeling of benefits, modified visual contents improved some evaluation results without reducing any evaluations.

Table 8. Feeling of the trust for proactive steering intervention

	Participants ID											
	1	2	3	4	5	6	7	8	9	10	11	12
The degree of the trust	7→7	9→9	7→7	3→6	4→7	9→9	9→9	8→8	7→9	9→9	7→7	9→9
	0	0	0	+3	+3	0	0	0	+2	0	0	0

4.5 Acceptability

Table 9 shows the evaluation results of acceptability of proactive braking intervention. Larger value indicates better evaluations. Cells colored in blue, green, and red indicate respectively negative, neutral, and positive evaluations. Although evaluations results of acceptability regarding the proactive braking intervention are relatively good, modified visual contents improved the evaluations furthermore. Fig. 13 shows the comparison results regarding the provision of modified visual contents. As is observable in Fig. 13, significant difference under the 5% significance level are confirmed for these results.

Table 9. Acceptability of proactive braking intervention

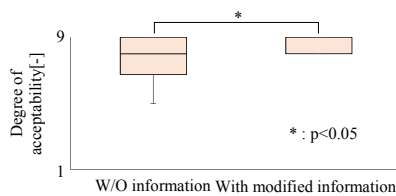| Acceptability	Participants ID											
	1	2	3	4	5	6	7	8	9	10	11	12
No information	5	9	5	8	7	9	8	6	8	9	7	9
Previous Contents	7	9	7	9	9	9	8	7	9	9	8	9
Modified Contents	8	9	8	9	9	9	9	8	9	9	8	9

Fig. 13. Comparison of acceptability of proactive braking intervention

Similarly, table 10 shows the corresponding results of proactive steering intervention. Regarding the proactive steering intervention, though evaluation results of the condition with previous contents contains some negative ones, modified visual contents improved the evaluation results to the positive level. Fig. 14 shows the comparison results regarding the provision of modified visual contents. As is observable in Fig. 14, significant difference under the 5% significance level are confirmed for these results.

Table 10. Acceptability of proactive steering intervention

Acceptability	Participants ID											
	1	2	3	4	5	6	7	8	9	10	11	12
No information	3	5	3	3	4	9	8	5	4	9	4	9
Previous Contents	5	9	4	3	7	9	9	7	8	9	7	9
Modified Contents	6	9	6	8	9	9	8	9	9	9	8	9
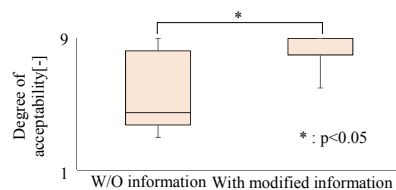
Fig. 14. Comparison of acceptability of proactive steering intervention

5. CONCLUSIONS

To improve the acceptability of the proactive intervention systems, we focused on the information sharing. Based on the experimental results of our previous researches, we modified visual contents of two kinds of proactive intervention systems: namely proactive braking intervention and proactive steering intervention. Then, we conducted the driving simulator experiment to investigate the effectiveness of modified ones. Important points that we confirmed from the experimental results are as follows.

- Modified visual contents basically kept the evaluation results of telling the intended meanings.

- Compared to previous visual contents, modified visual contents basically improved the evaluation results of feeling of the disturbance, the benefits, and the trust; further, they improved the acceptability of proactive intervention systems to the elderly drivers.

From our initial research of proactive intervention to this research, we investigated the acceptability of proactive

intervention systems to the elderly drivers, and proposed the information sharing as the technological solution for improving the acceptability. Based on the results of these researches, we need to take the next step to the further problems.

In this research, although we assumed the perfect performance of the intelligence of automated vehicle, it sometimes fails to behave adequately in the real world. Similarity, prediction of surrounding traffic situation for proactive vehicle controls does not always have right answers. Thus, we need to investigate the characteristics on the condition of false alarms.

In addition, although this research assumed the intervention systems by switching control, our final goal is to realize the intervention systems by shared control. In contrast to the switching control, since the drivers need to drive the vehicle appropriately to a certain degree, drivers need to acquire the information actively. To this end, we need to investigate the characteristics of active information sharing based on the results of this passive information sharing.

REFERENCES

Inoue, H. (2014), "Research into ADAS with Driving Intelligence for Future Innovation", *2014 IEEE International Electron Devices Meeting*, pp. 1.3.1-1.3.7.

Shino, T., Ito, T., and Kamata, M. (2014 a), "Acceptability of Proactive Collision Avoidance for Elderly Drivers", *12th International Symposium on Advanced Vehicle Control*.

Ito, T., Shino, T., and Kamata, M. (2014), "Effectiveness of Passive Information Sharing for Elderly Drivers from the Viewpoint of Acceptability for Proactive Braking Assistance", *Society of Automotive Engineers of Japan Spring Convention Proceedings,* Vol.2014 (139-14), pp.1-4. (in Japanese)

Shino, T., Ito, T., and Kamata, M. (2014 b), "Effectiveness of Passive Information Sharing for Elderly Drivers from the Viewpoint of Acceptability for Proactive Steering Assistance", *Society of Automotive Engineers of Japan Spring Convention Proceedings,* Vol.2014 (139-14), pp.5-8. (in Japanese)

Hasegawa, T., Raksincharoensak, P., and Nagai, M. (2014), "Risk-Potential Based Motion Planning and Control of Proactive Driving Intelligence System for Enhancing Active Safety", *12th International Symposium on Advanced Vehicle Control*.

Satomi, Y., Murano, T., Aga, M., and Yonekawa, T. (2009), "A characteristic analysis of driving behavior to rear-end collision warning using a driving simulator", *JSME Transportation and Logistics*, Vol. 18, pp. 283-286. (in Japanese)

Towards autonomous driving: an Augmented Reality Interface Design for lane change

Raïssa POKAM*, Christine CHAUVIN,
Serge DEBERNARD***, Sabine LANGLOIS******

**IRT SystemX, Renault, France
(e-mail : raissa.pokam@irt-systemx.fr).
**Lab-STICC UMR CNRS 6285, Université Bretagne Sud, France
(e-mail: christine.chauvin@univ-ubs.fr)
*** LAMIH UMR CNRS 8201, Université de Valenciennes et du Hainaut Cambrésis, France
(e-mail: Serge.Debernard@univ-valenciennes.fr}
****Human Factor, Renault, IRT SystemX, France
(e-mail:sabine.langlois@renault.com)*

Abstract: Autonomous vehicles allow the driver to be out of the loop of the driving task, under particular conditions. Interaction between the driver and the technical agent is crucial especially in autonomous mode and in handover processing. It is essential to identify the information requirements to meet the driver's needs. Technology advancement has introduced Augmented Reality, which is said to enhance vision. In this paper, we explore the use case of lane change. By applying a cognitive method, we extract information related to lane change maneuver. We present what the Augmented Reality representation will potentially look like at the end of our study. Finally, future research avenues are outlined.

Keywords: Autonomous vehicles, Human-machine co-operation, Human-machine interface, Augmented Reality

1. INTRODUCTION

Nowadays, highly automated vehicles are increasingly in evidence. This kind of vehicle allows the drivers or human agents to relinquish control to an automated system or technical agent when they wish to and when it is technically possible. Considering the number of functions delegated by the human agents to the technical agents, there are numerous levels of automation. Some taxonomies define these levels: the National Highway Traffic and Safety Administration (NHTSA) taxonomy, the Society of Automotive Engineers (SAE) taxonomy, and taxonomies such as those of Sheridan and Verplanck (1978), Endsley (1999), Gasser and Westhoff (2012), and Riley (1989). At the highest level of automation, the technical agent is solely responsible for the entire driving task; we then talk about self-driving, fully autonomous, or driverless vehicles. We expect to see fully autonomous vehicles driving on open roads by 2030.

Manufacturers and researchers focus their research on the intermediary levels of automation. In this perspective, many projects have been conducted. Among these, the LRA project (French acronym for Localization and Augmented Reality), a French collaborative project, aims to design an Augmented Reality Interface for autonomous driving. The present work is part of this project. The 10-member team of academics and manufacturers who work together has chosen to investigate Level 3 of automation in the NHTSA taxonomy. The

NHTSA specifies that *vehicles at this level of automation enable the driver to cede full control of all safety-critical functions under certain traffic or environmental conditions and in those conditions to rely heavily on the vehicle to monitor for changes in those conditions requiring transition back to driver control* (Marinik, Bishop, Fitchett, Morgan, Trimble, & Blanco, 2014). This automation level involves four major phases:

- The **manual driving phase** where the human agent is responsible for the driving task. The driver has to monitor the road environment and the other vehicles to avoid accidents and carry out proper maneuvers. The driver is *in-the-loop*.

- The **transition from manual to automated driving** where the human agent prepares to turn away from the driving task. It is then possible for the driver to take his/her hands off the steering wheel and his/her feet off the pedals.

- The **automated driving phase** where the technical agent controls the vehicle. Consequently, the driver can carry out some secondary and tertiary activities. It is said that the driver is *out-of-the-loop*.

- The **transition from automated to manual driving** where the human agent should reengage cognitively and physically in the driving task. This phase, if not completed properly, can lead to accidents.

Each phase requires an appropriate interface to allow the driver to be aware of what is going on inside the car and outside the car, i.e. to establish accurate *situation awareness* (Endsley, 1995). It is thus critical to convey the right information, in a suitable form and at the right time, especially in the autonomous driving phase and in the transition from automated to manual driving. These particular phases are the core focus of our work regarding the human-machine interface (HMI) design issue.

In the project, Augmented Reality allows the insertion of virtual objects into the real world in terms of their movements. This definition is similar to Azuma's (Azuma, 1997). It has been demonstrated the usefulness of using Augmented Reality in order to *alert drivers and guide their attention to dangerous situations*. Consequently, we can assume that Augmented Reality can enhance global situation awareness. In light of all these considerations, we identified three fundamental research questions to orientate the interface design:

a. In autonomous mode and in handover processing, which sufficient representation should the driver maintain or establish? According to the Situation Awareness model defined by Endsley (1995), this question may be subdivided into three sub-questions: (i) What should the driver perceive? (ii) What should he/she understand? (iii) Which projection of the external environment and the system should he/she perform?

b. How should we design the displays? (i) What should be displayed? (ii) How should that information be displayed? (ii) When should it be displayed? With which prioritization?

c. What is the added-value of Augmented Reality in the displays? In others words, can driver maneuvers be impacted by Augmented Reality?

These are valid questions for each phase of driving mentioned above. In this paper, we examine the particular case of lane change in autonomous mode.

The paper is structured as follows: first, a literature review on lane change is presented. Then, our methodology to extract the information needed by the drivers is described. Next, we present our results and the Augmented Reality expected outcome. In conclusion, future research avenues are outlined.

2. LITERATURE REVIEW ON LANE CHANGE

Accident statistics reveal that lane change is a very dangerous maneuver. It increases the drivers' mental load as they have to carry out many tasks in parallel: monitor vehicles in their current lane and in the adjacent lane, perform a cognitive calculation to work out whether lane change is possible or not, etc. (Henning, 2009, cited by Habenicht, Winner, Bone, Sasse & Korznietz 2011). This maneuver changes the lateral position of the vehicle. It is why we assume that, in autonomous mode, executing such a maneuver can be

"surprising" for drivers, even more so if they were engaged in another activity. In this section, we present the basic elements of lane change in manual mode, which constitute a prerequisite for the automated mode.

2.1 Definition

Many researchers have tried to define lane change and/or to describe it. Chovan, Tijerina, and Hendricks (1994) define lane change as *a deliberate and substantial movement in the lateral position of a vehicle.* Naranjo (2008) defines lane change as a maneuver in three steps: exiting a lane, entering another lane, and cruising in the new lane.

Lane change can be carried out for many reasons:

- To enter a highway,
- To prepare to exit or to exit a highway (Naranjo, 2008),
- To avoid a vehicle merging onto the highway in front of us,
- To avoid obstacles,
- To go back to a privileged lane,
- To avoid a vehicle arriving at high speed behind us,
- Etc.

2.2 Cognitive processes and driver behaviors

While lane changing, driving requires more visual and attentional resources than during simple cruising (Shinar, 1978, cited by Olsen, 2003). To change lanes safely, drivers have to monitor the other vehicles and obstacles carefully to avoid any collision. Then, there are a number of functions that need to be applied. Olsen (2003) presents the ideal sequence of lane change, which associates cognitive processes and driver behaviors, arising out of Chovan, Tijerina, Alexander & Hendricks's (1994) work and Wierwille's (1984) work. We have adapted this sequence by using a flowchart representation (see Figure 1).

The acronyms used in the figure are defined below:

- EV: Ego Vehicle
- POV LO: Principal Other Vehicles Leading (the ego vehicle) in the Original lane
- POV FO: Principal Other Vehicles Following (the ego vehicle) in the Original lane.
- POV LD: Principal Other Vehicles Leading (the ego vehicle) in the Destination lane.
- POV FD: Principal Other Vehicles Following (the ego vehicle) in the Destination lane.
- EV-POV LO: EV-POV LO distance.
- EV-POV FO: EV-POV FO distance.

The figure shows that drivers have to execute many parallel actions. The real process is not as linear as we have presented it, and loops can be observed. We also assume that expert drivers will make shunts in the whole process in terms of their experience. In the following section, the methodology

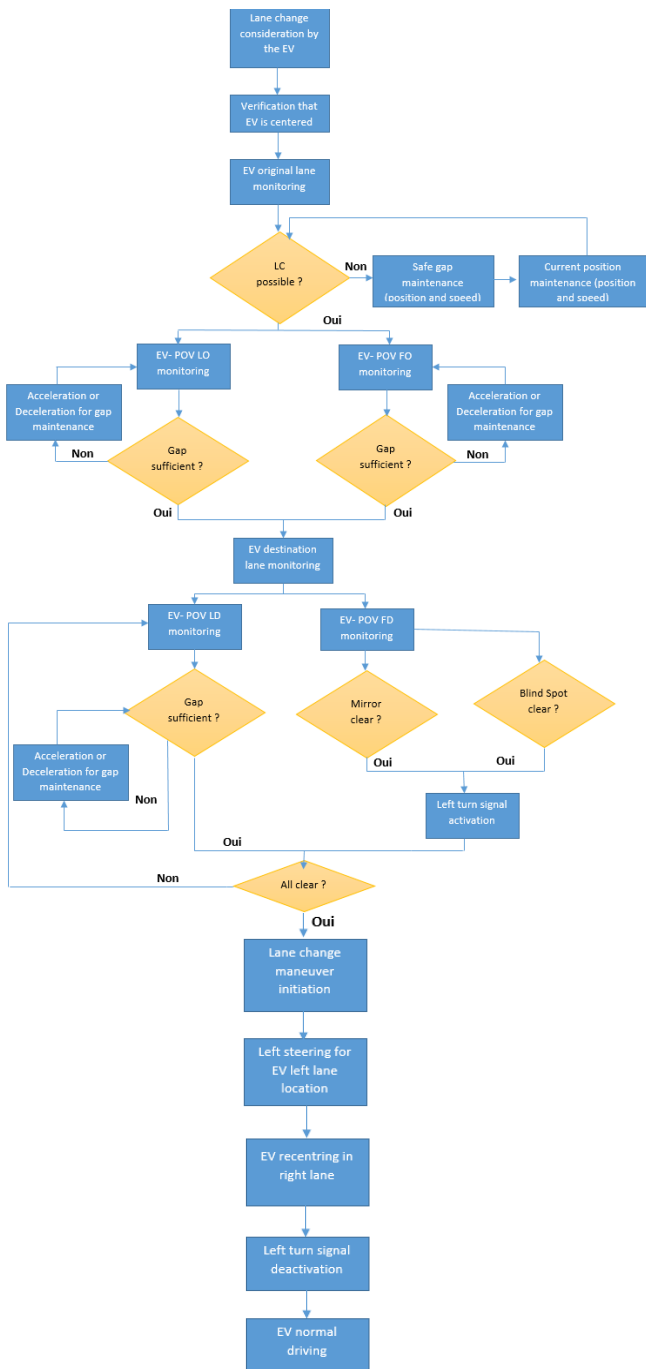used to design the interface in general and the lane change in particular is presented.

Fig. 1. Right to left lane change flowchart

3. METHODOLOGY AND RESULTS

In this section, we describe the methodology used to solve the problem. We also present the results obtained from the various steps.

3.1 General approach

At the outset, we defined some generalized use cases. Among those, we chose the ones we wanted to investigate in greater depth.

The next essential step was to define the methodology used to treat the interface design problem. The different steps of our methodology are shown in Figure 2.

- The first step involves the extraction of information required by drivers. For this purpose, we decided to apply Cognitive Work Analysis (CWA) to determine the driver requirements from which the interface requirements are then derived.
- The step following the information requirements is rule-based prioritization through a strong algorithm. In this step, we also defined the information format, its display modality and its output channel by taking into account Driver-Vehicle-Environment (DVE) conditions and the driver's state.
- Next, there is the step of interface specification where interaction between the technical agent and the human agent is designed according to the relevant use cases chosen.
- The last step consists in users' tests to assess the interface and improve it. In a simulated environment, some tests are conducted in order to refine our previous rules.

It is important to point out that sometimes, it is possible to loop through these steps. In this paper, we focus on the first step and its results.

3.1.1 Cognitive Work Analysis

CWA is a formative framework that considers work from the perspective of how it can be done. Hence, CWA is different from normative frameworks, which consider work from the perspective of how it should be done, and descriptive frameworks, which consider work from the perspective of how it is done. It is a framework from which the Ecological Interface Design approach or *EID-approach* first proposed by Rasmussen and Vicente (1989) came from. The Ecological Interface Design attempts to "minimize the potential for control interference, as well as supporting recovery from human errors" through system design (Rasmussen and Vicente, 1989).

CWA is made up of five phases: Work Domain Analysis, Control Task Analysis, Strategies Analysis, Social and Cooperation Analysis, and Worker Competencies Analysis. Throughout each phase, CWA determines the constraints that are associated with a socio-technical system. These constraints affect the behaviors of the actors (human and/or technical).
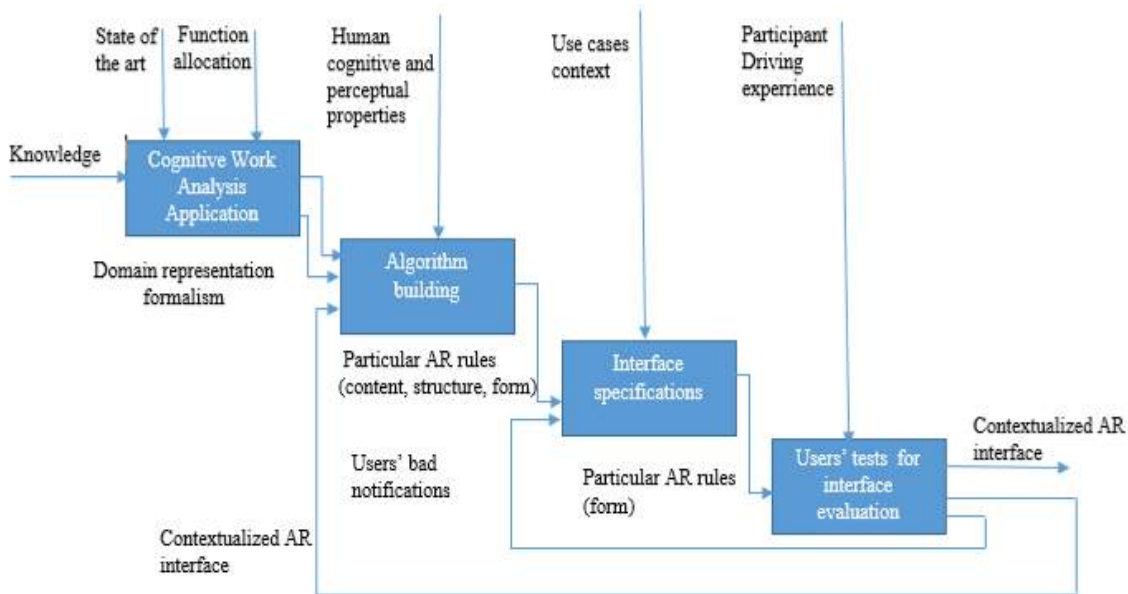
Fig. 2. HMI design methodology

3.1.2 Rationale for the use of Cognitive Work Analysis in the design process

CWA is a multifaceted purpose framework. It can be used to improve an existing system, to understand the functioning of a system, or to design a new, currently non-existent system. Some researchers have examined the bridge that CWA can establish between analysis and design. Read, Salmon, and Lenné (2012) define some roles that CWA can play in the design process:

- Going step by step, the CWA "result" can be directly mapped to design.
- Design requirements can be iteratively determined through CWA.
- Associated with human factors guidelines or other specific criteria, CWA has a design support role.

We used CWA to extract inputs for the design. Bisantz and Burns (2008) explain that design inputs can be found from the decision ladder. It is the reason why we focused on the first phases of the framework: Work Domain Analysis and the Control Task Analysis associated with the decision ladder.

- **Work Domain Analysis**: It is the first phase of CWA. It determines the factors that constrain the actors of a system to behave in certain ways. This analysis deals with the structural properties of the environment in which tasks are accomplished. The Abstraction

Hierarchy, which is the main tool of this phase, explores the system from its purpose(s) to its physical device(s) (Jenkins, 2009).
- **Control Task Analysis**: The second phase of CWA determines the factors that constrain the tasks. It answers the question "What needs to be done in the system?" (Naikar, 2013). Control Task Analysis defines the activity that is required for achieving a system's purposes (Naikar, 2013).

3.2 Cognitive Work Analysis on lane change manoeuver

Lane change is a manoeuver autonomous vehicles need to accomplish in the LRA project. Hence, we needed to carry out a CWA on autonomous vehicles. In order to explore fully function decomposition as related to lane changing, we decided to consider lane change as a system. We examined a lane change as performed by a driver and derived from this description the pieces of information that are necessary to design such a system. We integrated the autonomous aspect afterwards.

3.2.1 Work Domain Analysis

We conducted the WDA of autonomous vehicles but we do not report on WDA in detail because it is not the core of this paper. Figure 3 represents the Work Domain Analysis of lane change.

The Word Domain Analysis is divided into five levels ranging from the most abstract to the most concrete:
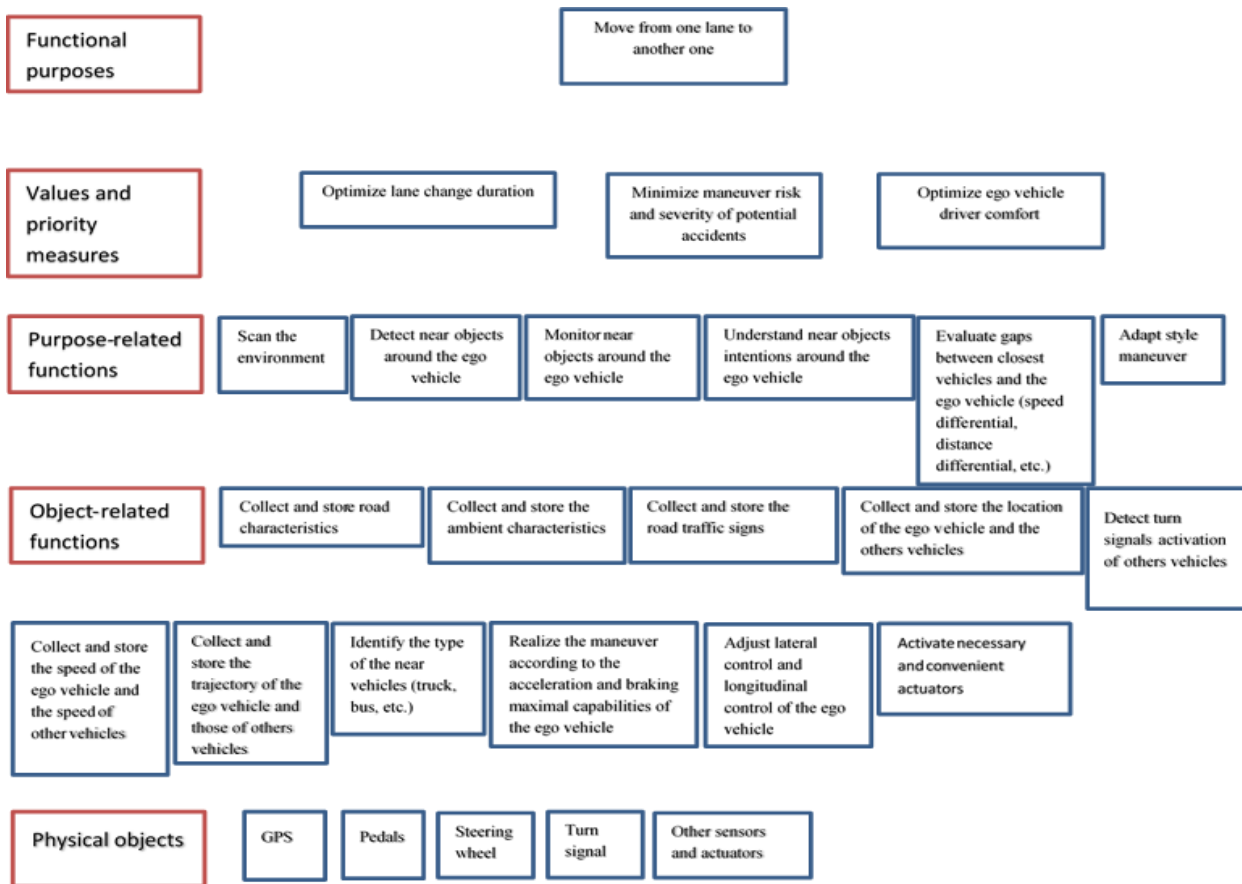
Fig. 3. Lane change Work Domain Analysis

- **Functional purposes**. It is the most abstract level. It corresponds to the main purpose of the system. In other words, it answers the question: "Why has this system been designed?" In our case, the functional purpose is a shift, a movement from one lane to another.
- **Values and priority measures**. At this level, the elements that help to know how the system progresses towards its goals are mentioned. Within the values and priority measures of the lane change system, we include "Optimize lane change duration".
- **Purpose-related functions**. It is the level of all functions that a system must accomplish to achieve its functional purposes. Within these functions, we include "Scan the environment", "Detect near objects around the ego vehicle", "Monitor near objects around the ego vehicle", etc.
- **Object-related functions**. To find the elements that constitute this level, Naikar suggests asking the following question, for example: "What functional purposes or functional capabilities of physical objects are necessary for the system to achieve its purpose-related functions?" (Naikar, 2013). Examples include "Collect and store road characteristics" (such as access type (freeway, highway, arterial, ramp, secondary road), road type (weaving, rural) and number of lanes), "Collect and store ambient characteristics" (ambient characteristics refer to the weather (rain, sun,

ice, snow, cold), visibility (sun, dust, rain, fog) and the time of day), "Collect and store the road traffic signs and signals" (such as speed limitation traffic signs, direction traffic signs, traffic markings and stationary cameras/police cars).
- **Physical objects**: Situated at the top of the figure, the physical objects refer to all the devices that allow the system to accomplish object-related functions. Among the components involved in lane change, we can cite a camera, Radar, LIDAR, etc.

3.2.3 Control Task Analysis

Control Task Analysis uses two major tools: the Decision Ladder (DL) and the Contextual Activity Template (CAT).

- The decision ladder was introduced by Rasmussen (1986). It represents the information-processing stages of a decision task (represented by the rectangles) and the knowledge states following them (represented by the ovals). The decision ladder for lane changing is shown in Figure 4.
- We adapted the usual contextual activity template that associates the work situations to work tasks or to work functions. In our study, we associated the use cases to the adequate component of the oval components, previously numbered. An extract of that table is shown in Table 1.
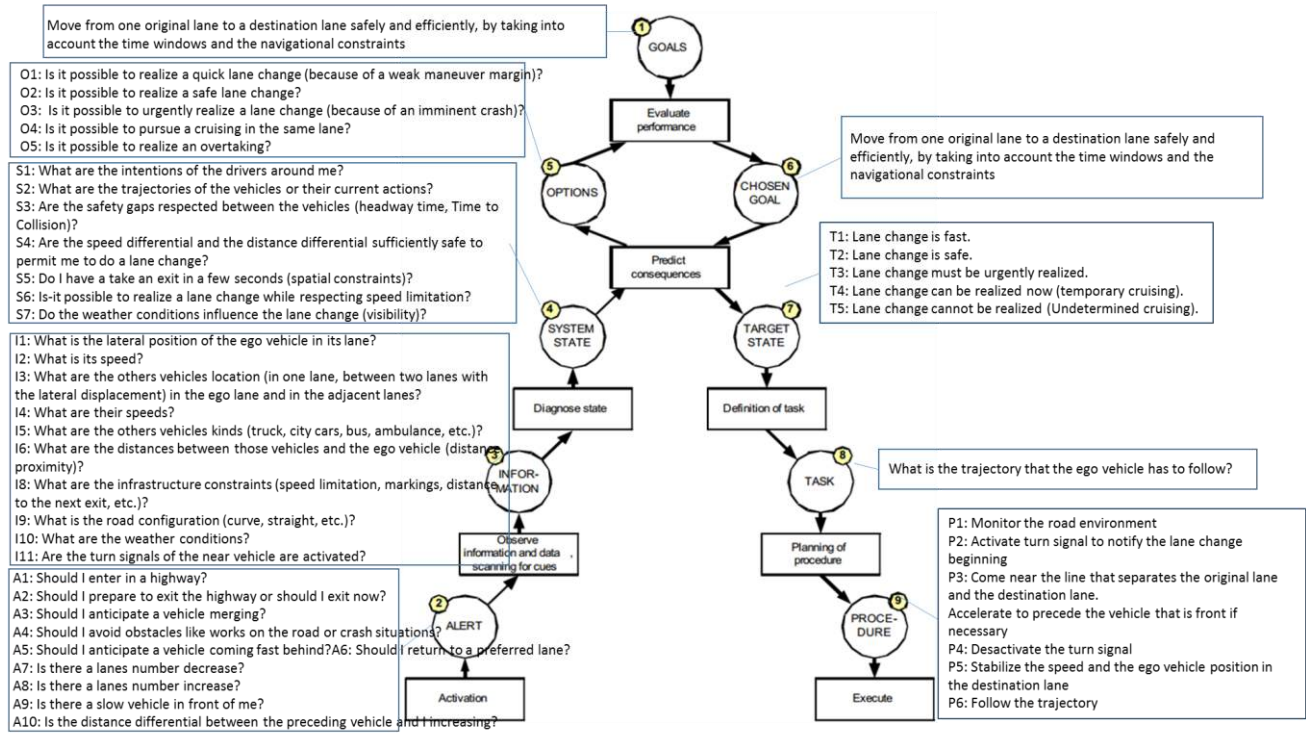
Fig. 4. Lane change Decision Ladder

Table 1. Extract of adapted Contextual Template

Scene number	Scene description	Alert	Information	System state	Target State
4	Overtaking of a slow vehicle by the ego vehicle	A10	I1,I2,I3,I4,I5, I6, I7, I8, I10,I11,I12	S1; S3; S4; S6	T1/T2
4'	Overtaking of a slow vehicle by the ego vehicle with restricting vehicles	A10	I1,I2,I3,I4,I5, I6, I7, I8, I10,I11,I12	S1; S3; S4; S6	T4
5	Overtaking of many vehicles once	A9	I1,I2,I3,I4,I5, I6, I7, I8, I10,I11,I12		T1/T2

Where:

A9 refers to "Is there a slow vehicle in front of me?"

A10 refers to "Is the distance differential between the preceding vehicle and I increasing?"

I1 refers to "What is the lateral position of the ego vehicle in its lane?"

I2 refers to "What is its speed?"

I3 refers to "What are the locations of the other vehicles (in one lane, between two lanes with the lateral displacement) in the ego lane and in the adjacent lanes?"

I4 refers to "What are their speeds?"

I5 refers to "What category do the other vehicles belong to (truck, city car, bus, ambulance, etc.)?"

I6 refers to "What are the distances between those vehicles and the ego vehicle (distance proximity)?"

I8 refers to "What are the infrastructure constraints (speed limitation, markings, distance to the next exit, etc.)?"

I10 refers to "What are the weather conditions?"

I11 refers to "Are the turn signals of the near vehicle activated?"

S1 refers to "What are the intentions of the drivers around me?"

S3 refers to "Are the safety gaps respected between the ego vehicle and the other ones?"

S4 refers to "Are the speed differential and the distance differential sufficiently safe to allow me to do a lane change?"

S6 refers to "Is it possible to execute a lane change while respecting the speed limitation?"

T1 refers to "Lane change is fast."

T2 refers to "Lane change is safe."

T4 refers to "Lane change can be carried out now (temporary cruising)."

3.3 Results

The first two phases of CWA enabled us to identify functions and objects that define a lane change maneuver. From these elements, we derived information requirements, including the AR and non-AR information. We took an element from the decision ladder and extracted all the physical components and abstract ones. Those pieces of information can be classified into three categories: ego vehicle, other vehicles, and infrastructure.

- For the ego vehicle
  - Vehicle condition: fuel level
  - Vehicle components condition: if components work well or not
  - Current location and desired end point
  - Own dynamics: speed, velocity, lateral displacement
- For the other vehicles
  - Their type
  - Their location
  - Their relative proximity to the ego vehicle in terms of speed, distance, or time
  - Their intentions
  - Their actions
- For the infrastructure
  - Road signage presentation
  - Road type
  - Infrastructure-related warning
  - Lane width

There are also information requirements related to the automated system and the ego vehicle driver. Considering that the autonomous mode should be an enjoyable experience, drivers need to have access to information they require; for example, drivers should know how long they have to plan their leisure activity. It is also necessary to check driver vigilance, especially when the transition from autonomous to manual mode is required. Other information should be conveyed:

- For the automated system
  - Its intentions
  - Its current action
  - Its comprehension of road rules
  - Its road perception
  - The remaining time in autonomous mode
- For the ego vehicle driver
  - Its distraction level
  - Its protection information: information related to the   seatbelt lock or unlock, hands on steering wheel or not, feet on pedals or not.

4. AUGMENTED REALITY EXPECTED OUTCOME

Many modern cars (Audi Q7, BMW M3 Berline, etc.) are equipped with a Head-Up Display (HUD) device. This device enables Augmented Reality implementation (Tönnis, Sandor, Lange, & Bubb, 2005). The expansion of Augmented Reality

in manual mode suggests that AR positively supports drivers by highlighting salient objects in the road environment. We thus hypothesize that AR will have a similar effect on drivers in the different phases of driving of an autonomous vehicle. In particular, we assume that AR will improve the takeover process. In lane change, we assume that AR will help to determine the vehicles, lanes, or lines so that the drivers may want to understand the current activity of the system and will easily understand the intention and the action of the ego vehicle.

In an exploratory phase, we implemented a few elements and obtained Augmented Reality representation samples. Figures 5 and 6 show two examples of these elements.

Fig. 5. Trajectory indication in fog manual driving

Fig. 6. Vehicle identification in autonomous mode

5. CONCLUSION

Autonomous driving interaction involves a number of challenges. One of these challenges is the HMI design to allow accurate communication between the human agent and the technical one. A well-designed HMI will enhance drivers' situation awareness of the environment. At this stage of our work, by applying a cognitive analysis, we have extracted all the information requirements necessary for drivers. The next step is to continue with other stages in order to have a strong AR HMI that takes into account the context and the dynamics of the environment.

REFERENCES

Azuma, R. T. (1997). *A survey of augmented reality.* Presence, 6(4), 355-385.

Bisantz, A. M., & Burns, C. M. (Eds.). (2008). *Applications of cognitive work analysis.* CRC Press.

Chen, J.Y.C, Boyce, Wright, J., Procci, K., Barnes, M. (in prep.). *SA-based Agent Transparency.* ARL Technical Report.

Chovan, J. D., Tijerina, L., Alexander, G., & Hendricks, D. L. (1994). *Examination of lane change crashes and potential IVHS countermeasures* (DOT HS 808 071) Washington, DC: National Highway Traffic Safety Administration. Available online at: http://www.itsdocs.fhwa.dot.gov/\JPODOCS\REPTS_ TE/61B01!.PDF.

Elix, B., & Naikar, N. E. E. L. A. M. (2008). Designing safe and effective future systems: A new approach for modelling decisions in future systems with Cognitive Work Analysis. In *Proceedings of the 8th international symposium of the Australian Aviation Psychology Association.*

Endsley, M. R. (1995). Toward a theory of situation awareness in dynamic systems. *Human Factors: The Journal of the Human Factors and Ergonomics Society*, 37(1), 32-64

Endsley, M. R. (1999). Level of automation effects on performance, situation awareness and workload in a dynamic control task. *Ergonomics*, *42*(3), 462-492.

Jenkins, D. P., Stanton, N. A., Salmon, P. M., Walker, G. H., & Rafferty, L. (2010). Using the decision-ladder to add a formative element to naturalistic decision-making research. *Intl. Journal of Human Computer Interaction*, 26(2-3), 132-146.

Gasser, T., & Westhoff, D. (2012). BASt-study: Definitions of automation and legal issues in Germany. In *Presentation at the Road Vehicle Automation Workshop*.

Habenicht, S., Winner, H., Bone, S., Sasse, F., Korzenietz, P. (2011). A maneuver-based lane change assistance system. In *Intelligent Vehicles Symposium* (IV), 2011 IEEE (pp. 375-380). IEEE.

Henning, M. (2009). Preparation for lane change manoeuvres: Behavioural indicators and underlying cognitive processes.Lee, S. E., Olsen, E. C., & Wierwille, W. W. (2004). *A comprehensive examination of naturalistic lane changes* (No. HS-809 702,).

Marinik, A., Bishop, R., Fitchett, V., Morgan, J. F., Trimble, T. E., & Blanco, M. (2014, July). *Human factors evaluation of level 2 and level 3 automated driving concepts: Concepts of operation*. (Report No. DOT HS 812 044). Washington, DC: National Highway Traffic Safety Administration.

Michon, J. A. (1985). A critical view of driver behavior models: what do we know, what should we do?. In *Human behavior and traffic safety* (pp. 485-524). Springer US.

Naikar, N. (2013).*Work domain analysis: Concepts, guidelines, and cases.* CRC Press.

Naranjo, J. E., Gonzalez, C., Garcia, R., & De Pedro, T. (2008). Lane-change fuzzy control in autonomous vehicles for the overtaking maneuver. *Intelligent Transportation Systems, IEEE Transactions on*, 9(3), 438-450.

Olsen, E. C. (2003). *Modeling slow lead vehicle lane changing* (Doctoral dissertation, Virginia Polytechnic Institute and State University).

Rasmussen, J. (1986). Information processing and human-machine interaction. *An Aproach to Cogntive Engineering, Amsterdam, Nom Holland*.

Rasmussen, J., & Vicente, K. J. (1989). Coping with human errors through system design: implications for ecological interface design. *International Journal of Man-Machine Studies*, 31(5), 517-534.

Read, G. J., Salmon, P. M., & Lenné, M. G. (2012, September). From work analysis to work design: A review of cognitive work analysis design applications. In *Proceedings of the Human Factors and Ergonomics Society Annual Meeting* (Vol. 56, No. 1, pp. 368-372). SAGE Publications.

Riley, V. (1989). A general model of mixed initiative human-machine systems. In *Proceedings of the Human Factors and Ergonomics Society Annual Meeting* (Vol. 33, No. 2, pp. 124-128). SAGE Publications.

Salmon, P. M., Regan, M., Lenné, M. G., Stanton, N. A., & Young, K. (2007). Work domain analysis and intelligent transport systems: implications for vehicle design. *International journal of vehicle design*, 45(3), 426-448.

Sheridan, T. B., & Verplank, W. L. (1978). *Human and computer control of undersea teleoperators*. Massachusetts Institute of Technology Cambridge Man-Machine Systems Lab.

Shinar, D. (1978). *Psychology on the Road: The Human Factor in Traffic Safety*. New York: Wiley.

Tijerina, L., Garrott, R, W., Glecker, M., Stoltzfus, D., Parmer, E. (1997). Van and passenger car driver eye glance behavior during lane change decision phase (Revised DRAFT: INTERIM REPORT). Transportation Research Center, Inc. and National Highway Transportation Safety Administration, Vehicle Research and Test Center.

Tonnis, M., Sandor, C., Lange, C., & Bubb, H. (2005, October). Experimental evaluation of an augmented reality visualization for directing a car driver's attention. In *Proceedings of the 4th IEEE/ACM International Symposium on Mixed and Augmented Reality* (pp. 56-59). IEEE Computer Society

Van Winsum, W. (1999). The human element in car following models. *Transportation research part F: traffic psychology and behaviour*, 2(4), 207-211.

Wierwille, W. W. (1984). Driver steering performance (Chapter 16). In G. A. Peters & B. J. Peters (Eds.), *Automotive Engineering and Litigation*, 1, 407-434. New York: Garland Law.

Vehicle Controllability Assessment Using Detailed Multibody Vehicle Simulations

G. Chrysakis* H. Monkhouse **
S. Kanarachos ***

*Mechanical Automotive Manufacturing Department, Coventry University,
Coventry, CV1 5FB, UK (Tel: +44 (0) 2477658377; e-mail: g.chrysakis@coventry.ac.uk)
** Protean Electric Limited, Farnham, Surrey, GU10 5EH,
UK, (e-mail: helen.monkhouse@proteanelectric.com)
*** Mechanical Automotive Manufacturing Department, Coventry University,
Coventry, CV1 5FB, UK (Tel: +44 (0) 2477657720; e-mail: stratis.kanarachos@coventry.ac.uk)}

Abstract: ISO 26262, the functional safety standard for automotive electric and electronic (E/E) systems, requires a controllability assessment to be made as part of the hazard and risk classification process. As well as influencing the function's Automotive Safety Integrity Level (ASIL), the verifiable controllability may also limit the functions intervention options and intensity during normal operation. For electric driven vehicles this limits their accident-avoidance/-mitigation potential. For an in-wheel motor driven electric vehicle it is questioned whether the failure of a motor could lead to a risk. It is obvious that the result of the risk assessment depends on the operating scenarios chosen. As numerous factors define a driving situation, the possible detailing of these factors is unlimited. In a previous paper, the results of a study regarding the controllability of a vehicle driven by in-wheel motors using a simplified linear bicycle model were presented. In this paper we extend the previous work by qualitatively and quantitatively identifying the hazards associated with in-wheel motors and by quantify the vehicle level effects that could be expected using validated detailed multibody vehicle models in both straight line and cornering events.

Keywords: vehicle controllability, vehicle dynamics, ISO26262, in-wheel motors, multibody vehicle simulations.

1. INTRODUCTION

For public traffic it is necessary to prove that the residual risk, due to hazardous failures or unintended reactions of automotive systems, is acceptably low. Requirements for the risk assessment of safety-related electric and electronic systems in case of failure are provided in ISO 26262 (ISO 26262: 2011).

Electric in-wheel drive systems are flexible, modular vehicle propulsion systems that revolutionize the way vehicles are driven today. Among their advantages are increased manoeuvrability and design freedom, and a reduction in the packaging space required. In-wheel drive systems need to comply with ISO 26262 and therefore research needs to be undertaken to ensure sufficient system safety (Hirano 2012), (Watts et al. 2010). Of concern is the case where one motor fails - besides not meeting the vehicle's acceleration/deceleration requirements - a yaw moment is introduced which acts as a disturbance and causes the vehicle unintendedly to turn. A question that arises during early risk analyses of such a system is the controllability of such system hazards. While this question is answered subjectively in early stages, very often using worst-case risk graphs, the question comes back later in a much more precise way: in cases where an in-wheel motor component failure would produce a deviation between desired and actual vehicle position, and that deviation can be measured in terms of amplitude and/or time, how much deviation can be controlled by the driver? (Reinelt et al. 2006)

A literature survey has shown that similar questions have arisen for active steering systems, automatic braking systems, and active safety systems (Neukum et al. 2008), (Weitzel et al. 2013). In many cases empirical studies have been conducted that assessed the controllability using a group of drivers and vehicles. Objective and subjective measurements have led to the definition of maximum allowable limits for different vehicle dynamics metrics e.g. yaw disturbance.

As numerous factors define a driving situation, the possible detailing of these factors is unlimited. A side-effect of increased detailing is to decrease the rate of occurrence of single situations; thereby lowering the perceived risk and overall safety level required. Hence, a method is needed that allows for the systematic and verifiable derivation of test situations, including traceability of the detailing. Automated controllability assessment using numerical models might be a possible solution, in case they represent reality well.

In a previous paper, the results of a study regarding the controllability of a vehicle driven by in-wheel motors using a simplified bicycle model have been presented and discussed

(Ellims et al. 2013). It is well known that the validity of the bicycle model is restricted only in the linear range e.g. for lateral accelerations up to 0.4g and in case of dry road conditions (Kanarachos 2009). In this paper, we extend the previous work by identifying the hazards associated with in-wheel motors and by quantifying the vehicle level effects that could be expected using validated detailed multibody vehicle models. Furthermore, we expand the risk analysis scope by considering that the vehicle is equipped with an electronic stability control system, like in (Alirezaei et al. 2013), which is now mandatory in Europe.

The rest of the paper is organized as follows: In the second chapter the problem is formulated by presenting the vehicle, driver, driveline and motor failure models used. In Section 3 the scenarios used for evaluating the controllability are described and the maximum allowable limits are shown. These scenarios include the application of torque applied due to fault of the in-wheel motor electric driveline during straight line and cornering events at 150 km/h. The response of the vehicle during low mu surface is also investigated. Section 4 the numerical results are illustrated and discussed while in Section 5 conclusions are drawn.

In order to reduce the risk of a system component failure two possible options exist. The first is to make the component physically redundant (Hirano 2012). The second one it to reallocate the control commands to the remaining actuators in such a way that risk is minimized (Watts et al. 2010). In case, of an electric vehicle driven by one or two pairs of in-wheel motors the redundancy exists.

2. CASE STUDY DEFINITION

2.1 Vehicle Specifications

The multibody model selected represents a GAC Trumpchi. The vehicle is selected as an average sedan vehicle with rear wheel drive (RWD) internal combustion driveline, also equipped with in-wheel motors at each rear wheel (RWDEV). The vehicle specifications used are:

- Aggregate mass: 1870kg

- Front / Rear weight distribution: 53.86% / 46.14%

- Wheelbase: 2.7m

For the scenarios evaluated in this paper the internal combustion driveline is considered to be inactive. Only the in-wheel electric motors propel the vehicle. The in-wheel electric motors used are from Protean Electric and their performance is shown in Figs. 1 and 2.
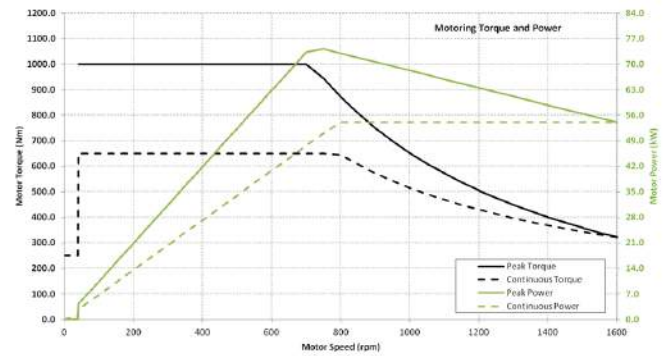
Fig. 1. Driving performance of the in-wheel electric motor
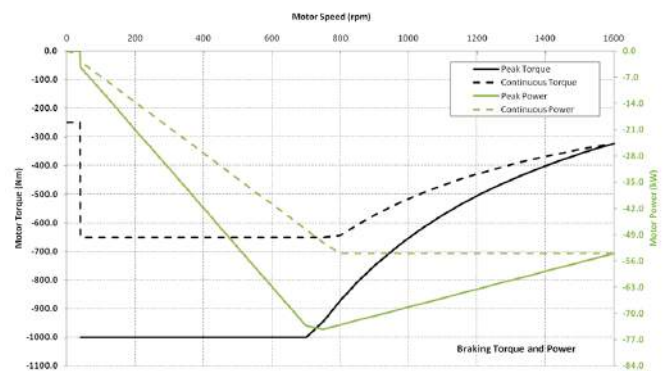
Fig. 2. Braking performance of the in-wheel electric motor

2.2 Electric motor failure scenarios

Two electric motor failure scenarios are evaluated. The first scenario is an almost instantaneous increase of the braking force by the motor, followed by controlled decay within 1.5 seconds as shown in Fig. 3. This is performed while the vehicle attempts to maintain velocity during the event. The reason for 'switching off' the torque after a time period is simply that the response of the driver controller to a fixed torque that remains on, is relatively straightforward and the driver is able to control the vehicle with much more ease. The removal of the failure torque is, in reality a much more likely scenario as the vehicle electronics will have intervened. The duration of the time before the fault is injected is simply to allow the vehicle to settle and the use of 10 seconds is arbitrary – it facilitates location of the fault in the results. The vehicle usually starts 'in the air and at speed' and some time is required at the start of the simulation for the tyre forces to initialise and also for the controller gains to take appropriate control of the model. This is to prevent the controller 'battling' the fault and is more reflective of the operator removing drive torque upon detection of a problem.
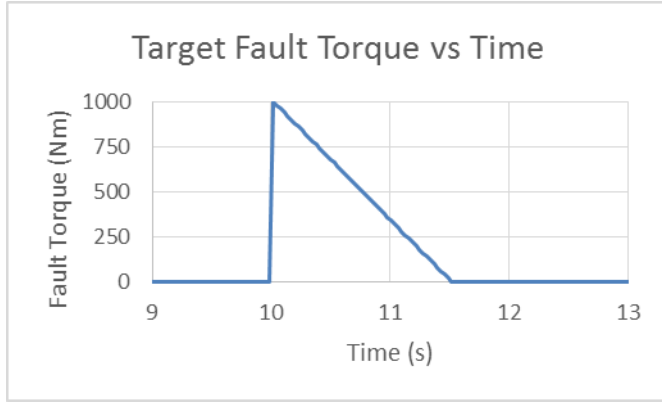
Fig. 3. Intermittent fault torque target versus time

The fault torque applied is limited by the performance of the motor. The target maximum torque is selected according to the maximum torque the motor can provide. However, following the maximum power profile of the motor, the maximum torque applied in this scenario is limited according to the angular velocity of the motor (Fig. 4).
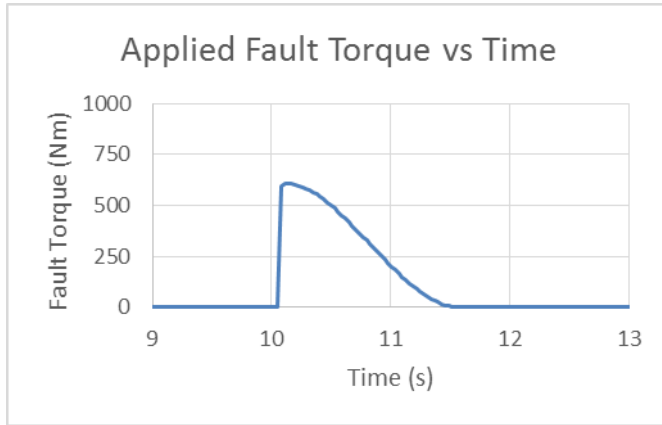
Fig. 4. Applied intermittent fault torque versus time

The second scenario represents a failure of the inverter controlling the electric motor. In case of an inverter failure the control of the electronics is disabled and a passive return of current from the motor to the battery. The magnitude of the current of the system is defined by the difference of the back- electromotive force generated by the motor relative to the voltage of the tractive system energy accumulator. In this scenario the motors are driven at their maximum power rating until the fault occurs. The failure is initially applied to the internal wheel (rear left) motor. The safety monitoring system recognises the torque difference across the axle and disables the second motor across the axis (rear right) after 200ms (Fig. 5) in order to minimise the yaw momentum applied on the vehicle.
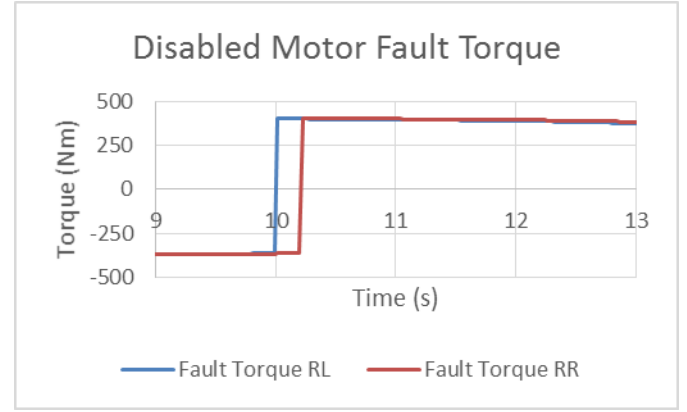
Fig. 5. Torque application due to disabled motors

2.3 Driver model

A detailed analysis with a 2 degree of freedom (Harty & Gade, 2013) vehicle model reveals that in order to reproduce the Neukum results the simplified PID Heading Controller (outlined in Fig. 6 below) has an infinite bandwidth – in other words, the response of the operator is simply too good to reflect a typical driver and some tuning of the model is required. Consequently, the controller model is tuned (via a second order differential equation) to have a specific natural frequency at 2Hz and some damping ratio.
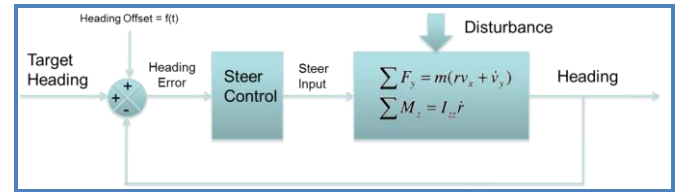
Fig. 6. Heading control model to represent the human operator defined by Neukum.

For the straight line event the model behaves very well. However for the cornering event the filter implementation applied delays the response of the driver. This results in a non-decaying oscillation of the steering input (and of the vehicle) which human drivers would eventually damp out by minimising both the steering torque input and the applied steering angle oscillation amplitude. This is implemented by an additional low gain PID controller controlling the angle of the steering wheel that corresponds to cornering yaw rate. This steering angle controller is tuned in line with the heading controller in order to damp the steering angle oscillation while having minimum impact on the response of the driver due to the fault.

3. SCENARIO DEFINITIONS

The scenarios investigated include the application of fault torque as described in section 2, during straight line and cornering events at initial speed of 150 km/h. The cornering event target is 0.4g of lateral acceleration. The response of the vehicle during low mu surface is also investigated up to the point that the vehicle stability is compromised when an Electronic Stability Control (ESC) system is also applied.

The 10 seconds fault injection is selected in order to allow the vehicle model and controllers to settle.

For the first fault scenario the fault is applied to the rear left motor. The same motor is again used as the disabled motor in the second scenario. The rear left motor is selected due to the increased yaw moment it applies during the failure as in Fig. 7. When a motor fault torque is applied a negative longitudinal force component is applied at the tyre's contact patch proportional to the radius of the tyre. The applied longitudinal force component applies yaw moment, in relation to the distance from the centre of mass, but also as a reduction of the lateral forces at rear axle compared to the front axle because of the friction ellipse. During the second fault scenario, the reduction of the lateral force due to the longitudinal component is similar before and after the fault application due to the similar absolute torque applied. However, the yaw moment caused by the longitudinal force component is still applied because of the opposite torque application across the rear axle. In addition due to the reversal of the longitudinal acceleration vector there is a longitudinal load transfer, unloading the rear tyres and loading the front ones affecting the peak lateral force capability of the tyres.
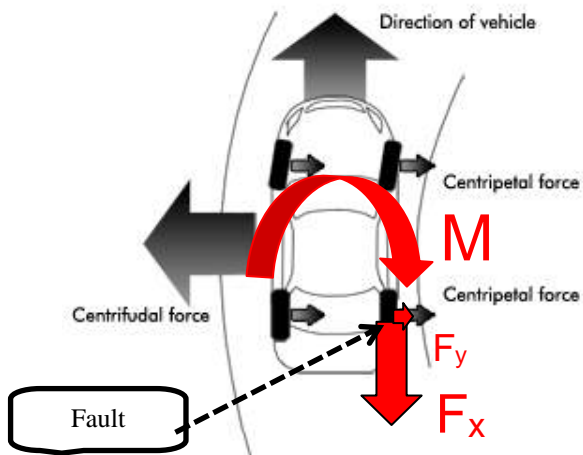
Fig. 7. Yaw disturbance caused by a motor's fault torque

According to Neukum, the peak yaw rate induced for irreversible steering fault at 150 kph is 2.5 deg/s, beyond which the safety of the vehicle is deemed unstable and difficult to control by the driver..

4. RESULTS

4.1 Straight line scenarios

The first set of scenarios are set on a straight line at 150km/h and only high coefficient of friction with the road mu = 1 is considered. Fig. 8 demonstrates the results of the intermittent fault application and Fig. 9 the results during the motor disabling sequence.
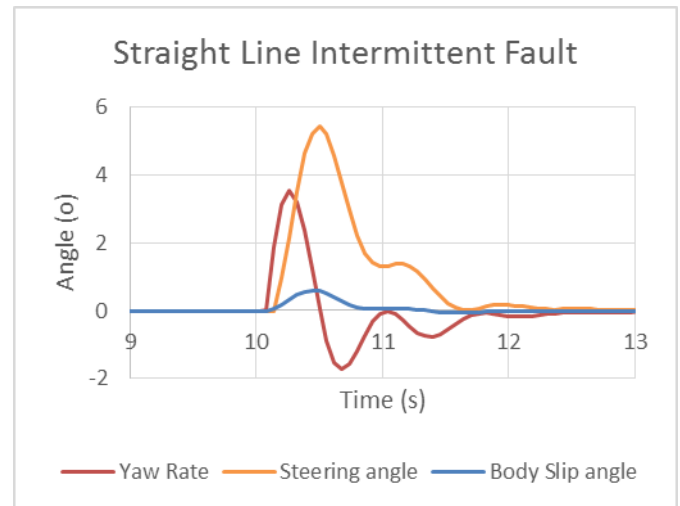
Fig. 8. Straight line performance with intermittent fault

During the intermittent fault at straight line it is understood that the fault injection creates a yaw moment that disturbs the vehicle. The sudden wheel deceleration accelerates the yaw rate up to 3.5° which is above the threshold defined by Neukum, but drops to -1.7° within 0.35s. However the body slip angle raises to only 0.6° posing no controllability issues. The amplitude of the yaw rate and body slip angle reduce to significantly low values as the fault torque also reduces and return back to normal within a second after the end of the fault torque. This scenario does not reflect any controllability issues.
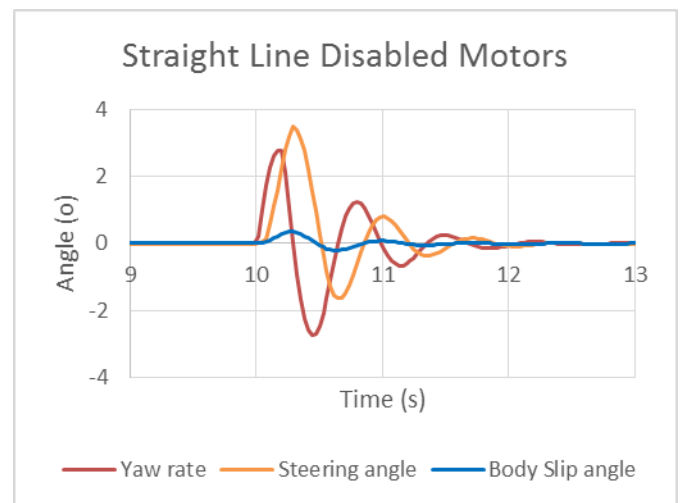
Fig. 9. Straight line performance with disabled motors

Compared to the intermittent fault, disabling permanently the motor creates a yaw moment that raises the yaw rate to 2.7° due to the longitudinal force created by the braking fault torque. However, the safety monitoring system disables the second motor across the driving axle creating a balance of longitudinal forces across the driving axle, canceling the yaw moment due to differential braking. This creates a decaying oscilation of the yaw rate and the body slip angle. The oscilation amplitude of the body slip angle ranges from 0.35°

to -0.2º. The vehicle returns back to its initial stability state at a similar time as the intermittent fault despite the different nature of the fault. This scenario does not reflect any controllability issues.

4.2 Cornering scenarios

4.2.1 Intermittent fault torque

For the cornering scenarios the two types of motor fault are investigated separately. Starting with the intermittent fault the model has been tested in numerous road friction coefficients before selecting the results demonstrated in this paper. At high mu the vehicle does not pose any risk of controllability as it is demonstrated in Fig. 10. The range of added yaw rate is 2.8º to -2.3º and added body slip angle is 0.42º to -0.13º which is slightly above Neukum's range of a permanent fault, however the above mentioned peak values are experienced for a very short time and decay with a high damping ratio.

The tyres operate within to just above their linear region entering without requiring disproportional increase of slip angle in order to provide the additional required lateral force for the stability of the vehicle. At lower mu scenarios the tyre is already operating at its non-linear region and close to its friction limit. At the high mu scenario the yaw moment developed by the reduction of lateral forces due to the fault times the wheelbase is less significant compared to the yaw moment produced by the longitudinal force applied by the fault torque times the halftrack distance. This is because the tyre operates within the linear region of its cornering stiffness and the additional longitudinal force due to the fault will not affect significantly the lateral forces applied. On low mu scenarios however, as the tyre is operating closer to its friction limit, any additional longitudinal forces will significantly reduce the lateral forces as the combined force applied by the tyre will reach the friction limit.

The above is demonstrated in Fig. 11, where the vehicle is controllable until the application of the intermittent fault when the yaw moment applied cannot be controlled because of the lack of the rear tyres to produce any additional lateral forces. The sudden increase of both the yaw rate and body slip angle demonstrate the loss of control of the vehicle despite the efforts of the driver. It should be noted that the response time of the driver is aided by the behaviour of the vehicle as with the increase of yaw rate due to the fault, the steering wheel feedback torque is also increased.
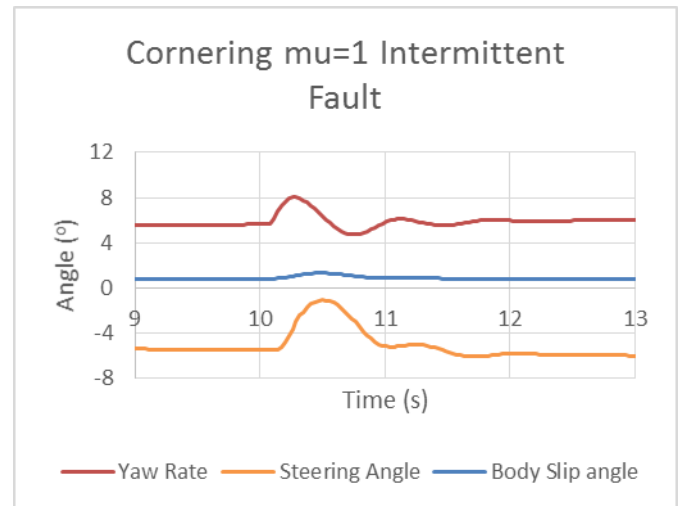
Fig. 10. Cornering performance with intermittent fault at mu = 1
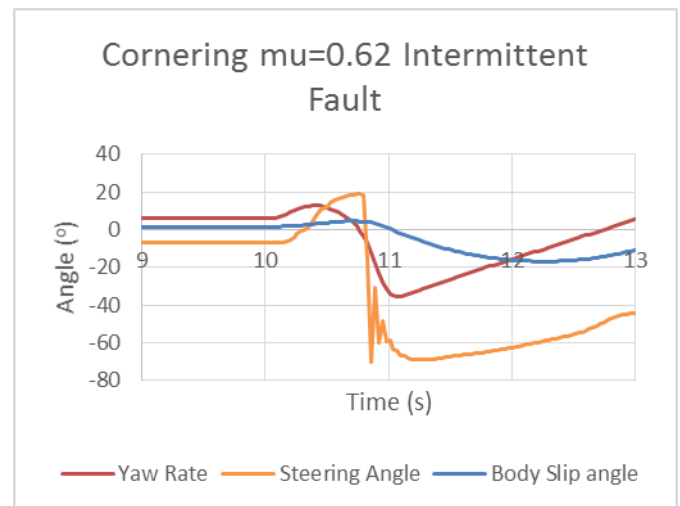
Fig. 11. Cornering performance with intermittent fault at mu = 0.62 without ESC

In Fig. 12 the uncontrolled scenario at reduced mu is attempted to be controlled with an ESC control algorithm. The resulst demonstrate that the vehicle can be controlled and provide safe performance as the added yaw rate (2.76º to -2.76º) and added body slip angle (0.57º to -0.19º) control peak limits are close to Neukum's recommendations. The oscilations of the yaw rate are caused by the delayed response of the driver attempting to control the yaw rate of the vehicle. Because of this delay in the driver's feedback, the yaw rate becomes excited by the driver's input corresponding to undamped oscilation with constant amplitude. The small gain steering angle control applied by the driver corresponds to the emotional response of the driver to maintain the initial steering wheel relative to the chosen path. This is despite the steering wheel feedback torque as it has been concluded from experimental results.
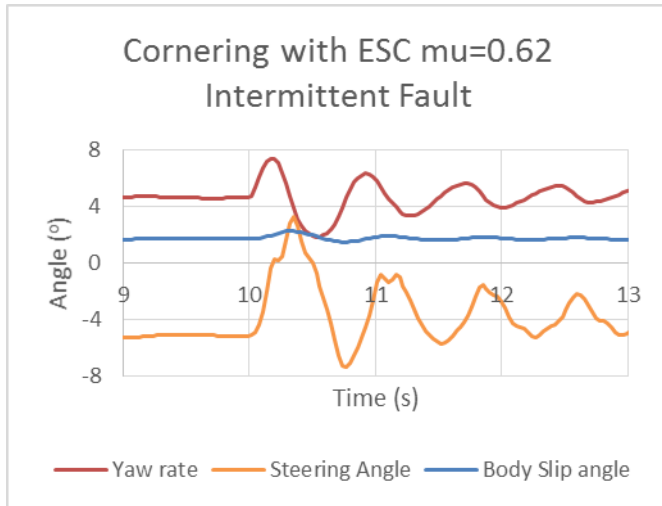
Fig. 12. Cornering performance with intermittent fault at mu = 0.62 with ESC

Fig. 13 demonstrates an attempt to tune the driver model heading feedback by reducing the filter frequency to 0.5Hz and significantly increasing the damping ratio causing the driver to respond slower to heading deviations. Despite the slower response of the yaw rate osclation frequency has increased even if the steering angle curve is now smoother.
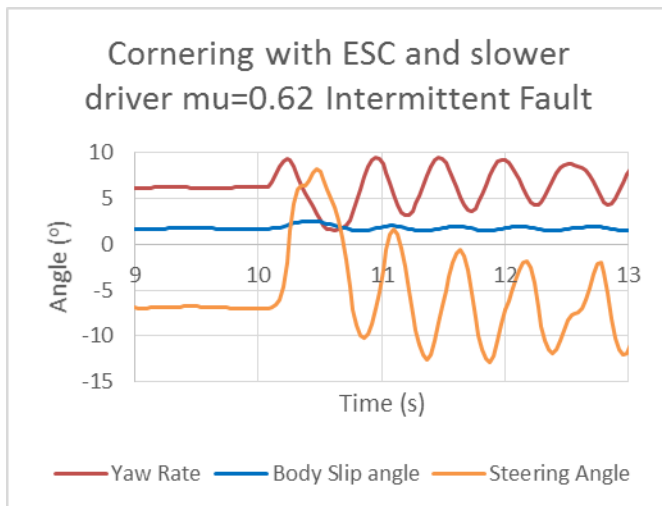

Fig. 13. Cornering performance with intermittent fault at mu = 0.62 without ESC

At this stage it is important to understand that the cornering scenario at mu = 0.62 is performed while the tyres are already close to their friction limit and within their highly non-linear cornering stiffness. A scenario like this would be difficult to control even with skilled physical driver on a vehicle with such behaviour on the friction limit. Fig. 14 demonstrates an a cornering scenario at mu = 0.7, with and without ESC where with the same driver model the ESC manages succesfully to control the yaw rate of the vehicle.
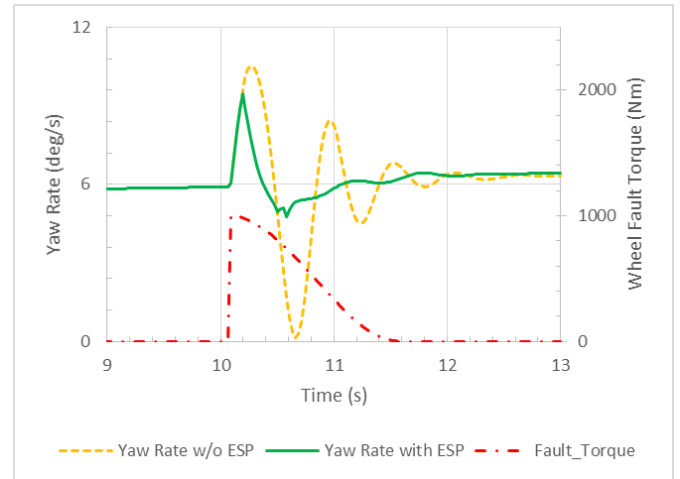
Fig. 14. Cornering performance with intermittent fault at mu = 0.65 with and without ESC

4.2.2 Disabled Motors fault

Performing the same coefficient of friction as at the intermittent fault scenarios, the disabled motors fault is deomnstrated below. Fig. 15 results at mu = 1 of the yaw rate and body slip angle indicate that there is no controllability issue. The range of the added yaw rate is 2.42° to -0.87° and added body slip angle is 0.48° to -0.03° which are within Neukum's recommendations. The disturbance is also smaller compared to the intermittent scenario. This is because the driver is already controlling the vehicle with recuded lateral forces at the rear axle, as the fault changes the direction of the applied torque, due to the motor similar limitation of torque on both driving and disabled when it is operating at the specific angular velocity corresponding to 150km/h. The longitudinal load transfer however is affecting the balance of the front to rear vertical forces causing a further reduction of the friction limit on the rear tyres.
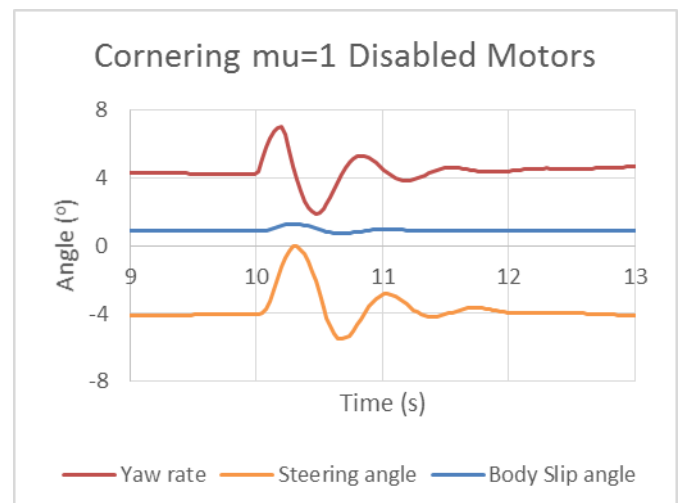
Fig. 15. Cornering performance with disabled motors at mu = 1

The above is also demonstrated at reduced mu of 0.62 in Fig. 16 where the vehicle does not need the use of ESC to maintain stability. In this scenario, the added yaw rate range is 3.87º to -3.83º and added body slip angle of 0.90º to -0.32º which is beyond Neukum's recommendations, however, the vehicle manages to return back to its initial state within reasonable time after the start of the fault.
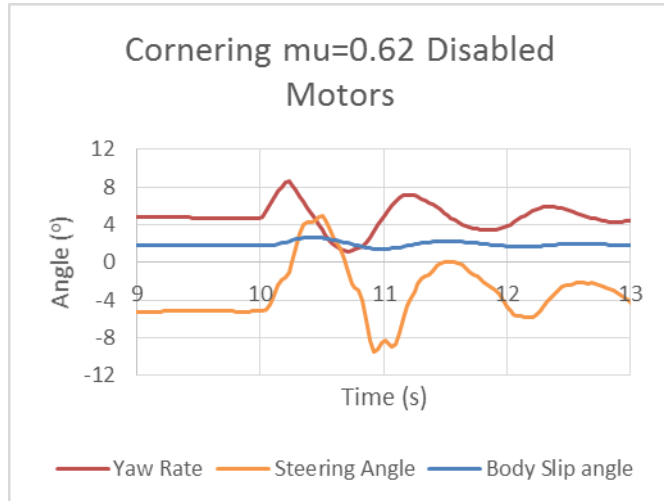
Fig. 16. Cornering performance with disabled motors at mu = 0.62 without ESC

5. CONCLUSIONS

Two different fault scenarios have been demonstrated in both high and low mu surface. The intermittent fault proved to cause significant consern of controlability especially at low mu where even skilled drivers will have difficulty controlling the vehicle without an ESC. A driver model sensitivity study is performed at the low mu cornering event with ESC in attempt to demonstrate the relationship between driver behaviour and ESC operation. From further simulations it is understood that the better the driver manages to hold the steering angle during the fault the better the ESC will manage to control the vehicle. Once the driver starts to attempt to control the heading of the vehicle by his feedback, the system enters a loop of non decaying yaw rate oscilation that can become unstable in real life.

The significant difference of the applied faults during cornering causing the intermittent fault to be less controllable during low mu scenarios is caused by the suddent change of the balance of the lateral forces applied by the tyres. This suddent change causes greater yaw momentum and grater yaw rate overshoot that can be very difficult to control at low mu due to high slip angle of the tyre close or even beyond the friction limit. On the other hand, the disabled motors scenario by inverting the applied torque direction causes less overshoot due to the small yaw momentum applied and the similar lateral forces applied by the tyres, where the slip angle of the tyres do not exceed the friction limit.

Most of the investigated scenarios can be considered to be within or just above the "disturbing" operational limits of yaw rate according to Neukum but should be considered safe.

REFERENCES

Alirezaei, M., Kanarachos, S., Scheepers, B., Maurice, J.P. (2013). Experimental evaluation of optimal Vehicle Dynamic Control based on the State Dependent Riccati Equation technique, *Proceedings of the American Control Conference*, art. no. 6579871, pp. 408-412

Ellims, M., Monkhouse, H., Harty, D., and Gade, T. (2013). "Using Vehicle Simulation to Investigate Controllability," *SAE Int. J. Alt. Power.* 2(1), pp.18-36.

Harty, D., Gade, T. (2013). *"Review of Stability Risks with In-Wheel Motors"*.

Hirano, Y. (2012). Integrated vehicle control of an in-wheel-motor vehicle to optimize vehicle dynamics and energy consumption, *Proceedings of the World Congress on Intelligent Control and Automation (WCICA)*, art. no. 6358264, pp. 2335-2339.

ISO 26262: 2011 (2011), Road vehicles -Functional safety.

Kanarachos, S.A. (2009). A new method for computing optimal obstacle avoidance steering manoeuvres of vehicles, *International Journal of Vehicle Autonomous Systems*, Vol. 7 (1-2), pp. 73-95.

Neukum, A., Ufer, E., Paulig, J., & Krüger, H.-P. (2008). Controllability of superposition steering system failure. In ATZ/TUEV SUED (Ed.), steering.tech. Available: http://www.psychologie.uni-wuerzburg.de/izvw/texte/2008_Neukum_etal_Controllability_of_superposition_steering_failures.pdf.

Reinelt, W., Lundquist, C. (2006). Controllability of active steering system hazards: From standards to driving tests, *SAE Technical Papers*.

Watts, A., Vallance, A., Whitehead, A., Hilton, C., Fraser, A. (2010). The technology and Economics of In-Wheel Motors, *SAE International Journal of Passenger Cars - Electronic and Electrical Systems*, Vol. 3 (2), pp. 37-54.

Weitzel, Alexander1; Winner, Hermann (2013). Controllability assessment for unintended reactions of active safety systems, *Proceedings of the 23rd International Technical Conference on the Enhanced Safety of Vehicles* (ESV), Available: http://www-esv.nhtsa.dot.gov/Proceedings/23/files/23ESV-000042.PDF

Creation of pre-crash simulations in global traffic accident scenarios based on the iGLAD database

Dipl.-Ing. F. Spitzhüttl*. Dipl.-Ing. H. Liers*
Dipl.-Ing. (FH) M. Petzold*

*Traffic Accident Research Institute at University of Technology Dresden, Dresden, Germany (Tel: +49 351 438989 0; e-mail: florian.spitzhuettl@vufo.de).

Abstract: Due to the globalized development of vehicles and advanced driver assistance systems (ADAS) in combination with the large variety of traffic situations all over the world, there is an increasing need of evaluating the effectiveness of ADAS on the basis of international real traffic data. This can be done with the help of so-called pre-crash matrices (PCM), which describe the vehicle dynamics in a defined time before the collision. After the publication of the first IGLAD data (1.550 accidents) a study was done dealing with the creation of pre-crash simulations out of international accidents. For the first time the benefit of an ADAS can be evaluated prospectively in the wide variety of global traffic accident scenario. This paper provides an overview of the challenges that come with merging data from different investigation areas. The main focus will be on the methodology to derive PCM from this international database. This also includes the definition of minimum requirements to enable the simulation of the vehicle behavior in the pre-crash phase. Furthermore, methods were developed how to deal with unknown data with regard to the different data quality and quantity. Finally the paper shows the unique possibility to analyze active safety systems from a global point of view by implementing and assessing an exemplary ADAS for different global traffic accident scenarios.

With the work done within the study, especially with the definition of minimum requirements and the developed methods, it is possible to create pre-crash simulations not only for upcoming iGLAD releases but also for other international accident databases.

Keywords: accident scenario, road traffic, vehicle dynamics, advanced driver assistance systems, active safety, global traffic scenario, pre-crash phase, in-depth accident data.

1. INTRODUCTION

For the development of advanced driver assistance systems (ADAS) information of the pre-crash phase are required. Therefore so-called pre-crash-matrices (PCM) can be used, as shown in (C. Erbsmehl et al., 2012). They describe the motion of participants of the accident just before collision. Additionally, current or future ADAS can be implemented in the pre-crash phase and thus an evaluation of their efficiency, as described in (Dr. H. Schittenhelm et al., 2008), is possible.

Applying that methodology to the data of the German In-Depth Accident Study (GIDAS) already produced significant results, but only for German traffic accident scenario. However, international traffic scenario is also important for the development of vehicles and their ADAS. After the first publication of the "Initiative for the Global Harmonization of Accident Data" (iGLAD), see (Bakker, 2012), it would be possible to prospectively analyze the safety potential of ADAS within the variety of road traffic accidents from around the world for the first time. Due to a smaller data volume of the iGLAD database compared with the GIDAS database, missing data is expected and the formulation of minimum requirements and the development of compensation methods seem to be necessary.

In the framework of this study a methodology for the creation of pre-crash simulations out of international accident databases is developed. The depth of information of the iGLAD data (phase I – 1.550 accidents) shall be determined and a PCM shall be created. The efficiency of an exemplarily ADAS in the field of global accident scenarios will be simulated and analyzed.

2. INITIATIVE FOR THE GLOBAL HARMONIZATION OF ACCIDENT DATA (iGLAD)

The motivation for founding an initiative like iGLAD is that traffic safety becomes more and more important from a global point of view. While fatalities due to traffic accidents are slightly decreasing in high-income countries they are strongly increasing in middle-income and low-income countries, see figure 1. Even with pessimistic predictions the worldwide number of traffic fatalities will increase tremendously in the next decade(s). The publication of the World Health Organization (WHO) "World report on road traffic injury prevention" of 2004 estimated the annual number of fatalities up to 1.3 million and around 20-50 million injured people (World Health Organization, 2004). Eighty-eight countries have reduced the number of deaths on their roads, but the total number of road traffic deaths remains unac-

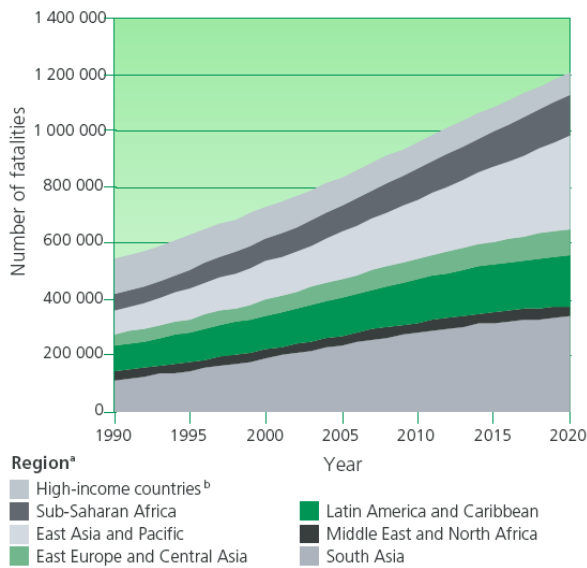ceptably high at 1.24 million per year (World Health Organization, 2013).

Fig. 1. Road traffic fatalities, 1990–2020 (World Health Organization, 2004)

Current trends suggest that by 2030 road traffic deaths will become the fifth leading cause of death unless urgent action is taken (World Health Organization, 2008). Therefore the need for action in this field and by association for an international in-depth database and its further improvement process is still very high or even increasing.

Therefore the "Initiative for the Global Harmonization of Accident Data" (iGLAD) was launched in 2011 as a collaborative project of the European Automobile Manufacturers Association (ACEA) and the Fédération Internationale de l'Automobile (FIA). Currently ten traffic accident research institutes from Europe, North America, Australia and Asia take part in the project (see figure 2).
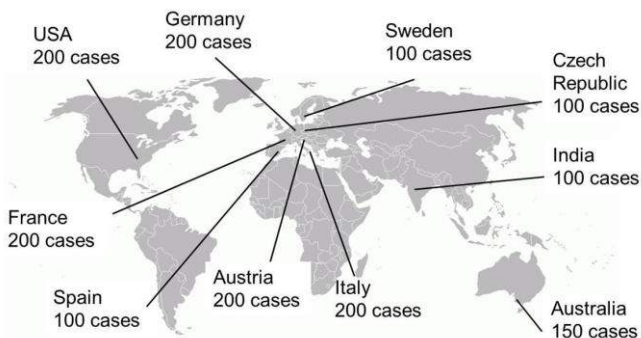
Fig. 2. Data providers of iGLAD phase I *("Data description, Data providers 2007-2012 data," 2014)*

The aim is to merge high-quality data from different national in-depth investigations. The big challenge of a harmonized accident database is the different data content of the single in-depth investigation projects. So on the one hand side it is important to ensure a minimal quality standard, but on the other hand side it is necessary to enable a useful comparison and evaluation of the efficiency of ADAS on several markets (Ockel et al., 2011). The iGLAD project members currently finished phase I. The database of phase I contains 1550 cases from 10 countries, like shown in figure 2. The inquiry period was 2007 to 2012 and each case includes information on 75 variables regarding accident, road, participants (information about vehicles and pedestrians), occupants and safety systems. Coming phases are in progress.

3. PRE-CRASH SIMULATION

ADAS are systems which assist the driver in the driving process to improve vehicle safety. Most of them have substantially reduced or will reduce the number of seriously and fatally injured persons. Therefore further development and improvement is important to support this progress. To prospectively determine the effect of an ADAS it is possible to estimate the benefit by contrasting the original scenario (no ADAS implemented) with the virtual situation with an implemented system and to compare significant parameters (see figure 3). Benefit estimations based on actual (crash) tests are limited due to small number of test scenarios and very high costs. Contrary to that simulations of accident scenarios give the possibility to estimate the benefit in a nearly infinite variety of scenarios representative for the real traffic accident scenario. Therefore, the actual vehicle behaviour in real traffic accidents has to be simulated and information about the pre-crash-phase is needed necessarily.
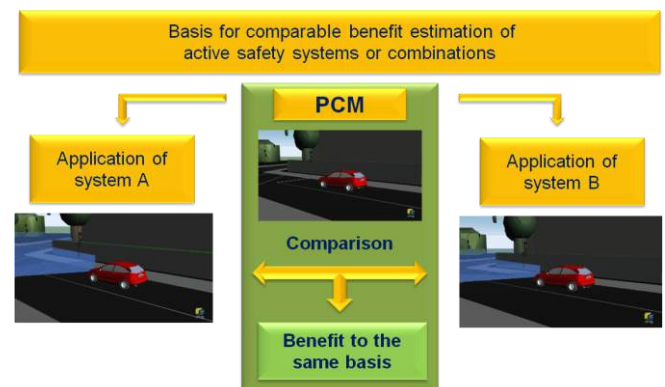
Fig. 3. Comparable benefit estimation of active safety systems

In-depth accident databases mostly contain much information about the in-crash and post-crash phases. Based on reconstruction of accident's chronological sequence it is possible to simulate the pre-crash-phase and to create so called Pre-Crash-Matrices (PCM). PCM contains information about vehicle dynamics of all participants for discrete time steps in a defined time before crash. Additionally information about surroundings, view obstacles and road markings can be contained. This data source can be used then to virtually implement ADAS into one or a large number of accident scenarios and to simulate the influence on driver and/or vehicle behavior. Afterwards, the simulation results can be used for further

analyses, e.g. for benefit estimations using Injury Risk Functions (IRF).

Pre-crash simulation and evaluation of the efficiency of several ADAS based on the German In-Depth Accident Study (GIDAS) have already been established and produce significant results, but only for German traffic accident scenario. The challenge is to adapt its methodology to the iGLAD database.
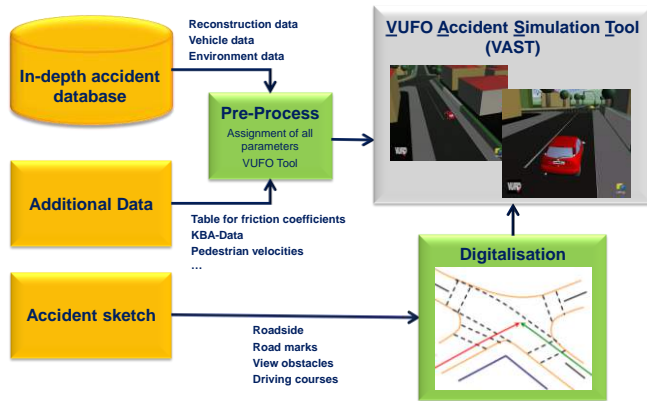

Fig. 4. Methodology of pre-crash simulation

4. PRE-CRASH MATRICES (PCM) FROM IGLAD DATABASE

4.1 Minimum requirements

The depth of information in the iGLAD database is not as high as in other real-world accident databases. For example the iGLAD database contains 71 variables within four tables, whereas the GIDAS database contains around 2,600 variables within 31 tables. This is no statement about the quality of included information but gives an indication that within iGLAD not all necessary information is available. It is expected that compensation methods as well as assumptions may be necessary. So minimum requirements are defined, characterizing necessary information which at least have to be available to enable pre-crash simulations.

The global data give some general information of the accident like the number of involved participants, combination of collision (meaning the part types of participants), number of collisions, collision type, accident type and some more.

The participant data contains all relevant information to parameterize the vehicles. Beside the numbers of the participants, which had the first collision of the accident, their geometry and further attributes of the participants are stored.

The dynamics data should give the motion characteristics of each participant. It contains global position, velocity, acceleration and global yaw angle of the vehicles. Furthermore the steering angle of the left and right front wheel should be specified. Another necessary information is, at which point the brake is actuated by the driver, so the point of reaction is specified.

The surroundings/environments data contains all the information about the surroundings like view obstacles, road geometry or marks. Roadside defines the relevant boundaries of the road, view obstacles describe relevant line-of-sight obstructions and marks define the relevant continuous, long interrupted and short interrupted road markings.

4.2 Analyses of the iGLAD database

According to the minimum requirements analyzing the released iGLAD phase I database is useful. Most of necessary global data is available for the majority of iGLAD phase I cases. The analysis shows that most vehicle data are not included in the iGLAD phase I data, see table 1.

Table 1. Analyses of participant data

NECESSARY DATA	iGLAD VARIABLE	AVAILABLE [QTY.] ✔	NOT AVAILABLE ✘	ALTERNATIVE SOURCE
PARTICIPANT NUMBER	PARTNR	2,881	0.0 %	-
TYPE OF PARTICIPANT	PARTTYPE	2,820	2,1 %	-
VEHICLE DIMENSIONS	✘	✘	✘	VEHMAKE + MODEL + REGYEAR EXTERNAL CAR DATABASES APPROXIMATION FORMULA
CENTER OF GRAVITY	✘	✘	✘	
INERTIA TENSOR I (Ixx, Iyy, Izz)	✘	✘	✘	
TRACK WIDTH	✘	✘	✘	
WHEELBASE	✘	✘	✘	
WEIGHT OF VEHICLE	VEHMASS	2,414	6.5 %	
VEHICLE ENGINE POWER	POWER	2,267	21.3 %	
COEFFICIENT OF FRICTION	✘	✘	✘	ROADCOND, WEATHER + RECONSTRUCTION

Only the type of participant, weight of vehicle and vehicle engine power are included but also not available for all cases. Therefore, all information for the parameterization of the vehicle dimensions, center of gravity, inertia tensor and so on have to be compensated or approximated. Most efficient method seems to be the use of the type of the participant, the vehicle make, the vehicle model and the year of first registration in combination with external car database. The big issue for an automated research is the variable for vehicle model which is saved as text in string format. Another challenge are different car markets, because there is no suitable global car database available. As a consequence the definition of default models seem to be necessary.

Dynamics data generally exist as parameters, but only available for around two third of all cases. Further information about global yaw angle and steering angles are not available. The global position of the vehicle has to be determined from the digitalized sketch. For motion characteristics available data does not automatically mean correct data. Therefore the data is checked to its plausibility regarding the iGLAD definitions of an uniformly accelerated (/decelerated) motion, see (1).

$$\vec{a} = \frac{d\vec{v}(t)}{dt} = \frac{d^2\vec{s}(t)}{dt^2} \qquad (1)$$

where $\vec{a}$ is the mean deceleration/acceleration (m/s2), $\vec{v}$ is the velocity (m/s), $\vec{s}$ is the distance (m) and t is the time (s).

Figure 5 shows the completeness and plausibility of the available dynamics data within the iGLAD database. It can be seen that completeness and plausibility is strongly varying across the data providers. It can be seen, that compensation methods are necessarily needed for dynamics data of the participants.
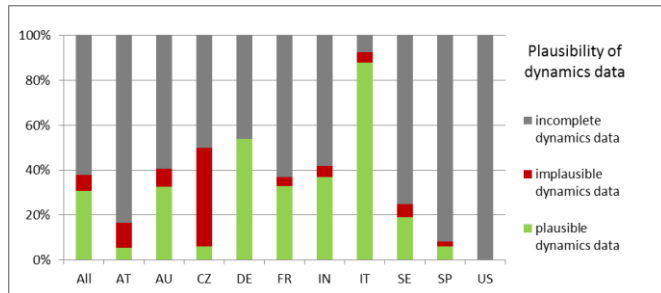
Fig. 5. Plausibility of dynamics data

The surroundings/environments data is mainly contained within the sketches. Therefore, the content of the provided sketches was analyzed. Table II shows the analysis of the minimum requirements for surroundings/environments, but only for potential cases regarding criteria named above (global data, participant data and dynamics data). It can be seen, that sketch content and quality varies strongly.

Table 2. Content of potential sketches

COUNTRY	NO. OF POT. CASES	TRA-JEC-TORY	IM-PACT POS.	CON-TACT POINT	FINAL POS.	ROAD SIDE	SCALE	POT. SKET-CHES
AT	16	9	6	1	9	10	10	0
AU	28	28	28	28	28	28	28	28
CZ	0	0	0	0	0	0	0	0
DE	59	56	52	47	54	59	59	43
FR	44	15	22	18	18	36	33	10
IN	0	0	0	0	0	0	0	0
IT	141	55	111	100	112	118	80	35
SE	4	1	1	1	1	4	1	1
SP	0	0	0	0	0	0	0	0
US	0	0	0	0	0	0	0	0
SUM	292	164	220	195	214	255	211	117

All these points clarifies compensation methods are absolutely essential to enable pre-crash simulation of global accident scenario. Without such methods there are just 117 cases (meaning less than 10 % of the whole iGLAD database) from mainly three data providers available for simulation.

4.3 Development of compensation methods

Due to non-fulfilment of the minimum requirements of the majority of the iGLAD cases, a defined dealing with missing data and the development of compensation methods are necessary to enable pre-crash simulations.

As already stated global data is existent for a high number of iGLAD cases. So generalized compensation methods are not necessary for such data. For missing information a single-case analysis is sufficient, if needed.

In contrast participant data has a lack of information within the database, so alternative data sources have to be found. It turned out that an appropriate method is the definition of standardized vehicle models which only depend on the type of participant. By this method the accuracy of the vehicle model decreases, but makes data available for a high number of cases. For passenger cars three example types have been defined for this study (mini model, compact model and maxi model). For further improvements vehicle body dependent models and also market specific models would be conceivable. This could improve the accuracy of the simulation.

The coded dynamics data within iGLAD and many other accident databases orientate on an uniformly accelerated (/decelerated) motion, see equation (1). Regarding to that, four values are defined as follows:

- the initial speed $\Rightarrow \vec{v}_0 = \vec{v}\,(t = 0)$

- the collision speed $\Rightarrow \vec{v}_k = \vec{v}\,(t = t_k)$

- the mean deceleration $\Rightarrow \vec{a}(t)\,(= \text{const.})$

- the deceleration distance $\Rightarrow \vec{s}_k = \vec{s}(t = t_k)$

This means that one missing value is possible to be calculated by three known values without losing accuracy. But for all cases with more missing information it cannot be handled like this. So the next step is to make assumptions and to define default driver and vehicle behaviour. Useful assumptions are:

1) No deceleration/acceleration
$$\Rightarrow \vec{v}_0 = \vec{v}_k = \text{const.}$$

2) Full braking
$$\Rightarrow a = f(\text{road condition})$$

3) Default velocity
$$\Rightarrow \vec{v}_0 = f(\text{road type})$$

 "1) No deceleration/acceleration" means, that there might be no reaction of the driver and the initial speed equals the collision speed. If there is no information about any deceleration or drivers reaction this is an easy assumption to compensation this missing information. Nevertheless it is clear that this decreases the accuracy of the real motion heavily. "2) Full braking" means that an emergency braking of the driver is assumed defining the deceleration as a function of the road condition, which gives a hint for the maximum coefficient of friction. "3) Default velocity" will just be used when nearly no information about the dynamics data is existing. In these cases a default initial speed as function of the type of road and the existing speed limit will be assumed. This assumption would be the worst case and the simulated vehicle behaviour might be far away from real vehicle motion characteristics.

Missing surroundings/environments data can only be compensated by single case analyses and high effort of re-drawing the sketches with the help of all other database information including the accident description, global data, participants data, dynamics data and other information. If there is not enough information available at all, it is not useful to simulate such a low case quality anymore.

The more compensation methods and assumptions have to be used, the less accurate is the simulation of a case and both accuracy and reliability are not assessable anymore. The pre-crash simulation equals more generalized scenarios than the real traffic accident. On the other hand side with such methods about 600 further cases, meaning more than 35 % of the whole iGLAD phase I database, could be used for pre-crash simulation. Finally, a sensible grade of using compensation methods has to be found.

4.4 Creation of pre-crash matrices

Building up on the previous results pre-crash simulations are performed methodically. For cases with non-fulfilment compensation methods and assumptions were applied. A look on the originally available data and the used compensation methods per case is taken. So the simulation quality can be assessed, to have an idea of the accuracy of the resulting pre-crash simulation per case.

Figures 6 to 9 visualize schematically the methodology to create pre-crash simulations for the iGLAD database divided to the dynamics data, participant's data, sketches, and the overview. Within them the different possibilities for processing can be seen. If the information is available you can use the "✔"-path. If the information is not available the " ✘- path" has to be followed and an alternative source has to be used or at least the case cannot be simulated because of too much missing data. If all necessary information from dynamics, participant data and the sketch are available and complete (see figure 10), it is possible to create pre-crash simulation for this case.

The developed methodology cannot only be adapted to upcoming iGLAD releases but also to other international accident databases.
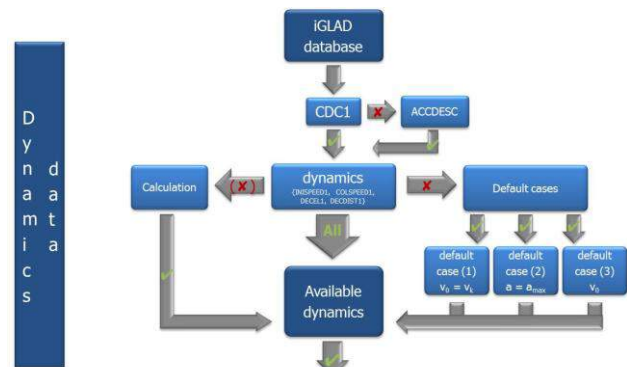
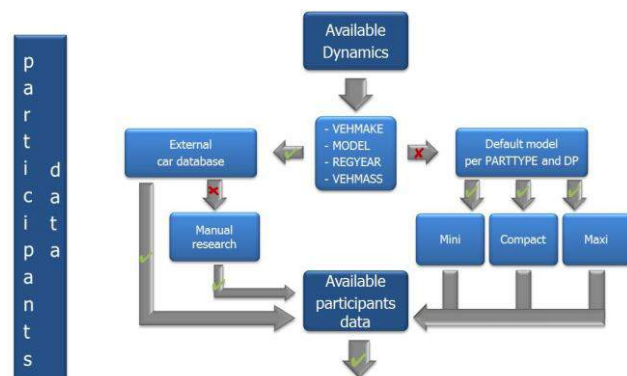Fig. 6. Methodology of creating pre-crash simulations 1

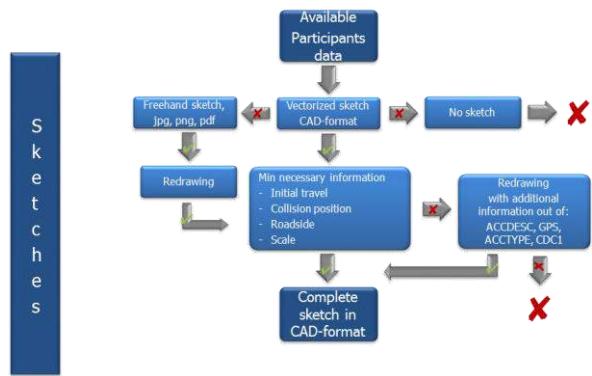Fig. 7. Methodology of creating pre-crash simulations 2

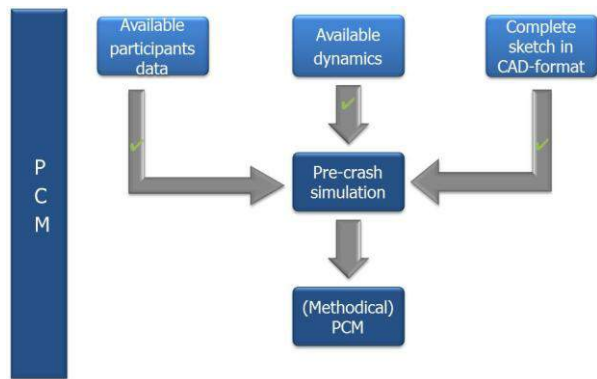Fig. 8. Methodology of creating pre-crash simulations 3

Fig. 9. Methodology of creating pre-crash simulations 4

Figure 10 shows the quality evaluation of the simulated cases, basing on the originally available data content and the used compensations methods and assumptions. Finally every simulated case has a quality number, which represents the lowest quality of the out of dynamics quality, sketch quality and simulation quality.

Fig. 10. Quality results of the Methodical PCM

4.5 Application of ADAS to pre-crash simulation

By using the created pre-crash simulations it is now possible to evaluate the effectiveness of an ADAS. Therefore two cases are representatively shown in this paper with and without an implemented Advanced Emergency Braking system (AEB). This demonstrates the benefit of pre-crash simulations from iGLAD database for the development of global road traffic safety. The implemented pedestrian-AEB system has the following characteristics:

- sensor range: 50 m
- sensor opening angle: 60 °
- sampling rate: 0.1 sec
- triggering AEB @ TTC <= 1.2 sec
- minimum object width: 0.5 m

Figures 11 and 12 show the collision position of both participants of a passenger car – pedestrian accident (country of origin: Italy). The original collision speed was 31 kph. With the virtually implemented AEB system the speed was reduced to 24 kph. So the benefit in this example is a reduction of the collision speed of 7 kph. This information can be used as input parameter for an evaluation with the help of an injury risk function.
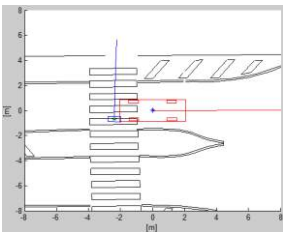
Collision speed: 31 kph   Collision speed: 24 kph

Fig. 11. Implemented ADAS – braking without AEB System

Fig. 12. Implemented ADAS – braking with AEB System

Figure 13 and 14 show the same implemented AEB for another passenger car – pedestrian accident (country of origin: France). In the original accident the passenger car collides with the pedestrian at a speed of 15 kph. With the implemented AEB system the collision could be avoided. So the benefit in this case is the complete prevention of the collision.
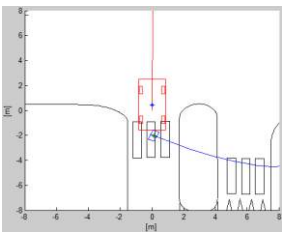
Collision speed: 15 kph   no collision

Fig. 13. Implemented ADAS – braking without AEB System
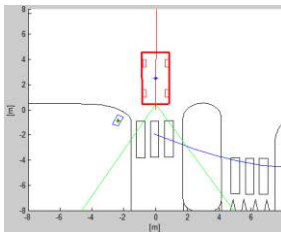
Fig. 14. Implemented ADAS – braking with AEB System

5. DISCUSSION

Pre-crash simulation and evaluation of the effectiveness of several ADAS based on the German In-Depth Accident Study (GIDAS) has already been established and produced significant results, but only for German traffic accident scenario. This study shows the possibility to do pre-crash simulation and furthermore evaluation of the effectiveness of ADAS by a reduced dataset of international data. The results exemplarily show the methodology for the iGLAD database and can also be adapted to other accident databases. For the first time it is now possible to prospectively analyze the safety potential of ADAS within the variety of road traffic accidents from around the world.

Due to a reduced dataset compensation methods and assumptions had to be introduced at the expense of accuracy and reliability of the results. The more data has to be compensated and the more assumptions have to be made, the more the results are brought closer to standard cases. To address this inaccuracy a quality criterion was introduced.

The representativeness of the iGLAD database was not analyzed within this study and thereby is unknown at this point. However, one main goal of the iGLAD project is to sample representative cases from every data provider to enable representative results in the future.

With the work done within the study, especially with the definition of minimum requirements and the developed compensation methods, it is possible to create pre-crash simulations not only for upcoming iGLAD releases but also for other international accident databases. Thus for the first time the safety potential of ADAS can be evaluated retrospectively and prospectively in the wide variety of global traffic accident scenario.

6. CONCLUSIONS

After the publication of the first iGLAD dataset a study was done dealing with the creation of pre-crash simulations out of international accidents. The main focus is on the methodology to create a Pre-Crash-Matrix (PCM) from this international database. This also includes the definition of minimum requirements to enable the simulation of vehicle behaviour in the pre-crash phase. Compensation methods were developed how to deal with unknown data with regard to the different data quality and quantity. Finally the paper shows the unique possibility to analyze active safety systems from a global point of view by implementing and assessing an exemplary ADAS for different global traffic accident scenarios. Thereby already existing ADAS and also systems which are in stage of development can be simulated and their expected benefit can be evaluated on global market.

Due to the increasing need of a high quality global in-depth database iGLAD is a continuously advancing project. Several groups (the technical working group, the steering committee, the data administration team) work together at further improvements. This means the database has no finished format and will improve with every period. Many improvements will result from this study, especially in terms of data quality,

plausibility checks and requirements on sketches and reconstruction. The phase II will be finished within 2015, containing accidents from 2012 to 2013. Based on the results of this study some decisions were made by the iGLAD consortium to improve the data quality. Many of them are already included in the current phase II.

REFERENCES

Bakker, J., 2012. iGLAD - A pragmatic approach for an international accident database.

C. Erbsmehl, A. Schubert, Dr. L. Hannawald, M. Wagner, 2012. Nutzung des IPG CarMaker zur Simulation realer Verkehrsunfälle der GIDAS Datenbank, in: IPG Technology Conference. Presented at the apply & innovate 2012.

Data description, Data providers 2007-2012 data [WWW Document], 2014. . www.iglad.net. URL http://iglad.net/web/page.aspx?refid=2 (accessed 11.1.14).

Dr. H. Schittenhelm, J. Bakker, H. Bürkle, P. Frank, J. Scheerer, 2008. Methods for analyzing the efficiency of primary safety measures based on real life accident data, in: ESAR. Presented at the Expert Symposium on Accident Research.

Ockel, D., Bakker, J., Schöneburg, R., 2011. Internationale Harmonisierung von Unfalldaten; Fortschrittsbericht des FIA / ACEA Projekts iGLAD (Initiative for the Global Harmonization of AccidentData). VDI Kongress, Berlin.

World Health Organization, 2013. Global status report on road safety 2013: supporting a decade of action.

World Health Organization, 2008. The global burden of disease 2004 update. World Health Organization, Geneva, Switzerland.

World Health Organization, 2004. World report on road traffic injury prevention. World Health Organization, Geneva, Switzerland.

Driving operations and parietal lobe activity correlate with driving skill during curve driving

Shuguang Li[*], Toshiyuki Sugimachi[*], Kimihiko Nakano[*], Yoshihiko Tabuchi[*], Yoshihiro Suda[*], Kouji Yamamoto[**], Hideki Takahashi[**], Yoshitomo Orino[**], Noriyuki Oka[***], Kayoko Yoshino[***], Toshinori Kato[***]

* Institute of Industrial Science, the University of Tokyo, Tokyo, Japan
(Tel: +81-03-5452-6098 ext: 57422; e-mail: lsg04@iis.u-tokyo.ac.jp).
** Central Nippon Expressway Co., Ltd., Nagoya, Japan.
*** Department of Brain Environmental Research, KatoBrain Co., Ltd., Japan.

Abstract: Elucidation of the relationship between brain activity and driver behavior may assist in the development of new driver models for next-generation driving-assistant systems that adapt to drivers' individual characteristics. However, multiple regions of the brain are involved in driving, so it is first necessary to investigate the role of each region. In this paper, we examined the relationship between driving skill and parietal lobe activity. We performed experiments using a driving simulator featuring a curved course modeled on a real test course. When drivers steered around the curve, data on their driving operations and the state of their vehicle were recorded, and their cortical activity was measured using functional near-infrared spectroscopy. Subsequently, jerk, which is the derivative of acceleration with respect to time, was utilized to divide drivers into the high-skilled and low-skilled groups. We found that high-skilled drivers operated the accelerator pedal and steering wheel smoothly while steering into the curve. Simultaneously, the parietal lobe was more active in the high-skilled group than in the low-skilled group at the entrance to the curve. The parietal lobe is known to integrate sensory information from various modalities. Therefore, our findings suggest that the integration of sensory information strongly influences driving skill.

Keywords: Driving Skill, Brain Activity, Driving Simulator, Near-Infrared Spectroscopy, Curve Driving

1. INTRODUCTION

Driver models that can be adapted to drivers' individual characteristics are central to next-generation driving-assistant systems. To date, several intelligent transport systems have been developed to improve vehicle safety, such as collision-avoidance and lane-departure warning systems. Researchers have identified that an embedded driver model could make such systems satisfy drivers' specific needs. For example, Zhang *et al.* (2010) proposed driving assistant systems that integrate a dynamic driver model capable of distinguishing drivers of different skill. Similarly, Fuwamoto *et al.* (2015) suggested a brake-assistant system that adjusts braking based on the evaluation of near misses or the detection of changes in physical capacity. Such driving-assistant systems could adjust their parameters for individual drivers depending on their driving skill or physical capacity, thereby meeting the requirements of different drivers and improving driving safety. Improving traffic safety is crucial, particularly in developed countries with an increasing proportion of elderly drivers and in developing countries with a growing population of novice drivers. Analysis of the driving characteristics of drivers of different driving skill may assist in the development of such driver models.

Elucidation of the relationship between brain activity and driver behavior is one way to build more effective driver models. Many studies have tried to extract driving characteristics from driving operation data. For example, Zhang *et al.* (2010) reported that the frequency of steering operations differs significantly between expert and low-skilled drivers. Chandrasiri *et al.* (2012) advocated a machine-learning approach to construct a driver-classification model based on driver behavior. In our previous research, we also developed a technology to extract characteristics that differ between high- and low-skilled drivers during curve driving (Li *et al.*, 2014). These studies yielded many interesting findings about the significant differences in the driving operations between drivers of different driving skill. Brain activity also has a significant effect on driving behaviour. However, little is known about the differences in brain activity between drivers of different driving skill. To complete even a tiny steering maneuver, drivers must gather road and traffic information in the brain, and plan and execute their decision while judging the distance and speed. In this study, we investigated differences in brain activity between high- and low-skilled drivers.

To observe drivers' brain activity during driving, it was necessary to develop noninvasive neuroimaging methods. Currently, the most commonly used noninvasive neuroimaging methods are functional magnetic resonance imaging (fMRI) and functional near-infrared spectroscopy (fNIRS; Strangman *et al.*, 2002). Uchiyama *et al.* (2003) used fMRI to identify activity in regions of the brain that correlated with drivers' ability to maintain a safe distance

from a preceding car. Calhoun & Pearlson (2012) reviewed studies that employ fMRI and simulated driving. fMRI is a powerful tool to measure drivers' brain activity; however, technical constraints mean that fMRI has many shortcomings for evaluating driving performance. In experiments using fMRI, drivers must lie in a cylinder and remain still. Therefore, simulated driving monitored using this technique is unrealistic. Conversely, fNIRS has attracted attention in this field, as the conditions of its use are relatively unconstrained. For example, Kojama *et al.* (2006) and Tsunashima *et al.* (2009) conducted experiments using fNIRS to measure brain activity in train operators and drivers. Similarly, Yoshino *et al.* (2013) observed drivers' brain activity in real highway experiments. In a driving simulator (DS) experiment, Oka *et al.* (2015) observed the brain activity of drivers steering around left curves. These reports suggested that the use of fNIRS enhances the identification of driving characteristics. Therefore, we introduced fNIRS in our research to record drivers' brain activity.

To determine the relationship between brain activity and driver behavior, it is first necessary to investigate the role of each region in driving, because driving is a complex action that involves multiple regions of the brain. This is an interdisciplinary topic, particularly concerning neuroscience. Neuroscientists have reported that the parietal lobe, which is involved in the integration of multimodal information, plays an important role in the performance of professional activities. As shown in Fig. 1, the location of the parietal association cortex is between the somatosensory cortex and visual cortices. Calvo-Merino *et al.* (2005) observed that the parietal lobes of expert dancers were more active while they were watching dance videos. Similarly, in an investigation of the differences in brain activity between expert softball players and nonathletes, Urata (2006) found that the parietal lobe was more active in the former. Furthermore, fundamental research in neuroscience found that "bimodal neurons" in the parietal lobe of monkey played an important role in tool use (Iriki *et al.*, 1996). These neurons respond to somatosensory and visual stimuli (Maravita & Iriki, 2004). Through bimodal neurons, the parietal lobe integrates sensory information of various modalities, such as visual and somatosensory information, to yield body image (Iriki *et al.*, 1996). Body image is the perception of the location and movement of the anatomic elements of the body by the brain. Iriki *et al.* (1996) found that body image can be dynamically modified and extended to tools during tool use. Motivated by these observations, we attempted to verify that parietal cortex (Brodmann Area 7, BA7) activity has a significant effect on driving operations and driving skill.
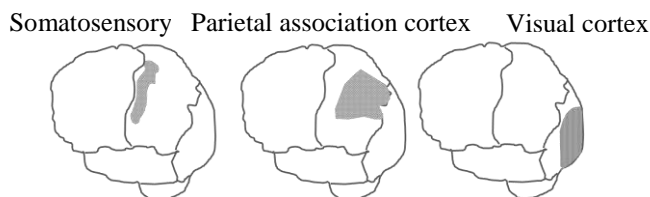
Fig. 1 The Location of Parietal association cortex (BA7)

To validate the relationship between driving skill level and BA7 activity, we performed a series of experiments using a DS featuring a course modeled on a real test course. When drivers steered around the curved course, we recorded data on driving operations and the state of their vehicle, such as speed, accelerator pedal use, and steering angle. Simultaneously, cortical brain activity was measured using fNIRS. Jerk, which is the derivative of acceleration with respect to time, was introduced to define driving skill. Subsequently, we compared driving operations and brain activity between high- and low-skilled drivers. We also examined drivers' BA7 activity during curve driving.

2. FUNCTIONAL NEAR-INFRARED SPECTROSCOPY

The principle of fNIRS is that irradiating 700–900 nm near-infrared rays pass into the scalp, then the light that has passed through these tissues is received. Using the absorption spectra of the light-absorbing chromophores present in these tissues, it is then possible to measure changes in oxy- and deoxyhemoglobin (Hb) in the cerebral blood flow, as shown in Fig. 2 (Kato, 2004).

Fig. 2 Principles of Functional Near-Infrared Spectroscopy

3. DRIVING SIMULATOR

The DS used in this study is shown in Fig. 3. It was equipped with a 6 degree-of-freedom motion platform, which was able to realize lateral and longitudinal accelerations and yaw rate. With three screens and projectors, drivers had a 140° field-of-view. It was also possible to create a realistic acoustic environment that included wind and engine noise.

Fig. 3 Driving simulator

4. EXPERIMENTS

4.1 Course

The experiments were conducted on the course shown in Fig. 4. This course was modeled on the peripheral oval road of the test course at the Japan Automobile Research Institute. First, we drove around the course and recorded the horizontal alignment and gradients of the road using vehicle-mounted global-positioning system (GPS) apparatus (RTK-GPS). Using the GPS-recorded data, we were able to entirely rebuild the alignment and gradients of the test course. The overall dimensions of the course were approximately 5.7 km long and 9.5 m wide. There were two lanes 3.5 m wide and shoulders on both sides.
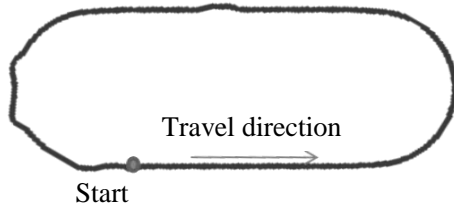
Fig. 4 Test Course for Experiments

In addition to the horizontal alignment and gradients, we also endeavored to make the illumination environment similar to that of the real road when we built the compute graphic (CG) model for the DS. The real road and CG model for the DS are compared in Fig. 5. We measured the luminance of the major components of the real road and the CG model projected on to a screen from the driver viewpoint and adjusted to a rational rate. Here, the major components included the road surface, white lines, and sky. Because of the limitations of the illumination capabilities of the projector equipped in the DS, we set the maximum illumination in the scenario at 200 cd/m^2 and other major components at the same rate. The luminance of the real course and actual DS scenario are listed in Table 1.

Fig. 5 Rebuilt Course versus Real Road Scene

Table 1 Luminous Environment of the Driving Simulator and Real Road

components	real course luminance (cd/m^2)	rate	DS scenario [actual/ (calculated)] cd/m^2	
Road surface	2000	0.16	32.1	(32)
White line	7300	0.58	116	(117)
sky	5000	0.4	79.8	(80)
Reference	12500	1	199	(200)

4.2 Outline of the Experiment

Eight healthy adults (four male and four female; average age, 33.3 ± 4.6 years) participated in the experiments. Drivers were instructed to speed up to 80 km/h after starting and to maintain this speed while avoiding veering out of their lane.

All participants practiced driving for one clockwise lap and one counterclockwise lap. Next, each driver finished 16 experimental laps (eight clockwise and eight counterclockwise). The traveling direction (clockwise or counterclockwise) of each lap was randomized.

4.3 Brain Activity Measurement

A multichannel fNIRS system (FOIRE-3000; Shimadzu Corporation, Kyoto, Japan) was used to measure hemodynamic responses and was placed behind the DS during experiments (Fig. 6). The equipment irradiated the cerebral cortex with three wavelengths of near-infrared light (780, 805, and 830 nm), and monitored changes in Hb concentrations. The sampling interval for measuring changes in Hb concentrations was 70 ms. The measurement area covered the prefrontal, motor, and parietal cortices and the occipital lobe using 96 channels. Fig. 7 shows the positions of the probes mounted on the head during an experiment. Because of the limitations of the number of channels of the fNIRS system, the 96 channels were divided into two probes that we denoted Probe-M and Probe-V. Probe-M measured the motor and parietal cortical areas using 52 channels, whereas Probe-V measured the frontal cortex and lobe using 46 channels. The position of optic fibers and channels is shown in Fig. 8. For each trail, just one probe was measured. In our experiments, both Probe-M and Probe-V measured four trails for each driver.

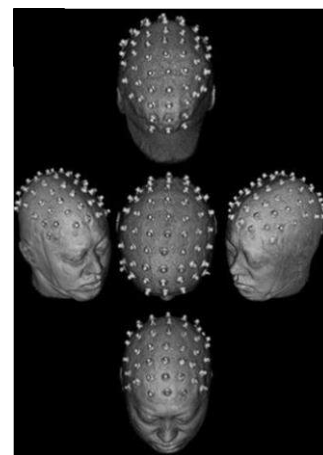Fig. 6 Multichannel Functional Near-Infrared Spectroscope and Image of an Experiment
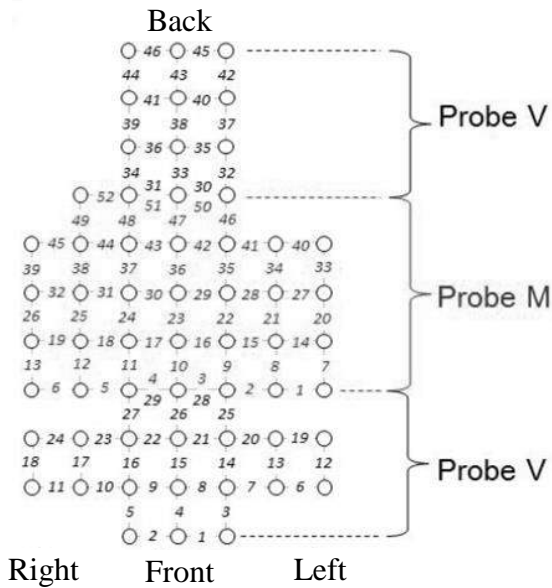

Fig. 7 Probes Mounted on the Head

Back

Fig. 8 Position of the Optic Fibers and Channels

5. RESULTS

5.1 Subject Section

In our previous research, we found that most features that differed between high- and low-skilled drivers were apparent at the entrance to the curves (Li *et al.*, 2014). To investigate the difference in brain activity between high- and low-skilled drivers while steering into the curve, a subject section of the track was selected, as shown in Fig. 9, which included: a 400-m straight section; 1 km after the start of the easement curve. The radius of the curve of the subject section was approximately 400 m. Sixty trails in the direction of travel shown in Fig. 9 were successfully measured and recorded for the eight drivers.
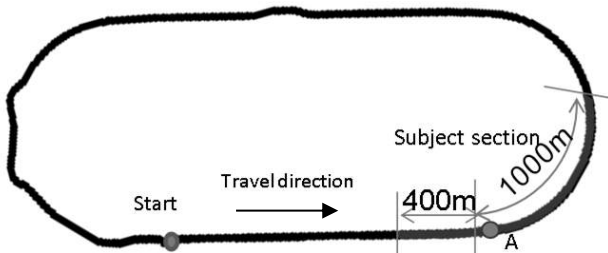
Fig. 9 Experimental Course

5.2 Definition of Driving Skill

The definition of driving skill is a complex issue. Most researchers use driving experience as a criterion, but this is variable and subjective. Researchers have found that less fuel is consumed and safety is improved if a vehicle is driven smoothly, which means a relatively smaller jerk (Murphey *et al.*, 2009). In this study, we defined the high- and low-skilled groups using a summation of the total jerk. Here we introduce the parameter *J*, which is the integrated value of all the jerk data:

$$J = \sum_{i=1}^{N} \sqrt{J_{lateral-i}^2 + J_{longitude-i}^2} \quad (1)$$

where $J_{lateral-i}$ and $J_{longitude-i}$ function as the *i-th* sample of the normalized lateral and longitude jerk, respectively, and N is the total number of the normalized jerk samples from start to finish (Li *et al.*, 2014).

To separate the high- and low-skilled drivers, all 60 trails were divided into two groups using the median of *J*. As shown in Fig. 10, 30 trails with bigger summations were defined as belonging to the low-skilled group and the rest were defined as belonging to the high-skilled group.
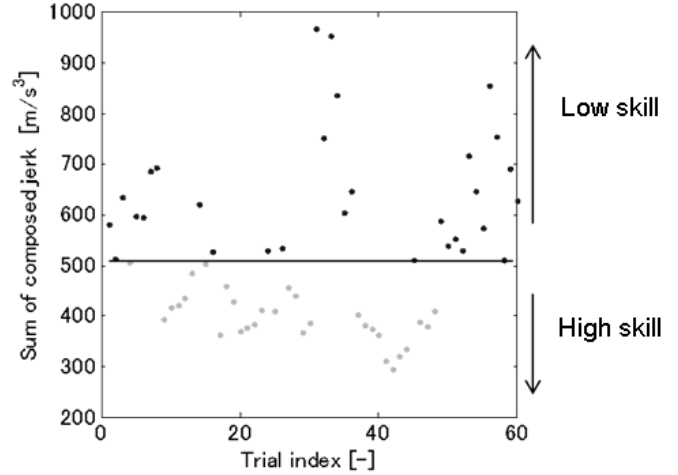
Fig. 10 Driving Skill Defined by Jerk

Next, we counted laps for each driver in the two groups. As shown by the bar graph in Fig. 11, all trails from D1, D2, D3, and D5 were defined as high-skilled trails, while all trails from D6, D7, and D8 were defined as low-skilled trails. Therefore, we defined D1, D2, D3, and D5 as the high-skilled driver group, and D6, D7, and D8 as the low-skilled driver group. We then compared driving operations and brain activity between the two groups. However, trails from D4 were not utilized, because it was hard to decide to which group this driver belonged. Here, the first two laps of all drivers were considered practice laps and not counted.

Fig. 11 Definition of the High- and Low-Skilled Driver Groups

5.3 Characteristics of Driving Operations

We compared the characteristics of driving operations between the high- and low-skilled groups. The average speed, percentage accelerator pedal, and steering angle in the subject

section of the two groups are shown in Fig. 12. The *x*-axis is the distance from the beginning of the subject section. The locations at which the significant difference (Mann–Whitney *U*-test, p < 0.05) between the two groups became apparent are marked by a dotted line. Our results show that the two groups performed almost identically in the straight section, which corresponds to the interval from 0~400 m. But from approximately 500 m, when drivers started steering into the curve, the speed of low-skilled drivers markedly diminished and their accelerator pedal percentage decreased. Conversely, high-skilled drivers maintained their speed and accelerator pedal percentage. In the same duration, drivers were steering into the curve. Therefore, high-skilled drivers maintained accelerator pedal use while steering smoothly, but low-skilled drivers frequently adjusted the accelerator pedal and tended to slow down while steering.
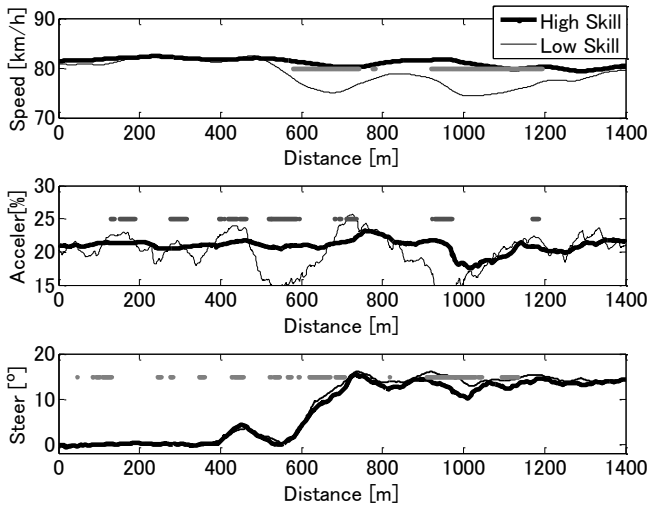
*dotline: significant (Mann–Whitney U-test, p < 0.05)
Fig. 12 Operations Performed by High- and Low-Skilled Drivers

5.4 Parietal Lobe Activity

Reportedly, cerebral oxygen exchange (ΔCOE) is an effective index of local brain activity (Kato, 2004; Sano *et al.*, 2013). We used ΔCOE to evaluate the BA7 activity of our drivers. ΔCOE was calculated using the following equation:

$$\Delta COE = \frac{[\Delta DeoxyHb] - [\Delta OxyHb]}{\sqrt{2}} \qquad (2)$$

where Δdeoxy-Hb and Δoxy-Hb are raw waveform data for changes in oxy-Hb and deoxy-Hb recorded using fNIRS. A positive ΔCOE value indicates brain activity. Previous research showed that the main causes of fluctuation of the optic signals obtained are oscillations of 0.1 Hz resulting from regional cerebral blood flow (Mayhew *et al.*, 1996). Based on this finding, we subjected the raw Δoxy-Hb and Δdeoxy-Hb data to low-pass filtering at 0.1 Hz to remove high-frequency components.

Using ΔCOE data, we compared BA7 activity between the high- and low-skilled groups. ΔCOE measured at the beginning of the subject section was considered the baseline. Then, ΔCOE was integrated every 100 m for each trail. Next,

significant differences (Mann–Whitney *U*-test, p < 0.05) between the two groups were examined. The distribution of significantly activated locations in the Brodmann area 7 (BA7) of high-skilled drivers is shown in Fig. 13. The *x*-axis of Fig. 13 is the distance from the beginning of the subject section. The *y*-axis indicates 17 channels of data corresponding to the BA7. Our results show that, in the straight section from 0~400 m, ΔCOE in the two groups almost didn't exhibit any significant difference. From 400 m, at the start of the easement curve, the BA7 of high-skilled drivers was more active, particularly after 600 m. Fig. 14 shows the average ΔCOE for the two groups, in which brightness indicates higher activity. Our results show that the BA7 was more activated in both the left and right hemispheres of high-skilled drivers.
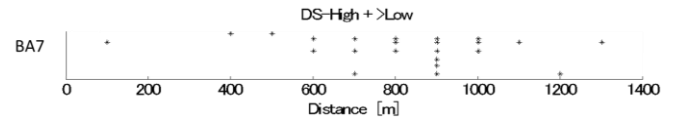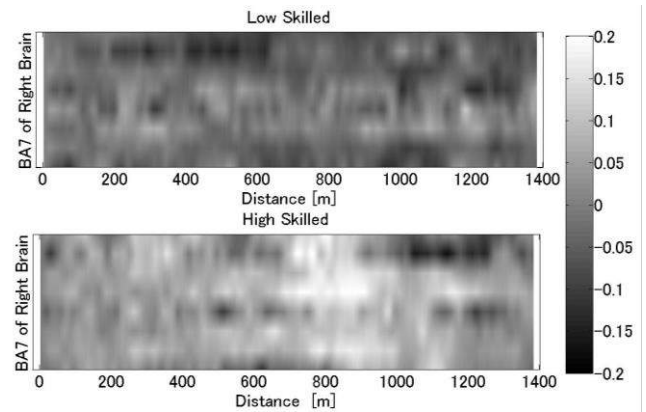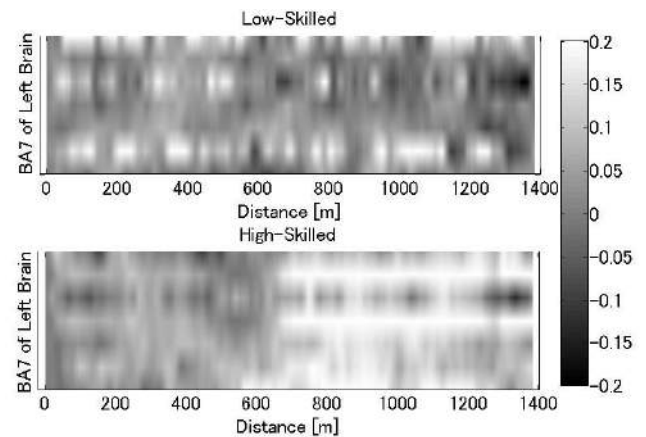

Fig. 13 Distribution of Significantly Activated Locations in the Brodmann Area 7 of High-Skilled Drivers


(a) BA 7 in the Right Hemisphere

(b) BA 7 in the Left Hemisphere

Fig. 14 Comparison of BA 7 Activity between the High- and Low-Skilled Driver Groups

Furthermore, considering the BA7 as a unit, we calculated the average ΔCOE of the BA7 for each trail along the course. Graphs of the average ΔCOE of the high- and low-skilled groups are shown in Fig. 15. A significant difference (Mann–Whitney *U*-test, p < 0.05) between the two groups was detected. Our results show that, in the interval from

600~1200 m, more oxygen was consumed in the BA7 of drivers in the high-skilled group. This suggests that the BA7 of high-skilled drivers was more active in this interval.
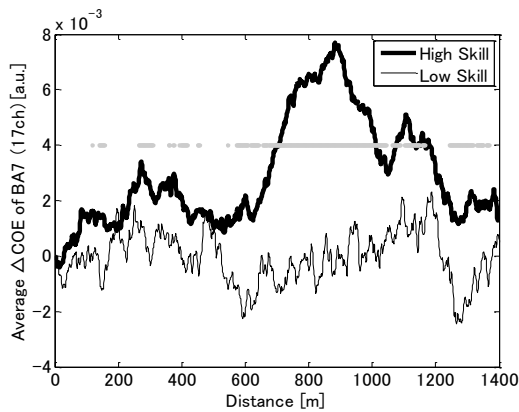
*dotline: significant (Mann–Whitney U-test, p < 0.05)

Fig. 15 Activity of the BA7 in the Two Groups

6. DISCUSSION

We analyzed the characteristic differences in driving operations and BA7 activity between high- and low-skilled drivers. Our findings show that high-skilled drivers operate the accelerator pedal and steering wheel smoothly while steering into the curve, and that the BA7 of high-skilled drivers is more active. Because the BA7 is involved in the integration of multimodal information, our results suggest that the integration of information has a significant effect on driving skill.

We constructed a block diagram (Fig. 16) to describe the relationship between brain activity involved with the integration of information related to perception and driving skill. Drivers perceive environmental information, integrate this in the BA7, and prepare these materials for judgment. The BA7 of high-skilled drivers was more active, suggesting that their ability to integrate this information is enhanced. This is a potential explanation of why high-skilled drivers drive more smoothly at the entrance to a curve. Therefore, the ability to integrate information must be an important factor determining driving skill.

*IIBA: Information Integration Brain Activation
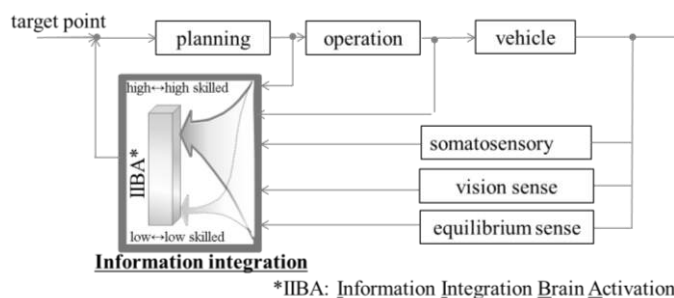
Fig. 16 Relationship between Information Integration and Driving Skill

Furthermore, information integration in the BA7 is known to contribute to the construction of body image. Therefore, based on the results of this research, body image must also influence driving skill. To act efficiently in space, our brain must both localize any objects of interest in our extra

personal space and hold a constantly updating idea of our body shape and posture, or body image, defined as a body map in the brain (Maravita & Iriki, 2004). When researchers trained Japanese Macaques to be dexterous tool users, they found that their parietal lobe integrated information from multiple sensory modalities (typically somatosensory and visual). Particularly, they found that their body image was not limited to the body profile, but extended to the tool (Iriki *et al.*, 1996; Maravita & Iriki, 2004). Similarly, when we learn to use a vehicle as a tool, it is reasonable to consider that our body image is remodeled. Drivers integrate information from multiple sensory modalities and construct a body image that extends to include the shape of the vehicle. This "extended body image" would permit drivers to consider the position and size of the vehicle from a body-centered perspective. Such a sensation is easily demonstrated while parking or driving through a narrow gap. In this study, drivers constructed an extended body image while driving through a curve, but discrepancies in the precision of this extended body image may reflect differences in driving skill. High-skilled drivers were able to construct a more accurate extended body image and experience a high sense of unity with the vehicle: these drivers more often adopted good positioning and therefore frequent adjustment operations weren't necessary, resulting in smoother driving. In conclusion, a high sense of unity with the vehicle leads to high-skilled driving. We believe that the precision of the extended body image constructed through the integration of information in the BA7 affected driving skill. Our results suggest that this sense of unity could be estimated by investigating brain activity in the BA7.

7. CONCLUSIONS

To validate the relationship between driving skill and BA7 activity, we performed experiments using a DS and measured cortical activity using fNIRS. We found that high-skilled drivers can operate the accelerator pedal while steering smoothly during curve driving. Simultaneously, the BA7 was more active in the high-skilled group than in the low-skilled group at the entrance to the curve. Our results suggest that activity of the BA7, which is involved in the integration of multimodal information and constructing body image, contributes to driving skill.

Our findings suggest that the ability to integrate information differs in drivers of different driving skill. Our findings will assist in the development of driver models that reflect individual driving characteristics for use in next-generation driving-assistant systems. Future work must investigate the relationship between driving behavior and brain activity during interactions with traffic lights, pedestrians, traffic signs, and other vehicles.

ACKNOWLEDGMENTS

REFERENCES

Zhang, Y., Lin, W. C., & Chin, Y. K. (2010). A pattern-recognition approach for driving skill characterization. Intelligent Transportation Systems, IEEE Transactions on, 11(4), 905-916.

Fuwamoto,Y., Moriizumi, K., & Ito, S. (2015). Driving simulator study on the braking behavior of drivers toward unexpected brake lamp of lead vehicle, 2015 JSAE Annual Congress (Spring) Proceedings, 210-212.

Chandrasiri, N. P., Nawa, K., Ishii, A., Li, S., Yamabe, S., Hirasawa, T., & Taguchi, K. (2012). Toyota InfoTechnology Center, Co., Ltd., Toyota, Japan. In ITS Telecommunications (ITST), 2012 12th International Conference on (pp. 542-547). IEEE.

Li, S., Yamabe, S., Sato, Y., Suda, Y., Chandrasiri, N. P., & Nawa, K. (2014). Learning Characteristic Driving Operations in Curve Sections that Reflect Drivers' Skill Levels. International Journal of Intelligent Transportation Systems Research, 12(3), 135-145.

Strangman, G., Boas, D. A., & Sutton, J. P. (2002). Non-invasive neuroimaging using near-infrared light. Biological psychiatry, 52(7), 679-693.

Uchiyama, Y., Ebe, K., Kozato, A., Okada, T., & Sadato, N. (2003). The neural substrates of driving at a safe distance: a functional MRI study. Neuroscience Letters, 352(3), 199-202.

Calhoun, V. D., & Pearlson, G. D. (2012). A selective review of simulated driving studies: combining naturalistic and hybrid paradigms, analysis approaches, and future directions. Neuroimage, 59(1), 25-35.

Tsunashima, H., & Yanagisawa, K. (2009). Measurement of brain function of car driver using functional near-Infrared spectroscopy (fNIRS). Computational intelligence and neuroscience, 2009.

Kojama, T., et al. (2006) A study on measurement of higher brain function in train operation, 15th The Transportation and Logistics Conference, (15), 313-316 (in Japanese)

Yoshino, K., Oka, N., Yamamoto, K., Takahashi, H., & Kato, T. (2013). Functional brain imaging using near-infrared spectroscopy during actual driving on an expressway. Frontiers in human neuroscience, 7: 882.doi:10.3389/fnhum.2013.00882..

Oka, N., Yoshino, K., Yamamoto, K., Takahashi, H., Li, S., Sugimachi, T., Nakano, K., Suda, Y., & Kato, T. (2015). Greater Activity in the Frontal Cortex on Left Curves: A Vector-Based fNIRS Study of Left and Right Curve Driving, 10 (5), e0127594. doi: 10.1371/journal.pone.0127594.

Calvo-Merino, B., Glaser, D. E., Grèzes, J., Passingham, R. E., & Haggard, P. (2005). Action observation and acquired motor skills: an FMRI study with expert dancers. Cerebral cortex, 15(8), 1243-1249.

Urata, H., (2006) Differences in Brain Activation between Expert Softball Players and Non-athletes: an fMRI Study Using GO/NO-GO task, Waseda journal of human sciences, 19, 96.

Iriki, A., Tanaka, M., & Iwamura, Y. (1996). Coding of modified body schema during tool use by macaque postcentral neurones. Neuroreport, 7(14), 2325-2330.

Kato, T. (2004). Principle and technique of NIRS-Imaging for human brain FORCE: fast-oxygen response in capillary event. In International Congress Series (Vol. 1270, pp. 85-90). Elsevier.

Murphey, Y. L., Milton, R., & Kiliaris, L. (2009). Driver's style classification using jerk analysis. In Computational Intelligence in Vehicles and Vehicular Systems, 2009. CIVVS'09. IEEE Workshop on (pp. 23-28). IEEE.

Sano, M., Sano, S., Oka, N., Yoshino, K., & Kato, T. (2013). Increased oxygen load in the prefrontal cortex from mouth breathing: a vector-based near-infrared spectroscopy study. Neuroreport, 24(17), 935-940.

Mayhew, J. E., Askew, S., Zheng, Y., Porrill, J., Westby, G. M., Redgrave, P., Rector, D.M., & Harper, R. M. (1996). Cerebral vasomotion: a 0.1-Hz oscillation in reflected light imaging of neural activity. Neuroimage, 4(3), 183-193.

Maravita, A., & Iriki, A. (2004). Tools for the body (schema). Trends in cognitive sciences, 8(2), 79-86.

Characterization of Driving Dynamics on road incidents collected by EDR

**Daniel LECHNER*, Claire NAUDE*, Thierry SERRE*, Maxime DUBOIS-LOUNIS*,
Michèle GUILBOT*, Jean-Yves FOURNIER*, Vincent LEDOUX****

**IFSTTAR Laboratory of Accident Mechanism Analysis, Salon de Provence,
France (Tel : 33 (0)4 90 56 86 14;e-mail : daniel.lechner@ifsttar.fr, www.ifsttar.fr)*
**CEREMA DTTV, Lyon, France (e-mail:vincent.ledoux @cerema.fr , www.cerema.fr)

Abstract: French government decided to support the SVRAI project (Saving Lives through Road Incident Analysis Feedback) to answer the question "Can incident data analysis help to avoid accidents?" Thus a 12 months data collection involving 50 public vehicles, fitted with a dedicated EDR named EMMA, was carried out. This paper focuses on results concerning vehicle dynamics: 339 incidents were collected, among which 70 % concern the lateral direction, with 70 % in right hand turns vs 30 % in left ones. Based on additional data synthesizing complete travels, 3D representations of dynamic parameters are also shown interesting to characterize driver performance.

Keywords: Vehicle dynamics, Active Safety, Accident, Incidents, Event Data Recorder.

1. INTRODUCTION

Accident data are useful to define road safety policies and particularly to identify where the road infrastructure should be improved. But the international trend of reduction of accidents during this last decade induced a lack of reliable data. They are more diffuse and local authorities can face difficulties to set priorities in their intervention policy on their road network.

In light of the fact that for 1 fatality there are many incidents, i.e. dangerous or hazardous driving situations, the French government (DSCR) decided to support the SVRAI project (Saving Lives through Road Incident Analysis Feedback) to complete accidentology with incidentology data. The SVRAI challenge is to answer to the question: Can incident data collection and analysis help to avoid accidents?

This study is based on a recording device named EMMA (Embedded data logger for accident mechanisms), specifically designed to detect driving situations considered as risky, during which the vehicle reaches high dynamics demands in longitudinal, lateral or combined directions. Among the large panel of data processing enabled by the SVRAI data collection, this paper focuses on the *characterization of driving dynamics on the road incidents collected by the 50 vehicles of public fleets* involved in the project.

2. MATERIAL AND METHODS

The SVRAI project relies on the Event Data Recorder (EDR) EMMA which was designed in 2007 by IFSTTAR-LMA with help of KERLINK, a small business society specialized into "Machine to Machine"

(Lechner & Naude, 2011).

Fig. 1.   The EMMA device.

In the first phase of the SVRAI project, 50 EMMA were implemented on public fleets of vehicles on 3 sites in France, Rouen, Clermont-Ferrand, and Salon-de-Provence. The data collection started in August 2012 and lasted one year. EMMA acquires:

- Analog data from low cost sensors directly integrated into the EDR (accelerometers and gyrometers), with a 100 Hz frequency,

- Data provided by low-cost GPS: trajectory and speed,

- Data available on vehicle on-board diagnostic system (CAN bus), which depend on the car model.

The data are analyzed, using real-time processing performed by the embedded software, to detect potential situations of interest (events). The processing is based on the following principles: when acceleration and jerk signals exceed simultaneously thresholds given hereafter, an event is triggered. The data acquired 30 seconds before and 15 seconds after the trigger are

stored in the device. These thresholds are the following:

- Speed <= 80 km/h and acceleration norm > 0.6 g and jerk > 2 g/s,

- Speed > 80 km/h and acceleration norm > 0.5 g and jerk > 2 g/s,

- Speed > 100 km/h and acceleration norm > 0.4 g and jerk > 2 g/s.

The file containing the whole data set is automatically sent to a secured server using GSM network. The event is then examined by an operator and, if considered of interest, classified as incident and stored as such in the global database.

Simple Events are mostly characterized by very short durations of acceleration peaks, generally not produced by a driver action, but however felt by the driver (often road infrastructure defaults), while genuine incident criteria are higher durations of accelerations, resulting from driver actions (up to 3 Hz). These differences were detailed in Serre and *al.* (2013).

Genuine incidents are clearly of major interest for the SVRAI Project. In addition the GPS data of all the itineraries are recorded, but stored with 1 position per minute only. Finally, the data collection comprises a file named "Travel Synthesis", concerning each itinerary, which allows characterizing the dynamic demands on many different samples of itineraries: over the whole database, or on travels performed on a given car, by different drivers, on the same itinerary... These data are not stored as time history, but under matrix form, aggregating the time spent at a given longitudinal and lateral acceleration combination, with 0.1 g intervals. The vehicle speed can also be taken into account in this collection, as an additional option, using 10 km/h intervals.

All the legal conditions to implement EDR in French public fleets of vehicles were respected during SVRAI, in accordance to the prescriptions of the CNIL (French administrative authority protecting privacy and personal data), integrating European regulations and respect of Human Rights.

The data collection is therefore limited to driving situations of interest from a research point of view. Moreover to ensure personal data protection, drivers should be informed about the experiment objectives and be volunteers: their consent should be free, enlightened and specific. EDR are thus inactivated by default, and volunteer drivers have to opt-in by pushing a button to start the recording at each itinerary. Anonymity is also guaranteed: Drivers are free to authenticate themselves using a RFID badge; this action gives access to their gender, age and driving license date to the researchers in charge of the specific driver data analysis.

These constraints induced consequences on the data

collection: EMMA average activation rate appeared to be only about 33 % and driver authentication rate covers only 17 % of the mileage (inside time where EMMA was activated). 221 drivers were volunteers to take part to the experiment and 154 got a RFID badge. Finally only 51 drivers self-authenticated. Among them, 48 produced travel syntheses and 18 experienced incidents.

3. SYNTHESIS OF RESULTS ON INCIDENTS

The whole SVRAI database for one year represents 3052 itineraries and 106645 km, apportioned on the 50 vehicles fitted with EMMA. It enabled to collect 339 incidents and 1237 simple events. The analysis of mileage, performed on the 26 vehicles on which the information was available on the CAN bus, reveals one incident every 300 km or every 5 hours of driving.

Figure 2 presents the breakdown for the 339 incidents collected as a function of the main dynamical demand on the vehicle in longitudinal, lateral or combined directions. The circles with 0.4, 0.5 and 0.6 g radius represent the level of acceleration beyond which an incident is triggered, if speed exceeds 100 and 80, or is lower than 80 km/h respectively. It can be noticed that 70 % of the incidents concern lateral accelerations (237 cases), 25 % longitudinal (85) and 5 % a combination of both (17). Among the lateral incidents, the right hand side turns represent 70 % against 30 % for the left hand side turns. The triggering speed exceeds 100 km/h for 11 % of cases, and 80 km/h for 9 %. For longitudinal triggering, speed exceeds 100 km/h for 16 % of braking incidents. The 3 positive longitudinal accelerations beyond 0.6 g correspond to one slight collision, one pothole and one abrupt start with wheel spin.
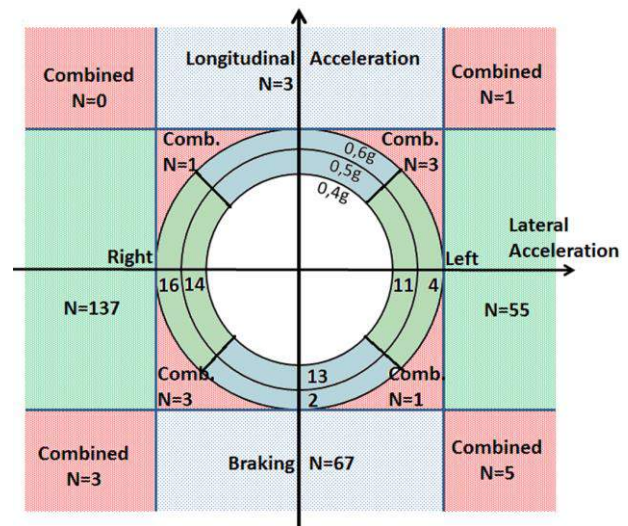

Fig. 2. Breakdown of incidents as a function of the main dynamical demand on the vehicle

Figure 3 provides additional knowledge about the breakdown of incidents as a function of the road layouts involved. Pure braking actions on a straight line

represent 19 % of incidents. Right/left bends are involved in 41/14 % of cases, whereas turns to right/left on crossroads are the theater of 8/4 % of incidents respectively. The remaining (14 %) are roundabouts, with only 2 % in the right bend entrances, 6 % in the right bend exits, and 6 % in the central left turns. While roundabout entrances and exits are generally transient manoeuvers, the central parts induce generally more steady state behaviors.

The large difference between the numbers of incidents in right/left bends (i.e. 41/14 %) can mainly be explained by the fact that the vehicles circulate on the right side of the road in France. This point has several consequences:

- All the motorway or main road exits are right hand bends, and these designs often provoke high dynamic demands on the car,

and on 2 way traffic roads:

- The drivers can feel more confident to reach high lateral accelerations in right bends, as the opposite lane of traffic on the left may act as a possible recovery area,

- The right hand side driving offers more capabilities to increase the radius of curvature of left bends by cutting the path using the opposite lane of traffic,

- Considering a given bend, when a vehicle turns on the right, the radius of curvature is slightly lower than when the vehicle turns on the left; consequently the lateral acceleration (equal to V^2/R if one neglects the side slip and the road banking) is slightly higher.
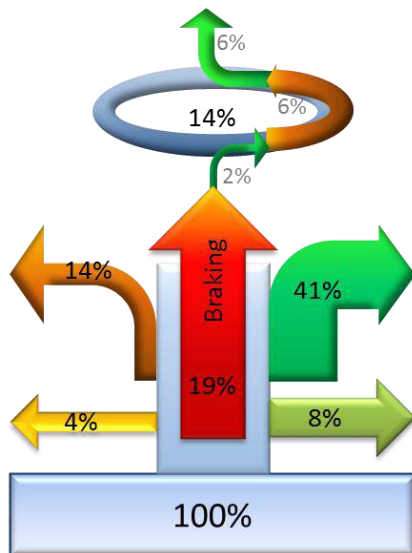
Fig. 3. Breakdown for incidents as a function of the type of road infrastructure layouts (bend, crossroad, roundabout…)

If 70 % of lateral incidents happened in right side turns, the levels of lateral acceleration, when EMMA triggered, are also higher in right turns than in left turns, as illustrated on figure 4. For instance lateral acceleration exceeds 0.7 g for 48 % of incidents in right turns and only 24 % of incidents in left turns.
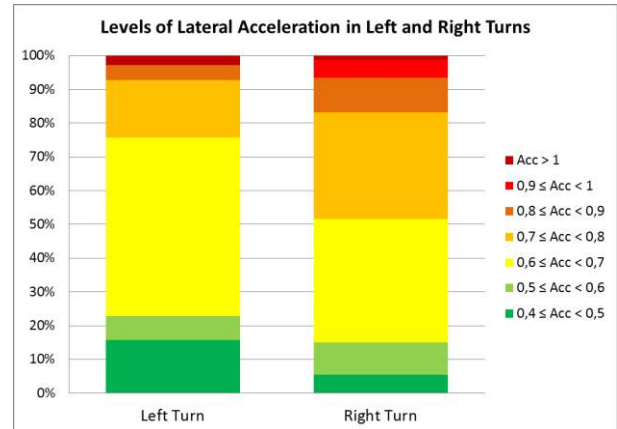
Fig. 4. Comparison of lateral acceleration in left (30 %) and right bends (70 %) when incidents are triggered

4. CHARACTERIZATION OF DRIVING DYNAMICAL PARAMETERS

The concept of "Travel Synthesis" was presented in Lechner and Naude (2011): the algorithm takes into account only the periods of braking (identified when brake lights are on), significant positive longitudinal acceleration (with throttle exceeding 60 %) and lateral acceleration (when the steering angle exceeds +/-30°).

To illustrate how this data collection enables to characterize driving dynamics, Figure 5 presents the 3D representation of dynamic parameters obtained from the matrices of Travel Synthesis, *by cumulating all the itineraries collected during 12 months by all the vehicles.* Three typical incidents, illustrating a braking, a right hand side bend and a combined demand on the car, were added, also under the form of the crossing of longitudinal AccX and lateral AccY accelerations.
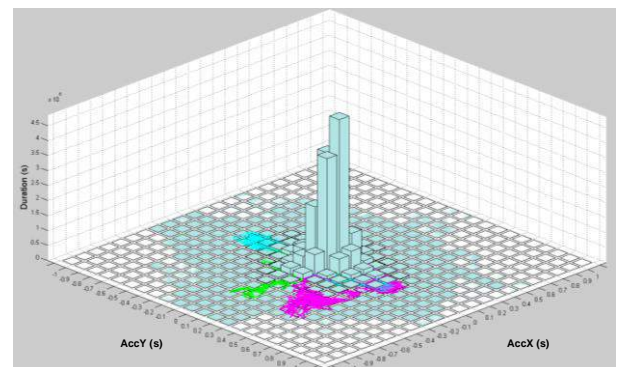

Fig. 5. 3D representation of dynamical parameters for the overall SVRAI database on which 3 typical incidents were added: braking (g) bend (c) and combined demand (m).

To illustrate more deeply the potential of this data collection, we will focus on four complementary data exploitations:

- Several incidents generated by one specific driver on one itinerary,

- Several incidents generated by one specific driver at the same location,

- Comparison of the vehicle operating area experienced by different drivers along their whole data collection,

- Comparison of the vehicle operating area experienced by two drivers on the same itinerary.

4.1 Several incidents generated by one driver on one itinerary

The example displayed on Figure 6 concerns one specific driver generating several incidents on a two hours long itinerary. It shows the 3D representation of dynamic parameters obtained from Travel Synthesis data, on which the three incidents occurring during the itinerary were added under lateral vs longitudinal accelerations form. The time history of speed, steering action and lateral acceleration during the three incidents are also shown in the upper part and the paths obtained from GPS appear in the lower part using Google Earth.
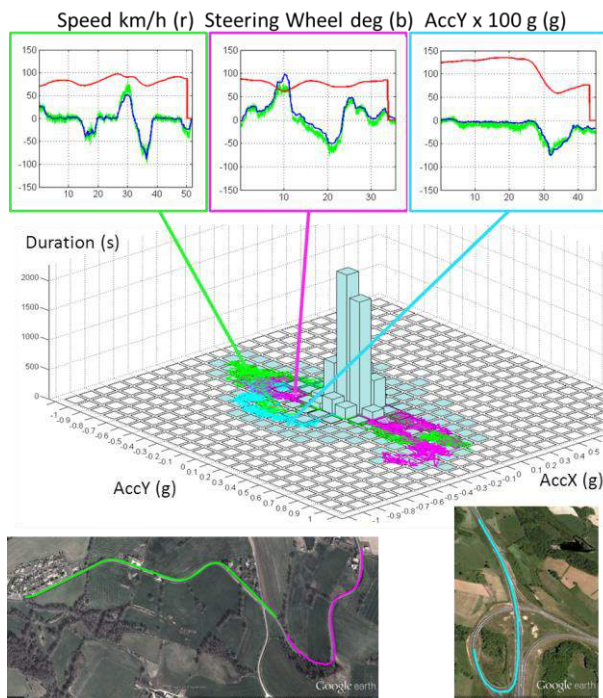
Fig. 6. 3D representation of dynamical parameters for one 2 hours long travel on which 3 incidents occurred

The incident in green produces lateral accelerations beyond 0.7 g with a speed over 90 km/h, and a light braking in the last right bend. The magenta one triggers

on both left (at 10 s) and right (20 s) bends, with 0.7 g lateral accelerations combined with light braking inside the bend to reduce speed to 60 and 70 km/h respectively. The cyan one takes place on a motorway exit; the driver enters the right bend at 130 km/h and brake simultaneously as he turns the wheel, during 200 meters, which reduces speed to 60 km/h. Dynamic demands during these three incidents are not far from the highest ones but this driver reaches the limits of the vehicle operating area in lateral at other moments on this travel.

4.2 Several incidents generated by one driver at the same location

Figure 7 shows the 3D representation of dynamical parameters for one driver, cumulating three occurrences of the same itinerary, each on which an incident occurred (upper part). The speed profiles and braking actions are also given in lower part. The site in hand is shown on Figure 8 revealing a transition between urban and rural areas. Moreover the slope is very steep with a 10 % average value.

The speeds are around 65 km/h when approaching, between 42 and 45 km/h when triggering the EMMA device in the left hand side bend (outlined by the yellow arrow on Figure 8), and go down to 32 km/h, in the following right bend, which is more tight. It should be noticed that for the 3 journeys shown, EMMA also triggered in this right bend, but the driver had a short braking action only on the cyan colored one, with a speed decreasing under 20 km/h as a consequence. This action is also visible on the 3D view of dynamic parameters, the two other cases showing more pure lateral demands. The differences in the three colored paths showing the whole 45 second long data set of each incident are not significant, since they are due to variable GPS accuracy. However the fact that each path begins at the same points is of particular interest, proving the similarities between speed profiles when approaching the point where 3 incidents are triggered.
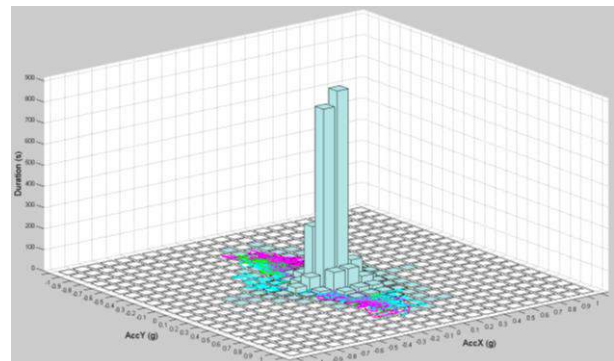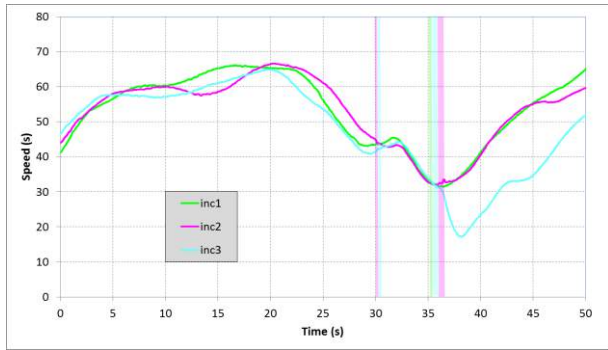
Fig. 7. 3D dynamical parameters and speed profiles for one driver on 3 occurrences of the same itinerary, on each of which an incident occurred (shown in green, magenta and cyan)
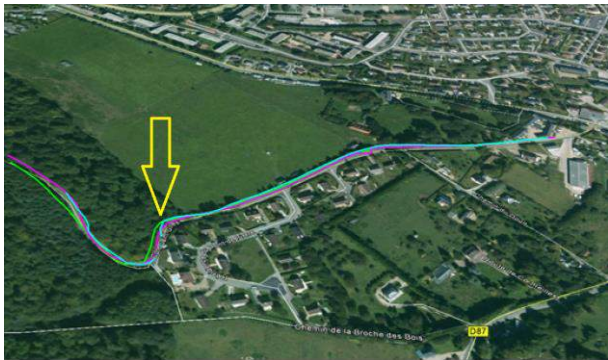

Fig. 8. Location of the 3 incidents with GPS paths

Figure 9 presents the crossing of vehicle yaw rate and driver steering-wheel angle for the 3rd incident, shown previously in cyan color, the only one during which the windscreen wipers worked.

The "Neutral Vehicle reference yaw rate" concept is very useful to analyze dynamic behavior (Van Zanten and *al.* 1995, Alberti and *al.* 1996). The definition of $\dot\psi_{refVN}$ is given hereafter, with δ the steering angle taken to the wheel, V the speed and L the wheelbase of the vehicle: $\dot\psi_{refVN} = V. \delta / L$.

It is clear that to analyze the vehicle response, the variable speed should be taken into account during steering actions. On the upper part of Figure 9, we defined 3 areas inside which the average speed is 43, 34 and 20 km/h, corresponding to the whole left bend (cyan), right bend entrance (magenta) and exit (yellow) respectively. The corresponding reference yaw rate of the neutral vehicle for each of these 3 areas is reported on the lower part, and enables to characterize vehicle response compared to neutral (understeer or understeer). This proves that the driver experienced slight under-steering behavior during this incident, with yaw response delayed from steering action, which probably explains his short braking at the apex of the right bend.
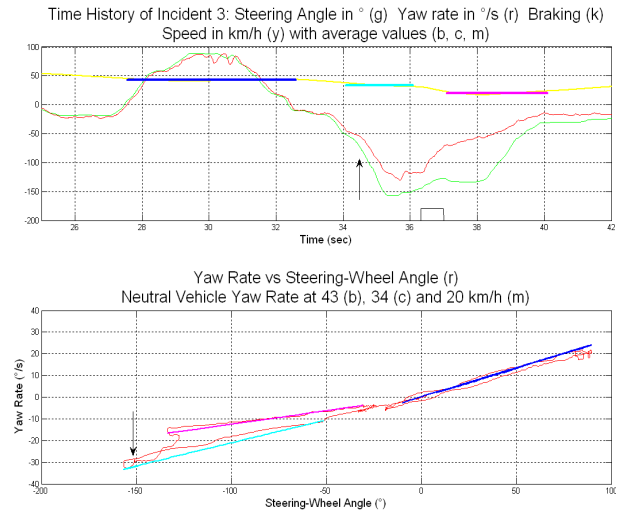
Fig. 9. Definition of 3 areas to average speed during steering (upper) - Crossing of vehicle yaw rate and steering-wheel angle, illustrating understeering behavior (black arrows)

This analysis shows that such an incident comes up to a potential loss of control of the vehicle in a bend.

### 4.3 Comparison of the vehicle dynamic operating area experienced by different drivers

Figure 10 presents the 3D dynamical parameters (with influence of speed, as the legend before the first graphic hereafter indicates) for 4 drivers among the 48 producing Travel Syntheses. For each driver are indicated an identification number, their age, years of driving license, number of travels (Iti), time of driving, mileage performed and number of incidents (Inc).
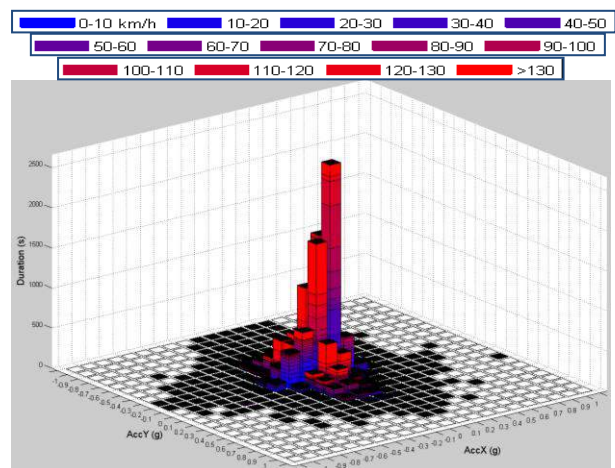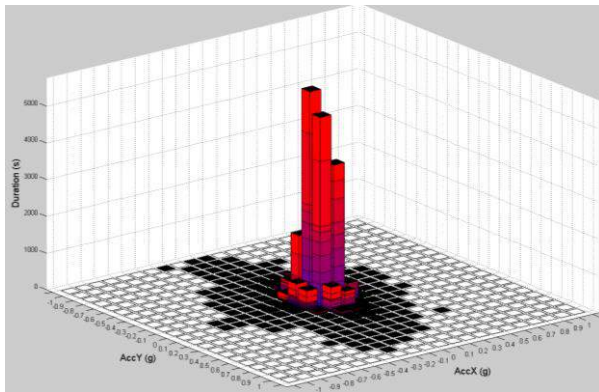

D1, 23, 5: 10 iti, 14h, 1308 km, 11 inc
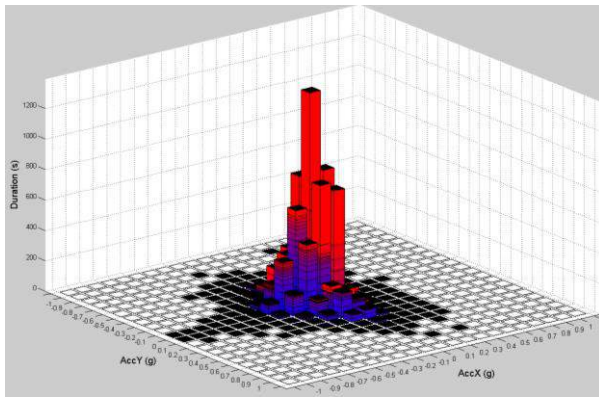
D11, 47, 29: 20 iti, 19h48, 2128 km, 2 inc
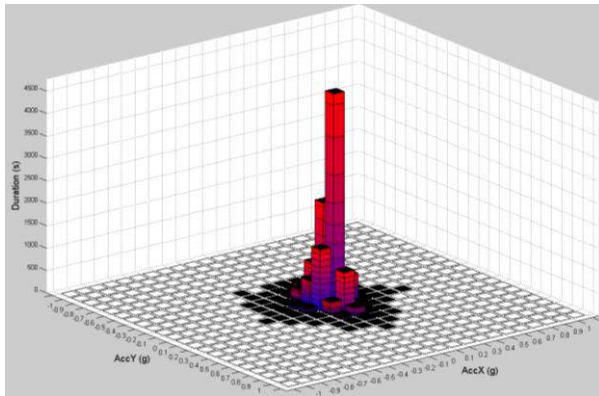
D15, 40, 22: 7 iti, 7h47, 745 km, 0 inc

D17, 33, 15: 11 iti, 8h06, 744 km, 7 inc

Fig. 10. Dynamical parameters for 4 drivers among the 42 self-authenticated in the SVRAI data collection

These 4 male drivers show very different behaviors: D1, who is only 23 years old, has the widest operating area, experiencing braking and lateral accelerations nearly beyond 1 g, whereas D15 has the smallest one, reaching quite never 0.5 g, whichever the direction of demand. D11 accepts higher acceleration in braking (beyond 1 g) than in bends (rarely up to 0.8 g). On the contrary, D17 experiences higher lateral accelerations (beyond 1 g) than braking decelerations (never exceeding 0.8 g). This typology looks like the one we published previously (Lechner and *al*., 1993, 2011).

4.4 Comparison of the operating area experienced by two drivers on the same itinerary

Figure 11 presents the 3D dynamical parameters for 2 drivers on the same itinerary (49 km long, located mainly on motorways). The upper graphic cumulates 4 occurrences of this travel by driver D34, with an average duration of almost 40 min and an average speed of 74 km/h, whereas the lower graphic cumulates 2 travels by driver D10, with an average duration of 29 min and an average speed of 90 km/h. One can notice a more reduced operating area for D34 (up to 0.6 g in bend and 0.9 g in braking) and a speed breakdown mostly under 90 km/h (in blue colors), when D10 shows a more spread out lateral operating area (up to 0.9 g in bend and 0.8 g in braking) and much higher speeds. None of these 2 drivers experienced incidents on these journeys.
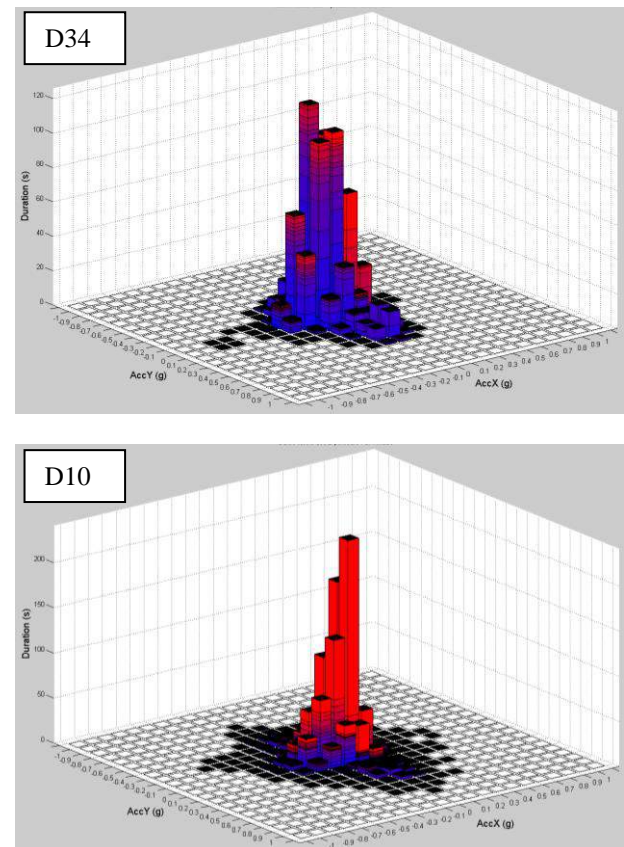

Fig. 11. Dynamical parameters for 2 drivers on the same itinerary

5. DISCUSSION AND CONCLUSION

The typology of driver performances and behaviors presented in paragraph 3 and 4 looks like, in some ways, to the ones already published from previous experiments with non-professional drivers on the open road field (Lechner and *al.* 1993, 2011). However the focus of SVRAI data collection on incidents (defined as situations in which the vehicle reaches high dynamics

demands in longitudinal, lateral or combined directions) enables to collect much more demanding situations, than most other naturalistic driving studies.

If EDR provides relevant information on driver's behavior, they can also detect infrastructure defects or failures considering they strongly contribute to driver's behavior as shown by (Ledoux and *al.*, 2014). This last study allows to assess if usual parameters recorded by EDR can identify road locations where infrastructure could be improved.

Results of this study show also that incidents represent an original and new source of information complementary to the ones already used like accidents, reports from road patrol … In future research work, the breakdown of incidents collected in SVRAI as a function of road infrastructure layouts (Fig.4) should be compared to the ones obtained on accident data, with or without injuries and fatalities.

Moreover the results presented in this paper proved that such a data collection on incident enables to perform in depth analyses of the driver-vehicle system in pre-critical driving situation and to provide original knowledge.

Additional vehicle dynamics investigation will be achievable from now on, with EMMA devices, since embedded calculation capabilities afford to develop an observer of sideslip angle based on Kalman Filter. This specific development was achieved in collaboration with HEUDIASYC (UTC/ CNRS 7253), from previous work validated on LMA Laboratory Vehicle (Doumiati and *al.* 2012).

In the future, in a possible second phase of the SVRAI project, further data collections on road incidents could be carried out with EMMA devices at the level of French Prefectures, with funding provided by the local authorities in charge of road infrastructure.

ACKNOWLEDGEMENTS

REFERENCES

Alberti V., Babbel E., (1996). Improved driving stability by active braking of the individual wheels. *Proceedings of AVEC'96*, Aachen. pp. 717-732.

Doumiati, M., Charara, A., Victorino, A., Lechner, D., (2012). Vehicle dynamics estimation using Kalman filter: practical applications. *Wiley-ISTE*.

Lechner, D., Perrin, C., (1993). The actual use of the dynamic performances of vehicles. *Journal of Automobile Engineering, Proceedings Part D*, Issue D4, IMechI 1993. SAE Paper 18-207-D4-249.

Lechner, D., Naude, C., (2011). Road incident analysis between naturalistic driving study and accident in-depth investigation. *Proc. FASTzero'11*. Tokyo, Japan.

Ledoux, V., Subirats, P., Violette, E., Bonin, Y., Serre, T., Naude, C., Guilbot, M., Lechner, D. (2014) Using event data recorder to detect road infrastructure failures from a safety point of view. AET/European Transport Conference. 29 sept-1st oct, Francfort, Germany.

Serre, T., Naude, C., Chauvet, S., Fournier, J.Y., Guilbot, M., Lechner, D., (2013). Towards a classification of road incidents acquired from public fleets of vehicles. *Proc. FASTzero'13.* Nagoya, Japan.

Van Zanten A. T., Erhardt R., Pfaff G., (1995). VDC, the vehicle dynamics control system of Bosch. *SAE Paper 950759.*

Green Phase Countdown Timer for Reducing Drivers' Dilemma at Signalized Intersection

Hironori Suzuki*. Takaya Ishikura**

** Nippon Institute of Technology, Saitama, Japan
(Tel: 81480-33-7734; e-mail: viola@nit.ac.jp).
** Graduate School of Nippon Institute of Technology, Saitama, Japan
(e-mail: ishikura.takaya@nit-trlab.net)*

Abstract: This paper developed a driving support system to reduce the driver's dilemma at signalized intersection. When facing an amber signal phase, the drivers occasionally come across the dilemma whether they should stop or pass the intersection stop line. The proposed system provides the remaining green time (RGT) to the drivers in real-time to support the stop/pass decision making. Driving simulator experiment equipped with the RGT indication system showed that the proposed system significantly reduced the probability of facing the dilemma and encouraged the drivers to decelerate earlier and stop before entering the intersection. Also, logistic regression analysis (LRA) revealed that approaching speed of a vehicle is the most significant factor to affect the stop/pass decision before the amber onset whereas remaining distance and acceleration rate affect it much more after fallen into the amber phase.

Keywords: Driver behaviour, Human factors, Green phase countdown timer, Dilemma zone

1. INTRODUCTION

The number of fatalities in traffic accidents has been gradually reduced since early 1990s in Japan due to the rapid progress and installation of various active safety measures. Around 30% of fatal accidents have still occurred at signalized intersections where the accidents that vehicle collides with human consists 40% of total crashes.

One of the possible reason of the accidents is the drivers' dilemma when facing the amber signal at signalized intersection (Long et al., 2013; Papaioannou, 2007). Driver has to make a decision whether he or she stops or passes the intersection at the moment when the signal turns into amber. In a special zone, however, the driver falls into the dilemma because he or she needs an unusual hard braking for a complete stop or infrequent acceleration to pass the intersection. This is referred to as the dilemma zone and the decision error at the zone occasionally causes the accidents with pedestrians or vehicles. Papaioannou (2007) applied the binary choice logit model to analyse the factors that affect the driver decision making at the dilemma zone. Long et al. (2013) introduced a green phase countdown timer to some real intersections in China, and also investigated the factors of stop/go decision making at the dilemma by the binary choice model as the function of some parameters. Regardless of the existing of dilemma, Mabuchi and Yamada (2013) estimated the driver's intent of stop/go decision after the signal phase turns into amber.

The literatures demonstrated here are mainly limited to the analyses of driver behaviour when facing the amber phase at the dilemma zone. The effective measures to reduce the drivers' dilemma has not been proposed yet except the study by Long et al.(2013) which introduced the green phase countdown timer (CDT). However, the effect of CDT seems to be insignificant in the China implementation because the drivers are more likely to cross the stop line when the CDT is present. It is obvious that the testing at real-world intersection equipped with the CDT convinces us of the effectiveness of the CDT. Collecting the remaining time of signal phase from the traffic light may also be an easy technical task. In our country Japan, however, it is a quite difficult mission to receive an authorisation from the police department to implement such a test at the real intersection. Instead, a simulator experiment should be carried out in advance before the installation of CDT to the real-world.

This study proposed the green phase CDT in order to reduce the drivers' dilemma when approaching to the signalized intersection. It is expected that presenting the remaining green time (RGT) encourages the driver to make an appropriate decision whether stopping or crossing the stop line before entering the dilemma zone. The effectiveness of the CDT is evaluated through the driving simulator (DS) experiment. Also, a logistic regression analysis (LRA) investigates what variables affect the drivers' stop/go decision making most when focusing on the acceleration rate, velocity and the remaining distance to the stop line of a vehicle after the amber phase onset.

2. THEORETICAL BACKGROUND

2.1 Definition of Dilemma Zone

The shaded region in Fig.1 illustrates the dilemma zone. The curve L1 defines the stopping distance L when a vehicle

approaches the stop line with the velocity v and the normal deceleration rate a. L2 is the distance that a vehicle can traverse during the amber time Y with its speed v. The area above L1 and below L2 can be defined as the dilemma zone where the driver needs an unusual hard braking for a complete stop or infrequent acceleration to cross the stop line. L1 and L2 are defined as follows:

$$L_1 = \tau v + \frac{v^2}{2a} \text{ and } L_2 = Yv . \tag{1}$$

where, a is the normal deceleration rate 3m/s^2; v is the velocity (m/s) of a vehicle approaching to the intersection; Y is amber time 3s; τ is driver's reaction time 0.75s.
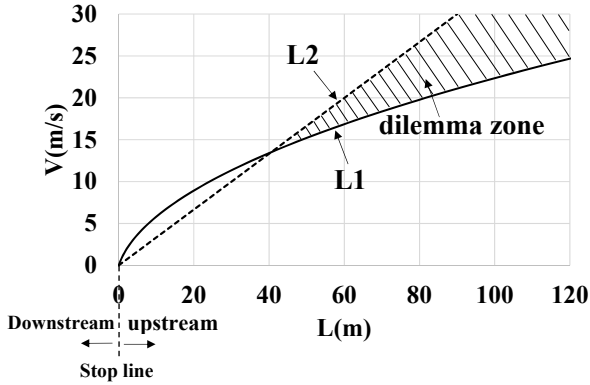
Fig.1. Definition of dilemma zone

2.2 Evaluation Indices

Margin to Stop (MTS) and Margin to Enter (MTE) defined by (2) are mainly employed as the evaluation indices (Ohtake et al., 2011). They all express the degree of safe capability for a vehicle to stop or enter the intersection immediately ahead. The fact that MTS is below 1 means that the vehicle is not able to stop at the stop line with the normal deceleration rate 3m/s^2. Also, the MTE lower than 1 expresses that a vehicle hardly enters the intersection during the amber phase if the speed v remains kept.

$$\text{MTS} = \frac{L(t)}{v(t)^2/2a} , \text{ MTE} = \frac{Y(t)v(t)}{L(t)} . \tag{2}$$

where $L(t)$ is the remaining distance to stop line (m) at time t and $Y(t)$ is the remaining amber time which satisfies:

$$Y(t) = \begin{cases} Y - t & (\text{if } t < Y) \\ 0 & (\text{o.w.}) \end{cases} . \tag{3}$$

Margin to Pass (MTP) evaluates whether the vehicle is able to cross the entire intersection during the all red signal phase as defined by (4). Similar to another indices, the MTP which is equals to 1 distinguishes the region of safety and danger for passing through the intersection.

$$\text{MTP} = \frac{Y(t)v(t) + AR(t)v(t)}{L(t) + L_i} , \tag{4}$$

where $AR(t)$ is the remaining all-read time defined by:

$$AR(t) = \begin{cases} AR & (\text{if } t > Y) \\ AR - (t - Y) & (\text{if } Y \leq t \leq Y + AR) \\ 0 & (\text{o.w.}) \end{cases} . \tag{5}$$

Here, AR is the time duration of all-read signal phase.

2.3 Zone Evaluation Using MTS, MTE and MTP

Consider the XY plot taking the MTS as the horizontal axis and MTE and MTP as the vertical axis, the XY chart can be divided into four regions; P-P, I-P, I-I and P-I zones, as depicted in Fig. 2. It should be noted that the centre of the chart is equal to 1.

The PP zone is the region where a vehicle is able to stop safely as well as to pass or enter the intersection without any unusual accelerations. This zone is considered as the most safe region, whereas the I-I zone is the dilemma where a vehicle can neither stop nor enter/pass the intersection safely with its current velocity and acceleration rate. In the P-I zone, a vehicle can stop before the intersection by the normal deceleration rate 3m/s^2 but is unable to enter/pass it. The I-P zone is vice versa. The data plot on the chart enables us to evaluate how safe the vehicle approaches and traverses the intersection.
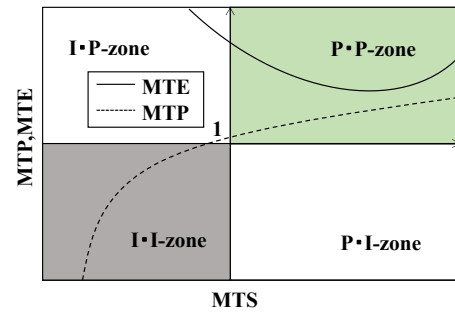

Fig.2. Zone Evaluation Using MTS, MTP and MTE

3. DRIVING SIMULATOR EXPERIMENT

3.1 CDT Design

The proposed CDT is solely to present the remaining green time (RGT) to the upper side of a front glass of a car as depicted in Fig.3. The CDT appears 250m upstream the stop line and remains indicated until the remaining time reaches zero and finally vanished immediately after the signal turns to amber. The amber phase has been introduced between blue and red to induce the driver to prepare the deceleration toward a complete stop during the red signal. As illustrated in Fig.1, however, the dilemma zone at the amber onset unexpectedly appears and expands as the approaching speed is increased. As long as the amber phase exists, the dilemma zone never disappears. The RGT could be one of the solutions to encourage the driver to decelerate or accelerate much earlier before he or she falls into the dilemma zone.

The RGT is supposed to be displayed on the front glass of a car through the device such as a head up display (HUD). The HUD is intended to prevent drivers' distraction and inattention as the deviation of eye glance direction is very small between the displayed RGT and the traffic light ahead. An alternate approach is to place the RGT besides the traffic light, but it is too difficult for drivers to identify the numbers of RGT as the remaining distance to the intersection is increased.

Fig.3. Design of CDT: Indication of remaining green time

3.2 Scenario and Experiment Condition

The host vehicle follows the preceding car which travels at 20m/s and is also followed by another car with 5m headway to consist 3-vehicle platoon on a two-lane road as shown in Fig. 4. Ten participants are required to keep the velocity 20m/s even after the preceding vehicle makes a lane-changing and to decide whether he or she stops or crosses the stop line according to the traffic lights and regulation regardless of CDT indication. On coming right-turn and thru vehicles randomly appear at the intersection. A participant experiences five trials each in two scenarios; with and without CDT, but encounters the dilemma only two cases out of five at random. Duration of amber is set to 3 seconds.

The driving behaviour with and without the CDT is compared and evaluated by some indices including not only MTS, MTE, MTP and their zone evaluation but also the occurrence rate of dilemma and error in judgement etc. It should be noted that the experiment was approved by the research ethics committee of Nippon Institute of Technology.
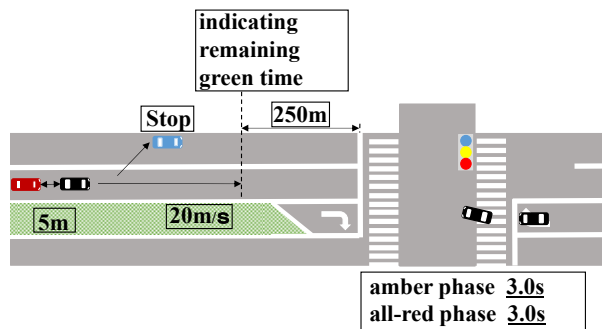
Fig.4. Scenario and the experimental conditions

3.3 Evaluation Results

Fig.5 illustrates an example of MTS, MTE and MTP versus the elapsed time after the amber onset with and without CDT. Without CDT, MTS and MTP already exceed 1 during the green phase showing that the vehicle was able to stop with normal deceleration rate or pass the intersection before the amber starts. Due to the confusion of decision making, however, the both MTS and MTP fall below 1 and finally the driver resulted in making a very hard braking to make a complete stop. The assistance by CDT encouraged the driver to decide to stop earlier so that the MTS never falls below 1 and the vehicle stopped safely. Since MTEs in both cases are always below 1, the vehicle was not able to enter the intersection all the time.
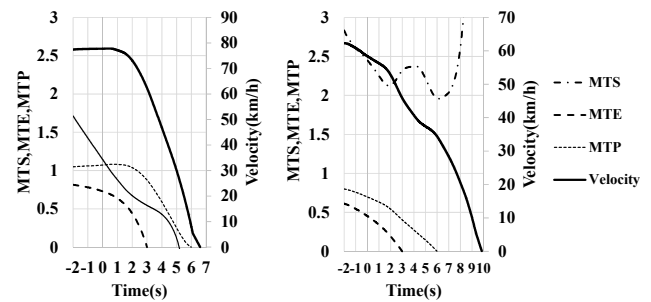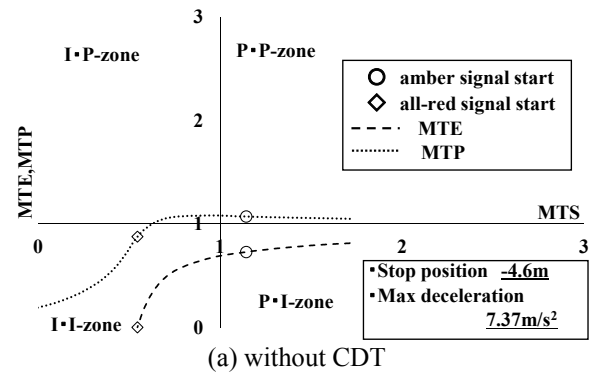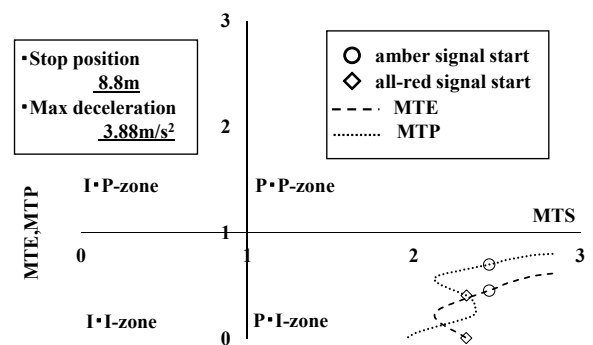

Fig.5. MTS, MTE and MTP with and without CDT (left; without CDT, right; with CDT)

Fig.6 (a) and (b) illustrate the transition of MTE and MTP versus MTS with and without CDT in a dilemma case. A

(a) without CDT

(b) with CDT

Fig.6. MTE and MTP versus MTS with and without CDT

circle and diamond show the amber and red onsets, respectively. Without CDT in Fig.6 (a), the driver could stop or pass very safely at the amber onset because both MTS and MTP exceed 1. After MTE and MTS fall into the I-I zone, the only safe way is to "pass" the intersection since MTP still remains exceeded 1. However, the driver decided to "stop" and started decelerating very hard at 7.4m/s^2 but came to a complete stop beyond the stop line. It was completely an error in judgement. With CDT depicted in Fig.6 (b), MTE and MTP were always in the P-I zone until the red onset where the vehicle was not able to enter nor pass but stop very safely. The driver could decide to stop much earlier with the assistance by CDT.

The occurrence rate of dilemma was significantly decreased from 75% to 10% by the presence of CDT as depicted in Fig. 7. The CDT is quite helpful in eliminating the confusion and dilemma of stop/pass decision making.

The CDT assistance was succeeded in inducing the drivers to choice "stop" rather than "pass" as shown in Fig. 8 (a). Also, Figs.8 (b) and (c) showed that the maximum deceleration rate and the error in judgement were both significantly reduced with the assistance. The CDT induced the driver to decide "stop" much earlier before the amber onset and to eliminate the error in judgement.
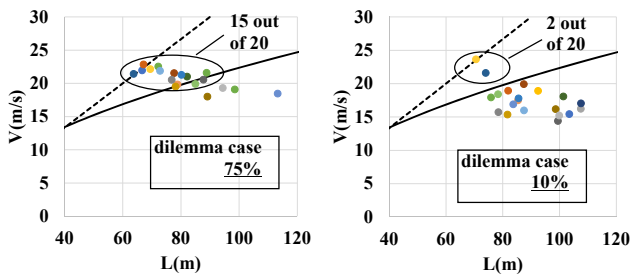
Fig.7. Occurrence rate of dilemma (left; without CDT, right; with CDT)

4. FACTORS AFFECTING THE STOP/PASS DECISION

The previous chapter showed that indicating the RGT reduced the drivers' dilemma when facing an amber phase and induced them to decide stop rather than pass the intersection. This chapter attempts to investigate what factors affect their stop/go decision in terms of some selected variables such as remaining distance to stop line (*L*), velocity (*v*) and acceleration rate (*a*) of a vehicle.

4.1 Logistic Regression Analysis (LRA)

LRA has been widely used as a binary or a multiple choice models to describe the human behaviour of selecting one thing among binary or multiple candidates. In this paper, for instance, each driver selects "stop" or "pass" among two alternatives in real-time given the new measurements of *L*, *v* and *a*. Then, the probability of "stop" can be modelled as:

(a) stop/pass ratio   (b) Maximum deceleration rate
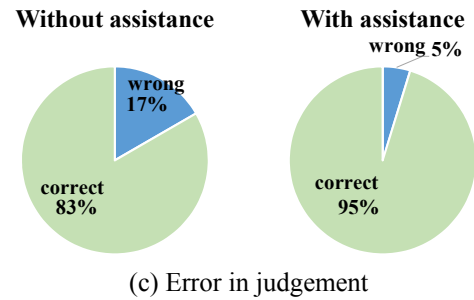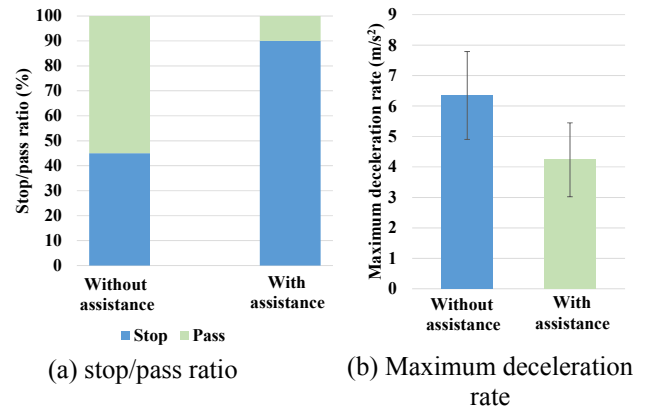

(c) Error in judgement

Fig.8. Stop/pass ratio, maximum deceleration rate and error in judgement with and without CDT

$$P(stop) = \frac{1}{1 + \exp\left(-\left(a_1 L + a_2 v + a_3 a + a_4\right)\right)}, \qquad (6)$$

where, P(stop) is the probability of selecting "stop", a_i (i=1 to 4) is the parameters of the LRA model. The stop/pass decision problem was defined by a simple LRA model.

4.2 Parameter Identification

The data on *L*, *v*, *a* were recorded every 10ms for all drivers through the DS experiment. The final decision whether he or she stopped or passed was also observed. The parameters a_i of (6) then can be identified using the data set of total five seconds; from two seconds before the amber onset until the end of amber.

The Newton-Raphson method which is one of the maximum likelihood method is used for the parameter identification. Starting with $a_i = 0$, a number of iterations is continued until the likelihood comes to maximum and gets convergence.

4.3 Results

Table 1 shows the identified parameters of (6) with and without CDT. a_1 corresponds to the remaining distance *L*, and a_2, a_3 are for the velocity *v* and acceleration rate *a*, respectively. If the sign of parameter is positive, the probability of stop P(s) increases as the corresponding variable is enlarged. For instance, the probability is to increase if the remaining distance *L* is longer because a_1 is positive for all five intervals.

Table 1. Parameters of LRA model

without CDT					
time (s)*	-2 to -1	-1 to 0	0 to 1	1 to 2	2 to 3
a_1 (L)	0.0492	0.0570	0.114	1.02	0.673
a_2 (v)	-1.13	-1.17	-1.09	-0.800	-1.91
a_3 (a)	-2.18	0.589	-3.11	-8.30	-3.08
a_4 (const.)	17.0	18.0	13.4	-49.1	3.40
with CDT					
time (s)*	-2 to -1	-1 to 0	0 to 1	1 to 2	2 to 3
a_1 (L)	0.0840	0.0976	0.187	0.431	0.202
a_2 (v)	-8.12	-6.60	-2.59	-1.56	-1.91
a_3 (a)	-1.22	1.84	-7.50	-6.29	-3.90
a_4 (const.)	163	133	43.3	9.74	30.4

* 0s is the amber onset

The LRA also evaluates the reliability of model parameter a_i based on the absolute t-value. Assuming the null hypothesis H_0 that the parameter a_i is equal to zero, the LRA calculates the t-value for each variable *L*, *v* and *a*. If the absolute t-value is large enough, then H_0 is rejected and the alternative hypothesis H_1 is accepted, meaning that the variable *L*, *v* or *a* are absolutely confident to explain the drivers' stop/go decision. Otherwise, they are useless.

Fig.9 (a) illustrates the absolute t-value without CDT. During the green phase; two seconds before the amber onset, the velocity contributes to the driver decision most because the absolute t-value is extremely high. Also, a_2 is negative so that if the approaching speed is increased the driver tends to "pass" the intersection. After the amber onset, however, the contribution of velocity is rapidly decreased and instead the influence of distance and acceleration rate are increased until two seconds after the amber onset. It can be concluded that the driver made a stop/pass decision mainly with his/her approaching speed before the amber onset whereas paid attention to the remaining distance and acceleration rate more than the speed after fallen into the amber. In the last second of amber time, no variable has much contribution because the driver has already decided to stop or pass at this stage regardless of whatever *L*, *v* and *a* are.

In the case with assistance of CDT, the absolute t-values are all much lower so that no variables are effective even during the green phase as illustrated in Fig. 9 (b). This clearly suggests that the driver has already made a decision prior to the amber onset due to the effect of the proposed CDT. It was concluded that the proposed CDT has a significant potential that allows a driver to shift the termination of stop/pass decision much earlier even to the region of green phase.

5. CONCLUDING REMARKS

This paper proposed a green phase countdown timer (CDT) which is expected to reduce drivers' dilemma whether he or she should stop or cross the intersection during the amber phase. Assuming a device like HUD, the remaining time to green is provided to the driver in real-time to support the stop/pass decision. A DS experiment was carried out to evaluate the effectiveness of the proposed CDT. Also, the factors affecting the stop/go decision is investigated through

a logistic regression analysis (LRA) when focusing on the remaining distance to stop line, approaching speed and acceleration rate. Numerical analyses showed that:

- The CDT significantly reduced the occurrence of dilemma and induced drivers to select "decelerate and stop" rather than "pass" the intersection. Maximum deceleration rate until the complete stop was also alleviated by the CDT.

- In the ordinary case without CDT, the approaching speed affects the stop/pass decision most during the green phase, whereas the remaining distance and the acceleration rate are much more effective for their decision making after the amber onset.

- With the assistance of CDT, the drivers tend to terminate their stop/pass decision prior to the amber onset even during the green phase.
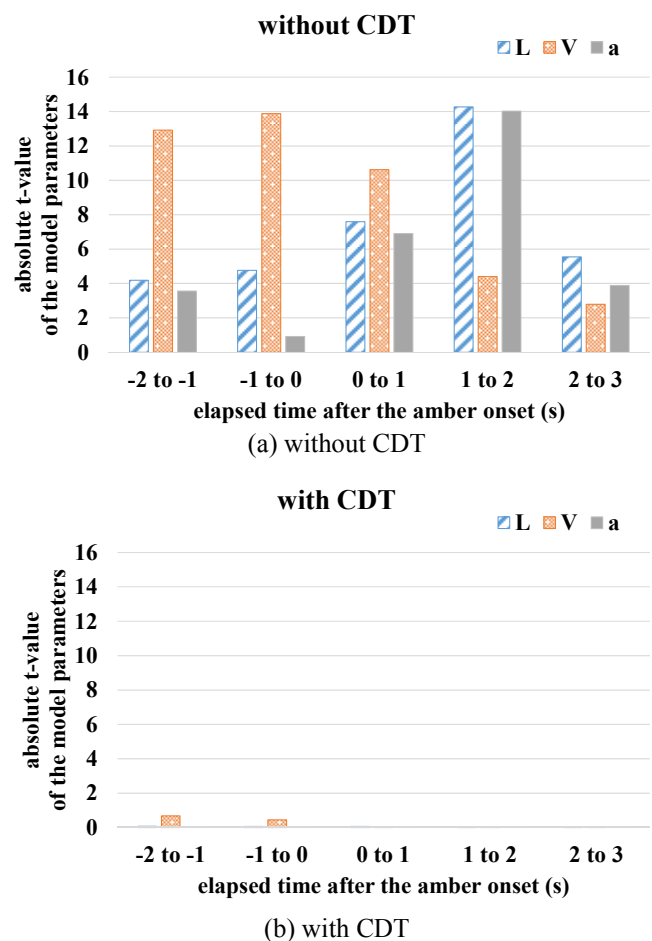

(a) without CDT

(b) with CDT

Fig.9 Absolute t-value of the model parameter L, v and a

It was concluded that the proposed system based on the CDT induced the drivers to make decision much earlier and to eliminate their error and dilemma in stop/pass judgement when approaching to a signalized intersection.

Further research will be addressed to infer drivers' stop/pass intent by applying a dynamic state space model including unscented Kalman filter or particle filtering algorithm.

REFERENCES

Mabuchi, R., and Yamada, K. (2011). Study on driver-intent estimation at yellow traffic signal by using driving simulator. 2011 IEEE Intelligent Vehicles Symposium (IV) Baden-Baden, Germany, 95-100.

Long, K., Liu, Y., and Han, L.D. (2013). Impact of countdown timer on driving manoeuvres after the yellow onset at signalized intersections: An empirical study in Changsha, China. *Safety Science*, vol.54, 8-16.

Ohtake, M, Michitsuji, Y., and Raksincharoensak, P. (2011). Proposal on driver's risk evaluation indices to crossing pedestrians at signalized intersection. Proceedings of the 20th transportation and logistics conference, The Japan Society of Mechanical Engineers, 31-34. (in Japanese)

Papaioannou, P. (2007). Driver behaviour, dilemma zone and safety effects at urban signalized intersections in Greece. *Accident analysis and prevention*, vol.39, 147-158.

Characteristics of Crash Data Collected by Event Data Recorders in Airbag Control Modules during Collision with a Tubular Metal Guardrail

Ryo Oga*, Kenshiro Kato*, Takaaki Terashima*, Nobuaki Takubo*

*National Research Institute of Police Science, Japan
Chiba Pref., Japan, (e-mail: oga@nrips.co.jp)

Abstract: Post-crash safety technologies are an important part of efforts to eliminate traffic accident-related fatalities. They are developed to enhance crash safety, and are therefore based on data collected from airbag control module (ACM) operation. In particular, delta-V (technically defined as the velocity vector difference before and after impact) data are very important in determining that a collision has occurred and evaluating accident severity. The aim of this study was to assess delta-V characteristics and to clarify the performance of event data recorders in ACM operation with focus on delta-V values recorded during collision with a tubular metal guardrail.

Keywords: road traffic, safety, traffic accident, crashworthiness, post-crash safety, event data recorder

1. INTRODUCTION

Post-crash safety technologies are an important part of efforts to eliminate traffic-related fatalities.

One example is automatic crash notification (ACN), which automatically determines that a vehicle has been in a collision, notifies emergency services and establishes a voice link between the vehicle and emergency response personnel. Advanced automatic collision notification (AACN) – the successor to ACN (CDC, 2008) – involves the use of an algorithm to perform triage for the vehicle's occupants so that emergency personnel can respond more quickly and more effectively.

Post-crash braking (PCB) technology prevents secondary accidents, or at least moderates their effects, thereby reducing risk to vehicle occupants and other road users (Häussler, 2011). If a system in a vehicle fitted with PCB functionality detects a collision, it activates an electronic stability control (ESC) system to prevent vehicle spin and automatically applies the brakes after impact to avoid a secondary collision or to reduce the speed at which any secondary collision occurs. For buses and trucks, PCB technology also reduces the risk of override accidents after rear-end collisions (Hino Motors, 2015).

Post-crash safety technologies are designed to enhance crash safety, and are therefore based on data collected from airbag control module (ACM) operation. In particular, delta-V (technically defined as the velocity vector difference before and after impact) data collected in this way are very important in determining that a collision has occurred and evaluating accident severity.

However, it is necessary to examine the reliability and accuracy of delta-V data collected from ACM operation (Ishikawa, 2009; Takubo, 2011). Accordingly, the aim of this study was to evaluate delta-V characteristics and to clarify

the performance of ACM operation for the assessment of collision severity. Focus was placed on delta-V values recorded during collisions with a tubular metal guardrail in actual car crash tests, and the resulting data were evaluated.

2. EXPERIMENTAL PROCEDURE

Typical real-life accidents such as single-car collisions with a tubular metal guardrail were simulated in four crash tests to enable evaluation of ACM data. The test conditions are listed in Table 1. The angle of impact with the guardrail was 90 degrees (Figure 1).

Table 1. Crash test conditions

Test no.	Gp-1	Gp-2	Gp-3	Gp-4
Vehicle	Toyota Corolla			
Target object (Japanese regulation code)	Guardrail (Gp-C-3E)		Guardrail (Gp-C-3B)	
Fixation method	Sunk in soil		Sunk in concrete	
Vehicle speed (m/s)	8.3	11.1	11.1	8.3

The Toyota Corollas used as test vehicles were equipped with ACMs in the floor center in front of the shift lever box under the console. The modules had an event data recorder (EDR) to collect collision information, including the maximum delta-V value and the delta-V time history curve with a 100 Hz sampling rate and a measurement duration of 200 ms. The measurement condition for delta-V is typical by Toyota Motor (Takubo 2011).

Crash test data were used for EDR data comparison. Accelerometers with a 10 kHz sampling rate were attached to the ACMs, and the acceleration data obtained from the

sensors were integrated to determine delta-V values. The accelerometers were triggered with a contact switch on the front bumper of the test vehicles. Vehicle crash behavior and guardrail deformation were captured using a high-speed video camera at 1,000 fps.

Fig. 1. Crash test

The guardrail was made of STK400 steel with a structure consisting of five vertical poles joined by three crossbars (Figure 2). The poles were 3 m apart (Figure 2 (a)) with a diameter of 114.3 mm and a metal thickness of 4.5 mm. The crossbars had a diameter of 48.6 mm and a metal thickness of 2.4 mm with heights of 450, 600 and 750 mm.
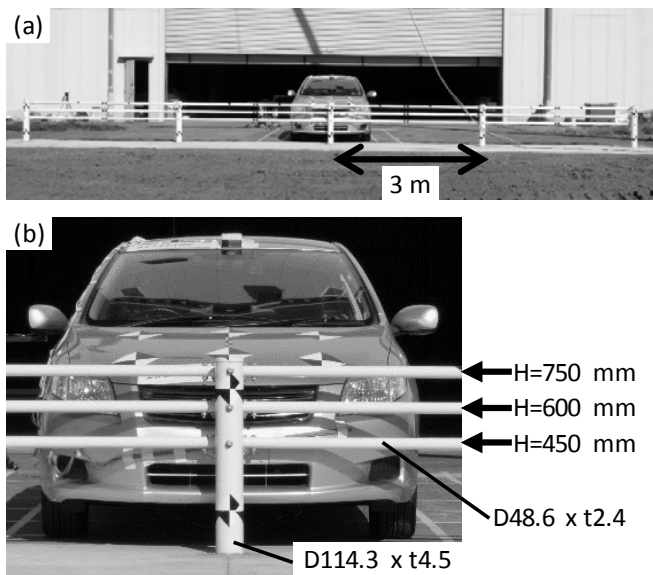
Fig. 2. Guardrail structure

3. RESULTS

Figure 3 shows images from high-speed video at the point of maximum guardrail deformation, whose duration exceeded 200 ms. The test vehicles rebounded in the reverse direction after this point.

Figure 4 shows the central vertical pole after collision. In test Gp-1 and test Gp-2, the poles deformed below ground level at depths of 390 and 400 mm, respectively. Meanwhile, deformation was observed at the surface of concrete pavement in test Gp-3 and test Gp-4.

As shown in Table 2, the maximum delta-V values from the EDRs were compared with accelerometer-derived data. EDRs

have two memory resources for delta-V data, referred to as Page.0 and Page.1. First, collision data are recorded on Page.0. If the airbags deploy upon collision, recording is stopped and the data stored on the page are saved in a freeze state. If the airbags do not deploy, the EDR continues to record secondary data on Page.1 after recording on Page.0.

Comparison of the maximum delta-V values recorded by the EDRs on Page.0 with accelerometer-derived data ([D] in Table 2) indicates non-negligible error in the former for a collision with a guardrail. This is attributable to the long duration of impact stemming from the large deformation of the guardrail.

As the airbags did not deploy in test Gp-1 and test Gp-2, two sets of data were recorded on Page.0 and Page.1 in each test. Comparison of the total values of Page.0 and Page.1 with the accelerometer-derived data ([E] in Table 2) verifies the accuracy of the data in both tests.

Figure 5 shows time history curves for the accelerometers fixed to the ACMs. The duration of acceleration was around 300 ms.

The vertical pole hit by the front bumper of the test vehicle was deformed in the collision at a rate calculated from the bending angle measured from a side-view high-speed video image. Figure 6 shows time history curves of this deformation. Some data are missing because the bumper obscured the vertical pole during collision. The peak deformation rate was between 48 and 70 ms.

Figure 7 shows delta-V time history curves. In test Gp-1 and test Gp-2, delta-V data on Page.1 were connected with the data on Page.0. Squares represent data recorded with the EDR on Page.0, and triangles represent data on Page.1. Solid lines represent accelerometer-derived data.

Table 2 Comparison of maximum delta-V values

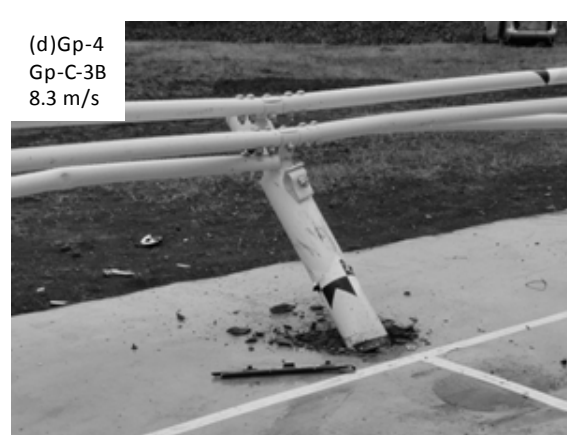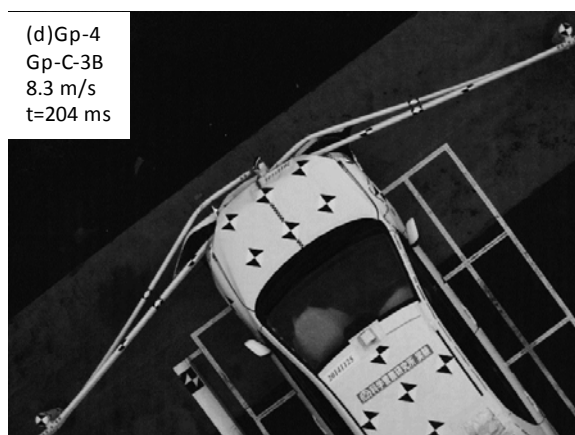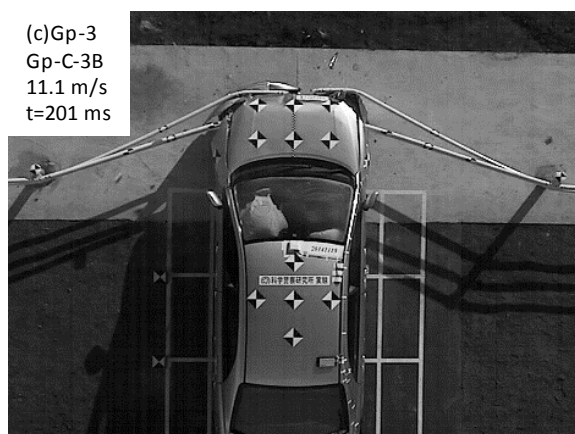| Test no.	Gp-1	Gp-2	Gp-3	Gp-4
Max. delta-V value integrated with accelerometer data (m/s) [A]	10.3	13.5	12.9	10.0
Max. delta-V value on EDR Page.0 (m/s) [B]	7.6	10.0	10.4	7.9
Max delta-V value on EDR Page.1 (m/s) [C]	1.6	2.5	No data	No data
Difference of Page.0 (m/s) [D] = [A] − [B]	2.7	3.5	2.5	2.1
Difference of total value of Page.0 and Page.1 (m/s) [E] = [A] − {[B] + [C]}	1.1	1.0	-	-

(a)Gp-1
Gp-C-3E
8.3 m/s
t=204 ms

(a)Gp-1
Gp-C-3E
8.3 m/s

(b)Gp-2
Gp-C-3E
11.1 m/s
t=215 ms

(b)Gp-2
Gp-C-3E
11.1 m/s

(c)Gp-3
Gp-C-3B
11.1 m/s
t=201 ms

(c)Gp-3
Gp-C-3B
11.1 m/s
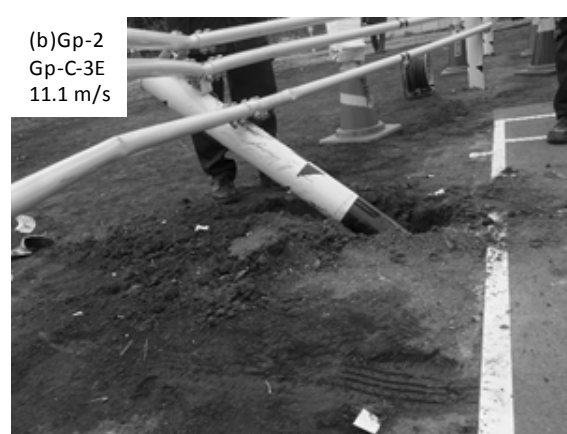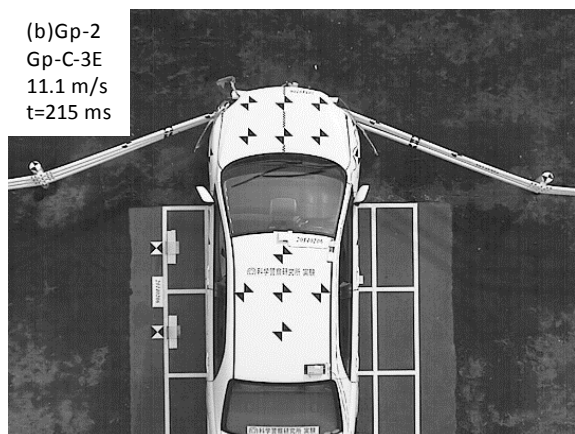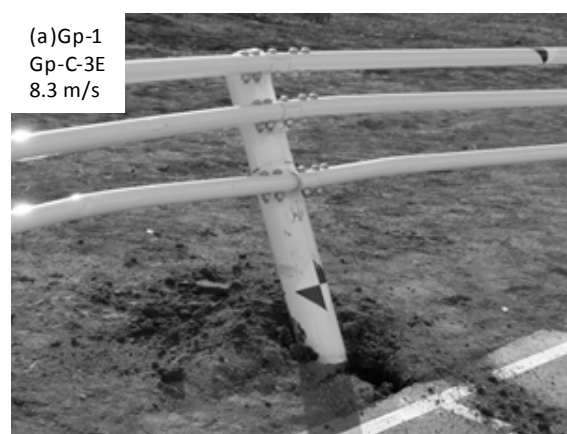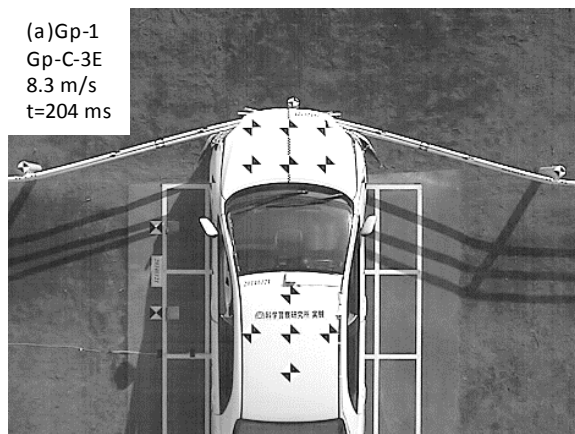
(d)Gp-4
Gp-C-3B
8.3 m/s
t=204 ms

(d)Gp-4
Gp-C-3B
8.3 m/s

Fig. 3. High-speed video at maximum deformation
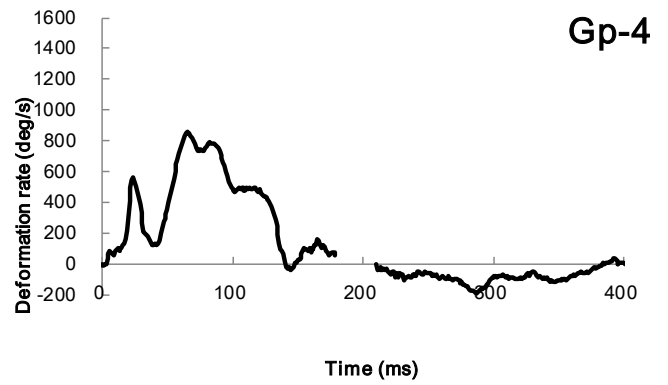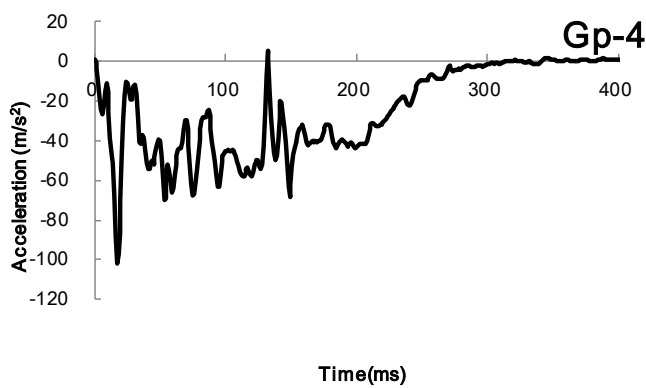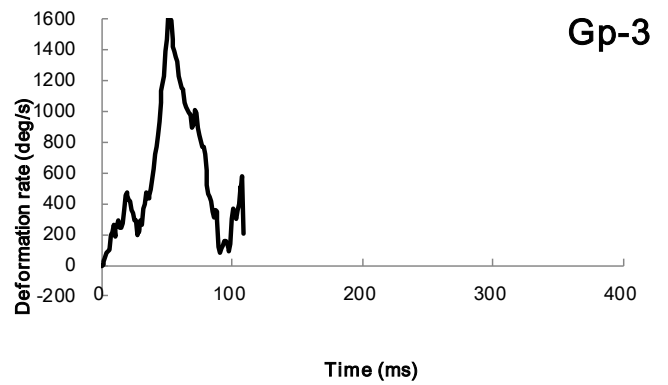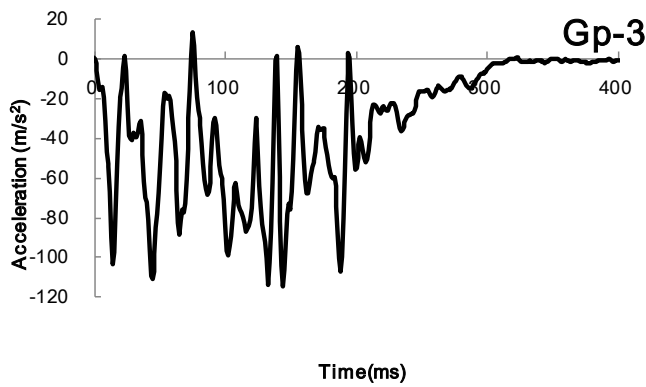
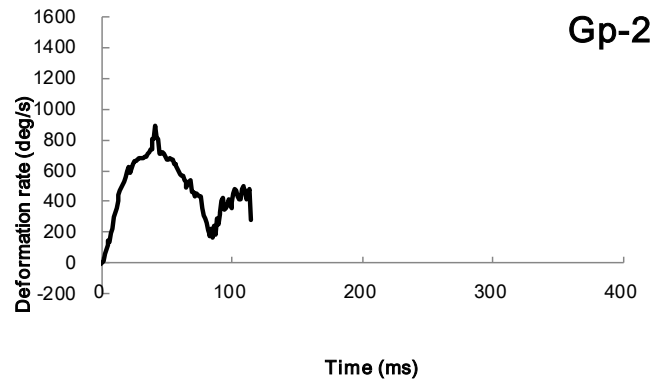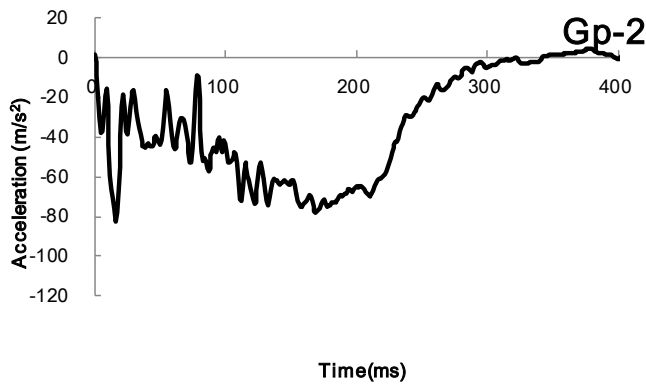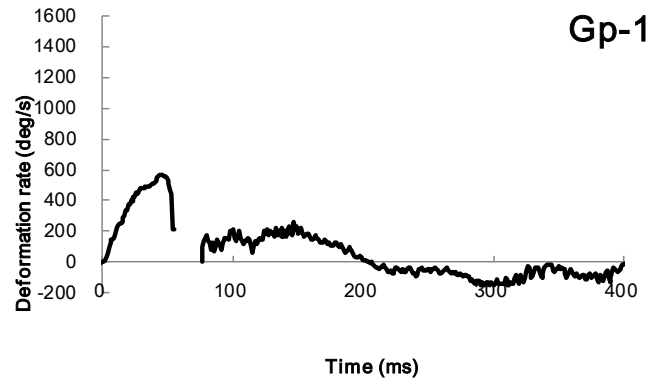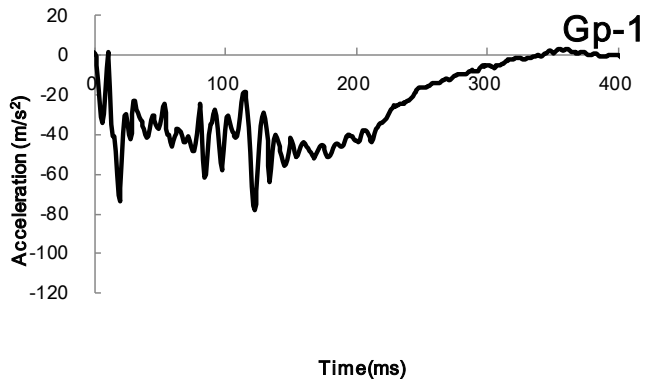Fig. 4. Central vertical pole after collision

Fig. 5. Time history of test vehicle acceleration

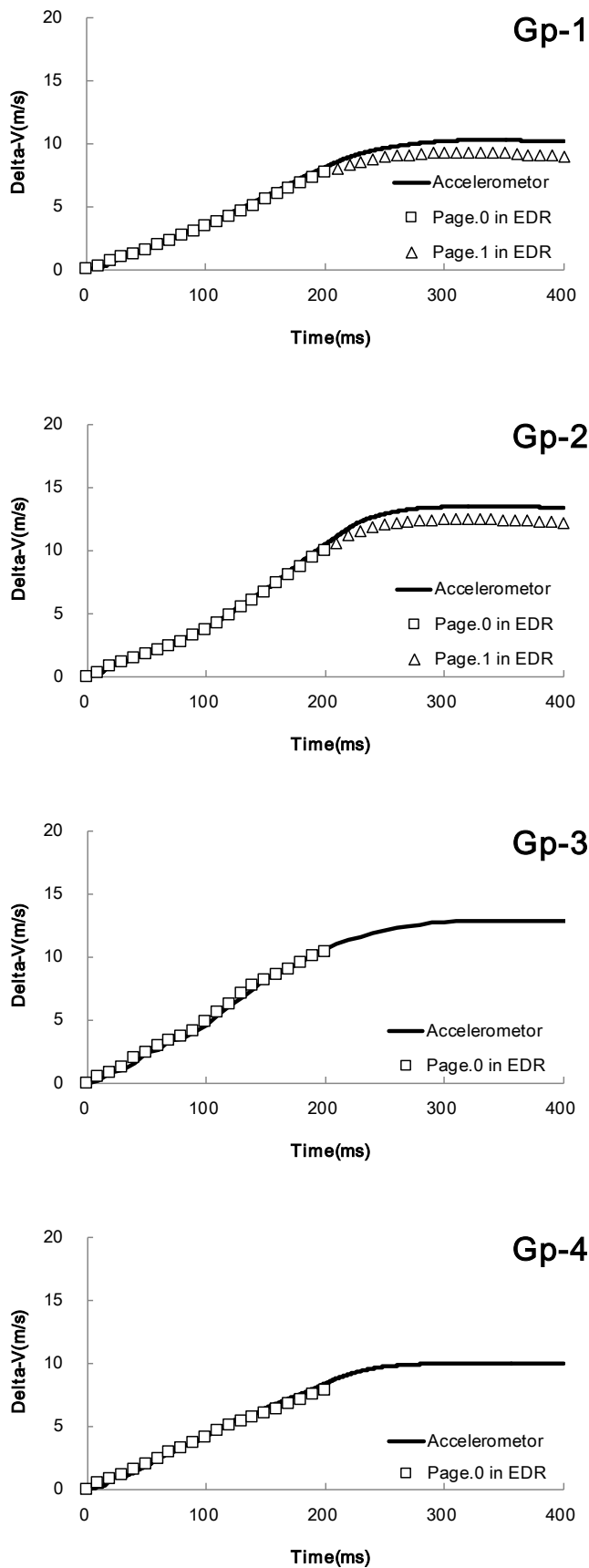Fig. 6. Time history of vertical pole deformation rate

Fig. 7. Time history curves of test-vehicle EDR delta-V values

4. DISCUSSION

Acceleration pulses were maintained for around 300 ms, and the peak intensities of acceleration were less than 120 m/s^2 (Figure 5). In a typical collision (vehicle-to-vehicle or a single vehicle with a barrier), the duration of collision impact is about 100 ms with a few hundred m/s^2 of acceleration. Accordingly, tubular metal guardrails are not rigit against impact from vehicles.

The vertical pipes of the guardrail bent over a period of 100 ms (Figure 6), which suggests that such deformation helps to absorb the vehicle's kinetic energy in the initial stage of the collision.

The time history curves in Figure 7 show that the delta-V values increased by about 300 ms before flattening out. All delta-V time history curves show good accuracy. These results indicate that the ACM sensors accurately collected delta-V data in collisions against the guardrail.

However, the maximum delta-V values from the EDRs are lower than the correct values measured by the accelerometers (see [D] in Table 2). This is attributable to the EDRs' short recording time, which was set in consideration of a typical collision with a duration of 100 ms or less. Accordingly, the recording time was fixed at 200 ms in the test vehicles.

It should be noted that the accuracy of delta-V data is very important for AACN, which involves the use of an algorithm to gauge the probable extent of occupant injury. The algorithm requires the following electronic information (CDC, 2008):

- Maximum delta-V value
- Principal direction of force (PDOF)
- Status of seatbelt usage
- Number of crash impacts
- Vehicle type

The severe injury risk curve with the AACN algorithm increases significantly for delta-V values exceeding 8.3 m/s (Tominaga et al., 2014). As shown by [D] in Table 2, the maximum EDR delta-V values in collisions with a tubular metal guardrail were lower than the corresponding accelerometer-derived values, which may result in the underestimation of injury in post-collision triage.

The risk of injury underestimation in triage can be addressed in a number of ways. A simple method of improving the accuracy of maximum delta-V values is to extend the EDR recording duration from 200 to 400 ms. However, this solution increases the cost of ACMs. Another approach involves connecting the data on Page.0 and Page.1 as in Gp-1 or Gp-2 (Figure 7 and [E] in Table 2). However, the memory is frozen and recording stops in EDR in the event of a severe accident in which airbags deploy (NHTSA, 2006; J-MLIT, 2008). Another method is to change the risk curve of the AACN algorithm toward overestimation of injury in triage if the time history curve is not saturated at 200 ms. In future work, such an algorithm change needs to be evaluated for collisions with guardrails.

5. CONCLUSIONS

Four crash tests involving single-car collisions with a tubular metal guardrail were performed to evaluate delta-V data collected by ACMs. It was found that although the ACM sensors collected the data accurately during the collisions, the recording time was insufficient. As a result, comparison of maximum delta-V values from ACMs with accelerometer-derived data indicated non-negligible errors in the former. In some cases, better results were observed when delta-V data from the two ACM memory resources were connected.

5. ACKNOWLEDGEMENT

REFERENCES

Alexander Häussler et al., (2011), Networking of airbag and ESP for prevention of further collisions, Bernd Heißing and Metin Ersoy (eds.) *Chassis Handbook Fundamentals, Driving Dynamics, Components, Mechatronics, Perspectives*, Vieweg+Teubner, 22 – 26.

Centers for Disease Control and Prevention, U.S., (2008), *Recommendations from the expert panel: Advanced automatic collision notification and triage of the injured patient*, online at http://www.cdc.gov/injuryresponse/pdf/aacn-report_final-a.pdf, 5. (Accessed: 6th February 2015)

Hino Motors, (2015), online at http://www.hino.co.jp/profia/safety/index.html. (Accessed: 6th February 2015)

Ishikawa, Hirotoshi, et al., (2009), *The 21st ESV Conference Proceedings*, 15 – 18 June 2009, Stuttgart, Germany.

MLIT (Ministry of Land, Infrastructure and Transport, Japan), (2008), *J-EDR technical requirements*, online at http://www.mlit.go.jp/kisha/kisha08/09/090328_.html. (Accessed: 6th February 2015)

NHTSA, (2006), 49 CFR Part 563, *Event Data Recorder Final Rule*, [Docket No. NHTSA-2006-25666] RIN 2127-AI72, August 2006.

Takubo, Nobuaki et al., (2011), *SAE Paper*, No. 2011-01-0810, SAE International.

Tominaga, Shigeru et al., (2014), *2014 JSAE Annual Congress (autumn)*, 22 – 24 October 2014, Sendai, Japan.

Age and Gender Difference in Braking Behavior from the 100-Car Naturalistic Driving Study: The Implication for Autonomous Braking System Design

Rong Chen, Kristofer D. Kusano
Hampton C. Gabler

Virginia Tech, Blacksburg, VA 24061
USA (e-mail: rjchen@vt.edu).

Abstract: Autonomous braking systems have potential benefits in active safety systems and Advanced Driver Assistance Systems. Ideally, emerging driver assistance systems which can automate certain driving aspects would apply braking in a human-like fashion. A better understanding of driver braking behavior can assist active safety and driver assistance system designers to better tailor the vehicle braking pattern to the driver and driving context. The objective of this study was to determine the potential effect of driver age and gender on braking profile. The approach of this study was to extract braking patterns in normal driving from the 100-Car Naturalistic Driving Study. Braking events with a closing lead vehicle were identified and extracted from the database. For each braking event, maximum brake force and braking profile was calculated from the instrumented vehicles. The result of the study shows that driver age and gender, as well as vehicle speed at start of braking, all have a statistically significant effect on driver braking profile. The results of this study have substantial implications for improving future autonomous braking system design to better tailor the system activation time to individual driver according to age, gender, and vehicle speed.

Keywords: autonomous braking, active safety system, naturalistic driving data, driver behavior, 100-Car.

1. INTRODUCTION

Autonomous braking is an integral component of active safety systems such as Dynamic Brake Support (DBS) and Autonomous Emergency Braking (AEB). These systems are designed to reduce the incidence and severity of collisions by automatically apply the brake in situations where the driver cannot apply sufficient brake force or were not able to brake in time. As vehicles begin to increase the level of automation, emerging Advanced Driver Assistance System (ADAS), may rely on autonomous braking systems to maintain following distance or navigate through "stop-and-go" traffic.

One of the challenges in designing an ideal autonomous braking system is to achieve automation which is human-centered (Goodrich & Boer 2000, Bainbridge 1983). An ideal autonomous braking system would be able to apply braking, both in magnitude and pulse shape, similar to a human driver to achieve a comfortable driving experience. A better understanding of driver braking behavior can assist active safety system and ADAS designers to better tailor the vehicle braking pattern to the driver and driving context. Previous studies have characterized driver braking behavior in crash avoidance scenarios, using test track and/or simulator (Wada et al. 2009, Kassaagi et al. 2003, Lee et al. 2002). Other studies have modeled car following behavior using traffic flow data (Gazis et al. 1961), or by numerical simulations (Hiraoka et al. 2005). Currently, no large scale study has been conducted on driver braking behavior in normal driving scenario.

One of the factors which may influence driver brake force and braking profile is driver age. Studies have suggested that muscle mass declines at approximately 1% per year after the age of 30 (Morley et al. 2011). The effect of this age related muscle mass loss, or sarcopenia, is directly correlated with loss of strength. In addition, difference in strength also exists across gender (Miller et al. 1993). Both age and gender difference can contribute to driver braking capacity and influence autonomous braking activation time. The objective of this study is to characterize braking pattern in normal driving, and analyze the potential difference in braking profile between drivers of different age group and gender.

2. METHODOLOGY

2.1 Data Source

This study was based on data extracted from the 100-Car Naturalistic Driving Study (NDS). The 100-Car NDS was a large-scale naturalistic driving study conducted by the Virginia Tech Transportation Institute (Dingus et al. 2006). The database contains approximately 2,000,000 vehicle miles of driving and 43,000 hours of data collected from 241 drivers. Drivers were recruited from the Washington D.C metropolitan area and were divided into male and female, and the following four age categories: Novice (age 18-20), Young (ages 21-30), Middle (ages 31-50), and Senior (ages 51-61+).

The 100-Car NDS oversampled younger drivers by design. The following analysis employed a weighting factor to adjust for the oversampled young drivers in the dataset. The weighting factor was calculated based on a post stratification strategy, in which we compared the distribution of age and gender between licensed drivers nationwide in 2012, the most recent year available (Federal Highway Administration 2012), and the current sample of drivers from the 100-Car NDS. Each driver was assigned a weight, w, as shown in (1),

$$w = \frac{p_{reg}}{p_{sample}} \quad (1)$$

where p_{reg} represents the proportion of registered drivers, and p_{sample} represents the proportion of drivers in the sample. The complete tabulation of weighting factor for age and gender is shown in Table 1.

Table 1. Post Stratification Weights

Age Group and Gender	% Drivers	% Sample	Weight
Novice, Female	2.8%	9.4%	0.30
Novice, Male	2.9%	9.4%	0.31
Young, Female	7.7%	7.8%	0.98
Young, Male	7.7%	23.4%	0.33
Middle, Female	17.7%	4.7%	3.78
Middle, Male	17.6%	21.9%	0.8
Senior, Female	22.3%	10.9%	2.03
Senior, Male	21.4%	12.5%	1.71

Vehicles in the 100-Car NDS were instrumented with cameras and inertial measurement devices and equipped with a PC-based computer to collect and store the data. Information such as vehicle speed and brake pedal switch was collected from the vehicle CAN bus. Other inertial measurements, such as longitudinal acceleration and yaw rate, was recorded by the on-board instrumentation installed by the researchers at VTTI. All data were recorded at a rate of 10 samples per second. Most sensors update at the same rate of 10 samples per second. However, some of the sensors update at lower rates. These data were still recorded at 10 samples per second, therefore would have multiple samples with equal magnitude until the sensor reports the next data point.

2.2 Data Selection

A total of 108 primary drivers were included in the 100-Car study period (McClafferty and Hankey 2010). Primary drivers were the primary owners or leasers of the instrumented vehicles, and accounted for 89% of all miles driven during the study period. The entire 100-Car database contains approximately 1.2 million miles of driving, 1,119,202 miles of which were driven by primary drivers in 139,367 trips (McClafferty and Hankey 2010). Some primary drivers drove in multiple vehicles. In order to extract the largest sample of drivers who consistently drove the same vehicle, the current study only includes trips where a primary driver was driving in the vehicle that he or she most frequently drove during the study, i.e. their primary vehicle, were selected.

Prior to the analysis, the status of all time-series data was inspected. Instrumentation data, including the front facing radar, vehicle speed, brake switch status, yaw rate signals, and lane tracking, were checked for missing or invalid data. The current study only included drivers in vehicles which had valid data in at least 60% of all trips and 60% of all distance travelled.

2.3 Automated Lead Vehicle Identification

The following study includes only braking events where the driver was approaching a lead vehicle. Lead vehicles were identified using a previously developed methodology (Kusano et al. 2014). The lead vehicle detection algorithm utilizes the on-board instrumentation, including the radar, vehicle speed,

vehicle azimuth, and vehicle acceleration, to identify the correct lead vehicle at the start of the braking event. The lead vehicle identification algorithm was validated against 100 manually inspected trips, containing over 8,400 braking applications. Lead vehicles identified by the algorithm were compared against the lead vehicle identified by the manual video inspection, and we found that the search algorithm agreed with the visual inspection in 92% of braking events.

Braking force will be a function of driving context, e.g. how likely the driver perceives risk of colliding with the lead vehicle. For each braking event with a lead vehicle, the traffic context is measured in terms of time to collision (TTC) and vehicle speed at the start of the braking event.

TTC is a measure of time it would take two objects to collide if the objects' trajectory and speed remains constant. Previous study has shown TTC to be a useful metric for driver perception of collision risk (Lee, 1976). In this study, TTC was calculated as shown in (2), where x is the range between the instrumented vehicle and the lead vehicle, and $\dot{x}$ is the range rate, or rate of change of range, between the two vehicles.

$$TTC = \frac{x}{\dot{x}} \quad (2)$$

2.4 Brake Force Calculation

In this analysis, we refer to braking force as the change in vehicle acceleration due to driver braking. Maximum brake force was determined based on the longitudinal acceleration recorded from the on-board instrumentation. The acceleration data was normalized by subtracting the acceleration at the start of the braking event from the remaining data. This was done in order to reduce the effect of existing acceleration caused by road slope. A five point moving average was performed on each acceleration trace prior to extracting the maximum to reduce the noise. No moving average was performed for braking events less than five data points.

2.5 Braking Profile Calculation

For each braking event, the driver braking profile was characterized based on the time centroid of the acceleration vs. time curve, as shown in (3), where t is the time duration and a(t) is the acceleration with respect to time. The integrals shown in (3) were performed with trapezoidal integration.

$$t_c = \frac{\int ta(t)dt}{\int a(t)dt} \quad (3)$$

As a quality control, the integral of a(t) for each event was compared against the change in velocity as reported by the vehicle CAN bus.

In order to compare the centroid, t_c, of each event with the population of all events, we have normalized the centroid using the length of the braking event, t_m, as show in (4). A t_c/t_m of 0.2 indicates that the driver "front loaded" the brakes in this event, where the peak braking force occurred near the beginning of the braking event. On the other hand, $t_c/t_m = 0.8$ indicates the driver "back loaded" the brakes in the event, and the peak braking force occurred near the end of the braking event.

$$Normalized\ Centroid = \frac{t_c}{t_m} \quad (4)$$

3. RESULTS

3.1 Dataset Composition

Table 2 shows the data composition in the analysis. A total of 58,611 trips with valid data, driven by 64 different drivers were extracted from the 100-Car NDS. A total of 889,268 braking events with closing lead vehicles were found in these trips, totaling over 16,000 hours of data.

Table 2. Dataset Composition

Number of Trips	58,611
Number of Drivers	64
Number of Braking Events	889,268
Hours of Data	16,319

3.2 Braking Duration

Figure 1 shows the braking duration in all braking events with a closing lead vehicle. The median braking duration was approximately 2.6 seconds. Approximately 20% of the braking events were found to be less than 1 second, and 90% of the braking events lasted less than 11 seconds.
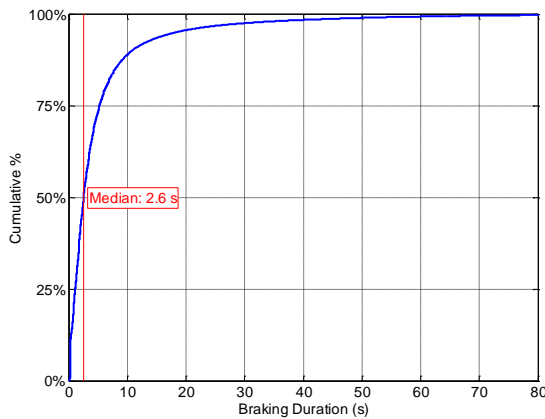

Figure 1. Distribution of Braking Duration

3.3 Braking Force

Figure 2 shows the distribution of maximum braking force for all braking events with closing lead vehicle. The median braking force was approximately 0.08 g. In 90% of the braking events, the maximum braking force was less than 0.2 g.
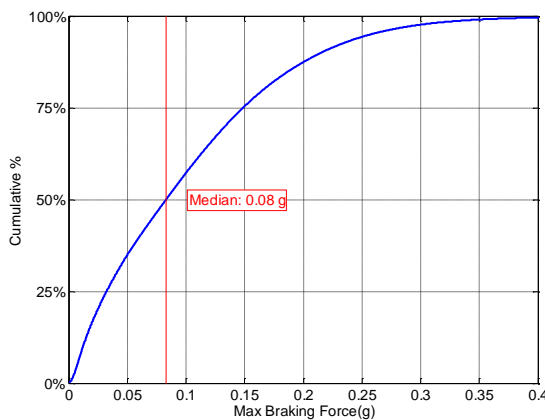

Figure 2. Distribution of Maximum Braking Force

3.4 Vehicle Change in Velocity

Figure 3 shows the vehicle change in velocity, or deltaV, in mph. For each braking event, the deltaV was computed by trapezoidal integration of the acceleration data. As shown in the figure, the median change in vehicle velocity was approximately 4 mph. As shown in Figure 1, approximately 20% of braking events in the sample had a change in vehicle speed of less than 1 mph. These low change in velocity braking events are tied to the short duration events, since it is unlikely to have made a significant change in vehicle speed in this short braking duration. Figure 4 shows a scatter plot of braking duration and vehicle deltaV. As shown by the figure, braking durations less than 1 s were generally associated with deltaV lower than 1 mph.
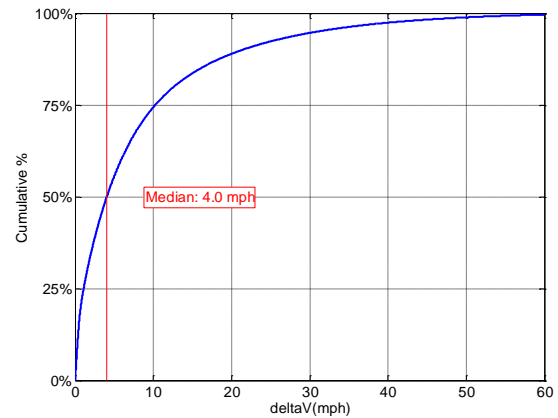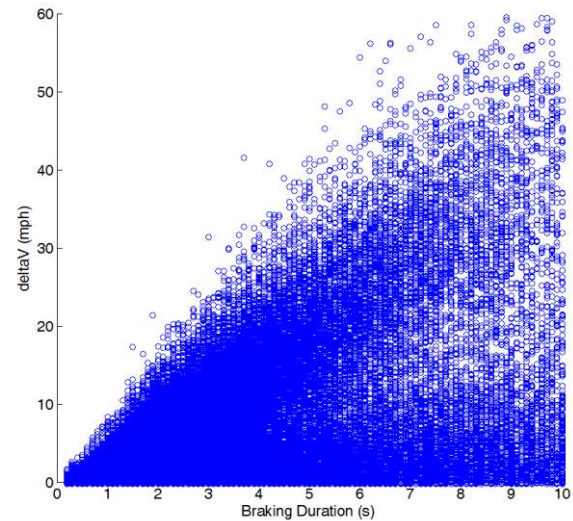

Figure 3. Distribution of Vehicle deltaV

Figure 4. Braking Duration and Vehicle deltaV

3.5 Braking Profile

Figure 5 shows the distribution of t_c/t_m. As shown by the figure, the median t_c/t_m is approximately 0.5. In other words, the median braking profile is one which the peak occurred neared the middle of the event.
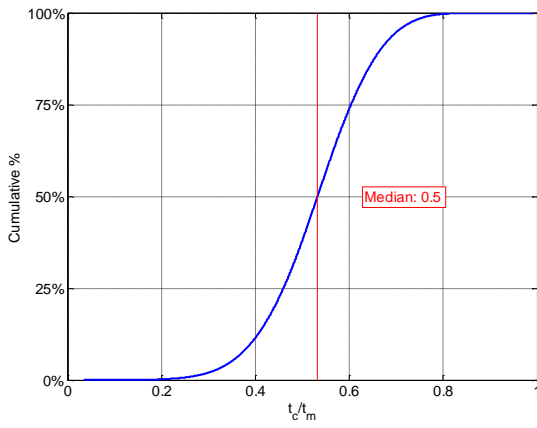
Figure 5. Distribution of t_c/t_m

Figure 6 shows a scatter plot of normalized t_c/t_m and TTC at the start of the braking event for all braking events in the sample. The figure also includes a "heat map" to indicate the density of braking events. Where red areas indicate more frequent occurrences, and blue areas indicate less frequent occurrences.

The relationship between TTC and t_c/t_m reveals several interesting characteristics about braking behavior. First, very few braking events were reported with t_c/t_m less than 0.25. This suggests that it is uncommon for drivers to "front load" brakes, or apply peak braking force early, in normal driving situations. The figure also shows that, the most frequent normal braking events have TTC's lower than 10 seconds and a t_c/t_m ranging from 0.4 to 0.6.
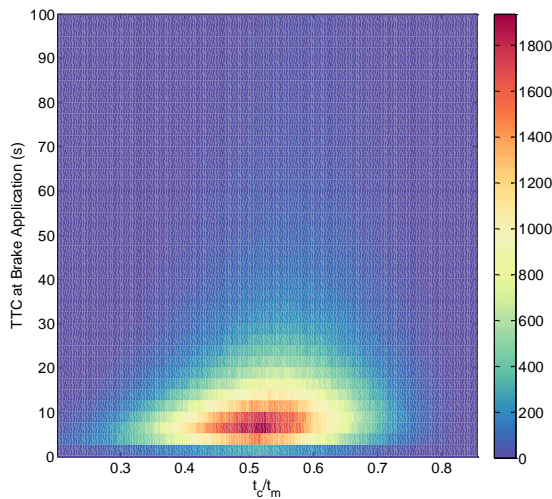

Figure 6. TTC at Braking and t_c/t_m

In order to further characterize these frequent braking events which has t_c/t_m ranging from 0.4 to 0.6, we have calculated the ratio of average braking force and peak braking force, as shown in Figure 7. An average/peak braking ratio of 1 indicate that the braking force is uniformly distributed with no obvious peak, similar to the left profile in Figure 8. Whereas a ratio greater than 1 would indicate that a sharp peak exist in the braking profile, similar to the right profile in Figure 8.

The distribution shown in Figure 7 shows that only a small percentage of mid loaded braking profile have a braking force ratio of 1, suggesting that majority of mid loaded braking include noticeable peaks near the middle of the braking event.
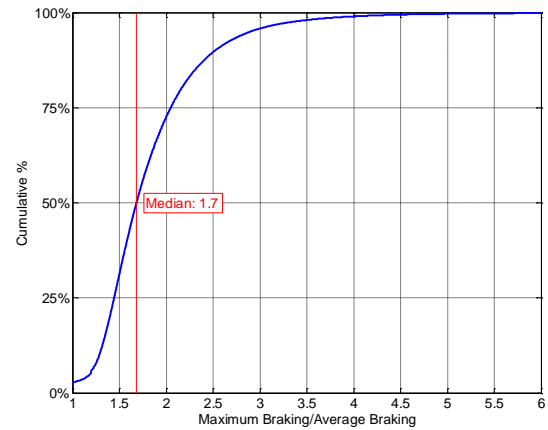

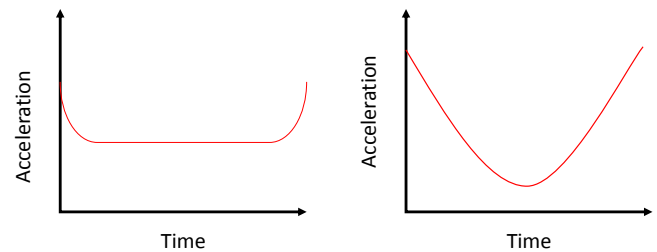Figure 7. Distribution of Maximum/Average Braking.

Figure 8. Idealized Example of Mid Load Braking Profiles

Figure 9 shows examples of braking profile for "front load", "mid load", and "rear load" events. The blue solid line shows the raw acceleration trace, the dashed red line shows the acceleration trace after the five point moving average filter, and the green star shows the location of the centroid.
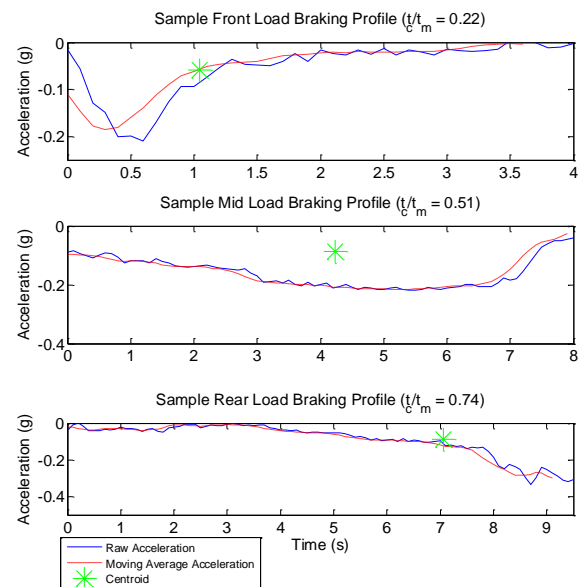

Figure 9. Sample Braking Profiles

3.6 Group Mean and Analysis of Variance

Table 3 shows the least square mean (LS mean) maximum braking force for each group. As shown, maximum braking force increases with increasing driver age. Middle age drivers (31-50) had the highest mean braking force. Female drivers also had slightly higher mean braking force than male.

The deceleration magnitudes shown in Table 3 are similar to values reported by previous studies. Wada et al. used test track data to model driver deceleration in car following scenarios and reported maximum decelerations ranging from 0.08g to 0.13g, for following distances of 50 m to 25 m, respectively (Wada et al. 2009). The numerical model by Hiroaoka et al., using minimum-jerk theory, reported a maximum deceleration of approximately 0.15g (Hiraoka et al. 2005). Similarly, the Gazis model, using traffic flow data, reported a maximum deceleration of approximately 0.2g (Gazis et al. 1961).

Table 3. LS Mean Maximum Braking Force

Groups	LS Mean Braking Force (g)
Novice (18-20)	0.084
Young (21-30)	0.093
Middle (31-50)	0.115
Senior (51+)	0.107
Male	0.093
Female	0.107

Similarly, Table 4 shows LS means of the t_c/t_m. The centroid locations for all age and gender groups were near the middle of the braking events.

Table 4. LS Mean t_c/t_m

Groups	t_c/t_m
Novice (18-20)	0.542
Young (21-30)	0.529
Middle (31-50)	0.518
Senior (51+)	0.526
Male	0.538
Female	0.519

A linear regression model was constructed in order to detect any potential significant difference in braking force between the driver demographic groups. "Age Group" and "Gender" was included in a linear regression model as categorical variables to control for driver characteristics, and vehicle speed and TTC was included as continuous variables in the model to control for traffic context. Table 5 shows the result of the Analysis of Variance (ANOVA). As shown by the figure, all main effect and interaction variables were statistically significant in influencing driver brake force at α level of 0.05.

Table 5. ANOVA for Linear Regression Model
(Response = Braking Force)

Parameter	DF	F Value	Pr(>F)	
Age Group	3	344.16	P < 0.0001	***
Gender	1	192.83	P < 0.0001	***
Vehicle Speed	1	7093.72	P < 0.0001	***
TTC	1	2984.36	P < 0.0001	***
(Age Group) *(Gender)	3	892.39	P < 0.0001	***
(Age Group) *(Vehicle Speed)	3	2075.87	P < 0.0001	***
(Age Group) *(TTC)	3	43.92	P < 0.0001	***
(Gender) *(Vehicle Speed)	1	313.89	P < 0.0001	***
(Gender) *(TTC)	1	31.53	P < 0.0001	***
(Vehicle Speed) *(TTC)	1	742.7	P < 0.0001	***

*** = P < 0.0001, ** = P < 0.05

Similarly, Table 6 shows the result of the ANOVA using centroid location, t_c/t_m, as the response. The only factor which was not statistically significant at alpha = 0.05 was the interaction between gender and TTC. All other factors were statistically significant at effecting t_c/t_m.

Table 6. ANOVA for Linear Regression Model
(Response = t_c/t_m)

Parameter	DF	F Value	Pr(>F)	
Age Group	3	326.31	P < 0.0001	***
Gender	1	2276.72	P < 0.0001	***
Vehicle Speed	1	13185.8	P < 0.0001	***
TTC	1	3722.76	P < 0.0001	***
(Age Group) *(Gender)	3	2364.18	P < 0.0001	***
(Age Group) *(Vehicle Speed)	3	118.88	P < 0.0001	***
(Age Group) *(TTC)	3	3.01	0.0288	**
(Gender) *(Vehicle Speed)	1	272.04	P < 0.0001	***
(Gender) *(TTC)	1	0.12	0.7251	
(Vehicle Speed) *(TTC)	1	1590.07	P < 0.0001	***

*** = P < 0.0001, ** = P < 0.05

Figure 10 shows the least square means estimates of maximum braking force with respect to vehicle speeds and age groups. Each '*' over top of the bars indicates that the groups were statistically different at alpha = 0.05. As shown in Figure 10, maximum braking force generally decreases with increasing vehicle speed. The change in braking force over different vehicle speed categories was more prominent for novice and young drivers. Middle age drives (age 31-50) had statistically higher maximum braking force compared to all other age groups in almost all speed ranges.

Similarly, Figure 11 shows the least square means estimate of t_c/t_m with respect to vehicle speed and age groups. In general,

t_c/t_m was approximately 0.5 for all age groups. We can see that the t_c/t_m generally increases with increasing speed for all age groups, suggesting that braking profile begins to "rear load" as vehicle speed increases. Contrary to other age

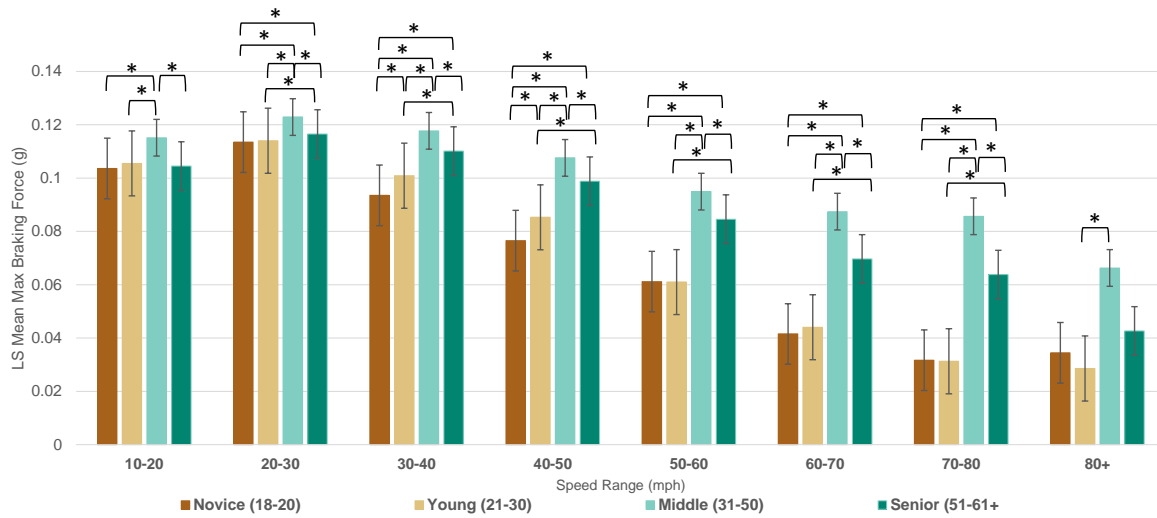groups, senior age drivers (51+) tends to "front load" braking as vehicle speed increases.

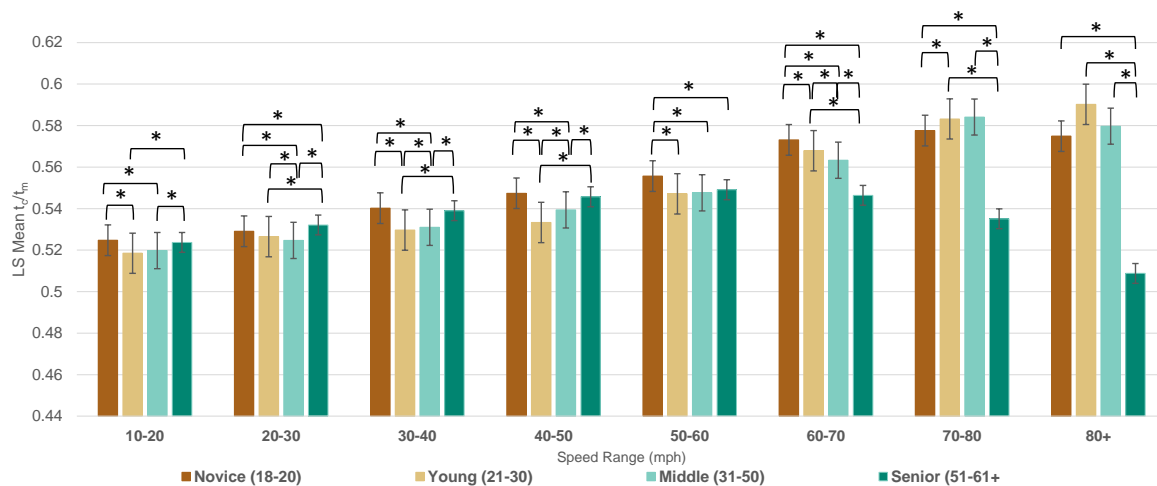Figure 10. LS Mean Estimate of Maximum Braking Force by Travel Speed and Age Group

Figure 11. LS Mean Estimate of t_c/t_m by Travel Speed and Age Group

4. DISCUSSIONS

This study has examined the braking behavior difference in driver age and gender demographic groups. The study shows that for braking events with a lead vehicle, driver braking force and braking profile is influenced by driver age and gender, as well as the traffic context, such as current vehicle speed and TTC with the lead vehicle.

The study also shows that, as driver age increases, the maximum braking force increases. A marginal difference in braking force between genders was also detected in the results. Using a linear regression model which controlled for vehicle speed and TTC, the difference between age and gender effect on braking was shown to be statistically significant.

Similarly, the study shows that driver braking profile varies with the driver demographic and driving context. For all age groups, the maximum braking force decreases as vehicle speed

increases. On the other hand, braking profile were shown to shift towards "rear load" as vehicle speed increases. The shift was not observed in senior drivers, who were shown to "front load" the brakes as vehicle speed increase.

One of the limitations of the study was that the results were based on normal driving data. It is possible that driver braking behavior is entirely different in crash imminent situations, therefore we cannot extend the conclusions from this study to crash imminent situations. In addition, information regarding cruise control activation was not available at the time of the study, which may help distinguish drivers' intention to cancel cruise control from crash avoidance braking. Nevertheless, the results from this study provides an good approximation of driver brake pulses in normal driving, and can still illustrate the differences in braking force across the demographic groups.

5. CONCLUSIONS

The objective of the current study was to determine the potential effect of age and gender on driver brake force. The study examined nearly 1 million braking events in over 58,000 trips extracted from the 100-Car NDS. The result of the study shows that maximum braking force generally increased with driver age. Women were found to have higher average braking force than men. Both age and gender were found to be statistically significant effects in influencing driver brake force.

The current study shows that there is a clear difference in braking profile between drivers of different age group and gender. The results of this study can help provide a better understanding of driver braking patterns in normal driving. The results of this study can support future automated braking systems and autonomous vehicle designers to better adapt vehicle driving behavior to be more human-like.

6. ACKNOWLEDGEMENTS

7. REFERENCES

Bainbridge L., 1983. Ironies of Automation. *Automatica,* 19, pp. 775-779

Dingus, T. et al., 2006. The 100-Car Naturalistic Driving Study, Phase II – Results of the 100-Car Field Experiment. , (DOT HS 810 593).

Federal Highway Adminstration (2012). Distriution of Licensed Drivers - 2012 by sex and percentage in each age group and relation to population. URL http://www.fhwa.dot.gove/policyinformation/statistics/2012/dl20.cfm. Accessed 12 February 2015

Gazis, D. C., Herman, R., & Rothery, R. W., 1961. Nonlinear follow-the-leader models of traffic flow, *Operation Research* 1(4), pp. 545-567

Goodrich, M. & Boer, E., 2000. Designing Human-Centered Automation: Tradeoffs in Collision Avoidance System Design. *IEEE Transaction on Intelligent Transportation Systems*, 1(1), pp. 40-54

Hiraoka, T., Kunimatsu, T., Nishihara, O., & Kumamoto, H., 2005. Modeling of Driver following behavior based on minimum-jerk theory. *12th World Congress on ITS*. Paper 3416.

Kassaagi, M., Brissart, G., & Popieul, J., 2003. A Study on Driver Behavior During Braking on Open Road. *18th International Technical Conference on The Enhanced Safety of Vehicles*. Paper No. 340

Kusano, K.D., Montgomery, J. & Gabler, H.C., 2014. Methodology for identifying car following events from naturalistic data. *IEEE Intelligent Vehicles Symposium, Proceedings*, (IV), pp.281–285.

Lee, D.N., 1976. A theory of visual control of brakign based on information about time-to-collision. *Perception,* 5, pp. 437-459

Lee, J. D., Hoffman, J. D., Brown, T. L., & McGehee, D. V., 2002. Comparison of Driver Braking Responses in a High Fidelity Driving Simulator and on a Test Track., (DOT HS 809 447).

McClafferty J, Hankey, J., 2010. 100-Car Reanalysis: Summary of Primary and Secondary Driver Characteristics. Blacksburg, VA: The National surface Transportation Safety Center for Excellence, Virginia Tech Transportation Institutte; Report No. 10-UT-007

Miller, a. E.J. et al., 1993. Gender differences in strength and muscle fiber characteristics. *European Journal of Applied Physiology and Occupational Physiology*, 66, pp.254–262.

Morley, J.E. et al., 2011. Sarcopenia With Limited Mobility: An International Consensus. *Journal of the American Medical Directors Association*, 12, pp.403–409.

Wada, T., Doi S.,Tsuru, N., Isaji, K., & Kaneko, H., 2009. Modeling of Expert Driver's Braking Behavior and Its Application to an Automatic Braking System. *SAE Technical Papers,* No. 2009-01-0785

Evaluation of Rear-End Collision Avoidance Technologies based on Real World Crash Data

I. Isaksson-Hellman*, M. Lindman**

**If P&C Insurance, Vikingsgatan 4, S-40536 Gothenburg
Sweden (Tel: +46-709-568648; e-mail: irene.isakssonhellman@if.se).
**Volvo Car Corporation, SE-405 31 Göteborg, Sweden (e-mail:magdalena.lindman@volvocars.com)*

Abstract: Over the last decade, collision avoidance technologies targeting rear-end collisions have been introduced by many vehicle manufacturers. However, evaluation of the real world performance of these systems are rare. The objective of this study was to evaluate the real world effectiveness of systems called Forward Collision Warning and Brake support combined with Adaptive Cruise Control (CWB+ACC). These systems were introduced as optional equipment in Volvo car models in 2006. The data analyzed comes from a detailed, representative dataset based on insurance claims. The rate of rear-end frontal collisions was compared for cars with and without CWB+ACC, controlling for different generations of CWB+ACC as well as presence of Low-speed Emergency Braking functionality. For cars with CWB+ACC, rear-end crashes with frontal impacts were reduced with 38%. Also, the data showed a clear progress in crash avoidance efficiency as a function of CWB+ACC development. For the third generation of CWB+ACC, the estimated collision avoidance effect was 45%. In future studies, the additional safety performance that collision avoidance technologies bring in the form of crash mitigation needs to be investigated.

Keywords*:* Insurance claims data, Safety efficiency analysis, Forward Collision Warning and Auto Brake

_____

1. INTRODUCTION

Collision avoidance systems help drivers to avoid or mitigate crashes using warnings and/or interventions, based on information about the traffic situation. Two major groups of systems addressing crashes with vehicles in front of the car that are positioned in, or traveling along the same path as the vehicle equipped with the functionality (i.e. rear-end frontal collisions) have been introduced **to** the market:

1. Collision Warning and Brake support combined with Adaptive Cruise Control (CWB+ACC)

2. Low-speed Emergency Braking (Low-speed_AEB)

Volvo Cars released a first version of CWB+ACC in 2006 (Coelingh et al., 2006), where the driver was assisted by a warning and brake support (pre-charge and increased sensitivity for the Emergency Brake Assist system). The functionality was restricted to objects moving in the same direction as the host vehicle. In the next generation of the system, introduced in 2007, standing still vehicles were distinguished, thus allowing for system activation for stationary vehicles as well (Coelingh et al., 2007). Also, auto brake up to 5m/s² was provided. In 2010, the third generation delivered full automatic emergency braking up to 10 m/s² and expanded to detect other conflict situations than rear-end scenarios (Lindman et al, 2010). All these systems were available as optional equipment in the car models presented in Fig1.

In addition to these functionalities, Low-speed_AEB operating at speeds up to 30 km/h was introduced as a standard mounted system in Volvo car models from 2008 and onwards, see Fig 1. In its second generation, Low-speed_AEB works at speeds up to 50 km/h. For cars equipped with both CWB+ACC and Low-speed_AEB, there is an overlap between the functionalities, Fig 1. Depending on various traffic situation parameters, e.g. travelling speed and speed reduction needed to avoid the crash, either one of the functionalities will intervene.

Numerous prospective studies have been performed, where the effectiveness of CWB+ACC was predicted, but research in the area of real world follow-up, i.e. summative evaluations of CWB+ACC studies are limited. One reason for this is that CWB+ACC often is offered as optional equipment and car individuals with the system need to be identified. Also take rates for these optional systems have been low, hence, the evaluation of the CWB+ACC system is hard to perform due to low numbers of equipped cars. Data from insurance claims is one good source of information for solving this issue. HLDI reported in 2012 a reduction in insurance claims for cars of different makes equipped with CWB+ACC systems (HLDI, 2012). Also, the real world effectiveness of the standard mounted Low-speed_AEB system was first evaluated in HLDI (2011, 2013) and in Isaksson-Hellman and Lindman (2012). Later, Low-speed_AEB was also evaluated in police reported data (Rizzi et al., 2014; Fildes et al., 2015).

The aim of this study was to investigate the crash reducing effect in real-world traffic of CWB+ACC systems, controlling for the crash conflict situation, car model and presence of Low-speed_AEB. The different generations of the CWB+ACC functionality were also evaluated.

2. METHOD

In this study, CWB+ACC were evaluated by using insurance claims from crashes in Sweden. The rate of rear-end frontal collisions per 1000 vehicle years was compared for vehicles with and without the technology. First, an overall evaluation of the CWB+ACC system was performed, by comparing car individuals with and without the optional system. All cars included in this evaluation were also equipped with the standard Low-speed_AEB system. Next, the development of CWB+ACC was evaluated by comparing different generations of the technology. Finally, for the most recent generation of CWB+ACC an analysis was performed within sedan-, station wagon- and cross country models separately.

2.1 Data

Insurance data was found to be valuable in safety performance evaluations based on real world crashes for collision avoidance technologies (HLDI, 2011-2013; Isaksson-Hellman and Lindman, 2012, 2015).

A comprehensive motor insurance for cars covers both injuries to people involved in a crash as well as damage to vehicles and property. The Collision Damage insurance pays for vehicle damage to the policy holder's own car, while the Third Party Liability insurance covers personal injuries and damage to other vehicles and property. In addition, Volvia/If Insurance handles a unique warranty, Car Damage Warranty, which provides an excellent opportunity to study the number of collisions for all new Volvo cars in traffic. This Car Damage Warranty is a unique Swedish concept, valid the first three years and covers damage to the policy holder's own car. The warranty is a Swedish standard and is funded by each car manufacturer.

The insurance claims data used for this study included information on crash type from two-vehicle collisions, car model, model year, date when the insurance started and ended, damaged parts, ownership, and estimated mileage per year. It was also possible to identify the car individuals equipped with the optional functionality CWB+ACC.

The introduction and occurrence of the different generations of CWB+ACC technologies for different car models and car model years is shown in Fig. 1. In parallel, the Low-speed_AEB functionality was successively introduced as standard equipment in Volvo models.
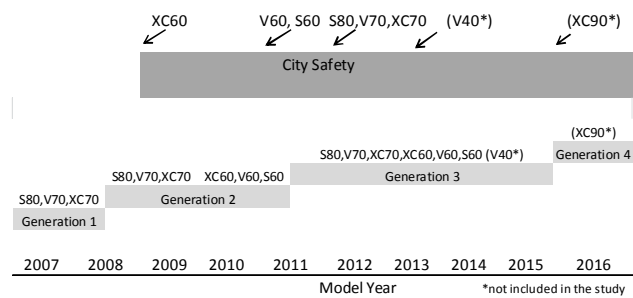

Fig. 1. Overview of the occurrence of the different generations of CWB+ACC and Low-speed_AEB for different Volvo car models and model years.

For the optional system CWB+ACC, the take rate, i.e. the share of cars equipped with the systems, has grown from 2% when it was introduced in 2006, up to approximately 15% in 2014, Fig. 2.
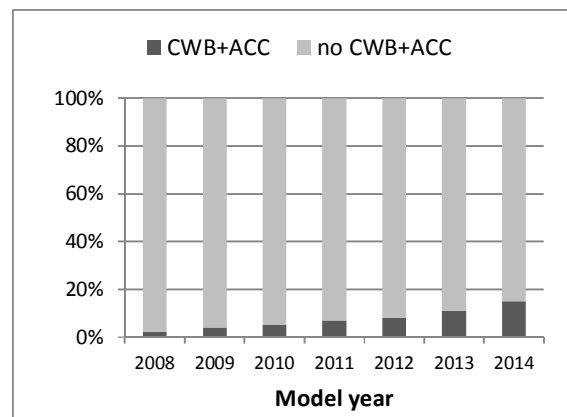

Fig. 2. Take rate for CWB+ACC systems by model year.

2.2 Data selection

Volvo car models selected for the study were new models launched before 2013, including car model years 2007-2014 where the CWB+ACC and/or Low-speed_AEB were provided. Data from crashes between 1 January, 2012 and 31 December, 2014, was used in this study. Rear-end frontal collisions were selected from two vehicle collisions in the database and the exposure was calculated by summing up the total number of insured vehicle years between 1 January, 2012 and 31 December, 2014.

An overall evaluation of the CWB+ACC system was performed by comparing car individuals with and without the optional system. All cars included in this evaluation were models also equipped with the standard Low-speed_AEB system. The exposure (number of insured vehicle years) for vehicle models and model years in the subset is presented in Table 1.

Table 1. Number of insured vehicle years (exposure) and model years for car models with and without CWB+ACC included in the overall evaluation of the CWB+ACC functionality

Exposure (Number of insured vehicle years) 1 Jan2012-31 Dec 2014			
Model	MY	With CWB+ACC incl. Low-speed_AEB	Without CWB+ACC incl. Low-speed_AEB
S80	2012-2014	650	1 748
S60	2011-2014	2 008	13 127
V70	2012-2014	2 821	41 773
V60	2011-2014	5 893	46 894
XC70	2012-2014	3 155	15 921
XC60	2010-2014	9 663	31 958
Total		24 190	151 421

The development of CWB+ACC was evaluated by comparing different generations of the technology. By using information on car individuals and start of production, subsets were generated for generation 1, 2 and 3 of CWB+ACC. Subsets were also created for cars without the system produced during corresponding time periods.

For the models equipped with generation 1 (S80, V70 and XC70, MY 2007-2008), the driver was assisted by a warning and brake support in situations where the object was moving in the same direction as the host vehicle. Also targeting rear-end frontal situations, the ACC functionality was a part of the optional equipment package while Low-speed_AEB was not available.

In CWB+ACC generation 2 (MY 2008-2011), rear-end situations with both stationary and moving vehicles were targeted. Also, auto brake up to 5m/s² was provided. Generation 2 was present in car models with Low-speed_AEB (S60, V60 and XC60) and in car models without Low-speed_AEB (S80, V70 and XC70).

The third generation of CWB+ACC that was introduced in MY 2011 delivers full automatic emergency braking up to 10 m/s². MY 2012-2014 was selected for the analysis in order to only include models with Low-speed_AEB, see Table 2.

Table 2. Number of insured vehicle years (exposure) and model years for car models with and without CWB+ACC generation 1-3, included in the dataset used for comparing different generations of CWB+ACC

Exposure (Number of insured vehicle years) 1 Jan2012-31 Dec 2014			
AEB generation/Model	MY	With CWB+ACC	Without CWB+ACC
Generation 1 CWB+ACC S80,V70,XC70 No Low-speed_AEB	2007-2008	1 475	33 628
Generation 2 CWB+ACC S60, V60, XC60 incl. Low-speed_AEB	2008-2011	6 153	31 404
Generation 2 CWB+ACC S60, V60, XC60 No Low-speed_AEB	2008-2011	4 609	116 231
Generation 3 CWB+ACC S80, V/XC 70, S/V/XC 60 incl. Low-speed_AEB	2012-2014	18 204	123 350

For the most recent generation of CWB+ACC, an analysis was performed for different types of car models, i.e. Sedan cars (S80, S60), Station wagon cars (V70, V60) and Cross country car models (XC70, XC60) separately.

Table 3. Number of insured vehicle years (exposure) and model years for *type* of car model with and without CWB+ACC, generation 3, included in the analysis of different types of car models

Exposure (Number of insured vehicle years) 1 Jan2012-31 Dec 2014				
Model	Type	MY	With CWB+ACC incl. Low-speed_AEB	Without CWB+ACC incl. Low-speed_AEB
S80/S60	Sedan	2012-2014	1 597	8 432
V70/V60	Station wagon	2012-2014	7 139	79 388
XC70/XC60	Cross country	2012-2014	9 468	35 530

2.3 Statistical methods

The evaluations were conducted by comparing rate of rear-end frontal collisions per 1,000 insured vehicle years for different groups of car models with and without the technologies under study. The rate of rear-end frontal collisions for CWB+ACC was defined as:

$$\text{Rate}_{w\,CWB+ACC} = (n_{w\,CWB+ACC} / VY_{w\,CWB+ACC}) \qquad (1)$$

where

$n_{w\,CWB+ACC}$ = Number of rear-end frontal collisions for cars with CWB+ACC

$VY_{w\,CWB+ACC}$ = Number of insured vehicle years for cars with CWB+ACC

The rate of rear-end frontals for cars without CWB+ACC was defined in the same way. The number of claims occurring can be considered using a Poisson distribution, and the 95% confidence interval for the rate was calculated by using a normal approximation to this distribution.

$$\text{Rate}_{w\,CWB+ACC} \pm 1.96 * \sqrt{\text{Rate}_{w\,CWB+ACC}/VY_{w\,CWB+ACC}} \quad (2)$$

To evaluate if CWB+ACC equipped vehicles have a different rate of rear-end frontal collisions, the difference between the rates for vehicles with and without the system was calculated together with a 95% confidence interval.

$$RD = \text{Rate}_{wo\,CWB+ACC} - \text{Rate}_{w\,CWB+ACC} \qquad (3)$$

Poisson distribution and test-based methods were used to construct the confidence interval. (Sahai and Kurshid, 1995).

$$\chi^2 = \frac{\left(n_{w\,CWB+ACC} - \frac{m*VY_{w\,CWB+ACC}}{VY}\right)^2}{\left(\frac{m*VY_{w\,CWB+ACC}*VY_{wo\,CWB+ACC}}{VY^2}\right)}$$

Where

m= the total number of events observed

VY= the total number of insured vehicle years

The confidence limits were then calculated by

$$RD_L = RD \pm 1.96 * \sqrt{RD^2/\chi^2} \qquad (4)$$

The effectiveness of CWB+ACC is calculated as a difference between rates for models without and with CWB+ACC divided by the rate for models without CWB+ACC:

$$e = \frac{Rate_{wo\ CWB+ACC} - Rate_{w\ CWB+ACC}}{Rate_{wo\ CWB+ACC}} \qquad (5)$$

The rates of rear-end frontal collisions were calculated during the same time period for the different groups with or without the system, from 1 January, 2012 to 31 December, 2014, in order to control for environmental conditions and other factors that could influence claim rates. The study also aimed at comparing vehicles age-wise as equal as possible

3. RESULTS

3.1 Overall evaluation of CWB+ACC, including Low-speed_AEB

A comparison of cars with and without the CWB+ACC technology, all with Low-speed_AEB as standard as listed in Table 1 was performed. The rate of rear-end frontal collisions estimated by insurance claims per 1,000 insured vehicle years, was 2.5, 95% CI [1.8, 3.1] for car models with CWB+ACC and Low-speed_AEB, as compared to 4.0, 95% CI [3.7, 4.3] for vehicle models without CWB+ACC and Low-speed_AEB only. A significant difference was estimated between the rates of rear-end frontal collisions in models with and without CWB+ACC on the 95% significance level;

$$RD = 4.0 - 2.5 = 1.5, 95\% \text{ CI } [0.7, 2.4]$$

The efficiency was 38%, calculated by using (5).

3.2 Evaluation of the development of CWB+ACC technology for the different generations 1 to 3.

Table 4. Rate differences (RD) and estimated effect (e) for car models with and without CWB+ACC for the three generations of CWB+ACC

Results / generation of CWB+ACC			
AEB generation/Model	MY	RD, CI	e
Generation 1 CWB+ACC S80, V70, XC70 no Low-speed_AEB	2007-2008	0.4, 95% CI [-2.8,3.7]	
Generation 2 CWB+ACC S60, V60, XC60 incl. Low-speed_AEB	2008-2011	0.0, 95% CI [-1.6, 1.6]	
Generation 2 CWB+ACC S80, V70, XC70 no Low-speed_AEB	2008-2011	**1.8, 90% CI [0.1, 3.6]**	**38%**
Generation 3 CWB+ACC S80, V70, XC70, S60, V60, XC60 incl. Low-speed_AEB	2012-2014	**1.9, 95% CI [0.9,2.8]**	**45%**

No significant effect was found for the first generation CWB+ACC technology, but there was an indication of a decrease in rate of rear-end frontal impacts of approximately 10%.

A reduction of 38%, significant on the 90% confidence level, was found for cars with the CWB+ACC system compared with cars without the system when *no* additional Low-speed_AEB was present. The rate difference was:

$$RD = 4.9 - 3.0 = 1.9, 90\% \text{ CI } [0.1, 3.6]$$

With Low-speed_AEB, no additional effect was found for the CWB+ACC generation 2 functionality, see Table 4.

For the third generation of CWB+ACC a significant reduction of 45% was found on a 95% level, see Table 4. The rate difference was:

$$RD = 4.1 - 2.3 = 1.8, 95\% \text{ CI } [0.9, 2.8]$$

3.3 Evaluation of the development of CWB+ACC technology for different types of car models.

Comparing types of car models, there was significant reduction of 43% on a 95% significance level for the station wagon models as well as a significant reduction of 45% for the cross country models, Table 5. Rate differences were:

RD (Station wagon) = 4.2 – 2.4 = 1.8, 95% CI [0.3, 3.3]

RD (Cross country) = 4.2 – 2.3 = 1.9, 95% CI [0.5, 3.3]

Due to low exposure (Table 3), no significant conclusion about the sedan models could be drawn, although a reduction of the rates at the same magnitude as for the other type of models was indicated.

Table 5. Rate differences (RD) and estimated effect (e) for different types of car models with and without CWB+ACC generation 3 (with Low-speed_AEB)

Results / Type of car generation 3 of CWB+ACC			
AEB generation 3 Type	MY	RD, 95% CI	e
Sedan S80, S60	2012-2014	1.7, 95% CI [-1.1, 4.5]	
Station wagon V70, V60	2012-2014	**1.8, 95% CI [0.3, 3.3]**	**43%**
Cross country XC70, XC60	2012-2014	**1.9, 95% CI [0.5, 3.3]**	**45%**

4. DISCUSSION

From the results presented in this report, it can be concluded that collision avoidance technologies targeting rear-end frontal collisions were effective in reducing the number of crashes. On average, a reduction of 38% rear-end frontal crashes was estimated for cars with both CWB+ACC and Low-speed_AEB technology. In a subset of cross country car models with the third generation of the system, an even higher crash reducing performance of 45% less rear-end frontal crashes was found. The progress in crash avoidance efficiency resulting from the evolution of the CWB-functionality was evident in the analysis of rear-end collision rates of different CWB+ACC generations. As anticipated,

there were more crashes avoided with the third system generation that provides full automatic emergency braking and identifies the opponent vehicle in moving as well as standing still scenarios compared to the first generation that only includes driver warning and brake support in situations where the opponent vehicle is moving.

The number of cars in the subsets representing cars equipped with different generations of CWB+ACC varied considerably, see Table 2. The estimated crash reduction for cars equipped with the first generation of CWB+ACC indicated a low effect of real world crash avoidance, although not significant. One reason for this is the small amount of cars equipped with FCW without Autobrake, see Table 2. Considering the uniqueness of the analysis on a real world crash data sample with cars equipped with Collision Warning and ACC without autonomous braking in rear-end frontal crashes, this was still a very interesting finding. A straight comparison of the crash avoidance effect of the first and the most recent CWB+ACC versions was not possible to perform, since the presence of Low-speed_AEB varied in cars of these two groups of the CWB+ACC generations. The crash avoidance effect of Low-speed_AEB was estimated to 28% less rear-end frontal crashes for cars with CWB+ACC and 25% for cars without CWB+ACC in a recent study (Isaksson-Hellman and Lindman, 2015), thus indicating the importance of controlling for the presence of Low-speed_AEB when evaluating CWB+ACC functionalities. Additionally, in the present study no significant effect of the CWB+ACC system was found when investigating the second generation of CWB+ACC, providing auto brake up to 5m/s², in a sample of cars equipped with Low-speed_AEB. In cars without Low-speed_AEB, a significant crash reducing effect on the 90% confidence level, of 38% was found. When comparing the second and third generation of CWB+ACC providing auto brake up to 5m/s² and 10 m/s² respectively, a significant larger effect was found in the latter, demonstrating the need for intervention performance in speeds beyond the range considered by Low-speed_AEB. As expected, the results showed that the CWB+ACC and Low-speed_AEB functionalities are working in combination and produce a total effect that not can be considered as additive.

In addition to the systems evaluated in this report, the car models with the second and third generation of CWB+ACC systems were also equipped with the active safety systems Lane Departure Warning and Driver Alert. Some of the car individuals studied were also equipped with Blind Spot Warning. However, these systems are not expected to influence the outcome of the CWB+ACC systems evaluation, since they target other crash conflict situations than rear-end frontal crashes.

Some limitations of the study were apparent. While the insurance data used for the present analysis were detailed enough for classifying the collision type of interest, rear-end frontal collisions, there was some information needed to perform further evaluations, e.g. to control for driving speed and ACC use. Also, it was not known whether the driver had turned off the systems prior to the crash. Yet, turning off the functionality is not expected to be a frequent behaviour. In a qualitative study on HMI concepts for Active Safety systems

(Lövsund and Wiberg, 2007), 15 out of 20 participants stated that they do not make any personal adjustments of the systems. So, theoretically there is a possibility that FCW and ACC settings varies for the cars in the datasets analysed and that this influence the results. Further, it can be assumed that the CWB+ACC systems that were optional features to a higher degree were chosen by persons driving their cars in a non-representative way. For example, it can be discussed whether or not these drivers were more aware of traffic safety, or if the drivers rely on the systems in a way that made them change their driving behaviour. These are all questions that are not possible to answer by using crash databases that are currently available.

In the present study, crashes not avoided but where collision avoidance technologies contributed to crash mitigation was not included in the scope of the analysis. A significant reduction of soft tissue neck injuries in rear-end impacts is expected since these are frequent in occupants of both the impacting and the impacted car, (Avery and Weekes, 2008; Jakobsson, 2004; Jakobsson et al., 2004; Kullgren et al., 2000). The total safety effect from CWB+ACC and Low-speed_AEB functionalities is therefore an important area for future studies. Also, other conflict situations than rear-end scenarios were not studied. Recent collision avoidance systems, such as the most recent generation of CWB+ACC, available as standard mounted equipment in the Volvo model XC90 MY2016, targets car to pedestrian-, car to cyclist crashes as well as crashes in intersections.

The unique study presented in this report met the challenges in real world safety performance follow-up methodology by using a representative dataset that included relevant details such as crash configuration, car equipment information and real exposure statistics. These are features of crash databases not found in other datasets available. The dataset used provided the possibility to compare cars with and without CWB+ACC in an efficient and unambiguous analysis.

6. CONCLUSIONS

This study is the first of its kind presenting real world traffic effects of non-standard mounted rear-end collision avoidance technologies in the relevant traffic conflict situation (rear-end frontal collisions). For vehicles with CWB+ACC, rear-end frontal collisions were reduced with 38%. For the third generation of CWB+ACC, the estimated collision avoidance effect was estimated to 45%. By providing relevant details in a representative dataset including real exposure statistics, insurance data proved to be an effective source of information when it comes to evaluating the effectiveness of collision avoidance technologies in real world traffic.

REFERENCES

Avery, M., Weekes, A. (2008). Volvo City Safety – Collision Avoidance Technology and its Potential to reduce Whiplash Injuries. *Conf. Neck Injuries in Road Traffic and Prevention Strategies*, Munich, Germany.

Coelingh E, Lind H, Wolfgang B, Wetterberg D. (2006). Collision Warning with Auto Brake. FISITA World

Congress, Paper No. F2006V130, Yokohama, Japan, 2006.

Coelingh, E., Jakobsson, L., Lind, H., Lindman, M. (2007)."Collision warning with auto brake – A real-life safety perspective". *International Technical Conference on the Enhanced Safety of Vehicles (ESV)*, Paper No. 07-0450, Lyon, France, 2007

Fildes, B., Keall, M., Bos, N., Lie, Y., Page, Y., Pastor, C., Pennisi, L. Thomas, P., Rizzi, M. and Tingvall, C. (2015). "Effectiveness of low speed autonomous emergency braking in real-world rear-end crashes". *Accident Analysis & Prevention* Volume 81, August 2015, p 24–29.

Insurance Institute of Highway Safety. (2011). *Status Report* Vol. 46. No.6.

Insurance Institute of Highway Safety. (2012). *Bullentin* Vol. 29. No.5.

Insurance Institute of Highway Safety. (2013). *Status Report* Vol. 48. No.3.

Isaksson-Hellman, I. and Lindman, M. (2012). The Effect of a Low-Speed Automatic Brake System Estimated from Real Life Data. *Proceedings of the Ann Adv Automot Med.* 56, 3-12.

Isaksson-Hellman, I. and Lindman, M. (2015). Real-World Performance of City Safety Based on Swedish Insurance Data. *International Technical Conference on the Enhanced Safety of Vehicles (ESV)*, Paper No. 15-0121, Gothenburg, Sweden, 2015.

Jakobsson, L. (2004). Evaluation of Impact Severity Measures for AIS1 Neck Injuries in Frontal Impacts using Crash Recorder Data. *Int. J of Crashworthiness*, *9(1)*: 105-111.

Jakobsson, L., Norin, H., Svensson, M. Y. (2004). Parameters Influencing AIS 1 Neck Injury Outcome in Frontal Impacts. *Traffic Injury Prevention*, *5(2):* 156-163.

Kullgren, A., Krafft, M., Malm, S., Ydenius, A., Tingvall, C. (2000). Influence of Airbags and Seatbelt Pretentioners on AIS1 Neck Injuries for Belted Occupants in Frontal Impacts. *Stapp Car Crash Journal 44,* 117-125.

Lindman, M., Ödblom, A., Bergwall, E., Eidehall, A., Svanberg, B., Lukaszewicz, T. (2010). "Benefit Estimation Model for Pedestrian Auto Brake Functionality". ESAR, Hanover, Germany, 2010.

Lövsund, K., and Wiberg, A. (2007). "Development of an integrated HMI-concept for Active Safety Systems". IT University of Göteborg, Report no. 2007:117.

Rizzi M, Kullgren A, Tingvall C. (2014). "The injury crash reduction of low-speed Autonomous Emergency Braking (AEB) on passenger cars". *Proc. of IRCOBI* Conference on Biomechanics of Impacts, Paper number IRC-14-73

Sahai, H., Kurshid, A. (1995). *Statistics in Epidemiology: Methods, Techniques and Applications.* CRC Press.

Towards a consistent threat assessment at traffic junctions using road information and naturalistic data:
A test example

Esteban R. Gelso * **Jonas Sjöberg** **

* *Advanced Technology and Research, Volvo Group Trucks Technology,*
SE-412 88 Göteborg, Sweden, (e-mail: esteban.gelso@volvo.com).
** *Department of Signals and Systems, Chalmers University of*
Technology, SE-412 96 Göteborg, Sweden, (e-mail:
jonas.sjoberg@chalmers.se)

Abstract: This paper presents enhanced versions of two metrics: the Time-to-Brake (TTB) and the Brake-Treat-Number (BTN), which are used as measures to describe the degree of being critical of traffic situations. The main idea is to include road information as input to obtain a more advanced prediction of the leading vehicle.
The results, illustrated by an example using real data, show a better assessment of the collision potential hazard and no false alarms.

Keywords: Active safety testing methods and tools, Field operational test, Driver behavior modeling.

1. INTRODUCTION

Rear-end crashes are one of the most frequent types of traffic accidents. Intending to reduce their occurrence, Advanced Driver Assistance Systems (ADAS) are being developed to assist the drivers; particularly, Collision Avoidance Systems (CAS).

Focusing specially on rear-end (near) crashes, the Brake-Threat-Number (BTN) and the Time-to-Brake (TTB) are typically used in CAS as measures of the situation criticality, and, equivalently, of the the need of automatic braking. When rear-end (near) crashes take place at traffic junctions, these measures often give false alarms, indicating a dangerous situation in cases where the driver has the situation under perfect control. Activating emergency braking in such situations can irritate the driver, and even compromise safety. Hence, there is a need of improvement of these measures.

This contribution analyses naturalistic traffic data collected in the framework of the European Field Operational Test on Active Safety Systems (EuroFOT) project to show that in situations where there is a traffic junction on the road, the typical BTN and TTB metrics overestimate the severity of hazard situations.

One reason for the deficiency of the BTN and TTB measures is that they are usually based on the assumption that the lead vehicle motion has constant acceleration (or even constant velocity), see, e.g., for BTN Brännström et al. (2010); Eidehall (2011); Seiler (2012), and for TTB Hillenbrand et al. (2006); Zhang et al. (2006).

This work proposes an enhanced model including road information to predict the braking behavior (deceleration pattern) of the lead vehicle. With this enhanced modeling of the lead vehicle, improved versions of BTN and TTB are proposed.

Summarizing, this paper is organized as follows. Section 2 describes how the BTN and the TTB are usually estimated. Section 3 presents the prediction model that approximates the braking behavior of the lead vehicle, whilst Section 4 explains how the model can be used to improve the BTN and TTB estimations. In Section 5 the enhanced estimations are applied and evaluated on a test example using real data from the EuroFOT project. Finally, Section 6 presents some conclusions and outlines the future work.

2. RISK METRICS FOR SITUATION AND THREAT ASSESSMENT

Two risk metrics commonly used in CAS, related to longitudinal motion, are used in this work to detect rear-end (near-) crashes; namely, the Brake–Threat–Number and the Time-to-Brake.

2.1 Brake–Threat–Number

The BTN estimates, for the host vehicle, the ratio of the needed acceleration to avoid a collision $a_{h,req}$, and the maximum achievable acceleration for a braking action $a_{h,max}$, as it is presented in (1). In other words, it is assumed that a hypothetical crash could be avoidable, and the worst case scenario would be a touching event between the participant vehicles at a time instant called Time–to–Touch (TTT). This means that the host vehicle touches the rear-end of the lead vehicle with relative velocity of zero.

$$BTN = \frac{a_{h,req}}{a_{h,max}} \qquad (1)$$

For the estimation of the BTN, the brake system can be approximated by different models. For instance, the longitudinal acceleration of the host vehicle $a_h(t)$ can be predicted to be piecewise constant. As well, as it is presented in Brännström et al. (2008), it could be approximated as a piecewise linear function where there is an initial delay, and after that, the acceleration decreases linearly with a constant rate up to a constant maximum level. The delay can model the driver perception-reaction time, or a time delay of the autonomous brake actuator.

In the piecewise constant case, method used in this work, $a_h(t) = a_h$ when $t > 0$, so the host vehicle position $x_h(t)$ is given by

$$x_h(t) = x_h(0) + v_h(0)\,t + \frac{a_h\,t^2}{2} \qquad (2)$$

where the velocity of the host vehicle is denoted as v_h.

Regarding the lead vehicle motion, a common assumption is that, the lead vehicle continues with constant longitudinal acceleration over the time until a hypothetical touching event in the worst case scenario; see for example Karlsson et al. (2004); Coelingh et al. (2007); Brännström et al. (2008). Consequently, the model of the lead vehicle position used in this event detection technique is a Taylor second degree expansion around the initial states at time $t = 0$

$$x_l(t) = x_l(0) + v_l(0)\,t + \frac{a_l(0)\,t^2}{2} \qquad (3)$$

where the position, velocity and acceleration of the lead vehicle are denoted as x_l, v_l, and a_l, respectively. The range or distance between the two participant vehicles, host and lead, $r(t)$ is given by (4), and the relative velocity is its derivative $\dot{r}(t)$.

$$r(t) = x_l(t) - x_h(t) \qquad (4)$$

Given (2), (3), and (4), the required host longitudinal acceleration is determined from (5), being *sol* the solution of the set of equations for a_h.

$$a_{h,req} = sol_{a_h}\left\{ (r(t), \dot{r}(t))^T = (0,0)^T \right\} \qquad (5)$$

In order to calculate the acceleration $a_{h,req}$, two cases are needed to be considered. In the first case, $a_{h,req}$ is defined by (6), where it is assumed that the lead vehicle comes to a standstill prior to the TTT (7).

$$a_{h,req} = -\frac{a_l(0)\,v_h(0)^2}{2\,a_l(0)\,r(0) - v_l(0)^2} \qquad (6)$$

$$TTT = \frac{2\,a_l(0)\,r(0) - v_l(0)^2}{a_l(0)\,v_h(0)} \qquad (7)$$

The time instant when the standstill occurs is labeled as Time–to–Stop (TTS), and defined as (8), with $a_l(0) < 0$.

$$TTS = -v_l(0)/a_l(0) \qquad (8)$$

In the second case, the lead vehicle continues in the same travel direction, without a stop, or stopping after the TTT. $a_{h,req}$ and the TTT are given by (9) and (10), respectively; on the condition that $v_h(0) > v_l(0)$.

$$a_{h,req} = a_l(0) - \frac{(v_l(0) - v_h(0))^2}{2\,r(0)} \qquad (9)$$

$$TTT = -\frac{2\,r(0)}{v_l(0) - v_h(0)} \qquad (10)$$

In practice, the BTN can vary in a range from 0 to 1 (theoretically, the BTN could take values greater than 1, but in practice it has no sense due to physical limitations of the brake system; in other words, a BTN value bigger than 1 indicates that the crash cannot be avoidable by a braking action alone). In this work, a given situation was considered as critical when the BTN was greater than or equal to 0.5. This is, 0.5 defines a risk threshold indicating a medium to high threat, as it is suggested by, for instance, Olsson (2008); Bengtsson et al. (2013).

2.2 Time-to-Brake

The TTB denotes the remaining time until an emergency braking at maximum deceleration must be applied to avoid the collision by braking Hillenbrand et al. (2005, 2006). In this case, the host vehicle must start its emergency braking maneuver at TTB in order to touch the lead vehicle with a relative velocity of zero at TTT. In cases when the crash is unavoidable, it is needed to apply the maximal deceleration in order to reduce the severity of the collision that would occur at a time instant Time–to–Impact (TTI).

Equations for the calculation of TTB and TTT for two special cases, under a set of particular initial conditions, are shown in Hillenbrand et al. (2005). In the first case, the lead vehicle comes to a standstill at time TTS, before TTT, but after the TTB. While, in the second case, the lead vehicle comes to a standstill at time TTS, after the TTT and the TTB.

Once calculated the TTB, it is possible to have a threat assessment using its value. As long as TTB > 0, it is theoretically possible to avoid an accident, but TTB close to zero means that there is little time to the driver to initiate a braking action; i.e. TTB is a measure of how critical the situation is. Specifically, according to Hillenbrand et al. (2005), if TTB $< \lambda$, where λ is a threshold value around $1s$, it indicates a medium to high hazard.

3. LEAD VEHICLE ACCELERATION ESTIMATION USING ROAD INFORMATION

The risk assessment obtained by using the BTN and TTB (described in the previous section) could be overestimated. As an example of that, considering the particular situations when $BTN > 1$, theoretically a collision cannot be avoided using only braking maneuvers, and it might be necessary to use steering maneuvers to prevent the imminent accident. But, in reality, despite the extremely

high risk assessment obtained, an accident could be even unlikely, for example, when the lead vehicle changes line, takes a highway exit, etc. This fact could be clarified under the light of the assumptions made for modelling the lead vehicle motion.

The assumptions of the threat assessment algorithms could be too pessimistic to overestimate the risk of collision. This overestimation could be related particularly to two assumptions. Firstly, when it is not possible to predict the lead vehicle driver behaviour and it is assumed that it continues in the same travel direction. And, secondly, when a constant lead vehicle longitudinal acceleration (or velocity) is assumed.

Regarding the prediction of driving behaviour, advances in wireless communication have opened an increasing number of new applications, focusing mainly on improving fuel economy and traffic safety, as well as reducing emissions. A new possibility is, for example, the use of wireless exchange of critical safety and operational data between vehicles and roadside infrastructure, i.e. infrastructure-to-vehicle communication.

Taking advantage of this kind of applications, road-traffic information has been used in Kamal et al. (2011), where a model predictive control (MPC) that reduces fuel consumption is presented. In the MPC, it is used an enhanced prediction model of the vehicle stopping motion, which is based on a set of patterns of driving data experimentally collected on urban roads.

Since a good prediction model not only benefits fuel efficiency and comfort, regarding safety, specifically intending to reduce false alarms activations, an approach to approximate the set of stopping behaviour patterns presented in Kamal et al. (2011) is proposed in this work to improve the threat assessment metrics already mentioned.

The proposed prediction model approximates the stopping velocity of the lead vehicle as a function of the stopping distance s_d. This function is obtained as an average of different drivers stopping behaviour, which is represented as a polynomial function. Thus, for this work purposes, the lead vehicle braking velocity v_l^* is approximated by a polynomial of degree 4 as

$$v_l^*(s_d) = c_0 + c_1 s_d + c_2 s_d^2 + c_3 s_d^3 + c_4 s_d^4 \qquad (11)$$

$$a_l^*(s_d) = \frac{dv_l^*(s_d)}{ds_d} v_l^*(s_d) \qquad (12)$$

In a more general way, for vehicles with higher or lower braking rates than the one in (12), the braking rate can be approximated by

$$a_l(s_d) = a_l^*(s_d) \left(\frac{v_l(s_d)}{v_l^*(s_d)} \right)^2 \qquad (13)$$

where $v_l(s_d)$ is the lead vehicle velocity at a stopping distance s_d. More details about this kind of approximation can be found in Kamal et al. (2011). Figure 1 shows the velocity v_l^* with a dashed line, whilst the continuous lines show the velocities predicted at different initial velocities and different initial stopping distances.
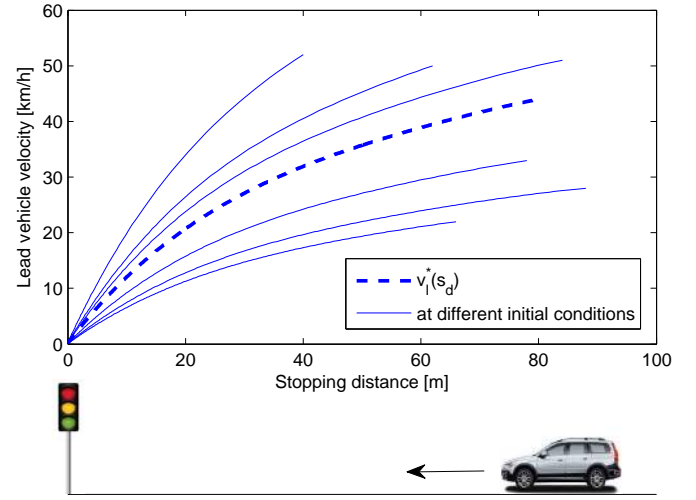

Fig. 1. Lead vehicle stopping patterns predicted at different initial conditions.

4. PROPOSAL: EVENT DETECTION USING BTN, TTB, AND ROAD INFORMATION

The prediction model presented in the previous section, is used to enhance the estimation of the BTN and TTB metrics. In this way, the assumption of constant lead vehicle longitudinal acceleration is avoided. Consequently, the host and lead vehicles longitudinal motion models can be expressed now in discrete-time form as

$$\begin{cases} x_h(k+1) = x_h(k) + Tv_h(k) \\ v_h(k+1) = v_h(k) + Ta_h(k) \end{cases} \qquad (14)$$

$$\begin{cases} x_l(k+1) = x_l(k) + Tv_l(k) \\ v_l(k+1) = v_l(k) + Ta_l(k) \end{cases} \qquad (15)$$

$$r(k) = x_l(k) - x_h(k) \qquad (16)$$

$$v_r(k) = v_l(k) - v_h(k) \qquad (17)$$

where T is the sampling time, and $a_l(k)$ is a function of the lead vehicle position and velocity at time instant k, and it is derived from (11)-(13)

$$a_l(k) = -\frac{\left(c_1 + c_2 s_d(k) + c_3 s_d(k)^2 + c_4 s_d(k)^3 \right) v_l(k)^2}{c_0 + c_1 s_d(k) + c_2 s_d(k)^2 + c_3 s_d(k)^3 + c_4 s_d(k)^4} \qquad (18)$$

The stopping distance at time instant k is calculated by subtracting the lead vehicle position $x_l(k)$ from the position of the stand-still place x_d (e.g. a traffic junction). i.e.

$$s_d(k) = x_d - x_l(k) \qquad (19)$$

These motion models are used to enhance the estimations of BTN and TTB as follows. In the case of the BTN calculation, the predicted $a_h(k)$ is assumed piecewise constant over time, and the required host longitudinal acceleration $a_{h,req}$ is obtained by (20), given (14)-(19), solving numerically the set of equations for a_h.

$$a_{h,req} = sol_{a_h}\{(r(k^*), v_r(k^*))^T = (0,0)^T,$$
$$\text{for a time instant } k^* > 0\} \qquad (20)$$

While, when the TTB is calculated, $a_h(k)$ is given by

$$a_h(k) = \begin{cases} a_h(0) & kT < TTB \\ a_{h,max} & kT \geq TTB \end{cases} \qquad (21)$$

and then, TTB is obtained in a similar way used for the BTN calculation; this is, solving numerically the set of equations for TTB.

$$TTB = sol_{TTB}\{(r(k^*), v_r(k^*))^T = (0,0)^T,$$
$$\text{for a time instant } k^* > 0\} \qquad (22)$$

5. RESULTS: TEST EXAMPLE

The test example used to evaluate the enhanced TTB and BTN metrics is part of the European Field Operational Test on Active Safety Systems (EuroFOT) data base. To create the part of this data base used in this work, Volvo cars type V70 and XC70 were equipped with data-loggers that record videos (e.g. rear-view, front-view, driver-view, and eye tracker), CAN signals, GPS positioning, and extra sensors data. Detailed information on the data acquisition system can be found in EuroFOT (2015).

The EuroFOT data set contains two types of available data, time-series data and video data. In order to illustrate the improvements proposed in this paper, time-series data, particularly the six required signals to estimate the enhanced metrics proposed in Section 4 are used. These are:

- Distance from the vehicle hosting data-loggers (host vehicle) to the main target (lead vehicle) in front.
- Longitudinal velocity of the main vehicle ahead.
- Longitudinal acceleration of the main vehicle ahead.
- Host vehicle longitudinal velocity (best estimate from available sensors, like GPS unit and wheel speed sensor).
- Host vehicle longitudinal translational acceleration from an accelerometer.
- Host vehicle location (estimated from the GPS unit).

Specifically the test example chosen for illustration purposes is the one called Event 22, where a rear-end near crash took place near to a traffic light triggering a false hazard alarm when the traditional BTN estimation is used. A satellite image of the place where the event was detected is shown in Figure 2. As it could be observed in the figure, the lead vehicle braking action is due to a traffic light.

Figure 3 shows the time histories of the event. Figure 3(a) shows the distance between the participant vehicles, velocity and acceleration of the host and lead vehicles during 4 s, starting 1 s before the event detection. Figure 3(b) illustrates, for the lead vehicle, with solid curves, its position being 0 m its location 1 s before the event is detected, its velocity and its acceleration. The blue dashed curves show the variables estimated using road information (from time $t = -1$ s). As observed, the proposed lead vehicle motion model shows a very good performance.

Fig. 2. Satellite images of the Event 22 taken from Google Earth.
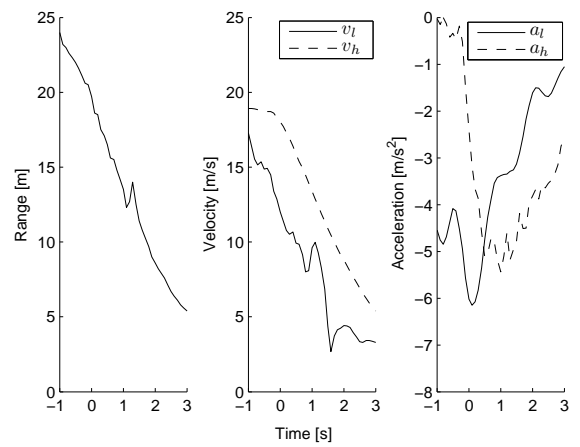
(a) Distance between vehicles, and velocity and acceleration of the lead vehicle (solid) and the host vehicle (dashed).
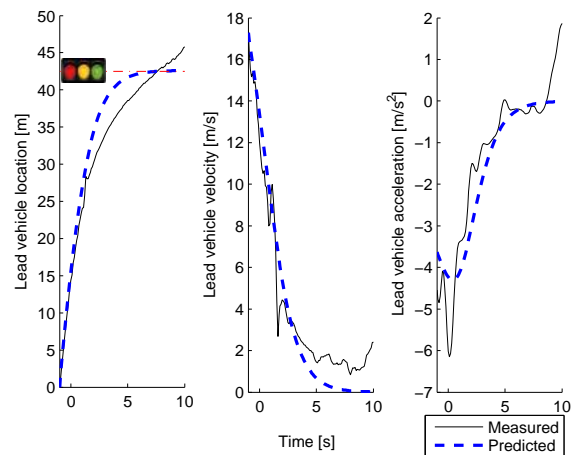
(b) Estimated (dashed) and measured (solid) values of position, velocity and acceleration of the lead vehicle.

Fig. 3. Event 22 from the EuroFOT data base: Time histories.

Figure 4 and Figure 5 are used to illustrate the criticality of Event 22. Image frames of this event are shown in Figure 4, the BTN profile for the event is shown in Figure 5(a), and the TTB profile is presented in Figure 5(b).

480

Fig. 4. Event 22 from the EuroFOT data base: Video frames at its detection, and at the traffic light.

(a) Traditional BTN (solid) and the enhanced BTN developed in this contribution (dashed).

(b) Traditional TTB (solid) and the enhanced TTB developed in this contribution (dashed).
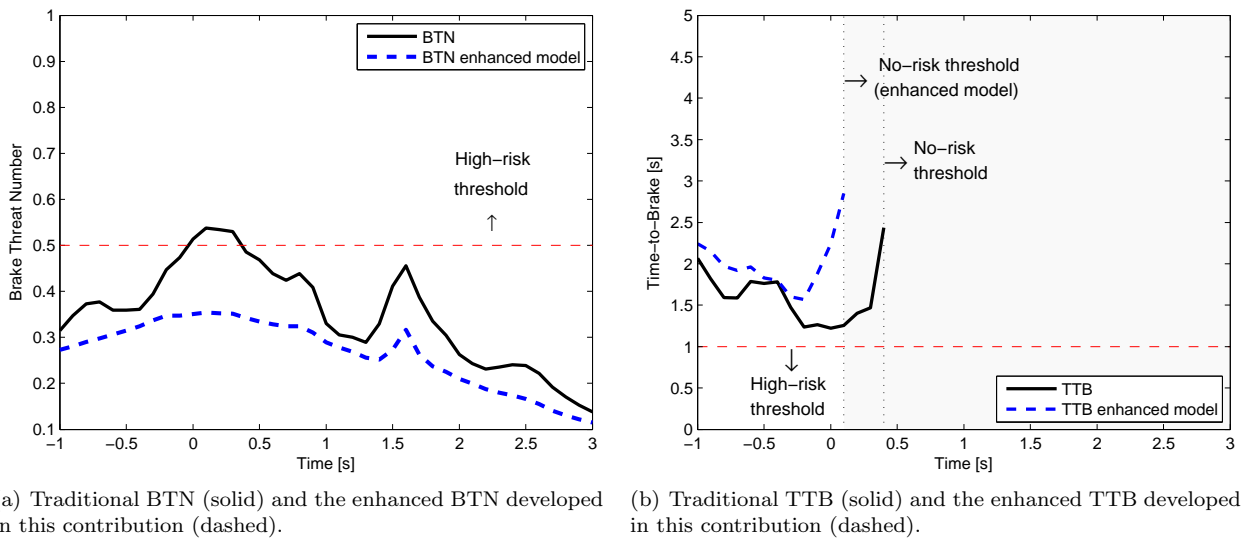
Fig. 5. Event 22 from the EuroFOT data base: BTN and TTB profiles.

Figure 4 shows video frames of the situation when the event is detected (using the traditional BTN metric, see Figure 5(a)), and 8.5 s after it, when the lead vehicle is at the traffic light.

When observing the traditional BTN and TTB profiles (solid black lines in Figure 5), it is found that the criticality of the event is evaluated as high just by the BTN, which exceeds the high-risk threshold (red dashed lines). This suggests that a false alarm has been triggered, and that the severity of the situation could not be so important, since it is not confirmed by the TTB evaluation.

As explained previously, the inconsistent hazard evaluation could be due to a lack of information about the road and the assumptions made to model the participant vehicles motion. This hypothesis could be validated by observing the Figure 4 which allows to infer that, the lead vehicle braking behaviour triggering a hazard alarm is due to the presence of a traffic light on the road.

Consequently, the enhanced hazard evaluation proposed in this work, including road information to estimate the BTN and the TTB (dashed blue lines in Figure 5) show a better assessment of the event severity. As observed, the enhanced BTN estimation does not reach the high-risk threshold, thus it does not trigger a false alarm.

6. CONCLUSIONS AND FUTURE WORK

The paper propose and evaluate enhanced versions of the BTN the TTB metrics to assess rear-end (near-) crashes by using a better prediction model of the leading vehicle built on road information. In the future, these new measures could make possible to propose an improved algorithm for consistent threat assessment for longitudinal motion, in cases where there are traffic junctions on the road.

ACKNOWLEDGMENT

REFERENCES

Bengtsson, M., Eidehall, A., and Agnvall, A. (2013). Forward collision risk reduction. US Patent 8,589,061.

Brännström, M., Coelingh, E., and Sjöberg, J. (2010). Model-based threat assessment for avoiding arbitrary vehicle collisions. *Intelligent Transportation Systems, IEEE Transactions on*, 11(3), 658–669.

Brännström, M., Sjöberg, J., and Coelingh, E. (2008). A situation and threat assessment algorithm for a rear-end collision avoidance system. In *Intelligent Vehicles Symposium, 2008 IEEE*, 102–107. IEEE.

Coelingh, E., Jakobsson, L., Lind, H., and Lindman, M. (2007). Collision warning with auto brake-a real-life safety perspective. In *20th International Technical Conference on the Enhanced Safety of Vehicles*, 1–9.

Eidehall, A. (2011). Multi-target threat assessment for automotive applications. In *Intelligent Transportation Systems (ITSC), 2011 14th International IEEE Conference on*, 433–438. IEEE.

EuroFOT (2015). EuroFOT - european large-scale field operational test on in-vehicle systems. URL http://www.eurofot-ip.eu/.

Hillenbrand, J., Kroschel, K., and Schmid, V. (2005). Situation assessment algorithm for a collision prevention assistant. In *Intelligent Vehicles Symposium, 2005. Proceedings. IEEE*, 459–465. IEEE.

Hillenbrand, J., Spieker, A.M., and Kroschel, K. (2006). A multilevel collision mitigation approachits situation assessment, decision making, and performance tradeoffs. *Intelligent Transportation Systems, IEEE Transactions on*, 7(4), 528–540.

Kamal, M., Mukai, M., Murata, J., and Kawabe, T. (2011). Ecological driving based on preceding vehicle prediction using MPC. *Proc. 18th World Congr. Int. Federat. Autom. Control*, 3843–3848.

Karlsson, R., Jansson, J., and Gustafsson, F. (2004). Model-based statistical tracking and decision making for collision avoidance application. In *American Control Conference, 2004. Proceedings of the 2004*, volume 4, 3435–3440. IEEE.

Olsson, P. (2008). Testing and verification of adaptive cruise control and collision warning with brake support by using HIL simulations. *SAE SP*, 2188, 1.

Seiler, R.L. (2012). Vehicle braking based on external object communications. US Patent App. 13/596,501.

Zhang, Y., Antonsson, E.K., and Grote, K. (2006). A new threat assessment measure for collision avoidance systems. In *Intelligent Transportation Systems Conference, 2006. ITSC'06. IEEE*, 968–975. IEEE.

Analysis and Modeling of Driver behavior on Pedestrian Crossing Road Situation
(1st report: Modeling Driver's Response)

First Ryo Iwaki*. Second Kenji Sato*
Third Takashi Wakasugi*. Fourth Nobuyuki Uchida

*Japan Automobile Research Institute, Safety Research Division
2530 Karima, Tsukuba, Ibaraki, 305-0822Japan
(e-mail: riwaki@jari.or.jp)

Abstract: This study analyzed drivers' actions to avoid pedestrians. Specifically, it studied these actions to construct models that would demonstrate drivers' avoidance of pedestrians crossing a road. An experiment was conducted to gather data on drivers' response to pedestrians. Actual cars were used, and a pedestrian dummy appeared before them at various times (2sec, 3.5sec, and 5sec). The time of lifting one's foot off the gas pedal, the time of braking, and the deceleration used to avoid colliding with pedestrians were individually examined using the acquired data. These three variables were analyzed in relation to time to collision with pedestrians. As a result, this study successfully produced models of a series of drivers' actions in response to pedestrians appearing before them, as well as time required to avoid a collision.

Keywords: Human factors, Driver behavior, Driver models

1. INTRODUCTION

During the past few years, the number of deaths from traffic accidents has been declining; however, this decline slowed after the number of deaths fell below 5,000 in 2009. In 2011, accidents involving pedestrians accounted for 36.6% of all accidents in Japan, where fatal accidents are examined in terms of accident percentage by conditions. Furthermore, accidents that occurred during pedestrian crossing accounted for 26.0% of all accidents. Both percentages involving pedestrians are high. The fatality rate also reflects an extremely high rate of pedestrian accidents, with such accidents being 4.6 times greater than the average for traffic accidents overall. To further reduce the number of fatal accidents, it is urgently necessary to prevent vehicular accidents involving pedestrians and to take measures to reduce damage

From a technological standpoint, measures to reduce vehicular accidents involving pedestrians include systems that detect pedestrians or assist in risk avoidance (e.g., warning signals and automatic brakes). However, to establish system-operating requirements and to predict the effects of accident reduction, it is essential to analyze drivers' behavior when they detect pedestrians and to ascertain the situation when an accident occurs.

Therefore, this study constructed models that simulated drivers' actions when they confronted pedestrians crossing the road, with the aim of analysing drivers' actions to avoid hitting pedestrians. Furthermore, the percentage of pedestrians who suddenly appear in front of a vehicle (a pressing situation from the driver's perspective) is extremely high. Therefore, this study focused on pedestrians suddenly crossing the road ("sudden crossing") and analyzed drivers' actions to avoid pedestrians in such instances.

2. EXPERIMENT

To investigate drivers' avoidance behavior in response to pedestrians on the road, an experiment using pedestrian dummies and actual cars was conducted on a test road (Fig. 1).

Fig. 1. Experiment field

2.1 Dummy Pedestrian

The dummy pedestrian depicted in Fig. 2 was used in an experiment that reproduced the condition in which a pedestrian would suddenly try crossing a road, while fully ensuring safety during the experiment. The dummy was a life-size picture of a man attached to a plastic board. When the experiment vehicle passed a prescribed point (above the photo sensor), the dummy was pulled toward the road using a rope wound around a reel. The experiment was configured so that the dummy pedestrian could be pulled at the same time and speed during the entire experiment, as long as the experiment conditions remained unchanged.
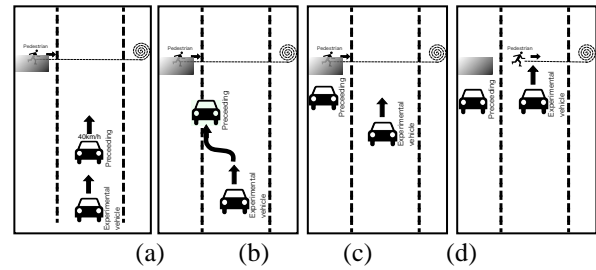
Fig. 2. Dummy pedestrian

Fig. 3. Means of running

2.2 Vehicle Running Pattern

The vehicle was running at 40km/h in a straight single lane. Drivers were instructed to drive the vehicle at a constant speed of 40km/h, to keep their eyes on the road, to follow a preceding vehicle, and to pass the preceding vehicle only after it started running along the curb (Fig. 3). The following specific instructions were given to the drivers.

(1) The purpose of this experiment is to check your bodily sensation of vehicle speed; thus, you must drive your vehicle at a constant speed to the extent possible without looking at the speedometer (Fig. 3 (a)).

(2) You should follow the preceding vehicle at a constant speed. When it starts to run along the curb (Fig. 3 (b)), you must stay in the same lane at the same speed and pass the preceding vehicle when the lane ahead of you is clear (Fig. 3 (c)).
(With these instructions given, it is expected that the driver will understand that the purpose of this experiment is to investigate the bodily sensation of speed.)

(3) During this experiment, you should drive the vehicle carefully, as if you were driving your car in an actual traffic environment.

The speedometer was covered during the experiment to prevent drivers from looking at it. The experiment consisted of 8 sections (Table 1), and every driver was asked to drive the vehicle 8 times. In the first section of the experiment, the speedometer was not hidden so that the driver could learn to drive at a constant speed. In the following seven sections of the experiment, the speedometer was hidden, and the driver had to be aware of maintaining a constant speed. In the fourth, sixth, and eighth sections, the dummy pedestrian suddenly tried crossing the road. The "pedestrian's road crossing TTC" in the fourth section was short (2.0 or 3.5sec), and the TTC in the sixth and eighth sections was long (5.0sec). The driver's response to the long TTC was thought to be affected by the driver's experience in the short TTC, so the experiment in the long TTC was carried out twice (sections 6 and 8).

Table 1. Section of running

Section	Running content
1	Training
2	Maintain velocity (cover story)
3	Maintain velocity (cover story)
4	Pedestrian crossing (TTC: short)
5	Maintain velocity (cover story)
6	Pedestrian crossing (TTC: long)
7	Maintain velocity (cover story)
8	Pedestrian crossing (TTC: long)

3. Driver's Behavior Analysis

3.1 Collision Avoidance Action of Driver

In the experiment, every driver avoided collision with the pedestrian only by putting on the brake when "TTC when pedestrian starts crossing the road (TTC pedestrian appears from the blind)" was long. When it was short (only 2.0sec), three of 11 drivers collided with the pedestrian. Also, when the "pedestrian's road crossing TTC" was 2.0sec, two drivers could avoid the pedestrian by controlling the steering wheel while braking. Sixty-three experiments (21 drivers x 3 runs) were conducted, and the drivers' responses to the pedestrian's sudden road-crossing were collected. 58 of 63 collision avoidance actions were just applying the brake, so we decided to focus on brake operations.

3.2 Analysis of Experimentl Data

As the first step of the analysis, drivers' collision avoidance actions were divided into the following phases, which were observed in this order of sequence (Fig. 4).

Phase 1   Pedestrian starts crossing (pedestrian appears: driver realizes pedestrian is about to cross the road).

Phase 2   Driver releases the accelerator (accelerator off).

Phase 3   Driver applies the brake (brake on).

Phase 4   Vehicle is brought to a stop (stop).

Under time-critical and unexpected urgent conditions (e.g., a pedestrian jumps out onto the road, and collision with the pedestrian may be imminent and expected), it is important to objectivelyanalyze the transfer timing from one phase to another, as well as the driver's behavior at that timing. We analyzed the following timings and driver behaviors.

(1) Transfer timing when a driver releases the accelerator after finding that a pedestrian is starting to cross the road ("accelerator off time") [Phase 1 to Phase 2]

(2) Transfer timing when a driver applies the brake after releasing the accelerator ("time to move from accelerator to brake") [Phase 2 to Phase 3]
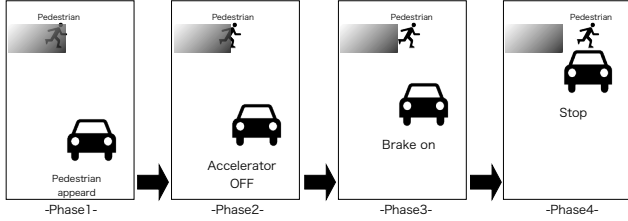
(3) Vehicle slowdown (deceleration) [Phase 3 to Phase 4]

Fig. 4. State transition

3.3 Analysis of Accelerator Off Time

"Accelerator off time" was calculated in every experiment. It was assumed that a driver releases the accelerator in response to detecting a pedestrian trying to cross the road. Thus, we focused on analysis of "accelerator off time" and "TTC when pedestrian appears." The distribution of "accelerator off time" is plotted in Fig. 5, in which the distribution is presented as a function of "TTC when pedestrian starts crossing the road." "TTC when pedestrian appears" is rather widely distributed, because the timing when a pedestrian starts crossing the road is determined by the vehicle position (detected by the photo sensor) and because the vehicle speed passing above the sensor varies. There is a correlation between the "TTC when pedestrian starts crossing the road" and "accelerator off time." In addition, results indicated that the larger the "TTC when pedestrian starts crossing the road," the wider the "accelerator off time" is distributed.

The average and standard deviation in every condition are indicated in Fig. 6. As TTC becomes small (the vehicle must be brought to a stop more quickly), "accelerator off time" becomes large. Differences among mean "accelerator off times" in each condition are statistically significant ($p<0.05$).
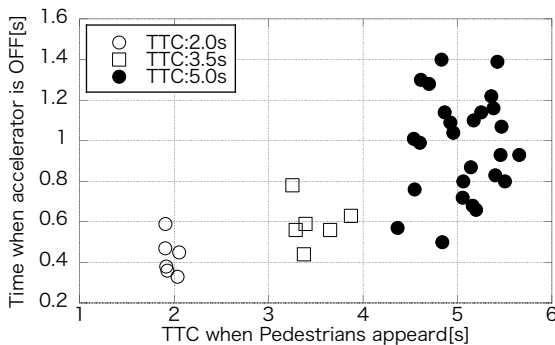
Fig. 5. Distribution of accelerator off timing
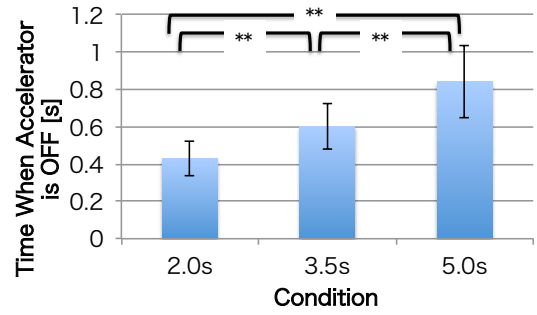
Fig. 6. Accelerator off timing for each condition

The average and standard deviation of the "accelerator off time" were studied for every "TTC when pedestrian starts crossing the road" condition (Fig. 7). Both average and standard deviation increase linearly as TTC increases. The linear regression operation of the average and standard deviation were calculated using Eqs. (1) and (2).

$$T_{accelerator} = 0.13 \cdot TTC_{ped} + 0.16 \qquad (1)$$
$$SD_{T_{accelerator}} = 0.032 \cdot TTC_{ped} + 0.025, \qquad (2)$$

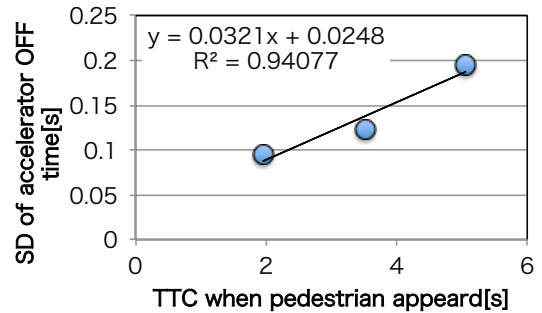$T_{accelerator}$: *Accelerator off time*
$SD_{T_{accelerator}}$: *Standerd deviation of Acceleration off time*
TTC_{ped} : *TTC when pedestrian starts crossing the road .*

In Fig. 8, the regression and +/-2σ lines, which were calculated using these equations, are presented as a function of "TTC when pedestrian starts crossing the road" and "accelerator off time." The trend of "accelerator off time" can be expressed roughly using the above linear regression equations.
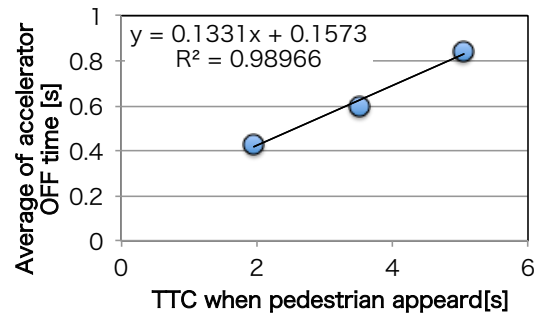
(a) Means

(b) Standard deviations
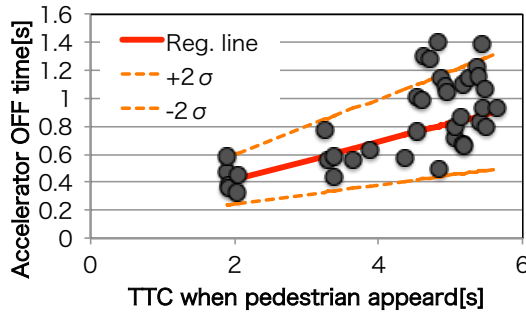Fig. 7. Accelerator off timing for each condition

Fig. 8. Accelerator off timing and TTC

Fig. 9. Distribution of " time to move from accelerator to brake"

3.4 Analysis of "Moving time of accelerator to brake"

The " time to move from accelerator to brake," which is the length of time from when a driver releases the accelerator to when the driver applies the brake, was calculated in every experiment. It was assumed that every driver would decide the "time to move from accelerator to brake" based on the pedestrian's position relative to the vehicle when the driver released the accelerator. Thus, we focused on the time from when the accelerator is released to the time when the brake is applied ("TTC during accelerator off").

The distribution of "moving time of accelerator to brake" is plotted in Fig. 9 as a function of "TTC during accelerator off." ??As "TTC during accelerator off' increases, " time to move from accelerator to brake" as well as its dispersion increases??. In addition, "TTC during accelerator off' in the same condition varies widely as "TTC when pedestrian starts crossing the road" is widely distributed. As indicated in Fig. 7 (b), the larger the "TTC when pedestrian starts crossing the road," the more widely the "accelerator off time" varies.

The average and standard variation of the " time to move from accelerator to brake" were studied for every "TTC when pedestrian starts crossing the road" condition. Results indicated no significant differences (p>0.1) in the average and standard variation among conditions. Therefore, the average and variation of " time to move from accelerator to brake" were studied regardless of "TTC when pedestrian starts crossing the road" to determine the general trend over the entire data of averages and variations of " time to move from accelerator to brake" due to "TTC during accelerator off." Since "TTC during accelerator off' varies widely with "TTC when pedestrian starts crossing the road," the linear regression operation was carried out using "TTC during accelerator off' as the explanatory variable and " time to move from accelerator to brake" as the response variable (Fig. 9). Distribution of " time to move from accelerator to brake" was evaluated using the regression line. The distribution of " time to move from accelerator to brake" was studied using the linear regression residuals, and the distribution index was studied using the root mean square of deviations from the regression line. If the deviation was calculated for a certain constant section of "accelerator off time," the number of elements varied between sections. Therefore, deviation from the line in terms of the root mean square of the regression residuals ("moving variance") was calculated for the moving data set that could keep the number of elements constant.
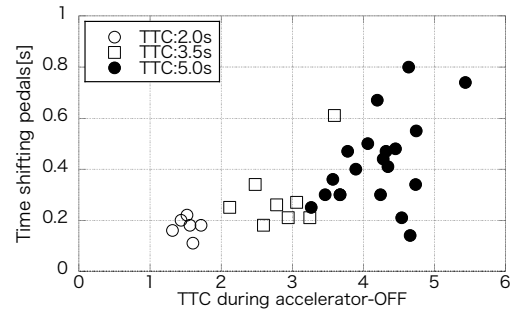
The moving variance of "TTC during accelerator off" and " time to move from accelerator to brake" is plotted in Fig. 10. The variance index of " time to move from accelerator to brake" increases as "TTC during accelerator off' increases. Therefore, "TTC during accelerator off' was used as the explanatory variable, and the variance index of "time to move from accelerator to brake" was used as the response variable in the linear regression (line in Fig. 11). As a result, the determination coefficient was found to be as high as 0.75, and the following equations were obtained to determine the relationship between "time to move from accelerator to brake" and "TTC during accelerator off."

$$T_{Shifting\_pedal} = 0.10 \cdot TTC_{throttle_{off}} \qquad (3)$$

$$SD_{T_{throttle}} = 0.050 \cdot TTC_{throttle_{off}} + 0.055 \qquad (4)$$

$T_{Shifting\_pedal}$: *Time* to move from *accelerator to brake*
$SD_{T_{shifting\_pedal}}$: *Standerd deviation of* $T_{shifting\_pedal}$
$TTC_{throttle_{off}}$: *TTC when accelerator off.*

These equations were used to find the regression line and deviations (+/-2σ); and Fig. 11 presents them as a function of "TTC during accelerator off" and " time to move from accelerator to brake." The trend of "accelerator off time" can be expressed roughly by the above linear regression equations.
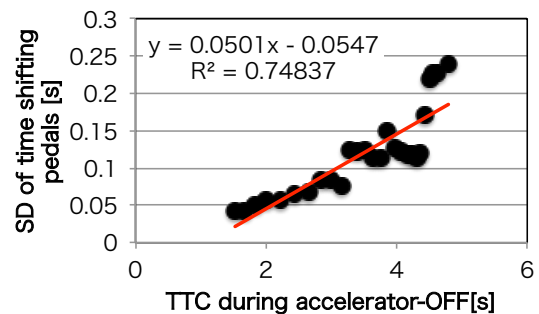

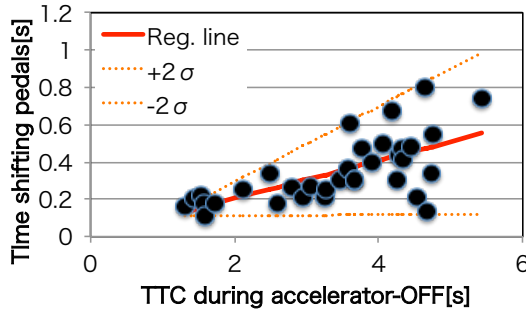Fig. 10. Standard deviation of time to move

Fig. 11. Results of moving time

3.5 Analysis of Vehicle Deceleration

In the first step of analysing vehicle deceleration, time-series changes of deceleration waveform were studied. In many waveforms the vehicle speed decreased at a constant rate until it reached its lowest value; then it was maintained at its lowest speed (Fig. 12). Thus, it was decided to divide the deceleration waveform into two parts, maximum deceleration and decreasing speed ("average jerk").

Vehicle deceleration was analyzed for each part.
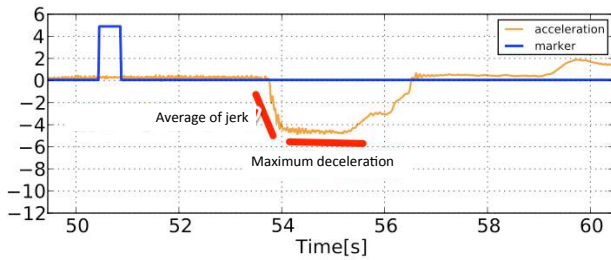
Fig. 12. Acceleration data

3.5.1 Maximum deceleration

Deceleration when a driver put on the brake to avoid collision with a pedestrian when the pedestrian started crossing the road was regarded as maximum deceleration. It was assumed that every driver would choose maximum deceleration based on the pedestrian's position relative to the vehicle when the driver put on the brake; thus, we focused on TTC of the pedestrian until the driver put on the brake ("TTC during brake on").

It was also assumed that drivers decelerate in response to their risk assessment of collision with a pedestrian; thus, "TTC^{-1}," which is often used as an index of collision risk, was used in this study. Figure 13 plots the distribution of maximum deceleration and "TTC^{-1}" when a driver applies the brake ("TTC^{-1} during brake on"). As "TTC^{-1} during brake on" increases, maximum deceleration also tends to increase linearly.
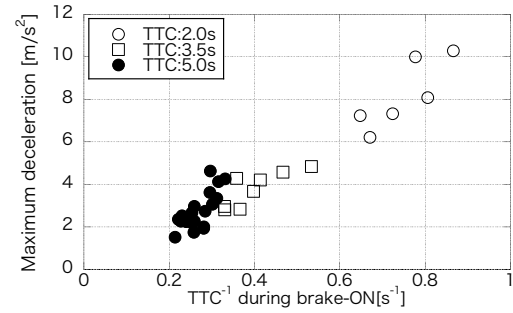

Fig. 13. Distribution of maximum deceleration

Linear regression was performed using "TTC^{-1} during brake on" as the explanatory variable and maximum deceleration as the response variable (Fig. 14). Since the determination coefficient was found to be high (0.91), we concluded that the trend of data was precisely expressed. The regression line was used to study variations in " time to move from accelerator to brake." In addition, deviations of data from the average, assumed to be the regression line, were used in the study.

Differences in the regression residuals among "TTC when pedestrian starts crossing the road" conditions were investigated. No significant differences (p>0.1) were found between conditions. Thus, the regression line derived from the entire data was regarded to be the average, and the standard deviation was calculated to be 0.68 (SD = 0.68). Based on the above observation, the trend of maximum deceleration variation could be expressed by

$$a_{max} = 11.5 \cdot TTC_{brake_{on}}^{-1} - 0.47 \qquad (5)$$
$$SD_{a_{max}} = 0.68, \qquad (6)$$

where

a_{max} : Max accerlation
$SD_{a_{max}}$: Standerd deviation
$TTC_{brake_{on}}^{-1}$: $1/TTC_{brake\_on}$.

These equations were used to find the regression line and deviations (+/-2σ), and they are presented in Fig. 14 as a function of "TTC^{-1} during brake on" and maximum deceleration. The trend of the maximum deceleration can be roughly expressed using "TTC^{-1} during brake on".
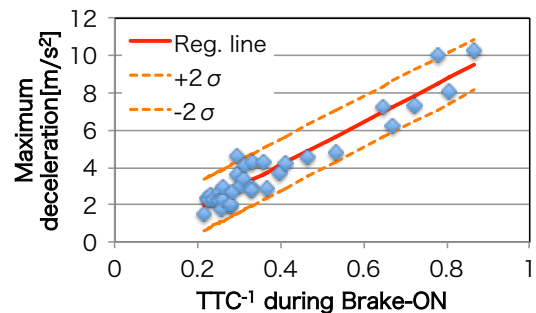

Fig. 14. Result of maximum deceleration

3.5.2 Average jerk

Average jerk is defined as a gradient of speed decelerated by collision avoidance braking for 0.5sec after the start of braking.

The distribution of the maximum deceleration and average jerk is plotted in Fig. 15. Maximum deceleration and average jerk are linearly related, and the linear regression provides a determination coefficient of 0.92. In the linear regression, the maximum deceleration was used as the explanatory variable, and average jerk was used as the response variable. This determination coefficient of 0.92 indicates a strong linear correlation between maximum deceleration and average jerk. Like the study discussed in the previous section, differences in regression residuals among "TTC when pedestrian starts crossing the road" were investigated, and no significant difference (p>0.1) was found among conditions. Thus, the regression line derived from the entire data was assumed to be the average, and the standard deviation was calculated to be 0.89 (SD = 0.89). Based on the above study, the following equations were obtained:

$$\bar{J} = 2.1 \cdot a_{max} - 2.6 \qquad (7)$$
$$SD_{a_{max}} = 0.89, \qquad (8)$$

where

a_{max} : max accerlation
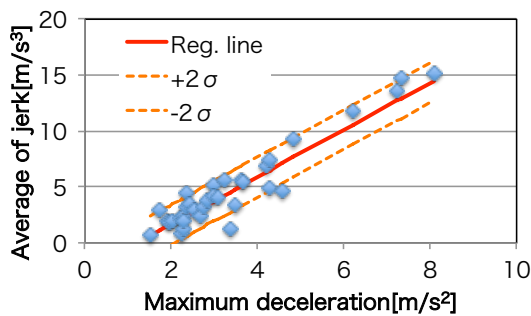$\bar{J}$: average of jerk.

Fig. 15. Liner regression between jerk and deceleration

5. CONCLUSION

Based on the results of this study, it is expected that the driver model extending from the entry of the pedestrian onto the road to the avoidance of a collision (braking) may prove useful in estimating the effectiveness of preventive safety measures in reducing accidents involving pedestrians, as well as support strategies for these accidents (Fig. 16).

In future studies, it will be necessary to increase the precision of the model by adding speed conditions and sample numbers, because the data obtained in this experiment was limited by short TTC conditions when the pedestrian entered the road and because there was only one speed (40 km/h).
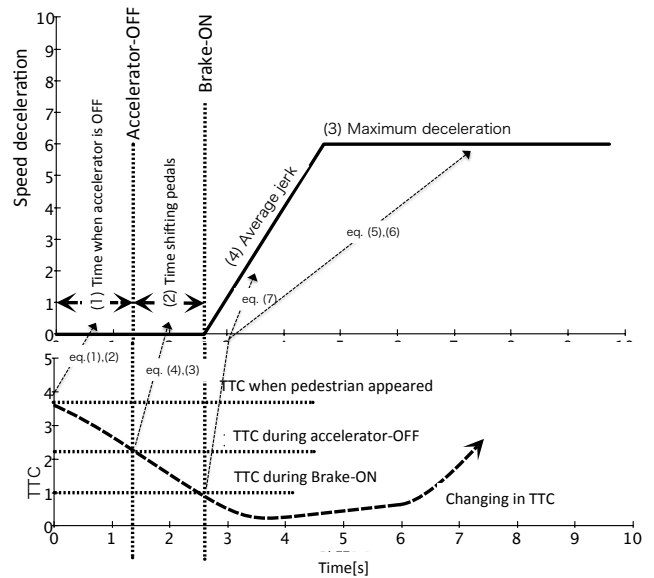

Fig. 16. Result of investigating driver model

Acknowledgments

Development of an instrumented vehicle with Augmented Reality (AR) for driver performance evaluation

Nobuyuki Uchida *, Takashi Tagawa *, Kenji Sato *

* Japan Automobile Research Institute, Safety Research Division
2530 Karima, Tsukuba, Ibaraki, 305-0822, Japan (E-mail: nuchida@jari.or.jp).

Abstract: Observing drivers' behaviours by reproducing traffic accidents and conflict situations is important for developing advanced driver assistance systems. For this purpose, an instrumented vehicle, named the JARI-ARV (Japan Automobile Research Institute - Augmented Reality Vehicle), was developed to reproduce realistic traffic accident and conflict scenarios without endangering the driver. In this study, we examined acceptability and controllability in the following cases: a right turn and encounter with a pedestrian by comparing the JARI-ARV with a normal (unaltered) same model vehicle. Results of the experiment indicated that drivers tend to react to virtual traffic participants in the same way as driving a normal vehicle. Applicability of the JARI-ARV for human factor research was confirmed.

Keywords: Driver behaviour, Accident scenario reproduction, Augmented Reality

1. INTRODUCTION

One current traffic safety research topic is driver assistance systems for collision avoidance. Observing drivers' behaviours by reproducing traffic accidents and conflict situations is effective for developing these systems. In some previous studies, realistic testing on a proving ground such as "surrogate target methodology" was developed to examine effective driver support (Kiefer et al., 1999). However, testing of realistic driver behaviour during critical traffic situations could endanger the participants because of possible physical contact.

Driving simulators are frequently used to evaluate driver assistance systems during product development. However, motion (simulator) sickness can be a serious practical problem with driving simulators. In general, rapid movement within the simulated scene, such as sharp decelerations for avoiding obstacles, easily produce sickness. It is proposed that motion sickness is the result of perceptual conflict between different sensory systems (Reason and Brand, 1975). Compared to visual information, vestibular and kinesthetic information is limited in a driving simulator because of difficulties in reproducing a vehicle's movements.

Therefore, an instrumented vehicle, named the JARI-ARV (Japan Automobile Research Institute - Augmented Reality Vehicle), was developed to reproduce realistic traffic accident and conflict scenarios without putting the driver at risk of an actual collision. In this study, we examined acceptability and controllability in 3 cases: a right turn, stopping at a stop line and an encounter with a pedestrian by comparing the JARI-ARV with a normal (unaltered) same model vehicle. A critical traffic situation where a pedestrian suddenly appears from behind a wall was reproduced to compare the driver's behaviours in the JARI-ARV to that in a normal vehicle.

2. CONFIGURATION OF THE INSTRUMENTED VEHICLE

The JARI-ARV is an augmented reality (AR) driving simulator, which is coupled with a real passenger car (Figure 1). The instrumented vehicle has three LCDs (42 inch) and three video cameras on its hood. A driver can operate the vehicle by viewing a frontal scene projected to these LCDs that cover almost a 110-degree horizontal field of view. This display system is defined as "Video see-through" (Rolland & Fuchs, 2000). The biggest advantage of the system is that a participant can drive without wearing any optical devices, such as a head mounted display (HMD). This is important to ensure natural visual behaviour while driving in a simulated traffic environment.

Figure 2 shows the configuration of the JARI-ARV. Forward view scenery is captured by a Full HD video camera, and sent to a workstation installed in the vehicle's cargo space. The workstation combines the real view scenery with 3D CGs (Car, Moped, Cyclist, Pedestrian etc.). The composite view, which consists of the real road lane and added virtual traffic participants, is projected to a LCD in front of the driver.

The representation of the virtual 3D objects (Figure 3) is calculated based on the position and orientation of the instrumented vehicle, so that the position and orientation of the JARI-ARV are accurately collected by real time kinematic GPS.

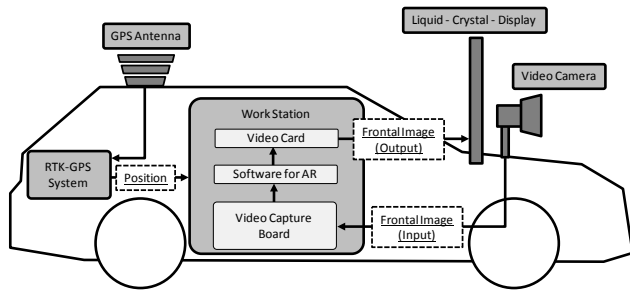Fig. 1. Overview of instrumented vehicle (JARI-ARV).

Fig. 2 System diagram of instrumented vehicle

Fig. 3. Frontal view with virtual traffic participants (cars in opposite lane) while driving the instrumented vehicle.

While driving the JARI-ARV, the driver has novel visual experiences compared to normal car driving. The explicit difference is that traffic situations in front of the driver are shown on the three LCDs. This requires the driver to perceive depth information from 2D visual images. Therefore, the performance of the vehicle control, especially while turning left or right, could be negatively affected by the visual display. A less obvious difference is encountering virtual traffic participants. Although the virtual 3D CG objects have realistic features, they are not exactly the same as real traffic. This could lead to differences in the driver's attention/reaction to the reproduced traffic participants in comparison with real human or objects. Therefore, we compared the JARI-ARV with a same model vehicle, in terms of vehicle controllability and reaction performance to other traffic participants.

The main objective was to validate applicability of the JARI-ARV for driver behaviour analysis and development of advanced driver assistance systems (ADAS).

3. METHOD

3.1 Experimental conditions

We examined the JARI-ARV in two types of traffic situations. The first type was normal driving situations that included a right turn at an intersection (Figure 4) and stopping at a stop line. The second type was an interactive (critical) traffic situation that included passing by a pedestrian on the roadside and an encounter with a pedestrian rushing out onto the road (Figure 5, Figure 6).
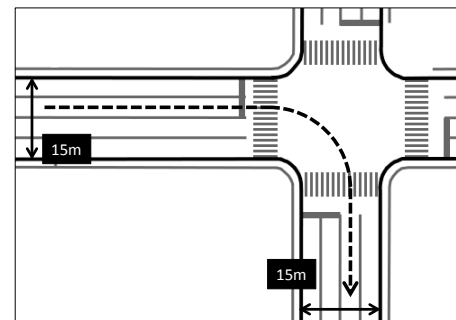

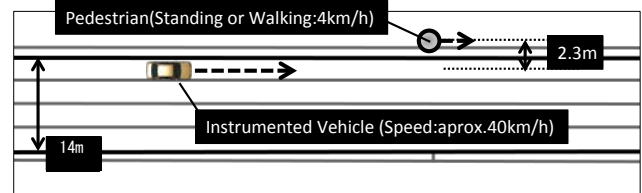
Fig. 4 Right turn at an intersection

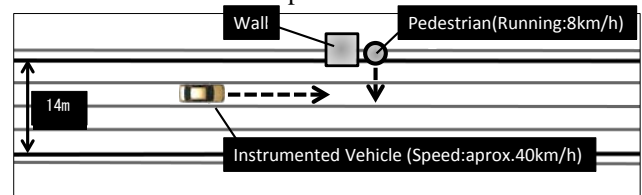Fig. 5 Configuration of traffic situations of passing a pedestrian

Fig. 6 Configuration of traffic situations of a pedestrian rushing out

3.2 Participants and Procedure

Ten male drivers, average age 37.5 years, participated in the experiment. Participants were instructed to follow rules and signs while driving on the JARI test field (simulated road in a residential area). Every participant drove two vehicles (JARI-ARV and same model normal vehicle) once, in turns. The order of driving was counterbalanced between the subjects. Although each test drive contained a normal and an interactive traffic situation, both tests were ended by the 'encounter with a pedestrian rushing out' scenario.

3.3 Analysis

3.3.1 Normal driving situation

To analyse ability of vehicle control, data for the running path of the right turn was collected. The initiation point of braking and steering before entering the intersection was also compared between the two vehicles.

3.3.2 Interactive (critical) traffic situation

(1) Passing by a pedestrian

If a driver meets a pedestrian and recognizes a potential risk, then the driver will pass by the pedestrian with adequate space. The distance from the roadside pedestrian to the passing vehicle was measured.

(2) Pedestrian rushing out

Brake reaction time was defined as the period between the appearance of the pedestrian and the onset of the driver braking.

4. RESULTS AND DISCUSSIONS

4.1 Normal driving situation

Figure 7 shows the running paths of ten participants in two vehicle conditions. The origin of the XY axis is the centre of the intersection. The distribution of turning paths in the JARI-ARV condition (bold lines) was found to be similar to the result in the normal vehicle condition (dotted lines). The initiation point of braking and steering before entering the intersection was not significantly different between the JARI-ARV and the normal vehicle (Figure 8, Figure 9). These results suggest that the JARI-ARV provides enough depth information for the driver to control the vehicle while turning right at an intersection, in spite of driving with the forward view projected on three LCDs.

On the other hand, the performance of the stop position control with the JARI-ARV was significantly inferior to that of the normal vehicle. As shown in Figure 10, the JARI-ARV stopped more than 1 meter before the stop line, which was more than the normal vehicle. The result suggested that the position of video cameras affected distance perception around the JARI-ARV. The video cameras were fixed 1 meter in front of the driver's eye point. The stop position deviation may have also been due to the lack of the front hood image of the JARI-ARV.

4. 2 Interactive (critical) traffic situation

Figure 11 shows the situation of approaching a roadside pedestrian who is standing still. For the pedestrian target, a 3D CG model and a real human were adopted in JARI-ARV and normal vehicle conditions, respectively. The distance from the roadside pedestrian to the passing vehicle was not significantly different between the two vehicles (Figure 12).
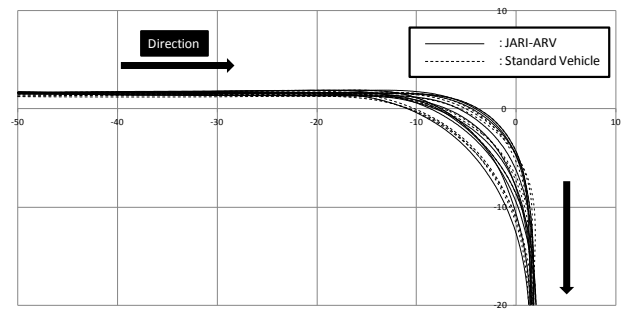

Fig. 7. Running paths of vehicles while right turning at an intersection.
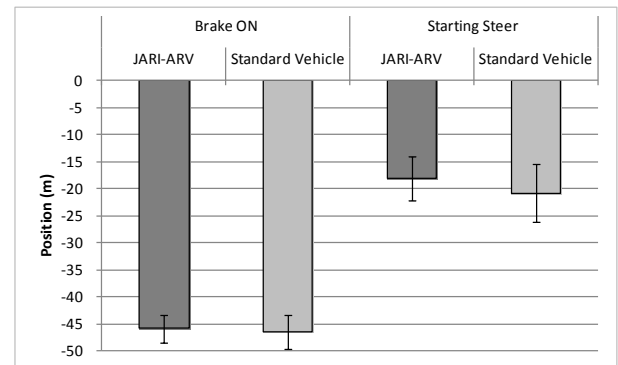

Fig. 8. Initiation point of driver behaviours from approaching intersection (x-axis).
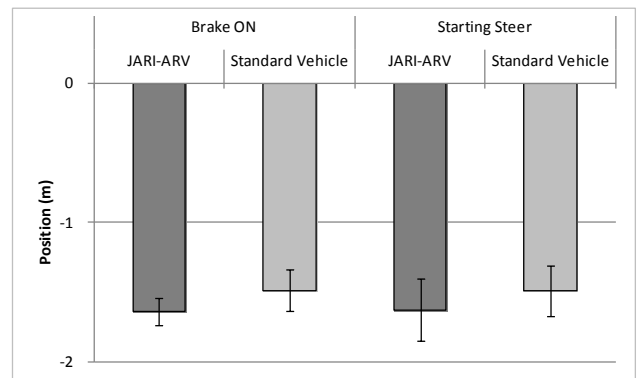

Fig.9 Initiation point of driver behaviours from approaching intersection (y-axis)

In a critical traffic situation, in which a roadside pedestrian rushed out (Figure 13), the same tendency was found. The reaction time to a pedestrian who rushed out in front of the vehicle was not significantly different between the JARI-ARV and the normal vehicle (Figure 14). These results suggest that drivers tend to react to virtual traffic participants in the same way as when driving a normal vehicle, even in a critical situation
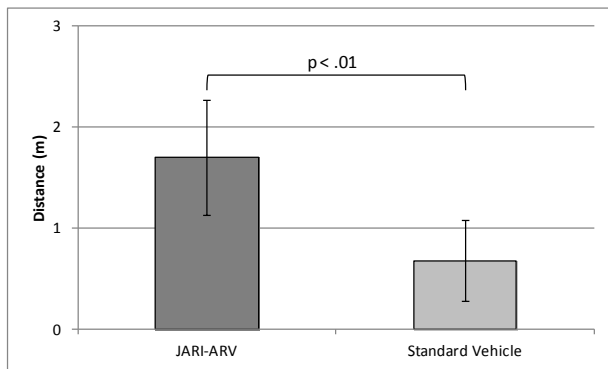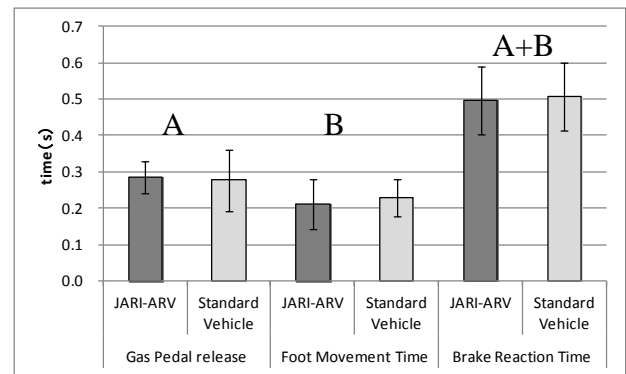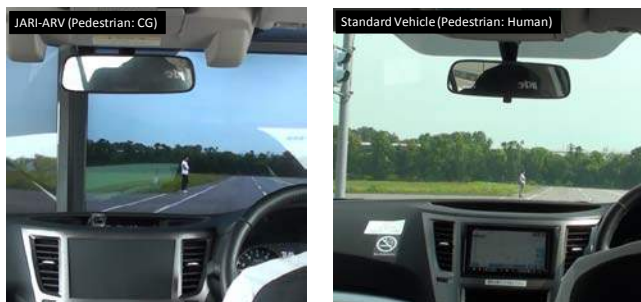
Fig.10 Stop position

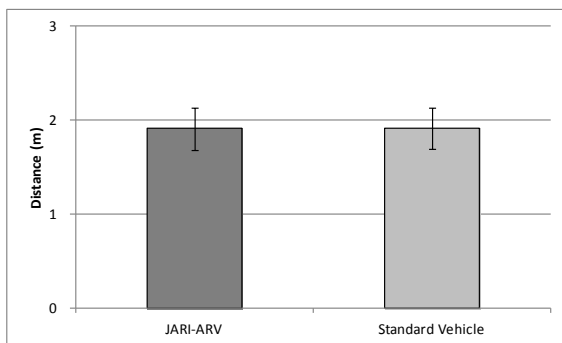Fig.11. Appearances of pedestrian standing still (Left: JARI-ARV, Right: Standard Vehicle).
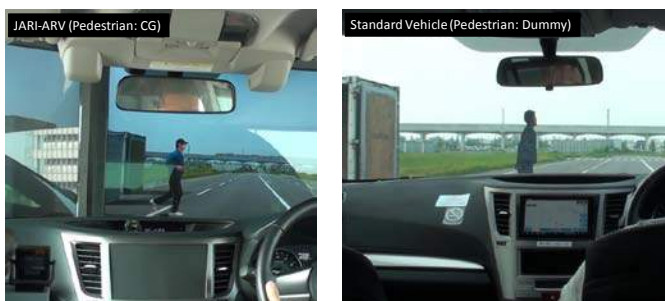

Fig. 12. Distance (for pedestrian standing still).

Fig. 13. Appearances of a pedestrian rushing out (Left: JARI-ARV, Right: Standard Vehicle).

Fig.14. Reaction time to a pedestrian appearing behind a visual obstruction.

5. CONCLUSIONS

Observing drivers' behaviours by reproducing traffic accidents and conflict situations is important for developing advanced driver assistance systems (ADAS). The JARI-ARV was developed to reproduce realistic traffic accident and conflict scenarios without putting the driver at risk of an actual collision. The main objective was to validate applicability of the JARI-ARV for this purpose.

We compared the JARI-ARV with a same model vehicle without alterations for the vehicle controllability and reaction performance to other traffic participants. Results of the experiment indicated that drivers tend to react to virtual traffic participants, in the same way as driving a normal vehicle. Applicability of the JARI-ARV for human factor research was confirmed.

REFERENCES

Kiefer, R., LeBlanc, D., Palmer, M., Salinger, J., Deering, R., & Shulman, M. (1999). Development and validation of functional definitions and evaluation procedures for collision warning/avoidance systems (DTNH22-95-H-07301). Washington DC: National Highway Traffic Safety Administration.

Reason, J. T., & Brand, J. J. (1975). Motion sickness. London: Academic.

Rolland, J.P. & Fuchs, H. (2000). Optical Versus Video See-Through Head-Mounted Displays in Medical Visualization. Presence: Teleoperators and Virtual Environments, pp.287–309.

Pedestrian Collision Risk Indices Based on
Driving Behavior During Right Turns at Intersections

Motoki Shino*, Yuta Shimazu*, Takashi Tagawa ** and Minoru Kamata*

**The University of Tokyo, 5-1-5 Kashiwanoha, Kashiwa-shi, Chiba 2778563,
JAPAN (e-mail: motoki@k.u-tokyo.ac.jp).
** Japan Automobile Research Institute, 2530 Karima, Tsukuba, Ibaraki 3050822
JAPAN (e-mail: ttagawa@jari.or.jp)*

Abstract: According to traffic accident statistics, 4481 fatal traffic accidents were reported in Japan in 2011—an extremely large number. Of these accidents, half occurred at intersections, and 40% of those were person-to-vehicle accidents, which typically result in high death rates. The causes of these accidents were judgment error, operation error, and particularly oversight, i.e., the driver not recognizing a pedestrian within a sufficient stopping distance. In this paper, pedestrian collision risk indices are proposed for use in identifying driving behavior that leads to collisions with pedestrians during right turns at intersections. These indices are based on the formulation of a strategy for passing through an intersection. The validity of the index was assessed using the Japan Automobile Research Institute's Augmented Reality Vehicle (JARI-ARV).

Keywords: Driving behavior, Collision risk assessment, Intersection, Human Factor, Pedestrian

1. INTRODUCTION

In Japan, the number of traffic accidents occurring annually remains high. According to traffic accident statistics, 4481 fatal accidents were reported in 2011—an extremely large number. To reduce the number of traffic accidents that occur, studies on active safety technologies, including driver assistance systems, are being carried out. Such systems can prevent accidents by checking for unsafe driving behavior by drivers. Of the 4481 accidents mentioned, half occurred at intersections, and 40% of those were person-to-vehicle accidents, which typically result in high death rates (ITARDA, 2011). The causes of these accidents were judgment error, operation error, and oversight, i.e., the driver not recognizing a pedestrian within a sufficient stopping distance. A large percentage of traffic accidents are characterized by driver oversight (Takubo, 2005). We hypothesized that this problem might be addressed by better detection of the potential for oversight and development of measures to assist drivers by informing them of the presence of pedestrians in intersections. Drivers vary their confirmation behavior and steering wheel and pedal operations based on the road environment and driving circumstances. Based on a driver's judgment process, the driver selects his or her driving behavior based on the road environment, so it is important to consider this judgment process (Shino et al., 2013, 2014). In this light, it is important to consider the road environment as well as driving behavior to prevent potential oversight of pedestrians while passing through an intersection. The purpose of this study was to develop risk indices based on driving behavior that leads to collisions with pedestrians while passing through intersections.

Figure 1 shows a schematic diagram of collision risk discrimination based on a driver's judgment process in a given traffic environment. A driving behavior database has been developed that contains not only driving behavior data but also road environment data. We used this database to identify driving behavior indices that relate the collision risk to the presence of pedestrians in specific traffic environments. The threshold value of such an index, the output, is determined by the relation between the index and the pedestrian collision risk assessment, for which the road environment is the input. The pedestrian collision risk assessment is performed by comparing the threshold value of the index to the measured value, based on the driving behavior. To apply this discrimination method, we first needed to identify driving behavior indices that were related to the collision risk while passing through an intersection. We evaluated the scenario of making a right turn while passing through an intersection because a great many vehicle–pedestrian accidents occur in Japan in this scenario.
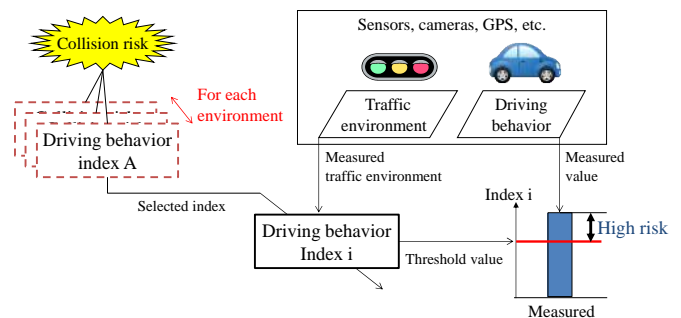

Fig. 1. Conceptual diagram of collision risk discrimination.

2. TRAFFIC ENVIRONMENTAL ELEMENTS AFFECTING DRIVING BEHAVIOR IN RIGHT TURNS

In general, driving is an adaptive behavior; the driver adapts his or her behavior to the traffic environment. The traffic environment in the vicinity of an intersection can be characterized in terms of object traffic (such as that of vehicles, bicycles and pedestrians), the road characteristics (such as the road width and the number of lanes), and traffic control characteristics (such as traffic signals and poles) (Nagayama, 1975). The driver adapts his or her driving behavior to the traffic circumstances by changing the velocity of his or her own vehicle (the host vehicle). Based on an analysis of traffic environment factors that influence vehicle velocity changes during right turns at intersections, as shown in Fig. 2, the presence of a crossing vehicle observed while passing the stop line and the presence of an oncoming vehicle and a proceeding vehicle while passing the center line were identified as influence factors, as shown in Fig. 3.
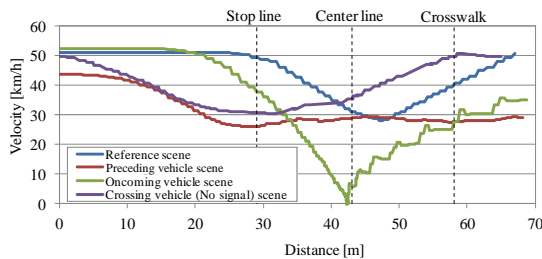

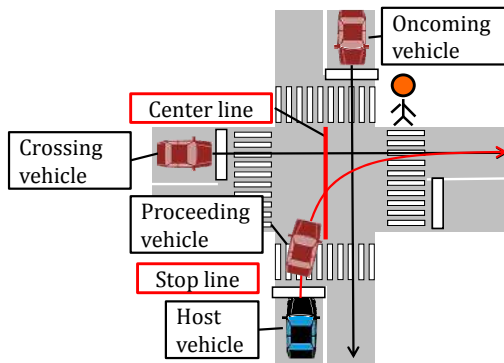Fig. 2. Change in velocity in each traffic environment.

Fig. 3. Traffic environmental elements selected as influence factors while turning right.

3. HYPOTHESIS OF PEDESTRIAN COLLISION RISK ASSESSMENT DURING RIGHT TURNS AT INTERSECTIONS

3.1 Driving Behavior Analysis with Near-miss Incident Database

We sought to develop an index for driving behavior that leads to collisions with pedestrians by focusing on the driver's judgment process relative to the road environment. To this end, a driving behavior index that satisfies the following two conditions was developed for assessment of the risk of a collision with a pedestrian:

- The index must be related to the road environment

- The index must indicate the risk of collision with a pedestrian

To examine whether the index satisfied these conditions in actual driving situations, we used a drive recorder database, which contains records of approximately 80,000 near-miss events collected by JSAE(Society of Japan Automotive Engineers of Japan)(Nagai et al., 2006). Because it was verified that the rate of near-miss patterns is similar to that of accident patterns, this was considered a valid approach to understanding the factors associated with accidents. We analyzed 77 events characterized by the following conditions: the incident involved making a right turn at a signalized intersection, the incident-induced object was a pedestrian, and it was possible to determine the direction toward which the driver's face was turned, as shown in Fig. 4. We classified them into 10 patterns as shown in Table 1, based on the driving behavior and the traffic environment elements selected as influence factors, as explained in the previous section.
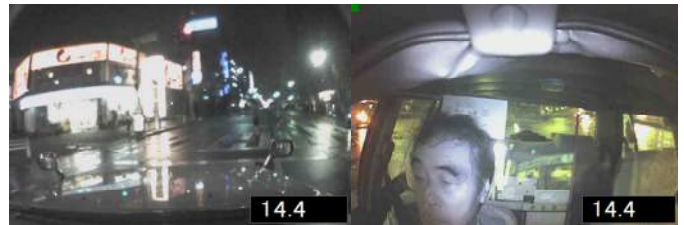
(a)   Front-view image   (b) Driver's face image
Fig. 4. Sample image data in the JSAE's near-miss database

Table 1. Classified patterns during right turns at intersections

Pattern	Environmental element	Driver's representative face direction	Host vehicle behavior
A1	Proceeding vehicle	Proceeding vehicle	Accelerating
A2	Proceeding vehicle (overtaken)	Blind spot behind leading vehicle	Low speed
B1	Oncoming vehicle (Going straight)	Traveling direction & oncoming direction	Accelerating
B2	Oncoming vehicle (Turning left)	Oncoming vehicle (Turning left)	Accelerating
B3	Oncoming vehicle (Turning right)	Oncoming direction	Accelerating
C1	Rare obstacle	Blind spot behind obstacle	Low speed
D1	—	Traveling direction	Accelerating or high speed
D2	—	Both side of crosswalk	Accelerating or high speed
E1	—	Other pedestrian	Very low speed
E2	—	Both side of crosswalk	Decelerating or very low speed
Others	Incidents caused by pedestrian's unexpected behavior		

In this study, we extracted the following three patterns based on the driver's visual search behavior, as estimated from the face direction and the traffic environment elements.

Pattern A1 (Fig. 5(a)): the driver recognizes a pedestrian who has crossed behind the preceding vehicle while the driver is approaching the crosswalk and following the proceeding vehicle.

Pattern B1 (Fig. 5(b)): the driver recognizes a pedestrian who starts crossing in the crosswalk while the host vehicle waits for an oncoming vehicle to pass through the intersection.

Pattern D (Fig. 5(c)): the driver seems to gaze in the traveling direction (D1) and increase the traveling velocity (D2) while turning right at an intersection, without a proceeding vehicle or oncoming vehicle being present.

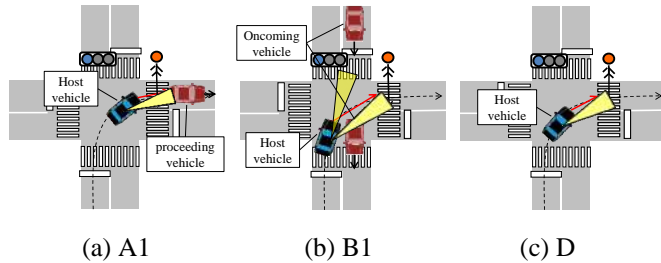
(a) A1   (b) B1   (c) D

Fig. 5. Typical patterns while turning right

Patterns A1, B1, and D were found to occur at the highest frequencies as shown in Table 1. In addition, most of these incidents occurred at pedestrian crossings while a vehicle was turning right at an intersection. With regard to the behavior pattern in which the driver looks away from the front, there is a practical system that has been developed to detect signs of oversight based on the driver's face direction (DENSO, 2013). One study has proposed a detection method based on the driver's operations in addition to the face direction (Horiguchi et al., 2007). However, for patterns A1, B1, and D, there has been little research conducted and there have been few systems developed to detect the risk of collision with a pedestrian.

3.2 Pedestrian Collision Risk Assessment

For the purpose of pedestrian collision risk assessment, we evaluated driving behavior with respect to traffic environmental elements during right turns at intersections. In this study, we focused on patterns A1, B1, and D, which enabled us to verify our hypothesis. Here, we will explain the driving behavior of pattern A1 and D as an example of the results obtained.

Driving behavior of pattern A1

The traffic environment element analysis results showed that this pattern, in which the host vehicle followed a proceeding vehicle, had a high frequency of occurrence when the proceeding vehicle accelerated after waiting for an oncoming vehicle. As a representative example, the driving behavior while turning right is shown in Fig. 6. While turning right, the driver gazes at the front of the preceding vehicle before crossing the stop line. After crossing the stop line, the driver gazes in turn at the opposite lane for an oncoming vehicle. The driver presses on the brake pedal at the same time as he/she recognizes that a pedestrian is present.

The time headway between the host vehicle and the proceeding vehicle is small, approximately 1.5 seconds, as shown in Fig. 7(a). The blind spot that the proceeding vehicle

generates grows as the time headway becomes smaller, which means that the time available to view the left side of the crosswalk occurs later as shown in Fig. 8.

This driving behavior is considered a factor in increasing the pedestrian collision risk during a right turn at an intersection. The face duration rates (the percentage of time that the driver's face is turned in a particular direction) with respect to elements of the traffic environment during visual search behavior while turning right are shown in Fig. 7(b). While turning right, the face duration rate for the proceeding vehicle rather than the crosswalk increases. This visual search behavior is considered a factor in increasing the pedestrian collision risk.

Based on the results of the examination of the near-miss database for instances of pattern A1, a hypothesis was formed that the time headway and the visual search behavior with respect to the proceeding vehicle are the best driving behavior indices for pedestrian collision risk assessment during right turns at intersections.

Fig. 6. Driver's face direction and vehicle velocity while turning right at an intersection (pattern A1)

(a) Distribution of THW   (b) Allocation of face direction

Fig. 7. Driving behavior analysis results for pattern A1

(a) Long THW   (b) Shorter THW

Fig. 8. Blind area behind preceding vehicle

Driving behavior for pattern D

The results of the traffic environment element analysis showed that this pattern, in which the host vehicle turns right in the absence of a proceeding vehicle and an oncoming vehicle at the intersection, as shown in Fig.5(c). Representative examples of patterns D1 and D2, which are driving behaviors while turning right, are shown in Fig. 9 (a) and (b). In the case of pattern D1, while turning right after crossing the stop line, the driver gazes at the opposite lane for any oncoming vehicles and then in the traveling direction, in spite of velocity being low. On the other hand, in the case of pattern D2, the driver tends to have a higher velocity (of more than 30 km/h) when passing the center line at the intersection while turning right. On the basis of the results of an analysis of the near-miss database for patterns D1 and D2, one can hypothesize that the face duration rates with respect to the elements of the traffic environment during a visual search while turning right are the ones shown in Fig.10(a). While turning right, the face duration rate for the traveling direction is higher than that for crosswalk. Moreover, the velocity of the host vehicle when it passes the center line at the intersection is high and more than 20km/h, as shown in Fig.10(b).

Based on the results of an analysis of the near-miss database for instances of patterns D1 and D2, a hypothesis was formed that the velocity of the host vehicle and a visual search along the travelling direction are the driving behavior indices for pedestrian collision risk assessment during right turns at intersections.
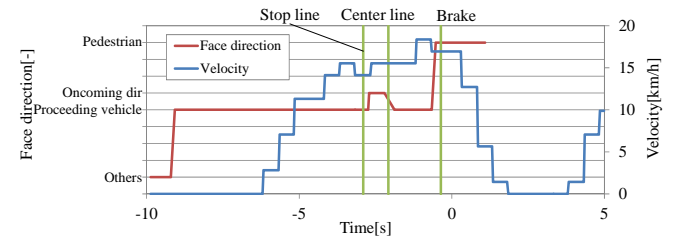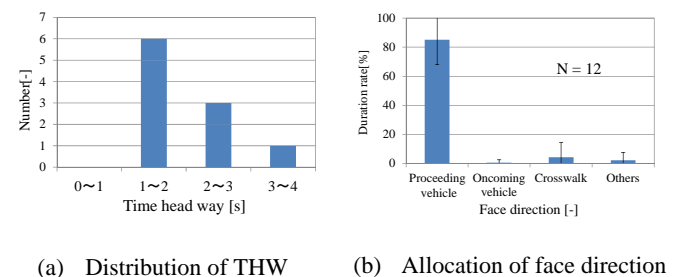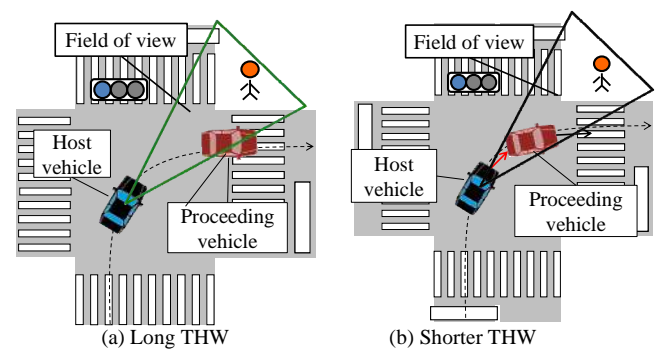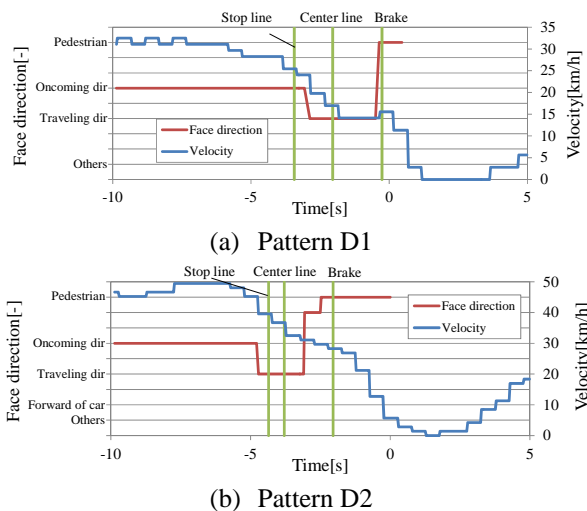

(a) Pattern D1

(b) Pattern D2

Fig. 9. Direction of the driver's face and vehicle velocity while turning right at an intersection (pattern D).

(a) Allocation of face direction

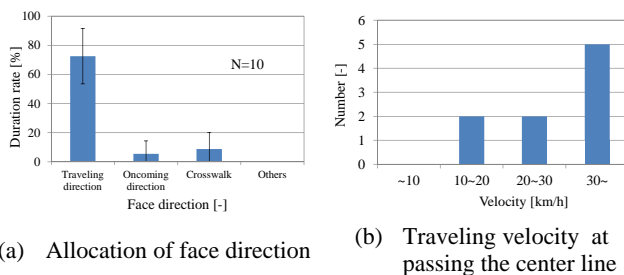(b) Traveling velocity at passing the center line

Fig. 10. Results of driving behavior analysis for pattern D.

4. VALIDATION OF DRIVING BEHAVIOR INDEX FOR COLLISION RISK ASSESSMENT FOR A PEDESTRIAN

4.1 Experimental Objective

The hypothesis concerning driving behavior indices in pattern A1 and D were developed based on a review of the near-miss incident database. However, in databases containing driving behavior data for various individuals, there is always noise of some variety. Therefore, we examined the validity of the driving behavior indices in each pattern A1 and D for pedestrian collision risk assessment on a test course.

4.2 Experimental Conditions and Method

The time to collision (*TTC*) during which the driver can avoid a collision with a pedestrian was defined as the reference measure for this type of traffic accident. To verify the effectiveness of the driving behavior index, we examined the relation between the *TTC* with a pedestrian and the index without a pedestrian during right turns at intersections. Each test consisted of one practical lap, three experimental laps without a pedestrian collision risk scenario, and finally, one experimental lap with the scenario.

The subjects were 21 people aged 22 to 42 years who possessed driving licenses and drove on a daily basis. We refer to 13 people by ID (D–P) for subjects in pattern A1 and 8 people by ID (JDA-JDH) for subjects in patterns D. We explained the nature of the experiment to the subjects and obtained their informed consent. To ensure a controlled environment, we used a test course. Because the near-miss database featured many cases of pedestrians crossing while a vehicle was turning right, the experimental course included two right turns at the target intersection, with two lanes on each side, as shown in Fig. 11.
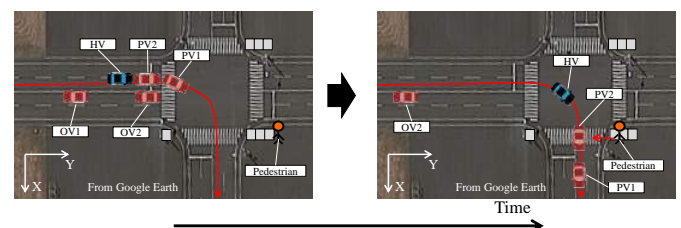
Fig. 11. Experimental scenario for pattern A1 while tuning right at an intersection (HV: Host Vehicle, PV: Proceeding Vehicle, OV: Oncoming Vehicle).

To reproduce conflict scenarios without putting actual pedestrians at risk, we used the JARI-ARV (Augmented Reality Vehicle) (Tagawa et al., 2014). To reproduce a critical scenario, computer graphics (CG) were superimposed on top of real frontal images. Such CGs are adapted from Augmented Reality (AR), and give the driver the impression that the pedestrians whose images shown are actually on the test field, as shown in Fig. 12.

(a) JARI-ARV

(b) Real frontal pedestrian image with AR technology

Fig. 12. Instrumented vehicle with AR used for driver performance evaluation

4.3 Results for Pattern A1 Based on Driving Behavior with JARI-ARV

To confirm the risk of a traffic accident with a pedestrian in pattern A1, we evaluated the *TTC* with a pedestrian based on the deceleration timing of each driver. We confirmed that three subjects collided with a pedestrian and three subjects performed sudden braking behavior during a near-miss event as shown in Fig.13.
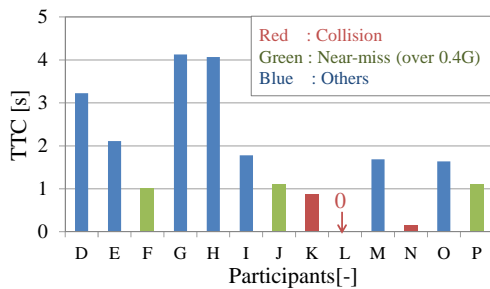

Fig. 13. *TTC* with a pedestrian for deceleration timing each driver in pattern A1

Figure 14(a) shows results for the relationship between *TTC* with a pedestrian and THW for the proceeding vehicle without the collision risk scene. There is a significant correlation between the *TTC* and the *THW* for the proceeding vehicle. This finding suggest that drivers tend decrease the *TTC* as the *THW* for the proceeding vehicle decreases ($r = 0.78$, $p < 0.01$). On the other hand, Fig. 14(b) shows results for the relationship between *TTC* with a pedestrian and the gaze duration rate (*GDR*) for the proceeding vehicle without the collision risk scene. There is a significant correlation between the *TTC* and the *GDR* ($r = -0.81$, $p < 0.01$). This suggests that drivers tend to decrease the *TTC* as the *GDR* for the proceeding vehicle increases. From the results of the examination of driving behavior with JARI-ARV, we verified our hypothesis concerning the driving behavior indices for pattern A1 for pedestrian collision risk assessment derived from the results of the near-miss analysis.
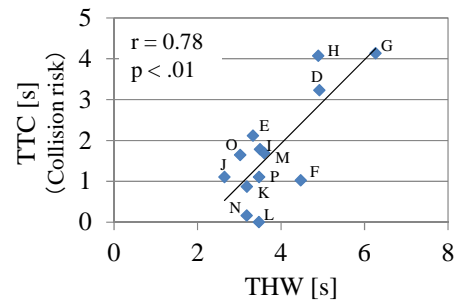
(a) *TTC* with a pedestrian vs. *THW* for a proceeding vehicle
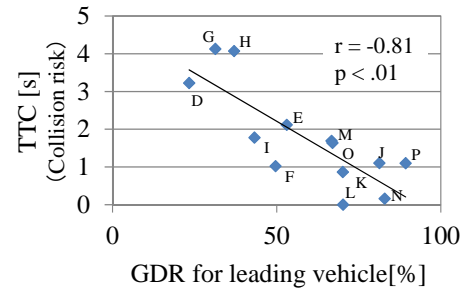
(b) *TTC with a pedestrian* vs. *GDR* for a proceeding vehicle

Fig. 14. Results of verification experiment for pattern A1

4.4 Results for Pattern D Based on Driving Behavior as Determined Using JARI-ARV

To confirm the risk for traffic accidents with pedestrians in the case of pattern D, we evaluated the *TTC* with a pedestrian based on the deceleration timing for each driver. Although we did not confirm whether each of the eight subjects collided with a pedestrian, some of the subjects braked suddenly during a near-miss event, as shown in Fig. 15
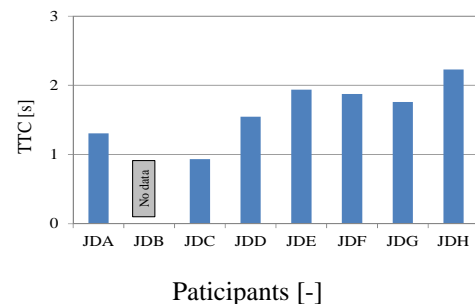
Fig. 15. *TTC* with a pedestrian based on the deceleration time of each driver for pattern D.

Figure 16(a) shows the relationship between the *TTC* with a pedestrian and the velocity at the center line. There is no significan correlation between the *TTC* and the velocity. On the other hand, Fig. 16(b) shows the relationship between the *TTC* with a pedestrian and the *GDR* for the traveling direction in the absence of collision risk. There is a significant correlation between the *TTC* and the *GDR* for the traveling direction ($r = -0.77$, $p < 0.01$). This suggests that the *TTC* decreases as the *GDR* for the traveling direction

increases. The results of the analysis of the driving behavior using JARI-ARV confirmed our hypothesis concerning the driving behavior index for pattern D for pedestrian collision risk assessment, as derived from the results of the near-miss analysis.
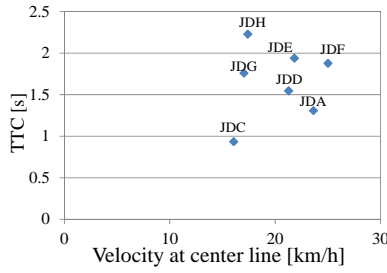
(a) *TTC* with a pedestrian vs. velocity at the center line at the intersection.
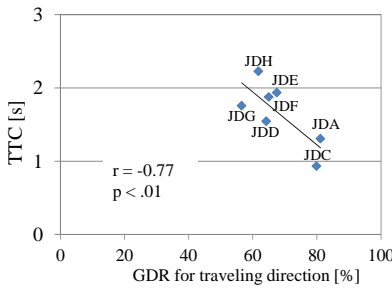
(b) *TTC* with a pedestrian vs. *GDR* for the traveling direction.

Fig.16. Results of the verification experiment for pattern D.

5. A PROPOSAL OF PEDESTRIAN COLLISION RISK ASSESSMENT BASED ON DRIVING BEHAVIOR DURING RIGHT TURNS AT INTERSECTIONS

5.1 Threshold Value for Pedestrian Collision Risk Assessment

To determine whether current driving behavior can predict the risk of pedestrian collision, the threshold value of an individual index needs to be determined with respect to the traffic environment. We set the threshold value based on the correlativity of the *TTC* with a pedestrian of each driver and the driving behavior index without a collision risk. If one sets the threshold, y_{th}, for the *TTC* such that the driver can avoid a collision with a pedestrian, the threshold, x_{th}, of the index can be calculated using the regression line of the relationship between the *TTC* and the indices with respect to the traffic environment.

$$x_{th} = \frac{1}{a}(y_{th} - b) \tag{1}$$

where *a* denotes the slope of the regression line and *b* is the intercept, as shown in Fig.17. Moreover, y_{th} is determined using the deceleration behavior dataset, which consists of the vehicle velocity, the deceleration, and the distance for deceleration when braking to avoid collision with a pedestrian.

$$y_{th} = TTC = \frac{V_0}{70.56 * D_{avg}} \tag{2}$$

where *Vo* denotes the vehicle velocity at the time of deceleration and D_{avg} denotes the average deceleration ratio during deceleration.
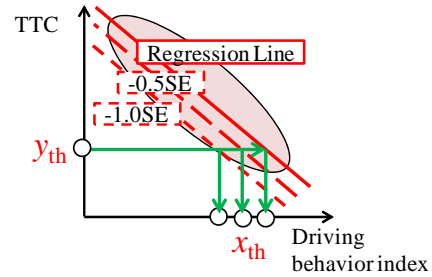
Fig.17. Inverse estimation considering a scatter of driving behavior

5.2 Possibility of Pedestrian Collision Risk Assessment Based on Driving Behavior Index

To determine whether it is possible to assess pedestrian collision risk based on the driving behavior index, we used the indices extracted in Section 4 in the case of the driving behavior for pattern A1. In particular, we examined whether the driving behavior indices during the 3rd experimental lap could be detected or not the collision with a pedestrian and the deceleration behavior of sudden braking for a pedestrian during the 4th experimental lap. The values of *Vo*, *a*, and *b* were determined using the dataset for pattern A1 and JARI-ARV on the basis of the driving behavior. D_{avg} was calculated and found to be 0.32G based on the dataset for sudden braking behavior in the case of a pedestrian [7]. Further, we determined the standard deviations for the three stages; these were found to be -0.0σ, -0.5 σ, and -1.0 σ for the threshold value for pedestrian collision risk when considering the scatter of the driving behavior.

We calculated a true detection ratio and a false detection ratio to confirm the viability of the proposed method by using the *THW* and *GDR* values for the proceeding vehicle as the driving behavior indices extracted in Section 4. The true detection ratio, R_t, and the false detection ratio, R_f, were defined using a Venn diagram as follows:

$$R_t = \frac{A}{A + B}, \quad R_f = \frac{C}{A + B + C + D} \tag{3}$$

The relationship between A, B, C, and D can be expressed as shown in Fig. 18

Fig. 18. Venn diagram showing the definition of the detection rate

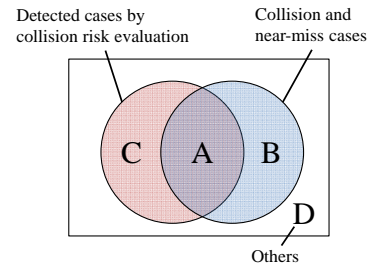Figure19 shows the discrimination results for pattern A1 based on the driving behavior, as determined using JARI-ARV. In this section, we compare the results obtained using R_t with *THW* and *GDR*, R_t with *THW* or *GDR*, R_t with only *THW*, and R_t with only *GDR* as the driving behavior indices for pattern A1. R_t increased in the case of the driving behavior where either *THW* or *GDR* was used as the index for the proceeding vehicle. This means that the proposed driving behavior indices such as the *THW* and the *GDR* for the proceeding vehicle can detect the pedestrian collision risk, which cannot be detected using either index alone. On the basis of the result shown in Fig. 19(d), it can be said that the proposed indices could detect the pedestrian collision risk at a true detection ratio of 83% and a false detection ratio of 8% for standard deviations of up to 0.5. It was confirmed that, when the proposed detection indices were used, the true detection ratio would be higher and the false detection ratio would be lower.

The proposed driving behavior indices confirmed the possibility of detecting the pedestrian risk scenarios during right turn at an intersection.
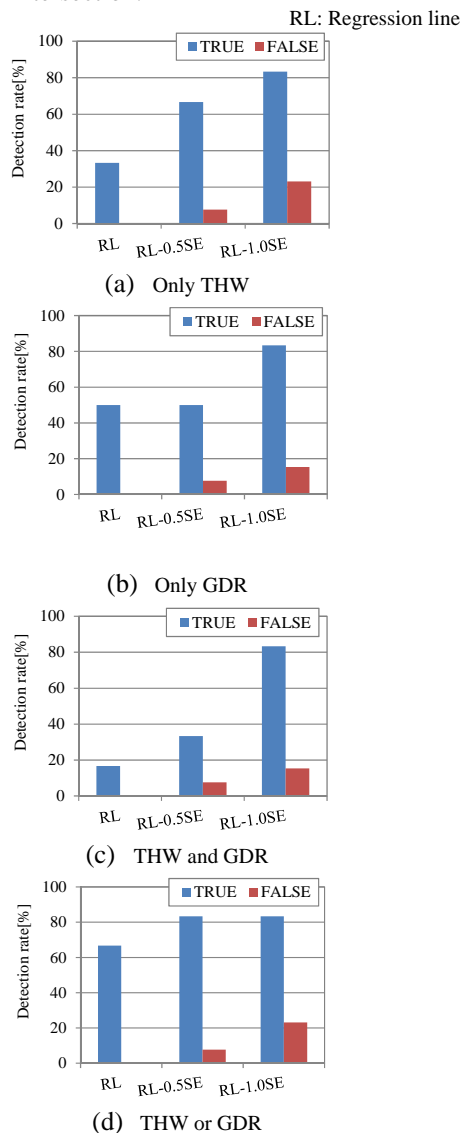

Fig.19. Discrimination result of collision risk detection

5. CONCLUSIONS

In this study, we examined driving behavior indices for pedestrian collision risk assessment during right turns at intersections and validated the indices using driving behavior examined with JARI-ARV. The major conclusions of this study are as follows:

- Based on an analysis of near-miss incidents, we extracted three patterns, identified as A1, B1, and D, for use in pedestrian collision risk assessment.

- The time headway and the duration rate of the gaze at the proceeding vehicle was proposed and validated as the indices for pattern A1.

- A gaze duration rate in the traveling direction was proposed as the index for pattern D and its suitability was confirmed.

- The proposed index for pattern A1 could detect pedestrian collision risk scenarios during right turn at an intersection.

REFERENCES

ITARDA. (2011). Annual statistics on traffic accidents (in Japanese). http://www.itarda.or.jp

Takubo, N. (2005). An analysis of traffic accident data for mental workload and human error by drivers (in Japanese). IATSS Review 30, 3, pp. 299-308.

Shino, M. et al. (2013). Formulation of Driver Judgement Process Around Curves For Deviated State Detection, 7th International Driving Symposium on Human Factors in Driver Assessment, Proceeding of USB.

Shino, M. et al. (2014). Driver State Detection Method Based on Naturalistic Driving Behavior during Approach to Intersection with ADAS, Proceedings of AVEC2014, CD-ROM.

Nagayama, Yasuhisa (1975). On Traffic Psychology, IATSS Review, Vol. 1, No. 2, pp. 325-335.

Nagai, Masao et al. (2006). Research on Incident Analysis Using Drive Recorder, Part2: Toward Active Safety Assessment, FISITA2006 World Automotive Congress, Proc. of CD-ROM

DENSO (2013). Driver states monitor (in Japanese). https://www.denso.co.jp/ja/aboutdenso/technology/product/electronics/safety2/commitment.html

Horiguchi, K. et al. (2007). Estimation of inattention in driving by using driver head pose and vehicle information (in Japanese). JSAE academic meeting papers (in Japanese), 110-07 (2007), pp. 1-6.

Tagawa, Takashiet et al. (2014). Reproducing Accident Situations Using Actual Vehicles: Developing test-vehicle adopted augmented reality and comparing driver behavior to that in a standard vehicle, Transaction of Society of Automotive Engineering of Japan, Vol.45，No.2, pp.419-424.

Driver Assistance System by Indicating Predicted Driving Evaluation Index at Rear-End of Preceding Vehicle

Takashi Nakano*. Yoshitaka Marumo**
Hironori Suzuki***

* Graduate School of Nihon University, Chiba, Japan
** College of Industrial Technology, Nihon University, 1-2-1 Izumi-cho, Narashino-shi, Chiba 275-8575, Japan
(e-mail: marumo.yoshitaka@nihon-u.ac.jp)
*** Faculty of Engineering, Nippon Institute of Technology, Saitama, Japan (e-mail: viola@nit.ac.jp)

Abstract: This study examines the driver assistance system to predict driving behavior considering information on the pre-preceding vehicle. The system indicates the predicted driving evaluation index at the rear-end of the preceding vehicle to avoid the driver's distraction. Driving simulator experiments are carried out with several participants who are instructed to follow a preceding and a visible pre-preceding vehicles with and without the driving assistance system. The participants with the assistance system could reduce the relative speed with the pre-preceding vehicle and acceleration of the following vehicle. These effects make it possible to suppress the variation of the collision risk to the preceding vehicle and to reduce fuel consumption of the following vehicle. In addition, the proposed assistance system shortened the drivers' reactions to the emergency deceleration of the preceding vehicle in comparison with the conventional assistance system, which is indicated at the onboard monitor in the following vehicle.

Keywords: Human factors, Driver behavior, Active safety, Pre-preceding vehicle, Following characteristics, Pedal operation

Topics: Cooperative Driver Assistance Systems, Cooperation between Drivers and Assistance Systems, Human Machine Interface.

1. INTRODUCTION

Driver assistance systems which encourage drivers to improve their driving behavior by indicating driving information to drivers have been developed and commercialized. Furthermore, ADAS (Advanced Driver Assistance Systems) such as AEBS (Autonomous Emergency Braking Systems) and ACC (Adaptive Cruise Control) spread out recently. A fuel economy meter and the indication of collision risk are well known as the fundamental measures for drivers to make an eco-friendly (Wada et al., 2011) and safe driving (Takada et al., 2012). In order to improve the fuel economy and the collision risk to the preceding vehicle, the driver should predict appropriate driving behavior such as the earlier deceleration by using the information on the ahead of the preceding vehicle. The predicted driving evaluation index which is referred to as the PRE3 (PREdiction by PRE-PREceding vehicle) was defined and proved that the driver assistance system which indicates the PRE3 in real time improved the driving behavior (Marumo et al., 2013). Further, numerical analysis using a traffic simulator showed the effect of installing PRE3-equipped vehicle on traffic flow is evaluated in terms of the efficiency, stability and safety (Suzuki et al., 2014).

The PRE3 was originally designed to be indicated through the monitor onboard the following vehicle. However, the onboard monitor may cause driver's distraction to be led to an unexpected accident. In addition, the following vehicle needs to have a special system to directly observe the vehicle ahead of the leading car. Recently, the assistance system which informs a driver of the emergency deceleration of the pre-preceding vehicle was developed (Nissan Motor Company). But, this assistance system used the special state-of-the-art technologies which directly measures the quantity of state of the pre-preceding vehicle.

This study proposed the system that the intermediate vehicle among three cars directly measures the relative speed with its forward and backward vehicles. The evaluation index PRE3 is then indicated at the rear-end of the intermediate vehicle. This study attempts to evaluate the effectiveness of the proposed assistance system through driving simulator experiments.

2. EVALUATION INDEX

A three-car platoon which consists of pre-preceding (1st), preceding (2nd) and the following (3rd) vehicles is assumed as illustrated in Fig. 1. Denoting i as the vehicle number, and v_i and $d_{i\,i+1}$ are defined as the velocity of the ith vehicle and the headway distance between the ith and $i+1^{th}$ vehicles.
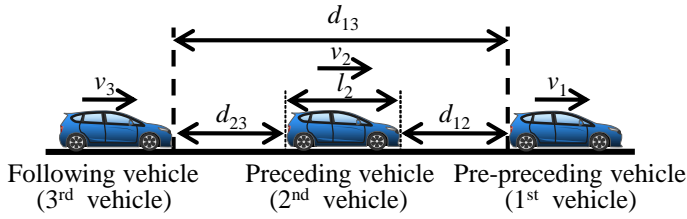
Fig. 1. Three-car platoon

One of the evaluation indices for the collision risk to the preceding vehicle (Kitajima et al., 2009) is the Risk Perception (RP) (Kondoh et al., 2008). The RP is defined as the weighted sum of the inverse of Time To Collision (TTC) and the inverse of the Time HeadWay (THW) as defined in Eq. (1). This index represents the driver's subjective risk to the preceding vehicle.

$$\text{RP} = \frac{a}{\text{THW}_{23}} + \frac{b}{\text{TTC}_{23}} = \frac{av_3}{d_{23}} + \frac{b(v_3 - v_2)}{d_{23}} \quad (1)$$

where THW_{23} is THW of the following vehicle to the preceding vehicle, and TTC_{23} is TTC of the following vehicle to the preceding vehicle. Coefficients a and b are equal to 1 and 5, respectively.

The predicted driving evaluation index PRE3, given in Eq. (2) is defined on the basis of the RP. The PRE3 considers not only the relationship (THW) between the preceding and following vehicles, but also the connection (TTC) between the pre-preceding and following vehicles. The coefficient b in Eq. (1) is twice because the TTC is applied to the pre-preceding vehicle.

$$\text{PRE3} = \frac{a}{\text{THW}_{23}} + \frac{2b}{\text{TTC}_{13}} = \frac{av_3}{d_{23}} + \frac{2b(v_3 - v_1)}{d_{13}} \quad (2)$$

where TTC_{13} is TTC of the following vehicle to the pre-preceding vehicle.

Fig. 2. PRE3 indication at the rear-end of preceding vehicle

Figure 2 shows the image of the PRE3 indication at the rear-end of the preceding vehicle. If the velocity of the following vehicle v_3 is slower than that of the pre-preceding vehicle v_1 or the following vehicle is away from the preceding vehicle (longer THW_{23}), the green arrow of the indicator scrolls upward. This is supposed to encourage the driver to accelerate to increase the PRE3 value. On the other hand, if the velocity of the following vehicle v_3 is faster than that of the pre-preceding vehicle v_1 or the following vehicle is close to the preceding vehicle (shorter THW_{23}), the red arrow of the indicator scrolls downward, and the driver should

decelerate to decrease the PRE3 value. If the driver performs the appropriate driving behavior, the indicator maintains the fixed grey arrow. The scroll speed of the arrow depends on the required operation.

3. EFFECTIVENESS OF ASSISTANCE SYSTEM

3.1 Experimental method

Experiment with a fixed-base driving simulator are examined with several participants who are instructed to follow the preceding vehicle and the visible pre-preceding vehicle as shown in Fig. 3. This experiment is evaluate the effectiveness when indicating PRE3 at the rear-end of the preceding vehicle. The participants are required to drive a car with and without the proposed assistance system.

The velocity of the pre-preceding vehicle is assumed as shown in Fig. 4. The pre-preceding vehicle repeats the acceleration and deceleration with 1m/s^2 and travels between 10m/s (36km/h) and 15m/s (54km/h). The driving course is a straight corridor. The pre-preceding vehicle is a tall minivan and the preceding vehicle is placed at the left side on the road to make the driver recognize the pre-preceding vehicle easily even without the assistance system.

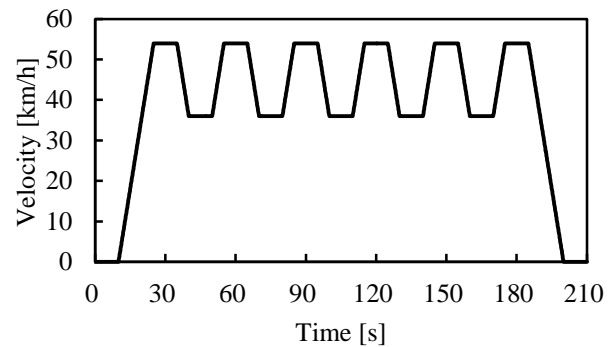Fig. 3. Overview of fixed-base driving simulator

Fig. 4. Velocity of pre-preceding vehicle

Eight males (Participant A through H) participated in the simulator experiments. All the participants gave their written informed consent before the experiments. The test drive was conducted to familiarize themselves with the simulator driving and the behavior of the PRE3 indicator. The

participants are to experience the trials with PRE3 assistance before the experiments without the assistant. These two driving conditions, i.e. with and without the assistance system, were repeated twice to make all four trials for each participant.

The participants were instructed to follow the rules and regulations below; "Look at the pre-preceding vehicle behavior carefully and predict appropriate driving behavior by the earlier acceleration and deceleration". "Drive the car so as to maintain the indicator arrow stay in the grey color". "In the trial without the assistance system, the driver refers to the driving behavior with the assistance system".

3.2 Experimental results

The time period used for the evaluation is between the 2nd and the last steady speed states of the first vehicle where all three-car platoon has a steady car-following.

3.2.1 Driving behavior of following vehicle

Figure 5 illustrates an example of the following vehicle with and without the assistance system (1st trial by Participant A). The solid line indicates the following vehicle velocity with the assistance system and the dashed line is without the assistance system. The assistance system prevents the delay of speed variation of the pre-preceding vehicle and reduces the relative velocity to the pre-preceding vehicle. This effect contributes the suppression of unnecessary acceleration.

The RMS of the relative velocity to the pre-preceding vehicle is depicted in Fig. 6. This figure shows the average of 16 trials (total of the two conditions for the eight participants). The assistance system reduces the RMS of the relative velocity to the pre-preceding vehicle with a significant difference under the 1% confidential level. This means that the assistance system makes the driver recognize the velocity change of the pre-preceding vehicle and prevents the unnecessary acceleration and deceleration.
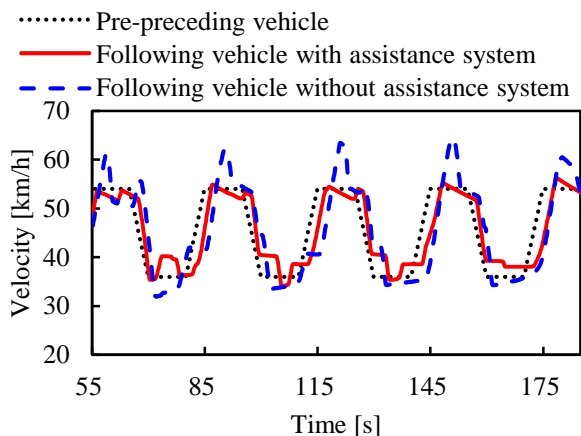
Fig. 5. Velocity with/without the assistance system (1st trial by Participant A)
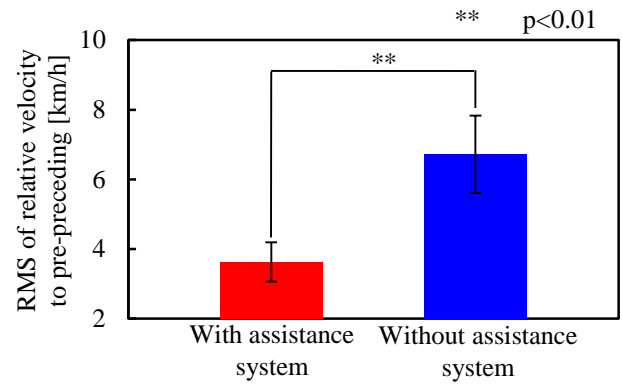
Fig. 6. RMS of relative velocity to pre-preceding vehicle (16 trials)

An example of the following vehicle acceleration (1st trial by Participant A) is shown in Fig. 7. The legend is same as the previous figure 5. The acceleration of the following vehicle are suppressed by the assistance system.

Figure 8 shows the RMS of the following vehicle acceleration, averaged by 16 trials. The assistance system could reduce the variation of acceleration with a significant difference under the 1% confidential level.
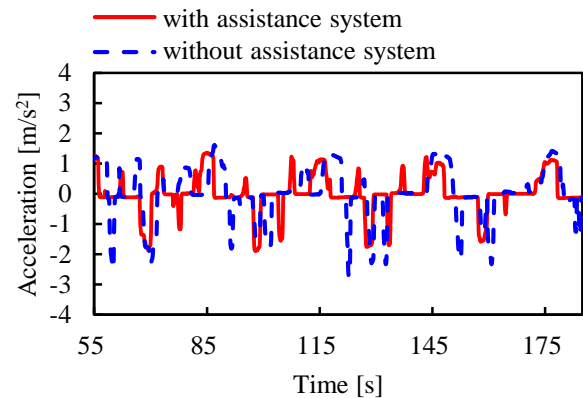
Fig. 7. Acceleration of following vehicle (1st trial by Participant A)
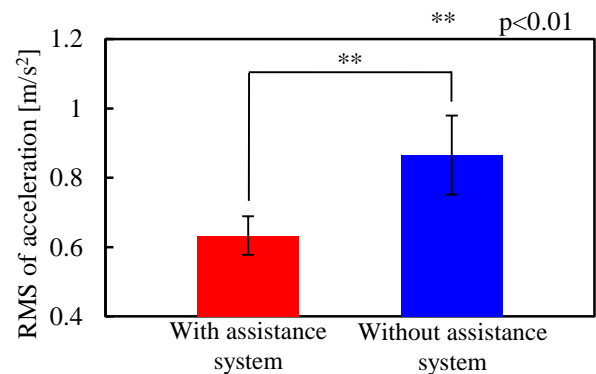
Fig. 8. RMS of acceleration (16 trials)

3.2.2 Effect of safety

Figure 9 illustrates an example of the RP (1st trial by Participant A). The legend is same as the previous Fig. 5. The variance of RP is also reduced by the assistance system. The driver with and without the assistance system maintains the RP around 0.5s^{-1}. Therefore, no significant difference is found in the mean of RP with and without the assistance.

Thought the mean of the RP with and without the assistance system has no significant difference, its standard deviation shows the large variation as depicted in Fig. 10. This figure shows the average of 16 running results. The assistance system also suppresses the standard deviation of the RP with a significant difference under the 1% level.
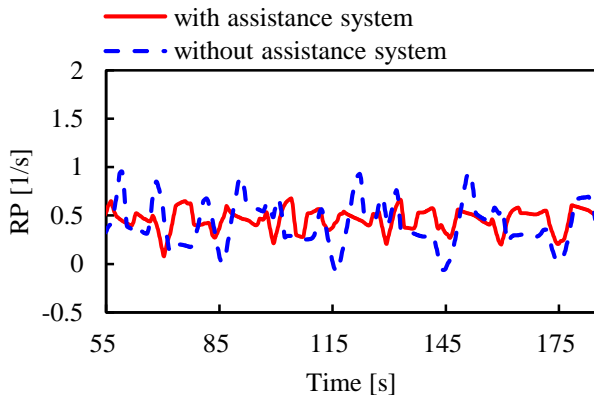
Fig. 9. RP to the preceding vehicle (1st trial by Participant A)
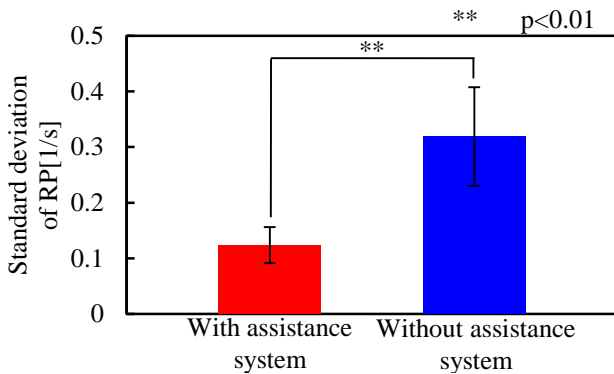
Fig. 10. Standard deviation of RP (16 trials)

These effects can be seen in the minimum value of the TTC to the preceding vehicle as shown in Figure 11. The assistance system increases the minimum value with a significant difference under the 1% level and suppresses the collision risk to the preceding vehicle.
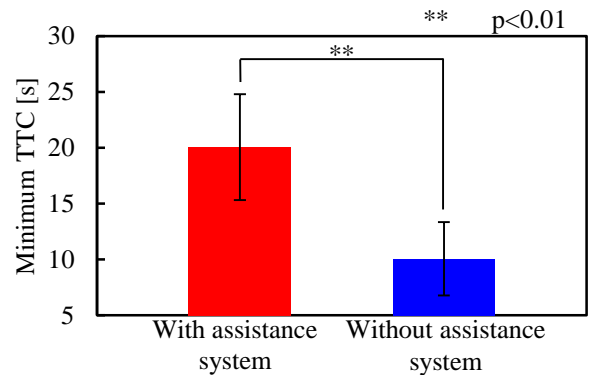
Fig. 11. Minimum TTC to the preceding vehicle (16 trials)

3.2.3 Fuel consumption

The fuel consumption is also calculated based on the fuel consumption rate map in the software (Mechanical Simulation Corporation, 2012) as shown in Fig. 12. The output of the engine this study uses is 150kW, and the density of the gasoline is 0.77kg/l. Figure 13 illustrates the fuel consumption of the following vehicle. This figure averaged by 16 trials. The assistance system improves the fuel consumption with a significant difference under the 1% level.

The proposed assistance system improves not only safety to the preceding vehicle, but also fuel consumption of the following vehicle.
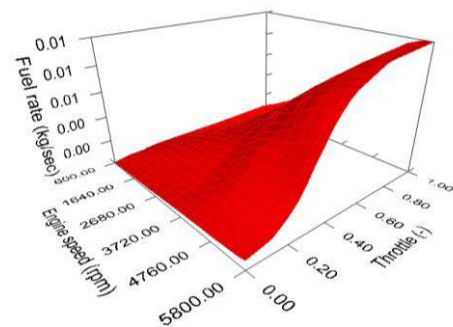
Fig. 12. Fuel consumption rate map (Mechanical Simulation Corporation, 2012)
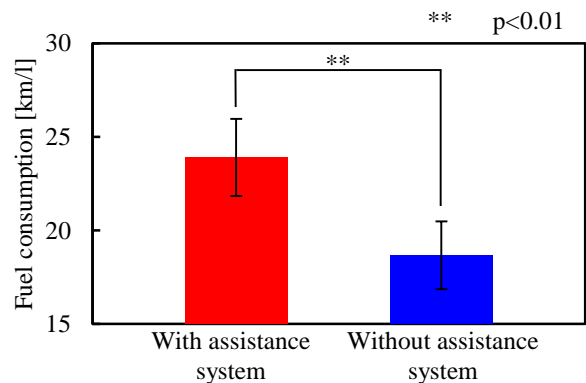
Fig. 13. Fuel consumption (16 trials)

4. COMPARISON OF THE INDICATING METHOD

4.1 Experimental method

Experiment with a fixed-base driving simulator are examined with several participants who are instructed to follow the preceding vehicle and the visible pre-preceding vehicle (Same as Fig. 2). This experimental purpose is to consider the proposed assistance system reduces drivers' reaction time to the emergency deceleration of the preceding vehicle compared with the conventional assistance system, in which PRE3 is indicated at the onboard monitor of the following vehicle. The participants are required to drive a car proposed assistance system (Same as Fig. 2) and conventional assistance system.

Figure 14 illustrates the image of the PRE3 indicator displayed in the following vehicle (conventional assistance system). If the velocity of the following vehicle v_3 is slower than that of the pre-preceding vehicle v_1 or the following vehicle is away from the preceding vehicle (longer THW_{23}), the green bar of the indicator is extended downward. This is supposed to encourage the driver to accelerate to increase the PRE3 value. On the other hand, if the red bar of the indicator is extended upward, the driver should decelerate to decrease the PRE3 value. If the driver performs the appropriate driving behavior, the bar remains grey.

Indicator in driver's view indicated at the onboard monitor of the following vehicle shown in Fig. 15. This study assumed as attached nearby an instrument panel such as a car navigation system. Therefore, onboard monitor located the screen lower right. The driving course is a straight corridor. The pre-preceding vehicle and the preceding vehicle condition is same as above experiment.
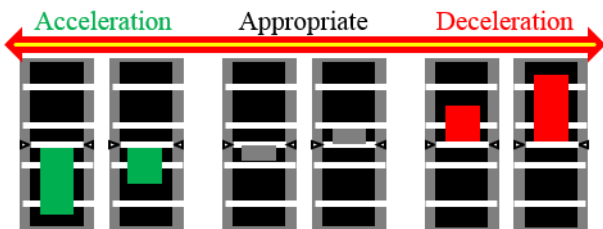
Fig. 14. PRE3 indicator displayed in the following vehicle

Fig. 15. Driver's view when indicated at the onboard monitor of the following vehicle

While two leading cars are traveling at 15m/s, only the preceding vehicle unexpectedly makes an emergency deceleration at 6m/s². This unpredictable deceleration is supposed to be some critical scenes such as a vehicle cut-in or a pedestrian jump in front of the car or an unexpected signal phase transition to amber.

Eight males (Participant A through H) participated in the simulator experiments (Same as section 3.1). All the participants gave their written informed consent before the experiments. The test drive was conducted to familiarize themselves with the simulator driving and the behavior of the PRE3 indicator. The participants are to experience the trials proposed assistance system before the experiments conventional assistance system. These two driving conditions were repeated twice to make all four trials for each participant.

The participants were instructed to follow the rules and regulations below; "Look at the pre-preceding vehicle and preceding vehicle behavior". "Drive the car so as to maintain the indicator arrow / bar stay in the grey color". "When the emergency deceleration, driver avoided the rear-end collision to the preceding vehicle only brake operation".

4.2 Experimental results

4.2.1 Driving behavior of following vehicle

Figure 16 illustrates an example of the following vehicle velocity when the preceding vehicle make an emergency deceleration (2nd trial by Participant A). The solid line indicates the following vehicle velocity when indicating at rear-end of preceding vehicle and the dashed line is following vehicle velocity when using the onboard indicator in the following vehicle. 0s in the horizontal axis means emergency deceleration timing of the preceding vehicle. The rear-end indicator is helpful to reduce the reaction time and to avoid the emergency deceleration much more than the onboard indicator.

Fig. 16. Comparison of velocity when the preceding vehicle made an emergency deceleration (2nd trial by Participant A)

Reaction time of brake pedal operation is depicted in Fig. 17. This figure shows the average of 16 trials (total of the two conditions for the eight participants). The drivers with the rear-end indicator initiates the brake pedal earlier than the onboard monitor system. The rear-end indicator system could reduce the reaction time of brake pedal operation with a significant difference under the 1% level.
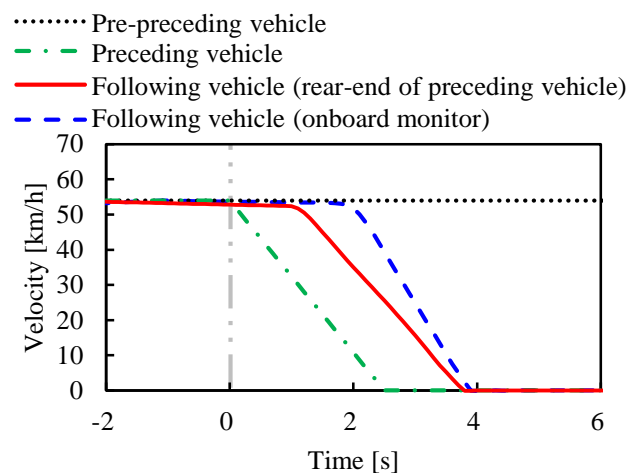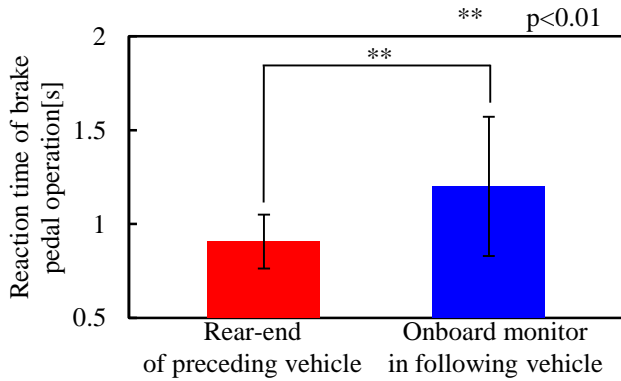

Fig. 17. Reaction time of brake pedal operation (16 trials)

4.2.2 Effect of safety

The maximum deceleration is depicted in Fig. 18. This figure shows the average of 16 running results. The rear-end indicator reduces the maximum deceleration with a significant difference under the 1% confidential level.

The minimum value of the TTC to the preceding vehicle as shown in Figure 17. This figure averaged by 16 trials. The rear-end indicator increases the minimum value with a significant difference under the 5% level and suppresses the collision risk to the preceding vehicle.
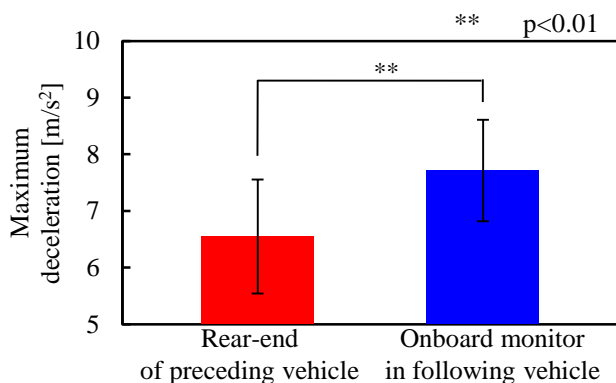
Fig. 18. Maximum deceleration (16 trials)
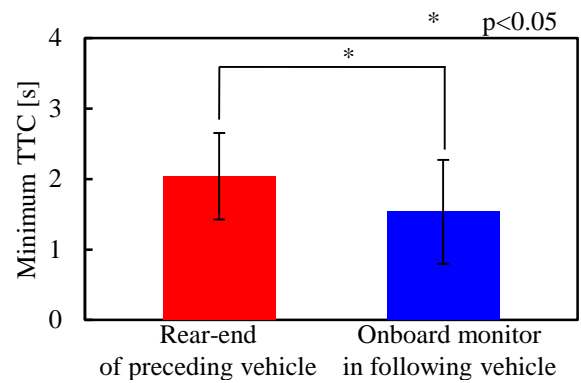
Fig. 19. Minimum TTC to the preceding vehicle (16 trials)

5. CONCLUSION

This study proposed the system that the intermediate vehicle among three cars directly measures the relative speed with its forward and backward vehicles. The evaluation index PRE3 is then indicated at the rear-end of the intermediate vehicle. This study attempts to evaluate the effectiveness of the proposed assistance system through driving simulator experiments.

The driving simulator experiments revealed that indicating the PRE3 reduces the unnecessary acceleration and deceleration to minimize the unexpected deterioration of traveling speed. The change of the RP is also suppressed, and the assistance system makes it possible to suppress the collision risk to the preceding vehicle. In addition, indicating the PRE3 also reduces the fuel consumption of the following vehicle.

In addition, the proposed assistance system reduces drivers' reaction time to the emergency deceleration of the preceding vehicle compared with the conventional assistance system, in which PRE3 is indicated at the onboard monitor of the following vehicle. Indicating PRE3 at rear-end of the preceding vehicle helps the driver to decelerate earlier and to avoid the high deceleration.

REFERENCES

Kitajima, S. et al. (2009). Comparison of Evaluation Indices concerning Estimation of Driver's Risk Perception -Risk perception of rear-end collision to a preceding vehicle-, *Review of Automotive Engineering*, 30(2), 191-198.

Kondoh, T. et al. (2008). Identification of visual cues and quantification of drivers' perception of proximity risk to the lead vehicle in car-following situations. *Journal of Mechanical Systems for Transportation and Logisics*, 1(2), 170-180.

Marumo, Y. et al. (2013). Assistance system to predict driving behavior considering information on pre-preceding vehicle. *Proceedings of the second international symposium on Future Active Safety Technology toward zero traffic accidents*, USB.

Mechanical Simulation Corporation, (2012). VehicleSim Browser Reference Manual Powertrain System, *CarSim 8.1.1 Driving Simulator*.

Nissan Motor Company. Predictive Forward Collision Warning. available at http://www.nissan-global.com/EN/TECHNOLOGY/OVERVIEW/predictiv e.html (accessed on 5 May, 2015).

Suzuki, H. et al. (2014). Driver assistance system to anticipate pre-preceding vehicle and its effect on traffic flow. *12th International Symposium on Advanced Vehicle Control (AVEC'14)*, 582-587.

Takada, S. et al. (2012). Effect of forward obstacles collision warning system based on deceleration for collision avoidance on driving behaviour. *Proceedings of 19th World Congress on Intelligent Transport Systems*, CD-ROM.

Wada, T. et al. (2011). Proposal of an eco-driving assist system adaptive to driver's skill. Proceedings of the IEEE International Conference on Intelligent Transportation Systems, 1880-1885.

Driver models based on lateral dynamics for adaptation of assistance systems

Proceedings of the 3rd International Symposium on Future Active Safety Technology Towards zero traffic accidents, 2015

Büyükyildiz, G.*, Pion, O.*
Henze, R.*, Küçükay, F.*

*Institute of Automotive Engineering, TU Braunschweig,
Germany (Tel: +49-531-391-2607; e-mail: g.bueyuekyildiz@tu-braunschweig.de).

Abstract: The continuous demand to increase the road safety induces that the driver in the vehicle development and research being taken increasingly in the focus. An important focus of research is to determine the driver's ability to respond to situations appropriately and thus to drive the vehicle safely in traffic.

At the Institute of Automotive Engineering (IAE) of the Technical University of Braunschweig, a driver model has been developed, which makes it possible to identify the specific driver characteristic in the form of an individual "fingerprint". By means of the knowledge of the "fingerprint" conclusions can be drawn on: the driving style, the driver's age/ driver control behaviour and the driver performance. Within the context of this paper, the relevant quantities are derived by means of a driver model that serves the adaptation of driver assistance systems. Furthermore, the existing correlations between the driver's performance and the driver control behaviour will be analysed as part of the driver's fingerprint. For this purpose, relevant vehicle and track camera signals are extracted from the CAN bus and used for the driver modelling. Genetic algorithm is used for the identification and optimization of the so-called "time-shifted driver model" control parameters. The brief presentation of a methodology used for calculating the individual driver condition parameter sets in real time on the test vehicle constitutes the conclusion of this article.

Keywords: Driver Monitoring, Driver State Detection, Driver Behaviour Modelling, Cooperation between Drivers and Assistance Systems.

1. INTRODUCTION

Both by the increasing traffic and by the objective to reduce traffic accidents, the driver moves nowadays in the vehicle development and research closer into the focus. An early study by Treat [7] shows with over 2250 accident records that the human factor and the driver have the largest contribution of accidents with 93%. The probability of an accident increases when the driving demands exceed the driver's performance capabilities [3]. "Looked-but-failed-to-See" [2] is also regarding accidents a frequent discussion phenomenon [9]. Thus, the ability to perceive and process information and therefore the driver's control behaviour seem to be affected. For this reason, there must be a connection between driver performance and driver control behaviour in this context (see the components of the "fingerprint" as shown in Fig. 1). Recent advanced driver assistance systems must consider therefore already in the application, this linkage between the performance of the driver and the driving requirements in order to assist the driver in terms of comfort and safety optimally. The ability of an adaptive adjustment of driver with such safety and comfort functions, depending on the current state of the driver (e.g. driver's performance or driving style) makes this assistance functions more interesting. An automatic adaptation enables fulfilling the needs and requests of the driver, so that a higher value and thus a higher acceptance can be achieved.

As an example one possible field of application in terms of longitudinal dynamics is to adapt the thresholds and intervention times of the Front Collision Warning (FCW) function according to the driver. Another example in terms of lateral dynamics could be to adapt the threshold and warning points of the Lane-Keeping Assist System (LKAS) with respect to the driver behaviour diversity for designing active safety functions. As a basis for such adaptation, the knowledge of the driver-specific fingerprint is required.
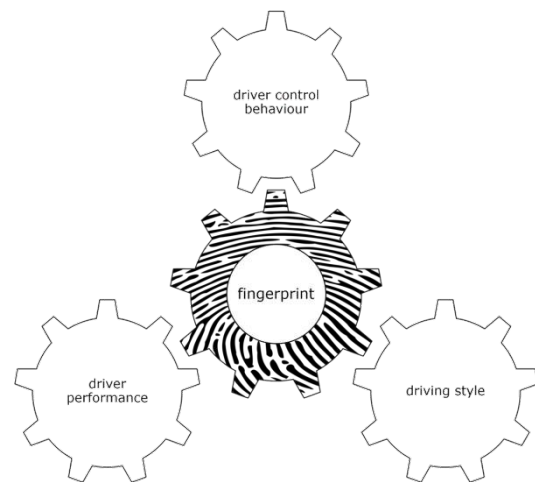
Fig. 1. Components of the fingerprint of the driver

In the literature driver models are used to investigate the drivers control activities to analyse his driving behaviour and to assess its adaptability to the vehicle and the driving task [5]. The driver models can be classified in longitudinal control and lateral control models. Whereas longitudinal control models consider the interaction of the pure driver-vehicle system or the interaction of the own vehicle with the leading vehicle, the focus of lateral control models highlights

the full interaction **d**river-**d**riven vehicle-**d**riving environs ("3d"). In the context of this paper a method is presented which identify the driver's characteristic control parameters using driver models within the frames of his fingerprint. In this case, possible relationships are examined with his performance. In order to figure out the mathematical description of the driver and illustration of his control behaviour by different means, the control system theory is used. To detect a significant change in the driver performance, long and monotonous drives are analysed. Therefore real data recordings from test vehicle on similar traffic conditions are used for modelling. This paper mainly focuses on the lateral-control of the driver, since an available fingerprint information signals exists as a result of the permanent lane keeping of the driver (also in case of reduced traffic volume, driving at constant speed etc.). The model input signals are pre-selected and outliers are corrected in order to improve the quality of the models. Moreover, in order to eliminate the effect of the dependence of the control parameter on the driving speed, a certain speed interval should be considered. Thus, in this paper the highway speed range is preferred for the selection. For that reason, very tight curves are not taken into account since the construction-based highway road conditions and physically constrains don't allow such curvatures.

Modern driver assistance systems regulate through algorithms, which are based on the profile of average drivers. The extracted control parameters using the described driver model for the driver's steering behaviour can be used for the adaptation of driver assistance systems.

2. MODELLING AND RESULTS

Based on a closed-loop model an application-specific model is developed as shown in Fig. 2, to consider the variation of the driver's control behaviour as a function of the driver's performance. In order to analyse the vehicle dynamics parameters, longitudinal and lateral accelerations a_x and a_y, the steering wheel angle δ_L, yaw rate ($\dot{\psi}$), the velocity (v) and

the lateral position of the vehicle in the lane Y and curvature (κ) from the track camera are required. Based on the curvature of the track camera the controlled portion of the steering angle is determined in the anticipation block and corresponds to the ideal driver, since no regulation is required. On the other hand, the anticipation is an inverse transfer function between the steering angle and the curvature. The reference trajectory $y_{reference}$ describes the target trajectory. The actual track $y_{current}$ is the prospective travelling trajectory, with an unchanged driver input, that is predicted through current vehicle states in case no further disturbances appear. Their difference is an input to the compensation block, which describes the feedback control of the steering angle.
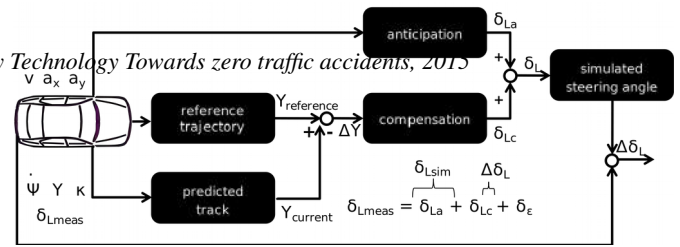

Fig. 2. *Time shifted driver model for lateral control*

The sum of the anticipation and the compensation is the total steering angle which is returned as input into the vehicle. The non-modelled difference between the measured steering angle δ_{Lmeas} and simulated by the model driver steering angle δ_{Lsim} is called the residual steering angle δ_ε. The factors influencing δ_ε, for example external disturbances such as lane grooves, side winds or road cambers.

At the Institute of Automotive Engineering various systematic series of test drives to identify the driver behaviour were carried out. For this purpose, within customer measurements extensive studies [4] have been carried out with over 1.5 million of measured kilometres with various vehicles in real traffic. In the context of this paper data driving scenarios addressed on well-developed national roads and motorways from this data recording. As a test vehicle, a BMW F11 for real-time parameterization for the fingerprint is used. The vehicle is equipped in addition to the standard sensors with additional measurement and visualization technologies. To parameterize the time shifted driver model genetic algorithm is used. This in biological evolution process is transferred as a principle to optimize the residual steering angle δ_ε.

Genetic algorithms are derived from the theory of evolution. Advantageous characteristics, i.e. better individuals, result from arbitrary variation of the natural selection. These characteristics are passed on to the next generation through mutation and genetic recombination. This principle from biological evolution is applied to optimisation of the objective function calculated by the minimum error between measured and simulated steering angle $min\left(\delta_{l,meas} - \left(\delta_a + \delta_c\right)\right)$.

Since these data were recorded in real traffic, a number of external disturbances affect the system, which cannot be physically represented. Control parameter identification without a model error is therefore not possible. Fig. 3 shows the comparison of the model error and the external disturbances of the steering angle. On the left side the model error -difference between the measured and simulated steering angle- is illustrated. The right side of the plot shows the steering angle, measured by holding the steering wheel tightly from the driver. The model error behaves as the same level as the external disturbances, which cannot be modelled easily.

The box plot on the right side of the figure shows the measured steering angle, as the driver was concentrated on a straight ahead driving, holding the wheel tightly against external disturbances. The model error has approximately the

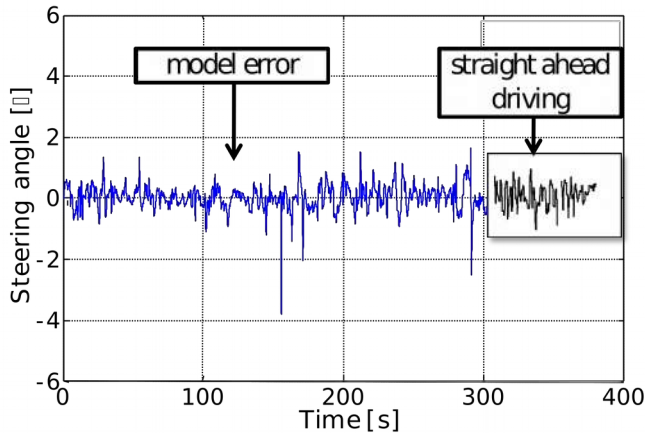same magnitude as the external disturbances, which cannot be modelled easily.

Fig. 3: Comparison of model error with external disturbances

The sensitivity analyses in advance have shown that four characteristic control parameters are sufficient for the driver parameterization. This includes the gain of the steering angle to lateral position V_R. A second parameter is the time constant T_K that represents the delays caused by the motor nerves and inertia of the neuromuscular system. The third parameter is the dead time τ or reaction time caused by the

excitation of the sensory organ, which describes the transmission of information in the sensory nerves and information processing in the central nervous system [6]. The prediction T_P considers as the fourth parameter, how foresighted the driver behaves, which is obtained from the prediction.

Fig. 4 visualizes the above mentioned driver identification parameters for each time segment (10 min each), with the aim to reach the minimum error between measured and simulated steering angle.
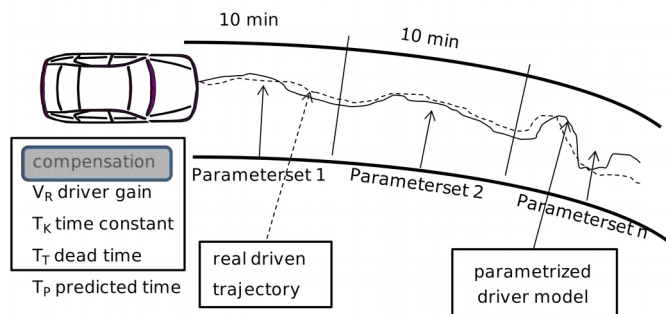
Fig. 4. *Identification of the control parameters*

Fig. 5 shows the cartesian representation of the driver gain and the predicted time for an exemplary driver. By certain preselections and outlier adjustments for input signals of the driver model, the modelling of the real driving data is improved. As the elapsed driving time increases, diameter of the plotted data points is then larger. With increasing travel time, the control parameters shift towards a shorter predicted time and higher driver gain.
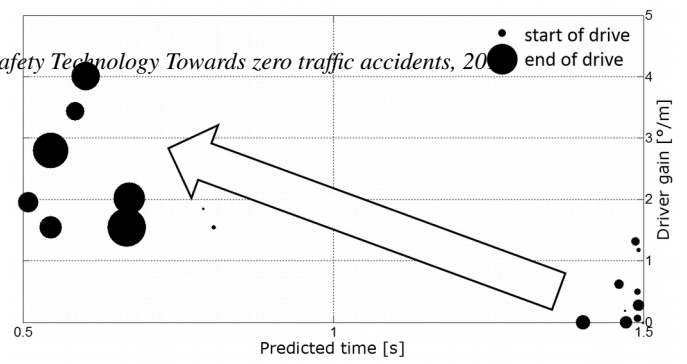
Fig. 5. *Cartesian representation of the driver gain and predicted time for an exemplary driver*

Analogous shifts of the control parameters to shorter predicted times and higher driver gains are observed among other drivers, but the difference in the predicted time is not always significant.

Fig. 6 shows another cartesian representation for a different test driver. The shift of the control parameters towards shorter prediction and higher driver gain can be also observed. However, it is not as obvious as for test driver before. At the start of the measurement, it is apparent, that the prediction time is less than the one for the test driver before. On the other hand, the control parameters are changing less amount during the measurement.
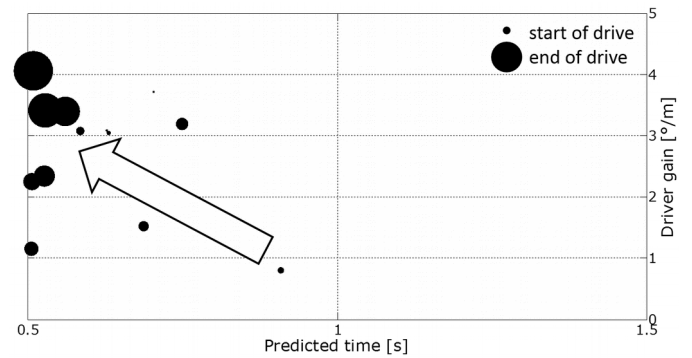
Fig. 6: *Cartesian representation of the driver gain and predicted time for a different exemplary driver*

There are test drivers, whose predicted time values remain almost constant with an increase of the driver gain. That means the change of the driver performance could only be observed by the parameter driver gain. The driver is going to compensate his fatigue only through regulating the parameter driver gain, without any need of being more foresighted. Once these individualities among the drivers can be clustered, a range of solutions can be created as patterns for the test vehicle. Due to depending on human characteristics, a driver specific driver model is implemented on the experimental vehicle at the first stage. With the same principle as in Fig. 2, the real time driver-specific parameterization on the experimental vehicle can be calculated using the driver input signals stated above. As a result, the current performance can be assigned to the driver to identify the fingerprint.

Implementation of the driver model into the fingerprint model

To identify the fingerprint, the driver is classified based on the individual driver behaviour. For this purpose, objective parameters are defined from longitudinal and lateral control behaviour, steering and lane keeping behaviour and usage of the active assistance systems, which are construct the basis for the adaptation of assistance systems [1].

In this section the fingerprint model is briefly presented to clarify advantages of the driver model. As Fig. 1 shows, the fingerprint model developed of three components. First sub-model aims to identify the driving style. To identify the driving style a "driving style identifier" will be used, which was developed. Basically, the driving style is defined as a natural and variable characteristic of the driver. The natural driving style might change suddenly, depending on the driving environment during the driving.

Fig. 7 shows the structure of "driving style identifier". The basis is the vehicle module (function block 1), including longitudinal and lateral acceleration and driving speed for classification. The usage of the friction circle or maximum use of the acceleration and deceleration potential are some examples for the criteria of the vehicle module to classify the driving style.
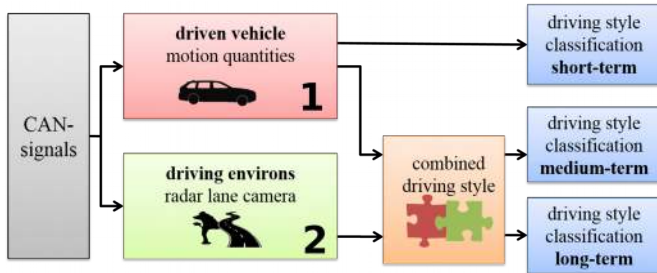
Fig. 7: Schematic illustration of the "driving style identificator"

However, the driving style, can be influenced by the driving environment (e.g. in urban traffic) in certain situations, which can be identified more precisely using the driving environment information (e.g. radar and/or camera data). In that case, a classification based on drive dynamics parameters is not sufficient. In addition to this, taking the driving environment information into account provides additional evaluable situations, so that the robustness of the detection is improved. In this context, the extension of the driving style identifier to an additional analysis and decision unit shown in function block 2 in Fig. 7. Relevant driving situations such as approach, follow-up, driving in a curve are used to classify the characteristics of the driver in terms of driving style. After the prioritization of the driving situations, the interaction of the driver with the driving environment (function block 2) and with the vehicle (function block 1) will be combined within a final classification. All related measured variables for the identification can be obtained by the vehicle CAN or Flexray.

Fig. 8 represents objective parameter examples of the time gap t_g for the driving situation "follow-up" after "approaching" a vehicle. Time gap t_g represents the time

required for the ego vehicle's front end to reach the current position of the rear of the leading vehicle in the front.
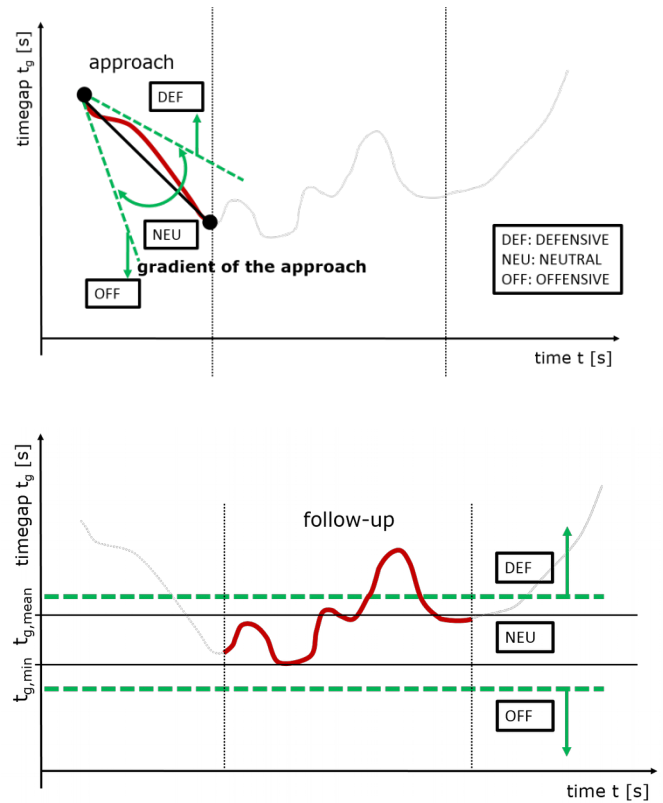
Fig. 8: Objective parameter examples of the time gap

The gradient of the time gap signal during approach and the absolute minimum $t_{g,min}$ and the average value of the signal $t_{g,mean}$ during follow-up represent the characteristics of the driver behaviour. In addition to the objective parameters related to the following behaviour mentioned above, objective parameters regarding lane keeping in curves can be also generated and used for classification. As an example offensive drivers tend to cut curves while defensive drivers rather follow the lane centre. According these objective parameters, it is possible to classify the driver with respect to the driving style.

Second sub model purposes to identify the driving performance. To identify the driving performance of the driver another sub model was also developed. Due to the focus on the driver models in this paper, the identification of the driving performance will not be handled at this point.

As the third and last sub model, the above mentioned driver model is used to identify the control behaviour and thus to complete the fingerprint of the driver.

Fig. 9 shows the test vehicle used for the fingerprint of the driver for a real-time experience. In addition to the standard sensors, the test vehicle is equipped with additional measurement and visualisation equipment.

Fig. 9: Experimental vehicle with measurement equipment

Finally, the fingerprint model is implemented into the test vehicle online (real time) and is being validated in various road test drivers. Buffers are used for signal processing and sequential evaluation. Fig. 10 illustrates the GUI for visualization of the final result. The benefit of the GUI is that the driver experiences the rating and classification in terms of his fingerprint in real time. The final classification result is provided as input to the associated safety and/or comfort functions for a possible adaptation of vehicle configuration and DAS (driving assistance system) functions.

Fig. 10: GUI of the fingerprint model for real-time experience

3. SUMMARY AND OUTLOOK

In this paper, the methodology used to generate the driver-specific fingerprint part (driver control behaviour) was presented. The objective of this contribution to identify the driver characteristic control parameter is carried out by means of an implemented driver model and using Genetic Algorithm. Based on four observed control parameters (driver gain V_R, time constant T_K, dead time τ and prediction

T_P) the driver was characterized within the driver-driven vehicle-driving environs control loop. Overall, it appears that for all drivers a change in the control parameters over the travel time exists. However, this shift or change in control behaviour possesses a very driver-specific characteristic, which can be distinguished by additional fingerprint information (e.g. driving style). The reliable knowledge of the driver control characteristic offers a great potential in the

adaptation of safety and comfort functions of assistance systems. It should be noted that the influence of traffic situations and weather conditions (driving environment) to the driver's control behaviour progressively to offer opportunities for improvement. The integration or fusion of diverse environment information from different sources could increase the classification quality. Another aspect is to take the driving environment related velocity dependence of the control parameters and the "risk homeostasis" effect [8] of adaptive systems into account. To test the adaptive assistance functions further and to ensure a wider range of driver types, extensive validation runs and acceptance studies are conducted. For this purpose, the presented driver model is implemented in the test vehicle and the solution spaces of the driver states are stored in the model for comparison. The usage of adaptive control approaches with MRAC ("model-reference adaptive control") and fuzzy controller for real-time parameterization of the driver is one of the other frameworks, which may play a role in the field of "autonomous driving", a theme with increasing importance. The matter of "how should the passengers be transported for their best satisfaction in case of autonomous driving?" probably concerns the information delivery by fingerprint sub models.

REFERENCES

[1] Bergholz, J., Pion, O., Küçükay,: Fingerprint des Fahrers zur Adaption von Assistenzsystemen. In 26. VDI/VW-Gemeinschaftstagung "Fahrerassistenz und Integrierte Sicherheit" (VDI-Berichte 2104). Düsseldorf: VDI-Verlag. 6-7 Oktober 2010, Wolfsburg

[2] Brown, I. D.: Review of the 'Looked-but-Failed-to-See' Accident Causation Factor. Road Safety Research Report No. 60, Department for Transport, London, 2005.

[3] Fuller, R.: Towards a general theory of driver behaviour. Acc. Anal. & Prev., 37, 2005.

[4] Henze, R.; Kollmer, H.; Küçükay, F.: Adaptation of ADAS-Functions by Monitoring Driver Characteristics, FAST-zero, September 5.-9. 2011, Shibaura Institute of Technology, Tokyo Japan

[5] Henze, R.; Bergholz, J.; Küçükay, F.: The Driver as the Basis for Objectification of DRV characteristics, FISITA 2010 World Automotive Congress, 30. Mai-04 Juni, Budapest

[6] Oppelt, W.; Vossius, G.: Der Mensch als Regler – VEB Verlag Technik, Berlin, 1970.

[7] Treat, J. R.: Tri-level study of the causes of traffic accidents: An overview of final results. Proceedings of the 21st Annual Conference of the American Association of Automotive Medicine/National Highway Safety Administration/Insurance Institute for Highway Safety, September 15 – 17, 1977, Illinois, USA.

[8] Wilde, G.: Risk homeostasis theory and traffic accidents: propositions, deductions and discussion of dissension in recent reactions, Volume 31, Issue 4, Journal Ergonomics, 1988.

[9] Winner, H., Hakuli, S.; Wolf, G.: Handbuch Fahrerassistenzsysteme, Grundlagen, Komponenten und Systeme für aktive Sicherheit und Komfort, Vieweg + Teubner Verlag, Wiesbaden, 2012.

Vehicle-in-the-Loop as a Method to Tangibly Experience Active Safety Systems at an Early Stage

Raphael J. Pfeffer* Tobias Leichsenring**, Sebastian Schwab***

*Product Manager TestSystems, IPG Automotive GmbH, Bannwaldallee 60, 76185 Karlsruhe, Germany (Tel: +49 721 98520610; e-mail: raphael.pfeffer@ipg.de).
**Engineer in the TestSystems & Engineering Department, IPG Automotive GmbH (e-mail: tobias.leichsenring@ipg.de)
*** Senior Engineer in the TestSystems & Engineering Department, IPG Automotive GmbH (e-mail: sebastian.schwab@ipg.de)

Abstract: Vehicle-in-the-Loop (VIL) is a method designed to consistently experience advanced driver assistance (ADAS) functions across all stages of the development process in the real-world vehicle. Consequently, VIL provides a useful complement to the development of ADAS along the V-Model. The possibility to have a real-world test vehicle autonomously driven by a driver model increases the highly desirable reproducibility in test driving. In addition, thanks to VIL, entire test catalogs (e.g. Euro NCAP tests) can be run in automated mode on a test track. Furthermore, VIL is a safe and resource-saving method for trials with test subjects. In contrast to using a driving simulator, the test subjects experience real-world vehicle dynamics in the vehicle itself. The utilization of Augmented Reality technologies complements the VIL tests in off-site terrain by virtual objects. This enables manufacturers and system suppliers to comprehensively investigate customer acceptance of new functions and to reduce the risk of developments heading in the wrong direction.

Keywords: Virtual Reality, Automatic Testing, Driver Models, Augmented Reality, Advanced Driver Assistance Systems, Active Safety, Human-Machine-Interface

1. INTRODUCTION

The research and development departments of all automobile manufacturers are currently testing a large number of advanced driver assistance systems (ADAS) as the basis for successful partially and fully automated driving. The objective is to transfer these driving modes from the test track into highly automated driving on normal roads in a few years from now. OEMs are highly committed to this endeavor, as everyone intends to keep pace with technology leadership in the field of automated driving.

The Euro NCAP (European New Car Assessment Programme) tests, in which vehicles are evaluated according to their safety, are another driver of this development. Good ratings relating to advanced driver assistance systems are important as the test results are widely known among consumers as well and seen as one of many criteria affecting their decisions. In addition to seatbelt tensioners, crumple zones and airbags, the focus has long been placed on active safety systems such as emergency brake assist (EBA) or systems like adaptive cruise control (ACC) to avoid accidents. The Euro NCAP requirements are further intensified as the testing regulations are to be extended starting in 2016. Emergency brake assist for crossing pedestrians (see Figure 1), for instance, will be a new test criterion.

The associated 'democratization' of advanced driver assistance systems not only requires the systems to be put on the road safely, but in time- and cost-efficient ways as well. In view of the challenges described below, this is no mean feat:

- ADAS increasingly interact with other domains of the vehicle (Human-Machine-Interface, Vehicle Dynamics).

- In the case of vehicles that increasingly act autonomously, there are high demands made on functional safety and its proof.

- The number of test cases in which the systems have to be validated is enormous, as the number of external environmental influences is countless.

- Innovative sensor concepts and algorithms pose a high development risk.

- There is relatively little experience available concerning customer acceptance of highly automated and autonomous functions.

2. VIRTUAL INTEGRATION AS A PROBLEM-SOLVING APPROACH

In view of the high system complexity, complexity of the test cases and the large scope of testing, advanced driver

assistance systems, today, are developed and validated based on models. Ideally, this is done by using a test and development environment that allows seamless investigations of the systems in virtual test driving. The basic idea behind virtual test driving is to transfer real-world road testing into the virtual world and to thereby benefit from the advantages which simulation offers in terms of reproducibility, flexibility and the reduced investment of time and costs [1].

A virtual vehicle prototype is the core of a test environment for virtual test driving, as CarMaker, the open integration and test platform by IPG Automotive. Here, the components under test are integrated as a model, software code or hardware, depending on the state of development. The virtual vehicle is operated by a driver model that is parameterized via a behavioral model (e.g. sporty, defensive). Like a driver in a real-world road test, the virtual driver executes a sequence of maneuvers. This maneuver-based test method provides the advantage that the results can be transferred to all stages of the simulation, as well as to the results of the real-world road test. Maneuver descriptions that have been defined once can always be used again. As a result, the test conditions are exactly reproducible in all development stages. This facilitates the collaboration between the vehicle manufacturer and the supplier as well. If both are working with the same integration and test platform, the OEM can provide virtual prototypes, maneuver catalogs and evaluation criteria so that the systems can already be integrated and tested in the whole virtual vehicle.

The virtual driver operates the vehicle on virtual roads in a virtual environment. The movements of the traffic objects (e.g. passenger cars, trucks, buses, pedestrians, bicycle riders) can be configured based on maneuver processes. These maneuvers are prompted by time, distance, route or event based triggers. Events such as the distance between two objects or the difference in speed between the ego vehicle and the preceding traffic object, for instance, will trigger defined braking, lane-change or acceleration maneuvers.

Figure 1 shows a test scenario for testing an emergency braking assist system with pedestrian recognition.

Figure 1: Simulated scenario for testing emergency braking assist systems in IPGMovie

While in early development stages all the elements of test driving are still virtual, the progressive integration of real-world test components follows during the course of the development. In this context, the process chain consisting of model- (MIL), software- (SIL) and hardware-in-the-loop (HIL) has become established practice.

But despite consistently increasing computing power and quality of the models real-world road testing will continue to play a crucial part in the development process of advanced driver assistance models, as models always imply a simplification of the complex real world. For this reason, the systems only receive their final approval in real-world road tests. Furthermore, road testing is indispensable when it comes to making the intervention behavior of the systems within the total vehicle context perceptible for the driver. Only a driver who physically experiences vehicle dynamics is able to evaluate ride. This subjective vehicle characteristic subsequently plays a crucial part in whether or not the assistance system is accepted by the customer.

However, the increasing complexity of the systems continually drives up the cost and effort involved in testing advanced driver assistance systems in conventional road tests. While in the case of parking assistance systems variations typically concern mostly stationary objects in order to represent various parking scenarios, accident avoidance systems such as emergency-braking assistance require at least one potential 'opponent' in the crash scenario. So-called dummy targets serve this purpose in currently used methods (Figure 2). These targets are mainly designed for rear-end collisions in longitudinal traffic. Other relevant traffic situations, such as traffic crossing at an intersection, vehicles suddenly cutting in, as well as the hazard of collisions with pedestrians or bicycle riders, can only be investigated to a limited extent or with a considerable investment of cost and effort.

Figure 2: Test method for emergency braking assist systems with dummy targets [2]

A suitable approach providing a useful complement to the established chain of MIL, SIL, HIL and real-world road testing is the Vehicle-in-the-Loop (VIL) method. VIL overcomes the limitations of simulation and test driving by combining the advantages of both approaches in a single method.

3. VIL TEST CONCEPT

When using the Vehicle-in-the-Loop method, a real-world test vehicle is integrated into a powerful simulation environment (in the implementation presented here: CarMaker). The test vehicle moves in real-world off-site terrain while other traffic objects such as other motor vehicles, pedestrians, bicycle riders, buildings, road signs, road markings, etc. are virtualized (Figure 3).

Figure 3: The VIL principle: a real-world test vehicle in a virtual environment, in this case used for testing a parking assist system

As a result, advanced driver assistance systems such as emergency brake assist can be tested safely and in a way that considerably saves resources. There are no dummy targets required to reconstruct the necessary test scenarios in reality, as in the VIL method the potential collision opponents are generated virtually. Sensor models acquire the simulated traffic objects and transmit the signals to the electronic control units (ECUs) in real time. The ECUs can be integrated into the real-world test vehicles as models (MIL), by software-in-the-loop as 'rapid prototypes' or as hardware (HIL) without extensive conversions or installations. These ECUs assess the perceived situation and, if necessary, trigger a braking intervention. The driver acts in a mixed reality of the virtual and real world, sensing real-world vehicle dynamics (the emergency braking event in this case) and viewing the virtual traffic objects that move on the real-world test track.

The driver is incorporated into the traffic simulation via various visualization media, depending on the application. If test driving is to be monitored or evaluated from the developer's perspective, monitors displaying the simulated scenarios within the driver's field of view provide a visualization option with relatively little effort. However, if the virtual and the real world are to merge with each other so that the driver will perceive the driving situation as a unit, a Head-Mounted-Display (HMD) will be used. The HMD displays the appropriate image section from the virtual world, depending on the orientation of the driver's head.

The depiction of the scenarios in CarMaker's 3D real-time animation is very realistic due to the sophisticated modeling of the 3D objects. Visual effects such as reflections from the surface of vehicles or water puddles (compare Figure 4),

dazzling effects caused by low sun, weather conditions, darkness and light sources of varying intensity, can be emulated. In addition to the physically correct movements of third-party vehicles, pedestrians walk by using typical movement patterns. Such a near-photorealistic depiction of the traffic scenarios is helpful for achieving a maximum degree of immersion in the VIL tests.

Figure 4: Realistic depiction using 3D real-time animation

Aside from a human driver, the driver model of CarMaker, IPGDriver, can assume control of the test vehicle as well. In this case, the driver model accesses the actuators of the real-world test vehicle in real time. The model-based control makes it possible to perform demanding closed-loop maneuvers in a reproducible manner even with real-world vehicles. Objective results in real-world road tests are typically ensured by sophisticated technologies such as steering and driving robots, etc. These technologies, however, only allow the performance of open-loop maneuvers. In contrast, the driver model IPGDriver interacts with the vehicle – and completes reproducible test runs even at the physical limits. IPGDriver allows ADAS interventions and realistically responds to them.

By means of the driver model interactions between driving style and the advanced driver assistance system can be systematically investigated. In this context, the following intriguing questions are raised for example: "How does emergency brake assist behave in the interaction with a 'sporty driver' who on the verge of performing an overtaking maneuver follows the preceding vehicle relatively closely? Might this even lead to a potentially dangerous situation because the system assumes the driver to be inattentive and erroneously applies the brakes? As situations like these are relevant particularly at high speeds, it is difficult to carry them out under completely real conditions. By contrast, in VIL mode, the collision opponents exist only in the virtual world and the real-world vehicle can be autonomously controlled with the driver model up to the limit range of vehicle dynamics.

The possibility of running the tests on the test track in automated mode is another advantage. In the simulation environment used, all tests and their maneuvers as well as the parameter variations can be managed by the TestManager. The driver model automatically executes the maneuver tasks of the TestManager and the results are captured in test logs and complete reports. This allows a very large number and long series of tests to be continually run.

The automated execution of entire test catalogs to validate functions is particularly productive. The TestManager, for instance, provides perfectly prepared tests according to the Euro NCAP protocol. Tests run as early as in the MIL, SIL, HIL or VIL stage give some indication of the NCAP active safety rating to be expected.

The Euro NCAP test protocols describe relatively simple test scenarios as they originate from real-world road testing. However, more complex situations can be varied from the simple scenarios, such as a third-party vehicle suddenly cutting in in front of the ego vehicle. These scenarios can be run in an automatic mode as well.

4. VIL IN THE MODEL-BASED DEVELOPMENT PROCESS

The VIL test concept implemented by IPG Automotive can consistently be used in all stages of model-based development. At the end of the V-Model, the VIL approach closes the gap between HIL simulation and test driving. In very early development stages, in which only models or algorithms are available, VIL, as a complement to pure office simulation, enables the investigation of new functions even in the real-world vehicle.

VIL in Early Development Stages

Consequently, the VIL tests offer function developers an otherwise rare opportunity to 'experience' functions at an early development stage. For this purpose models (e.g. a Simulink model or Functional Mock-Up Units) or virtual ECUs are integrated into the real-world test vehicle via the CarMaker simulation platform. In many cases, it is sufficient to incorporate the developers into the virtual world via monitors. The developer can experience the functions in an easy and safe manner, develop a feel for the function, and test various parameters and their effects on vehicle dynamics [3]. The same driving situation can be reproduced as many times as desired without requiring extensive test setups.

The focus of the development can thus be shifted from the specific single function to the product as a whole. In the best case, this promotes cross-domain collaboration of the teams involved and the functions achieve a higher level of maturity at an earlier stage.

The evaluation of the customer's experience can be included in the development by VIL tests at a very early stage as well. Today, tests are typically run with test subjects in driving simulators. There are various ways to realize this, depending on the application, starting with simple 'seat boxes' consisting of a static PC-based monitor/steering wheel/pedal combination, through to large-scale dynamic simulators. The latter use sophisticated immersion technologies to simulate the movements as well as the auditory, haptic and visual impressions for the test subject. For testing and validating advanced driver assistance systems in interaction with the driver, driving simulators enable precise adjustability and high reproducibility of the driving situations to be investigated. Critical situations can be safely represented and

the vehicle and environmental parameters easily varied [4]. However, driving simulators also have some disadvantages that make it more difficult to transfer the simulator results to reality.

The simple 'seat boxes' bear little resemblance to reality, which is problematic particularly for trials with test subjects. While professional testers can adapt to the driving tasks with greater ease, a higher level of immersion is desirable for trials involving (non-professional) test subjects. Dynamic simulators with powerful motion and projection systems are able to convey a very realistic feel for handling and ride which, however, due to limitations of the actuators and latencies in image transmission, can never correspond to reality 100 %. As a result, some test subjects suffer from so-called simulator sickness (aka kinetosis or motion sickness) which occurs whenever vestibular and visual sensory stimuli are not compatible with each other [4]. However, the greatest disadvantages of dynamic driving simulators are the high costs incurred and the test subject's awareness of not performing a real-world driving test.

In contrast, VIL tests can be performed at relatively low cost. After all, the test subject drives a real-world vehicle, which makes vehicle dynamics, vehicle and road noise, as well as haptics, 'real' as well. Only the aspect of visual stimulation is critical. As mentioned above, a high level of immersion in the VIL test is achieved by head-mounted displays. They generally offer the possibility of a 'virtual reality' projection, which means that the driver sees a complete virtual world on the display. However, studies have been reporting a higher incidence of simulator sickness in this case as well [3]. The solution preferred by the authors of this paper is the application of Augmented Reality (AR) technology which is currently establishing itself in other areas of automotive development as well (e.g. Augmented Reality Head-Up Displays [5]). In this case, the driver sees the real world, which is augmented by virtual elements. In the VIL test, optical see-through glasses are used as the display for this purpose (see Figure 5).

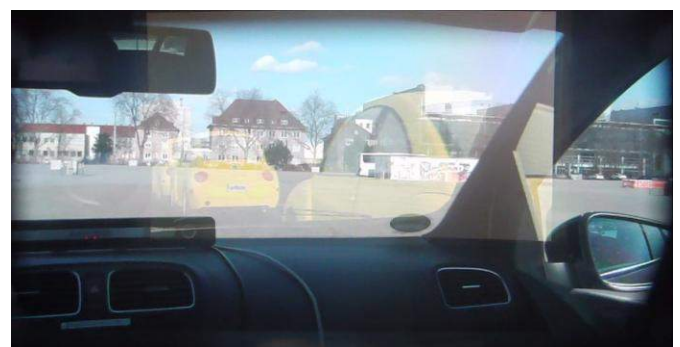Figure 5: View through AR glasses in a parking scenario

Simulator sickness issues have not occurred here so far. Furthermore, AR enjoys a high level of acceptance with test subjects because, as drivers, they do not have to 'blindly' rely on the information displayed on the glasses. They see the real-world test track/road with real-world obstacles. Consequently, potential failure of the display glasses is no

problem. Furthermore, it is ensured that in the event of any discrepancies between the test site and the simulated test track/road the driver will not unintentionally leave the test site. Through his integration by means of AR technology, the driver becomes a real road user in the simulation. He is no longer a 'spectator' watching the functions of the assistance systems but interacts with the ADAS under test in the virtual-real world.

Therefore, the VIL test is particularly well-suited to evaluate the Human-Machine-Interface (HMI) by test subjects in early development stages. An example would be the investigation of innovative display concepts such as the Augmented Reality-Head-Up Display (AR-HUD) which Continental introduced last year [6]. In this case, the real-world external view in front of the vehicle is complemented by virtual information. The information being fed in appears exactly where it is relevant to the driver. In the case of activated ACC, for instance, the AR-HUD indicates the preceding vehicle which the assistance system has currently adjusted to, as shown in the following Figure 6.

Figure 6: Augmented-Reality HUD with information about the ACC function (source: Continental AG)

In the VIL test, subjects can experience the functions of such an HUD display in that the HUD images are projected directly onto the AR glasses. The actual HUD display including the projection technology is not required for this purpose. The controllers of the assistance systems can also be operated as models in the real-world test vehicle. This allows customer requirements to be validated in early development stages when changes to the development can still be implemented with greater ease and at lower costs.

VIL for Application and final Validation of Customer Acceptance

While the VIL test in early development stages complements the simulation by the advantages of the real-world road test, the situation is reversed in subsequent stages of validation and verification when the ECUs are integrated into the vehicle as hardware. In this case, the disadvantages of conventional road testing are offset by the addition of virtual

components. In the VIL test, for example, even complex traffic scenarios can be reproducibly investigated in the real-world vehicle with real-world forces and accelerations.

The application which, today, in large part is still carried out in the real-world vehicle is a possible area for the utilization of VIL. In the field of advanced driver assistance systems, for instance, the determination of the right timing for a system intervention, e.g. by an emergency brake assist system, on the target ECU poses a major challenge. Optimal assistance by controlled intervention should be provided as early as possible, albeit avoiding so-called 'false positives.' False positives in particular can reduce acceptance of the assistance function because the driver perceives them. However, early interventions increase the effectiveness of the function. Intensive work to come up with solutions to this warning dilemma is in progress at the moment. Reinisch et al. [7], for instance, propose to alert an inattentive driver to an impending collision by the automatic transmission shifting into a lower gear. However, if the driver is not inattentive but deliberately follows the preceding vehicle closely in order to overtake it, he will benefit from the higher torque being made available.

The VIL test now offers a good opportunity to validate such concepts in the real-world vehicle and to apply the customer functions in the vehicle without a major effort. Applicators can subjectively and objectively evaluate the control systems and efficiently investigate a large number of variants and fine-tuning measures in the process.

Customer acceptance of the new function is typically tested towards the end of the development process. Ideally, this is done using a real-world vehicle in a real-world environment. However, the VIL method may well continue to be installed in order to present variants or alternatives to the customers that would otherwise require physical changes to be made to the target vehicle. [1]

5. TECHNICAL IMPLEMENTATION OF THE VIL CONCEPT

The implementation of the VIL method is based on CarMaker as it is an established simulation tool for MIL, SIL and HIL tests, which supports developers with cost and time savings. CarMaker is used in a broad field of vehicle dynamics and ADAS applications. For purposes of the VIL approach, the following functions have additionally been implemented:

- Acquisition of the movements of the test vehicle by an inertial navigation system (INS) and synchronous depiction in the simulation

- Sensoring of the virtual world in order to hand over the information about virtual objects to the real-world sensors and/or ECUs

- Integration of the human driver into mixed virtual/real-world test driving by an Augmented Reality interface

Integration of the Test Vehicle into the Virtual World

The real-world test vehicle is integrated into the virtual test environment via the vehicle model by projecting its movements onto the virtual vehicle. While it is being operated in an open space its virtual counterpart – the simulated ego vehicle – synchronously moves in the virtual environment. For this purpose, the exact position (+/- 1 to 2 cm) of the test vehicle is determined both translationally and rotationally by means of an installed inertial navigation system. The INS consists of an inertial measurement unit (IMU) to measure the relative movement and a system to determine the absolute global position by means of (D)GPS. From calculations of the acceleration and gyro sensors it determines the positional change and, by means of the DGPS system for adjustment of the drift that occurs over time, the absolute position. Via the (Xpack4-) real-time system this positional data is handed over to the simulation environment where it determines the position of the vehicle in the simulation via the corresponding inputs.

Sensor Interface

There are two possibilities to make the virtual environment detectable for the real-world test vehicle. One way is to cut off the real-world sensors of the ECU or the ECU array. The signals which are now lacking are modeled and, similar to an HIL test bench, transmitted to the corresponding ECUs via a real-time environment. This method is advantageous whenever the real-word sensors cannot be stimulated by artificial signals with a reasonable effort. Some kinds of sensors, e.g. ultrasonic, on the other hand can be stimulated by exposing them to response signals which are artificially generated. In this case, the real-world sensors are included in 'in-the-loop' testing.

Figure 7 shows a compact demonstrator parking assist system.

Figure 7: VIL system for a parking assist system, 1 = PDC sensor box, 2 = RoadBox (real-time computer), 3 = INS, 4 = Battery

It consists of a self-supporting system that can be integrated into various vehicles with very short set-up times. As a result, this implementation is particularly well suited for serial tests with changing vehicles.

Augmented Reality Interface

IPG Automotive has made the visualization of the virtual objects suitable for use in VIL testing by means of optical see-through technology and a head tracking system. In the implementation, which was realized as a demonstration (depicted in Figure 8), the SMARTTRACK tracking system (by ART) is utilized, which is mounted to the instrument panel of the test vehicle. The system acquires the position and orientation of the head (head pose) by tracking a target with 6 markers on a pair of AR glasses via two cameras. The head pose is transmitted via UDP to the host PC from which the simulation is configured, controlled and visualized by means of the IPGMovie animation tool. The virtual camera of IPGMovie is subsequently oriented in a way that corresponds to the driver's line of vision. This view of the virtual world is output on a pair of AR glasses (Vuzix Star 1200XLD).

Figure 8: Integration or AR visualization into the test concept

However, only the relevant virtual objects are projected onto the see-through glasses. All other objects that are normally shown in IPGMovie, such as the road or the sky, are hidden. Figure 5 by way of example shows the visualization of virtualized parking vehicles in an otherwise completely real environment.

A major challenge in the implementation was and is the continual minimization of the latencies which may result from delays in image projection, head tracking, data transmission, etc. The ideal state is that the driver's head movements are directly represented in the augmented environment so that the virtual and the real world become a unity for the driver.

6. CONCLUSION

The utilization of the VIL method enables the testing of advanced driver assistance systems as a tangible experience and to optimize them at very early stages of the development process. At the same time this results in a massive reduction

of the test effort compared with real-world road testing, as even highly complex test scenarios can be easily and efficiently defined and reproduced via the simulation environment. The proposed implementation of the VIL method is based on the CarMaker open integration and test platform which can seamlessly be used for MIL, SIL, HIL and VIL tests. As a result, maneuver and test scenarios only have to be defined once and can subsequently be re-used in all development stages. The results of the tests in the individual development stages are directly comparable.

In addition to the verification and validation of functions, VIL, by utilizing advanced AR technologies, makes it possible to comprehensively test the subsequent customer's acceptance of new functions at an early stage. The interaction of the driver and the assistance system can thereby be comprehensively investigated in a safe and effective process. As a result, the risk of pursuing new developments that will enjoy only minimal opportunities in the marketplace can be significantly reduced.

REFERENCES

[1] S. Hakuli and M. Krug, "Virtuelle Integration," in *Handbuch Fahrerassistenzsysteme*, H. Winner, S. Hakuli, F. Lotz, and C. Singer, published by Springer Fachmedien Wiesbaden, 2015, P. 125–138.

[2] P. Seiniger, O. Bartels, T. Unselt, C. Rodarius, J. Vissers, A. Aparicio, and S. Baurès, "Ein validiertes Testverfahren für Notbremssysteme – Ergebnisse des ASSESS-Projekts," held at the 5th Driver Assistance Convention, Munich, 2012.

[3] G. Berg and B. Färber, "Vehicle in the Loop," in *Handbuch Fahrerassistenzsysteme*, H. Winner, S. Hakuli, F. Lotz, and C. Singer, published by Springer Fachmedien Wiesbaden, 2015, P. 155–163.

[4] H.-P. Schöner and B. Morys, "Dynamische Fahrsimulatoren," in *Handbuch Fahrerassistenzsysteme*, H. Winner, S. Hakuli, F. Lotz, and C. Singer, published by Springer Fachmedien Wiesbaden, 2015, P. 139–154.

[5] C. Groenegress and S. Ritz, "Augmented Reality Transfer von Präsentations-techniken ins Cockpit," *ATZelektronik*, Bd. 8, No. 4, P. 258–263, Aug. 2013.

[6] Continental, "Continental zeigt erstmals Head-up-Display mit Augmented Reality für bessere Fahrerinformationen," 14-July-2014. [Online]. Available at : www.continental-presse.de. [Accessed: 28-Feb-2015].

[7] P. Reinisch, F. Kohlhuber, and P. Zahn, "Schaltvorgänge zur situationsangepassten Vorwarnung des Fahrers," *ATZ - Automob. Z.*, Volume 113, No. 3, P. 210–215, Feb. 2011.

What ADAS are the most promising for our future older drivers?
Evidences reported from France and Sweden

Tania Dukic Willstrand*, Thierry Bellet**, Thomas Broberg***/****,
Christina Stave*, Jean-Christophe Paris**, Björn Peters*, Claude Marin-Lamellet**

*Swedish National Transport Research Institute, Gothenburg, Sweden
(tania.willstrand@vti.se; christina.stave@vti.se: bjorn.peters@vti.se).
**IFSTTAR, Bron, France (thierry.bellet@ifsttar.fr; jean-christophe.paris@ifsttar.fr, claude.marin-lamellet@ifsttar.fr)
*** Volvo Car Corporation, Volvo Cars Safety Centre, Gothenburg, Sweden (thomas.broberg@volvocars.com)
****Chalmers University of Technology, Applied Mechanics Vehicle Safety, Gothenburg, Sweden.

Abstract: Focus groups were conducted in both France and Sweden as part of the SAFEMOVE project. The aim of the study was to identify and asses difficulties experienced by older drivers (+70) due to age-related declines in sensory, physical and cognitive abilities and potential consequences in terms of both traffic safety and mobility. Furthermore, the aim was to identify Advanced Driving Assistance Systems (ADAS) liable to improve safe mobility for the target group and to compare the situation between France and Sweden. Three main topics investigated were trip planning and navigation task, speed control and regulation, and intersection crossing (more particularly when turning on the left). For each one, data collected focused on both older drivers' experienced difficulties and their interests or expectations towards driver support like ADAS. There was in general a positive attitude to driver support systems but participants were also concerned about costs. Furthermore, several differences between French and Swedish older drivers were found.

Keywords: older drivers, focus group, driving support, navigation, intersections, speed, ADAS.

1. INTRODUCTION

During the last decades, more and more attention has been devoted to the older drivers' situation. The older drivers are usually experienced and careful drivers, without taking over-estimated risks (Langford, Methorst, & Hakamies-Blomqvist, 2006). However, aging is frequently associated with some declines in sensory, physical and cognitive capacities. For instance, Vrkljan and Miller-Polgar (2005) indicated that changes in the visual and cognitive systems may reduce the ability to drive a car safely. Physical abilities like neck flexibility can also affect various aspect of driving performance. For Baldwin (2002) age effect on information processing could be linked to an interaction between cognitive and sensory changes: if vision is affected by aging in all its components, it is higher order visual processes including dynamic visual acuity and the simultaneous use of central and peripheral vision which have been shown to have some correlation with accident rates. Audition is also affected by aging, notably pure tone detection and speech comprehension. As a consequence, a minimum of 10 Db increasing is requested by older people for an auditory presentation if they are involved in a multiple task in comparison to younger drivers. From Koppel et al (2010), it appears that when cognitive load increases, processing speed of older people decreases. This could be the result of slowed integration of relevant information, limited memory and attentional capacities as well as a decline in executive functions, high order cognitive processes like planning, inhibition of irrelevant information, mental flexibility, judgement and self-adaptation. Then older drivers could be more subject to distraction than other drivers because they have less spare attentional capacity, and multitask can be problematic because of the reduction of time-sharing skills. Another set of studies (Bolstad, 2001; Bailly, 2004; Kaber et al, 2012) also showed negative age effects on drivers' Situation Awareness (SA). Situation Awareness was defined by Endsely (1995) as 'the perception of elements in an environment within a volume of time and space, the comprehension of their meaning, and projection of their status in the near future'. In the frame of car driving activity, SA corresponds to mental representation of the road environment, as perceived and understood by the driver (Bellet et al, 2009). Through a simulator experiment, Bolstad (2001) showed that, due to age-related declines in perceptive and cognitive functions, older drivers' mental models of road environments are less complete of SA elaborated by youngest experienced drivers. Similar results were also found by Bailly (2004) in normal driving conditions and, more recently, by Kaber et al (2012) for hazardous situations: age negatively impacts the content and the adequacy of SA, more particularly for complex driving situations requiring high attentional demands. Facing the complexity of some traffic situations, older drivers may have difficulties to perceive and integrate all the relevant pieces of information required to make the right decision, resulting in higher involvement in

certain types of accidents. This is typically the case for accidents occurring at intersections with crossing traffic (Larsen & Kines, 2002; Preusser, Williams, Ferguson, Ulmer, & Weinstein, 1998). Braitman et al (2007) reported that failure to yield was found in more than half of the crashes involving drivers +80 in a US-study. These crashes occur more often when drivers are turning left and at stop signs. Braitman et al (2007) attribute this fact to misjudgements of the time needed to proceed through the turning manouver; moreover, they also reported that "look but failed to see" errors were predominant among drivers +80. Based on these characteristics, the development of driving assistance systems might be an option to support older drivers and prolong their time as active safe drivers (Simoes & Marin-Lamellet (2002), Davidse (2006)). To support older drivers, the driving aids have to be adapted to their characteristics, needs and expectations in order to be efficient and well accepted.

The overall aim of this focus group study conducted within the SAFEMOVE project was to acquire knowledge about the difficulties older drivers have when they drive their car in everyday life both in France and in Sweden to compare findings. A second aim was to identify existing or future Advanced Driving Assistance Systems (ADAS) capable in supporting older drivers and liable to help improve their mobility in a safe way. A first step to address safe mobility in the SAFEMOVE project was through a large survey reaching a total of 4200 persons in France and Sweden together. On-road observations with sub-sets of the survey respondents were performed in both countries as a next step. During the on-road experiments, participants drove a car in real traffic conditions on a specific route. A driving instructor was in the car to ensure safety and an occupational therapist was responsible to identify problematic situations and behaviours observed for the drivers. Based on the experience gained from the survey and the on-road experiments, complemented with a literature review (Chin et al, 2014), three common areas of interest were identified to be further investigated among older drivers through focus groups in Sweden and France (Stave et al., 2014; Bellet et al., 2014).

2. METHOD

Even if the approaches applied in France and Sweden were similar, there were some methodological specificities in each country concerning the way the focus group sessions were carried out, the type of data that was collected and the analysis performed by each team.

2.1 Focus groups

France: Focus group sessions as implemented in France, were organised around a set of main topics, briefly introduced by the experimenters, and then sub-divided in a sub-set of questions to be successively discussed by the participants. Data collected were both individual opinions per question and then common discussions between the participants dedicated to each main topic.

Sweden: For the Swedish focus group sessions, using an explorative approach, quality rather than quantity was the lead word striving for consensus where counting frequencies or categories was not of interest. Focus group interviews support interaction amongst participants, which can enrich data in a way individual interviews cannot (Kitzinger, 1994).

2.2 Recruitment of participants

France: 30 older drivers participated in the focus group sessions. All the French participants were recruited among a group of 76 older drivers who previously participated in the SAFEMOVE on-road driving experiment. These 76 participants were initially selected from a face-to-face survey (including interview, questionnaires and cognitive tests) implemented among 800 older drivers living in the Rhône area. Six sessions of five participants (from 4 to 6) were organized.

Sweden: The focus groups were conducted at two occasions, 2011 and 2013. The participants in the first round were recruited through two different national pensioners' organisations. The second round of participants was recruited among the 40 participants in the on-road assessment conducted in SAFEMOVE (Henriksson et al., 2014). In total 63 drivers living in the Gothenburg area participated. They were 70 years or older, had a valid drivers' licence and were still active drivers.

2.3 Procedure and themes

France: focus group sessions were organised in 7 "Blocks", each one dedicated to a specific topic, jointly defined with the Swedish team. The themes derived from the previous studies of Broberg and Willstrand, (2014) and Peters et al. (2015) where difficulties were observed during the on-road assessment performed in the SAFE MOVE project. The first one was dedicated to trip planning issues and the navigation task. The second topic concerned speed control and speed adaptation strategies of older drivers according to the traffic condition and the situational context, including their awareness of speed limit when driving. The last topic focused on intersection crossing issues, more specifically when turning to the left, involving complex interaction with other roads users. Each theme was organised in two parts: one focused on the difficulties met by the participants when driving and the second one was dedicated to their use and/or expectations regarding ADAS and future driving aids (Fig 1). Finally, each of these two parts were supported by a set of questions to be successively answered by the participants (around 12 questions per block). For each question, participants had first to provide an individual judgement (by using a Likert scale). Then, after each part (i.e. half-block), a common discussion between the participants was implemented under the moderation of the experimenters. The total duration of a session was half a day (4 hours), including two 15 minute breaks.

Fig 1: Example of illustration presented to the French participants to collect their opinions and their expectations on future navigation systems based on augmented reality (to the left) or on head-up display (to the right).

Sweden: A structured interview guide was used where the three pre-defined themes were introduced to get the discussion going (see the French description earlier). As an introductory "warm up" topic, participants were asked what kind of driver assistance or safety technology they have in their cars today. The moderator introduced themes and facilitated the discussion among the participants. The discussion last for two hours including a short break.

2.4 Analysis

France: Concerning the individual opinions collected among the participants based on Likert scales, they had to provide numerical values (from 0 % to 100 %) on an individual paper grid (one numerical value was collected for each question, among each participant). Concerning the common discussion phases (coming after each part of 6-10 questions), they were video recorded and notes were taken by the experimenter. Analysis implemented were primarily focused on individual opinions, and collective discussion were mainly used to assess if common consensus exist or not between the participants or if several contradictory point of views appeared.

Sweden: All focus groups were audio recorded and notes were taken. After each focus group, a debriefing was performed in order to see if the researchers had a common understanding of what they had just heard. Then, the researchers who performed the focus groups listened to the recordings to extract answers, first individually and secondly together. For the three pre-defined themes covered as well as the introductory question, a simple form of content analysis was performed.

3. RESULTS

3.1 Trip planning and navigation task

Difficulties for Navigation in France: The majority of older drivers participating did not experience navigation as a very difficult task. Indeed, for a large part of them, they primarily drive their car on familiar routes during their everyday life, and they can generally adapt their trip in order to avoid unfavourable driving conditions (like bad weather, night driving, or high congestion time). In addition, they generally have a good confidence in their own ability to navigate when driving. If they have to perform the driving task on unfamiliar

routes, the navigation task is assessed as significantly more difficult. In this case, they spend time to carefully plan their trips. More than half of them know and frequently use web services like *Mappy* or *ViaMichelin*, and they print the trip information to support them during the travel. All of them also have and use classical paper maps. However, despite this they declared a high level of confidence in their navigation skills, it should be noted that 4 participants tracked the trip for going to IFSTTAR, the day before the experiment.

Difficulties for Navigation in Sweden: The majority of the participants agreed that every activity take more time nowadays. They spend more time to plan their trips. They expressed a need to plan even for shorter trips, specifically if it concerned new destinations. However, generally it is not a big problem as they do not visit new locations very often and they tend to use the well-known roads as they have done for many years. They actually have more need to reroute when a sudden change occurs such as traffic accidents or a roadwork. They experience trouble when rerouting spontaneously in such situations. Planning a trip is about creating large margins to stay inside their comfort zones. They often take into account possible information about weather, distance, the traffic situation, parking, time of the day, specific roads or places to avoid, different kinds of breaks (rest, sleep, food, refuel). They try to avoid driving in darkness, especially if there is a risk of being blinded by headlights and if it is winter conditions.

Aid in France: Two thirds of the French participants declared they have a Navigation system. Moreover, a large part of them frequently use it, also for familiar routes. This high rate of equipment and use is partially due to the French law on speed limit. Indeed, the most popular Navigation systems in France are also equipped with warning functions informing the driver of the current speed limits (including radar detection until 2011), and several drivers primarily activate their GPS to better control their speed and to avoid speed tickets. In a general way, a majority of the participants have a positive opinion about GPS, in terms of both perceived utility and acceptability, even if they also sometimes detect some dis-functioning or sub-optimal route suggestions provided by their GPS. However, advanced HMI, like head up display or augmented reality technologies (presented to the participants from illustrative pictures during the focus groups), were assessed by seniors as very promising and liable to better support their own needs against the existing systems.

Aid in Sweden: Participants agreed that GPS is a solution for the future that will be good for route planning, travel time and refuel information and more. However, even if some participants tell they had a navigation system it was not clear how often they use them. However, to increase their use, they requested to have better interfaces and perhaps voice guided navigation.

Traffic information through radio was also considered a good source of information to plan or reroute. Traffic information regarding accidents on the road is automatic and sent to your radio automatically. Regardless if the radio is on or not it will stop broadcasting and send warnings regarding accidents, their location and measures to avoid the black spot if

possible. Older drivers using cell phones stated that "the cell phone gives a sense of security and you can call for help and communicate if you have any problems". Some participants would like to see better visible road signs that can be seen at a longer distance in complex traffic locations.

3.2 Speed control, regulation and adaptation

Difficulties in France: The main topic investigated during the Focus Groups in France regarding speed control was the difficulties the participants have (or not) to respect the legal speed limits. First at all, it must be noted that this issue appeared as one of the highest difficulty, and probably the main concern of older drivers in France, when they have to drive their car in their everyday life. This fact is surely due to strict French laws applied since 2005 regarding speed limit violations, and to the massive deployment - during the last ten years - of automatic speed-controls radars (speed ticket of 90 Euros and the lost on 1 point /12 since the first km/h exceeding the legal speed limit). As a consequence, the majority of the French older drivers are fully aware of the high probability to be controlled for their speed during driving (several of them received a speed ticket during the last 3 years), and they pay high attention to control and regulate their speed under the legal limit. In addition, the more the route they use is unfamiliar (i.e. difficulty to know the current speed limit) and/or includes frequent changes of speed limit (like short section of 70-km/h on rural road or urban highway, generally limited to 90-km/h, or 30-km/h sections in urban areas), the more they have to pay attention to regulate their own speed, and the more they have difficulties to adequately perform the driving task (however, proportionally, the 30-km/h sections generates more difficulties among men, against 70-km/h sections among women).

Difficulties in Sweden: There was a general high acceptance for driving too fast and the participants seldom discussed that their own high speed would be a problem. Quite the contrary, many considered people driving slowly as more dangerous, possibly causing dangerous situations. The participants felt that they have to follow the traffic flow even if it means driving too fast or driving over their own ability. However, they mentioned that it was important to respect 30-km/h signs posted at schools. Driving slowly wasn't perceived as good driving practice. The ideal driving was driving fast in a more offensive way, which indicates that you are a skilled driver with great control of the car and with an ability to quickly and accurately scan and perceive all road users. It creates a problem for those who need more time since the worst thing that could happen, according to the participants, is to obstruct the traffic flow. Some difficulty in speed adaptation was noticed during the on-road driving in SAFE MOVE, i.e. driving too fast in certain scenarios such as down town where many pedestrians and bicyclists are present. You do not necessarily exceed speed limit but you do not drive with a safe speed in this particular situation. Moreover with age you need more time to scan the traffic, to perceive other road users, especially bicyclists which suddenly appears, and at last to react to sudden event. Therefore recommendation are to decrease speed in order to give more time to react. There

were many different explanations as to why they were driving too fast. Difficulties in knowing the actual speed limit was one. Another reason often mentioned was the traffic rhythm, i.e. you have to follow the flow to keep your position in traffic, and it is perceived as more important than to respect the speed limit. The participants mentioned that if you do not follow the traffic flow, dangerous overtaking situations could appear. In addition, it was specifically mentioned that it was important to respect 30-km/h signs posted at schools.

Aid in France: Regarding driving assistance, one of the main results collected during the focus groups is that half of the participants have, and frequently use, a driving aid to support them in their speed regulation. The main systems used are the automatic cruise control, information or warning systems provided by a GPS, and the speed limiter. Regarding the perceived utility and the acceptance level of such driving aids, it must be noted that devices providing information (i.e. current speed limit) and warning (in case of over-speed) received highest values among the participants as a whole, against active ADAS based on partial automation (like speed limiter, cruise control, or adaptive cruise control).

Aid in Sweden: Aid mentioned were more signs to frequently remind drivers about the speed limit; an alternative considered was having a display in the car to inform the driver about the current speed limit. Many participants were positive to signs in the infrastructure that give feedback on actual speed. Cruise control and navigation system were also mentioned as means. They also mentioned 2+1 roads or highways where it is possible for other drivers to overtake safely so that they could keep driving at their own pace "without being in the way" for other road users. Infrastructure solutions such as speed bumps were suggested to help control speed but were also noted as negative if not correctly designed or easy to detect.

3.3 Intersection crossing and left turn

Difficulties in France: Intersection crossing, more particularly when they have to leave the priority to other road users, was assessed by the French participants as a potential difficult task during driving. Nevertheless, this task was assessed as less difficult than overtaking a vehicle, to respect the speed limits, or to merge on to an urban highway. The main difficulties they have are about identifying the priority rules in unfamiliar intersections, and to make decision for turning to the left at urban crossroads – more particularly to adequately assess in this last case the speed of incoming vehicles. In addition, difficulties for crossing intersections were assessed as significantly higher by women, compared to men. This was the case for all the types of crossroads and manoeuvres investigated during the focus groups.

Difficulties in Sweden: Most of the participants agreed that intersections could be difficult, especially when turning left on rural roads. "I feel stressed when the traffic is pushing from behind, trying to find a gap ahead while determining the speed of the oncoming cars". "There are also risks with those who are close behind, are there any driver assistance systems for that?" one driver asked reflecting on several comments regarding the problem with those who don't keep a safe

distance. They also blamed other road users (drivers, pedestrians and cyclists) for not giving way, which make them confused and create difficulties "It is mostly young people who drive very fast into the intersections and brake hard; you cannot trust that people will stop at the intersection".

Aid in France: For the French focus group sessions, driving aids to assist intersection crossing were primarily focused on the Left Turn (LT) manoeuvre. To support the discussions, three type of LT aids were first presented and explained in-depth to the participants: (1) a *perception support system*, providing information on approaching cars (having the priority), specifically regarding their distance and their speed, (2) a *decision support system*, assessing gaps and giving the time drivers have to safely cross the opposite lane, and (3) a *warning support system*, designed to detect potential collision risks and then to alert the driver in case of an erroneous decision or a critical behaviour. Data collected among the participants (having to give their opinion on each system and then to establish a hierarchy between the 3 devices) clearly showed the highest levels of interest, acceptance and perceived utility for the last warning support system. Then, the perception support system was assessed as very useful by women (close to the Warning system), but more poorly accepted by men. Finally, Decision support system (LT gap assessment) received the lowest judgement values from our participants as a whole.

Aid in Sweden: Automatic road signs actually showing that a cyclist is approaching were given as an example of a good solution. Another suggested solution was to drive through an intersection or roundabout with more care, looking more often to the sides and also using the rear mirrors, being more attentive and careful or trying to avoid those locations in the first place. One person suggested "having good foresight and automatic transmission so that no attention is spent on changing gears". From the infrastructure side, one could implement better and more signs to help inform about the way so that it becomes easier to plan the driving. One could also replace dangerous intersections with roundabouts which are highly appreciated and perceived as safer compared to other crossings. To build separate lanes to be able to turn left in a safe way without being in the way for other road users or to introduce traffic islands are other ways of improving infrastructure. Some participants stated that the visibility in new cars has been reduced and better mirrors could be a possible improvement. A slower pace in traffic as a whole was requested by many.

4. DISCUSSION

The aim of the present study was two folded: first, to identify potential areas were driver support system could contribute to an improved safe mobility for older (+70y) drivers and to identify possible communalities and differences among French and Swedish older drivers. On one side, similarities may indicate more universal difficulties when driving, or similar expectations towards driving aids liable to be shared by all older drivers living in different European countries. By contrast, differences may reveal some cross-cultural specificities between Swedish and French drivers that could be considered to adequately assist them or to support their respective needs for driving aids.

Concerning the demographic issues of older drivers, there has been a similar change in the two countries during the last decades. In Sweden, the proportion of license holders among older citizens and particularly among women has increased sharply in recent decades. Today, 83 percent of all those who are 67 years or older have a driving license, which can be compared with the share of 30 percent in 1980. Among women 67 and older, the proportion of the license increased from ten per cent in 1980 to 73 per cent in 2013 (facts from BilSweden). In a similar way, the number of older drivers also considerably increased in France during the last decades (Marin-Lamellet and Alauzet, 2011). This evolution is due to the increasing number of French households having a car (from 64 % of households in 1994 against 85 % in 2008), but also to the highest number of women who have a driving licence and who drive a car (42 % in 1982, 64 % in 1994 and 76 % en 2008). Despite these demographic similarities, there are differences in special driving conditions for Sweden and France which should be mentioned. For instance, the traffic situation is dramatically different in Sweden compared to France during winter. The poor weather conditions during winter with a long period of darkness, presence of snow and black ice in many places, significantly reduces driving for Swedish older drivers during wintertime. In France, and more particularly in the Lyon area, weather conditions are generally better and older drivers may drive to a larger extent all the year round. Other differences are related to specific traffic laws in each country. An example, recent changes in Sweden and in France regarding speed limits have influenced older drivers differently and their concerns towards speed limit respect for each country (see 4.2.).

4.1 Trip planning and navigation task

For older drivers in both countries planning the trip and performing the navigation task, especially on unfamiliar roads, is a situation of concern where the participants welcome support systems. However, it is generally not a major problem for them because they primarily drive in familiar places using well-known roads. In other cases, they spend more time carefully planning their trips before travelling (from map or web services). They often plan their trip according to weather, distance, or traffic conditions. Furthermore, they also consider places to avoid. Both Swedish older drivers and a large part of French older drivers (specifically women) avoid driving during night, especially if there is a risk of glare by headlights of other vehicles and if there is bad weather conditions.

Experience of navigation aid systems for support in this situation seems more positive in France than in Sweden, probably because French drivers have more experience in using GPS-navigation systems. Partly, because they have a specific concern to avoid speeding tickets. Moreover, both French and Swedish drivers pointed out the need to design a

better interface for the GPS navigation system (to avoid visual distraction or to facilitate GPS information matching with the road environment) and other support to really use them and avoid irritation. This comment is also common for all support systems where they do not want to be disturbed or overloaded too often by a visual or an auditive interface. In a recent study, tactile-based navigation system was tested with hearing impaired drivers (common impairment among older drivers) and normal hearing drivers, with very positive results for both groups (Thorslund et al., 2013).

4.2 Speed control, regulation and adaptation

For older drivers in both countries, there is a perceived difficulty to respect speed limits although the reasons are not completely similar. To be aware of the speed limit is a common explanation in both countries where they do not feel to have sufficient support today. Results in Sweden also show that the traffic rhythm is contributing to excessive speed. Regarding aid for speed control, drivers in both countries wants to get feedback and information on their own speed and the speed limits, from the vehicle. Despite these similarities, inter-country differences also appear clearly in the focus group data. These differences seem directly related to specific traffic laws in each country. For instance, in 2011, the Swedish authorities made a reform regarding speed limits where several new speed limits were implemented giving that signs posting 30, 40, 50, 60, 70, 80, 90, 100, 110 and 120 km/h are present on the roads. As a consequence, driving in Sweden requires frequent updating of speed limit from a large set of possible values, and it is not always easy for older drivers to be fully aware of the speed limit on the road section where they are currently driving. For France, the recent development and the massive deployment of automatic speed-control radars since 2005 on the French roads, have considerably impacted drivers' behaviour and their concern towards speed limits. Around ten percent of the older French drivers interviewed during the focus group had received a speed ticket during the past 5 years, and a large part of the others feel highly concerned by this potential risk. This concern is clearly due to the automatic "contrôle-sanction" policy in France that occurred during the last decade. There is no tolerance with the new radars that are able to automatically generate a speed ticket of 90 Euros – and the fact that you loose one point on a 12 point- scale- from the first km/h exceeding the legal speed limit. As a consequence, knowing the legal speed limit on the road section they drive is a major concern to older French drivers, and they allocate a lot of their capacity to the speed control task. In addition, several of the French drivers decided to equip their car with a GPS system including warning in case of speed-limit violation. This fact may explain the higher level of experience and the more frequent use of GPS navigation systems by French older drivers compared to Swedish.

4.3 Intersection crossing and left turn

The common difficulties at an intersection was to leave priority, especially when turning left, to other vehicles and at the same time find a gap to turn, assess speed of in-coming

vehicle and manoeuvre the own vehicle. Both French and Swedish drivers were interested to have support in this task. They were both open to have systems inside their car and also proposed road infrastructure solutions such as to remove "left turn intersections and introduce roundabouts instead. The results in Sweden and in France showed that no participants knew of any driver assistance system that could help them in intersections but confronted with such a possibility during the focus group, they were very positive. In France, intersection crossing in general, and left turn manoeuvre in particular, are assessed as more difficult by women.

Moreover, by considering the left turn manoeuvre successfully implemented by the French participants during the on-road experiment, it seems that some of the older drivers underestimate the difficulties they have to adequately perform the task. They indicated during the focus group that is not an easy task to perform, but they don't feel "highly" concerned about this situation (compared with speed limit respect, for instance). In contrast, several critical situations occurred during the on-road experiment when they had to turn left at urban crossroads with incoming traffic, and speed limit was generally well respected.

4.4 Method

Even though extracted from a larger cohort of older drivers in both countries all participants in this study were volunteers. Generalizing the application of the findings to older drivers in general is therefore to some extent restricted due to possible bias (i.e. those with most severe problems are less likely to attend). More so, it showed difficult within the focus groups to find ideas of specific solutions for driver aid. However, the focus groups made it possible to identify problems and needs for support to older drivers. The next step would therefore be to provide representatives of the target group with examples of technical solution they might not have any idea existed. One such next step within the SAFEMOVE project will be to create demonstrators of driver assistance concepts in vehicle and driving simulator environment for further studies using the results from the focus group as input.

5. CONCLUSION

Amongst both the French and Swedish drivers, there was a great variation in experience of own assistance technology but generally a positive attitude despite a fear of costs. Car manufacturers have to take the economic situation of older drivers into account when pricing the systems and designing the safety package as an option. When the French & Swedish participants were asked about future ADAS, they were positive if it increased safety. Information regarding ADAS effect has to reach the public and future users. By knowing the existence and understanding their effect, it would increase the penetration rate, which is still very low, and consequently has an effect on safety. ADAS systems have the potential to increase mobility for older drivers. The use of systems can delay driving cessation by maintaining the task difficulty within their ability. Future ADAS development has to include all travels with an holistic approach, from planning the travel to returning back home. New planning tools have to be

designed to plan the travel before sitting in the vehicle. Information has to be available during driving to increase situation awareness and increase perception when needed such as during turning left manoeuvre. Feedback during and after the drive has to be available as a training tool for the driver to learn from mistakes. This holistic approach is a key factor to increase safe mobility not only for older but for all drivers.

REFERENCES

Bailly, B. (2004). Conscience de la Situation des conducteurs: aspects fondamentaux, méthodes et applications pour la formation des conducteurs. PhD Thesis, University Lyon 2.

Baldwin, C. L. (2002). Designing in-vehicle technologies for older drivers: application of sensory-cognitive interaction theory. Theoretical Issues in Ergonomics Science, 3(4), 307-329.

Bellet T., Bailly-Asuni B., Mayenobe P., Banet A. (2009). A theoretical and methodological framework for studying and modelling drivers' mental representations. Safety Science, 47, pp. 1205–1221.

Bellet, T., Paris, J.C., Marin-Lamellet, C., Ojeda, L. (2014). Older drivers' needs and priorities for DVIS functionality (in french). SAFE MOVE deliverable D 3.1.1.

Bolstad, C. A. (2001). Situation awareness: does it change with age? Proceedings of the human factors and ergonomics society 45th annual meeting (pp. 272– 276). Minneapolis, Minnesota, USA.

Braitman, K.A., Kirley, B.B., Ferguson, S., Chaudhary, N.K., 2007. Factors leading to older drivers' intersection crashes. Traffic Injury Prevention 8 (3), 267–274.

Broberg,T. & Willstrand, T. (2014) Safe mobility for elderly drivers—Considerations based on expert and self-assessment. *Accident Analysis and* Prevention, 66, 104–113.

Chin, E., Marin-Lamellet, C., Bellet, T., Dukic Willstrand, T., Broberg, T., Boverie, S., Gurret, F., Ojeda, L., Stave, C. (2013). Potential benefit of driving assistance systems for older drivers in critical situations. SAFE MOVE deliverable D 3.1.2.

Davidse, R. J. (2006). Older drivers and ADAS-which systems improve road safety? IATSS, 30(1), 6-20.

Endsley, M. R. (1995). Toward a theory of situation awareness in dynamic systems. *Human Factors*, 37(1), 32–64.

Henriksson, P., Levin, L., Willstrand, T & Peters, B. (2014) Challenging situations, self-reported driving habits and capacity among older drivers (70+) in Sweden. A questionnaire study. VTI report nr VTI-notat 9 – 2014, Linköping, Sweden.

Kaber, D., Yu Zhang, Sangeun Jin, Prithima Mosaly, Megan Garner/ Transportation Research Part F 15 (2012) 600–611.

Kitzinger, J. (1994). The methodology of focus groups: the importance of interactions between research participants. Sociology of Health and Illness 16, p 103–121.

Koppel, S., Charlton, J., & Fildes, B. (2009). Distraction and the older driver. In M. A. Regan, J. D. Lee & K. S. Young (Eds.), *Driver distraction: Theory, Effects and Mitigation* (pp. 579-601). Florida, USA: CRC Press.

Langford, J., Methorst, R., & Hakamies-Blomqvist, L. (2006). Older drivers do not have a high crash risk--A replication of low mileage bias. *Accident Analysis & Prevention*, 38(3*), 574-578.*

Larsen, L., & Kines, P. (2002). Multidisciplinary in-depth investigations of head-on and left-turn road collisions. *Accident Analysis & Prevention*, 34, 367–380.

Marin-Lamellet C, Alauzet A (2011). La Mobilité Des Seniors : État des lieux et perspectives. In Les aînés : quels enjeux pour les décideurs publics? Contribution au débat national, Administration N°229; pp. 118–121.

Peters, B., Selander, H., Willstrand, T. and Broberg, T. (2015). On Road Assessment in Sweden - First Results. SafeMove Deliverable 1.3, under production.

Preusser, D. F., Williams, A. F., Ferguson, S. A., Ulmer, R. G., & Weinstein, H. B. (1998). Fatal crash risk for older drivers at intersections. *Accident Analysis and Prevention*, 30, 151–159.

Simoes, A., & Marin-Lamellet, C. (2002). Road users who are elderly: drivers and pedestrians. In Fuller. R. & Santos.J.A. (Eds.), Human factors for the highway engineer (pp. 255-275). Oxford: Elsevier Science Ltd.

Stave, C., Willstrand, T., Broberg, T., Peters, B. (2014) Older drivers' needs for safety and comfort systems in their cars – A focus group study in Sweden VTI Notat 31A-2014, Linköping, Sweden.

Thorslund, B., Peters, B., Herbert, N., Holmqvist, K., Lidestam, B., Black, A., Lyxell, B. (2013). Hearing loss and a supportive tactile signal in a navigation system: Effects on

driving behavior and eye movements. *Journal of Eye Movement Research, 6*(5), 1-9.

Vrkljan, B. H., & Miller-Polgar, J. (2005). Advancements in vehicular technology: potential implications for the older driver. Int. J. Vehicle Information and Communication Systems, 1, 88-105.

Human-machine Shared Driving Characteristics of Autonomous Driving Intelligence System in Collision Avoidance Manoeuvre

Pongsathorn Raksincharoensak*, Ko Iwano**,
Yuichi Saito***, Hiroshi Mouri**** and Masao Nagai

** Tokyo University of Agriculture and Technology, 2-24-16 Naka-cho, Koganei,
Tokyo, 184-8588, Japan (Tel: +81-42-388-7397; e-mail: pong@cc.tuat.ac.jp).
** Tokyo University of Agriculture and Technology, 2-24-16 Naka-cho, Koganei,
Tokyo, 184-8588, Japan (Tel: +81-42-388-7395; e-mail: 50013643012@cc.tuat.ac.jp).
*** Tokyo University of Agriculture and Technology, 2-24-16 Naka-cho, Koganei,
Tokyo, 184-8588, Japan (Tel: +81-42-388-7395; e-mail: y-saito@cc.tuat.ac.jp).
**** Tokyo University of Agriculture and Technology, 2-24-16 Naka-cho, Koganei,
Tokyo, 184-8588, Japan (Tel: +81-42-388-7032; e-mail: h-mouri@cc.tuat.ac.jp).
***** Japan Automobile Research Institute, 1-1-30 Shibadaimon, Minato-ku,
Tokyo, 105-0012, Japan (Tel: +81-3-5733-7932; e-mail: mnagai@jari.or.jp).*

Abstract: This paper investigates the effectiveness of shared driving characteristics in collision avoidance maneuver when the human and the autonomous driving system act in parallel. In the development of driver-in-the-loop ADAS, it is important to study how the autonomous steering assistance function should be designed in order to obtain good driver acceptance when both human and the system act in parallel as a shared control task. From the viewpoint of human-machine system, it is essential to investigate the shared control law for enhancing the collision avoidance performance while minimizing the conflicts between the control action of the driver and the system. This paper employs the steer-by-wire system in the experiment as it provides good robustness in vehicle dynamics control while the steering reaction torque characteristics can be designed independently. Based on the driving simulator experiment, the driver-vehicle interaction as well as the driving performance are discussed.

Keywords: Active Safety, Driver Assistance System, Shared Driving, Collision Avoidance.

1. INTRODUCTION

Today, based on a model of automation (Parasuraman et al., 2000), advanced driver assistance systems (ADAS) can be categorized into four classes: (a) perception enhancement, (b) arousing attention to potential risks, (c) setting off a warning, and (d) automatic safety control (Inagaki, 2006). ADAS are designed to complement driver capabilities for perception, cognition, action selection, and action implementation in a dynamic environment (Inagaki, 2008). In order to reduce the number of vehicle accidents, it is important to develop proactive safety technologies.

The target of this study is to develop the autonomous driving intelligence system which the driver is still in the control loop and has responsibility in driving. Moreover, when the assistance by autonomous driving technology is designed to act in parallel with the driver (Iwano et al., 2014), a dynamic balance of authority in vehicle control and responsibility between the driver and the driver assistance systems must be investigated, especially elderly drivers, in order to achieve good safety performance and driver acceptance.

Most of studies on vehicle automation focus on how to switch the authority in vehicle control between human and machine (Hayashi et al., 2012) while this research project focuses on how cooperative characteristics can be obtained by continuously assisting the driver. Haptic shared control of steering wheel as well as accelerator pedal is an important issue of shared control design that the human and the system work together simultaneously (Abbink et al., 2012, Mulder et al., 2010, Iwano et al., 2014). This paper investigates the shared control characteristics between the driver and the active steering control system for collision avoidance assistance by using the driving simulator reconstructing a pedestrian crash-relevant-event. The shared driving task ratio of steering torque between the human and the system is designed to obtain good collision avoidance performance with minimizing conflicts between the human and the system. The driving simulator experiment is conducted and the effect of the steering assistance system is discussed.

2. SHARED CONTROL DESIGN

2.1 Steer-by-wire System

Lateral control systems are classified according to whether they use (1) steering angle control or (2) steering torque control. Steering angle control provides superior robustness because the non-linearity of the steering system is compensated for a minor loop in the steering angle control

algorithm (Shimakage et al., 2002). However, the system does not allow driver's steering intervention (Shimakage et al., 2002). In contrast, steering torque control allows to some extent the driver's steering intervention because it does not include a minor loop for the steering angle (Shimakage et al., 2002). In this study, the steer-by-wire system is employed as there is no mechanical connection between the steering wheel and the front tyres, which can satisfy both the vehicle dynamics control performance based on steering angle control and the override performance based on steering torque control. Figure 1 shows a model of the steer-by-wire system.
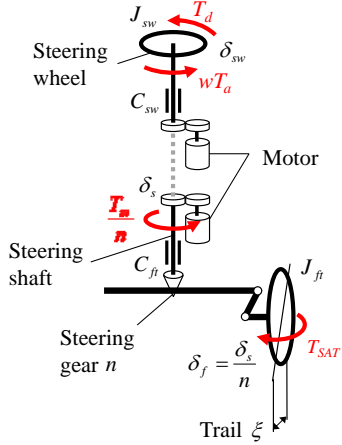
Fig.1 Steer-by-wire system.

In this study, the complicated power steering mechanism and the torsional stiffness of the steering are not considered. Moreover, the self-aligning torque is transferred from the front tyres to the steering shaft directly through the steering gear. Therefore, the equations of motion of the steer-by-wire system model on the steering wheel and the front tyres can be respectively expressed as follows:

$$J_{sw}\ddot{\delta}_{sw} = -C_{sw}\dot{\delta}_{sw} - T_r + wT_a \tag{1}$$

$$J_{fw}\ddot{\delta}_f = -C_{fw}n^2\dot{\delta}_f - T_{SAT} + T_m \tag{2}$$

where, J_{sw} is the moment of inertia of the steering wheel, C_{sw} is the viscous damping coefficient of steering wheel, J_{fw} is the moment of inertia of the front wheel, C_{fw} is the viscous damping coefficient of front wheel, ξ is the trail of front tyre, n is the overall steering gear ratio, δ_{sw} is the steering wheel angle δ_f is the front tyre angle, w denotes the weighting coefficient, T_a indicates the active steering assistance torque, T_r is the artificial reaction torque on the steering wheel, T_{SAT} is the self-aligning torque, and T_m is control input of front wheel.

Here, the self-aligning torque is transferred to the steering wheel in the general steering system. However in the steer-by-wire system, the self-aligning torque is not transferred to the steering wheel since there is not mechanical connection. Therefore, in this study, the reaction torque is expressed as follows:

$$T_r = c_r\dot{\delta}_{sw} + k_r\delta_{sw} \tag{3}$$

where, c_r indicates the viscous damping coefficient for simulating reaction torque and k_r indicates the spring constant for generating the artificial reaction torque equivalent to SAT.

2.2 Collision Avoidance Steering Assistance System

Figure 2 shows the block diagram of collision avoidance steering assistance system by using steer-by-wire configuration. If the system detects an obstacle ahead and finds that the collision cannot be avoided by only braking, the assistance system actively changes its driving lane to avoid collision with the obstacle by steering control, based on the assumption that there is no object existing in the adjacent lane. In this system, the front tyre angle is controlled based on the driver's input torque and the system's assisting torque as the shared control that the human and the system work together simultaneously.
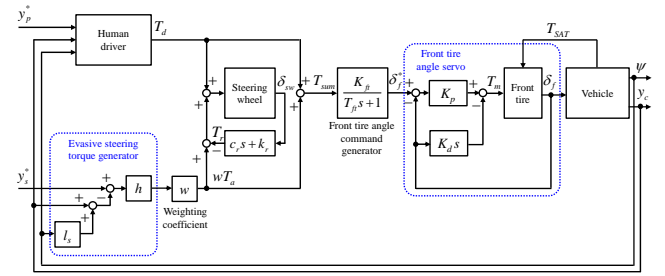

Fig.2 Block diagram of collision avoidance steering control.

2.3 Evasive Steering Torque Generator

The assistance torque is calculated based on the preview control, as similar to the general 1st order look-ahead driver model based on an assumption that the delay of the environment perception is negligible. Therefore, the look-ahead driver model with the steering torque input can be expressed as follows:

$$T_a = h\left(y_s^* - y_s\right) = h\left\{y_s^* - \left(y_c + l_s\psi\right)\right\} \tag{4}$$

where, y_s^* is the desired lateral position at the preview point, y_s is the predicted lateral position of the vehicle at the preview point, h denotes the corrective steering torque gain, y_c is the lateral position of center of gravity, ψ is the yaw angle, and l_s indicates the preview distance.

2.4 Shared Driving Law

The shared driving law can be expressed as follows:

$$T_{sum} = wT_a + (1-w)T_d \tag{5}$$

where, T_d is the driver's input steering torque. Here, the weighting coefficient w is a constant value and is variable between the ranges from 0 to 1. When the w is zero, it refers to the manual driving. On the other hand, for example, when the w is 0.5, it refers to the shared driving. Moreover, when

the w is one, it refers to the autonomous driving. Therefore, the w means the workload ratio for both the human and the system. After determining the intervention level of steering assistance, the desired front tyre angle is calculated. To simplify the collision avoidance steering assistance system design, by approximating that the relationship between the steering torque and the lateral acceleration as the first order lag system, the relationship between the steering torque and the lateral acceleration can be expressed as follows:

$$\ddot{y}_c = \frac{K_{acc}}{T_{acc}s+1}T_{sum} \tag{6}$$

where, K_{acc} is the lateral acceleration gain, and T_{acc} is the lateral acceleration time constant.

Here, to reduce the order of the controller as far as possible, by assuming that the response lag of vehicle is negligible in the target frequency range of steering manoeuvre, the relationship between the steering torque and the desired front tyre angle $\delta_f{}^*$ can be expressed as follows:

$$\delta_f^* = \left(1+KV^2\right)\frac{l}{V^2}\ddot{y}_c = \left(1+KV^2\right)\frac{l}{V^2}\cdot\frac{K_{acc}}{T_{acc}s+1}T_{sum} \tag{7}$$

where, K is the stability factor, and V is the vehicle velocity.

2.5 Front Tyre Angle Controller

Figure 3 shows the block diagram of steering angle servo control system.
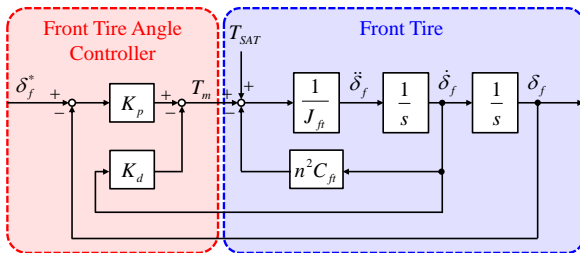
Fig.3 Block diagram of steering angle servo.

The front steering control law can be expressed as the following state feedback control law.

$$T_m = K_p\left(\delta_f^* - \delta_f\right) - K_d\dot{\delta}_f \tag{8}$$

where, K_p is the feedback gain of front wheel angle, K_d is the feedback gain of front wheel angular velocity. The transfer function of front tyre steering angle closed-loop system can be expressed as follows:

$$\frac{\delta_f}{\delta_f^*} = \frac{K_p/J_{fw}}{s^2 + \left\{\left(n^2C_{fw}+K_d\right)/J_{fw}\right\}s + K_p/J_{fw}}$$
$$= \frac{\omega_n^2}{s^2 + 2\zeta\omega_n s + \omega_n^2} \tag{9}$$

where, ω_n is the natural angular frequency, ζ is the damping ratio. From equation (9), the transfer function becomes the second-order transfer function. Therefore, by comparing the

coefficient in equation (9), the feedback gains K_p and K_d can be expressed as follows:

$$K_p = \omega_n^2 J_{fw} \tag{10}$$

$$K_d = 2\zeta\omega_n J_{fw} - n^2 C_{fw} \tag{11}$$

3. DRIVING SIMULATOR EXPERIMENT

The experiment was conducted to evaluate the shared driving characteristic between the drivers and the collision avoidance assistance system using the steer-by-wire system by using driving simulator. The experiment was conducted with the approval of the ethical committee at the Tokyo University of Agriculture and Technology.

3.1 Apparatus

This experiment was conducted with TUAT driving simulator. The driving simulator consists of a host computer, a visual and an audio system, a steering system and a motion controller. The driving simulator was equipped with the same driver operational interfaces as real vehicle. The host computer calculated the vehicle behaviour based on the input of driver operational interfaces and consequently generated the driving screen images and conducted the motion cueing based on the calculated vehicle dynamics. In addition, any scene or traffic situation was reconstructed by setting the road environment and the traffic flow of other vehicles.
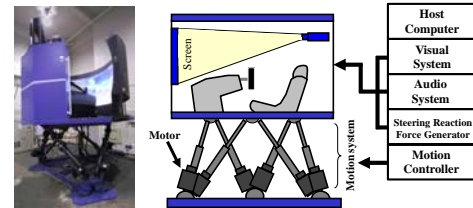

Fig. 4 TUAT driving simulator

3.2 Experimental Conditions

Seven participants (S1 – S7) as a young driver and ten participants (O1 – O10) as an elderly driver of 65 ages and older who drives daily participated in this experiment. The driving scenario is shown in Figure 5. The experiment was conducted under the condition that the vehicle was running at a constant speed of 60 km/h on a two-lane straight road and there was an obstacle which randomly darted out from a number of occlusions located on the left side of road.
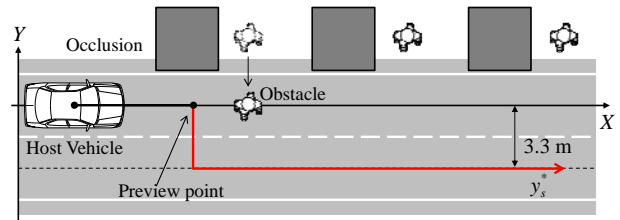

Fig.5 Experimental scenario.

The obstacle darted out at the front side of the vehicle at a time instant that the time-to-collision is lower than 2 seconds. The assistance system was activated at the same time instant of the obstacle appearance. At this condition setting, the vehicle cannot avoid the collision by only braking due to the limited braking capability. The subjects were instructed to avoid the obstacle and to change the lane by steering without brake pedal operation, in order to focus the steering behaviour of the drivers when the obstacle darted out, although common drivers might avoid the obstacle by implementing the brake pedal operation besides steering. Additionally, after avoidance, the subjects were instructed to keep on running in the adjacent lane. The experiment was conducted three times per a subject under the condition that the weighting coefficient w was changed at 0, 0.5, and 1. During the experiment, the subjects were not informed about the changed value of weighting coefficient w.

3.3 Experimental Results

Figures 6 and 7 are typical examples of the results for the lateral displacement and the steering torque respectively, and show the measurement data by two elderly drivers. The zero time instant indicates the time instant that the pedestrian appears from behind the occlusion.

(a) Subject O5

(b) Subject O10
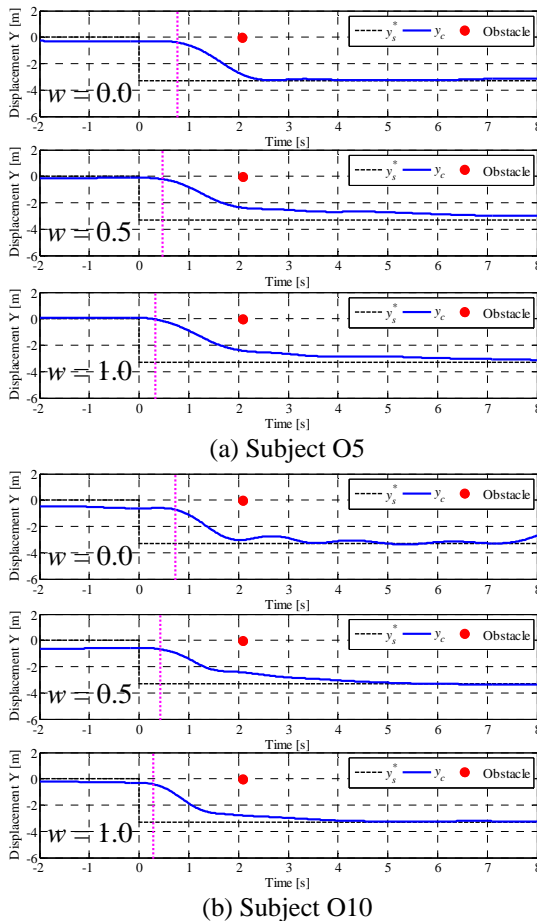
Fig. 6 Comparison of obstacle avoidance trajectory

As can be noticed from Figure 6 (a) and (b), when increasing the level of steering assist (increase the weighting coefficient

$w = 0$ to 1), the vehicle lateral movement to avoid the collision with pedestrian becomes more agile as the evasive manoeuvre reaction time to the pedestrian becomes shorter, indicated by the pink lines. After the steering avoidance manoeuvre, it was obvious that the vehicle stability was improved by adding the steering assist torque to the driver-vehicle system as shared control.

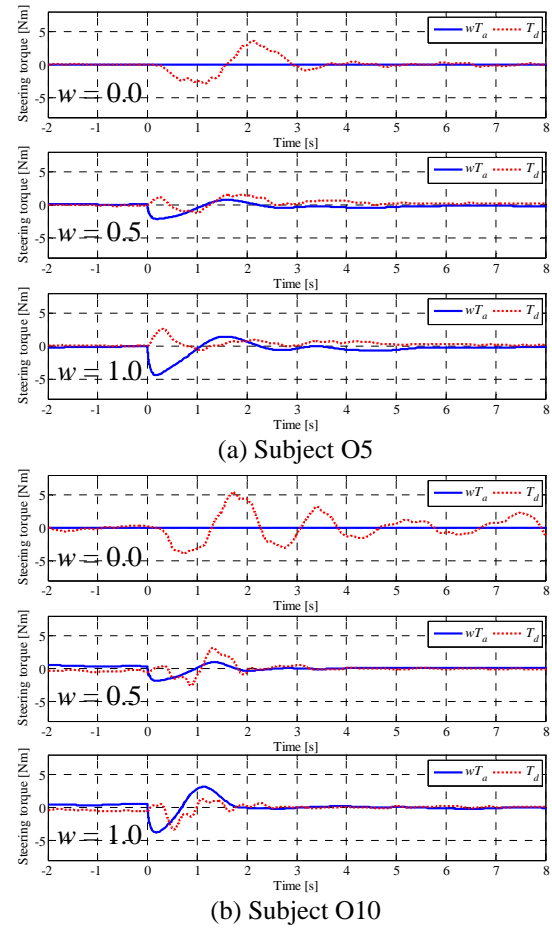(a) Subject O5

(b) Subject O10

Fig. 7 Driver and Assist torque during obstacle avoidance

As can be noticed from Figure 7 (a) and (b), in the case without steering assist (the weighting coefficient $w = 0$), the driver's input torque was large and fluctuating. In addition, Figure 7 (a) and (b) shows that there was the delay time in steering torque of the elderly driver. On the other hand, when the steering intervention was added (the weighting coefficient $w = 0.5$ or 1), the driver's input torque became significantly smaller. Also, we can confirm that the assistance system implemented the steering avoidance manoeuvre without delay. However, the driver's input steering torque was applied in the opposite direction with the assistance torque in the primary evasive steering manoeuve phase. The conflicts between the driver and the system occurred since the assistance system implemented the steering avoidance manoeuvre earlier than the driver as there is a certain reaction time from when the drivers recognize the pedestrian until the driver steer. As the result, the drivers have tendency to dampen the steering wheel movement to keep the vehicle go straight until the driver reacts to the pedestrian appearance and then takes the steering avoidance manoeuvre. After the system's steering avoidance manoeuvre, we can confirm

from Figure 7 (b) that the elderly driver O10 input the torque on steering wheel so that he/she was derived by the assistance system. In contrast, when the weighting coefficient w was 0.5 or 1, we can confirm from Figure 7 (a) that the elderly driver O5 did not implement the steering action actively to avoid the pedestrian.

<div align="center">4. DISCUSSIONS</div>

4.1 Avoidance Performance

This measure was evaluated as the delay time from when the pedestrian appeared from behind the occlusion until the vehicle initiated to move the desired lateral position. As delay time becomes short, it means that the vehicle could avoid the pedestrian as well as maintain the time margin enough to cope with any given situation. In this paper, the delay time τ is defined as the time from when the pedestrian appeared until the vehicle's lateral position moved 0.1 m toward the desired lateral position. Figure 8 shows the delay time per the elderly driver and the mean value and the standard deviation for the delay time τ. It is clear that it is possible to shorten the avoidance delay by increasing the weighting coefficient w.
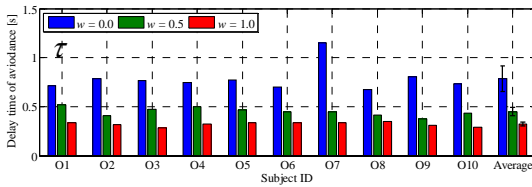
Fig. 8 Delay time of avoidance of elderly drivers

4.2 Vehicle Stability Performance

This measure was evaluated as integral of squared yaw rate during the time period of 10 seconds after the vehicle has passed the pedestrian. As the value is small, it means that the vehicle's lateral fluctuation decreases and the vehicle stability improves. Figure 8 shows the integral of squared yaw rate per the elderly driver and the mean value and the standard deviation for the integral of squared yaw rate. It is clear from Figure 9 that it is possible to decrease the lateral fluctuation of the vehicle by the system's assist. It is assumed that to decrease the vehicle lateral fluctuation is the result which the elderly driver's steering delay was compensated and the driver's steering action was derived appropriately toward the desired trajectory.
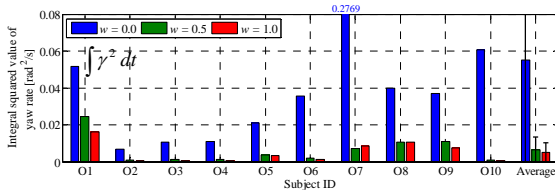

Fig. 9 Integral of squared yaw rate as a stability index

4.3 Driver's Workload and Steering Feeling

This measure was evaluated as integral of squared steering torque as steering effort of elderly driver during the time period of 10 seconds after the pedestrian appeared. As the value is small, it means that the driver's workload reduced by the system assistance torque. Figure 10 shows the integral of squared steering torque per the elderly driver and the mean value and the standard deviation for the integral of squared steering torque. It is clear from Figure 10 that the elderly driver's workload reduced by the system's assist.
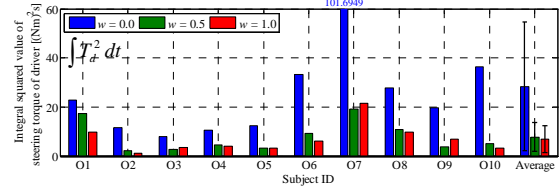

Fig. 10 Integral of squared steering torque as steering effort

Next, the steering feeling of the driver in shared control is discussed. The steering feeling was evaluated by using the Lissajous diagram for steering torque versus yaw rate, as shown in Figure 11. The areas of the second and fourth quadrants mean that the yaw rate occurs in the opposite direction with the driver's input torque, and the linear relationship between both variables means good manoeuvrability of the vehicle. In general, the Lissajous diagram has a hysteresis waveform because the yaw rate occurs in the same direction for the steering torque with the delay. When the weighting coefficient w as the steering assistance level is at 0.5, the Lissajous diagram appears to the linear relationship between both variables as compared with the weighting coefficient w is at 0. Therefore, it means that the driver can be steer with a smaller torque and can be recognize the steering feeling like the vehicle response is fast by the system's assist. On the other hand, when the steering assistance level is strong (w=1), the yaw rate becomes nonlinear with respect to the steering torque which means it is more difficult to control the vehicle. This reveals that the assistance level must be compromised to achieve good avoidance performance and good manoeuvrability.
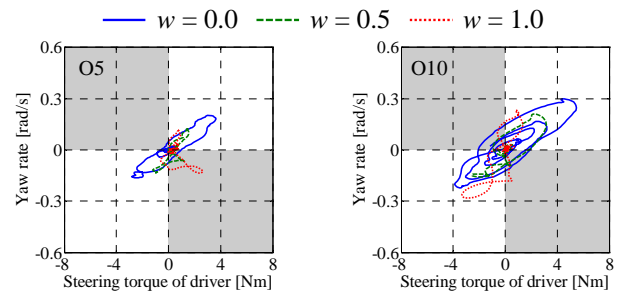

Fig. 11 Lissajous diagram for steering torque and yaw rate of subjects O5 and O10

4.4 Change of Driver Steering Characteristics

This subsection is described how the steering characteristics of the driver change by the assistance torque. Assuming that the driver takes the steering action as a preview-predictor

model, we conducted the parameter identification based on the minimization problem of non-linear functions. In this paper, the driver model is represented as

$$T_{dm} = \frac{1}{T_n s + 1} \left[He^{-\tau_d s} \left\{ y_s^* - \left(y_c + T_p V\psi \right) - y_{offset} \right\} + K_h w T_a \right] \quad (12)$$

where, y_{offset} is the lateral offset value, K_h is the haptic gain, and it means that the driver input the torque on the steering wheel so that he/she is led toward appreciate direction when the haptic gain K_h is at between 0 and 1. On the other hand, when the haptic gain K_h is at between -1 and 0, it means that the driver continued to hold the steering wheel. The identified parameters are the delay time τ_d, the first order lag time constant T_n, the steering gain H, the haptic gain K_h, and the lateral offset value y_{offset}. Figure 12 shows the identified steering gain H for elderly drivers. The steering gain H means that the driver can take a steering action with the smaller steering torque as the gain H is small. It appears from Figure 12 that the reducing effect of the steering gain was small when the system was active. On the other hand, Figure 13 shows the identified haptic gain K_h. There were many cases that the elderly driver haptic gain K_h is a negative value. It means that there were the conflicts between the driver and the system that he/she input the torque on the steering wheel toward the opposite direction for the appropriate vehicle trajectory. It is assumed that the elderly driver could not react quickly to the system's assist and maintained the current handle position because of age-related decreases in cognitive, visual, and physical functions. Therefore, from these results, it suggested that it is necessary to develop the driver-adaptive manner based shared control low which takes into account the driver steering characteristics.
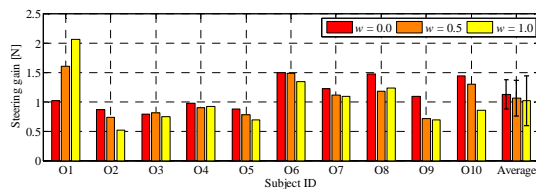

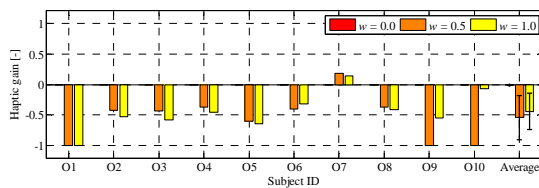Fig. 12 Identified steering gain (*H*) of all elderly drivers

Fig. 13 Identified haptic gain (*K_h*) of all elderly drivers

5. CONCLUSIONS

Haptic shared control of steering wheel as well as accelerator pedal is an important issue of shared control design. To investigate the shared control characteristics of driver assistance system, this paper examined the feasibility of using steer-by-wire in the collision avoidance by steering. The shared driving task ratio or intervention level of steering torque between the human and the system was designed to obtain good collision avoidance performance with

minimizing conflicts between the human and the system. The effect of steering control system with different intervention level of the steering assistance on the driving performance and manoeuvrability was investigated by using driving simulator. It was found that moderate steering intervention enhances avoidance performance and vehicle stability while maintain good vehicle manoeuvrability for elderly drivers. However, there was the conflict between the driver and the system that he/she input the torque on the steering wheel toward the opposite direction for the appropriate vehicle trajectory, since the elderly drivers could not react immediately to the system control intervention.

As the next step of the study, the adaptation of the intervention level depending on the driver state and the collision risk as well as the override characteristics will be studied.

REFERENCES

D. A. Abbink, M. Mulder and E. R. Boer, (2012). Haptic shared control: smoothly shifting control authority?, *Cognition, Technology, & Work,* vol. 14, no. 1, pp. 19-28.

K. Iwano, P. Raksincharoensak and M. Nagai, (2014). Study on Shared Driving Characteristics between Driver and Collision Avoidance Steering Control Using Driving Simulator, *Proc. the 12th International Symposium on Advanced Vehicle Control*, 6 pages.

M. Mulder, J. J. A. Pauwelussen, M. M. van Paassen, M. Mulder, D. A. Abbink, (2010). Active Deceleration Support in Car Following, *IEEE Transactions on Systems, Man and Cybernetics, Part A: Systems and Humans*, Vol .40, No. 6, pp. 1271-1284.

M. Shimakage, S. Satoh, K. Uenuma and H. Mouri, (2002). Design of lane-keeping control with steering torque input, *JSAE Review*, vol. 23, no. 3, pp. 317-323.

R. Parasuraman, T. B. Sheridan and C. D. Wickens, (2000). A model for types and levels of human interaction with automation, *IEEE Transactions of Systems, Man, and Cybernetics*, vol. 30, no. 3, pp. 286-297.

R. Hayashi, J. Isogai, P. Raksincharoensak and M. Nagai, (2012). Autonomous Collision Avoidance System by Combined Control of Steering and Braking using Geometrically-Optimized Vehicular Trajectory, *Vehicle System Dynamics*, Vol. 50, pp. 151-168.

T. Inagaki, (2006). Design of human-machine interactions in light of domain-dependence of human-centered automation, *Cognition, Technology & Work*, vol. 8, no. 3, pp. 161-167.

T. Inagaki, (2008). Smart collaborations between humans and machines with mutual understanding, *Annual Reviews in Control*, vol. 32, pp. 253-261.

A Lane-Change Gap Acceptance Scenario Developed for Heavy Vehicle Active Safety Assessment: A Driving Simulator Study

Jesper Sandin*. Bruno Augusto*
Peter Nilsson**, Leo Laine**

*The Swedish National Road and Transport Research Institute (VTI), Gothenburg, Sweden.
(Tel: +46 31 750 2610; e-mail: jesper.sandin@vti.se).
** Volvo Group Trucks Technology, Gothenburg, Sweden.
(Tel: +46 31 3234752; e-mail: peter.q.nilsson@volvo.com).

Abstract: The aims of this study were to develop a lane-change scenario for driving simulators in order to analyse the characteristics of lane-change manoeuvres performed with heavy vehicles. The scenario was set up based on information from lane-change accidents and on-road lane-change observations. The gap acceptance scenario consisted of two consecutive lane changes were the intention was to study truck drivers' accepted gap between two vehicles in the adjacent right lane, at the initiation of each lane change. An experiment was conducted with 18 truck drivers in a full-motion driving simulator with implemented high fidelity models of an 80tonnes and 32m long vehicle combination and a 40tonnes and 22m tractor semi-trailer. The results showed no statistically significant difference in the accepted gaps to the lead and lag vehicles in the target lane. For both heavy vehicles, the overall average lead gap and lag gap was estimated to 0.85s and 0.83s respectively, at the average velocity of 17.3m/s. The difference in lane-change duration for the two vehicles was statistically significant and estimated to an average of 8.7s for the tractor semi-trailer, and 10.5s for the A-double. The conclusion from the present study is that the drivers performed the lane changes equally well with the tractor semi-trailer and the long vehicle combination. There were no major differences between the manoeuvres other than the duration times, which can be justified by the difference in vehicle length. Future studies are able to use this scenario as a non-critical reference to more critical events in the development and assessment of active safety functionality and automated driving systems.

Keywords: Higher Capacity Vehicles, HCV, High Capacity Transport, HCT, LCV, Articulated vehicles, Merge lane, Rearward amplification

1. INTRODUCTION

Higher Capacity Vehicles (HCVs) are road transport vehicles with weights and/or dimensions outside that permitted in conventional regulation. HCVs are expected to increase transport and energy efficiency and thereby decrease costs as well as carbon dioxide emissions (OECD 2009). Since about two decades, Sweden and Finland allow a maximum length of 25.25m and a gross vehicle weight of 60tonnes within the Europe and Modular System (EMS). The standard of heavy vehicles in the EU is 18.75m and 40tonnes.

In Sweden, an increasing number of different HCVs (+60tonnes/25.25m) are permitted for transport on designated roads. One of those is an A-double transporting goods between the cities Göteborg and Malmö. The A-double falls under the category of Long Combination Vehicles (LCVs). It consists of a 6x4 tractor unit followed by a three-axle semi-trailer, two-axle dolly and a three-axle semi-trailer unit. It is 32m long, and has a maximum allowed gross vehicle weight of 80tonnes.

There are concerns among researchers, politicians, stakeholders and the public that HCVs are more dangerous than conventional transport vehicles because of their larger size and/or weight (Grislis 2010). There is however a lack of information that can confirm or falsify several of these concerns.

Looking at the accident involvement of today's heavy vehicles, accident statistics from the US show that lane change/merging crashes are most frequent, closely followed by rear-end crashes (Blower and Kostyniuk 2007). Combinations-unit trucks (i.e. tractor-trailers) are more involved in lane-change crashes than passenger cars and single-unit trucks (Bie et al. 2013).

Regarding the accident involvement of heavy vehicles in Sweden, Sandin (2015) conducted a detailed analysis of around 10 500 Swedish police-reported accidents involving heavy vehicles during the years 2003-2013. The preliminary results indicate that the top three accident types are rear-end crashes (25%), single-vehicle crashes (18.6%), followed by lane-change crashes (16.2%). In about half of the lane-change crashes, the truck had changed lane towards the right and collided with a passenger car, which in the majority of cases had been obscured by the truck cabin according to the accident narratives. The vast majority of the lane-change crashes occured on multi-lane highways passing through larger cities (Sandin 2015).

When it comes to accidents one could assume that the increased vehicle length of an LCV might increase the risk at lane-change manoeuvres. Due to their size, LCVs require more space and may be more difficult to monitor for the driver when compared to a conventional heavy vehicle. In addition, the lateral stability of some LCVs is sensitive to the steering input (Kharrazi et al. 2015), which may require additional driver attention and space to execute a stable lane-change manoeuvre.

There is a general lack of on-road lane-change data for passenger cars as well as heavy vehicles. This represents an important limitation to studies that use these data to develop and evaluate driver assistance systems (Toledo and Zohar 2007). Based on real road observations on a multilane Interstate highway in the US, Toledo and Zohar (2007) modelled lane change actions with heavy vehicles. They found that heavy vehicles lane change duration ranged from 1.1s to 11.8s, with a Mean of 3.8s, Median of 2.9s and SD of 2.4s (no distinction between heavy vehicles were made). They also found that it takes on average about one sec longer to change lane to the right compared with the left. They suggested that this finding might be related to the dimensions of heavy vehicles, as the drivers have a relatively limited field-of-view to the right when compared with the left.

When it comes to LCVs, there is no quantitative lane-change data available. Nilsson et al (2014a) measured the lane-change with the aforementioned 32m A-double on a straight road section of a Swedish two-lane highway. The measurements were carried out with one driver, at four lane changes and with no traffic in the destination lane. The measured lane-change durations turned out to be 10s or longer in order to maintain lateral stability. For the sake of comparison, this duration is in the upper range of Toledo and Zohars (2007) observations.

Thus, the question to address is if lane-change manoeuvres are more challenging and even hazardous with LCVs, in the presence of other vehicles as well as in comparison with conventional heavy vehicles. A safe way to evaluate such issues is to take advantage of advanced moving-base driving simulators (Jansson et al., 2014). Conducting realistic experiments with heavy vehicles, and in particular LCVs, put great demands on the simulator performance and fidelity regarding the representation of vehicle dynamics.

The aims of this study were to develop a lane-change scenario for driving simulators in order to analyse the characteristics of lane-change manoeuvres performed with heavy vehicles.

2. METHOD

2.1 Development of gap-acceptance scenario

The setup of the gap-acceptance scenario was based on information from lane-change accidents (e.g. Sandin 2015) and on-road lane-change observations (Toledo and Zohar 2007). Hence, the scenario was developed with the intention to study truck drivers' accepted gap between two vehicles in the adjacent right lane, at the initiation of a lane change.

The gap-acceptance scenario consists of two consecutive lane changes. A lane change is initiated by the time the driver turns on the indicator. At this moment, the lead and lag vehicle on the lane to the right of the truck will start displacing in order to create a gap where the truck can fit (Fig. 1).

At the indicator onset in the first lane change, the lead vehicle travelling in front of the tractor will accelerate from a Time Headway (THW) of 0.4 in order to create a target THW of 2.3s between its rear and the front of the tractor. In the second lane change, the lead vehicle accelerates from a THW of 0.35 to a THW of 0.9s. The lag vehicle behind the truck will decelerate from a THW of 0.35 in the first lane change, and a THW of 0.7 in the second lane change, in order to generate a target THW of 3s between the rear of the truck to the front of the lag vehicle in both the first and second lane change (Table 1). The differences in THWs between the two lane changes were implemented for the purpose of studying lane-change maneuvers in slightly different conditions.

Once the truck crosses into the target lane, the lead vehicle will no longer track a THW as a means of controlling its displacement. The lead vehicle will instead set its speed to either the current speed of the truck plus 3.6km/h or 62km/h, whichever yields the lowest value. These speed settings for the lead vehicle was implemented to ensure that the truck driver would always drive as close as possible to the speed limit since the lead vehicle slowly creates some slack for the truck if the latter is driving slower than the intended speed.

In order to add some realism during the experiments, a number of additional surrounding vehicles were implemented that adjusted their relative position and speed to the simulated heavy vehicle.
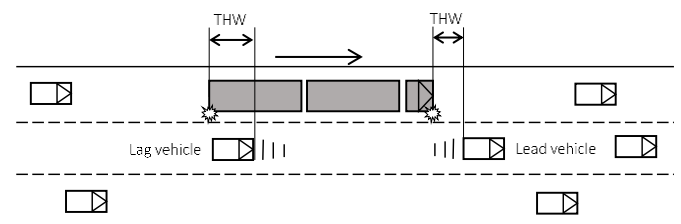

Fig. 1. Illustration of the first lane change (to the right) out of two in the gap-acceptance scenario. When the driver turns on the indicator, the lead and lag vehicle on the lane to the right will start displacing in order to create a gap where the truck can fit.

Table 1. The setting of the initial and target Time Headway (THW) for lead and lag vehicle during the first and second lane change

Lane change	Initial THW (s)		Target THW (s)	
	Lead vehicle	Lag vehicle	Lead vehicle	Lag vehicle
First	0.4	0.3	2.3	-3.0
Second	0.35	0.7	0.9	-3.0

2.2 Driving simulator and vehicle models

The study was conducted in the advanced moving-base driving simulator SimIV, located at VTI in Göteborg, Sweden. In SimIV, the heavy vehicle mock-up is a Volvo FH12, where the left and right hand side mirrors are replaced with LCD screens. The motion system, delivered by Bosch-Rexroth, combines the possibilities of a hexapod motion base with the extended motion envelope in x- and y-direction through a 5x5 m sled-system. The visual system gives the driver a 210-degree forward field of vision. Sound simulating the own vehicle and the directional sound of surrounding traffic is given via a 6.1 speaker system integrated in the truck cabin. An electric motor is installed on the steering-wheel column to present feedback torque to the driver (Jansson et al. 2014).

High fidelity models of a tractor semi-trailer and a 32m A-double were used to emulate the vehicle dynamics. The tractor (two axles) and a semi-trailer had a combined length of roughly 22m and weight of 40tonnes. The A-double consisted of a tractor (three axles) and three towed units in the following order – semi-trailer, dolly and semi-trailer, for a total length of 32m and weight of 80tonnes. See Nilsson et al (2014b) for more details of the A-double model. The performance of both vehicle models was validated against real world measurements. To improve the realism further, the motion cues generated by the driving simulator were tuned with the help of professional test drivers.

2.3 Experiment setup

The simulator experiment took place on three-lane road sections passing through a virtual version of Göteborg. The experiment was divided in two parts: one training part and one part with the gap-acceptance scenario. The training part consisted of two braking exercises and three single lane-change manoeuvres. The first two lane change manoeuvres were towards the right and the last was towards the left. The lane changes were guided with cones, which flew up if they were hit. The purpose of the training was for the driver to get a sense of the vehicle dynamics of the tractor semitrailer and the A-double in the simulator. The exact same training manoeuvres were conducted with both vehicles. After the training, there was a short break and a questionnaire regarding vehicle handling was given to the drivers.

After the training, the driver's task was to enter a three-lane road section and subsequently reach an exit ramp towards another highway. The three-lane road section was entered in the leftmost lane, so in order to reach the exit ramp the driver had to change lanes two times in accordance with the scenario. The total distance of the road section is 2.3km with a driving time of 2min at the speed limit 70km/h. This particular road section was selected as it has frequent lane-change crashes involving heavy vehicles (Sandin 2015). The intention was also to make the two consecutive lane changes more challenging when they had to be carried out on a limited distance. Upon completing the driving task, the drivers were asked to fill in questionnaires about their experience of the scenarios, assessment of scenario hazardousness and their own performance.

The study was a within-subject design, i.e. all subjects drove both vehicle types through the experiment setup. All subjects started with the tractor semi-trailer.

2.4 Data collection

Simulator data were logged to accurately represent driver manoeuvres, position and speed of the heavy vehicle as well as information of surrounding traffic relative to the simulated heavy vehicle. The drivers were asked to fill in questionnaires about truck handling, as well as their experience of the scenarios, e.g. Self-Assessment Manikin (SAM) (Bradley and Lang 1994), assessment of scenario hazardousness and their own performance, as well as simulator realism.

2.5 Subjects

Subjects were recruited from VTIs database of professional truck drivers, through advertisement, and via personal contacts.

In total 18 subjects with truck license participated in the study, whereof 15 were, or had been, working as professional truck drivers. Two subjects were Volvo GTT employees and two subjects were truck-driving instructors. The subjects included 17 men and one woman with an average of 46.3 years of age (SD = 10.5 years) with an annual average mileage of 56 000km, ranging from 10 to 200 000km.

Four of the subjects regularly drove tractor semi-trailer, nine subjects drove rigid trucks and eight subjects drove truck and trailers. None of the subjects had driven an A-double or any other long vehicle combination.

3. ANALYSIS

The simulator log data were analysed around the time of the lane changes. The following variables were retrieved for each lane change:

- The lead and lag gap measured as Time Headway (THW) at lane change initiation.
- The heavy vehicles' velocities at lane change initiation and completion.
- The duration between the lane change initiation and completion.

According to Toledo and Zohar (2007) and Bie et al. (2013) the initiation and completions points of a lane change should be defined as the time instances when the lateral movement of the subject vehicle begins and ends, respectively. The lane-change duration is the time lapse between its initiation and completion (Fig. 2). Accordingly, in the present study, the initiation and completion of the lane change was measured as the deviation of heading relative to the road, modified for the last axle.

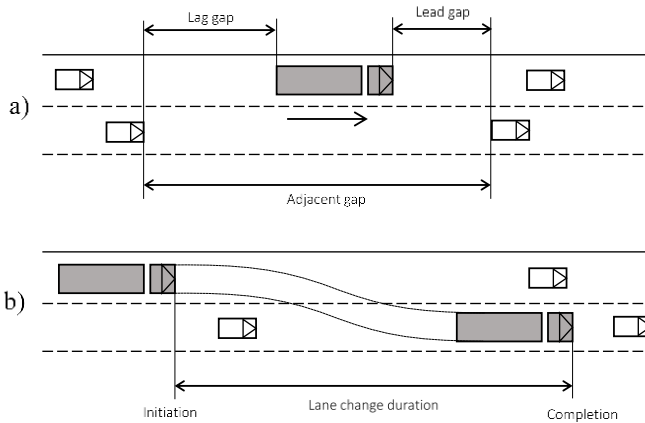Selected questions from questionnaires that were relevant for this study were compiled and analysed.

Fig. 2. a) Gap acceptance in a lane change. Both the lead gap and the lag gap have to be accepted. b) Initiation and completion of a lane change represented by the start and end time of the lateral movement respectively. The lane-change duration is the time lapse between its initiation and completion (based on Bie et al. 2013).

4. RESULTS

4.1 Lead and lag gaps

The following results are based on data from 17 drivers, as the data from one experiment session were corrupt.

Table 2 and 3 show the lead and lag gap respectively at the initiation of the first and second lane change, for the tractor semi-trailer (Semi) and the A-double (LCV). The lead and lag gap is measured as temporal time headway (THW) in sec as defined in Fig 1. No differences were found that were statistically significant between the first and second lane change carried out with the same vehicle, or within the two lane changes carried out with different vehicles.

With reference to Table 2 and the first lane change, the mean THWs for both vehicles (Semi = 0.8s and A-double = 0.93s) are within the lead vehicle's target THW of 2.3s as set for the first lane change in the scenario. In the second lane change, the mean THWs for both vehicles (Semi = 0.91s and A-double = 0.77s) are close to the lead vehicle's target THW of 0.9s as set for the second lane change. A measured THW above 0.9s indicates that, during the lane change, the driver first brakes and then steers, or brakes and steers at the same time, within a very short period. The max THWs for both vehicles (Semi = 1.5s and A-double = 1.37s) are both higher than 0.9s. A closer examination of the measured THWs reveals that the THW was higher than 0.9s in five instances for each vehicle, i.e. in 10 instances in total. This indicates that the drivers in these 10 instances braked and then steered, or braked and steered at the same time.

With reference to Table 3 and the first and second lane change, the mean THWs are all within the lag vehicles' target THW of -3.0s. It can be noted that three out of four max

THWs have small positive values, indicating that the driver in these instances initiated the lane change just before the lag vehicle was completely behind the last trailer.

Table 2. Lead gap at lane change initiation measured as temporal time headway (THW) between the front of truck to the rear of the lead vehicle.

Lane change	Vehicle	Lead gap THW at initiation (s)				
		Mean	Median	SD	Min	Max
First	Semi	0.8	0.54	0.69	-0.09	2.14
	LCV	0.93	0.92	0.45	0.18	1.67
Second	Semi	0.91	0.89	0.29	0.55	1.5
	LCV	0.77	0.73	0.38	0.2	1.37

Table 3. Lag gap at lane change initiation measured as temporal time headway (THW) between the rear of truck to the front of the lag vehicle.

Lane change	Vehicle	Lag gap THW at initiation (s)				
		Mean	Median	SD	Min	Max
First	Semi	-1.07	-1.07	0.68	-2.84	0.04
	LCV	-0.77	-0.76	0.46	-1.35	-0.06
Second	Semi	-0.81	-0.66	0.58	-2.1	0.38
	LCV	-0.67	-0.65	0.52	-1.61	0.16

4.2 Velocities at lane change initiation and completion

Table 4 shows the velocities at the initiation and completion associated with the first and second lane change, divided for the tractor semi-trailer (Semi) and the A-double (LCV). At the initiation of the first lane change, the velocities of the A-double (M = 15.3m/s) is statistically different from the other velocities. No other statistically significant differences were found.

Table 4. Velocity at lane change initiation and completion.

Lane change	Vehicle	Velocity at initiation (m/s)			Velocity at completion (m/s)		
		Mean	Median	SD	Mean	Median	SD
First	Semi	18.2	18.1	1.77	19.0	19.0	1.34
	LCV	15.3	14.7	2.30	17.7	17.8	2.25
Second	Semi	17.3	18.8	2.31	17.6	18.5	2.25
	LCV	17.4	17.3	1.78	17.5	17.9	2.23

4.3 Lane-change durations

Table 5 shows the lane change duration between its initiation and completion, measured as deviation of heading relative to the road, modified for the last axle.

There is a statistically significant difference in the lane change duration between the tractor semi-trailer (Semi) and

the A-double (LCV) in the first lane change (paired t(16) = 3.10, p = 0.01). There is also a notable difference in the lane change duration between the vehicles in the second lane change but which is not statistically different (paired t(16) = 2.08, p = 0.054). No other statistically significant differences were found.

Table 5. Duration of lane change between its initiation and completion.

Lane change	Vehicle	Lane change duration (s)				
		Mean	Median	SD	Min	Max
First	Semi	8.42	7.43	2.38	5.27	12.7
	LCV	10.4	10.1	2.42	5.41	14.9
Sec-ond	Semi	8.99	9.5	3.23	3.47	16.5
	LCV	10.6	10.5	1.96	7.85	16.3

4.4 Questionnaires

This section describes the results from the questionnaires, beginning with the drivers' experience of carrying out lane changes in the gap acceptance scenario with two different vehicles.

The ratings of the SAM scale for positive vs negative emotions were below average (M = 3.3; Median =3.0; SD = 1.9 on the scale from 1 = positive, to 9 = negative) associated with the tractor semi-trailer and the A-double (M = 2.89; Median = 2.0; SD = 2.0). The ratings of the active vs passive/calm emotions were above average (M = 5.8; Median =6.0; SD = 2.1 on the scale from 1 = positive, to 9 = negative) associated with the tractor semi-trailer and the A-double (M = 7.3; Median =7.5; SD = 1.6).

The experienced riskiness of the lane changes was rated as below average (M = 3.2; Median =3.0; SD = 1.8 on the scale from 1 = not risky at all, to 7 = very risky) associated with the tractor semi-trailer and the A-double (M = 2.89; Median =2.0; SD = 1.45).

The self-rated handling of the lane changes was just above average (M = 4.9; Median =5.0; SD = 1.3 on the scale from 1 = very bad, to 7 = very good) associated with the tractor semi-trailer and the A-double (M = 5.7; Median =6.0; SD = 0.75).

Continuing with the realism of the lane changes which was rated just above average (M = 4.6; Median =5.0; SD = 1.2 on the scale from 1 = not realistic at all, to 7 = very realistic). The general realism of driving in the simulator was rated above average (M = 5.4; Median =6.0; SD = 1.3 on the scale from 1 = not realistic at all, to 7 = very realistic). Some drivers mention a poor sense of speed and that the steering was too sensitive and not matching the movements of the simulated vehicle as in a real vehicle.

Finally, common driver comments reveal that the tractor semi-trailer is perceived as very sensitive to brake and steering input as well as wobbly in comparison with the A-double, which felt more like a real heavy vehicle. Some

drivers mentioned the lack of a red lamp placed on the rear corner of the last trailer (such a lamp does not exist on the simulated heavy vehicles). This red lamp is used for keeping track of the rear of the trailer when doing lane-changes and driving in curves. During the lane changes, the vehicles in the target lane were by some drivers perceived as being annoying and driving very slow.

5. DISCUSSION

The aims of this study were to develop a lane-change scenario for driving simulators in order to analyse the characteristics of lane-change manoeuvres performed with heavy vehicles.

The characteristics of a lane change were in the present study described by lead and lag gap measured as Time Headway (THW) at lane change initiation, the heavy vehicle velocity at lane change initiation and completion, and finally the lane-change duration. In the following sections, the measured values of these variables will be discussed.

Regarding the lead gap, the results showed that there were no significant differences for this gap between any of the vehicles or lane changes. Thus, the overall average lead gap is estimated to 0.85s. Nevertheless, in the scenario's second lane change, the lead vehicle's target THW was set to 0.9s. A closer examination of the measured lead gap in the second lane change revealed that the lead gap was higher than 0.9s in 10 instances in total. This indicates that the drivers in these 10 instances braked and then steered, or braked and steered at the same time. An analysis of the drivers' brake and steering input is required to confirm this.

As with the lead gap, there were no significant differences for the lag gap between any of the vehicles or lane changes. Thus, the overall average lead gap is estimated to 0.83s. In three instances, it was noted that the driver initiated a lane change just before the lag vehicle was completely behind the last trailer. This can possibly be explained in one of two ways. The first is that the drivers could not perceive the relative distance to the lag vehicle in the simulator's right side mirror. Moreover, as mentioned by some drivers, the lack of a red lamp placed on the rear corner of the last trailer, may have hampered this further. The other explanation is that the drivers perceived that the lag vehicle was decelerating, allowing for an early initiation of the lane change. A more thorough analysis would be required to clarify this.

It should be noted that the estimated accepted lead and lag gap of 0.85s and 0.83s respectively are only average values, which to some degree can be used for comparison with measurements from other studies and observations. In reality, the lead and lag gap can vary a great deal during the lane change, as they are dependent on the relative velocity between the heavy vehicle and the lead and lag vehicles (see e.g. Moridpour et al. 2010).

At the initiation of the first lane change, the A-double's average velocity (M = 15.3m/s) was significantly different from the velocities in the other three conditions. At the corresponding occasion, the tractor semi-trailer's average

velocity was somewhat higher (M = 18.2 m/s). One possible reason for this is that the drivers were more careful at the initiation of the first lane change with the tractor semi-trailer and the A-double as this was the first lane change with each respective vehicle. This reasoning is strengthened by the fact that the average velocities for both vehicles were around 17.3m/s in the second lane change, which will be the estimate for the average velocity at lane-change initiation.

When it comes to the lane-change duration, there was a statistically significant difference between the tractor semi-trailer and the A-double in the first lane change. There was also a tendency of statistical difference between the vehicles in the second lane change. Assuming that this difference exists in both lane changes, the overall average lane-change duration is estimated to 8.7s for the tractor semi-trailer, and 10.5s for the A-double. This is in line with Aghabayk et al. (2011) who observed that the time needed to complete a lane-change manoeuvre increased with the size of the subject vehicle on arterial roads and freeways. Their observations were however limited to heavy vehicles up to 12m in length. The lane-change durations in the present study are in the upper range of the durations estimated by Toledo and Zohar (2007) as ranging from 1.1s to 11.8s (M = 3.8s) for heavy vehicles. However, the authors made no distinction between heavy vehicles of different size. Thus, in conclusion, it is difficult to find observations of lane-change duration for vehicles that are in the same size-range as in the current study.

Yet, it is probable that the lane-change duration of the tractor-semitrailer is somewhat longer than would be the case in reality. One reason for this may be that the drivers drove the tractor semi-trailer more cautiously in the simulator because they, according to their comments, perceived the tractor semi-trailers as rather sensitive in lateral direction.

The A-double's estimated lane-change duration of 10.5s seems to be in accordance with expectations. The duration is in line with the real world measurements by Nilsson et al. (2014a), which were 10s or longer. A professional driver carried out the lane changes and the authors pointed out that the long lane-change durations were necessary in order to maintain lateral stability. The equivalence of the durations indicates that the drivers in the simulator took the vehicle dynamics, and in particular the lateral stability, into consideration when performing the lane changes. Such subtle vehicle dynamics are made possible in an advanced full-motion simulators with high-fidelity vehicle-models.

According to the questionnaires, the drivers found it easier to carry out the lane changes with the A-double in comparison with the tractor semi-trailer. Moreover, the drivers felt that the lane-changes involved a low risk, and the ratings of the SAM-scales show that their emotions during the lane changes were in the positive and calm direction. While the lane changes were performed easily by the drivers with both vehicles, the realism of the lane-changes was rated just above average. The realism was to some extent restrained by the rather complicated scenario setup involving two consecutive lane changes. The general realism of driving in the simulator was rated higher.

6. CONCLUSIONS

In order to develop the safety of articulated heavy vehicles it is important to study drivers' gap acceptance during lane changes in the absence of critical events, as well as their avoidance manoeuvres when critical events occur. A safe way to evaluate such issues is to take advantage of advanced moving-base driving simulators. Conducting realistic experiments with heavy vehicles, and in particular long vehicle combinations, puts great demands on the simulator performance regarding the representation of vehicle dynamics.

The aims of this study were to develop a lane-change scenario for driving simulators in order to analyse the characteristics of lane-change manoeuvres performed with heavy vehicles. The conclusion from the present study is that the drivers performed the lane changes equally well with the 22m tractor semi-trailer and the 32m A-double. There were no major differences between the manoeuvres other than the duration times, which can be justified by the difference in vehicle length.

Future studies are able to use this scenario as a non-critical reference to more critical events in the development and assessment of active safety functionality and automated driving systems, with the aim to reach high driver acceptance.

ACKNOWLEDGEMENTS

REFERENCES

Aghabayk, K., Moridpour, S., Young, W., Sarvi, M., and Wang, Y. B. (2011). Comparing heavy vehicle and passenger car lane-changing maneuvers on arterial roads and freeways. *Transportation Research Record*: Journal of the Transportation Research Board, (2260), 94-101.

Bie, J., Roelofsen, M., Jin, L. and van Arem, B. (2013). Lane Change and Overtaking Collisions: Causes and Avoidance Techniques. In Naja, R., *Wireless Vehicular Networks for Car Collision Avoidance,* 143-187. Springer, New York.

Blower, D.F. and Kostyniuk, L.P. (2007). Strategies to Reduce CMV –involved Crashes, Fatalities and Injuries in Michigan, the University of Michigan Transportation Research Institute, Ann Arbor.

Bradley, M. M. and Lang., P. J. (1994). Measuring emotion: the self-assessment manikin and the semantic differential. *Journal of behavior therapy and experimental psychiatry,* 25(1), 49-59.

Grislis, A. (2010). Longer combination vehicles and road safety. *Transport,* 25(3), 226-343.

Jansson, J., Sandin, J., Augusto, B., Fischer, M., Blissing, B. and Källgren, L. (2014). Design and performance of the VTI Sim IV, Driving Simulation Conference 2014, Paris, France.

Kharrazi, S., Karlsson, R., Sandin, J. and Aurell, J. (2015). Performance Based Standards for High Capacity Transports in Sweden FIFFI project 2013-03881 – Report 1, Review of existing regulations and literature. Swedish National Road and Transport Research Institute (VTI), Linköping.

Nilsson, P., Laine, L., Benderius, O. and Jacobson, B. (2014a). A Driver Model Using Optic Information for Longitudinal and Lateral Control of a Long Vehicle Combination, IEEE 17th International Conference on Intelligent Transportation Systems (ITSC), October 8-11, 2014. Qingdao, China, 1456-1461.

Nilsson, P., Laine, L. and Jacobson, B. (2014b). Performance characteristics for automated driving of long heavy vehicle combinations evaluated in motion simulator, 2014 IEEE Intelligent Vehicles Symposium, 2014, Dearborn, Michigan, USA.

Moridpour, S., Rose, G., and Sarvi, M. (2010). Effect of surrounding traffic characteristics on lane changing behavior. *Journal of Transportation Engineering*, 136(11), 973-985.

OECD (2009). Working Group on Heavy Vehicles: Regulatory, Operational and Productivity Improvements, Moving freight with better trucks improving safety, productivity and sustainability, Organization for Economic Cooperation and Development (OECD).

Sandin, J. (2015). Heavy-vehicle lane-change accidents identified and classified from police reported accidents. Unpublished working paper.

Toledo, T. and Zohar, D. (2007). Modeling Duration of Lane Changes. *Transportation Research Record*: Journal of the Transportation Research Board. No. 1999, 71–78.

Evaluation of a Run-off-Road Scenario for Driving Simulators used for the Assessment of Automatic Steering-Wheel Interventions

Jesper Sandin*, Bruno Augusto*
Regina Johansson**, Bo Svanberg**, Mats Petersson**

*The Swedish National Road and Transport Research Institute (VTI), Gothenburg, Sweden
(Tel: +46 31 750 2610; e-mail: jesper.sandin@vti.se).
**Volvo Cars Corporation, VCC Safety Centre, Gothenburg, Sweden
(Tel: +46 31 3253616; e-mail: mats.r.petersson@volvocars.com).

Abstract: The setup of a run-off-road scenario was based on the current knowledge about critical run-off-road situations and accidents. The scenario was initiated by a visual secondary task. During the task, an added clockwise yaw deviation, intended to create the run-off-road scenario, was presented visually but not by the vehicle dynamics or the lateral acceleration of the simulator's motion system. Results from two experiments show that the drivers frequently neutralised the yaw deviation because of their lack of full attention to the secondary task, the occasionally rough yaw deviation, or a combination of both. Because of the frequently neutralised yaw deviations, the number of steering-wheel interventions from an implemented system, intended to steer back into the lane in run-off-road situations, became limited in number. The system generated in total 14 steering-wheel interventions, ranging from torque levels of 0.3 to 3.7Nm. During ten of the interventions, the driver counteracted the torque with one hand. Nevertheless, the drivers that had experienced the interventions would like to have a system that could steer back to the lane when approaching the road edge, and accept that it takes control of the steering wheel. Further research on shared steering control is required so that driver responses to interventions does not neutralise the intended safety benefit of the system.

Keywords: Single-vehicle accidents, Lane departure, Crash avoidance, Crash Mitigation, Distraction, Attention, Muscle response, Reaction time, Advanced Driving Assistance Systems, Active safety,

1. INTRODUCTION

Single vehicle accidents lead to severe casualties and high economic costs. Common risk factors associated with these crashes are driver fatigue and distraction (Najm et al. 2007, McCarthy et al. 2009, Sandin and Ljung 2007)

Petersson et al. (2013) presented an analysis of around 70 critical, but non-accident, run-off-road situations identified in data from the EU project EuroFOT. The analysis showed that about 70% of the drivers had been engaged in a secondary task that involves both a visual and a manual component, typically leading to situations where the driver has the left hand on the steering wheel while looking and grasping after something with the right hand.

A crash avoidance system that, in emergency situations, prevents the vehicle from leaving the lane by controlling the vehicle heading through an automatic regulation of the steering-wheel angle could be an efficient countermeasure.

Crash mitigation systems that apply automatic braking of the vehicle have been available for some years. These systems are expected to be effective countermeasures, and drivers generally accept brake interventions (Coelingh et al. 2007, Blower 2014). In comparison, applying automatic steering

interventions is a greater challenge when it comes to driver interaction (Benderius 2014). Test track and simulator studies within the EU project interactIVe (Hesse et al. 2014) have shown that drivers tend to counteract automatic steering interventions in critical rear-end collision situations and avoidance situations. Because of the driver counteraction, low and medium level torque overlays had little effect, and high-level overlays (up to 9.9Nm) led to controllability issues. In the studies described by Hesse et al. (2014), the drivers looked forward in the absence of visual secondary tasks.

Thus, previous studies have shown that the drivers are likely to counteract an automatic steering-wheel intervention. One remaining question is if this result holds for situations where the driver is visually distracted from the main driving task and without knowing it ends up in potentially dangerous situations where a safety system can intervene.

For the sake of safety, critical run-off-road situations are suitable to test in advanced moving-base driving simulators. There may however be challenges in directing the simulated vehicle towards the road edge without the driver noticing it - even during a secondary task. Fischer et al. (2011) suggested an algorithm for an advanced head-on scenario where the simulator vehicle was deviated towards oncoming traffic in

the opposite lane risking a collision, during a visual secondary task. Variations of that scenario were used by Eriksson et al. (2013), but not with the purpose of studying the effect of automatic steering interventions.

Thus, the aims of this study were to i) develop a critical run-off-road scenario for driving simulators, and by means of two experiments ii) evaluate the scenario with respect to driver performance with and without the presence of automatic steering-interventions, and iii) study the driver response to steering-wheel interventions during the scenario.

2. METHOD

2.1 Driving simulator

The advanced moving-base simulator SimIV at VTI was used for the purpose of this study. The motion system of SimIV is composed by a hexapod mounted on a sledge for a total of 8 Degrees of Freedom (DOF). The simulator dome is designed to host a passenger vehicle cabin, which was used in the present study, or a truck cabin. The visual system is independent of the cabin choice and provides the driver with a field of view of almost 180deg (Jansson et al. 2014).

In SimIV, an electric motor is installed on the steering wheel column to present feedback torque to the driver. Five eye-tracker cameras are installed in the cabin for eye tracking.

2.2 Run-off-road scenario

The setup of the run-off-road scenario was based on the current knowledge about critical run-off-road situations and accidents. The timing of the vehicle position during the scenario was based on previously set requirements to trigger a steering-intervention system.

The run-off-road scenario was initiated by a visual secondary task during which an added yaw deviation was presented visually but not by the vehicle dynamics or the corresponding lateral acceleration of the simulator's motion system.

The visual secondary task was shown on a display positioned sufficiently far down and to the right of the driver's forward view to draw the driver's attention from the forward roadway. Thus, the driver was not supposed to notice the change in vehicle heading until s/he looks up from the display.

At the start of the secondary task, the drivers were prompted by a pre-recorded voice to read back a sequence of 6 numbers (randomised single digits between 1 and 9) appearing on the display. Each number was displayed for 0.3 seconds, with 0.2 seconds of blank screen in between numbers. The total time of the secondary task from the start of the pre-recorded voice until the display of the last number was 5.1s, whereof the visual reading task lasted 2.8s. In addition, the drivers had to hold their right index finger on the screen to activate the display and see the numbers. With this setup, they only had their left hand on the steering wheel during the yaw deviation.

The added yaw deviation was activated 3.1s after the start of the pre-recorded voice. Once active, the yaw of the simulated vehicle was changed in increments for a period of 2.0s. The yaw increments were computed in open loop assuming that the initial longitudinal speed was kept constant throughout the whole manoeuvre. With the previous assumption, by the end of the manoeuver the vehicle should have travelled to the right road line, have a relative heading to the road of 5deg and a value of lateral acceleration equal to zero (Fig. 1).
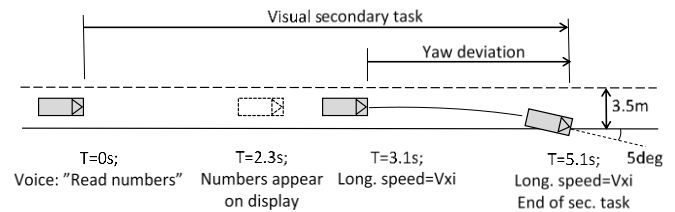

Fig. 1. Illustration of the run-off-road scenario where the added yaw deviation is initiated at T=3.1s during the visual secondary task.

2.3 Steering intervention system

A system was implemented in the simulator environment that could intervene in run-off-road situations. This system acted by regulating the vehicle heading through control of the steering wheel angle, with the purpose of returning the vehicle to the lane (Fig. 2). The generated steering-wheel angle and torque overlay depended on the vehicle's angle and position relative to the road edge. When active, the system only intervened when the vehicle was heading towards the left road edge, and not towards the road centre line.
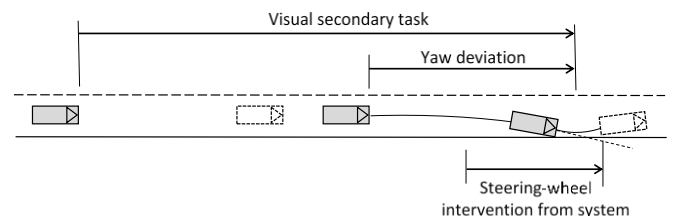

Fig. 2. Illustration of the effect of the steering intervention system relative to the run-off-road scenario (the position of intervention is approximate).

2.4 Experiments

In order to evaluate the run-off-road scenario with respect to driver performance with and without the presence of automatic steering-interventions, two groups of drivers were selected from two experiments with slightly different setup. Group 2 had the steering intervention system activated in the run-off-road-scenario, while Group 1 had not. Group 1 is in the present study intended as a reference in the evaluation of the run-off-road scenario without the presence of an intervention system.

Both experiments were divided in two parts; one training part and one part with repeated secondary tasks. The training part was exactly the same for Group 1 and 2. The purpose of the training was for the drivers to become acquainted with the simulated vehicle by doing braking and steering manoeuvres.

They also trained on the visual secondary task three times during standstill and three times while driving.

During the experiment, both groups experienced ten visual secondary tasks. The drivers in Group 1 were subjected to the yaw deviation Y_0 only during the last instance of the secondary task (Table 1). The reason for this is that the drivers in Group 1 were subjected to steering wheel interventions as a part of another study (indicated with an "I" in Table 1), just before this last event. For Group 2, four yaw deviations Y_1, Y_2, Y_3, and Y_4 was activated during secondary tasks number 4, 6, 8 and 10 (Table 1).

Table 1. Order of secondary tasks and events during the experiment for Group 1 and 2.

	Order of secondary tasks during experiment									
	1	2	3	4	5	6	7	8	9	10
Group 1	I			I	I		I		I	**Y_0**
Group 2				**SI, Y_1**		**SI, Y_2**		**SI, Y_3**		**SI, Y_4**

Events:
SI: steering intervention system active,
I: other automatic steering interventions (as part of another study)
Y: yaw deviation, where the index number indicates the repetition of yaw events that are analysed in the present study

The study took place on the outer track of a virtual version of the Swedish proving ground AstaZero (Fig. 3). The outer track is appr. 5.7km long and built as a typical Swedish rural road with normal road safety standards and with a lane width of 3.5m. Half of the rural road is designed for 70kph and half for 90kph. In several places there are scrub or broadleaf trees growing near the track.

The run-off-road- scenario was triggered by road position. It was required that the test sections would be straight and able to sustain 5s of driving at roughly 75kph with no major curvature changes. In this way, it was possible for the driver to feel comfortable while looking down at the secondary task, as well as effectively decouple the effects of road geometry from the test setup. Yaw repetition Y_0, Y_1 and Y_3 occurred on one and the same position, while and Y_2 and Y_4 occurred on another track section as illustrated in Fig. 3. Because of this setup, the experiment required several laps around the outer track.

The drivers were told that the purpose of the experiment was to study the effect of the visual secondary task on their steering behaviour and to evaluate a newly installed eye-tracker equipment. Therefore, the drivers were urged to look at the display during the whole secondary task and read as many of the six numbers as possible. They were told that the secondary task only appeared on straight road sections and that no other vehicles are on the test track. Therefore it was safe to do the secondary task. None of the driver groups were informed about the run-off-road scenario or any steering-wheel interventions. The drivers were instructed to drive 75-80kph. There were no other vehicles on the road during any

part of the experiment. The study took appr. 1.5 hours in total including introduction, training (12min), driving the experiment (17min), and answering questionnaires.
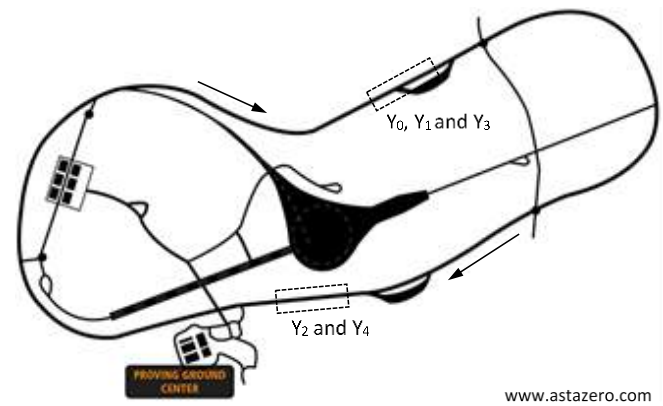
Fig. 3. Illustration of the AstaZero proving ground and the appr. positions of the run-off-road events and yaw repetitions. The arrows indicate the driving direction.

2.5 Subjects

The subjects were employees at Volvo Cars Corporation, recruited randomly from administrative and technical departments (none of them working with development associated with this study). The subjects in Group 1 included eight men and four women with an average of 42.4 years of age (SD = 5.4 years) and an average annual mileage of around 20 000km. The subjects in Group 2 included eight men and four women with an average of 43.7 years of age (SD = 9.5 years) and an annual mileage of between 20 000 and 30 000km.

3. ANALYSIS

The simulator log data were analysed in a time window of eight sec. around the time of the run-off-road scenario. Variables of interest for the present study were steering-wheel angle and torque applied to the steering wheel column by the driver and/or system intervention. The gaze direction vector was also analysed in order to determine if the drivers diverted their eyes back to the road during the visual secondary tasks. Selected questions from questionnaires that were relevant for this study were compiled and analysed.

4. RESULTS

Table 2 describes the characteristics of the steering-wheel interventions. There were in total 14 system interventions over all the yaw repetitions, ranging from torque levels of 0.3 to 3.7Nm. The driver counteracted the torque during ten of the 14 interventions. In these cases the torque was about 1Nm or above.

Fig. 4 shows that during the four yaw repetitions Y_0, Y_2, Y_3, and Y_4, almost 90% of the drivers neutralises the yaw deviation. More than 50% of those drivers look up at one or several occasions during the yaw deviation. The rest of the drivers neutralise the yaw deviation even when they are not looking up. This is in contrast to yaw repetition Y_1 , where

one third of the drivers in Group 2 look up and/or neutralise the yaw deviation.

Fig. 4 also shows steering-wheel interventions in almost half of the yaw deviations at repetition Y_1 and Y_3, which is more frequent than at Y_2 and Y_4.

Table 2. The number and characteristics of the steering-wheel interventions by system during the yaw deviations at repetition Y_1, Y_2, Y_3, and Y_4 for Group 2.

		Group 2 (n=12)			
Yaw repetition		Y_1	Y_2	Y_3	Y_4
Steering-wheel interventions (n)		5	1	6	2
Torque (Nm)	Range	0.7-3.7	3	0.4-2.1	0.3-3.2
	Average	2,06	-	1,08	-
	SD	1,07	-	0,62	-
Driver counteracts torque (n)		4	1	4	1
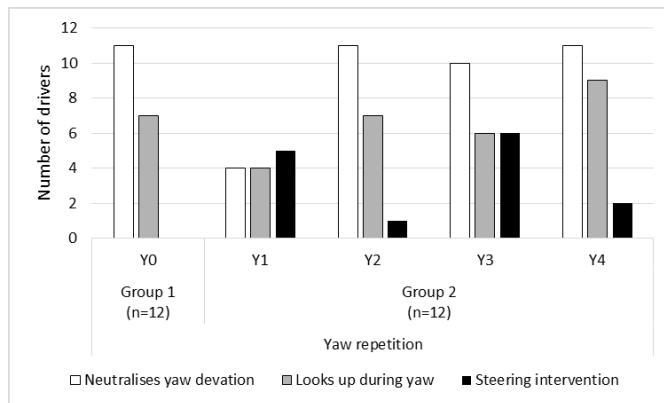
Fig. 4. The number of drivers in each group per yaw repetition that neutralised the yaw deviation (by turning left), looked up and/or had a system steering-intervention respectively during the yaw deviation.

The 14 interventions are associated with nine of the 12 drivers in Group 2. This means that three drivers never received interventions during any of the yaw repetitions. The questionnaire after driving revealed that four of those nine drivers had felt a steering-wheel torque during at least one of the yaw repetitions.

Moreover, the questionnaire reveals that 11 of the 12 drivers would like to have a system that could steer back to the lane when approaching the road edge. They would also accept that a system takes control of the steering wheel and vehicle in a critical situation. All of the 12 drivers had experienced unintentional, but non-accident, critical lane departures in real driving, whereof some report distraction as the cause and being upset or frightened as a result of the lane deviation.

The self-rated driving performance was just above average (M = 4.9; SD = 0.9 on the scale from 1 = very bad, to 7 = very good).

The realism of driving the simulator and test track compared to real driving was rated as just above average (M = 4.7, SD = 1.3 on the scale from 1 = not at all similar, to 7 = very similar). Some drivers mention a poor sense of speed and that the steering was too sensitive and not matching the movements of the simulated vehicle as in a real vehicle.

The self-rated stress during driving was below average (M = 2.8; SD = 1.5 on the scale from 1 = no, not stressed at all, to 7 = yes, very stressed).

How easy it was to stay in the lane while performing the secondary task was rated just below average (M = 3.2; SD = 1.1 on the scale from 1 = very difficult, to 7 = very easy).

5. DISCUSSION

Thus, the aims of this study were to i) develop a critical run-off-road scenario for driving simulators, and by means of two experiments ii) evaluate the scenario with respect to driver performance with and without the presence of automatic steering-interventions, and iii) study the driver response to steering-wheel interventions during the scenario.

The run-off-road scenario was initiated by a visual secondary task during which an added yaw deviation was presented visually but not by the vehicle dynamics or the lateral acceleration of the simulator's motion system.

Beginning with the driver responses to the steering-wheel interventions. The results show that there were in total 14 steering-wheel interventions over all 48 repetitions of the run-off-road scenario for the 12 drivers in Group 2, which had the steering intervention system active. The intervention ranged from torque levels of 0.3 to 3.7Nm. During ten of the interventions, the driver counteracted the torque while they were holding the steering wheel with one hand. The torque in these cases was about 1Nm or above. Four drivers reported that they had felt a steering-wheel intervention.

The number of interventions were fewer than anticipated because the drivers frequently neutralised the yaw deviations. Except for the first repetition (Y_1) for the drivers that had a safety system active (Group 2), almost 90% of the drivers neutralised the yaw deviation in the three remaining repetitions and the reference scenario, even in instances when they were not looking up. As a result, either the run-off-road scenarios did not become critical enough to activate a steering-wheel intervention from the system, or the intervention torques varied more than preferred in size and/or appearance.

There are two probable main causes for the frequently neutralised yaw deviation: the drivers' lack of full attention to the secondary task, the yaw deviation algorithm, or a combination of both. The yaw deviation was induced 0.8s after the moment the first number appeared on the screen, provided that the driver had activated the screen with their right index finger. When deemed necessary, the drivers were

urged to focus on the secondary task during training. This was generally not done during the experiment as the drivers seemed to direct their gaze towards the screen at the onset of the secondary task. The eye-tracker data show however that 50% of the drivers looked up one or several times before the end of the secondary task. This was difficult to observe directly during the experiments. According to the questionnaire, the drivers thought it was relatively difficult to stay in lane while performing the secondary task. This can further have been hampered while taking into account the poor feedback from steering and vehicle dynamics as commented by some drivers. As a consequence, they probably had to check their heading more frequently than what they would have in a real car. The poor sense of vehicle dynamics can to some extent be explained by the fact that the feedback gain from the motion system had to be reduced so that the induced yaw deviation would not be noticed physically.

For the sake of comparison, Eriksson et al. (2013) noticed in their study that the instructions to the driver, the design of the secondary task and the timing of the yaw deviation during the secondary task affected the outcome of their scenarios. They observed that drivers easily neutralised the induced yaw deviation when s/he did not perform the secondary task within about 0.2-0.3s after the task onset. Thus, they had to urge the drivers to initiate the task as quickly as possible during the course of the experiment. The authors further discussed the difficulty of introducing secondary tasks without giving any prioritization rules. In the present study, the drivers were told that the secondary task only appear on straight road sections and that no other vehicles are on the test track. Therefore it was safe to perform the secondary task. The drivers generally accepted this motivation.

The additional explanation to why the drivers looked up or was able to neutralise the yaw deviation, even when looking down, is the way the yaw deviation was implemented. On closer examination, the added yaw deviation became somewhat rough on a number of occasions. This led to the risk that the yaw deviation was perceived in the drivers' peripheral vision, or that they felt some small lateral acceleration from the simulator's motion system (although this was not intended). In order to study the effect of the intervention system, the yaw deviation was programmed to ensure the same final conditions for all drivers. This means that the yaw deviation algorithm was more sensitive to the starting conditions, creating a wider range of vehicle trajectories. Consequently, there was more variation in the yaw deviations between the drivers and repetitions, thus presenting some drivers with more rough and easy to perceive yaw deviations, and others with less noticeable ones.

For the evaluation of an active safety system, the choice of yaw deviation strategy would ideally be related to the way a system intervention is activated. However if the driver and/or the system is able to change the heading of the vehicle at all times, as was the case in the current study, the driver's attention has to be fully directed somewhere else than towards the critical event. This is a challenge as can be seen from the results from this study, and others. So perhaps the

first question one should raise when planning a test or experiment is whether it is primarily the system functionality that is being evaluated - or primarily the driver response. For example, if the driver response is of primary interest, then a more generic intervention profile would be preferred which does not require precise conditions for the activation of a certain level of intervention.

Regarding driver responses to steering-wheel interventions, previous studies have shown that drivers are likely to counteract an automatic steering-wheel intervention (e.g. Hesse et al. 2014). Benderius (2014) thoroughly examined the reaction to a sudden and unexpected torque disturbance in the steering wheel. Benderius found that the observed counteraction could be attributed to the stretch reflex, associated with the muscle *biceps brachii*, and an automatic subconscious cognitive action - a response that the author suggested is neurologically hard-wired.

Unlike the studies described by Hesse et al. (2014), the drivers were in the present study intended to be visually distracted from the main driving task under which an automatic steering intervention was initiated. Despite the limited number of interventions, the results indicate that the drivers did counteract the steering interventions, in line with previous research, even while holding the steering wheel with one hand. However, because the drivers neutralised the yaw deviation during the run-off-road scenario, one cannot draw too far-reaching conclusions. For the same reason, it was not possible to analyse the preventive safety effect of the system.

From the questionnaires it is interesting to see that that all of the 12 drivers in Group 2 had experienced unintentional, but non-accident, critical lane departures in real driving, whereof some report distraction as the cause of the departure, and being upset or frightened as a result. Moreover, 11 of the 12 drivers would like to have a system that could steer back to the lane when approaching the road edge. They would also accept that a system takes control of the steering wheel and vehicle in a critical situation.

Thus, there seems to be a contrast between drivers' conscious acceptance of steering-wheel interventions and what their muscles do, which is not controlled by will.

Steering-wheel interventions are probably an efficient measure in certain critical situations. However, further research on shared steering control is required so that driver responses to interventions does not neutralise the intended safety benefit of the system. The issue of shared steering control almost certainly needs to be handled also in higher levels of automation when driving conditions changes from normal to critical.

6. CONCLUSIONS

The run-off-road scenario evaluated in this study was initiated by a visual secondary task during which an added yaw deviation was presented visually but not by the vehicle dynamics or the lateral acceleration of the simulator's motion system. The results show that the yaw deviation was frequently neutralised because of the drivers' lack of full

attention to the secondary task, the occasionally rough yaw deviation, or a combination of both. Because of the frequently neutralised yaw deviations, the number of steering-wheel interventions from an implemented system became fewer than anticipated. The system generated in total 14 steering-wheel interventions, ranging from torque levels of 0.3 to 3.7Nm. During ten of the interventions, all with torque levels above 1Nm, the driver counteracted the torque while holding the steering wheel with one hand. Given these experiences, the first question one should raise when planning a test or experiment is whether it is primarily the system functionality that is being evaluated - or primarily the driver response.

ACKNOWLEDGEMENTS

REFERENCES

Benderius, O. (2014). *Modelling driver steering and neuromuscular behaviour*. Doctoral Thesis. Chalmers University of Technology, Göteborg.

Blower, D. (2014). Assessment of the effectiveness of advanced collision avoidance technologies. UMTRI-2014-3. The University of Michigan Transportation Research Institute, Ann Arbor.

Coelingh, E., Jakobsson, L., Lind, H., and Lindman, M. (2007). Collision Warning with Auto Brake - A Real-Life Safety Perspective. 20th International Technical Conference on the Enhanced Safety of Vehicles (ESV), Lyon, France.

Eriksson, L., Bolling, A., Alm, T., Andersson, A., Ahlström, C., Blissing, B. and Nilsson, G. (2013). Driver Acceptance and Performance with LDW and Rumble Strips Assistance in Unintentional Lane Departures. ViP publication 2013-4. Virtual Prototyping and Assessment by Simulation (ViP), Linköping.

Fischer, M., Sehammar, H., Ljung Aust, M., Nilsson, M., and Weiefors, H. (2011). Advanced driving simulators as a tool in early development phases of new active safety functions. *Advances in Transportation Studies,* Special Issue RSS2011, 171-182.

Hesse, T., Schieben, A., Heesen, M., Dziennus, M., Griesche, S. and Köster, F. (2013). Interaction design for automation initiated steering manoeuvres for collision avoidance. Institute of Transportation Systems, German Aerospace Center (DLR), Braunschweig, Germany.

Jansson, J., Sandin, J., Augusto, B., Fischer, M., Blissing, B. and Källgren, L. (2014). Design and performance of the VTI Sim IV, Driving Simulation Conference 2014, Paris, France.

McCarthy, M., Fagerlind, H., Heinig, I., Langner, T., Heinrich, S., Sulzberger, L. and Schaub, S. (2009). Preliminary Test Scenarios, Deliverable D1.1 of the EU FP7 project ASSESS, SST.2008.4.1.1: 233942.

Najm, W.G., Smith, J.D., and Yanagisawa, M. (2007), Pre-Crash Scenario Typology for Crash Avoidance Research, DOT HS 810 767. U.S. Department of Transportation Research and Innovative Technology Administration, Cambridge.

Petersson, M., Svanberg, B., and Johansson, R. (2013). Driver Reaction for Evaluating Autonomous Interventions − A Test-Track Method, Presented at the International Research Council on Biomechanics of Injury (IRCOBI) conference Sept 12, 2013.

Sandin, J., and Ljung Aust, M. (2007). Understanding the causation of single-vehicle crashes: a methodology for in-depth on-scene multidisciplinary case studies. *International Journal of Vehicle Safety,* 2 (3), 316-333.

Effect of Automatic Lane Changing on Driver's Behaviour Decision Process [⋆]

Kentarou Hitomi [*] **Hitoshi Terai** [**] **Hiroyuki Okuda** [***]
Takashi Bando [*] **Chiyomi Miyajima** [***]
Takatsugu Hirayama [***] **Yuki Shinohara** [*] **Masumi Egawa** [*]
Kazuya Takeda [***]

[*] *DENSO CORPORATION, 1-1, Showa cho, Kariya, Aichi, Japan
(e-mail: {kentarou_hitomi, takashi_bandou, yuki_shinohara,
masumi_egawa}@denso.co.jp).*
[**] *Kinki University, Fukuoka, Japan (e-mail: terai@fuk.kindai.ac.jp).*
[***] *Nagoya University, Aihci, Japan (e-mail:
h_okuda@nuem.nagoya-u.ac.jp, miyajima@nagoya-u.jp,
hirayama@is.nagoya-u.ac.jp, kazuya.takeda@nagoya-u.jp).*

Abstract: This paper analyses the driver's behavioural change about which the usage of automated driving system brings, focusing on the behaviours at changing lanes. Especially the relation between drivers' sensitivity to risk factors in surrounding environment and their gaze behaviour were analysed. We assumed, in this research, an automated driving of level 2 in the definition provided by NHTSA. At this level of automation, the drivers are required to monitor the driving situation and, when necessary, interrupt the system's automatic control and thereby recover the safety of the driving. We have conducted a simulation experiment with fifteen drivers, and compared their behaviours in two conditions; the conventional manual driving and the driving where automated driving system automatically changes lanes. By analysing collectively the risk factors at changing lanes, shift of each driver's sensitivity to risk at changing lanes were estimated. The experimental data shows the correlation between risk sensitivity and gaze behaviour.

Keywords: Driver Behavior Modeling, Cooperation Between Drivers and Assistance Systems, Driver Overdependence and Distrust on Assistance Systems

1. INTRODUCTION

Much research is currently being done on automated driving technologies, and vehicles with partially automated driving systems, capable of operating in limited environments, are already being marketed by automakers. Governments have also begun to modify traffic laws to accommodate automated driving on public roads [Smith (2014)].

Automated driving promises to improve driving safety, reduce driver stress and fatigue, and lower fuel consumption, but automation may have negative effects on driver performance which should also be evaluated. Studies have shown that drivers using advanced driver assistance systems (ADAS), such as adaptive cruise control (ACC), lane-keeping assist systems (LKAS), or automated driving systems, sometimes become overly dependent on these systems [Inagaki (2010); Abbink and Mulder (2008); NHTSA (July 2014)]. As National Highway Traffic Safety Administration (NHTSA) of the United States described in its policy statement concerning automated vehicles [NHTSA (May, 2013)], there are several levels of automation in

driving from level 0 (*No-Automation*) to level 4 (*Full Self-Driving Automation*). The problem of over-reliance matters especially in lower levels of automation, such as levels 1 (*Function-specific Automation*) and 2 (*Combined Function Automation*), the drivers are required to monitor the roadway and vehicle behaviour, and "to be available for control at all times and on short notice". Driver over-reliance on such automated systems may reduce driver awareness and decreased sensitivity, and may result in drivers being unable to respond quickly enough in the event of system failures. Negative adaptation on the part of drivers to automation needs to be further investigated in order to improve human-machine interfaces and avoid problems such as over-reliance, disuse and misuse. Therefore, the driver's behavioural change including the negative adaptation, about which the usage of automated driving system brings, needs to be understood, in order to avoid discordance among human, system, and the driving environment. Especially it needs to be analysed in relation to risk in driving situation.

The purpose of this study is the development of a possible method of detecting negative adaptation to an automated driving system. Most driver behaviour studies rely on the monitoring of vehicle operation signals by the driver to collect data for analysis, but since drivers are usually disengaged from vehicle operation during automated driving,

other methods of driver evaluation must be developed. When an automated system operating at a lower level of vehicle automation is engaged, drivers still need to keep their eyes on the road, even if they are not actively controlling the vehicle. Therefore, in this study we focus on driver gaze behaviour while driving as a means of measuring driver attentiveness in relation to risk in driving situation. Our analysis focuses on the driver's sensitivity to risks at changing lanes, such as the vehicle approaching from behind in the neighbouring lane, and its variation brought by the introduction of automatic lane changing system, assuming the automation of level 2 in definition provided by NHTSA.

We conducted a simulation experiment to collect drivers' behaviours under two conditions; conventional manual driving condition and automated driving condition. In the manual driving the driver manually operates the vehicle, and in the automated driving the simulated automated driving system autonomously operates the vehicle and changes lanes frequently. Also, the drivers are required, in automated driving, to monitor driving situation and to avoid risky situation by interrupting the system's driving operation when necessary. Based on the situations where the vehicle changed lanes and where it did not, decision boundaries on risk factors for lane-changing are estimated as the boundary of these situations using logistic regression. By comparing these boundaries between the two driving conditions, variation of decision boundary are estimated as the variation in sensitivity to risks brought about by the automated system. Furthermore the driver's gaze behaviour was recorded and modelled using Gaussian Mixture Model (GMM) and Hidden Markov Model (HMM). The variation of the gaze behaviour brought about by the automated system is evaluated using HMM built on the learnt GMM. It is shown that the quantified variation of gaze behaviour has high correlation to the variation to risk factors in the driving environment.

2. MODEL ASSUMPTION AND ANALYSIS TARGET

2.1 Decision model of the driver

We set the analysis target under following assumption on driver's behaviour model. It is reasonably assumed that the driver operates the vehicle keeping the risk of driving situation under certain risk level where he/she can handle the situation in safe. The risk of driving situation depends on the state of the vehicle. For example, when host vehicle is following its leading vehicle, the inter-vehicle distance to the leading vehicle, their velocities and accelerations are the dominant variables for representing the risk, and other variables such as those of vehicles in neighbouring lane are of little relevance. When host vehicle is changing lanes, in addition to the leading vehicle, such variables of vehicles in neighbouring lane are also substantial to the risk of driving situation. Those values contributes to each driver's subjective risk recognition via Time-To-Collision for instance, and the drivers' decision boundaries at which the driver's behaviour switches (e.g. whether to apply deceleration or not, whether to start changing lanes or not) are dependent on drivers [Mima et al. (2009)]. Each driver operates the vehicle keeping the risk of driving situation under subjective threshold.
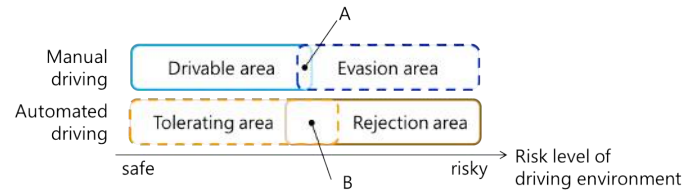
Fig. 1. Hypothetical model of driver's behaviour decision based on risk of driving environment, in manual driving and in automated driving. A & B indicates driver's decision transition area on risk level.
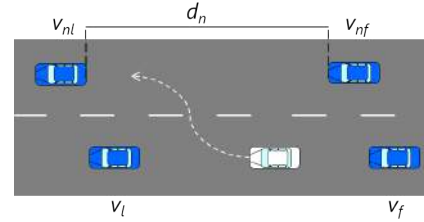
Fig. 2. The presumed risk factors in the surrounding situation at changing lanes.

Figure 1 shows our hypothetical model of driver's decision in relation to risk level of driving environment. In conventional manual driving where the driver him/herself operates the vehicle, the driver keeps the risk lower than certain level and avoid driving in riskier situation (*Drivable area* and *Evasion area*). In automated driving, the vehicle is operated by the automated driving system and the driver monitors the roadway and the vehicle system behaviour. If the driver is comfortable with the system behaviour, the driver tolerates the system's operation, and if the driver is uncomfortable with the system behaviour, the driver intervenes the operation of the system to reject the automated behaviour of the system (*Tolerating area* and *Rejection area*). In the case of lane changing, the driver changes lanes normally in *Drivable area* and intervenes in *Rejection area*.

2.2 Analysis target

In our experiment, the negative adaptation to the automated system of the driver is represented by the variation of the driver's decision boundary on the risks in the driving environment, for changing lanes. By estimating and comparing the decision boundaries in manual driving and automated driving, the variation in sensitivity to risk factors are evaluated as the shift of the decision boundaries, as the effect of introduction of automated driving system.

The presumed risk factors in our analysis in the surrounding situation at changing lanes are depicted in the Fig.2; the velocities of leading and following vehicles in current lane v_l, v_f, the velocities of leading and following vehicles in neighbouring lane v_{nl}, v_{nf}, and inter-vehicle distance of the destination of lane changing d_n. For a reason in implementation in our experiment, we further simplified and analysed the velocity difference between lanes $\delta v = (v_{nl} + v_{nf})/2 - (v_l + v_f)/2$ and d_n. The drivers' decision boundaries for changing lanes are estimated on those variables.

Fig. 3. A screenshot of a scenery projected in DS.

Fig. 4. Snapshot of the driving simulator equipments. Three eye-tracking device, Tobii X2-30 are placed on around the driving seat.
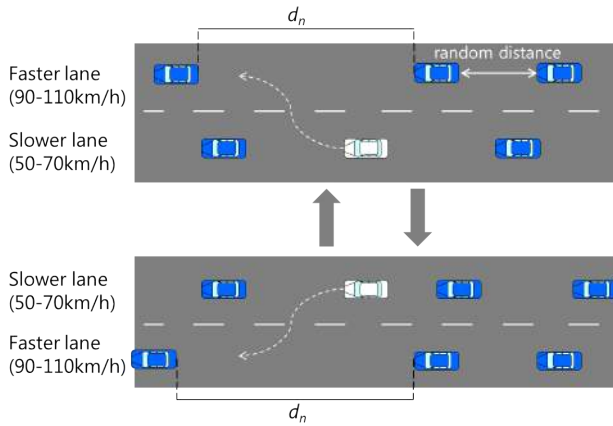

Fig. 5. The transition of situations in driving simulation; Faster lane and slower lane flips according to the host vehicle's driving lane.

Additionally, we investigated the proactive sign of variation of sensitivity to risk, into driver's appearance. A gaze behavioural feature which correlates to change in sensitivity to risk can be expected to be useful cue to detect the behavioural change.

3. EXPERIMENT SETUP

3.1 Simulator setting

In the experiment, we used a driving simulator to collect driving behaviour data. Figure 3 shows a scene in simulated driving, which is projected over the screens around the driver seat of the simulator. The simulation system is built on CarSim [Virtual Mechanics Corp. (2014)], a high-fidelity vehicle dynamics simulator. Figure 4 shows
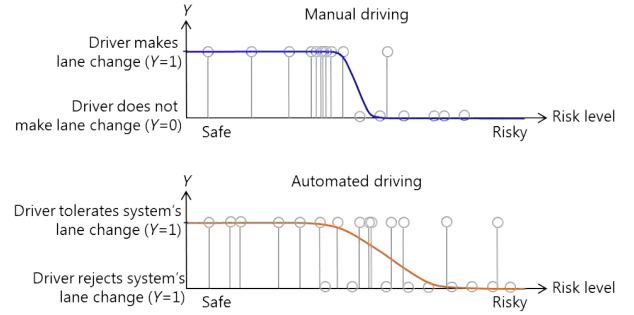
Fig. 6. negative adaptation image.

the used driving simulator with three eye trackers Tobii X2-30 (Tobii Technology (2014)) mounted on it. It has three screens which provide 180 degrees of front field of view, and the interior equipments around driver seat is the same as a real car. The steering wheel has torque feedback system which reflects the physical status of the vehicle in the simulation in real-time.

The simulated driving environment was implemented with straight two-lane highway in one direction and surrounding other cars (Fig.3 and 5). In each lane, surrounding vehicles travel at the same speed and never collide with each other. The lane in which host vehicle is driving is set to the "slower lane". The slower lane is relatively congested and surrounding vehicles in this lane travel at the speed selected randomly between 50 km/h and 70 km/h. The other lane is set to the "faster lane". The faster lane is relatively sparse and vehicles in this lane travel at the randomly-selected speed between 90 km/h and 110 km/h. In both lanes, inter-vehicle distances are randomly set at the distances between 30 m and 100 m. During 10 to 20 seconds after host vehicle's lane changing, the host vehicle can drive in the fast lane from the slow lane to the fast lane. After this period of time, the setting of both lanes are flipped; the velocity of vehicles in the fast lane gradually shifts into the velocity range of the slower lane, and vice versa. Therefore, the simulator forces the host vehicle to drive in the slower lane most of the time.

The simulation has two conditions; the manual driving and the automated driving. In the manual driving condition, the driver operates the steering wheel and gas and braking pedals as normally as usual driving. In the automated driving condition, the simulated automated driving system, which was implemented in our experiment, autonomously generates the operational input to the host vehicle and it follows leading vehicles and changes lanes when the system considers the appropriate situation for them. The simulator is equipped with a speaker to simulate the sound of turning signal so that the driver can notice the initiation of automatic lane change. Also, the steering wheel rotates automatically according to the operational input from the automated driving system. During the simulation of driving (in both conditions), the driving simulator records the status of each vehicle (e.g. position, velocity, acceleration, orientation), the driver's operational signals (e.g. steering wheel, gas pedal and braking pedal), and the driver's gaze direction. The sampling rate of recording is 100 Hz. In analysis, they are down-sampled to 10 Hz in the analysis.

3.2 Simulation scenario

The drivers were instructed in manual condition as follows, to keep the velocity of the vehicle at 100 km/h as possible as he/she can.

"Imagine that you are going to take an important exam at your university this morning, but you woke up late. You have to rush to your university by car or you will be late for the exam and fail the class. The speed limit on the highway is 100 km/h. Please drive safely, but try to arrive at the university as quickly as possible by travelling at around the speed limit and by passing other vehicles in front of you by making lane changes if possible. During automated driving, you can take your feet off the gas and brake pedals and hands off the steering wheel, but keep monitoring the roadway so that you can take control of the vehicle at any time, such as when the automated control of the vehicle is risky. Please intervene in control of the vehicle by operating the pedals and steering wheel yourself when you feel there is any danger."

Therefore the drivers were pushed to change lanes frequently. In the automated driving, the background story in the instruction is the same. Concerning the automated driving system, the drivers were told as follows:

"Use the automated driving system whose preferred velocity is set to 100 km/h. However, the automated system is not perfect for any possible situation. If you notice any risk of collision, use the steering wheel, gas pedal and braking pedal in order to recover safety. After the risk diminishes enough, please take you hands and foot off from the steering wheel and pedals to let the automated driving system operate the vehicle again."

3.3 Analysis of negative adaptation

Through the manual driving trials, we collected the samples of situation at initiation of lane changing and situation before the host vehicle was passed on by the neighbouring vehicle. The former situation indicates that the driver was comfortable to change lanes in that situation, i.e. the situation is in his/her drivable area for changing lanes. The latter situation indicates that the driver was uncomfortable to change lanes in that situation, i.e. the situation was in his/her evasion area. Hence, the decision boundary for lane change is estimated as the boundary between those two situations. In the upper panel in Fig.6, the situation where the driver made lane changes and the situation where the driver did not make lane changes are depicted as circles at $Y = 1$ and $Y = 0$ on the vertical axis against the corresponding risk level on the horizontal axis. Risk level in our experiment consists of velocity difference between lanes δv and the inter-vehicle distance of the destination of lane changing d_n, as described in the section 2.2.

In the automated driving, we collected the samples of situation at the initiation of automatic lane changes which the driver tolerated and those which the driver did not. The lower panel in Fig.6 depicts the driver's decision boundary for lane changes in the same manner.

Our focus in negative adaptation is the variation of decision boundary on risk of the situation, i.e. the variation of the sensitivities to the risk factors in the driving situation.

They are estimated by applying logistic regression to the collected data. Let $p = P(Y = 1|\delta v, d_n)$, which is, in the manual driving, the probability that the driver changes lanes given the risk of driving situation $(\delta v, d_n)$, i.e. $1 - p$ is the probability that the driver does not change lanes. Logistic regression is the probabilistic plane expressed as

$$\log \frac{p}{1 - p} = \beta_0 + \beta_{\delta v} \cdot \delta v + \beta_{d_n} \cdot d_n, \tag{1}$$

where $\beta_{\delta v}$ and β_{d_n} represent the driver's sensitivity to risk factors δv and d_n, respectively. The coefficients β_0, $\beta_{\delta v}$ and β_{d_n} are estimated from the collected behaviour data of $(Y, \delta v, d_n)$. In the automated driving, p is the probability that the driver tolerates the automated lane change by the system, and $1 - p$ is the probability that the driver will interrupt and refuse the automated lane change. Our analysis investigate the driver's negative adaptation by comparing the sensitivities to the risk factors obtained using logistic regression.

Additionally the gaze behaviour of the driver was investigated as the indicator of negative adaptation on the driver's appearance. This also includes the comparison of the gaze behaviours in the two conditions of driving. The difference of the gaze behaviours in two conditions were evaluated in relation to the negative adaptation represented as the insensitivity to risk factors. The gaze direction is recorded at 30 Hz and down-sampled to 10 Hz in the analysis.

4. EXPERIMENT RESULTS

Fifteen subjects with driving license participated in our experiment as the drivers in the driving simulator. Each driver is required to drive the simulator for four trials in total; two trials for each driving conditions and each trial continues about twenty minutes. They made about twenty lane changes in one trial. Each driver is given five minutes of practice to get used to the simulator itself, and another five minutes to get used to the simulated automated driving system.

4.1 Variation of decision boundaries

Examples of the probability surfaces estimated using logistic regression for Subjects 05 and 08 are shown in Figs. 7 and 8. Lane change decisions made by these drivers in manual and automated driving are shown in the graphs on the left and on right, respectively. Samples of left and right lane changes have been combined into one data set and are included in the same graph. Each dot in the graph shows the result of a driver's decision whether or not to make a lane change, based on their assessment of the risk level of the surrounding environment, (i.e. based on δv and d_n as described in the section 2.2). A red dot indicates the driver decided to make a lane change, either manually or by allowing the vehicle to automatically change lanes in the case of automated driving. A blue dot indicates the driver decided not to make a lane change during conventional driving, or intervened to prevent an automated lane change during automated driving. These red and blue dots correspond to the samples of $Y = 1$ and of $Y = 0$ in the Fig.6, explained in the section 3.3. The more the red and blue dot distributions overlap, the more inconsistent

a driver was when making lane change decisions (i.e. the more randomly the subject made or avoided lane changes in relation to the subjective risk level). Figure 7 shows that Subject 05 displayed relatively consistent behaviour regarding lane change decisions during both manual and automated driving, but seemed somewhat more conservative during automated driving than during manual driving. Although he tended to avoided making lane changes when it was risky, and tended to make lane changes when it was safe, he also tended to make a greater number of risky lane changes during conventional driving. Accordingly, his decision plane obtained by logistic regression has relatively more sharp slope in manual driving. In contrast, Subject 08 exhibited more random risk taking behaviour during automated driving, as shown by the overlapping of the red and blue dots, compared to her behaviour during manual driving. We can see how the decision surface became more uniform during automated driving as her decision threshold became more ambiguous.

Table 1. Regression coefficients estimated for each driver using logistic regression. "M" and "A" in the "Condition" column indicate manual and automated driving, respectively.

Subject #	Condition	$\exp(\beta_0)$	$\exp(\beta_{\delta v})$	$\exp(d_n)$
01	M	0.032	0.838	1.094
	A	0.193	0.972	1.034
02	M	0.019	1.034	1.062
	A	0.064	0.937	1.077
03	M	0.033	0.954	1.065
	A	0.034	0.927	1.066
04	M	0.377	0.763	1.065
	A	0.330	0.819	1.054
05	M	0.040	0.989	1.079
	A	0.003	0.876	1.128
06	M	0.024	0.993	1.069
	A	0.041	1.002	1.052
07	M	0.010	1.037	1.063
	A	0.022	0.783	1.110
08	M	0.090	0.863	1.088
	A	0.519	0.941	1.036
09	M	0.051	0.952	1.071
	A	0.057	0.980	1.054
10	M	0.171	0.754	1.124
	A	0.158	0.893	1.051
11	M	0.047	0.958	1.083
	A	0.107	0.836	1.067
12	M	0.009	0.980	1.088
	A	0.046	0.854	1.081
13	M	0.153	0.875	1.043
	A	0.083	0.963	1.028
14	M	0.044	0.991	1.067
	A	0.272	1.010	1.026
15	M	0.145	0.993	1.062
	A	0.124	1.117	1.028

Regression coefficients (odds ratios $\exp(\beta_i)$ where $i \in \{0, \delta v, d_n\}$) estimated for each driver are listed in Table 1. Regression coefficients for manual driving ($\exp\left(\beta_i^{(M)}\right)$) and automated driving ($\exp\left(\beta_i^{(A)}\right)$) are compared. Odds ratio $\exp(\beta_{\delta v})$ represents inconsistency in a driver's lane change decision making for given differences in relative velocity between the two lanes (δv), while $\exp(\beta_{d_n})$ represent inconsistencies in decision making based on distance between vehicles in the faster lane (d_n). Risk level of the
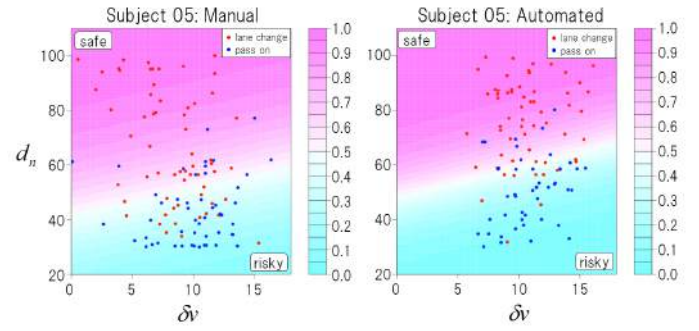
Fig. 7. Subject 05's decision boundaries on risk plane; red dots indicate that the driver decided to make a lane change and blue dots indicate that the driver decided not to make a lane change.
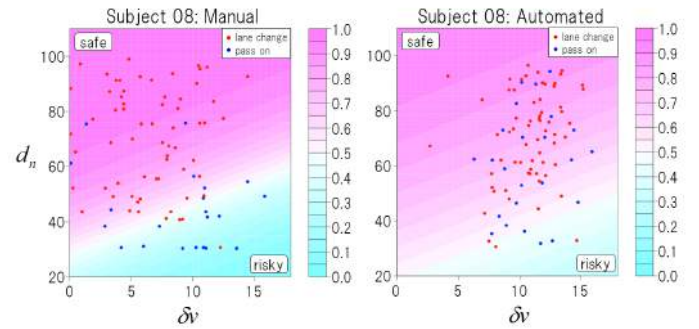
Fig. 8. Subject 08's decision boundaries on risk plane; red dots indicates that the driver decided to make a lane change and blue dots indicate that the driver decided not to make a lane change.

surrounding environment increases as relative velocity δv increases and distance d_n decreases, thus we can infer that drivers with larger odds ratios $\exp(\beta_{\delta_v})$ and small odds ratios $\exp(d_n)$ are more inconsistent in their decision making in relation to these risk factors (i.e. they are less sensitive to the relative velocity of vehicles and to the distance between vehicles when making lane changes).

4.2 Variation of gaze behaviour

The data of gaze direction is recorded as the sequence of positions on the simulator's screen. It is converted and categorized into one of the following five categories, according to the positions of equipments on the simulator.

(1) To the front (the road ahead)
(2) Into the rear-view mirror
(3) To the right (including right rear-view mirror)
(4) To the left (including left rear-view mirror)
(5) Other (out of range or unknown)

The gaze coordinates of the driver's focus on the screen of the simulator were used to classify gaze direction into one of these five categories. Figures 9 and 10 show examples of the gaze behaviour data collected from Subjects 8 and 12, respectively. The relative frequencies of driver gaze into each of the five directions was calculated for each point in time during both right lane changes (a) and left lane changes (b), with the top and bottom graphs corresponding to conventional and automated driving,

(a) Right lane change

(b) Left lane change
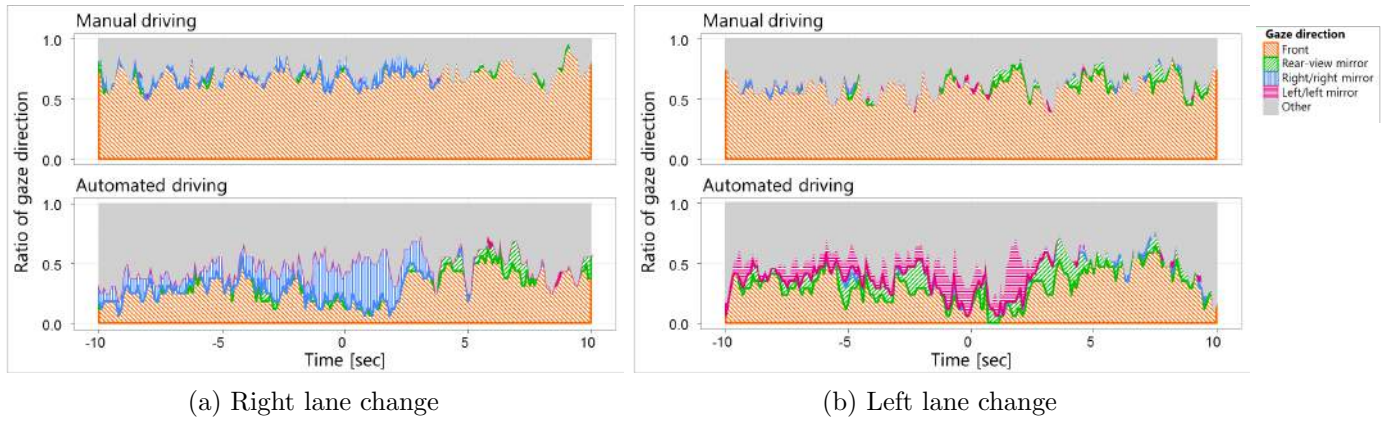
Fig. 9. Subject 08's gaze direction during lane changes
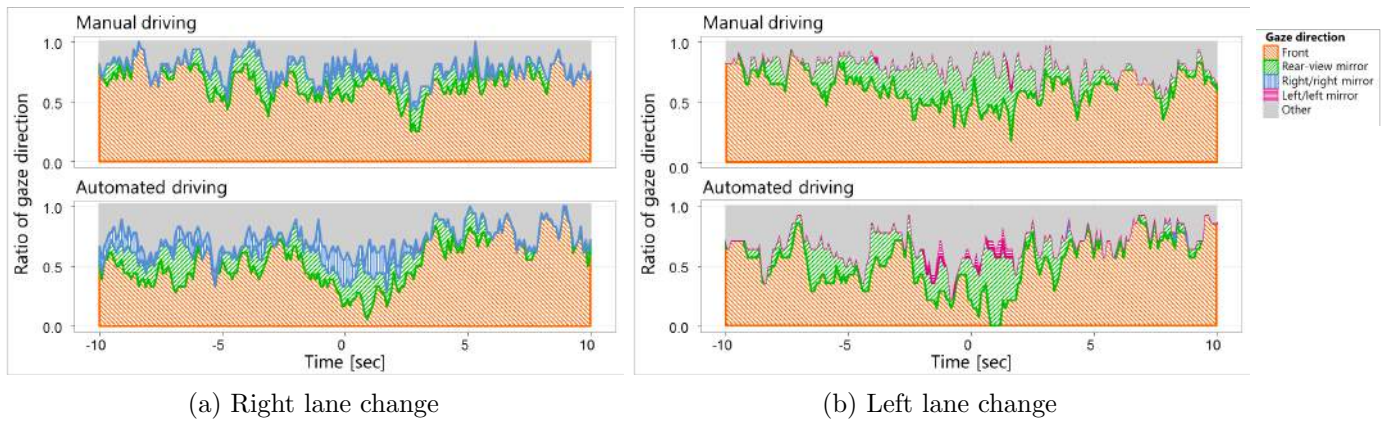

(a) Right lane change

(b) Left lane change

Fig. 10. Subject 12's gaze direction during lane changes

respectively. We analysed driver gaze direction during the ten seconds before and after the beginning of each lane change. 0 seconds on the horizontal axes represents the beginning of these lane changes, with negative values representing the seconds preceding those lane changes. We can see from Figs. 9 and 10 that the gaze behaviour of both drivers varied between conventional and automated driving. Subject 08's gaze was directed to the front about 70 % of the time during manual driving, but only about 30 % of the time during automated driving. This subject also tended to look to the right or into the right rear-view mirror more often when the vehicle was making automated right lane changes than when he made manual right lane changes, and he exhibited parallel behaviour when making automated lane changes to the left. Fig.10, which shows the data for Subject 12, reveals that this driver also looked more often to the right and left during automated lane changes compared to when she made manual lane changes. However, this driver did not exhibit a significant decrease in attention to the front during automated driving. We can also see that Subject 12 looked into the rear-view mirror more often than Subject 08 during both automated and manual lane changes.

4.3 Relation between Decision Making Behaviour and Gaze Behaviour

The gaze behaviour of the drivers are further investigated in relation to the negative adaptation appeared on the

decision boundaries. To quantify the difference of gaze behaviours between two driving conditions, they are modelled using Gaussian Mixture Model (GMM) and Hidden Markov Model (HMM). The process for evaluating the difference is as follows.

For each subject,

(1) Relative frequency of five gaze direction during lane changes in automated and manual driving (e.g. Fig.9) are merged into one data set. A GMM with ten Gaussian distributions is trained on the data set (i.e. each component is a distribution on five dimensional space).

(2) Using the obtained ten Gaussian distributions for relative frequencies as the emission probabilities of hidden states in HMM, its transition probabilities are learnt based on the relative frequency of gaze direction in manual driving.

(3) For each state of the learnt HMM, the number of frames where it is visited is counted in manual and automated driving respectively.

(4) The difference of histograms of states visited in the two driving conditions are evaluated using Hellinger distance metric.

The gaze direction time sequences used for learning the transition probabilities are the same sequences used for generating the relative frequency of gaze direction during lane changes (such as shown in Figs. 9 and 10 for the
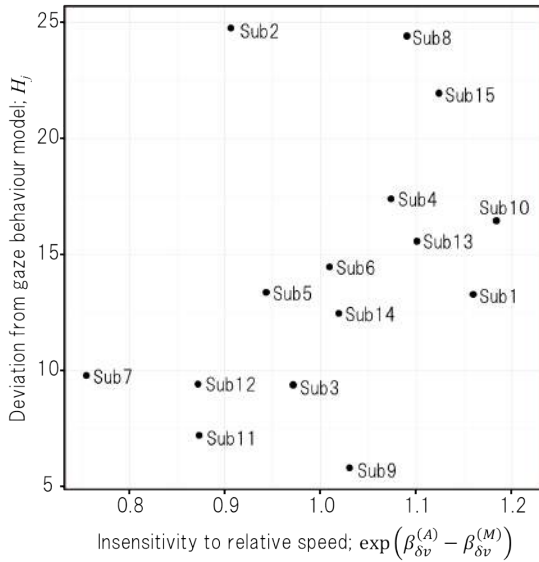
Fig. 11. Correlation between driver's sensitivity to relative speed and driver's behavioural deviation from his/her gaze model.

Subjects 08 and 12). The Hellinger distance is a metric to measure the distance between two probability distributions, which is expressed as follows when the distributions are discrete,

$$H(P,Q) = \frac{1}{\sqrt{2}} \sqrt{\sum_{i=1}^{k} (\sqrt{p_i} - \sqrt{q_i})^2}, \qquad (2)$$

where P and Q are the discrete probability distribution with p_i and q_i as their i-th component.

The relationship between the variation of gaze behaviour, evaluated as the Hellinger distance H_j for the driver j, and the variation of decision boundary, evaluated as the variation of odds ratio $\exp\left(\beta_{\delta v}^{(A)} - \beta_{\delta v}^{(M)}\right)$, is shown in Fig.11. The value of $\exp\left(\beta_{\delta v}^{(A)} - \beta_{\delta v}^{(M)}\right)$ represents the increase in inconsistency in driver decision making regarding lane changes, when inconsistency in decision making during automated and manual driving are compared for given differences in relative velocities between two lanes. Note that Subject 02, an outlier in the graph, fell asleep during last half of the automated driving session, and the subject's gaze direction during drowsy driving could not be properly measured. The correlation coefficient between these values including the data of Subject 02 is 0.40. Excluding the data of Subject 02, it is 0.72.

Figure 11 reveals that drivers whose gaze behaviour differs more in automated driving from that in manual driving also tend to be less sensitive to risk factors in the surrounding environment. This suggests that negative adaptation to an automated driving system can be detected by measuring the deviation in driver gaze behaviour between automated and manual driving.

5. CONCLUSION

In order to develop a method for detecting negative driver adaptation to an automated driving system, we inves-

tigated the driver's negative adaptation in the decision boundaries for changing lanes and the driver gaze behaviour, using a driving simulator experiment. We found that drivers who paid less attention to the road ahead during automated driving tended to be more dependent on the automated system. Compared to their driving behaviour during conventional manual driving, these drivers were less consistent when making lane change decisions during automated driving, and less sensitive to risk factors in the surrounding environment, such as differences in relative speeds and distances between nearby vehicles. Changes in driver adaptation to automated driving systems over time, as well as adaptation to different levels of automation, should be examined in future research.

REFERENCES

Abbink, D.A. and Mulder, M. (2008). Motivation for continuous haptic gas pedal feedback to support car following. In *Proc. IEEE Intelligent Vehicles Symposium.*

Inagaki, T. (2010). Traffic systems as joint cognitive systems: Issues to be solved for realizing human-technology coagency. *Cognition, Technology, & Work*, 12(2), 153162.

Mima, H., Ikeda, K., Shibata, T., Fukaya, N., Hitomi, K., and Bando, T. (2009). A rear-end collision warning system for drivers with support vector machines. In *Proc. IEEE Workshop on Statistical Signal Processing*, 650–653.

NHTSA (July 2014). Human factors evaluation of level 2 and level 3 automated driving concepts.

NHTSA (May, 2013). Preliminary statement of policy concerning automated vehicles.

Smith, B. (2014). Automated vehicles are probably legal in the united states. 1 tex. a&m l. rev. 411.

Tobii Technology (2014). X2-30 Eye Tracker. URL http://www.tobii.com/en/eye-tracking-research/global/products/hardware/tobii-x2-30-eye-tracker/. (accessed Jun. 7, 2015).

Virtual Mechanics Corp. (2014). CarSim. URL http://carsim.jp/. (accessed Jun. 7, 2015).

Analysis and modeling of driver behavior on pedestrian crossing situations (2nd report: Analysis of a crossing diagonally situation using JARI-ARV)

First Kenji Sato*. Second Ryo Iwaki *
Third Takashi Wakasugi *. Fourth Nobuyuki Uchida*

* Japan Automobile Research Institute, Safety Research Division
2530 Karima,Tsukuba,Ibaraki, 305-0822, Japan (E-mail: ksato@jari.or.jp).

Abstract: Pedestrian-crossing-related accidents were 26.0% of all fatal accidents that occurred in Japan in 2012. To prevent pedestrian-versus-vehicle accidents, several driver-support systems (alarms and automatic brakes) have recently been commercialized. For verification of the validity of these driver support systems, it is important to understand driver behavior regarding pedestrian crossing. In this study, we examined driving performance for situations where pedestrians suddenly crossed the road to construct a driving behavior model. Experiments were implemented using an instrumented vehicle, JARI-ARV, which was able to reproduce critical situations where pedestrians suddenly crossed the road in front of the instrumented vehicle using augmented reality technologies (computer graphics). Several walking patterns including diagonal crossing of the road were set up as experiment conditions. Consequently, a collision avoidance behavior model for a particular complex crossing pattern was determined.

Keywords: Human factors, Driver behavior, Driver models

1. INTRODUCTION

Pedestrian-versus-car fatal traffic accidents accounted for 36.6% of all fatal traffic accidents in Japan in 2012. Furthermore, accidents involving pedestrians crossing the road accounted for 26.0% of all fatal traffic accidents (approximately 1000 accidents) [1]. The fatality rate during walking is extremely high. Preventing fatal pedestrian traffic accidents and implementing measures for reducing the extent of damage caused by accidents are matters of considerable urgency and must be implemented in order to reduce fatal traffic accidents. Systems that assist drivers in detecting pedestrians and avoiding danger (alarms and automatic brakes) are measures that can be implemented on vehicles to prevent pedestrian traffic accidents. To verify the validity of these driving support systems, it is important to assess driver behavior for detecting pedestrians.

This study focused on an analysis of evasive actions taken by drivers to avoid pedestrians and examined the building of a driver avoidance behavior model to avoid pedestrians crossing the road. A high proportion of the causes of accidents involving pedestrians crossing a street has been reported to be the timing of the pedestrian, entering the road relatively early (an urgency situation from the perspective of drivers), and consideration was focused on such a sudden crossing by pedestrians (pedestrian sudden entry) to analyze the evasive actions taken by drivers in such instances. Past studies have considered evasive actions taken by drivers, using actual vehicles and pedestrian dummies. However, there are limits to the degree of danger that can be tolerated and the level of reproducibility available with such methods, so the experiments performed in this study were conducted using augmented-reality instrumented vehicles of the Japan Automobile Research Institute ("JARI-ARV").

2. EXPERIMENT METHOD

2.1 Experiment equipment

Liquid crystal displays (LCD) were installed in front of the driver's seat of an actual vehicle on the JARI-ARV, enabling the driver to drive an actual vehicle while looking at the displays (Fig. 1). The equipment used augmented reality technology and could reproduce a variety of traffic environments, adding pedestrians, cars and the like using computer graphics (CG) to the image of the actual scenery shown on the LCD. Furthermore, trials were conducted under experiment conditions identical to past studies (for cases involving pedestrians entering the street from a blind spot and crossing the street in the vertical direction) in order to gain understanding of the vehicle characteristics of the JARI-ARV. We also verified the deceleration of the instrumented vehicle when pedestrian sudden entry (using pedestrian dummies in actual vehicle experiments but CG pedestrians with JARI-ARV) was introduced. As seen in Fig. 2, the results were equivalent to those of actual vehicle experiments, thus confirming that an analysis can be performed using the JARI-ARV.

Fig. 1. JARI-ARV
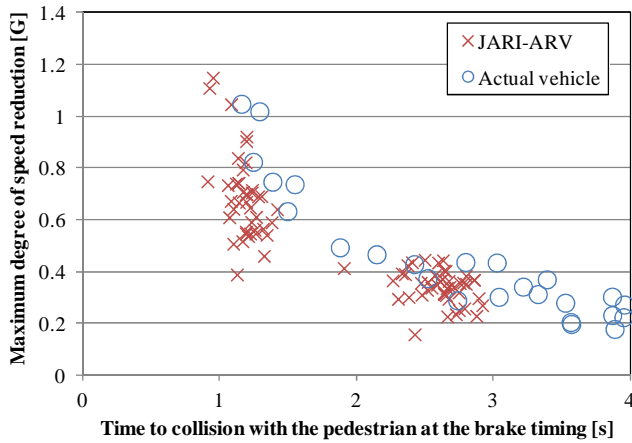
Fig. 2. Verification of the JARI-ARV apparatus

Table 1. Experiment conditions

Pedestrian position	Sudden entry timing[s]	Road crossing angle [deg]	
Left / Right	2.0 / 3.5	9	
		23	Pedestrians going away
		45	
		9	
		23	Pedestrians coming
		45	

Fig. 3. Experiment conditions

2.2 Subjects

The experiment was conducted with 35 male and female participants (Average age 42.0 ± 16.8) who drive routinely, after obtaining their informed consent. The contents and safety of experiments conducted in this study were deliberated on and approved by the Ethical Review Board, which was appointed by the Japan Automobile Research Institute.

2.3 Experiment conditions

The scene in which a pedestrian suddenly entered the roadway was considered, with the condition of the pedestrian "crossing the road diagonally starting from a blind spot". Two sudden entry conditions were set for the pedestrian, pedestrian position conditions were set for both sides of the road with respect to the traveling direction of the vehicle, and six pedestrian road-crossing angles were set (Table 1, Fig. 3). Only one walking velocity (6.3km/h) and one vehicle velocity (40km/h) were set, with the focus of this examination concentrated on the starting timing of the pedestrian and the influence of the crossing pattern on the outcome.

2.4 Evaluation items

The driving behavior of the driver, the state quantity of the vehicle, and the state quantity of the CG pedestrian shown in Table 2 were measured. The following four phases were established considering the status transition that occurred as the driver took evasive actions when the pedestrian suddenly entered the roadway, as the acquired data was analyzed. Phase 1 was the timing at which the pedestrian jumped into the roadway (with the driver being aware of the presence of the pedestrian), Phase 2 was the timing at which the driver released the accelerator, Phase 3 was the timing at which the driver stepped on the brake pedal, and Phase 4 was the timing at which the vehicle halted. The transition between these phases was considered important in order to objectively analyze the actions taken by the driver, since the dangerous condition of the pedestrian suddenly jumping into the roadway (i.e., the risk of the vehicle colliding with the pedestrian) changed from moment to moment. This examination was conducted using the following analysis indices.

(1) Time of release of the acceleration pedal [s] : The time from pedestrian appearance until release of the acceleration pedal.

(2) Time of pedal switch [s] : The time it took from releasing the accelerator until depressing the brake.

(3) Maximum deceleration [G] : Maximum deceleration of vehicles.

Table 2. Measurement item

State quantity		Driving behavior	Video
Vehicle	CG pedestrian		
Position [m]	Position [m]	Acceleration pedal position [%]	Face
Velocity [m/s]	Velocity [m/s]	Brake pedal force [N]	Front view
Acceleration [m/s²]		Steering wheel angle [deg]	Foot
Yaw / Roll / Pitch [deg]			

The predicted time to collision (TTC) was believed to be important in considering the avoidance behavior of the driver as a pedestrian suddenly entered the roadway, so it was necessary to sort out the respective indices with respect to the TTC. Since the traveling direction of the pedestrian and that of the vehicle do not form a 90-degree angle when the pedestrian crosses the road diagonally, the velocity vector of the pedestrian is affected with respect to the vehicle travel direction (> 0km/h). The three definitions described below can be considered (Fig. 4).

(1) The predicted arrival time for the vehicle to reach the position where the pedestrian enters (TTW). TTW is calculated below. The distance between the blind spot and the vehicle was divided by the vehicle speed when a pedestrian appeared from a blind spot.

(2) TTC is calculated based on the relative velocity and relative distance of the vehicle and the pedestrian with respect to the travel direction of the vehicle (TTI). TTI is calculated below. The distance between the vehicle and the pedestrian was divided by the vehicle speed when the driver release of the acceleration pedal.

(3) The predicted time for the vehicle to arrive at the collision point with the pedestrian (assumed to be at the center of the roadway; hereinafter referred to as "TTCP"). TTCP is calculated below. The distance between the vehicle and the collision point was divided by the vehicle speed when the driver applied the brakes.

TTW[s]= Lw / V   TTI[s]= Li / (V+Vp)   TTCP[s]= Lcp / V
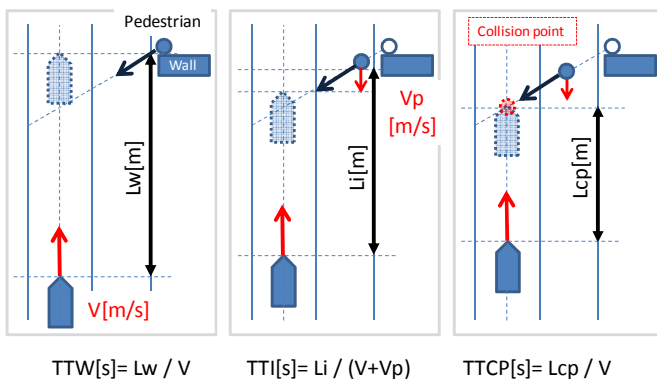
Fig. 4. Risk indices

2.5 Driving method

The vehicle was driven on a test course belonging to the Japan Automobile Research Institute (Fig. 5), with the drives divided into two runs of about 30 minutes each. The instructions given to the driver were as follows.

・"We are conducting an investigation to see if it is possible to drive the JARI-ARV similarly to an actual vehicle."

・"Please drive the vehicle as if you are driving in a real traffic environment. Please drive as you would normally."
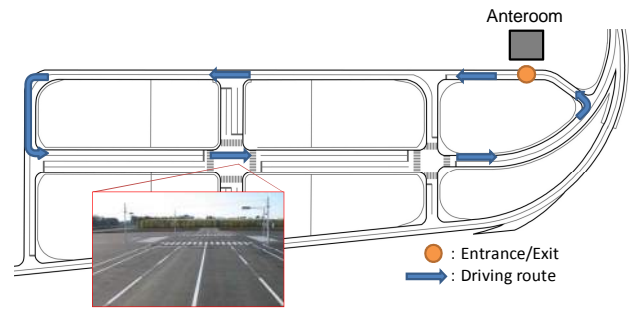
Fig. 5. Driving path diagram

3. ANALYSIS

To build the driver's avoidance behavior model, we screened the avoidance behavior measurement data. The conditions for screening were as follows.

・Collision accident data.

・Deceleration before the pedestrian enters.

・Driver does not perform a brake avoidance maneuver.

・Inattentive driving when pedestrian enters.

From the distribution of the measurement data, we could understand that the avoidance behavior data tended to follow a straight linear approximation in the analysis. We discuss the results in the next section.

4. RESULTS

The experiment clarified that the timing of the driver's response behavior was influenced by the risk indices for the pedestrian with regard to the start time of driving operations such as deceleration and braking, as well as speed reduction behavior for the avoiding a collision. The details are as follows.

It was apparent that the time at which the driver release of the acceleration pedal was influenced by the TTW of the pedestrian entry as a risk index (Fig. 6 (a)), the time at which the driver switched pedals was influenced by the TTI at the time the driver ceased to accelerate (Fig. 6 (b)), and the degree of speed reduction when the driver avoided a pedestrian was influenced by the TTCP at the time of braking (Fig. 6 (c)).
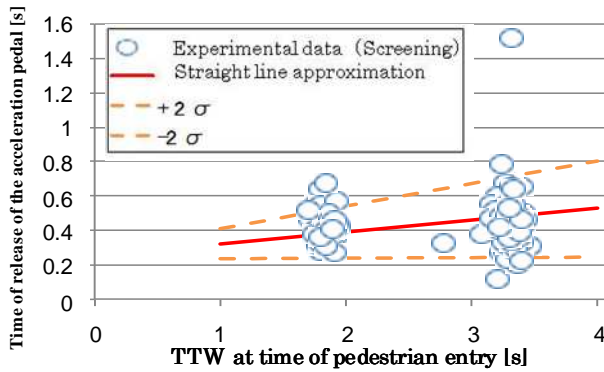
Fig. 6 (a) Tme of release of the acceleration pedal and TTW relation
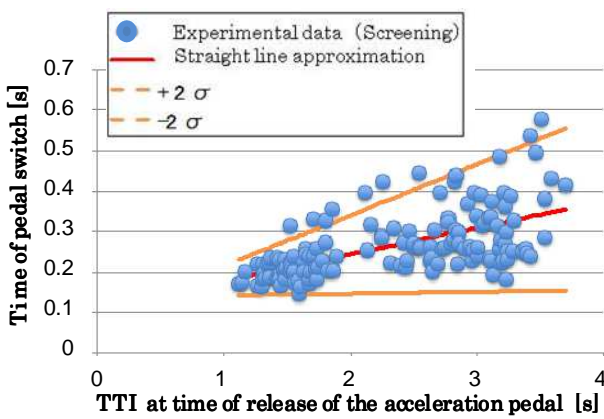
Fig. 6 (b). Straight line approximation of pedal switching time
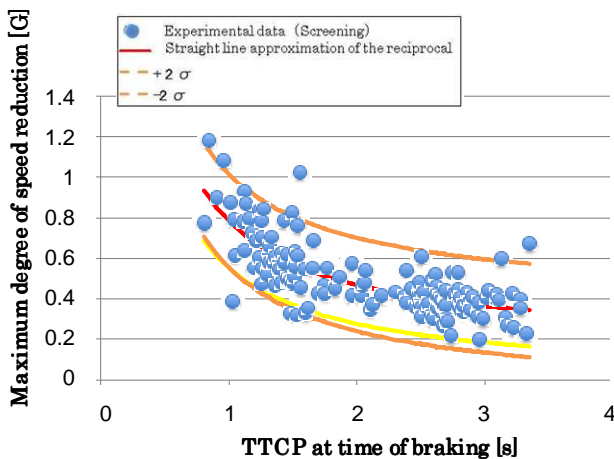
Fig. 6 (c). Distribution of maximum speed reduction
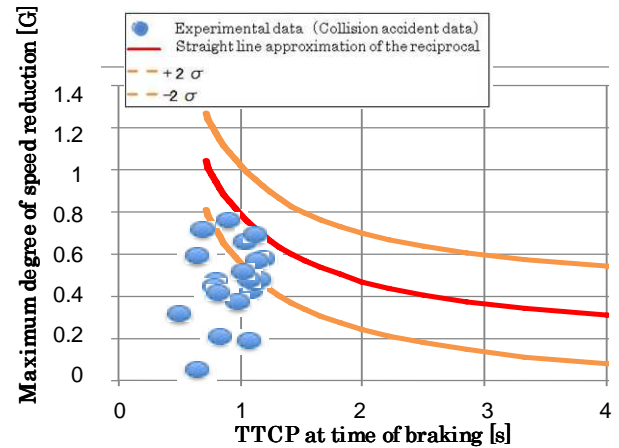
Fig. 7. Distribution of collision accident data

An analysis of the data for situations where the pedestrian and the vehicle collided suggested that the collisions were caused by delays in the timing of the various driving operations and slower deceleration (Fig. 7).

5. CONCLUSION

A model for assessing driver collision avoidance behavior in response to a pedestrian's time of entry was constructed. The model can be applied even in a complicated situation such as a diagonal entry by using TTW, TTI, and TTCP according to driver collision avoidance behavior.

To further develop these results, it will be necessary to increase the precision of the model by adding speed conditions and sample numbers because the data obtained in this experiment was limited by short risk index conditions when the pedestrian entered the road and because there was only one speed (40km/h) and only one entry location.

REFERENCES

1. National Police Agency. (2014). Traffic accidents situation

Motion Planning Method for Overtaking Bicycles in Urban Driving Scenario Based on Potential Field Framework

Vachirawat Lertsilpachalearn[*]**. Yasuhiro Akagi**[**]**. Pongsathorn Raksincharoensak**[***]

[*]*Department of Mechanical Systems Engineering, Tokyo University of Agriculture and Technology, Tokyo, Japan (Tel: +81-42-388-7395; e-mail: 50014833014@st.tuat.ac.jp).*
[**]*Department of Mechanical Systems Engineering, Tokyo University of Agriculture and Technology, Tokyo, Japan (Tel: +81-42-388-7395; e-mail: akagi-y@cc.tuat.ac.jp).*
[***]*Department of Mechanical Systems Engineering, Tokyo University of Agriculture and Technology, Tokyo, Japan (Tel: +81-42-388-7395; e-mail: pong@cc.tuat.ac.jp).*

Abstract: Autonomous driving in urban environment is more complicated due to the unpredictable movements of obstacles such as pedestrians and bicycles. This paper focuses on a motion planning of a vehicle for overtaking a bicycle in a straight road. The motion of the vehicle is determined based on an artificial potential field model considering the movement of the bicycle. By sequentially determining the location of the bicycle then applying the potential field model of a static obstacle, our method simulates the safe path for overtaking the bicycle. Furthermore, the more complex condition such as the oncoming vehicle is presence at the opposite lane is also considered for the overtaking path planning algorithm. Finally, the vehicle motion is compared with the actual driving data of expert drivers to verify the effectiveness of the proposed method.

Keywords: Active safety, Autonomous Driving, Driver Assistance Systems, Motion Planning, Potential Field

1. INTRODUCTION

In recent years, the amount of population with age over 65 is increasing gradually in Japan, whereas the statistical data also shows that road accident rate of aged drivers are increasing annually. As the fact that elderly drivers tend to decrease the physical and mental abilities (e.g. the recognition, decision and response time to avoid obstacles), it is strongly affected to the driving performance. Thus, in order to compensate the degradation in those abilities, intelligence driving technologies consists of high-precision sensory devices and real-time systems are developed. With the driver assistance systems such as Adaptive Cruise Control (ACC), which helps keeping safe speeds and safe distances to a preceding vehicle, the workload of the drivers operating pedals is reduced and the drivers can focus on the steering control task. Furthermore, Autonomous Emergency Braking (AEB) has been developed to avoid forward collision from frontal obstacles such as preceding vehicle suddenly braking. By using the driving assistance systems, the vehicle can response to the rapidly change of the speed of the preceding vehicle faster than the driver. This system recovers the declination of the physical abilities of elder drives. However, ACC is capable only for car-following situation with the less complexity environments, mainly in highway driving and AEB has the effectiveness in only high-hazard situations. Thus, in order to prevent the mis-conducted behaviour that lead the drivers and the vehicles to the high-hazard situations and expand the performance boundary of the driving assistance systems, driving assistance for the complex situations such as the overtaking scenario is required.

In urban area, since the road width is limited by the residence building, either footpath or cycling lane cannot be provided for the pedestrians and the bicycles. Thus, it is the difficult task for elder drivers to plan the overtaking route for passing the pedestrians and bicycles safely. Since the movements of pedestrians and bicycles are more complicated than vehicles to predict, the algorithms to plan the overtaking path and speeds to avoid the accidents related to pedestrians and bicycles are required.

This paper focuses on the overtaking maneuver of a vehicle for avoiding the bicycle, as a part of the construction of urban ACC. The rest of the paper is organized as follows, section 2 describes the experiment vehicle for collecting the real driving data and the driving scenario analysis. Section 3 describes the algorithm for overtaking the bicycle based on the artificial potential field. Then the simulation result of the path planning for the overtaking based on the potential field is described. Furthermore, the calculated overtaking path and vehicle motion is compared with the actual driving data of expert drivers to verify the effectiveness of the proposed path planning method.

2. EXPERIMENTAL VEHICLE AND REAL WORLD DRIVING DATA

This section mainly explains on the experimental vehicle and the method of collecting the driving data in the real world.

2.1 The experimental vehicle configuration

The vehicle using for this study is a typical hybrid-electric

vehicle that currently available in the markets, as shown in Fig. 1. For the environment sensing and data collection, vehicle is equipped with various sensors. A stereo camera is installed at the base of rear-view mirror for recording the front-view of the vehicle. A LIDAR (Light Image Detecting And Ranging) sensor is attached at the front grille of the vehicle for detecting obstacles around the vehicle in the field of view of 180 degrees. A high-precision GNSS devices is attached at the roof of the vehicle for determining vehicle location. Velodyne is attached to the roof of the vehicle for creating the surrounding world model and allocating the obstacles around the vehicle.

For measuring vehicle status, CAN data of the vehicle is collected including velocity, pedal input quantity and steering angle. In addition to the factory on-board sensors, the inertial measurement unit (IMU) is equipped near the center of the gravity of the vehicle to measure the yaw rate and the acceleration in each direction. The controller board dSPACE is used for digital signal processing and installed with the on-board PC to acquire the vehicle status from CAN and external sensors mentioned above.

Fig. 1 The experimental vehicle

2.2 Driving data from real world

For the data collection, the group of driving school instructors, which has the high tendency to drive with the safe driving pattern, were asked to drive the experimental vehicle on a specific route in residential area, shown in Fig. 2. By conducting the experiment during rush-hour in the morning and late-afternoon, the sharing of the road between pedestrians, bicycles and vehicle is relatively high.

Fig. 2 Driving course for the experiment

2.3 Analysis of the driving data from real world

In urban area, due to the limited space, most of the minor roads (road that connect between wide major roads) have the same traffic pattern, consists of one lane per direction without the separation between footpath and road itself. The result is the road sharing between motor vehicles and bicycles is unavoidable. Since the typical speed limit in urban area in Japan is 40 km/h or 30km/h and the typical speed of the bicycle is around 15~20 km/h, there are many situations the motor vehicles overtake the bicycles.

We classify the four types overtaking scenarios based on the direction of the bicycle movements and the oncoming vehicle. Fig. 3 shows the four types of the overtaking scenarios.
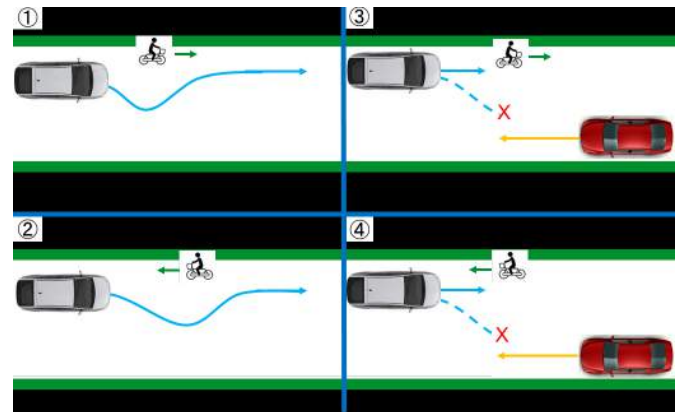
Fig. 3 The bicycle overtaking pattern

Pattern 1) Overtaking the bicycle moving towards without oncoming vehicle – This types is the most common, overtaking the slower bicycle in front of vehicle.

Pattern 2) Overtaking the bicycle moving against the vehicle without oncoming vehicle – This types is occurred when the bicycle travels opposite to the direction of the vehicle.

Pattern 3) Overtaking the bicycle moving towards with oncoming vehicle – The overtake timing is decided based on the oncoming vehicle

Pattern 4) Overtaking the bicycle moving against with oncoming vehicle – The bicycle travels opposite to the direction of the vehicle and the overtaking is decided based on both bicycle the oncoming vehicle

From the collected data, the most frequently occurred pattern is pattern 1 whereas pattern 2 and 3 have nearly the same amount. However, there is no pattern 4 data as the fact that it is the traffic law violation for travelling opposite direction and the experiment route has the less amount of the vehicle passing. For analysing the overtaking path planning, four patterns are divided into two approaches, as shown in Fig. 4.
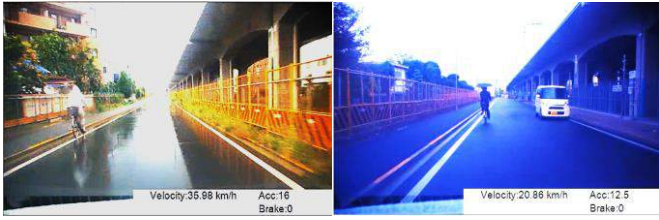
Fig. 4 Left : Approach A   Right : Approach B

Approach A : Free overtaking – In case of the slow bicycle travelling in front of the vehicle and there is no oncoming vehicle, the overtaking maneuver is conducted with using the opposite lane for making the proper distance to pass the bicycle. When the vehicle finished to overtake the bicycle, the vehicle returns to the original lane.

Approach B : Occupied overtaking – Since the road width in urban area is limited, the overtaking vehicle occupied the free space of the opposite lane. If the bicycle is travelling in front of vehicle and the other vehicle is approaching (Fig.5), how to decide the overtaking timing and location is difficult problem. To overtake the bicycle, the arrival time of the oncoming vehicle to the side of the bicycle must be investigated. If the investigation is wrong, the vehicle intercepts the travelling path of the oncoming vehicle or it is difficult to keep enough margin to the bicycle.

2.4 Approach selection based on the oncoming vehicle movement

As mentioned above that time-to-arrival of the oncoming vehicle is the main factor to decide whether the overtaking is possible or not. The motion of the oncoming vehicle must be take into account for calculating the time-to-arrival. Fig. 5 shows the pictorial diagram of the parameters for the decision make.
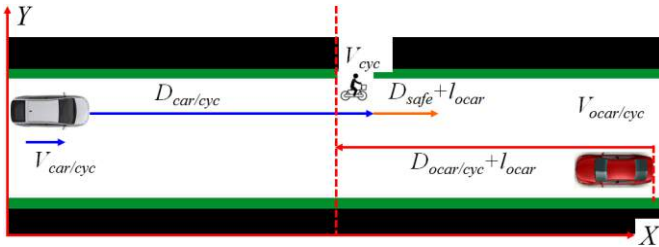
Fig. 5 The pictorial diagram of the approach selection

The algorithm of the overtaking maneuver are as follows. First, we regured the velocity of bicycle is constant and it is a fixed object as an observer. Then, the velocity of the vehicle can be converted into the relative velocity $V_{car/cyc}$. Finally, time to finish overtaking the bicycle T_{to} with the constant acceleration is defined as follows:

$$T_{to} = -V_{car/cyc} \pm \sqrt{V_{car/cyc}^2 + 2a_{car}\left(D_{car/cyc} + D_{margin}\right)} \quad (1)$$

where, $V_{car/cyc}$ is the relative velocity of the vehicle to the bicycle, $D_{car/cyc}$ is the distance to bicycle, D_{margin} shows the distance between the bicycle and the vehicle after the overtaking is finished. Next, T_{ta} of the oncoming vehicle is calculated using the equation below:

$$T_{ta} = -V_{ocar/cyc} \pm \sqrt{V_{ocar/cyc}^2 + 2a_{ocar}\left(D_{ocar/cyc} + l_{ocar}\right)} \quad (2)$$

where, $V_{ocar/cyc}$ is the relative velocity of the oncoming vehicle to the bicycle, $D_{ocar/cyc}$ is the distance between the bicycle and the oncoming vehicle. l_{ocar} shows length of the oncoming vehicle. Finally, the criteria for the approach selection is defined below;

➔ If $T_{to} \leq T_{ta}$,then the approach A is selected.

➔ If $T_{to} > T_{ta}$,then the approach B is selected.

Based on the driving data from the expert drivers, in cases that the overtaking cannot be performed (approach B), there are some behaviours that are quite interesting during the passing of the oncoming vehicle to the start of overtaking. At the experiment route, there are some sections that the road has no centerline. In this case, many drivers tend to overtake the middle of the road to make the space between roadside and vehicle. The reason is to avoid the collision in case bicycle or pedestrian darts out from the occlusion.

For such the behaviour, if the oncoming vehicle is coming while there is the slow bicycle in front of the vehicle, expert drivers decelerate the speed to follow the forward bicycle while keeping the vehicle to the left for allowing the oncoming vehicle to pass the bicycle. Thus, it is important to consider this behaviour as the one of strategy for the path planning algorithm and for the driver acceptance of the system.

3. VEHICLE MOTION PLANNING IN BICYCLE OVERTAKING MANEUVER

To realize an ACC which can handle urban road situation, it is required to take the motion of the traffic participants into account to avoid accidents. Therefore, this paper proposes a method to create bicycle overtaking maneuver in terms of autonomous driving system. The schematic diagram of the system is shown in Fig. 6. First, the overtaking approach mentioned in the section 2 is selected based on the surrounding, either there is an oncoming car in hazard range or not.
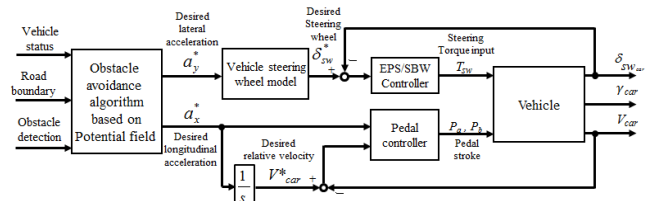
Fig. 6 The schematic diagram for the overtaking path planning

3.1 Motion planning using the potential field method

In this paper, the overtaking path is calculated based on the potential field around obstacles (Noto, et al. (2011) and Hasegawa et al. (2014)). The sensory equipment attached to the vehicle is used to create the world model for the vehicle including the surroundings information, including the position and velocity of the bicycle.

For free overtaking approach, vehicle path is determined by simulating the artificial potential field around the moving bicycle. Next, the situational risk assessment algorithm based on potential fields determines the desired acceleration and deceleration for overtaking the bicycle. Finally, the desired lateral acceleration is converted into steering wheel input via steering model. The longitudinal acceleration is also converted into pedal input quantity for controlling the vehicle velocity. Fig. 7 shows the conversion from real world scenario into the potential field for overtaking the bicycle.
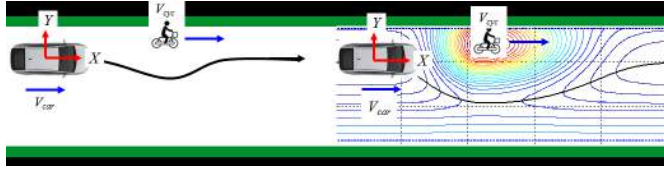
Fig. 7 Potential field for moving bicycle

For occupied overtaking, as the fact that the oncoming vehicle plays a vital role for the start timing of the overtaking maneuver, vehicle path is determined by not only the potential field around the moving bicycle but also the oncoming vehicle. Then, the desired acceleration/deceleration for the path planning is calculated based on the sum of the potential field from each obstacle. Finally, the vehicle motion is controlled in the same way as free overtaking approach. Fig. 8 shows the conversion from real world scenario into the potential field with both the bicycle and the oncoming vehicle.
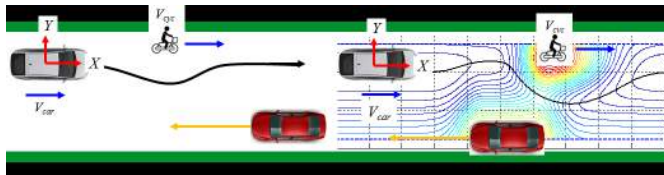
Fig. 8 Potential field for the moving bicycle and the oncoming vehicle

For the first step, the system will be corresponding with the assumption that bicycle is moving forward without lateral movement. With the information from vehicle sensors, surrounding world model is created and the locations of the obstacles around the vehicle can be obtained.

To calculate the path to avoid the bicycle, the desired lateral and longitudinal acceleration are calculated using the artificial potential field with respect to the bicycle position. The potential field is defined as the repulsive force from the obstacle and road boundaries. The longitudinal and lateral acceleration of the vehicle is determined by the repulsive force which is the gradient of the potential field function.

3.2 The potential field for lateral motion control

First, the risk potential used in the lateral motion control system is described. For free overtaking approach, under the condition that obstacles exists in front of the vehicle on a straight road, the vehicle path is determined by two factors: road boundaries and an forward bicycle. Actual drivers determined the optimal path reducing the risk of collisions with the obstacles and lane borders. Therefore, artificial potential fields are formulated by using these two factors.

The repulsive potential field of road boundaries is defined as follows:

$$U_w(X,Y) = w_w\left[1 - \exp\left\{-\frac{(Y - Y_{cr})^2}{2\sigma_w^2}\right\}\right] \quad (3)$$

where, w_w σ_w are the weight and the variance of the repulsive potential field of road boundaries respectively, and Y_{cr} is the Y-coordinate offset of the road centerline to the travelling lane centerline.
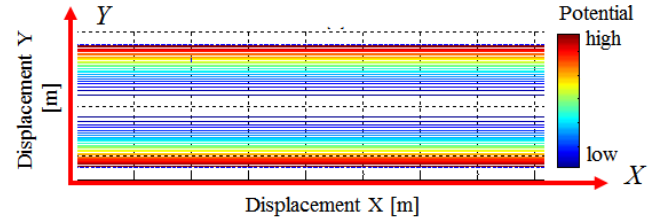
Fig. 9 Potential field for road boundaries

Fig. 9 shows the contour of the repulsive potential field of the road boundaries. This potential field has the maximum value at the position of the road boundaries to express risk of lane departure and has the minimum value at the position of the travelling path in normal condition, i.e. middle of the travellng lane.

Next, the repulsive potential field of the bicycle is defined as follows:

$$U_c(X,Y) = w_c\left[\exp\left\{-\frac{(X - X_c)^2}{\sigma_{cX}^2} - \frac{(Y - Y_c)^2}{\sigma_{cY}^2}\right\}\right] \quad (4)$$

where, w_c indicates the weight of the repulsive potential field of the bicycle, σ_{cX}, σ_{cY} are the variances of X direction and Y direction respectively, X_c, Y_c indicates the X-Y coordinate position of the obstacle with respect to time. As can be noticed from equation (2), the repulsive potential field of the obstacle is also defined as an exponential function of X and Y.
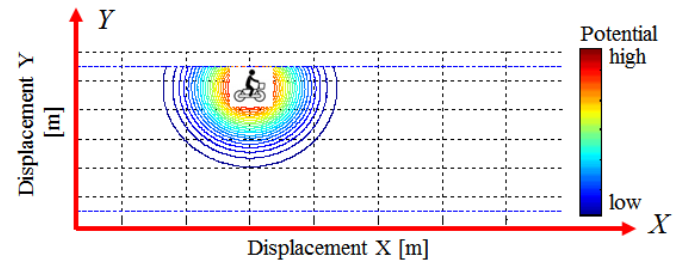
Fig. 10 Potential field for bicycle

Fig. 10 shows the contour of the repulsive potential field of the the bicycle. This potential field has the maximum value at the position of the bicycle to express risk of collision.
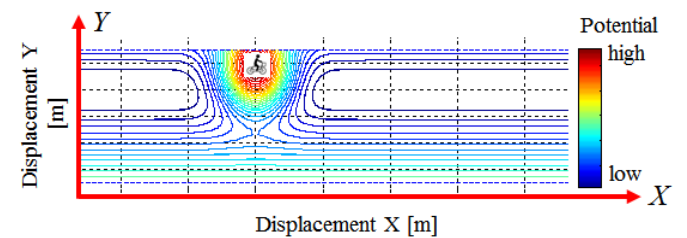
Fig. 11 Combined of Potential field

Finally, the overall risk potential field for free overtaking is defined as follows:

$$U_{risk}(X,Y) = U_c(X,Y) + U_w(X,Y) \quad (5)$$

As can be noticed from Equation (4) and (5), the overall risk potential field is the summation of the repulsive potential field of the road boundaries U_r and the repulsive potential field of the obstacles U_c, U_o, w_r, w_c, w_c, σ_r, σ_{cX} and σ_{cY} included in Equations (3) and (4) are the parameters to vary the shape and height of the risk potential field. These parameters are determined for manipulating the driving data of the actual expert drivers.

After obtained the risk potential function of the environment field, the virtual force acting on the vehicle is expressed as follows:

$$\begin{bmatrix} F_X \\ F_Y \end{bmatrix} = - \begin{bmatrix} \left. \dfrac{\partial U_{risk}}{\partial X} \right|_{(X,Y)=(X_p, Y_p)} \\ \left. \dfrac{\partial U_{risk}}{\partial Y} \right|_{(X,Y)=(X_p, Y_p)} \end{bmatrix} \quad (6)$$

where X_p, Y_p represent the preview position of the vehicle. Then the desired lateral acceleration is calculated as shown below.

$$a_y^* = \frac{1}{m}\left(-F_X \sin\psi + F_Y \cos\psi\right) \quad (7)$$

Finally, the obtained desired lateral acceleration is converted to the desired steering wheel angle. If the side slip angle at the gravity center and the change rate of the vehicle velocity are negligible, the desired steering wheel angle δ_{sw}^* can be expressed using the equivalent linear two-wheel vehicle model as follows:

$$\delta_{sw}^*(t) = n(1 + KV(t)^2)\frac{l}{V(t)}\gamma^*(t) \quad (8)$$

where, K indicates the stability factor, n is the steering gear ratio. Finally, based on the application, various steering control algorithm can be applied. For the autonomous driving, the steer-by-wire system is employed for controlling the steering wheel. In case of the driving assistance system development, desired steering wheel angle can be converted into steering torque assist for leading the driver to turn the steering wheel to the desired path.

3.3 The potential field for longitudinal motion control

This section shows the method for calculating the desired longitudinal acceleration. For free overtaking approach, the desired longitudinal acceleration is calculated from;

$$a_x^* = \frac{1}{m}\left(-F_X \cos\psi + F_Y \sin\psi\right) \quad (9)$$

On the other hand, in case of the occupied overtaking, as mentioned earlier that drivers keep the vehicle to the left while following the bicycle, this behavior is represented in risk potentfield as a "preview potential field". From the driving data, when both the bicycle and the oncoming vehicle can be

seen by the driver, they decelerate while keep left. Based on this fact, the artificial potential field regarding the oncoming vehicle is also introduced in the motion planning computation algorithm.

First, the system calculates the passing point of the vehicle and the oncoming vehicle by using the relative motion. By fixing the bicycle as an observer, suppose the oncoming is moving at the constant velocity, the time that the oncoming vehicle reaches the bicycle is calculated as follows:

$$t_p = -V_{ocar/cyc} \pm \sqrt{V_{ocar/cyc}^2 + 2a_{ocar}D_{ocar-cyc}} \quad (10)$$

where $V_{ocar/cyc}$ is the velocity of the oncoming with the bicycle as an observer, a_{ocar} is the acceleration of the oncoming vehicle and the $D_{ocar-cyc}$ is the distance from the bicycle to the oncoming vehicle. Then, the location of the preview potential field can be determined by using the movement of the bicycle, defined as follows:

$$X_{preview} = V_{cyc}t_p + \frac{a_{cyc}t_p^2}{2} \quad (11)$$

where V_{cyc} is the bicycle velocity and a_{cyc} is the acceleration of the bicycle. After obtain the location of the preview potential field, the preview potential field then occupy the opposite lane where the oncoming vehicle is travelling.

The repulsive potential field of the preview oncoming vehicle is defined as follows:

$$U_o(X,Y) = \begin{cases} w_o\left[\exp\left\{-\dfrac{(X-X_{preview})^2}{\sigma_{oX}^2} - \dfrac{(Y-Y_{ocar})^2}{\sigma_{oY}^2}\right\}\right] & X < X_{preview} \\ w_o\left[\exp\left\{-\dfrac{(Y-Y_{ocar})^2}{\sigma_{oY}^2}\right\}\right] & X_{ocar} > X \geq X_{preview} \\ w_o\left[\exp\left\{-\dfrac{(X-X_{ocar})^2}{\sigma_{oX}^2} - \dfrac{(Y-Y_{ocar})^2}{\sigma_{oY}^2}\right\}\right] & X \geq X_{ocar} \end{cases} \quad (12)$$

where, w_o indicates the weight of the repulsive potential field of the oncoming vehicle, σ_{oX} and σ_{oY} are the variances of X direction and Y direction respectively and X_{ocar}, Y_{ocar} indicates the X-Y coordinate function of the oncoming vehicle.
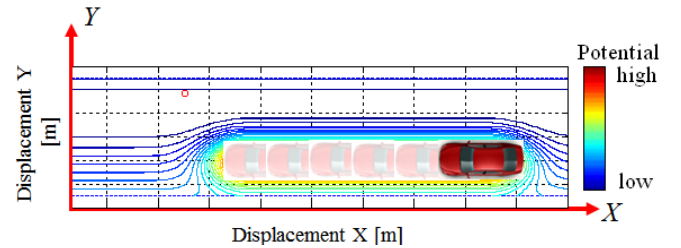

Fig. 12 Potential field for oncoming vehicle

Fig. 12 shows the contour of the repulsive potential field of the preview oncoming vehicle and the real oncoming vehicle in one set. This potential field has the maximum value at the position of the obstacle.

Finally, for occupied overtaking, the sum of the potential field is defined as follows.

$$U_{risk}(X,Y) = U_c(X,Y) + U_w(X,Y) + U_o(X,Y) \quad (13)$$

For the desired lateral acceleration, the method of calculation is the same as free overtaking approach. Fig. 13 shows the

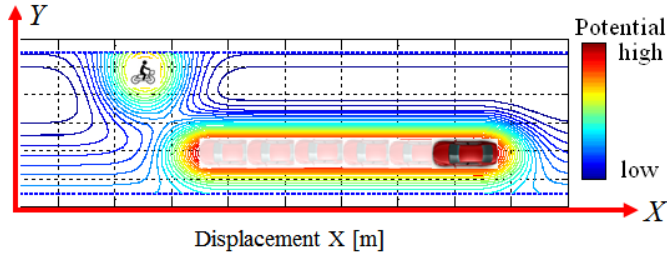combined of the potential field considering the preview potential field and the oncoming vehicle.

Fig. 13 Combined of Potential field considering the oncoming vehicle

For the risk potential used in the lateral motion control of occupied overtaking, the different potential based on the bicycle is used. Since the method of generating the potential field around the bicycle is calculated based on the size of the bicycle, if the vehicle try to approach the bicycle, instead of braking, the vehicle path may be deviated to the left-right. Thus, by separating the lateral maneuver and the longitudinal maneuver, the vehicle velocity can be directly controlled.

The repulsive potential field of the bicycle for longitudinal maneuver is defined as follows:

$$U_b(X,Y) = \begin{cases} w_b\left[\exp\left\{-\dfrac{(X-X_c-X_{safe})^2}{\sigma_{bX}^2}\right\}\right] & X < X_c \\ w_b & X_c \le X < X_{preview} \\ w_b\left[\exp\left\{-\dfrac{(X-X_{preview}-X_{safe})^2}{\sigma_{bX}^2}\right\}\right] & X \ge X_{preview} \end{cases} \quad (14)$$

where, w_b indicates the weight of the repulsive potential field of for braking, σ_{bX} is the variance of X direction. X_c, represents the current position of the bicycle in X direction and $X_{preview}$ represents the preview position of the overtaking maneuver, which are sequentially calculated while X_{safe} keeps the safe distance between the vehicle and the bicycle. Fig. 14 shows the potential field the velocity control during the bicycle approaching.
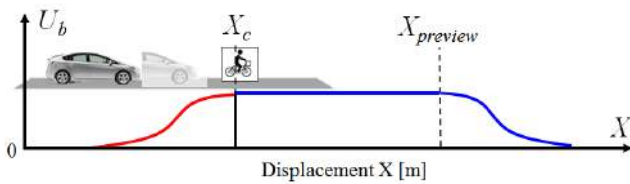
Fig. 14 Potential field of the bicycle in longitudinal axis

Then, the virtual force acting on the vehicle in longitudinal axis is expressed as

$$F_x = -\left[\frac{\partial U_b(X_e,Y_e)}{\partial X_e}\right] \quad (15)$$

Finally, the desired longitudinal acceleration is defined as

$$a_x^* = \frac{1}{m}F_x \quad (16)$$

As shown in Fig. 14, by calculating the desired acceleration at the first section of the potential field, the result is the negative. This section represents the way driver reduce the velocity to follow the bicycle. For the next section, the calculated desired deceleration is equal to zero. It means there is no force to accelerate/decelerate the vehicle. This section represents the behaviour that driver is waiting until the opposite lane is vacancy to operate the overtaking. For the last section, the calculated desired acceleration becomes positive. This result shows the acceleration of the vehicle for overtaking the bicycle.

4. EXPERIMENT VALIDATION OF FREE OVERTAKING APPROACH

The experiment validation is performed by implementing the simulation based on vehicle dynamics to verify the effectiveness of the system. The vehicle parameters are based on the real passenger vehicle.

4.1 Free overtaking maneuver simulation

The simulation is conducted with the moving bicycle as an obstacle. The initial parameters of the simulation is shown in Fig. 15. However, for the simplification, the bicycle acceleration and the lateral movement of the bicycle are neglected. Thus, the bicylce is moving forward with the constant velocity for this simulation.
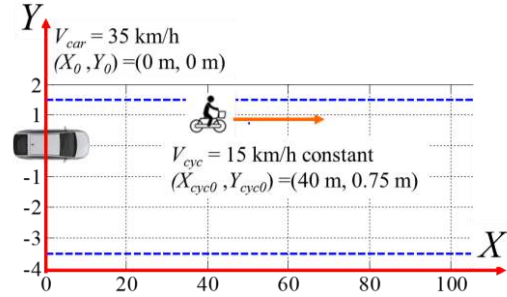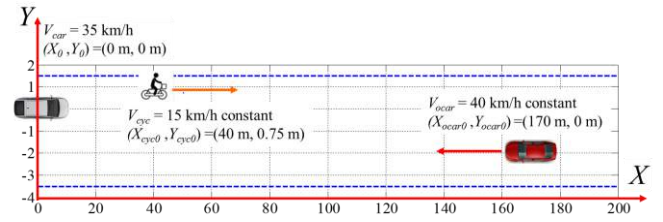

Fig. 15 The vehicle parameters from simulation

The experimental results of the trajectory of the vehicle and the shape of the potential field are shown in Fig. 16. and the parameters for the result in Fig.16 are shown in Fig.17.
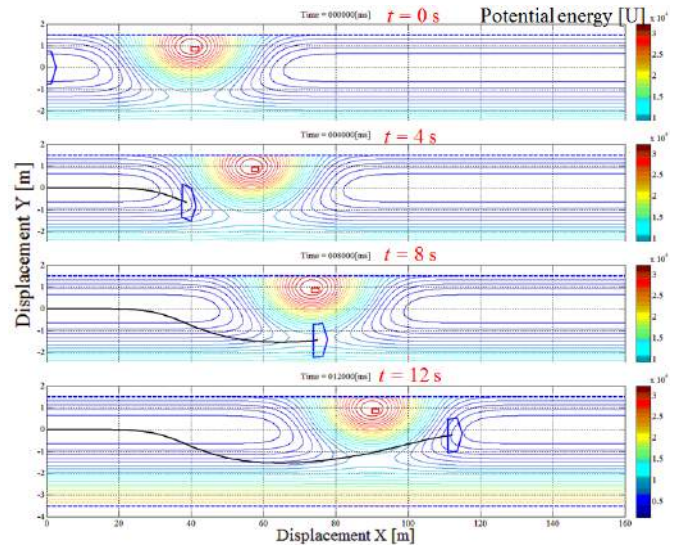
Fig. 16 The vehicle position during the free overtaking
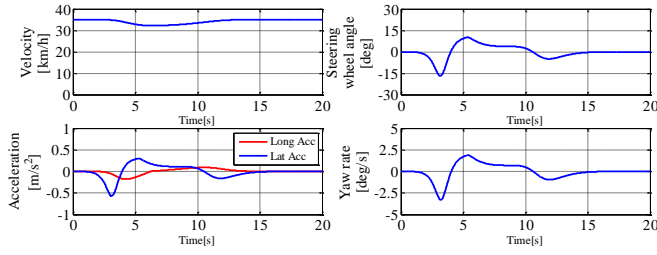
Fig. 17 The vehicle parameters from simulation

The overtaking path as shown in the Fig.16 shows that the vehicle smoothly overtook the bicycle with proper margin to the bicycle along the generated trajectory. The potential field of the Fig.16 shows that the generated trajectory is generated along the lower area of the risk levels.

4.2 Free overtaking maneuver comparison

In order to prove the effectiveness of the proposed system, the real driving data from the expert drivers is compared. Fig. 18 shows the vehicle parameters of the free overtaking approach from real world driving data. For the lateral movement, the results shows that the steering wheel motions of both the simulation and the actual data is similar in trend and the maximum of the angle. For the longitudinal movement, as there is no velocity change during the overtaking for both the real world driving and the simulation. Thus, the proposed path planning method is correctly representing the driving behaviours of the expert drivers.
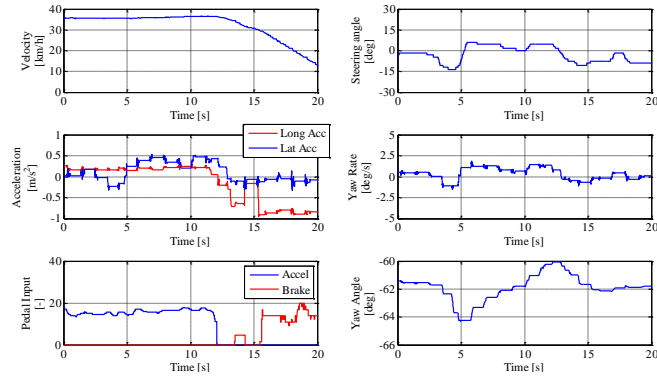
Fig. 18 The vehicle parameters from free overtaking real driving

5. EXPERIMENT VALIDATION OF OCCUPIED OVERTAKING APPROACH

5.1 Occupied overtaking maneuver simulation

For occupied overtaking approach, the simulation is constructed in the same way as free overtaking approach in the previous section with the addition of the oncoming vehicle movement. Fig. 19 shows the initial parameters of the simulation. For the simplification, both the bicycle and the oncoming vehicle are travelling with the constant velocity and no deviation to left-right.

Fig. 19 The vehicle parameters from simulation

The experimental results of the trajectory of the vehicle and the shape of the potential field of the both bicycle and the preview potential field from the oncoming car are shown in Fig. 20. and the parameters for the result in Fig.20 are shown in Fig.21.

For the overtaking path, as shown in the Fig.20, the vehicle slightly keep left while reducing the velocity to follow the forward bicycle while the oncoming vehicle is approaching. After the oncoming vehicle is passed, the vehicle starts overtaking the bicycle with the enough side-by-side distance. However, there is the difference in velocity between the vehicle and the oncoming vehicle. The reason might be the oncoming vehicle is passed the vehicle before the vehicle reaches the desired velocity (bicycle velocity).
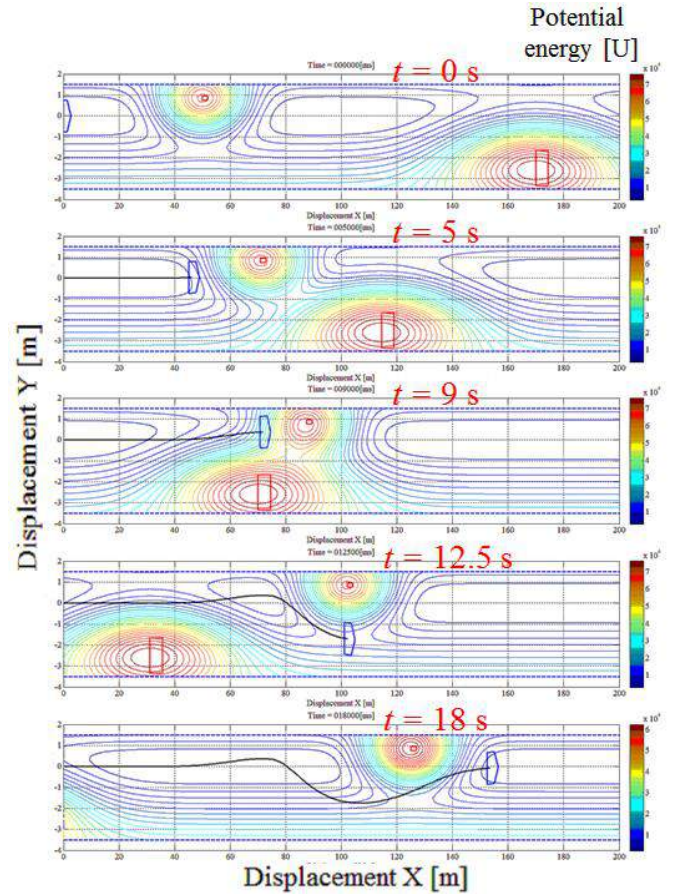
Fig. 20 The vehicle position during the occupied overtaking
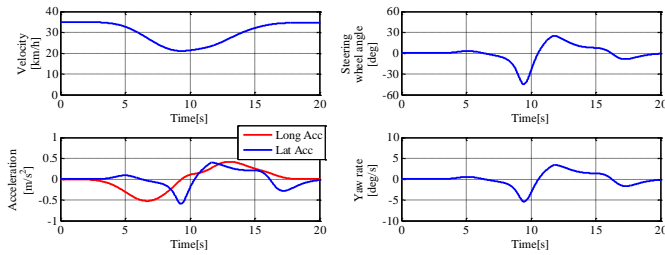
Fig. 21 The vehicle parameters from simulation

5.2 Occupied overtaking maneuver comparison

From Fig. 22, the vehicle parameters from the simulation show nearly the same behaviour compare with the real world driving data. For the longitudinal axis, the vehicle velocity is dropped to about 20 km/h which is regenerated by the simulation. For the lateral axis, the maximum steering angle of the vehicle is around 45 degree which is almost the same as the simulation. However, for yaw rate, there is some different with the peak value, the reason can be the calculation of the steering model of the
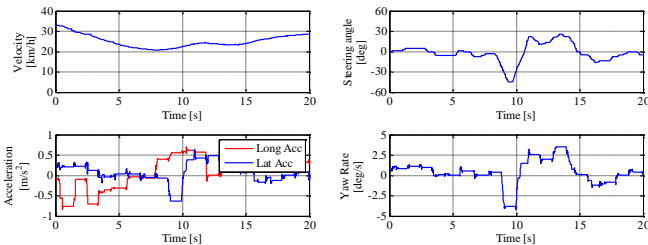
Fig. 22 The vehicle parameters from occupied overtaking real driving

6. CONCLUSIONS

This paper proposed the obstacle avoidance algorithms for the overtaking maneuver of the bicycles in typical urban driving scenarios by using the potential field. Based on the position and the velocity of the bicycle, the potential field is sequentially calculated and the overtaking path is generated. Then the lateral and longitudinal acceleration of the vehicle is calculated from the surroundings including the bicycle. The results show that vehicle can pass by the moving bicycle smoothly without collision.

Moreover, in case that the opposite lane is occupied by the oncoming vehicle, the system considers the movement of the oncoming vehicle for determining the overtaking timing by predicting the time-to-arrival of the oncoming vehicle. Then, the potential field for the vehicle control is calculated according to the bicycle present position and the overtaking preview position. During the bicycle approaching, the vehicle can simulate the expert drivers driving behaviour by keeping to the left while waiting until the oncoming car passes. After the oncoming vehicle completely passes, the bicycle overtaking maneuver is conducted based on the risk potential around the bicycle.

However, the simulation must be conducted with the various pattern of the bicycle and the oncoming vehicle such as the sudden change in the bicycle direction or the change in velocity of each obstacle to verify the effectiveness of the

system. Also, the system can be improved for the velocity and steering profile in order to deal with the driver acceptance, which is the big issue for both autonomous driving and driving assistance systems.

REFERENCES

Traffic Bureau, National Police Agency, Statistics 2007 road accidents Japan, International Association of Traffic and Safety Sciences (IATSS), (2008)

Noriyasu Noto, Hiroyuki Okuda, Yuichi Tazaki, Tatsuya Suzuki (2011), *"Identification of Personalized Potential Field and Its Application to Obstacle Avoidance Assisting Control"*, 2011 JSAE Annual Congress (Spring) Manuscript, No.138-11(2011), pp.11-14. (in Japanese)

Hasegawa Takahiro, Pongsathorn Raksincharoensak (2014), *"Risk-Potential Based Motion Planning and Control of Proactive Driving Intelligence System for Enhancing Active Safety"*, AVEC'14

Khatib, O., "Real-Time Obstacle Avoidance for Manipulators and Mobile Robots", International Journal of Robotics Research, Vol.5, No.1, pp.90-98.

Ribeiro, M.I., "Obstacle Avoidance", (2005) available from <http://users.isr.ist.utl.pt/~mir/pub/ObstacleAvoidance.pdf>, (accessed 2014-5-26)

Iwasawa Issei, Pongsathorn Raksincharoensak (2012), *"Study on Hazard-Anticipatory Driving Assistance System for Preventing Pedestrian Collisions in Unsignalized intersection"*, SI2012

Detailed Investigation of Real-time Steering Entropy Sensitivity in Calling Events

Takayuki Kondoh* ** Shane McLaughlin* Tomohiro Yamamura**
Nobuyuki Kuge** Miguel Perez * Takashi Sunda**

*Virginia Tech Transportation Institute, Blacksburg, VA 26041 USA
(Tel: +1(540)-231-1091; e-mail: {tkondo, smclaughlin, mperez }@vtti.vt.edu).
**Nissan Motor Co., Ltd., Atsugi, Kanagawa 2430123 JAPAN
(e-mail:{t_kondoh, t-yamamura, n-kuge, t-sunda}@mail.nissan.co.jp)

Abstract: On-board driver state monitoring is considered one of technologies that could reduce traffic accidents caused by human errors, particularly in cases of higher workload due to driver distraction. An approach to assessing driver workload using a real-time steering entropy (RSE) method has been proposed by the authors. RSE quantifies the nature of a driver's corrective steering with an index of relative entropy (*RHp*) from information theory. The higher the driver workload, the higher the *RHp*. In this paper, the RSE method was applied to naturalistic driving database gathered from 18 drivers in the United States under joint research between Virginia Tech Transportation Institute (VTTI) and Nissan Motor. *RHp* was calculated in off line simulation, and cases where the diver's state indicated higher *RHp* were reviewed in through using video. The result indicates that the RSE method detected over 80% of the cases within 300 sec from when the handheld call started. There may also be differences in the onset of *RHp* behavior between calls initiated by the driver (outgoing) and incoming calls.

Keywords: Driver Workload, Driver Monitoring and Driver State Detection

1. INTRODUCTION

Pickrell & Ye (2013) estimated 660,000 drivers in U.S. use cell phones or manipulating electronic devices while driving during daytime hours. And National Safety Council (2013) reported that 3,154 people died by motor vehicle crashes involving distracted drivers and approximately 424,000 crashed in 2013. Active safety techniques are needed to reduce the number of traffic accidents involving distracted driving. Techniques for accurately monitoring the driver's condition could be used to recognize lower levels of attention, distraction, or other factors.

The steering entropy (SE) method (Nakayama et al. 1999) has been proposed as one technique for estimating a driver's physical or mental condition. The SE method is an excellent technique for quantifying driver workload without the driver being conscious of any measurement because it makes use of the steering angle signal, which is a readily obtainable vehicle signal. On the other hand, the SE method cannot calculate driver workload in real time. In addition, it is difficult to obtain measurements in real-world driving due to the wide variety of roadway environments. Therefore, the authors have developed a real-time steering entropy (RSE) method which capable of real time measurement of driver workload in typical traffic environments. The practical utility of the RSE method was evaluated by applying the algorithm to naturalistic driving data, thereby providing a simulation or bench test of the algorithm.

In this paper, the RSE method is described with comparison with other measurements and the conventional steering entropy method. An overview of the RSE calculations is provided and a description of a previous RSE study, which identified a set of cases used in the present work. Finally, a review of RSE cases is conducted to investigate performance around making and receiving calls while driving.

2. CONVENTIONAL DRIVING WORKLOAD EVALUATION METHODS AND ISSUES

2.1 Driver Workload Evaluation Methods

Various methods have been proposed to date for evaluating the driver's condition, including techniques for assessing driver workload. Methods of evaluating driver workload include subjective evaluations, physiological indexes, driver behavior indexes and estimations based on vehicle behavior. Subjective evaluation methods include the National Aeronautics and Space Administration Task Load Index (NASA-TLX) (Hart et al. 1998) and the use of the rating scale mental effort (RSME) (Zijlstra 1993). While simple measurements can be made with these methods, they cannot be directly applied to vehicle systems because they are based on self-reports given by drivers. Evaluation methods based on physiological indexes include the use of brain waves, blood pressure and salivary cortisol, among other things. While quantitative data can be obtained with these indexes, it is necessary for the driver to wear some type of measuring

equipment, which can interfere with the driving task or change the workload. Methods using estimations based on whole vehicle measures assume that driver workload is pass on to driving operations, and so would be reflected in vehicle kinematics. However, based on the mass of the vehicle and complex kinematic interactions of subsystems, it is difficult to detect subtle changes in the driver's condition through vehicle kinematics.

On the other hand, measures of driving operations such as the driver's operation of the pedals or steering maneuvers can be obtained non-intrusively and without requiring the driver to alter his or her behavior. Therefore, they are regarded as the most promising candidates for application to vehicle systems.

2.2 Overview and Issues of SE Method

The SE method is a technique for estimating driver workload from steering operations. Specifically, it is method for indirectly measuring driver workload by quantifying the smoothness of the driver's steering control as an entropy value. This method was developed in the 1990s at Nissan Technical Center North America-Cambridge Basic Research (NTCNA-CBR). Entropy (*Hp*) (Shannon 1948) refers to entropy in the context of information theory and represents the degree of uncertainty, randomness or disorder. The SE method is based on the characteristic that entropy values decrease when steering operations are smooth (i.e., not random). Situations involving high driver workload, such as when performing a secondary task while driving, can be detected on the basis of SE because they are often accompanied by the execution of sudden corrective steering maneuvers. The results of a previous study by Nakayama et al. (1999) suggested that increasing the frequency of mental arithmetic tasks while driving increased *Hp* values. However, the SE method computes the magnitude of entropy with a widely varied set of conditions that include the road type, vehicle speeds and other factors. This variance and the computational requirements have made it difficult to use this method in real-time in actual driving environments.

3. OVERVIEW OF REAL-TIME STEERING ENTROPY METHOD

3.1 Aims and Features

The real-time steering entropy (RSE) method used in this work reduces some of the challenges to the SE method through use of baseline data for an individual driver that are collected in real-time, monitoring a recent and a long term time window, and limiting use to situations that will support application (e.g., straight segments and expressways).

These features make it possible to quantify driver workload in real time using a vehicle system without being affected by the driving environment or individual driver differences.

3.2 Relative Entropy

The RSE method calculates probability distributions *PE* for two time windows. One is a long-term time window that

calculates a baseline steering behavior of an individual driver. The other is a short-term time window that calculates the driver's steering behavior in the most recent time period. The difference in the *PE* distributions in these two time windows represents relative entropy (*RHp*), which is calculated with Eq. (1) below (Kullback and Leibler 1951, Kullback 1968) and expresses the change in steering characteristics due to the driver's current condition.

$$D_{KL} = \sum Q(i) \cdot \log \frac{Q(i)}{P(i)} \qquad (1)$$

In probability theory and information theory, relative entropy, also referred to as Kullback-Leibler divergence, is a measure of the difference between two probability distributions *P* and *Q*. Here, *Q* represents data or a currently observed value while *P* is given as a model or baseline value. In the RSE method developed in this study, *Q* corresponds to the most recent steering behavior and *P* to the longer time window description of the individual driver's steering behavior. The selection of appropriate durations for the two windows is a balance between avoiding momentary disturbances, establishing a baseline, and achieving fairly rapid recognition of disturbances. The approach used in this evaluation to resolve this dilemma was to define a long time window for *P* in the initial learning phase so as to effect an early transition to the evaluation phase, then extending the time window of *P* to the desired length as needed. As one example, the short time windows and the long time windows are set 90 sec and 180 sec in the initial learning phase, and after the learning phase, they are set 90 sec and 2160 sec, respectively. These time windows were determined on the basis of data obtained in driving situations involving high levels of driver workload in tests conducted on the company's proving ground and from the standpoints of the detection sensitivity of *Q* and the convergence time and stability of *P*.

3.3 Calculation of Frequency Distributions Using a Recursive Calculation Procedure

In calculating the *Hp* value with the conventional SE method, it is necessary to measure all the *PE* values within a certain predetermined time frame and then calculate the frequency distribution. For example, if a time frame of 180 sec is defined, there must be sufficient system memory capacity for 3,600 pieces of *PE* data (in case of sampling by 50 msec). Moreover, it is necessary to set a longer time frame in order to measure the individual steering characteristics of a driver, which requires enormous memory capacity. In order to minimize the memory requirements, the frequency distributions calculated the previous time samples were updated recursively using newly measured *PE* values.

3.4 Driving Condition Targeted for RSE Method

The RSE method processes small changes in steering angle to evaluate workload. Large steering wheel movements such as are found when cornering and changing lanes cannot be reasonably incorporated into the distributions, and so are not passed to the RSE algorithm. Based on this approach, the

RSE method is designed for use when driving on straight segments of expressways where the steering angle does not change greatly.

3.5 Calculation Procedure

Calculations of the RSE are performed at a 50 msec cycle as is done in the conventional SE method (Nakayama et al. 1999). The following section provides an overview of the calculations. For a detailed description, see Kondoh et al. (2015). Figure 1 shows a flowchart of real-time steering entropy.

Calculation of steering angle prediction error (*PE*) is performed by retaining previous steering angle points and performing a second-order Taylor expansion on the average steering angles to predict the present steering angle. The difference between the actual steering angle and the predicted steering angle is the *PE*. The *PE* value is a signed quantity because there are times when it contains error on the right side and times when it contains error on the left side.

As mentioned previously, the RSE method does not evaluate *PE* in situations where the steering angle changes greatly such as when driving at low speed, cornering and changing lanes. In this study, the *RHp* value was regarded as being zero and the *PE* distribution was not updated when the vehicle speed was less than 60 km/h, the steering angle was greater than 12 deg. or a turn signal indicator was on.

PE distribution values are saved in nine bins and only for the most recent probability density values, thereby minimizing memory requirements. With this procedure, the *PE* is characterize in two *PE* distributions, i.e., *Q* for the most recent steering characteristics and *P* for individual steering characteristics.

The updated *PE* distributions are treated as the latest distributions and saved.

The absolute entropy of the two *PE* distributions is then calculated and then followed by relative entropy (*RHp*) is calculated below using the updated *PE* distributions and the absolute entropy values

If the *RHp* value exceeds a certain given threshold, the event is judged to have high driver workload.

Repeating the procedure above makes it possible to calculate *RHp* in real time. The logic was installed in a vehicle controller and it was confirmed that the calculations were performed in real time.

4. SIMULATION PERFORMED USING ACTUAL DRIVING DATA

4.1 Driver Behavior Database Used in RSE Method Evaluation by Simulation

The driver behavior database used in this evaluation contains naturalistic driving study data collected jointly with the Virginia Tech Transportation Institute (VTTI) in the United States. Driver behavior was measured using two instrumented
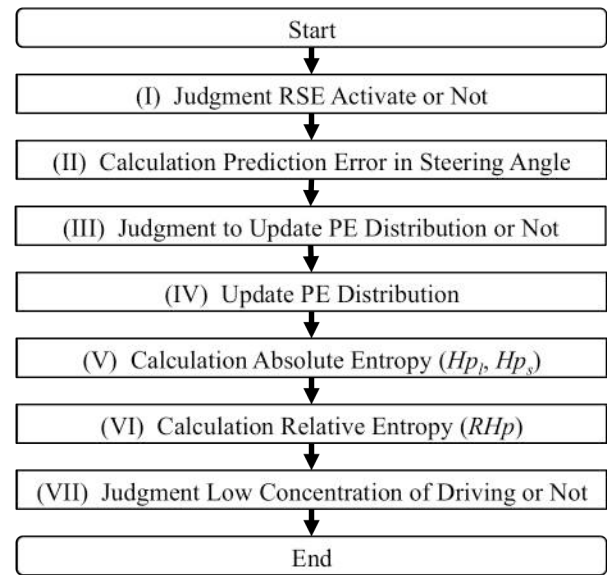
Fig. 1. Flowchart of real-time steering entropy.

Infiniti M35 cars (Figure 2) fitted with five video cameras (Figure 3) and measuring instruments. The participants in the experiment were 18 ordinary drivers (10 males; 8 females) living in the Washington, D.C. area. They ranged in age from 35 to 70 years old (49.8 ±10.8 years) and all of them were current owners and drivers of Infiniti vehicles. Data collection and analysis were conducted with the approval (IRB#: 10-624) of the Virginia Tech Institutional Review Board and under the assurance of the ethical, safety and privacy rights of the participants who gave their written informed consent to participate in the study. The instrumented cars were lent to the participants each of whom was allowed to use the car as they normally would during a study period of 14 days. In total, naturalistic driving behavior data were collected for 2,303 trips covering an aggregate driving distance of 39,000 km and an aggregate driving time of 730 hours.

The evaluation of the RSE method required a learning phase. Accordingly, the data targeted for use in the simulation were for trips in which the vehicle speed was 60 kph or higher for a period of 15 min. or longer. Because trips meeting these conditions were not measured for three of the participants, the simulation was conducted using the data recorded for the remaining 15 participants. Therefore, the driver behavior data used in the evaluation were for 265 trips covering an aggregate driving distance of 10,418 km and an aggregate driving time of 190 hours.

4.2 Evaluation Method Used in Simulation

Following the collection of driver behavior data, the viability of using the RSE method to quantify driver workload was examined. The RSE method was activated in an off-line simulation to detect events in which the *RHp* value exceeded the given threshold. The actual driving situation in the detected events was then confirmed using video and recorded

driving data. Driver behavior in addition to driving operations was identified by watching the video.

4.3 Previous Simulation Results

As mentioned in the introduction, in a previous study (Kondoh, et al., 2015), a total of 233 events were recorded in which *RHp* exceeded the threshold for 10 participants among the 15 whose data were used in the simulation. Such events were not observed for the other five participants. The driver's condition was judged to be the cause of the high *RHp* value in 211 of the events and the driving environment, including a rough road, was judged to be the cause in 22 events.

Figure 8 presents the results of a video analysis of the 211 events in which the driver's condition was judged to be the cause of the high *RHp* value. The major reasons were observed to be calling on a cellphone or talking to a passenger (39%; 83 events), looking aside or continuous operation of the navigation system controls (22%; 46 events), detection of reduced alertness or fatigue (31%; 65 events), and others (8%; 17 events). The total of 211 detected events corresponds to 1.1 detection per hour of driving.

This result made it clear that the RSE method is capable of detecting most of the secondary tasks that are observed in actual driving situations.

4.4 Analysis of RHp Behavior Involving Calling Events

According to previous study, 55 events (26% of all detected events) were judged the calling as primary cause. In order to explore the sensitivity of *RHp* around calling events behavior of *RHp* on calling events was investigated in additional detail. These analysis were conducted with the approval of the Virginia Tech Institutional Review Board (IRB#: 15-460).

Calling events were categorized as outgoing calls (the driver calls someone) and incoming calls (someone calls the driver). Calling events were categorized through review of video. In addition to determining how the call originated the time stamp at which the call started was noted. Note that the vehicles did not record audio, so the video was used to determine when calls began. For both outgoing and incoming calls, the timestamp at which the call started was identified as when the driver's hand movement towards a phone or mouth movement.

Fifty-five calling events were analyzed. 28 handheld calling events (outgoing calls and incoming calls are 8 and 20, respectively) were used on this study. Other 19 events were detected within a single call and for eight events it was not possible to determine when the call started (e.g., the call had already started when the video recording began, the hands-free call was hard to identify when the calls start).

Figure 5 presents that the histogram of the relationship between starting to call and detected timing by RSE. 80% of calling events were detected before 300 sec passed since the call started.

Figure 6 presents examples of time histories of the simulation results for outgoing calls. This example is typical outgoing calls. In this figure, the zero point on horizontal axis

Fig. 2. Instrumented car (Infiniti M35).
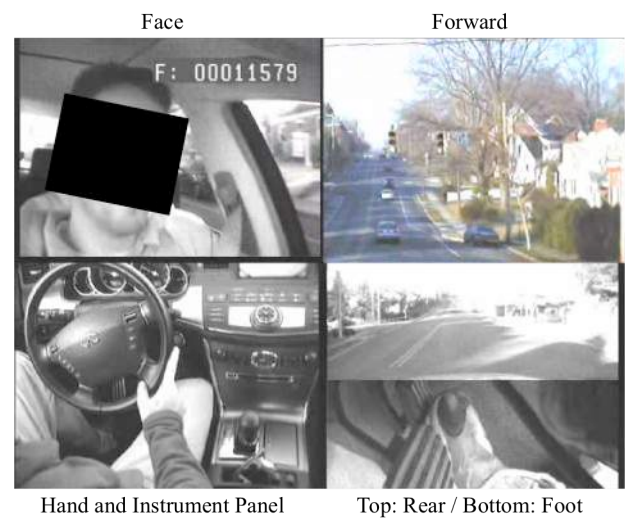
Fig. 3. Video views collected.
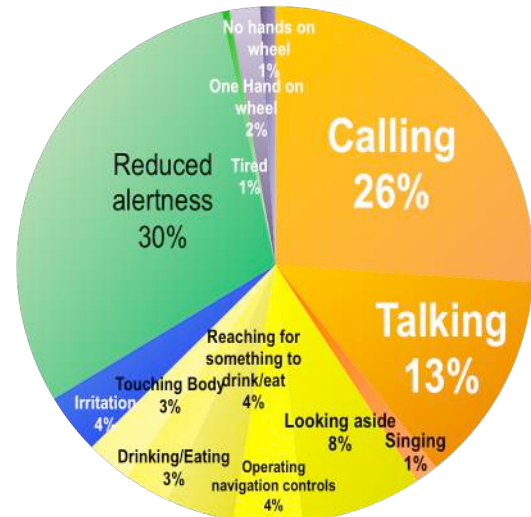
Fig. 4. Detected conditions in which drivers encountered high workload on driving.

indicates the point in time when the call started. In this example, *RHp* started to increase before call started. After 49.9 sec passed from the start of the call, the RSE value exceeded the threshold indicating high workload. Around 90 sec in this figure, it seems that *RHp* suddenly went to zero.

In this case, RSE computation was zeroed while the turn signal was activated during a lane change (see green line on second panel).

Figure 7 presents examples of time histories of the simulation results for incoming calls. In this figure, zero point on lateral axis shows the timing of the call started. In this figure, the relative entropy was observed to increase after the call started. This example is typical incoming calls. *RHp* started to increase after the call started. In this example, after 75.5 sec passed since the call started, RSE values indicated a high workload event.

Figure 8 provides an overlay of *RHp* behavior from at the start of multiple calls, both incoming (cyan) and outgoing (magenta). In general, the trend observed for outgoing and incoming calls is portrayed in this figure. Increases in *RHp* were found before the start of the call for outgoing calls. Additionally, the slope of the two cases. The incoming calls may have an increase in *RHp* over a shorter period of time than for the outgoing calls.

4.5 Discussion

Figure 5 shows the response performance of *RHp* for calling. Over 80% of detected calling events are detected less than 300 sec after the call started based on the threshold in this simulation. This performance could be adjusted through the adjustment of the selected threshold. The current threshold appears to provide a reasonable balance, detecting distraction within an effective period of time, and minimizing annoyance for the driver.

Figure 6 and Figure 7 present typical *RHp* behavior in case of outgoing calls and incoming calls. *RHp* behavior appears to follow with what would be expected of the onset of distraction for the two cases. In the case of outgoing calls, prior to initiation of the call, the driver is thinking about the call content, looking for the cell phone, dialing, and waiting for the person to answer. For incoming calls, the additional workload is minimal until the driver detects the incoming call, looks for the cell phone, and pushing the answer button. Nakayama et al.(1999) demonstrated that *Hp* (conventional SE) increased during various activities while driving (i.e. conversation, thinking, eye diversion, operation of equipment). *RHp* values would also be expected to indicate changes due to these driver behaviors. *RHp* was also observed to increase in an accelerated manner after answering an incoming call. Based on this, it appears that incoming calls may create a time pressure for the driver that is not as pressing as in situations where the driver is planning to make an outgoing call).

Schroeder et al.(2013) reported that 14.3% of drivers send text message or e-mail while driving. This study also reported that 35.3% of drivers continue to drive while completing the message. Texting while driving contributes considerable risk. RSE has possibility to identify these situations.
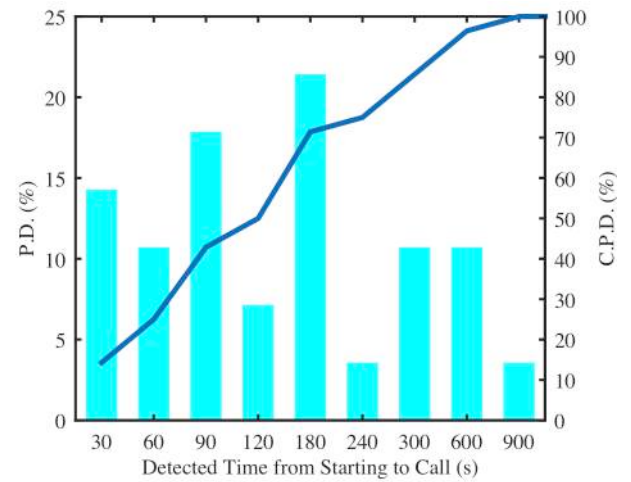
Fig. 5. Detection characteristic of sensitivity after call started.
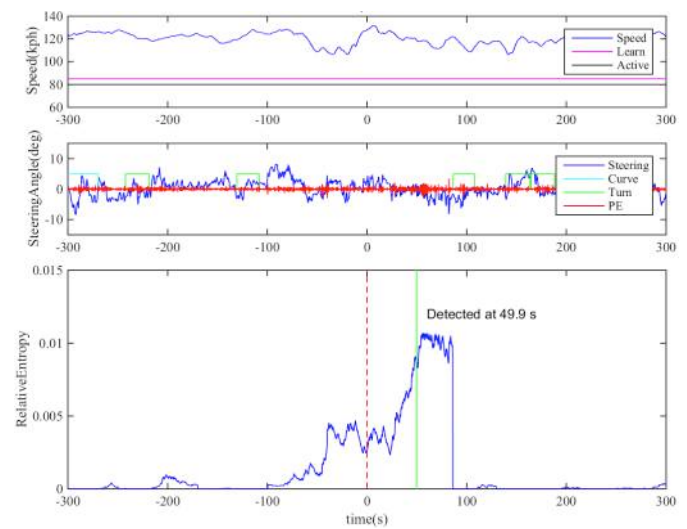
Fig. 6. Time histories of vehicle speed, steering angle and *RHp* in outgoing calls.
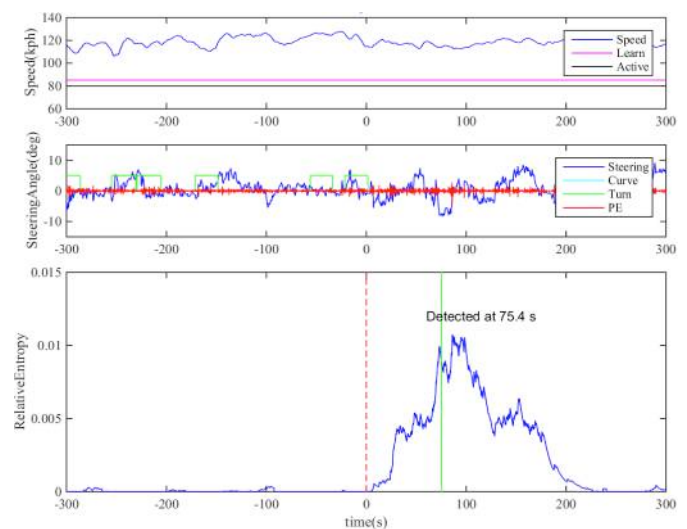
Fig. 7. Time histories of vehicle speed, steering angle and *RHp* in incoming calls.

5. CONCLUSIION

This paper has described a real-time steering entropy (RSE) method that has good sensitivity for quantifying driver workload in real-world driving environments. In a simulation conducted using actual naturalistic driving study data, the results confirmed that *RHp*, which was calculated as a degree of workload by the RSE method, can recognize changes in driver behavior when involved in making and receiving calls.

It is envisioned that the RSE method for quantifying driver workload can also be useful in detecting issues such as reduced alertness and distracted driving. In addition to issuing attention alerts to drivers, this method can also presumably be used in driver support systems to vary the method and degree of assistance according to the driver's workload level, or it could be applied to in-vehicle infotainment (IVI) systems to control the quantity and timing of information provided to drivers according to their current level of workload.
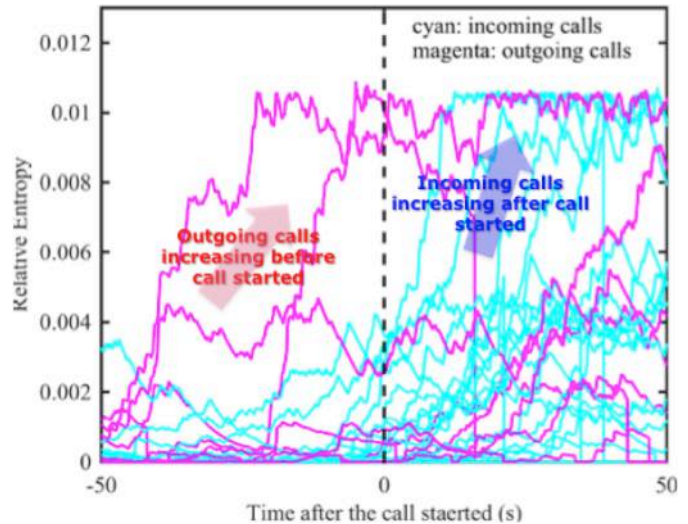
Fig. 8. Comparison *RHp* behavior around call started between outgoing calls and incoming calls.

REFERENCES

Hart, S. G. and Saveland, L. E. (1998). Development of NASA-TLX (Task Load Index): Results of empirical and theoretical research, Human Mental Workload, North Holland Press, Amsterdam.

Kullback, S. and Leibler, R. A. (1951). On information and sufficiency, *The Annals of Mathematical Statistics*, vol. 22, pp. 79-86.

Kullback, S. (1968). *Information Theory and Statistics*, Dover Publications, New York.

Kondoh, T., Yamamura, T., Kuge, N., Perez, M., Sunda, T. (2015). Development of a Real-time Steering Entropy Method for Quantifying Driver's Workload, *Transactions of the Society of Automotive Engineers of Japan*, 46(1), pp.167-172. (in Japanese)

Nakayama, O., Futami, T., Nakamura, T., and Boer, E. (1999). Development of a Steering Entropy Method for Evaluating Driver Workload, *SAE Technical Paper*, 1999-01-0892.

National Safety Council. (2014). Crashes Involving Cell Phones.

Pickrell, T. M., & Ye, T. J. (2013). Driver Electronic Device Use in 2011. (Report No. DOT HS 811 719). Washington, DC: National Highway Traffic Safety Administration.

Schroeder, P., Meyers, M., Kostyniuk, L. (2013). National survey on distracted driving attitudes and behaviors – 2012, NHTSA, DOT HS 811 729.

Shannon, C. E. (1948). A Mathematical Theory of Communication, *The Bell System Technical Journal*, Vol. 27, pp.379-423.

Zijlstra, F.R.H. (1993). Efficiency in work behavior, Delft University Press, The Netherlands.

Analysis of Driver Behavior for Joint Human–machine Systems Design of Intelligent Driving System

Tsukasa Shimizu*, Masayuki Okuwa*, Pongsathorn Raksincharoensak**

* Toyota Central R&D Labs., Inc., 41-1 Yokomichi, Nagakute,
Aichi 480-1192, JAPAN (e-mail: {shimizu, okuwa}@mosk.tytlabs.co.jp)
** Department of Mechanical Systems Engineering, Tokyo University of Agriculture
and Technology, 2-24-16 Naka-cho, Koganei, Tokyo, 184-8588, JAPAN
(e-mail: pong@cc.tuat.ac.jp)

Abstract: An intelligent driving system that combines the AEB function and the preventive driving assistance system (PDAS) that assists a driver to drive like experienced drivers can improve traffic safety in hazardous situations. We aim to develop PDAS in the shared control approach. This study analyzed driver behaviors in the passing-a-car scenario as an example of a potentially hazardous situation to assess the interaction between the driver and PDAS. Using driving data collected from 29 participants in a controlled test course environment, drivers were categorized into four driver groups based on their safety margins in the passing-a-car scenario. Then the driver behaviors were compared among driver groups. Some drivers belonging to unsafe driver groups passed the parked car with insufficiently reduced speed for their lateral gap. Examining their pedal operations, we found two patterns of unsafe pedal operations resulting in the insufficient speed reduction: delayed pedal-off and no pedal-off. For these unsafe pedal operations, we proposed a speed reduction support strategy.

Keywords: Driver behavior, Shared control, Active safety, Advanced driver assistance system

1. INTRODUCTION

Passing a blind area, such as one behind a parked car or a blind corner at an intersection, is a potentially hazardous situation because other road users such as pedestrians and bicycles might suddenly emerge. Although automatic emergency brake (AEB) systems for pedestrians (Coelingh et al., 2010) have been available on the market and although their collision mitigation effectiveness has been demonstrated (Rosén et al., 2010), current AEB systems are less effective to avoid or mitigate a collision when a pedestrian suddenly emerges from a blind area. For a preliminary experiment for AEB tests for pedestrians that Euro NCAP plans to conduct from 2016, the test scenario with a child emerging from behind parked cars was found to be the most demanding for AEB systems (Lemmen et al., 2013).

In such hazardous situations, however, experienced drivers drive in a preventive manner, slowing and maintaining a lateral safety margin, preparing for the possible sudden appearance of other road users (Shimizu et al., 2013). Hasegawa et al. (2014) demonstrated that a combination of AEB systems with preventive driving simulated from experienced drivers' driving data can avoid collisions with a pedestrian emerging from behind a parked car. Therefore, an intelligent driving system that combines the AEB function and the preventive driving assistance that assists a driver to drive like experienced drivers can be expected to improve traffic safety in potentially hazardous situations.

We intend to develop a preventive driving assistance system (PDAS) using a shared control approach (Abbink et al., 2012), by which a driver is always in the control loop and the assistance system cooperates as needed. To develop our PDAS, reference motion planning (Hasegawa et al., 2014) is necessary for assistance. Moreover, investigating how drivers who are presumed to be assisted by PDAS behave in potentially hazardous situations is important for the design of driver–PDAS interactions. This study examines driver behaviors in a scenario where a driver passes a parked car (passing-a-parked-car scenario) as a typical case of the potentially hazardous situations. Based on those results, we discuss the design of driver–PDAS interactions.

The paper is structured as follows: Section 2 presents our motivations and goals of this study. Section 3 describes an experiment used for driving data collection. Section 4 explains our examination of driver behaviors in the passing-a-parked-car scenario. Section 5 presents discussion of the PDAS design. Finally, we conclude our study in Section 6.

2. MOTIVATIONS AND GOALS

Several studies have analyzed driver behaviors of normal drivers (not expert drivers or commercial drivers) in potentially hazardous situations. Takemoto et al. (2012) investigated unsafe behaviors of normal drivers in the passing-a-parked-car scenario in actual traffic environments with specific examination of the vehicle speed (passing speed) and lateral gap (passing gap) to the parked car at the moment of passing it, each of which is a key point for safe

driving in the scenario emphasized by driving school instructors. Comparing the passing speed and passing gap between a normal driver and the driving school instructors revealed that unsafe normal drivers often pass by the parked car with an insufficient lateral gap for high speed.

Herein, we also examine driver behaviors in a passing-a-parked-car scenario, but our study differs from the previous study in several ways: First, we examine driving data collected at a controlled test course environment. In the previous study, driving data were collected on public roads and were screened for elimination of effects by other traffic factors besides the parked car. However, they could not be controlled adequately. Second, we collected driving data repeatedly from each participant (driver). In contrast, the previous study examined driving data of each driver, constituting a small sample. Consequently, we can verify the repeatability of characteristic driver behaviors of the respective drivers. Third, we assess vehicle motion and driver operations not only at the moment of passing by the parked car, but also during the process of approaching it because understanding of vehicle motion and driver operations while approaching is necessary for the design of driver–PDAS interactions.

In the analysis (Section 4), we first verify the within-driver repeatability of driver behaviors and clarify differences among drivers. Next, drivers are categorized into four groups based on the passing speed and passing gap to examine between-group differences in driver behaviors. Furthermore, we select typical drivers from each driver group to compare their vehicle motion and operations that produce the passing speed and passing gap.

3. EXPERIMENT FOR DRIVING DATA COLLECTION

3.1 Participants

This study examined 20 elderly drivers (15 men, 5 women; average age of 70.85 years, range 62–80 years) who participated in the driving data collection experiment. In addition, 6 normal drivers (4 men and 2 women in their 30s and 40s) and three expert drivers (3 men in their 20s, 40s and 50s) were recruited as non-elderly drivers. We obtained informed consent from all participants before the experiment.

3.2 Experimental settings

The experiment was conducted on a straight course in a controlled test course environment (Fig. 1). Figure 2 shows the driving course settings used for the experiment. Two lanes divided by a white line were regarded as a two-lane road (both lanes had the same travelling direction). The course comprises three zones: a 67-m-long acceleration zone (from starting point to steering-onset point); a 50-m-long passing zone (from steering-onset point to the parked car); and an 80-m-long post-passing zone (from the parked car to goal). Pylons were located as landmarks at the starting point, steering-onset point, and goal. In the middle of the course about 120 m distant from the starting point, a minivan type vehicle (4.77 m long, 1.80 m wide, 1.55 m high) was situated to represent a parked car. A car (Prius; Toyota Motor Corp.)

equipped with a CAN data logger (30 Hz) and a RTK-GPS receiver (10 Hz) was used to produce and record driving data.
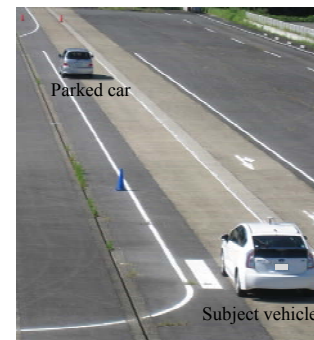
Fig. 1. Experimental environment.
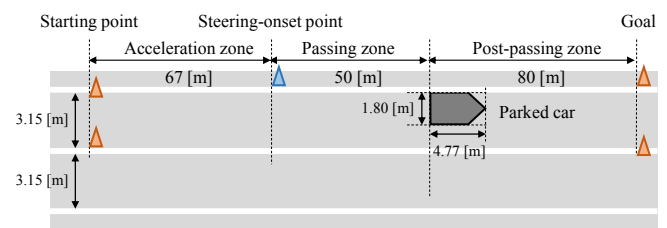
Fig. 2. Driving course settings.

3.3 Procedure

For the experiment, each driver completed five runs after three practical runs. In each run, drivers were instructed to accelerate up to around 40 km/h in the acceleration zone on the left lane. Then they were requested to pass the parked car while slowing and steering at their own judgment in the passing zone. After passing the parked car, they were instructed to drive through the goal, demonstrating control of the final vehicle status between drivers. In addition, the drivers were instructed to drive in a modestly safe manner according to their own criteria to avoid overly safe driving.

4. ANALYSIS OF DRIVER BEHAVIORS

4.1 Driving Data

RTK-GPS data are used for vehicle trajectory (change in position) analysis, and for assessing the speed and lateral gap to the parked car. Vehicle position data were resampled at 30 Hz from the smoothened raw data. Vehicle speed data were calculated based on time differences of the resampled vehicle position data. Lateral gap data were obtained by subtracting the resampled vehicle position from the parked car position. Steering wheel angle signals, accelerator pedal position signals and brake pedal pressure signals from CAN data were used, respectively, for analyses of steering operations, accelerator pedal operations, and brake pedal operations.

Figure 3 shows the coordinate system used in the analysis. The X-axis is for the longitudinal position of the vehicle. The Y-axis shows the lateral position. The origin is set at the front left corner point of the parked vehicle. The vehicle position is set at its front center point shown as (X_{vhc}, Y_{vhc}) in Fig. 3. Consequently, while the vehicle approaches the parked car, the X-position of the vehicle (X_{vhc}) is always a negative value.

When the front end of the vehicle reaches the front end of the parked car, $X_{vhc} = 0$. We regard the moment when $X_{vhc} = 0$ as the moment of passing the parked car.
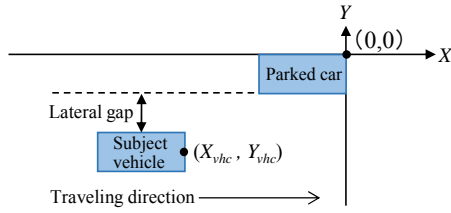

Fig. 3. Coordinate system.

4.2 Repeatability of Vehicle Motion

Figure 4 presents vehicle trajectories (left) and speed profiles (right) of three drivers as examples. Results of five runs for a driver are graphed together in each panel. The vehicle trajectory and speed profile in every run are nearly constant for a single driver, although they can vary among drivers. This within-driver repeatability and variation among drivers indicate that a driver passes the parked car in a stable manner, but the driving behavior can differ among drivers. Driver characteristics are manifested in the driver behaviors shown in the passing-in-a-car scenario.
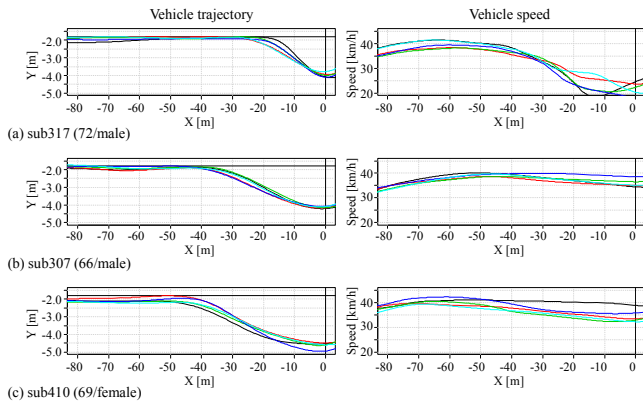
Fig. 4. Vehicle trajectories (left) and speed profiles (right) of three drivers. Age and sex of the drivers are noted in brackets after driver IDs (subNNN).

4.3 Driver Categorization

It is desirable to categorize drivers into several groups and to examine the characteristics of the group of drivers who are presumed to be assisted by PDAS instead of individual drivers. Such a categorization should be performed based on the degree of driving safety in the passing-a-parked-car scenario. As described in Section 2, driving school instructors emphasize the passing speed and passing gap as key points of safe driving in the passing-a-parked-car scenario (Takemoto et al., 2012). Therefore, in this study, we categorize drivers based on passing speed and passing gap.

Before driver categorization, safety in the passing-a-parked-car scenario is considered from the perspective of the passing speed and passing gap. Figure 5 is a two-dimensional plot of the average passing speed and average passing gap for all drivers. The points are widely spread, indicating that passing

speed and passing gap vary among drivers. The closer a point is shown to the bottom right in Fig. 5, the larger safety margin is when passing by the parked car; such drivers use a lower passing speed and larger passing gap. However, points shown along an upward-sloping line, such as points sub317, sub706, and sub407, do not clarify which driver is safer. Sub407 has a safety margin by keeping a large lateral gap, whereas sub317 does so by slowing down. Sub706 can be regarded as equally safe to sub407 and sub317 because sub706 takes a safety margin by slowing moderately while keeping a moderate lateral gap.
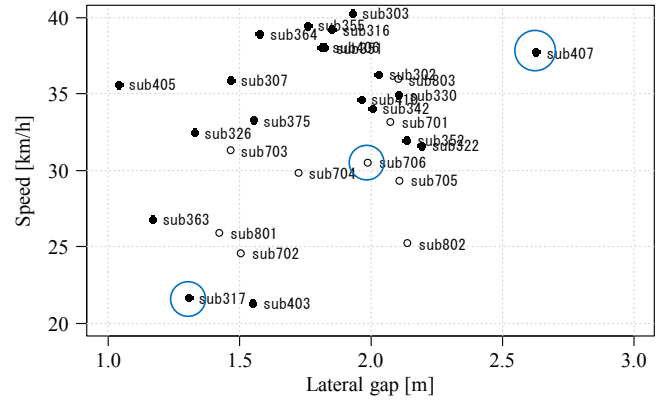
Fig. 5. Average passing speed and average passing gap. Filled points represent data for elderly drivers and open points represent data for non-elderly drivers.

Based on the idea of a safety margin when passing the parked car described above, assuming that drivers shown along some upward-sloping line in Fig. 5 allow equal safety margins, we can categorize drivers into four driver groups using repeated linear regression methods. The driver categorization procedure is the following (Fig. 6):

1. Regression line l_0 is obtained from all points in Fig. 5.

2. Points above l_0 are categorized as group A; those below l_0 are in Group B.

3. Regression line l_1 is obtained from all points in Group A.

4. For points in group A, points above l_1 are categorized as Group A1; those below l_1 are categorized as Group A2.

5. Regression line l_2 is obtained from all points in Group B.

6. For points in group B, points above l_2 are categorized as Group B1; those below l_2 are categorized as Group B2.
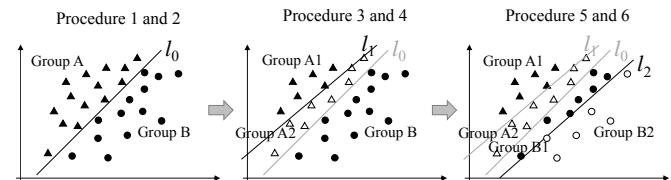
Fig. 6. Steps of driver categorization.

The driver categorization results are portrayed in Fig. 7. Regression lines obtained from data points in each driver group are also portrayed in Fig. 7. Because data points belonging to each driver group are roughly located along the

corresponding regression line, drivers have been categorized into four groups based on the idea of safety margin: Group A1, Group A2, Group B1, and Group B2. The Group A1 and Group A2 drivers allow smaller safety margins than Group B1 and Group B2 drivers do: the former pass the parked car at higher speed than the latter, given the same lateral gap. Categorization results show that Group A1 and Group A2 drivers can be assisted by PDAS.

The numbers of drivers categorized into driver groups are shown by driver type (elderly, normal, and expert) in Table 1. The proportion of Group A1 and Group A2 drivers is higher for elderly drivers than for non-elderly drivers, indicating that elderly drivers might be the main target of PDAS.
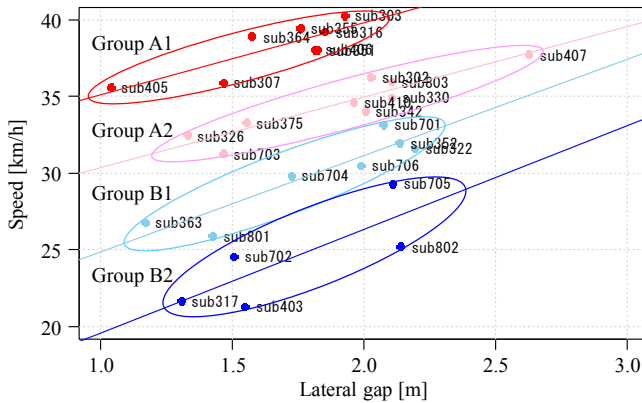
Fig. 7. Driver categorization result. Lines are regression lines obtained from data points belonging to the corresponding groups.

Table 1. Summary of driver categorization

Group	Elderly	Normal	Expert
A1	8	0	0
A2	7	1	1
B1	3	3	1
B2	2	2	1

4.4 Passing Gap and Passing Speed

Figure 8 presents boxplots of the passing gap and passing speed by driver groups. For the passing gap (Fig. 8(a)), ANOVA showed a significant main effect of driver group $(F(3,140) = 3.75, p < 0.05)$. Tukey's test was performed for pairwise comparisons between driver groups. Results show a significant difference between Group A1 and Group A2 $(p < 0.05)$. Differences of average passing gaps between them are 0.25 m, which is not much different practically from the perspective of the PDAS design. Consequently, all the driver groups are nearly identical in terms of the passing gap. Regarding passing speed (Fig. 8(b)), ANOVA showed a significant main effect of the driver group $(F(3,140) = 113.4, p < 0.01)$ and Tukey's test showed significant differences for all pairs of driver groups $(p < 0.01)$. It is readily apparent that Group A1 and Group A2 speeds are much higher than those of Group B1 and Group B2. According to results, a major problem of Group A1 and Group A2 in the passing-a-car scenario is insufficient speed reduction for their lateral gap.
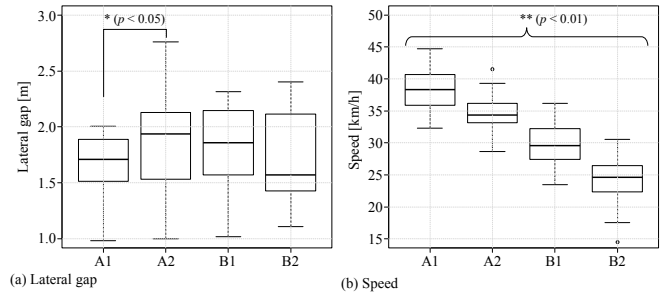
Fig. 8. Comparison of (a) passing gap and (b) passing speed among driver groups.

4.5 Speed and Lateral Gap at Onset of Steering

Insufficient speed reduction of Group A1 and Group A2 drivers described in the previous subsection is explainable by their delay of preparing to pass by the parked car or their speed choice. Consequently, in this subsection, we compare the timing of intending to passing by the parked car between driver groups. Then, we examine the speed and lateral gap at this moment. The onset of steering, which is determined as the moment of reaching at 15 percent of the maximum steering wheel angle to the right, are used as the timing of intention to pass it.

Figure 9 depicts barplots of X-position (longitudinal distance to parked car) and THW at the onset of steering by driver groups. An ANOVA showed no significant main effect of driver groups on X-position $(F(3,140) = 1.00, p > 0.05)$ and THW $(F(3,140) = 0.53, p > 0.05)$. As the maximum difference of average THWs between driver groups (Group B1 and Group B2) is 0.24 s, the onset of steering, i.e., the timing of intending to passing by the parked car is almost identical, on average, among driver groups.
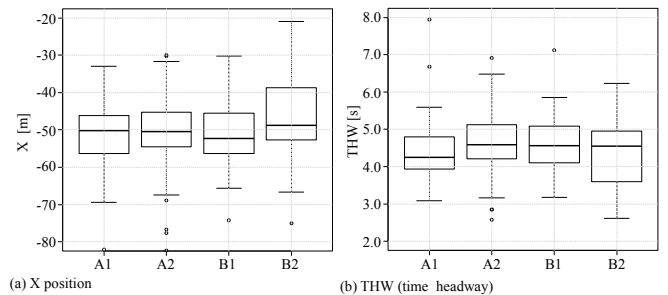
Fig. 9. Onset of steering in terms of (a) longitudinal distance to the parked car (X-position) and (b) time headway (THW).

Figure 10 portrays barplots of the lateral gap to the parked car and speed at the onset of steering by driver groups. An ANOVA showed a significant main effect of driver groups on lateral gap $(F(3,140) = 9.8, p < 0.01)$) and post hoc Tukey's test showed significant differences in several pairs of driver groups. However, as the maximum difference of average lateral gap separating them is 0.19 m (Group A1 and Group B1), the lateral gap at the onset of steering can be regarded as being almost identical among driver groups. For speed, a significant main effect of driver groups by ANOVA $(F(3, 140) = 12.96, p < 0.01)$ and Tukey's test showed significant differences in several pairs of driver groups. The maximum

difference of average speed between them, which is 4 km/h (Group A1 and Group B2) is much less than that for the average passing speed. Consequently, the large difference of passing speed between driver groups is attributed to driver operations after the onset of steering.
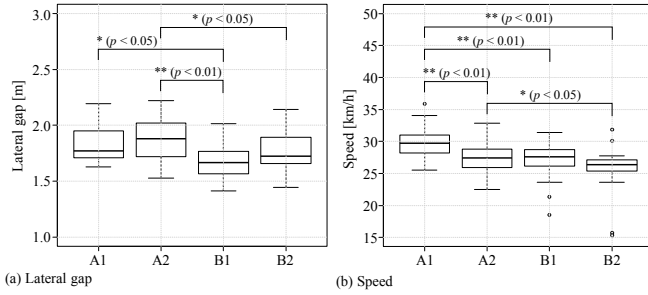

(a) Lateral gap   (b) Speed

Fig. 10. Comparison of (a) passing gap and (b) speed at the onset of steering between driver groups.

4.6 Steering Operations and Pedal Operations

To examine driver operations after the onset of steering, a typical driver is selected from each driver group and compared to assess their operation patterns. We select drivers in accordance with the criterion of nearly identical average passing gap (approx. 1.5 m). Table 2 shows selected drivers (see also Fig. 7)

Table 2. Selected drivers

Group	Driver ID	Driver type	Lateral gap (avg.) [m]	Speed (avg.) [km/h]
A1	sub307	Elderly	1.47	35.93
A2	sub375	Elderly	1.55	33.30
B1	sub801	Expert	1.42	25.93
B2	sub702	Normal	1.51	24.59

Before examining their operations, let us confirm their vehicle trajectories and speed profiles (Fig. 11). As shown in Fig. 4, repeatability of the vehicle trajectories and speed profiles within a driver is also shown. Because the selected drivers have a nearly identical average passing gap, their vehicle trajectories are also almost identical, with a slight difference in the onset of steering. However, speed profiles are much different between them and are representative speed patterns for the corresponding driver groups.

Figure 12 shows steering operation profiles (steering wheel angle) and pedal operation profiles while approaching the parked car. For visual comprehension, weighted combinations of accelerator pedal position profiles (positive values) and brake pedal pressure profiles (negative values) are used for pedal operation profiles. Within-driver repeatability of steering operations and pedal operations, which contribute to within-driver repeatability of vehicle motions, is shown. Steering operation profiles are roughly identical between the drivers, except for sub375, while pedal operation profiles greatly differ among drivers. Differences among drivers are more prominent in pedal operation profiles than in speed profiles. Sub801 (Group B1) and sub701 (Group B2) slowed by pushing the brake pedal after taking the foot off the accelerator pedal. In contrast, sub307 (Group

A1) and sub375 (Group A2) did not push the brake pedal at all while approaching the parked car. They slowed only by taking the foot off accelerator pedal. Moreover, sub307 did not take his foot off accelerator pedal twice in five runs.
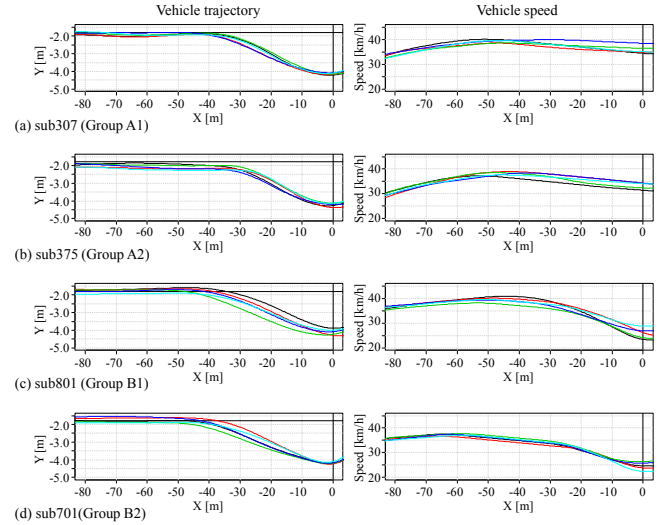
Fig. 11. Vehicle trajectories (left) and speed profiles (right) of typical drivers in different driver groups. Results of five runs for each driver are shown together in each panel.
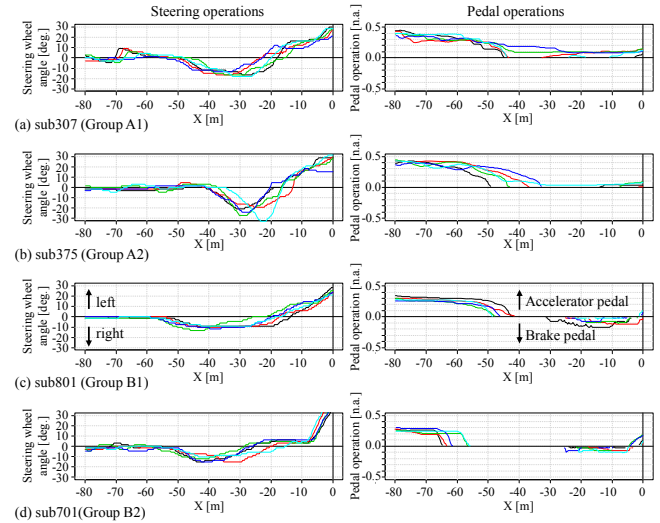
Fig. 12. Steering operations (left) and pedal operations (right). Positive values for the steering angle denote steering to the left, negative values denote steering to the right. Positive values in pedal operations denote accelerator pedal operations, with negative values denoting brake pedal operations.

5. SYSTEM DESIGNS

In the section, based on an understanding of unsafe driver behaviors in the passing-a-parked-car scenario, possible designs of driver–PDAS interactions are discussed. The main findings from the analysis are summarized as shown below.

1. Vehicle motion (vehicle trajectory and speed) and driver operations (steering operations and pedal operation) are nearly constant for a single driver, but vary among drivers.

2. Results of driver categorization based on the assumption of the same safety margin show that some driver groups (Group A1 and Group A2) pass by the parked car at overly high speed for the lateral gap (insufficient speed reduction).

3. Elderly drivers are much more likely to be in Group A1 and Group A2.

4. Insufficient speed reduction by drivers in Group A1 and Group A2 is attributed to speed adjustment after the onset of steering because the onset of steering and speed at this moment do not differ much among driver groups.

5. Drivers in Group A1 and Group A2 take the foot off the accelerator pedal after some delay (delayed pedal-off). Some do not take the foot off the accelerator pedal (no pedal-off).

Group A1 and Group A2 drivers are the main targets for PDAS. For those drivers, a speed reduction support system expected to be more effective rather than a lateral gap support system because of the high passing speed for the lateral gap. As the vehicle motions and the driver operations before the onset of steering maneuver are mostly identical between all driver groups, the driver support should be provided based on the vehicle motion states and driver operations after the onset of steering maneuver. For unsafe pedal operation patterns (delayed pedal-off and no pedal-off), different support strategies can be found as described below.

[Support for delayed pedal-off]

A certain amount of additive deceleration is provided after a driver takes the foot off the accelerator pedal to compensate for insufficient speed reduction because of the delayed pedal-off (Fig. 13 (a)). In this case, because the driver's intention of speed reduction is shown by the pedal-off action, the driver would not feel unpleasantness or discomfort from the added deceleration. However, such a support system also must judge whether the driver will take the foot off the accelerator pedal in the case of no pedal-off action (as explained below).

[Support for no pedal-off]

When the support system judges that the driver will not take a foot off the accelerator pedal, it provides haptic feedback such as vibration or reaction force using an active accelerator pedal to prompt the driver to take the foot off the accelerator pedal (Fig. 13(b)). The above support for delayed pedal-off is performed if the driver does so. Otherwise, the system automatically intervenes to slow down to an optimal speed for lateral gap (Fig. 13(b)). For such support, an optimal speed estimator based on road surrounding recognition is needed.

(a) Delayed pedal-off   (b) No pedal-off
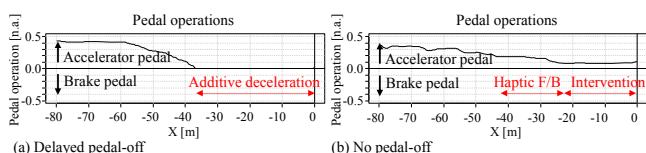
Fig. 13. Speed reduction support in passing the car. (a) Support for the case of delayed pedal-off. (b) Support for the case of no-pedal-off.

6. CONCLUSIONS

In this study, we examined the vehicle motion and driver operations in the passing-the-car scenario as an example of a potentially hazardous traffic situation to design interactions between a driver and a preventive driving assistance system (PDAS). Some drivers passed by it at high speed because of insufficient speed reduction after the onset of steering operations. Delayed pedal-off and no pedal-off actions have been found to be unsafe pedal operations patterns resulting in insufficient speed reduction. For the unsafe patterns, a speed reduction support strategy was proposed. To realize the support system, the development of a judgment algorithm for the appropriate timing of pedal-off remains as a research issue for future works.

ACKNOWLEDGMENTS

REFERENCES

Abbink, D.A., Mulder, M., and Boer, B.R. (2012). Haptic shared control: smoothly shifting control authority? Cognition, Technology & Work, Vol.14, No.1, pp.19-28.

Coelingh, E., Eidehall, A., and Bengtsson, M. (2010). Collision Warning with Full Auto Brake and Pedestrian Detection - a practical example of Automatic Emergency Braking. Proceedings of ITSC 2010, pp.155-160.

Hasegawa, T., Raksincharoensak, P., and Nagai, M. (2014). Risk-potential based motion planning and control of proactive driving intelligence system for enhancing active safety, Proceedings of AVEC'14, No.20149224.

Lemmen, P., Stoll, J., Bergelt, U., Seiniger, P., Wisch, M., Bartels, O., Schubert, E., Kunert, M., Knight,I., Brookes, D., Ranovona, M., Okawa, T., Domsch, C., and Schaller, T. (2013). Evaluation of pedestrian targets for use in autonomous emergency brake system testing – A report from the Harmonisation Platform 2 dealing with test equipment. Proceedings of the 23rd ESV Conference, No.13-0124-W.

Rosén, E., Källhammer, J.E., Eriksson, D., Nentwich, M., Fredriksson, R., and Smith, K. (2010). Pedestrian injury mitigation by autonomous braking. Accident Analysis and Prevention, Vol.42, Issue 6, pp.1949-1957.

Shimizu, T., Ohama, Y., Hatakeyama, Y., and Kumai, Y. (2013). Promoting safe driving: Informing rationale and tactic effects on safe driving behaviors, Proceedings of FAST-zero '13, No. 20134661.

Takemoto, M. and Higuchi, K. (2012). Analysis of unsafe driver behavior when passing through parked vehicle. Japan Ergonomics Society, Vol.48, No.1, pp.7-16. (in Japanese)

The Influence of Roadway Characteristics on Potential Safety Benefits of Lane Departure Warning and Prevention Systems in the U.S. Vehicle Fleet

John M. Scanlon Kristofer D. Kusano
Hampton C. Gabler

Biomedical Engineering and Mechanics Department, Virginia Tech, Blacksburg, VA 24060 USA (e-mail: john91@vt.edu)

Abstract: **Nearly one-third of all fatal crashes in the U.S. are a result of road departures. Lane departure warning (LDW) and lane departure prevention (LDP) have the potential to mitigate crashes and seriously injured drivers that result from road departures. However, the effectiveness of these systems are dependent on roadway characteristics, such as shoulder width and the presence of lane markings. In the U.S., road shoulders are often narrow, and lane markings are frequently not present. The objective of this study was to determine the limiting influence of shoulder width and lane markings on the effectiveness of LDW and LDP. Real-world road departure crashes were simulated without LDW/LDP, with LDW, and with LDP. These crashes were then simulated again on roads with improved infrastructure, i.e. with lane markings and a 3.6 m shoulder width. LDW and LDP were estimated to prevent 53% and 68% of crashes, respectively, when the shoulder width was at least 3.6 m. In contrast, when no shoulder was present (29% of departure crashes), LDW was found to have no effectiveness and LDP was estimated to prevent only 1% of crashes. When the crashes were simulated again with roadway infrastructure modifications, the number of crashes that could be prevented with LDW/LDP were found to double. The results of this paper highlight the importance of roadway characteristics on potential safety benefits of LDW and LDP, and should inform policy on roadway design.**

Keywords: **Safety Impact Assessment of Active Safety Devices, On-Board Sensing Driver Assistance Systems, Lane departure warning, lane departure prevention, roadway design**

1. INTRODUCTION

Road departure crashes are among the most deadly crash modes in the United States, accounting for nearly one-third of all fatal crashes (Kusano and Gabler 2014). Lane departure warning (LDW) and lane departure prevention (LDP) systems are active safety systems that have the ability to mitigate crashes and injuries by alerting drivers of a lane departure and/or directly modulating vehicle trajectory.

Deficient roadway infrastructure, such as narrow shoulders or the absence of lane markings, may restrict the effectiveness of LDW and LDP. Lane markings give a positional reference for LDW and LDP, which enable these systems to activate when a lane departure is imminent or has occurred. Although advancements in road edge detection algorithms may eventually solve the issue of no lane markings, a lack of adequate shoulder width for recovery is less easily solvable and extremely costly.

Previous works (Kusano and Gabler 2014, Scanlon et al. 2015) have examined road departure crashes from a database containing a U.S. nationally representative sample of road departure crashes. Figure 1 shows a breakdown of shoulder widths on the roadways where these road departures occurred. A majority of road departure crashes happen on roadways with shoulder widths less than 0.3 m (1 ft) wide. Additionally, this dataset also indicated that only 70% (shown in Figure 2) of vehicles crossed over lane markings prior to road departure crashes. The objective of this study was to investigate the impact of roadway design on the predicted safety benefits of

LDW and LDP if all vehicles in road departure crashes in the U.S. fleet were equipped with either system.
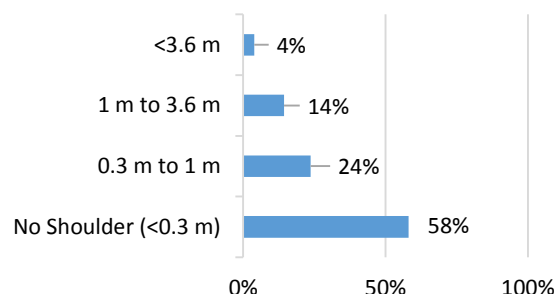

Fig. 1. Distribution of Shoulder Widths in U.S. road departure crashes (NASS/CDS 2012).
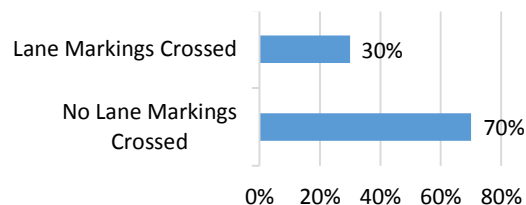

Fig. 2. Road markings crossed prior to U.S. road departure crashes (NASS/CDS 2012).

2. METHODS

2.1 Modelling Framework

Figure 2 summarizes the process for the LDW and LDP benefits computations developed for this project. Two sets of

simulations were run in this study. First, road departure crashes from a U.S. nationally representative database were retrospectively simulated as if the vehicle had been equipped with an LDW or LDP system. Second, crashes were simulated again with improved roadway infrastructure. Specifically, all non-curbed roadways were assumed to have lane markings present and a shoulder width of 3.6 m (highway lane width maximum in the U.S.). No roadway infrastructure modifications were assumed to be made if the road had a curb. In summary, this set of simulations aimed to determine how effective LDW and LDP would be if these road infrastructure improvements were made.
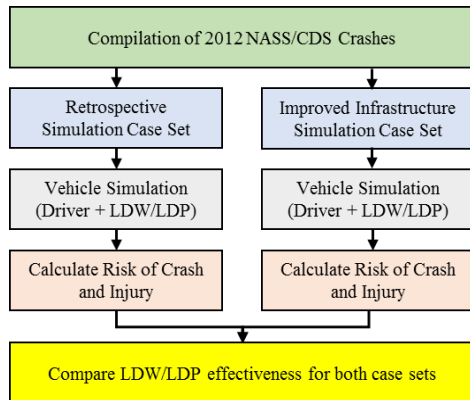
Fig. 2. Modelling framework used to estimate the effectiveness of LDW/LDP with and without roadway infrastructure improvements.

2.2 Data Source

The 2012 National Automotive Sampling System Crash Worthiness Data System (NASS/CDS) was used to formulate the simulation case sets. The database is comprised of approximately 5,000 new U.S. crashes each year, and includes detailed medical records and information from the crash environment, such as road characteristics. In order to be included in this database, at least one vehicle involved in the crash had to be towed away from the scene. Each case is additionally assigned a national weight factor, which was used in this paper to make the results nationally representative.

This study exclusively analysed single vehicle crashes where the driver drifted out of their lane and departed the roadway. Crashes that involved control loss or animals in the roadway were excluded.

2.3 Formulating a Simulation Case Set

Two pieces of information were required for formulating a simulation case set for this study. First, the NASS/CDS database contains much of the information required to run the simulations in this study. In order to effectively model each crash, a review of event records from each case was performed. Three parameters were determined during the review, including the travel lane of the vehicle, the presence of lane markings, and road shoulder width. Second, statistical models were used to determine departure conditions, i.e. departure angle and speed. These methods have been previously described Kusano et al. (2014) and Scanlon et al. (2015).

Because most crashes occurred on two-lane undivided roads, determining travel lane was typically unnecessary. In road departure cases on multi-lane roads, the scene narrative and scene diagram prepared by the crash investigator were used to determine the initial travel lane.

The lane marking was identified at the approximate location of the first lane departure. No evaluation of the painted lane marking clarity or quality was made.

Shoulder width was estimated from scene photographs showing the location of vehicle departure. Shoulder width was divided into four separate categories, including (1) less than 0.3 m wide, (2) between 0.3 and 1 m wide, (3) between 1 and 3.6 m wide, and (4) over 3.6 m wide. The 3.6 m threshold was selected because a typical U.S. highway lane is no wider than 3.6 m. For the retrospective simulation case set, crashes with labelled shoulder widths of 0.3 m to 1 m and 1 m to 3.6 m were simulated twice, once with each width to account for uncertainty in the actual should width. Shoulder widths less than 0.3 m were assumed to be negligible, and were simulated as 0 m. Shoulder widths greater than 3.6 m were simulated as being 3.6 m wide.

Departure conditions, i.e. departure angle and velocity, were determined using statistical models generated from the National Cooperative Highway Research Program (NCHRP) Project 17-22. The dataset consists of 890 reconstructed road departure crashes of cases included in the NASS/CDS database. One-way ANOVAs were then used to determine predictor variables that significantly influence each departure conditions. Last multivariate linear regression models were formed that maximized the adjusted-R^2. These models are presented in Kusano et al. (2014).

2.4 Performing Vehicle Simulations

Vehicle kinematics simulations were performed using CarSim vehicle simulation software. Driver control was modelled using a previously implemented driver recovery model developed by Volvo, Ford, and University of Michigan Transportation Research Institute (VFU) through the Advanced Crash Avoidance Technologies (ACAT) Program (Gordon et al. 2010). As the vehicle approaches the edge lines of the road, the driver model considers the yaw of the vehicle, identifies if that yaw will cause lane departure, and makes a proportional change to the yaw rate to maintain vehicle position in the lane. Driver steering was assumed to begin after the driver departed the paved roadway or after being alerted by LDW or LDP.

The LDW system was modelled as alerting the driver at the instance the leading wheel touched the lane markings. The LDP system was assumed to work in conjunction with the LDW system, i.e., the driver was alerted of a lane departure. Additionally, when LDP became active and prior to driver steering, the system was assumed to directly modulate steering wheel angle. The LDP system was assumed to linearly increase lateral acceleration over a 0.5 s interval to a maximum of 0.1 g, which is depicted in Figure 3.
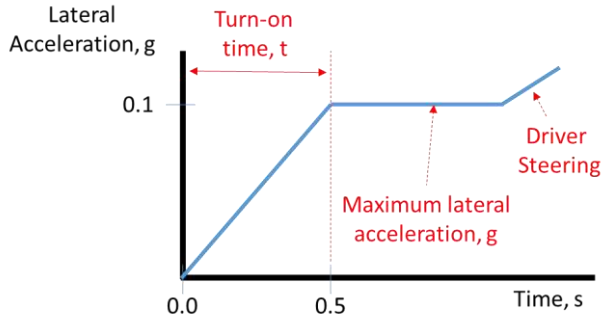
2.5 Benefits Estimates

Fig. 3. LDP lateral acceleration kinematics.

Benefits estimates were performed in three steps. These steps are illustrated in Figure 4. These methods have been previously detailed by Kusano et al. (2014) and Scanlon et al. (2015).

First, a probability of crash was computed for each of the simulated trajectories. Trajectories from NCHRP Project 17-22 were used to estimate collision risk. Probability of a crash was assumed to be dictated by 1) the distance travelled laterally from the road, and 2) the total distance travelled off-road. In summary, Using the number of crashes in each of the roadside zones (C_k), the distance travelled in each of the roadside zones (γ_k), and the total simulated trajectory length in each zone k ($L_{i,k}$) the probability of a crash P[Crash$_i$] for a given trajectory could be calculated using Equation 1.

$$P[Crash_i] = 1 - \prod_{k=1}^{K} \exp\left(-\frac{C_k L_{i,k}}{\gamma_k}\right) \qquad (1)$$

Second, probability of a seriously injured driver (Maximum Abbreviated Injury Score of 3 or greater, MAIS3+) was estimated from previously developed logistic regression functions. Departure velocity and seat belt were used as predictors for the model, and serious injury was the dependent variable. After determining the probability of a serious injury, P[injury$_{IC}$], the injury probability for the simulated trajectory, P[injury$_i$], could be calculated using Equation 2.

$$P[Injury_i] = P[Injury_{IC}] \, P[Crash_i] \qquad (2)$$

Third, benefits estimates were computed to determine the proportion of crashes and seriously injured drivers that could have been prevented if the vehicle had been equipped with LDW/ LDP. An effectiveness measure, ε, was used to compute the proportion of crashes or injuries reduced given the presence of LDW or LDP. Equation 3 shows the calculation of this effectiveness measure and utilizes counts of the number of crashes with LDW/LDP, N$_{with LDW/LDP}$, and the number of crashes without LDW/LDP, N$_{without LDW/LDP}$.

$$\epsilon = \frac{N_{without LDW/LDP} - N_{with LDW/LDP}}{N_{without LDW/LDP}} \qquad (3)$$

3. RESULTS

A total of 478 crashes from NASS/CDS 2012 were used in this study. These crashes are representative of 147,662 crashes
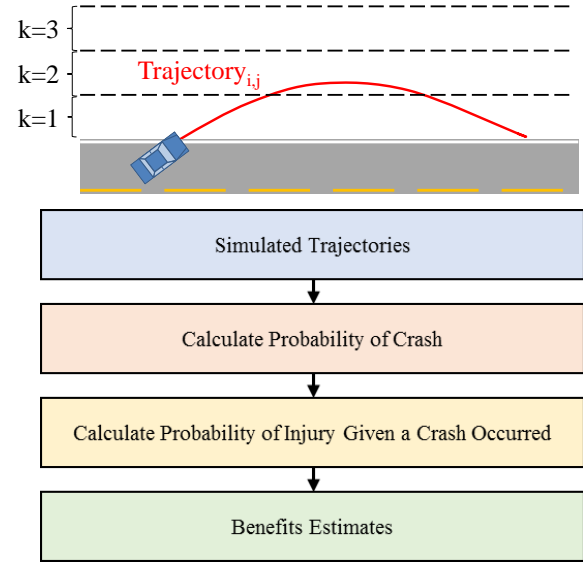
Fig. 4. Overview of methods for generating benefits estimates.

nationally in the U.S. Approximately 20% (30,167 nationally) of these crashes resulted in the driver being seriously injured.

Table 1 gives a breakdown of the cases in the dataset by shoulder width. Over half of the departure crashes happened on roadways with no shoulder width. Only 3.9% of the roadways had shoulder widths greater than 3.6 m.

Lane markings were found to be present in 70.5% (103,511 nationally) of road departure crashes. Of the crashes without lane markings, 60.5% of the crashes occurred roadways with curbs.

Table 2 lists the number of crashes and injuries without LDW/LDP systems along with the predicted effectiveness of LDW and LDP systems. The retrospective simulation of real-world crashes and the simulation of crashes with improved roadway infrastructure are both shown in the table.

Figures 5 and 6 show the effectiveness of LDW and LDP by shoulder width for the retrospective simulation case set. Only simulations that had no adjacent travel lanes crossed prior to departure, i.e. traveling in rightmost or leftmost lane, are tabulated to isolate the effect of shoulder width from number of lanes crossed before departure. In total, three-fifths (63%) of the road departure crashes occurred without any adjacent travel lanes being crossed.

Table 1. Breakdown of Cases by Shoulder Width.

Shoulder Width Category	Count	Proportion
No Shoulder (<0.3 m)	85,730	58.1%
0.3 m to 1 m	34,937	23.7%
1 m to 3.6 m	21,195	14.4%
<3.6 m	5,800	3.9%
Total	**147,662**	**100.0%**

4. DISCUSSION AND LIMITATIONS

The potential benefits of LDW and LDP were found to be dramatically influenced by the presence of lane markings and shoulder width. A total of 30.9% of road departures took place on roadways without lane markings. On roads with no lane markings, LDW and LDP were assumed to not activate. This indicates that, if an LDW/LDP system requires lane marking to be present, a maximum of 69.1% of crashes could have been prevented by LDW/LDP.

LDW and LDP were estimated to prevent 59% and 67% of crashes, respectively, when the shoulder width was at least 3.6 m. In contrast, when no shoulder was present, LDW was found to have no effectiveness and LDP was estimated to prevent 1% of crashes. The influence of shoulder width on benefits is especially important when considering that 29% of crashes occurred on roads with no shoulder. On roads with lane markings but no shoulder, only LDP was assumed to be activated.

Our simulations indicate that LDW and LDP would be substantially more effective if all roadways included lane markings and had expanded shoulders (> 3.6 m). The number of crashes that could be prevented by LDW with these roadway infrastructure modifications was found to double (28.4% to 59.2% of crashes prevented). Likewise, the number of crashes that could be prevented by LDP with these roadway infrastructure modifications was found to nearly double as well (32.1% to 63.2% of crashes prevented).

It is important to note that instituting the roadway infrastructure improvements discussed in this study would be extremely costly. Specifically, expanding roadway shoulders to be the width of a highway lane would not be practical. However, this analysis highlights the importance of these roadway attributes for the effectiveness of LDW and LDP. Additionally, this analysis shows the opportunities for greatly enhancing the effectiveness of LDW/LDP by developing
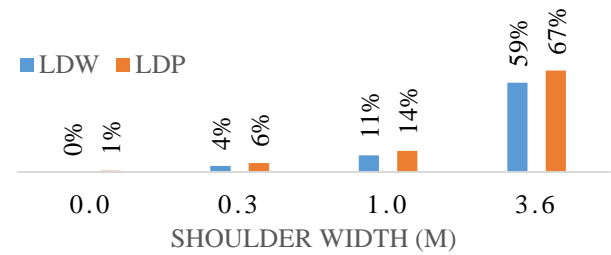
Fig. 5. Effectiveness of LDW/LDP in reducing the number of crashes as a function of shoulder width.
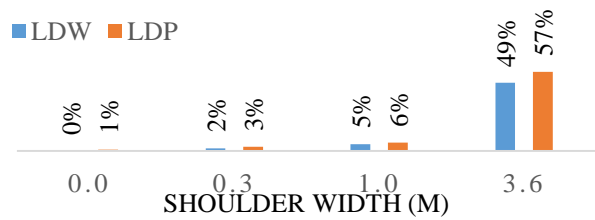
Fig. 6. Effectiveness of LDW/LDP in reducing the number of seriously injured drivers as a function of shoulder width.

systems which can detect the road edge in the absence of lane markings.

There were some limitations to the model. First, the modelled LDW and LDP systems were assumed to function independent of visibility (e.g. fog or snow). LDW and LDP currently rely on video-based lane detection, which makes them highly dependent on the clarity of the line and visibility issues. These issues were not considered in this study. Second, not all equipped vehicles will have LDW or LDP enabled, because some drivers may disable the systems. Third, modifying roadway infrastructure may prevent some road departures for

Table 2. Effectiveness of LDW/LDP by Simulation Case Set.

Measure	Values	Effectiveness (% Improvement)	Measure	Values	Effectiveness (% Improvement)
Baseline Infrastructure			*Lane Markings + Expanded Shoulder Width*		
Crashes					
No LDW or LDP	147,662	---	No LDW or LDP	147,662	---
with LDW	105,657	28.4%	with LDW	60,314	59.2%
With LDP	100,261	32.1%	With LDP	54,279	63.2%
Injuries (MAIS3+)					
No LDW or LDP	30,167	---	No LDW or LDP	30,167	---
with LDW	23,871	20.7%	with LDW	14,711	51.5%
with LDP	21,722	27.8%	with LDP	13,390	55.9%

vehicles not equipped with LDW or LDP. This model assumed that drivers without either system would not be alert until the road departure occurs. However, this additional time prior to a road departure may have allowed some drivers to realize an imminent crash and steer back into the lane.

5. CONCLUSIONS

The results of this paper highlight the crucial influence of roadway characteristics on potential safety benefits of LDW and LDP. Federal and state transportation agencies seeking to maximize the benefit of emerging fleets with automated crash avoidance technologies, e.g. LDW or LDP, should consider the effect of these infrastructural characteristics when planning roadway improvements. This work also highlights the opportunities for LDW/LDP developers to improve the crash and safety benefits of these systems by determining ways to detect road edges on roadway without lane markings.

6. ACKNOWLEDGEMENTS

7. REFERENCES

Gordon, T., Sardar, H., Blower, D., Ljung Aust, M., Bareket, Z., Barnes, M., Blankespoor, A., Isaksson-Hellman, I., Ivarsson, J., Juhas, B., Nobukawa, K., Theander, H (2010). Advanced Crash Avoidance Technologies (ACAT) Program - Final Report of the Volvo-Ford-UMTRI Project: Safety Impact Methodology for Lane Departure Warning - Method Development and Estimation of Benefits. Department of Transportation. Report DOT HS 811 405.

Kusano, K.D., and Gabler, H.C. (2014). Comprehensive Target Populations for Current Active Safety Systems using National Crash Databases. . Traffic injury prevention., 15(7), 753–761.

Kusano, K. D., Gorman, T. I., Sherony, R., & Gabler, H. C. (2014). Potential Occupant Injury Reduction in the US Vehicle Fleet for Lane Departure Warning–Equipped Vehicles in Single-Vehicle Crashes. Traffic injury prevention, 15(sup1), S157-S164.

Scanlon, J. M., Kusano, K. D., Sherony, R., & Gabler, H. C. (2015). Potential Safety Benefits of Lane Departure Warning and Prevention Systems in the U.S. Vehicle Fleet. Proceedings of the 24th International Enhanced Safety of Vehicles Conference. Gothenburg, Sweden, Paper Number 15-0080.

Dynamic Crash Target for the Assessment, Evaluation and Validation of ADAS and Safety Functions

Dipl.-Ing. (FH) Marvin Rabben, M.Sc.*, Dr.-Ing. Roman Henze,
Prof. Dr.-Ing. Ferit Küçükay

Institute of Automotive Engineering, TU Braunschweig, Hans-Sommer-Str. 4, 38106 Braunschweig
Germany (Tel: +49 531-391-2610; e-mail: iae@tu-bs.de).

Abstract: The advancing integration of ADAS (Advanced Driver Assistance Systems) and the increasingly complex E/E architecture across all vehicle classes require a reliable and safe method for the assessment, evaluation and validation of said systems. At the Institute of Automotive Engineering (IAE), a test tool that functions as a full-size vehicle replacement has been developed allowing the full scope of tests to be performed while minimizing the risk to the test personal and vehicles involved. The test tool consists of three separate modules: a driving module, a soft crash target carrier and the soft crash target itself. The soft crash target carrier holding the soft crash target is connected to the driving module via detachable links. Considering a collision scenario as use case, the driving module separates from the soft crash target carrier just moments before a collision is imminent, performs evasive manoeuvres and thus leaves the possibly harmful collision area. The soft crash target is quickly exchanged according to the use case under consideration and is visible to common sensor technologies (radar, lidar, camera etc.). The developed test tool can furthermore be used for controllability studies according to ISO 26262 in cases where a second vehicle or collision partner is necessary.

Keywords: Automated guided vehicles, Controllability, Crash-Target, Functional Safety, ADAS

1. INTRODUCTION

With the increasing market penetration of Advanced Driver Assistance Systems (ADAS) such as ACC (Adaptive Cruise Control) or Autonomous Emergency Braking (AEB) as well as the increasing number of further assistance systems and safety relevant functions implemented into nowadays vehicles, realistic full-scale test methodologies continue to be high in demand. In order for the test methodologies to be a suitable replacement for a real vehicle, quite a few challenges need to be addressed. First, a representation of a vehicle chassis must be propelled and guided precisely and reliably along a trajectory allowing the vehicle-under-test (VUT) and the vehicle representation to intersect at a pre-defined point to recreate different scenarios of interest. These scenarios of interests can represent any kind of real world behaviour including but not limited to collisions, near misses, crossing path, side swipes, etc. Second, the vehicle representation must not pose any substantial physical risk to the test personnel involved or the VUT. This holds especially true in scenarios where the system under test must be evaluated well into the crash imminent phase of the conflict and a collision might not be avoided.

At the Institute of Automotive Engineering (IAE), a full-scale test methodology that meets the aforementioned requirements has been developed and successfully tested in different scenarios. The test methodology consists of three individual modules which together form the dynamic crash-target (DCT) which will be outlined hereafter. Centre of the DCT is its electrically self-propelled, autonomously guided, programmable driving module (DM). Attached to the DM is the soft crash target carrier (SCTC), a low profile interchangeable two-part platform carrying a soft crash target (SCT). The SCTC can be attached to the side, rear or front of the DM for different usage scenarios (i.e. rear- or front-end collisions, side swipes, etc.). The arrangement of the two platforms of the SCTC can likewise be changed to support different soft crash targets for the aforementioned use cases. The soft crash target is made of several blocks of foam interlinked with each other via a tongue and groove mechanism and is a realistic representation of a real vehicle both for the driver of the VUT and the system under test. The driving module serves as a means of propulsion and guidance for the attached SCTC and SCT allowing the SCT to be brought up to the desired test speed and pre-defined point of interest. Shortly before a collision is imminent the DM disconnects from the SCTC and leaves the collision area. Thus, a collision only involves the SCTC and the SCT as far as the dynamic crash-target is concerned, reducing the risk to the test equipment and driver. As long as the DM and the SCTC are coupled, the DCT coordinates its motions with the VUT allowing identical initial conditions in the pre-crash phase from test run to test run. In the case that the VUT's systems react to the conflict ahead, the DCT can either keep on coordinating its motions with the VUT or automatically switch to a semi-autonomous mode in which its speed and course are no longer coordinated with the VUT. Within the semi-autonomous mode of operation, the DCT will arrive at a pre-defined ground-fixed impact point while using a speed-time-distance trajectory which has been set up beforehand. This method of operation allows determining the benefits of a

system under test or comparing different parameter sets and sensor technologies in one specific scenario.

Over the last years a number of different test methodologies for the evaluation of ADAS have been developed, all of them trying to minimise the risk to the test personnel involved as well as avoiding damage to the VUT or the collision partner. These methodologies include the use of stationary or pulled balloon cars (Pawellek 2014; Sandner 2013), dedicated test facilities where the VUT is held stationary and the collision partner moves relative to it (Gietelink et al. 2004), parts of a real vehicle being towed behind another vehicle (Hoffman 2008; Sandner 2013) and also a few autonomous flat platforms carrying soft crash targets which mainly vary in their size and especially height (AEDesign 2015; Anthony Best Dynamics 2014; Steffan 2012). The height is an important factor considering that a VUT should be able to drive over the platform without any damage to it in general and in particular to its suspension and axle components. This is fairly easy achieved considering a VUT driving over the platform at constant speed, but becomes more complicated in a braking scenario. Braking scenarios occur quite often while evaluating collision mitigation and avoidance systems as the system under test might reduce the velocity of the VUT but not enough to fully prevent a collision. Thus, the VUT drives over the platform in a braked condition. Due to the occurring pitch, the ground clearance at the front of the VUT is reduced, leading to lower permissible overrun height of the platform. The developed SCTC provides such a low overrun height, allowing it to be driven over by the VUT (braked and unbraked) at very high speeds without any damage to the SCTC or the VUT's suspension (tested). Combined with the realistic movement of the DM and the realistic appearance of the SCT for a certain scenario, the DCT allows the evaluation of ADAS at high speeds up to and through the point of impact, while minimising physical risk to test personnel and equipment.

2. SYSTEM ARCHITECTURE

For a meaningful operation of the DCT, additionally a VUT with systems to be tested as well as a base station from which the DCT is controlled and programmed needs to be present. If the VUT is equipped with the proper equipment, it can also be controlled via the base station. However, one can use the DCT without a VUT that is controlled from the base station, thus using the DCT as a standalone unit following its pre-programmed trajectory without coordinating its movements with any other vehicles. Fig. 1 shows the overall system layout with its respective nodes and peripheral equipment including the network architecture within and in-between each node.
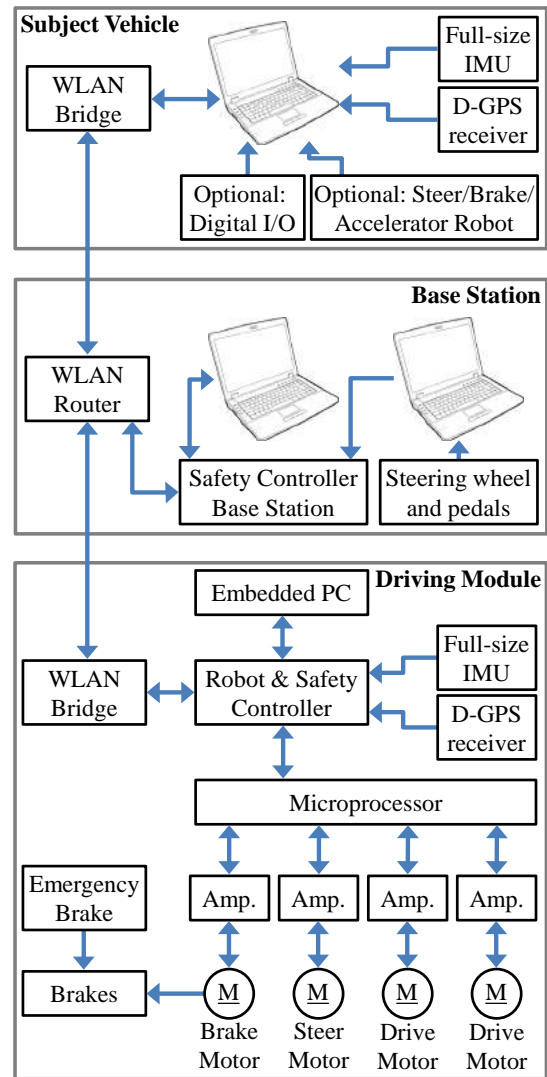
Fig. 1. System architecture of the DCT

In the case of the VUTs movements being coordinated with the DCT, the VUT comprises the following components:

- Notebook computer

- Full-size inertial measurement unit (IMU)

- Differential GPS receiver

- Wireless LAN Bridge

- Optional: Steer/Brake/Accelerator-Robot

- Optional: Digital I/O board

The VUT can either be driven by a human driver or can be set up to act as a semi- or fully autonomous, driverless vehicle. The latter requires specific robots to be fitted to the vehicle or a vehicle capable of drive-by-wire. In the case that the VUT is driven by a human, the notebook computer is used to set up the tests that should be performed, to monitor the test procedure and give (corrective) instructions to the driver. The IMU provides precise measurements of the acceleration as well as the rotational motion while the D-GPS

signal is used to improve the positional accuracy of the VUT. The WLAN bridge transmits the measurements to the base station and DCT where, if necessary, it is used to adapt the driving strategy. The D-GPS signal can either be received from a local D-GPS base station or via mobile radio. The VUT can additionally be fitted with a digital I/O board that records or triggers discrete events such as an audible alert signalling the driver to perform a certain driving manoeuvre, ADAS warnings or open-loop steering/braking/accelerating manoeuvres. If the VUT is operated driverless, a remote connection to the VUT computer from the base station allows the configuration of the tests.

The base station serves as the central hub for all in- and outputs to and from the VUT and DCT. It is where the test engineer controls and supervises the movements of the vehicles. The base station is comprised of the following components:

- Two notebook computers

- Steering wheel and pedals

- Wireless LAN Router

- Safety controller base station

One of two notebook computers establishes a remote connection to the DCT computer, thus allowing the operator to set up the tests for the DCT. The second notebook computer runs the software that allows the engineer to start and stop the previously selected tests remotely and allows the DCT to be driven manually via the steering wheel and pedals. The safety controller base station transmits a watchdog signal to the DCTs safety controller. If the watchdog signal is not received by the DCTs safety controller within the required time, the DCTs emergency protocol is activated which first activates the regular on-board braking system and, if it does not suffice, the emergency brake is fired bringing the DCT to a safe and quick stop.

Although a fully operational DCT consists of the DM, the SCTC and the SCT, only the DM has active components. The driving module comprises the following components:

- Two DC drive motors and amplifiers

- One brushless DC steering motor and amplifier

- One brushless DC braking motor and amplifier

- Hydraulic disc brake with master brake cylinder

- Spring-loaded emergency brake system

- Full-size inertial measurement unit (IMU)

- Differential GPS receiver

- Wireless LAN Bridge

- Robot & Safety Controller

- Microprocessor controlling the on-board CAN bus

- Embedded computer

The embedded computer runs the same software as the notebook computer in the VUT and is accessed remotely form the base station to set up the tests and monitor the DM. Information about the test to be performed is then loaded into the robot controller which in turn calculates the required drive motor torque, steering angle and brake level to fulfil the time-space trajectory of the test. The drive motor torque command, steering angle command and brake level command are transmitted via CAN bus to a microprocessor that actuates the corresponding components and also receives feedback from these components about their current status which is relayed back to the robot controller to achieve a closed-loop control. Identical to the VUT, the safety controller on the DM receives a watchdog signal from the base station and activates the emergency protocol if it is not received within a given timeframe. The D-GPS signal can again be received from a local base station or via mobile radio and increases the positional accuracy of the DM to up to 2 cm.

3. DYNAMIC CRASH-TARGET

3.1 Driving Module (DM)

The Driving Module (Fig. 2) is the core element of the DCT as it is responsible for the reliable and precise guidance of the attached SCTC carrying the Soft Crash Target.

Fig. 2. Driving Module with enclosure

The DM's is electrically driven by two DC motors and is built upon a customary kart chassis that has been modified to accommodate all actuators, controllers, sensors, batteries and further equipment. All components are protected against splash water as well as environmental factors such as dust and small stones that may be present at the proving ground by a two-piece enclosure made from polystyrene (PS) coated with UV-resistant paint. The whole operational principle of the DCT is based on the fact that the DM disconnects from the SCTC moments before a collision is imminent and leaves the probable collision area via an evasive manoeuvre. Hence, it never runs the risk of being crashed into.

Each of the two DC motors drives one of the rear wheels as the DM features a split rear axle to allow for torque vectoring, increasing the DM's manoeuvrability. Steering of the front wheels is achieved by a brushless DC servo motor. A set of disc brakes at the front wheels and both drive motors at the rear wheels provide enough braking performance in

order to bring the DM to a quick and safe stop after a test scenario has been completed or to avoid reaching the collision area after disconnecting from the SCTC. The hydraulic brake system at the front wheels is actuated by means of a master brake cylinder. The master brake cylinder is either activated by the brushless DC brake motor or the spring-loaded emergency brake system. Both brake systems are connected to the master brake cylinder via a fixed linkage. They are not exclusive to each other and permanently run in parallel. The emergency brake however can at any time overpower the DM's system brake. The system brake is actuated autonomously by the robot controller according to the space-time trajectory that has been set up and can also be activated manually by the operator using the brake pedal at the base station.

All components draw their power from two centrally placed battery packs in between the front and rear wheels of the kart chassis. The battery packs are easily accessed and exchanged reducing downtime to a minimum. The steering and brake motors as well as the emergency brake sit in front of the battery pack. The two drive motors as well as the robot and safety controller are mounted behind the battery pack. As a result the DM features a slightly tail-heavy weight distribution.

The DM has the SCTC attached to its front, rear or one of its sides by means of a magnetic spring-loaded coupling mechanism. To connect the DM and the SCTC, the coupling mechanism is pressed into a fitting on the SCTC where it is held in place by a permanent electromagnet. Once the decoupling event has been triggered, as per the pre-programmed trajectory, a current is applied to the magnet cancelling out the magnetic field. Due to the utilised spring, the coupling mechanism is pulled out of the fitting and the DM and SCTC are separated allowing the DM to leave the collision area.

3.2 Soft Crash Target Carrier (SCTC)

The Soft Crash Target Carrier features two identical flat platforms made from PVC (polyvinyl chloride) which are connected to each other via additional links. Each platform is fitted with six ball bearing mounted wheels. The wheels are connected to the platform through a spring steel wheel suspension. This allows the platform to hunker down when driven over by a VUT, reducing the load on the SCTC's wheels by creating a direct load path from the VUT's tyre to the ground. Under normal operating conditions the ground clearance is about 1 cm with the overrun height for the most part being equal to the material thickness of the platforms (1 cm) except for a small area around the six wheel assemblies. To prevent any damage to the wheel assemblies due to the VUT driving over them, a small rugged enclosure made from PVC has been put in place around each wheel assembly. The enclosures are angled on each side to reduce the load into the suspension of the VUT even further. The overrun height in these areas increases to 3 cm.

The platforms can easily be rearranged to suit different usage scenarios. For rear and front end scenarios the platforms are

put next to each other, as seen in Fig. 3. An appropriate soft crash target for said scenarios is then mounted on the edge of the SCTC. For side crash scenarios the two platforms are mounted behind each other (Fig. 4), resulting in a long, narrow SCTC allowing a full size side soft crash target to be fitted. Scenarios requiring a rear and side view of a soft crash target at the same time can be represented by combining the side configuration with parts of the rear configuration leading to an L-shaped platform structure.
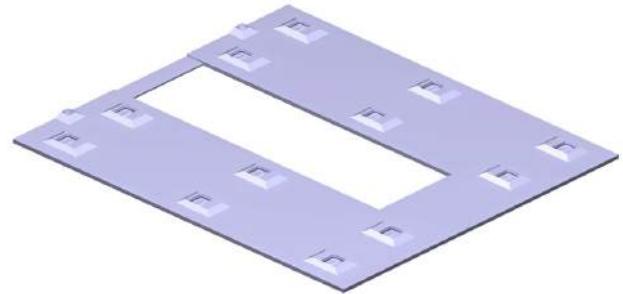
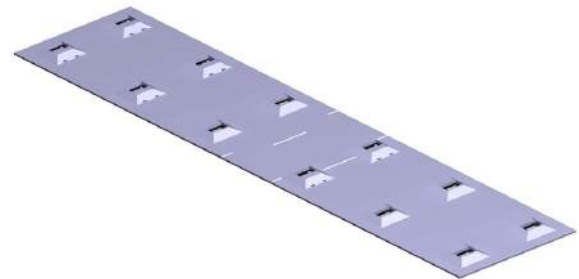Fig. 3. SCTC for rear- and front end collisions

Fig. 4. SCTC for side impacts and sideswipes

As the SCTC is disconnected from the DM moments before a possible collision, it is no longer actively guided and thus small deviations from the final collision point may occur. Although these small deviations are well within the tolerance range for quite a large number of tests and therefore do not significantly affect the performance of the system under test, a large portion of those deviations can be determined before a series of test runs and can subsequently be taken into account for the test setup. However, for the few test that require high-precision guidance up to the collision point, an enhanced version of the SCTC that is actively guided after the separation from the DM has been developed (2nd generation SCTC). It features two brushless DC drive motors as well as one brushless linear DC steering motor on each platform supplemented by one D-GPS receiver for positional control. After separation from the DM, the actively guided SCTC holds the velocity according to the space-time trajectory and performs corrective steering measures. Also, the actively guided SCTC allows intersection scenarios with turning vehicles to be realised. To accommodate the additional components (actuators, battery, D-GPS) the overrun height has increased slightly to 5.3 cm.

3.3 Soft Crash Target (SCT)

The Soft Crash Target consists of several individual blocks of low density polyethylene (PE) foam which separate on impact to reduce stress on the VUT and the SCT itself. The blocks are interlocked among themselves and connected to the carrier by a tongue and groove mechanism (Fig. 5) providing sufficient support for high velocity operations of the DCT.
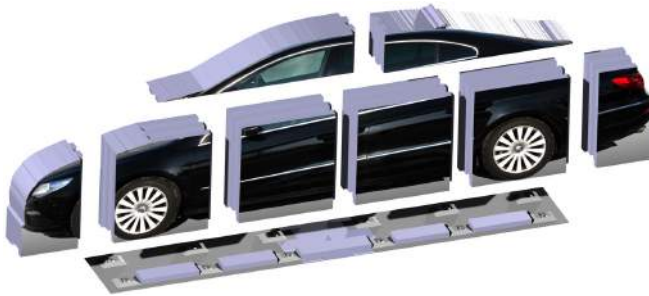
Fig. 5. Soft crash target side view with tongue and groove mechanism

The SCT is visible to common sensor technologies such as radar and lidar by means of built-in triple mirrors providing a very similar reflecting surface as a real vehicle. Visibility and plausibility for a camera system has been achieved by imprinting high quality images on a film attached to the individual blocks representing a certain view of a vehicle (rear, side, front or any combination of these), see Fig. 6. The SCT is changed according to the driving scenario or function under test (e.g. crossing-paths, sideswipes, rear-end, front-end, convoy-driving, etc.). As has been outlined before, use cases requiring a side and rear view at the same time use an L-shaped Soft Crash Target. Due to the simple structure, the SCT can be reassembled by one person within two minutes.

Fig. 6. Soft crash target for rear end collisions

4. METHOD OF OPERATION

4.1 Trajectory Planning

Before a test can be run, the appropriate space-time trajectories for the DCT and if applicable, the VUT have to be generated. The test runs can be reconstructed real world accident scenarios or hypothetical ones. In any case they need to be physics-based, i.e. the DCT and VUT have to be at certain waypoints with a certain velocity to fulfil the end condition (e.g. collision, near miss, beginning of the beam opening angle of a sensor, etc.) of the test run. The trajectories can have any shape, the DCT and VUT trajectory do not necessarily have to intersect and they can include variations in speed for both vehicles. Additionally the trajectories also store information about discrete events that need to be triggered at specific waypoints along the trajectory. These can be messages to the driver of the VUT that a certain task is required (e.g. braking, steering), but also the point in time when the DM should disconnect from the SCTC is defined as such a discrete event.

4.2 Testing with the DCT

After the initialisation procedures of the DCT have been completed, it is put into driverless mode and connected to the SCTC. Once in driverless mode, the previously created trajectory and selected test are downloaded onto the robot controller. For the DCT to travel along its path it needs to be within a certain start zone allowing it to spline onto the pre-defined trajectory. This is achieved by utilising the manual control at the base station (steering wheel and pedals). The procedure for the VUT is quite similar. The DCT and, if applicable, VUT are then set to the fully autonomous mode.

Due to the high performance of the DCT, the VUT in most cases starts to travel first along its trajectory constantly transmitting its position and inertial measurements to the DCT. Precisely timed to arrive at the pre-defined point where the separation of the SCTC from the DM takes place, the DCT starts to travel along its path adjusting for small longitudinal and lateral errors. Immediately after separation the DM takes evasive measures in order to leave the possibly harmful collision area. Furthermore, the motions of the VUT and DCT resp. DM are no longer coordinated with each other, i.e. the VUT automatically switches to sub-autonomous mode in which the velocity of the VUT is controlled by the information contained in the trajectory file. This sub-autonomous mode is also available for the DCT and is always triggered by pre-determined discrete events (e.g. time-to-collision less than a threshold, ADAS warnings, separation command, etc.). The SCTC, being it the passive or actively guided version, continues to travel along the path up to the collision point or point of interest.

After a collision has taken place or the test run is finished, the SCT is reassembled (if needed) and the operator manually drives the DM near the SCTC so it can be reconnected for subsequent test runs. Afterwards the operator can either manually drive the DCT back to the start zone or use a pre-

programmed reverse trajectory that is autonomously driven by the DCT. From this point on, the aforementioned process repeats.

4.3 Use Cases

First and foremost the DCT is used for the evaluation and validation of current and future ADAS. Application examples of some of the possible driving scenarios for current and future ADAS are shown in Fig. 7.
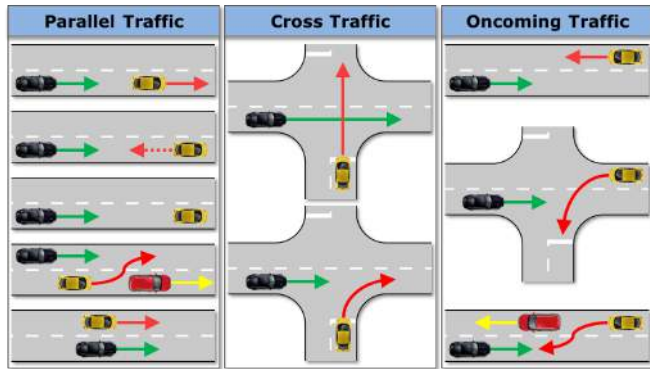

Fig. 7. Driving situations for current and future ADAS

Additionally the usefulness of new sensor concepts and the combination of different sensor technologies via sensor fusion is another field of application. With the actively guided SCTC the DCT can furthermore be used for a preliminary performance assessment of ADAS in accordance with Euro NCAP (European New Car Assessment Program), NHTSA (National Highway Traffic Safety Administration) and IIHS (Insurance Institute for Highway Safety).

In respect to the increasing efforts that are being made towards highly automated and autonomous driving, the application of the DCT provides a safe and quick method to test specific functions on the one hand and on the other hand generate data (e.g. in controllability studies) which subsequently can be used in the homologation process of said functions. In accordance with ISO 26262 the OEMs are required to prove that their functions are safe or in the case of a malfunction (e.g. erroneous steering or brake inputs, etc.) can be controlled. Fig. 8 shows an example of such a use case. Two vehicles drive in a convoy with a time headway (THW) significantly less than one second and an erroneous acceleration of the following vehicle occurs.

The driver of the following vehicle has to react to the increasingly more critical becoming situation either by braking or performing an evasive maneuver. If the driver does not react at all, not quick or not sufficient enough, the situation quickly becomes uncontrollable, likely leading to a collision with the vehicle in front. Making use of the DCT as the second vehicle actually allows a collision to happen whereas intervening action, either by a safety concept or a co-driver, has to be taken in case of a real vehicle. Performing experimental studies with a large number of normally practiced drivers or a small sample of expert drivers varying

the erroneous acceleration, can yield the controllability of said driving scenario. Using the collisions velocity as a measure and correlating it with known accident severity at certain speeds, the severity of the aforementioned driving scenario can also be determined.
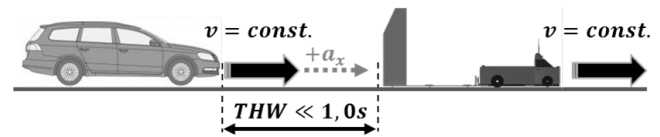
Fig. 8. Example for a controllability study: Erroneous acceleration of the following vehicle

5. PERFORMANCE

Table 1. Performance Specification of the DCT

Longitudinal acceleration (with SCTC and SCT)	+0.4g
Longitudinal deceleration under braking (without SCTC and SCT)	-0.8g
Lateral acceleration (with SCTC and SCT)	±0.4g
DM top speed (alone)	> 100 km/h
DCT top speed (with SCTC and SCT)	80 km/h
SCTC top speed (actively propelled version)	65 km/h
D-GPS positional accuracy	2 cm
Drive motor performance	Two DC drive motors, totalling: 30 kW peak 9,5 kW continuous
Bus voltage	48 VCD
Turning radius (without torque vectoring)	< 6 m
Battery charge time	60 min (full charge)
Battery switch time	5 min
SCT reassembly time	2 min

6. SUMMARY AND CONCLUSION

The developed Dynamic Crash Target (DCT) allows the assessment, evaluation and validation of current and future ADAS with minimal risk to the test personal and vehicles

involved. It does so by utilising a three-part structure consisting of a Driving Module, a Soft Crash Target Carrier and a Soft Crash Target that is suitable for the driving scenario and system under test. The DCT can be driven manually or fully autonomous utilising a pre-programmed space-time-trajectory. The vehicle under test can be driven by a human driver or semi-/fully autonomous by means of respective driving robots or drive-by-wire. The DM disconnects from the SCTC just moments before a collision or a near miss is imminent and thus the sensitive and expensive measurement equipment is never at risk. For driving scenarios that require high positional accuracy and driving performance, an actively guided SCTC (2nd generation) has been developed. The low overrun height of both the 1st and 2nd generation SCTC allows running over it in a braked or unbraked condition without any damage to the VUT or the SCTC even at high velocities. In addition to the test of current and future ADAS, the DCT can also be used in controllability studies for homologation purposes according to ISO 26262.

REFERENCES

AEDesign (2015). *AVCASS – Autonomous Vehicle for the Certification of Active Safety Systems*. Available from: <http://www.aedesign.com.pk/AVCASS large.html>. [15.01.2015].

Anthony Best Dynamics (2014). *Guided Soft Target Vehicle*. Outline Specification SP6011 – Issue 4. <http://www.abd.uk.com> [August 2014]

Gietelink, O., Ploeg, J., De Schutter, B. Verhaegen, M. (2004). *VEHIL: A test facility for validation of fault management systems for advanced driver assistance systems*. Proceedings of the 4th IFAC Symposium on Advances in Automotive Control. 19 – 23 April. Salerno, Italy.

Hoffmann, J. (2008). *Das Darmstädter Verfahren (EVITA) zum Testen und Bewerten von Frontalkollisionsgegenmaßnahmen*. Fachgebiet Fahrzeugtechnik, TU Darmstadt, Dissertation.

Pawellek, T., Henze, R.Küçükay, F. (2014). *Testing and Optimization of ADAS for Longitudinal Guidance (ACC, AEB)*. International Conference – The Road to Automated Drive 2014. 30 June – 2 July. Stuttgart, Germany.

Sandner, V. (2013). *Development of a test target for AEB systems: development process of a device to test AEB systems for consumer tests*. Proceedings of the 23rd International Technical Conference on the Enhanced Safety Vehicles (ESV). 27 May – 30 May. Soeul, South Korea.

Steffan, H., Moser, A., Ebner, J., Sinz, W. (2012). *UFO – ein neues System zur Evaluierung von Assistenzsystemen*. Braunschweiger Symposium Automatisierungssysteme, Assistenzsysteme und Eingebettete Systeme für Transportmittel. 8 – 9 February. Braunschweig, Germany.

Reconstructing Accidents by Simulation for Developing Active Safety Systems

Shin Tanaka*

*TOYOTA MOTOR CORPORATION, 1200, Mishuku, Susono, Shizuoka 410-1193, JAPAN
(Tel: +55-997-7929; e-mail: shin_tanaka_aa@mail.toyota.co.jp).

Abstract: This paper describes the development of a method to reconstruct accident scenarios by simulation as a means of helping to develop more effective active safety systems through quantitatively estimating the potential real-world accident reduction benefit of a system. This method enhances the validity of benefit estimation results by defining the road environment as well as the characteristics of the vehicle, system, and driver behavior based only on actual data. The validity of the method was also ensured by increasing the number of parameters considered and analyzing the dependency relationships between parameters, so that the simulation results reproduce the same characteristics as actual accident data. The robustness of this method was verified by inputting accident data from other regions around the world and confirming its ability to simulate accident scenarios in these regions. As a result, a method capable of simulating crossing pedestrian accidents, lane departure accidents, and rear-end accidents was developed using accident data from Japan, the U.S., and Europe. This method helps to identify the effectiveness of active safety systems in different accident scenarios and the type of support that is necessary to reduce accidents further. This information can then be fed back into active safety system development.

Keywords: benefit estimation, crossing pedestrian, lane departure, rear-end.

1. INTRODUCTION

A key part of active safety system development is accurately identifying the system benefit. By doing so, the types of accident that the system can help to avoid or reduce can be better understood, and the support required to enhance the system benefit can be fed back into the system development. The benefit of an active safety system is defined as the accident reduction potential that may be achieved if that system becomes widely adopted in the market. In conventional system development, the operation of the controls can be verified on a test course or tests on actual roads. However, the real-world accident reduction benefit of a system cannot be verified until after it is launched on the market as an actual product. Therefore, it tends to take a long period of time before the results of a system under actual usage conditions can be fed back into system development.

For this reason, Toyota Motor Corporation is developing a method of reconstructing traffic environments and accident scenarios by simulation based on road environments as well as vehicle and driver characteristics (Yuhara et al., 2006). The benefit of an active system in the real-world can be estimated during development by evaluating the effect on the number of accidents, fatalities, and injuries if the system is introduced, and measures can be taken to further enhance its potential active safety performance.

One critical aspect of this method is the validity of the simulated accident scenarios. Toyota has developed a method of reconstructing various accident scenarios in multiple regions around the world by simulation based only on actual data. This paper describes this method and analyses its validity.

2. RECONSTRUCTING ACCIDENTS BY SIMULATION

The developed method uses the Advanced Safety-System & Traffic REaltime Estimation Tool (AS-STREET) to reconstruct the traffic scenarios (Tajima, 2012). This tool is composed of road environment, vehicle, and driver behaviour models (Fig. 1). The driver perceives the surrounding environment, before judging and then carrying out the appropriate operation. As the individual characteristics of each driver are different, traffic flows can be reconstructed on a macro level by building up separate micro-level traffic scenarios based on individual driver behaviour (Fig. 2).
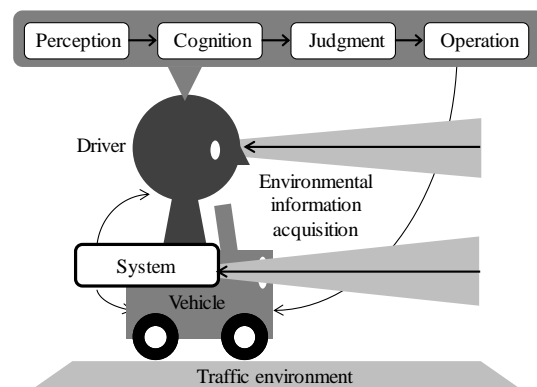

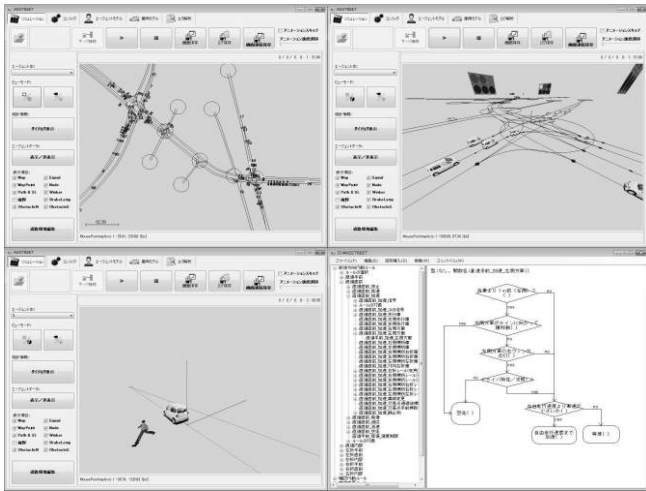Fig. 1. Configuration of models in the AS-STREET simulation tool.

Fig. 2. Examples of AS-STREET tool operation.

Fig. 3. Simulation of Reconstructing Accidents (SORA).

In general terms, traffic accidents occur due to a combination of driver error and the traffic situation at that moment. For example, even if a driver is distracted, an accident will not occur unless a slow moving vehicle is present in front of the driver's vehicle. The developed simulation method also combines driver error with the traffic situation to generate accidents. As a result, the accident frequency of the simulation method is as low as in the real-world.

Therefore, this tool extracts scenarios in which an accident has occurred from the generated traffic scenarios and simulates the benefit of active safety systems against that scenario (Fig. 3). The potential accident reduction benefit of an active safety system in the real world can be estimated by comparing the results (i.e., the number of accidents, fatalities, and injuries) with and without that active safety system installed. This allows the real-world benefit of the system to be confirmed efficiently and quantitatively even at the development phase.

This method of efficiently estimating the benefit of active safety systems by reconstructing accident scenarios through simulation is called "Simulation of Reconstructing Accidents" (SORA).

The distinguishing feature of SORA is its capability to reconstruct both accident scenarios based only on actual data and scenarios in which active safety systems are activated. These scenarios are reconstructed by combining real-world traffic and accident data with data of vehicle and system control models and driver behaviour measured in tests. The validity of the accident scenario reconstruction is described below. The characteristics of driver behaviour with respect to the activation of an active safety system are obtained using actual data through a driving simulator (Murano et al., 2009).

The scenarios in which these systems are activated are reconstructed using the Toyota Dynamic Driving Simulator (TDDS, Fig. 4). Data about the driver reaction time, behaviour, and the like are measured during the active safety simulation and reflected in the accident scenario simulation.
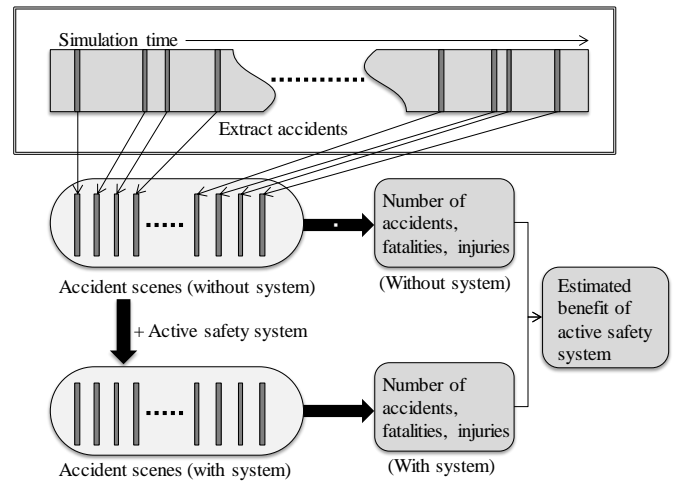
Fig. 4. Toyota Dynamic Driving Simulator (TDDS).

3. VERIFICATION OF VALIDITY OF SORA

To demonstrate the validity of the accident scenario reconstruction, the simulated accident scenes in Fig. 3 must be compared with actual accidents to check that the same trends are generated. In addition, to confirm the robustness of the method, it is also necessary to verify that the simulation can obtain the appropriate results even after changing the input data (e.g., the target region).

Although this simulation uses only actual data, the types of parameters that must be considered and the logic that defines the mutual dependency relationships have multiple solutions. Therefore, the following procedure was adopted to verify the validity and robustness of the accident scenario reconstruction.

3.1 Verification of Accident Scenario Reconstruction Validity

This research confirmed whether the accident situation of a target country could be reconstructed using accident data from that country.

If the accident situation could not be reconstructed, the number of parameters considered or dependency relationships was increased.

3.2 Verification of Robustness

This research confirmed if the accident situation of a different country could be reconstructed using data from that country

If the accident situation could not be reconstructed, the number of parameters considered or dependency relationships was increased.

The developed method was refined through these verifications and measures to boost simulation accuracy, and is now capable of reconstructing various types of accidents in various regions around the world.

4. RECONSTRUCTION OF CROSSING PEDESTRIAN ACCIDENT SCENARIOS

4.1 Confirmation of Crossing Pedestrian Accident Scenario Reconstruction Validity

Crossing pedestrian accident scenarios were reconstructed using accident data from Japan. As shown in Fig. 5, vehicle and pedestrian parameters have to be set before an accident scenario can be reconstructed. Although vehicle-related parameters were analysed from accident data, this data contains virtually no information about the pedestrians involved. Therefore, the characteristics of pedestrians crossing roads in the real-world were measured, and the walking speed distribution and crossing start judgment criteria were analysed from the obtained data.
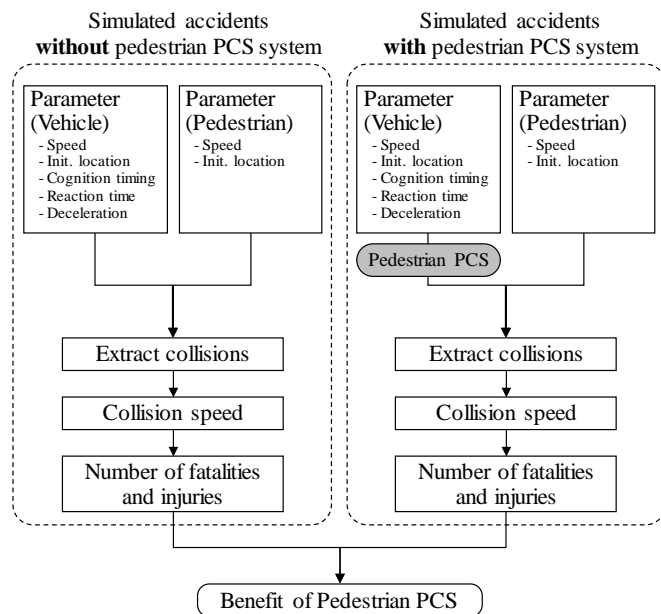
Fig. 5. Reconstruction of crossing pedestrian accident scenarios.

Although the obtained parameters were then incorporated into the system, these were not sufficient to properly reconstruct the accident scenarios. For example, even when the speed distributions when the accidents occurred were compared, the simulation results could not obtain the same trends as the actual accident data at the initial development

phase. This error was gradually reduced by adding parameters to be considered by the simulation and by analysing and defining the dependency relationships between the parameters. Figure 6 shows the parameters considered in the crossing pedestrian accident scenario reconstruction and the dependency relationships between the parameters. For example, actual vehicle test results of the driver's deceleration response to a crossing pedestrian identified that the rate of deceleration depends on the braking timing, and that the braking timing depends on the appearance timing of the pedestrian. The results also found that the brake pedal depression time also depends on the appearance timing of the pedestrian. The logic for these dependencies was incorporated into the simulation to help improve its reconstruction performance. Iwaki et al. (2013) reported that the trends of accident states (e.g., the speed distribution when an accident occurs) generated by simulations in this way match those of actual accidents.

When comparing the number of fatalities and injuries, it is necessary to calculate casualty figures based on the collision speed. Initially, a casualty map was calculated based on the speeds described in accident data and the proportion of fatalities and injuries (Fig. 7). However, these results did not match those of real-world accidents. A subsequent analysis of accident data found that a distinguishing characteristic of the casualty data is a dependence on the age of the pedestrian. This analysis also identified differences in crossing pedestrian accidents between night and daytime. The accident conditions were sub-divided as shown in Fig. 8, producing the casualty calculation shown in Fig. 9. These results confirmed that the targeted accident scenario could be reconstructed (Teraoka et al., 2013).
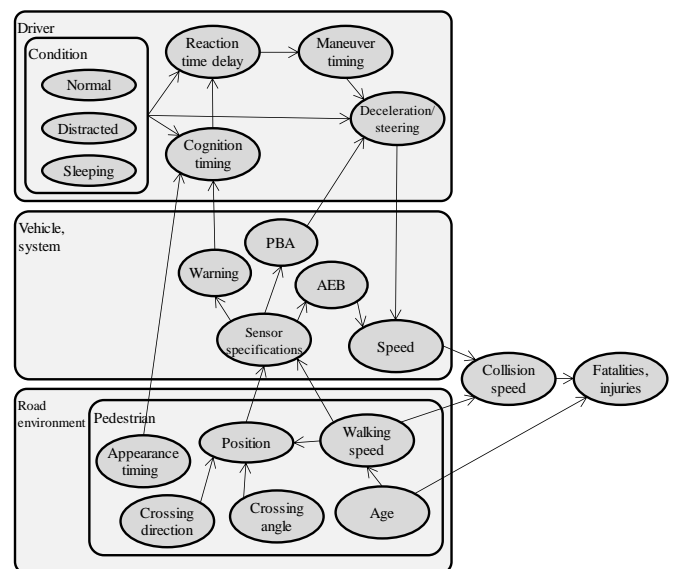
Fig. 6. Parameters and dependency relationships considered in crossing pedestrian accident scenario reconstruction.
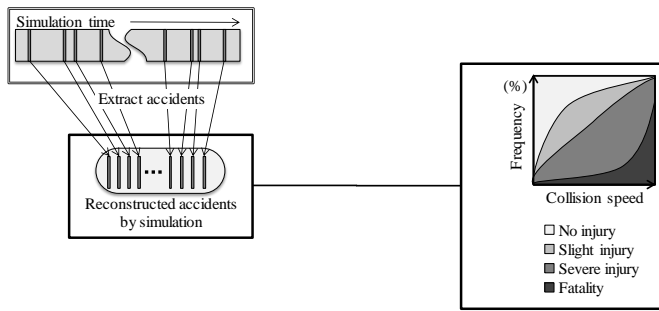
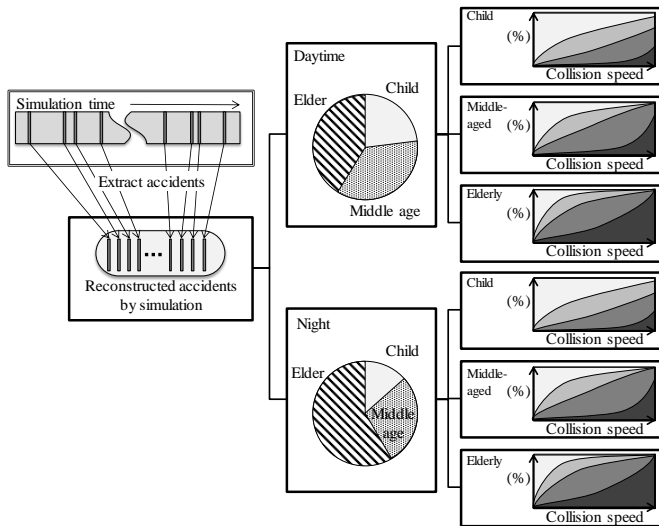Fig. 7. Calculation of fatalities and injuries in crossing pedestrian accidents.

Fig. 8. Sub-division of conditions for calculating fatalities and injuries in crossing pedestrian accidents.
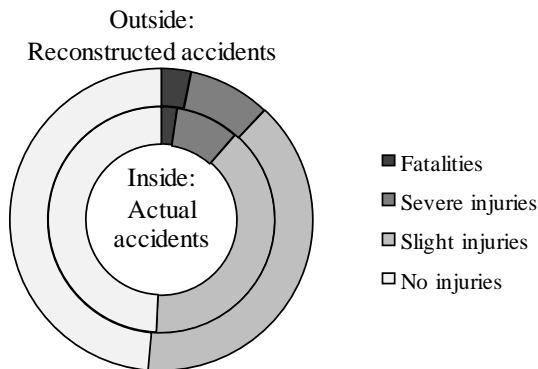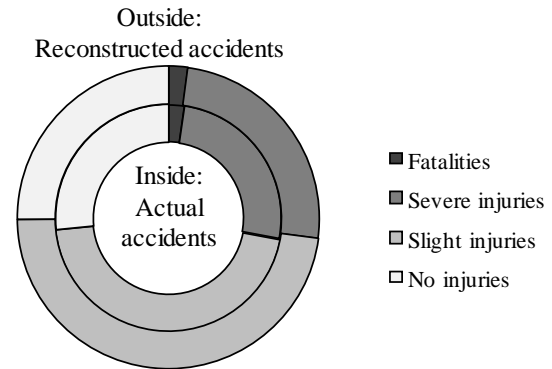

Fig. 9. Confirmation of crossing pedestrian accident reconstruction performance (comparison of fatalities and injuries in Japan).

4.2 Confirmation of Crossing Pedestrian Accident Scenario Reconstruction Robustness

The robustness of the crossing pedestrian accident scenario reconstruction was validated using German In-Depth Accident Study (GIDAS) accident data from Europe to verify this method in European accident scenarios. A robust simulation method should be capable of using the same

method as described above to reconstruct European accident scenarios. Assuming no significant differences in driver behaviour, Japanese driver data was also applied to the European accident scenarios. The results of the accident scenario reconstruction are shown in Fig. 10 (Tanaka et al., 2014). The simulation results showed the same trends as actual accidents in Europe as well, indicating that the parameters and dependency relationships considered for crossing pedestrian accident scenario reconstruction were sufficient and that the simulation method is robust.
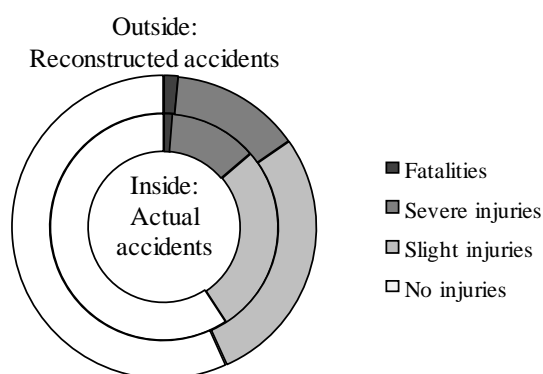

Fig. 10. Confirmation of crossing pedestrian accident reconstruction performance (comparison of fatalities and injuries in Europe).

5. RECONSTRUCTION OF LANE DEPARTURE ACCIDENT SCENARIOS

5.1 Confirmation of Lane Departure Accident Scenario Reconstruction Validity

Lane departure accident scenarios were reconstructed using accident data from Japan. Figure 11 shows the considered parameters and dependency relationships, and Fig. 12 compares the number of fatalities and injuries.
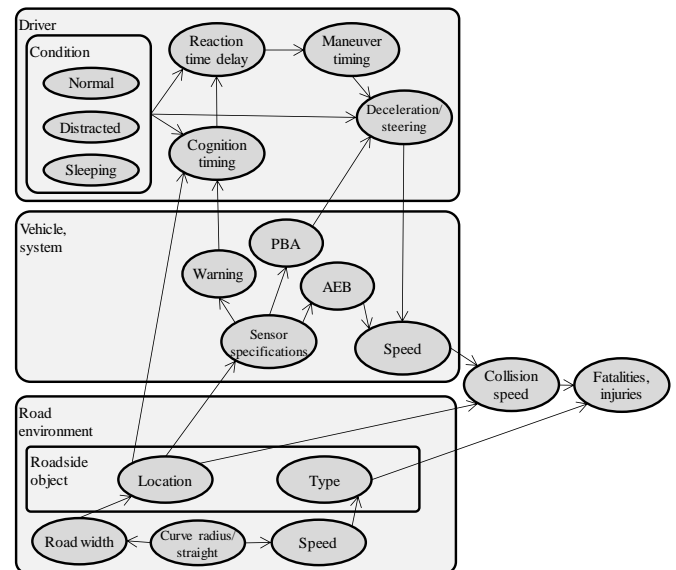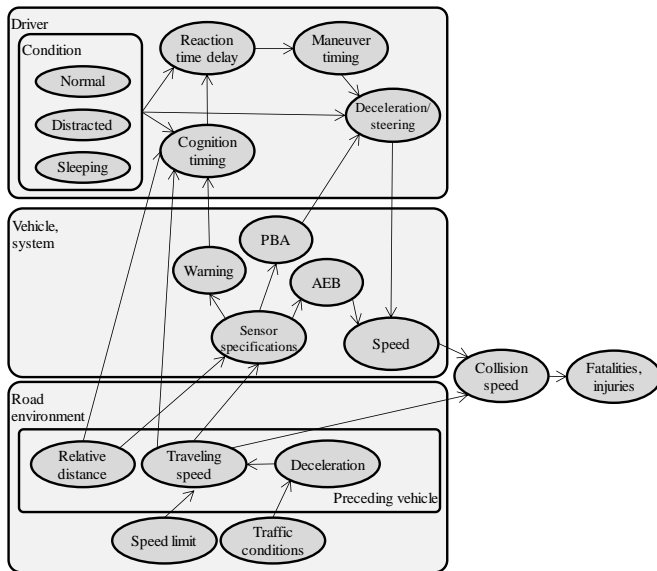

Fig. 11. Parameters and dependency relationships considered in lane departure accident scenario reconstruction.
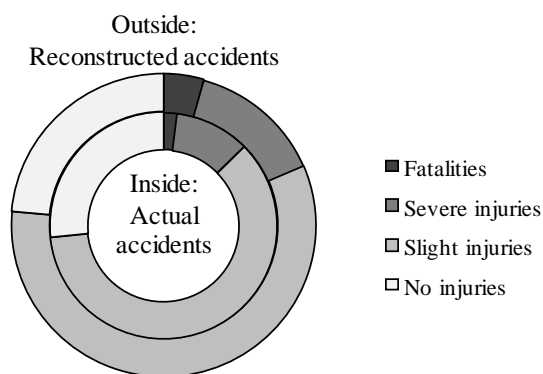
Fig. 12. Confirmation of lane departure accident reconstruction performance (comparison of fatalities and injuries in Japan).

The number of fatalities and injuries in lane departure accidents depends on the type of object involved in the collision. The type of object depends on the speed of the vehicle (i.e., the type and characteristics of the road). The reconstruction performance was enhanced by incorporating the relationships shown in Fig. 13 (Tanaka et al., 2012).
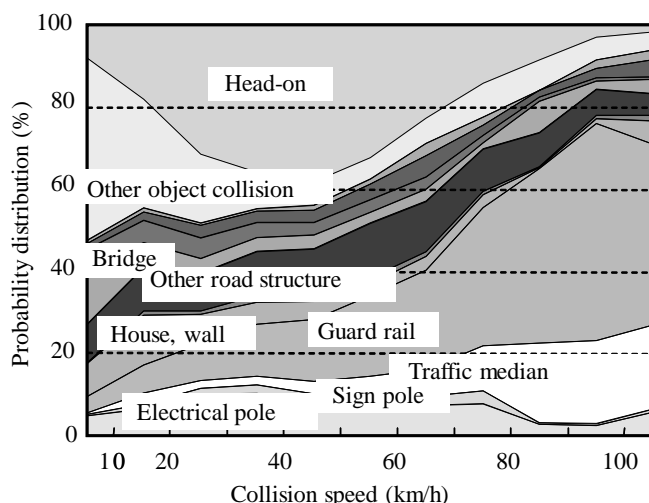
Fig. 13. Relationship between collision object and collision speed in lane departure accidents.

5.2 Confirmation of Lane Departure Accident Scenario Reconstruction Robustness

Figure 14 shows the simulation results using accident data from the U.S. It was confirmed that the same trends were reconstructed (Teraoka et al., 2014).

When European accident data was used, the same simulation method as for Japan and the U.S. did not achieve valid results. The difference between the two results was the state of the driver. In Japan and the U.S., drowsiness and carelessness affected a majority of drivers involved in an accident. However, in Europe, most drivers were alert. This indicated that the model did not adequately simulate the state of driver alertness. This issue was analysed and additional parameters

incorporated until the method was capable of adequately reconstructing accidents in Europe as well (Fig. 15).
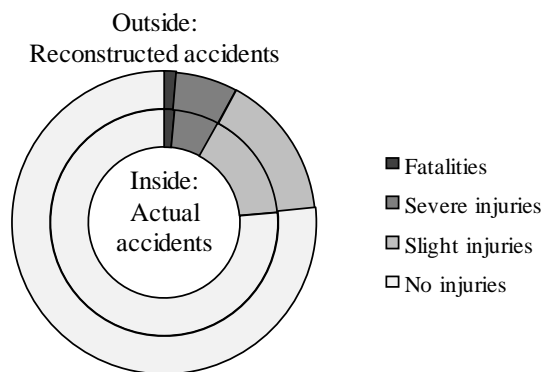
Fig. 14. Confirmation of lane departure accident reconstruction performance (comparison of fatalities and injuries in U.S.).

Fig. 15. Confirmation of lane departure accident reconstruction performance (comparison of fatalities and injuries in Europe).

6. RECONSTRUCTION OF REAR-END ACCIDENT SCENARIOS

6.1 Confirmation of Rear-End Accident Scenario Reconstruction Validity

Rear-end accident scenarios were also reconstructed using accident data from Japan. Figure 16 shows the considered parameters and dependency relationships, and Fig. 17 compares the number of fatalities and injuries. The method reconstructed the same trends as the actual accidents.

6.2 Confirmation of Rear-End Accident Scenario Reconstruction Robustness

Figures 18 and 19 show the results of accident scenario reconstruction performed using accident data from the U.S. and Europe. In both cases, the reconstructed results match the actual accident data, thereby demonstrating the robustness and validity of this simulation.

Fig. 16. Parameters and dependency relationships considered in rear-end accident scenario reconstruction.
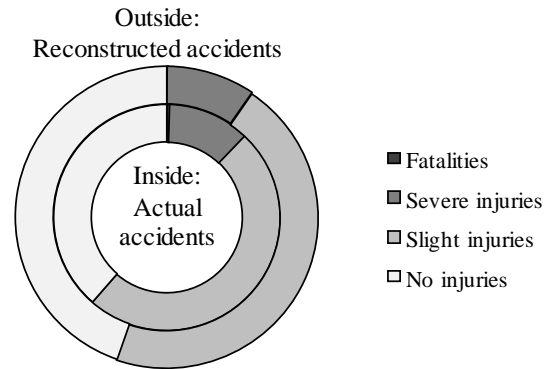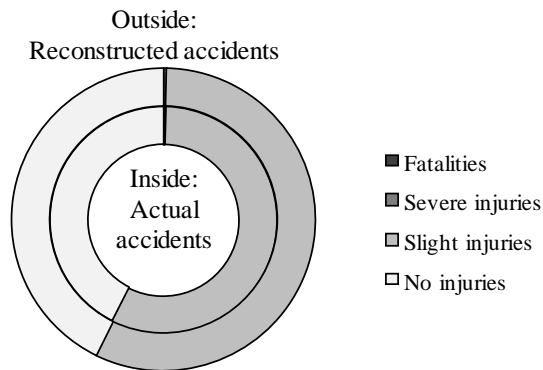

Fig. 17. Confirmation of rear-end accident reconstruction performance (comparison of fatalities and injuries in Japan).
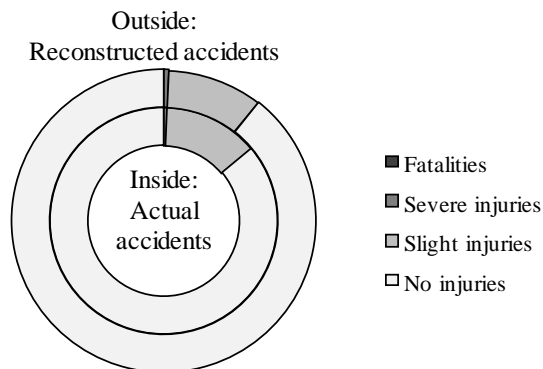

Fig. 18. Confirmation of rear-end accident reconstruction performance (comparison of fatalities and injuries in U.S.).

Fig. 19. Confirmation of rear-end accident reconstruction performance (comparison of fatalities and injuries in Europe).

7. CONCLUSION

This paper has described an accident scenario reconstruction method based on actual data, which was developed to help estimate the potential accident reduction benefit of active safety systems in the real world. The validity and robustness of this method were also demonstrated.

These simulations are performed using only combinations of actual data, consisting of road environment, vehicle and system, and driver behaviour characteristics. The parameters considered by the simulation, and the mutual dependency relationships between the parameters were defined to enable the reconstruction of the same accident scenarios as in the real world. In addition, this method is also capable of reconstructing accident scenarios from different regions around the world by inputting data from those regions. These results demonstrate that this is a robust simulation method that uses the appropriate parameters to reconstruct the target accident scenarios. This paper described the verification of this system using accident data from Japan, the U.S., and Europe. However, providing that accident conditions resemble those in these three regions, it should be possible to reconstruct accident scenarios in those regions by inputting the relevant accident data. This should help to develop active safety systems appropriate for those regions. In contrast, the existence of accident data for a region that cannot be reconstructed by this simulation indicates that the accident conditions and characteristics for that region differ from Japan, the U.S., and Europe. In this case, this method can be used to verify what the differences are, which can then be incorporated into active safety system development. This method focuses on pedestrian crossing, lane departure, and rear-end collision accidents, which make up a large proportion of the total number of accidents. However, this method can also be enhanced to reconstruct accidents at intersections between vehicles going straight on and between vehicles crossing and turning, enabling it to cover most accident scenarios occurring in the real-world. Ultimately, this method has the potential to help reduce accidents around the world by enhancing the effectiveness of active safety systems in these scenarios.

REFERENCES

Iwaki, R., Wakasugi, T., Teraoka, E., Tanaka, S., and Uchida, N. (2013). Analysis of driver response to road crossing pedestrian. *JSAE Paper* No. 20135756.

Murano, T., Yonekawa, Aga, M., and Nagiri, S. (2009). Development of high-performance driving simulator. *SAE 2009 World Congress*, SAE 09AC-0133.

Tajima, J. (2012). Verification of ASSTREET driver-agent model by collaborating with the driving simulator. *SAE International Journal of Passenger Cars - Electronic and Electrical Systems*, Vol. 5(2), 553-560.

Tanaka, S., Aga, M., Mochida, T., Yasuda, H., and Tajima, J. (2011). Benefit estimation of a pre-crash safety system for rear-end collisions by ASSTREET. *Proceedings of the First International Symposium on Future Active Safety Technology toward Zero-Traffic-Accidents*.

Tanaka, S., Mochida, T., Aga, M., and Tajima, J. (2012). Benefit estimation of a lane departure warning system using ASSTREET. *SAE Int. J. Passeng. Cars - Electron. Electr. Syst.* Vol. 5(1), 133-145.

Tanaka, S. and Teraoka, E. (2014). Benefit estimation of active safety systems. *FISITA 2014 World Automotive Congress*, F2014-AST-006.

Teraoka, E., Tanaka, S., Mochida, T. (2013). Benefit estimation of active safety systems for crossing-pedestrian scenarios. *FAST-Zero'13 Proceedings*, JSAE Paper No. 20134631.

Teraoka, E., Tanaka, S., and Mochida, T., (2014). Benefit estimation method for lane departure warning systems in the American traffic environment. *SAE Technical Paper* 2014-01-0172.

Yasuda, H., Kozato, A., Tanaka, S., Mochida, T., and Tajima, J. (2011). A generative approach to estimate effects of safety systems for rear-end collisions using ASSTREET. *Proceedings of the 22nd International Technical Conference on the Enhanced Safety of Vehicles*.

Yuhara, N. and Tajima, J. (2006). Multi-driver agent-based traffic simulation systems for evaluating the effects of advanced driver assistance systems on road traffic accidents. *International Journal of Cognition, Technology and Work*, Vol. 8(4), 283-300.

H

Primitive Modeling of Driver's Steering Torque using Front Field of View and Reaction Torque

Hidehisa YOSHIDA*. Hideya YAMAGUCHI*

*National Defense Academy, Yokosuka, 239-8686
Japan (Tel: 81-486-41-3810; e-mail: yoshida@ nda.ac.jp).

Abstract: The cooperative driver steering assistance system takes various steering characteristics and improves driving performance with less disturbance. This research uses the driver's steering torque for the driver model construction. The proposed basic driver model considers lateral deviation, as viewed from the front of the vehicle, for the model input, and steering function for position changes in two models based on the lateral deviation and reaction torque. Driving simulator experiments are shown**.**

Keywords: Driver model, Steering torque, Lateral deviation, Driving simulator.

1. INTRODUCTION

Collision avoidance systems using autonomous braking have been widely recognized to reduce accidents while driving in emergency situations. The need for steering avoidance technology exists for situations such as high-speed driving or low road surface friction. Future research and development are expected.

The purpose of the driver assistance system is to keep safe driving conditions and ensure the vehicle does not come into dangerous driving conditions. Braking assistance systems are directionally one-dimensional and decrease the kinetic energy of the vehicle, regardless of the driver's ability. It is assumed that steering performance degrades in vehicles with a steering intervention assistance system. In order to design a high precision driving assistance system, it is necessary to take various driving characteristics and how they effect steering into consideration.

The premise of the driver assistance system is to allow for allowances and judgment of the driver such that attention and operational ability of the driver are not lowered. It is necessary that stability and safety of the vehicle are improved as the operational characteristics of the driver are modified by the assistance effect.

Much knowledge has been accumulated by examining many models that handle the steering operation via the steering wheel angle using control theory. While travelling at high speeds, a driver need only to alter the steering angle a small amount in order to change lanes; it is empirically understood that steering work is achieved through torque, not by the steering wheel's angular change. The steering action is created by the feedback to the reaction torque. The feedback received from the steering wheel causes a reaction in steering, and stimulates the warning system's steering vibration. The assistance system indicates the steering direction needed, based the torque of the steering wheel.

It is the goal of this research that the steering torque model of the driver is accomplished over a series of steering actions in order to construct the necessary driver model in this research of design, effect, evaluation, and verification of steering assist under high speed driving. The first step for modeling the driver steering, high speed driving of a typical automobile is examined by modeling the driver via steering torque during lane-changing, which steers based on the front field of view and reaction torque of the steering wheel where the driver actively steers.

2. STEERING MODEL IN A LANE CHANGE SITUATION

Lateral deviation ε is registered by a driver as visual information, and is regarded as steering torque T_d, which increases in order to make the lateral deviation ε zero. A driver steering model under various conditions may be considered using a transfer function regarded as feedback action by the lateral deviation. This modeling is described in Equation (1). By considering the proportion element and the delay element, which is related to reaction delay time, the differential element, which is related to the time lead of the reaction, and dead time component based on the model in the control engineering, it is possible to understand features of the driver's steering using the control theory, in respect of the physical meaning, when it is described in the transfer function. It is also possible to evaluate the steering assistance system by this physical meaning when a driver assistance system is designed.

$$T_d(s) = G(s)\,\varepsilon(s) \qquad (1)$$

In this research, modeling of the driver's steering torque is based on the transfer function expression. This research examines both a model identification and a modeling of steering torque in which the driver inputs to the steering wheel in the driving simulator experiment.

2.1 Steering Model using a Front Field of View

Most studies of a driver model using steering angle input are based on the driver's steering to maintain a desired course and the lateral position input from the front viewpoint. The steering model in this research is also based on this.

Figure 1 shows the driver's steering input based on the deviation to the desired course in the front viewpoint. Where the center of gravity of lateral position in the vehicle is y_c, desired lateral position in the front viewpoint is y_{ref}, vehicle yaw angle between a centerline of the vehicle body and X axis of a fixed coordinate system is ψ.

It is possible to describe Equation (2), lateral deviation, with the front viewpoint with a desired course in the front view distance L from the present center of gravity of the vehicle position.

$$\varepsilon(t) = y_c + L\psi - y_{ref} \tag{2}$$

$$L = vt_p \tag{3}$$

The driver model using a front view model by the first prediction for straight line driving. The front view distance L multiplied by front view time t_p in vehicle speed v as Equation (3) is applied. A block diagram of the driver and vehicle system is shown in Figure (2).
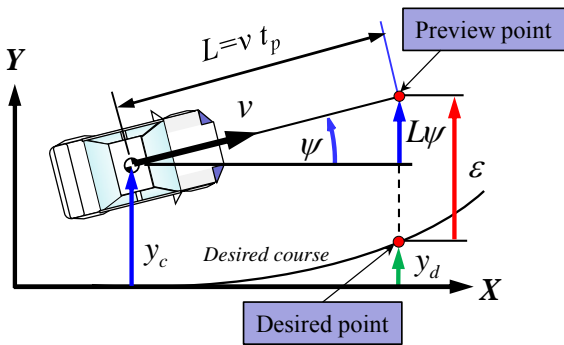
Fig. 1 The driver's steering input based on the deviation to the desired course in the front view point.
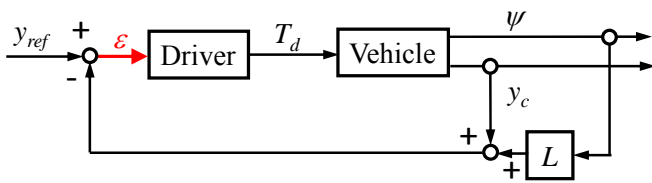
Fig. 2 A block diagram of a driver's steering and vehicle behavior. The input of a driver's steering is lateral deviation ε and the output of a driver's steering is steering torque T_d.

2.2 Driving Simulator

A lane-changing experiment at a constant speed of 100km/h is carried out by the driving simulator (DS) shown in Figure 3 in order to collect steering action of the driver under high speed driving. The DS used in this study reproduces a front

field of view on the monitor, the noise of the vehicle and the steering reaction torque from the steering wheel.

On the steering shaft, the reaction torque based on self-aligning torque shown by multiplying the caster trail ξ and front tire lateral force F_{yfl}, F_{yfr} of right and left is reproduced.

$$T_{SAT} = -\xi\left(F_{yfl} + F_{yfr}\right) \tag{4}$$

During the DS experiment, the examinees drive on a 2 lane expressway. The drive line is straight, and the width of a lane is 3.6m. It is asked of the examinee to keep a constant speed of 100 km/h by their own pedal operation. The driver is also asked to change to the adjacent lane (single lane change) by the steering wheel operation equal to an expressway situation in which the examinee normally uses.

The approval of the National Defense Academy ethics committee has been received for this research. The experiments are carried out with the informed consent of the examinees.

Fig. 3 Driving simulator (DS) for this research

2.3 Transition Steering Transfer model

It is possible to interpret lane changing in high speed driving scenerio by dividing it into two segments. One segment is when the lane-changing starts (course changing operation) and the other is when the driving course is corrected in order to keep driving in the new lane (lane keeping operation). In the initial course change operation, a comparatively large steering operation is carried out, and vehicle body attitude angle increases. After the course change operation, a steering correction is conducted for the purpose of keeping the lane so that the vehicle will not deviate from the desired course.

The course change operation and lane keeping operation are modeled in the driver's steering behavior in proportion to the lateral deviation ε in the front viewpoint. The steering operation of the driver model is divided into two parts and the model identification is examined. One part is the course change operation expressed by Equation (5), the other part is the lane keeping operation expressed by Equation (6).

$$T_{dmc}(s) = G_c \frac{1}{(\tau_{2c}s+1)(\tau_{2c}s+1)} e^{-\tau_{L_1}s} \varepsilon(s) \tag{5}$$

$$T_{dmk}(s) = G_k \frac{\tau_{1k}s+1}{(\tau_{2k}s+1)(\tau_{2k}s+1)} e^{-\tau_{L_2}s} \varepsilon(s) \tag{6}$$

Figure 4 shows the lane change response of a driver, lateral deviation ε in the front viewpoint, lateral position y, desired lateral position y_r, reaction torque of steering T_r and steering

torque in the experiment T_d. Steering torque in the model T_{dm} with model at Equation (5) and (6) are also shown together. It is assumed and it is used for the model identification at front preview time t_p=1.5[s], and dead time τ_{L1}= τ_{L2}=0.2[s]. And, the driving experiment result by typical passenger vehicle speeds of 80km/h are also shown in Figure 5. It can be confirmed that steering behavior by the DS experiment validates the modeling. And, it can be confirmed that response delay increases during the lane keeping operation.
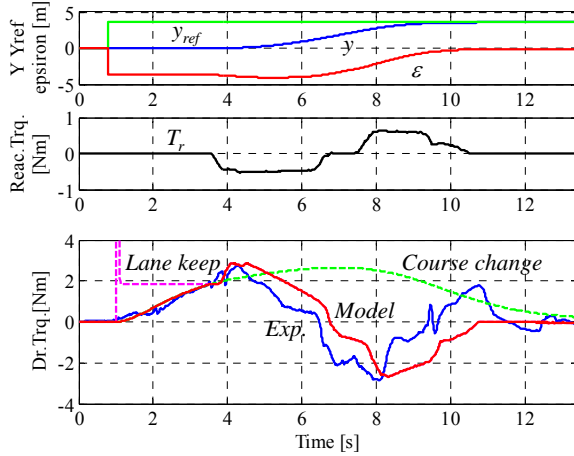
Fig. 4 Lane change DS experimental result with model response
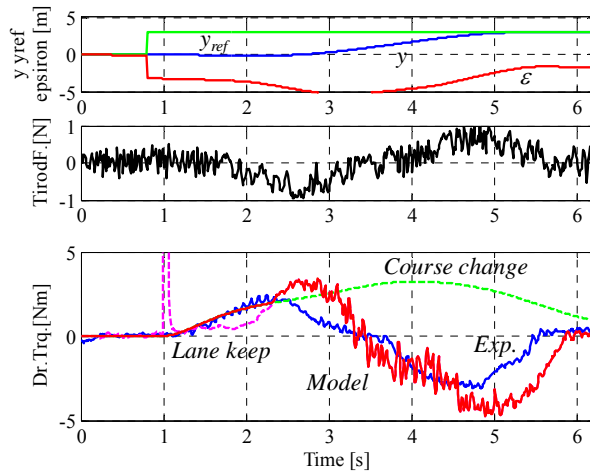
Fig. 5 Lane change car experimental result with model response

2.4 Effect on the model parameters by the existence of the reaction torque

In the DS experiment, two cases are compared. In the first case the reaction torque is presented in the steering wheel in which the driver steers and in the second, it is not presented. The results of driver parameters of Equation (5) and Equation (6) are shown in Figure 6. The significance was confirmed in the proportional gain G_c, G_k, and reaction delay time τ_2 by the existence of the reaction torque. But, the significance by the existence of the reaction torque could not be seen on lead time τ_1.

According to these results, when there is no information on the reaction torque, the torque gain tended to be small and response delay is shown by the parameter change of the model.
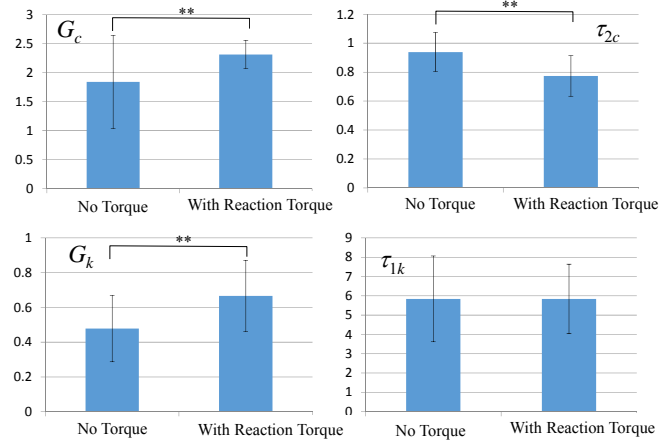
Fig. 6 Driver parameter change with/without reaction torque

3. PROPOSING A STEERING TORQUE MODEL THAT CONSIDERS THE TRANSFER OF STEERING OPERATION MODES

3.1 Transfer of steering operation modes

It was proven that the operating condition is transferred between course change operation just after the start and lane keeping operation after the course change operation, when the driver carried out the lane-changing. It was then proposed that the two steering operation mode transfer be considered in the driver model. The concept of steering operation mode transition in a lane change experiment is shown in Figure 7.
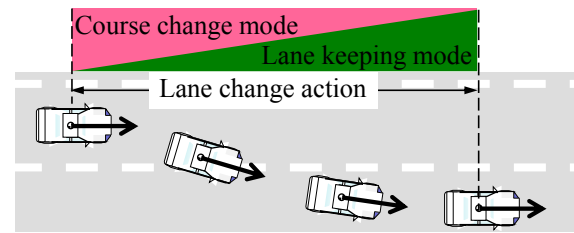

Fig. 7 Outline of steering model transition in the lane change

We considered the driver, under high speed driving conditions, has a sense for the risk of change of the moving speed of an object recognized in the visual field. In this experiment, the driving lane line can be seen on the road, and during lane changing, the driver seems to have recognized the relative moving speed change between the vehicle body and the lane. Then, it is considered that the driver recognizes the rate of changing for the lateral deviation ε.

The vehicle carries out a rotational motion in proportion to the frictional force (lateral force in which the tire generates) between the tire and road surface. With vehicle motion, the lateral force that occurs in the tire and generates within the

steering axle creates a self-aligning torque. The driver recognizes this self-aligning torque as a steering reaction torque in the steering wheel. Then, a steering model is devised, according to this effect and the tactile sense devised from it. The block diagram of the driver and vehicle system which considers this effect by the reaction torque in Figure 8 is shown.

Considering the effect of the visual information and tactile sense information, a new driver model of the driver's steering torque which includes course change operation mode and lane keeping operation mode is proposed in Equation (7).

$$T_{dm}(s) = G_h \frac{\alpha\tau_1 s + 1}{(\tau_2 s + 1)(\tau_3 s + 1)} e^{-\tau_{L1}} \varepsilon(s)$$
$$- G_r e^{-\tau_{L2}} T_r(s) \tag{7}$$
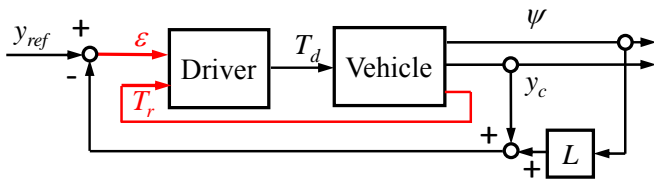
Fig. 8 Block diagram of a driver's steering model and vehicle behavior with reaction torque T_r.

3.2 Transition weight function of the steering operation

In proposing this driver model, the transition weight function in which the steering action is made to continuously transit from lateral deviation ε in the front viewpoint, which is where the visual information of the driver is introduced.

Just after the lane change start ($|\varepsilon|>0$), the course change operation is done in $\alpha=0$. When the vehicle is moved to the target lane, with $y_c=y_{ref}=y_d$ and with $\varepsilon=0$ condition, the course change operation is unnecessary and it becomes the lane keeping operation. This driver model is renewed at $\alpha=1$, and is work on the lane keeping operation.

From the above situation, the transition weight function α, which carries out the weighting of the model by the condition ε, is proposed in Equation (8). Transition weight function α is the parameter that corresponds to the ratio of the two modes of driver models. It is the parameter which is made dimensionless by taking to the numerator for the sum of the time history of desired course y_{ref} and the lateral deviation with the front fixation point ε, and to the denominator for the lateral step distance of the desired course y_d. Since the steering operation of the driver transits from the course change mode to the lane keeping mode, in the lane change operation, the transition weight function α changes by the condition of ε.

$$\alpha = \frac{y_{ref}(t) + \varepsilon(t)}{y_d} \tag{8}$$

For the experimental result of the lane change operation, time history responses that are applied to this model are shown in Figure 9. Identified driver parameters are shown in Table 1. Figure 9(a) shows the lateral displacement y_c of the car body's center of gravity and desired course y_{ref}, (b) shows yaw angle of the vehicle body, (c) shows the lateral deviation in the front view point, (d) shows the reaction torque T_r and (e) shows the transition weight function ε.

The change of transition weight function α gradually increases from $\alpha=0$ in the course change mode start at the $t=1[s]$, and it has transferred to $\alpha=1$ lane keeping mode near the $t=9[s]$ in which the course change mode finishes. In proportion to the change of transition weight function α, the model output of the steering torque shows the same tendency of the response of the experimental result. Two models transit by transition weight function α; it is proven that the steering torque behavior, of which the response of the model is similar to the experimental result, is shown.

It is possible to transform from Equation (7) to Equation (8), when the breakdown of composing driver model of steering torque is divided into every element.

$$T_{dm}(s) = G_h \frac{\alpha\tau_1 s + 1}{(\tau_2 s+1)(\tau_3 s+1)} e^{-\tau_{L1}s}\varepsilon(s) - G_r e^{-\tau_{L2}s}T_r(s)$$
$$= (1-\alpha)\left\{G_h \frac{1}{(\tau_2 s+1)(\tau_3 s+1)} e^{-\tau_{L1}s}\right\}\varepsilon(s)$$
$$+ \alpha\left\{G_h \frac{\tau_1 s+1}{(\tau_2 s+1)(\tau_3 s+1)} e^{-\tau_{L1}s}\right\}\varepsilon(s) \tag{9}$$
$$+ \left\{-G_r e^{-\tau_{L2}s}\right\}T_r(s)$$
$$= T_{dmc} + T_{dmk} + T_{dmr}$$

T_{dmc} can explain steering torque by the course change mode, T_{dmk} can explain steering torque by the lane keeping mode and T_{dmr} can explain steering torque in proportion to the reaction torque.

Table 1 Parameters of proposed lane change driver model

G_h [Nm/m]	τ_1 [s]	τ_2 [s]	τ_3 [s]	τ_{L1} [s]	G_r [Nm/Nm]	τ_{L2} [s]
0.25	5.0	0.5	0.1	0.2	3.0	0

(a) Reference course, Lateral position

(b) Yaw angle

(c) Lateral deviation

(d) Reaction torque

(e) Transition weight function

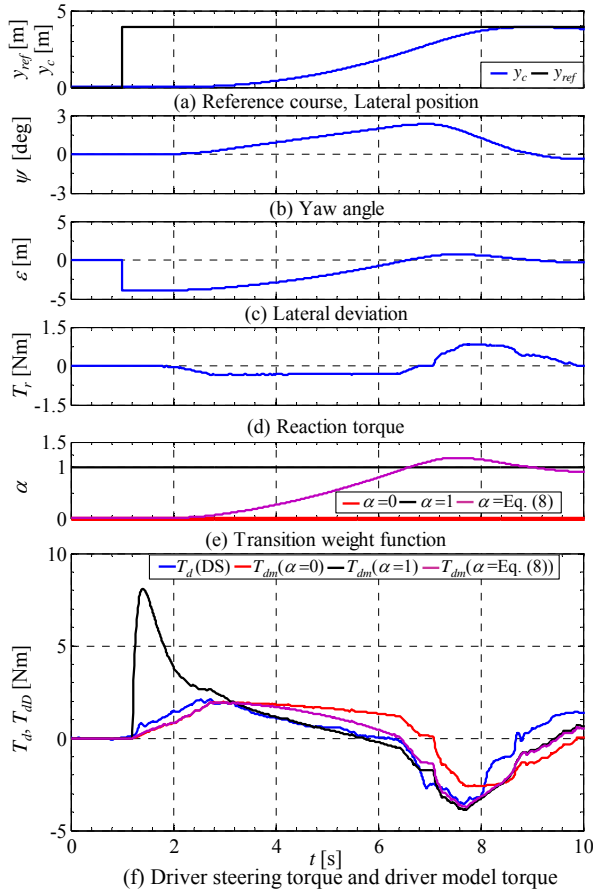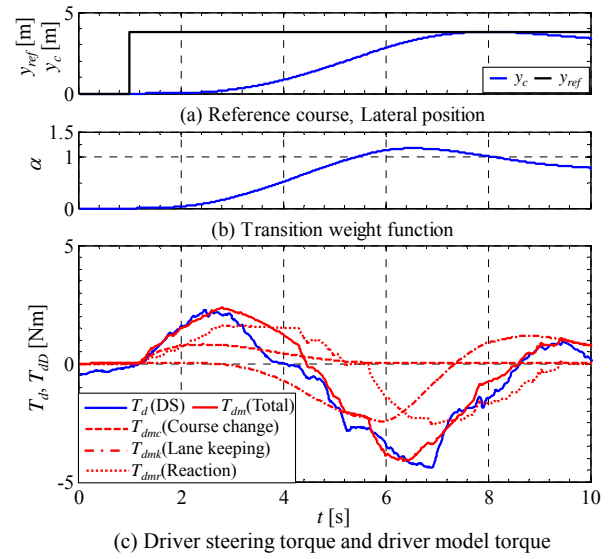(f) Driver steering torque and driver model torque

Fig. 9   Time history of lane change at driving model transition from course change mode to lane keeping mode

The result of calculating Equation (9) using examples of experimental results is shown in Figure (10). The blue line at Figure 10(c) is steering torque T_d, obtained by a DS experiment. The red broken line has shown steering torque T_{dmc} for the course change operation mode. The red dashed line shows steering torque T_{dmk} for the lane keeping operation mode. The redspot line has shown steering torque T_{dmr} in proportion to the reaction torque. The red continuous line has shown steering torque T_{dm} which the mode of these three are totaled.

It may be confirmed that steering torque T_{dmc} for the course change mode becomes almost zero after about t=5.5[s]. In this time, it may be understood that the driver intends the end of the course change operation. The steering torque of the lane keeping mode T_{dmk} generates reverse-directional course change mode near t=3[s], and becomes a maximum near t=6[s]. This situation is possible to understand that the steering torque is being generated, in order to suppress exceeding the desired course of the lane change. In addition, it may be understood that steering torque in proportion to the reaction torque causes an effect which guarantees the delay of the lane keeping operation.

From them, it was confirmed that the steering torque by the driver could be reproduced on course change operation and lane keeping operation in the lane change by considering lateral deviation in the front view point and reaction torque

by considering the transition weight function. There seems to be the validity on understanding in this model in which the steering operation of the driver transits from the course change operation mode to the lane keeping operation mode in the lane change steering.

(a) Reference course, Lateral position

(b) Transition weight function

(c) Driver steering torque and driver model torque

Fig. 10   Time history of each steering torque at the driving model transition from course change mode to lane keeping mode

3.3 Driver parameters

The model identification on the steering torque during lane-changing was carried out. For proportional gain G_h for the lateral deviation ε, lead time τ_1, reaction delay time τ_2, and the proportional gain G_r for the steering reaction torque are examined. The preview time as t_p=1.5[s] (fixed) in the front view point and the lag time as τ_{L1} =0.2[s] (fixed) for lateral deviation in the front view point are set. In order to ensures properness of the transfer characteristic, it has be made to be τ_3 =0.1[s] (fixed).

The lane-changing experiment by the five examinees whom they showed in Table 2 was carried out.

Table 2   Subjects for DS lane change experiment

	Gender	Age	Driving experience [Years]	Driving frequency [per week]
A	Male	33	16	2
B	Male	42	22	1
C	Male	29	6	2
D	Male	27	7	5
E	Male	63	40	7

It is necessary to understand features of the steering torque in the lane-changing by the driver are for proportional gain G_h, for the lateral deviation, for the phase lead time τ_1, reaction delay time τ_2 and proportional gain G_r for the steering reaction torque.

Each driver parameter is examined. Mean value and standard deviation of each examinee of the driver parameter are shown in Figure 11, and test result of the 5% significance for examinee A is written together.

Though there is not any significance to G_h in proportion to lateral deviation in the front viewpoint, the lead time τ_1, reaction delay time τ_2 are not observed as significant by the examinee. These parameters are regarded as applying to the model as a general purpose characteristic value which is not based on every examinee. In the meantime, on proportional gain G_r for the steering reaction torque, there is a significance by the examinee, and it is considered that this value in proportion to each examinee must be applied to this model.

The next two points were confirmed above the result approach. The remainder of the individual characteristic differences were not observed in dead time and reaction delay time for lateral deviation in front view point and for the reaction torque. It is observed unique of the individual for the proportional gain and especially, it is shown that features of the driver remarkably appeared in the proportional gain for the reaction torque.

(a) Driver gain G_h
(b) Lead time τ_1
(c) Reaction delay time τ_2
(d) Reaction torque gain G_r
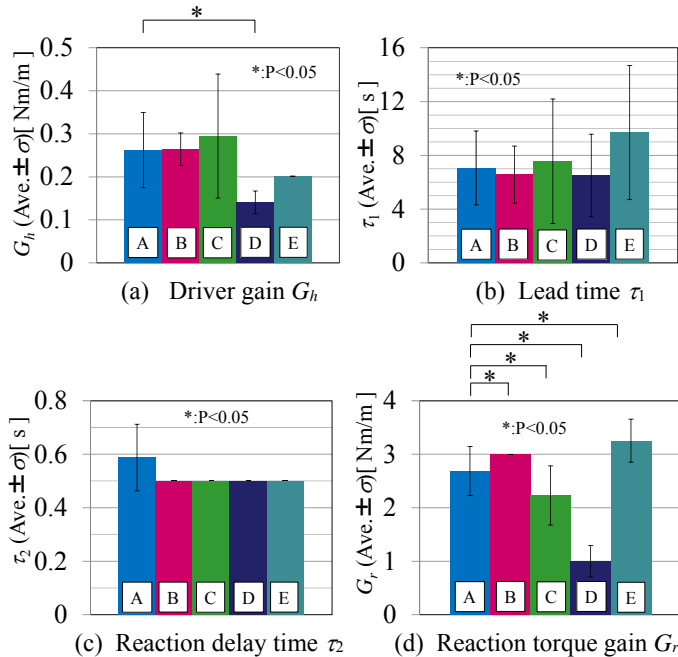
Fig. 11 Difference every subject of a driver parameters on proposed driver model

4. CONCLUSIONS

In this research, in order to construct necessary driver model for design, effect evaluation and verification of the steering assist system under high speed driving, the driver's steering torque model is made to be a goal of our research that a series of steering actions of the driver are modelled.

The steering torque model which reproduced the steering torque of the driver considering the lateral deviation in the front viewpoint and reaction torque from the steering wheel was proposed. Based on the idea that driver's steering operation makes the transition of course change operation

mode to the adjacent lane and afterwards the lane keeping operation mode and carries out the lane change steering, the transitional steering torque model was devised, and the effect was confirmed.

From the results of the significance test of driver parameter of model identification from the lane change experiment, it was proven that the proportional gain for the reaction torque may be unique to every examinee, dead time and reaction delay time for lateral deviation in front viewpoint and that the reaction torque is not observed in individual characteristic differences.

REFERENCES

Harada, H., (1992). Stability Criteria and Evaluation of Steering Maneuver in Driver –Vehicle System. *Transactions of the Japan Society of Mechanical Engineers*, Series C, Vol.58, No.546 (1992), pp.418–424 (in Japanese).

Iguchi. M., (1970). Man-machine systems, pp.14-45., Kyoritsu Shuppan Co., Ltd. (in Japanese).

Kondo, M., (1958). Basic relation which exists between the steering of a car and the dynamics, *Transactions of Society of Automotive Engineers of Japan*, No.5, pp.40-43 (in Japanese).

McRuer, D. T. and Jex, H. R., (1967). A review of quasi-linear pilot models, *IEEE Trans.*, HFE-8-3, pp.231-249.

Nagai, M., Shitamitsu, K., Yoshida, H. and Mouri, H., (2003). Over-ride characteristics of Lane-Keeping control system using steering torque input : A studey on lateral wind response with a driving simulator, *Transactions of Society of Automotive Engineers of Japan*, Vol. 34, No.1, pp.157-162 (in Japanese).

Yoshida, H., Nagai, M., Mouri, H. and Sato, S., (2006). A study on vehicle lane departure delay system, *Review of Automotive Engineering*, Japan Society of Automotive Engineers, Vol.27, No.2, pp.273-248.

Safe Driving Evaluation System to Enhance Motivation for Safe Driving

Toshihiro Hiraoka * **Keita Nozaki** ** **Shota Takada** ***
Hiroshi Kawakami ****

* *Kyoto Univ., Kyoto, Japan (hiraoka@sys.i.kyoto-u.ac.jp).*
** *Kyoto Univ., Kyoto, Japan (nozaki@sys.i.kyoto-u.ac.jp).*
*** *West Nippon Expressway Engineering Kansai Company Ltd.,*
Ibaraki, Osaka, Japan (sho_takada@w-e-kansai.co.jp).
**** *Kyoto Univ., Kyoto, Japan (kawakami@design.kyoto-u.ac.jp).*

Abstract: Systems to enhance a driver's motivation to drive safely are expected to be effective in reducing the number of traffic accidents. With the aim of encouraging drivers to drive in a pleasant and safe manner, the present study modifies the safe driving evaluation indices proposed in a previous study, and constructs a safe driving evaluation system based on game design methodologies and presents a novel design for guidelines governing a human-machine system. Driving simulator experiments were conducted to ascertain the effectiveness of the proposed system.

Keywords: Human-machine interface, User interfaces, Driver behavior, Human-centered design.

1. INTRODUCTION

The number of deaths and casualties caused by automotive accidents remains at a high level in Japan. In order to enhance vehicle safety inherently, it is important to encourage spontaneous safe behavior on the part of drivers in light of the fact that some reports [Wilde (2001); Smiley (2000); Saad (2006); Hiraoka (2010)] have pointed out that the introduction of safety devices can provoke unsafe behavior by drivers.

Previous research proposed quantitative evaluation indices of safe driving [Hiraoka (2013)], and verified that visual feedback of the index values could encourage drivers' behavioral adaptation for safer driving [Takada (2013, 2014)].

The present study improves the evaluation indices and modifies the interface of the safe driving evaluation system (SDES) based on game design methodologies and presents novel design methods of a human-machine system in order to enhance motivation for safe driving. Moreover, driving simulator experiments are performed to verify the effectiveness of the proposed SDES.

2. IMPROVEMENT OF SAFE DRIVING EVALUATION INDICES

This paper focuses on the four safe driving evaluation indices that were proposed in a previous study [Hiraoka (2013)]. The four indices, shown in Fig. 1, are non-dimensional parameters, and their range of the four following indices is from zero to one, with the higher value represents safer driving behavior.

(1) Index I_F: *Proper deceleration*
(2) Index I_B: *Deceleration with consideration for backward vehicle*
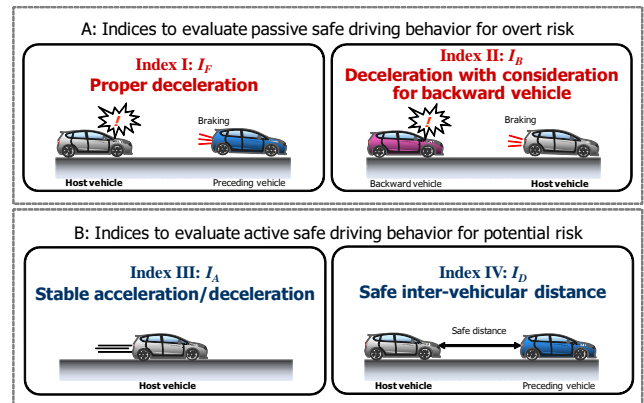
Fig. 1. Four indices to evaluate safe driving behavior

(3) Index I_A: *Stable acceleration/deceleration*
(4) Index I_D: *Safe inter-vehicular distance*

The present study modifies the above indices to better evaluate safe behavior on the part of drivers: 1) the index I_A considers not only stability but also smoothness of acceleration/deceleration; 2) the modification solves the problem of indices I_F and I_B, which tend to underestimate the safeness of driving behavior when the driver reacts quickly to an overt danger because the evaluation time becomes too short.

3. SYSTEM DESIGN FOR IMPROVEMENT OF DRIVERS' MOTIVATION

3.1 Self-Determination Theory

The self-determination theory (SDT) [Deci (2004)] is one of the most representative theories with respect to motivation. The theory states that individuals have innate psychological needs:

S1) Autonomy: this becomes high when individuals feel that they have elected to do something and do so by themselves

S2) Competence: a perceived self-belief in one's ability to perform well in an activity

S3) Relatedness: a sense of shared experience

3.2 Gamenics Theory

Gamification is defined as a term for the use of game elements in a non-game system to improve user experience and engagement. Saito [Saito (2007)] proposed a gamenics theory, which is a massive body of know-how related to the user interface design. It consists of five principles as follows:

G1) Intuitive and comfortable user interface
G2) Operability that does not require a manual
G3) Techniques to get the players hooked on the game
G4) Promotion of gradual learning
G5) Linking the virtual world to the real world

3.3 Benefit of Inconvenience: Fuben-eki

Fuben-eki (FUrther BENEfit of a Kind of Inconvenience) is a design concept for constructing and evaluating a system that enable users to gain subjective benefits such as self-determination, competence, and fun [Kawakami (2013)]. According to the concept, it is preferable to leave a margin to devise safe-driving mannerisms by the drivers themselves in order to obtain better subjective benefits.

3.4 Design Guidelines to Encourage Safe Driving

A good interface gives user-appropriate and system-appropriate communication of knowledge or information. In the field of road traffic safety and psychology, six interface design indices have been proposed [Hiraoka (2012)]:

D1) Incentives for safe driving
D2) Entertainment for improving the feeling of competence
D3) Continuous and multi-modal information presentation
D4) Interface to satisfy S-R compatibility
D5) Intuitive mechanism and control law
D6) Illusion for increasing the perceived risk

4. PREVIOUS VERSION OF SDES INTERFACE

4.1 Features

Figure 2 shows the version of the SDES interface proposed in the previous study [Takada (2014)]. This version displays interval scores and average scores of the above-mentioned four indices to evaluate safe driving behavior by conversion to 100 points. The interval score means the points of the latest evaluation interval, and the average score means the points averaged from the start to the latest evaluation interval. The variance in average score becomes smaller as the travel time becomes longer, and it represents a driver's average driving skill level with respect to the index. The variance of the interval score becomes larger
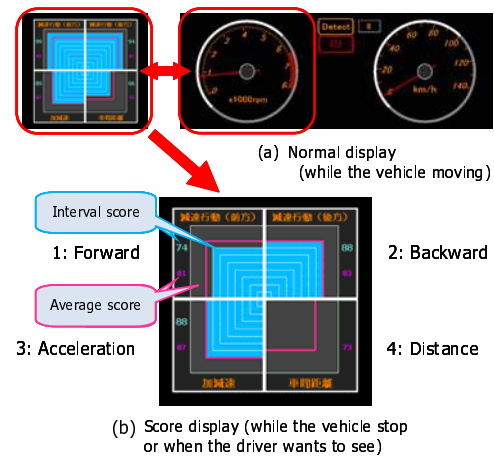
Fig. 2. Previous version of SDES interface

compared to the average score, because the evaluation interval is short.

As mentioned above, the interval score is equivalent to feedback of the most recent score with respect to safe driving. The driver can feel an increase in skill or a decrease in skill with respect to safe driving by comparing the interval score and the average score and therefore it is possible to increase a driver's motivation to improve safe driving.

Complex visual information while driving increases the visual workload on a driver and might distract a driver from the primary task of operating a vehicle. Therefore, the visual information of the SDES appears only when the vehicle stops or the driver pushes the display information button.

4.2 Problems

The driving simulator experiments [Takada (2013, 2014)] showed that the SDES shown in Fig. 2 could encourage participants to drive safely spontaneously. However, there were some participants who felt that the score evaluation system of the SDES was bothersome, and only half of the participants replied that they would want to use the system in an actual driving situation. Further investigation clarified two main reasons for this: 1) it is difficult for users to understand the evaluation algorithm of the SDES; and 2) users do not feel the necessity for the SDES. The investigation also found that the system and the interface must be improved in order to enhance the motivation for usage of the SDES.

5. PROPOSAL OF NEW SDES INTERFACE

5.1 Intuitive User Interface

Figure 3 shows the visual information display of the SDES proposed in this study. Three vehicles arranged vertically on the left side of the screen correspond to the longitudinal relationship among a preceding vehicle, a driver's vehicle, and a backward vehicle. This display is intended to help the driver understand the display contents intuitively, and therefore it will not disturb motivation to utilize the system.
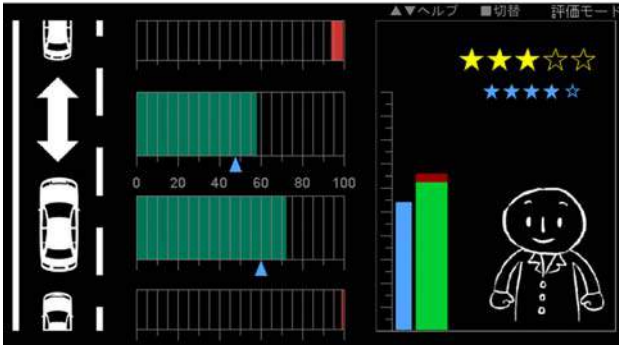
Fig. 3. Advanced version of SDES interface

5.2 Easy Understanding of Operations without Manuals

In order to improve understanding of the SDES, only scores for two indices, I_A and I_D, are displayed when a driver starts using the system. The display contents increase along with an increase in safe driving skills until finally the scores of all four indices are displayed on the screen. The scores of I_A and I_D, which represent a potential risk, are enlarged to be easily noticeable in order to emphasis active safe driving behavior.

The system also can display help information on the screen, which eliminates the need for reading an operation manual (Fig. 4).

(a) advice about I_F (b) advice about I_B

(c) advice about I_A (d) advice about I_D
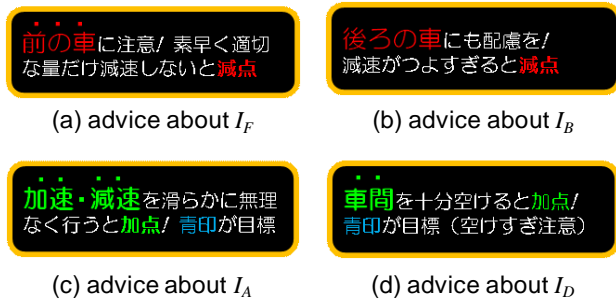
Fig. 4. Help information display

5.3 Absorbed Production and Gradual Learning Effects

The SDES provides the driver with a performance goal according to her/his score history, and adjusts the difficulty of the goal to encourage gradual learning for safe driving. Figure 5 shows a flow of the achievement evaluation and a renewal of the target value.
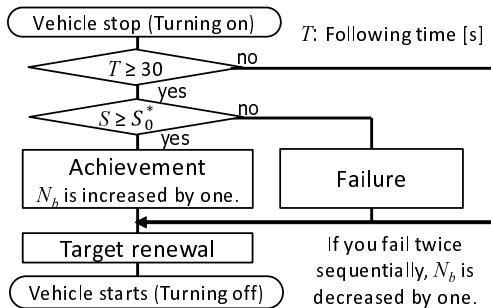
Fig. 5. Flow of evaluation and target renewal

Score Presentation   Interval scores of the indices are calculated at the moment the vehicle stops and are illustrated by green or red bars as shown in Fig. 3. The SDES does not evaluate driving behavior if the duration of the following state is less than 30 [s]. The indices I_A and I_D for active safe driving are calculated by point-addition scoring and green bars, and the indices I_F and I_B for overt risks are calculated by point-deduction scoring and red bars. As shown in Fig. 6, the total score S is defined by

$$S = I_A + I_D - (1 - I_F) - (1 - I_B). \qquad (1)$$
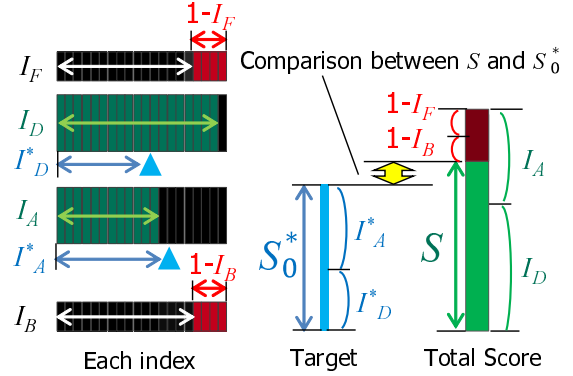
Fig. 6. Calculation of total score S and target value S_0

Target Value Presentation   The target values I_A^* and I_D^* are calculated according to driving skill. Figure 7 shows the calculation method for the target values based on the score histories [Hiraoka (2011)].
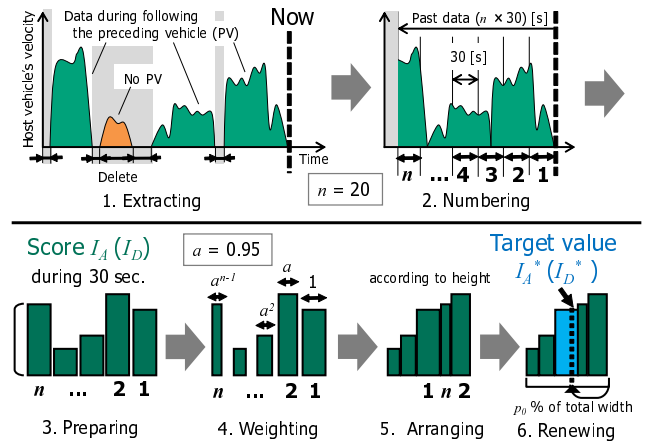
Fig. 7. Extraction of evaluation object (upper) and calculation method of target value (lower)

The simple sum of the two target values I_A^* and I_D^*, which are depicted by blue triangles, is defined as target total score S_0^*, and it is illustrated by a blue vertical bar. They are updated by every stop.

Evaluation of Target Achievement   The SDES evaluates goal achievement at every stop. The number of blue stars is increased by one when the total score S exceeds the target value, and it is decreased by one when the total score does not exceed the target value twice in a row. At the same moment, the system provides sound effects to inform the driver of goal achievement or a failure. Five blue stars ($N_b = 5$) is equivalent to one yellow star ($N_y = 1$).

The number of yellow stars also represents the achievement level D.

Support for Gradual Learning   In order to promote gradual learning for safe driving, the task difficulty of the SDES is set according to a driver's skill level, which is equivalent to the achievement level D. At the levels $D = 1$–3, the achievement possibility p_0 used for calculation of the target value, as shown in Fig. 8, is defined to be 70%. At the easiest level $D = 1$, the total score S is defined by only two indices I_A and I_D. At the levels $D = 2$ and 3, the evaluation indices I_F and I_B, which are point-deduction scores, are also considered sequentially to calculate the total score S. Additionally, at the levels $D = 4$ and 5, the achievement possibility p_0 becomes 60% and 50% in order to inspire the driver to more difficult task.
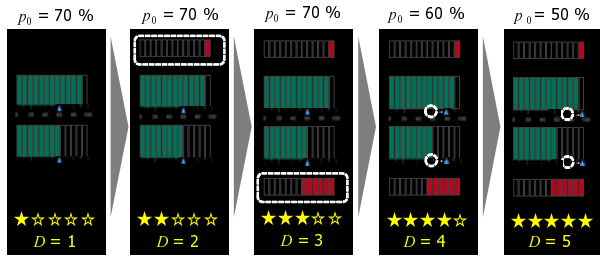
Fig. 8. Evaluation method at each achievement level D

6. DRIVING SIMULATOR EXPERIMENT #1: EVALUATION OF USER ACCEPTANCE

This section describes driving simulator experiment #1 conducted to ascertain user acceptance of the proposed SDES.

6.1 Conditions

The experimental participants were ten men and one woman, ranging in age from 21 to 30 years old, with an average driving experience of 39 months. They gave informed consent before the experiment started.

Each participant drove a host vehicle (HV) along a course consisting of a two-lane, one-way straight road. The width and length of which were 7 [m] and 8 [km], respectively. A preceding vehicle (PV) traveled in front of the host vehicle, and the PV's velocity pattern was predefined to simulate a general velocity pattern on urban and suburban roads. In addition, a backward vehicle (BV) followed the HV according to the following model.

The participants were given the following instructions: a) drive in the left lane and follow the PV, b) the BV passes the HV and cuts in ahead of the HV when the inter-vehicular distance between the HV and the PV becomes greater than the threshold, c) restart the experimental driving from the beginning when there are many collisions with other vehicles and when being constantly overtaken by the BV, and d) perform the subtask [1] provided that it does not interfere with one's driving ability.

---

[1] The participant adjusts a dial switch located beside the steering wheel to match the number displayed on road traffic signs.

6.2 Procedure

The experiment consisted of 12 conditions for three days; **cond. 1 and 2:** normal driving without the SDES × 2 times (n1, n2), **cond. 3–11:** driving with the SDES × 9 times (s1–s9), and **cond. 12:** normal driving without the SDES (n3). The participants practiced to become familiar with driving on the simulator before the experiment started.

After the experimental driving, the participants answered a questionnaire with a seven-point scale, which consisted of questions relevant to '*degree of utilization*', '*motivation for usage*', '*game elements*', and other such items.

6.3 Results

Overall Results   Figure 9 shows transitions of total score S, achievement level [2] L, and the four indices I_F, I_B, I_A, I_D, which were averaged for each condition. The total score S and the achievement level L increased and the number of down points of I_F and I_B decreased with driving repetitions, while the indices I_D and I_A remained unchanged.

Table 1 lists the results of the subjective evaluations. It shows that the motivation to use the SDES continuously was relatively low and many participants did not feel any sense of competence even though they had used the SDES and tried to achieve the target by using the device.

As shown in Table 1, the average score for 'understanding of operation by using SDES' (Q1-b1) was 5.5, which is relatively high compared to the understanding of the four indices. The results might be derived from individual differences caused by the complaint about the insufficiency of the help contents and doubts about the evaluation methods of the indices.

The scores for 'fun' (Q1-c1) and 'degree of enthusiasm for using SDES' (Q1-c2), which represent the absorbed production and the gradual learning effects mentioned in 5.3, tended to be clearly split into two groups. The results might be derived from difficulty using the SDES, which six out of eleven participants said was difficult to use.

Comparison due to difference in enthusiasm   The participants were split into two groups, G1 and G2, according to the score for feeling of enthusiasm for using the SDES. This subsection clarifies the factors that influenced the degree of enthusiasm, and verifies the differences in safe driving mindset and driving behavior according to the degree of enthusiasm.

- Group G1: five participants who used the SDES with a feeling of enthusiasm (the Q1-c2 score was 5 or more)
- Group G2: six participants who used the SDES without a feeling of enthusiasm (the Q1-c2 score was 3 or less)

The experimental results for each group are shown in Fig. 10. Two-way ANOVA with respect to the total score S showed that there is no correlation between the group and the driving condition, and that a simple main effect of the

---

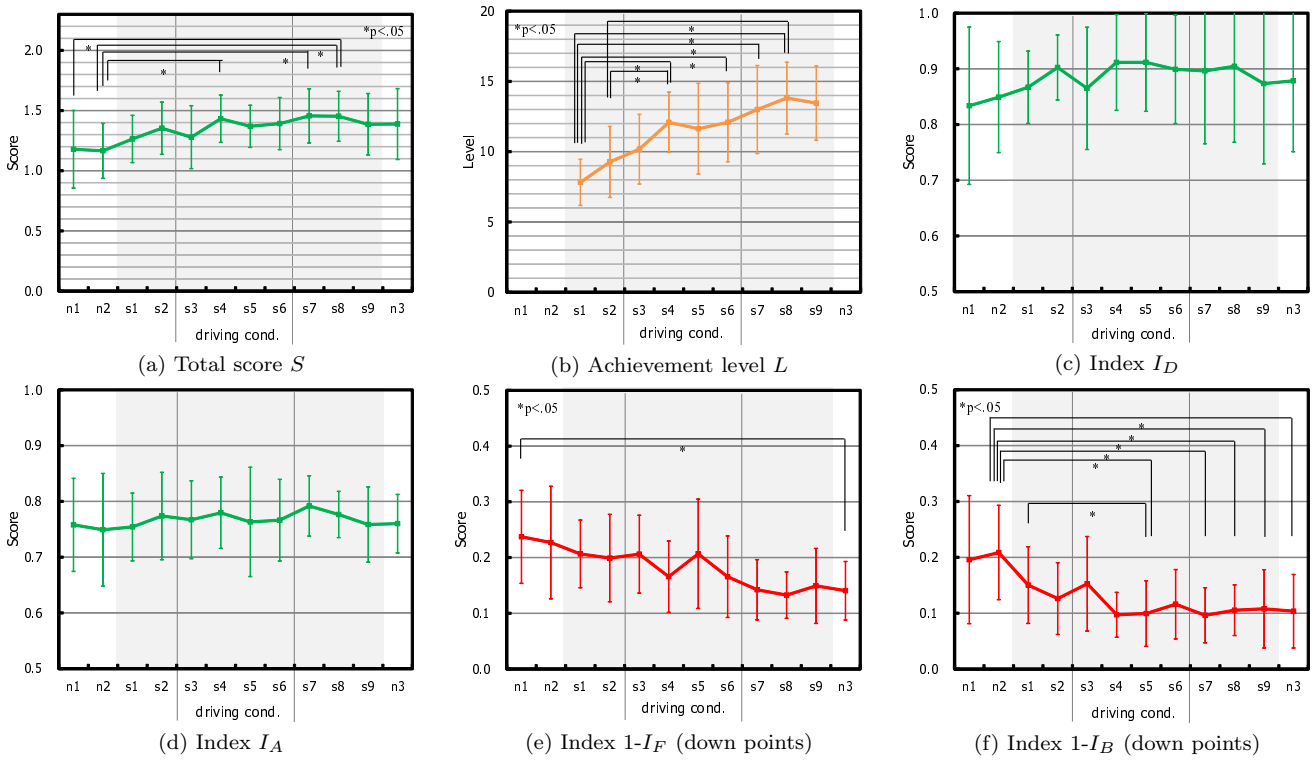[2] The number of blue stars at the end of the experiment.

Fig. 9. Results of Exp. #1: all participants

Table 1. Subjective evaluation results of Exp. #1 (7-point scale)

No.	Question	Mean (total)	S.D.	Mean (G1)	Mean (G2)	t-test
Q1-a1	degree of utilization	5.4	1.5	6.2	4.7	+
Q1-a2	motivation for usage	3.6	1.3	4.7	2.7	*
Q1-a3	satisfaction with autonomy	4.4	1.0	5.2	3.8	**
Q1-a4	satisfaction with competence	3.2	1.0	3.7	2.8	ns
Q1-b1	understanding of operation using SDES	5.5	1.0	5.8	5.2	ns
Q1-b2	understanding of Index I_D	5.5	1.4	6.4	4.7	*
Q1-b3	understanding of Index I_A	4.6	1.4	4.8	4.5	ns
Q1-b4	understanding of Index I_F	4.5	1.6	5.8	3.3	**
Q1-b5	understanding of Index I_B	4.4	1.8	5.8	3.2	**
Q1-c1	fun	4.2	1.7	5.4	3.2	*
Q1-c2	degree of enthusiasm for using SDES	3.9	1.5	5.4	2.7	***
Q1-c3	feeling of accomplishment when using SDES	3.6	1.6	5.2	2.3	***
Q1-c4	feeling of usefulness	4.5	0.9	5.2	3.8	**
Q1-c5	proficiency in safe driving	4.4	1.0	5.0	3.8	+
Q1-c6	safe driving mindset	4.8	1.3	5.6	4.2	+

+: $p < .1$, *: $p < .05$, **: $p < .01$, ***: $p < .001$

group was slightly significant ($F(1,9) = 3.75, p < .10$). This indicates that the safe driving skills of G1 members who used the system with enthusiasm was higher than that of G2 members. The total scores S of G2 members who used the system without enthusiasm declined from s8 to n3, and this implies that the G2 participants ceased to improve safe-driving skills in the middle and the end of the experiments. The scores for the achievement level L of G1 members increased with driving repetition, whereas those of G2 members hit a wall in the middle of the experiments. The results might be derived from the fact that the number of failures in goal achievement in the case of G2 participants were relatively more than those of G1 members.

As for the results of the four indices, I_D and I_A for both groups remained at a constant score of n1 to n3 and the

down points of I_F and I_B of both groups decreased, while the combined score of G1 was better than that of G2.

Table 1 shows that the subjective evaluation scores of G1 are generally better than those of G2. In particular, the scores of G1 was higher than those of G2 at a 10% or less significant level with respect to the following questions: 'fun' (Q1-c1), 'feeling of accomplishment' (Q1-c3), 'feeling of usefulness' (Q1-c4), 'proficiency in safe driving' (Q1-c5), and 'safe driving mindset' (Q1-c6). For G1 members, whose driving skills were improved by using the SDES with enthusiasm, the usefulness of the system became higher and they obtained subjective benefits such as fun and a feeling of competence in being able to change their driving behavior for the better. On the other hand, three out of six participants in the G2 group gave up on improving their safe driving skills because their understandings of

(a) Total score S

(b) Achievement level L

(c) Index I_D

(d) Index I_A

(e) Index 1-I_F (down points)
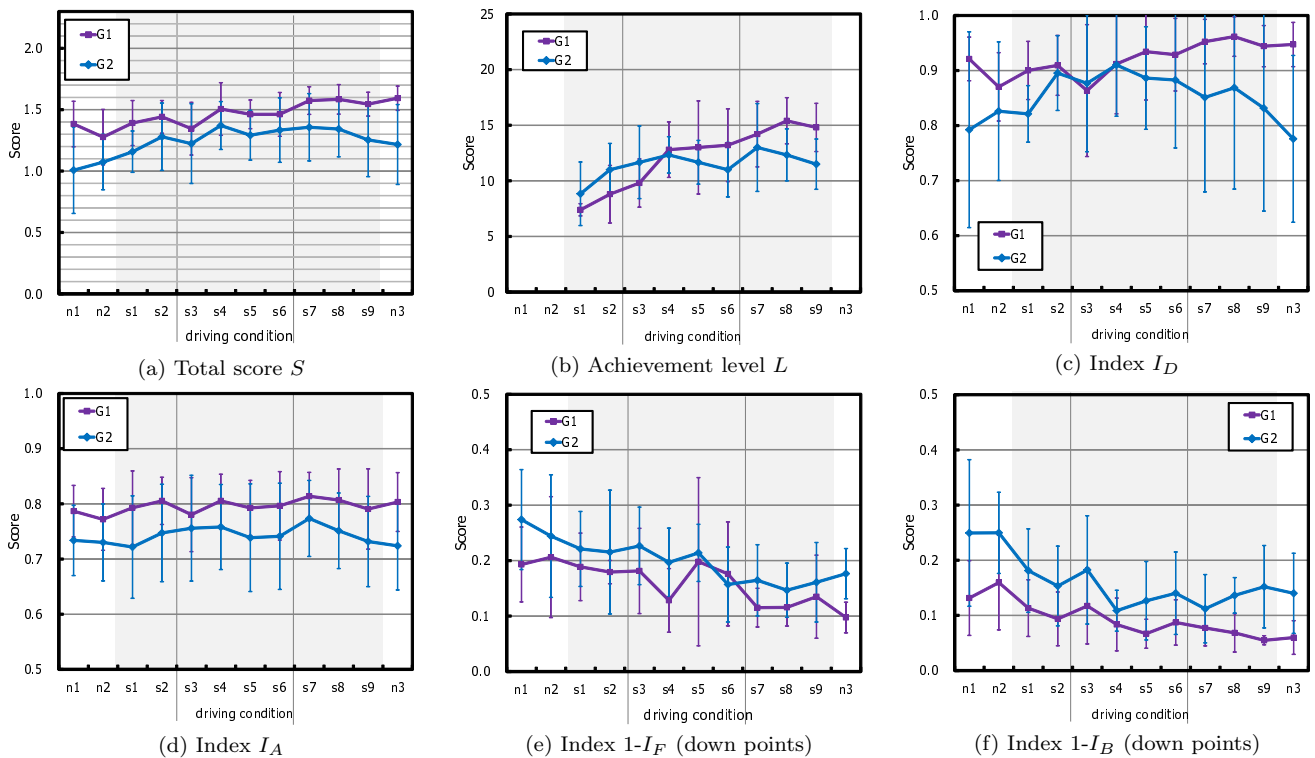
(f) Index 1-I_B (down points)

Fig. 10. Results of Exp. #1: comparison between G1 and G2

the indices were low and they felt that the difficulty in obtaining the target was too high.

7. DRIVING SIMULATOR EXPERIMENT #2: EFFECTIVENESS OF GAME ELEMENTS OF SDES

This section details improvements to the SDES by enhancing the game elements and reports on the driving simulator experiments conducted to ascertain the effects of the introduction of the games elements.

7.1 Improved SDES

Based on the results of experiment #1, the SDES is improved as follows: 1) provision of detailed help contents (Fig. 11), 2) preparation of an instruction manual, 3) target value calculation that considers the history of down points with respect to indices I_F and I_B, and 4) the achievement possibility p_0 is defined to be 60% at $D = 1$–3, 50% at $D = 4$, and 40% at $D = 5$.

7.2 Conditions

The experimental participants were eighteen men and two women, ranging in age from 19 to 24 years old, with an average driving experience of 34 months. They gave informed consent before the experiment started.

The participants were separated into two groups by balancing the average driving experience of each group, and the intersubject experiments were performed by using the same driving simulator as in experiment #1.

- Experimental group E: used the improved SDES
- Control group C: used the simple SDES

(a) advice about I_F

(b) advice about I_B

(c) advice about I_A

(d) advice about I_D

Fig. 11. Detailed help display

Compared to the improved SDES, the simple SDES does not have functions such as 'help display', 'target setting and display', and 'gradual learning support'. That is, the simple SDES has few game elements.

The experimental procedure was completely the same as for experiment #1.

7.3 Results

Driving Performance   Figures 12 (a) and (b) show transitions in the total score S and achievement level L. Both groups increased their total score S with repetitions of driving using the system.

The average scores S of Group E were higher than those of Group C after s2, while a two-way ANOVA did not

(a) Total score S

(b) Achievement level L

(c) Evaluation time of Index I_D

(d) Evaluation time of Index I_A

(e) Evaluation time of Index I_F

(f) Evaluation time of Index I_B
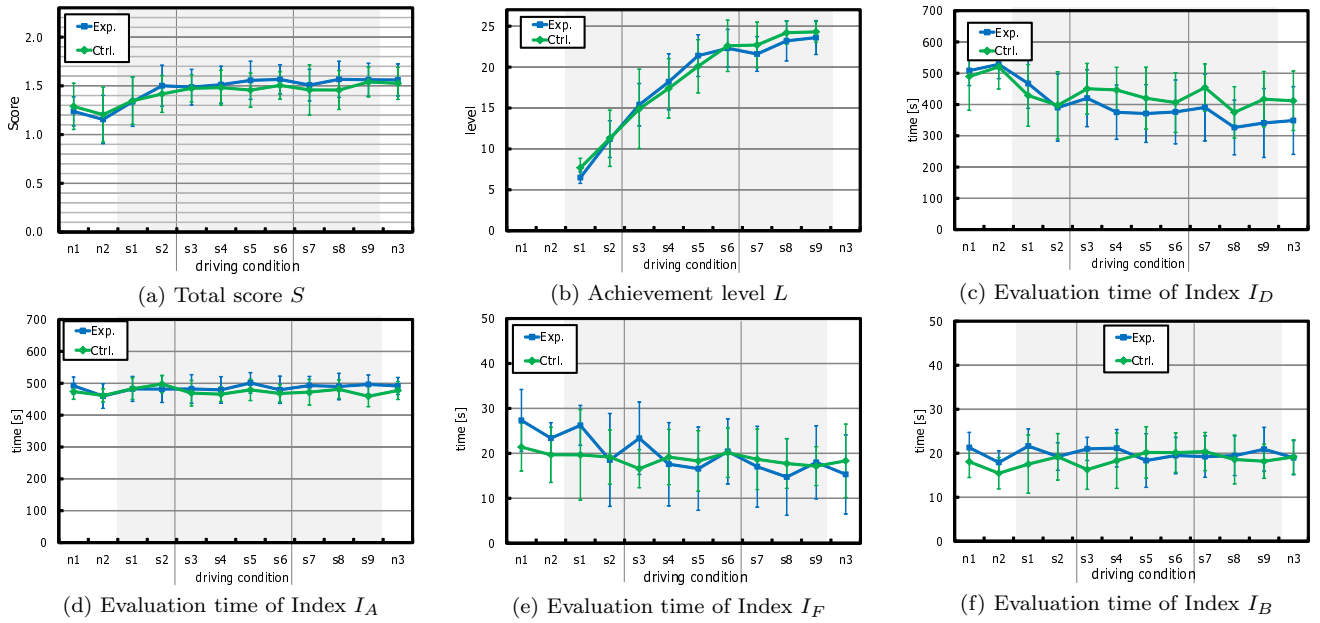
Fig. 12. Results of Exp. #2: comparison based on system differences

find any interaction between the group and the driving condition. As for the achievement level L, Group E improved its level a little bit earlier than Group C. However, the total score S of Group E decreased temporarily after achievement level L was reached around the upper limit in driving condition s6, and then the score S and the level L increased again. The scores of five participants of Group E decreased just after reaching the upper limit, and the decline was statistically significant. This phenomenon was not found in Group C. The results imply the effectiveness of the system with the game elements and the necessity of continuous support for the driver.

As for the transitions of the four indices, I_D and I_A of Group E were better than those of Group C from the middle to the end of the experiments, and I_B of Group E was overall higher than that of Group C. However, in all indices, there were no statistically significant differences between the two group.

Here, let us analyze the evaluation times of the four indices (Fig. 12 (c)–(f)). As for the evaluation times of I_D, I_F, and I_B, two-way ANOVA found that interactions between the group and the driving condition were significant. The evaluation time of I_D of Group E decreased with driving repetition, which suggests that the participants of Group E extended the inter-vehicular distance compared to those of Group C. Figure 12 (e) shows that the evaluation time of I_F of Group E decreased with driving repetition, while that of Group C remained constant. This denotes the effectiveness of the system in that the participants of Group E maintained a proper inter-vehicular distance and paid more attention to the front of their own vehicle.

Accordingly, the experimental results showed that the improved SDES with game elements (Group E) was more effective than that of the simple SDES without game elements (Group C), although both SDES encouraged the drivers to drive safer. Moreover, they also clarified that the participants ceased pursuit of safe driving temporarily

when the achievement level reached the upper limit and the game elements disappeared. This is a problem to be solved in the future.

Subjective Evaluation   As shown in Table 2, the scores of the both groups exceeded 4.0 for many questions. This means both SDES had high acceptability and that they also brought many subjective benefits and showed their effectiveness for safe aspects. Furthermore, the scores of Group E were higher than those of Group C at a statistically significant level for the following questions: 'degree of utilization' (Q2-a1), 'satisfaction with autonomy' (Q2-a3), 'satisfaction with competence' (Q2-a4), 'understanding of Index I_B' (Q2-b5), 'degree of enthusiasm for using SDES' (Q2-c2), 'feeling of accomplishment when using SDES' (Q2-c3), and 'proficiency in safe driving' (Q2-c5). That is to say, when the participants used the improved SDES with more game elements, they were enthused about the improved SDES and therefore the acceptability and the subjective benefits increased. Moreover, it produced the effect whereby the participants learned safe driving through the utilization of the system.

8. CONCLUSIONS

This study improved the safe driving evaluation indices to measure not only dangerous situations but also common driving situations. In addition, the interface of the SDES was modified based on psychological theories and game design methods in order to enhance the subjective benefits for drivers and improve their motivation for using the system.

The driving simulator experiment #1 showed that the SDES encouraged many drivers to proactively devise safe driving techniques, and that the degree of enthusiasm on using the SDES varied considerably individual to individual.

Next, an SDES equipped with more game elements was proposed in order to solve the problems found in experi-

Table 2. Subjective evaluation results of Exp. #2 (7-point scale)

No.	Question	Group E	Group C	t-test
Q2-a1	degree of utilization	6.1	4.9	*
Q2-a2	motivation for usage	4.7	4.0	ns
Q2-a3	satisfaction with autonomy	5.8	5.2	*
Q2-a4	satisfaction with competence	5.1	3.8	**
Q2-b1	understanding of operation by using SDES	6.1	5.4	ns
Q2-b2	understanding of Index I_D	6.3	5.4	+
Q2-b3	understanding of Index I_A	5.4	4.6	ns
Q2-b4	understanding of Index I_F	6.0	5.2	ns
Q2-b5	understanding of Index I_B	6.3	5.0	*
Q2-c1	fun	5.8	5.1	ns
Q2-c2	degree of enthusiasm for using SDES	5.5	3.6	**
Q2-c3	feeling of accomplishment when using SDES	5.5	3.1	**
Q2-c4	feeling of usefulness	6.0	5.2	ns
Q2-c5	proficiency in safe driving	5.6	4.4	*
Q2-c6	safe driving mindset	5.8	6.0	ns

+: $p < .1$, *: $p < .05$, **: $p < .01$

ment #1, and driving simulator experiment #2 was performed to ascertain the effectiveness of the game elements. The results showed that the subjective benefits and the safe driving mindset increased and a behavioral adaptation for safer strongly was encouraged in the case when drivers used the improved SDES with more game elements.

The following are considered as tasks for future work: 1) a method of providing visual information about midterm and long-term driving history, 2) a method to satisfy the needs to the relatedness by using functions such as a ranking system, 3) realtime feedback by using multi-modal information provision, and 4) validity verification in a real car environment.

ACKNOWLEDGEMENT

REFERENCES

Deci, E. L. and Ryan, R. M. (2004). *Handbook of self-determination research.* University Rochester Press.

Hiraoka, T., Masui, J. and Nishikawa, S. (2010). Behavioral adaptation to advanced driver-assistance systems. *Proc. of SICE Annual Conference 2010*, pages 930–935.

Hiraoka, T., Nishikawa, S. and Kawakami, H. (2011). Driver-assistance system to encourage spontaneous eco-driving behavior. *Proc. of 18th World Congress on Intelligent Transport Systems*, CD-ROM.

Hiraoka, T. (2012). Driver-Assistance System to Encourage Drivers to Perform Safe Driving. *Journal of the Society of Instrument and Control Engineers*, Vol. 51, No. 8, pages 742–747. (in Japanese)

Hiraoka, T., Takada, S. and Kawakami, H. (2013). Proposal of non-dimensional parameter indices to evaluate safe driving behavior. *Human Interface and the Management of Information (Information and Interaction for Health, Safety, Mobility and Complex Environments)*, LNCS, Vol. 8017, pages 470–479.

Kawakami, H. (2013). Further Benefit of a Kind of Inconvenience for Social Information Systems. *Human-Computer Interaction (Users and Contexts of Use)*, LNCS, Vol. 8006, pages 301–306.

Saad, F. (2006). Some critical issues when studying behavioural adaptations to new driver support systems. *Cognition Technology and Work*, Vol. 8, No. 3, pages 175–181.

Saito, A. (2007). *What is Gamenecis?* Gentosha. (in Japanese)

Smiley, A. (2000). Behavioral adaptation, safety, and Intelligent Transportation Systems. *Transportation Research Record: Journal of the Transportation Research Board*, Vol. 1724, No. 1, pages 47–51.

Takada, S., Hiraoka, T., Nozaki, K. and Kawakami, H. (2013). Safe driving evaluation system to encourage spontaneous behavioral adaptation (2nd report) - Effect of evaluation system on driving behavior -. *Trans. of JSAE*, Vol. 44, No. 2, pages 673–678. (in Japanese)

Takada, S., Hiraoka, T., Nozaki, K. and Kawakami, H. (2014). Safe driving evaluation system to encourage spontaneous behavioral adaptation (3rd report) - Effect of Active Understanding of the System on Drivers' Motivation -. *Trans. of JSAE*, Vol. 45, No. 2, pages 411–417. (in Japanese)

Wilde, G. J. S. (2001) *Target Risk 2 -A new psychology of safety and health-.* PDE Publications.

The Effect of Advanced Automatic Collision Notification (AACN)
on Road Fatality Reduction in Sweden

J. Jonsson[1], N. Lubbe[1,2], J. Strandroth[1,3], R. Thomson[1]

[1]*Chalmers University of Technology, Department of Applied Mechanics, Hörsalsvägen 7A, 412 96 Gothenburg, Sweden*
[2]*Toyota Motor Europe NV/SA, Technical Affairs Planning Dept., Hoge Wei 33, 1930 Zaventem, Belgium*
[3]*Swedish Transport Administration, Röda vägen 1, 781 70 Borlänge, Sweden*

Corresponding author: J. Jonsson, jonsson.jonathan@gmail.com

Abstract: This paper aims at estimating the effect of the Advanced Automatic Collision Notification (AACN) post–crash system on road fatality reduction in Sweden. The analysis was based on the Swedish Traffic Accident Data Acquisition (STRADA) database in combination with in-depth studies of fatal accidents. Logistic regression with backward selection was used to identify relevant variables and develop a statistical model. The variables 'admission to trauma center', 'age' and 'injury severity' were identified as significant and by applying the final model on fatalities in passenger cars the estimated fatality reduction due to AACN was calculated. AACN was estimated to potentially reduce road fatalities by 8.6% (95% CI = -0.3-16.4%).

Keywords: Advanced Automatic Collision Notification, AACN, post-crash, injury prediction, fatality reduction, hospital classification, emergency medical service

1. INTRODUCTION

Road traffic injuries account for approximately 1.3 million fatalities each year and are the eighth most common cause of death globally and the leading cause of death for young people between the age of 15 and 29 (WHO, 2013). The outcome of a collision is affected by actions taken before, during, and after the collision. By optimizing these actions fatalities and injuries in traffic can be reduced. In addition to injury reduction due to active and passive safety systems, emergency medical service providers play an important role for the medical outcome of persons involved in collisions.

In the event of a collision, notification to the rescue services and pre-hospital triage are most likely to be performed by a vehicle occupant or bystander that has observed the collision. If no one has observed the collision and the occupants are unable to notify rescue services, the notification time (i.e. the time between the collision and the notification to the rescue services) is extended which negatively affects the chance of survival (Ohlin et al., 2014; Wu et al., 2013; Lahausse et al., 2008; Clark et al., 2002). The estimated effect of enabling earlier notification (< 1 min) differs between studies but is suggested to be between 1.87% (Wu et al., 2013) and 11% (Lahausse et al., 2008). In 2014 Ohlin et al. conducted a case-by-case study based on Swedish accident data from 2011 and suggested that early notification could have reduced road traffic fatalities by 3.2%.

Even if occupants would be able to notify rescue services, they do not necessarily do so perfectly. Schulman et al. (2010) found that 13% of the occupants who felt they were uninjured actually required hospitalization, indicating that in some cases occupants cannot estimate their own injuries and

that AACN (Advanced Automatic Collision Notification) can provide important triage decision-support

AACN is a system that, given a collision, can establish a communication link with the rescue services and forward the collision location as well as an estimation of the injury severity of the occupants involved. The injury severity estimation is based on an algorithm using a number of parameters obtained from the in-vehicle sensors, such as delta v, principal direction of force, seatbelt use, airbag deployment, roll-over, multiple impacts etc. Different car manufactures may use different algorithms and set of variables but the objective remains the same, to determine the probability of severely injured occupants. AACN functionality is offered by several car manufactures, such as GM with their OnStar and BMW with their ConnectedDrive services, but the overall market penetration is still very low (European Commission, 2013). An AACN system is able to provide information to aid pre-hospital triage and give the emergency service operator information that is vital when deciding on appropriate action. Using this information it is more likely that appropriate medical service units can be dispatched to the collision scene and that patients in need of trauma care can be identified at an early stage, possibly enabling swifter transport to a medical facility with adequate trauma care level.

Both means of transport and target hospital are suggested to affect the fatality risk for seriously injured patients (German Trauma Society, 2015; MacKenzie et al., 2006; Hilbert et. al., 2010). MacKenzie et al. (2006) compared the difference in mortality risk between level 1 trauma centers and non-trauma centers in the US and suggested that the in-hospital mortality

rate and one-year mortality rate are 20% and 25% lower, respectively, at a level 1 trauma center compared to a non-trauma center. A German study by Hilbert et al. (2010) comparing the mortality rate for severely injured (AIS3+) at Germany's ten top-scoring trauma centers to the ten lowest-scoring trauma centers found that the fatality rate was almost twice as high (16.6% compared to 8.7%) at the ten lowest-scoring centers. The consequences of a road traffic collision are thus partly depended on which hospital trauma patients are admitted to. Hence, AACN systems can provide vital information for the occupants involved in a road traffic collision.

AACN has potential to decrease the fatality risk of occupants involved in a collision, both by shortening the notification time (Wu et al., 2013; Ohlin et al., 2014) and by estimating injury severity (Schulman et al. 2010). Because collision characteristics and rescue service operation differ from country to country, the potential benefit of AACN is most likely country dependent. Since no study has investigated the potential benefit of AACN in Sweden this paper aims at conducting such a study. The main purpose is to estimate the benefit of AACN in Sweden, in terms of how the fatality risk would be affected by the implementation of such a system.

2. METHOD AND MATERIAL

A benefit analysis based on accidents during the years 2006 to 2014 was conducted. Two different databases were used: 1) the statistical database STRADA (Swedish Traffic Accident Data Acquisition) (Transportstyrelsen, 2015) and 2) the in-depth database of fatal accidents in the Swedish road transport system (Trafikverket, 2012). The two databases were matched to identify the cases relevant for the analyses. Variables assumed to affect the outcome were selected and included in a statistical model. Thereafter, backward selection with stepwise exclusion of variables with $p > 0.1$ was carried out to obtain the final model. In addition to exclusion based on significance, variables with an estimated effect that were not consistent with previous research were excluded. Using the final model *P(fatality)* was calculated for all fatalities in passenger cars, first by using the actual outcome parameters obtained from STRADA, and then by changing the outcome parameters affected by AACN, such as target hospital. The two probabilities were then compared to obtain an estimated fatality reduction due to AACN. Fig. 1 illustrates on a high level how the analysis was performed.

2.1 Dataset

The in-depth database provided by the Swedish Transport Administration (STA), which collects information on all road traffic fatalities in Sweden since 1997, was used to identify the location of death ('accident scene', 'transport', 'hospital' or 'unknown') for all fatalities. Crash investigators at STA systematically inspect the vehicles involved in fatal crashes and record direction of impact, vehicular intrusion, seat belt use, airbag deployment, tire properties, etc. The crash site is also inspected to investigate road characteristics, collision objects, etc. Further information about injuries are provided from forensic examinations, questioning and witness

statements from the police and reports from the emergency services. The in-depth database contained 7 255 cases, of which 3 489 were fatalities. To analyze the effect of target hospital in treating injury and to avoid influencing results by hospitals being ineffective in treating patients dead at arrival, only deaths occurring after arriving to hospital were included. Cases where a person died of natural causes were also excluded. This resulted in 943 cases remaining, of which 404 were travelling in a passenger car.
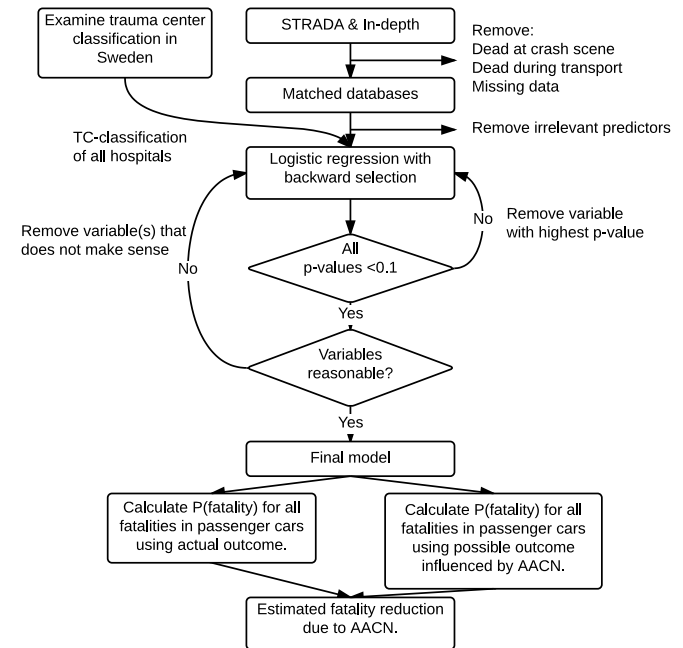
Fig. 1. High-level description of how the analysis was performed.

The statistical database STRADA, which is a Swedish national information system containing data of injuries and accidents in the entire road transport system, was used as primary data source. The database is based on information reported from both the police and the hospitals. Since 2003 all police districts are reporting to STRADA and today all emergency hospitals are reporting to STRADA as well, but during the years considered in this study, 2006 to 2014, the hospital 'Akademiska Sjukhuset' in Uppsala was not reporting to STRADA. Also, not all hospitals reporting in late 2014 were reporting in early 2006 as some hospitals started their reporting to STRADA during this period.

During the years 2006-2014 there were 69 040 cases reported to STRADA containing both police and hospital data. Excluding cases with age < 1 or age > 100 resulted in 69 011 cases, of which 946 were coded as fatalities and the rest as non-fatally injured. Of the fatally injured, 463 were travelling in a passenger car and 483 were other road users. Fatalities from the in-depth studies (n=943) were matched with fatalities in STRADA using the accident unique STRADA-id. In accidents with multiple fatalities the parameters age, gender and occupant position were used to identify the correct match. Of those travelling in a passenger car 154 died in a hospital and the corresponding number for the other road

users was 222, giving a total of 376 people deceased in hospital. The total number of cases in the matched dataset was thus 68 441. In Fig. 2 a flowchart is illustrating how the cases in STRADA and in-depth database were selected and matched. The patient characteristics in the matched dataset are presented in Table 1.

When calculating 'Rescue time' the difference between police-reported 'time of accident' and hospital reported 'time of hospital admission' was used. However, due to poor reporting, mostly of 'time of accident', not all cases contained a proper 'Rescue time'. In addition, if 'Rescue time' exceeded 720 minutes it was excluded and treated as a misreporting. The number of cases containing a proper rescue time was 64 124, of which 360 were fatalities. The reporting of means of transport was also incomplete. Only 55 256 cases, of which 367 were fatalities, were reported with either helicopter or ambulance transport.
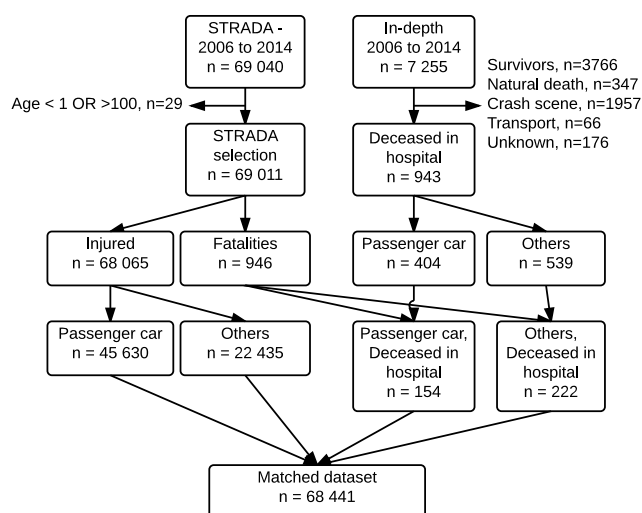
Fig. 2. STRADA and in-depth case selection, exclusion and matching.

Table 1. Patient characteristics in the dataset.

Variable	Entire road transport system		Passenger cars only	
	Dead N=376	All N=68441	Dead N=154	All N=45784
Dispatched to TC %	48,7	28,4	47,2	25,7
Transported by helicopter %	16,2	1,4	26,1	1,2
Distance to target hospital [km]	30,5	17,8	36,8	19,2
Age	52,1	37,2	45,1	37,5
Male %	67,5	56,7	69,7	54,0
Rescue time [min]	53,6	67,4	65,8	70,3
ISS	33,4	3,2	34,8	2,6

2.2 Hospital classification

In Sweden there is no official trauma classification of hospitals and thus no obvious way to divide the hospitals into different trauma levels. Furthermore, there is no coherent system used to classify the resources available in each hospital, preventing a third party to quantitatively classify the hospitals according to other countries' trauma level standards. To qualitatively examine and classify each hospital was beyond the scope of this paper. A trauma classification was however essential in order to include the effect of target hospital in the benefit estimation of AACN. Two different approaches were considered: Mortality rate per hospital and the use of University Hospitals as a proxy for trauma centers. Due to the low number of fatalities available for the analysis (e.g. only 10 out of the 73 hospitals had 10 or more fatalities) it was not possible to make a reasonable classification of hospitals based on mortality rate per hospital. Thus the classification of University Hospitals as trauma centers was used as University Hospitals possess the resources needed to treat major trauma. The University Hospitals are located in Stockholm (Solna), Gothenburg, Malmö/Lund, Uppsala, Linköping, Örebro and Umeå.

One prerequisite for the classification of University Hospitals as trauma centers was that they could cover most of the accident locations, i.e. that the distance between accident location and nearest trauma center was short enough so that the patient could have been transported to a TC within reasonable time, either by ground ambulance or helicopter. To determine that the distance between all fatal accident locations involving a passenger car and the nearest University Hospital was computed using GPS-coordinates. The distance was measured both as a straight line, representable when transporting by helicopter, and as actual road distance, representing transport distance by ground ambulance. The road distance was obtained from Google Maps via the Google Distance Matrix API.

2.3 Statistical model design

To examine how the variables possibly influenced by AACN, e.g. target hospital and means of transportation, affect the fatality risk other variables not influenced by AACN, e.g. age and injury severity, had to be accounted and adjusted for. Multivariable logistic regression with backward predictor selection was used to perform such analysis. Multivariable logistic regression is a widely used method to relate one or several variables of interest to a binary outcome while accounting for confounding variables (Vittinghoff et al. 2011). The logistic regression was performed using the function 'fitglm' in MATLAB R2014b. The model used in the analysis was *logit*, defined as

$$\text{logit}(Y) = \log\left(\frac{Y}{1-Y}\right) = Xb \tag{1}$$

where *Y* is the fatality outcome, *X* the input variables and *b* the coefficients calculated by the regression model. A similar approach, with backward stepwise logistic regression, was used by Alghnam et al. (2014) when they examined the in-hospital death among traffic crash victims in Saudi Arabia.

The outcome of interest in this analysis was whether or not a person involved in a traffic accident died as a result of the accident after arrival to hospital.

Only variables assumed to influence the outcome were included in the model. Moreover, parameters possibly affecting injury severity, such as belt use, helmet use, over speeding, drink-driving etc., were not included, only injury severity itself was considered. The following variables were included: admitted to a TC (1=yes, 0=no), transported by helicopter (1=yes, 0=no), distance to hospital [km], age, gender (1=female, 0=male), rescue time [min] (time from accident to hospital arrival), ISS categorized (1-3 as reference group, 4-6, 7-9,..., 73-75). The variables distance, age and rescue time were treated as continuous, the variable ISS as categorical and the rest as binary.

Backward selection was used to determine the final input variables. The procedure works as follows: Starting from a set of variables the one with the highest p-value is removed until all variable's p-values are below 0.1 (Vittinghoff et al. 2011). After removing a variable the regression model is recalculated using the variables left to obtain the new p-values. In addition to backward selection variables estimated to affect the fatality risk in an unreasonable way (based on previous research) were excluded from the model.

The effect of each independent variable in the final model was expressed as an odds ratio (OR). The OR, and corresponding confidence interval (CI), for a variable x_n was calculated from (2) (Vittinghoff et al. 2011).

$$OR = \exp(\beta_n) \tag{2}$$

When developing the statistical model injured and fatalities from the entire road transport system were considered, i.e. the whole data set containing 68'441 cases. Using only passenger car related injuries and deaths did not provide enough data to get statistically significant results, possibly due to the low number of fatalities (n=154).

The final model performance was evaluated using the area under the receiver operating characteristics curve (AUC). AUC is a measure of how well the model discriminate between the two outcomes. A value of 1 indicates perfect discrimination and a value of 0.5 implies that the model does not perform better than a guess.

2.4 Benefit estimation

With the statistical model the effect of AACN on road fatality reduction was calculated based on fatalities in passenger cars. The number of road fatalities in passenger cars included in this analysis was 154. The effect was obtained by first calculating *P(fatality, no AACN)* for all cases using the actual outcome, i.e. using the parameter values obtained in STRADA and then calculating *P(fatality, AACN)* using an alternative outcome, i.e. changing the parameters affected by AACN. *P(fatality)* was obtained from

$$P(fatality) = P(x_1, \dots, x_n)$$
$$= \frac{\exp(\beta_0 + \beta_1 x_1 + \cdots + \beta_n x_n)}{1 + \exp(\beta_0 + \beta_1 x_1 + \cdots + \beta_n x_n)} \tag{2}$$

where x_n is the value of the variable and β_n the corresponding coefficient from the statistical model.

P(fatality, no AACN) and *P(fatality, AACN)* were then averaged to get P_{NoAACN} and P_{AACN} which were used to calculated the effect of AACN. The effect was expressed both as OR, calculated from (3), and as relative risk (RR), calculated from (4) (Vittinghoff et al. 2011). The change in fatality risk was also expressed in percentage by taking 1-RR. Confidence intervals for P_{NoAACN}, P_{AACN}, OR and RR were calculated using bootstrap with resampling (*bootstrp* in MATLAB) and 10 000 iterations.

$$OR = \exp\left(\log\left(\frac{P_{AACN}}{1 - P_{AACN}}\right) - \log\left(\frac{P_{NoAACN}}{1 - P_{NoAACN}}\right)\right) \tag{3}$$

$$RR = \frac{P_{AACN}}{P_{NoAACN}} \tag{4}$$

2.5 Assumed AACN functionality

When considering the alternative outcome in the benefit estimation all cases where the target hospital could have been affected by AACN were revised. Fatalities that had sustained less severe injuries, defined as ISS < 9, would possible not have been identified by an AACN system and were thus not modified. Furthermore, the distance between accident location and nearest trauma center was sometimes too long, defined as > 150 km. These cases were not modified either, unless the distance to target hospital exceeded 150 km and the distance to nearest TC was shorter than the distance to target hospital.

2.6 Sensitivity analysis

To evaluate how and to what extent different assumptions and decisions regarding variables and their representation affected the final model and the benefit estimation a sensitivity analysis was included. Four different aspects were considered. Firstly, the use of MAIS as injury classification instead of ISS was evaluated. Secondly, the effect of different ISS-intervals on parameter estimation and fatality reduction was examined. Thirdly, a regression model based only on fatalities and injured from passenger cars was compared with the model including fatalities and injured from the entire road transport system. Lastly, the consequences of treating Örebro University Hospital as non-TC was investigated. The reason for the latter is that Örebro is the only University Hospital without a neurosurgery (Swedish Neurosurgical Society, 2015) and a neurosurgery can potentially be seen as a requirement for a TC.

3. RESULTS

3.1 Trauma center coverage

In Fig. 3 the coverage of nearest hospital, target hospital and nearest TC are illustrated. Given that the mean rescue time for fatal accidents involving passenger cars in this study is approximately 66 minutes (Section 2.1) and that the ambulance helicopters operating in Sweden have a cruising speed of approximately 250 km/h (Scandinavian AirAmbulance, 2015) it is reasonable to assume a helicopter coverage of 125-150 km. The trauma centers can then cover around 85-88% of the accidents by helicopter transport. Thus it appears reasonable to assume that more than 85% of all

patients involved in a motor vehicle crash could be transported to a TC if ambulance helicopter is used.
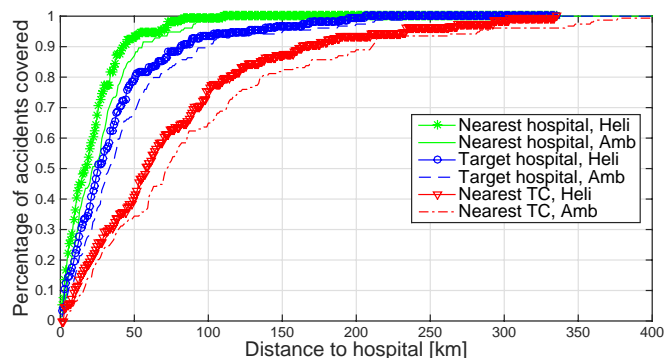

Fig. 3. Hospital coverage measured as percentage of fatal accidents covered at a given distance from the nearest hospital (green), target hospital (blue) and nearest TC (red).

3.2 Statistical model

The backward selection procedure identified the variables 'TC', 'Age' and 'ISS' as significant. The variables 'Helicopter' and 'Rescue time' were excluded due to implausible parameter estimation. The estimated effect of helicopter transport on survival probability was negative, but since the vast majority of studies regarding ambulance helicopter transport suggests increased survival probability with helicopter transport (German Trauma Society, 2015) the variable was removed from the analysis. Also, longer rescue times were associated with higher survival probability. It was not possible to model quality and time spent for treatment at the accident location which could explain such effects, as extended treatment at the accident scene might be beneficial. Thus, 'Rescue time' was removed from the model as implausible.

In Table 2 the final logistic regression model with variables 'TC', 'Age' and 'ISS' is presented. Patients admitted to a trauma center instead of a non-trauma center were less likely to die (OR = 0.781, 95% CI = 0.609-1.003) and older patients were more likely to die than younger patients (OR=1.030 per one year increase, 95% CI = 1.024-1.036). Finally, higher ISS value was associated with a higher risk of death (OR = 1.898 per three unit increase on average, 95% CI = 1.897-2.290).

The AUC for the final model was 0.9808 suggesting excellent discrimination and model performance.

3.3 Benefit estimation

The probability to die when not making use of AACN information was on average $P_{NoAACN} = 0.151$ (95% CI = 0.026-0.395) whereas the probability was $P_{AACN} = 0.138$ (95% CI = 0.023-0.366) on average when using AACN information to reroute seriously injured patients to a trauma center if possible. The corresponding OR was 0.904 (95% CI = 0.816-1.004) and the corresponding RR was 0.914 (95% CI = 0.836-1.003). Thus AACN in Sweden was estimated to lead to a 8.6% fatality reduction (95% CI = -0.3-16.4%).

Table 2. Model specifications for the final logit regression model with input variables 'TC', 'Age' and 'ISS'

Variable	Estimate	SE	P-value	N cases
Constant	-10.377	0.468	<0.001	68 411
TC	-0.247	0.128	0.053	68 411
Age	0.030	0.003	<0.001	68 411
ISS 1-3	Reference	Reference	Reference	50 911
ISS 4-6	1.574	0.606	0.009	10 166
ISS 7-9	3.683	0.528	<0.001	2 450
ISS 10-12	4.342	0.523	<0.001	1 450
ISS 13-15	4.955	0.503	<0.001	1 056
ISS 16-18	5.719	0.486	<0.001	784
ISS 19-21	6.284	0.509	<0.001	306
ISS 22-24	6.347	0.496	<0.001	365
ISS 25-27	7.060	0.491	<0.001	251
ISS 28-30	7.368	0.488	<0.001	217
ISS 31-33	7.916	0.541	<0.001	68
ISS 34-36	8.019	0.494	<0.001	142
ISS 37-39	8.978	0.524	<0.001	64
ISS 40-42	8.789	0.553	<0.001	46
ISS 43-45	9.039	0.529	<0.001	58
ISS 46-48	9.070	1.078	<0.001	5
ISS 49-51	9.296	0.557	<0.001	40
ISS 52-54	9.250	0.909	<0.001	7
ISS 55-57	9.041	0.802	<0.001	10
ISS 58-60	8.737	0.841	<0.001	9
ISS 64-66	9.583	1.126	<0.001	4
ISS 73-75	11.079	0.709	<0.001	32

3.4 Sensitivity analysis: MAIS as injury classification

When using MAIS as injury classification instead of ISS the backward selection procedure identified the variables 'Distance', 'Age' and 'MAIS' as significant. 'Helicopter' and 'Rescue time' were excluded due to implausible parameter estimation. The model parameters are presented in Table 4. The AUC for this model was 0.9781 suggesting very good discrimination and model performance but not as good as the final model presented in section 3.2. The fact that only 'Distance', 'Age' and 'MAIS' are significant when using 'MAIS' as injury classification makes this model useless to evaluate the benefit of AACN since none of these variables are directly affected by AACN.

Table 4. Model specifications for the logit regression model with input variables 'Distance, 'Age' and 'MAIS'

Variable	Estimate	SE	P-value	N cases
Constant	-10.351	0.466	<0.001	68 318
Distance	0.004	0.001	0.007	68 318
Age	0.026	0.003	<0.001	68 318
MAIS 1	Reference	Reference	Reference	50 843
MAIS 2	2.025	0.540	<0.001	11 898
MAIS 3	5.053	0.462	<0.001	4 176
MAIS 4	6.795	0.462	<0.001	892
MAIS 5	8.323	0.459	<0.001	478
MAIS 6	10.841	0.707	<0.001	31

3.5 Sensitivity analysis: The effect of different ISS-intervals

In the final model described in section 3.2 the ISS-interval was set to three. Changing the interval affects the model

coefficients and thus the estimated fatality reduction. In Fig. 4 the change in coefficient estimation and p-value for the variable 'TC' (the most affected variable) are illustrated along with the estimated fatality reduction. The values are steady until the ISS-interval exceeds six after which fluctuations increases.
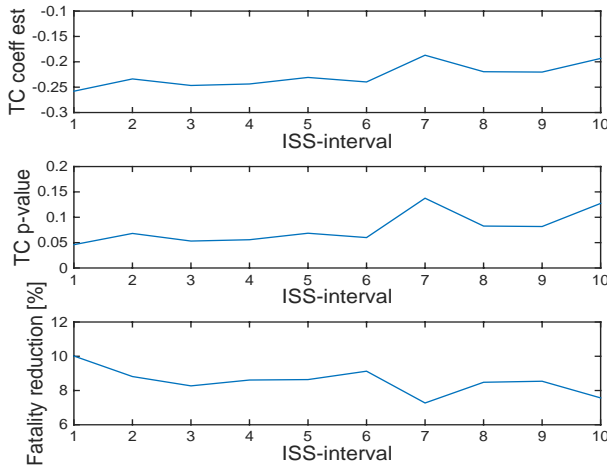
Fig. 4. The effect of ISS-interval on coefficient estimation and p-value for the variable 'TC' and on the estimated fatality reduction.

3.6 Sensitivity analysis: Regression model using only passenger cars

If only fatalities and injuries from passenger cars were used in the regression model the backward selection procedure identified the variables 'Age', 'Gender' and 'ISS' as significant. 'Helicopter' and 'Rescue time' were excluded due to implausible parameter estimation. The model parameters are presented in Table 5. The AUC for this model was 0.9788 suggesting very good discrimination and model performance but not as good as the final model presented in section 3.2. The fact that only 'Age, 'Gender' and 'ISS' are significant makes this model useless to evaluate the benefit of AACN since none of these variables are affected by AACN.

Table 5. Model specifications with input variables 'Age', 'Gender' and 'ISS' when only fatalities and injuries from passenger cars were included in the analysis.

Variable	Estimate	SE	pValue	N cases
Constant	-9.732	0.537	<0.001	68 411
Age	0.019	0.005	<0.001	68 411
Gender	-0.398	0.207	0.055	68 411
ISS 1-3	Reference	Reference	Reference	50 911
…	…	…	…	…
ISS 73-75	11.414	1.161	<0.001	32

3.7 Sensitivity analysis: Örebro University Hospital

Treating Örebro University Hospital as a non-TC does not change the variables included in the final model but affects the estimated effect of the variables slightly. Based on this model the estimated fatality reduction was 7.9% (95% CI = -0.8-15.8%), thus a little lower than when Örebro University Hospital was treated as a TC.

4. DISCUSSION

4.1 Parameter estimation in final model

The final model estimated that the in-hospital fatality rate was lower at a TC compared to a non-TC, OR = 0.781 (95% CI = 0.609-1.003), after adjusting for age and injury severity (ISS). This finding is in line with the 20% estimated by MacKenzie et al. (2006) but lower than the suggested 91% by Hilbert et al. (2010). As in many other findings regarding health outcome, advanced age was associated with an increase in fatality risk, OR=1.030 per one year increase on average (95% CI = 1.024-1.036). Further, a three-unit increase in ISS-value was associated with a high increase in fatality, OR = 1.898 on average (95% CI = 1.897-2.290). A somewhat higher risk increase than the OR = 2.0 per five unit increase suggested by Alghnam et al. (2014).

In the final model the estimated coefficient for ISS does not always increase with increased ISS-value (Table 2) as expected. However, looking at the overall trend there is a clear increase in the ISS-coefficient with increased ISS-value. Regardless of how the ISS-interval was chosen the trend was the same. The fluctuations are probably caused by the difference in the number of cases for each ISS-value (Table 4) along with rather few cases available for ISS>50 (n=64).

An ISS-interval of three was used and whether or not this was the best parameter choice is difficult to say. A larger ISS-interval will cause information to be lost but a too small interval will give too little cases per interval. In Fig. 4 the fluctuations are rather small for ISS-interval less than seven but above that the fluctuations increases. An ISS-interval of three was thus considered suitable to group values together while still containing the information in the ISS-values.

4.2 Benefit estimation of AACN

The study suggests that transporting seriously injured patients to a trauma center, whenever possible, is beneficial and can potentially reduce the number of road fatalities by 8.6%. However, the confidence interval ranges from -0.3 to 16.4% indicating a fairly large uncertainty in the estimation. Since no similar study (i.e. evaluating the possible effect of AACN by a retrospective analysis) was found it is difficult to evaluate the suggested fatality reduction.

The fact that the benefit estimation is solely based on whether or not a patient is transported to a trauma center makes the result heavily depended on trauma center classification and assumptions regarding transport possibilities for injured occupants. For example, the difference in distance between target hospital and nearest TC is not taken into account, meaning that if target hospital is located 1 km from the accident scene it is still considered beneficial to transporting patients to a TC located 140 km away, which perhaps is not the case. Further, the benefit estimation assumes that it is always possible to transport a patient with a helicopter if needed. This is probably not realistic though, since helicopters have other missions possibly preventing them to respond and the weather does not always allow for helicopter use.

In the analysis it is assumed that an AACN system can always identify seriously injured (ISS≥9) occupants. A more realistic approach would have been to account for expected AACN performance. Buendia et al. (2015) suggested based on Swedish accident data that injuries with ISS≥9 can be predicted with an AUC of 0.78. Including this in the benefit study would decrease the expected fatality reduction. On the other hand, the study does not account for the benefit of reduced notification time, which could be beneficial also for people that died of natural causes, at crash scene or during transport. Furthermore, an AACN system has potential to reduce not only fatalities but also injury severity and length of stay in hospital; these advantages were not included in the study either.

4.3 Hospital classification

Since the emergency hospitals in Sweden are not classified according to a national trauma classification or similar system, the effect of trauma center admission are based on the classification made by the authors. The use of University Hospitals as trauma centers can be questioned and does not necessary conform with a potential future trauma center classification. However, since no thorough investigation was possible within the scope of this paper the classification used was considered the most reasonable. In Sweden each county determines how the trauma care should be handled, thus there is no national coordination of trauma care (Regeringskansliet, 2015). The trauma care organization in Sweden is under review by the Swedish national board of health and welfare and their findings will be presented in the summer of 2015 (Regeringskansliet, 2015).

The use of only two trauma center levels, i.e. TC or non-TC, is a limiting factor preventing the analysis to account for intermediate trauma level hospitals. It is reasonable to assume that the hospitals can be divided into more than two trauma levels, as in Germany or the US, which would plausibly affect the overall benefit of AACN. To further investigate the effect target hospital has on fatality risk a more thorough classification of the emergency hospitals, preferably including several trauma levels, is needed.

The classification of Örebro University Hospital as TC can be debated. Because Örebro is a University Hospital, it appeared reasonable to include it as TC even though it lacks a neurosurgery. However, treating Örebro as non-TC did not change the outcome much (7.9% fatality reduction vs. 8.6%).

4.4 Trauma center coverage

TC coverage is an essential part to justify the use of University Hospitals as TCs. If the coverage is too low there will still be a lot of people that cannot be transported to a TC and thus not benefit from the initial assessment possible thanks to AACN. When examining the coverage of fatal accident locations only fatalities in passenger cars were included in the analysis. Including fatalities in the entire road transport system increased the coverage of TC since most of the fatal accidents involving pedestrians and cyclist occur in cities where the distance to nearest TC is often shorter. To only include fatalities in passenger cars seemed most

reasonable since an AACN system currently only can affect the outcome of occupants travelling in a passenger car.

A reasonable flight distance for ambulance helicopters is hard to derive. Since no relevant literature was found regarding the subject an estimation was made based on mean rescue time for fatalities in passenger cars and the cruising speed of a typical ambulance helicopter used in Sweden. Whether or not this estimation is representable for real world cases can be discussed. For example, the mean flight distance between accident location involving passenger cars and target hospital was 47 km whereas the ten longest flight distances ranges from 190 km to 319 km. Also, the flight distance is dependent on where the helicopters are stationed and where they are located at the time of the alarm. The assumption that over 85% can be transported to a TC may not hold when taking these factors into account.

4.5 Databases

Two different data sources were used to identify the relevant cases, thus the matching process was of great importance for the subsequent analysis. Ideally, most fatalities in STRADA should match the in-depth cases coded as 'deceased in hospital' but that was not the case as only 376 of the 946 fatalities in STRADA were matched. This is partly explained by the number of cases in the in-depth database coded as 'unknown location of death' (n=176). Also, fatalities coded as 'deceased during transport' (n=66) are presumably reported in STRADA since these most likely are transported to an emergency department. However, there are still very many cases left to explain. No thorough examination of the non-matching cases was performed and to further enlarge the dataset such examination is probably needed.

Only fatalities matching the in-depth were included but all non-fatal injured from STRADA were included. No other cause than pure chance is known for some fatalities in STRADA to be matched and some not, thus the matching itself was not considered a cause for bias.

When classifying the cases in the in-depth database the notes from the investigator were sometimes hard to interpret, thus the location of death was not always clear. Only cases that clearly stated the location of death were coded as 'deceased in hospital'. All cases described as 'dead on arrival', 'declared dead on arrival' or similar were not coded as 'deceased in hospital'. All these factors probably contribute to the low number of matches and presumably the cases identified as 'deceased in hospital' in the in-depth database are not all persons that died at a hospital.

4.6 Using only accidents involving passenger cars

To obtain as good picture as possible over how different variables affects the fatality risk a large dataset was essential. Including injuries and fatalities from the entire road transport system instead of only passenger cars increased the dataset from 46 000 to 68 000 but most importantly the number of fatalities increased from 154 to 376. It was assumed that independent of how the injures were sustained the medical outcome for persons with similar injuries and demography

were the same when treated at the same hospital. However, it is plausible that injuries sustained in a passenger car are different from injures sustained on a motorcycle even though the ISS-values are the same. The benefit of a larger dataset was though considered more valuable than the potential drawback of including injuries of road users other than passenger car occupants.

4.7 Exclusion of 'Helicopter transport' and 'Rescue time'

Helicopter transport was associated with increased fatality risk, thus the opposite of what several recent studies (Desmettre et al. 2012; Andruszkow et al. 2014; Abe et al. 2014) and the German Trauma Society (2015) suggest. The fact that injured people transported by helicopter had more severe injuries than those transported by ground ambulance (mean ISS = 12.45 vs. 3.45) should not affect the estimation since injury severity is adjusted for in the model, unless the adjustment is flawed by ISS not being an accurate predictor of injury severity. From the data available, no obvious cause for this result was found.

Longer rescue times were associated with higher survival probability, thus not consistent with the assumption that swifter hospital care is beneficial. Rescue time was calculated from data relying on two different time reports (police and hospital) thus the reliability in this variable can be questioned. It is plausible that a longer rescue time can be beneficial if an extended on-scene medical care is of high quality but since no information regarding on-scene medical care and the time spent on this was available for the analysis this effect could not be evaluated.

5. CONCLUSION

This is the first study evaluating the effect of the post crash system Advanced Automatic Collision Notification (AACN) on road fatality reduction in Sweden. Admission to a TC of people sustaining road traffic injuries, when adjusted for injury severity and age, was associated with an OR of 0.781 (95% CI = 0.609-1.003) compared to a non-TC. When AACN was assumed to predict injuries only for cases with ISS≥9, limiting possible transportation to 150km distances, and applying benefit only to those people not transported to a TC already without AACN, the estimated effect of AACN in Sweden was 8.6% fatality reduction, with a 95% confidence interval spanning from -0.3 to 16.4%. To further improve the estimation model a better defined trauma classification is needed along with additional accident data.

REFERENCES

Abe T., Takahashi O., Saitoh D., Tokuda Y. (2014). Association between helicopter with physician versus ground emergency medical services and survival of adults with major trauma in Japan. *Critical Care,* 18:R146

Alghnam S., Palta M., Hamedani A., Alkelya M., Remington P.L., Durkin M.S. (2014). Predicting in-hospital death among patients injured in traffic crashes in Saudi Arabia. *Injury*, 45 (11), 1693-1699.

Andruszkow H., Hildebrand F., Lefering R., Pape H-C., Hoffmann R., Schweigkofler U. (2014). Ten years of helicopter emergency medical services in Germany: Do we still need the helicopter

rescue in multiple traumatized patients?. *Injury*, 45 (sup3), S53-S58.

Buendia R., Candefjord S., Fagerlind H., Bálint A., Sjöqvist B.A., (2015). On scene injury severity prediction (OSISP) algorithm for car occupants. *Accident Analysis and Prevention*, 81, 211-217.

Clark D.E., Cushing B.M. (2002). Predicted effect of automatic crash notification on traffic mortality. *Accident Analysis and Prevention*, 34 (4), 507-513.

Desmettre T., Yeguiayan J-M., Coadou H., Jacquot C, Raux M., Vivien B., Martin C., Bonithon-Kopp C., Freysz M. (2012). Impact of emergency medical helicopter transport directly to a university hospital trauma center on mortality of severe blunt trauma patients until discharge. *Critical Care*, 16:R170

European Commission (2013). 112 eCall – Frequently Asked Questions. http://europa.eu/rapid/press-release_MEMO-13-547_en.htm (2015-05-05).

German Trauma Society (2015). S3 – Guideline on Treatment of Patients with Severe and Multiple Injuries. http://www.awmf.org/leitlinien/detail/ll/012-019.html (2015-05-06).

Hilbert P., Lefering R., Stuttman R. (2010). Trauma care in Germany: Major Differences in Case Fatality Rates Between Centers. *Dtsch Arztebl Int.,* 107 (26), 463-469.

Lahausse J.A., Psych D., Fildes B.N., Page Y., Fitzharris M.P. (2008). The Potential for Automatic Crash Notification Systems to Reduce Road Fatalities. *Association for the Advancement of Automotive Medicine (AAAM),* 52, 85-92.

MacKenzie E.J., Rivara F.P., Jurkovich G.J., et al. (2006). A national evaluation of the effect of trauma-center care on mortality. *The New England Journal of Medicine*, 354 (4), 366-378.

Ohlin M., Strandroth J., Lie A. (2014). Potential Safety Benefits of Automatic Collision Notification – A Case by Case Analysis. *Intelligent Transport Systems World Congress*, September 7-10, 2014, Detroit.

Regeringskansliet (2015). Uppdrag att utarbeta ett planeringsunderlag för traumavård. http://www.regeringen.se/regeringsuppdrag/2013/04/s20133285fs/ (2015-05-28)

Scandinavian AirAmbulance (2015). http://www.airamb.se (2015-05-28)

Schulman C.I., Bahouth G., Digges K., Augenstein J. (2010). Improving Pre-Hospital Triage Using Advanced Automatic Collision Notification. *Journal of Surgical Research*, 165 (2), 209-210.

Swedish Neurosurgical Society (2015). http://www.swedishneurosurgicalsociety.se/kliniker/ (2015-05-06).

Trafikverket (2012). Djupstudier av vägtrafikolyckor. http://www.trafikverket.se (2015-05-06).

Transportstyrelsen (2015). Strada – informationssystem för olyckor och skador i trafiken. https://www.transportstyrelsen.se (2015-05-06).

Vittinghoff E., Glidden D.V., Shiboski S.C., McCulloch C.E. (2011). *Regression Methods in Biostatistics: Linear, Logistic, Survival, and Repeated Measures Models*. Second edition. Berlin: Springer Science+Business Media.

World Health Organization (2013). Global status report on road safety 2013: supporting a decade of action. http://www.who.int (18 Dec. 2014)

Wu J., Subramanian R., Craig M., Starnes M., Longthorne A. (2013). The Effect of Earlier or Automatic Collision Notification on Traffic Mortality by Survival Analysis. *Traffic Injury Prevention*, 14 (sup1), 50-57

Extending Vehicle Linear Behaviour: A Retrospective Approach through Design and Simulation Strategies

Ahsan ud-Din Qazi*. Mike Blundell**.
Gary Wood***.

*Department of Mechanical Automotive and Manufacturing Engineering
Faculty of Engineering and Computing, Coventry University
Priory Street CV1 5FB, Coventry, West Midlands,
United Kingdom of Great Britain.
(Tel: +44(0)7466780163; e-mail: qazia@uni.coventry.ac.uk)
**Department of Mechanical Automotive and Manufacturing Engineering
Faculty of Engineering and Computing, Coventry University
Priory Street CV1 5FB, Coventry, West Midlands,
United Kingdom of Great Britain.
(e-mail: cex403@coventry.ac.uk)
***Department of Mechanical Automotive and Manufacturing Engineering
Faculty of Engineering and Computing, Coventry University
Priory Street CV1 5FB, Coventry, West Midlands,
United Kingdom of Great Britain.
(e-mail: aa6661@coventry.ac.uk)

Abstract: Full Electric Vehicles (FEVs) with in-wheel motors offer more choices to dynamists and control engineers to fine tune the vehicle for better performance during steady state and transient manoeuvres. This paper investigates the design and simulation strategies to extend vehicle dynamics linear behaviour. A set of linear, non-linear and Multi-Body System (MBS) models are used to examine the lateral dynamics. A fully featured model of Subaru Impreza is constructed in MSC-Adams and various ISO standard test manoeuvres are performed and the response is validated against the test track data for Subaru Impreza. A torque biasing mechanism is implemented to extend the linear handling response of the vehicle and yaw rate gain associated with the vehicle architecture is improved.

Keywords: **Vehicle Dynamics, Active Control, Torque Vectoring, In-wheel Motors, Vehicle Linearity.**

I. INTRODUCTION

Environmental concerns, depleting natural resources and increasing petroleum prices augmented with governmental legislations across Europe and America is bringing in stringent regulations and practices for the automotive industry to align themselves to (Ivanov et al. 2014 and Jalali et al. 2013). The results are cleaner, energy efficient and dynamically stable electric vehicles as the promising platforms offer advanced traction control systems implemented by controlling the electric motors torques to maintain the optimal traction of each tyre (Jalali et al. 2013).

A vehicle's handling behaviour at low levels of lateral accelerations is approximated by geometric Ackerman angle. As the vehicle speed increases and approaches 30mph, the behaviour depicted by the vehicle deviates from what is known as the linear behaviour (Blundell and Harty, 2004). The in-wheel motors provide an opportunity for a drive by wire system to extend the linear handling response of the vehicle. The quick torque build-up, left-right torque vectoring or for-aft torque vectoring utilises the maximum potential of

a wheel and brings in the desired yaw dynamics without the expense of longitudinal speed of the vehicle (Sabbioni et al. 2014, De Novellis et al. 2014).

The paper is structured as follows. Section II describes various vehicle dynamics system models used for the this study. Section III briefly discusses the analyses performed for characterising the handling and control. Proposed simulation strategy through torque vectoring for the vehicle is presented in Section IV. Concluding remarks of this study in Section V highlight the potential of the proposed concept and provides future research directions.

II. VEHICLE MODELLING

2.1 Co-ordinate system

The Newtonian formulations are based on a combination of vehicle fixed (x, y) and ground fixed coordinates (X,Y) coordinates as shown in Fig. 1 and Fig. 2 respectively by ISO 8855 standard with z-axis pointing vertically upward.
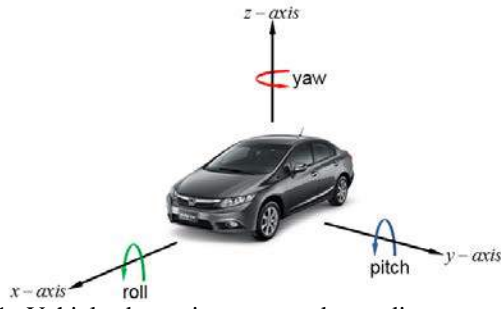
Figure 1: Vehicle dynamics axes and coordinates as in ISO 8855 (modified from Blundell and Harty 2004)

Vehicle heading angle 'ψ' and the vehicle trajectories (X,Y) are calculated from vehicle states (lateral velocity 'V_y' and yaw 'r').
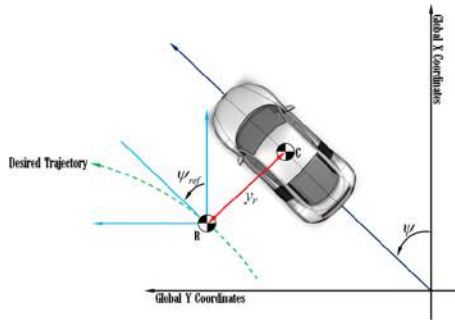
Figure 2: Global coordinates and vehicle coordinates (modified from Gillespie 1992)

2.2 Vehicle System Models

A number of different models are used to suit different but associated tasks. A set of simplifying assumptions to enable the representation of the lateral dynamics to be appropriate for the handling analysis are made. These include; vehicle symmetry with no heave degree of freedom; rigid vehicle links; negligible aerodynamic forces and constant longitudinal velocity. However, it is acknowledged that longitudinal weight transfer, acceleration and brake torques do implicate the lateral dynamics and considered in high degree of freedom model.

2.2.1 2 DOF bicycle model

The Newtonian formulations of motion for the bicycle model as shown in Fig. 3 are developed from the first principles using Euler's equations.
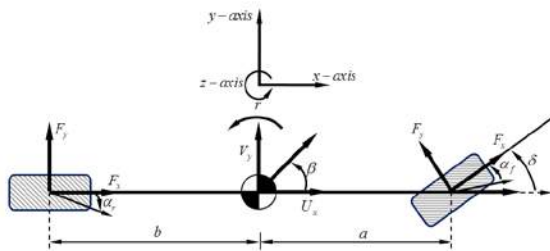
Figure 3: Bicycle model and vehicle axis system in two dimensions (modified from Blundell, Harty 2014)

These equations are

$$\sum F_y = ma_y \tag{3}$$

$$\sum M_z = I_{zz}\dot{r} \tag{4}$$

The lateral acceleration of the vehicle in such a moving frame with rotational dynamics involved is given by

$$a_y = \dot{V_y} + rU_x \tag{5}$$

The total lateral force '$\sum F_y$', and total moment '$\sum M_z$' at the centroidal axis are given by

$$\sum F_y = F_{yf} + F_{yr} \tag{6}$$

$$\sum M_z = aF_{yf} - bF_{yr} \tag{7}$$

The model states are defined in terms of the longitudinal velocity of the vehicle in x-direction at vehicle centre of gravity (CG) as 'U_x', lateral velocity in y-direction at CG as 'V_y', and 'r' yaw at CG. From the vector analysis of Fig. 4, a quantitative formulation for the front and rear slip angles in association to the vehicle parameters, states and kinematics is extracted and given below.

(a): Front tyre slip angle   (a): Rear tyre slip angle
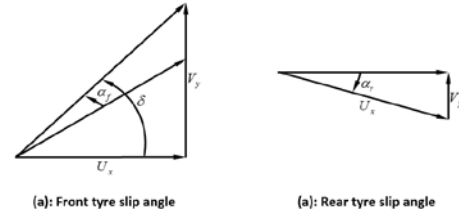
Figure 4: Vector representation for response angles at front and rear tyres

$$\alpha_f = \left(\frac{V_y + ar}{U_x}\right) - \delta \tag{8}$$

$$\alpha_r = \left(\frac{V_y - br}{U_x}\right) \tag{9}$$

The small angles are assumed for the linear approximation of the vehicle sideslip angle 'β' as

$$\beta = \tan^{-1}\left(\frac{U_x}{V_y}\right) \text{ to } \beta = \left(\frac{U_x}{V_y}\right) \tag{10}$$

The applications of a steer angle 'δ' at the wheel contact patch results in lateral forces 'F_{yf}' and 'F_{yr}' at front and rear axles respectively. These non-linear forces are approximated by an semi-empirical Magic Formula implemented by author later in the discussion but is considered linear at low levels of lateral accelerations. The magnitudes of the lateral forces at front and rear axles are

$$F_{yf} = C_{\alpha f}\alpha_f \tag{11}$$

$$F_{yr} = C_{\alpha r}\alpha_r \tag{12}$$

The coupling nature of the planar vehicle dynamics with lateral velocity and yaw are influenced by a single control element - the hand wheel. Substituting the value of lateral

acceleration 'a_y', front axle lateral force 'F_{yf}' and rear axle lateral force 'F_{yr}' in (5) results in

$$C_{\alpha f}\alpha_f + C_{\alpha r}\alpha_r = m\left(\dot{V}_y + rU_x\right) \quad (13)$$

Similarly substituting the values of moments about the yaw axis from (7) in equation (4) results in

$$aC_{\alpha f}\alpha_f - bC_{\alpha r}\alpha_r = I_{zz}\dot{r} \quad (14)$$

The values of front and rear slip angles from (8) and (9) when substituted in (13) and (14) results in

$$C_{\alpha f}\left(\left(\frac{V_y + ra}{U_x}\right) - \delta\right) + C_{\alpha r}\left(\left(\frac{V_y - rb}{U_x}\right)\right) \quad (15)$$

$$. = m(rU_x + \dot{V}_y).$$

$$aC_{\alpha f}\left(\frac{V_y + ra}{U_x} - \delta\right) - bC_{\alpha r}\left(\frac{V_y - rb}{U_x}\right) = I_{zz}\dot{r} \quad (16)$$

Combining similar terms and the equations can be written in the standard form as

$$\left(\frac{C_{\alpha f} + C_{\alpha r}}{mU_x}\right)V_y + \left(\frac{aC_{\alpha f} - bC_{\alpha r}}{mU_x} - U_x\right)r$$

$$. - \left(\frac{C_{\alpha f}}{m}\right)\delta = \dot{V}_y \quad (17)$$

$$\left(\frac{aC_{\alpha f} - bC_{\alpha r}}{I_{zz}V_x}\right)V_y + \left(\frac{a^2C_{\alpha f} + b^2C_{\alpha r}}{I_{zz}U_x}\right)r$$

$$. - \left(\frac{aC_{\alpha f}}{I_{zz}}\right)\delta = \dot{r}. \quad (18)$$

Equations (17) and (18) are coupled first order differential equations with 'V_y'; the vehicle's lateral velocity and 'r'; the vehicle's yaw as the two states. The equations are produced below in a standard system notation as

$$\begin{pmatrix} \left(\dfrac{C_{\alpha f} + C_{\alpha r}}{mU_x}\right) & \left(\dfrac{aC_{\alpha f} - bC_{\alpha r}}{mU_x} - U_x\right) \\ \left(\dfrac{aC_{\alpha f} - bC_{\alpha r}}{I_{zz}U_x}\right) & \left(\dfrac{a^2C_{\alpha f} + b^2C_{\alpha r}}{I_{zz}U_x}\right) \end{pmatrix}\begin{pmatrix} V_y \\ r \end{pmatrix}$$

$$. - \begin{pmatrix} \dfrac{C_{\alpha f}}{m} \\ \dfrac{aC_{\alpha f}}{I_{zz}} \end{pmatrix}\delta = \begin{pmatrix} \dot{V}_y \\ \dot{r} \end{pmatrix}. \quad (19)$$

2.2.2 3 DOF yaw-roll model

The limitations of the two degree of freedom model are removed by incorporating a number of suggestions into the new model. A three degree of freedom model (Gillespie 1992) is used for taking into considering the vehicle body roll motion and any effects thereby transferring from lateral load transfer. The model is non-linear and the assumptions for the 2DOF model are applicable unless otherwise stated with only exception which is consideration of vehicle roll included in this representation.
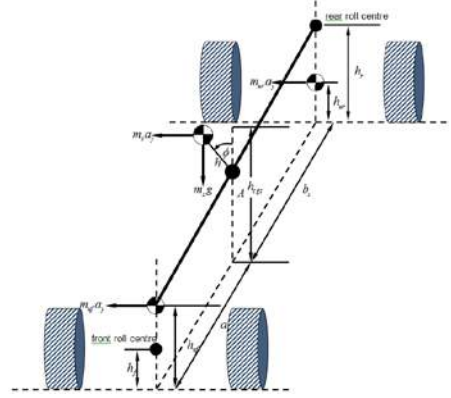
Figure 5: Lateral load transfer model for a full vehicle (modified from Gillespie 1992)

The mass centres move with a constant linear velocity in longitudinal direction and hence the longitudinal slip ratio due to variation in longitudinal velocity is eliminated. A sprung mass and total vehicle mass are two separate masses considered for this model and are at separate distances from the vehicle CG. The total mass is constrained to the x-y plane of the vehicle with only longitudinal velocity 'U_x', lateral velocity 'V_y', side-slip angle 'β' and yaw rate 'r'. The external tyre forces are 'F_{yf}' and 'F_{yf}' act on the total mass 'm'. The motion of the sprung mass 'm_s' is constrained to rotation about the roll axis, i.e x-axis by the roll angle 'ϕ'. Roll stiffness 'K_ϕ' and roll damping 'C_ϕ' constants are assumed and are fixed values.

By equating the internal and external force-moment using Lagrangian-Newtonian formulations with small angle assumptions are written as

$$\sum F_y$$

$$mU_x\left(\dot{\beta} + r\right) + m_s h_s \ddot{\phi} = 2C_f(\delta_f + \alpha_f\phi - \beta - \frac{a}{U_x}r)$$

$$. + 2C_r(\alpha_r\phi - \beta + \frac{b}{U_x}r). \quad (20)$$

$$\sum M_z$$

$$I_z\dot{r} = 2aC_f(\delta_f + \alpha_f\phi - \beta - \frac{a}{U_x}r)$$

$$. - 2bC_r(\alpha_r\phi - \beta + \frac{b}{U_x}r). \quad (21)$$

$$\sum M_x$$

$$I_x \ddot{\phi} + m_s h_s V_x (\dot{\beta} + r) = -K_\phi \phi - C_\phi \dot{\phi} \qquad (22)$$

The system equations written in standard matrix notation are

$$E \dot{x} = A_0 x + B_0 u$$

$$y = C_p x + D_p u$$

where the matrices are defined as

$$
A_0 = \begin{bmatrix}
-\left(\dfrac{C_f + C_r}{U_x}\right) & -\left(mU_x + \dfrac{aC_f}{U_x} - \dfrac{bC_r}{U_x}\right) & \alpha_f C_f + \alpha_r C_r & 0 \\[2mm]
-\left(\dfrac{aC_f - bC_r}{U_x}\right) & -\left(\dfrac{a^2 C_f + b^2 C_r}{U_x}\right) & \alpha_f aC_f + \alpha_r bC_r & 0 \\[2mm]
0 & 0 & 0 & 1 \\[2mm]
0 & -m_s h_s U_x & -K_\phi & -C_\phi
\end{bmatrix} ;
$$

$$B_0 = \begin{bmatrix} 0 & 0 & 0 & 1 \end{bmatrix}^T \qquad C_0 = \begin{bmatrix} 0 & 0 & 1 & 0 \end{bmatrix}$$

$$D_0 = \begin{bmatrix} 0 \end{bmatrix} \qquad E_0 = \begin{bmatrix} m & 0 & 0 & m_s h_s \\ 0 & I_z & 0 & 0 \\ 0 & 0 & 1 & 0 \\ m_s h_s & 0 & 0 & I_x \end{bmatrix}$$

The state matrix is given by

$$x = \begin{bmatrix} V_y & r & \phi & \dot{\phi} \end{bmatrix}^T$$

The effect of the roll angle on slip angles of the vehicle is termed as the 'roll steer' of the vehicle and is considered for the 3DOF model. The total vertical dynamic load acting on the individual wheels due to the combined effects of the lateral load transfer is given by

$$F_{zfl} = \left(\frac{1}{2}\frac{mgb}{a+b}\right) - \left(\frac{1}{2}\frac{ma_x h_{cg}}{a+b}\right)$$
$$+ \frac{a_y}{t_f}\left(\frac{m_s b h_f}{a+b} + m_{uf} h_{uf}\right) + \frac{1}{t_f}\left(-K_{\phi f}\phi - C_{\phi f}\dot{\phi}\right). \qquad (23)$$

$$F_{zfr} = \left(\frac{1}{2}\frac{mgb}{a+b}\right) - \left(\frac{1}{2}\frac{ma_x h_{cg}}{a+b}\right)$$
$$- \frac{a_y}{t_f}\left(\frac{m_s b h_f}{a+b} + m_{uf} h_{uf}\right) - \frac{1}{t_f}\left(-K_{\phi f}\phi - C_{\phi f}\dot{\phi}\right). \qquad (24)$$

$$F_{zrl} = \left(\frac{1}{2}\frac{mga}{a+b}\right) + \left(\frac{1}{2}\frac{ma_x h_{cg}}{a+b}\right)$$
$$+ \frac{a_y}{t_r}\left(\frac{m_s a_s h_r}{a+b} + m_{ur} h_{ur}\right) + \frac{1}{t_r}\left(-K_{\phi r}\phi - C_{\phi r}\dot{\phi}\right). \qquad (25)$$

$$F_{zrr} = \left(\frac{1}{2}\frac{mga}{a+b}\right) + \left(\frac{1}{2}\frac{ma_x h_{cg}}{a+b}\right)$$
$$- \frac{a_y}{t_r}\left(\frac{m_s a_s h_r}{a+b} + m_{ur} h_{ur}\right) - \frac{1}{t_r}\left(-K_{\phi r}\phi - C_{\phi r}\dot{\phi}\right). \qquad (26)$$

1.2.3 Multi-Body System (MBS) model

The preceding level and degrees of freedom of models delivered a great deal of clarity but did not include the high fidelity and compliance of a modern day passenger vehicle. A large amplitude Multi-Body System (MBS) model is prepared using MSC-ADAMS, a modern suite of industrial grade software widely used as standard automotive software. The model is represented in Fig. 6.
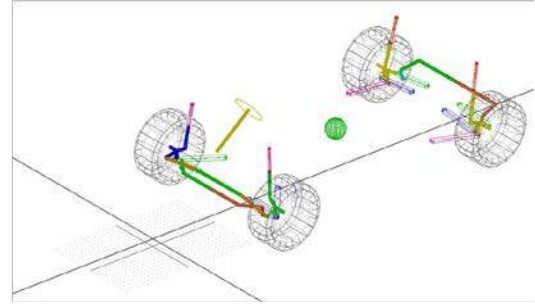
Figure 6: Large amplitude MBS model of Subaru Impreza implementation in MSC ADAMS

The model for Subaru Impreza is later modified to accommodate the battery mass, in-wheel motors mass and inertial elements added to the wheel assembly. The revised weight distribution needed recalibration of the vehicle front and rear anti-roll bars and adjusting spring-damper characteristics to regain the original satisfactory ride and handling behaviours.

The data set used for a Subaru Impreza is used to establish its conformity to the test track data available for the vehicle. The vehicle is a nose heavy variant with 52.40 % front mass distribution. The detailed data set is represented in Table 4.4 given below.

Table 4.4: Vehicle dynamics model parameters. The values correspond to a Subaru Impreza.

Symbol	Description	Units
m	Mass of the vehicle	893 kg
I_{zz}	Moment of inertia around z-axis at CG	1297.58 kgm^2
a	Distance of front axle from CG	1.19 m
b	Distance of rear axle from CG	1.31 m
l	Wheelbase	2.51 m

C_{af}	Cornering stiffness at front axle	-150,000 $Nrad^{-1}$
C_{ar}	Cornering stiffness at rear axle	-150,000 $Nrad^{-1}$

1.2.4 Tyre Model

The Magic Formula model is an empirical model based on transcendental functions and is used in this work. The input quantities for the Magic Formula are the longitudinal slip ratio 'κ', lateral slip angle 'α', camber angle 'γ' and the acting normal load 'F_z'. For the case of pure sideslip or the pure longitudinal condition and a given vertical load and camber angle the Magic Formula as described by Bakker et al. (1986) is

$$y(x) = D \sin \left[C \arctan \left\{ Bx - E \left(Bx - \arctan \left(Bx \right) \right) \right\} \right] \quad (27)$$

$$y(x) = y(X) - S_v \quad (28)$$

$$x = X + S_h \quad (29)$$

$y(X)$ is the longitudinal force 'F_x', lateral force 'F_y' or aligning moment 'M_z', 'X' is either the longitudinal slip ratio 'κ', lateral slip angle 'α' and 'B', 'C', 'D' and 'E' are tyre coefficients and the significance become meaningful when considering Fig. 7.
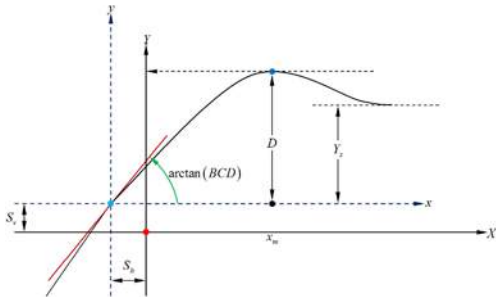
Figure 7: Graphical interpretation of coefficients in tyre Magic Formula (modified from Blundell and Harty 2004)

These factors are related to the shape of the characteristic curve and are detailed below in Table 1.

Table 1: Magic Formula Shape Factors

Factors	Name	Effect
B	Stiffness Factor	BCD is the slop at orgin, i.e cornering stiffness
C	Shape Factor	Controls the stretching in x-direction.
D	Peak factor	
E	Curvature Factor	It effects the transition in the curve and the determines the position of peak value

Apart from these factors, there are two values related to the lateral force or aligning moment. These are given below in Table 2.

Table 2: Magic Formula Offset Factors

Factors	Name	Reason
S_h	Horizontal Shift	Shifts the curve towards along x-axis
S_v	Vertical Shift	Shifts the curve towards along y-axis

The tyre model implemented for a 205/55 R16 tyre resulted in the following values for the lateral tyre force and slip angle curve.
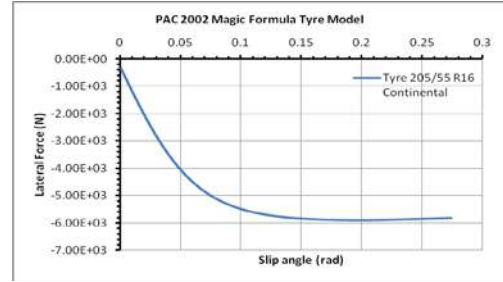
Figure 8: Lateral force curve for tyre used for simulation

III. ANALYSES

3.1 Eigen Analysis

State variables represent dynamics characteristics of a system and design variables are specified from the design criteria. This relationship suggests that initial values of design variables govern the characteristics of variables. The theory of linear systems provides an insight into the homogeneous solution of the vehicle dynamics problem −no steer input at handhwheel which implies an eigen formulation as

$$A - \lambda I = 0$$

Equation (19) is re-written as

$$\left(\begin{pmatrix} \dfrac{C_{af} + C_{ar}}{mU_x} \end{pmatrix} \begin{pmatrix} \dfrac{aC_{af} - bC_{ar}}{mU_x} - U_x \end{pmatrix} \\ \begin{pmatrix} \dfrac{aC_{af} - bC_{ar}}{I_z U_x} \end{pmatrix} \begin{pmatrix} \dfrac{a^2 C_{af} + b^2 C_{ar}}{I_z U_x} \end{pmatrix} \right) \begin{pmatrix} V_y \\ r \end{pmatrix}$$
$$. - \lambda \begin{pmatrix} 1 & 0 \\ 0 & 1 \end{pmatrix} = \begin{pmatrix} 0 \\ 0 \end{pmatrix} \quad (30)$$

The frequency and damping ratio from eigen solutions for 2 DOF vehicle is given below in Fig. 9 and Fig. 10 respectively.
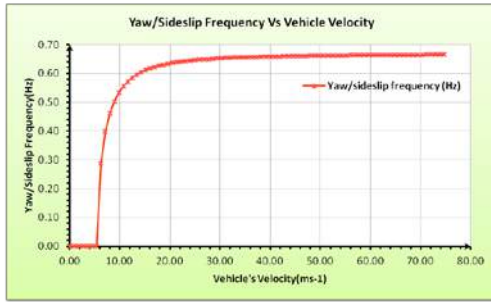
Figure 9: Eigen solution for the 2 DOF model-frequency for a 52:40 mass distribution vehicle architecture
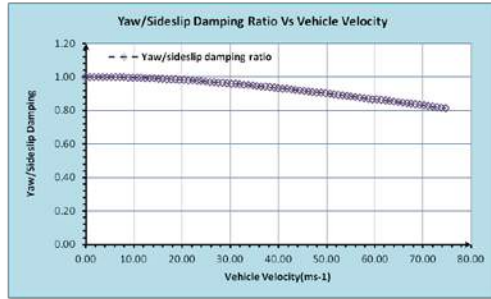
Figure 10: Eigen solution for the 2 DOF model-damping for a 52:40 mass distribution vehicle architecture

The vehicle has a constant yaw/sideslip frequency of oscillation around and below 0.67 Hz and damping degrades gracefully and remains above 0.8 for a wide range of longitudinal speeds. The pole plot signifies it as a stable vehicle over the entire range of vehicle operation. The frequency of oscillation of the modes dies out and does not proceed into an unstable region as shown in Fig. 11 below.
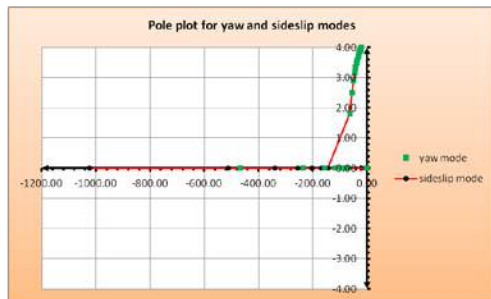
Figure 11: Poles plot from eigen solution for the 2 DOF model for a 52:40 mass distribution vehicle architecture

3.2 Vehicle Handling and Control

Vehicle handling is primarily a combination of vehicle steerability and control. Considering the time domain solution by subjecting the vehicle travelling at 157 mph (approx. 70 m/s) to a hand wheel steering input application (0.1 seconds) to yield a 0.4 g lateral acceleration. The internal dynamics evident from the analysis of the response angles and response variables plotted in Fig. 12 and Fig. 13 respectively suggest a contact patch angle of 0.19 degrees (with a steering ratio of 15.6:1), a handwheel steering input of about 2.93 degrees; the control gains are very high at the speed.
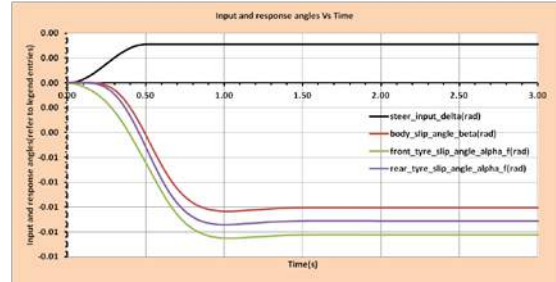
Figure 12: Time domain response angles for a steering input to give 4 ms^{-2} lateral response at 70 ms^{-1}.
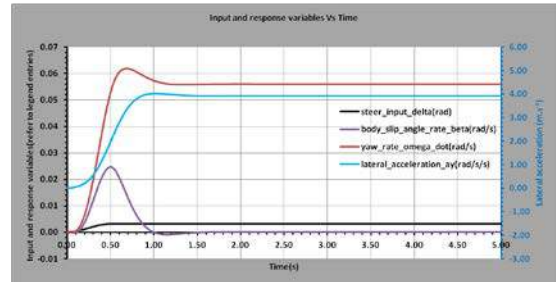
Figure 13: Time domain response variables for a steering inputs to give 4 ms^{-2} lateral response at 70 ms^{-1}.

The vehicle was driven at lower velocity of 79 mph (approx. 35 m/s) and the application of 0.57 degrees at contact patch by inducing a handwheel steer input of 8.62 degrees. The control gains are much reasonable as shown in Fig. 14 and Fig. 15 given below.
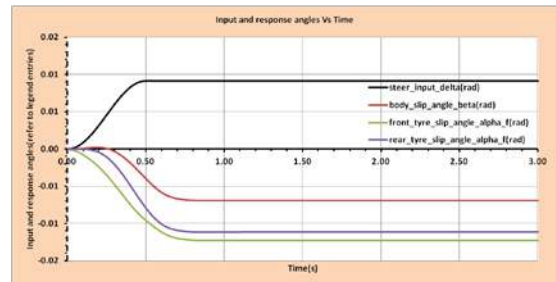
Figure 14: Time domain responses for steering inputs to give 4 ms^{-2} lateral response at 35 ms^{-1}.
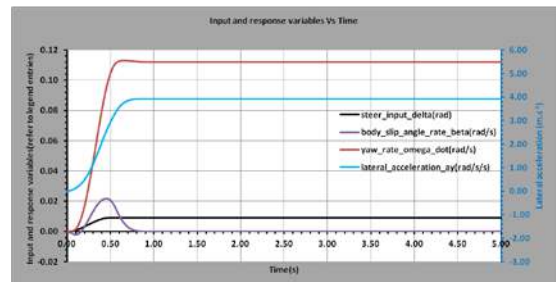
Figure 15: Time domain response variables for a steering inputs to give 4 ms^{-2} lateral response at 70 ms^{-1}.

The high control gains and long settling times associated with the response variables make the control task difficult for drivers. The aircraft dynamics suggest a delay of 0.1 seconds is inevitable to the pilot but a delay in response of over 0.3 seconds render a workload on the operator progressively

higher (Blundell and Harty 2014). This concept of yaw rate gain, which is a normalized on the basis of steering input characterizes the vehicle objectively and is shown in Fig. 16 below.
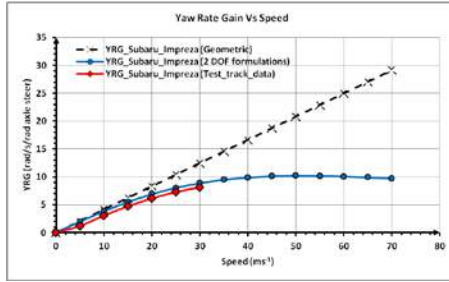
Figure 16: Geometric yaw rate gain, yaw rate gain based on 2DOF bicycle model formulations and yaw rate gain from test track data.

The overwhelming majority of driving community expects the vehicle to respond geometrically to the steering demand requests. As the vehicle longitudinal speed increases, the vehicle needs more steering input to respond to the vehicle yaw demand to match the linearised and expected yaw rate. The SAE J670 defines the understeer situation if the actual yaw rate gain of the vehicle is less than the geometric yaw rate gain. A very important conclusion on the significance of SAE understeer is detailed by Blundell and Harty (2014) as the perception of the technical SAE understeer and defined by the standard as experienced by a real driver is that the driver of the vehicle adapts to this objective notion of the vehicle undertseer which is not observable.

3.3 Sensitivity Studies

The yaw rate gain of the vehicle depends on a large set of parameters investigated through sensitivity analysis.These parameters include

- Mass of the vehicle
- Mass moment of inertia of the vehicle
- Front axle cornering stiffness of the vehicle
- Rear axle cornering stiffness of the vehicle
- Distance from the front axle to the CG of the vehicle
- Distrance of the rear axle to the CG of the vehicle

The sensitivity is defined as

$$\text{Sensitivity of a parameter} = \left| \frac{\text{Percent change in response}}{\text{Percent change in input parameter}} \right| * 100$$

The sensitivity of the vehicle is detailed below in Fig. 17 to Fig. 22.
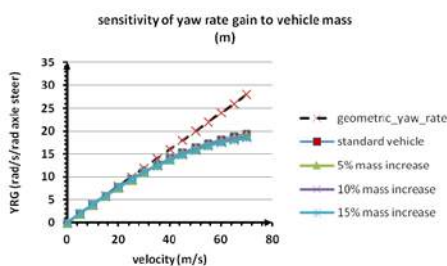
Figure 17: Influence of vehicle mass on yaw rate gain
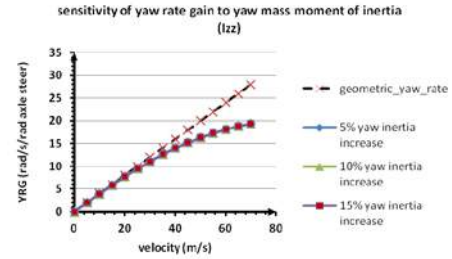
Figure 18: Influence of vehicle mass moment of inertia on yaw rate gain
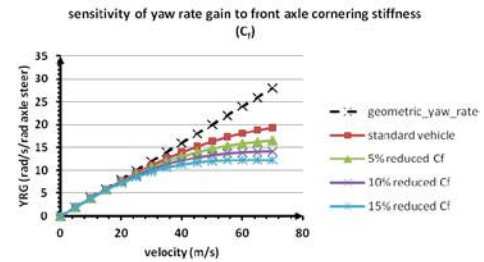
Figure 19: Influence of front axle cornering stiffness on yaw rate gain
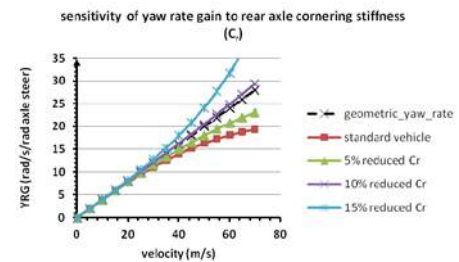
Figure 20: Influence of rear axle cornering stiffness on yaw rate gain
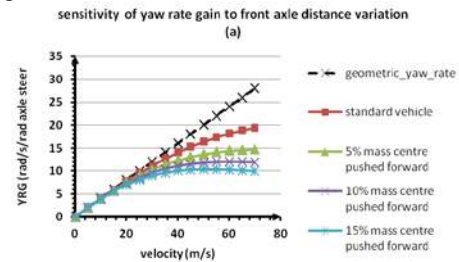
Figure 21: Influence of CG distance from front axle on yaw rate gain
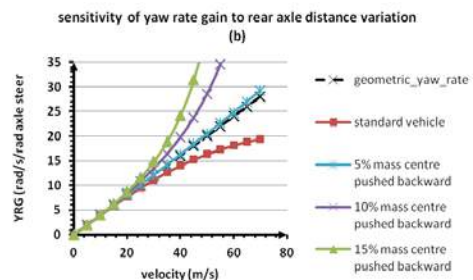
Figure 22: Influence of CG distance from rear axle on yaw rate gain

IV. SIMULATION STRATEGY AND TORQUE VECTORING

4.1 ISO 4138(2012)Steady State Cornering-Open Loop Test -Constant Steer Angle

The simulation strategy was implemented through the ISO 4138(2012) test implemented in MSC ADAMS that requires driving the test vehicle at several discrete speeds with a single selected steering wheel angle to remain fixed for each longitudinal speed.

A torque biasing is implemented based on the sensor feedback from the virtual yaw rate sensor of the vehicle by comparing it against the reference yaw rate based on 2 DOF formulations as

$$\dot{r}_{ref} = \frac{U_x l C_f C_r \delta_f}{l^2 C_f C_r + m U_x^2 \left(b C_r - a C_f \right)} \quad (31)$$

A simple PID control based on the the torque biasing applicable to the wheels through an In-wheel motor is proposed to improve the yaw rate gain of the vehicle.The result for the torque vectoring implemented in MSC ADAMS for steady state cornering is detailed below in Fig. 23.
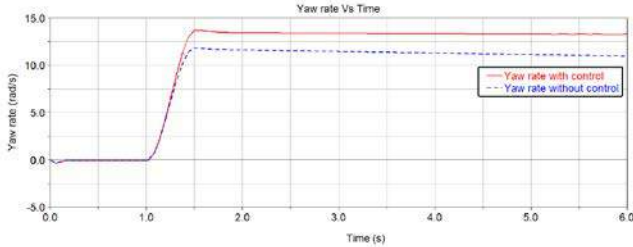
Figure 23:   Yaw rate for steady state cornering with and without control in MSC ADAMS.

The simulation was carried for a large set of longitudinal speeds and steady state values for normalised yaw rate were plotted against the vehicle longitudinal speed. An improvement in yaw rate gain of the vehicle is observed by simulating a torque biasing strategy through ISO 4138(2012) and by using the yaw rate gain concept as shown in Fig. 24 below.
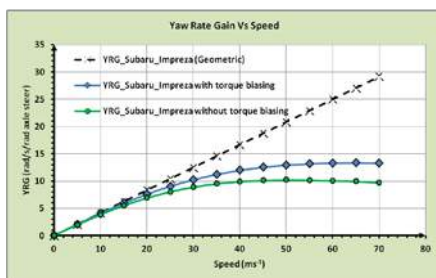
Figure 24:   Yaw rate gain improvement by implementing torque biasing for Subaru Impreza.

V. CONCLUSIONS

The yaw rate gain concept to investigate the linear handling response of the vehicle is robust and novel in totality. The sensitivity studies reveal strong correlation between the yaw rate gain and the cornering stiffness of tyres and the CG placement of the vehicle. The strategy can be used to suggest the design modifications for new vehicles and as a retrospective tool to improve the design of an existing vehicle. An improvement in torque vectoring control can be useful by borrowing the robust concepts from non-linear control, adaptive control and model predictive control to improve the controller performance in tracking the desired yaw rate of the vehicle and reduce the actuator saturation linked to in-wheel motors.

REFERENCES

Blundell, M. & Harty, D. 2004, *Multibody Systems Approach to Vehicle Dynamics,* Ist edn, Elsevier Butterworth-Heinemann, Oxford.

Blundell, M. & Harty, D. 2014, *Multibody Systems Approach to Vehicle Dynamics,* (2nd Edition), Cambridge, GBR: Butterworth-Heinemann.

Gillespie, T.D., 1992. *Fundamentals of Vehicle Dynamics.* Society of Automotive Engineers.

De Novellis, L., Sorniotti, A., Gruber, P. & Pennycott, A. 2014, "Comparison of Feedback Control Techniques for Torque-Vectoring Control of Fully Electric Vehicles", *Vehicular Technology, IEEE Transactions on,* vol. 63, no. 8, pp. 3612-3623.

Ivanov, V., Shyrokau, B., Savitski, D., Orus, J., Meneses, R., RodrÃguez-FortÃºn, J., Theunissen, J. & Janssen, K. 2014, "Design and Testing of ABS for Electric Vehicles with Individually Controlled On-Board Motor Drives", *SAE Int.J.Passeng.Cars - Mech.Syst.,* vol. 7, no. 2, pp. 902-913.

Jalali, K., Uchida, T., McPhee, J. & Lambert, S. 2013, "Development of an Integrated Control Strategy Consisting of an Advanced Torque Vectoring Controller and a Genetic Fuzzy Active Steering Controller", *SAE International Journal of Passenger Cars,* vol. 6, no. 1, pp. 222-240.

Li, Y., Zhang, J., Guo, K. & Wu, D. 2014, *A Study on Force Distribution Control for the Electric Vehicle with Four In-wheel motors*, - SAE International.

Park, J., Yoon, J., Kim, D. & Yi, K. 2008, "Roll state estimator for rollover mitigation control", *Proceedings of the Institution of Mechanical Engineers, Part D: Journal of Automobile Engineering,* vol. 222, no. 8, pp. 1289-1312.

Sabbioni, E., Cheli, F., Vignati, M. & Melzi, S. 2014, "Comparison of Torque Vectoring Control Strategies for a IWM Vehicle", *SAE Int.J.Passeng.Cars ΓÇô Electron.Electr.Syst.,* vol. 7, no. 2, pp. 565-572.

Effects of hearing loss shown in both driving simulator and real traffic

B. Thorslund*& J. Jansson *

*VTI, Olaus Magnus väg 35 SE-581 95 Linköping Sweden (e-mail: birgitta.thorslund@vti.se).

Abstract: This paper describes two studies, one conducted in VTI driving simulator III and the other on roads in and around Linköping city center. In both studies two groups were included, one with age related hearing loss and one control group with normal hearing. The purpose was to examine differences between the groups in driving behavior, visual behavior and also to evaluate the effectiveness and acceptance of a tactile driver assistance system The driving scenario in the simulator was a 35 km long rural road with a speed limit of 70 km/h. Twice per minute drivers were prompted by a vibration in the seat to perform a secondary task by first look at and then read back a complete sequence of four letters. On road, all participants undertook two drives of 14 km each while they performed two pre-programmed navigation tasks guiding them around two different routes. The same navigation system was used for both drives but during one drive the navigation system presented only the visual information and during the other drive there was an additional vibration in the seat to guide the driver in the right direction. Effects of Hearing Loss was seen on driving speed and on visual search behavior in both simulator and in real traffic. In the driving simulator, during secondary task and when passing a parked car, participants with HL drove 5-6 km/h slower. In real traffic, on road sections with a speed limit of 70 km/h, participants with HL drove 4 km/h slower. This more cautious driving behavior suggests that drivers with HL use compensatory strategies. The fact that corresponding results can be seen both in the simulator and on real road is interesting, on one hand for simulator validity in general but also for the opportunity to further study these issues in controlled simulator experiments.

Keywords: Driving simulator, Validity, Hearing loss, Driving speed, Visual search behavior

1. INTRODUCTION

Several studies have provided support for relative validity of driving simulators and suggest their potential role as assessment tool. In terms of driving speed, some studies have shown higher speed in the simulator compared to on road (Bella, 2008; Diels & Parkes, 2010) and others have shown the opposite (Godley, Triggs, Fildes, 2002; Hakamies-Blomqvist, Östlund, Henriksson, Heikkinen, 2000; Klee et al, 1999). The validity of VTIs driving simulator III has, in one validation study, been suggested very high except from lower risk perception resulting in higher speed (Östlund, Nilsson, Törnros, Forsman, 2006), while in another, no significant difference was found between simulator and real road on sections with constant speed limit (Ahlström, Bolling, Sörensen, Eriksson, Andersson, 2012).

Advantages of simulator studies commonly mentioned are that they are safer, more economical and more replicable (e.g. Lee, H.C. Cameron, Lee, 2003; Dela, Laine, Bruzelius, Sehammar, Renner, Markkula, Karlsson, 2009). Driving simulators have also been found valid means of studying visual search strategies (Carter; Underwood, Crundall, Chapman), identifying age-related changes in driving performance and cognition (Johnson et al., 2011; Casutt, Martin, Keller, Jäncke, 2014) and for studying increased and high visual and cognitive demands (Landsdown, Flyte, 1996).

The prevalence of HL in Europe is roughly 30% for men and 20% for women at the age of 70 years, and 55% for men and 45% for women at the age of 80 years (Roth, 2001). The effects of hearing loss (HL) on driving behavior has until now received very limited attention in the literature. Increasing numbers of advanced information systems are becoming available in modern vehicles. These often have an auditory output, which may make them less accessible for drivers with HL.

According to motivational driver behaviour models, drivers aim to maintain a preferred level of risk. Lewis-Evans (2012) suggest time-based safety margins as relevant measures of this individual level of risk, and visual search is proposed as a valid indicator of risk awareness (Lidestam et al., 2010). Manipulation of both driving speed (e.g., Fuller, 2008; Summala, 2007; Levis-Evans, 2012) and degree of engagement in secondary tasks (Fuller, 2005) may be most important in maintaining the preferred level of risk. This is all in line with Gibson and Crooks' field of safe travel (Gibson & Crooks, 1938) and also relevant for understanding the effect of HL on driving behavior and for the evaluation of driver support systems. Recurring in the models is the driving speed, and several studies have linked speed perception to the amount of noise in car cabins or to the driving sound (Evans, 1970; Ohta & Komatsu, 1991). Thus, speed might be perceived differently by drivers with hearing loss, due to a reduced sensitivity to sounds.

2. AIM

This paper describes two studies, one conducted in VTI driving simulator III (Nordmark, Jansson, Palmkvist, & Sehammar, 2004) and the other on roads in and around Linköping city center. In both studies two groups were included, one with age related HL and one control group with normal hearing (NH). The purpose was to examine differences between the groups in driving behavior, visual behavior and also to evaluate the effectiveness and acceptance of a tactile driver assistance system.

3. METHOD

The simulator study was conducted in SIM III, a high fidelity moving base simulator, at VTI, see Fig. 1. In total, 48 participants took part (24 with NH and 24 with HL). The mean age was approximately 60 in both groups. Thirty-two participants (16 with NH and 16 with HL) participated in the study in real traffic and the mean age was approximately 55 years. There was no significant difference between groups in terms of mileage per year, age or years with a driving license. The inclusion criterion for the NH group was a hearing threshold of maximum 20 dB at each frequency (500, 1000, 2000 and 4000 Hz) measured with a pure tone audiometer. Inclusion criterion for the HL group was a moderate HL (41–60 dB) according to WHO categories (Arlinger, 2007). The driving scenario in the simulator was a 35 km long rural road with a speed limit of 70 km/h. The traffic density was low with no traffic in the same lane and approaching cars approximately every 22 seconds. Twice per minute drivers were prompted by a vibration in the seat to perform a secondary task by first look at and then read back a complete sequence of four letters.

Fig. 1 VTI driving simulator, Sim III

On road, all participants undertook two drives of 14 km each while they performed two pre-programmed navigation tasks guiding them around two different routes in the city of Linköping in Sweden. The same navigation system was used for both drives but during one drive the navigation system presented only the visual information and during the other drive there was an additional vibration in the seat to guide the driver in the right direction. This tactile support was given in either the left or the right side of the driving seat, to indicate the direction of the next turn. The order in which the two routes where driven as well as the order of system information presented was balanced between the groups.

A questionnaire was included in both studies, with the aim to gather the drivers' subjective experience of their driving performance, realism (only simulator study), and of the information presented by the different systems in terms of feelings of safety, usefulness and comfort. In the simulator, a 5 camera system from Smarteye was used for eye tracking (see Fig. 2) and on road SMI ETG glasses

(SensoMotoricInstruments, 2013) was used (see Fig. 3). The Smarteye-system was mounted in SIM III and the reason for using SMI glasses in the field study was mainly that we were interested in pre-defined targets both inside and outside the car.
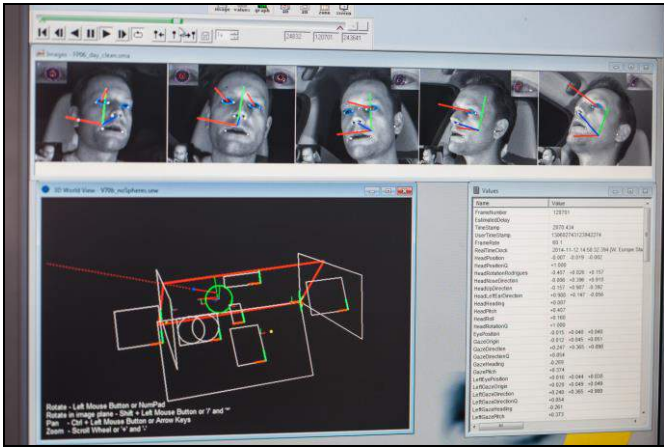
Fig. 2 Eye tracking in SIM III with Smarteye

Fig. 3 Eye tracking on road with SMI ETG glasses

4. RESULTS

In the driving simulator, during baseline driving, there was no significant effect of HL on driving speed. With increased complexity, that is by adding either a secondary task or passing a parked car, participants with HL drove 5-6 km/h slower, on a 70 km/h road. In real traffic, on road sections with a speed limit of 70 km/h, participants with HL drove 4 km/h slower compared to participants with NH. The same tendency could be seen also on sections with a speed limit of 50 km/h, however this was not significant, see Fig. 4. There was no effect of route or navigation system information on the speed.
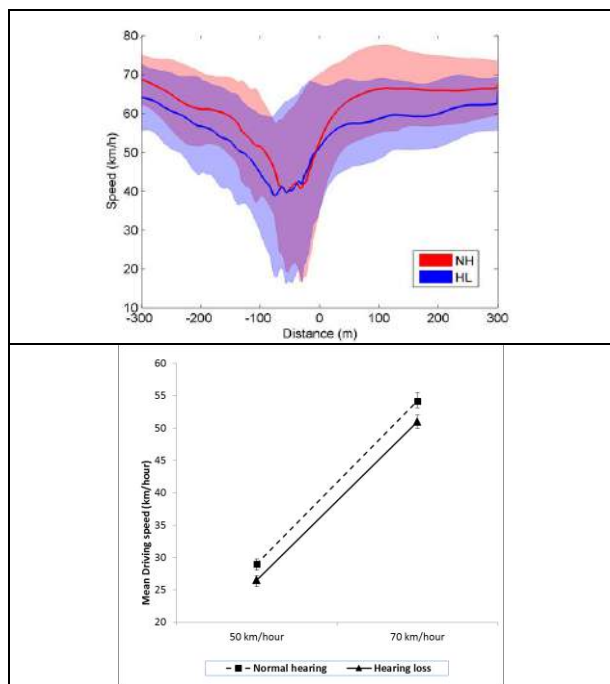
Fig. 4 Mean driving speed during parked car event in simulator (top) and in real traffic (bottom).
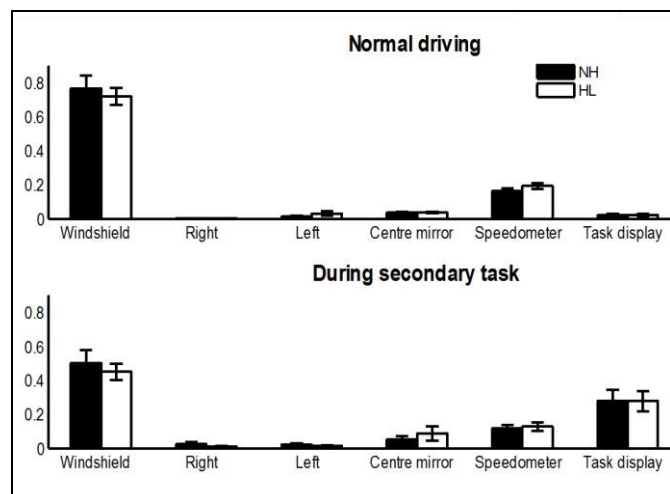
Fig. 5 distribution of glances at simulator drive.

In the simulator, drivers with HL looked away from road as much as NH drivers, however with more frequent glances of shorter duration. The distribution of glances is displayed in Fig. 5.

The results also indicated that drivers with HL perform a visual scan of the surrounding traffic environment before looking away towards the secondary task display. This can be seen in the probability matrixes in Fig. 6. Before looking at the secondary task display, participants with HL have a higher probability to look at the rear view mirror and to the right side compared to participants with NH.
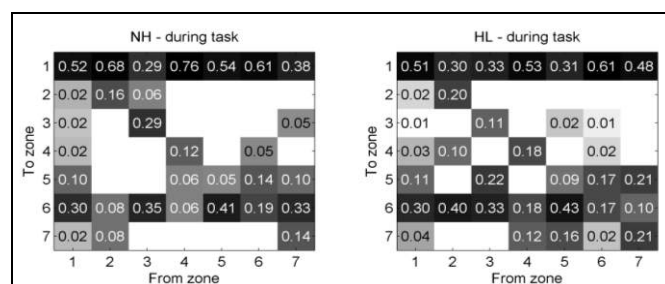
Fig. 6 Matrix showing the probability of looking at one specific target after one other target; 1 Windshield, 2 Right, 3 Left, 4 Rear view mirror, 5 Speedometer, 6 Secondary task display.

In real traffic, participants with HL looked on average 1.4% more in the rear view mirror compared to participants with NH. On average HL participants looked three times as often (0.3 compared to 0.1 times per minute) in the rear view mirror compared to the NH group, but there was no effect on the duration of glances. There was no effect of navigation system information on these measures.

The tactile signal showed high effectiveness and acceptance both in the simulator when used to alert the driver and on real road when used for navigation support.

5. DISCUSSION

Drivers with HL, compared to NH drivers show a more cautious behaviour including lower driving speed and a more comprehensive visual search behaviour. This effect was seen both in the simulator and in real traffic. The difference in driving speed between the groups was similar in the simulator and in real traffic, which is in line with previous studies in Sim III suggesting high speed validity on sections with constant speed limit (Ahlström, Bolling, Sörensen, Eriksson, Andersson, 2012).

The cautious glance behaviour shown by drivers with HL is more pronounced in the on road results. This could be an indication that the difference in perceived risk associated with HL is more apparent on road although the effects on driving speed was comparable (c.f. Östlund, Nilsson, Törnros, Forsman, 2006). However, it could also be an effect of the fact that the computer graphics is not as detailed as the real world e.g. in terms of moving actors (the simulator study

was set-up so that no vehicles where catching up from behind).

These results, might suggest that drivers with HL are safer drivers. However, this is not our interpretation. In line with the research on driving behavior models and the aim to maintain a certain level of risk, we suggest that drivers with HL choose a lower driving speed and use a more comprehensive visual search behavior to compensate for the loss of hearing. The fact that a similar adaptation strategy is seen both in the simulator and on road is an important result for simulator validity. This suggest that driving behavior related to perceived risk, for some situations also for people with disabilities, can be studied in a driving simulator.

The tactile signal used in both studies, in the simulator study to call for driver attention and in the field study to indicate the direction when navigating, was both effective and well accepted by the drivers. This is further discussed in the thesis by Thorslund (2014).

6. CONCLUSION

Effects of HL on driving behaviour that could be seen both in driving simulator and on real road include lower driving speed and a more comprehensive visual search behaviour. The corresponding results in simulator and on real road strengthen the validity of the simulator experiment. This suggests the simulator as a useful tool to evaluate effects of HL on driving behaviour. Tactile information was effective and very accepted both for alerting and for guidance, in the simulator and on real road.

7. REFERENCES

Ahlström, C. Bolling, A., Sörensen, G., Eriksson, O., Andersson, A. (2012). Validating speed and road surface realism in VTI driving simulator III. VTI report 745A.

Arlinger, S. (Ed.). (2007). Nordisk Lärobok i Audiologi. Nordic Textbook of Audiology. Bromma: C-A Tegnér AB.

Bella, F. (2008). Driving simulator for speed research on two-lane rural roads. *Accident Analysis and Prevention, 40*(3), 1078-1087.

Carter, C.J., Laya,O. (1998). Drivers visual search in a field situation and in a driving simulator. Vision in vehicles, 21-31.

Dela, N., Laine, L., Bruzelius, F., Sehammar, H., Renner, L., Markkula, G., Karlsson, A. (2009). A pilot evaluation of using large movement driving simulator experiments to study driver behaviour influence on active safety systems for commercial heavy vehicles. Proceedings of the 21st International Symposium on Dynamics of Vehicles on Roads and Tracks (IAVSD'09), Stockholm, Sweden, August 17-21, 2009.

Casutt, G., Martin, M., Keller, M., Jäncke, L. (2014). The relation between performance in on-road driving, cognitive screening and driving simulator in older healthy

drivers. *Transportation Research Part F: Traffic Psychology and Behaviour, 22*, 232- 244.

Diels, C., Parkes, A.M. (2010). Matching speed production in real and simulated driving. TRL Published Project Report.

Fuller, R. (2005). Towards a general theory of driver behaviour. *Accident Analysis & Prevention, 37*(3), 461–472.

Fuller, R., McHugh, C., & Pender, S. (2008). Task difficulty and risk in the determination of driver behaviour. *Revue Européenne De Psychologie Appliquée/European Review of Applied Psychology*, 58(1), 13–21.

Gibson, J.J., & Crooks, L.E. (1938). A theoretical field-analysis of automobile-driving. *The American Journal of Psychology, 51*(3), 453–471.

Godley, S.T., Triggs, T.J. Fildes, B.N. (2002). Driving simulator validation for speed research. *Accident Analysis and Prevention, 34*(5), 589-600.

Hakamies-Blomqvist, L., Östlund, J., Henriksson, P., Heikkinen, S. (2000). Äldre bilförare i simulator: en valideringsstudie. Older drivers in simualtor: A validity study. VTI report 464.

Johnson, M.J., Chahal, T., Stinchcombe, A., Mullen, N., Weaver, B., Bédard, M. (2011). Physiological responses to simulated and on-road driving. *International Journal of Psychophysiology, 81*(3), 203-208.

Klee, H. (1999). Preliminary validation of driving simulator based on forward speed. Transportation Research Record.

Landsdown,T.C., FLYTE, M.G. (1996). Evaluating in-vehicle information systems: a comparison of road and simulator based experiments. Conference proceedings, Combined 18TH ARRB Transport Research Conference and Transit New Zealand Land Transport Symposium.

Lee, H.C., Cameron, D., Lee, A.H. (2003). Assessing the driving performance of older adult drivers: On-road versus simulated driving. *Accident Analysis and Prevention, 35*(5), 797-803.

Lewis-Evans, B. (2012). *Testing models of driver behaviour.* (Doctoral dissertation). University of Groningen.

Lidestam, B., Lundqvist, A., & Rönnberg, J. (2010). Concepts from research literature and practical assessment of risk awareness: the Swedish driving test from the perspective of cognitive psychology. *Transportation Research Part F: Traffic Psychology and Behaviour, 13*(6), 409–425.

Nordmark, S., Jansson, H., Palmkvist, G., & Sehammar, H. (2004). "The new VTI Driving Simulator - Multi Purpose Moving Base with High Performance Linear Motion". Driving Simulator Conference, Paris

Ohta, H., & Komatsu, H. (1991). *Speed perception in driving*. Vision in vehicles, vol. III. Amsterdam: Elsevier Science Publishers; pp. 415–426.

Roth, T. N., Hanebuth, D., Probst, R. (2001). Prevalence of age-related hearing loss in Europe: a review. *Eur Arch Otorhinolaryngol, 268*(8), 1101–1107.

Summala, H. (2007). Towards understanding motivational and emotional factors in driver behaviour: Comfort through satisficing. In C. Cacciabue (Ed.), *Modelling Driver Behaviour in Automotive Environments*. London: Springer; pp. 189–207.

Thorslund, B. (2014). Effects of Hearing Loss on Traffic Safety and Mobility (Doctoral dissertation). Linköping: Linköping University Electronic Press.

Underwood, G., Crundall, D., Chapman, P. (2011). Driving simulator validation with hazard perception. *Transportation Research Part F: Traffic Psychology and Behaviour, 14*(6), 435-446.

Östlund, J. Nilsson, L., Törnros, J., Forsman, Å. (2006). Effects of cognitive and visual load in real and simulated driving. VTI report 533A

A Methodology for Simulation and Validation of a Safety-Critical Electronic Control Unit for Integration Testing in Connected Hardware-in-the-Loop Environments

Jan Schroeder * **Christian Berger** * **Thomas Herpel** **

* *University of Gothenburg, Department of Computer Science and Engineering, {jan.schroder, christian.berger}@gu.se*
** *Automotive Safety Technologies GmbH, thomas.herpel@astech-auto.de*

Abstract: Model-based software using Matlab & Simulink is indispensable in the automotive sector. Hence, the approaches for requirements engineering, development, verification, and validation in this area are deeply studied. This study focuses on their specific application for simulation models of safety-critical software and hardware components in the domain. A methodology for the above-mentioned software development steps is proposed. Each step is explained and considerations regarding safety are outlined. The study concludes with showing the feasibility of combining stakeholder knowledge with current literature on model-based development.

Keywords: ECU simulation, hardware-in-the-loop, verification, validation, safety

1. INTRODUCTION

Electronic control units (ECUs) responsible for safety-critical functionality in vehicles become more and more common. As they undergo continuous evolution, permanent verification and validation are required in order to ensure their functionality and quality.

1.1 Problem Domain & Motivation

In industry, verification and validation of ECUs is done using highly specialized Hardware-in-the-loop (HIL) test systems during integration and testing phases. Additionally, to ensure correct operation of the ECUs in an interconnected system like a complete vehicle, connected HILs are used. To ensure an efficient utilization of the connected HIL as a resource, real ECUs are complemented with simulations realized in Simulink. Simulations enable testing of single or multiple ECUs in a real-car environment even if not all ECUs are fully developed.

The general development process for an ECU involves the steps depicted in Figure 1. After the design has been created from the requirements, the development process is split up into a hardware and a software part. For an ECU to be used on a HIL, the software part has to be integrated with the hardware after both parts have been tested separately. This dependency bears the risk of delays if either the hardware or the software development is not finished in time. Hence, a different approach for the connected HILs was introduced depicted by the dashed lines in Figure 1. Simulations of the ECU software and its physical surroundings called plant models are created and connected to real ECUs or other simulations at the connected HILs.

These simulations enable testing functionality at connected HILs without the ECUs hardware. The approach depends on existing interfaces for the bus communication. Hence, the design, containing clearly defined specifications of the communication from and to the ECU is required to apply this approach.

1.2 Goal and Research Question

The goal of this work is to analyze the process of realizing a simulation model for the safety-critical ECU, like the Airbag control. Experience from existing projects showed that lack of maintainability can lead to severe problems in later development phases. If a model is difficult to maintain, small flaws in code and structure can accumulate and high effort is required if solving the issues becomes inevitable. This kind of problems is also called Technical Debt (cf. Kruchten et al. (2012)).

From the statements above, the following research question emerges.

RQ: How can best practice from literature and from stakeholders familiar with existing preconditions in industry be combined to a methodology for simulation and validation of a simulation model?

Hence, it is analyzed which approach for the simulation of model-based software results from an investigation in the given context. The methodology shall include a structured approach for requirements engineering, requirements prioritization, software development, verification, and validation. As the ECU to be created is a safety-critical component in the car, considerations in this regard are part of the study as well simulating safety-critical ECUs.
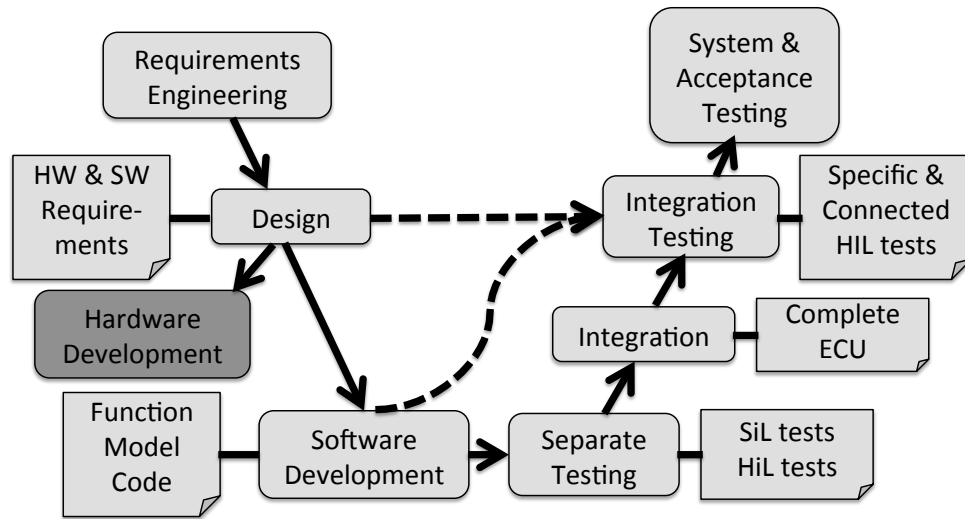
Fig. 1. V-model for the ECU development process following the solid lines. The dashed lines show the approach for ECU testing using simulation investigated in this study. The hardware development step highlighted is not split up any further as it is out of the scope of this study.

1.3 Contribution

This study focuses on a problem in industry. Hence, it contributes with a process ready to be applied to projects creating simulation models in industry. Additionally, each step in the process is examined attentively, to provide additional background on limitations and delimitations of a method. Those limitations and delimitations might be generalizable to other projects outside the domain as well.

1.4 Scope

This study covers simulation models of ECUs in the context of automotive software engineering. The models simulate software and also hardware parts of the ECUs, like sensors and actors. Still, the hardware and software development of the real ECUs are not in the scope of this work.

1.5 Structure of the Article

This article is structured as follows. In Section 2, the design and methodology of the study is outlined. Section 3 describes the results received from applying the methodology in the context described in Section 1. In Section 4, the results are analyzed and the study is concluded. The study is summarized in Section 5.

2. DESIGN OF THE STUDY

To understand the process of the creation of simulation models, the relevant data-flows and its required behavioral models need to be identified, iteratively realized, and validated in the HIL environment. This includes requirements engineering, software development using Simulink, verification, and validation.

Continuous integration and incremental development are necessary as features are realized iteratively and evolve over time. This and the multiple different variants require the software to be maintainable. Hence, these considerations shall be part of the study as well.

The process of mapping the safety-critical ECU to a simulation model for the connected HIL is studied with a strong focus on incremental realization and continuous validation. Therefore, relevant stakeholders are involved and complemented by findings from similar safety-critical systems found in literature. In addition, the influence of the safety standard ISO-26262 on the simulation model is investigated. Each step is validated in stakeholder workshops and by a second researcher, to increase its applicability in the context of the study and to ensure method and data triangulation. Existing development processes mentioned in the literature are mostly meant for creating ECU software and not their accompanying simulations (cf. Lee et al. (2014) and Köhl and Jegminat (2005)). In this study, those processes will provide considerable input, as a gap was identified in literature for processes specifically designed for the creation of ECU simulations.

A stakeholder workshop in this case means a meeting in which at least one but mostly multiple engineers come together and discuss intermediate results with one of the researchers.

Next to other less frequently involved stakeholders, seven participated repeatedly in the workshops. They are three software developers, three software testers, and one department manager. On average they have a work experience of 4.5 years in the context of model-based software engineering for the automotive industry.

3. RESULTS

The result of this study is a systematic process for creating a simulation model. It has to fulfill properties relevant for a safety-critical ECU used in connected HIL environments. All relevant stakeholders and current literature are considered. The investigations resulted in the following list of activities part of the process. The process is also summarized in Figure 2.

(1) Requirement Prioritization
    The correct features have to be selected for imple-
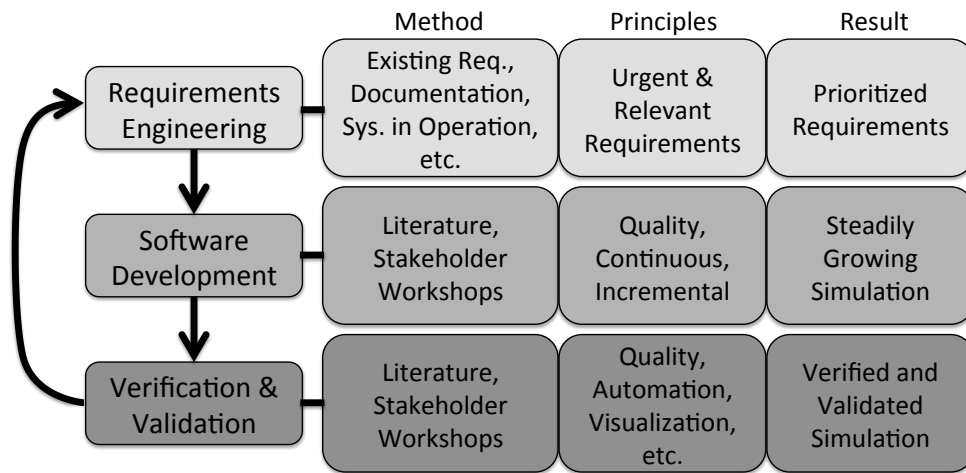
Fig. 2. Summary of the process resulting from the analysis.

mentation in the simulation. How to prioritize which feature to implement first will be decided based on:

- How relevant is a feature for the ECU in general and for the ECU in an interconnected environment?
- How urgent is the feature to be tested?

The following methodology is used in this step:

- Stakeholder interviews on best practices for feature selection and prioritization
- Stakeholder workshops to verify the lists of prioritized requirements
- System in operation analysis, in order to compare which of the requirements other simulations realize

The outcome expected from this step are:

- Validated and prioritized requirements

(2) Development of the simulation

The development process shall follow these principles:

- The process has to be continuous and incremental
- The created simulation has to follow guidelines for maintainable software, elicited from the industry's best practices and from literature

The following methodology is used in this step:

- Stakeholder interviews on best practices for the creation of simulation models and to which extend they address maintainability.
- Literature review on designing and developing model-based software for maintainability
- Validation of the applicability of the elicited approaches from industry and literature using comparison in an experiment

The outcome expected from this step are:

- An incrementally growing simulation of the ECU developed while having focus on maintainability

(3) Verification and Validation

The validation has to ensure that the implemented simulation is a plausible representation of the original ECU and thus, functional and quality requirements have to be verified. This step consists of:

- Validation and verification of both, the simulated ECU alone and in combination with other modules on a connected HIL.
- Assessment of the simulation's maintainability
- Automation of the validation process
- Visualization of results received

The following methodology is used in this step:

- Stakeholder interviews on best practices for the model validation in industry
- Literature review on software engineering approaches for the validation of simulation models and model-based software in general
- Validation of the elicited approaches in an experiment comparing expert opinion and literature
- Validation of the resulting approaches for applicability in industry in stakeholder workshops

The outcome expected from this step are:

- A verified and validated simulation model for relevant properties of the Airbag ECU.

3.1 Requirements Elicitation and Prioritization

For requirements elicitation and prioritization, techniques are used that have proven as being useful in the automotive industry, as outlined by (Schroeder et al. (2015b)). The elicitation is based on triangulation of data gathered from existing requirements, documentation, systems in operation, and from stakeholder interviews. In this case existing requirements play a major role as the real ECUs are usually specified already. These existing specifications facilitate the elicitation process. Still, as the simulations are reduced versions of them, the other sources are used as well. Additionally, the prioritization becomes important. The set of requirements the final simulation has to fulfill will be ordered by urgency and relevancy.

3.2 Development of Simulation Models

The vastly observed approach for developing simulations at the studied company comes with the nature of its structure. The department for testing ECUs in connection receives test assignments from the departments responsible for the actual ECU development.

That means, that functionality is added to the simulations as needed. Either caused by software evolution or because of extension of the test requirements. Therefore, some simulations might not be changed for months, while the ones that are part of the current test assignment might experience multiple changes. Hence, in reality the development parts of the results vary.

As in this case, the ECU simulation is not an extension of an existing one but a new development, the respective development steps have to be described as well.

3.3 Verification

Software verification can be defined as "The process of evaluating a system or component to determine whether the products of a given development phase satisfy the conditions imposed at the start of that phase." IEEE (1990)

If not done manually, testing and verification of model-based software systems is naturally based on model-based testing approaches. There is a wide range on literature regarding general approaches testing for different coverage criteria of the models. When it comes to testing of safety-relevant software, this is realized using formal methods and model checking. For example, there are methods applied in software for railway stations (cf. Cimatti et al. (1998)) or systems in the healthcare, nuclear, and military industry (cf. Bowen and Hinchey (1997)). They can be used to formally proof that the system works correctly.

Formal methods do not come without drawbacks, though. Amongst others, the literature mentions a lack of scalability, understandability and proper tools (cf. Snook and Harrison (2001); Broadfoot and Broadfoot (2003); Heitmeyer (1998)). Earlier research has started to look into these problems. In their paper, Whalen et al. (2008) analyze the integration of formal methods into the industrial context. Additionally, for simulations as mentioned in this study, which are usually realizing only parts of the functionality and proportionally smaller compared to the real ECUs, scalability issues might only apply for simulations of high complexity.

3.4 Validation

Software validation can be defined as "The process of evaluating a system or component during or at the end of the development process to determine whether it satisfies specified requirements." IEEE (1990).

The issue that the simulations implement only a subset of requirements distinguish the validation approaches from them applied to the real ECUs. It might actually occur, that next to different functional requirements also different quality are required in the simulation. Hence, the question arises, how can it be ensured, that the simulation actually reflects the reality?

In their literature study, Mohagheghi et al. (2009) found six quality requirements, which current literature presents assessment strategies for. They are correctness, completeness, consistency, comprehensibility, confinement, and changeability. As mentioned earlier, maintainability is an important attribute of the simulations studied. In a previous study it was shown that maintainability can be assessed by measuring complexity Schroeder et al. (2015a). Hence, literature provides existing approaches to support validation of model. In most cases, their applicability in industry still has to be shown.

3.5 Safety

The simulations are not going to be used in a real car. Still, to ensure that the final vehicle software fulfills the safety requirements and to increase amount of recognized safety-related issues as early as possible, it seems reasonable to apply methods common in the ECU development for the simulations, as well. Rana et al. (2014) use fault injection and mutation testing for validation and verification early in the software development life cycle. They follow the recommendation of the ISO-26262 standard. Their approach could be applied to simulations in integration testing. A mutated simulation could reveal faults in the interconnected system.

4. ANALYSIS AND CONCLUSIONS

This study presents one possible approach for development of simulations for safety-critical ECUs in the context of integration testing using hardware-in-the-loop test rigs. Analyzing the process showed that special attention has to be paid to validation and verification of simulation models as required functionality and quality might differ from the real ECU. Regarding safety, approaches from the regular ECU software development seem to be applicable for most of the verification and validation steps.

Regarding threats to validity, using findings from stakeholder workshops from a single company can bias the methodology, as those stakeholders are the ones using the current process that is thought to be improved. The workshops were necessary though, in order to ensure that the new process fits the context and the needs of the respective stakeholders. This threat of bias is mitigated by including a second independent researcher to discuss each finding received.

Generalizability is limited as stakeholder workshops have been performed in one company. According to Wieringa and Daneva (2015), it could be achieved by repeating the study using different cases in similar contexts. As no similar studies could be identified, this threat is not negligible.

5. SUMMARY AND FUTURE WORK

In this study we combined stakeholder knowledge in the automotive domain with current literature to create an approach of developing simulation models of ECUs. In order to ensure the applicability of the process, it will be validated by simulating a real ECU in the same field as part of future work.

6. ACKNOWLEDGMENTS

REFERENCES

Bowen, J. and Hinchey, M. (1997). The use of industrial-strength formal methods. In *Computer Software and Applications Conference, 1997. COMPSAC '97. Proceedings., The Twenty-First Annual International*, 332–337.

Broadfoot, G. and Broadfoot, P. (2003). Academia and industry meet: some experiences of formal methods in practice. In *Software Engineering Conference, 2003. Tenth Asia-Pacific*, 49–58.

Cimatti, A., Giunchiglia, F., Mongardi, G., Romano, D., Torielli, F., and Traverso, P. (1998). Model checking safety critical software with spin: an application to a railway interlocking system. In W. Ehrenberger (ed.), *Computer Safety, Reliability and Security*, volume 1516 of *Lecture Notes in Computer Science*, 284–293. Springer Berlin Heidelberg.

Heitmeyer, C. (1998). On the need for practical formal methods. In A. Ravn and H. Rischel (eds.), *Formal Techniques in Real-Time and Fault-Tolerant Systems*, volume 1486 of *Lecture Notes in Computer Science*, 18–26. Springer Berlin Heidelberg. URL http://dx.doi.org/10.1007/BFb0055332.

IEEE (1990). IEEE standard glossary of software engineering terminology. *IEEE Std 610.12-1990*, 1–84.

Köhl, S. and Jegminat, D. (2005). How to do hardware-in-the-loop simulation right. Technical Report SAE Technical Paper 2005-01-1657, SAE International.

Kruchten, P., Nord, R.L., and Ozkaya, I. (2012). Technical debt: From metaphor to theory and practice. *IEEE Software*, 29, 18–21.

Lee, K., Ki, Y., Cheon, J., Hwang, G., and Ahn, H. (2014). Approach to functional safety-compliant ecu design for electro-mechanical brake systems. *International Journal of Automotive Technology*, 15(2), 325–332.

Mohagheghi, P., Dehlen, V., and Neple, T. (2009). Definitions and approaches to model quality in model-based software development a review of literature. *Information and Software Technology*, 51(12), 1646 – 1669.

Rana, R., Staron, M., Berger, C., Hansson, J., Nilsson, M., and Trner, F. (2014). Early verification and validation according to iso 26262 by combining fault injection and mutation testing. In J. Cordeiro and M. van Sinderen (eds.), *Software Technologies*, volume 457 of *Communications in Computer and Information Science*, 164–179. Springer Berlin Heidelberg.

Schroeder, J., Berger, C., Herpel, T., and Staron, M. (2015a). Comparing the applicability of complexity measurements for simulink models during integration testing – an industrial case study. In *Proceedings of the 2nd International Workshop on Software Architecture and Metrics (SAM)*.

Schroeder, J., Holzner, D., Berger, C., Hoel, C.J., Laine, L., and Magnusson, A. (2015b). Design and evaluation of a customizable multi-domain reference architecture on top of product lines of self-driving heavy vehicles an industrial case study. In *Proceedings of the 37th International Conference on Software Engineering (ICSE)*.

Snook, C. and Harrison, R. (2001). Practitioners' views on the use of formal methods: an industrial survey by structured interview. *Information and Software Technology*, 43(4), 275 – 283.

Whalen, M., Cofer, D., Miller, S., Krogh, B., and Storm, W. (2008). Integration of formal analysis into a model-based software development process. In S. Leue and P. Merino (eds.), *Formal Methods for Industrial Critical Systems*, volume 4916 of *Lecture Notes in Computer Science*, 68–84. Springer Berlin Heidelberg.

Wieringa, R. and Daneva, M. (2015). Six strategies for generalizing software engineering theories. *Science of Computer Programming*, 101(0), 136 – 152.

Introduction of Intelligent Adaptive Cruise Control (i-ACC) – a predictive safety system

Marcus Kleinehagenbrock*, Morimichi Nishigaki*, Robert Kastner*, Jens Schmuedderich**, Sven Rebhan**, Thomas Weisswange**, Hiroyuki Kamiya***, Naoki Mori***, Shunsuke Kusuhara*** and Shinnosuke Ishida***

*Honda R&D Europe (Deutschland) GmbH, Offenbach/Main, Germany (e-mail: <first name>_<last name>@de.hrdeu.com)
**Honda Research Institute Europe GmbH, Offenbach/Main, Germany (e-mail: <first name>.<last name>@honda-ri.de)
***Honda R&D Co., Ltd. Automobile R&D Center, Tochigi, Japan (e-mail: <first name>_<last name>@n.t.rd.honda.co.jp)

Abstract: In 2015 Honda introduced their new intelligent Adaptive Cruise Control (i-ACC) to the market. It is the world's first cut-in prediction system which can anticipate the behavior of other vehicles in a neighboring lane. More precisely, i-ACC can predict if a vehicle is about to change lane from a neighboring lane to the lane of the own vehicle. This way, i-ACC can react earlier than conventional ACC systems and, therefore, ensure increased safety and comfort. In stereotypical situations it can even react before the other vehicle starts moving to the own lane. This means that the system sometimes starts to decelerate before the driver even realizes that a cut-in will take place. Such situations were one reason to carry out a comprehensive subjective evaluation in order to verify the acceptance of i-ACC by test subject drivers. The results of this acceptance test are our focus point in this contribution. We will also compare these results to the outcome of an objective evaluation which was carried out before.

Keywords: Driver Assistance Systems, Adaptive Cruise Control, Predictive Control System

1. INTRODUCTION

Driver assistance systems, such as autonomous emergency braking (AEB), see for example Doi et al. (1994), Fujita et al. (1995), Seiler et al. (1998); adaptive cruise control (ACC), see for example Winner et al. (1996), Haney et al. (2000), Iijima et al. (2000); and lane keeping assist (LKA), see for example Ishida et al. (2003), Mineta et al. (2003), Pohl (2003); have been gaining popularity recently. These systems support drivers to make their driving comfortable and safe in a variety of traffic situations. There are about two decades of history of those driver assist systems on the market, and they keep being improved, see Vahidi et al. (2003), van Arem et al. (2006), Vasudevan et al. (2012), Rosenfeld et al. (2015). To our knowledge, however, all of the existing driver assistance systems are still reactive systems which control the vehicle in order to adapt to the current or immediate future situation. Take AEB as an example of such reactive systems which brakes for obstacles in front of the own vehicle. It applies the brake only for cases where a collision is inevitable. In this sense it is reactive, but not proactive. ACC systems also mainly work reactively to preceding vehicles.

A conventional ACC is a comfort system for longitudinal velocity control. It keeps a velocity chosen by the driver and additionally maintains the distance to preceding vehicles. Some ACC systems on the market consider the lateral motion of preceding vehicles. However, as far as we know, for those systems the future position of a preceding vehicle is estimated by physically extrapolating its previous motion. The physical extrapolation enables a system to predict the future only for a short time around a second. Therefore, one issue on existing ACC systems is about the late reaction on a

vehicle that cuts in to the own lane from a lower-speed lane in close distance to the own vehicle. This situation often arises on highways and results in either an uncomfortable strong braking maneuver by the system or the driver braking by himself which deactivates ACC. Human drivers can usually foresee such a cut-in even before the cut-in vehicle starts moving to the own lane and prepare for it by adapting the vehicle speed. But up to now, existing systems have not been intelligent enough to do so.

For increasing safety and comfort in cut-in situations, we have researched on making ACC more intelligent. We realized this by mimicking processes of the human brain such as perception, situation understanding, judgment, and action selection (see Fig. 1).
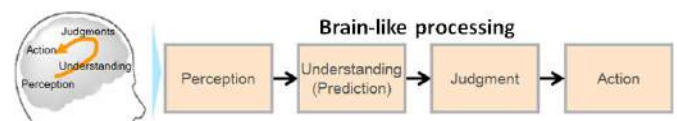
Fig. 1. Brain-like processing.

The benefit of using a general system architecture based on brain-like processing is that it reduces the effort to adapt to new situations. For example, it would be possible to update judgment and action modules to change the behavior of the own vehicle based on the existing prediction without changing perception and understanding modules. In another example, the perception module could be adapted to new sensors without changing any of the downstream modules.

This paper is organized in the following way: In section 2 we will present our processing architecture in more detail.

Section 3 focuses on the functionality, the HMI, and the limitations of i-ACC. In section 4 we will show the results of a subject test conducted with i-ACC. Section 5 then compares conventional ACC to i-ACC. Finally, section 6 concludes the paper with an outlook.

2. PROCESSING ARCHITECTURE

The actual processing architecture for i-ACC which is motivated by brain-like processing concepts is depicted in Fig. 2.

Fig. 2. Processing architecture.

The perception module applies sensor fusion for combining data provided by the monocular camera and the radar sensor of the own vehicle. Fig. 3 shows the sensor setup used by the i-ACC system. The module also applies smoothing to noisy measurements of perceived vehicles, so that they will be usable by the situation understanding module.

Fig. 3. Sensors used by i-ACC: The camera is located behind the windscreen. The radar sensor is mounted behind the grill.

Data provided by the perception module is interpreted as representation of the current traffic situation in front of the own vehicle. The situation understanding module classifies that situation into pre-defined situation models. For those models, which were designed based on expert knowledge, it is known how they will develop in the near future. This means that it can be derived from those models whether a car in a neighboring lane will cut-in to the own lane or not. We call this kind of reasoning context-based prediction. For a thorough situation prediction the context-based prediction is complemented by a physical prediction in order to increase its robustness. The physical prediction classifies the lateral motion of a preceding vehicle into models representing lane change trajectories. More details on the prediction can be found in the companion contribution by Schmuedderich et al. (2015). Finally, the results of both prediction modules are passed on to the judgment module.

The judgment module decides whether to react on a predicted cut-in or not. In certain situations it is not needed to react, for example, if the cut-in vehicle is far enough away and faster

than the own vehicle. The need to react on a potential cut-in vehicle is determined based on the distance and relative speed between the own vehicle and the cut-in vehicle, as well as on the likelihood of the cut-in. However, the distance and speed values are not only considered for the current point of time, but also for the point of time for which the cut-in is predicted to take place. If the judgment module decides to react, it also determines the deceleration rate of the ego vehicle. A combined evidence for a cut-in is calculated from the output of the context-based and physical prediction. If the evidence is below a certain threshold then only a mild declaration is activated. If the combined likelihood is above that threshold then the ego vehicle is allowed to perform a stronger deceleration.

If the judgment module decides to react on a vehicle that is predicted to cut in to the own lane then information on that cut-in vehicle and the maximum allowed deceleration rate are provided to a control module. Finally, this module executes the desired action by controlling throttle and brake of the own vehicle accordingly. The control module is basically the same as for conventional ACC.

By realizing the above processing architecture for i-ACC, we improved conventional ACC to be a proactive system for cut-in situations.

3. i-ACC FUNCTIONALITY

In this section we will explain the mode of operation, the HMI, and the limitations of i-ACC.

3.1 Mode of operation

The buttons used to operate i-ACC are located on the right side of the vehicle's steering wheel. They are the same as used for conventional ACC. The system can be activated for speeds above 30 km/h. For speeds between 30 km/h and 80 km/h, only the conventional ACC functionality is available. For speeds higher than 80 km/h, the cut-in prediction is automatically activated. The cut-in prediction is turned off again if the vehicle speed drops below 60 km/h. This minimum speed is required by the system, because the cut-in prediction is designed for highway roads which have at least two lanes. i-ACC can be deactivated at any time by pressing the brake pedal or by hitting the *Cancel* button on the steering wheel. The system can be temporarily overridden by pressing the gas pedal. The cut-in prediction is also temporarily deactivated if the driver activates a turn signal or changes the lane. A reaction to a predicted cut-in can also be aborted by shortly tipping the gas pedal. The cut-in prediction can also be permanently turned off in the vehicle settings.

If i-ACC is active then it will predict cut-ins from the slower neighboring lane. As the system is designed for European traffic and driving style, it has to behave differently for the UK and continental Europe. For the UK i-ACC has to predict cut-ins from the left neighboring lane, for continental Europe it has to predict cut-ins from the right neighboring lane (see Fig. 4).

In order for i-ACC to be able to successfully predict a cut-in, the cut-in vehicle as well as the vehicle preceding the cut-in

vehicle has to be in the field of view of the sensors. In addition to that, the cut-in vehicle has to be faster than its predecessor and slower than the own vehicle. If a cut-in is predicted, the ego vehicle decelerates at an adequate rate and informs the driver about the predicted cut-in via the HMI (see Fig. 4).

Fig. 4. Cut-in prediction: i-ACC senses all vehicles in front of the ego vehicle, informs the driver about a predicted cut-in and reacts on it.

3.2 Human-machine interface

Because i-ACC is a novel function, it should be made easy for the driver to understand it. Although the reaction of the system is designed to match with the driver's expectation, it might happen that the driver does not understand why the vehicle decelerates before the cut-in actually occurs. The best way to communicate the behavior of i-ACC would be if the function could explain itself to the driver via a human-machine interface (HMI). Another reason for introducing an HMI for i-ACC is that a driver might sometimes prefer to close the gap to a preceding vehicle instead of allowing a vehicle from the slower lane to cut-in. Therefore, i-ACC should indicate when it predicts that a vehicle is about to cut in, so that the driver could override i-ACC early and speed up by pressing the gas pedal. In another case, i-ACC might wrongly predict a cut-in and slow down the vehicle, for example, due to a wrong perception of the current situation. Also in this case i-ACC should communicate to the driver when it predicts a vehicle to cut in, so that the driver could understand that i-ACC causes the slowdown. Then the driver could again override the system early by pressing the gas pedal. It might also happen that i-ACC misses to predict a cut-in (cf. section 3.3). In such cases the system would react late, because it would then fall back to conventional ACC behavior. If i-ACC would indicate a detected cut-in via an HMI, then the absence of an indication showed to the driver that the system would not react early on the cut-in vehicle. Hence, the driver could still react early by pressing the brake pedal or the *Cancel* button and thereby deactivate i-ACC.

Based on the previous argumentation, a new visual HMI was developed for i-ACC which is depicted in Fig. 5. The HMI informs the status of the cut-in prediction to the driver through a display in the instrument cluster. Basically, the conventional ACC view was extended by an icon that is shown if i-ACC predicts a cut-in. This way, the driver can

recognize that the system is causing a deceleration, because it assumes that a vehicle from the slower lane is about to cut in to the own lane. As a result, the new HMI allows every person driving the vehicle to understand how i-ACC works.

Fig. 5. Display in the cluster instrument showing the cut-in icon on the right side.

3.3 Limitations

i-ACC is designed to adapt to cut-in situations, but not to all. As described in Section 3.1, certain conditions must be met for the system to predict a cut-in. Therefore, the system is limited to react on specific, foreseeable cut-in situations from the slower neighboring lane, where a certain relation between the potential cut-in vehicle, its predecessor, and the own vehicle exists. In more detail, the following situations are not addressed by the cut-in prediction: Cut-ins from acceleration lanes at highway entrances; cut-ins from vehicles that do not drive faster than their predecessor; and cut-ins in construction sites.

Cut-ins from acceleration lanes at highway entrance cannot be predicted by i-ACC, because in this case the cut-in vehicle usually does not have a predecessor. The predecessor needs to be detected in order to predict a cut-in, because the end of the acceleration lane cannot be detected by the system. Cut-ins from vehicles that do not drive faster than their predecessor are usually not even foreseeable for human drivers. Therefore, also i-ACC cannot predict them. Cut-ins in construction sites can only be predicted in rare cases. Usually the differences in speed between cut-in vehicle, its predecessor, and the own vehicle do not match those for typical cut-in situations. Also, the reduced width of lanes in construction sites makes it difficult to predict the intention of a cut-in. Moreover, as already mentioned, i-ACC is adapted to European traffic and driving style. This means that i-ACC would show a reduced performance in countries outside of Europe.

As mentioned before, i-ACC only reacts to cut-ins from the slower neighboring lane if certain relations between the own vehicle, the cut-in vehicle, and its predecessor exist. These requirements must not be understood as limitations. We found out that, for example, a reaction to a cut-in from the faster neighboring lane is counterproductive, because the cut-in vehicle is usually faster than the own vehicle. Therefore, such situations resolve by itself to a high extend without any intervention by i-ACC. Similarly, a cut-in from the slower neighboring lane is ignored if the cut-in vehicle is faster than the own vehicle.

As indicated in Sections 3.2 and 3.3, the reaction of i-ACC might not always be understood by the driver. Moreover, the system's perception and prediction modules have to deal with uncertainties, so that even not all targeted cut-in situations will always be predicted correctly. Due to said limitations of the system and uncertainties in data processing, the question arose, whether i-ACC would be accepted by the customer. In order to answer this question, we performed a subject test for evaluating the acceptance of the newly developed function.

4. SUBJECTIVE EVALUATION

A subject test was conducted were each subject had to drive with i-ACC for about one hour on different highways. Subjects which did not know Honda's conventional ACC beforehand were asked to test it first, so all subjects had (at least a little) experience with ACC. Also, only subjects were chosen that had a certain level of driver training due to the prototype status of the test vehicle. The test drives were mostly done in light traffic. The weather was mostly sunny; there were just a few rainy days. A supervisor attended the test drives in order to instruct the subjects in i-ACC, ask questions to the subjects, and fill out a driving log. After each test drive the subject was asked to fill out a questionnaire.

4.1 Questions answered while test driving

While driving with i-ACC, the subjects were asked to tell the supervisor each time they notice one of the following conditions:

- i-ACC reacted early on a predicted cut-in (= True Positive reaction, TP)

- i-ACC missed to predict a cut-in and the subject considered a reaction necessary. The cut-in was in sensor range (= False Negative reaction, FN)

- i-ACC predicted a cut-in that did not occur. The cause was a wrong prediction by i-ACC (= False Positive reaction, FP)

When a subject noticed a TP, they were asked two questions: "How appropriate was the applied braking force?" and "How appropriate was the braking timing?" The answers were scaled according to the Likert scale, see Likert (1932). The distribution of the answers can be seen in Fig. 6 and Fig. 7, respectively. As a result, the braking force applied by i-ACC seems to be well adjusted and the braking timing seems to be appropriate.
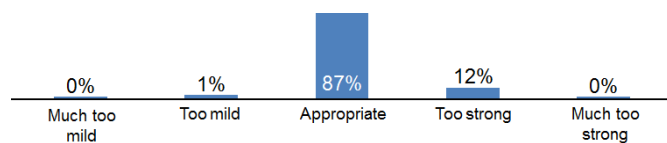
Fig 6. Event: Subject noticed that i-ACC reacted early on a predicted cut-in. Answers to question: "How appropriate was the applied braking force?"
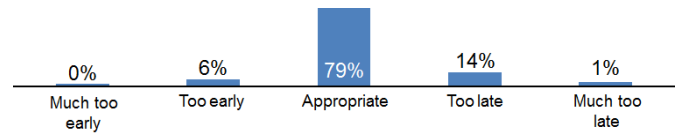
Fig 7. Event: Subject noticed that i-ACC reacted early on a predicted cut-in. Answers to question: "How appropriate was the braking timing?"

When a subject noticed an FN, they were asked the following question: "Was the miss acceptable or not?" The meaning of "acceptable" was defined in the following way: A failure is *not* acceptable if the failure is a reason to switch off i-ACC permanently. The answers were scaled according to the Guttman scale, see Guttman (1950). The distribution of the answers can be seen in Fig. 8. As a result, all missed cut-ins were accepted due to the benefit of i-ACC.

Fig 8. Event: Subject noticed that i-ACC missed to predict a cut-in and considered a reaction necessary. The cut-in was in sensor range. Answers to question: "Was the miss acceptable or not?"

When subjects noticed an FP, they were asked the following question: "Was the reaction acceptable or not?" The meaning of "acceptable" was again defined in the following way: A failure is *not* acceptable if the failure is a reason to switch off i-ACC permanently. The answers were scaled according to the Guttman scale. The distribution of the answers can be seen in Fig. 9. As a result, all reactions on non-occurring cut-ins were accepted due to the benefit of i-ACC. Some reactions on FP predictions were even considered as good. For example, two comments that were made were: "I also expected a cut-in and would have braked too!" and "Ah, the system plays safe. Good!"

Fig 9. Event: Subject noticed that i-ACC predicted a cut-in that did not occur. The cause was a misprediction by i-ACC. Answers to question: "Was the reaction acceptable or not?"

From the answers given during the test drives, the prediction hit rate (TPs / TPs + FNs) and the false activation rate (FPs / FPs + TPs) were calculated. These rates were compared to corresponding objective measures that were calculated from recorded data based on predefined criteria. The distribution of the rates is depicted in Fig. 10. As a result, subjects estimated the performance of i-ACC to be higher than the objective measures. The main reason for this is, that some false reactions were so mild or short that they were not noticed and some false reactions were comprehensible for the subjects.
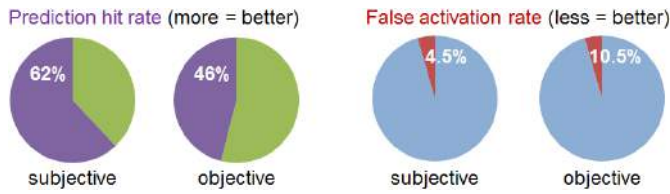
Fig 10. Comparison of subjective and objective prediction hit rates and the false activation rates.

4.2 Questionnaire answered after test driving

After their test drives the subjects were asked to fill out a questionnaire which contained seven statements and three questions. The seven statements and the first question were scaled according to the Likert scale. The answers to the last two questions were used to evaluate the attractiveness of the i-ACC function according to the Kano model, see Kano *et al.* (1984). The statements were:

- i-ACC is a useful function.

- I want to have i-ACC for my vehicle.

- i-ACC increases the safety of a vehicle.

- i-ACC helps me while driving.

- I am pleased if i-ACC reacts early on a predicted cut-in.

- I am annoyed if i-ACC misses to predict a cut-in.

- I am annoyed if i-ACC predicts a cut-in that does not occur.

The distribution of the rating for each statement can be seen in Fig. 11 to Fig. 17, respectively.
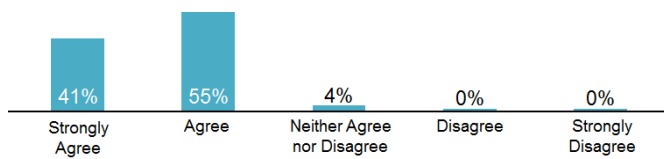
Fig 11. Rating of statement: "i-ACC is a useful function."
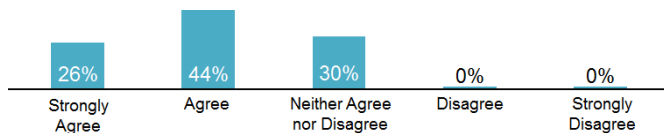
Fig 12. Rating of statement: "I want to have i-ACC for my vehicle."

The responses to the seven statements show that i-ACC is seen as a useful, desired, safety-increasing, and helpful function. All false reactions (FNs and FPs) by i-ACC are seen as acceptable, so subjects allow/accept mispredictions.
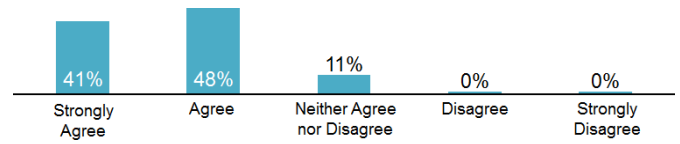
Fig 13. Rating of statement: "i-ACC increases the safety of a vehicle."
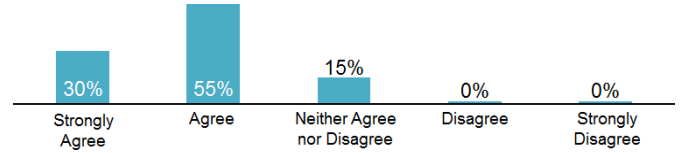
Fig 14. Rating of statement: "i-ACC helps me while driving."
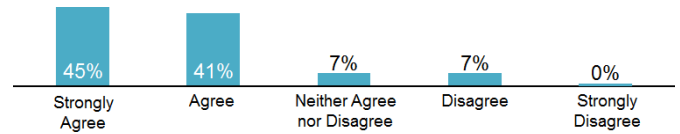
Fig 15. Rating of statement: "I am pleased if i-ACC reacts early on a predicted cut-in."
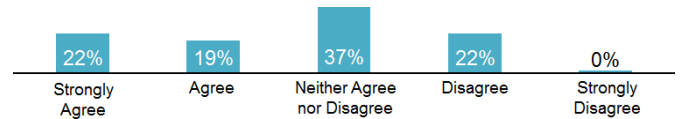
Fig 16. Rating of statement: "I am annoyed if i-ACC misses to predict a cut-in."
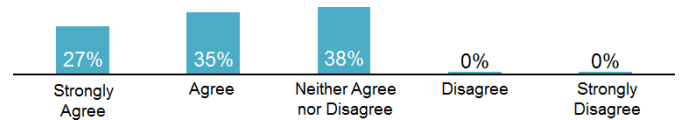
Fig 17. Rating of statement: "I am annoyed if i-ACC predicts a cut-in that does not occur."

The question which was scaled according to the Likert scale was: "How appropriate was the cut-in icon display duration?" The distribution of the answers to that question can be seen in Fig. 18. As a result, the cut-in icon display duration is acceptable but could be a bit longer. As a countermeasure the minimum display duration was increased after the subject test.
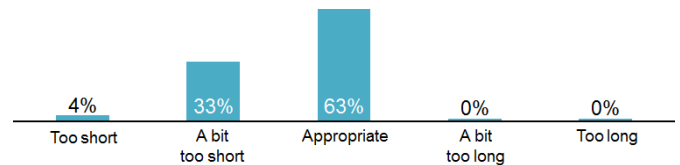
Fig 18. Answers to question: "How appropriate was the cut-in icon display duration?"

The two questions which were used to evaluate the attractiveness of i-ACC were: "How would you feel if your vehicle *had* i-ACC?" and "How would you feel if your

vehicle *did not have* i-ACC?" The answers to these two questions were evaluated and the corresponding responses calculated. The responses were depicted in a spider diagram and can be seen in Fig. 19. As a result, according to Kano's customer satisfaction model, i-ACC is seen as an attractive function.
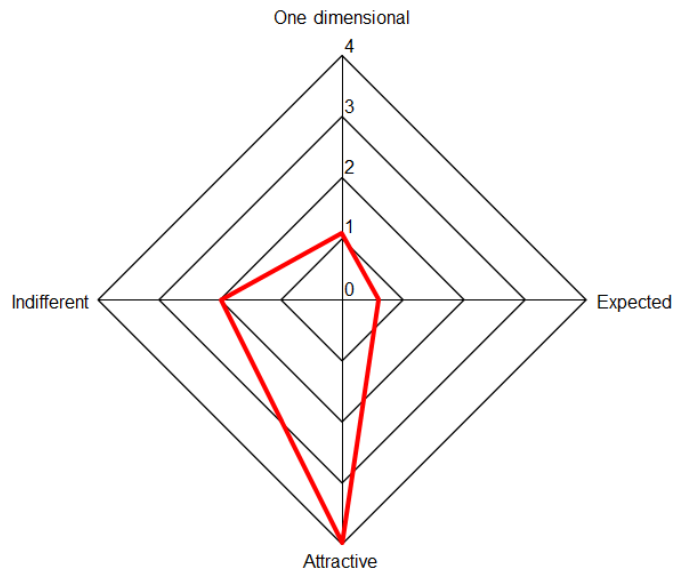
Fig 19. Responses on attractiveness of i-ACC, normalized to [0, 4].

All in all, the results of the subjective evaluation show that the quality of the i-ACC function is high. The benefit of the system is well understood and the performance is accepted by the test subjects to a large extend.

5. COMPARISON OF CONVENTIONAL ACC TO i-ACC

In cut-in situations, conventional ACC usually estimates if and when a vehicle on a neighboring lane might change lane to the own lane based on physical extrapolation. This means that those systems estimate the future position of a potential cut-in vehicle (for example, vehicle A in Fig.20a) from its current motion. In more detail, the future position of the cut-in vehicle is estimated from its current direction, current speed, and current acceleration. Consequently, a cut-in can only be detected *after* the cut-in vehicle started to change the lane. Vehicles preceding the cut-in vehicle (for example, vehicle B in Fig. 20a) are not considered for the cut-in detection.

In contrast to conventional ACC, i-ACC applies situation understanding and situation prediction in order to determine if a vehicle on a neighboring lane will cut in to the own lane. This means that i-ACC estimates the future position of a potential cut-in vehicle (for example, vehicle A in Fig.20b) from anticipating the behavior of other drivers. In order to predict the behavior of a potential cut-in vehicle, certain relations between all relevant vehicles (for example, all vehicles in Fig. 20b) have to be considered, such as the time gaps. Additionally, the occupancy of lanes is taken into account. All this information is evaluated all the time and not just when the cut-in vehicle starts to change the lane to the

own lane. Therefore, i-ACC can predict a lane change *before* the cut-in vehicle actually starts with a lateral motion.
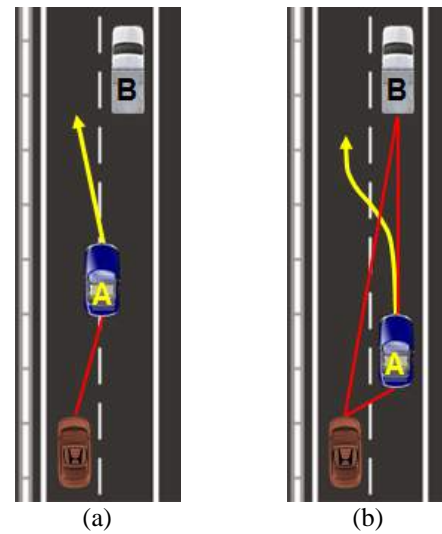
Fig. 20. (a) Conventional ACC is usually limited to physical extrapolation; (b) i-ACC performs behavior anticipation by analyzing vehicle relations. The red lines indicate the vehicle relations considered by the corresponding system; the yellow lines illustrate the estimated trajectory.

As a result of the function design, i-ACC has a much larger prediction horizon than conventional ACC which can only detect cut-ins based on physical extrapolation. Due to the larger prediction horizon, i-ACC can perform at a level comparable to human drivers which can often foresee certain cut-in types. For these typical cut-in situations, the system can predict a cut-in up to five seconds before it takes place and, therefore, react even before the cut-in vehicle starts moving to the ego lane (see Fig. 21). Because i-ACC can react much faster than conventional ACC, the system can also maintain a safety margin to cut-in vehicles more easily. Also, because the system has more time to adapt the vehicle speed to the cut-in vehicle, the deceleration profile can be made smoother than for conventional ACC which increases the comfort of the vehicle control. Another benefit is that the average vehicle speed for i-ACC is higher than for conventional ACC which has positive effects on the vehicle's fuel consumption.
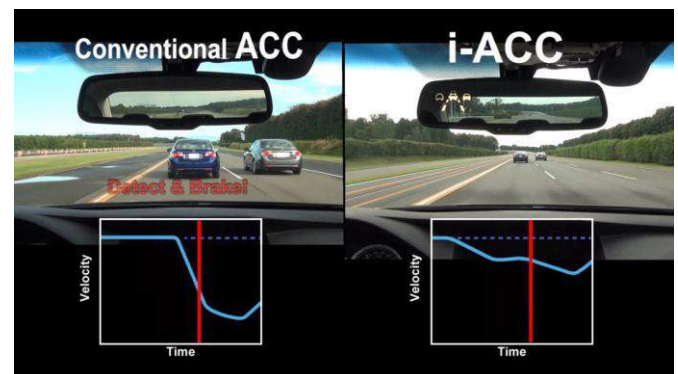
Fig 21. Comparison: i-ACC reacts up to 5 seconds earlier than conventional ACC.

6. SUMMARY AND OUTLOOK

Our newly developed prediction technology was introduced to the market together with i-ACC as a first step towards proactive systems. The benefit of situation prediction was confirmed by conducting a subjective evaluation of i-ACC. We aim to further improve our prediction technology and apply it to other types of advanced driver assistance systems as well. Prediction allows us to make existing functions smarter and to develop new kinds of functions. We are convinced that this technology is a significant step forward towards automated driving.

REFERENCES

Doi, A., Butsuen, T., Niibe, T., Yakagi, T., Yamamoto, Y., and Seni, H. (1994). Development of a Rear-End Collision Avoidance System with Automatic Braking Control. *JSAE Review*, 15(4), 335–340.

Fujita, Y., Akuzawa, K., and Sato. M. (1995). Radar Brake System. *Proceedings of the 1995 Annual Meeting of ITS America*, 1, 95–101.

Guttman, L. (1950). The basis for scalogram analysis. In Stouffer et al. (ed.), *Measurement and Prediction. The American Soldier Vol. IV*. New York: Wiley.

Haney, P.R. and Richardson, M.J. (2000). Adaptive Cruise Control, System Optimisation and Development for Motor Vehicles. *Journal of Navigation*, 53(1), 42–47.

Iijima, T., Higashimata, A., Tange, S., Mizoguchi, K., Kamiyama, H., Iwasaki, K., and Egawa, K. (2000). Development of an Adaptive Cruise Control System with Brake Actuation. *SAE Technical Paper Series*, Paper No. 2000-01-1353.

Ishida, S., Tanaka, J., Kondo, S., and Shingyoji, M. (2003). Development of a Driver Assistance System. *SAE Technical Paper Series*, Paper No. 2003-01-0279.

Kano, N., Seraku, N, Takahashi, F., and Tsuji, S. (1984). Attractive quality and must-be quality. *Journal of the Japanese Society for Quality Control* (in Japanese), 14 (2), 39–48.

Likert, R. (1932). A Technique for the Measurement of Attitudes. *Archives of Psychology,* 140, 1–55.

Mineta, K., Unoura, K., and Ikeda, T. (2003). Development of a Lane Mark Recognition System for a Lane Keeping Assist System. *Intelligent Vehicle Initiative,* 39–48. Society of Automotive Engineers, Warrendale, PA.

Pohl, J. and Ekmark, J. (2003). Development of a Haptic Intervention System for Unintended Lane Departure. *SAE Technical Paper Series*, Paper No. 2003-01-0282.

Rosenfeld, A., Bareket, Z., Goldman, C.V., LeBlanc, D.J., and Tsimhoni, O. (2015). Learning Drivers' Behavior to Improve Adaptive Cruise Control. *Journal of Intelligent Transportation Systems*, 19 (1), 18–31.

Schmuedderich, J., Rebhan, S., Weisswange, T., Kleinehagenbrock, M., Kastner, R., Nishigaki, M., Kamiya, H., Mori, N., Kusuhara, S., and Ishida, S. (2015). A novel approach to driver behavior prediction using scene context and physical evidence for intelligent Adaptive Cruise Control (i-ACC). *Proceedings of the 3rd International Symposium on Future Active Safety Technology Towards zero traffic accidents*.

Seiler, P., Song, B., and Hedrick, J.K. (1998). Development of a Collision Avoidance System. *Automotive Engineering International*, 106(9), 24–28.

Vahidi, A. and Eskandarian, A. (2003). Research advances in intelligent collision avoidance and adaptive cruise control. *IEEE Transactions on Intelligent Transportation Systems*, 4(3), 143–153.

van Arem, B., van Driel, C.J.G., and Visser, R. (2006). The Impact of Cooperative Adaptive Cruise Control on Traffic-Flow Characteristics. *IEEE Transactions on Intelligent Transportation Systems*, 7(4), 429–436.

Vasudevan, S., Vasudevan, S.K., and Arumugam, B. (2012). *Design of Adaptive Cruise Controller: With Stop & Go Scenarios.* LAP Lambert Academic Publishing, Germany.

Winner, H., Witte, S., Uhler, W., and Lichtenberg, B. (1996). Adaptive Cruise Control System Aspects and Development Trends. *SAE Technical Paper Series*, Paper No. 961010.

High-level Automated Driving on Complex Urban Roads with LiDAR, Vision, and GPS/map based Environment Representation

Beomjun Kim. Dongwook Kim, Junyung Lee, Kyuwon Kim
Kyongsu Yi ***

* Department of Mechanical and Aerospace Engineering, Seoul National University, 301-dong 113-ho, Gwanak-ro 1, Gwanak-gu, Seoul, Korea (Tel: 82-2-880-1941; e-mail: kyi@snu.ac.kr).

Abstract: This paper proposes a fully automated driving algorithm which is capable of automated driving on urban roads with guaranteed safety. The proposed algorithm consists of the following three steps: an environment representation, a motion planning, and a vehicle control. An environment representation system consists of three main modules: object classification, vehicle/non-vehicle tracking and map/lane based localization. A motion planning modules derives an optimal trajectory as a function of time, from the environment representation results. A safety envelope definition module determines the complete driving corridor that leads to the destination while assigning all objects to either the left or right corridor bound. In the case of moving objects such as other traffic participants, their behaviors are anticipated in the near future. An optimal trajectory planner uses the safety envelop as a constraint and computes a trajectory that the vehicle stays in its bounds. The vehicle control module feeds back the pose estimate of the localization module to guide the vehicle along the planned trajectory. The effectiveness of the proposed automated driving algorithm is evaluated via vehicle tests. Test results show the robust performance on an inner-city street scenario.

Keywords: autonomous vehicles, environment representation.

1. INTRODUCTION

Recently, the interest of automotive researches changes from the passive safety system to the active safety system and, by extension, automated driving system due to advances in sensing technologies. For example, active safety applications, such as vehicle stability control (VSC), adaptive cruise control (ACC), lane keeping assistance (LKA) and lane change assistance (LCA) system), automated parking assist system (APA) and blind spot intervention (BSI), already have been commercialized by major automakers (Enache et al., 2010, Hoedemaeker and Brookhuis, 1998, O'Malley et al., 2010, Yoon et al., 2007, Jung et al., 2006).

Furthermore, there are various ongoing projects which are trying to achieve the zero fatality. There is an ongoing project called 'Vision Zero' in Sweden of which objective is to reduce fatalities to zero by 2020 (Tingvall and Haworth, 2000). The research initiative PReVENT is one step closer to market-ready automated vehicles. In this project low-cost sensors such as cameras or radio-based car to car communication were used (Schulze et al., 2005).

And some of major automakers have been researching to integrate individual active safety system for the enhancement of safety. GM is trying to develop and introduce 'Super Cruise' system which can drive on the highway without human driver's intervention. In this system, adaptive cruise control technology and active lane keeping control technology would be combined. Toyota has undertaken researches to develop 'Automatic Highway Driving Assist' technology. The objective of this system is to maintain safety

of the subject vehicle and reduce fatigue on the driver. This system is developed by integrating cooperative adaptive cruise control technology, which communicates with surrounding vehicles wirelessly, and lane trace control technology. And the Mercedes Benz developed 'Intelligent Drive' system and followed the route from Mannheim to Pforzheim, Germany, in fully autonomous manner (Ziegler et al., 2014)

From a considerable amount of literature, automated driving technology has the potential to reduce the environmental impact of driving, reduce traffic jams, and increase the safety of motor vehicle travel. However, the current state-of-the-art in automated vehicle technology requires precise, expensive sensors such as differential global positioning systems, and highly accurate inertial navigation systems and scanning laser rangefinders. While the cost of these sensors is going down, integrating them into cars will increase the price and represent yet another barrier to adoption (Furgale et al., 2013).

Therefore, in this research, we focus on developing a fully automated driving algorithm which is capable of automated driving in complex scenarios while a chosen sensor configuration is closer to current automotive serial production in terms of cost and technical maturity than in many autonomous vehicles presented earlier.

Mainly three research issues are considered: an environment representation, a motion planning, and a vehicle control. The system architecture of the algorithm is outlined in Fig.1. The environment representation system consists of three main modules: object classification, vehicle/non-vehicle tracking
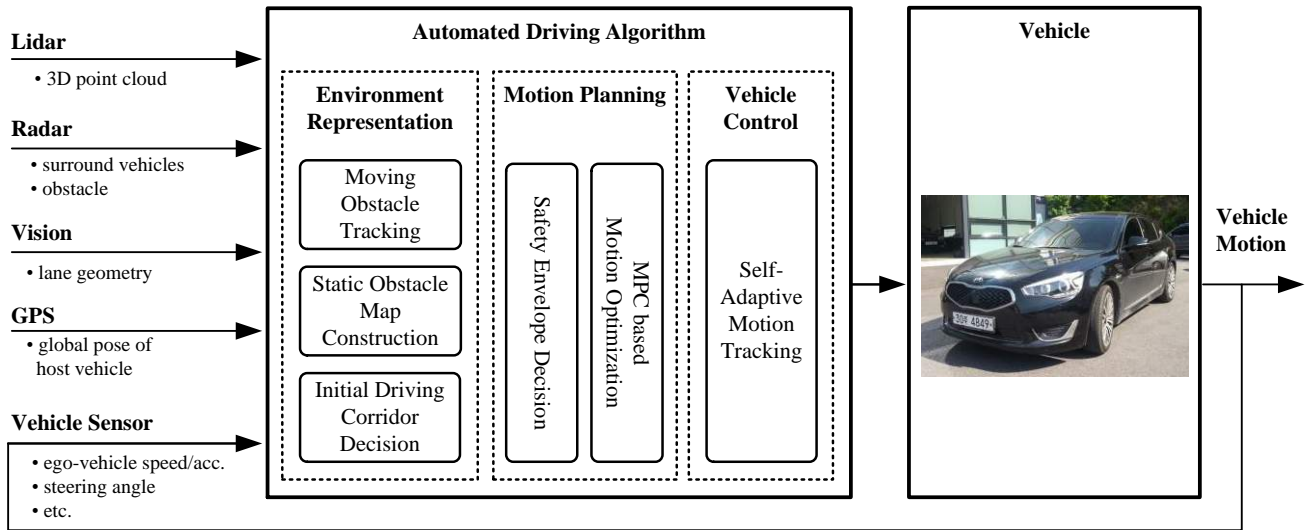
Fig.1. System overview of the proposed automated driving system. The proposed algorithm consists of the following three steps: an environment representation, a motion planning, and a vehicle control.

and map/lane based localization. All system modules make use of information from equipped various sensors. The main sensing components are a vision, radars and vehicle sensors. The chosen sensor configuration is closer to current automotive serial production in terms of cost and technical maturity than in many autonomous robots presented earlier. The objective of the motion planning modules is to derive an optimal trajectory as a function of time, from the environment representation results. A safety envelope definition module determines the complete driving corridor that leads to the destination while assigning all objects to either the left or right corridor bound. In the case of moving objects such as other traffic participants, their behaviors are anticipated in the near future. An optimal trajectory planner uses the safety envelop as a constraint and computes a trajectory that the vehicle stays in its bounds. The vehicle control module feeds back the pose estimate of the localization module to guide the vehicle along the planned trajectory.

In the remainder of this paper, we will provide an overview of the overall architecture of the proposed automated driving control algorithm and the experimental results which shown the effectiveness of the proposed automated driving algorithm.Environment Representation

Precise and comprehensive environment perception is the basis for safe and comfortable autonomous driving in complex traffic situations such as busy cities (Ziegler et al., 2014). We modified the serial-production sensor setup already available in our test vehicles as follows: A multilayer laser scanner was added for monitoring static obstacles with increased precision. For lane detection, an additional monocular vision system was mounted on the windshield. And a low-cost-GPS was equipped for a rough-precision ego-localization which is used for initial corridor decision. The complete sensor setup is shown in Fig.2. Depicted in yellow is a monocular vision system for lane detection. Front radar system is depicted in blue and two rear-side radars are depicted in green. A multilayer laser scanner for obstacle

monitoring is shown in red and low-cost GPS is depicted in purple signal. The main objectives of these sensors are lane-level localization, static/moving obstacle detection, and drivable area representation for safe and comfortable autonomous driving.
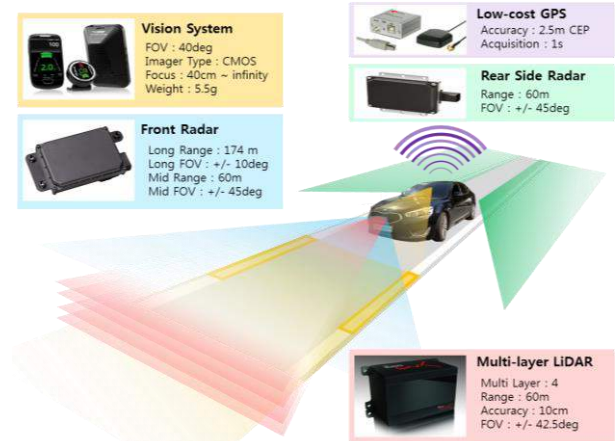
Fig.2. The experimental vehicle and its sensor-setup.

2.1. *Initial Driving Corridor Decision*

An initial driving corridor is determined from detected lanes, rough-precision localization, and digital map which is stored in advance. The map contains properties of the environment that are necessary for driving, but cannot be reliably detected by sensors such as road width, and global waypoint of centerline of total route.

The rough-precision localization is accomplished with ego chassis sensor signals and low-cost GPS. The state vector for localization are defined as follows:

$$\mathbf{x} = \begin{bmatrix} p_x & p_y & \psi & v_x & \gamma & a_x \end{bmatrix}^T \tag{1}$$

where, subscript x and y denote x-axis and y-axis of each frame, p denotes the relative position θ denotes the relative yaw angle, v denotes the velocity, γ denotes the yaw rate, and a denotes the acceleration. The process model is discretized based on no-slip assumption as follows:

$$\begin{aligned}\mathbf{x}[k] &= \mathbf{f}\left(\mathbf{x}[k-1]\right) + \mathbf{w}[k] \\ &= \mathbf{x}[k-1] + \Delta T \cdot \left(\mathbf{a}\left(\mathbf{x}[k-1]\right)\right) + \mathbf{w}[k]\end{aligned} \tag{2}$$

where,

$$\mathbf{a}_1 = v_x \cos\psi \quad \mathbf{a}_2 = v_x \sin\psi \quad \mathbf{a}_3 = \gamma \quad \mathbf{a}_4 = a_x \quad \mathbf{a}_5 = 0 \quad \mathbf{a}_6 = 0$$
$$\mathbf{w}[k] \sim \left(\mathbf{0}, \mathbf{W}[k]\right)$$

where, $\mathbf{a}$ is the nonlinear process vector equation, and $\mathbf{w}$ is the process noise vector which is the white noise of covariance $\mathbf{W}$. The measurement model for the dead-reckoning is derived as follows:

$$\mathbf{z}_{DR}[k] = \mathbf{h}_{DR}\left(\mathbf{x}[k]\right) + \mathbf{v}_{DR}[k] \tag{3}$$

where,

$$\mathbf{h}_{DR,1} = v_x - \frac{w}{2}\cdot\gamma \qquad \mathbf{h}_{DR,2} = v_x + \frac{w}{2}\cdot\gamma \qquad \mathbf{h}_{DR,5} = \gamma \quad \mathbf{h}_{DR,6} = a_x$$

$$\mathbf{h}_{DR,3} = \begin{pmatrix}\cos\delta\left(v_x - \frac{w}{2}\cdot\gamma\right) \\ +\sin\delta\left(l\cdot\gamma\right)\end{pmatrix} \qquad \mathbf{h}_{DR,4} = \begin{pmatrix}\cos\delta\left(v_x + \frac{w}{2}\cdot\gamma\right) \\ +\sin\delta\left(l\cdot\gamma\right)\end{pmatrix}$$

$$\mathbf{v}_{DR}[k] \sim \left(0, \mathbf{V}_{DR}[k]\right)$$

where, $\mathbf{h}$ is nonlinear measurement vector where the elements are rear-left wheel speed, rear-left wheel speed, front-left wheel speed, front-right wheel speed, yaw rate, and longitudinal acceleration in numeric order. When the GPS is updated, an augmented measurement model is modified as follows:

$$\begin{aligned}\mathbf{z}_{+GPS}[k] &= \mathbf{h}_{+GPS}\left(\mathbf{x}[k]\right) + \mathbf{v}_{+GPS}[k] \\ &= \left[\mathbf{h}_{DR}\left(\mathbf{x}[k]\right) \quad \mathbf{h}_{+GPS,7} \quad \mathbf{h}_{+GPS,8} \quad \mathbf{h}_{+GPS,9}\right]^T + \mathbf{v}_{+GPS}[k]\end{aligned} \tag{4}$$

where,

$$\mathbf{h}_{+GPS,7} = p_x \qquad \mathbf{h}_{+GPS,8} = p_y \qquad \mathbf{h}_{+GPS,9} = \psi$$

$$\mathbf{v}_{+GPS}[k] \sim \left(0, \begin{bmatrix}\mathbf{V}_{+DR}[k] & 0 \\ 0 & \mathbf{V}_{+GPS}[k]\end{bmatrix}\right)$$

From the global pose estimate of the ego vehicle, a nearest segment is selected from the map and transformed to local coordinate. From the detected lane information, distances and angle deviation between the vehicle's pose and the centerline of the local segment are updated with improved accuracy.

It is common practice to describe the forward road geometry by a 2nd-order polynomial (Swartz, 2003). The relation between the host vehicle and the road center line can be described by two factors: the relative lateral position and the relative heading angle. With these two factors, the road geometry, which has a curvature radius R, can be approximated by (Swartz, 2003):

$$\begin{aligned}y_r(x) &= \frac{1}{2R}x^2 - \tan e_\theta \cdot x - e_y \\ &= a_2\cdot x^2 + a_1\cdot x + a_0\end{aligned} \tag{5}$$

Where x is the down-range distance, and y_r is the lateral position of the corresponding road center in the current body coordinates. As a result, the estimate of the initial driving corridor coefficients is recursively estimated using the Kalman filter (RE, 1960). Both detected lane and selected local segment are used for measurement update. Note that the covariance of the measurement noise should be well defined so that it can represent each of two errors: the localization error and lane detection error.

(a) Nearest segment selection

(b) Lane detection

(c) Segment transformation to local coordinate

(d) Lane-level segment matching
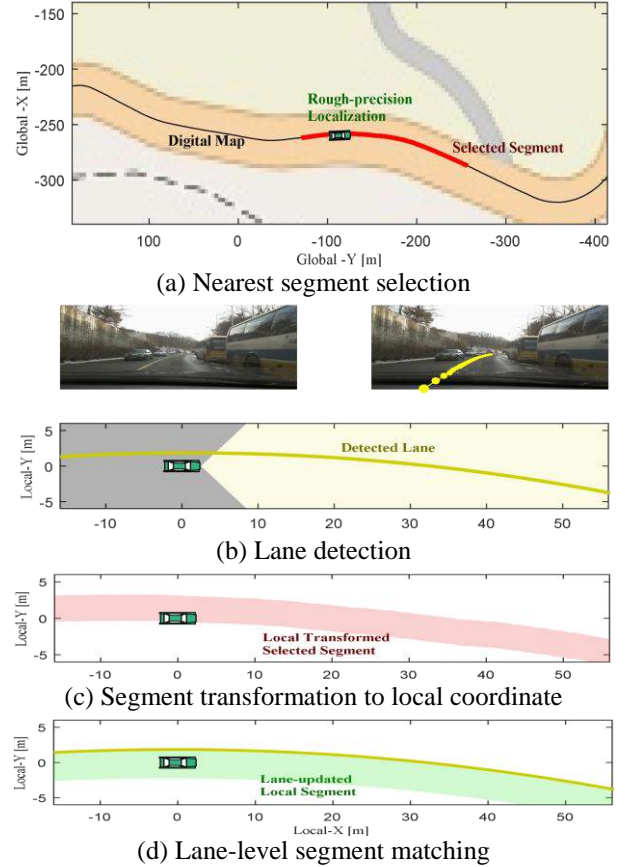
Fig.3. Sequences of initial driving corridor decision.

Fig.3 shows an example of sequence of initial driving corridor decision. Fig.3-(a) shows a nearest segment selection from the map data. Digital map is depicted as black line, rough-precision global pose estimate result is depicted as green vehicle, and the selected nearest segment is depicted as red-thick line. Fig.3-(b) shows a lane detection results. From the figure, we can see that yellow centerline is detected. Fig.3-(c) shows transformed segment to local coordinate. Due to the error of the global pose estimate, it seems that the ego-vehicle deviated from the lane (actually not). Fig.3-(d) shows lane-level segment matching result. Because the locally transformed segment is updated with the detected lane, the updated local segment has more improved accuracy.

2.2. Moving Object Tracking and Prediction

One important factor in autonomous driving in rural roads is all-around monitoring for other traffics. One long-range radar (front) and a set of three mid-range radars (front, rear-left, and rear-right) were selected to fulfil these perception tasks.

The reliable detection and tracking of other traffics like preceding vehicle and oncoming vehicle is one of the most important tasks. And another essential task is to estimate and predict the target vehicles' overall behaviors such as heading, yaw rate, absolute velocity and acceleration as well as relative position and relative velocity.

To achieve these tasks, an interacting multiple model (Furgale et al.) approach using extended Kalman filters (EKF) was employed to improve multi-target states estimation performance.

Various driving patterns of a vehicle including straight line, curve, cut-in/out, U-turn and interchange can be represented by a combination of a constant velocity rectilinear motion, a constant acceleration rectilinear motion, a constant angular velocity curvilinear motion and a constant angular acceleration curvilinear motion. To describe all these motions, the state vector and input vector of target n are defined as follows:

$$\mathbf{x}_n = \begin{bmatrix} p_{n,x} & p_{n,y} & \theta_n & v_{n,x} & \gamma_n & a_{n,x} & \dot{\gamma}_n \end{bmatrix}^T \tag{6}$$

$$\mathbf{u} = \begin{bmatrix} v_x & \gamma \end{bmatrix}^T \tag{7}$$

where subscript x and y denote x-axis and y-axis of each frame, subscript n denotes "of target n ", p denotes the relative position θ denotes the relative yaw angle, v denotes the velocity, γ denotes the yaw rate, a denotes the acceleration, and $\dot{\gamma}$ denotes the yaw acceleration. And variable without subscript n means "variable of the host vehicle". Therefore v_x denotes the longitudinal velocity of host vehicle and γ denotes the yaw rate of host vehicle. Note that $p_{n,x}$, $p_{n,y}$ and θ_n are defined on the host vehicle's body-fixed moving frame, and other elements are defined on the ground-based fixed frame.

In an automotive target tracking, changes in the target aspect with respect to the radar can cause the apparent point of radar reflections (relative position seen by the antenna) to wander significantly. To represent these characteristics, the measurement model can be elaborated by introducing new parameters to specify the sensor position and the measured point. As the result, the measurement vector of target n is defined as follows.

$$\mathbf{z}_n[k] = \mathbf{h}(\mathbf{x}_n[k], \mathbf{u}[k]) + \mathbf{v}_n[k]$$
$$= \begin{bmatrix} \mathbf{h}_{n1} & \mathbf{h}_{n2} & \mathbf{h}_{n3} \end{bmatrix}^T + \mathbf{v}_n[k] \tag{8}$$
$$\mathbf{v}_n[k] \sim (0, \mathbf{V}_n[k])$$

where,

$$\mathbf{h}_{n1} = p_{n,x} - s_x + b_{n,x} \cos\theta_n - b_{n,y} \sin\theta_n$$

$$\mathbf{h}_{n2} = p_{n,y} - s_y + b_{n,x} \sin\theta_n + b_{n,y} \cos\theta_n$$

$$\mathbf{h}_{n3} = v_{n,x} \cos\theta_n - v_x + p_{n,y} \cdot \gamma + (b_{n,x} \sin\theta_n + b_{n,y} \cos\theta_n)(\gamma - \gamma_n)$$

where $\mathbf{h}$ is nonlinear measurement equation which describe the state of measured point on the sensor based moving frame. $\mathbf{s}$ is sensor position vector defined on the host vehicle's body-fixed moving frame and $\mathbf{b}_n$ is measured point vector of target n defined on the target vehicle's body-fixed moving frame. The first order approximation of the measurement error covariance has been presented in previous works as follows:

$$\mathbf{V}_n = \begin{bmatrix} \dfrac{\sigma_r^2 - r_n^2 \sigma_\theta^2}{2} \begin{bmatrix} b_n + \cos 2\theta_n & \sin 2\theta_n \\ \sin 2\theta_n & b_n - \cos 2\theta_n \end{bmatrix} & \mathbf{0}_{2\times 1} \\ \mathbf{0}_{1\times 2} & \sigma_v^2 \end{bmatrix} \tag{9}$$

where,

$$b_n = \frac{\sigma_r^2 + r_n^2 \sigma_\theta^2}{\sigma_r^2 - r_n^2 \sigma_\theta^2} \quad r_n = \sqrt{\mathbf{h}_{n1}^2 + \mathbf{h}_{n2}^2} \quad \theta_n = \tan^{-1}\left(\frac{\mathbf{h}_{n2}}{\mathbf{h}_{n1}}\right)$$

where, r_n and θ_n are the range and azimuth measurements, respectively. σ_r, σ_θ and σ_v are the standard deviations of the range, the azimuth and the relative velocity, respectively. The approximation is validated to be useful for practical parameters. The various measurement patterns due to the target aspect with respect to radar can be represented by the above standard measurement model by adjusting the measured point vector $\mathbf{b}_n$. A detailed description of the IMM/EKF based multi-target tracing algorithm can be found in (Kim et al., 2015)

And the possible behaviors of surrounding vehicles are predicted considered in determining the safe drivable area decision. In predicting reasonable ranges of the future states of surrounding vehicles, driving data is collected on test track and real roads to analyze the probabilistic movement characteristics of the vehicle.

The future vehicle states are described as a stochastic multi-stage process via Taylor Methods. At every time step of the prediction time horizon, a desired yaw rate is determined by the lane-keeping driver model. Suppose that the measurement noise has a normal distribution with zero mean. Hence, the predictive measurement is linearly related to the time-updated predictive state. Then, the maximum likelihood prediction of the future state is calculated by the Kalman filtering equations.

That is, behavior restrictions due to road geometry and driver characteristics such as reasonable acceleration input range are replaced with multi-stage of Kalman filtering problem by the proposed prediction algorithm. A detailed description of the vehicle's behavior prediction can be found in (Kim and Yi, 2014).

Fig.4 shows test results of other traffic tracking and its possible motion prediction. The sensing area of long range radar is depicted as green region and mid-range radar is

depicted as blue region. Red squares are current observation of radar. Blue-filled-vehicle is the estimated oncoming vehicle and blue-lined-vehicles are prediction results at 0.5s time interval. From the front cam view of Fig.4, we can see that all predicted positions are in the center of the lane. In this way, the prediction performance can be said to be clearly reasonable indirectly.
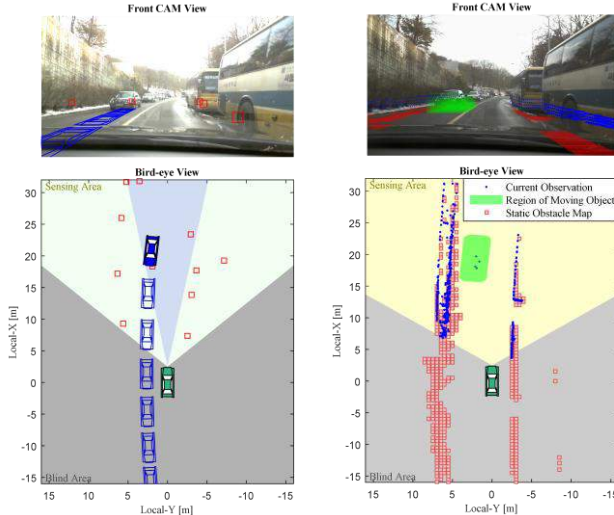
Fig.4. An example of moving object tracking and prediction.

Fig.5. An example of static obstacle map construction.

2.3. *Static Obstacle Map Construction*

A grid map representation was used for the static obstacle recognition. To cope with noisy measurement of laser scanner, we accumulate multiple observations to obtain reliable map information. Each grid of the map has the counter which indicates how many times obstacles have been observed in that grid. At each observation, the counter of each grid where obstacles exist is incremented. If the counter value of a grid is higher than a certain threshold, the grid is considered unsafe. The set of unsafe grids constitutes the current static obstacle map.

In the case of the candidates for moving objects, they are detected by comparing the current observation with estimated moving objects from radar. If the point is completely inside the region of estimated moving object, the point is considered as a part of a moving object.

Since the vehicle generates a map while it moves, we first transform the existing map to the current local position (including orientation) of the vehicle. And then current measured data is integrated to the transformed map. The position deviation of the vehicle is estimated from the odometry. To reduce the effect of accumulated error when the vehicle moves by a long distance, only thirteen latest observations are used for making the static obstacle map construction.

Fig.5 shows an example of static obstacle map construction. The sensing area of laser scanner is depicted as yellow region. Blue dots are current observation while the red squares are unsafe-grids of the constructed static obstacle map. We can

see that parked-buses on the right side and left-barrier are well tracked though they are hidden in blind area. And the part of a moving object is recognized very well.

3. Safety Driving Envelope Decision and Motion Optimization

Our approach to motion planning was to separate it into two distinct tasks (cf. Fig.1). Firstly, it is responsible for translating perceived moving objects and their prediction, static obstacles from the laser scanner, information from the digital map and vision, etc. into geometric constraints. This top level module is called as *safety driving envelope decision*. Subsequently, the *motion optimization* module computes the desired path and desired velocity of the ego-vehicle as a function of time. This trajectory is obtained by solving a geometric problem that has been posed as a convex optimization problem with linear equality/inequality constraints. These two components are addressed in the following subsections.

3.1. *Safety Driving Envelope Decision*

In order to develop a highly automated driving system, a safe driving envelope which indicates the drivable boundaries for safe driving over a finite prediction horizon should be determined with the consideration of not only current states of traffic situation surrounding the subject vehicle but also probable future states of that simultaneously (Ferguson and Dolgov, 2014).

The safety envelope decision module uses the initial driving corridor (described in section 2.1) as a constraint, and asserts that the vehicle stays in its bounds.

Starting from this initial driving corridor, static obstacles, which are represented as grid map, are combined with either the left or right corridor bound. For this coupling, for all obstacles grids, it is decided whether the ego-vehicle is supposed to pass them on the left or right. After having assigned all obstacle grids to either the left or right corridor bound, geometric constraints for motion optimization are newly computed considering driver acceptance, sensor uncertainty, and control uncertainty, etc.

To handle the probable risky situation due to surrounding vehicles whiten the finite time-horizon, the probable future states of other traffic participants should be considered. To achieve this, as described in subsection 2.2, every moving object estimated from the sensor system is associated with one lane and a future motion for the object is predicted in probabilistic methodology, assuming that the vehicle follows the lane with acceptable deviation. Similar to the static obstacles, safety envelopes are created for each of the prediction results. However, because the object is in motion, each envelop is active for a specific time step only.

Then the relative complement of predicted area of moving object and unsafe region due to static obstacle in the initial driving corridor is the set of drivable area at each time step, also termed "*safety driving envelope*".

In Fig.6, these safety envelop decision results are presented for the case of an oncoming vehicle and right side static obstacles (parked buses). All variables are expressed in term of the current local coordinate of ego vehicle. In the figure, the initial driving corridor is depicted as green area, newly computed geometric constraints due to static obstacle as red area, and active constraints due to moving object at each time step as blue area. And the blue vehicles mean the predicted oncoming vehicle and the green vehicle is the predicted ego-vehicle. Note that active constraints due to moving object is propagated as the prediction interval grows longer. Then the safety driving envelope can be defined as the relative complement of blue and red area in green area, at each time step.
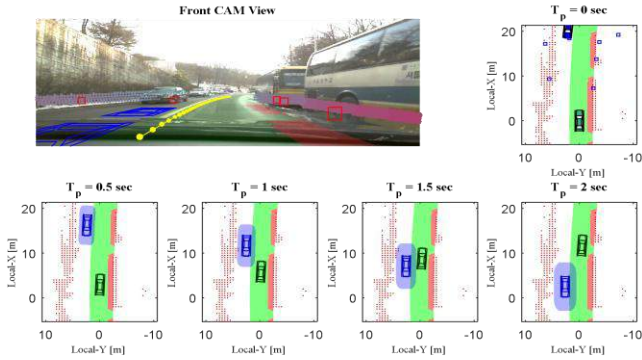
Fig.6. Safety envelop decision results at different time steps.

3.2. Model Predictive Control based Motion Planning

In order to determine the desired motion to track, a control architecture based on MPC approach is adopted. The sampling time is chosen as 0.1s and the length of the prediction horizon, N_p, is chosen as 21. These receding horizon optimization problems are solved at each time step and the first terms of the optimal control sequences are applied to the system. Then receding horizon optimization problems for a shifted prediction horizon are solved to obtain new optimal control inputs at next time step. To solve MPC problem in MATLAB, CVXGEN which is designed to be utilizable in MATLAB is used as solver (Mattingley and Boyd, 2012). The MPC problem is defined using CVXGEN syntax, and the CVXGEN returns convex optimization solver for the defined optimization solver for the defined optimization problem.

Particle motion model is used as the system model for MPC approach. State vector, input vector, and dynamic model are defined as follows:

$$\mathbf{x}_{\text{MPC},[j|k]} = \begin{bmatrix} p_{x,[j|k]} & p_{y,[j|k]} & v_{x,[j|k]} & v_{y,[j|k]} \end{bmatrix}^T \quad (10)$$

$$\mathbf{u}_{\text{MPC},[j|k]} = \begin{bmatrix} a_{x,[j|k]} & a_{y,[j|k]} \end{bmatrix}^T \quad (11)$$

$$\mathbf{x}_{\text{MPC},[j|k+1]} = \mathbf{A}_{\text{MPC},[j|k]}\mathbf{x}_{\text{MPC},[j|k]} + \mathbf{B}_{\text{MPC},[j|k]}\mathbf{u}_{\text{MPC},[j|k]} \quad (12)$$

where the system matrices are defined as follows:

$$\mathbf{A}_{\text{MPC},[j|k]} = \begin{bmatrix} 1 & 0 & \Delta t_{MPC} & 0 \\ 0 & 1 & 0 & \Delta t_{MPC} \\ 0 & 0 & 1 & 0 \\ 0 & 0 & 0 & 1 \end{bmatrix} \quad \mathbf{B}_{\text{MPC},[j|k]} = \begin{bmatrix} \dfrac{\Delta t_{MPC}^{\,2}}{2} & 0 \\ 0 & \dfrac{\Delta t_{MPC}^{\,2}}{2} \\ \Delta t_{MPC} & 0 \\ 0 & \Delta t_{MPC} \end{bmatrix}$$

MPC approach determines optimal control sequences which minimize the predefined cost function while satisfying constraints. Therefore, before the formulation of MPC problem, we should design the cost function corresponding to the objective of the control algorithm. The predictive expression of the cost function can be represented as follows:

$$
\begin{aligned}
J = &\sum_{j=1}^{N_p} \left\{ \left(\mathbf{x}_{\text{MPC},[j|k]} - \mathbf{x}_{\text{model},[j|k]} \right)^T \mathbf{Q}_{[k]} \left(\mathbf{x}_{\text{MPC},[j|k]} - \mathbf{x}_{\text{model},[j|k]} \right) \right\} \\
&+ \sum_{j=0}^{N_p-1} \left(\mathbf{u}_{\text{MPC},[j|k]}^T \mathbf{W}_{\mathbf{u},[j|k]} \mathbf{u}_{\text{MPC},[j|k]} \right) \\
&+ \sum_{j=1}^{N_p-1} \left\{ \left(\mathbf{u}_{\text{MPC},[j|k]} - \mathbf{u}_{\text{MPC},[j-1|k]} \right)^T \mathbf{W}_{\Delta\mathbf{u},[j|k]} \left(\mathbf{u}_{\text{MPC},[j|k]} - \mathbf{u}_{\text{MPC},[j-1|k]} \right) \right\}
\end{aligned}
\quad (13)
$$

where, $\mathbf{x}_{\text{model},[j|k]}$ is the initial guessed ego-vehicle states of jth prediction time step, which predicted by the methodology described in section.2.2. $\mathbf{Q}$ is predefined weighting matrix, which penalize the differences between states and rule-based predicted states, $\mathbf{W}_{\mathbf{u}}$ and $\mathbf{W}_{\Delta\mathbf{u}}$ are predefined weighting matrices for the reduction of magnitudes of control input sequences and the rate of change in control sequences respectively. These matrices are positive-definite symmetric.

The driving limit usually becomes dominated by the friction limit of the tires. This limit can be thought of as a circle of forces (Pacejka, 2005), and these constraints are given as follows:

$$\left\| \mathbf{u}_{\text{MPC},[j|k]} \right\| < u_{\max} \quad (14)$$

Safety driving envelope decision results at each predated time step should be representable as Quadratic Program to be solved with CVXGEN.
Safety driving envelope decision results at each predated time step should be representable as Quadratic Program to be solved with CVXGEN. For these QP representation, the constraints due to safety driving envelope are approximated as maximal rectangles as shown in Fig.7. The rotation of each rectangle is given from initial prediction of ego-vehicle and the maximal rectangle is decided by iterative method. Consequently, the rectangle representations can be expressed as two inequality linear equations as follows:

$$\left| \left\{ \mathbf{R}_{\text{model},[j|k]} \left(\mathbf{x}_{\text{MPC},[j|k]} - \mathbf{x}_{\text{center},[j|k]} \right) \right\}^1 \right| < p_{x,\text{margin}} \quad (15)$$

$$\left| \left\{ \mathbf{R}_{\text{model},[j|k]} \left(\mathbf{x}_{\text{MPC},[j|k]} - \mathbf{x}_{\text{center},[j|k]} \right) \right\}^2 \right| < p_{y,\text{margin}} \quad (16)$$

where the initial guessed ego-vehicle's states based rotation matrix $\mathbf{R}_{\text{model}}$ is defined as follows:

$$\mathbf{R}_{\text{model},[j|k]} = \begin{bmatrix} +\cos(\mathbf{x}_{\text{model},[j|k]}^3) & +\sin(\mathbf{x}_{\text{model},[j|k]}^3) \\ -\sin(\mathbf{x}_{\text{model},[j|k]}^3) & +\cos(\mathbf{x}_{\text{model},[j|k]}^3) \end{bmatrix}$$

As aforementioned, Fig.7 shows an example of MPC based motion planning results at the instance of meeting an oncoming vehicle. The maximal rectangle at each predicted time step is depicted as a sky-color-filled square and a cyan vehicle is the MPC solution at that time step. As can be seen in the figure, the ego-vehicle is guided along the safe region with appropriate control input sequences.

(a) at $t_p = 0.0$s

(c) at $t_p = 1.0$s

(e) at $t_p = 2.0$s
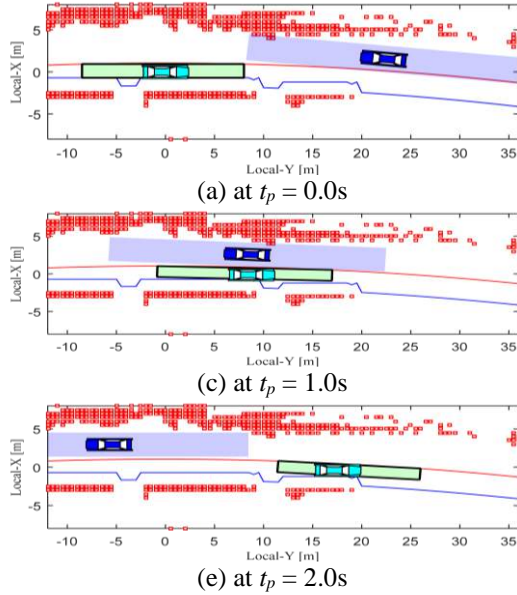
Fig.7. An example of MPC based motion planning at the instance of meeting an oncoming vehicle.

4. VEHICLE TESTS

Vehicle tests have been conducted for several times at the internal road of Seoul National University. The details of test roads are depicted in Fig.8. The given test roads have quite complicated environments to drive automatically. As can be seen in Fig.8-(b), the test vehicle drives the given route fully autonomously without a driver manipulation. The lanes were hard to be distinguished because of faded paint. There are a lot of buses parked along the road as shown in Fig.8-(c). In Fig.8-(d), there exist non-vehicle obstacles such as pedestrian and guardrail. Also, we need to consider other traffic participants like oncoming and preceding vehicles as described in Fig.8-(e).

The proposed automated driving algorithm has shown the satisfactory control performance and the test results are given in Fig.9. As shown in Fig.9, the ego-vehicle drives through a narrow urban environment with static infrastructure (buildings, trees, poles, etc.), parking cars on the right, and a preceding vehicle. Furthermore comparisons with center path tracking with the detected lane (without information fusion with GPS/Map) are given. Control input sequences from MPC solver are depicted as red line with circle marker and center-path tracking inputs as blue solid line.

Fig.9-(a) shows the result at a driving scene with two oncoming vehicles with right side static obstacles. From the figure, we can see that MPC approach guarantee the safety with oncoming vehicle by giving defense steering command.

(a) Test routes in SNU

(b) Inside of test vehicle   (c) Highly extreme condition

(d) Non-vehicle obstacles   (e) Other traffic participants
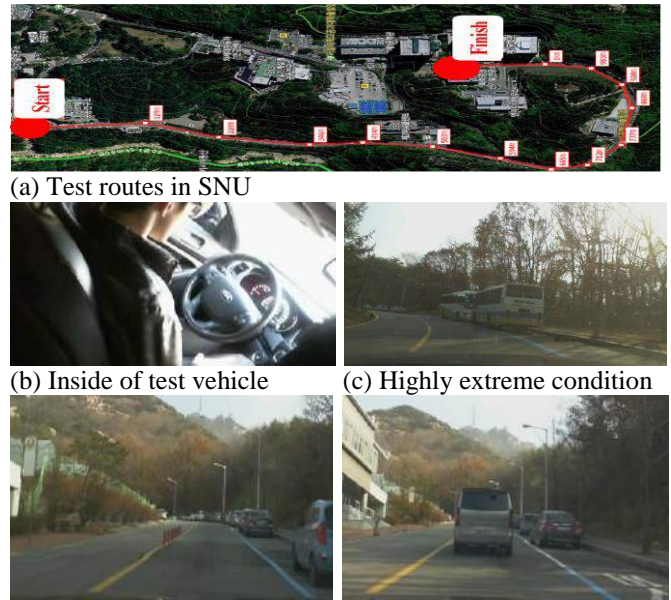
Fig.8. Configuration of vehicle tests

This results suggest that proposed algorithm may enhance the driver acceptance and driver comfort. Fig.9-(b) obtained from the situation with a preceding vehicle at the curved roads. In the case of the normal lane keeping, the proposed algorithm shows the smaller range of control while the center path tracking shows the frequent changes. Fig.9-(c) provides the driving scene with a preceding vehicle with both side obstacles (parked buses). Also in this case, the proposed algorithm shows the smaller range of control with higher speed while the center path tracking shows the frequent changes of steering with lower speed. Fig.9-(d) presents the stop control behind the decelerating preceding vehicle. In this situation, the lane is invisible due to close preceding vehicle. Consequently, the center path tracking shows the weird steering input while the proposed algorithm gives a stable performance. From the test results, it is apparent that the test vehicle successfully completed the test route with the proposed automated driving algorithm.

(a) Two oncoming vehicles   (b) Following at curved roads

(c) Both side obstacles   (d) Stopped preceding vehicle
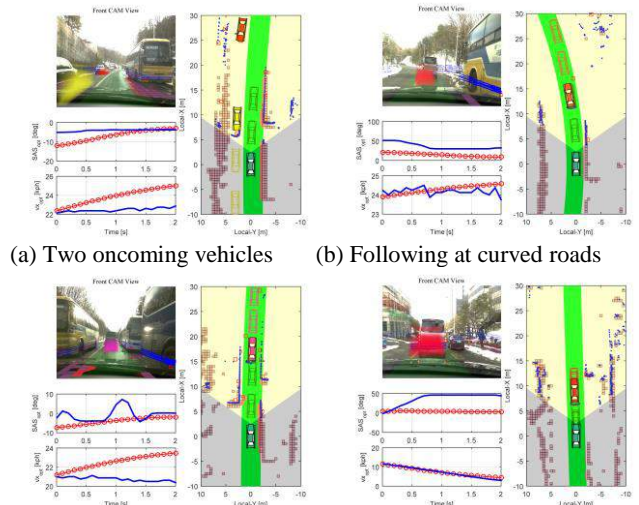
Fig.9. Test results with proposed automated driving algorithm

5. CONCLUSION

This paper has proposed a fully automated driving algorithm which is capable of automated driving on urban roads with guaranteed safety.

The proposed algorithm consisted of the following three steps: an environment representation, a motion optimization, and a vehicle control. In an environment representation, algorithms for lane-level localization, static/moving obstacle detection, and drivable area representation for safe and comfortable autonomous driving has been developed. And a motion optimization algorithm which is separated into two distinct tasks (safety driving envelope decision and motion optimization) has been proposed. The proposed motion optimization algorithm solves a geometric constraint problem as a convex optimization problem with linear equality/inequality constraints. The effectiveness of the proposed automated driving algorithm is evaluated via vehicle tests. From the test results it is shown that proposed automated driving algorithm can shows the robust performance on an inner-city street scenario.

A further improvement of the autonomous vehicle's ability to interpret a given traffic scenario and to obtain a meaningful behavior prediction of other traffic participants is imperative to achieve incomparable performance and to extend the covering area of autonomous driving.

ACKNOWLEDGMENT

REFERENCES

ENACHE, N. M., MAMMAR, S., NETTO, M. & LUSETTI, B. 2010. Driver steering assistance for lane-departure avoidance based on hybrid automata and composite Lyapunov function. *Intelligent Transportation Systems, IEEE Transactions on,* 11**,** 28-39.

FERGUSON, D. I. F. & DOLGOV, D. A. 2014. Modifying behavior of autonomous vehicle based on predicted behavior of other vehicles. Google Patents.

FURGALE, P., SCHWESINGER, U., RUFLI, M., DERENDARZ, W., GRIMMETT, H., MUHLFELLNER, P., WONNEBERGER, S., TIMPNER, J., ROTTMANN, S. & LI, B. Toward automated driving in cities using close-to-market sensors: An overview of the V-Charge Project. Intelligent Vehicles Symposium (IV), 2013 IEEE, 2013. IEEE, 809-816.

HOEDEMAEKER, M. & BROOKHUIS, K. A. 1998. Behavioural adaptation to driving with an adaptive cruise control (ACC). *Transportation Research Part F: Traffic Psychology and Behaviour,* 1**,** 95-106.

JUNG, H. G., KIM, D. S., YOON, P. J. & KIM, J. Parking slot markings recognition for automatic parking assist system. Intelligent Vehicles Symposium, 2006 IEEE, 2006. IEEE, 106-113.

KIM, B. & YI, K. 2014. Probabilistic and Holistic Prediction of Vehicle States Using Sensor Fusion for Application to Integrated Vehicle Safety Systems. *Intelligent Transportation Systems, IEEE Transactions on,* 15**,** 2178-2190.

KIM, B., YI, K., YOO, H.-J., CHONG, H.-J. & KO, B. 2015. An IMM/EKF Approach for Enhanced Multitarget State Estimation for Application to Integrated Risk Management System. *Vehicular Technology, IEEE Transactions on,* 64**,** 876-889.

MATTINGLEY, J. & BOYD, S. 2012. CVXGEN: a code generator for embedded convex optimization. *Optimization and Engineering,* 13**,** 1-27.

O'MALLEY, R., JONES, E. & GLAVIN, M. 2010. Rear-lamp vehicle detection and tracking in low-exposure color video for night conditions. *Intelligent Transportation Systems, IEEE Transactions on,* 11**,** 453-462.

PACEJKA, H. 2005. *Tire and vehicle dynamics*, Elsevier.

RE, K. 1960. A New Approach to Linear Filtering and Prediction. *Transection of the ASME-Journal of Basic Engineering***,** 35-45.

SCHULZE, M., NOCKER, G. & BOHM, K. PReVENT: A European program to improve active safety. Proc. of 5th International Conference on Intelligent Transportation Systems Telecommunications, France, 2005.

SWARTZ, D. Clothoid road geometry unsuitable for sensor fusion. IEEE Intelligent Vehicles Symposium, 2003. 484-488.

TINGVALL, C. & HAWORTH, N. Vision Zero: an ethical approach to safety and mobility. 6th ITE International Conference Road Safety & Traffic Enforcement: Beyond, 2000.

YOON, J., KIM, D. & YI, K. 2007. Design of a rollover index-based vehicle stability control scheme. *Vehicle system dynamics,* 45**,** 459-475.

ZIEGLER, J., BENDER, P., SCHREIBER, M., LATEGAHN, H., STRAUSS, T., STILLER, C., DANG, T., FRANKE, U., APPENRODT, N. & KELLER, C. G. 2014. Making bertha drive—An autonomous journey on a historic route. *Intelligent Transportation Systems Magazine, IEEE,* 6**,** 8-20.

Index of Authors

FAST-zero' 15

3rd International Symposium on
Future Active Safety Technology
Toward zero traffic accidents

www.fastzero15.net